



Vibration Theory and Applications with Finite Elements and Active Vibration Control

Alan Palazzolo



WILEY

Vibration Theory and Applications with Finite Elements and Active Vibration Control

Vibration Theory and Applications with Finite Elements and Active Vibration Control

Alan B. Palazzolo

*Mechanical Engineering
Texas A&M University
College Station, TX, USA*

WILEY

This edition first published 2016
© 2016 John Wiley & Sons, Ltd

Registered Office

John Wiley & Sons, Ltd, The Atrium, Southern Gate, Chichester, West Sussex, PO19 8SQ, United Kingdom

For details of our global editorial offices, for customer services and for information about how to apply for permission to reuse the copyright material in this book please see our website at www.wiley.com.

The right of the author to be identified as the author of this work has been asserted in accordance with the Copyright, Designs and Patents Act 1988.

All rights reserved. No part of this publication may be reproduced, stored in a retrieval system, or transmitted, in any form or by any means, electronic, mechanical, photocopying, recording or otherwise, except as permitted by the UK Copyright, Designs and Patents Act 1988, without the prior permission of the publisher.

Wiley also publishes its books in a variety of electronic formats. Some content that appears in print may not be available in electronic books.

Designations used by companies to distinguish their products are often claimed as trademarks. All brand names and product names used in this book are trade names, service marks, trademarks or registered trademarks of their respective owners. The publisher is not associated with any product or vendor mentioned in this book.

Limit of Liability/Disclaimer of Warranty: While the publisher and author have used their best efforts in preparing this book, they make no representations or warranties with respect to the accuracy or completeness of the contents of this book and specifically disclaim any implied warranties of merchantability or fitness for a particular purpose. It is sold on the understanding that the publisher is not engaged in rendering professional services and neither the publisher nor the author shall be liable for damages arising herefrom. If professional advice or other expert assistance is required, the services of a competent professional should be sought.

Library of Congress Cataloging-in-Publication Data

Palazzolo, Alan B., author.

Vibration theory and applications with finite elements and active vibration control / Alan B. Palazzolo, Texas A&M University, TX, USA.

pages cm

Includes bibliographical references and index.

ISBN 978-1-118-35080-5 (cloth)

1. Vibration—Mathematical models. 2. Finite element method. I. Title.

TA355.P235 2016

531'.320151825—dc23

2015025684

A catalogue record for this book is available from the British Library.

Set in 10/12pt Times by SPi Global, Pondicherry, India

Contents

Preface xv

Acknowledgments and Dedication xxi

About the Companion Website xxiii

List of Acronyms xxv

1 Background, Motivation, and Overview 1

- 1.1 Introduction 1
- 1.2 Background 1
 - 1.2.1 Units 5
- 1.3 Our Vibrating World 6
 - 1.3.1 Small-Scale Vibrations 6
 - 1.3.2 Medium-Scale (Mesoscale) Vibrations 8
 - 1.3.3 Large-Scale Vibrations 8
- 1.4 Harmful Effects of Vibration 9
 - 1.4.1 Human Exposure Limits 9
 - 1.4.2 High-Cycle Fatigue Failure 11
 - 1.4.3 Rotating Machinery Vibration 21
 - 1.4.4 Machinery Productivity 27
 - 1.4.5 Fastener Looseness 28
 - 1.4.6 Optical Instrument Blurring 28
 - 1.4.7 Ethics and Professional Responsibility 29
 - 1.4.8 Lifelong Learning Opportunities 29
- 1.5 Stiffness, Inertia, and Damping Forces 29
- 1.6 Approaches for Obtaining the Differential Equations of Motion 34
- 1.7 Finite Element Method 35
- 1.8 Active Vibration Control 37
- 1.9 Chapter 1 Exercises 37
 - 1.9.1 Exercise Location 37
 - 1.9.2 Exercise Goals 37
 - 1.9.3 Sample Exercises: 1.6 and 1.11 38
- References 38

2 Preparatory Skills: Mathematics, Modeling, and Kinematics 41

- 2.1 Introduction 41
- 2.2 Getting Started with MATLAB and MAPLE 42
 - 2.2.1 MATLAB 42
 - 2.2.2 MAPLE (Symbolic Math) 45
- 2.3 Vibration and Differential Equations 50
 - 2.3.1 MATLAB and MAPLE Integration 50

2.4	Taylor Series Expansions and Linearization	56
2.5	Complex Variables (CV) and Phasors	60
2.6	Degrees of Freedom, Matrices, Vectors, and Subspaces	63
	2.6.1 <i>Matrix–Vector Related Definitions and Identities</i>	69
2.7	Coordinate Transformations	75
2.8	Eigenvalues and Eigenvectors	79
2.9	Fourier Series	80
2.10	Laplace Transforms, Transfer Functions, and Characteristic Equations	83
2.11	Kinematics and Kinematic Constraints	86
	2.11.1 <i>Particle Kinematic Constraint</i>	86
	2.11.2 <i>Rigid Body Kinematic Constraint</i>	90
	2.11.3 <i>Assumed Modes Kinematic Constraint</i>	96
	2.11.4 <i>Finite Element Kinematic Constraint</i>	98
2.12	Dirac Delta and Heaviside Functions	100
2.13	Chapter 2 Exercises	101
	2.13.1 <i>Exercise Location</i>	101
	2.13.2 <i>Exercise Goals</i>	101
	2.13.3 <i>Sample Exercises: 2.9 and 2.17</i>	101
	References	102

3 Equations of Motion by Newton’s Laws 103

3.1	Introduction	103
3.2	Particle Motion Approximation	103
3.3	Planar (2D) Rigid Body Motion Approximation	107
	3.3.1 <i>Translational Equations of Motion</i>	107
	3.3.2 <i>Rotational Equation of Motion</i>	108
3.4	Impulse and Momentum	129
	3.4.1 <i>Linear Impulse and Momentum</i>	129
	3.4.2 <i>Angular Impulse and Momentum</i>	134
3.5	Variable Mass Systems	138
3.6	Chapter 3 Exercises	140
	3.6.1 <i>Exercise Location</i>	140
	3.6.2 <i>Exercise Goals</i>	140
	3.6.3 <i>Sample Exercises: 3.8 and 3.21</i>	141
	References	141

4 Equations of Motion by Energy Methods 143

4.1	Introduction	143
4.2	Kinetic Energy	143
	4.2.1 <i>Particle Motion</i>	143
	4.2.2 <i>Two-Dimensional Rigid Body Motion</i>	144
	4.2.3 <i>Constrained 2D Rigid Body Motion</i>	146
4.3	External and Internal Work and Potential Energy	147
	4.3.1 <i>External Work and Potential Energy</i>	150
4.4	Power and Work–Energy Laws	151
	4.4.1 <i>Particles</i>	151
	4.4.2 <i>Rigid Body with 2D Motion</i>	153

4.5	Lagrange Equation for Particles and Rigid Bodies	157
4.5.1	<i>Derivation of the Lagrange Equation</i>	158
4.5.2	<i>System of Particles</i>	160
4.5.3	<i>Collection of Rigid Bodies</i>	162
4.5.4	<i>Potential, Circulation, and Dissipation Functions</i>	168
4.5.5	<i>Summary for Lagrange Equation</i>	182
4.5.6	<i>Nonconservative Generalized Forces and Virtual Work</i>	183
4.5.7	<i>Effects of Gravity for the Lagrange Approach</i>	195
4.5.8	<i>“Automating” the Derivation of the LE Approach</i>	201
4.6	LE for Flexible, Distributed Mass Bodies: Assumed Modes Approach	211
4.6.1	<i>Assumed Modes Kinetic Energy and Mass Matrix Expressions</i>	212
4.6.2	<i>Rotating Structures</i>	215
4.6.3	<i>Internal Forces and Strain Energy of an Elastic Object</i>	216
4.6.4	<i>The Assumed Modes Approximation</i>	219
4.6.5	<i>Generalized Force for External Loads Acting on a Deformable Body</i>	221
4.6.6	<i>Assumed Modes Model Generalized Forces for External Load Acting on a Deformable Body</i>	221
4.6.7	<i>LE for a System of Rigid and Deformable Bodies</i>	223
4.7	LE for Flexible, Distributed Mass Bodies: Finite Element Approach—General Formulation	267
4.7.1	<i>Element Kinetic Energy and Mass Matrix</i>	267
4.7.2	<i>Element Stiffness Matrix</i>	269
4.7.3	<i>Summary</i>	272
4.8	LE for Flexible, Distributed Mass Bodies: Finite Element Approach—Bar/Truss Modes	275
4.8.1	<i>Introduction</i>	275
4.8.2	<i>1D Truss/Bar Element</i>	276
4.8.3	<i>1D Truss/Bar Element: Element Stiffness Matrix</i>	276
4.8.4	<i>1D Truss/Bar Element: Element Mass Matrix</i>	277
4.8.5	<i>1D Truss/Bar Element: Element Damping Matrix</i>	277
4.8.6	<i>1D Truss/Bar Element: Generalized Force Vector</i>	278
4.8.7	<i>1D Truss/Bar Element: Nodal Connectivity Array</i>	279
4.8.8	<i>System of 1D Bar Elements: Matrix Assembly</i>	280
4.8.9	<i>Incorporation of Displacement Constraint</i>	285
4.8.10	<i>Modeling of 2D Trusses</i>	289
4.8.11	<i>2D Truss/Bar Element: Element Stiffness Matrix</i>	292
4.8.12	<i>2D Truss/Bar Element: Element Mass Matrix</i>	293
4.8.13	<i>2D Truss/Bar Element: Element Damping Matrix</i>	294
4.8.14	<i>2D Truss/Bar Element: Element Force Vector</i>	295
4.8.15	<i>2D Truss/Bar Element: Element Action Vector</i>	296
4.8.16	<i>2D Truss/Bar Element: Degree of Freedom Connectivity Array and Matrix Assembly</i>	296
4.8.17	<i>2D Truss/Bar Element: Rigid Region Modeling for 2D Trusses</i>	303
4.9	Chapter 4 Exercises	306
4.9.1	<i>Exercise Location</i>	306
4.9.2	<i>Exercise Goals</i>	307
4.9.3	<i>Sample Exercises: 4.43 and 4.52</i>	307
	References	308

5 Free Vibration Response 309

- 5.1 Introduction 309
- 5.2 Single Degree of Freedom Systems 309
 - 5.2.1 *SDOF Eigenvalues (Characteristic Roots)* 310
 - 5.2.2 *SDOF Initial Condition Response* 311
 - 5.2.3 *Log Decrement: A Measure of Damping—Displacement-Based Measurement* 313
 - 5.2.4 *Log Decrement: A Measure of Damping—Acceleration-Based Measurement* 315
- 5.3 Two-Degree-of-Freedom Systems 319
 - 5.3.1 *Special Case I ($\underline{C} = \underline{G} = \underline{K}_C = \underline{0}$) (Undamped, Nongyroscopic, and Noncirculatory Case)* 322
 - 5.3.2 *Special Case II $\underline{C} = \underline{K}_C = \underline{0}$ (Undamped, Gyroscopic, and Noncirculatory Case)* 332
 - 5.3.3 *Special Case III $\underline{C} = \underline{G} = \underline{0}$ (Undamped, Nongyroscopic, and Circulatory Case)* 342
- 5.4 *N-Degree-of-Freedom Systems* 346
 - 5.4.1 *General Identities* 346
 - 5.4.2 *Undamped, Nongyroscopic, and Noncirculatory Systems—Description* 346
 - 5.4.3 *Undamped, Nongyroscopic, and Noncirculatory Systems—Solution Form* 347
 - 5.4.4 *Undamped, Nongyroscopic, and Noncirculatory Systems—Orthogonality* 349
 - 5.4.5 *Undamped, Nongyroscopic, and Noncirculatory Systems—IC Response* 351
 - 5.4.6 *Undamped, Nongyroscopic, and Noncirculatory Systems—Rigid Body Modes* 352
 - 5.4.7 *Summary* 353
 - 5.4.8 *Undamped, Nongyroscopic, and Noncirculatory Systems—Response to an IC Modal Displacement Distribution* 363
 - 5.4.9 *Orthogonally Damped, Nongyroscopic, and Noncirculatory Systems—Description* 364
 - 5.4.10 *Orthogonally Damped, Nongyroscopic, and Noncirculatory Systems—Eigenvalues and Eigenvectors* 365
 - 5.4.11 *Orthogonally Damped, Nongyroscopic, and Noncirculatory Systems—IC Response* 366
 - 5.4.12 *Orthogonally Damped, Nongyroscopic, and Noncirculatory Systems—Determination of \underline{C}_0* 367
 - 5.4.13 *Nonorthogonally Damped System with Symmetric Mass, Stiffness, and Damping Matrices* 377
 - 5.4.14 *Undamped, Gyroscopic, and Noncirculatory Systems—Description* 379
 - 5.4.15 *Undamped, Gyroscopic, and Noncirculatory Systems—Eigenvalues and Eigenvectors* 380
 - 5.4.16 *Undamped, Gyroscopic, and Noncirculatory Systems—Biorthogonality* 385
 - 5.4.17 *General Linear Systems—Description* 388
 - 5.4.18 *General Linear Systems—Biorthogonality* 389

5.5	Infinite Dof Continuous Member Systems	390
5.5.1	<i>Introduction</i>	390
5.5.2	<i>Transverse Vibration of Strings and Cables</i>	390
5.5.3	<i>Axial Vibration of a Uniform Bar</i>	394
5.5.4	<i>Torsion of Bars</i>	396
5.5.5	<i>Euler–Bernoulli (Classical) Beam Theory</i>	400
5.5.6	<i>Timoshenko Beam Theory</i>	404
5.6	Unstable Free Vibrations	408
5.6.1	<i>Oil Film Bearing-Induced Instability</i>	411
5.7	Summary	418
5.8	Chapter 5 Exercises	418
5.8.1	<i>Exercise Location</i>	418
5.8.2	<i>Exercise Goals</i>	418
5.8.3	<i>Sample Exercises: 5.25 and 5.35</i>	419
	References	419

6 Vibration Response Due to Transient Loading 421

6.1	Introduction	421
6.2	Single Degree of Freedom Transient Response	421
6.2.1	<i>Direct Analytical Solution Method</i>	422
6.2.2	<i>Laplace Transform Method</i>	428
6.2.3	<i>Convolution Integral</i>	434
6.2.4	<i>Response to Successive Disturbances</i>	438
6.2.5	<i>Pulsed Excitations</i>	440
6.2.6	<i>Response Spectrum</i>	444
6.3	Modal Condensation of N dof: Transient Forced Vibrating Systems	451
6.3.1	<i>Undamped and Orthogonally Damped Nongyroscopic, Noncirculatory Systems</i>	452
6.3.2	<i>Unconstrained Structures</i>	465
6.3.3	<i>Base Excitation</i>	475
6.3.4	<i>Participation Factor and Modal Effective Mass</i>	477
6.3.5	<i>General Nonsymmetric, Nonorthogonal Damping Models</i>	488
6.4	Numerical Integration of N dof Transient Vibration Response	493
6.4.1	<i>Second-Order System NI Algorithms</i>	494
6.4.2	<i>First-Order System NI Algorithms</i>	500
6.5	Summary	521
6.6	Chapter 6 Exercises	522
6.6.1	<i>Exercise Location</i>	522
6.6.2	<i>Exercise Goals</i>	522
6.6.3	<i>Sample Exercises: 6.18 and 6.21</i>	522
	References	523

7 Steady-State Vibration Response to Periodic Loading 525

7.1	Introduction	525
7.2	Complex Phasor Approach	525
7.3	Single Degree of Freedom Models	527
7.3.1	<i>Class I ($f(t) \neq 0, y(t) = 0$): No Support Excitation—Only External Forcing</i>	529

7.3.2	<i>Class II ($f(t) = 0, y(t) \neq 0$): Only Support Excitation—No External Forcing</i>	535
7.3.3	<i>Half Power Point Damping Identification</i>	538
7.3.4	<i>Phase Slope Damping Identification</i>	541
7.3.5	<i>Accurate Measurement of ω_n</i>	541
7.3.6	<i>Experimental Parameter Identification: Receptances</i>	543
7.3.7	<i>Steady-State Harmonic Response of a Jeffcott Rotor and Rotor Balancing</i>	545
7.3.8	<i>Single Plane Influence Coefficient Balancing</i>	549
7.3.9	<i>Related American Petroleum Institute Standards for Balancing</i>	551
7.3.10	<i>Response of an SDOF Oscillator to Nonsinusoidal, Periodic Excitation</i>	552
7.3.11	<i>Forced Harmonic Response with Elastomeric Stiffness and Damping</i>	556
7.4	<i>Two Degree of Freedom Response</i>	559
7.4.1	<i>Vibration Absorber: Principles</i>	560
7.4.2	<i>Vibration Absorber: Mass Ratio Effect</i>	563
7.5	<i>N Degree of freedom Steady-State Harmonic Response</i>	566
7.5.1	<i>Direct Approach</i>	566
7.5.2	<i>Modal Approach</i>	570
7.5.3	<i>Receptances</i>	572
7.5.4	<i>Receptance-Based Synthesis</i>	575
7.5.5	<i>Dominance of a Single Mode in the Steady-State Harmonic Response</i>	577
7.5.6	<i>Receptance-Based Modal Parameter Identification: Method I</i>	578
7.5.7	<i>Receptance-Based Modal Parameter Identification: Method II</i>	585
7.5.8	<i>Modal Assurance Criterion for Mode Shape Correlation</i>	590
7.6	<i>Other Phasor Ratio Measures of Steady-State Harmonic Response</i>	591
7.7	<i>Summary</i>	593
7.8	<i>Chapter 7 Exercises</i>	593
7.8.1	<i>Exercise Location</i>	593
7.8.2	<i>Exercise Goals</i>	594
7.8.3	<i>Sample Exercises: 7.9 and 7.23</i>	594
	<i>References</i>	594

8 Approximate Methods for Large-Order Systems 595

8.1	<i>Introduction</i>	595
8.2	<i>Guyan Reduction: Static Condensation</i>	596
8.3	<i>Substructures: Superelements</i>	608
8.4	<i>Modal Synthesis</i>	609
8.4.1	<i>Uncoupled System Equations</i>	610
8.4.2	<i>Coupled System Equations: Displacement Compatibility at Junction</i>	611
8.4.3	<i>Coupled System Equations: Subspace Condensation</i>	611
8.5	<i>Eigenvalue/Natural Frequency Changes for Perturbed Systems</i>	620
8.5.1	<i>Undamped, Nongyroscopic, Noncirculatory \underline{M} and \underline{K} Type Systems</i>	620
8.5.2	<i>Orthogonally Damped Systems</i>	624
8.5.3	<i>Rayleigh's Quotient</i>	631

- 8.6 Summary 633
- 8.7 Chapter 8 Exercises 634
 - 8.7.1 Exercise Location 634
 - 8.7.2 Exercise Goals 634
 - 8.7.3 Sample Exercises 8.4 and 8.13 634
- References 635

9 Beam Finite Elements for Vibration Analysis 637

- 9.1 Introduction 637
- 9.2 Modeling 2D Frame Structures with Euler–Bernoulli Beam Elements 637
 - 9.2.1 2D Frame Element Stiffness Matrix and Strain Energy: Transverse Deflection 639
 - 9.2.2 2D Frame Element Stiffness Matrix and Strain Energy: Axial Deflection 641
 - 9.2.3 2D Frame Element Stiffness Matrix and Strain Energy 642
 - 9.2.4 2D Frame Element Mass Matrix 642
 - 9.2.5 2D Frame Element Force Vector 644
 - 9.2.6 2D Frame Element Stiffness and Mass Matrices and Force Vector: Transformation to Global Coordinates 646
 - 9.2.7 2D Frame: Beam Element Assembly Algorithm 654
 - 9.2.8 Imposed Support Excitation Modeling 666
- 9.3 Three-Dimensional Timoshenko Beam Elements: Introduction 670
- 9.4 3D Timoshenko Beam Elements: Nodal Coordinates 672
- 9.5 3D Timoshenko Beam Elements: Shape Functions, Element Stiffness, and Mass Matrices 679
 - 9.5.1 Strain–Displacement Relations and Shear Form Factors 681
 - 9.5.2 \tilde{x}_1 – \tilde{x}_2 Plane, Translational Differential Equations, Shape Functions, and Stiffness and Mass Matrices 684
 - 9.5.3 \tilde{x}_1 – \tilde{x}_3 Plane, Translational Differential Equations, Shape Functions, and Stiffness and Mass Matrices 691
 - 9.5.4 Axial (Longitudinal) \tilde{x}_1 Differential Equation, Shape Functions, and Stiffness and Mass Matrices 696
 - 9.5.5 Torsional $\tilde{\theta}_1$ Differential Equation, Shape Functions, and Stiffness and Mass Matrices 698
 - 9.5.6 Twelve-Dof Element Stiffness Matrix 700
 - 9.5.7 Twelve-Dof Element Mass Matrix 703
- 9.6 3D Timoshenko Beam Element Force Vectors 704
 - 9.6.1 Axial Loads 706
 - 9.6.2 Torsional Loads 706
 - 9.6.3 \tilde{x}_1 – \tilde{x}_2 Plane Loads 707
 - 9.6.4 \tilde{x}_1 – \tilde{x}_3 Plane Loads 709
 - 9.6.5 Element Load Vector 711
- 9.7 3D Frame: Beam Element Assembly Algorithm 713
- 9.8 2D Frame Modeling with Timoshenko Beam Elements 725
- 9.9 Summary 748
- 9.10 Chapter 9 Exercises 749
 - 9.10.1 Exercise Location 749
 - 9.10.2 Exercise Goals 749
 - 9.10.3 Sample Exercises: 9.4 and 9.15a 749
- References 750

10 2D Planar Finite Elements for Vibration Analysis 751

- 10.1 Introduction 751
- 10.2 Plane Strain ($P\epsilon$) 751
- 10.3 Plane Stress ($P\sigma$) 753
- 10.4 Plane Stress and Plane Strain: Element Stiffness and Mass Matrices and Force Vector 754
 - 10.4.1 External Forces 760
 - 10.4.2 Concentrated Forces 760
 - 10.4.3 General Volumetric Loading 761
 - 10.4.4 Edge Loads 762
- 10.5 Assembly Procedure for 2D, 4-Node, Quadrilateral Elements 763
- 10.6 Computation of Stresses in 2D Solid Elements 768
 - 10.6.1 Interior Stress Determination 768
 - 10.6.2 Surface Stresses 770
- 10.7 Extra Shape Functions to Improve Accuracy 774
- 10.8 Illustrative Example 776
- 10.9 2D Axisymmetric Model 786
 - 10.9.1 Axisymmetric Model Stresses and Strains 786
 - 10.9.2 4-Node, Bilinear Axisymmetric Element 788
- 10.10 Automated Mesh Generation: Constant Strain Triangle Elements 801
 - 10.10.1 Element Stiffness Matrix 803
 - 10.10.2 Element Mass Matrix 803
 - 10.10.3 System Matrix Assembly 804
- 10.11 Membranes 810
 - 10.11.1 Kinetic Energy and Element Mass Matrix 810
 - 10.11.2 Strain Potential Energy and Element Stiffness Matrix 811
 - 10.11.3 Matrix Assembly 812
- 10.12 Banded Storage 815
- 10.13 Chapter 10 Exercises 820
 - 10.13.1 Exercise Location 820
 - 10.13.2 Exercise Goals 821
 - 10.13.3 Sample Exercises: 10.5 and 10.8 821
- References 822

11 3D Solid Elements for Vibration Analysis 823

- 11.1 Introduction 823
- 11.2 Element Stiffness Matrix 825
 - 11.2.1 Shape Functions 825
 - 11.2.2 Element Stiffness Matrix Integral and Summation Forms 828
- 11.3 The Element Mass Matrix and Force Vector 835
 - 11.3.1 Element Mass Matrix 836
 - 11.3.2 Element External Force Vector 836
 - 11.3.3 Force Vector: Concentrated Nodal Forces 837
 - 11.3.4 Force Vector: Volumetric Loads 838
 - 11.3.5 Force Vector: Face Loading 839
- 11.4 Assembly Procedure for the 3D, 8-Node, Hexahedral Element Model 842
- 11.5 Computation of Stresses for a 3D Hexahedral Solid Element 846
 - 11.5.1 Computation of Interior Stress 846
 - 11.5.2 Computation of Surface Stresses 848

11.5.3	<i>Coordinate Transformation</i>	849
11.5.4	<i>Geometry Mapping in Surface Tangent Coordinates</i>	850
11.5.5	<i>Displacements in the Surface Tangent Coordinate System</i>	851
11.5.6	<i>Strains in the Surface Tangent Coordinate System</i>	851
11.5.7	<i>Surface Stresses Obtained from Cauchy's Boundary Formula</i>	852
11.5.8	<i>Surface Stresses Obtained from the Constitutive Law and Surface Strains</i>	853
11.5.9	<i>Summary of Surface Stress Computation</i>	854
11.6	3D Solid Element Model Example	856
11.7	3D Solid Element Summary	864
11.8	Chapter 11 Exercises	865
11.8.1	<i>Exercise Location</i>	865
11.8.2	<i>Exercise Goals</i>	865
11.8.3	<i>Sample Exercises: 11.2 and 11.3</i>	865
	References	866

12 Active Vibration Control 867

12.1	Introduction	867
12.2	AVC System Modeling	871
12.3	AVC Actuator Modeling	874
12.4	System Model with an Infinite Bandwidth Feedback Approximation	878
12.4.1	<i>Closed-Loop Feedback Controlled System Model</i>	882
12.5	System Model with Finite Bandwidth Feedback	886
12.6	System Model with Finite Bandwidth Feedback and Lead Compensation	893
12.6.1	<i>Transfer Function Approach</i>	893
12.6.2	<i>State Space Approach</i>	897
12.7	Sensor/Actuator Noncollocation Effect on Vibration Stability	901
12.8	Piezoelectric Actuators	907
12.8.1	<i>Piezoelectric Stack Actuator</i>	908
12.8.2	<i>Piezoelectric Layer (Patch) Actuator</i>	915
12.9	Summary	923
12.10	Chapter 12 Exercises	923
12.10.1	<i>Exercise Location</i>	923
12.10.2	<i>Exercise Goals</i>	923
12.10.3	<i>Sample Exercise: 12.1</i>	923
	References	924

Appendix A Fundamental Equations of Elasticity 927

Index 941

Preface

The material in this text is drawn from the author's 35 years of teaching, research, and industrial experiences in the areas of vibrations, finite elements, dynamics, and feedback control. The teaching experiences include both undergraduate and graduate course instruction in vibrations, graduate courses in finite elements and boundary elements, and undergraduate courses in controls and dynamics. The research experiences include performing sponsored research for NASA Glenn and Marshall, ONR, ARL, DOE, and a host of industrial companies. The industrial experience is drawn from employment at Southwest Research Institute, Bently Nevada, and Allis-Chalmers Corp.

The pedagogical motivation for this book resulted from a desire to fulfill the following perceived needs of college and university students and practicing engineers and scientists for learning vibrations and finite elements:

1. Provide a convincing and motivational first chapter about “why” the material presented in the book is important. As was so eloquently expressed in the writings of John Henry Newman, learning for the sake of exercising the intellectual dimension of the person is an important activity which enriches our life experience and strengthens our reasoning faculties with endless benefits. This is very true; however, the application of this knowledge to better understand nature and direct it to better the human condition through engineering practice is also an important motivational benefit for the reader. For this reason, Chapter 1 provides an overview of everyday vibration experiences, fundamental concepts, deleterious effects of vibrations, and industrial standards. A brief introduction to the concept of finite elements is also included, which is the most common tool for vibration analysis in industry and research. Finally, Chapter 1 concludes with a discussion of the concept of active vibration control, which is one area of “smart” technologies that seem ubiquitous in engineering and popular news.
2. Provide a chapter that contains subjects that need to be initially grasped in order to more quickly comprehend and utilize the core material that appears in the later chapters. The preparation subjects include computer coding, mathematical theory, modeling, and kinematic constraints. Quite often, the above subjects are folded into the major areas such as free and forced vibration theory or are relegated to appendices that in the author's experience are rarely referenced. Chapter 2 presents these preparatory subjects in an isolated, front, and center manner with the goal of providing a solid background for the reader before he or she embarks on using them in sometimes subtle steps, nested in more complicated vibration theory and problems. Divide and conquer is a very effective strategy in vibrations, as in all educational pursuits!

This chapter also introduces the student to the use of the symbolic math codes MAPLE and MATLAB symbolic. These tools are utilized in many of the chapters to facilitate complicated and tedious algebraic and differential and integral calculus calculations in an elegant and minimal error manner. Working knowledge of these tools will aid the reader in many areas of engineering practice which fulfills a holistic learning goal of engineering education.

The common thread for implementation of structural modeling methods is kinematic constraints (deformation assumptions). As discussed in Chapter 2, rigid body, assumed modes (Rayleigh–Ritz), finite elements, and boundary element models all impose

kinematic constraints (deformation assumptions) that reduce the dimensionality of a structural model in order to provide a practical solution path to its governing differential equations. Understanding this common thread removes some of the apprehension for learning or instructing assumed modes or finite elements, when they are viewed as extensions of more elementary and familiar kinematic constraints. These may include coupled rigid body systems or examples from strength of materials, for example, plane sections remain plane in the beam deformation theory.

3. Provide initial chapters that elucidate the understanding and application of Newton's laws (Chapter 3) and the energy-based (Chapter 4) approaches (conservation and Lagrange equations) for deriving governing differential equations. Instructional experience has so often exposed the inability of students to derive accurate governing differential equations, prior to utilizing them to obtain vibration-related response characteristics such as natural frequencies, transient response, etc. The student's solution is maimed by an erroneous governing equation from the start, and the ensuing results are misleading and often nonsensical. This occurs in spite of the possible mastery of other modeling, simulation, and presentation skills. Frankly speaking, garbage in leads to garbage out (no matter how polished and visual is its presentation format).

Chapter 4 demonstrates that the most widely used engineering vibration simulation tool—finite elements—follows naturally from Lagrange equations with the removal of the kinematic (deformation) constraints (assumptions) of the simpler models. This requires a somewhat rigorous demonstration that Lagrange's equations are valid for flexible members and their assemblages in structural systems. Most texts leap over this demonstration by implicitly invoking a variant of "it can be shown." Thus, it is presupposed that the demonstration of the generalized force of a coil spring being obtained from the derivative of its potential energy is sufficient for justifying the application of the same approach for modeling the elastic properties of a 10 000-degree-of-freedom solar panel array on a satellite. This approach, although ultimately valid, is deficient for leaving an important gap in the sound understanding of the approach by the reader. The chapter also provides detailed derivations of the Lagrange equations for rigid body, assumed modes, and finite element-type models with a wide variety of stiffness and damping interconnections.

The assumed modes section of Chapter 4 is included for its intrinsic modeling value and as an introduction to the finite element approach. The chapter also utilizes bar/truss elements for the initial presentation of deriving finite element stiffness and mass matrices and force vectors and for the matrix assembly procedure. The assembly procedure is presented with significant detail for fully automating in a computer code, for both free and constrained structures. The method presented is nearly universal and is applied without significant modification for beams in Chapter 9, 2D and axisymmetric solids and membranes in Chapter 10, and 3D solids in Chapter 11.

Symbolic math examples are provided in both **Chapters 3** and **4** to demonstrate their usage for automating steps in deriving equations of motion, such as substitutions, combination, sorting, integrations, and differentiations, which typically are steps prone to error when worked by hand.

4. Provide a more pedagogically effective approach for instructing free, transient, and harmonic vibrations as compared with the traditional approach. The major simulation application areas of vibrations—free vibrations (F), transient forced vibrations (T), and steady-state forced harmonic vibrations (SSH)—are treated in **Chapters 5, 6, and 7**, respectively. A pedagogical goal for this arrangement of the text was to provide uninterrupted treatments of these three major areas of vibrations. The format of many

vibrations textbooks is frequently to present F, then T, and then SSH for single-degree-of-freedom models; next to present F, then T, and then SSH for 2-degree-of-freedom models; then to present F, then T, and then SSH for multiple-degree-of-freedom models; and finally to present F, then T, and then SSH for continuous member models. The author's pedagogical experience is that a more effective approach is to cover F for 1, 2, and multiple degree of freedom and continuous members and then present similar learning sequences for T and finally for SSH. Instructing free vibrations from single degree of freedom through continuous members without multiple circulations through transient and SSH vibrations seems far less confusing and more effective and logical. A similar conclusion holds for treatments of transient vibrations and steady-state harmonic vibrations. In the author's opinion, the format of prior texts, as outlined above, has lost a significant justification with the advent of modern math tools, which have greatly lessened the solution difficulties encountered in transitioning from single-degree-of-freedom to 2-degree-of-freedom to N -degree-of-freedom models.

Chapter 5 expands the conventional content covered in free vibrations by including treatment of rotating systems with gyroscopic moments, the destabilizing effect of circulatory forces, flexible unconstrained structures, orthogonal damping matrices, and unstable systems. Likewise, Chapter 6 expands the conventional content covered in transient vibrations by including response spectrums, modal condensation for general \underline{M} , \underline{K} , and \underline{C} systems, flexible unconstrained structures, base excitation, participation factor and modal effective mass, and numerical integration methods. Finally, Chapter 7 expands the conventional content covered in steady-state harmonic response by including peak amplitude and frequency for the simple single-degree-of-freedom oscillator (SDOFO), parameter identification methods for the SDOFO, high spot-heavy spot and influence coefficient balancing for a simple Jeffcott rotor, demonstration that resonance may occur in any general \underline{M} , \underline{K} , and \underline{C} linearized vibrating system, use of receptances for the synthesis of substructures and mode shape identification, and use of the modal assurance criterion (MAC) for mode shape correlation.

5. Provide a treatment of techniques for improving computational efficiency for larger-order models by utilizing approximate methods. Large-scale finite element models are utilized throughout industry and in research and economic solutions are typically a necessity. Long run times inhibit use of optimization approaches such as genetic algorithm guided design which requires a large multitude of simulations with parameter variations. Modal condensation for accelerating system transient solutions is covered very thoroughly in Chapter 6, including use of the modal acceleration method. Chapter 7 also introduces a receptance approach for economically determining the response of coupled substructures through receptance synthesis. Chapter 8 covers other areas for economic, large-order system model solutions including Guyan reduction-static condensation, substructures-superelements, modal synthesis, eigenvalue-eigenvector perturbations with reanalysis, and the Rayleigh quotient approach.
6. Provide an in-depth presentation of finite elements that far surpasses the conventional content of only 2D Euler-Bernoulli beams and present an implementation algorithm that is universally applicable among the various types of elements and treats both fixed and time-varying boundary conditions. This goal reflects the author's experiences with finite elements in industry and research, namely, various types of elements are utilized and in most cases 3D models are inevitably required. Chapter 9 presents theory and examples for 2D Euler-Bernoulli and 2D and 3D Timoshenko beams with shear deformation effects. The Timoshenko beam development includes a truly "consistent mass matrix" utilizing the Timoshenko shape functions, derived from the solution of the beam's static

governing equations, in the kinetic energy expression for deriving the element mass matrix. Most developments employ a lumped mass formulation or an “inconsistent” mass matrix formulation utilizing Timoshenko beam shape functions for displacements and Euler–Bernoulli (Hermite cubic polynomials) shape functions for velocities in the beam’s kinetic energy expression. A general approach and accompanying 2D beam-frame example are provided for the case of imposed motion excitation at boundary points in a finite element model. The Timoshenko beam theory presented is for general 3D frames including I beams, box beams, etc. The matrix assembly algorithm presented in Chapter 4 is again utilized for all beam-frame models in Chapter 9. The standard format of only including 2D Euler–Bernoulli beams in vibration texts is clearly surpassed in Chapter 10 which includes treatment of 2D solid elements for plane stress and plane strain and axisymmetric and 2D vibrating membranes. Detailed algorithms are provided for determining stresses at interior and surface points for use in high-cycle fatigue studies. Both bilinear (2 node) and quadratic (9 node) isoparametric element formulations are presented. The extra (incompatible) shape function approach is utilized in order to accelerate convergence especially in 2D bending-type problems. Most commercial finite element codes utilize automated mesh generators with lower-order finite element models. The formulation for a constant strain triangle is presented for this purpose. The MATLAB code MESH2D is utilized for creating an automated triangular element mesh, which is then solved for natural frequencies and mode shapes. Large-order problems create large systems of linear algebraic equations that must be solved for the unknown nodal vibrations. The corresponding matrices may be highly sparse as described by a small bandwidth to order ratio. This fact may be exploited to economize on the required computation time for solving the equations. A banded solver assembly procedure and coding are provided and demonstrated with a steady-state harmonic vibration response example.

Chapter 11 provides theory, assembly procedures, and an example for a general 8-node, 3D solid (brick) hexahedral isoparametric element including extra (incompatible) shape functions for improved bending deformation modeling. The example reveals modes and natural frequencies that are absent from the corresponding 2D solid and Timoshenko beam models. A detailed discussion is provided for determining interior and surface point stresses for usage in high-cycle fatigue studies.

7. Provide an intermediate-level treatment of active vibration control (AVC) which is often categorized as an area of smart structures and materials. The need for lightweight, high-performance structures, vehicles, machines, and devices that may be required to function in extreme environments and adapt to various operating conditions has spawned a vast amount of research and development efforts in AVC. Chapter 12 provides in-depth treatments of both electromagnetic and piezoelectric actuator types, ideal (infinite) and finite bandwidth modeling and effects, and closed-loop stability and steady-state response determination. Closed-loop feedback control models that assume infinite bandwidths for all feedback components (sensors, controllers, power amplifiers, and actuators) are prone to miss unstable poles that appear in the as-built system and preclude the use of predetermined design feedback gains. This point is elucidated by both theory and example in Chapter 12. Examples are provided for systems with electromagnetic actuators or with piezoelectric stack or patch (layer) actuators.
8. Provide an appendix which contains a summary of the basic equations of elasticity (equilibrium, constitutive law, strain displacement, compatibility, strain energy) for easy reference when deriving the assumed modes and finite element stiffness matrices.

All chapters have a generous number of EXERCISES. Limitations on the size and cost of the textbook precluded including the EXERCISES within the textbook. The exercises are

accessible from a dedicated website (www.wiley.com/go/palazzolo), which is maintained by Wiley. The website contains a wide variety of intermediate to challenging exercises. A typed solution manual for the exercises is available from Wiley for instructors.

MATLAB and MAPLE codes are utilized in the examples throughout the text and in the exercise solutions. Many of the code listings are contained in the chapters or in Appendices B–F. The remaining codes are provided in a dedicated website (www.wiley.com/go/palazzolo) maintained by Wiley for instructors.

Limitations on the size and cost of the textbook precluded including sections on test instrumentation and sensors, nonlinear vibrations, and random vibrations. These are all very important subjects although much can be obtained on instrumentation and sensors by web search. Other texts that are readily accessible to students have introductory sections on nonlinear and random vibrations. The author has taught nonlinear vibrations at Texas A&M for the past 12 years and is planning a specialized book in this area.

Acknowledgments and Dedication

The author acknowledges the dedicated and excellent effort provided by his wife Changchun “Esther” Palazzolo in preparing the figures, typing, formatting, and detailed submission of this book. The author dedicates this book to his parents, Jerome and Beverly Palazzolo; his loving wife, Esther; his children, Stephanie, Elizabeth, and Justin; his siblings, Thomas, Steven, Jerome, and Marianne; and his friends, Msgr. John McCaffrey and Marty and Karen Smith. The author also dedicates the book to all those whose enthusiasm sparked and sustained his interest in vibrations, dynamics, and finite elements instruction and research:

Mr. Jerome J. Palazzolo, his lifelong mentor, friend, and expert in strain measurements
Prof. Demetrios D. Raftopoulos, his first research coordinator in vibrations
Prof. Edgar Gunter, his adviser and rotordynamicist extraordinaire
Prof. John Junkins, his longtime mentor and dynamicist extraordinaire
Mr. Donald Bently, inventor and founder of Bently Nevada Corp.
Mr. Bob Eisenmann, his leader at Bently Nevada and renown field vibration expert
Prof. Walter Pilkey, his adviser and solid mechanics expert extraordinaire
Dr. Tony Smalley, his leader at Southwest Research and renown vibrations specialist
Mr. Albert Kascak, his colleague at NASA Glenn and research scientist specialist
Dr. Make McDermott, colleague and engineering instructor extraordinaire
Prof. John Vance, his colleague and rotordynamicist expert extraordinaire
Prof. Dara Childs, his colleague and rotordynamicist expert extraordinaire
Prof. J. N. Reddy, his colleague and mechanics expert extraordinaire
Prof. Kumbakonam Rajagopal, his friend and mechanics expert extraordinaire
Many past and present graduate students, all very special sources of enthusiasm,
imagination and hope

About the Companion Website

This book is accompanied by a companion website:

www.wiley.com/go/palazzolo

This website includes:

- Appendices B through F which contain listings of MATLAB and MAPLE Codes for major examples in the text
- Exercises
- Matlab and Maple Codes

Exercises will be updated to reflect reader comments and the database of exercises will be expanded. This technological innovation will make the text a 'living' document, whilst having an expanding and polished Exercises section on a website reduces the size and cost of the book.

List of Acronyms

AF	amplification factor
AFM	atomic force microscope
AM	amplitude modulation
ANS	American National Standard
API	American Petroleum Institute
AVC	active vibration control
BC	boundary conditions
CCW	counterclockwise
COAM	conservation of angular momentum
COLM	conservation of linear momentum
CS	commercial software
CV	complex variables
DCTM	direction cosine transformation matrices
DE	differential equation
DFCA	“degree of freedom” connectivity array
DOF(s)/dof(s)	degree(s) of freedom
DSP	digital signal processor
EA	electrorestrictive actuator
EM	electromagnetic
ENI	Euler numerical integration
EOM(s)	equation of motion(s)
ES	equilibrium state
FBD(s)	free body diagram(s)
FE	finite element
FEM(s)	finite element method(s)
FRF(s)	frequency response function(s)
FS	Fourier series
GP	Gauss points
GQ	Gauss quadrature
GRSC	Guyan reduction and static condensation
HAVS	hand-arm vibration syndrome
HCF	high-cycle fatigue
HP	high pressure
HST	Hubble space telescope
HVAC	heating, ventilation and air-conditioning
IC(s)	initial condition(s)
IP	Intermediate pressure
ISO	International Standard Organization
ISS	international space station
JRM	Jeffcott rotor model
LE	Lagrange’s equation
LHS	left-hand side
LP	low pressure
LPF	low-pass filters

xxvi List of Acronyms

LT	Laplace transform
LTM	Laplace transform method
MA	mode acceleration
MAC	modal assurance criterion
MB	magnetic bearings
ME	microgravity experiment
MIMO	multiple input multiple output
MSF	mode scale factor
NASA	National Aeronautics and Space Administration
NB	Newmark beta
NCA	“nodal” connectivity array
NI	numerical integration
NIOSH	National institute of occupational safety and health
ODE(s)	ordinary differential equation(s)
OP	operating point
OSR	operating speed range
PD	proportional-derivative
PDE	partial differential equation
PE	potential energy
PID	proportional-integral-derivative
PLA	piezoelectric layer (patch) actuator
RB	rigid body
RBM	rigid body model
RBMPI	receptance-based modal parameter identification
REOM	rotational equation of motion
RHS	right hand side
RK	Runge-Kutta
RK4NI	fourth-order Runge-Kutta numerical integration
rms	root mean square
SDOF	single-degree-of-freedom
SDOFO	single-degree-of-freedom oscillator
SEP	static equilibrium position/static equilibrium reference
SISO	single input single output
SM	separation margin
SPA(s)	servo power amplifier(s)
SSB	simply supported beam
SSHR	steady-state harmonic response
SSME	space shuttle main engine
TB	Timoshenko beam
TEOM	translational equation of motion
VDV	vibration dose value
VM	Von Mises
WBV	whole body vibration

Chapter 1

Background, Motivation, and Overview

1.1 INTRODUCTION

The word “university” is derived from the word “universal” (Newman, 1927) in that the university is the foremost setting for teaching universal knowledge. Philosophy, chemistry, agriculture, mechanics, theology, biology, and so on are all topics of learning, teaching, and exploring at the true university. The study of vibrations is a microcosm of the ideal university, encompassing aspects of dynamics, fluid mechanics, structural deformation and fatigue, electromagnetism, feedback control, sound, and other phenomena. Confronting this, the eager investigator feels great satisfaction in drawing ideas from each area and then forging solutions to vibration problems. As an athlete develops calves and biceps, shoulders, and forearms and then enjoys using these in harmony and mutual support in competition, so the vibration engineer delights in recognizing and using many disciplines to tame vibrations.

With its arsenal of anomalies—fastener looseness, structural member fatigue and failure, noise, internal rubs in machinery, human fatigue and distractions, optical instrumentation and machining errors, and so on—vibration continues to present formidable engineering challenges and to limit energy efficiency and cost reduction in machinery and structures in the twenty-first century. New machinery that pushes the envelopes of efficiency and power density; new structures that stretch the imagination in size, materials, light weights, and locations; and new vehicles that propel us through land, air, sea, and space with ever increasing speed and comfort level all hold great promise for an efficient and convenient future. These advances will come at a price though and vibration will be there to collect its due. *The author extends his best wishes for success to those who meet the vibration challenges that continue to arise in mankind’s quest to subdue nature and use its awesome forces for peace, human dignity, and prosperity.*

1.2 BACKGROUND

The following sections provide discussions of many important aspects of vibration. The intent of this section is to provide some basic background material to facilitate understanding of the following sections. Vibration is the study of dynamic motions of mechanical, structural, or anatomical components or systems about their static equilibrium configurations. The motion may be sinusoidal periodic, complex periodic, quasiperiodic, transient, chaotic, or random. Monotone (single-frequency) sinusoidal vibration is characterized by an equilibrium position x_{eq} and the dynamic displacement *amplitude* (A_x), *phase angle* (ϕ_x), *frequency* (f), and *period* (T) as shown in Figure 1.2.1.

2 Vibration Theory and Applications with Finite Elements and Active Vibration Control

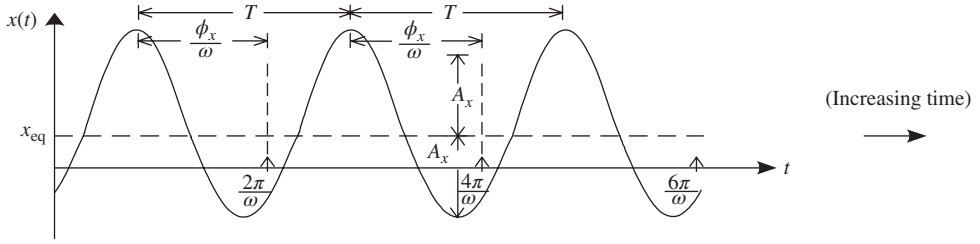


Figure 1.2.1 Pure tone sinusoidal vibration

The period and frequency are related by

$$f = \frac{1}{T} \text{ cycles/s or Hz, } \omega = 2\pi f \text{ circular frequency in rad/s} \quad (1.2.1)$$

Period markers are seen to occur at $0, 2\pi/\omega, 4\pi/\omega, \dots$. This may represent a once per revolution event on a rotating shaft or just some arbitrarily referenced pulse that indicates the beginning of a new forcing period. The motion is described using the expression

$$x(t) = A_x \cos(\omega t + \phi_x) \quad (1.2.2)$$

The positive peaks occur when the argument of the cosine function is a multiple of 2π , that is,

$$\omega t_{pn} + \phi_x = 2\pi n \quad n = 1, 2, \dots \quad (1.2.3)$$

which implies

$$t_{pn} \in \left\{ \frac{2\pi}{\omega} - \frac{\phi_x}{\omega}, \frac{4\pi}{\omega} - \frac{\phi_x}{\omega}, \frac{6\pi}{\omega} - \frac{\phi_x}{\omega}, \dots \right\} \quad (1.2.4)$$

Thus, it is seen by comparison of (1.2.4) and Figure 1.2.1 that the phase angle ϕ_x has a physical interpretation, namely, it provides a measure of the time between $x(t)$ experiencing a positive peak and the occurrence of a period marker. This time lag is

$$\Delta t_p = \frac{\phi_x}{\omega} \quad (1.2.5)$$

The velocity and acceleration expressions are obtained by differentiating (1.2.2)

$$v(t) = \dot{x}(t) = A_v \cos(\omega t + \phi_v) \quad (1.2.6)$$

$$a(t) = \dot{v}(t) = \ddot{x}(t) = A_a \cos(\omega t + \phi_a) \quad (1.2.7)$$

where

$$\begin{aligned} A_v &= \omega A_x, & \phi_v &= \phi_x + \frac{\pi}{2} \\ A_a &= \omega A_v = \omega^2 A_x, & \phi_a &= \phi_v + \frac{\pi}{2} = \phi_x + \pi \end{aligned} \quad (1.2.8)$$

The motion depicted in Figure 1.2.1 could result from displacing or striking the component and allowing it to freely vibrate as in the case of a swing, traffic light, car antenna,

cantilevered ruler, bell, or guitar string. The frequency of this natural or “free” motion is called a “natural frequency.” Alternatively, the motion could result from being forced by some source that has a frequency ω , as in the case of a washing machine with an unbalanced load, a vehicle with a slightly oval tire, or an offshore platform subjected to periodic wave forces at frequency ω . The oval tire would actually induce a vibration at frequency 2ω if its rotation frequency is ω .

So what happens if the forcing (source) frequency nearly equals the structural component’s natural frequency? The answer is that the vibration may become very large and even cause failure of the component. This phenomenon is called *resonance*, and it was a major reason for the spectacular failure of the Tacoma Bridge in Washington, United States, on November 7, 1940. Many years later, resonance still persists as a common source of failure for many structures and machines. An explanation for the increase in vibration amplitude at resonance accentuates a major distinction between static deflection and dynamic motion, namely, the existence of an *inertial force*. The *stiffness* force in a component is proportional to its deflection and acts to restore it to its equilibrium state when deflected. The inertial force is proportional to acceleration which is 180° out of phase with the displacement as shown by (1.2.8). The inertial force may become large and cancel the restoring stiffness force. This causes the dynamic motion (vibration) to become very large and destructive. This simplified example of resonance is extended to complex systems in Chapter 7.

Free (unforced) vibration decays with time due to energy dissipating forces such as:

- Viscous, dry, or atmospheric friction
- Material hysteresis
- Eddy current generated magnetic forces of an electrically conductive component that vibrates in a magnetic field

This vibration decay is illustrated in Figure 1.2.2. The presence of the *damping* force prevents exact cancellation of the stiffness restoring force by the inertial force at resonance. This, and nonlinear effects, reduces the infinite amplitude, resonant vibrations to finite values. Thus, damping is generally good for attenuating resonant vibrations. As with most things in life though, too much of a good thing may be bad, and damping is no exception. The velocity at the point where a viscous damper is attached to a flexible body will become zero as the damper strength increases. The energy dissipated by the damper is proportional to the square of the velocity of the attachment point. Therefore, very little energy is dissipated and all other points on the flexible body may vibrate severely. Thus, an optimum level of damping is sought in practice.

Systems may vibrate with many *free and/or forced frequencies* simultaneously. This results because:

- Actual components such as buildings, piping systems, shafts, blades, guitar strings, and so on have many natural frequencies.

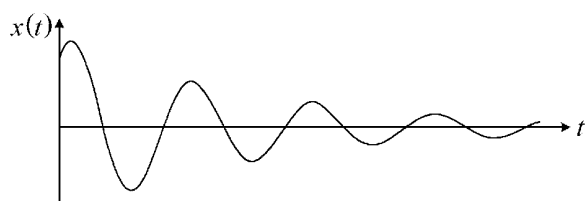


Figure 1.2.2 Damped free vibrations

4 Vibration Theory and Applications with Finite Elements and Active Vibration Control

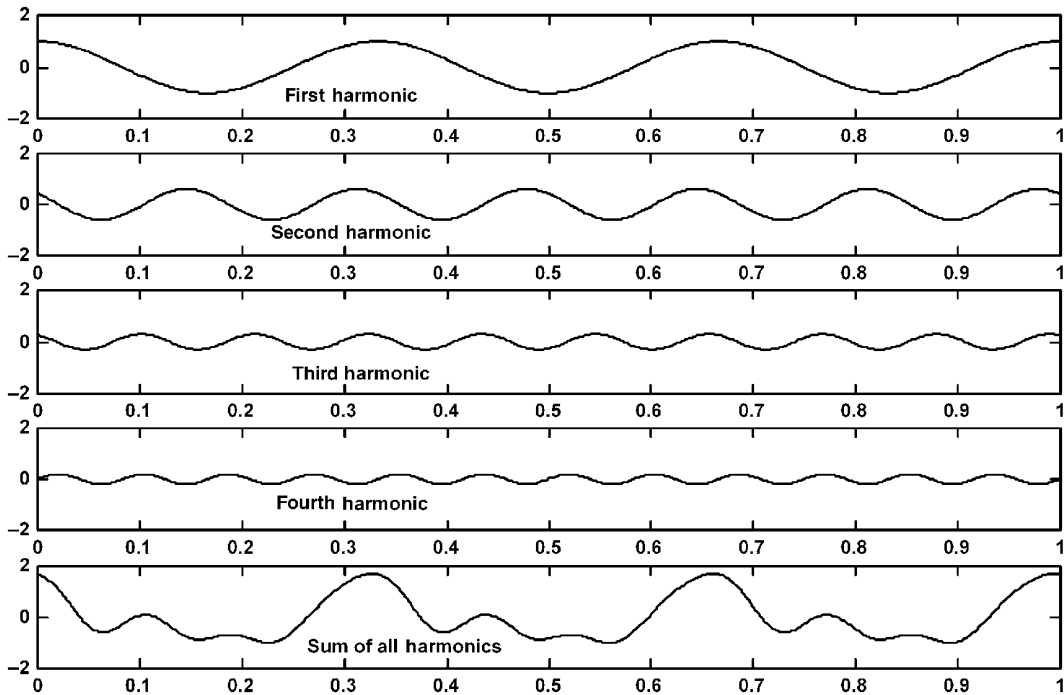


Figure 1.2.3 Lowest four constituent harmonics and their sum

- Some systems are excited by multiple sources at different frequencies. For example, a jet engine generally has two coaxial shafts: one a power turbine and the other a gas generator. Mass imbalances on the two shafts exert forces on the engine at the power turbine spin frequency and at the gas generator spin frequency.
- Some forces are periodic but not purely sinusoidal such as piston pressure or crankshaft/connecting rod/piston inertial forces in a vehicle engine or reciprocating pump or compressor, or a jack hammer striking building flooring, and so on.

Multifrequency vibration is referred to generally as complex periodic and is illustrated by Figure 1.2.3. A *Fourier series* expansion (see Chapter 2) will reveal all of the amplitudes, phase angles, and frequencies of the constituent sine waves that are superimposed to form the complex waveform.

Some vibrations are not entirely periodic since these result from nonperiodic excitations such as step, impulse, ramp, or more general shock inputs. Finally, some excitations such as atmospheric buffeting of airplanes or helicopters may be random, which causes the responses also to be random. Complex and random vibration waveforms may display many sinusoidal components of varying amplitude and duration. A common measure of severity determined from these responses is the *root mean square (rms) value*

$$x_{\text{rms}} = \sqrt{\frac{1}{T} \int_0^T x^2(t) dt} \quad (1.2.9)$$

where T is the period of measurement. For single-frequency sinusoidal motion, (1.2.9) yields

$$x_{\text{rms}} = \sqrt{\frac{1}{T} \int_0^T [A_x \cos(\omega t + \phi_x)]^2 dt} = \frac{A_x}{\sqrt{2}} \quad (1.2.10)$$

where T is one cycle of the motion. For multiharmonic complex motion, (1.2.9) yields

$$\begin{aligned} x_{\text{rms}} &= \sqrt{\frac{1}{T} \int_0^T [A_{x1} \cos(\omega t + \phi_{x1}) + A_{x2} \cos(2\omega t + \phi_{x2}) + \cdots + A_{xn} \cos(n\omega t + \phi_{xn})]^2 dt} \\ &= \sqrt{\frac{1}{2} (A_{x1}^2 + A_{x2}^2 + \cdots + A_{xn}^2)} \end{aligned} \quad (1.2.11)$$

where T equals the period of the lowest (fundamental) harmonic

$$T = \frac{2\pi}{\omega} \quad (1.2.12)$$

which is also the period of the complex, multiharmonic waveform.

1.2.1 Units

The vast majority of the units in this text are metric. Some helpful conversions are given below:

$$1g \text{ (gravity constant)} = 9.81 \text{ m/s}^2 = 386 \text{ in./s}^2 \text{ (on earth)}$$

$$1 \text{ mil} = 0.001 \text{ in.} = 0.0254 \text{ mm} = 25.4 \mu\text{m}$$

$$1 \text{ in.} = 0.0254 \text{ m} = 2.54 \text{ cm} = 25.4 \text{ mm}$$

$$1 \text{ m} = 39.37 \text{ in.} = 3.281 \text{ ft}$$

$$1 \text{ km} = 0.62 \text{ miles}$$

$$1 \text{ N} = 0.219 \text{ lbf}$$

$$1 \text{ lbf} = 4.54 \text{ N}$$

$$1 \text{ N/m} = 0.0056 \text{ lb/in.}$$

$$1 \text{ lb/in.} = 178.6 \text{ N/m}$$

$$1 \text{ N/m}^2 = 1 \text{ Pa} = 1.42 \times 10^{-4} \text{ lb/in.}^2$$

$$1 \text{ lb/in.}^2 = 7032.3 \text{ N/m}^2$$

$$1 \text{ in.}^4 = 4.162 \times 10^{-7} \text{ m}^4$$

$$1 \text{ m}^4 = 2.403 \times 10^6 \text{ in.}^4$$

$$1 \text{ lb.s/in.} = 178.6 \text{ N.s/m}$$

$$1 \text{ N.s/m} = 0.0056 \text{ lb.s/in.}$$

$$1 \text{ in.lb/rad} = 0.1153 \text{ N.m/rad}$$

$$1 \text{ N.m/rad} = 8.672 \text{ in.lb/rad}$$

$$\text{Weight of } 1 \text{ kg} = 9.81 \text{ N} = 2.161 \text{ lbf (on earth)}$$

1.3 OUR VIBRATING WORLD

The term vibration has many different connotations but is most often connected with oscillatory motion of an object about some equilibrium position and/or operating point. The Merriam-Webster dictionary entry for vibration provides a commendable description for the “vibrations” studied in this text, that is, “periodic motion of the particles of an elastic body or medium in alternately opposite directions from the position of equilibrium when that equilibrium has been disturbed (as when a stretched cord produces musical tones or molecules in the air transmit sounds to the ear).” A vibration engineer might add “a source of cyclic fatigue, looseness, human health or contact damage which limits the performance of machines and people.”

Vibrations are often related to a natural frequency and resonance. Objects vibrate at certain characteristic frequencies due to the periodic exchange of energy between kinetic and potential forms. So bells, traffic lights, pendulums, car antennas, turbine blades, and so on sway and ring at certain frequencies when displaced and released. Resonance occurs when an excitation or disturbance acts on an object with nearly the same frequency as the object’s natural frequency. The result may be large, damaging, and sometimes catastrophic vibrations.

1.3.1 Small-Scale Vibrations

The potential energy that is created when atoms are collected in a lattice produces forces that act like spring connecting the atoms. These masses connected by “springs” vibrate and are particularly sensitive to certain excitation frequencies referred to as resonance frequencies. Cesium 133 atoms have a resonant frequency at 9,192,631,770 cycles/s. When excited at this frequency, the atoms change state. A voltage applied to a piezoelectric crystal causes it to deform. The vibrating piezoelectric is utilized to create microwaves which impinge on the cesium atoms. If the frequency of the voltage varies near 9,192,631,770 Hz, the microwaves cause the cesium 133 to experience a peak in the number of transformed atoms as resonance occurs at the atomic natural frequency. These atoms are continuously counted as the frequency of the voltage applied to the piezoelectric is varied. A peak count indicates that the frequency is exactly 9,192,631,770 Hz (cesium 133 atomic resonant frequency). The cycles are counted and every 9,192,631,770 cycles form 1 second. Hence, vibrations even on the atomic level reveal a practical usage, that is, an *atomic clock*.

The lens-free atomic force microscope (AFM) employs a tiny 100 μm length cantilever beam to measure local sample height (topography) at the atomic level. The beam has a very low spring stiffness (0.1 N/m) yet very high natural frequency. Mounted on the end of the cantilever is a sharp tip that is typically a 3 μm tall pyramid with 10–30 nm end radius. The deflection of the tip is measured with a laser. The beam and tip may also function in a non-contact mode where topographic images are derived from measurements of attractive forces. Environmental vibration, that is, due to a passing truck, can cause severe distortion of the images produced by an AFM.

On a slightly larger scale, a tiny quartz crystal in a watch may vibrate (ring) for minutes similar to a tuning fork due to a lack of damping. Deflection of the quartz (piezoelectric) crystal creates a voltage that can be amplified and reapplied to the crystal to sustain the vibration at its “natural” frequency. This frequency is known and constant so a count of the number of cycles executed provides a means to determine the passing of 1 second—that is, the fundamental time unit for the watch.

Vibrations occur in the human body on a very small scale yet they are also very important. Consider the auditory system consisting of the external, middle, and inner ear. The

outer portion of the external ear (auricle) directs sound waves to the 2.5 cm long ear canal, passing to the ear drum (tympanic membrane). The ear drum is about 1 cm in diameter, has a concave shape, and vibrates in response to the incoming sound waves. Its displacement amplitude during normal speech (~60 dB sound level) is estimated to be about equal to the size of a molecule of hydrogen. The middle ear consists of three solid material “ossicles,” the hammer (malleus), the anvil (incus), and the stirrup (stapes), which increase the vibratory force about 20 times as it is transmitted from the ear drum to the “oval window.” This results from lever action of the ossicles and the decrease in area between the ear drum and oval window. The stapes displaces the oval window as it transmits the sound waves (vibration). This oval window acts as a piston oscillating the fluid (perilymph) within the snail-shaped cochlea which winds about $2\frac{3}{4}$ turns. The fluid causes the “basilar membrane” in the cochlea to vibrate in different manners according with the frequency of the exciting sound wave. Frequencies below 50 Hz cause vibration of the entire membrane, whereas higher frequencies (15–24 KHz) cause the membrane to vibrate only at its base attachment point. The membrane is covered with hair cells that move against a second membrane (tectorial). Microvilli (minute projections of cell membranes that greatly increase surface area) that are embedded in the tectorial membrane bend in response to movement of the basilar membrane. Bending of the microvilli causes ionic actions that stimulate nerves connected to the acoustic cortex in the brain, via the basilar hair cells. As mentioned, different frequencies cause different parts of the basilar membrane to deflect which in turn bends different microvilli, which in turn affect different nerves that synapse (membrane-to-membrane contact of two nerve cells that promotes transmission of nerve impulses) with the basilar hair cells. These nerves are connected to different positions along the acoustic cortex. Thus, the frequency of the sound waves determines which part of the basilar membrane vibrates, which tectorial membrane microvilli bend, which basilar membrane hairs synapse with nerves to the acoustic cortex, and which portion of the acoustic cortex is stimulated. The audible frequency range extends from 20 Hz to 24 KHz. For reference, the lowest frequency of a piano is 27.5 Hz and the highest is 4186 Hz. In addition, middle C is 400 Hz, and the next C is one octave (factor of 2) higher at 800 Hz. J. S. Bach divided each octave into 12 equal frequency intervals to include flats and sharps (Cannon, 1967). Each note is then $2^{1/12}$ (1.0595) higher in frequency than the next lower note. From this discussion, it is clear that the ear acts as a transduction device that converts vibrations into nerve impulses.

Small vibrations also occur in the vocal folds (chords) of the human throat. The left and right vocal folds are made of muscles and form a “V” when viewed from above. The folds are pulled apart from one another when breathing and are pulled together during speech. Talking, singing, and humming cause the two folds to open and close very quickly as air passes from the lungs through the windpipe and then through the folds. The folds are forced open by the higher air pressure in the windpipe but quickly close as the pressure decreases due to the escaping air. The windpipe pressure builds up again and the pattern is repeated at a high frequency. Thus, sound is produced as the small jets of air pass through the moving vocal folds. The shape of the vocal tract changes as the tongue, jaw, palate, and lips are moved. This causes the air in the voice tract to resonate (resonate) at different frequencies (acoustic natural frequencies) to the vocal fold vibration and corresponding air jets. This is similar to blowing across the openings of several bottles that are filled to different levels with water, each producing a distinct pitch due to the difference in cavity shape. The lowest (fundamental) spoken frequency is about 100 Hz and the highest about 3000 Hz. Articulation is the action of changing the vocal tract geometry to produce desired sounds. Vowels resonate in the throat and consonants in the nasal passages.

1.3.2 Medium-Scale (Mesoscale) Vibrations

Trucks, autos, buses, trains, and amusement park rides bounce and buzz due to road or track unevenness and machinery forces developed in the engine, transmission, and auxiliary equipment. Airplanes shake and vibrate due to air turbulence and dynamic forces in their engines. The same scenario exists for helicopters with the addition of torque transmission-related dynamic forces for the main and tail rotor. Ships utilize many machines (turbines, gear boxes, propellers, pumps, ventilation fans, and so on) that cause vibration and also experience sea wave excitation. Industrial chemical, petroleum, paper product, and power plants utilize hundreds of compressors, turbines, pump, fans, and so on that vibrate due to rotating imbalance, misalignment, gear and blade forces, and so on and in turn excite many kilometers of attached piping and vessels. Mills, lathes, drill presses, and saws shake and vibrate due to imbalance and cutting forces in thousands of machine shops and manufacturing facilities. This may cause delirious effects on surface finish, and limit the depth and rate of cut, and consequently the tool performance. Buildings for the most part buzz and vibrate due to HVAC equipment and sway due to wind buffeting. Precision optical instruments such as lasers, telescopes, microscopes, and interferometers vibrate due to transmission of forces from neighboring machinery and forces, oftentimes degrading the instrument's performance. Musical instruments (strings and drums) vibrate but in a (hopefully) pleasant manner. Skis, baseball bats, tennis rackets, and golf clubs also vibrate in response to impact loading. These medium-scale vibrations typically occur with an amplitude range of 0.01–10.0 mm and a frequency range of 2–2000 Hz. These vibrations are rarely detectable with the naked eye but can have catastrophic consequences.

1.3.3 Large-Scale Vibrations

About 100 earthquakes occur each year with the strength to cause significant damage. The earth's crust (outer layer) surrounds its hot liquid inner core and is broken up into giant plates of rock. Sometimes two plates collide along a fault and pressure builds up until the plates snap into a new position. The release of this traction (pressure) causes vibrations that we feel as an earthquake. When the vibration of the earth has the same frequency as the natural frequency of a building, a resonance occurs and the building vibrations may become very destructive. The Mexico City earthquake of 1985 was especially destructive for buildings 10–14 stories tall since they had natural frequencies near the ground shake frequency. The Northridge, California, earthquake of 1994 registered 6.7 on the Richter scale and yielded motions up to 0.35 m. Typical earthquake frequencies range from 0.2 to 5.0 Hz.

The field of helioseismology has discovered that the sun, being a deformable ball of hot gas, vibrates in millions of resonant modes with the major ones ringing at frequencies between 1 and 5 milli-hz. These modes may ring for days or even months before decaying away. Similar phenomena have been observed by astronomers noting the brightness of other very distant stars. The radial vibration velocity observed in one case was in the 1–3 km/s range.

Our universe is filled with vibrating objects: some big—some small, some near—some far, some good—some bad, shaking an atom and shaking a star! Feel like vibrating? Place your fingertips on your throat and say a long “e” with a big cavity and with a small cavity-shaped throat. Feel the vibes! *This level of vibration would be considered as severe if it was measured on the bearing housings of a large industrial turbine or compressor.*

1.4 HARMFUL EFFECTS OF VIBRATION

Some beneficial reasons to create vibrations include:

- (a) Music
- (b) Radar/sonar/radio/microwaves
- (c) Back massagers
- (d) Lithotripsy (for kidney stone fragmentation)
- (e) Industrial vibrators for clearing blockages and hang-ups of grain screenings, soya meal, gypsum coal, refined ore, and other materials in bins, chutes, hoppers, and silos

These are the good vibrations. In contrast, most vibrations are adverse to human, machinery, and structural health, and an important engineering objective is to reduce them to harmless levels.

1.4.1 Human Exposure Limits

Body vibration is usually classified according to “whole body vibration” (WBV) or “local vibration” (Griffin, 1990). The three principal possibilities for WBV are sitting on a vibrating seat, standing on a vibrating floor, or lying on a vibrating surface. Local vibration results when a limb or the head contacts a vibrating surface. Effects of vibration on the body depend on frequency, amplitude, and duration and range from “motion sickness” (low frequency–high amplitude) to fatigue-decreased proficiency and permanent damage to hands and arms (high frequency–low amplitude).

The International Standard Organization’s (ISO) Standard ISO 2631-1, 1997 “Mechanical Vibration and Shock—Evaluation of Human Exposure to Whole Body Vibration” provides a quantitative, measurable means to determine how severe a particular vibration may be on human health, based on statistical surveys. This document should be directly consulted in an actual design study; however, some general guidelines are that WBV acceleration vibrations less than 0.75 m/s^2 may be mildly disagreeable, from 0.75 to 1.5 m/s^2 may be disagreeable, and higher levels may be very disagreeable. The Standard parses these general divisions into much more finely divided levels and is a “living document” that is periodically updated. Continuous exposure to vibration over some duration of time may be risky to health as illustrated by the ISO standards.

A measure of vibration exposure that includes both amplitude and duration is the vibration dose value (VDV). This is defined as (Griffin, 1990)

$$\text{VDV} = \left[\int_{t=0}^T a^4(t) dt \right]^{1/4} \quad (1.4.1)$$

where $a(t)$ is the vibration acceleration in m/s^2 . The caution zone is reached when the VDV is $8.5 \text{ m/s}^{1.75}$ and a health risk occurs for VDV greater than $17 \text{ m/s}^{1.75}$. Referring to British standard 6472, Guide to evaluation of human exposure to vibration in buildings, Hassan (2009) provides VDV levels for the threshold of “adverse comment” of people working in various types of buildings and offices. These values range from $0.1 \text{ m/s}^{1.75}$ for residential buildings at night to $0.8 \text{ m/s}^{1.75}$ for busy offices or workshops.

The transportation safety department of the Australian Transport Safety Bureau identified potential WBV-related health problems as:

- (a) Discomfort and interference with activities
- (b) Disorders of the joints and muscles and especially the spine

- (c) Cardiovascular, respiratory, endocrine, and metabolic changes
- (d) Problems in the digestive system
- (e) Reproductive damage in females
- (f) Impairment of vision or balance
- (g) Low back pain arising from early degeneration of the lumbar system
- (h) Muscular fatigue and stiffness

The motions referred to thus far represent input motions to the whole body. The vibrations of certain parts of the body could be much worse if internal resonance occurs. Griffin (1990) states that a human body should only be considered to act rigidly for frequencies less than 2 Hz. For instance, the eye's natural frequency (f_n) falls in the range 20–70 Hz, the head relative to shoulders f_n lies between 20 and 30 Hz, and the trunk's f_n lies between 4 and 6 Hz.

Local body vibration may also cause serious health problems. An example of this is vibration that is localized to the hand and arm. Prolonged exposure may result in the hand–arm vibration syndrome (HAVS), which is also known as “white finger,” “dead finger,” or “Raynaud’s syndrome” (Griffin, 1990). HAVS is a vascular (blood vessel) disorder-related disease of increased risk with exposure to cold, loud noise, and tobacco smoke (CDC, 1994). Early signs of HAVS include:

- Tingling fingertips
- Fingertips turning white or blue
- Trouble picking up small objects
- Numbness
- Clumsiness with hands
- Trouble buttoning and zipping clothes
- Reduced sense of heat, cold, and pain in hands

According to the US National Institute of Occupational Safety and Health (NIOSH, 1989), HAVS reduces blood circulation due to narrowing of the blood vessels. This results in one or more fingers becoming white and cold. This condition may become irreversible with long-term vibration exposure. The disease is prevalent among workers using chipping hammers, drills, riveters, grinding wheels, chain saws, and driving motorcycles. Relevant information on HAVS exposure limits may be found in ISO Standards 5349 and 8662 and ANSI S3.34-1986 (American National Standard) as well as in Griffin (1990). Thus, for example, these references indicate that a vibration acceleration level of 30 m/s^2 ($\approx 3g$) is generally safe for 1 hour exposure but it may be unsafe for 2 hours or more of exposure. The actual standards should be referenced in any industrial design study. Appropriate use of the standards requires measurement of the acceleration component directed into the hand so as to generate compression rather than shear motion. The standard should be applied to the worst frequency component of the acceleration signal's Fourier series (spectrum). There is also a probabilistic aspect to interpreting the standards. This is illustrated by noting, for instance, that for the 4–8-hour exposure zone, a latency period of 10–20 years is expected to yield vascular symptoms in 10% of the exposed population. The harmful effects of long-term exposure to hand and arm vibration extend beyond blood circulation (vascular) disorders to include a large number of bone and joint disorders (Griffin, 1990).



Figure 1.4.1 Simple cantilever pipe subjected to bending, axial, and torsional loads

1.4.2 High-Cycle Fatigue Failure

The intent here is to present a primer on high-cycle fatigue (HCF) to illustrate the practical importance of studying vibrations. More advanced texts such as Nicholas (2006) or Lee et al. (2012) should be referenced for a more in-depth understanding and for applications. Stress is a measure of the internal or surface force density in an object. For example, the beam shown in Figure 1.4.1 has a cantilever support and a circular cross section and is subjected to a transverse force $F(t)$, axial force $P(t)$, and twisting torque $\tau(t)$. The vibrations caused by these excitations create an internal shear force $V(x, t)$, internal bending moment $M(x, t)$, internal axial force $f(x, t)$, and internal torque $\Gamma(x, t)$ at position x . These internal actions create stresses in beams described by the strength of materials type formulas

$$\sigma_{\text{bend}}(t) = \frac{M(t)c}{I}, \quad \sigma_{\text{axial}}(t) = \frac{P(t)}{A}, \quad \tau_{\text{shear}}(t) = \frac{V(t)}{A}, \quad \tau_{\text{tors}}(t) = \frac{\Gamma(t)c}{J} \quad (1.4.2)$$

where A is the cross-sectional area, I is the bending area moment of inertia, and J is the torsion constant. As implied by (1.4.2), loads and resulting stresses generally vary with time.

Materials are compared and characterized by the amount of stress they can withstand before breaking. For example, the ultimate strength (stress) for high-strength 340 Aermet steel is $\sigma_{\text{ut}} \approx 325000 \text{ lb/in.}^2$, where the more common A36 steel has an ultimate strength $\sigma_{\text{ut}} \approx 56000 \text{ lb/in.}^2$. Guess which costs more, or which is more likely to be found in a high-performance aircraft, given that they both have the same density? The amount of stress that a component can tolerate is reduced if the stress varies cyclically with time. This important fact gave birth to the entire subject of fatigue. To demonstrate this, bend an ordinary metal coat hanger by 180° , and you'll find it does not break. However, if the bending deformation is repeated many times, failure will occur, even for angles that are much less than 180° . This phenomenon is referred to as low-cycle fatigue failure if the bent section breaks in less than approximately 1000 cycles and the maximum stress is near the tensile (ultimate) strength S_{ut} . HCF represents the same phenomena of cyclic stress; however, failures occur after 10^3 , 10^4 , 10^5 , 10^6 or higher cycles and the failure stress may be much less than S_{ut} or even much less than the yield stress.

How does this relate to vibrations? Well, within the limits of linear theory, stresses are proportional to strains, which are in turn proportional to displacements, aka vibration. Thus, the larger the vibration deformation becomes, the larger the stress. HCF failures may occur when vibrations become excessive as will be the case if the component has low damping and is being forced at a frequency near to one of its free vibration (natural) frequencies, that is, near resonance.

Several practical examples from industry will illustrate the importance of HCF considerations. Gas turbine engines mix compressed air with fuel, combust the mixture, and expel

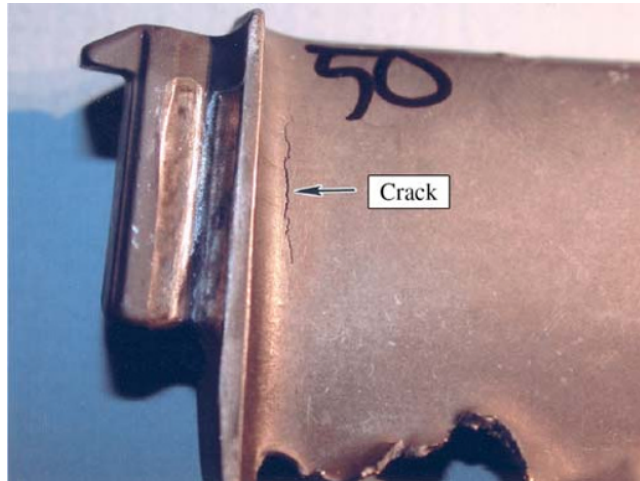


Figure 1.4.2 Turbine blade with high-cycle fatigue crack. Reproduced with permission from Transport Safety Board of Canada

the resulting hot gases through a turbine wheel. The torque that this causes on the turbine wheel may spin a compressor creating compressed air or a generator creating electricity. The air that flows through the compressor is directed by stationary (nonrotating) stator vanes to optimally impinge on the rotating blades. A similar situation occurs with the hot gases in the turbine. Any rotating blade experiences an impulse-type force as it collides with the flow through the passage between two stator vanes. The rotor blade is then excited at the frequency

$$f_{\text{excit}} = (\text{Rotor spin frequency}) * (\text{Number of stator vanes}) \quad (1.4.3)$$

which is referred to as the blade-pass frequency. This excitation causes the blades to vibrate causing time-varying (alternating) stresses along with the static, centrifugal-induced stress in the blades. The level of alternating stress that is tolerable is reduced by the presence of the static (mean), tensile, and centrifugal stresses. Figure 1.4.2 shows an HCF crack on a blade from an aircraft gas turbine engine.

The combination of *alternating stress and mean stress* may cause an HCF failure (catastrophic crack) if the rotor blade is not properly designed. The vibration (and stress) level will substantially increase if f_{excit} or one of its harmonics is in the vicinity of a rotor blade natural frequency, that is, a resonant condition. HCF of blades is a constant concern of all turbine and compressor designers with applications to steam or gas turbines for power generation, aircraft, helicopters, ships, chemical processing, or even to the space shuttle main engines. The consequences of “throwing off” a cracked blade are frequently catastrophic and sometimes fatal. The US Air Force has determined that more than 50% of accidents involving aircraft damage result from HCF.

Piping and tubing systems are also subjected to vibration-induced cyclic stress due to pressure pulsation forces generated by attached machinery, such as reciprocating compressors, or from internally generated vortices. These systems are also subjected to static stress from internal pressure and partially constrained thermal expansion. Experienced chemical plant personnel know that an HCF-induced crack in a high-pressure gas line will sometimes emit a high-pitch whistle as the gas escapes through the crack, signaling all nearby workers to shut down the machinery and flee.

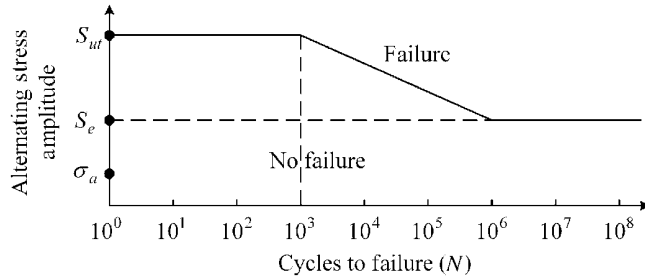


Figure 1.4.3 Simplified S–N curve for HCF failure evaluation plotted on log–log format

These examples illustrate cases where vibration of machinery and structures induces cyclic stress, which may cause HCF failure. This may occur at stress levels well below the yield stress or ultimate/tensile strength (S_{ut}), which is illustrated by the simplified S – N (*alternating stress amplitude vs. number of cycles to cause failure*) diagram in Figure 1.4.3. The sloped portion of the curve is of primary interest and has the general form

$$S_{\text{failure}} = \gamma N^\alpha \quad (1.4.4)$$

where the constants γ and α are determined experimentally and are a property of the material.

The *endurance limit* stress S_e is defined as the level below which failure will not occur independent of the number of cycles. The value of S_e is most accurately obtained by experiment with the material and geometry of interest; however, it is sometimes approximated for steels as (Shigley, 1989)

$$S'_e = \begin{cases} 0.50 * S_{ut}, & S_{ut} \leq 1400 \text{MPa (200kpsi)} \\ 700 \text{MPa}, & S_{ut} > 1400 \text{MPa} \\ 100 \text{kpsi}, & S_{ut} > 200 \text{kpsi} \end{cases} \quad (1.4.5)$$

$$S_e = k S'_e$$

where k is a series product of modifying factors and S'_e is the endurance stress limit of a highly polished, cylindrical specimen at room temperature. The modifying (*Marin*) factors account for surface condition, size, load types, temperature, plating, corrosion, and so on. In addition, a modifying factor also may be applied to account for the reliability of S'_e , which is a statistical quantity, typically provided in tables as a mean value over many tests of “identical” specimens. This modifying factor is usually based on the assumption of a Gaussian distribution for the measured endurance limit and a ratio of its standard deviation to the mean value of, for instance, 8%. The maximum value of stress taken over the entire component should be utilized in Figure 1.4.3 since stress varies spatially.

Figure 1.4.4 shows a weight attached to the end of a cantilevered beam. The static weight causes a static deflection and strain, which causes a constant mean stress σ_m that is maximum at the wall since the moment is largest there and the nominal beam stress is magnified by the local geometry (stress concentration) at the connection to the wall. The weight vibrates about its statically deflected position creating a time-varying deflection and corresponding alternating stress.

14 Vibration Theory and Applications with Finite Elements and Active Vibration Control

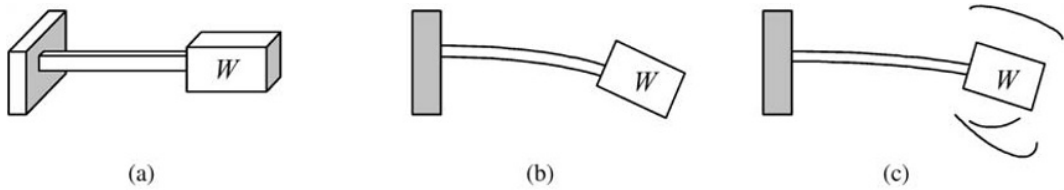


Figure 1.4.4 (a) Cantilevered block with (b) static (mean) and (c) static plus dynamic deflections and stresses

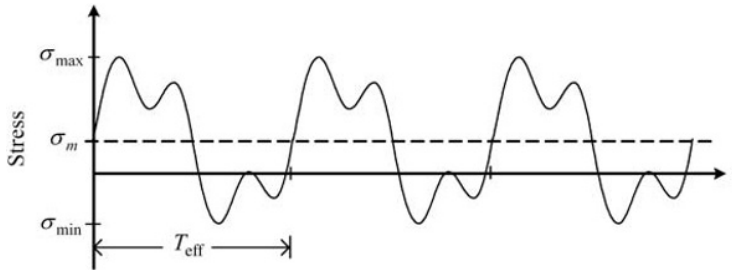


Figure 1.4.5 Stress response with multiple frequencies and a static component

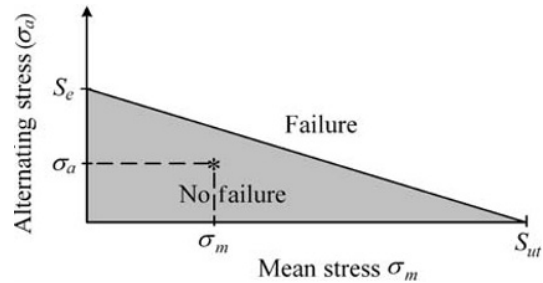


Figure 1.4.6 Modified Goodman diagram for combined static and dynamic stresses

Stress waveforms may contain components at several frequencies including a static component as illustrated in Figure 1.4.5. Define the alternating stress amplitude as

$$\sigma_a = \frac{\sigma_{\max} - \sigma_{\min}}{2} \quad (1.4.6)$$

Then σ_a can be utilized in Figure 1.4.3 to estimate the life of the component. Collins (1981) states that the minor “frequency component” (small bumps) in Figure 1.4.5 may be ignored if they are substantially smaller than the primary component. The effective cycle period becomes T_{eff} as shown in Figure 1.4.5. The effect of the “static” or “mean” stress in Figure 1.4.5

$$\sigma_m = \frac{\sigma_{\max} + \sigma_{\min}}{2} \quad (1.4.7)$$

is to reduce the alternating stress level below which HCF failure will not occur, that is, reduce the infinite life stress threshold to a value less than S_e . This is illustrated by the modified *Goodman diagram* in Figure 1.4.6. The failure line connecting S_e and S_{ut} provides the effective endurance limit $S_{e,\text{eff}}$ as a function of the mean stress σ_m .

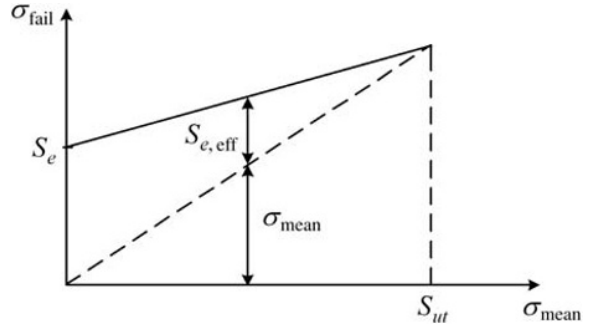


Figure 1.4.7 Peak stress at failure versus mean tensile stress

This figure is only applicable for positive values of σ_m (tensile stress). For compressive σ_m values, the part will eventually fail if $\sigma_a > S_e$ or will fail if $\sigma_m > S_{ut}$, that is, the static and dynamic failure criteria are uncoupled. The obvious implication of the Goodman diagram is that the effective endurance limit $S_{e,eff}$ decreases as mean stress increases. Another view is that the alternating stress amplitude should be divided by this same reduction factor when using the S–N curve in Figure 1.4.3, that is, utilize the following effective alternating stress in Figure 1.4.3:

$$\sigma_{a,eff} = \frac{\sigma_a}{1 - \sigma_m/S_{ut}} \quad (1.4.8)$$

Although the endurance limit may decrease with increasing tensile mean stress, the maximum total stress (mean plus alternating) for which failure will eventually occur typically increases with mean stress as indicated by Figure 1.4.7.

Fatigue test data is generally consistent with Figure 1.4.7. Fatigue data is available from several sources and is generally presented in the form depicted in Figure 1.4.8. This figure is “Figure 2.3.1.3.8(l). Best-fit S–N curves for notched, $K_T = 3.3$, AISI 4340 alloy steel bar, $F_{TU} = 200$ ksi, longitudinal direction” in the extensive database supported by MMPDS-08, Battelle Memorial Institute, at www.mmpds.org. The “stress ratio” R is defined by

$$R = \frac{\sigma_{\min}}{\sigma_{\max}} = \frac{\sigma_m - \sigma_a}{\sigma_m + \sigma_a} = \frac{1 - \sigma_a/\sigma_m}{1 + \sigma_a/\sigma_m} \quad (1.4.9)$$

which increases monotonically as σ_a/σ_m decreases. Note that $R = -1$ corresponds to a zero mean stress, $\sigma_m = 0$, condition, that is, the maximum stress is the amplitude of the alternating stress. Similarly, $R = 1$ corresponds to a zero alternating stress, $\sigma_a = 0$, condition, that is, the maximum stress is the mean stress. The test data is typically accompanied by curve fits in forms similar to

$$\text{Cycles to failure} = 10^{\{a_1 - a_2 * \log_{10}[\sigma_{\max} * (1-R)^{a_3} - a_4]\}} \quad (1.4.10)$$

where σ_{\max} is in units of ksi and the a_i are constants. Care must be taken to utilize the curve fit equation only when the argument $[\sigma_{\max} * (1-R)^{a_3} - a_4]$ of the logarithm is positive.

Note that the peak allowable stress increases as R increases, indicating an increase in total allowable stress as σ_a/σ_m decreases. Some components experience a nearly pure state of torsional shear stress such as a shaft in an industrial machinery train. The shear stress in a circular shaft or coupling due to pure torsional torque loading is given by

$$\tau = \frac{T r_{\text{outer}}}{J} \quad \text{where } J = \frac{\pi}{2} (r_{\text{outer}}^4 - r_{\text{inner}}^4) \quad (1.4.11)$$

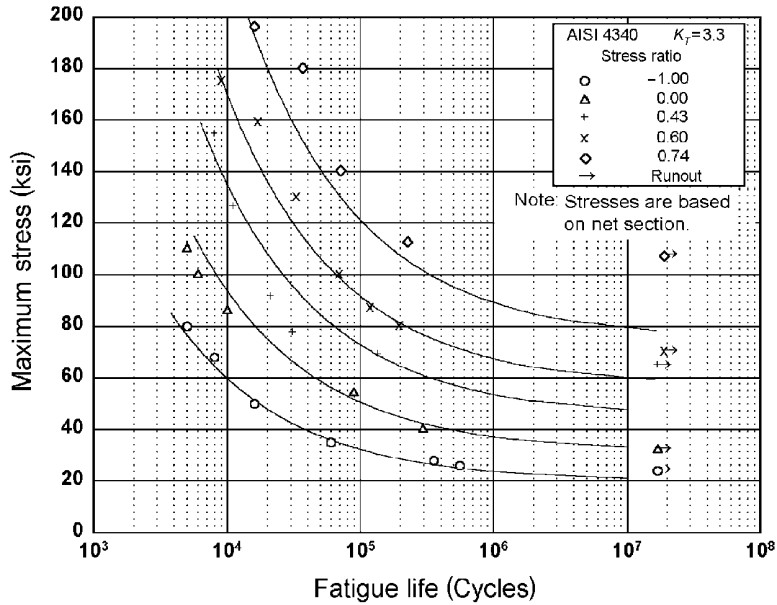
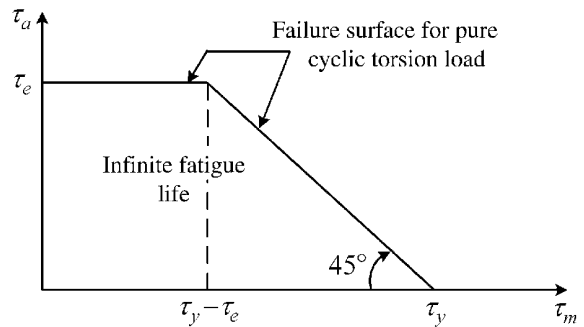


Figure 1.4.8 Typical S–N curves for various R values MMPDS-08. (Figure 2.3.1.3.8(I). Best-fit S–N curves for notched, $K_T=3.3$, AISI 4340 alloy steel bar, $F_{TU}=200$ ksi, longitudinal direction.) Reproduced with permission of Battelle Memorial Institute

Figure 1.4.9 Plot of effective torsional stress endurance limit (solid line) versus mean torsional shear stress



where τ is the shear stress, T is the transmitted torque through the coupling/shaft, r_{outer} is the outer radius of the coupling/shaft, r_{inner} is the inner radius of the coupling/shaft, and J is the torsion constant. For this case, Wang (2006) states that “Experimental results tend to show that the value of the mean shear stress has no influence on the fatigue life of a ductile structural component subjected to cyclic torsional loading as long as the maximum stress is less than the yield strength of the material. Hence, the plot of the alternating shear stress τ_a versus mean shear stress τ_m is bound by a horizontal line with $\tau_a = \tau_e$ and a 45 deg yield line.” This is illustrated in Figure 1.4.9.

The parameters in Figure 1.4.9 are τ_e , the torsional endurance limit; τ_y , the torsional yield strength; τ_m , the torsional mean stress; and τ_a , the torsional alternating stress. The material will fail after a finite number of stress cycles if either

if

$$\tau_m < \tau_y - \tau_e \text{ and } \tau_a > \tau_e \quad (1.4.12)$$

then $\tau_{a,\text{eff}} = \tau_a$ (*mean stress has no influence*)

or if

$$\tau_m > \tau_y - \tau_e \text{ and } \tau_a > \tau_y - \tau_m \quad (1.4.13)$$

then $\tau_{a,\text{eff}} = \tau_a \frac{\tau_e}{\tau_y - \tau_m}$ (*mean stress has influence*).

Most components of structural systems are subjected in general to complex states of combined normal and shear stresses. The above approach for evaluating HCF failure may still be utilized by employing the equivalent, or “von Mises (VM)”, stress utilized in the von Mises–Hencky, or distortion energy yielding failure theory. This failure theory states that the material will yield if the actual structure’s local, distortion-strain energy density, due solely to distortion and not to the hydrostatic stress components, exceeds the distortion-strain energy density in a uniaxially loaded test specimen, at the yield condition. This condition produces the following condition for yield failure

$$\sigma' \geq \frac{S_Y}{n} \quad (1.4.14)$$

where S_Y is the yield strength of the material (in general another statistical quantity), n is the selected design safety factor, and σ' is the so-called von Mises, or equivalent, stress

$$\begin{aligned} \sigma' &= \frac{1}{\sqrt{2}} \sqrt{(\sigma_1 - \sigma_2)^2 + (\sigma_2 - \sigma_3)^2 + (\sigma_3 - \sigma_1)^2} \\ &= \frac{1}{\sqrt{2}} \sqrt{(\sigma_X - \sigma_Y)^2 + (\sigma_Y - \sigma_Z)^2 + (\sigma_Z - \sigma_X)^2 + 6(\tau_{XY}^2 + \tau_{YZ}^2 + \tau_{XZ}^2)} \end{aligned} \quad (1.4.15)$$

where (1, 2, 3) indicates principal normal stresses and (X, Y, Z) indicates Cartesian coordinate, component stresses. The alternating amplitude and mean value for each component or principal stress in (1.4.15) are evaluated by applying equations (1.4.6) and (1.4.7) to the respective stress’s time history. These alternating and mean values are then utilized to determine the *equivalent mean VM stress* and the *equivalent alternating VM stress* as follows:

$${}^m\sigma' = \frac{1}{\sqrt{2}} \sqrt{({}^m\sigma_X - {}^m\sigma_Y)^2 + ({}^m\sigma_Y - {}^m\sigma_Z)^2 + ({}^m\sigma_Z - {}^m\sigma_X)^2 + 6({}^m\tau_{XY}^2 + {}^m\tau_{YZ}^2 + {}^m\tau_{XZ}^2)} \quad (1.4.16)$$

$${}^a\sigma' = \frac{1}{\sqrt{2}} \sqrt{({}^a\sigma_X - {}^a\sigma_Y)^2 + ({}^a\sigma_Y - {}^a\sigma_Z)^2 + ({}^a\sigma_Z - {}^a\sigma_X)^2 + 6({}^a\tau_{XY}^2 + {}^a\tau_{YZ}^2 + {}^a\tau_{XZ}^2)} \quad (1.4.17)$$

Then ${}^m\sigma'$ and ${}^a\sigma'$ are employed in Figure 1.4.6, in place of σ_m and σ_a , respectively, to determine whether HCF failure will occur, including the effects of the corresponding safety factor and the reduced value of the endurance limit due to the mean stress ${}^m\sigma'$. Vibration simulation models are frequently assembled from beam, plate, bar, or other structural modeling components that provide nominal stress values. Consideration of abrupt changes in geometry such as holes, fillets, welds, and so on requires multiplication of the nominal stresses by respective *stress concentration factors* to obtain accurate stress values (Budynas and

Nisbett, 2008). The equivalent stresses in (1.4.16) and (1.4.17) then assume the more complicated forms

$${}^m\sigma' = \frac{1}{\sqrt{2}} \sqrt{\left({}^m\sigma_X K_X - {}^m\sigma_Y K_Y \right)^2 + \left({}^m\sigma_Y K_Y - {}^m\sigma_Z K_Z \right)^2 + \left({}^m\sigma_Z K_Z - {}^m\sigma_X K_X \right)^2 + 6 \left[\left({}^m\tau_{XY} K_{XY} \right)^2 + \left({}^m\tau_{YZ} K_{YZ} \right)^2 + \left({}^m\tau_{XZ} K_{XZ} \right)^2 \right]} \quad (1.4.18)$$

$${}^a\sigma' = \frac{1}{\sqrt{2}} \sqrt{\left({}^a\sigma_X K_X - {}^a\sigma_Y K_Y \right)^2 + \left({}^a\sigma_Y K_Y - {}^a\sigma_Z K_Z \right)^2 + \left({}^a\sigma_Z K_Z - {}^a\sigma_X K_X \right)^2 + 6 \left[\left({}^a\tau_{XY} K_{XY} \right)^2 + \left({}^a\tau_{YZ} K_{YZ} \right)^2 + \left({}^a\tau_{XZ} K_{XZ} \right)^2 \right]} \quad (1.4.19)$$

where the K terms are stress concentration factors derived from test data or analysis (Pilkey, 1997). The K factors can also be modified from their static load values for application to fatigue problems as indicated in Budynas and Nisbett (2008).

1.4.2.1 Miner–Palmgren Rule

Suppose an object is exposed to N_{loads} distinct sets of loadings characterized by effective alternating stress amplitudes σ_{ai} , actual number of load cycles n_i at this stress amplitude, and number of load cycles N_i for failure at this stress amplitude. Define the damage done by the i th load set as

$$R_i = \frac{n_i}{N_i} \quad (1.4.20)$$

Then the object is predicted to fail by the *Miner–Palmgren rule* when the damage

$$D = \sum_{i=1}^{N_{\text{loads}}} R_i = \beta \quad (1.4.21)$$

where typically $\beta = 1$; however, for a more conservative approach, some researchers utilize 0.6 or 0.7 instead. Stress will be calculated at many locations in the component's model, and the part will be predicted to fail if any of these locations have a cumulative fatigue damage that exceeds β . A thorough fatigue analysis requires that the damage be evaluated at many locations.

1.4.2.2 Rainflow Cycle Counting

In general, loading may be nonperiodic (Chapter 6) but recurring and cause vibratory deflections and stresses. The most common example is random excitation as might occur on a wind turbine blade or offshore platform. Another occurrence is a system subjected to a transient load that causes vibratory stresses and is applied at well-separated and varying time intervals, such as the transient start-up torque applied by an electric motor to a machinery train. It is not obvious how one should properly identify load cycles and equivalent alternating stress amplitudes to utilize (1.4.20), (1.4.21), and Figure 1.4.2 to predict damage and life for this type of loading. The “rainflow method” is the most common of the “cycle counting” techniques that provide a systematic means to identify arrays of alternating stress amplitudes and corresponding mean stresses during an arbitrary varying stress time history.

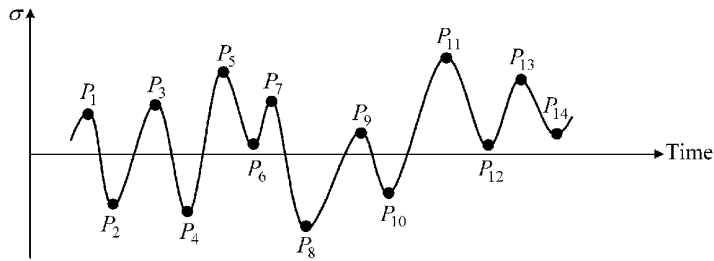


Figure 1.4.10 Stress extrema set in a stress versus time history

Consider the following definitions:

Extremum: a point P_i in a stress versus time history when the stress is either a local maximum or minimum. The plural of extremum is extrema. Reference Figure 1.4.10.

Extrema set: collection of extremum points in a stress versus time history.

Extrema pair: two members in an extrema set.

Extrema trio: three consecutive members (a, b, c) in an extrema set.

Begin point: first point in an extrema set.

Change C: absolute value of the difference between two stresses in an extrema pair.

Mean stress: average of the two stresses in an extrema pair.

Alternating stress: one-half of the absolute difference of the two stresses in an extrema pair.

The overarching logic of the method is to systematically locate extrema trios (a, b, c) such that the change C_{bc} between (b, c) is greater than the change C_{ab} between (a, b). This justifies counting C_{bc} as $\frac{1}{2}$ load cycle. The rainflow procedure is illustrated by the example given below. Start with the extrema set that contains all extrema in a stress versus time history, for example, P_1 through P_{14} in Figure 1.4.10. These extrema and their values (in ksi) are given in row 1 of Table 1.4.1. Table 1.4.1 lists the 14 steps needed to identify the equivalent load cycles for given stress time history. The extrema set of step i is given by the numbers in row i of Table 1.4.1. The number of members in the extrema set diminishes as the rainflow process proceeds. Each step considers a new trio (a, b, c) of points in the current extrema set and compares the respective changes C_{ab} and C_{bc} of extrema pairs (a, b) and (b, c). The trio (a, b, c) are boldened for each step in Table 1.4.1.

As demonstrated in Table 1.4.2 for each rainflow step:

- Trio (a, b, c) are *always* three consecutive points in the updated extrema set.
- The trio (a, b, c) is updated in going from step i to step $i + 1$ in the following manner: Point “ c ” is the next point in the extrema set in going from step i to step $i + 1$, with the exception that if in step i (point “ a ” is not the begin point of the extrema set and $(C_{bc}/C_{ab}) \geq 1$), then in step $i + 1$ point “ a ” is set equal to the begin point.
- If $(C_{bc}/C_{ab}) \geq 1$ and the begin point and “ a ” are the same, then remove point “ a ” from the extrema set, and accumulate $\frac{1}{2}$ cycle of stress with the mean and alternating stress of extrema pair (a, b).
- If $(C_{bc}/C_{ab}) \geq 1$ and the begin point and “ a ” are different, then remove points “ a ” and “ b ” from the extrema set, and accumulate 1 cycle of stress with the mean and alternating stress of extrema pair (a, b).
- If $(C_{bc}/C_{ab}) < 1$, then no points are removed from the extrema set and no load cycles are accumulated.

Table 1.4.1 Rainflow points for Figure 1.4.10

Point step	1 (8)	2 (-12)	3 (14)	4 (-14)	5 (18)	6 (4)	7 (15)	8 (-16)	9 (5)	10 (-8)	11 (20)	12 (3)	13 (16)	14 (7)
1	1	2	3	4	5	6	7	8	9	10	11	12	13	14
2	—	2	3	4	5	6	7	8	9	10	11	12	13	14
3	—	—	3	4	5	6	7	8	9	10	11	12	13	14
4	—	—	—	4	5	6	7	8	9	10	11	12	13	14
5	—	—	—	4	5	6	7	8	9	10	11	12	13	14
6	—	—	—	4	5	6	7	8	9	10	11	12	13	14
7	—	—	—	4	5	—	—	8	9	10	11	12	13	14
8	—	—	—	—	5	—	—	8	9	10	11	12	13	14
9	—	—	—	—	5	—	—	8	9	10	11	12	13	14
10	—	—	—	—	5	—	—	8	9	10	11	12	13	14
11	—	—	—	—	5	—	—	8	—	—	11	12	13	14
12	—	—	—	—	—	—	—	8	—	—	11	12	13	14
13	—	—	—	—	—	—	—	8	—	—	11	12	13	14
14	—	—	—	—	—	—	—	8	—	—	11	12	13	14

Parentheses: stress value in *ksi*.

Bold indicates “a,” “b,” and “c” points of current step.

Table 1.4.2 Rainflow cycle counts for Figure 1.4.10

Step	Begin point	<i>a</i>	<i>b</i>	<i>c</i>	C_{ab}	C_{bc}	Removed ^a point “a” or “a” and “b”	Number of cycles of (<i>a</i> , <i>b</i>) ^a	σ_{\min}^b	σ_{\max}^b	σ_m^b	σ_a^b
1	1	1	2	3	20	26	1	½	-12	8	-2	10
2	2	2	3	4	26	28	2	½	-12	14	1	13
3	3	3	4	5	28	32	3	½	-14	14	0	14
4	4	4	5	6	32	22	—	—	—	—	—	—
5	4	5	6	7	14	11	—	—	—	—	—	—
6	4	6	7	8	11	31	6 and 7	1	4	15	9.5	5.5
7	4	4	5	8	32	34	4	½	-14	18	2	16
8	5	5	8	9	34	21	—	—	—	—	—	—
9	5	8	9	10	21	13	—	—	—	—	—	—
10	5	9	10	11	13	28	9 and 10	1	-8	5	-1.5	6.5
11	5	5	8	11	34	36	5	½	-16	18	1	17
12	8	8	11	12	36	17	—	—	—	—	—	—
13	8	11	12	13	17	13	—	—	—	—	—	—
14	8	12	13	14	13	9	—	—	—	—	—	—
15	8	8	11	—	36	—	8	½	-16	20	2	18
16	11	11	12	—	17	—	11	½	3	20	11.5	8.5
17	12	12	13	—	13	—	12	½	3	16	9.5	6.5
18	13	13	14	—	9	—	13	½	7	16	11.5	4.5

^a Only if $C_{bc} > C_{ab}$.

^b Values for extrema pair interval (*a*, *b*).

Table 1.4.3 Load cycles for example in Table 1.4.1

j	1	2	3	4	5	6	7	8	9	10	11
No. of cycles n_i	½	½	½	1	½	1	½	½	½	½	½
σ_m (ksi)	-2	1	0	9.5	2	-1.5	1	2	11.5	9.5	11.5
σ_a (ksi)	10	13	14	5.5	16	6.5	17	18	8.5	6.5	4.5
$\sigma_{a,eff}$ (ksi)	10	13.5	14	8.9	17.4	6.5	17.7	19.6	15.7	10.5	8.3
$N_i \times 10^5$	0.33	0.07	0.06	0.60	0.02	2.82	0.019	0.011	0.034	0.259	0.815

The above procedure is repeated until point “c” of the trio (a, b, c) is the last extrema point. A ½ load cycle is counted for each of the surviving consecutive extrema pairs in the final extrema set. This is illustrated by steps 15–18 in Table 1.4.2.

For the sake of illustration, assume that $S_e = 5$ ksi, $S_{ut} = 25$ ksi and the S–N curve follows the following common form (Budynas and Nisbett, 2008):

$$\gamma = \frac{(\phi S_{ut})^2}{S_e} = 80000, \quad \alpha = -\frac{1}{3} \log_{10} \left(\frac{\phi S_{ut}}{S_e} \right) = -0.200$$

$$\text{Cycles to failure} = N = \begin{cases} \left(\frac{\sigma_{a,eff}}{\gamma} \right)^{1/\alpha} & \text{if } \sigma_{a,eff} > S_e \\ \infty & \text{if } \sigma_{a,eff} < S_e \end{cases}$$

where ϕ is a constant that is taken as 0.8 for this example. The effective alternating stress is obtained from the modified Goodman formula (1.4.8) as

$$\sigma_{a,eff} = \begin{cases} \frac{\sigma_a}{1 - (\sigma_m/S_{ut})} & \text{if } \sigma_m > 0 \\ \sigma_a & \text{if } \sigma_m \leq 0 \end{cases}$$

Table 1.4.3 summarizes the load cycles obtained by the rainflow method in Table 1.4.2, the corresponding effective alternating stresses, and the cycles to failure.

The damage as given by (1.4.21) is

$$D = \sum_{i=1}^{11} \frac{n_i}{N_i} = .0013$$

This implies that for a $D = 1$ failure criteria, $1/D = 765$ repetitions of the sample load set would be required to fail the component.

The rainflow counting algorithm is tedious by hand for a large data set and is frequently implemented in an automated form such as found in the MATLAB code (Nieslony, 2010). Additional reading on the rainflow method may be found in ASTM E-1049–85 (2011).

1.4.3 Rotating Machinery Vibration

Spinning shafts of industrial, aviation, and aerospace machinery such as turbines, compressors, motors, fans, and so on vibrate due to their inherent imbalance, misalignment, looseness, resonance, inadequate damping, interaction with the transmitted liquid or gas, gear

forces, failed bearings, and so on. Most of the machines mentioned above operate at high speeds (1000–50 000 rpm) and have very small clearances between the spinning (rotor) and stationary (stator) components. These clearances may be as small as 0.01 mm per 1 cm of shaft diameter. This accentuates the potential seriousness of controlling vibration, which may lead to internal rubs followed by loss of machinery, product, and, in rare instances, lives. For this reason, standards have been established to aid in purchasing and operating various types of rotating machine. The American Petroleum Institute (API) *standards* are often utilized throughout the petrochemical and process industries. Some API standards include:

- API STD 610—Centrifugal Pumps for General Refinery Service
- API STD 611—General Purpose Steam Turbines for Petroleum, Chemical, and Gas Industry Services
- API STD 617—Axial and Centrifugal Compressors and Expander—Compressors for Petroleum, Chemical, and Gas Industry Services
- API Standard Paragraphs Rotordynamic Tutorial: Lateral Critical Speeds, Unbalance Response, Stability, Train Torsionals, and Rotor Balancing. API Recommended Practice 684, 2nd Ed., August 2005, Reaffirmed, November 2010

An example rule from API STD 617 is as follows: Let x represent the peak-to-peak vibration of the rotating shaft relative to the stator at the bearing locations, and then the maximum allowable value for x is

$$x \leq 25 * \sqrt{\frac{12000}{N_{\max}}} (\mu\text{m, p-p}) \quad (1.4.22)$$

where N_{\max} is the maximum continuous speed of the compressor in revolutions per minute. It is very important to note that the API standards are “living documents” that are being continuously updated by panels of experts and that the standards should be consulted directly for use of the most up-to-date formulas for actual industrial applications.

Recall the phenomenon of resonance that was discussed in Sections 1.2 (Tacoma Narrows Bridge), 1.3 (clocks and earthquakes), and 1.4 (human body). Machinery resonance is a particularly detrimental problem, which may lead to premature and possibly catastrophic failure. Resonance occurs when an excitation (forcing) frequency coincides with a natural frequency. An excitation frequency in rotating machinery is the spin (rotational speed) frequency since mass imbalance forces of the rotor vary sinusoidally at the spin frequency. Consequently, the operating speed range of most machinery is kept well separated from any bending natural frequencies of the spinning shaft. API 684 provides rules pertaining to designing and operating rotating machinery in a manner to avoid resonance, which for rotating machinery is referred to as “critical speed.” The API standards account for the possible presence of a resonance both above and below the operating speed (rpm) range (OSR) of the machine, by defining a below OSR *minimum separation margin* (SM) and an above OSR minimum SM. As one might expect, the specified minimum SM increases as the intensity (danger) of the resonance increases. Intensity is quantified as the amplification factor AF, which increases as the resonance peak increases in relative height, and is calculated using the half power point method (Eqs. (7.3.52) and (7.3.53), Figure 7.3.9).

A second source for vibration severity guidelines in rotating machinery is the International Organization for Standardization (ISO). The ISO Standard ISO 3945-1977(E) entitled “Mechanical Vibration for Large Rotating Machines with Speed Ranges from 10 to 200 rev/s—Measurement and Evaluation of Vibration Severity in situ” bases vibration

Table 1.4.4 Example vibration severity table—in terms of peak, RMS vibration velocity

v_{rms} (mm/s)	v_{rms} (in./s)	Condition
<1.27	<0.05	Smooth
>1.27 and <3.8	>0.15 and <0.15	Mild
>3.8 and <10.2	>0.15 and <0.4	Rough
>10.2 and <15.2	>0.4 and <0.6	Severe
>15.2	>0.6	Unacceptable

severity on the measured velocity of vibration *on all bearing housings* of a machine. Specifically, the rms velocity

$$v_{\text{rms}} = \sqrt{\frac{1}{T} \int_0^T v^2(t) dt} \quad (1.4.23)$$

is utilized, where T is the total measurement period and $v(t)$ is the measured vibration velocity in the frequency range 10–1000 Hz. The velocity severity measure v_{rms} may also be evaluated from the relation (1.2.11)

$$v_{\text{rms}} \approx \sqrt{\frac{1}{2} (v_1^2 + v_2^2 + \dots + v_n^2)} \quad (1.4.24)$$

if the Fourier frequency component amplitudes $v_1 \ v_2 \ \dots \ v_n$ of $v(t)$ are known. Let $v_{\text{rms}}^{\text{max}}$ represent the maximum value of v_{rms} over all measurement locations (typically two bearing housings) and directions (typically horizontal, vertical, and axial) on a machine. Similar standards are published by other organizations and vibration instrumentation manufacturers. Table 1.4.4 shows a sample chart presented only for illustration purposes. Actual standards from ISO or other sources should be consulted in practice.

It is notable that the intent of the standard is to provide an evaluation of machinery health based upon a relatively easily taken set of measurements and the accumulated experience of the standard's authors. This approach is clearly justified by the time and cost associated with surveying large numbers of rotating machines in chemical, refinery, paper processing, power, steel, and equipment manufacturing plants and also on ships. A more detailed set of measurements such as stress, force, and so on should be made if high vibration is indicated by use of tables in the standards.

Vibration in rotating machinery most often results from mass imbalance of the spinning shaft. This causes centrifugal forces that deflect the shaft and react against the bearings and machinery support structure in a sinusoidally varying manner. The corresponding excitation frequency is the rotational speed frequency of the shaft. ISO has developed standards to specify acceptable *imbalance* levels since the imbalance force is an important driver (source) of vibrations. For process equipment such as gas and steam turbines, turbo-compressors, turbine-driven pumps, and so on, ISO 1940-1973(E) recommends

$$e\omega \leq 2.5 \text{ mm/s} \quad (1.4.25)$$

where

$$e = \text{offset of the rotating assembly's mass center} \\ \text{relative to its geometric center (spin axis) in mm} \quad (1.4.26)$$

$$\omega = \text{spin frequency of the rotating assembly in rad/s} \quad (1.4.27)$$

For example, consider a steam turbine rotor that weighs 1000 N and spins at 10 000 rpm (1047 rad/s). The recommended maximum eccentricity level becomes

$$e = \frac{2.5 \text{ mm/s}}{1047 \text{ rad/s}} = 2.4 \mu\text{m} \quad (1.4.28)$$

The centrifugal force corresponding to this mass eccentricity and speed is

$$F_c = me\omega^2 = \frac{1000 \text{ N}}{9.8 \text{ m/s}^2} * 2.4 \times 10^{-6} \text{ m} * (1047 \text{ s}^{-1})^2 = 268 \text{ N} \quad (1.4.29)$$

This represents the dynamic force transmitted through the bearings only if the rotational speed frequency is well below all rotating assembly or support natural frequencies. The transmitted force may be much higher at resonance and much lower at shaft speeds well above resonance.

It is important to note that most standards are “living documents” that evolve as the understanding of related anomalous vibrations is increased through experience and research. The latest standards should be referred to in actual practice.

EXAMPLE 1.4.1 *Effective Endurance Limit, Safety Factor, and Vibration Severity*

A large, motor-driven fan is supported at the end of a uniform pipe, which is fastened to a fixed wall. The pipe is modeled as a massless, cantilevered Euler beam (Figure E1.4.1(a)).

The pipe may eventually fail (crack) due to HCF if the alternating component of the von Mises stress $^a\sigma'$ at the wall exceeds the effective endurance limit for the pipe material accounting for the mean von Mises stress $^m\sigma'$. The equation for the boundary curve in the modified Goodman diagram of Figure 1.4.6 provides the effective endurance limit as

$$S_{e,\text{eff}} = S_e - \frac{S_e}{S_{ut}} (^m\sigma') \quad (1)$$

The vertical, transverse deflection $\delta_{\text{tip}}^T(t)$ at the tip of the beam has a mean (constant) component δ_m^T due to the weight of the motor/fan assembly and a sinusoidally varying component $\delta_a^T(t)$ due to the rotating imbalance force of the fan

$$\delta^T(t) = \delta_m^T + \delta_a^T(t) = \bar{\delta}_m^T + \bar{\delta}_a^T \sin(\omega t) \quad (2)$$

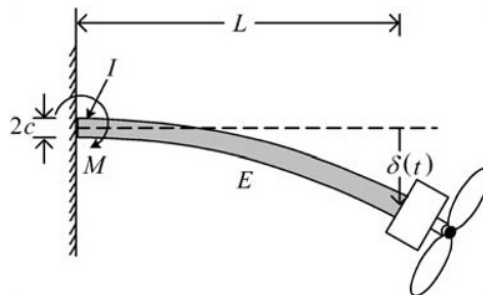


Figure E1.4.1(a) Motor supported by cantilever pipe

The term $\bar{\delta}_a^T \sin(\omega t)$ represents the *vibration*. In addition, the fan blade–air interaction forces cause a static torque Γ_{fan} about the pipe axis and a static, tensile force F_{fan} along the pipe axis. These cause the constant axial and torsional deflections δ_m^A and θ_m^A , respectively, at the tip of the beam.

Let F_{wall} , M_{wall} , and Γ_{wall} be the axial force, bending moment, and torque at the wall, respectively. Then the maximum values of the component, nominal stresses at the wall become

$$\sigma_{\text{axial}} = \frac{F_{\text{wall}}}{A}, \quad \sigma_{\text{bend}} = \frac{M_{\text{wall}} * D_O}{2I}, \quad \tau_{\text{shear}} = \frac{\Gamma_{\text{wall}} * D_O}{2J} \quad (3)$$

where

$$\begin{aligned} I &= \text{bending moment of inertia} = \frac{\pi}{64} (D_O^4 - D_I^4) \\ J &= \text{torsion moment of inertia} = \frac{\pi}{32} (D_O^4 - D_I^4) \\ A &= \text{pipe cross-sectional area} = \frac{\pi}{4} (D_O^2 - D_I^2) \\ D_O, D_I &= \text{outer and inner diameters of the pipe} \end{aligned} \quad (4)$$

The load combination described above only produces a normal stress σ_X along the direction of the pipe axis and a shear stress τ_{XY} on the pipe cross section. The corresponding stress concentration factors at the pipe-wall connection plane are K_X and K_{XY} , respectively. All of the remaining stress components are zero. The parameter values for this problem are

$$E = 30.0 \times 10^6 \text{ psi}, \quad G = 12.0 \times 10^6 \text{ psi}, \quad K_X = 3.0, \quad K_{XY} = 2.0, \quad L = 40 \text{ in.}, \quad D_O = 3.5 \text{ in.}, \quad D_I = 3.0 \text{ in.}$$

$S_{\text{ut}} = 100000 \text{ psi}$, $S_e = 25000 \text{ psi}$ (for a zero mean stress state and includes Marin correction factors)

$$\bar{\delta}_m^T = 0.080 \text{ in.}, \quad \bar{\delta}_a^T = 0.020 \text{ in.}, \quad \delta_m^A = 0.0005 \text{ in.}, \quad \theta_m^A = 0.002 \text{ rad} \quad (5)$$

where X is the axial direction along the pipe axis and Y is the vertical direction. In general, K_X will be different for axial and bending loads, in which case the component stresses are amplified (multiplied) by their respective K_X values prior to forming σ_X . For the sake of simplicity, the K_X values are the same in this problem:

- (a) Determine the amplitude of the alternating and the mean (steady) *transverse* forces that the motor/fan exerts on the free end of the pipe:

$$\begin{array}{cc} \text{Alternating} & \text{Mean} \\ F_a^{\text{tip}} = \frac{3EI}{L^3} * \bar{\delta}_a^T & F_m^{\text{tip}} = \frac{3EI}{L^3} * \bar{\delta}_m^T \\ F_a^{\text{tip}} = 95.3 \text{ lb} & F_m^{\text{tip}} = 381 \text{ lb} \end{array} \quad (6)$$

- (b) Determine the mean (steady) *axial* force and torque exerted by the wall on the pipe:

$$F_{\text{axial}} = \frac{EA}{L} * \delta_m^A = 957.2 \text{ lb}, \quad \Gamma = \frac{GJ}{L} \theta_m^A = 4068 \text{ in.} \cdot \text{lb} \quad (7)$$

- (c) Determine the maximum x component of mean pipe stress including both bending and axial load contributions:

$$\sigma_m^{\text{axial}} = \frac{F_{\text{axial}}}{A}, \sigma_m^{\text{bend}} = \frac{M_m * D_0/2}{I}, \sigma_m^x = \sigma_m^{\text{axial}} + \sigma_m^{\text{bend}}, \sigma_m^x = 8250 \text{psi} \quad (8)$$

- (d) Determine the maximum x component of alternating pipe stress:

$$\sigma_a^{\text{bend}} = \frac{M_a * D_0/2}{I}, \sigma_a^x = \sigma_a^{\text{bend}}, \sigma_a^x = 1969 \text{psi} \quad (9)$$

- (e) Determine the pipe's mean shear stress at the wall:

$$\tau_m = \frac{\Gamma * D_0/2}{J}, \tau_m = 1050 \text{psi} \quad (10)$$

- (f) Determine the maximum von Mises, mean pipe stress:

$$\sigma'_m = \frac{1}{\sqrt{2}} \sqrt{2(K_X * \sigma_m^x)^2 + 6(\tau_m * K_{XY})^2}, \sigma'_m = 25016 \text{psi} \quad (11)$$

- (g) Determine the maximum von Mises, alternating pipe stress:

$$\sigma'_a = \sigma_a^x * K_X, \sigma'_a = 5906 \text{psi} \quad (12)$$

- (h) Determine the effective endurance limit " $S_{e,\text{eff}}$ " at the wall where the above von Mises stresses occur:

$$S_{e,\text{eff}} = -\frac{S_e}{S_{\text{ut}}} \sigma'_m + S_e, S_{e,\text{eff}} = 18746 \quad (13)$$

Note that this is lower than the endurance limit ($S_e = 25000 \text{psi}$) in the absence of a mean stress.

- (i) What is the safety factor on the vibration amplitude $\bar{\delta}_a^T$ relative to the effective endurance limit, that is, what factor applied to $\bar{\delta}_a^T$ will cause the alternating von Mises stress to exceed the effective endurance limit " $S_{e,\text{eff}}$."

The alternating stress increases in proportion to $\bar{\delta}_a^T$; therefore, the factor on $\bar{\delta}_a^T$ to exceed $S_{e,\text{eff}}$ is

$$\frac{S_{e,\text{eff}}}{\sigma'_a} = 3.17$$

- (j) Assume that the fan spins and the beam vibrates at $\omega = 100 \text{rad/s}$. Also assume that the vibration amplitude on the fan bearing is the same as $\bar{\delta}_a^T$, and the supports are considered to be flexible. Provide a qualitative description of the vibration severity level. Provide a numerical justification for your answer.

The vibration velocity amplitude is $v = \omega \bar{\delta}_a^T$ so its rms value is

$$v_{\text{rms}} = \frac{\omega \bar{\delta}_a^T}{\sqrt{2}} = \frac{100 * 0.020}{\sqrt{2}} = 1.414 \text{in./s} = 36 \text{mm/s}$$

Table 1.4.4 shows this is an unacceptable level of v_{rms} .

Military standard MIL-STD-810D “Environmental Test Methods and Engineering Guidelines” provides guidance for inspectors and vendors of jet engine aircraft, propeller aircraft, and helicopters. Specifically, its objectives are:

- (a) “To disclose deficiencies and defects and verify corrective actions”
- (b) “To assess equipment suitability for its intended operational environment”
- (c) “To verify contractual compliance”

Excessive vibration is considered to be potentially harmful due to the possibility of

- Wire chafing
- Loosening of fasteners
- Intermittent electrical content
- Touching and shorting of electrical parts
- Seal deformation (leakage)
- Component fatigue
- Optical misalignment
- Cracking and rupturing

Although these considerations concern mechanical distress, pilot fatigue is also a major concern. Standard MIL-STD-810D is a very comprehensive document, which contains a section on vibrations (section 514). Category 6 of section 514 considers helicopter vibration, which has a broadband random nature with strong sinusoidal vibrations due to onboard rotating machinery. This machinery includes engines, main and tail rotors, and meshing gears (transmission). The major peaks in the vibration spectrum are usually harmonics of the main rotor’s blade-pass frequency (no. of blades * main rotor spin frequency); however, different areas of the helicopter will have different sources at different frequencies as shown in Figure 1.4.11. The standard contains severity tables similar with Table 1.4.4 for various types of helicopters and general locations on the helicopters.

1.4.4 Machinery Productivity

Tool speed and depth of cut play a major role in productivity in machining and woodworking processes. Both of these factors are limited due to vibration. Chatter type vibrations result as the tool bit interacts with previously cut paths in milling, drilling, and boring operations. Suppressing these vibrations can yield a significant payoff in increased productivity.

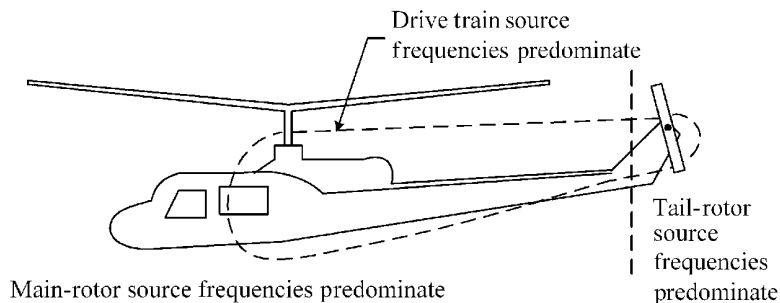


Figure 1.4.11 Helicopter dominant vibration zones

1.4.5 Fastener Looseness

Preloaded bolts (or nuts) rotate loose, when relative motion between the male and female threads takes place. This motion reduces the friction grip and permits the off-torque, which is proportional to the preload and thread pitch, to loosen the fastener. Transversely applied alternating forces generate the most severe condition for self-loosening. Appropriate choice of washers, installation of tie wires, and use of special bolts with more uniform load distributions between mating thread surfaces are some means to reduce bolt loosening. Attenuation of vibration treats this problem at its source. Fastener looseness is an especially important concern in high-performance machinery such as aircraft, helicopters, space shuttle, race cars, trains, roller coasters, and so on.

1.4.6 Optical Instrument Blurring

Lasers, telescopes, microscopes, interferometers, mirrors, and so on require a nearly vibration-free environment. This is typically accomplished by passive or active isolation of the equipment. Vibration has been called “the curse” in airplane- or helicopter-based aerial photography. Engine dynamic forces are transmitted through the airframe and into the camera resulting in blurry photos. High shutter speeds alleviate this problem at the expense of grainy photographs with less contrast. The camera must be soft mounted (isolated), which is more of a challenge for helicopter installations since the main rotor has a typically low frequency (e.g., ~ 30 Hz) and the camera must also be isolated from the tail rotor and engine frequencies (e.g., ~ 150 and ~ 250 Hz).

On the very small level, the lens-free AFM employs a tiny $100\ \mu\text{m}$ length cantilever beam to measure local sample height (topography) at the atomic level. The beam has a very low spring stiffness ($0.1\ \text{N/m}$) yet very high natural frequency. Mounted on the end of the cantilever is a sharp tip that is typically a $3\ \mu\text{m}$ tall pyramid with $10\text{--}30\ \text{nm}$ end radius. The deflection of the tip is measured with a laser. The beam and tip may also function in a noncontact mode where topographic images are derived from measurements of attractive forces. Environmental vibration can cause severe blurring of the topographic image produced by an AFM.

The space-based Hubble Space Telescope (HST) (Figure 1.4.12) experienced poor imaging due to vibrations of its original solar panels. The “jitter” interfered with operation

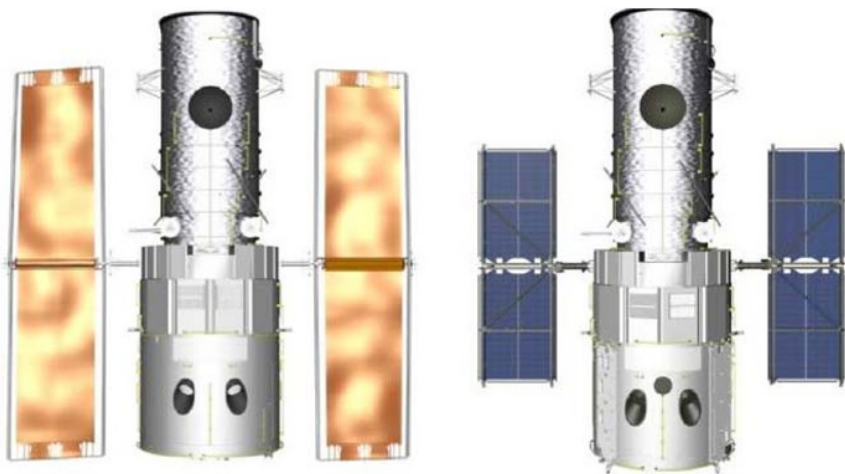


Figure 1.4.12 Hubble space-based telescope with original flexible and new rigid, smaller, and more powerful solar arrays. Reproduced with permission from NASA Goddard Space Flight Center

of the onboard optical instrumentation. The vibrations were induced by thermal deformations resulting from its cyclic exposure to 45 minutes of searing heat and 45 minutes of frigid cold during every 90 minutes orbit around the earth. The transition from extreme hot to extreme cold occurs almost instantaneously subjecting the solar arrays to a transient thermal shock load in a very low vacuum. The vibration frequency of the arrays occurred at about 0.1 Hz (1 cycle/10 seconds).

1.4.7 Ethics and Professional Responsibility

Section 1.4 has stressed some practical aspects of vibrations and why they should be tamed. I once heard a person say “why worry about standards, there are not the law.” This is true however from a commercial and sometimes litigation standpoint they have very high importance. It may be quite difficult to sell a machine that vibrates in excess of the limits defined by the standards during commissioning of the machine to industry or government users. Similarly, it may be challenging to defend operation of a machine prior to failure that may have resulted in loss of millions of dollars of products, facility damage, injury, or even death, if vibrations were related to the failure and the operating vibrations exceeded the limits provided in the standards. Insurance companies which pay for failures and accidents and judicial arbiters view industry and government standards with great seriousness, sometimes even more so than arguments based on detailed testing or simulation model results.

1.4.8 Lifelong Learning Opportunities

The list of vibration standards and related materials is very long and includes documents from many countries. A web search at the time of the writing of this book identified the following:

- (a) International Organization for Standardization (ISO—130 member countries)
http://www.iso.org/iso/home/store/catalogue_ics.htm (search vibration)
- (b) US Military Standards (MIL)
<http://quicksearch.dla.mil/> (search vibration)
- (c) UK Health and Safety Executive
www.hse.gov.uk/index.htm (search vibration)
- (d) American Petroleum Institute (API)
<http://www.api.org/Standards/>

This large number of standards is just one example of the fact that it is truly a lifelong learning experience to be a vibrations expert.

1.5 STIFFNESS, INERTIA, AND DAMPING FORCES

Systems vibrate due to the interplay (energy exchange) between *stiffness* (restoring), *inertia* (mass), and *damping* (drag) related forces. Figure 1.5.1 shows the top view of a horizontal spring/mass/damper system. The deflection of the spring in Figure 1.5.1(a) would always be

$$x(t) = \frac{F(t)}{k} \quad (1.5.1)$$

in a world without mass. This follows from *Newton's second law* (with mass = 0) and the spring's force–deflection relation. Equation 1.5.1 shows that point *p* will vibrate (oscillate) only if the external force *F* is oscillatory (periodic). Experience reveals that real systems oscillate even in the absence of oscillatory external forces, that is, the occurrence of natural

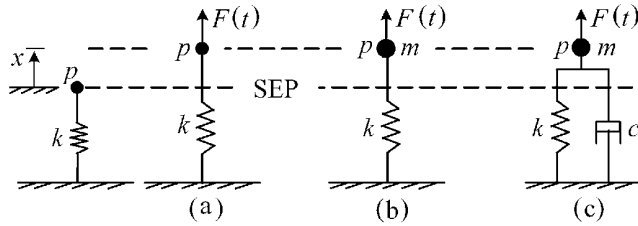


Figure 1.5.1 Response of spring/mass/damper system to external force $F(t)$

vibrations or vibrations due to a nonperiodic force. To understand why, consider the following discussion.

The spring stiffness acts to pull point p back toward its *static equilibrium position* (SEP). In fact, if k became infinite, it would pull x to the SEP independent of a finite valued $F(t)$. Equation (1.5.1) implies that

$$x = \begin{cases} F_0/k, & F(t) = F_0 \\ 0, & F(t) = 0 \end{cases} \quad (1.5.2)$$

so that x would instantaneously become zero at the moment $F(t)$ was removed. Suppose a mass is now attached to point p as shown in Figure 1.5.1(b). This mass will deflect by $x_0 = F_0/k$ if $F(t)$ is pseudostatically increased from zero to F_0 . Should the response in (1.5.2) still be expected if F_0 is suddenly removed with m attached? Intuition tells us no for several reasons:

- (a) The spring has potential energy ($PE = (1/2)kx_0^2$) when deflected at $x = x_0$. If x becomes zero, its P.E. is zero. Where did the potential energy go? The answer is kinetic energy, which implies that $\dot{x}(t)$ is not equal to zero at $x = 0$.
- (b) By (a) m has velocity ($-v_0$), that is, momentum as it passes through $x = 0$ at $t = t_0$. The spring force needs time to change the momentum of m from zero at $x = x_0$ to $-mv_0$ at $x = 0$. This results from the *impulse and momentum theorem*

$$I_k = \text{impulse on } m \text{ from spring } k = \int_0^{t_0} -kx dt = \Delta(mv) = m\Delta v = -mv_0 \quad (1.5.3)$$

Thus, x cannot return to zero instantaneously as was the case with no mass m in (1.5.2). The spring force exerts a positive impulse as soon as x becomes less than zero so m begins to decelerate. This implies that v_0 is the maximum velocity of m . The potential energy of the spring will become $(1/2)kx_0^2$ at $x = -x_0$. Therefore, the mass must have zero *kinetic energy* at $x = -x_0$ by conservation of energy, so its velocity is zero. The spring's impulse increases and m 's velocity again becomes positive. In this manner, the impulse of the spring force periodically changes m 's momentum (velocity direction) alternately positive and negative. This is the mechanism of free vibration. Both k and m influence the period of free vibration as can be seen from Equation (1.5.3).

The *work* performed on m by the damper in Figure 1.5.1(c) is negative since

$$W_c = \int_{x_1}^{x_2} F_c dx = \int_{t_1}^{t_2} -c\dot{x}dx = -c \int_{t_1}^{t_2} \dot{x}^2 dt < 0 \quad (1.5.4)$$

Energy is therefore removed from the system by damper c and the vibration diminishes to zero. This diminution to zero will not occur if another external force performs positive work on the system.

The word stiffness typically invokes an image of a coil spring that may deform in stretch or compression creating a force or in torsion creating a torque. Ultrahigh-strength springs as shown in Figure 1.5.2 are used in a myriad of machinery, instrument, transportation, and/or other applications.

In general, stiffness results from the restoring force capability of strain energy in a deformed elastic object. Table 1.5.1 shows an assortment of typical stiffness elements.



Figure 1.5.2 Assortment of extension–compression and torsion springs. Reproduced with permission from Murphy & Read Spring Manufacturing Co.

Table 1.5.1 Assorted stiffness elements

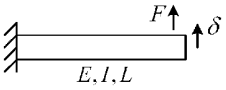
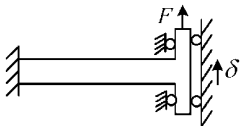
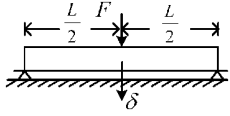
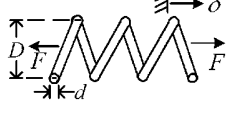
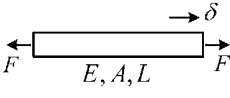
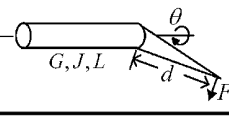
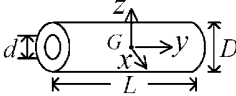
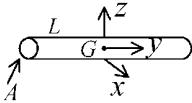
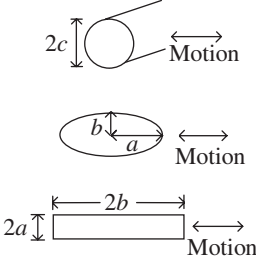
Entry	Description	Figure	Stiffness
1	Free cantilever		$k = \frac{F}{\delta} = 3 \frac{EI}{L^3}$
2	Guided cantilever (zero rotation at tip)		$k = \frac{F}{\delta} = 12 \frac{EI}{L^3}$
3	Simply supported beam		$k = \frac{F}{\delta} = 48 \frac{EI}{L^3}$
4	Coiled spring (round wire) G = shear modulus N = number of coils		$k = \frac{F}{\delta} = \frac{Gd^4}{8D^3N}$
5	Stretched rod		$k = \frac{F}{\delta} = \frac{EA}{L}$
6	Torsion spring G = shear modulus J = torsion constant		$k_T = \frac{Fd}{\theta} = \frac{GJ}{L}$

Table 1.5.2 Assorted mass elements

Entry	Description	Figure	Inertia
1	Hollow cylinder ρ = mass density G = mass center		$m = \frac{\rho\pi L(D^2 - d^2)}{4}$ $I_y = \frac{m}{8}(D^2 + d^2)$ $I_x = I_z = m\left(\frac{L^2}{12} + \frac{(D^2 + d^2)}{16}\right)$
2	Long slender rod G = mass center		$m = AL\rho$ $I_x = I_z = \frac{mL^2}{12}$
3	Vibration of soil in liquid ρ = density of liquid	Cross-sections 	Added mass per unit length $\rho\pi c^2$ $\rho\pi b^2$ $1.15 \rho\pi a^2, (a = b)$ $1.14 \rho\pi a^2, (a = 10b)$

Likewise, Tables 1.5.2 and 1.5.3 show assortments of mass and damping elements. Finally, Table 1.5.4 shows a table of force expressions.

The following analysis shows a derivation of entry 2 (Table 1.5.3). A liquid flowing with velocity u and laminar Reynolds (R_e) number ($(\rho u d_H)/\mu$) experiences the pressure drop

$$\Delta p = \rho \frac{L}{d_H} \frac{u^2}{2} f \quad (1.5.5)$$

as it flows through a pipe of length L . The laminar flow friction factor may be obtained from most fluid mechanics text as

$$f = \frac{64}{R_e} = \frac{64\mu}{ud_H\rho} \quad (1.5.6)$$

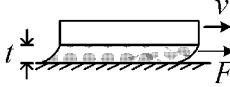
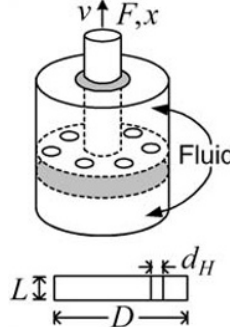
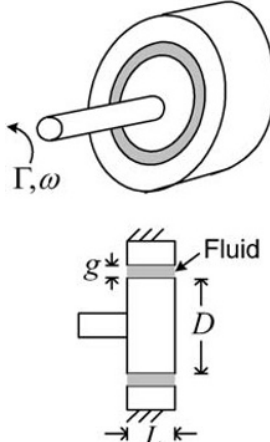
Substitute (1.5.6) into (1.5.5) to obtain

$$\Delta p = 32 \frac{L\mu u}{d_H^2} \quad (1.5.7)$$

Let A be the entire area of the piston and “ a ” the area of a single hole. Then the time rate of change of the upper volume is

$$\frac{\Delta V}{\Delta t} = vA = \frac{\Delta x}{\Delta t} A \quad (1.5.8)$$

Table 1.5.3 Assorted damping elements

Entry	Description	Figure	Damping
1	Parallel plate damper A = plate wetted area μ = absolute viscosity		$C = \frac{F}{v} = \frac{\mu A}{t}$
2	Orifice damper μ = fluid absolute viscosity n = no. of orifice holes		$C = \frac{F}{v} = \frac{8\pi L\mu}{n} \left(\frac{D}{d_H}\right)^4$
3	Torsional damper μ = fluid absolute viscosity		$C_T = \frac{\Gamma}{\omega} = \frac{2\pi\mu L D^3}{8g}$

The volumetric flow rate through the n holes is

$$Q_H = nua \quad (1.5.9)$$

Conservation of the mass for an incompressible liquid requires that

$$Q_H = \frac{\Delta V}{\Delta t} \Rightarrow u = \frac{vA}{na} = \frac{v}{n} \cdot \frac{\pi D^2/4}{\pi d_H^2/4} = \frac{v}{n} \left(\frac{D}{d_H}\right)^2 \quad (1.5.10)$$

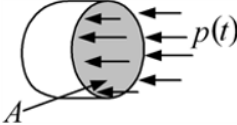
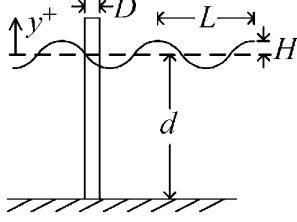
Substitute (1.5.10) into (1.5.7)

$$\Delta p = \frac{32L\mu}{d_H^2} \frac{v D^2}{n d_H^2} \quad (1.5.11)$$

The net force on the piston is

$$F = \Delta p A = \frac{\pi D^2}{4} \Delta p \quad (1.5.12)$$

Table 1.5.4 Assorted force expressions

Entry	Description	Figure	Force
1	Pressure force		$F(t) = pA(t)$
2	Wave force on circular cylinder		$F(y, t) = \text{force per unit length}$ $= g_1(y)g_2\left(\frac{\pi D}{L}\right) * \cos(\omega t - g_3)$ $g_1(y) = \frac{2\rho g H \cosh(k(d+y))}{k \cosh(kd)}$ $g_2\left(\frac{\pi D}{L}\right) = \left\{ \left[J'_1\left(\frac{\pi D}{L}\right) \right]^2 + \left[Y'_1\left(\frac{\pi D}{L}\right) \right]^2 \right\}^{-1/2}$ $g_3 = \tan^{-1} \left(\frac{J'_1\left(\frac{\pi D}{L}\right)}{Y'_1\left(\frac{\pi D}{L}\right)} \right)$
	$T = \text{wave period}$		
	$\omega = \text{wave frequency}$ $= 2\pi/T$		
	$k = \text{wave frequency}$ $= 2\pi/L$		
	$\rho = \text{mass density of water}$		$J'_1 = \text{derivative of the first order Bessel function of the first kind}$
	$g = \text{gravity constant}$		$Y'_1 = \text{derivative of the second order Bessel function of the second kind}$

if $na \ll A$. Insert (1.5.11) into (1.5.12) to obtain

$$F = cv \quad (1.5.13)$$

where

$$c = \frac{8L\mu\pi}{n} \left(\frac{D}{d_H} \right)^4 \quad (1.5.14)$$

1.6 APPROACHES FOR OBTAINING THE DIFFERENTIAL EQUATIONS OF MOTION

The equations of motion for a vibrating system model provide a starting point for simulating the system's response to initial conditions, external forces, or parametric excitation (time-dependent system parameters). Approaches for deriving the equations of motion for a model of a vibrating system are discussed below.

(a) Newton's Laws (Chapter 3)

These laws represent the balance between external and inertial forces as first proposed by Sir Isaac Newton. Practical applications required extension of this balance from a particle to a collection of particles and finally to a rigid body. The translational and rotational forms of Newton's laws for rigid bodies are presented in Chapter 3.

(b) *The Power Conservation Approach (Chapter 4)*

Applying power conservation for deriving the equations of motion has a physical intuition appeal. The potential and kinetic energy expressions form the starting point for applying the method. This approach has an advantage of being able to disregard all forces that perform a net work of zero, as discussed in Chapter 4.

(c) *The Lagrange–Hamilton Approach (Chapter 4)*

The Lagrange–Hamilton approach utilizes expressions for kinetic and potential energy to develop the equations of motion for the system. This approach may be interpreted as a restatement of Newton’s laws or an entirely different physical principle based on making an “action” integral stationary, using the calculus of variations.

The Lagrange approach for formulating the equations of motion of a rigid or flexible body model circumvents some tasks for direct application of Newton’s law. These include:

- No direct evaluation of acceleration vectors for the mass center(s)
- Less applications of Newton’s third law for equal and opposite reactions in many instances
- Less sign determination for many forces
- Direct use of potential energy to evaluate internal force effects in a flexible body
- Direct means to formulate equations of motion in terms of any generalized coordinate, which may consist of an actual physical coordinate or of a parameter that governs a distributed shape for deflections (this is a key capability in the assumed modes and finite element methods)

The Lagrange approach is discussed extensively in Chapter 4.

1.7 FINITE ELEMENT METHOD

The finite element method (FEM) is widely used in industry for avoiding machinery and structural vibration problems. User-friendly graphically driven interfaces have greatly facilitated the efficient use of this method. Direct conversion of solid modeler geometry descriptions into finite element “meshes” is quickly becoming standard practice for the simulation of vibrations of components and systems of all sizes and shapes. This is illustrated in Figure 1.7.1.

The meshes consist of discrete node points that define finite-sized subvolumes referred to as elements. The motions within any element are approximated by interpolation functions, which interpolate the displacements at the node points throughout the element. The interpolation functions are generally linear or quadratic functions of position but may be more complex as a result of “isoparametric” transformations that enable the element to possess general 2- or 3-dimensional shapes. The FEM has its theoretical foundations in the more general areas of energy principles and weighted residual methods. The former utilizes the variational approach of determining the solution of the equilibrium equations by finding solutions that make a companion functional stationary (maximum or minimum), as in the case of the principle of virtual work, Hamilton’s principle, or the principle of minimum total potential energy. The latter develops a “weak” form of the original equilibrium equations by integrating products of weight functions times the equilibrium equations while lowering continuity requirements on the interpolation functions utilizing integration by parts (divergence theorem). The net result is typically a very large order system of linear differential equations that are numerically integrated to obtain the time-varying displacements at the node points. These displacements can then be utilized to solve for stresses, which are in

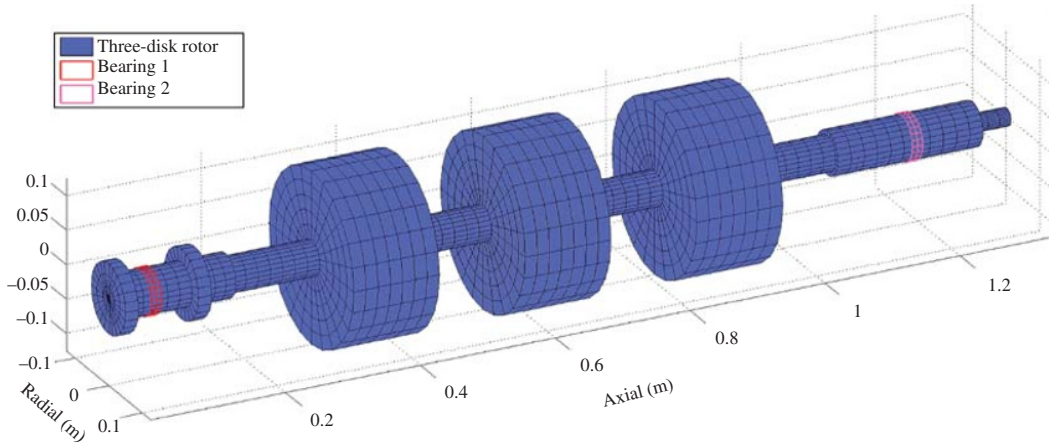


Figure 1.7.1 Finite element mesh generated from a solid model of a shaft

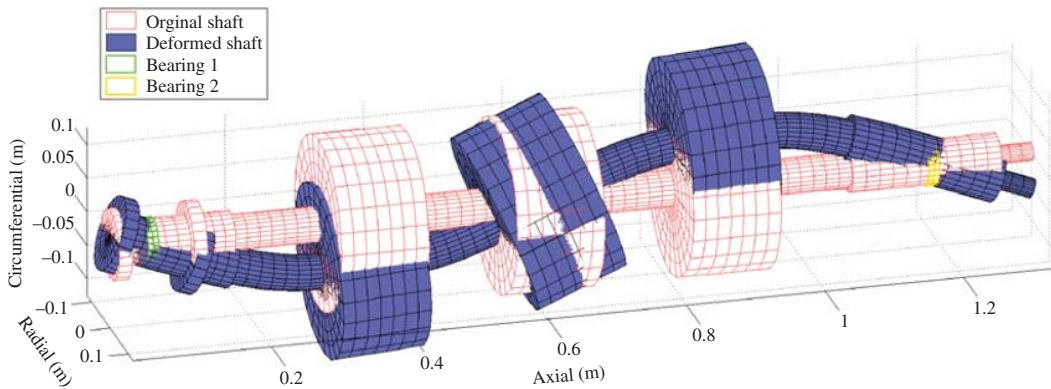


Figure 1.7.2 Vibration “mode shape” obtained from a finite element model

turn utilized to predict fatigue life. The system of equations can also be solved to obtain eigenvalues and eigenvectors, which describe the “mode” shapes and “natural” frequencies of the modeled system in free (unforced) vibration. This is illustrated in Figure 1.7.2 for the finite element model in Figure 1.7.1.

So why study finite element theory when its application tools are quickly progressing toward a nearly automated state? There are several very good reasons, including:

- (a) **Cost:** The “honeymoon is over” as far as cheap software when one leaves the university and enters industry or private practice. Single seat, annual licensing fees in the tens of thousands of dollar range for industrial users are common.
- (b) **Proper usage of commercial software (CS):** CS can be easily misused by not understanding the limitations (assumptions) of the theory implemented by the CS. Understanding the theory will guide one to utilize the appropriate software options and avoid the ineffective ones.
- (c) **Advancement and customization:** Engineering technology is advancing at an incredible rate requiring the use of novel materials, smart and multidisciplinary systems, newly

discovered empirical force descriptions, and so on. CS sometimes lags behind these needs requiring engineers to develop their own finite element software. Customer input and output requirements may also motivate engineers to develop their own finite element software.

- (d) General innovation: Who knows what new methods of modeling and simulation lies over the horizon? It's hard to say, however, chances are good that it will build on the theory of existing methods. Knowledge of finite element theory will provide a foothold to reach out and develop new theoretical approaches for simulation.

The book provides the necessary theory and implementation tools required to develop your own finite element codes. The progression of element sophistication is ordered from simple spring mass systems to general 3D solids in the book to facilitate comprehension and to provide results of significant practical value.

1.8 ACTIVE VIBRATION CONTROL

Passive vibration control seeks to achieve vibration mitigation goals via structural modification and installation of devices such as absorber masses, spring, and dampers to reduce the system sensitivity to external disturbances and to self-excitation forces, that is, instability. Passive devices have limits though in adaptability and environmental operating conditions. Active vibration control AVC devices can replicate the behavior of a passive device as described and also produce forces with a more general dependence on motion variables. AVC devices may also adapt to changing operating condition variables and function well even in extreme temperature and pressure environments, including vacuum conditions. Chapter 12 provides an in-depth introduction to the methodology of AVC. This includes discussions of modeling methods, common architecture, simulation and solution procedures, and analysis of electromagnetic and piezoelectric actuators.

1.9 CHAPTER 1 EXERCISES

1.9.1 Exercise Location

All exercises may be conveniently viewed and downloaded at the following website: www.wiley.com/go/palazzolo. This new feature greatly reduces the length of the printed book, yielding a significant cost savings for the college student and allows the author to provide additional exercises.

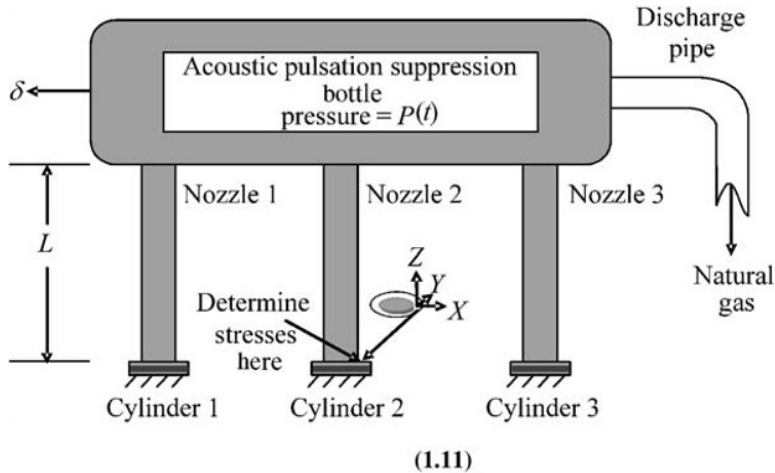
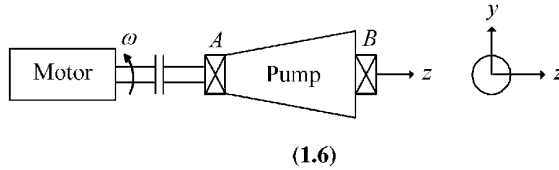
1.9.2 Exercise Goals

The goal of the Exercises in Chapter 1 is to strengthen the student's understanding and related engineering problem-solving skills in the following areas:

- (a) The presence of vibrations in natural and industrial processes and devices
- (b) The deleterious effects of vibration on the reliability, efficiency, and safety of industrial processes and devices and on human health
- (c) The quantified descriptions of vibrations
- (d) The determination of failure and life of a vibrating object
- (e) The use of vibration standards established by industry and government

1.9.3 Sample Exercises: 1.6 and 1.11

Exercise 1.6 illustrates the use of machinery vibration standards for multiharmonic vibrations of an electric motor-driven pump. Exercise 1.11 considers a vibrating, pulsation suppression vessel for a natural gas transmission compressor. This exercise requires evaluation of component and von Mises (equivalent) stresses and component life, given mean and alternating (vibrating) motions. This exercise should impress on the student the role that vibration analysis plays in designing machines for greater reliability and sharpen skills in fatigue-related failure.



REFERENCES

- ASTM E-1049–85, *Standard Practices for Cycle Counting in Fatigue Analysis*, (Reapproved 2011), <http://www.astm.org/DownloadStandardB.html?ASTM%20HC=ASTM&DESIGNATION=E1049&AdID=&Split=&Campaign=Individual%20Standards%207&gclid=COF9kujhlgCFYM-aQodJ5cD4w> (accessed 15 October 2015).
- BUDYNAS, R. and NISBETT, J., *Shigley's Mechanical Engineering Design*, 8th ed., McGraw Hill, New York, 2008.
- CANNON, R. H., *Dynamics of Physical System*, 1st ed., McGraw Hill, New York, 1967.
- CDC, *Health Hazard Report No. 94-0425*, 1994.
- COLLINS, J. A., *Failure of Materials in Mechanical Design*, 1st ed., John Wiley & Sons, New York, 1981.
- GRIFFIN, M. J., *Handbook of Human Vibration*, 1st ed., Academic Press, London, 1990.
- HASSAN, O. A. B., *Building Acoustics and Vibrations*, 1st ed., World Scientific Publishing, Singapore, 2009.

- LEE, Y.-L., BARKEY, M. E., and KANG, H. T., *Metal Fatigue Analysis Handbook: Practical Problem-Solving Techniques for Computer-Aided Engineering*, Elsevier, Waltham, MA, 2012.
- NEWMAN, CARDINAL, J. H., *The Idea of a University*, edited by D. M. O'Connell, Loyola University Press, Chicago, IL, 1927.
- NICHOLAS, T., *High Cycle Fatigue: A Mechanics of Materials Perspective*, Elsevier, Oxford, 2006.
- NIESLONY, A., *Rainflow Counting Algorithm*, MATLAB, Mathworks, Inc., Natick, MA, 2010.
- NIOSH, *Occupational Exposure to Hand-Arm Vibration*, US Department of Health and Human Services, Cincinnati, OH, 1989. <http://www.cdc.gov/niosh/docs/89-106/89-106.pdf>. Accessed August 4, 2015.
- PILKEY, W. D., *Peterson's Stress Concentration Factors*, 2nd ed., John Wiley & Sons, Inc., New York, 1997.
- SHIGLEY, J. E., *Mechanical Engineering Design*, McGraw Hill, New York, 1989.
- WANG, S., Mean Shear Stress Effect for a Notch-Free Ductile Material Under Pure Cyclic Torsional Loads, *Journal of Pressure Vessel Technology*, Vol. **128**, pp. 667–669, 2006.

Chapter 2

Preparatory Skills: Mathematics, Modeling, and Kinematics

2.1 INTRODUCTION

Mathematics is often referred to as the “language of science.” This description is very accurate with regard to the science of vibrations, where the capability to predict responses of complex systems is made possible through specialized mathematical methods. This chapter provides a foundation for understanding mathematical-based solutions and derivations in subsequent chapters. Modern tools for mathematical manipulation and solution are becoming essential parts of the efficient solution of vibration problems. The two commercial software packages that are integrated into the text are MATLAB and MAPLE due to their generality and popularity. Short primers in the usage of these programs are presented first since subsequent sections utilize these codes. Notably, an introduction for the usage of these codes with symbolic operations is included. This chapter also presents some key aspects of modeling, specifically degrees of freedom (dofs) and motion constraints. Motion constraints are the basis for approximation in solving vibration problems and have the form of boundary and interconnection conditions, particle and RBMs, and flexible body models utilizing the assumed modes and finite element methods (FEMs). Some believe that simpler forms of modeling are approaching obsolescence as advanced finite element modeling tools have evolved to yield highly detailed models requiring only a solid model input. Without denying the great value of sophisticated finite element models, one should also consider that

- Engineering intuition is required to form the solid models and is typically based on simple model approximations.
- Many practical problems can be solved with simple models that combine engineering experience with knowledge of the related natural laws and analytical techniques.
- Commercial finite element codes are quite expensive so they may not be available to some analysts, designers, or problem troubleshooters.
- Design is an iterative process, requiring variation of possibly many parameters, so that use of highly detailed models may become computationally time prohibitive.
- Highly complex model responses generally behave similar to simpler models. The simpler models provide a “reality check” for verifying the complex models.

Simple models still play a key role in shaping intuition and for design and retrofitting systems via vibration engineering.

2.2 GETTING STARTED WITH MATLAB AND MAPLE

This section provides a foothold to get started using math software for vibration problem solution. It is placed here, and not in an appendix, to address the reality that mathematical/numerical simulation plays an essential role in vibration engineering and in the examples provided in the text. It is also placed front and center to motivate the students to initiate learning computational skills very early in the course. *This section also provides explanations for symbolic operations utilizing these codes. This capability is used often in Chapters 4, 5, 6, 7, and 12 and can reduce the analyst/student workload tremendously and increase the accuracy of derivations.*

2.2.1 MATLAB

Real Scalar Operations

(1) addition, (2) subtraction, (3) multiplication, (4) division, (5) exponentiation, (6) absolute value, (7) sign, (8) \log_{10} , (9) \log_e , (10) square root, (11) cosine, (12) sine, (13) tangent, (14) \tan^{-1} , (15) cosh, (16) sinh

Code:

```
y1 = 2+5 , y2 = 2-5 , y3 = 2*5 , y4 = 2/5
y5 = 2^3 , y6 = abs(-8) , y7 = sign(-8)
y8 = log10(1000) , y9 = log(2.7183) , y10 = sqrt(144)
y11 = cos(3.1416) , y12 = sin(-3.1416/2) , y13 =
tan(45/57.2956)
y14a = atan2(-1,0)*57.2956 , y14b = atan2(1,1)*57.2956
y14c = atan2(0,0) , y15 = cosh(0) , y16 = sinh(0)
```

Output:

```
y1 = 7, y2 = -3, y3 = 10, y4 = 0.4000
y5 = 8, y6 = 8, y7 = -1
y8 = 3.0000, y9 = 1.00, y10 = 12
y11 = -1.0000, y12 = -1.00, y13 = 1.0000
y14a = -89.9997, y14b = 44.9999
y14c = 0, y15 = 1, y16 = 0
```

Complex Scalar Operations

(1) addition, (2) subtraction, (3) multiplication, (4) division, (5) exponentiation, (6) magnitude, (7) angle, (8) conjugate

Code:

```
z1 = (3+i*4)+(5-i*8) , z2 = (3+i*4)-(5-i*8) , z3 = (3+i*4)*(5-i*8) ,
z4 = (3+i*4)/(5-i*8) , z5 = (3+i*4)^3 , z6 = abs(3+i*4)
z7 = angle(2+i*2)*57.2956 , z8 = conj(2+i*2)
```

Output:

```

z1 = 8.0000 - 4.0000i, z2 = -2.0000 +12.0000i,
z3 = 47.0000 - 4.0000i
z4 = -0.1910 + 0.4944i, z5 = -1.1700e+002 + 4.4000e + 001i , z6 = 5
z7 = 44.9999, z8 = 2.0000 - 2.0000i

```

Matrix Operations

(1) addition, (2) transpose^{***}, (3) multiplication, (4) inverse, (5) eigenvalues, (6) eigenvectors, (7) rank, (8) null matrix, (9) unit matrix, (10) ones, (11) partition matrix assembly, (12) partition matrix extraction, (13) element-wise multiplication, (14) element-wise sine

****Taking the transpose A' of a complex array A will yield the transpose of the complex conjugate of the original array. Utilize A.' in order to suppress the complex conjugate operation.*

$$\underline{a} = \begin{bmatrix} 1 & 2 & 3 \\ 4 & 5 & 6 \end{bmatrix}, \underline{b} = \begin{bmatrix} 2 & -3 \\ -5 & 7 \end{bmatrix}, \underline{c} = \begin{bmatrix} 22 & -8 & -9 \\ -8 & 19 & -12 \\ -9 & -12 & 30 \end{bmatrix},$$

$$\underline{d} = \begin{bmatrix} 1 & 2 & 4 \\ 7 & 4 & 18 \\ 9 & -3 & 15 \end{bmatrix}, \underline{e} = \begin{bmatrix} 0 & \pi/2 & \pi \\ -\pi/2 & \pi/4 & 0 \\ \rho & 3\pi/2 & 0 \end{bmatrix}, \underline{f} = \begin{bmatrix} \underline{a} & \underline{c} \\ \underline{a} & \underline{d} \\ \underline{a} & \underline{d} \end{bmatrix}$$

Code:

```

a = [ 1 2 3 ; 4 5 6 ] , b = [ 2 -3 ; -5 7 ]
c = [ 22 -8 -9 ; -8 19 -12 ; -9 -12 30 ] , d = [ 1 2 4 ; 7 4 18 ; 9 -3 15 ]
e = [ 0 pi/2 pi ; -pi/2 pi/4 0 ; pi 3*pi/2 0 ]

```

```

m1 = c + d, m2 = a' % transpose of a, m3 = b*a
m4a = inv(c) % inverts matrix c
m5 = eig(c) % eigenvalues of c
[m6,evalues] = eig(c) ; % eigenvectors and eigenvalues of c
m6 % print matrix of eigenvectors of c
m7 = rank(d) % the rank of matrix d
m8 = zeros(3,4) % matrix of zeros
m9 = eye(3) % the unit matrix
m10 = ones(3,4) % matrix of ones

```

% Form a partitioned matrix:

```

m11(1:2,1:3) = a ; , m11(3:4,1:3) = a ; , m11(5:6,1:3) = a ;
m11(1:3,4:6) = c ; , m11(4:6,4:6) = d ;
m11

```

```

% Extract a part of a partitioned matrix m12 = m11(2:4,3:6)

```

```

% Element-wise multiplication of 2 arrays    m13 = c.*d
% Element-wise sine of an array            m14 = sin(e)
a = 1   2   3       b = 2  -3           c = 22  -8  -9
    4   5   6       -5   7           -8   19  -12
                                -9  -12  30

d = 1   2   4       e = 0   1.5708   3.1416
    7   4   18      -1.5708  0.7854   0
    9  -3   15      3.1416  4.7124   0

m1 = 23  -6  -5     m2 = 1  4           m3 = -10 -11 -12
    -1  23  6       2  5              23  25  27
    0 -15  45      3  6

m4a = 0.1018  0.0832  0.0638           m5 = 28.6036
      0.0832  0.1384  0.0803           38.6066
      0.0638  0.0803  0.0846           3.7898

m6 = -0.7964  0.2666  0.5429     m7 = 2       m8 = 0  0  0  0
      0.6029  0.4217  0.6773           0  0  0  0
      0.0484 -0.8667  0.4965           0  0  0  0

m9 = 1  0  0           m10 = 1  1  1  1
     0  1  0           1  1  1  1
     0  0  1           1  1  1  1

m11 = 1  2  3  22  -8  -9
      4  5  6  -8  19 -12
      1  2  3  -9 -12  30
      4  5  6  1  2  4
      1  2  3  7  4  18
      4  5  6  9 -3  15

m12 = 6  -8  19 -12   m13 = 22 -16 -36   m14 = 0  1  0
      3  -9 -12  30     -56  76 -216     -1  .7071  0
      6  1  2  4       -81  36  450     0  -1  0

```

Miscellaneous

- Always start your code with “clear.” This will eliminate accumulated operations.
- Utilize “whos” command to obtain list of dimensions of all variables.
- Utilize “help” command to understand the usage of any MATLAB command. For example, to understand how to use the matrix inverse command inv, type:

```
help inv
```

in the MATLAB workspace.
- The “global” command allows arrays or scalars to be transferred between the main code and subfunctions.
- Use syms commands for all symbolic variables

- Loops may be defined as for example:
for i=1:1:100 , a(i) = i^2 + 3, end
- Conditional statements may be defined as for example:
if i+3 ==5 , jj = 5 + I, end
- MATLAB has a symbolic option as illustrated by the matrix multiplication, determinant, derivative, and integration examples given below. *MATLAB symbolic is utilized in Chapters 6 and 12.*

```
clear all
syms x1 y1 x2 y2 x3 y3 x4 y4 z1 z2 b1 b2 b3 g1 g2 g3 e1 e2
      e3 nu E Q
H = [x1 y1; x2 y2]
Q = 1/4*[ z2-1 -z2+1 ; z1-1 -z1-1 ]
J = Q*H
det_J = det(J)
HH = [x1^2 0; x2^2 0];
int(HH, x1)
diff(HH, x1)
```

Outputs

```
H = [ x1, y1]
      [ x2, y2]
Q = [ z2/4 - 1/4, 1/4 - z2/4]
      [ z1/4 - 1/4, - z1/4 - 1/4]
J = [ x1*(z2/4 - 1/4) - x2*(z2/4 - 1/4), y1*(z2/4 - 1/4) -
      y2*(z2/4 - 1/4)]
      [ x1*(z1/4 - 1/4) - x2*(z1/4 + 1/4), y1*(z1/4 - 1/4) -
      y2*(z1/4 + 1/4)]
det_J = (x1*y2)/8 - (x2*y1)/8 - (x1*y2*z2)/8 + (x2*y1*z2)/8
ans = [x1^3/3, 0]
      [ x1*x2^2, 0]
ans = [ 2*x1, 0]
      [0, 0]
```

2.2.2 MAPLE (Symbolic Math)

This section provides a foothold for using the symbolic math code MAPLE for vibration applications. Symbolic manipulation is used in several key areas in the text, including automated formulation of equations of motion (EOMs), the assumed modes method, and for obtaining orbital equilibrium states for harmonically forced nonlinear systems. *MAPLE symbolic is utilized in Chapters 3, 4, 5, and 9.* Alternatively, one may prefer to use MATLAB's symbolic math features (see above MATLAB code).

2.2.2.1 Solving Systems of Nonlinear Algebraic Equations

The commands below illustrate how to solve simultaneous linear or nonlinear algebraic equations. This tool is useful for obtaining algebraic expressions for natural frequency,

damping, and other characteristics in terms of system parameters. The subs command is included to illustrate how to substitute a numerical value into a symbolic variable in your code.

```
> eqs := {y=zeta*theta^2, y-alpha*theta-.25=0};

          eqs := {y - alpha*theta - 0.25 = 0, y = zeta*theta^2}

> eqs1 := subs(zeta=2., alpha=0.1, eqs);

          eqs1 := {y - 0.1*theta - 0.25 = 0, y = 2.*theta^2}

> solve(eqs1, {y, theta});

{theta = -0.3294361720, y = 0.2170563828}, {y = 0.2879436172, theta = 0.3794361720}
```

2.2.2.2 Symbolic Differentiation

This tool is very useful for applying Lagrange's equations to obtain EOMs.

```
> g := cos(beta) + 2*y + 3.*beta^3 + b*sin(beta);

          g := cos(beta) + 2y + 3.*beta^3 + 5 sin(beta)

> der_g_wrt_beta := diff(g, beta);

          der_g_wrt_beta := -sin(beta) + 9.*beta^2 + 5 cos(beta)
```

2.2.2.3 Symbolic Integration

This tool is very useful for implementing the assumed modes method for obtaining EOMs for generalized coordinates.

```
> g := cos(beta) + 2*y + 3.*beta^3 + b*sin(beta);

          g := cos(beta) + 2y + 3.*beta^3 + 5 sin(beta)

># Integrate this function with respect to beta
> int_g_wrt_beta := int(g, beta);

          int_g_wrt_beta := sin(beta) + 2.y*beta + 0.7500000000 beta^4 - 5.cos(beta)
```

```

># Integrate this function with respect to  $\beta$  from  $\beta = 0$  to  $\beta = 5.0$ 

> g:= cos(beta) + 2*y + 3.*beta^3 + b*sin(beta);

      g:= cos( $\beta$ ) + 2y + 3. $\beta^3$  + b sin( $\beta$ )

> int_g_wrt_beta:= int(g,beta=0..5.0);

      int_g_wrt_beta:= 0.7163378145 b + 467.7910757 + 10.y

```

2.2.2.4 Evaluation of the Jacobian Matrix

The Jacobian matrix is very helpful for identifying the stability and “domains of attraction” for the multiple equilibrium points of a nonlinear dynamical system and for simple linearization of force expressions.

```

> # The Jacobian matrix for 2 functions (g1(x,y), g2(x,y)) of
> 2 independent variables x and y is defined by the 2 by 2 matrix:
> #      J = [ d(g1)/dx   d(g1)/dy
> #            d(g2)/dx   d(g2)/dy ]

> # Consider the following example.
> g1:= 5*x^2+x - 5.*y^3 ; g2:= 5.*sin(x) + 3.*cos(y) ;

      g1:= 5x2 + x - 5.y3
      g2:= 5.sin(x) + 3.cos(y)

> # The Maple linear algebra package must be entered in order to
> form the Jacobian matrix.
> with(linalg): # enter into the Maple linear algebra pkg.
> # Then the Jacobian Matrix may be formed as follows:
> Jmat:= jacobian([g1,g2], [x,y]);

```

$$Jmat := \begin{bmatrix} 10x+1 & -15.y^2 \\ 5.\cos(x) & -3.\sin(y) \end{bmatrix}$$

2.2.2.5 Eigenvalues and Eigenvectors

This tool is very useful for calculating natural frequencies and mode shapes of a vibrating system.

```

> with(linalg): # enter into the Maple linear algebra pkg.
> # Next consider evaluation of the eigenvalues of the jacobian
> matrix at x = 5 and y = -3

```



```
> Jmat1:= simplify(subs(x=5.,y=-3.,evalm(Jmat)) );
```

$$Jmat1 := \begin{bmatrix} 51. & -135. \\ 1.418310928 & 0.4233600243 \end{bmatrix}$$

```
> # The simplify command simplifies the expression, i.e. in this case it causes the sin and cos expressions to be numerically evaluated.
```

```
> # The evalm command implies "evaluate numerical value of matrix"
```

```
> # Next evaluate the eigen-solutions of matrix Jmat1
```

```
> eigenvectors(Jmat1);
```

$$\begin{aligned} & [46.87833191, 1, \{[9.564175146, 0.2920026335]\}], \\ & [4.545028115, 1, \{[3.334295489, 1.147367431]\}] \end{aligned}$$

```
> # Note that each of the output groups contain an eigenvalue, its algebraic multiplicity (no. of times its repeated) and its corresponding eigenvector
```

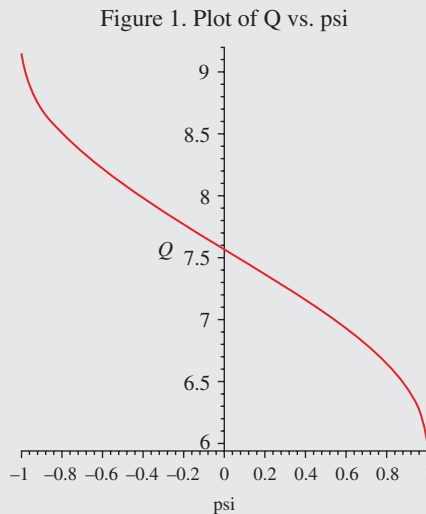
Simple Y versus X Type Plot

```
# A simple plot of one quantity (Q) vs. another (psi) is illustrated next
```

```
> Q:= 2. + arccos(psi) +4;
```

$$Q := 6. + \arccos(\psi)$$

```
> plot(Q,psi=-1..1, title = "Figure 1. Plot of Q vs. psi", labels=["psi", "Q"] );
```



Miscellaneous

MAPLE has a very useful “help” feature that is accessible at the upper toolbar.

```
> # The following topics may be viewed via the help icon and
clicking " new users tour"
> # These tours provide useful instructions and examples for many
engineering math
> # related operations
```

- (1) Working Through the New User’s Tour
- (2) Numerical Calculations
- (3) Algebraic Computations
- (4) 2-D Graphics
- (5) 3-D Graphics
- (6) Calculus
- (7) Vector Calculus
- (8) Differential Equations
- (9) Linear Algebra
- (10) Programming
- (11) Programming the Maple Graphical User Interface
- (12) Help System
- (13) Summary

General:

```
> # The pounce (#) symbol is for writing comments .
> restart ; # The restart command is employed to clear all arrays
of their present values . It is recommended to always employ this
command at the very beginning of your codes
> # In order to execute the command at the present position of
the cursor click the ! icon on the tool bar .
> # In order to execute the entire code click the !!! icon on the
tool bar
> # Click the [> icon on the above toolbar to add a line below the
current position of the toolbar
> # Subscripted symbols may be utilized by employing brackets .
Warning there are some Maple commands that will not work with
subscripted variables .
> a[1,1] := 3*5 ; b[1][2] := a[1,1]/2 ;
```

$$a_{1,1} := 15 \quad b_{1,2} := \frac{15}{2}$$

```
> # Floating point results may be obtained by employing the feval
command or by expressing numerical values with a decimal . Some
examples are
> a := 4 ; b := 5 ; c := a/b ; d := evalf(a/b) ; e := 4./5. ;
```

$$a := 4 \quad b := 5 \quad c := \frac{4}{5} \quad d := 0.8000000000 \quad e := 0.8000000000$$

> # Terminate a command with a semi-colon for display of results.
 Terminate a command with a colon for no display of results.

2.3 VIBRATION AND DIFFERENTIAL EQUATIONS

Two principles presented in a second year course on static and dynamic are:

(a) Static equilibrium implies that all forces and moments on a body sum to zero:

$$\sum \vec{F} = \vec{0}, \quad \sum \vec{\Gamma} = \vec{0} \quad (2.3.1)$$

(b) Dynamic equilibrium implies that all forces on a body sum to *mass times acceleration* and all moments sum to *mass moment of inertia times angular acceleration*:

$$\sum \vec{F} = m \vec{a}, \quad \sum \vec{\Gamma} = I \vec{\alpha} \quad (2.3.2)$$

The acceleration term in that course is typically treated as a constant, or the force balance is considered at one instant (snapshot) in time in (2.3.2). The result is that (2.3.2) yields one or more algebraic equations for unknown forces, moments, or accelerations. Vibration analysis seeks to determine motions as time varies, which requires that the acceleration be expressed as the second derivative of position or the first derivative of velocity in (2.3.2). The left-hand side of (2.3.2) may contain terms that are explicit functions of time or functions of velocities and displacements. The net result is that (2.3.2) becomes a differential equation. Depending on the coordinates selected, the left- and right-hand sides of (2.3.2) may have nonlinear and linear functions of position and its first and second derivatives. Thus, (2.3.2) may be a linear or nonlinear differential equation.

The use of differential equations in vibration theory should be of no surprise to the student who has completed a first course in differential equations and is familiar with the following simple cases:

(a) $\ddot{x} + 2\xi\omega\dot{x} + \omega^2x = 0$

with solution form $C * e^{-\xi\omega_n t} \cos(\omega_d t + \phi)$

(b) $\ddot{x} + 2\xi\omega\dot{x} + \omega^2x = \tilde{F} \cos(\omega t)$

with solution form $C * e^{-\xi\omega_n t} \cos(\omega_d t + \phi) + B \cos(\omega t + \beta)$

These examples have decaying (damped) response, free and forced frequencies, and phase angle, which are all characteristics of vibration behavior.

2.3.1 MATLAB and MAPLE Integration

Instructions for utilizing MATLAB and MAPLE for integration are provided below. This subject is treated in greater detail in Chapter 6 on transient vibrations and is required prior to Chapter 6 to integrate EOM for obtaining responses to initial conditions or forced excitation.

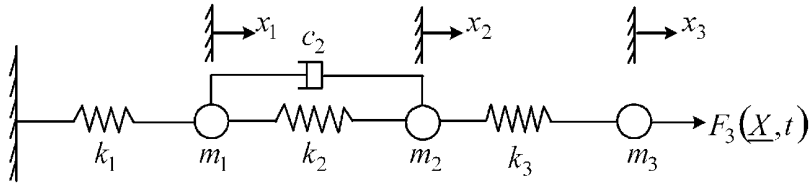


Figure E2.3.1(a) Simple vibratory system model

EXAMPLE 2.3.1 *MATLAB Numerical Integration*

The governing differential equations for the system in Figure E2.3.1(a) may be obtained by the methods presented in Chapter 3.

The results are

$$\underline{M} \dot{\underline{V}} + \underline{C} \underline{V} + \underline{K} \underline{X} = \underline{F}(\underline{X}, t) \quad (1)$$

where

$$\underline{M} = \begin{bmatrix} m_1 & 0 & 0 \\ 0 & m_2 & 0 \\ 0 & 0 & m_3 \end{bmatrix}, \quad \underline{C} = \begin{bmatrix} c_2 & -c_2 & 0 \\ -c_2 & c_2 & 0 \\ 0 & 0 & 0 \end{bmatrix}, \quad \underline{K} = \begin{bmatrix} k_1 + k_2 & -k_2 & 0 \\ -k_2 & k_2 + k_3 & -k_3 \\ 0 & -k_3 & k_3 \end{bmatrix}, \quad (2)$$

$$\underline{X} = \begin{Bmatrix} x_1 \\ x_2 \\ x_3 \end{Bmatrix}, \quad \underline{V} = \begin{Bmatrix} v_1 \\ v_2 \\ v_3 \end{Bmatrix}, \quad \underline{F} = \begin{Bmatrix} 0 \\ 0 \\ F_3 \end{Bmatrix} = \begin{Bmatrix} 0 \\ 0 \\ F_0 \sin \omega t - \alpha(x_3 - x_2)^3 \end{Bmatrix}$$

Use of MATLAB's ordinary differential equation (ODE) suite requires that a subfunction file be written defining the first derivative expressions (right-hand side of (3)). For example, in this problem,

$$\frac{\dot{\underline{q}}}{6 \times 1} = \begin{Bmatrix} \dot{\underline{V}} \\ \underline{X} \end{Bmatrix} = \begin{Bmatrix} \underline{M}^{-1} [\underline{F}(\underline{X}, t) - \underline{C} \underline{V} - \underline{K} \underline{X}] \\ \underline{V} \end{Bmatrix} \quad (3)$$

The initial condition for this example depicts the system being released from rest with an initial displacement at x_3 .

$$\underline{q}(0) = (0 \ 0 \ 0 \ 0 \ 0 \ x_{30})^T \quad (4)$$

Main File (see code output in Figure E2.3.1(b))

```
clear
global M K C F0 alpha omega
format short
% define parameters to be transferred to the subfunction file
% through global
m1 = 5 , m2 = 3 , m3 = 7 ;
k1 = 30000 , k2 = 20000 , k3 = 10000;
```

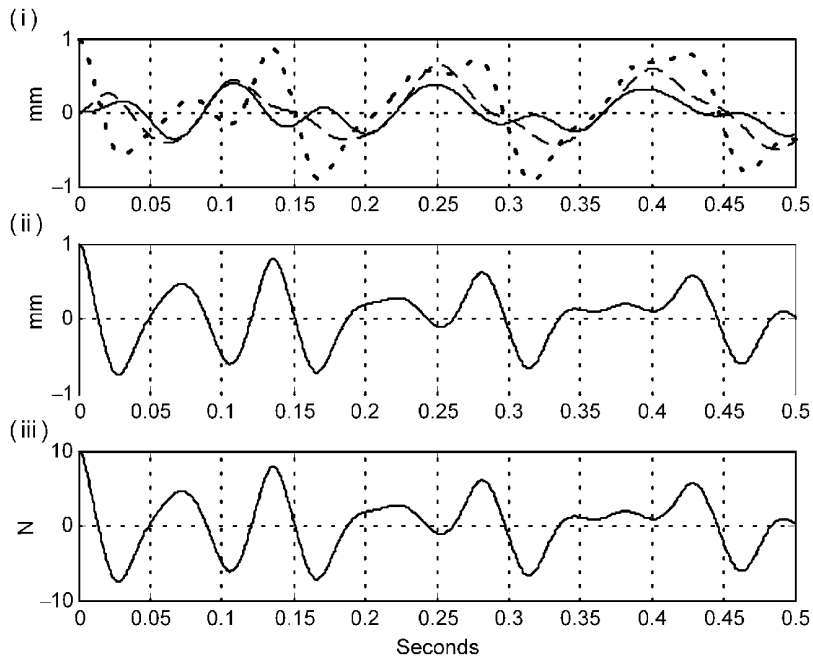


Figure E2.3.1(b) Response plots: (i) x_1 (solid), x_2 (dashed), and x_3 (dotted) displacements, (ii) relative displacements $x_3 - x_2$, and (iii) spring force in k_3

```

c2 = 100;
F0 = 10 , alpha = 1.0e+11 , f = 20 , omega = 2*pi*f ;

% define system matrices
M = zeros(3,3) , M(1,1) = m1 , M(2,2) = m2 , M(3,3) = m3 ;
C = zeros(3,3) , C(1,1) = c2 , C(1,2) = -c2 , C(2,1) = -c2 ,
C(2,2) = c2 ;
K = zeros(3,3) , K(1,1) = k1+k2 , K(1,2) = -k2 , K(2,1) = -k2 ,
K(2,2) = k2+k3 ;
K(2,3) = -k3 , K(3,2) = -k3 , K(3,3) = k3 ;

% define integration time range , (nplot = no. of points to be
% plotted)

tbegin = 0 , tfinal = 0.5 , nplot = 1000 ;
tspan=linspace(tbegin,tfinal,nplot) ; % creates an array of
nplot % equally spaced points

% define initial conditions
x30 = .001 , q0 = [0 0 0 0 0 x30] ;

% call Matlab ODE45 numerical integrator (explicit Runge Kutta
% (4,5) formulation)

```

```

% The sub-function that defines qdot has the filename
%Ch2MatlabODEsub
% Both the main and sub-function files must reside in the same % %
directory. The sub function filename is Ch2MatlabODEsub
[t,q] = ode45('Ch2MatlabODEsub',tspan,q0) ;

% plot results
subplot(3,1,1)
plot(t,q(:,4)*1000,'k-',t,q(:,5)*1000,'k--',t,q
(:,6)*1000,'k:');
grid on
title('Ch.2 Matlab ODE Example');
ylabel('x1,x2,x3 in mm');
msg = sprintf('x1(solid) x2(dashed) x3(dotted) ');
gtext(msg)

subplot(3,1,2)
plot(t,(q(:,6)-q(:,5))*1000,'k-');
grid on
ylabel('relative disp. x3-x2 in mm');

subplot(3,1,3)
plot(t,(q(:,6)-q(:,5))*k3,'k-');
grid on
ylabel('k3 spring force in N');
xlabel('time in seconds');

```

Subfunction file: Store this file in the same directory as the main file.

```

%This filename is Ch2MatlabODEsub
function qdot = Ch2MatlabODEsub(t,q)
global M K C F0 alpha omega
tee = t % displays the current integration time
qdot = zeros(6,1); % initialize qdot
F = [0 0 F0*sin(omega*t)-alpha*(q(6,1)-q(5,1))^3]';
qdot(1:3,1) = inv(M)*(F-C*q(1:3,1)-K*q(4:6,1));
qdot(4:6,1) = q(1:3,1);

```

EXAMPLE 2.3.2 MAPLE Symbolic Differential Equation Solution

Determine the analytical solution for the following differential equations and initial conditions:

$$3\ddot{x} + \dot{x} + 20x = 3\cos(100t), \quad x(0) = 1, \quad \dot{x}(0) = 0$$

```
> restart:
> with(DEtools):
> with(plots):
> diff_eq:= 3.*D(D(x))(t)+1.0*D(x)(t)+20.*x(t)=
3.*cos(100.*t);
```

$$\text{diff_eq} := 3 \cdot (D^{(2)})(x)(t) + 1.0D(x)(t) + 20 \cdot x(t) = 3 \cdot \cos(100 \cdot t)$$

```
> init_con:=x(0)=1.0, D(x)(0)=0.0;
```

$$\text{init_con} := x(0) = 1.0, D(x)(0) = 0.$$

```
> dsolve({diff_eq, init_con}, {x(t)});
```

$$x(t) = \frac{44936017}{10740784280} e^{\left(-\frac{t}{6}\right)} \sin\left(\frac{\sqrt{239}t}{6}\right) \sqrt{239} + \frac{44945017}{44940520} e^{\left(-\frac{t}{6}\right)} \cos\left(\frac{\sqrt{239}t}{6}\right) - \frac{4497}{44940520} \cos(100t) + \frac{3}{8988104} \sin(100t)$$

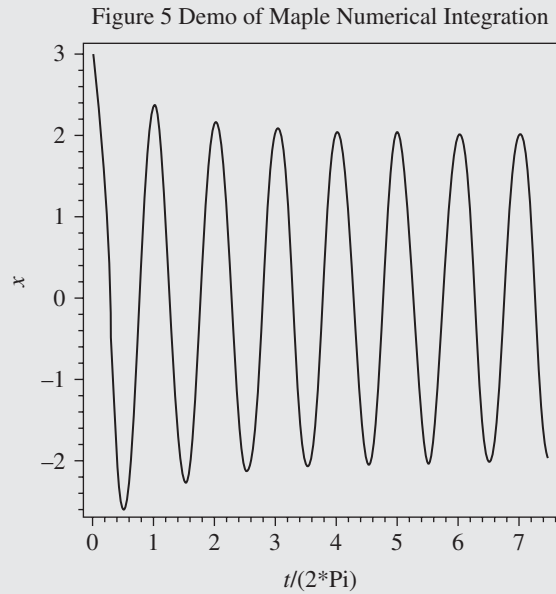
EXAMPLE 2.3.3 *MAPLE Numerical Differential Equation Solution*

Determine the numerical integration solution for the following differential equations and initial conditions:

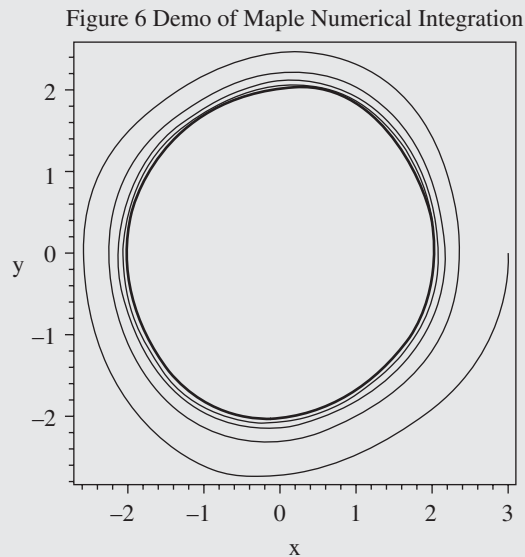
$$\dot{x} = y \quad \dot{y} = -\varepsilon(x^2 - 1)y - x, \quad x(0) = 3 \quad y(0) = 0$$

```
> # The Maple commands for simply numerically integrating the
state equations is illustrated below.
> restart:
> with(DEtools):
> with(plots):
> epsilon:= 0.1:
> sola:=dsolve({diff(x(t),t)=y(t),diff(y(t),t)=-epsilon*
(x(t)^2-1.)*y(t)-x(t),x(0)=3.0,y(0)=0.0},{x(t),y(t)},
numeric):
>
ppa:=odeplot(sola,[t/2./Pi,x(t)],0..15.0*Pi,numpoints=500,
thickness=1,color=black,axes=boxed,title="Figure 5 Demo of
Maple Numerical Integration",labels=["t/(2*Pi)","x"]):
```

```
> display(ppa); # Display X(t) vs. t
```



```
>
ppb:=odeplot(sola, [x(t), y(t)], 0..15.0*Pi, numpoints=500,
thickness=1, color=black, axes=boxed, title="Figure 6 Demo of
Maple Numerical Integration", labels=["x", "y"]):
> display(ppb); # Display Y(t) vs. X(t) (Phase Plot)
```



2.4 TAYLOR SERIES EXPANSIONS AND LINEARIZATION

Motion-dependent forces always become nonlinear as the magnitude of the motion increases. This is common, for example, in *Hertzian contact forces*, aerodynamic damping, and rubber vibration mounts. The Hertzian contact force is the repulsive force that occurs at the interface between two bodies that are compressed against each other. The nonlinearity is readily apparent in the compression test data, and mildly apparent in the shear test data in Figure 2.4.1, for an isolation mount used to reduce vibrations due to forces in machinery. Figure 2.4.1 (i) and (ii) illustrates *hardening* (stiffness increasing with deflection) and *softening* (stiffness decreasing with deflection) springs, respectively.

Figure 2.4.2 shows a similar nonlinear curve for a Belleville washer, which is a component frequently employed to provide a preload force in ball bearings and other devices.

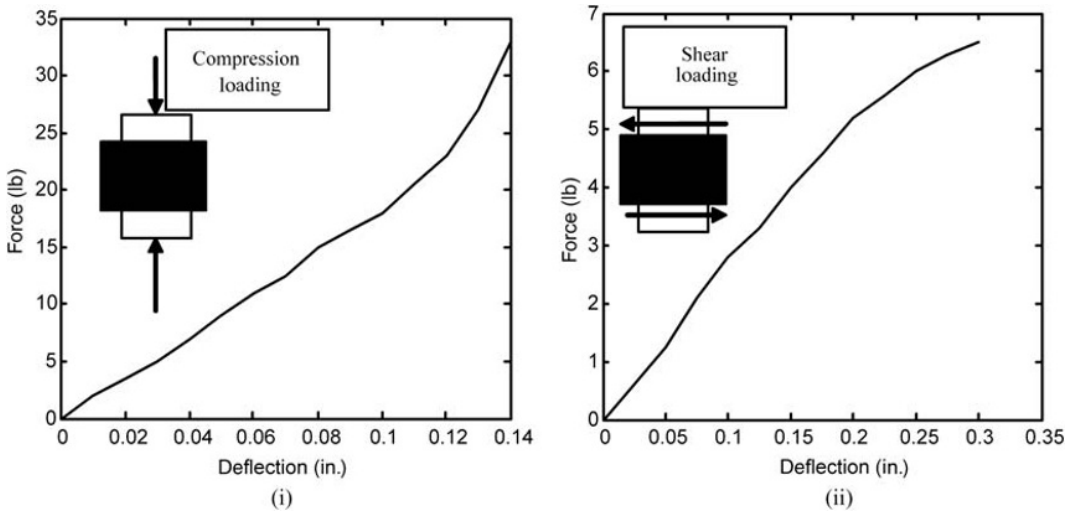


Figure 2.4.1 Nonlinear test data for vibration isolation mount with (i) hardening and (ii) softening nonlinear load versus deflection curves

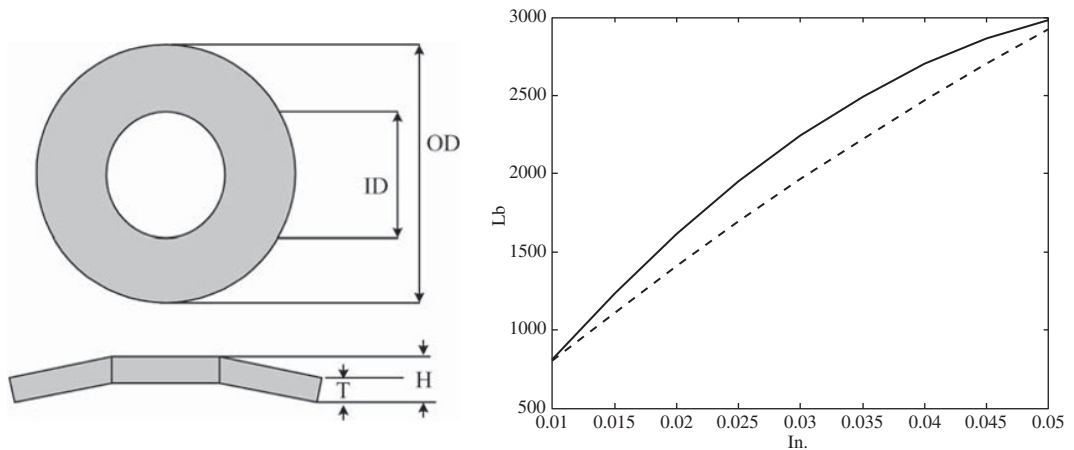


Figure 2.4.2 Nonlinear load versus deflection curve for a steel (solid) and composite (dashed) Belleville washer

A Taylor series expansion is frequently utilized to simplify a nonlinear force expression and express it as a truncated polynomial series, the most common form being a two-term series that provides a linear approximation of the force, about some operating point (OP). The OP force is typically a larger constant force that would deflect the springs in Figures 2.4.1 and 2.4.2 to a constant deflection. A smaller dynamic force is then included as the source of the linearized vibrations about the OP. The single variable Taylor series formula is (Hildebrand, 1976; Kreyzig, 1972)

$$f(x) = f(x_0 + \Delta x) = f(x_0) + \left. \frac{df}{dx} \right|_{x_0} \Delta x + \frac{1}{2!} \left. \frac{d^2 f}{dx^2} \right|_{x_0} \Delta x^2 + \cdots + \frac{1}{(n-1)!} \left. \frac{d^{n-1} f}{dx^{n-1}} \right|_{x_0} \Delta x^{n-1} + \cdots \quad (2.4.1)$$

EXAMPLE 2.4.1 *Inclined Spring Force*

A mass vibrates in the horizontal direction and is attached to ground via an inclined stiffness, utilizing a Taylor series expansion to obtain a polynomial approximation for the horizontal component of the spring force in terms of the mass's displacement x (Figure E2.4.1(a)).

The exact expressions for the spring force and its horizontal component are

$$\begin{aligned} F_k(x) &= f\delta = k \left(\sqrt{a^2 + b^2} - \sqrt{(a-x)^2 + b^2} \right) \\ F_{kx}(x) &= F_k \cos(\theta) = k \left(\sqrt{a^2 + b^2} - \sqrt{(a-x)^2 + b^2} \right) \frac{a-x}{\sqrt{(a-x)^2 + b^2}} \end{aligned} \quad (1)$$

The Taylor series for F_{kx} in (1) is obtained from the MAPLE code shown below.

```
> restart;
> :simplify(taylor(k*(sqrt(a^2+b^2)-sqrt((a-x)^2+b^2))*
(a-x)/sqrt((a-x)^2+b^2), x=0, 4));
```

$$F_{kx} = \frac{ka^2}{a^2 + b^2}x - \frac{3kb^2a}{2(a^2 + b^2)^2}x^2 - \frac{kb^2(4a^2 - b^2)}{2(a^2 + b^2)^3}x^3 + O(x^4) \quad (2)$$

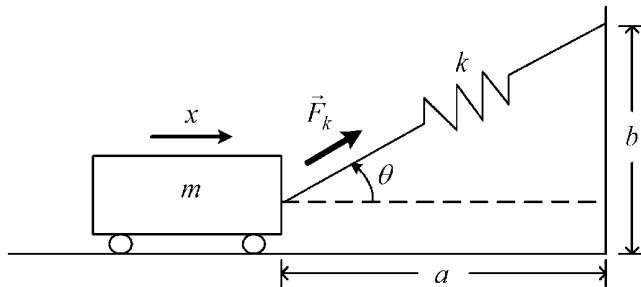


Figure E2.4.1(a) Inclined spring that causes a nonlinear force on mass m in the x direction

The Taylor series for a function of two variables is given by

$$\begin{aligned}
 f(x, y) = f(x_0 + \Delta x, y_0 + \Delta y) &= f(x_0, y_0) + \frac{\partial f}{\partial x} \Big|_{x_0, y_0} \Delta x + \frac{\partial f}{\partial y} \Big|_{x_0, y_0} \Delta y \\
 &+ \frac{1}{2!} \left(\frac{\partial^2 f}{\partial x^2} \Big|_{x_0, y_0} \Delta x^2 + 2 \frac{\partial^2 f}{\partial x \partial y} \Big|_{x_0, y_0} \Delta x \Delta y + \frac{\partial^2 f}{\partial y^2} \Big|_{x_0, y_0} \Delta y^2 \right) + \dots \\
 &+ \frac{1}{n!} \left(\Delta x \frac{\partial}{\partial x} + \Delta y \frac{\partial}{\partial y} \right)^n f(x, y) \Big|_{x_0, y_0} + \dots
 \end{aligned} \tag{2.4.2}$$

The most common use of Taylor series in vibration is for linearization of force functions that are nonlinear functions of position and velocity. Only the first two terms of the Taylor series expansion are utilized for linearized model applications, that is,

$$f(x) = f(x_0 + \Delta x) \approx f(x_0) + \frac{df}{dx} \Big|_{x_0} \Delta x \tag{2.4.3}$$

$$f(x, y) = f(x_0 + \Delta x, y_0 + \Delta y) \approx f(x_0, y_0) + \frac{\partial f}{\partial x} \Big|_{x_0, y_0} \Delta x + \frac{\partial f}{\partial y} \Big|_{x_0, y_0} \Delta y \tag{2.4.4}$$

or in the case of n functions of m independent variables

$$\underline{f}(\underline{x}) = \underline{f}(\underline{x}_0 + \Delta \underline{x}) \approx \underline{f}(\underline{x}_0) + \underline{J} \Big|_{\underline{x}_0} \Delta \underline{x} \tag{2.4.5}$$

where

$$\underline{x} = (x_1 \ x_2 \ \dots \ x_m)^T, \quad \underline{x}_0 = (x_{10} \ x_{20} \ \dots \ x_{m0})^T, \quad \Delta \underline{x} = (\Delta x_1 \ \Delta x_2 \ \dots \ \Delta x_m)^T \tag{2.4.6}$$

$$\underline{f}(\underline{x}) = \begin{cases} f_1(x_1, \dots, x_m) \\ f_2(x_1, \dots, x_m) \\ \vdots \\ f_n(x_1, \dots, x_m) \end{cases} \tag{2.4.7}$$

and the ‘‘Jacobian’’ matrix is

$$\underline{J} = \begin{bmatrix} \frac{\partial f_1}{\partial x_1} & \frac{\partial f_1}{\partial x_2} & \dots & \frac{\partial f_1}{\partial x_m} \\ \vdots & \vdots & \ddots & \vdots \\ \frac{\partial f_n}{\partial x_1} & \frac{\partial f_n}{\partial x_2} & \dots & \frac{\partial f_n}{\partial x_m} \end{bmatrix} \tag{2.4.8}$$

Some care must be exercised in applying linearization since sufficiently large vibrations may violate the linearization assumptions yielding unusual vibrations such as chaos.

EXAMPLE 2.4.2 Two Variable Linearization of a Magnetic Force

Statement: This example illustrates the use of the Taylor series to obtain an approximate, linear representation of a nonlinear force containing two variables. The results are also

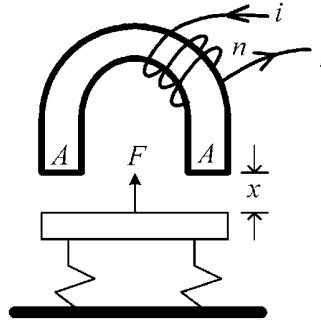


Figure E2.4.2(a) C-core electromagnetic generating force F

utilized in the electromagnetic actuator-based active vibration control (AVC) examples in Chapter 12.

Objective: Obtain a two-term Taylor series approximation for the force of an electromagnet.

Motivation: Linearization of the given force will greatly simplify the dynamic equilibrium equations for the system containing the force.

Solution: The magnetic force developed by the C-core arrangement in Figure E2.4.2(a) is

$$F(x, i) = \frac{N^2 i^2 \mu_0 A}{4x^2} \quad (1)$$

where N is the number of turns in the coil, i is the electric current in the wire, μ_0 is the magnetic permeability in free space ($4\pi \cdot 10^{-7} \text{ m kgs}^{-2} \text{ A}^{-2}$), A is the cross-sectional area of a pole, and x is the air gap distance.

Equation (1) shows that the force varies nonlinearly with both gap x and current i . Let x_0 and i_0 represent the OP (steady-state) values of x and i , respectively, and Δx and Δi perturbations about x_0 and i_0 . Then by (2.4.3),

$$\begin{aligned} F(x, i) &= F(x_0 + \Delta x, i_0 + \Delta i) \approx F(x_0, i_0) + \left. \frac{\partial F}{\partial x} \right|_{x_0, i_0} \Delta x + \left. \frac{\partial F}{\partial i} \right|_{x_0, i_0} \Delta i \\ &= \frac{N^2 i_0^2 \mu_0 A}{4x_0^2} + \left(-\frac{N^2 i_0^2 \mu_0 A}{2x_0^3} \right) \Delta x + \left(\frac{N^2 i_0 \mu_0 A}{2x_0^2} \right) \Delta i \end{aligned} \quad (2)$$

The coefficients in (2) are commonly referred to as stiffnesses or force gains, that is,

$$k_{\text{pos}} = \text{position stiffness} = -\frac{N^2 i_0^2 \mu_0 A}{2x_0^3} \quad (3)$$

$$k_i = \text{current stiffness} = \frac{N^2 i_0 \mu_0 A}{2x_0^2} \quad (4)$$

so that (2) may be written as

$$F(x, i) \approx F(x_0, i_0) + k_{\text{pos}} \Delta x + k_i \Delta i \quad (5)$$

Summary: The approximate force expression in (5) allows the analyst to evaluate system vibration stability by calculating eigenvalues or to determine steady-state harmonic response. These are essential steps for assuring the goodness of a system's design with regard to vibrations.

EXAMPLE 2.4.3 Euler's Identity

Here is a Taylor series expansion for a very familiar identity used extensively in Chapter 7 on steady-state harmonic response. The MAPLE command `taylor(exp(beta * x), x=0,6)` yields the lowest six terms of the Taylor series for $e^{\beta x}$ about $x = 0$, as

$$e^{\beta x} = 1 + \beta x + \frac{(\beta x)^2}{2} + \frac{(\beta x)^3}{6} + \frac{(\beta x)^4}{24} + \frac{(\beta x)^5}{120} + \dots \quad (1)$$

substitute the imaginary unit i for β to obtain

$$e^{ix} = 1 + ix - \frac{(x)^2}{2} - i\frac{(x)^3}{6} + \frac{(x)^4}{24} + i\frac{(x)^5}{120} + \dots = \cos(x) + i\sin(x) \quad (2)$$

which follows from the Taylor series expansions for $\sin(x)$ and $\cos(x)$. This identity is very useful for determining forced harmonic responses, natural frequencies, and mode shapes in vibration analyses.

2.5 COMPLEX VARIABLES (CV) AND PHASORS

The concept of phase (time) lag was initially discussed in Section 1.2. The concept may be understood by considering the vertical oscillation of a buoy as it experiences a train of water waves traveling left to right as shown in Figure 2.5.1. The figure depicts “wave-powered buoys” that are used for an energy harvesting application. The peak upward displacement (heave) of the buoy occurs *after* the crest of the wave passes beneath it due to inertia and damping forces. Thus, a time lag occurs between the wave crest and the peak displacement events. This time lag can be expressed as a “phase angle” with one complete wave period equivalent to 360° and the phase lag angle = wave frequency \times time lag. Chapter 7 shows how measurement of the phase lag angle can be used to identify damping, mode shapes, natural frequencies, mass imbalance in a rotating shaft, and so on, so it is a very important quantity. Phase lag occurs in all physical devices since no device can react instantaneously to an input. There is always an inertia or inductance like action that delays the response of a

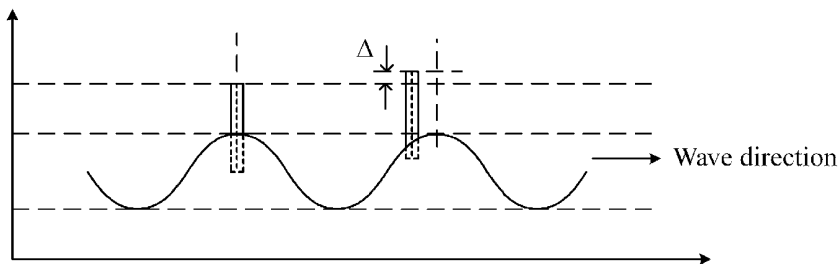


Figure 2.5.1 Buoys with peak vertical heave motion delayed by a time lag after occurrence of the peak wave crest force

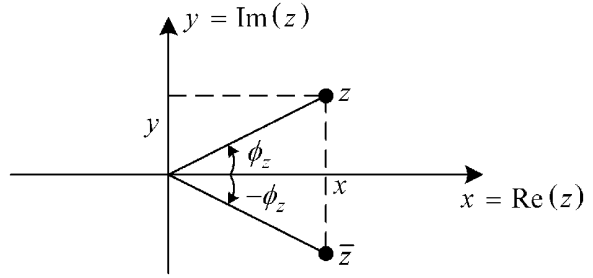


Figure 2.5.2 Illustration of complex numbers z and \bar{z}

system, which is the root cause of phase lag. There also exists a time lag (phase angle) between harmonically varying displacement, velocity, and acceleration. Descriptions of harmonic motion thus require both amplitude and phase angle for completeness. This has long been referred to as utilizing “phasor” quantities, having amplitude and phase, in the study of electric circuits.

A complex number has both a magnitude and phase angle ϕ , which allows it to represent the magnitude of a vibratory response and its time lag relative to inputs, or other responses. Figure 2.5.2 shows a typical complex number z .

In rectangular form,

$$z = x + iy, \quad i = \sqrt{-1} \quad (2.5.1)$$

and in polar (phasor) form,

$$z = |z|e^{i\phi_z}, \quad |z| = \sqrt{x^2 + y^2}, \quad \phi_z = \tan^{-1}\left(\frac{y}{x}\right) \quad (2.5.2)$$

This may be proven by the use of Euler’s identity (Example 2.4.3). The conjugate of z is defined by

$$\bar{z} = x - iy = |z|e^{-i\phi_z} \quad (2.5.3)$$

so that

$$z\bar{z} = |z|^2 e^{i(\phi_z - \phi_z)} = |z|^2 \quad (2.5.4)$$

Let

$$z_1 = |z_1|e^{i\phi_1}, \quad z_2 = |z_2|e^{i\phi_2} \quad (2.5.5)$$

be two complex numbers. Then,

$$z_1 z_2 = |z_1| |z_2| e^{i(\phi_1 + \phi_2)} \quad (2.5.6)$$

$$\frac{z_1}{z_2} = \frac{|z_1|}{|z_2|} e^{i(\phi_1 - \phi_2)} \quad (2.5.7)$$

The utility of complex variables may be demonstrated by considering the solution for the particular (steady-state) part of the common vibration differential equation:

$$m\ddot{q} + c\dot{q} + kq = A \cos(\omega t) + B \sin(\omega t) \quad (2.5.8)$$

The real variable solution proceeds by substituting the assumed form of the particular solution

$$q_p(t) = \alpha \cos(\omega t) + \beta \sin(\omega t) \quad (2.5.9)$$

into (2.5.8) and equating coefficients of the sin and cos terms. This yields two linear algebraic equations for the real constants α and β . A simpler approach consists of making the following substitutions

$$q(t) \Rightarrow Q(t) = Q_r(t) + iQ_i(t), \quad \cos(\omega t) \Rightarrow e^{i\omega t}, \quad \sin(\omega t) \Rightarrow -ie^{i\omega t} \quad (2.5.10)$$

yielding

$$m\ddot{Q} + c\dot{Q} + kQ = Ae^{i\omega t} - iBe^{i\omega t} \quad (2.5.11)$$

Equate the real parts of both sides of this equation to obtain

$$m\ddot{Q}_r + c\dot{Q}_r + kQ_r = A \cos(\omega t) + B \sin(\omega t) \quad (2.5.12)$$

This demonstrates that the real part of the complex variable $Q(t)$ has the same differential equation as the original real variable $q(t)$, which suggests the alternative approach of obtaining $q(t)$ by solving (2.5.11) for $Q(t)$ and then taking its real part to obtain $q(t)$. The particular solution for (2.5.11) is obtained by substituting the assumed form

$$Q = \tilde{Q}e^{i\omega t} \quad (2.5.13)$$

into (2.5.11) yielding

$$(-\omega^2 m + i\omega c + k)\tilde{Q} = A - iB \quad (2.5.14)$$

Then, solve for $\tilde{Q}(t)$:

$$\tilde{Q} = \frac{A - iB}{(-\omega^2 m + i\omega c + k)} \quad (2.5.15)$$

The term $\tilde{Q}(t)$ may be written in polar form:

$$\tilde{Q} = |\tilde{Q}|e^{i\angle\tilde{Q}} \quad (2.5.16)$$

Then, the solution for the original real variable $q(t)$ becomes

$$q(t) = \text{Real}(Q(t)) = \text{Real}(\tilde{Q}e^{i\omega t}) = |\tilde{Q}|\cos(\omega t + \angle\tilde{Q}) \quad (2.5.17)$$

Thus, by (2.5.5)–(2.5.7) and (2.5.15), the amplitude of the displacement response is

$$|q| = |\tilde{Q}| = \sqrt{\frac{A^2 + B^2}{(k - m\omega^2)^2 + (c\omega)^2}} \quad (2.5.18)$$

and the phase angle of the displacement response is

$$\begin{aligned}\angle q = \angle \tilde{Q} &= \angle \text{numerator of } \tilde{Q} - \angle \text{denominator of } \tilde{Q} \\ &= \tan^{-1}\left(\frac{-B}{A}\right) - \tan^{-1}\left(\frac{\omega c}{k - \omega^2 m}\right)\end{aligned}\quad (2.5.19)$$

2.6 DEGREES OF FREEDOM, MATRICES, VECTORS, AND SUBSPACES

Mechanical and structural systems may vibrate in simple or complex ways. This is typically quantified by identifying the number of independent dofs that are required to capture all important motions of the system. “Independent dof” refers to the ability of the corresponding motion (dof) to occur, when all other dofs are intentionally held fixed. A familiar example is the 6 dofs of a rigid body with longitudinal travel such as an auto, ship, train, or plane, as shown in Figure 2.6.1.

Translations: (1) Heave (vertical up/down), (2) Sway (side to side), (3) Surge (front to back)

Rotations: (4) Roll (about front/back longitudinal axis), (5) Pitch (about side to side axis), (6) Yaw (about up/down axis)

Figure 2.6.2 shows a ship undergoing predominantly roll and heave motions. A model consisting of only heave and roll dofs or even just a roll dof may be adequate to predict wave amplitudes or frequencies that may cause the ship to capsize: an important vibration problem! A 4-dof surge direction model may be adequate for modeling the three-trailer truck shown in Figure 2.6.3 for a fatigue-related failure or crashworthiness enhancement simulation. The springs in this model represent the compliance that exists in the hitches that connect the trailers with each other and the cab. The model could be further generalized

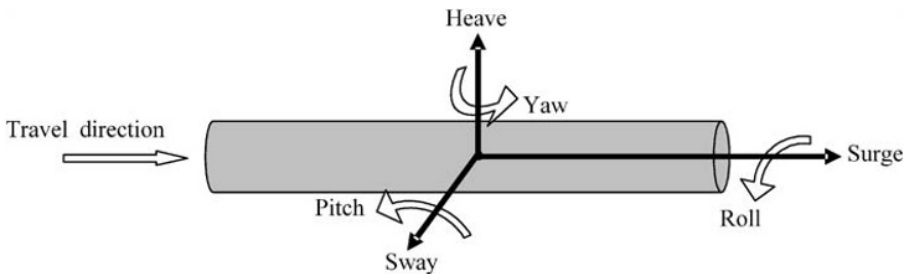


Figure 2.6.1 Six rigid body degrees of freedom (dof) of body with longitudinal travel

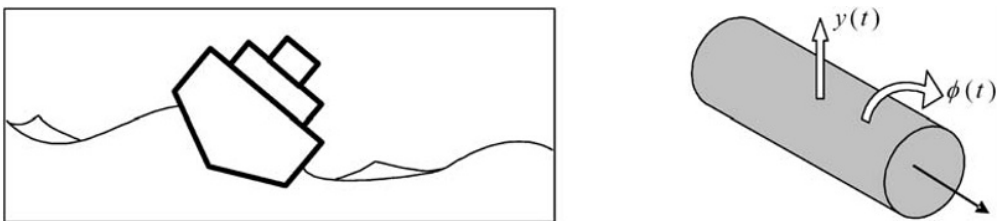


Figure 2.6.2 Ship in rough seas and simplified roll and heave model

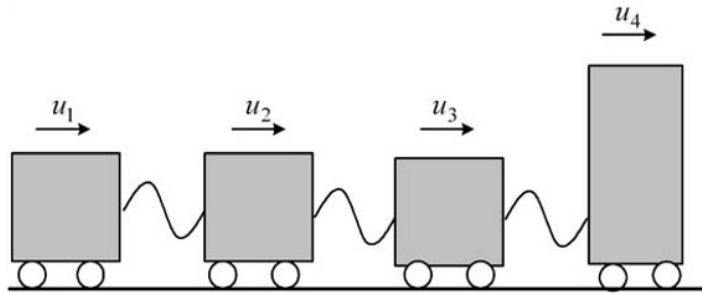


Figure 2.6.3 Three-trailer truck and simplified surge motion model

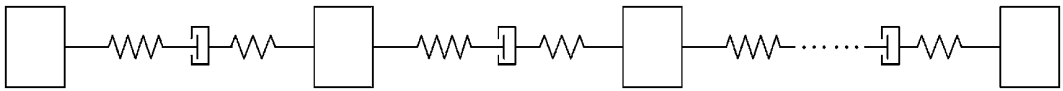


Figure 2.6.4 Model of train undergoing start-up conditions

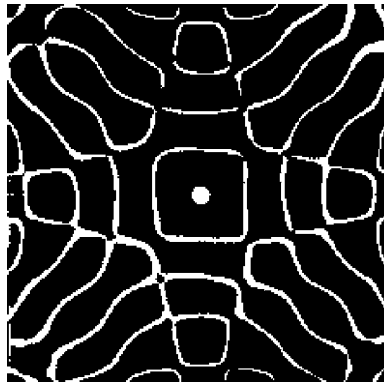


Figure 2.6.5 Sand pattern (nodal lines) of plate in a resonance state. Reproduced with permission of Professor Stephen Morris, Nonlinear Physics, University of Toronto © Prof. Stephen W. Morris

to model the surge motion of a train as depicted in Figure 2.6.4 to mitigate vibration-induced wear during start-up or to improve shock- and vibration-related crashworthiness for locomotive occupant safety. The train hitches may intentionally have gaps in order for the inertia load pulled by the locomotive to increase gradually instead of all simultaneously on start-up of the train. Even a simplified rigid body, surge motion only model may contain 100s of dofs to represent the train vibration. A more complex rigid body model (RBM) could include heave and pitch motions of each car, which are supported on springs and able to vibrate independent of the wheeled bogies that provide a moving suspension for the cars and locomotives. Models obtain even a greater number of dofs when flexibility of each component is accounted for. Each point on a component may vibrate totally independent of other points, requiring a far greater number of dofs than the six rigid body ones. This has been illustrated by the sand pattern on the rectangular steel plate shown in Figure 2.6.5. Sand is spread

uniformly on a plate, which is then subjected to a vertical shaking force. The frequency of the force is varied until it matches a resonant frequency (Section 1.2), under which condition, a standing wave pattern appears where peak vibrations (antinodes) occur at certain locations and no motion occurs along “node” lines. The sand migrates away from the antinodes and collects along the nodal lines due to the vertical shaking motion. The nodal lines are clearly shown in the plate photo in Figure 2.6.5.

Finite element models as shown in Figure 1.7.1 include 3 translation dofs at each node point in the model, where node point in the finite element context is different than the zero vibration node points in the sand patterns. The finite element node points are locations where the displacements in the elements are interpolated from. The points where the lines intersect in Figure 1.7.1 are some of the finite element model’s node points.

The dofs of a model can be arranged as members of an $n \times 1$ array:

$$\underline{U}(t) = (u_1(t) \ u_2(t) \ u_3(t) \ u_4(t) \ \cdots \ u_n(t))^T \quad (n \times 1) \quad (2.6.1)$$

where the u_i typically represent physical translations or rotations. A “linear model” is one that expresses forces as either explicit functions of time or linear functions of the motion variables, that is, displacements, velocities, and accelerations. Thus, equilibrium equations for the linear model must have the general form

$$\begin{bmatrix} m_{11} & m_{12} & \cdots & m_{1n} \\ m_{21} & m_{22} & \cdots & m_{2n} \\ \vdots & \vdots & \ddots & \vdots \\ m_{n1} & m_{n2} & \cdots & m_{nn} \end{bmatrix} \begin{Bmatrix} \ddot{u}_1(t) \\ \ddot{u}_2(t) \\ \vdots \\ \ddot{u}_n(t) \end{Bmatrix} + \begin{bmatrix} c_{11} & c_{12} & \cdots & c_{1n} \\ c_{21} & c_{22} & \cdots & c_{2n} \\ \vdots & \vdots & \ddots & \vdots \\ c_{n1} & c_{n2} & \cdots & c_{nn} \end{bmatrix} \begin{Bmatrix} \dot{u}_1(t) \\ \dot{u}_2(t) \\ \vdots \\ \dot{u}_n(t) \end{Bmatrix} + \begin{bmatrix} k_{11} & k_{12} & \cdots & k_{1n} \\ k_{21} & k_{22} & \cdots & k_{2n} \\ \vdots & \vdots & \ddots & \vdots \\ k_{n1} & k_{n2} & \cdots & k_{nn} \end{bmatrix} \begin{Bmatrix} u_1(t) \\ u_2(t) \\ \vdots \\ u_n(t) \end{Bmatrix} = \begin{Bmatrix} f_1(t) \\ f_2(t) \\ \vdots \\ f_n(t) \end{Bmatrix} \quad (2.6.2)$$

or be written in an abbreviated manner as

$$\underline{M}\ddot{\underline{U}} + \underline{C}\dot{\underline{U}} + \underline{K}\underline{U} = \underline{f}(t) \quad (2.6.3)$$

An objective of the FEM is to define the matrices $(\underline{M}, \underline{C}, \underline{K}, \underline{f}(t))$ given an FE mesh and load description. A first impression may be that organization of coefficients and motion variables into vectors and matrices in (2.6.2) and (2.6.3) is merely a bookkeeping aid. Although there are some bookkeeping advantages for using vectors and matrices, a more important reason is to bring the powerful theories and techniques of linear algebra to bear on the efficient and comprehensive solution of the equations. Rewrite (2.6.1) using the modification shown in (2.6.4). This new form expresses the system’s physical coordinate displacement vector as the sum of contributions from a set of “basis vectors” $\underline{e}_1, \underline{e}_2, \dots, \underline{e}_n$, each being multiplied by its respective physical coordinate, which varies with time. Clearly any \underline{U} in (2.6.4) can be exactly represented by the correct choice of the u_i , so the \underline{e}_i is said to form a complete set of basis vectors, or equivalently to *span* “ n -space.”

$$\begin{aligned}
 \underline{U}(t) &= \begin{Bmatrix} u_1(t) \\ u_2(t) \\ \vdots \\ u_n(t) \end{Bmatrix} = \begin{bmatrix} 1 & 0 & \cdots & 0 \\ 0 & 1 & \cdots & 0 \\ \vdots & \vdots & \ddots & \vdots \\ 0 & 0 & \cdots & 1 \end{bmatrix} \begin{Bmatrix} u_1(t) \\ u_2(t) \\ \vdots \\ u_n(t) \end{Bmatrix} \\
 &= \begin{Bmatrix} 1 \\ 0 \\ \vdots \\ 0 \end{Bmatrix} u_1(t) + \begin{Bmatrix} 0 \\ 1 \\ \vdots \\ 0 \end{Bmatrix} u_2(t) + \cdots + \begin{Bmatrix} 0 \\ 0 \\ \vdots \\ 1 \end{Bmatrix} u_n(t) = u_1(t)\underline{e}_1 + \cdots + u_n(t)\underline{e}_n \quad (2.6.4)
 \end{aligned}$$

For the sake of illustration, Figure 2.6.6 depicts the terms in (2.6.4) for 3-space. Note that the vector \underline{U} could also be expressed in terms of a second set of basis vectors \underline{v}_i , as

$$\begin{aligned}
 \underline{U}(t) &= \eta_1(t)\underline{v}_1 + \eta_2(t)\underline{v}_2 + \eta_3(t)\underline{v}_3 = \begin{Bmatrix} v_{11} \\ v_{21} \\ v_{31} \end{Bmatrix} \eta_1(t) + \begin{Bmatrix} v_{12} \\ v_{22} \\ v_{32} \end{Bmatrix} \eta_2(t) + \begin{Bmatrix} v_{13} \\ v_{23} \\ v_{33} \end{Bmatrix} \eta_3(t) \\
 &= [\underline{v}_1 \ \underline{v}_2 \ \underline{v}_3] \begin{Bmatrix} \eta_1(t) \\ \eta_2(t) \\ \eta_3(t) \end{Bmatrix} = \begin{bmatrix} v_{11} & v_{12} & v_{13} \\ v_{21} & v_{22} & v_{23} \\ v_{31} & v_{32} & v_{33} \end{bmatrix} \begin{Bmatrix} \eta_1(t) \\ \eta_2(t) \\ \eta_3(t) \end{Bmatrix} = \underline{V}\underline{\eta}(t) \quad (2.6.5)
 \end{aligned}$$

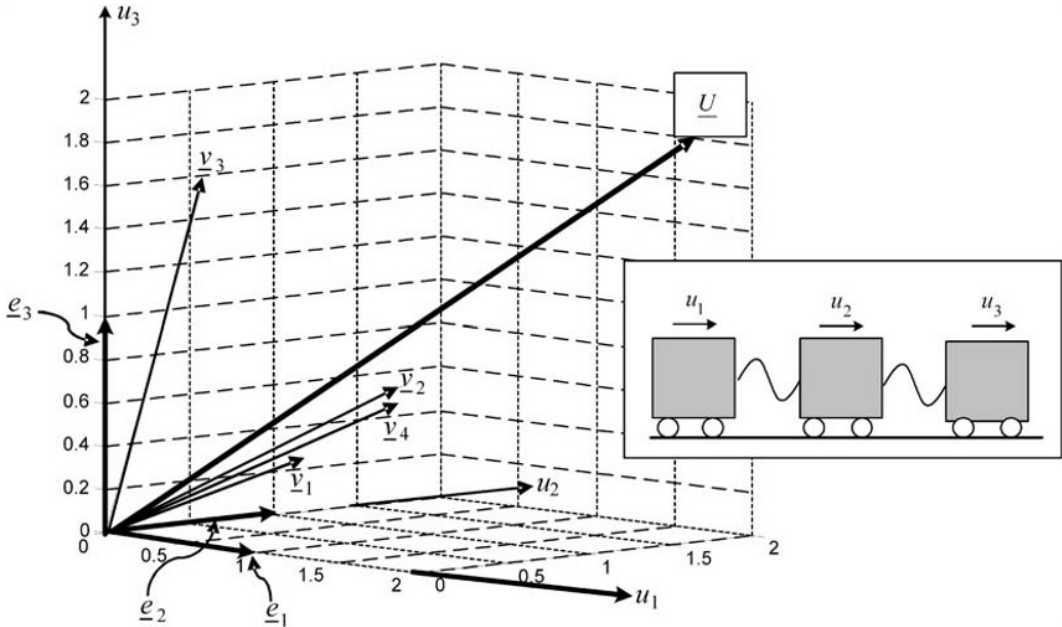


Figure 2.6.6 The vector \underline{U} and basis vectors \underline{e}_i and \underline{v}_i .

Thus, given the basis vector set \underline{v}_i , the corresponding “generalized coordinates $\eta_i(t)$ ” required to form \underline{U} may be determined from

$$\underline{\eta}(t) = \begin{bmatrix} v_{11} & v_{12} & v_{13} \\ v_{21} & v_{22} & v_{23} \\ v_{31} & v_{32} & v_{33} \end{bmatrix}^{-1} \begin{Bmatrix} u_1(t) \\ u_2(t) \\ u_3(t) \end{Bmatrix} = \underline{V}^{-1} \underline{U}(t) \quad (2.6.6)$$

This “transformation of coordinates” or “change of basis” fails if the inverse of the matrix \underline{V} does not exist, that is, the matrix \underline{V} is singular, which occurs if the columns of \underline{V} are linearly dependent. This has a geometric interpretation in 3-space; namely, the three basis vectors lie in the same plane. This is illustrated by the alternative set of basis vectors \underline{v}_1 , \underline{v}_2 , and \underline{v}_4 that are coplanar in Figure 2.6.6. Clearly there is no way that a linear weighted sum of \underline{v}_1 , \underline{v}_2 , and \underline{v}_4 , as in (2.6.5), can equal \underline{U} if \underline{U} has a component out of (perpendicular to) the plane containing \underline{v}_1 , \underline{v}_2 , and \underline{v}_4 . The condition that \underline{v}_1 , \underline{v}_2 , and \underline{v}_4 lie in a plane is mathematically expressed as

$$\underline{v}_4 = \alpha_1 \underline{v}_1 + \alpha_2 \underline{v}_2 \quad (2.6.7)$$

for some real constants (α_1, α_2) , since clearly \underline{v}_4 will lie in the plane formed from \underline{v}_1 and \underline{v}_2 if (2.6.7) is satisfied. The condition (2.6.7) may be stated in a more general form as

$$\alpha_1 \underline{v}_1 + \alpha_2 \underline{v}_2 + \alpha_4 \underline{v}_4 = \underline{0} \quad (2.6.8)$$

and these vectors are then said to be “linearly dependent.” The change in basis in (2.6.5) is valid only if the basis vectors \underline{v}_i form a *linearly independent set*.

The above discussion is generally valid for n -space where the transformation becomes

$$\underline{U}(t) = \sum_{i=1}^n \eta_i(t) \underline{v}_i = \begin{bmatrix} \underline{v}_1 & \underline{v}_2 & \cdots & \underline{v}_n \end{bmatrix} \begin{Bmatrix} \eta_1(t) \\ \eta_2(t) \\ \vdots \\ \eta_n(t) \end{Bmatrix} = \underline{V} \underline{\eta}(t) \quad (2.6.9)$$

and \underline{v}_i must form a linearly independent set. This discussion begs the questions: If \underline{U} can be expressed with any set of valid basis vectors and corresponding generalized coordinates, are there preferred basis vectors, or are the physical coordinate basis vectors \underline{e}_i always preferred? Solutions of large finite element models may be performed efficiently if a set of basis vectors provides accurate predictions when the number m of basis vectors and generalized coordinates is much smaller than the number n of physical coordinates. In this case, (2.6.9) becomes

$$\underline{U}(t) = \sum_{i=1}^m \eta_i(t) \underline{v}_i = \begin{bmatrix} \underline{v}_1 & \underline{v}_2 & \cdots & \underline{v}_m \end{bmatrix} \begin{Bmatrix} \eta_1(t) \\ \eta_2(t) \\ \vdots \\ \eta_m(t) \end{Bmatrix} = \underline{V} \underline{\eta}(t) \quad (2.6.10)$$

This restricts the response to the *subspace* spanned by the m basis vectors. Substitution of (2.6.10) into the equilibrium equation (2.6.3) yields

$$\underline{\bar{M}} \ddot{\underline{\eta}} + \underline{\bar{C}} \dot{\underline{\eta}} + \underline{\bar{K}} \underline{\eta} = \underline{\bar{f}}(t) \quad (2.6.11)$$

where

$$\bar{\underline{M}} = \underline{V}^T \underline{M} \underline{V}, \quad \bar{\underline{C}} = \underline{V}^T \underline{C} \underline{V}, \quad \bar{\underline{K}} = \underline{V}^T \underline{K} \underline{V}, \quad \bar{\underline{f}} = \underline{V}^T \underline{f} \quad (2.6.12)$$

The matrices $\bar{\underline{M}}$, $\bar{\underline{C}}$, and $\bar{\underline{K}}$ are all of dimensions $m \times m$, and the vector $\bar{\underline{f}}$ is of dimension $m \times 1$. The reduction in the number of coupled differential equations in (2.6.11) will greatly reduce the computation time required to solve for the η_i , and the physical coordinates are then easily obtained from (2.6.10). The computational time can be reduced further if the matrices in (2.6.12) are diagonal, implying that η_i could be obtained by solving an uncoupled set of m ODEs. The mathematical condition for this is obtained from (2.6.10) and (2.6.12) as

$$\begin{aligned} (\bar{\underline{M}})_{i,j} &= \underline{V}_i^T \underline{M} \underline{V}_j = 0, \quad \text{for } i \neq j \\ (\bar{\underline{K}})_{i,j} &= \underline{V}_i^T \underline{K} \underline{V}_j = 0, \quad \text{for } i \neq j \\ (\bar{\underline{C}})_{i,j} &= \underline{V}_i^T \underline{C} \underline{V}_j = 0, \quad \text{for } i \neq j \end{aligned} \quad (2.6.13)$$

These are the so called “orthogonality” conditions. Though seemingly improbable, nature does provide a suitable set of basis vectors to condense and uncouple the generalized coordinates, which is applicable to a large class of vibration problems. To illustrate this, consider the spring-mass model of the space station module treated in Chapter 7 and shown in Figure 2.6.7. Resonances occur at natural frequencies as the frequency of the force F at mass 2 is slowly increased from 0 to 100 Hz as shown in Figure 2.6.8(a).

The vibrations at the nine masses are dominated by a unique pattern of relative amplitudes and phases at each resonance (peaks in Figure 2.6.8(a)). These patterns are called the “mode shapes” that correspond with their respective natural frequencies in Table 2.6.1 and are shown in Figure 2.6.8(b).

The first mode shape (lowest curve in Figure 2.6.8(b)) is called a *rigid body mode* since all of its values are identical and its natural frequency is zero (0). The other mode shapes all have relative motions indicating that the body is straining and storing strain energy as it vibrates in these “flexible” modes. For example, mode shape 8 has the properties

$$f_8 = 64.4 \text{ Hz}, \quad \underline{V}_8 = (0.214, -0.662, -0.243, 0.973, -1.00, 0.741, -0.292, 0.110, -0.028) \quad (2.6.14)$$

The mode shapes form a linearly independent set of basis vectors if all of the natural frequencies are distinct. Furthermore, the contribution of any mode to the system response

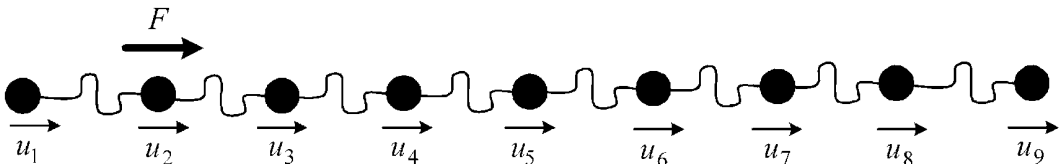


Figure 2.6.7 Spring-mass model of a space station module for modal basis vector example

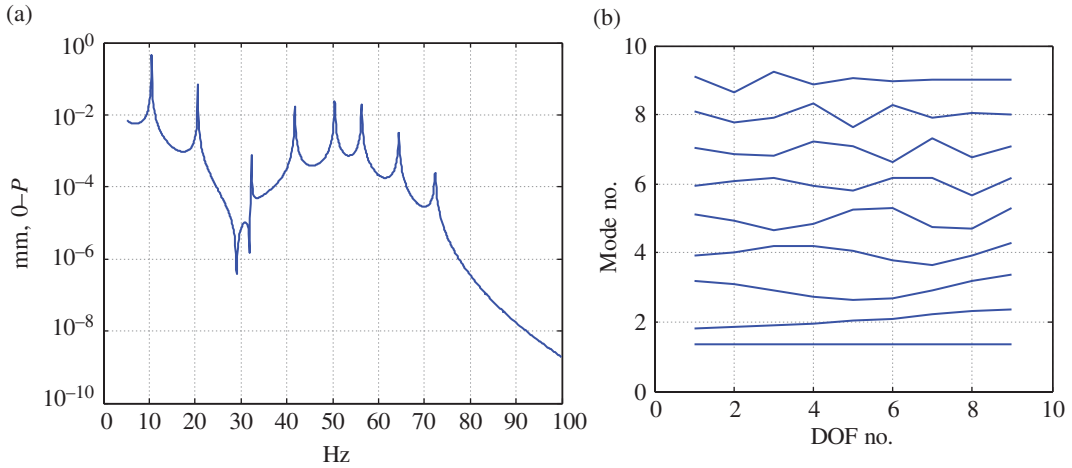


Figure 2.6.8 (a) Displacement amplitude of mass 8 versus forcing frequency and plots of (b) all nine mode shapes

Table 2.6.1 Natural frequencies (in Hz) for space station module model

(1) 0	(2) 10.5	(3) 20.6	(4) 32.3	(5) 41.8	(6) 50.4	(7) 56.3	(8) 64.4	(9) 72.3
-------	----------	----------	----------	----------	----------	----------	----------	----------

diminishes as the forcing frequency is displaced further away from the natural frequency of that mode shape. Then, for instance, the contributions of modes 3–9 may be negligible if the forcing frequency range is limited to 1–25 Hz. Thus the approximation

$$\underline{U}(t) \approx \sum_{i=1}^{m=2} \eta_i(t) \underline{v}_i = \begin{bmatrix} v_1 & v_2 \end{bmatrix} \begin{Bmatrix} \eta_1(t) \\ \eta_2(t) \end{Bmatrix} = \underline{V} \underline{\eta}(t) \quad (2.6.15)$$

may yield highly accurate results and reduces the dimension of the equilibrium equations in (2.6.11) from 9 to 2. In addition, under certain conditions on damping, all of the matrices in (2.6.12) may also become diagonal by using the mode shapes as basis vectors. Thus the mode shapes form an orthogonal set of basis vectors satisfying (2.6.13). Utilizing a reduced set of basis vectors is termed “subspace condensation,” since the response $\underline{U}(t)$ of the physical coordinates is restricted to lie in the subspace spanned by the m basis vectors, as indicated in (2.6.10). The mode vectors are the most commonly used subspace basis vectors in vibration practice; however, others such as *Guyan basis vectors* (Chapter 8) are also utilized.

2.6.1 Matrix–Vector Related Definitions and Identities

The earlier discussion provided an introductory explanation to the importance of matrices and vectors in vibration theory and modeling. The remainder of the text extends this discussion to many other aspects of vibration analyses. The identities provided below will facilitate the understanding of these topics.

2.6.1.1 Definitions and Usages

Consider the “ n ” dimensional vectors

$$\underline{\underline{A}}_{n \times 1} = \begin{bmatrix} a_1 \\ a_2 \\ \vdots \\ a_n \end{bmatrix}, \quad \underline{\underline{B}}_{n \times 1} = \begin{bmatrix} b_1 \\ b_2 \\ \vdots \\ b_n \end{bmatrix}, \quad \underline{\underline{C}}_{n \times 1} = \begin{bmatrix} c_1 \\ c_2 \\ \vdots \\ c_n \end{bmatrix} \quad (2.6.16)$$

where an underbar ($\underline{\underline{\quad}}$) indicates a vector or matrix array. The “dot” or “inner” product is defined by

$$\underline{\underline{A}}^T \underline{\underline{B}} = \underline{\underline{B}}^T \underline{\underline{A}} = \sum_{i=1}^n a_i b_i \quad (2.6.17)$$

and is utilized extensively for obtaining generalized forces that correspond to generalized coordinates and nodal coordinates in finite element and assumed modes models.

Define the matrix

$$\underline{\underline{D}} = \begin{bmatrix} d_{11} & \cdots & d_{1n} \\ \vdots & \ddots & \vdots \\ d_{n1} & \cdots & d_{nn} \end{bmatrix} \quad (2.6.18)$$

Some types of matrices and applications are provided below:

$\underline{\underline{D}}$ symmetric ((mass $\underline{\underline{M}}$, damping $\underline{\underline{C}}$, and stiffness $\underline{\underline{K}}$) matrices for nonrotating structures)

$$\underline{\underline{D}}^T = \underline{\underline{D}} \quad (2.6.19)$$

$\underline{\underline{D}}$ skew-symmetric ((gyroscopic $\underline{\underline{C}}$ and circulatory $\underline{\underline{K}}$) matrices for some rotating structures)

$$\underline{\underline{D}}^T = -\underline{\underline{D}} \quad (2.6.20)$$

$\underline{\underline{D}}$ orthogonal (coordinate transformation matrices for truss, plate, and beam finite elements)

$$\underline{\underline{D}}^T = \underline{\underline{D}}^{-1} \quad (2.6.21)$$

$\underline{\underline{D}}$ positive definite ($\underline{\underline{M}}$ and $\underline{\underline{K}}$ matrices are generally positive definite, which ensures positive kinetic and potential energy)

$$\underline{\underline{x}}_{1 \times nn}^T \underline{\underline{D}}_{nn \times nn} \underline{\underline{x}}_{nn \times 1} > 0, \quad \text{for all } \underline{\underline{x}} \quad (2.6.22)$$

$\underline{\underline{D}}$ positive semi-definite (makes potential energy zero when applied to the $\underline{\underline{K}}$ matrix with rigid body (strain-free) motion)

$$\underline{\underline{x}}_{1 \times nn}^T \underline{\underline{D}}_{nn \times nn} \underline{\underline{x}}_{nn \times 1} \geq 0, \quad \text{for all } \underline{\underline{x}} \quad (2.6.23)$$

2.6.1.2 Identities

- (a) Identities (a)–(d) are useful in demonstrating some unique properties of spinning (gyroscopic) vibrating systems.

Let \underline{x} and \underline{y} be real $N \times 1$ vectors and \underline{D} a real, skew-symmetric $N \times N$ matrix, that is,

$$\underline{D}^T = -\underline{D} \quad (2.6.24)$$

Then since a scalar equals its transpose,

$$\underline{x}^T \underline{D} \underline{y} = \underline{y}^T \underline{D}^T \underline{x} = -\underline{y}^T \underline{D} \underline{x} \quad (2.6.25)$$

Note that if \underline{x} equals \underline{y} , (2.6.25) yields

$$\underline{x}^T \underline{D} \underline{x} = -\underline{x}^T \underline{D} \underline{x}$$

or

$$\underline{x}^T \underline{D} \underline{x} = 0 \quad (2.6.26)$$

- (b) Let $\underline{\psi}$ be a complex vector and \underline{D} skew-symmetric, then

$$\begin{aligned} \bar{\underline{\psi}}^T \underline{D} \underline{\psi} &= \left(\underline{\psi}_R^T - i \underline{\psi}_I^T \right) \underline{D} \left(\underline{\psi}_R + i \underline{\psi}_I \right) \\ &= \left(\underline{\psi}_R^T \underline{D} \underline{\psi}_R + \underline{\psi}_I^T \underline{D} \underline{\psi}_I \right) + i \left(\underline{\psi}_R^T \underline{D} \underline{\psi}_I - \underline{\psi}_I^T \underline{D} \underline{\psi}_R \right) \end{aligned}$$

The use of (2.6.25) and (2.6.26) simplifies this to

$$\bar{\underline{\psi}}^T \underline{D} \underline{\psi} = i 2 \underline{\psi}_R^T \underline{D} \underline{\psi}_I = \text{pure imaginary constant} \quad (2.6.27)$$

where $\underline{\psi} = \underline{\psi}_R + i \underline{\psi}_I$

- (c) Let \underline{x} and \underline{y} be real $N \times 1$ vectors and \underline{E} a real, symmetric $N \times N$ matrix, that is,

$$\underline{E}^T = \underline{E}$$

Then since a scalar equals its transpose,

$$\underline{x}^T \underline{E} \underline{y} = \underline{y}^T \underline{E}^T \underline{x} = \underline{y}^T \underline{E} \underline{x} \quad (2.6.28)$$

- (d) If $\underline{\psi}$ is a complex vector and \underline{E} symmetric,

$$\bar{\underline{\psi}}^T \underline{E} \underline{\psi} = \left(\underline{\psi}_R^T \underline{E} \underline{\psi}_R + \underline{\psi}_I^T \underline{E} \underline{\psi}_I \right) + i \left(\underline{\psi}_R^T \underline{E} \underline{\psi}_I - \underline{\psi}_I^T \underline{E} \underline{\psi}_R \right)$$

The use of (2.6.28) simplifies this result to

$$\bar{\underline{\psi}}^T \underline{E} \underline{\psi} = \underline{\psi}_R^T \underline{E} \underline{\psi}_R + \underline{\psi}_I^T \underline{E} \underline{\psi}_I = \text{pure real constant} \quad (2.6.29)$$

- (e) An important identity for subspace condensation methods in vibrations.

Let \underline{A} be a $n \times m$ matrix and \underline{x} a $m \times 1$ vector; then

$$\underline{A} \underline{x} = \begin{bmatrix} \underline{A}_1 & \underline{A}_2 & \cdots & \underline{A}_m \end{bmatrix} \underline{x} = \sum_{i=1}^m x_i \underline{A}_i \quad (n \times 1) \quad (2.6.30)$$

where \underline{A}_i is column i of \underline{A} .

- (f) An important identity used for decoupling equations of motion (EOMs). Let
- \underline{A}
- be a
- $n \times m$
- matrix and
- \underline{B}
- a
- $m \times r$
- matrix; then

$$\underline{A} \underline{B} = \underline{A} \begin{bmatrix} \underline{B}_1 & \underline{B}_2 & \cdots & \underline{B}_r \end{bmatrix} = \begin{bmatrix} \underline{A} \underline{B}_1 & \underline{A} \underline{B}_2 & \cdots & \underline{A} \underline{B}_r \end{bmatrix} \quad (n \times r) \quad (2.6.31)$$

where \underline{B}_i is column i of \underline{B} . This product may also be written as

$$\underline{A} \underline{B} = \begin{bmatrix} \underline{A}_1 \\ \underline{A}_2 \\ \vdots \\ \underline{A}_n \end{bmatrix} \underline{B} = \begin{bmatrix} \underline{A}_1 \underline{B} \\ \underline{A}_2 \underline{B} \\ \vdots \\ \underline{A}_n \underline{B} \end{bmatrix} \quad (n \times r) \quad (2.6.32)$$

where \underline{A}_i is the i th row of \underline{A} .

- (g) An important identity used for decoupling EOMs. Let
- $\underline{\text{diag}}(\alpha_i)$
- be an
- $m \times m$
- diagonal matrix; then

$$\underline{\text{diag}}(\alpha_i) \underline{A} = \underline{\text{diag}}(\alpha_i) \begin{bmatrix} \underline{A}_1 \\ \underline{A}_2 \\ \vdots \\ \underline{A}_m \end{bmatrix} = \begin{bmatrix} \alpha_1 \underline{A}_1 \\ \alpha_2 \underline{A}_2 \\ \vdots \\ \alpha_m \underline{A}_m \end{bmatrix} \quad (2.6.33)$$

where \underline{A}_i is the i th row of \underline{A} . Similarly

$$\underline{A} \underline{\text{diag}}(\alpha_i) = \begin{bmatrix} \underline{A}_1 & \underline{A}_2 & \cdots & \underline{A}_m \end{bmatrix} \underline{\text{diag}}(\alpha_i) = \begin{bmatrix} \alpha_1 \underline{A}_1 & \alpha_2 \underline{A}_2 & \cdots & \alpha_m \underline{A}_m \end{bmatrix} \quad (2.6.34)$$

- (h) An important identity used for decoupling EOMs. Let
- \underline{A}
- be an
- $m \times n$
- matrix with columns
- \underline{A}_j
- and
- \underline{B}
- be an
- $n \times r$
- matrix with rows
- \underline{B}_j
- ; then

$$\begin{aligned} \underline{A} \underline{B} &= \begin{bmatrix} \underline{A}_1 & \underline{A}_2 & \cdots & \underline{A}_n \end{bmatrix} \begin{bmatrix} \underline{B}_1 \\ \underline{B}_2 \\ \vdots \\ \underline{B}_n \end{bmatrix} \\ &= \left\{ \begin{bmatrix} \underline{A}_1 & \underline{0} & \cdots & \underline{0} \end{bmatrix} + \begin{bmatrix} \underline{0} & \underline{A}_2 & \cdots & \underline{0} \end{bmatrix} + \cdots + \begin{bmatrix} \underline{0} & \underline{0} & \cdots & \underline{A}_n \end{bmatrix} \right\} \begin{bmatrix} \underline{B}_1 \\ \underline{B}_2 \\ \vdots \\ \underline{B}_n \end{bmatrix} \\ &= \sum_{j=1}^n \underline{A}_j \underline{B}_j \end{aligned} \quad (2.6.35)$$

- (i) An important identity used for developing concise frequency response equations for harmonically forced systems. Let \underline{A} , \underline{R} , \underline{B} , and $\underline{\text{diag}}(\alpha_i)$ be $n \times n$ invertible matrices. If

$$\underline{B} \underline{R} \underline{A} = \underline{\text{diag}}(\alpha_i) \quad (2.6.36)$$

then

$$\underline{A}^{-1} \underline{R}^{-1} \underline{B}^{-1} = \underline{\text{diag}}\left(\frac{1}{\alpha_i}\right) \quad (2.6.37)$$

or using (2.6.34) and (2.6.35)

$$\underline{R}^{-1} = \underline{A} \underline{\text{diag}}\left(\frac{1}{\alpha_i}\right) \underline{B} = \begin{bmatrix} \frac{1}{\alpha_1} \underline{A}_1 & & & \\ & \frac{1}{\alpha_2} \underline{A}_2 & & \\ & & \cdots & \\ & & & \frac{1}{\alpha_n} \underline{A}_n \end{bmatrix} \begin{bmatrix} \underline{B}_1 \\ \underline{B}_2 \\ \vdots \\ \underline{B}_n \end{bmatrix} = \sum_{i=1}^n \frac{1}{\alpha_i} \underline{A}_i \underline{B}_i \quad (2.6.38)$$

where \underline{A}_i is the i th column of \underline{A} and \underline{B}_i is the i th row of \underline{B} .

- (j) An important identity used for combining substructure models to form a system model. Two partitioned matrices may be multiplied together by treating the partitions as scalars if all matrix multiplications agree in dimension. For example, if

$$\begin{bmatrix} \underline{A}_{11} & \underline{A}_{12} & \underline{A}_{13} \\ \underline{A}_{21} & \underline{A}_{22} & \underline{A}_{23} \\ \underline{A}_{31} & \underline{A}_{32} & \underline{A}_{33} \end{bmatrix} \begin{bmatrix} \underline{B}_{11} & \underline{B}_{12} & \underline{B}_{13} \\ \underline{B}_{21} & \underline{B}_{22} & \underline{B}_{23} \\ \underline{B}_{31} & \underline{B}_{32} & \underline{B}_{33} \end{bmatrix} = \begin{bmatrix} \underline{C}_{11} & \underline{C}_{12} & \underline{C}_{13} \\ \underline{C}_{21} & \underline{C}_{22} & \underline{C}_{23} \\ \underline{C}_{31} & \underline{C}_{32} & \underline{C}_{33} \end{bmatrix} \quad (2.6.39)$$

then

$$\underline{C}_{ij} = \sum_{k=1}^3 \underline{A}_{ik} \underline{B}_{kj} \quad (2.6.40)$$

under the condition that matrices \underline{A}_{ik} and \underline{B}_{kj} have dimensions that are compatible for matrix multiplication.

- (k) The Lagrange equation approach requires differentiation of energy and work-type expressions appearing as quadratic forms or inner products. The following identity facilitates this process. Let r be the *quadratic form*

$$r = \frac{1}{2} \underset{1 \times n}{\underline{q}}^T \underset{n \times n}{\underline{G}} \underset{n \times 1}{\underline{q}} \quad (2.6.41)$$

and utilize the *vector differentiation notation*

$$\frac{\partial r}{\partial \underline{q}}_{n \times 1} = \left\{ \begin{array}{c} \frac{\partial r}{\partial q_1} \\ \frac{\partial r}{\partial q_2} \\ \vdots \\ \frac{\partial r}{\partial q_n} \end{array} \right\} \quad (2.6.42a)$$

then

$$\frac{\partial r}{\partial \underline{q}} = \underline{G} \underline{q} \quad (2.6.42b)$$

(l) An identity for applying the assumed modes and FEMs to vibration models. Let

$$\underline{u} = \underline{\Phi} \underline{q} \quad (2.6.43)$$

then

$$\underline{u}^2 = \underline{u}^T \underline{u} = \underline{q}^T \underline{\Phi}^T \underline{\Phi} \underline{q} \quad (2.6.44)$$

Apply (2.6.42b) to (2.6.44) to obtain

$$\frac{\partial \underline{u}^2}{\partial \underline{q}} = 2 \underline{\Phi}^T \underline{\Phi} \underline{q} \quad (2.6.45)$$

(m) An identity for applying the assumed modes and FEMs to vibration models.

Let $u = \alpha_1 q_1 + \alpha_2 q_2 + \alpha_3 q_3 + \dots + \alpha_n q_n$, then

$$\underline{u}^2 = (q_1 \ q_2 \ q_3 \ \dots \ q_n) \begin{bmatrix} \alpha_1 \alpha_1 & \alpha_1 \alpha_2 & \dots & \alpha_1 \alpha_n \\ \alpha_2 \alpha_1 & \alpha_2 \alpha_2 & \dots & \alpha_2 \alpha_n \\ \cdot & \cdot & \dots & \cdot \\ \cdot & \cdot & \dots & \cdot \\ \cdot & \cdot & \dots & \cdot \\ \alpha_n \alpha_1 & \alpha_n \alpha_2 & \dots & \alpha_n \alpha_n \end{bmatrix} \begin{Bmatrix} q_1 \\ q_2 \\ \cdot \\ \cdot \\ \cdot \\ q_n \end{Bmatrix} = \underline{q}^T \underline{\hat{\alpha}} \underline{q} \quad (2.6.46)$$

Apply (2.6.42b) to (2.6.45) to obtain

$$\frac{\partial \underline{u}^2}{\partial \underline{q}} = 2 \underline{\hat{\alpha}} \underline{q} \quad (2.6.47)$$

(n) An identity for applying the assumed modes and FEMs to vibration models. Let

$$\underline{X} = \begin{Bmatrix} x_1 \\ x_2 \\ \vdots \\ x_n \end{Bmatrix} \quad \text{and} \quad \underline{Y} = \begin{Bmatrix} y_1 \\ y_2 \\ \vdots \\ y_n \end{Bmatrix} \quad (2.6.48)$$

then

$$\frac{\partial(\underline{Y}^T \underline{X})}{\partial \underline{X}} = \begin{Bmatrix} \frac{\partial(\underline{Y}^T \underline{X})}{\partial x_1} \\ \frac{\partial(\underline{Y}^T \underline{X})}{\partial x_2} \\ \vdots \\ \frac{\partial(\underline{Y}^T \underline{X})}{\partial x_n} \end{Bmatrix} = \underline{Y} \quad (2.6.49)$$

(o) Other useful matrix identities:

$$(\underline{A}^T)^{-1} = (\underline{A}^{-1})^T = \underline{A}^{-T} \quad (2.6.50)$$

The row i , column j entry of the triple matrix product

$$\underline{D} = \underline{A} \underline{C} \underline{B} = \begin{bmatrix} \underline{A}_1 \\ \underline{A}_2 \\ \vdots \\ \underline{A}_m \end{bmatrix} \underline{C} [\underline{B}_1 \quad \underline{B}_2 \quad \cdots \quad \underline{B}_r] \quad (2.6.51)$$

is

$$D_{ij} = \underline{A}_i \underline{C} \underline{B}_j \quad (2.6.52)$$

where \underline{A}_i is the i th row of \underline{A} and \underline{B}_j is the j th column of \underline{B} .

2.7 COORDINATE TRANSFORMATIONS

A coordinate transformation provides a means to express motion sensed in a fixed frame in terms of motions sensed in a rotating frame. The motions sensed in the rotating frame are typically much simpler than in the fixed frame, and the fixed frame motions are typically needed to properly apply Newton's law. A simple example is the simple up/down motion of a mechanical horse as sensed in the rotating frame of a merry-go-round. The horse's motion has a simple description in the reference (viewing) frame attached to the merry-go-round, but has a very complex description to a viewer in a fixed, nonmoving reference frame. Vibration of blades attached to a spinning turbine disk presents a more practical example. Another important application of coordinate transformations is in finite elements. Element stiffness and mass matrices may be more easily derived in an element-based frame and then transformed to a system frame of reference. A vector may be expressed with components in any number of coordinate systems. For example, the vector \vec{G} in Figure 2.7.1 is shown with components in the unprimed frame and in the rotated primed frame.

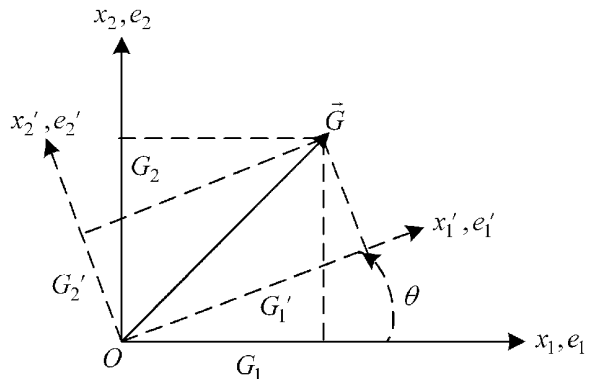


Figure 2.7.1 Components of vector \vec{G} in the rotated and fixed coordinate frames: 2D case

The two sets of components are related by the transformation

$$\begin{Bmatrix} G'_1 \\ G'_2 \end{Bmatrix} = \begin{bmatrix} \cos\theta & \sin\theta \\ -\sin\theta & \cos\theta \end{bmatrix} \begin{Bmatrix} G_1 \\ G_2 \end{Bmatrix} \quad (2.7.1)$$

or

$$\underline{G}' = \underline{C} \underline{G} \quad (2 \times 1) \quad (2.7.2)$$

Note that

$$\underline{C}^T \underline{C} = \begin{bmatrix} 1 & 0 \\ 0 & 1 \end{bmatrix} \quad (2.7.3)$$

so \underline{C} is an orthogonal matrix, that is, $\underline{C}^{-1} = \underline{C}^T$. Matrix \underline{C} may also be defined by

$$C_{ij} = \cos\angle(x'_i, x_j) = \text{cosine of the angle between } x'_i \text{ and } x_j \quad (2.7.4)$$

The rotating observer o frame and fixed n frame are shown in Figure 2.7.2 for the 3D case.

In general

$$\begin{Bmatrix} G_{o1} \\ G_{o2} \\ G_{o3} \end{Bmatrix} = \begin{bmatrix} C_{11} & C_{12} & C_{13} \\ C_{21} & C_{22} & C_{23} \\ C_{31} & C_{32} & C_{33} \end{bmatrix} \begin{Bmatrix} G_{n1} \\ G_{n2} \\ G_{n3} \end{Bmatrix} \quad (3 \times 1) \quad (2.7.5)$$

where the direction cosine matrix entries are

$$C_{ij} = \cos\angle(x'_{oi}, x_{nj}) = \cos(\theta_{ij}) \quad (2.7.6)$$

Figure 2.7.3 illustrates a sequence of three rotation angles that will reorient the n frame into the o frame. This has application in the modeling of beams in finite element frame models and in modeling vibrations of components attached to rotating bodies such as airplanes, satellites, and ships.

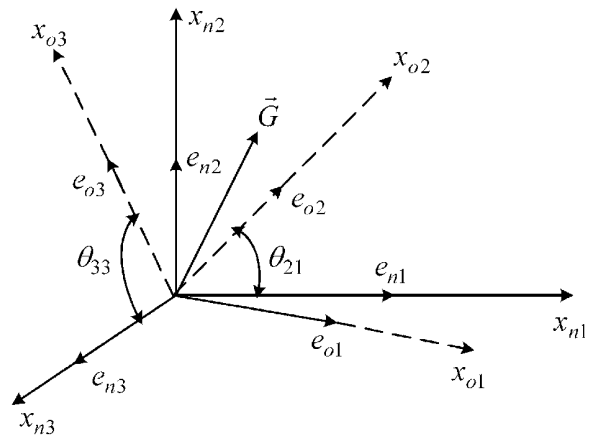


Figure 2.7.2 Components of vector \bar{G} in the rotated and fixed coordinate frames: 3D case

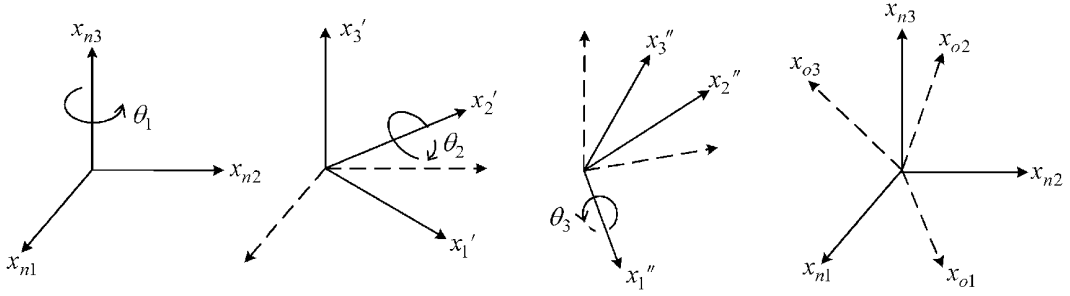


Figure 2.7.3 Euler angle rotation sequence 3-2-1 from frame “*n*” to frame “*o*”

The *n* to *o* transformation matrix \underline{C} is obtained from the Euler angles $(\theta_1, \theta_2, \theta_3)$ as

$$\begin{Bmatrix} e_{o1} \\ e_{o2} \\ e_{o3} \end{Bmatrix} = \begin{bmatrix} 1 & 0 & 0 \\ 0 & c\theta_3 & s\theta_3 \\ 0 & -s\theta_3 & c\theta_3 \end{bmatrix} \begin{bmatrix} c\theta_2 & 0 & -s\theta_2 \\ 0 & 1 & 0 \\ s\theta_2 & 0 & c\theta_2 \end{bmatrix} \begin{bmatrix} c\theta_1 & s\theta_1 & 0 \\ -s\theta_1 & c\theta_1 & 0 \\ 0 & 0 & 1 \end{bmatrix} \begin{Bmatrix} e_{n1} \\ e_{n2} \\ e_{n3} \end{Bmatrix} = [\underline{c}_{ij}] \begin{Bmatrix} e_{n1} \\ e_{n2} \\ e_{n3} \end{Bmatrix} \quad (2.7.7)$$

where $c\theta$ and $s\theta$ represent $\cos(\theta)$ and $\sin(\theta)$, respectively, and

$$\begin{aligned} c_{11} &= \cos\theta_1 \cos\theta_2 \\ c_{12} &= \sin\theta_1 \cos\theta_2 \\ c_{13} &= -\sin\theta_2 \\ c_{21} &= -\cos\theta_3 \sin\theta_1 + \sin\theta_2 \sin\theta_3 \cos\theta_1 \\ c_{22} &= \cos\theta_1 \cos\theta_3 + \sin\theta_1 \sin\theta_2 \sin\theta_3 \\ c_{23} &= \sin\theta_3 \cos\theta_2 \\ c_{31} &= \sin\theta_1 \sin\theta_3 + \cos\theta_1 \sin\theta_2 \cos\theta_3 \\ c_{32} &= -\cos\theta_1 \sin\theta_3 + \sin\theta_1 \sin\theta_2 \cos\theta_3 \\ c_{33} &= \cos\theta_2 \cos\theta_3 \end{aligned} \quad (2.7.8)$$

It can be shown by direct multiplication that

$$\underline{C}\underline{C}^T = \underline{I}_3 \Rightarrow \underline{C}^{-1} = \underline{C}^T \quad (\text{i.e., } \underline{C} \text{ is orthogonal}) \quad (2.7.9)$$

and from (2.7.7) and (2.7.9)

$$\underline{e}_o = \underline{C}\underline{e}_n, \quad \underline{e}_n = \underline{C}^{-1}\underline{e}_o = \underline{C}^T\underline{e}_o \quad (2.7.10)$$

For airplane, train, vehicle, or ship motion, θ_1 is the yaw angle, θ_2 is the pitch angle, and θ_3 is the roll angle for the fore and aft of the body along the + and $-x_1$ direction, respectively. Chapter 9 utilizes the aforementioned sequence of rotations for transforming 3D beam elements from a local element-based frame to the system frame.

The vector \vec{G} in Figure 2.7.2 may be expressed in two ways with vector notation and two ways with array notation:

(a) Vector Notation

$$\vec{G}_n = G_{n1}\hat{e}_{n1} + G_{n2}\hat{e}_{n2} + G_{n3}\hat{e}_{n3}, \quad \vec{G}_o = G_{o1}\hat{e}_{o1} + G_{o2}\hat{e}_{o2} + G_{o3}\hat{e}_{o3} \quad (2.7.11)$$

(b) Array Notation

$$\underline{G}_n = \begin{Bmatrix} G_{n1} \\ G_{n2} \\ G_{n3} \end{Bmatrix}_n, \quad \underline{G}_o = \begin{Bmatrix} G_{o1} \\ G_{o2} \\ G_{o3} \end{Bmatrix}_o \quad (2.7.12)$$

The coordinate transformation can be applied to the unit vectors for the vector representation, that is,

$$\begin{Bmatrix} \hat{e}_{o1} \\ \hat{e}_{o2} \\ \hat{e}_{o3} \end{Bmatrix} = \begin{bmatrix} c_{11} & c_{12} & c_{13} \\ c_{21} & c_{22} & c_{23} \\ c_{31} & c_{32} & c_{33} \end{bmatrix} \begin{Bmatrix} \hat{e}_{n1} \\ \hat{e}_{n2} \\ \hat{e}_{n3} \end{Bmatrix} \quad (2.7.13)$$

The vector \vec{G} with components in frame o is given by (2.7.12). Substitute (2.7.13) into (2.7.11) to obtain \vec{G} with components in frame n :

$$\begin{aligned} \vec{G}_n &= G_{o1}(c_{11}\hat{e}_{n1} + c_{12}\hat{e}_{n2} + c_{13}\hat{e}_{n3}) + G_{o2}(c_{21}\hat{e}_{n1} + c_{22}\hat{e}_{n2} + c_{23}\hat{e}_{n3}) \\ &\quad + G_{o3}(c_{31}\hat{e}_{n1} + c_{32}\hat{e}_{n2} + c_{33}\hat{e}_{n3}) \\ &= (c_{11}G_{o1} + c_{21}G_{o2} + c_{31}G_{o3})\hat{e}_{n1} + (c_{12}G_{o1} + c_{22}G_{o2} + c_{32}G_{o3})\hat{e}_{n2} \\ &\quad + (c_{13}G_{o1} + c_{23}G_{o2} + c_{33}G_{o3})\hat{e}_{n3} \\ &= G_{n1}\hat{e}_{n1} + G_{n2}\hat{e}_{n2} + G_{n3}\hat{e}_{n3} \end{aligned} \quad (2.7.14)$$

The coordinate transformation can be applied to the arrays

$$\begin{Bmatrix} G_{o1} \\ G_{o2} \\ G_{o3} \end{Bmatrix}_o = \begin{bmatrix} c_{11} & c_{12} & c_{13} \\ c_{21} & c_{22} & c_{23} \\ c_{31} & c_{32} & c_{33} \end{bmatrix} \begin{Bmatrix} G_{n1} \\ G_{n2} \\ G_{n3} \end{Bmatrix}_n \quad (2.7.15)$$

$$\underline{G}_o = \underline{C} \underline{G}_n$$

and since \underline{C} is orthogonal $\underline{C}^{-1} = \underline{C}^T$, it follows that

$$\begin{Bmatrix} G_{n1} \\ G_{n2} \\ G_{n3} \end{Bmatrix}_n = \begin{bmatrix} c_{11} & c_{21} & c_{31} \\ c_{12} & c_{22} & c_{32} \\ c_{13} & c_{23} & c_{33} \end{bmatrix} \begin{Bmatrix} G_{o1} \\ G_{o2} \\ G_{o3} \end{Bmatrix}_o \quad (2.7.16)$$

$$\underline{G}_n = \underline{C}^T \underline{G}_o$$

From (2.7.16)

$$\begin{aligned} G_{n1} &= c_{11}G_{o1} + c_{21}G_{o2} + c_{31}G_{o3} \\ G_{n2} &= c_{12}G_{o1} + c_{22}G_{o2} + c_{32}G_{o3} \\ G_{n3} &= c_{13}G_{o1} + c_{23}G_{o2} + c_{33}G_{o3} \end{aligned} \quad (2.7.17)$$

Note that the results of (2.7.14) and (2.7.17) are identical. The magnitude of any vector is invariant in any coordinate system, that is,

$$|\underline{\bar{G}}| = \sqrt{\underline{\bar{G}}_o^T \underline{\bar{G}}_o} = \sqrt{\underline{G}_n^T \underline{C}^T \underline{C} \underline{G}_n} = \sqrt{\underline{G}_n^T \underline{G}_n} \quad (2.7.18)$$

since \underline{C} is orthogonal.

2.8 EIGENVALUES AND EIGENVECTORS

Displacing the tip of a car antenna and releasing it will result in it vibrating at nearly a single frequency and shape, and the vibration will decay with time. Displacing the same car antenna near its center while holding the tip fixed and then releasing it will result in vibration at a different frequency, shape, and decay rate. This phenomenon occurs with all flexible structures and machinery components and is termed natural or free vibrations. Its measurement or prediction is commonly referred to as modal analysis. Resonance occurs when the frequency of an external force and a natural frequency become nearly coincident. The stiffness-related restoring forces are nearly cancelled by the inertia forces under these conditions and the vibrations may become dangerously large. Determining natural frequencies and their respective damping and characteristic mode shapes is an essential step in the design of critical machines and structures. The frequencies, shapes, and decay rates are characteristic (eigen) properties of the object itself, where “eigen” is the German expression for characteristic. The frequency, decay rate, and vibrating shape are referred to as natural frequency, damping, and mode shape, respectively. The unforced (free) form of the equilibrium equation (2.6.3) is

$$\underline{M}\ddot{\underline{U}} + \underline{C}\dot{\underline{U}} + \underline{K}\underline{U} = \underline{0} \quad (2.8.1)$$

This second-order form is converted into a first-order form in Chapter 6. The results are

$$\underset{n \times 1}{\dot{\underline{X}}} = \underset{n \times n}{\underline{D}} \underset{n \times 1}{\underline{X}} \quad (2.8.2)$$

or

$$\underset{n \times n}{\underline{A}} \underset{n \times 1}{\dot{\underline{X}}} = \underset{n \times n}{\underline{B}} \underset{n \times 1}{\underline{X}} \quad (2.8.3)$$

Substitution of the solution form

$$\underset{n \times 1}{\underline{X}} = \underset{1 \times 1}{e^{\lambda t}} \underset{n \times 1}{\underline{\psi}} \quad (2.8.4)$$

into (2.8.2) or (2.8.3) yields

$$\lambda \underline{\psi} = \underline{D} \underline{\psi} \quad (2.8.5)$$

or

$$\lambda \underline{A} \underline{\psi} = \underline{B} \underline{\psi} \quad (2.8.6)$$

where λ is an eigenvalue and $\underline{\psi}$ is an eigenvector of either $(\underline{A}, \underline{B})$ or \underline{D} . Equations (2.8.5) and (2.8.6) are referred to as a standard form and generalized form eigenvalue problem,

respectively. Clearly, $\underline{\psi} = \underline{0}$ is a solution to either (2.8.5) or (2.8.6); however by (2.8.4), this would imply that the system does not respond, that is, a cantilever beam does not vibrate if its tip is released from some initial deflection, or a bell does not ring if it is suddenly tapped. Hence, if $\underline{\psi} \neq \underline{0}$, the condition

$$(\lambda \underline{I} - \underline{D})\underline{\psi} = \underline{0} \quad (2.8.7)$$

$$(\lambda \underline{A} - \underline{B})\underline{\psi} = \underline{0} \quad (2.8.8)$$

can be solved only if $(\lambda \underline{I} - \underline{D})$ and $(\lambda \underline{A} - \underline{B})$ are noninvertible, that is, singular matrices with

$$\det(\lambda \underline{I} - \underline{D}) = 0 \quad (2.8.9)$$

$$\det(\lambda \underline{A} - \underline{B}) = 0 \quad (2.8.10)$$

These expressions are often referred to as *characteristic equations* and their n roots (λ_j) as “eigenvalues,” that is, characteristic roots. Substitution of an eigenvalue λ_j into (2.8.7) or (2.8.8) allows the corresponding “eigenvector” $\underline{\psi}_j$ to be determined. Clearly, if $\underline{\psi}_j$ satisfies (2.8.7) or (2.8.8), so will $\alpha \underline{\psi}_j$ where α is an arbitrary complex constant. Thus, $\underline{\psi}_j$ is unique only to within a multiplication constant. The eigenvector $\underline{\psi}_j$ is referred to as the j th *mode shape*.

The complete solution for $\underline{X}(t)$ in (2.8.4) is by linear superposition

$$\underline{X}(t) = \sum_{j=1}^n \gamma_j e^{\lambda_j t} \underline{\psi}_j \quad (2.8.11)$$

where γ_j are constants determined by the value of \underline{X} at $t=0$.

In general, the eigenvalues and eigenvectors are complex, that is,

$$\lambda_j = c_j + id_j \quad (2.8.12)$$

Then from (2.8.11) and Euler’s identity (Example 2.4.3),

$$\underline{X}(t) = \sum_{j=1}^n \gamma_j e^{c_j t} [\cos(d_j t) + i \sin(d_j t)] \underline{\psi}_j \quad (2.8.13)$$

Note that if c_j are all less than or equal to zero, $\underline{X}(t)$ remains bounded (stable response). However, if any λ_j lies in the right-hand side of the complex plane (Figure 2.5.2), that is, $c_j > 0$, the $e^{c_j t}$ and consequently $\underline{X}(t)$ will become unbounded (unstable response) as $t \rightarrow \infty$. Eigenvalues are routinely calculated in vibration and control studies to determine if the free vibration response is stable.

2.9 FOURIER SERIES

Many forces in machinery and nature are not sinusoidal but recur periodically, that is, with a fixed period. A reciprocating compressor (Figure 2.9.1) has reciprocating pistons that periodically compress gas in its cylinders and discharge the gas into the attached piping through valves.

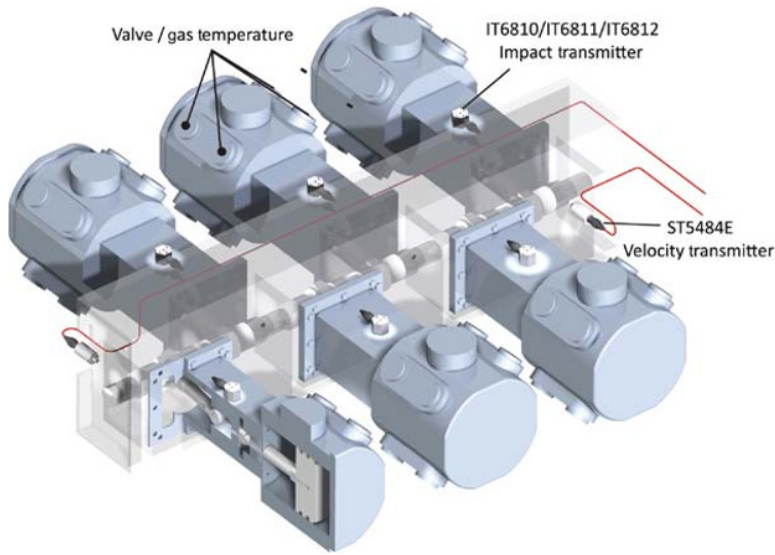


Figure 2.9.1 Six-cylinder industrial reciprocating compressor. Reproduced with permission of Metrix Instrument Co., LP. © Adriana Romero-Metrix Instrument Co.

The fundamental gas pressure frequency is the rpm of the compressor's crankshaft, which pushes and pulls the pistons as it rotates. The piping has acoustic natural frequencies, similar to a flute. Coincidence of a harmonic of the periodic pressure frequency with an acoustic natural frequency causes acoustic resonance, which can cause high-cycle fatigue HCF cracking of piping. Not a good thing when the pipe holds 1200 psi natural gas or hydrogen sulfide gas! The author is acquainted with an incidence of a 36th pressure harmonic causing an HCF crack in a compressor piping network on an offshore platform. Similarly a concrete-busting jackhammer produces a periodic, nonsinusoidal force on the flooring, which may cause excessive noise radiation or damage to nearby precision instrumentation or computer hard drives. Fourier series (FS) provides a mathematical tool to decompose a periodic force or response into a sum of sinusoidal contributions. The amplitudes, phase angles, and frequencies of the Fourier components are all determined by the FS technique. The number of mode shape basis vectors to include in a subspace, as in (2.6.10), can be estimated by FS, since it will show the frequency above which the component force amplitudes are negligible.

Any periodic waveform ($Y(t) = Y(t+T)$, where T is the period) may be expressed as the sum of sinusoids

$$Y(t) = \frac{A_0}{2} + \sum_{n=1}^{\infty} (A_n \cos(n\omega t) + B_n \sin(n\omega t)) = \frac{A_0}{2} + \sum_{n=1}^{\infty} C_n \cos(n\omega t - \phi_n) \quad (2.9.1)$$

where

$$C_n = \sqrt{A_n^2 + B_n^2} \quad (2.9.2)$$

$$\phi_n = \tan^{-1} \frac{B_n}{A_n} \quad (2.9.3)$$

$$A_0 = \frac{2}{T} \int_0^T Y(t) dt, \quad A_n = \frac{2}{T} \int_0^T Y(t) \cos\left(\frac{2\pi}{T} nt\right) dt, \quad B_n = \frac{2}{T} \int_0^T Y(t) \sin\left(\frac{2\pi}{T} nt\right) dt \quad (2.9.4)$$

$n = 1, 2, 3, \dots, \infty$

The frequency and period are related by

T = fundamental period of the complex waveform

$$f = \frac{1}{T} = \text{fundamental frequency in Hz} \quad (2.9.5)$$

$$\omega = 2\pi f = \frac{2\pi}{T} = \text{circular fundamental frequency in rad/s}$$

The formulas in (2.9.1)–(2.9.4) result from the “orthogonality” relations

$$\int_0^T \cos(n\omega t) \cos(m\omega t) dt = \begin{cases} 0, & m \neq n \\ \frac{T}{2}, & m = n \end{cases}$$

$$\int_0^T \sin(n\omega t) \sin(m\omega t) dt = \begin{cases} 0, & m \neq n \\ \frac{T}{2}, & m = n \end{cases} \quad (2.9.6)$$

$$\int_0^T \sin(n\omega t) \cos(m\omega t) dt = 0 \quad \text{for all } m \text{ and } n$$

where m and n are integers and $\omega = 2\pi/T$.

EXAMPLE 2.9.1 *Fourier Series for Sawtooth Function*

Derive the Fourier sinusoid amplitudes and phase angles for a repeated ramp waveform. This might represent the dynamic component of a periodic pressure-induced force. The static pressure component will exceed the dynamic component so that the total (static plus dynamic) pressure will not become negative. For example, Figure E2.9.1(a) could represent a dynamic pressure waveform.

For this example,

$$Y(t) = A - \frac{2A}{T}t, \quad 0 \leq t < T \quad (1)$$

Determine the A_n and B_n by inserting (1) into (2.9.4):

$$A_0 = \frac{2}{T} \int_0^T \left(A - \frac{2A}{T}t\right) dt = \frac{2A}{T} \left(t - \frac{1}{T}t^2\right) \Big|_0^T = 0 \quad (2)$$

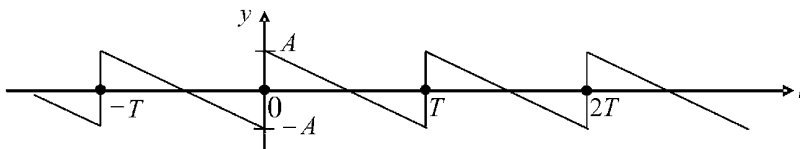


Figure E2.9.1(a) Periodic sawtooth waveform with amplitude A and period T

$$\begin{aligned}
A_n &= \frac{2}{T} \int_0^T A \left(1 - \frac{2}{T}t\right) \cos\left(\frac{2\pi}{T}nt\right) dt \\
&= \frac{2A}{T} \int_0^T \cos\left(\frac{2\pi}{T}nt\right) dt - \frac{4A}{T^2} \int_0^T t \cos\left(\frac{2\pi}{T}nt\right) dt \\
&= \frac{2A}{T} \left[\frac{T}{2\pi n} \sin\left(\frac{2\pi n}{T}t\right) \right] \Big|_0^T - \frac{4A}{T^2} \left[\left(\frac{T}{2\pi n}\right)^2 \cos\left(\frac{2\pi n}{T}t\right) + \left(\frac{T}{2\pi n}\right)t \sin\left(\frac{2\pi n}{T}t\right) \right] \Big|_0^T \quad (3) \\
&= \frac{2A}{T} (0-0) - \frac{4A}{T^2} \left[\left(\frac{T}{2\pi n}\right)^2 + 0 - \left(\frac{T}{2\pi n}\right)^2 - 0 \right] \\
&\Rightarrow A_n = 0, \quad n = 1, 2, 3, \dots
\end{aligned}$$

$$\begin{aligned}
B_n &= \frac{2}{T} \int_0^T A \left(1 - \frac{2}{T}t\right) \sin\left(\frac{2\pi}{T}nt\right) dt \\
&= \frac{2A}{T} \int_0^T \sin\left(\frac{2\pi}{T}nt\right) dt - \frac{4A}{T^2} \int_0^T t \sin\left(\frac{2\pi}{T}nt\right) dt \\
&= \frac{2A}{T} \left[\frac{-T}{2\pi n} \cos\left(\frac{2\pi n}{T}t\right) \right] \Big|_0^T - \frac{4A}{T^2} \left[\left(\frac{T}{2\pi n}\right)^2 \sin\left(\frac{2\pi n}{T}t\right) - \left(\frac{T}{2\pi n}\right)t \cos\left(\frac{2\pi n}{T}t\right) \right] \Big|_0^T \quad (4) \\
&= \frac{2A}{T} \left[\frac{-T}{2\pi n} - \left(\frac{-T}{2\pi n}\right) \right] - \frac{4A}{T^2} \left[\left(\frac{T}{2\pi n}\right)^2 * 0 - \left(\frac{T}{2\pi n}\right)T(1) - \left(\frac{T}{2\pi n}\right)^2 * 0 - 0 \right] \\
&= \frac{-4A}{T^2} \left(\frac{-T^2}{2\pi n}\right) = \frac{2A}{\pi n} \\
&\Rightarrow B_n = \frac{2A}{\pi n}, \quad n = 1, 2, 3, \dots
\end{aligned}$$

Insert (2), (3), and (4) into (2.9.1):

$$Y(t) = 0 + \sum_{n=1}^{\infty} \left(0 * \cos(n\omega t) + \frac{2A}{\pi n} \sin(n\omega t) \right) = \frac{2A}{\pi} \sum_{n=1}^{\infty} \frac{1}{n} \sin(n\omega t) \quad (5)$$

2.10 LAPLACE TRANSFORMS, TRANSFER FUNCTIONS, AND CHARACTERISTIC EQUATIONS

Multidisciplinary interaction problems generally model multiple domains of different physical natures. For example, AVC seeks to reduce the vibration of structures or machines by measuring the vibrations and applying actuator forces determined by controllers. The controller output power is inadequate for powering the actuators, so the controller outputs are routed through servo power amplifiers (SPAs) to drive the actuators as discussed in Chapter 12 on AVC. The SPAs are dynamic systems themselves as characterized by frequency response functions (FRFs) that vary in amplitude and phase angle as a function of frequency as shown in Figure 2.10.1. The FRFs are the ratios of output over input for the

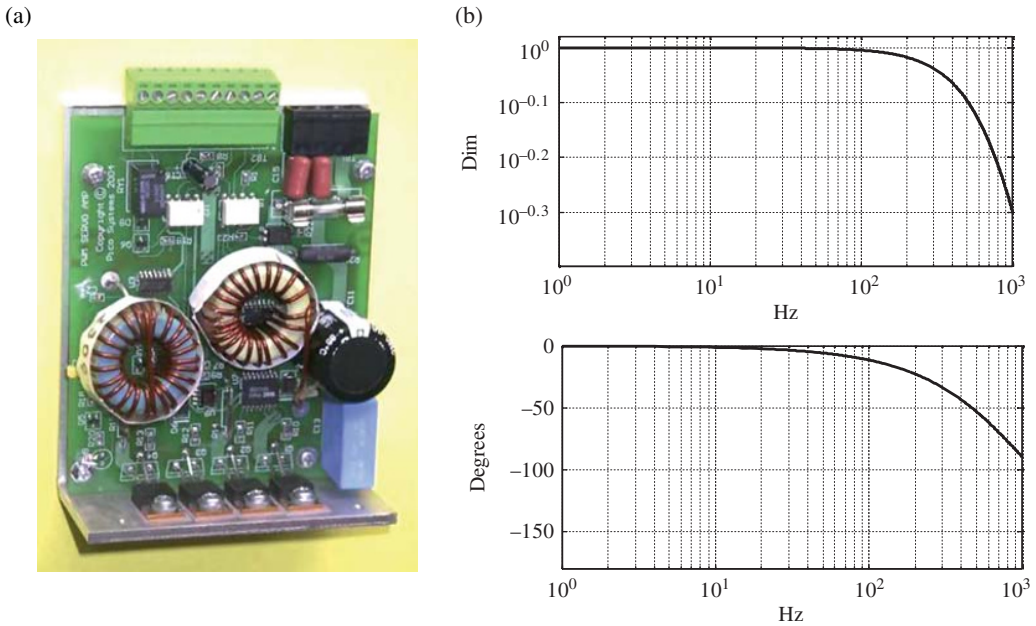


Figure 2.10.1 (a) Servo power amplifier and its (b) output current/input voltage amplitude and phase angle versus frequency. Photograph reproduced with permission of Jon Elson of Pico Systems © John Elson

given device. A transfer function may be obtained from the FRF via curve fitting algorithms and codes such as MATLAB's `invfreqs`. A challenge is combining the dynamics model of the structure being controlled with the dynamics model of the controller and power amplifier, which may contain 1000s of components. The structural model is typically described by a set of ODEs, which have the general form of (2.6.3) for a linear model. The SPA is too complex of a system to likewise describe with coupled differential equations. The remedy for this is to treat the SPA as a “black box” and experimentally measure its FRF. Curve fitting this provides the equivalent transfer function for the SPA. The transfer function may be converted to an equivalent set of first-order state differential equations that are readily coupled to the structural component differential equations as in Chapter 12. Conversely, for small-order models the structural equations may be converted into transfer functions and then combined with the SPA transfer function to obtain a system model.

The earlier discussion is equally valid for soil–structure and fluid–structure interaction problems where the soil or fluid is governed by laws described with complex sets of differential equations; however, their output (typically force)/input (typically motion) frequency response characteristics may be relatively easily measured. An example is the force generated by the leakage flow in a liquid seal on a high-speed pump shaft in response to transverse vibration of the spinning shaft. The FRF of this force may be measured and then included in the fluid–structure interaction model.

The conversion of an experimentally derived transfer function to an equivalent set of first-order state differential equations is given below. The transfer function has the general form

$$T(s) = \frac{\text{Output}}{\text{Input}} = \frac{y(s)}{u(s)} = \frac{b_1 s^{n-1} + b_2 s^{n-2} + \dots + b_n}{s^n + a_1 s^{n-1} + a_2 s^{n-2} + \dots + a_n} \quad (2.10.1)$$

Given the input $u(t)$, the output $y(t)$ may be obtained by solving the following (*canonical form*) state equations:

$$\dot{\underline{X}} = \underline{A}\underline{X} + \underline{B}u \quad (2.10.2)$$

$$y = \underline{C}\underline{X} \quad (2.10.3)$$

where

$$\underline{A} = \begin{bmatrix} -a_1 & -a_2 & -a_3 & \cdots & -a_{n-1} & -a_n \\ 1 & 0 & 0 & \cdots & 0 & 0 \\ 0 & 1 & 0 & \cdots & 0 & 0 \\ \vdots & \vdots & \vdots & \ddots & \vdots & \vdots \\ 0 & 0 & 0 & \cdots & 1 & 0 \end{bmatrix} \quad (2.10.4)$$

$$\underline{B} = (1 \ 0 \ 0 \ \dots \ 0)^T, \quad \underline{C} = (b_1 \ b_2 \ b_3 \ \dots \ b_n)$$

The Laplace transform method (LTM) also provides a convenient way to solve EOMs. The Laplace transform (LT) of the EOM is performed, and the result is solved for the LT of the response variable. The response is obtained by comparing the LT of the response variable with a table of LTs. The following list contains some LTs and LT properties.

The LT of a function $f(t)$ is defined by

$$F(s) = L(f) = \int_0^{\infty} e^{-st} f(t) dt \quad (2.10.5)$$

(a) If α is a constant,

$$L(\alpha f) = \int_0^{\infty} e^{-st} \alpha f dt = \alpha \int_0^{\infty} e^{-st} f dt = \alpha F(s) \quad (2.10.6)$$

(b) If f_1 and f_2 are two functions and β_1 and β_2 are two constants,

$$\begin{aligned} L(\beta_1 f_1 + \beta_2 f_2) &= \int_0^{\infty} (\beta_1 f_1 + \beta_2 f_2) e^{-st} dt = \beta_1 \int_0^{\infty} f_1 e^{-st} dt + \beta_2 \int_0^{\infty} f_2 e^{-st} dt \\ &= \beta_1 F_1(s) + \beta_2 F_2(s) \end{aligned} \quad (2.10.7)$$

(c) If \dot{f} is the time derivative of f and using integration by parts $\left(\int u dv = uv - \int v du \right)$

$$L(\beta \dot{f}) = \int_0^{\infty} \beta \dot{f} e^{-st} dt = \beta \left[f e^{-st} \Big|_0^{\infty} - \int_0^{\infty} f (-s e^{-st}) dt \right] = \beta [sF(s) - f(0)] \quad (2.10.8)$$

(d) If \ddot{f} is the second time derivative of f and using two integrations by parts,

$$\begin{aligned} L(\beta \ddot{f}) &= \int_0^{\infty} \beta \ddot{f} e^{-st} dt = \beta \left[\dot{f} e^{-st} \Big|_0^{\infty} - \int_0^{\infty} \dot{f} (-s e^{-st}) dt \right] \\ &= \beta \left\{ -\dot{f}(0) + s \left[f e^{-st} \Big|_0^{\infty} - \int_0^{\infty} f (-s e^{-st}) dt \right] \right\} = \beta [s^2 \bar{F}(s) - \dot{f}(0) - s f(0)] \end{aligned} \quad (2.10.9)$$

Table 2.10.1 Table of common Laplace transforms

$f(t)$	$F(s)$
1. e^{-at}	$\frac{1}{s+a}$
2. $t^n \quad n=0,1,2,\dots$	$\frac{n!}{s^{n+1}}$
3. $\cos \omega t$	$\frac{s}{s^2 + \omega^2}$
4. $\sin \omega t$	$\frac{\omega}{s^2 + \omega^2}$
5. $\frac{\omega_n}{\sqrt{1-\xi^2}} e^{-\xi\omega_n t} \sin(\omega_d t) \quad \text{where } \omega_d = \omega_n \sqrt{1-\xi^2}$	$\frac{\omega_n^2}{s^2 + 2\xi\omega_n s + \omega_n^2}$
6. $-tf(t)$	$\frac{dF(s)}{ds}$
7. $(-1)^n t^n f(t)$	$\frac{d^n F(s)}{ds^n}$
8. $\delta(t-a)$ = unit impulse (Dirac delta function) at $t=a$	e^{-as}
9. $u(t) = \begin{cases} 0, & t < a \\ 1, & t \geq a \end{cases}$ Unit step or Heaviside function	$\frac{e^{-as}}{s}$
10. $\frac{1}{\omega_n^2} (1 - \cos \omega_n t)$	$\frac{1}{s(s^2 + \omega_n^2)}$
11. $\frac{1}{\omega_n^3} (\omega_n t - \sin \omega_n t)$	$\frac{1}{s^2(s^2 + \omega_n^2)}$
12. $\frac{1}{(s+a)(s^2 + \omega_n^2)}$	$\frac{e^{-at}}{(a^2 + \omega_n^2)} + \frac{a \sin \omega_n t}{\omega_n (a^2 + \omega_n^2)}$

Some common LTs are given in Table 2.10.1. Taking the LT of a linear ODE will yield a relationship between the LTs of the output (y) and input (u),

$$G(s) = \frac{\bar{y}(s)}{\bar{u}(s)} = \frac{N(s)}{D(s)} \quad (2.10.10)$$

where $G(s)$ is referred to as the transfer function and $N(s)$ and $D(s)$ are its numerator and denominator polynomials, respectively. The denominator $D(s)$ is often referred to as the characteristic polynomial.

2.11 KINEMATICS AND KINEMATIC CONSTRAINTS

Imagine modeling an automobile for vibrations by starting with relative motions of atoms! From a computational view, one would quickly replace the quantum mechanics descriptions and models with continuum models that in some manner impose reasonable motion constraints. The motion constraints are typically based on experiment and/or intuition and greatly reduce the number of dofs to a manageable level.

2.11.1 Particle Kinematic Constraint

The simplest model of a finite-sized object is that it behaves as a “particle.” The underlying assumptions are that the object does not deform or rotate. The point “particle” model can

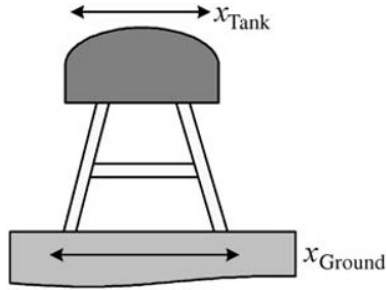


Figure 2.11.1 Horizontal translation of water tower tank due to earthquake motion

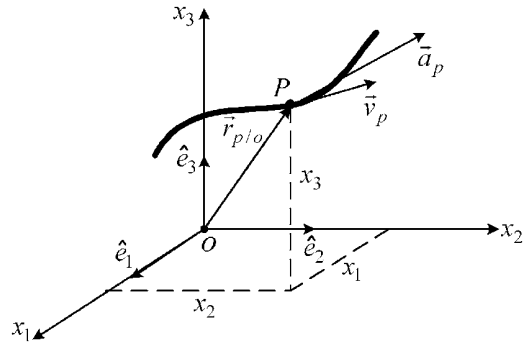


Figure 2.11.2 Particle motion in 3D space

represent the motion at any location on the body since the motion is the same over the entire body. Some examples might include a boat, plane, car, or train car translating along a straight or curved path with negligible rotation or deformation. Even large masses such as the water tower tank in Figure 2.11.1 can be treated as a particle as long as it only translates, without rotation.

The following list contains some mathematical relationships for particle motion. Figure 2.11.2 shows a particle traversing a path in three dimensions. The position, velocity, and acceleration of this point are given by the following formulae:

2.11.1.1 Rectilinear Coordinates

$$\vec{r}_{p/o} = x_1 \hat{e}_1 + x_2 \hat{e}_2 + x_3 \hat{e}_3, \quad \vec{v}_p = \dot{x}_1 \hat{e}_1 + \dot{x}_2 \hat{e}_2 + \dot{x}_3 \hat{e}_3, \quad \vec{a}_p = \ddot{x}_1 \hat{e}_1 + \ddot{x}_2 \hat{e}_2 + \ddot{x}_3 \hat{e}_3 \quad (2.11.1)$$

The following formulas relate the position, velocity, or acceleration quantities.

(a) Functions of time

$$x_i = \int v_i dt, \quad v_i = \int a_i dt, \quad v_i = \frac{dx_i}{dt}, \quad a_i = \frac{dv_i}{dt} \quad (2.11.2)$$

(b) Functions of position

$$v_i(x_i) = \frac{dx_i}{dt} \Rightarrow t = \int \frac{dx_i}{v_i(x_i)} \quad (2.11.3)$$

$$a_i(x_i) = \frac{dv_i}{dt} = \frac{dv_i dx_i}{dx_i dt} = v_i \frac{dv_i}{dx_i}, \quad \int v_i dv_i = \int a_i(x_i) dx_i, \quad \frac{v_i^2}{2} = \int a_i(x_i) dx_i \quad (2.11.4)$$

(c) Functions of velocity

$$a_i(v_i) = \frac{dv_i}{dt} \Rightarrow t = \int \frac{dv_i}{a_i(v_i)} \quad (2.11.5)$$

or from (2.11.4)

$$a_i(v_i) = v_i \frac{dv_i}{dx_i} \Rightarrow x_i = \int \frac{v_i}{a_i(v_i)} dv_i \quad (2.11.6)$$

2.11.1.2 Cylindrical Coordinates

Often, it is more convenient to use a curvilinear coordinate system to describe particle motion as illustrated by the cylindrical and normal–tangential systems shown in Figure 2.11.3. The cylindrical coordinate unit vector's directions vary with time as they follow the particle, although their magnitudes remain equal to one, as shown in Figure 2.11.4.

Note that

$$\Delta \hat{e}_r = (1 \Delta \theta) \hat{e}_\theta \quad (2.11.7)$$

so

$$\frac{d\hat{e}_r}{dt} = \lim_{\Delta t \rightarrow 0} \frac{\Delta \hat{e}_r}{\Delta t} = \dot{\hat{e}}_r = \dot{\theta} \hat{e}_\theta \quad (2.11.8)$$

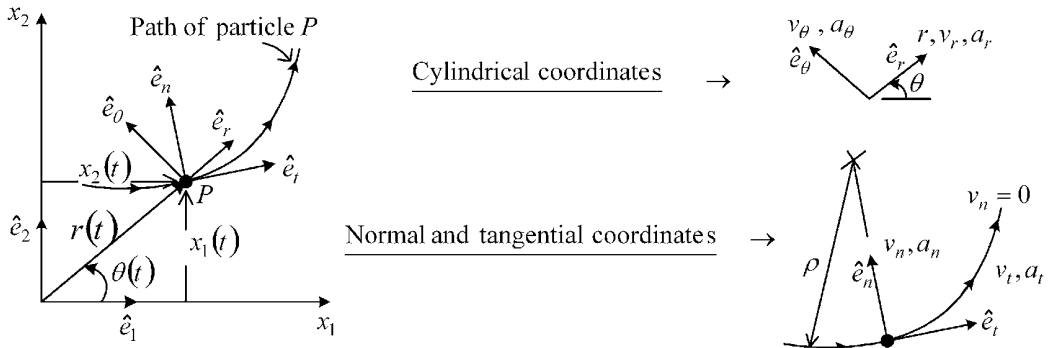


Figure 2.11.3 Cylindrical and normal–tangential coordinates for point motion

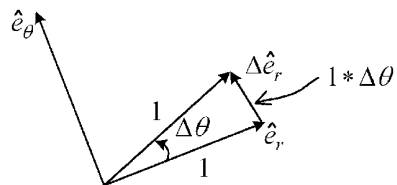


Figure 2.11.4 Cylindrical coordinate unit vectors

Likewise,

$$\frac{d\hat{e}_\theta}{dt} = -\dot{\theta}\hat{e}_r \quad (2.11.9)$$

and therefore

$$\vec{R}_p(t) = r\hat{e}_r \quad (2.11.10)$$

$$\vec{V}_p(t) = \dot{r}\hat{e}_r + r\frac{d}{dt}(\hat{e}_r) = \dot{r}\hat{e}_r + r\dot{\theta}\hat{e}_\theta = V_r\hat{e}_r + V_\theta\hat{e}_\theta \quad (2.11.11)$$

$$\vec{a}_p = \frac{d}{dt}(\vec{V}_p) = a_r\hat{e}_r + a_\theta\hat{e}_\theta = \ddot{r}\hat{e}_r + \dot{r}\dot{\theta}\hat{e}_\theta + r\ddot{\theta}\hat{e}_\theta + r\dot{\theta}\dot{\theta}\hat{e}_r + r\dot{\theta}\dot{\theta}\hat{e}_\theta + r\dot{\theta}\dot{\theta}\hat{e}_\theta \quad (2.11.12)$$

$$\Rightarrow a_r = \ddot{r} - r\dot{\theta}^2, \quad a_\theta = r\ddot{\theta} + 2r\dot{\theta}$$

2.11.1.3 Normal–Tangential Coordinates

The tangential and normal unit vectors vary in direction with time as they follow the path or particle P , although their magnitudes remain equal to one, as shown in Figure 2.11.5.

The parameter S represents distance along the path and the radius of curvature is given by

$$\rho = \frac{\left[1 + \left(\frac{dx_2}{dx_1}\right)^2\right]^{3/2}}{\left|\frac{d^2x_2}{dx_1^2}\right|} \quad (2.11.13)$$

Note that

$$\dot{\hat{e}}_t = \lim_{\Delta t \rightarrow 0} \frac{\Delta \hat{e}_t}{\Delta t} = \frac{(1)\Delta\phi}{\Delta t}\hat{e}_n = \frac{\Delta S/\rho}{\Delta t}\hat{e}_n = \frac{\dot{S}}{\rho}\hat{e}_n \quad (2.11.14)$$

and since

$$v = \dot{S} \quad \text{and} \quad \vec{V}_p = V\hat{e}_t \quad (2.11.15)$$

$$\Rightarrow \vec{a}_p = \dot{V}\hat{e}_t + V\dot{\hat{e}}_t = a_t\hat{e}_t + a_n\hat{e}_n \quad (2.11.16)$$

where

$$a_t = \dot{v}, \quad a_n = \frac{v^2}{\rho} \quad (2.11.17)$$

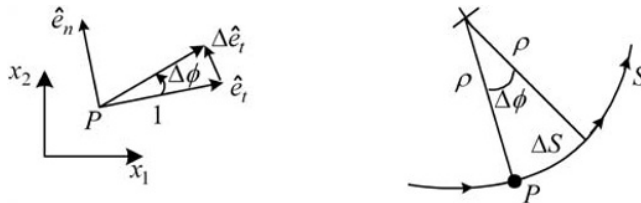


Figure 2.11.5 Normal–tangent unit vectors

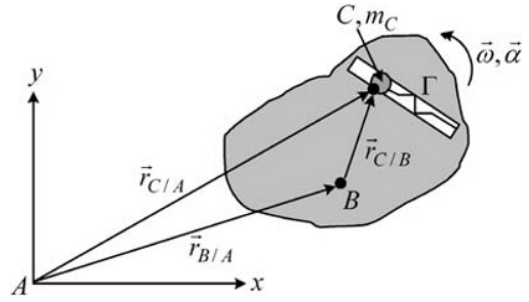


Figure 2.11.6 Point C moving along a path Γ on a rigid body

2.11.2 Rigid Body Kinematic Constraint

The RBM is a zero strain model in which an observer fixed to the body does not sense any relative deflections of the body itself. A point C moves along path Γ on the rigid body shown in Figure 2.11.6

2.11.2.1 Position, Velocity, and Acceleration

The position of C is given by

$$\vec{r}_{C/A} = \vec{r}_{B/A} + \vec{r}_{C/B} \quad (2.11.18)$$

The velocity and acceleration expressions for point C are

$$\vec{V}_C = \vec{V}_B + \vec{V}_{C/B} + \vec{\omega} \times \vec{r}_{C/B} \quad (2.11.19)$$

where

$\vec{\omega}$ = angular velocity of the rigid body

$\vec{V}_{C/B}$ = velocity of C as sensed in a reference frame attached to the rigid body

$$\vec{a}_C = \vec{a}_B + \vec{\alpha} \times \vec{r}_{C/B} + \vec{\omega} \times (\vec{\omega} \times \vec{r}_{C/B}) + 2\vec{\omega} \times \vec{V}_{C/B} + \vec{a}_{C/B} \quad (2.11.20)$$

where

$\vec{a}_{C/B}$ = acceleration of C as sensed in a reference frame attached to the rigid body

$\vec{\alpha} = (d/dt)(\vec{\omega})$ = angular acceleration of the rigid body

2.11.2.2 Transport Theorem

The *transport theorem* is a very useful tool for analyzing motions of masses that vibrate with respect to a rigid body that is itself undergoing general translational and rotational motions as illustrated by mass m_C in Figure 2.11.6. The vector \vec{G} may represent any vector quantity

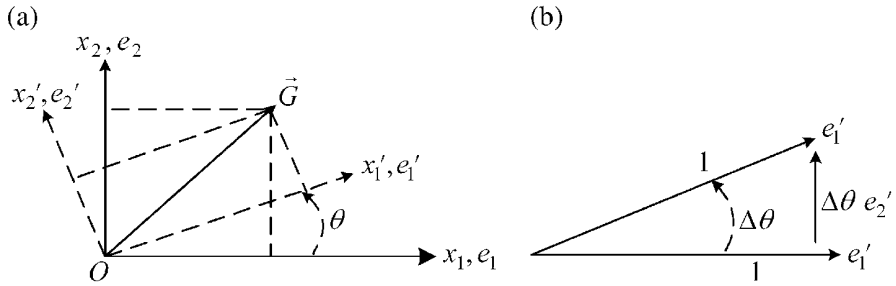


Figure 2.11.7 (a) Vector \vec{G} defined in two reference frames with relative angular velocity $\vec{\omega}$ and (b) infinitesimal rotation of unit vector e'_1

such as position, velocity, force, momentum, and so on and is defined in the primed and unprimed frames in Figure 2.11.7 as

$$\vec{G} = G_1 e_1 + G_2 e_2 \quad (2.11.21)$$

$$\vec{G} = G'_1 e'_1 + G'_2 e'_2 \quad (2.11.22)$$

where e_1, e_2 and e'_1, e'_2 are unit vectors in the unprimed and primed frames, respectively.

The time rate of change of \vec{G} , as sensed by an observer in the $x_1 x_2$ frame, is

$$\frac{d\vec{G}}{dt} = \dot{G}'_1 e'_1 + G'_1 \dot{e}'_1 + \dot{G}'_2 e'_2 + G'_2 \dot{e}'_2 \quad (2.11.23)$$

From Figure 2.11.7(b), it is seen that

$$\dot{e}'_1 = \lim_{\Delta t \rightarrow 0} \frac{\Delta e'_1}{\Delta t} = \lim_{\Delta t \rightarrow 0} \frac{\Delta \theta e'_2}{\Delta t} = \dot{\theta} e'_2 \quad (2.11.24)$$

Similarly

$$\dot{e}'_2 = -\dot{\theta} e'_1 \quad (2.11.25)$$

Substitution of (2.11.24) and (2.11.25) into (2.11.23) yields

$$\frac{d\vec{G}}{dt} = \dot{G}'_1 e'_1 + \dot{G}'_2 e'_2 - \dot{\theta} G'_2 e'_1 + \dot{\theta} G'_1 e'_2 = \dot{G}'_1 e'_1 + \dot{G}'_2 e'_2 + \dot{\theta} e'_3 (G'_1 e'_1 + G'_2 e'_2) \quad (2.11.26)$$

or

Transport Theorem

$${}^{(0)} \frac{d\vec{G}}{dt} = {}^{(0)} \frac{d\vec{G}}{dt} + \vec{\omega} \times \vec{G} \quad (2.11.27)$$

or as expressed in words

The time rate of change of vector \vec{G} as sensed by an observer in the unprimed frame equals

the time rate of change of \vec{G} as sensed by an observer in the primed frame plus

the cross product of the (angular velocity of the primed frame relative to the unprimed frame) with the vector \vec{G} . A consistent set of unit vectors should be employed in this manipulation.

This result is applicable to 3D as well as 2D vectors.

2.11.2.3 Constraints

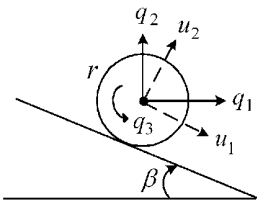
Reduction of dofs in a structural component or system model may result from geometrical constraint considerations. These cases usually involve the implicit assumption of rigidity of one or more components. This is illustrated by the following example:

EXAMPLE 2.11.1 Natural Motion Constraints

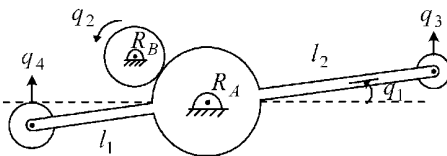
Statement: The following simple systems illustrate how the number of dofs in a model may be reduced by imposing natural constraint conditions.

Objective: Determine the mathematical constraint conditions for the systems in Figure E2.11.1(a).

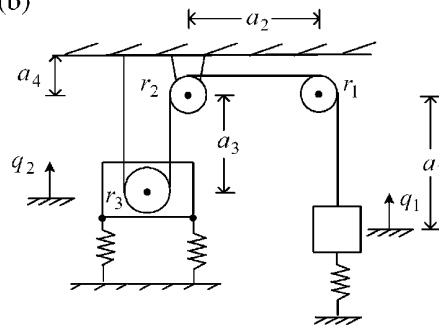
(a)



(c)



(b)



(d)

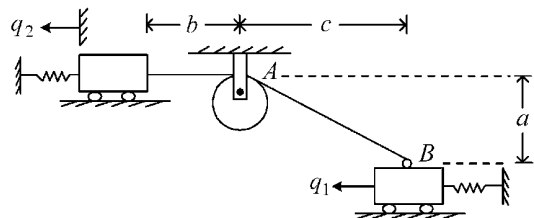


Figure E2.11.1(a) (a–d) Motion constraints in four subsystem models

Motivation: Imposing natural constraint conditions on a system dynamics model, via essential boundary conditions or linear constraint equations, reduces the number of unknowns and ensures kinematic agreement between the model and actual system.

Solution: *System (a)* has 3 dofs, which are interdependent due to the rolling contact condition and to the incline. Application of the coordinate transformation in Equation (2.7.1) yields

$$\begin{Bmatrix} u_1 \\ u_2 \end{Bmatrix} = \begin{bmatrix} \cos\beta & -\sin\beta \\ \sin\beta & \cos\beta \end{bmatrix} \begin{Bmatrix} q_1 \\ q_2 \end{Bmatrix} = \begin{Bmatrix} u_1 \\ 0 \end{Bmatrix} \quad (1)$$

This implies

$$q_1 \sin\beta + q_2 \cos\beta = 0 \Rightarrow q_2 = -\tan\beta q_1 \quad (2)$$

The rolling contact condition and Equation (1) yields

$$u_1 = \cos\beta q_1 - \sin\beta q_2 = -rq_3 \quad (3)$$

$$\Rightarrow q_3 = -\frac{1}{r}(\cos\beta + \sin\beta \tan\beta)q_1 \quad (4)$$

Equations (2) and (4) show that there is only one independent dof in this subsystem.

System (b) has 2 dofs, which are interdependent if the cable is assumed to be inextensible. The springs in this system are pretensioned to prevent the cable from becoming slack. The cable length in the static equilibrium state is

$$l = a_1 + \frac{\pi}{2}r_1 + a_2 + \frac{\pi}{2}r_2 + a_3 + \pi r_3 + a_3 + a_4 \quad (5)$$

and in the displaced state is

$$l = (a_1 - q_1) + \frac{\pi}{2}r_1 + a_2 + \frac{\pi}{2}r_2 + (a_3 - q_2) + \pi r_3 + (a_3 - q_2) + a_4 \quad (6)$$

Equating (5) and (6) yields

$$-q_1 - 2q_2 = 0 \Rightarrow q_2 = -\frac{q_1}{2} \quad (7)$$

which again demonstrates that there is only one independent dof in the subsystem.

System (c) has 4 dofs, which are interdependent due to the gear and lever actions, that is, for small motions

$$q_2 = -\frac{R_A}{R_B}q_1, \quad q_3 = (R_A + l_2)q_1, \quad q_4 = -(R_A + l_2)q_1 \quad (8)$$

System (d) has pretensioned springs and 2 dofs, which are interdependent due to the inextensible cable of length l . At static equilibrium,

$$l = b + (a^2 + c^2)^{1/2} \quad (9)$$

In a displaced state,

$$l = b + q_2 + [(c - q_1)^2 + a^2]^{1/2} \quad (10)$$

Equate (9) and (10) to obtain

$$0 = (a^2 + c^2)^{1/2} - [(c - q_1)^2 + a^2]^{1/2} - q_2 \quad (11)$$

The second term in this equation may be approximated by a two-term Taylor series expansion (2.4.3) for small q_1 values, that is,

$$f(q_1) = f(q_1 = 0) + \left. \frac{\partial f}{\partial q_1} \right|_{q_1=0} q_1 \quad (12)$$

so that

$$\begin{aligned} [(c - q_1)^2 + a^2]^{1/2} &\approx (a^2 + c^2)^{1/2} + \frac{1}{2} [(c - q_1)^2 + a^2]^{-1/2} 2(c - q_1)(-1) \Big|_{q_1=0} q_1 \\ &= (a^2 + c^2)^{1/2} - \frac{cq_1}{(a^2 + c^2)^{1/2}} \end{aligned} \quad (13)$$

Substitute (13) into (11):

$$q_2 \approx \frac{cq_1}{(a^2 + c^2)^{1/2}} = q_1 \cos \alpha \quad (14)$$

where

$$\alpha = \tan^{-1} \left(\frac{a}{c} \right) \quad (15)$$

Summary: These simple examples have shown how model dofs may be reduced by imposing *geometric constraint conditions*. For small motions these constraint conditions could all be expressed by the set of linear constraint conditions

$$\underline{q} = \underline{T}_G \underline{q}_r \quad (16)$$

where the subscript r represents retained dofs. For examples (a)–(d),

$$\underline{q}_r = q_1 \quad (17)$$

and

$$\text{(a)} \quad \underline{q} = \begin{Bmatrix} q_1 \\ q_2 \\ q_3 \end{Bmatrix}, \quad \underline{T}_G = \begin{Bmatrix} 1 \\ -\tan \beta \\ -\frac{1}{r}(\cos \beta + \sin \beta \tan \beta) \end{Bmatrix} \quad (18)$$

$$\text{(b)} \quad \underline{q} = \begin{Bmatrix} q_1 \\ q_2 \end{Bmatrix}, \quad \underline{T}_G = \begin{Bmatrix} 1 \\ -1/2 \end{Bmatrix} \quad (19)$$

$$\text{(c)} \quad \underline{q} = \begin{Bmatrix} q_1 \\ q_2 \\ q_3 \\ q_4 \end{Bmatrix}, \quad \underline{T}_G = \begin{Bmatrix} 1 \\ -R_A/R_B \\ R_A + l_2 \\ -(R_A + l_1) \end{Bmatrix} \quad (20)$$

$$(d) \quad \underline{q} = \begin{Bmatrix} q_1 \\ q_2 \end{Bmatrix}, \quad \underline{T}_G = \begin{Bmatrix} 1 \\ c/(a^2 + c^2)^{1/2} \end{Bmatrix} \quad (21)$$

The above constraints are called scleronomic constraints since they do not contain any explicit function of time t .

EXAMPLE 2.11.2 Hinged Beam–Pulley System

Statement: Figure E2.11.2(a) and E2.11.2(b) depicts a hoist system that is driven by an electric motor. The cable is assumed to be inextensible. Horizontal beam 1 shown is free to rotate about pivot 4. Pulley 2 is free to rotate about pivot 5; however, pulley 3 is fixed against rotation, that is, the motor has a brake applied. Pivot 6 and its support block can only translate vertically, without rotation.

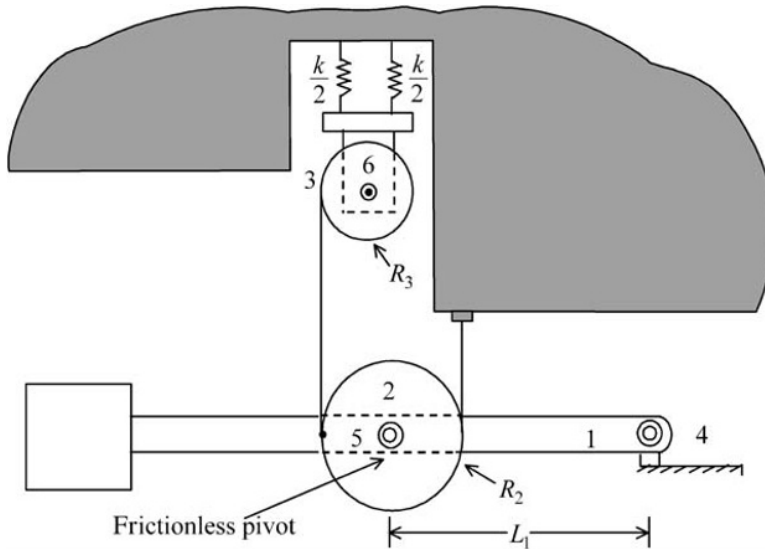


Figure E2.11.2(a) Hoist system model

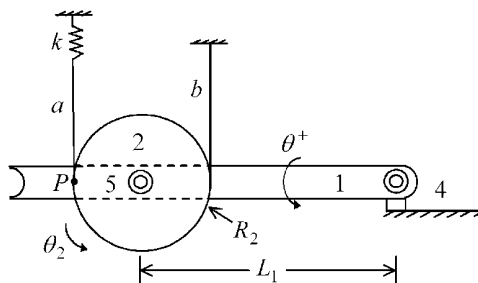


Figure E2.11.2(b) Hoist system—simplified model

Objectives

- (a) Derive an expression for the cable force that results due to a small, static, downward rotation θ of the beam.
- (b) Show the complete derivation and express the answer in terms of θ and the system constants.

Motivation: Understand the importance of the kinematic step for modeling a system in a vibration analysis study.

Solution: Consider the simplified diagram shown below.

Consider pivot 5 as fixed on beam 1. Then the arc that it sweeps through is

$$s_5 = L_1\theta \quad (1)$$

Next consider pulley 2 as “rolling” on cable segment b . Then the distance that “5” traverses is

$$d_5 = R_2\theta_2 \quad (2)$$

for small angles

$$d_5 \approx s_5 \quad (3)$$

so

$$\theta_2 \approx \frac{L_1}{R_2}\theta \quad (4)$$

Again assume that pulley 2 rolls on segment b ; then the downward motion of P may be expressed utilizing (4) as

$$\Delta P = 2R_2\theta_2 = 2L_1\theta \quad (5)$$

So the cable force is

$$F_c = k\Delta P = 2L_1k\theta \quad (6)$$

As will be shown in Chapter 3, the force expression in (6) is required to obtain a statement of dynamic equilibrium for this system utilizing Newton’s law.

2.11.3 Assumed Modes Kinematic Constraint

Chapter 4 shows how the assumed modes method constrains the infinite number of dofs of a flexible structural member to deflect accordingly with the weighted sum of analyst selected displacement patterns that extend over the entire member. For example, the assumed form for the (x_1, x_2, x_3) direction displacements (u_1, u_2, u_3) is

$$\begin{aligned} u_1(x_1, x_2, x_3, t) &= \sum_{i=1}^{N_1} q_{i1}(t) * \phi_{i1}(x_1, x_2, x_3) = \sum_{i=1}^{N_1} u_{i1}(x_1, x_2, x_3) \\ u_2(x_1, x_2, x_3, t) &= \sum_{i=1}^{N_2} q_{i2}(t) * \phi_{i2}(x_1, x_2, x_3) = \sum_{i=1}^{N_2} u_{i2}(x_1, x_2, x_3) \\ u_3(x_1, x_2, x_3, t) &= \sum_{i=1}^{N_3} q_{i3}(t) * \phi_{i3}(x_1, x_2, x_3) = \sum_{i=1}^{N_3} u_{i3}(x_1, x_2, x_3) \end{aligned} \quad (2.11.28)$$

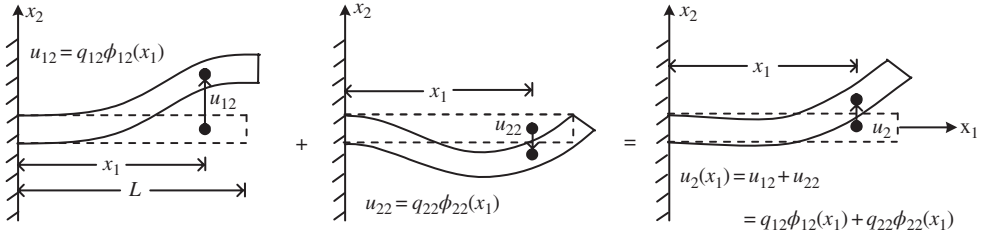


Figure 2.11.8 Approximate deflection of a beam utilizing two global shape functions

where the displacement patterns are ϕ_{ij} and the weighting factors $q_{ij}(t)$ vary with time, are referred to as generalized coordinates, and determine the contribution of any given displacement pattern to the overall displacement field. The ϕ_{ij} are selected by the analyst's intuition and must form a set of linearly independent functions of position. These functions may also form an orthogonal set

$$\int_V \phi_{i1} \phi_{k1} dm \begin{cases} 1, & i \neq k \\ \tilde{m}_i, & i = k \end{cases} \quad (2.11.29)$$

if it is desired to uncouple the generalized coordinate EOMs, where V is the volume of the structural member. Note that ϕ_{ij} are functions only of the coordinates x_1, x_2 , and x_3 and are referred to as "global shape functions" since they are defined over the entire structural member. A simple example of this is the beam deflection shown in Figure 2.11.8.

In this case $\phi_{12}(x_1)$ and $\phi_{22}(x_1)$ are selected to be

$$\phi_{12}(x_1) = \frac{3x_1^2}{L^2} - \frac{2x_1^3}{L^3} \quad (2.11.30)$$

$$\phi_{22}(x_1) = \frac{-x_1^2}{L} + \frac{x_1^3}{L^2} \quad (2.11.31)$$

where

$$u_2(x_1) = q_{12}\phi_{12}(x_1) + q_{22}\phi_{22}(x_1) \quad (2.11.32)$$

Note that

$$\phi_{12}(0) = \phi_{22}(0) = \phi'_{12}(0) = \phi'_{22}(0) = 0 \quad (2.11.33)$$

which by (2.11.32) implies

$$u_2(0) = u'_2(0) = 0 \quad (2.11.34)$$

Since ϕ_{12} and ϕ_{22} satisfy the zero deflection and slope conditions at the wall, they are referred to as "kinematically admissible shape functions." Also since they provide an approximate value of u_2 over the entire member, they are referred to as "global shape functions." Note that the deflection of any point along the beam may be obtained if the two generalized coordinates $q_{12}(t)$ and $q_{22}(t)$ are known. Therefore, it can be said that this model has $N = 2$ independent dofs. As in the case of the rigid body approximation, the effect of the deflection assumption is to reduce the number of dofs from ∞ to a small finite number, $N = 2$ in this example and $N = N_1 + N_2 + N_3$ in general. The assumed modes method uses a global (over the entire body) interpolation approximation. Figure 2.11.9 shows a general 3D body, with point P located by position vector \vec{R}_P .

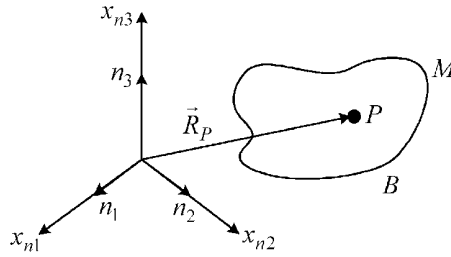


Figure 2.11.9 Point P located by \vec{R}_P on body B

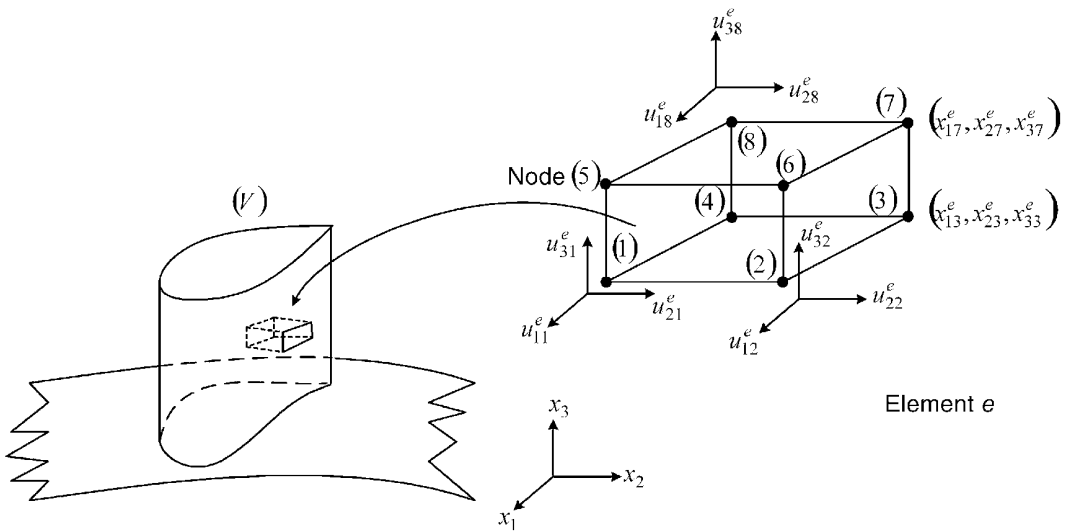


Figure 2.11.10 Blade FE model composed of 8-node, 3-dof/node brick elements

The velocity of P as expressed with the assumed modes approximation is

$$\begin{aligned} \vec{V}_P &= \dot{\vec{R}}_P = \dot{u}_1 n_1 + \dot{u}_2 n_2 + \dot{u}_3 n_3 \\ &= \left\{ \sum_{i=1}^{N_1} \dot{q}_{i1}(t) \phi_{i1}(x_1, x_2, x_3) \right\} n_1 + \left\{ \sum_{i=1}^{N_2} \dot{q}_{i2}(t) \phi_{i2}(x_1, x_2, x_3) \right\} n_2 + \left\{ \sum_{i=1}^{N_3} \dot{q}_{i3}(t) \phi_{i3}(x_1, x_2, x_3) \right\} n_3 \end{aligned} \quad (2.11.35)$$

The form for the velocity field in (2.11.35) facilitates the evaluation of the kinetic energy of the body, which will be utilized to derive the EOMs for the assumed modes generalized coordinates $q_{ij}(t)$, via the Lagrange equation method.

2.11.4 Finite Element Kinematic Constraint

The FEM subdivides a continuous member into a large number of small subvolumes called elements. This is illustrated for a blade model in Figure 2.11.10. The FE method then employs a local (element-based) set of “shape functions” to interpolate displacements

within the element. This is in contrast to the assumed modes approach where the “global” shape function must approximate a likely deflection pattern for the entire member and also satisfy displacement and slope “essential” boundary conditions. Each element possesses a finite set of nodes, and displacements at any nonnodal point positions in the element are obtained by interpolation from the nodal point displacement values. The node point displacements become the model’s coordinates to be solved for. The node point displacements at node k in Figure 2.11.10 are represented by $u_{jk}^e(t)$, where $j = 1, 2, 3$ and $k = 1, 8$.

The displacements at any location (x_1^e, x_2^e, x_3^e) within element e are given by

$$u_j^e(x_1^e, x_2^e, x_3^e, t) = \sum_{k=1}^8 u_{jk}^e(t) N_k^e(x_1^e, x_2^e, x_3^e) \quad j = 1, 2, 3 \quad (2.11.36)$$

The “shape functions” N_k^e are known functions of position, which are selected by the analyst and must satisfy the *shape function consistency condition*

$$N_k^e(x_{1i}^e, x_{2i}^e, x_{3i}^e) = \begin{cases} 1, & i = k \\ 0, & i \neq k \end{cases} \quad (2.11.37)$$

in order for (2.11.36) to yield the nodal point displacements $u_{jk}^e(t)$ when the formula is evaluated at the nodal point coordinates $(x_{1i}^e, x_{2i}^e, x_{3i}^e)$, where index “ i ” indicates node i . From (2.11.36) the deflections at any location within element e can be obtained once the twenty-four nodal displacements in e are known. The nodal displacements u_{jk}^e are the generalized coordinates for the displacements in element e . If the entire blade model has N nodes, there will be $3N$ nodal displacements in the model from which all other displacements in the model may be obtained by the interpolation formula (2.11.36) for each element. The $3N$ generalized coordinates of the model are

$$(q_1, q_2, q_3, \dots, q_{3N}) = (u_{11}, u_{12}, \dots, u_{1N}, u_{21}, u_{22}, \dots, u_{2N}, u_{31}, u_{32}, \dots, u_{3N}) \quad (2.11.38)$$

where u_{ij} is the i direction displacement at node j of the model. These values determine the motions over the entire blade model by (2.11.36). The motion approximation of (2.11.36) constrains the actual deflections to some assumed pattern and reduces the number of dofs from ∞ to a finite number ($n = 3N$). The velocity of some point P in Figure 2.11.10 is given via the FE approximation of (2.11.36) as

$$\frac{{}^n d}{dt} \vec{R}_P = {}^n v_1^e n_1 + {}^n v_2^e n_2 + {}^n v_3^e n_3 \quad (2.11.39)$$

where

$${}^n v_j^e(x_1^e, x_2^e, x_3^e, t) = \frac{{}^n d}{dt} u_j^e(x_1^e, x_2^e, x_3^e, t) = \sum_{k=1}^8 \dot{u}_{jk}^e(t) N_k^e(x_1^e, x_2^e, x_3^e) \quad (2.11.40)$$

and $\dot{u}_{jk}^e(t)$ is the velocity in direction j at node k of element e , as sensed in frame n . The form for the velocity field in (2.11.40) facilitates the evaluation of the kinetic energy of the body, which will be utilized to derive the EOMs for the generalized coordinates in (2.11.38) utilizing the Lagrange equation method.

2.12 DIRAC DELTA AND HEAVISIDE FUNCTIONS

A concentrated (point) force or mass is a mathematical idealization of a physical force or mass distribution. For instance, all forces are applied over finite-sized areas and thus are more accurately considered to be resultants of pressure or traction distributions, as illustrated in Figure 2.12.1.

Pressures and tractions have units of force per area and produce a force(s) when integrated over their areas of application. The Dirac delta function is a special mathematical device that is employed to represent the corresponding pressure, traction, or force per length for an idealized concentrated (point) force. The Dirac delta function has the following special properties:

$$\delta(z-d) = 0, \quad z \neq d \quad (2.12.1)$$

and

$$\int_{-\infty}^{\infty} \delta(z-d) dz = 1 \quad (2.12.2)$$

In view of (2.12.1), (2.12.2) may be written as

$$\int_0^L \delta(z-d) dz = 1 \quad (2.12.3)$$

where $0 < z < L$ is a finite interval that contains $z = d$. Multiply (2.12.3) by $F(t)$, noting that F is not a function of z .

$$\int_0^L F(t) \delta(z-d) dz = F(t) \quad (2.12.4)$$

Therefore, $F(t)\delta(z-d)$ is the force per unit length for the point force $F(t)$ since when integrated from 0 to L it yields $F(t)$. Another important property of the Dirac delta function is

$$\int_0^L f(z) \delta(z-d) dz = f(d) \quad (2.12.5)$$

The Dirac delta function is utilized with the assumed modes method in Chapter 4, the FEM in Chapter 9, and the AVC in Chapter 12. An important Dirac delta function identity utilized in Chapter 12 for piezoelectric AVC is

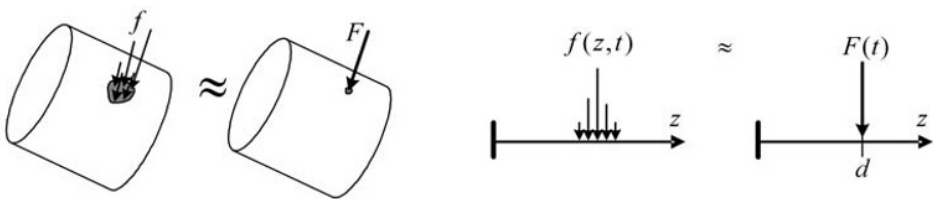


Figure 2.12.1 Actual force distributions and their concentrated (point) representation

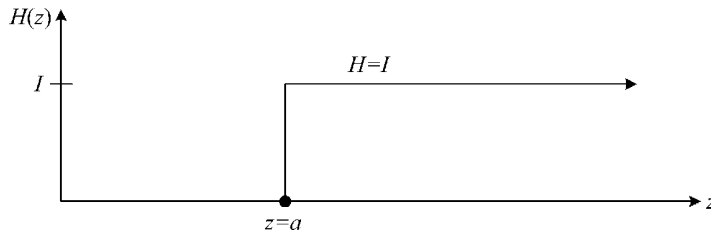


Figure 2.12.2 Heaviside function $H(z - a)$ with argument $z = a$

$$\int_{-\infty}^{\infty} f(z) \frac{d}{dz} \delta(z-a) dz = -\left. \frac{df}{dz} \right|_{z=a} \quad (2.12.6)$$

The Dirac delta function is the derivative of the Heaviside function H , which is shown in Figure 2.12.2. The Heaviside function is utilized for transient response analysis in Chapter 6 and in AVC in Chapter 12.

2.13 CHAPTER 2 EXERCISES

2.13.1 Exercise Location

All exercises may be conveniently viewed and downloaded at the following website: **www.wiley.com/go/palazzolo**. This new feature greatly reduces the length of the printed book, yielding significant cost savings for the college student, and is updated.

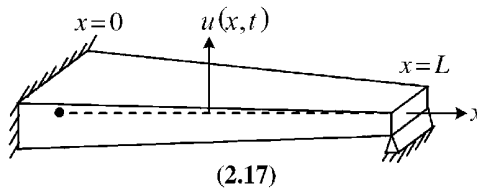
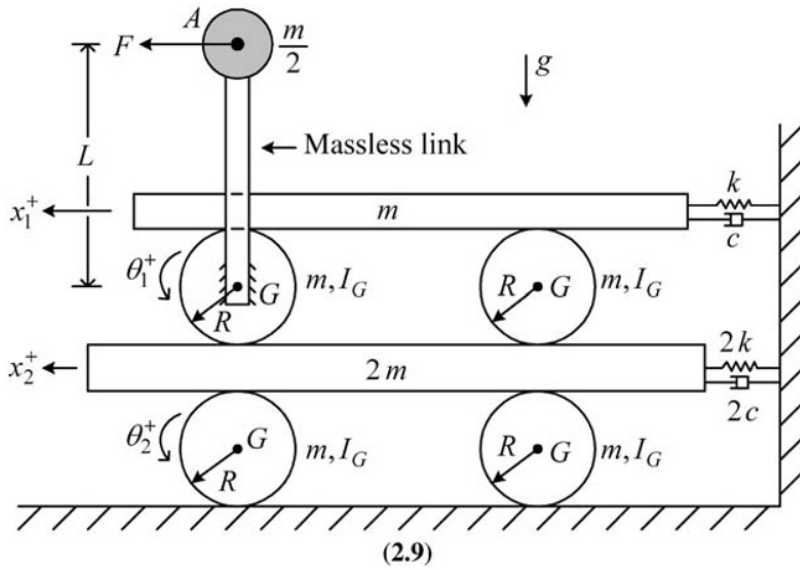
2.13.2 Exercise Goals

The goal of the exercises in Chapter 2 is to strengthen the student's understanding and related engineering problem-solving skills in the following areas:

- (a) Areas of math that are frequently used for vibration analysis and measurements.
- (b) Identification of kinematic constraint conditions in order to remove redundancy in the description of a system's motion and determine a set of independent coordinates.
- (c) Utilize linearization to approximate nonlinear forces when considered for small motions about an OP, thus making the problems solvable within the vast framework of linear differential equations.
- (d) Extend the concept of kinematic constraints in (b) to include motions of deformable objects via the assumed modes and the finite element FEM methods.

2.13.3 Sample Exercises: 2.9 and 2.17

Although the system in (2.9) appears to have many dofs, the student is tasked to demonstrate that only two are independent. Likewise, the deformable beam in (2.17) has an infinite number of dofs; however, the student is tasked to formulate an approximate model with just three generalized coordinates using the assumed modes approach.



REFERENCES

HILDEBRAND, F. B. *Advanced Calculus for Applications*. 2nd ed. Prentice Hall, Englewood Cliffs, NJ, 1976.
 KREYZIG, E. *Advanced Engineering Mathematics*. John Wiley & Sons, Inc., New York, 1972.

Chapter 3

Equations of Motion by Newton's Laws

3.1 INTRODUCTION

The governing equations of motion (EOMs) provide a bridge between modeling and vibration response simulation (Figure 3.1.1). Solution of the EOM provides natural frequencies, mode shapes, stability, steady-state harmonic, and transient responses. Computational tools such as MATLAB and MAPLE greatly facilitate solution of the EOM whether in numerical form or symbolic form. EOMs are derived from Newton's laws in this chapter and by energy and variational approaches in Chapter 4. The impulse–momentum principle is discussed and follows from integration of Newton's law for an aggregate of moving particles. The result provides a convenient way to write EOMs for system which gain or lose mass and for providing initial conditions for impact problems. The usage of a symbolic math code is demonstrated for reducing the workload and improving the accuracy in deriving EOM.

3.2 PARTICLE MOTION APPROXIMATION

The motions of many objects may be accurately modeled as a “particle.” The key assumptions for utilizing this approximation are that the body is rigid and rotational inertia effects are negligible. Figure 3.2.1 shows three examples of “particle” motion.

These particles are acted on by the forces shown in the free body diagrams (FBD) of Figure 3.2.2.

Newton's law states in each of these cases

$$m\vec{a} = \sum \vec{F}_{\text{ext},i} \quad (3.2.1)$$

where \vec{a} is the particle's acceleration vector and $\vec{F}_{\text{ext},i}$ is the i th external force acting on the particle. Therefore, for Figure 3.2.2(a)

$$ma_1 = -F_{\text{drag}} + F_{WR} \quad (3.2.2)$$

and for Figure 3.2.2(b)

$$ma_{x1} = R_{x1}, \quad ma_{x2} = R_{x2}, \quad m \cdot 0 = R_{x3} - W \quad (3.2.3)$$

and for Figure 3.2.2(c)

$$ma_{x1} = F_{\text{drag}x1}, \quad ma_{x2} = F_{\text{drag}x2}, \quad ma_{x3} = -W + F_{\text{drag}x3} \quad (3.2.4)$$

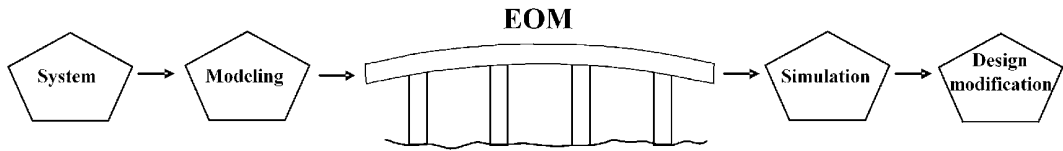


Figure 3.1.1 EOM bridges system modeling and vibration response simulation

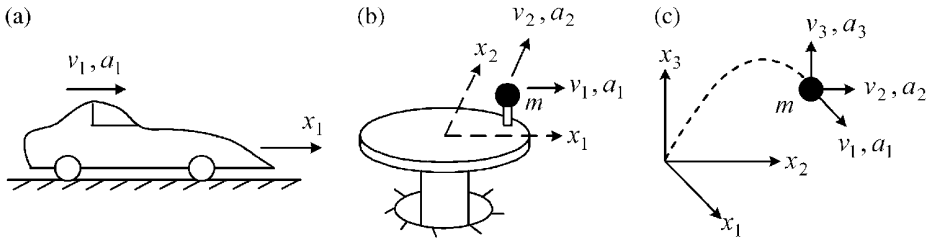


Figure 3.2.1 (a–c) Three examples of particle motion approximation

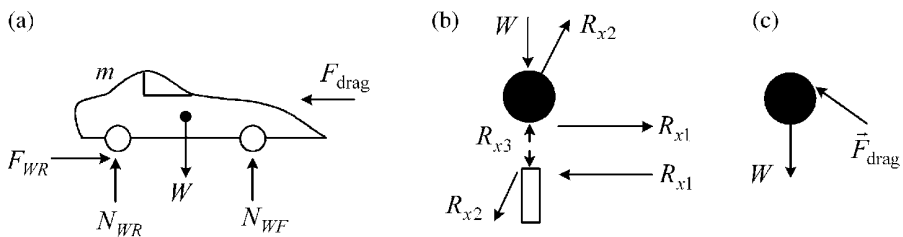


Figure 3.2.2 (a–c) Free body diagrams (FBDs) of particles in Figure 3.2.1

The motions $x_j(t)$ and $v_j(t)$ are obtained by solving the above differential equations given expressions for all forces.

EXAMPLE 3.2.1 Jet Landing on Aircraft Carrier

Statement: A jet lands on a carrier deck and is quickly decelerated by a constant friction braking force F_B and a tailhook device which utilizes a hydraulic cylinder and cable mechanism. The tailhook device is represented by a simplified model consisting of a spring and damping force

$$F_k = -k_1x - k_3x^3 - c\dot{x} \quad (1)$$

as shown in Figure E3.2.1(a). The cubic spring stiffness term is used to provide a hardening effect that is small for small deflections but increases rapidly for large deflections. This lowers the deceleration effect on the pilot yet still performs the function of stopping the plane.

Objective: Derive two first-order differential equations that govern the landing dynamics.

Motivation: This problem represents a classic engineering design trade between minimizing the landing distance and minimizing the acceleration ($|\ddot{x}|$) loading on the jet structure (and its occupants!). The solution can provide useful quantities such as the maximum deceleration and stopping distance for various values of F_B and k . In practice, F_B becomes zero as the jet slows to a stop and the jet is secured by some mechanical means.

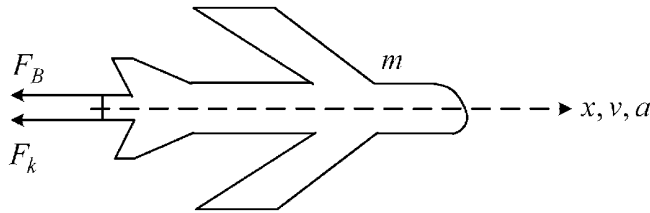


Figure E3.2.1(a) Jet landing on carrier deck

Solution: By Newton's law,

$$ma = m\ddot{x} = -F_B - c\dot{x} - k_1x - k_3x^3 \quad (2)$$

The two first-order (state) equations are

$$\dot{x} = v, \quad \dot{v} = -\frac{F_B}{m} - \frac{c}{m}v - \frac{k_1}{m}x - \frac{k_3}{m}x^3 \quad (3)$$

These equations can be solved given initial conditions $x_0 = 0$ and v_0 .

EXAMPLE 3.2.2 Engine on Nonlinear Isolation Mounts

Description: Vehicle and industrial engines are commonly “soft” supported on rubber isolation mounts to attenuate the transmission of forces originating in the engine to the surrounding environment. These mounts may be filled with liquid that circulates through internal orifices and passages to provide low- and high-frequency attenuation of forces as discussed in Kim and Singh (1995). Figure E3.2.2(a) illustrates a simplified model of a soft mounted engine subjected to input (chassis) motion $y(t)$ and crankshaft/piston unbalanced loads $F(t)$. The nonlinear stiffness characteristic of the isolation mount is expressed by

$$F_k = -\left[k_1(x-y) + k_3(x-y)^3\right] \quad (1)$$

Objective:

- Derive the equation of motion for this system by the Newton approach.
- Linearize (Section 2.4) the nonlinear EOM about the static deflection position x_s to obtain the linearized EOM for the displacement perturbation

$$\delta_x(t) = x - x_s \quad (2)$$

where x_s is the static deflection due only to the engine weight W , that is, $F(t) = y(t) = 0$.

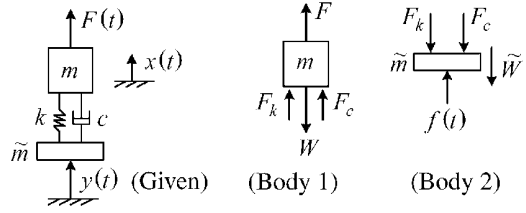
Motivation: Ride quality based on minimum noise and vibration sells. The EOM can be used to determine and hopefully reduce forces transmitted to the chassis from the engine.

Solution: The coordinate reference here at $x=0$ corresponds to the undeflected isolation mount, that is, without weight W , force $F(t)$, or support input $y(t)$ applied.

- From the free body diagrams (FBD),

$$\begin{aligned} + \uparrow \text{Engine} \quad m\ddot{x} &= F + F_k + F_c - W \\ &= F - k_1(x-y) - k_3(x-y)^3 - c(\dot{x}-\dot{y}) - W \end{aligned} \quad (3)$$

Figure E3.2.2(a) Soft mounted engine with support input motion



(b) Consider the static equilibrium case with $(\dot{x} = \ddot{x} = F = y = 0)$. Then (3) becomes

$$0 = -k_1 x_s - k_3 x_s^3 - W \quad (4)$$

This is a cubic algebraic equation which can be easily solved by MATLAB, MAPLE, MATHCAD, and so on for the static deflection x_s . The nonlinear term in (3) is Q^3 where

$$Q = x - y \quad (5)$$

which can be approximated by a two-term Taylor series expansion (2.4.1) about

$$Q_s = x_s - y_s = x_s \quad (6)$$

that is,

$$Q^3 \approx Q_s^3 + \frac{\partial Q^3}{\partial Q} \Big|_{Q_s} (Q - Q_s) = Q_s^3 + 3Q_s^2 (Q - Q_s) \quad (7)$$

Insert (5)–(7) and

$$x = x_s + \delta_x(t) \quad (8)$$

into (3) to obtain

$$m(\ddot{x}_s + \ddot{\delta}_x) = F - k_1(x_s + \delta_x - y) - k_3[x_s^3 + 3x_s^2(x_s + \delta_x - y - x_s)] - c(\dot{x}_s + \dot{\delta}_x - \dot{y}) - W \quad (9)$$

Simplifying (9) by substituting (4) and

$$\dot{x}_s = \ddot{x}_s = 0 \quad (10)$$

since x_s is a constant to obtain

$$m\ddot{\delta}_x = F - k_1(\delta_x - y) - 3k_3x_s^2(\delta_x - y) - c(\dot{\delta}_x - \dot{y}) \quad (11)$$

or

$$m\ddot{\delta}_x + c\dot{\delta}_x + (k_1 + 3k_3x_s^2)\delta_x = F(t) + (k_1 + 3k_3x_s^2)y + c\dot{y} \quad (12)$$

The final EOM (12) for the perturbation δ_x of x about x_s is a linear EOM as compared with (3) which is nonlinear in x . This provides an EOM from which approximate responses may be readily solved for. The approximation is only valid for small motions about the statically deflected position.

3.3 PLANAR (2D) RIGID BODY MOTION APPROXIMATION

Consider a rigid body moving in the x_1, x_2 plane as shown in Figure 3.3.1.

3.3.1 Translational Equations of Motion

This body may represent a part in a machine, or an entire machine or structure. Let n represent an inertial reference frame (fixed, or translating with constant velocity without rotation) and dm a differential mass within the body. The forces on dm can be of an external type ($d\bar{F}$), that is, from tractions, pressures, gravity, magnetic fields, and so on, or an internal type ($d\bar{f}$), that is, from interaction with neighboring dm . The $d\bar{f}$ are assumed to satisfy Newton's third law of equal and opposite reactions, and point G represents the instantaneous location of the mass center. From Newton's second law for particle kinetics,

$$dm \frac{{}^n d^2}{dt^2} \bar{R} = d\bar{f} + d\bar{F} \quad (3.3.1)$$

or

$$dm \frac{{}^n d^2}{dt^2} (\bar{R}_G + \bar{q}) = d\bar{f} + d\bar{F} \quad (3.3.2)$$

Integrate this equation over the body to obtain

$$m \frac{{}^n d^2}{dt^2} \bar{R}_G + \int_B \frac{{}^n d^2 q}{dt} dm = \int_B d\bar{f} + \int_B d\bar{F} \quad (3.3.3)$$

where m is the total mass of body B . The second integral in this expression may be written as

$$\frac{{}^n d^2}{dt^2} \left(\int_B q dm \right) = \frac{{}^n d^2}{dt^2} (0) = 0 \quad (3.3.4)$$

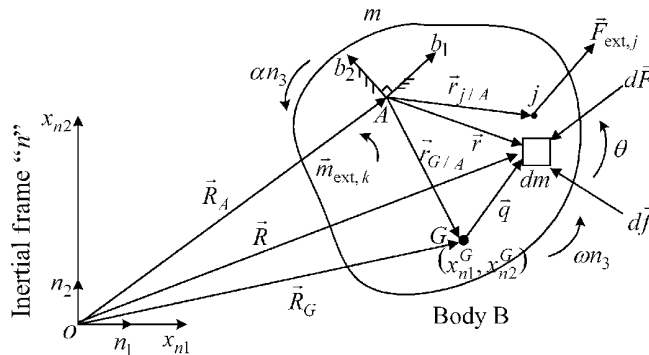


Figure 3.3.1 Illustration of general shaped rigid body for 2D kinetic analysis

by definition of the mass center and by virtue of the invariance of the integration domain, that is, a rigid body. The third integral in (3.3.3) is zero if all internal interaction forces satisfy Newton's third law. The fourth integral is the resultant (\vec{F}_{ext}) of all external forces acting on the body. Then (3.3.3) reduces to:

2D Translational Equation of Motion (TEOM)

$$m\vec{a}_G = \vec{F}_{\text{ext}} \quad (3.3.5)$$

where

$$\begin{aligned} m &= \text{mass of body } B \\ \vec{F}_{\text{ext}} &= \text{resultant of all external forces acting on body } B = F_{\text{ext}1}n_1 + F_{\text{ext}2}n_2 \end{aligned} \quad (3.3.6)$$

and

$$\begin{aligned} \vec{a}_G &= \frac{{}^n d^2}{dt^2} \vec{R}_G = \text{acceleration of mass center } G, \text{ in inertial frame } n \\ &= \frac{{}^n d^2}{dt^2} (x_{n1}^G n_1 + x_{n2}^G n_2) = \ddot{x}_{n1}^G n_1 + \ddot{x}_{n2}^G n_2 \end{aligned} \quad (3.3.7)$$

3.3.2 Rotational Equation of Motion

Define the “angular momentum vector” of body B relative to moment point A and sensed in frame n as

$${}^n \vec{H}^{B/A} = \int_B \vec{r} \times \left(dm \frac{{}^n d\vec{r}}{dt} \right) \quad (3.3.8)$$

Let (b_1, b_2) be the unit vectors of a reference frame that is fixed to the body and has its origin at A , as shown in Figure 3.3.1. Then $\vec{\omega}_{b/n}$ is the angular velocity of body B relative to inertial frame n . Apply the transport theorem (2.11.27) to the derivative term in (3.3.8)

$$\frac{{}^n d}{dt} \vec{r} = \frac{{}^b d}{dt} \vec{r} + \vec{\omega}_{b/n} \times \vec{r} \quad (3.3.9)$$

If B is a “rigid” body

$$\frac{{}^b d}{dt} \vec{r} = 0 \quad (3.3.10)$$

substitute (3.3.10) and (3.3.9) into (3.3.8) to obtain

$${}^n \vec{H}^{B/A} = \int_B \vec{r} \times \left(\vec{\omega}_{b/n} \times \vec{r} \right) dm \quad (3.3.11)$$

Apply the cross product formula

$$\vec{g} \times (\vec{c} \times \vec{d}) = (\vec{g} \cdot \vec{d}) \vec{c} - (\vec{g} \cdot \vec{c}) \vec{d} \quad (3.3.12)$$

to the integrand in (3.3.11) to obtain

$$\vec{r} \times (\vec{\omega}_{b/n} \times \vec{r}) = (\vec{r} \cdot \vec{r}) \vec{\omega}_{b/n} - (\vec{r} \cdot \vec{\omega}_{b/n}) \vec{r} \quad (3.3.13)$$

For 2D motion, \vec{r} is perpendicular to $\vec{\omega}_{b/n}$ so (3.3.13) reduces to

$$\vec{r} \times (\vec{\omega}_{b/n} \times \vec{r}) = r^2 \vec{\omega}_{n_3} \quad (3.3.14)$$

Substitution of (3.3.14) into (3.3.11) yields

$${}^n \vec{H}^{B/A} = I_A \vec{\omega} \quad (3.3.15)$$

where

$$I_A = \int_B r^2 dm = \text{mass moment of inertia of body } B \text{ about point } A \text{ on } B \quad (3.3.16)$$

$$\vec{\omega} = \omega n_3 = \dot{\theta} n_3 = \text{angular velocity of } B \text{ relative to inertial frame } n \quad (3.3.17)$$

In order to derive the rotational equation of motion (REOM or Euler's equation), take the time derivative in frame n of Equation (3.3.8):

$$\frac{{}^n d}{{}^n dt} {}^n \vec{H}^{B/A} = \frac{{}^n d}{{}^n dt} \int_B \vec{r} \times \frac{{}^n d}{{}^n dt} \vec{r} dm = \int_B \left(\frac{{}^n d}{{}^n dt} \vec{r} \times \frac{{}^n d}{{}^n dt} \vec{r} + \vec{r} \times \frac{{}^n d^2}{{}^n dt^2} \vec{r} \right) dm \quad (3.3.18)$$

The first term in the integrand is zero ($\vec{a} \times \vec{a} = 0$, for any \vec{a}), and use Figure 3.3.1 to obtain

$$\frac{{}^n d}{{}^n dt} {}^n \vec{H}^{B/A} = \int_B \vec{r} \times \left(\frac{{}^n d^2}{{}^n dt^2} \vec{R} - \frac{{}^n d^2}{{}^n dt^2} \vec{R}_A \right) dm \quad (3.3.19)$$

Substitute (3.3.1) and use the vector relation $a \times b = -b \times a$ to obtain

$$\frac{{}^n d}{{}^n dt} {}^n \vec{H}^{B/A} = \int_B \vec{r} \times (d\vec{f} + d\vec{F}) + \frac{{}^n d^2}{{}^n dt^2} \vec{R}_A \times \int_B \vec{r} dm \quad (3.3.20)$$

The first integral vanishes since neighboring dm have the same \vec{r} and equal and opposite $d\vec{f}$ or because $d\vec{f}$ is parallel to the relative position vector connecting neighboring dm . The second integral is the total moment acting on body B , as taken about point A . This includes all contributions from external forces and torques:

$$\begin{aligned} \vec{\Gamma}_A &= \int_B \vec{r} \times d\vec{F} \\ &= \text{resultant moment of all external forces and torques} \\ &\quad \text{acting on body } B, \text{ taken about point } A \end{aligned} \quad (3.3.21)$$

Finally, the third integral in (3.3.20) may be written according to Figure 3.3.1 as

$$\frac{{}^n d^2}{dt^2} \vec{R}_A \times \int_B (\vec{r}_{G/A} + \vec{q}) dm \quad (3.3.22)$$

$$\int_B \vec{q} dm = 0 \quad (3.3.23)$$

yielding

$$\frac{{}^n d^2}{dt^2} \vec{R}_A \times \vec{r}_{G/A} m \quad (3.3.24)$$

Collecting results into (3.3.20) yields

$$\frac{{}^n d}{dt} \left({}^n \vec{H}^{B/A} \right) = \vec{\Gamma}_A - \vec{r}_{G/A} \times m \frac{{}^n d^2}{dt^2} \vec{R}_A \quad (3.3.25)$$

Summarizing:

2D Rotational Equation of Motion—Form 1 (2D REOM-1)

$$I_A \vec{\alpha} + \vec{r}_{G/A} \times m \vec{a}_A = \vec{\Gamma}_A \quad (3.3.26)$$

where

$$I_A = I_{33}^{B/b} = \int_B r^2 dm = \text{mass moment of inertia of body } B \text{ about axis } n_3, \quad (3.3.27)$$

passing through point A

$$\vec{\alpha} = \ddot{\theta}_1 n_3 \quad (3.3.28)$$

$$\Gamma_A = \text{resultant moment of all external forces and torques acting on body } B, \quad (3.3.29)$$

taken about point A

$$\vec{a}_A = \frac{{}^n d^2}{dt^2} (\vec{R}_A) = \text{acceleration of point } A, \text{ as sensed in inertial frame } n \quad (3.3.30)$$

A second, common form for the 2D REOM is obtained as follows:

By the parallel axis theorem:

$$I_A = I_G + m r_{G/A}^2 \quad (3.3.31)$$

and from 2D rigid body kinematics:

$$\vec{a}_G = \vec{a}_A + \vec{\alpha} \times \vec{r}_{G/A} + \vec{\omega} \times (\vec{\omega} \times \vec{r}_{G/A}) \quad (3.3.32)$$

Insert (3.3.31) and (3.3.32) into (3.3.26) to obtain

$$(I_G + m r_{G/A}^2) \vec{\alpha} + m \vec{r}_{G/A} \times [\vec{a}_G - \vec{\alpha} \times \vec{r}_{G/A} - \vec{\omega} \times (\vec{\omega} \times \vec{r}_{G/A})] = \vec{\Gamma}_A \quad (3.3.33)$$

Utilize the following vector identity:

$$\vec{r}_{G/A} \times (\vec{\alpha} \times \vec{r}_{G/A}) = r_{G/A}^2 \vec{\alpha} - (\vec{r}_{G/A} \cdot \vec{\alpha}) \vec{r}_{G/A} \quad (3.3.34)$$

The second term on the RHS is zero since $\vec{r}_{G/A}$ and $\vec{\alpha}$ are perpendicular. Therefore,

$$\vec{r}_{G/A} \times (\vec{\alpha} \times \vec{r}_{G/A}) = r_{G/A}^2 \vec{\alpha} \quad (3.3.35)$$

Utilize the vector identity:

$$\vec{r}_{G/A} \times [\vec{\omega} \times (\vec{\omega} \times \vec{r}_{G/A})] = \vec{r}_{G/A} \times [(\vec{\omega} \cdot \vec{r}_{G/A}) \vec{\omega} - (\vec{\omega} \cdot \vec{\omega}) \vec{r}_{G/A}] \quad (3.3.36)$$

The first term on the RHS is zero since $\vec{r}_{G/A}$ and $\vec{\omega}$ are perpendicular, and the second term on the RHS is zero since $\vec{\omega} \times \vec{\omega} = 0$, for all $\vec{\omega}$. Therefore,

$$\vec{r}_{G/A} \times [\vec{\omega} \times (\vec{\omega} \times \vec{r}_{G/A})] = 0 \quad (3.3.37)$$

Substitution of (3.3.35) and (3.3.37) into (3.3.33) yields

$$I_G \vec{\alpha} + m r_{G/A}^2 \vec{\alpha} + \vec{r}_{G/A} \times (m \vec{a}_G) - m r_{G/A}^2 \vec{\alpha} = \vec{\Gamma}_A \quad (3.3.38)$$

Summarizing:

2D REOM—Form 2

$$I_G \vec{\alpha} + \vec{r}_{G/A} \times (m \vec{a}_G) = \vec{\Gamma}_A \quad (3.3.39)$$

where

$$I_G = \int_B q^2 dm = \text{mass moment of inertia of body } B \text{ about axis } n_3, \quad (3.3.40)$$

passing through its mass center G

$$\vec{\alpha} = \ddot{\theta}_1 n_3 \quad (3.3.41)$$

$$\vec{\Gamma}_A = \text{resultant moment of all external forces and torques acting on body } B, \quad (3.3.42)$$

taken about point A

$$\vec{a}_G = \frac{d^2}{dt^2} \vec{R}_G = \text{acceleration of point } G, \text{ as sensed in inertial frame } n \quad (3.3.43)$$

A third form of the 2D REOM is obtained by substituting (3.3.5) into (3.3.39):

2D REOM—Form 3

$$I_G \vec{\alpha} + \vec{r}_{G/A} \times \vec{F}_{\text{ext}} = \vec{\Gamma}_A \quad (3.3.44)$$

where

$$\vec{F}_{\text{ext}} = \text{resultant of all external forces acting on body } B \quad (3.3.45)$$

Inspection of REOM—Forms I, II, and III shows:

2D REOM—IV

$$I_A \ddot{\alpha} = \ddot{\Gamma}_A \quad (3.3.46)$$

if any of the following conditions are satisfied

1. Base point A is located at the mass center G .
2. Base point A is fixed or moving with a constant velocity vector as sensed in inertia frame n .

$$3. \vec{r}_{G/A} \text{ and } \frac{d^2}{dt^2} (\vec{R}_A) \text{ are always parallel.} \quad (3.3.47)$$

EXAMPLE 3.3.1 Resonant Vibrator for Compound Potting

Description: Various compounds are employed for potting components. These compounds flow more readily when vibrated with a high amplitude and frequency, providing an example of a “good vibration.” Figure E3.3.1(a) depicts a specialized device for vibrating parts (m_Q)

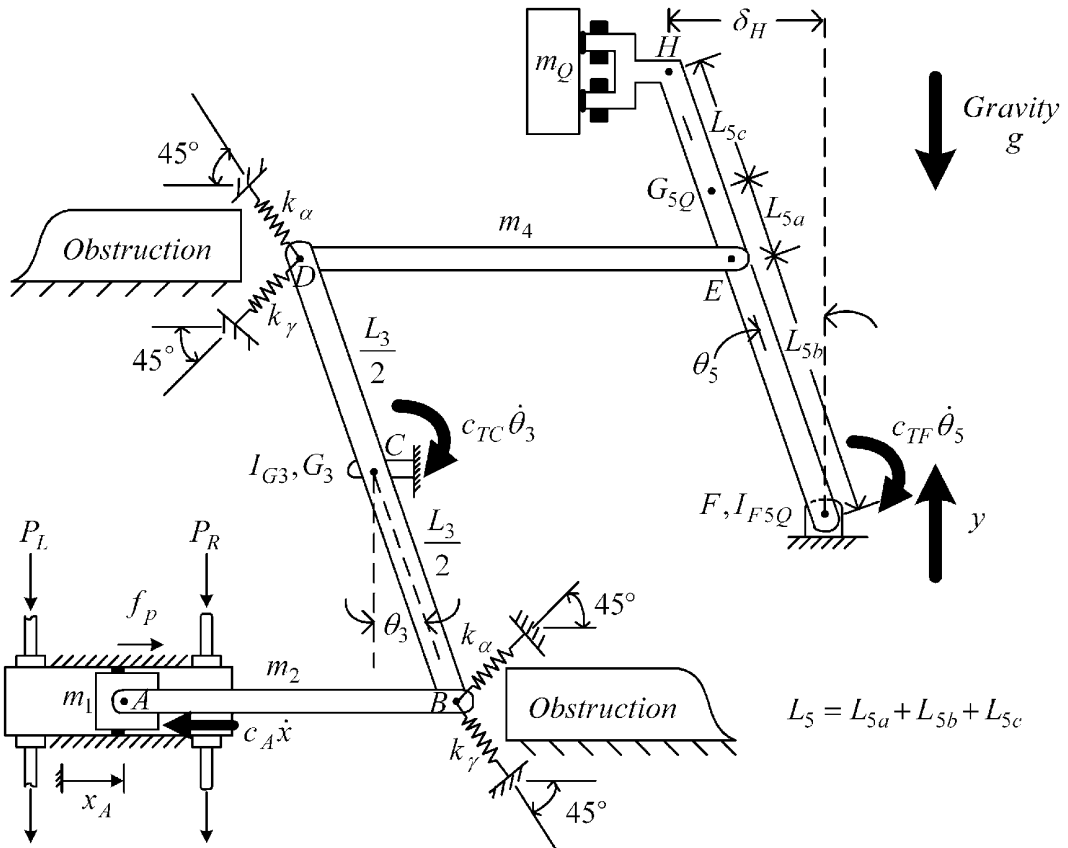


Figure E3.3.1(a) Resonant vibrator mechanism

that are being filled with potting compound. The container that is intentionally vibrated has mass m_Q and is held by arm FH using an electromagnetic. The mechanism is powered by the double-acting hydraulic piston—cylinder which produces the force $f_p(t)$ at A . Springs at B and D are installed to place the mechanism's natural frequency at 100 Hz. This frequency has been experimentally determined to be an optimal shaking frequency for the potting process. The alternating force f_p is operated near this frequency to drive the system into resonance, thereby yielding the highest vibration amplitudes at H . The shape of the mechanism results from accommodating obstructions that exist in the manufacturing facility. The springs are seen to be installed at 45° to the horizontal to avoid existing obstructions to the machine. Pivots C and F are assumed to produce drag (friction) torques proportional to their angular velocities.

Objective:

- (a) Derive the equation of motion (EOM) for this system by the Newton/Euler approach.
- (b) Determine an expression for the power required to drive this mechanism.

Motivation: The EOM provides a means to simulate the mechanism to obtain:

- (a) Power requirements, bearing loads, and motion amplitudes at H

Assumptions:

- (a) Small angular motions, Rods AB and DE , remain horizontal, all joints are ideal (zero rattle space), and Rods AB and DE are light in weight, so $m_2 = m_4 = 0$.
- (b) At static equilibrium,

$$x_A = \theta_3 = \theta_5 = 0 \quad (1)$$

Solution:

Stiffness Transformations

As shown in Figure E3.3.1(a), the springs are oriented at 45° to avoid obstructions in the machine. The effective stiffness in the x and y directions may be determined by considering Figure E3.3.1(b).

From this figure, it is seen that

$$\begin{Bmatrix} F_{x'} \\ F_{y'} \end{Bmatrix} = \begin{bmatrix} k_\beta & 0 \\ 0 & 0 \end{bmatrix} \begin{Bmatrix} x' \\ y' \end{Bmatrix} \quad (2)$$

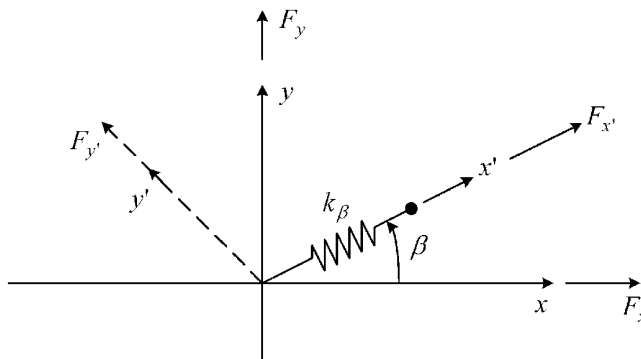


Figure E3.3.1(b) Transformation of stiffness in rotated frames

or

$$\underline{F}' = \underline{k}' \underline{x}' \quad (3)$$

The coordinate transformation for this case is (Eq. 2.7.1)

$$\begin{Bmatrix} x' \\ y' \end{Bmatrix} = \begin{bmatrix} \cos\beta & \sin\beta \\ -\sin\beta & \cos\beta \end{bmatrix} \begin{Bmatrix} x \\ y \end{Bmatrix} \quad (4)$$

or

$$\underline{x}' = \underline{c} \underline{x} \quad (5)$$

Similarly,

$$\underline{F}' = \underline{c} \underline{F} \quad (6)$$

where

$$\underline{F} = \begin{Bmatrix} F_x \\ F_y \end{Bmatrix} \quad (7)$$

Substitute (5) into (3) and premultiply by \underline{c}^T to obtain

$$\underline{c}^T \underline{F}' = \underline{c}^T \underline{k}' \underline{c} \underline{x} \quad (8)$$

$$\Rightarrow \underline{F} = \underline{k} \underline{x} \quad (9)$$

where

$$\underline{k} = \underline{c}^T \underline{k}' \underline{c} \quad (10)$$

$$\begin{bmatrix} \cos\beta & -\sin\beta \\ \sin\beta & \cos\beta \end{bmatrix} \begin{bmatrix} k_\beta \cos\beta & k_\beta \sin\beta \\ 0 & 0 \end{bmatrix} = \begin{bmatrix} k_\beta \cos^2\beta & k_\beta \cos\beta \sin\beta \\ k_\beta \cos\beta \sin\beta & k_\beta \sin^2\beta \end{bmatrix} \quad (11)$$

In general, if n_{spr} springs are attached at angles $\beta_1, \beta_2, \dots, \beta_{n_{\text{spr}}}$, the following relation holds:

$$\underline{k} = \sum_{i=1}^{n_{\text{spr}}} k_{\beta_i} \begin{bmatrix} \cos^2\beta_i & \cos\beta_i \sin\beta_i \\ \cos\beta_i \sin\beta_i & \sin^2\beta_i \end{bmatrix} = \begin{bmatrix} k_{xx} & k_{xy} \\ k_{xy} & k_{yy} \end{bmatrix} \quad (12)$$

where

$$\begin{Bmatrix} F_x \\ F_y \end{Bmatrix} = \underline{k} \begin{Bmatrix} x \\ y \end{Bmatrix} \quad (13)$$

For the small angle assumption, y_B and y_D are both approximately zero. Therefore, (12) and (13) imply

$$F_{Bx}^k = [k_\gamma \cos^2(315^\circ) + k_\alpha \cos^2(45^\circ)]x = \frac{1}{2}(k_\alpha + k_\gamma)x \quad (14)$$

$$F_{By}^k = [k_\gamma \sin(315^\circ)\cos(315^\circ) + k_\alpha \sin(45^\circ)\cos(45^\circ)]x = \frac{1}{2}(k_\alpha - k_\gamma)x \quad (15)$$

Similarly,

$$F_{Dx}^k = \frac{1}{2}(k_\alpha + k_\gamma)x, \quad F_{Dy}^k = \frac{1}{2}(k_\gamma - k_\alpha)x \quad (16)$$

Assume that for this mechanism

$$k_\alpha = k_\gamma = k \quad (17)$$

Then

$$F_{Bx}^k = F_{Dx}^k = kx, \quad F_{By}^k = F_{Dy}^k = 0 \quad (18)$$

Free Body Diagrams

Figure E3.3.1(c) shows the FBDs for the mechanism in Figure E3.3.1(a).

Kinematic Constraints

From Figures E3.3.1(a) and E3.3.1(c), it can be seen that

$$\begin{aligned} \frac{L_3}{2}\theta_3 &= x \\ \Rightarrow \theta_3 &= \frac{2x}{L_3} \end{aligned} \quad (19)$$

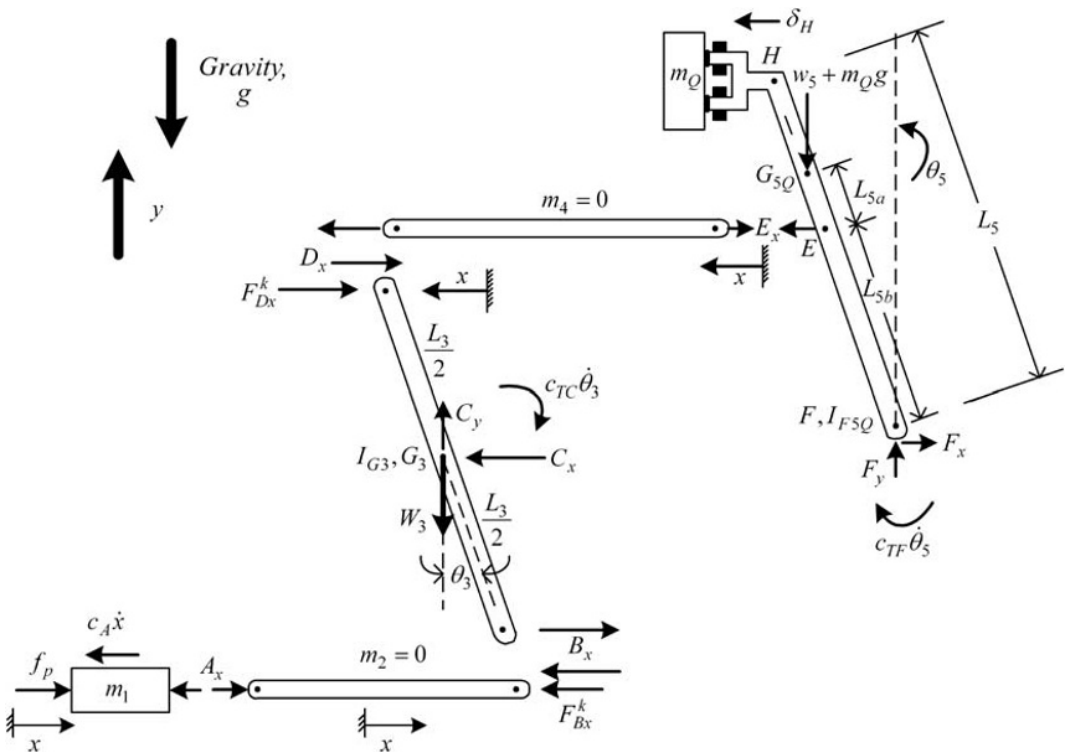


Figure E3.3.1(c) Free body diagrams for mechanism in Figure E3.3.1(a)

Similarly,

$$\begin{aligned} L_{5b}\theta_5 &= x \\ \Rightarrow \theta_5 &= \frac{x}{L_{5b}} \end{aligned} \quad (20)$$

and

$$\delta_H = L_5\theta_5 = \frac{L_5}{L_{5b}}x \quad (21)$$

From the FBDs,

$$+ \quad \Rightarrow \quad m_1\ddot{x} = -c_A\dot{x} + f_p - A_x \quad (22)$$

$$+ \quad \Rightarrow \quad m_2\ddot{x} = 0 * \ddot{x} = A_x - B_x - F_{B_x}^k \quad (23)$$

For the next EOM, use 2D REOM-II (Equation (3.3.39)) with $A = G$:

$$+ \quad \curvearrowright \quad I_{G3}\ddot{\theta}_3 = \frac{L_3}{2}B_x - c_{TC}\dot{\theta}_3 - (F_{D_x}^k + D_x)\frac{L_3}{2} \quad (24)$$

$$+ \quad \Rightarrow \quad m_4\ddot{x} = 0 * \ddot{x} = D_x - E_x \quad (25)$$

For the next EOM, use 2D REOM-I (Equation (3.3.26)) with $\vec{a}_A = \vec{0}$:

$$+ \quad \curvearrowright \quad I_{F5Q}\ddot{\theta}_5 = -c_{TF}\dot{\theta}_5 + L_{5b}E_x + (L_{5a} + L_{5b})\theta_5(w_5 + m_Qg) \quad (26)$$

where I_{F5Q} includes the inertias of bar FH and of m_Q . These five equations must be combined to eliminate all internal reaction forces and produce one EOM in terms of δ_H . From Equation (22),

$$A_x = -c_A\dot{x} + f_p - m_1\ddot{x} \quad (27)$$

From Equations (17), (23), and (27),

$$B_x = A_x - F_{B_x}^k = -c_A\dot{x} + f_p - m_1\ddot{x} - kx \quad (28)$$

From (17), (19), (24), and (28),

$$\begin{aligned} D_x &= \frac{2}{L_3} \left(\frac{L_3}{2}B_x - c_{TC}\dot{\theta}_3 - I_{G3}\ddot{\theta}_3 \right) - F_{D_x}^k \\ &= \frac{2}{L_3} \left[\frac{L_3}{2}(-c_A\dot{x} + f_p - m_1\ddot{x} - kx) - c_{TC}\frac{2\dot{x}}{L_3} - I_{G3}\frac{2\ddot{x}}{L_3} \right] - kx \\ &= \left(-m_1 - \frac{4}{L_3^2}I_{G3} \right) \ddot{x} + \left(-c_A - \frac{4c_{TC}}{L_3^2} \right) \dot{x} - 2kx + f_p \end{aligned} \quad (29)$$

From (25),

$$E_x = D_x \quad (30)$$

From (21), (26), (29), and (30),

$$\begin{aligned}
 I_{F5Q} \left(\frac{\ddot{\delta}_H}{L_5} \right) &= -c_{TF} \frac{\dot{\delta}_H}{L_5} \\
 &+ L_{5b} \left[\left(-m_1 - \frac{4}{L_3^2} I_{G3} \right) \frac{L_{5b}}{L_5} \ddot{\delta}_H + \left(-c_A - \frac{4c_{TC}}{L_3^2} \right) \frac{L_{5b}}{L_5} \dot{\delta}_H - 2k \frac{L_{5b}}{L_5} \delta_H + f_p \right] \\
 &+ (L_{5a} + L_{5b})(W_5 + m_Q g) \frac{\delta_H}{L_5}
 \end{aligned} \quad (31)$$

Summarizing:

$$M_{\text{eq}} \ddot{\delta}_H + C_{\text{eq}} \dot{\delta}_H + K_{\text{eq}} \delta_H = F_{\text{eq}} \quad (32)$$

where

$$M_{\text{eq}} = \frac{I_{F5Q}}{L_5^2} + \frac{L_{5b}^2}{L_5^2} \left(m_1 + \frac{4}{L_3^2} I_{G3} \right) \quad (33)$$

$$C_{\text{eq}} = \frac{c_{TF}}{L_5^2} + \frac{L_{5b}^2}{L_5^2} \left(c_A + \frac{4c_{TC}}{L_3^2} \right) \quad (34)$$

$$K_{\text{eq}} = 2k \frac{L_{5b}^2}{L_5^2} - \frac{(L_{5a} + L_{5b})}{L_5^2} (W_5 + m_Q g) \quad (35)$$

$$F_{\text{eq}} = \frac{L_{5b}}{L_5} f_p \quad (36)$$

The power required to drive this mechanism is

$$P_{\text{ow}}^{\text{in}} = f_p \dot{x} = f_p \frac{L_{5b}}{L_5} \dot{\delta}_H \quad (37)$$

To obtain this power, solve Equation (32) for $\dot{\delta}_H(t)$ and then evaluate Equation (37).

EXAMPLE 3.3.2 Labeling Mechanism

Description: The system shown in Figure E3.3.2(a) is part of a mechanism employed to attach labels in a manufacturing process. Vibration of the system results from actuator forces $f_1(t)$ and $f_2(t)$ and torque $\tau_1(t)$.

Objective: Derive the two equations of motion for coordinates q_1 and q_2 utilizing Newton's laws, and derive an equation for determining the horizontal reaction force at pin A.

Assumptions: q_1 and q_2 are small motions.

Newton's Law

It is helpful to employ the free body diagrams in Figure E3.3.2(b) for utilizing the Newton's law solution approach.

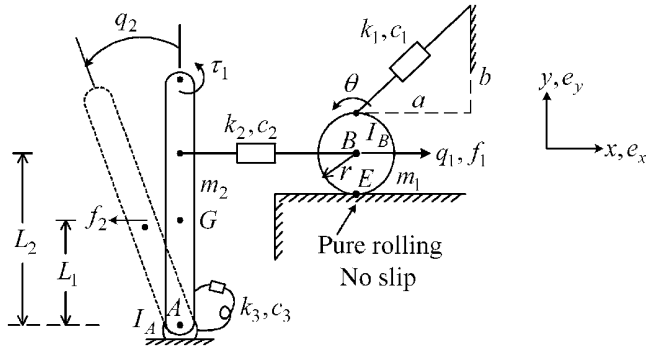


Figure E3.3.2(a) Vibrating mechanical system with two dofs and three excitations

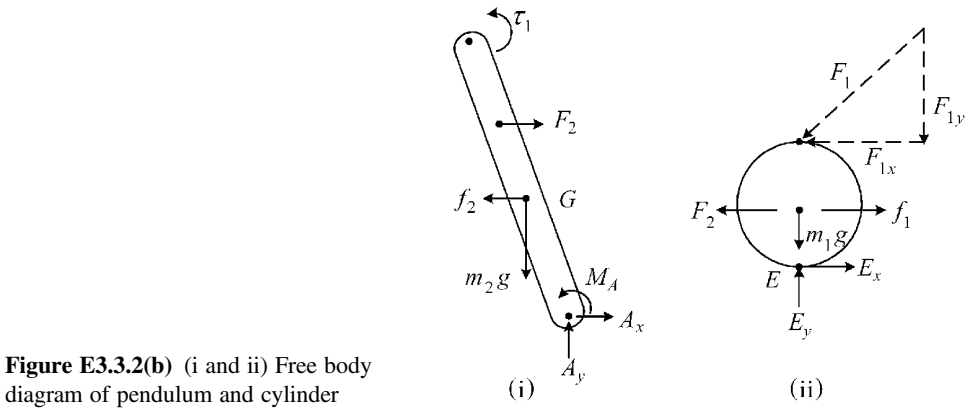


Figure E3.3.2(b) (i and ii) Free body diagram of pendulum and cylinder

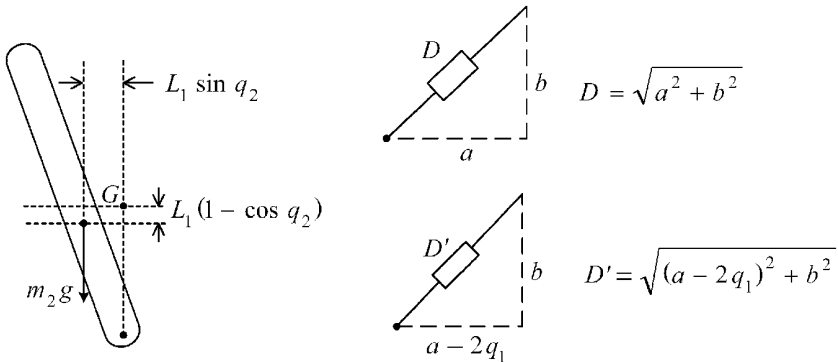


Figure E3.3.2(c) Inverted pendulum and k_1-c_1 impedance geometries

The change in length of the k_1-c_1 impedance in Figure E3.3.2(c) is approximated by a two-term Taylor series expansion (Example 2.4.1):

$$\begin{aligned} \Delta D &= D - D' \approx \Delta D|_{q_1=0} + \left. \frac{\partial \Delta D}{\partial q_1} \right|_{q_2=0} q_1 \\ &= (D - D') - \frac{1}{2} \left[(a - 2q_1)^2 + b^2 \right]^{-1/2} 2(a - 2q_1)(-2) \Big|_{q_1=0} q_1 = \frac{2a}{\sqrt{a^2 + b^2}} q_1 \end{aligned} \tag{1}$$

Therefore,

$$F_1 = k_1 \Delta D + c_1 \Delta \dot{D} = \frac{2a}{\sqrt{a^2 + b^2}} (k_1 q_1 + c_1 \dot{q}_1) \quad (2)$$

and then

$$F_{1x} \approx F_1 \frac{a}{\sqrt{a^2 + b^2}} = \frac{2a^2}{a^2 + b^2} (k_1 q_1 + c_1 \dot{q}_1) \quad (3)$$

The $k_2 - c_2$ force is given by

$$F_2 = k_2 (q_1 + L_2 q_2) + c_2 (\dot{q}_1 + L_2 \dot{q}_2) \quad (4)$$

The $k_3 - c_3$ moment is given by

$$+ \curvearrowright \quad M_A = -k_3 q_2 - c_3 \dot{q}_2 \quad (5)$$

The torque above A of the pendulum's weight is given, for small q_2 , by

$$+ \curvearrowright \quad M_G = m_2 g L_1 \sin q_2 \approx m_2 g L_1 q_2 \quad (6)$$

Newton's laws (3.3.5) and (3.3.46) as applied to the disk in Figure E3.3.2(b) yield

$$+ \rightarrow \quad m_1 \ddot{q}_1 = -F_{1x} - F_2 + E_x + f_1 \quad (7)$$

$$+ \curvearrowright \quad I_B \ddot{\theta} = I_B \left(\frac{-\ddot{q}_1}{r} \right) = r F_{1x} + r E_x \quad (8)$$

Divide (8) by $-r$ and add to (7)

$$\begin{aligned} \left(m_1 + \frac{I_B}{r^2} \right) \ddot{q}_1 &= -F_{1x} - F_2 + f_1 - F_{1x} \\ &= -2 \cdot \frac{2a^2}{a^2 + b^2} (k_1 q_1 + c_1 \dot{q}_1) - k_2 (q_1 + L_2 q_2) - c_2 (\dot{q}_1 + L_2 \dot{q}_2) + f_1(t) \end{aligned} \quad (9)$$

Newton's law as applied to the pendulum in Figure E3.3.2(b) yields

$$\begin{aligned} I_A \ddot{q}_2 &= M_A + \tau_1 - L_2 F_2 + L_1 f_2 + M_G \\ &= -k_3 q_2 - c_3 \dot{q}_2 + \tau_1 + L_1 f_2 - L_2 [k_2 (q_1 + L_2 q_2) + c_2 (\dot{q}_1 + L_2 \dot{q}_2)] + m_2 g L_1 q_2 \end{aligned} \quad (10)$$

Expressing (9) and (10) in matrix-vector form yields

$$\underline{M} \ddot{\underline{q}} + \underline{C} \dot{\underline{q}} + \underline{K} \underline{q} = \underline{F}(t) \quad (n \times 1) \quad (11)$$

where

$$n = 2 \quad (12)$$

$$\underline{q} = \begin{Bmatrix} q_1 \\ q_2 \end{Bmatrix} \quad (13)$$

$$\underline{M} = \begin{bmatrix} m_1 + I_B/r^2 & 0 \\ 0 & I_A \end{bmatrix} \tag{14}$$

$$\underline{C} = \begin{bmatrix} \alpha c_1 + c_2 & c_2 L_2 \\ c_2 L_2 & c_3 + c_2 L_2^2 \end{bmatrix} \tag{15}$$

$$\underline{K} = \begin{bmatrix} \alpha k_1 + k_2 & k_2 L_2 \\ k_2 L_2 & k_3 + k_2 L_2^2 - m_2 g L_1 \end{bmatrix} \tag{16}$$

$$\underline{F}(t) = \begin{Bmatrix} f_1 \\ \tau_1 + L_1 f_2 \end{Bmatrix} \tag{17}$$

$$\alpha = \frac{4a^2}{a^2 + b^2} \tag{18}$$

Equation (11) may be integrated to obtain $q_1(t)$, $q_2(t)$, $\dot{q}_1(t)$, and $\dot{q}_2(t)$, after which the reaction force A_x may be obtained via Newton's laws applied to Figure E3.3.2(b):

$$+ \quad \longrightarrow \quad m_2 \ddot{x}_G = m_2 (-L_1 \ddot{q}_2) = A_x - f_2 + F_2 \tag{19}$$

$$\rightarrow \quad A_x = -m_2 L_1 \ddot{q}_2 + f_2 - [k_2(q_1 + L_2 q_2) + c_2(\dot{q}_1 + L_2 \dot{q}_2)] \tag{20}$$

where \ddot{q}_2 may be obtained from Equation (10).

EXAMPLE 3.3.3 *Static Equilibrium Reference (SEP): Newton Approach*

Objective: A common practice in formulating equations of motion is to reference deflections relative to the static equilibrium state and to ignore the static forces (typically the weight) that caused the deflections at static equilibrium. The following examples illustrate the method and a possible pitfall:

EXAMPLE 1

Consider a mass m suspended by a linear spring and damper as shown in Figure E3.3.3(a).

Figure E3.3.3(a)-(i) shows the spring in its zero force state which establishes the unloaded (UL) reference line A-A. The weight of the mass compresses the spring by the

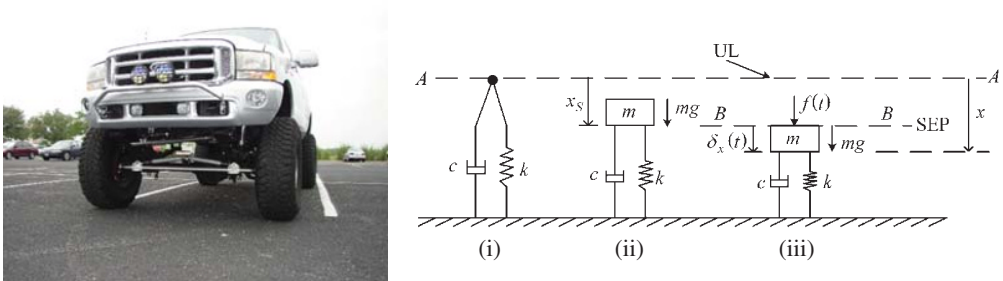


Figure E3.3.3(a) (i–iii) SEP and UL references for a simple m, k, c system

static deflection x_s and establishes the SEP reference line $B-B$. The dynamic force $f(t)$ is applied and m is displaced by δ_x away from the SEP. Static equilibrium in state (ii) requires that

$$kx_s - mg = 0 \quad (1)$$

Newton's law applied to state (iii) yields

$$m\ddot{x} = -kx - c\dot{x} + mg + f(t) \quad (2)$$

Substitute

$$x = x_s + \delta_x(t) \quad (3)$$

into (2) to obtain

$$m\ddot{\delta}_x = -k\delta_x - c\dot{\delta}_x + mg + f(t) \quad (4)$$

Substitute (1) into (4) to obtain

$$m\ddot{\delta}_x = -k\delta_x - c\dot{\delta}_x + f(t) \quad (5)$$

Equation (5) is also the result obtained simply by ignoring the mg force and writing the force expressions in terms of the coordinate δ_x referenced relative to SEP, instead of x referenced relative to UL.

EXAMPLE 2

The system in Figure E3.3.3(b) consists of a hinge supported bar, coil spring, damper, static torque Γ_s , and dynamic torque Γ_D . The static deflection angle α_s due to Γ_s may be large; however, deflections δ_α about α_s are assumed to be small (typically $< 5^\circ$), where

$$\alpha = \alpha_s + \delta_\alpha \quad (1)$$

Figure E3.3.3(b) shows the unloaded (UL) reference line AA with Γ_s , Γ_D , and mg removed. The combined actions of the weight (mg) and static torque Γ_s rotate the bar to the SEP reference AB . The dynamic torque $\Gamma_D(t)$ is applied and the bar is displaced away

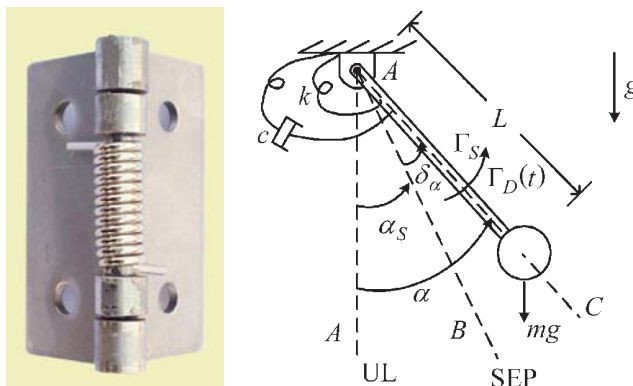


Figure E3.3.3(b) SEP and UL references for pendulum with static offset angle α_s

from SEP by the angle δ_α . Static equilibrium at the SEP requires that the sum of the moments about A equals zero:

$$\Gamma_s - mgL\sin\alpha_s - k\alpha_s = 0 \quad (2)$$

Newton's law (3.3.46) applied to state AC requires that

$$mL^2\ddot{\alpha} = \Gamma_s + \Gamma_D - mgL\sin\alpha - k\alpha - c\dot{\alpha} = 0 \quad (3)$$

Substitute

$$\alpha = \alpha_s + \delta_\alpha \quad (4)$$

into (3) to obtain

$$mL^2\ddot{\delta}_\alpha = \Gamma_s + \Gamma_D - mgL\sin(\alpha_s + \delta_\alpha) - k\alpha_s - k\delta_\alpha - c\dot{\delta}_\alpha \quad (5)$$

Substitute (2) into (5) to obtain

$$mL^2\ddot{\delta}_\alpha = -mgL[\sin(\alpha_s + \delta_\alpha) - \sin\alpha_s] - k\delta_\alpha - c\dot{\delta}_\alpha + \Gamma_D \quad (6)$$

Expand the first sine term

$$mL^2\ddot{\delta}_\alpha = -mgL(\sin\alpha_s \cos\delta_\alpha + \cos\alpha_s \sin\delta_\alpha - \sin\alpha_s) - k\delta_\alpha - c\dot{\delta}_\alpha + \Gamma_D(t) \quad (7)$$

For small δ_α , let

$$\cos\delta_\alpha \approx 1 \quad (8)$$

$$\sin\delta_\alpha \approx \delta_\alpha \quad (9)$$

Then (7) becomes

$$mL^2\ddot{\delta}_\alpha = -mgL\cos(\alpha_s)\delta_\alpha - k\delta_\alpha - c\dot{\delta}_\alpha + \Gamma_D(t) \quad (10)$$

Consider the result obtained by ignoring mg and Γ_s and evaluating the motions as referenced from SEP instead of UL. From Figure E3.3.3(b),

$$mL^2\ddot{\delta}_\alpha = \Gamma_D - k\delta_\alpha - c\dot{\delta}_\alpha \quad (11)$$

Note that the $mgL\cos(\alpha_s)\delta_\alpha$ term is missing in (11). Thus, by inspection of (10) and (11), the latter, SEP-referenced, approach is valid only if

$$k \gg mgL\cos(\alpha_s) \quad (12)$$

that is, a “stiff” spring system. These two examples illustrate that use of static equilibrium state-referenced variables simplifies the derivation of the equations of motion but may yield erroneous results in some cases.

EXAMPLE 3.3.4 *Symbolic Math Code Assistance for Writing Equations of Motion*

Motivation: The algebra involved with writing equations of motion for a single- or multiple-degree-of-freedom system may become very tedious and prone to human error. Use of a symbolic math code like MAPLE, MATLAB-Symbolic, or MATHEMATICA can greatly simplify this process and significantly reduce human errors.

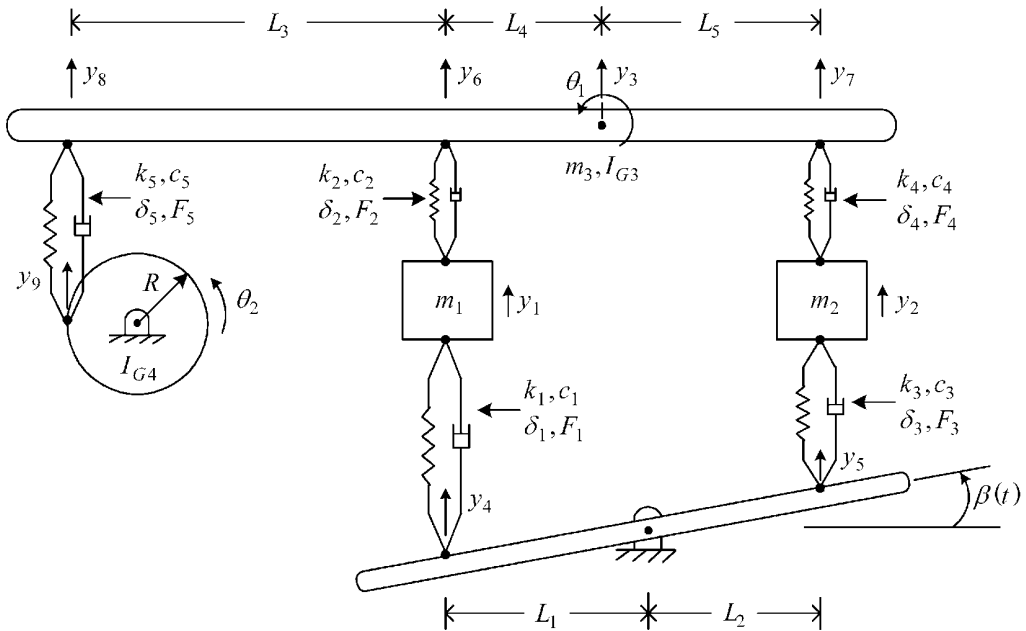


Figure E3.3.4(a) Multidegree-of-freedom vibrating system model

Objective: Figure E3.3.4(a) depicts a mechanical system with support excitation angle $\beta(t)$ and rigid masses m_1, m_2, m_3 , and I_{G4} . Assume that all coordinates are referenced to their static equilibrium positions and that all angles are small. Utilize the symbolic math code MAPLE to obtain the EOM for the coordinates $(y_1 \ y_2 \ y_3 \ \theta_1 \ \theta_2)$.

Solution Outline:

- (a) Code expressions for the following in MAPLE (or MATLAB-Symbolic – pg. 45):
 - (i) Absolute displacements y_4 through y_9 in terms of β , L_1 through L_5 , y_3 , θ_1 , θ_2 , and R
 - (ii) Relative displacements $(\delta_1$ through $\delta_5)$ across the springs and dampers, in terms of y_1 through y_9
 - (iii) Internal forces F_1 through F_5 in terms of δ_i , $\dot{\delta}_i$, c_i , and k_i
- (b) Code the y_1, y_2, y_3, θ_1 , and θ_2 equations of motion (EOM) in terms of F_i, L_i, y_i, θ_i and the inertias $(m_1, m_2, m_3, I_{G3}, \text{ and } I_{G4})$.
- (c) Code calculates five EOMs in (b) in terms of y_1 through $y_3, \theta_1, \theta_2, R, L_i, c_i, \beta$, and k_i .
- (d) Identify all r_i, M_{ii}, C_{ij} , and K_{ij} coefficients, for $j \geq i$, in the matrix expression

$$\underline{M} \ddot{\underline{q}} + \underline{C} \dot{\underline{q}} + \underline{K} \underline{q} = \underline{r}(t) \quad (5 \times 1)$$

for the five EOMs where

$$\underline{q} = (y_1 \ y_2 \ y_3 \ \theta_1 \ \theta_2)^T \quad (5 \times 1)$$

and rows 1–5 are the EOM's in the order y_1, y_2, y_3, θ_1 , and θ_2 .

Solution:

- (a) (i) This part of the problem seeks to reduce the number of coordinates by identifying dependency relations between the coordinates. The set of independent coordinates are $\theta_1, \theta_2, y_1, y_2,$ and y_3 :

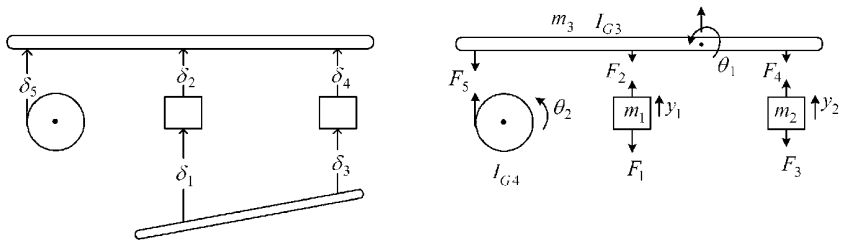
$$y_4 = -L_1\beta, \quad y_5 = L_2\beta, \quad y_6 = y_3 - L_4\theta_1, \quad y_7 = y_3 + L_5\theta_1,$$

$$y_8 = y_3 - (L_3 + L_4)\theta_1, \quad y_9 = -R\theta_2$$

- (ii) The relative displacements are required for evaluating the spring and damper forces:

$$\delta_1 = y_1 - y_4, \quad \delta_2 = L_6 - y_1, \quad \delta_3 = y_2 - y_5, \quad \delta_4 = y_7 - y_2, \quad \delta_5 = y_8 - y_9$$

- (iii) Now, the spring and damping forces may be expressed in terms of the relative displacements and relative velocities:



$$F_1 = k_1\delta_1 + c_1\dot{\delta}_1, \quad F_2 = k_2\delta_2 + c_2\dot{\delta}_2, \quad F_3 = k_3\delta_3 + c_3\dot{\delta}_3,$$

$$F_4 = k_4\delta_4 + c_4\dot{\delta}_4, \quad F_5 = k_5\delta_5 + c_5\dot{\delta}_5$$

- (b) The EOMs are obtained via application of (3.3.5) and (3.3.46) to the above free body diagrams:

$$+\uparrow \quad m_1\ddot{y}_1 = F_2 - F_1 \quad (1)$$

$$+\uparrow \quad m_2\ddot{y}_2 = F_4 - F_3 \quad (2)$$

$$+\uparrow \quad m_3\ddot{y}_3 = -F_2 - F_4 - F_5 \quad (3)$$

$$+\curvearrowright \quad I_{G3}\ddot{\theta}_1 = -L_5F_4 + L_4F_2 + (L_3 + L_4)F_5 \quad (4)$$

$$+\curvearrowright \quad I_{G4}\ddot{\theta}_2 = -RF_5 \quad (5)$$

- (c) MAPLE performs the derivatives of the relative displacement expressions, sums the terms in the EOMs from (b), and collects coefficients of like expressions in the EOMs:

```

> restart;
>
> # Absolute Displacements
> y[4] := -L[1]*beta(t);
> y[5] := L[2]*beta(t);
> y[6] := y[3](t) - L[4]*theta[1](t);
> y[7] := y[3](t) + L[5]*theta[1](t);
> y[8] := y[3](t) - (L[3] + L[4])*theta[1](t);
> y[9] := -R*theta[2](t);

y4 := -L1*beta(t)      y5 := L2*beta(t)      y6 := y3(t) - L4*theta1(t)
y7 := y3(t) + L5*theta1(t)  y8 := y3(t) - (L3 + L4)*theta1(t)  y9 := -R*theta2(t)

> # Relative Displacements

> delta[1] := y[1](t) - y[4];
> delta[2] := y[6] - y[1](t);
> delta[3] := y[2](t) - y[5];
> delta[4] := y[7] - y[2](t);
> delta[5] := y[8] - y[9];

delta1 := y1(t) + L1*beta(t)  delta2 := y3(t) - L4*theta1(t) - y1(t)  delta3 := y2(t) - L2*beta(t)
delta4 := y3(t) + L5*theta1(t) - y2(t)  delta5 := y3(t) - (L3 + L4)*theta1(t) + R*theta2(t)

> # Internal Forces

> F[1] := k[1]*delta[1] + c[1]*diff(delta[1], t);
> F[2] := k[2]*delta[2] + c[2]*diff(delta[2], t);
> F[3] := k[3]*delta[3] + c[3]*diff(delta[3], t);
> F[4] := k[4]*delta[4] + c[4]*diff(delta[4], t);
> F[5] := k[5]*delta[5] + c[5]*diff(delta[5], t);

F1 := k1(y1(t) + L1*beta(t)) + c1((d/dt)y1(t)) + L1(d/dt)beta(t)
F2 := k2(y3(t) - L4*theta1(t) - y1(t)) + c2((d/dt)y3(t) - L4(d/dt)theta1(t) - (d/dt)y1(t))
F3 := k3(y2(t) - L2*beta(t)) + c3((d/dt)y2(t) - L2(d/dt)beta(t))
F4 := k4(y3(t) + L5*theta1(t) - y2(t)) + c4((d/dt)y3(t) + L5(d/dt)theta1(t) - (d/dt)y2(t))
F5 := k5(y3(t) - (L3 + L4)*theta1(t) + R*theta2(t))
    + c5((d/dt)y3(t) - (L3 + L4)(d/dt)theta1(t) + R(d/dt)theta2(t))

> ### Y1 Equation of Motion
> e1 := m[1]*diff(y[1](t), t, t) + F[1] - F[2];
> e2 := collect(e1, theta[2](t));
> e3 := collect(e2, theta[1](t));

```

```

> e4:=collect (e3, y [3] (t)) :
> e5:=collect (e4, y [2] (t)) :
> e6:=collect (e5, y [1] (t)) :
> e7:=collect (e6, diff (theta [2] (t), t)) :
> e8:=collect (e7, diff (theta [1] (t), t)) :
> e9:=collect (e8, diff (y [3] (t), t)) :
> e10:=collect (e9, diff (y [2] (t), t)) :
> eY1_final:=collect (e10, diff (y [1] (t), t)) ;

eY1_final := (c1 + c2) \left( \frac{\partial}{\partial t} y_1(t) \right) - c_2 \left( \frac{\partial}{\partial t} y_3(t) \right) + c_2 L_4 \left( \frac{\partial}{\partial t} \theta_1(t) \right) + (k_1 + k_2) y_1(t)
            - k_2 y_3(t) + k_2 L_4 \theta_1(t) + m_1 \left( \frac{\partial^2}{\partial t^2} y_1(t) \right) + k_1 L_1 \beta(t) + c_1 L_1 \left( \frac{\partial}{\partial t} \beta(t) \right)

> ### Y2 Equation of Motion
> e1:= m [2] *diff (y [2] (t), t, t) +F [3] -F [4] :
> e2:=collect (e1, theta [2] (t)) :
> e3:=collect (e2, theta [1] (t)) :
> e4:=collect (e3, y [3] (t)) :
> e5:=collect (e4, y [2] (t)) :
> e6:=collect (e5, y [1] (t)) :
> e7:=collect (e6, diff (theta [2] (t), t)) :
> e8:=collect (e7, diff (theta [1] (t), t)) :
> e9:=collect (e8, diff (y [3] (t), t)) :
> e10:=collect (e9, diff (y [2] (t), t)) :
> eY1_final:=collect (e10, diff (y [1] (t), t)) ;

eY1_final := (c3 + c4) \left( \frac{\partial}{\partial t} y_2(t) \right) - c_4 \left( \frac{\partial}{\partial t} y_3(t) \right) - c_4 L_5 \left( \frac{\partial}{\partial t} \theta_1(t) \right) + (k_3 + k_4) y_2(t)
            - k_4 y_3(t) - k_4 L_5 \theta_1(t) + m_2 \left( \frac{\partial^2}{\partial t^2} y_2(t) \right) - k_3 L_2 \beta(t) - c_3 L_2 \left( \frac{\partial}{\partial t} \beta(t) \right)

> ### Y3 Equation of Motion
> e1:= m [3] *diff (y [3] (t), t, t) +F [2] +F [4] +F [5] :
> e2:=collect (e1, theta [2] (t)) :
> e3:=collect (e2, theta [1] (t)) :
> e4:=collect (e3, y [3] (t)) :
> e5:=collect (e4, y [2] (t)) :
> e6:=collect (e5, y [1] (t)) :
> e7:=collect (e6, diff (theta [2] (t), t)) :
> e8:=collect (e7, diff (theta [1] (t), t)) :
> e9:=collect (e8, diff (y [3] (t), t)) :
> e10:=collect (e9, diff (y [2] (t), t)) :
> eY1_final:=collect (e10, diff (y [1] (t), t)) ;

eY1_final := (c5 + c2 + c4) \left( \frac{\partial}{\partial t} y_3(t) \right) + (-c_2 L_4 + c_4 L_5 + c_5 (-L_3 - L_4)) \left( \frac{\partial}{\partial t} \theta_1(t) \right)
            + c_5 R \left( \frac{\partial}{\partial t} \theta_2(t) \right) + (k_2 + k_4 + k_5) y_3(t) + (-k_2 L_4 + k_5 (-L_3 - L_4) + k_4 L_5) \theta_1(t)
            + k_5 R \theta_2(t) + m_3 \left( \frac{\partial^2}{\partial t^2} y_3(t) \right) - k_2 y_1(t) - c_4 \left( \frac{\partial}{\partial t} y_2(t) \right) - k_4 y_2(t) - c_2 \left( \frac{\partial}{\partial t} y_1(t) \right)

```

```

> ### Theta1 Equation of Motion
> e1:= I [G3] *diff (theta [1] (t) , t, t) +L [5] *F [4] -L [4] *F [2] - (L [3]
+L [4] ) *F [5] :
> e2:=collect (e1, theta [2] (t) ) :
> e3:=collect (e2, theta [1] (t) ) :
> e4:=collect (e3, y [3] (t) ) :
> e5:=collect (e4, y [2] (t) ) :
> e6:=collect (e5, y [1] (t) ) :
> e7:=collect (e6, diff (theta [2] (t) , t) ) :
> e8:=collect (e7, diff (theta [1] (t) , t) ) :
> e9:=collect (e8, diff (y [3] (t) , t) ) :
> e10:=collect (e9, diff (y [2] (t) , t) ) :
> eY1_final:=collect (e10, diff (y [1] (t) , t) ) ;

```

$$\begin{aligned}
eY1_final := & (c_4 L_5 - c_2 L_4 - (L_3 + L_4) c_5) \left(\frac{\partial}{\partial t} y_3(t) \right) \\
& + (c_4 L_5^2 + c_2 L_4^2 - (L_3 + L_4) c_5 (-L_3 - L_4)) \left(\frac{\partial}{\partial t} \theta_1(t) \right) - (L_3 + L_4) c_5 R \left(\frac{\partial}{\partial t} \theta_2(t) \right) \\
& + k_2 L_4 y_1(t) - k_4 L_5 y_2(t) + (k_4 L_5 - k_2 L_4 - (L_3 + L_4) k_5) y_3(t) \\
& + (k_4 L_5^2 + L_4^2 k_2 - (L_3 + L_4) k_5 (-L_3 - L_4)) \theta_1(t) - (L_3 + L_4) k_5 R \theta_2(t) \\
& + I_{G3} \left(\frac{\partial^2}{\partial t^2} \theta_1(t) \right) - c_4 L_5 \left(\frac{\partial}{\partial t} y_2(t) \right) + c_2 L_4 \left(\frac{\partial}{\partial t} y_1(t) \right)
\end{aligned}$$

```

> ### Theta2 Equation of Motion
> e1:= I [G4] *diff (theta [2] (t) , t, t) +R *F [5] :
> e2:=collect (e1, theta [2] (t) ) :
> e3:=collect (e2, theta [1] (t) ) :
> e4:=collect (e3, y [3] (t) ) :
> e5:=collect (e4, y [2] (t) ) :
> e6:=collect (e5, y [1] (t) ) :
> e7:=collect (e6, diff (theta [2] (t) , t) ) :
> e8:=collect (e7, diff (theta [1] (t) , t) ) :
> e9:=collect (e8, diff (y [3] (t) , t) ) :
> e10:=collect (e9, diff (y [2] (t) , t) ) :
> eY1_final:=collect (e10, diff (y [1] (t) , t) ) ;

```

$$\begin{aligned}
eY1_final := & R c_5 (-L_3 - L_4) \left(\frac{\partial}{\partial t} \theta_1(t) \right) + R^2 c_5 \left(\frac{\partial}{\partial t} \theta_2(t) \right) + k_5 R y_3(t) \\
& + R k_5 (-L_3 - L_4) \theta_1(t) + k_5 R^2 \theta_2(t) + I_{G4} \left(\frac{\partial^2}{\partial t^2} \theta_2(t) \right) + R c_5 \left(\frac{\partial}{\partial t} y_3(t) \right)
\end{aligned}$$

(d) Use the EOMs from part (c) to identify all coefficient terms in the matrix–vector form of the system EOM:

$$\underline{M} \underline{\ddot{q}} + \underline{C} \underline{\dot{q}} + \underline{K} \underline{q} = \underline{r}(t) \quad (5 \times 1)$$

where

$$\underline{q} = (y_1 \ y_2 \ y_3 \ \theta_1 \ \theta_2)^T \quad (5 \times 1)$$

and rows 1–5 are the EOMs in the order $y_1, y_2, y_3, \theta_1, \theta_2$. The results of this matching process are

- From y_1 equation,

$$\begin{aligned} M_{11} &= m_1 \\ c_{11} &= c_1 + c_2, \quad c_{12} = 0, \quad c_{13} = -c_2, \quad c_{14} = c_2 L_4, \quad c_{15} = 0 \\ k_{11} &= k_1 + k_2, \quad c_{12} = 0, \quad k_{13} = -k_2, \quad k_{14} = k_2 L_4, \quad k_{15} = 0 \\ r_1(t) &= -k_1 L_1 \beta(t) - c_1 L_1 \dot{\beta}(t) \end{aligned}$$

- From y_2 equation,

$$\begin{aligned} M_{22} &= m_2 \\ c_{21} &= 0, \quad c_{22} = c_3 + c_4, \quad c_{23} = -c_4, \quad c_{24} = -c_4 L_5, \quad c_{25} = 0 \\ k_{21} &= 0, \quad k_{22} = k_3 + k_4, \quad k_{23} = -k_4, \quad k_{24} = -k_4 L_5, \quad k_{25} = 0 \\ r_2(t) &= k_3 L_2 \beta(t) + c_3 L_2 \dot{\beta}(t) \end{aligned}$$

- From y_3 equation,

$$\begin{aligned} M_{33} &= m_3, \quad r_3(t) = 0 \\ c_{31} &= -c_2, \quad c_{32} = -c_4, \quad c_{33} = c_2 + c_4 + c_5, \quad c_{34} = -c_2 L_4 + c_4 L_5 + c_5(-L_3 - L_4), \quad c_{35} = R c_5 \\ k_{31} &= -k_2, \quad k_{32} = -k_4, \quad k_{33} = k_2 + k_4 + k_5, \quad k_{34} = -k_2 L_4 + k_5(-L_3 - L_4) + k_4 L_5, \quad k_{35} = R k_5 \end{aligned}$$

- From θ_1 equation,

$$\begin{aligned} M_{44} &= I_{G3}, \quad r_4(t) = 0 \\ c_{41} &= c_2 L_4, \quad c_{42} = -c_4 L_5, \quad c_{43} = c_4 L_5 - c_2 L_4 - c_5(L_3 + L_4), \\ c_{44} &= c_4 L_5^2 + c_2 L_4^2 + c_5(L_3 + L_4)^2, \quad c_{45} = -(L_3 + L_4) R c_5 \\ k_{41} &= k_2 L_4, \quad k_{42} = -k_4 L_5, \quad k_{43} = k_4 L_5 - k_2 L_4 - k_5(L_3 + L_4), \\ k_{44} &= k_4 L_5^2 + k_2 L_4^2 + k_5(L_3 + L_4)^2, \quad k_{45} = -(L_3 + L_4) R k_5 \end{aligned}$$

- From θ_2 equation,

$$\begin{aligned} M_{55} &= I_{G4}, \quad r_5 = 0 \\ c_{51} &= c_{52} = 0, \quad c_{53} = R c_5, \quad c_{54} = -(L_3 + L_4) R c_5, \quad c_{55} = R^2 c_5 \\ k_{51} &= k_{52} = 0, \quad k_{53} = R k_5, \quad k_{54} = -(L_3 + L_4) R k_5, \quad k_{55} = R^2 k_5 \end{aligned}$$

3.4 IMPULSE AND MOMENTUM

3.4.1 Linear Impulse and Momentum

The Newton translational equation of motion (TEOM) was shown to be Equation (3.3.5) for the rigid body in Figure 3.3.1:

$$m \frac{d}{dt} {}^n \vec{V}_G = \vec{F}_{\text{ext}} = \text{resultant of all external forces acting on the body}$$

$m = \text{body mass}$ (3.4.1)

$${}^n \vec{V}_G = \frac{d}{dt} {}^n \vec{R}_G = \text{velocity vector of the body's mass center, as viewed in inertial frame } n$$

Integration of Newton's law between times t_1 and t_2 yields:

Linear Impulse and Momentum Principle

$${}^n \vec{P}_G(t_2) - {}^n \vec{P}_G(t_1) = \vec{I}_L(t_1, t_2) \quad (3.4.2)$$

where

$${}^n \vec{P}_G = m {}^n \vec{V}_G = \text{linear momentum vector of the rigid body as sensed in frame } n \quad (3.4.3)$$

$$\vec{I}_L(t_1, t_2) = \int_{t_1}^{t_2} \vec{F}_{\text{ext}} dt = \text{linear impulse received by the body from } \vec{F}_{\text{ext}} \text{ between times } t_1 \text{ and } t_2 \quad (3.4.4)$$

For external force-free motion

Conservation of Linear Momentum (COLM)

If

$$\vec{F}_{\text{ext}} = \vec{0} \quad (3.4.5)$$

then

$$\vec{I}_L(t_1, t_2) = \vec{0} \quad (3.4.6)$$

then Equation (3.4.2) implies

$${}^n \vec{P}_G = \text{a constant vector between times } t_1 \text{ and } t_2, \text{ as sensed in the inertial frame} \quad (3.4.7)$$

COLM is often utilized to solve multibody collision problems. Figure 3.4.1 depicts two bodies colliding with equal and opposite reaction forces (\vec{F}_C).

The forces \vec{F}_1 and \vec{F}_2 represent external forces such as arising from springs, dampers, gravity, or other sources. For body 1, Equation (3.4.2) implies

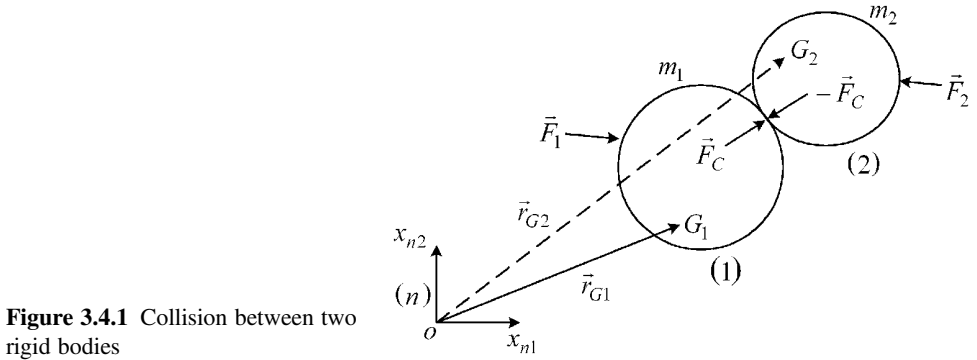


Figure 3.4.1 Collision between two rigid bodies

$${}^n\vec{P}_{G1}(t_2) - {}^n\vec{P}_{G1}(t_1) = \int_{t_1}^{t_2} (\vec{F}_1 + \vec{F}_C) dt \quad (3.4.8)$$

For body 2, Equation (3.4.2) implies

$${}^n\vec{P}_{G2}(t_2) - {}^n\vec{P}_{G2}(t_1) = \int_{t_1}^{t_2} (\vec{F}_2 - \vec{F}_C) dt \quad (3.4.9)$$

Summing these equations cancels the contact force, yielding

$$\Delta {}^n\vec{P}_{G1} + \Delta {}^n\vec{P}_{G2} = \int_{t_1}^{t_2} (\vec{F}_1 + \vec{F}_2) dt \quad (3.4.10)$$

If the collision duration is very small, an engineering approximation is that

$$\int_{t_1}^{t_2} (\vec{F}_1 + \vec{F}_2) dt \approx (\vec{F}_1 + \vec{F}_2) \Delta t \approx (\vec{F}_1 + \vec{F}_2) 0 = 0 \quad (3.4.11)$$

from which (3.4.10) becomes

$$\Delta {}^n\vec{P}_{G1} + \Delta {}^n\vec{P}_{G2} = \vec{0} \quad (3.4.12)$$

or

$${}^n\vec{P}_{G1}(t_2) - {}^n\vec{P}_{G1}(t_1) + {}^n\vec{P}_{G2}(t_2) - {}^n\vec{P}_{G2}(t_1) = \vec{0} \quad (3.4.13)$$

or

$$\left({}^n\vec{P}_{G1} + {}^n\vec{P}_{G2} \right) \Big|_{t_2} = \left({}^n\vec{P}_{G1} + {}^n\vec{P}_{G2} \right) \Big|_{t_1} \quad (3.4.14)$$

Therefore, the sum of the individual linear momentums is conserved. The system mass center location is given by

$$\vec{r}_G = \frac{(m_1 \vec{r}_{G1} + m_2 \vec{r}_{G2})}{m_1 + m_2} \quad (3.4.15)$$



Figure 3.4.2 Perfectly plastic collision of concrete rubble with trailer bed

Define the system linear momentum as

$${}^n\vec{P}_G = (m_1 + m_2){}^n\vec{V}_G = (m_1 + m_2)\frac{{}^n d}{dt}\vec{r}_G = m_1{}^n\vec{V}_{G1} + m_2{}^n\vec{V}_{G2} = {}^n\vec{P}_{G1} + {}^n\vec{P}_{G2} \quad (3.4.16)$$

so that (3.4.14) implies

$${}^n\vec{P}_G \Big|_{t_2} = {}^n\vec{P}_G \Big|_{t_1} \quad (3.4.17)$$

that is, the “total system” momentum is also conserved. To solve for the motions of both masses following collision requires at minimum one additional equation. The relation

$$e = \frac{v_{n1}^A - v_{n2}^A}{v_{n1}^B - v_{n2}^B} \quad (3.4.18)$$

is often used, where e is an experimentally measured coefficient of restitution; B and A refer to before and after collision, respectively; and n indicates the velocity components normal to the surfaces at the contact point. Only one velocity is unknown following collision if the impact is perfectly plastic (bodies stick together) as depicted in Figure 3.4.2. In this case, (3.4.18) is not required.

EXAMPLE 3.4.1 Platform Fire and Piping Damage

Statement: Forensic engineers perform accident reconstruction simulations and tests to explain sources of machinery, systems, or structural failures as requested by client companies or individuals involved in related lawsuits. To illustrate their work, consider the

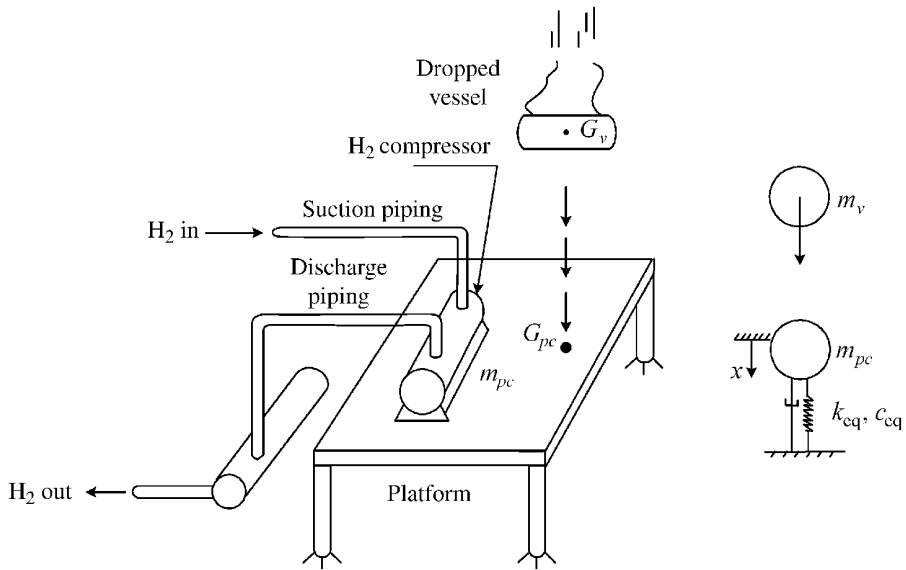


Figure E3.4.1(a) Illustration for machine dropped on platform and equivalent model

following hypothetical case history. A fire on a platform in a large petrochemical plant was traced to leakage of combustible gases through cracks in piping attached to a hydrogen gas compressor on the platform. Downtime for the platform cost the company \$10 M in lost product. The insurance carrier for the plant has sued the plant builder charging that inadequate piping bellows installation led to thermal expansion-induced, low-cycle fatigue failure (cracking) of the pipes. The builder on the other hand has learned that one week prior to the fire, a heavy vessel accidentally fell onto the platform while being transported over it by an overhead crane. Although the vessel did not hit any piping, it did cause a significant vertical vibration of the platform and attached piping. The piping stress due to the vibration may be determined via a finite element-based software package which requires the platform motion as input. The platform's motion after impact can be estimated utilizing the idealized model in Figure E3.4.1(a). The equivalent stiffness k_{eq} and damping c_{eq} represent the combined properties of the columns and attached piping. The mass m_{pc} is the mass of the platform and H_2 compressor, and the mass m_v is the mass of the dropped vessel.

Objective: Determine the initial velocity of vertical motion of the platform following impact by the dropped vessel. This and the zero initial position may be used to estimate the platform vibration following impact.

Solution:

- Draw FBDs for the impact process as shown in Figure E3.4.1(b).
- List assumptions: It is assumed that the time ($\Delta t = 0^+ - 0^-$) required for the vessel to “stick” onto the platform and form a single mass \bar{m} is very short.
- Apply the COLM to determine the velocity \bar{v} of \bar{m} at $t = 0^+$. Use “+” superscripts to denote just after impact ($t = 0^+$) and “-” superscripts to denote just before impact ($t = 0^-$). In considering the system of two masses, the impulse of the contact forces cancels as discussed in the derivation of Equation (3.4.10). The impulse of the external forces, that is,

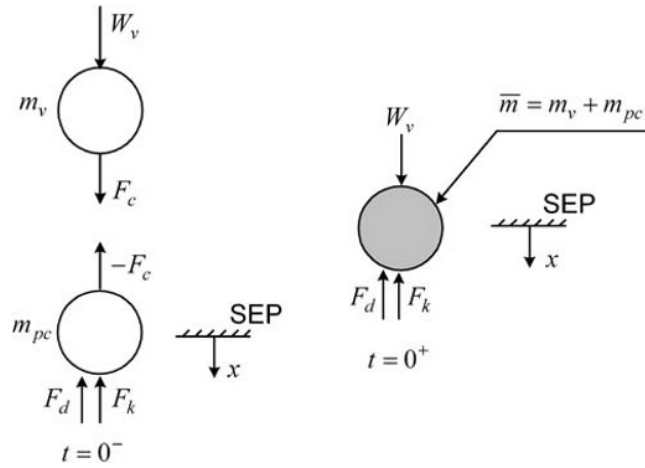


Figure E3.4.1(b) FBDs for the platform—vessel impact simulation

$$\int_{0^-}^{0^+} (W_v - F_d - F_k) dt \approx (W_v - F_d - F_k) \Delta t \approx 0 \quad (1)$$

since

- Δt is almost zero, and
- $F_d = c_{eq}\dot{x}$ and $F_k = k_{eq}x$ are both nearly zero because both x and \dot{x} were zero at $t = 0^-$ and barely change in the time interval Δt .

Under these assumptions, Equation (3.4.14) may be applied:

$$\left({}^n \vec{P}_{Gv} + {}^n \vec{P}_{Gpc} \right)_{0^-} = \left({}^n \vec{P}_{Gv} + {}^n \vec{P}_{Gpc} \right)_{0^+} \quad (2)$$

$$m_v v_v^- + m_{pc} v_{pc}^- = m_v v_v^+ + m_{pc} v_{pc}^+ \quad (3)$$

$$m_v v_v^- + 0 = (m_v + m_{pc}) \bar{v} = \bar{m} \bar{v}$$

or

$$\bar{v} = \frac{m_v v_v^-}{\bar{m}} \quad (4)$$

The same result is obtained using the “System” COLM form in (3.4.17), that is,

- The system mass center's position and velocity just before impact are

$$x_G^- = \frac{m_v x_v^- + m_{pc} x_{pc}^-}{m_v + m_{pc}} \Rightarrow v_G^- = \frac{m_v v_v^- + m_{pc} v_{pc}^-}{m_v + m_{pc}} = \frac{m_v v_v^-}{\bar{m}} \quad (5)$$

Therefore, the system's total momentum just prior to impact is

$${}^n P_G^- = \bar{m} v_G^- = m_v v_v^- \quad (6)$$

- The system mass center's position and velocity just after impact are

$$x_G^+ = \frac{m_v x^+ + m_{pc} x^+}{m_v + m_{pc}} \Rightarrow v_G^+ = \frac{m_v \bar{v} + m_{pc} \bar{v}}{m_v + m_{pc}} = \bar{v} \quad (7)$$

Therefore, the system's total momentum just after impact is

$${}^n P_G^+ = \bar{m} \bar{v} \quad (8)$$

Equate (6) and (8) by the System COLM in (3.4.17) to obtain

$$\bar{m} \bar{v} = m_v v_v^- \quad (9)$$

or

$$\bar{v} = \frac{m_v v_v^-}{\bar{m}} \quad (10)$$

which is the same as (4).

Summary: The result in (4) or (10) provides the initial velocity to determine the platform's motion for all time t , following the vessel impact. The piping stresses may then be determined given the platform's motion.

3.4.2 Angular Impulse and Momentum

The Newton REOM for a single rigid body was shown to be Equation (3.3.25):

$$\frac{{}^n d}{dt} \left({}^n \bar{H}^{B/A} \right) = \bar{\Gamma}_A \quad (3.4.19)$$

if

- (a) base point A is located at mass center G , or
- (b) base point A is fixed or moving with a constant velocity vector as sensed in inertial frame n , and where

$$\bar{\Gamma}_A = \text{resultant moment of all external forces and torques acting on body } B, \text{ taken about point } A \quad (3.4.20)$$

$$\begin{aligned} {}^n \bar{H}^{B/A} &= \int_B \bar{r} \times \left(dm \frac{{}^n d\bar{r}}{dt} \right) = I_A \bar{\omega} \\ &= \text{angular momentum vector of body } B \text{ relative to moment point } A, \text{ as sensed in inertial frame } n \text{ (ref. Eqs. (4.3.8) and (4.3.15))} \end{aligned} \quad (3.4.21)$$

Integration of (3.4.19) between times t_1 and t_2 yields:

Angular Impulse and Momentum Theorem

If

$${}^n\vec{H}^{B/A}(t_2) - {}^n\vec{H}^{B/A}(t_1) = \vec{I}_A(t_1, t_2) \quad (3.4.22)$$

where

$$\vec{I}_A(t_1, t_2) = \int_{t_1}^{t_2} \vec{\Gamma}_A dt = \text{angular impulse received by the body from } \Gamma_A \text{ between times } t_1 \text{ and } t_2 \quad (3.4.23)$$

For external moment-free motion

Conservation of Angular Momentum (COAM)

If

$$\vec{\Gamma}_A = 0 \quad t_1 < t < t_2 \quad (3.4.24)$$

then

$$\vec{I}_A(t_1, t_2) = \vec{0} \quad (3.4.25)$$

and Equation (3.4.22) implies

$${}^n\vec{H}^{B/A} = \text{constant vector between times } t_1 \text{ and } t_2, \text{ as sensed in inertial frame } n \quad (3.4.26)$$

The angular momentum of a point mass m , with position vector $\vec{r}_{c/o}$, about *fixed* point o is from (3.3.8)

$${}^n\vec{H}^{c/o} = \vec{r}_{c/o} \times (m\vec{v}_{c/o}) \quad (3.4.27)$$

where o is a point that is fixed in inertial space n . Differentiate (3.4.27) in frame n

$$\frac{{}^n d}{{}^n dt} {}^n\vec{H}^{c/o} = \dot{\vec{r}}_{c/o} \times (m\vec{v}_{c/o}) + \vec{r}_{c/o} \times (m\dot{\vec{v}}_{c/o}) = m\vec{v}_c \times \vec{v}_c + \vec{r}_{c/o} \times \vec{F}_c = \vec{r}_{c/o} \times \vec{F}_c = \vec{\Gamma}_{c/o} \quad (3.4.28)$$

Integrating from t_1 to t_2 yields:**Angular Impulse-Momentum Principle for a Point Mass about Fixed Point O**

$${}^n\vec{H}^{c/o}(t_2) - {}^n\vec{H}^{c/o}(t_1) = \vec{I}^{c/o} = \int_{t_1}^{t_2} \vec{\Gamma}_{c/o} dt \quad (3.4.29)$$

where

$$\vec{\Gamma}_{c/o} = \vec{r}_{c/o} \times \vec{F}_c \quad (3.4.30)$$

\vec{F}_c is the resultant of all forces acting on mass m which has position vector $\vec{r}_{c/o}$ and ${}^n\vec{H}^{c/o}$ is defined by (3.4.27).

EXAMPLE 3.4.2 *Ship Motion for Machinery Fault Study Following Cargo Drop Upset*

Statement: Continuous operation of onboard machinery is of prime importance following an upset event. Some typical machines on a ship may include pumps, compressors, turbines, motors, gearboxes, and so on. Critical machines may be soft mounted on the decks (as car chassis are on suspension springs and shock absorbers and as large buildings are near earthquake fault lines) to mitigate the force they experience during a support motion upset event. In approaching the problem of design for isolating shipboard machinery, the upset motions of the ship must first be calculated (it is much cheaper and less dangerous than performing a test!). Thus, here we consider a study of the accidental dropping of a heavy cargo load from an overhead crane onto the deck of a docked ship. This is depicted in Figure E3.4.1(a).

For simplicity, assume that the crate (1) falls in the center plane of the ship (plane of mass center G) so that the ship (2) only pitches (θ_2) and heaves (x_{3G}) but does not roll ($\theta_3 = 0$), or yaw ($\theta_1 = 0$). The ship's mass includes its structural mass, plus the "added mass" that results from accelerating the surrounding water when it oscillates:

$$\tilde{m} = m_s + m_A \quad (1)$$

Likewise, the ship's inertia includes an "added" mass contribution due to the water

$$\tilde{J} = I_{22} = J_s + J_A \quad (2)$$

The added mass is a significant amount and can be nearly equal to the mass of the water displaced by the vessel, that is, from Blagoveshchensky (1962), the mass of the water volume equivalent to the submerged portion of the vessel volume.

Objective: Simulation of the ship's motion after impact of the dropped cargo requires solution of its TEOM and REOM for a given set of initial conditions (ICs). The only objective of this example is to demonstrate how COLM and COAM may be utilized to determine the ICs:

$$v_{3G}(0) = v_{3G0} = \dot{x}_{3G}(0) \quad (3)$$

and

$$\omega_{b2}(0) = \omega_{b20} = \dot{\theta}_2(0) \quad (4)$$

Motivation: In actuality, the overarching motivation would be to determine the ship's motion at the location of some critical machine (point A in Figure E3.4.2(a)) and then to use this motion as the inputs for a study/simulation of the machine's response to the motion of the ship.

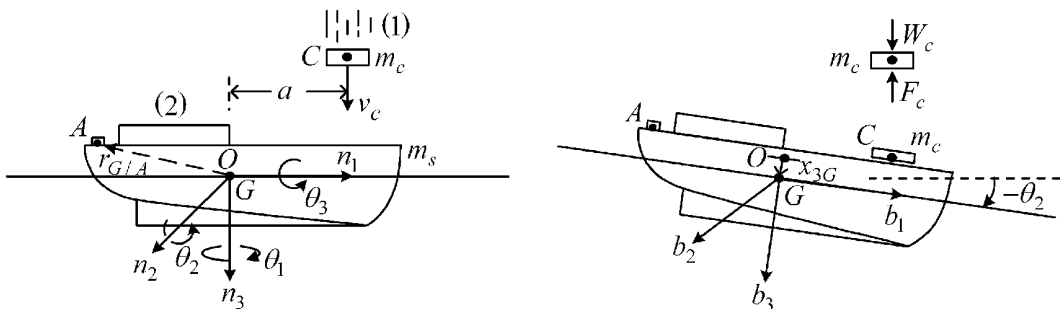


Figure E3.4.2(a) Ship subjected to sudden impact by dropped cargo load

Solution: The dropped cargo is treated as a point mass in the following analysis.

From (3.4.29),

$${}^n\vec{H}^{\bar{c}/o}(t_2) - {}^n\vec{H}^{\bar{c}/o}(t_1) = \vec{I}^{\bar{c}/o} = \int_{t_1}^{t_2} \vec{\Gamma}_{c/o} dt \quad (5)$$

Apply (5) to the cargo load from just prior to impact to just after impact:

$$(-am_c v_{c+}) - (-am_c v_{c-}) = \int_{0^-}^{0^+} (aF_c - aW_c) dt \approx aF_c \Delta t - aW_c \Delta t \quad (6)$$

The cargo is assumed to stick to the ship after impact so by (2.11.19)

$$t = 0^+, \quad {}^n\vec{v}_c = {}^n\vec{v}_G + {}^s\vec{v}_{c/G} + \vec{\omega}_{s/n} \times \vec{r}_{c/G} \quad (7)$$

where “s” indicates a frame of reference attached to the ship. Therefore,

$$v_{c+} = v_{3G0} + (-\omega_{b20}a) \quad (8)$$

and (6) becomes

$$am_c(v_{3G0} - a\omega_{b20}) = am_c v_{c-} - aW_c \Delta t - aF_c \Delta t \quad (9)$$

The angular momentum of the ship is from (3.3.15)

$$H_2 = \tilde{J}\omega_{b2} \quad (10)$$

so that from (3.4.22)

$$\tilde{J}\omega_{b2}(0^+) - \tilde{J}\omega_{b2}(0^-) = \int_{t_1}^{t_2} \vec{\Gamma}_G dt = \int_{t_1}^{t_2} (-aF_c + \Gamma_B) dt = -aF_c \Delta t + \Gamma_B \Delta t \quad (11)$$

where Γ_B is a buoyancy restoring torque which results from Archimedes principle and is proportional to x_{3G} and θ_2 . The terms $(aW_c \Delta t)$ and $(\Gamma_B \Delta t)$ are assumed to be negligible as $\Delta t \rightarrow 0$, so subtracting (9) from (11) yields

$$\tilde{J}\omega_{b20} - am_c v_{3G0} + a^2 m_c \omega_{b20} = -am_c v_{c-} \quad (12)$$

Apply the linear impulse–momentum principle (3.4.2)–(3.4.4) to the cargo

$$m_c v_{c+} - m_c v_{c-} = \int_{0^-}^{0^+} (-F_c + W) dt \quad (13)$$

or from (8)

$$m_c(v_{3G0} - a\omega_{b20}) \cong m_c v_{c-} - F_c \Delta t \quad (14)$$

Apply the linear impulse–momentum principle to the ship

$$\tilde{m}v_{3G+} - \tilde{m}v_{G-} = \int_{0^-}^{0^+} (F_c + W_c + F_B) \Delta t \quad (15)$$

where

$$F_B = \text{buoyant force} \quad (16)$$

Then, for $\Delta t \rightarrow 0$,

$$\tilde{m}v_{3G0} = F_c \Delta t \quad (17)$$

Add (17) and (14)

$$(\tilde{m} + m_c)v_{3G0} - am_c\omega_{b20} = m_c v_{c-} \quad (18)$$

Combine (18) and (12) to obtain

$$\begin{bmatrix} \tilde{m} + m_c & -am_c \\ -am_c & \tilde{J} + a^2m_c \end{bmatrix} \begin{Bmatrix} v_{3G0} \\ \omega_{b20} \end{Bmatrix} = \begin{Bmatrix} m_c v_{c-} \\ -am_c v_{c-} \end{Bmatrix} \quad (19)$$

Therefore,

$$v_{3G0} = \frac{\tilde{J}}{(\tilde{m} + m_c)\tilde{J} + \tilde{m}m_c a^2} (m_c v_{c-}) \quad (20)$$

$$\omega_{b20} = \frac{-a\tilde{m}}{(\tilde{m} + m_c)\tilde{J} + \tilde{m}m_c a^2} (m_c v_{c-}) \quad (21)$$

Summary: This example has demonstrated how to use the angular and linear impulse–momentum principles to obtain the ICs for solving for the motion of a ship when a cargo load is accidentally dropped onto one of its decks.

3.5 VARIABLE MASS SYSTEMS

Newton's law must be modified from its form in (3.3.5) for systems with time-varying mass. Consider the object that is gaining mass as depicted in Figure 3.5.1.

From (3.4.2)–(3.4.4), the impulse–momentum balance applied to Δm between t and $t + \Delta t$ becomes

$$\Delta m (\vec{V}_G + \Delta \vec{V}_G) - \Delta m \vec{V}_a = \int_t^{t+\Delta t} -\vec{F}_c dt \quad (3.5.1)$$

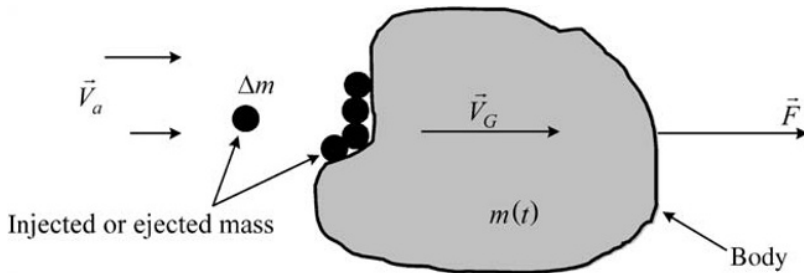


Figure 3.5.1 Variable mass object subjected to external force resultant \vec{F}

where $\Delta \vec{V}_G$ is the change in the velocity of the body's mass center between t and $t + \Delta t$. An impulse–momentum balance applied to the body between t and $t + \Delta t$ becomes

$$m(\vec{V}_G + \Delta \vec{V}_G) - m\vec{V}_G = \int_t^{t+\Delta t} \vec{F}_C dt + \int_t^{t+\Delta t} F dt \quad (3.5.2)$$

Adding these equations yields

$$(m + \Delta m)(\vec{V}_G + \Delta \vec{V}_G) - m\vec{V}_G - \Delta m \vec{V}_a = \int_t^{t+\Delta t} F dt \quad (3.5.3)$$

Divide by Δt , cancel terms, and take the limit as $\Delta t \rightarrow 0$ to obtain

$$m(t) \vec{a} = \dot{m} \vec{V}_{a/m} + \vec{F}(t) \quad (3.5.4)$$

where

\dot{m} = the rate of gaining or losing mass experienced by the body

$$\vec{a} = \frac{d\vec{V}}{dt}, \vec{V}_{a/m} = \text{relative velocity of the entering or exiting mass} \quad (3.5.5)$$

EXAMPLE 3.5.1 *Partially Lifted Vertical Chain Supported by Two Springs*

Description: The chain has mass per unit length \tilde{m} and is suspended above the floor by a length $y(t)$ (Figure E3.5.1(a)). The system is the suspended portion of the chain and gains or losses mass as the chain vibrates in the vertical direction.

Objective: To derive the equation of motion for the vertical movement of point A.

Solution: The system is the total length of chain that is suspended above the floor; therefore,

$$m(t) = \tilde{m}y(t) \quad (1)$$

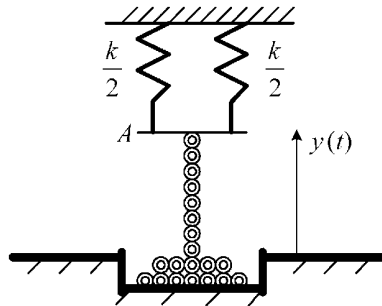


Figure E3.5.1(a) Vertical chain supported by two springs

The rate of change of mass experienced by the system (suspended part of the chain) is

$$\dot{m} = \tilde{m} \frac{dy}{dt} \quad (2)$$

The relative velocity of the entering or exiting mass is

$$\vec{V}_{a/m} = \vec{V}_a - \vec{V}_m = 0 - \frac{dy}{dt} \quad (3)$$

since the chain on the floor has zero velocity whether it is about to enter or after it has exited the suspended portion of the chain, as the chain vibrates vertically. The net external force is given by

$$F = -m(t)g + k(\bar{y} - y(t)) \quad \text{for } y < \bar{y} \quad (4)$$

where \bar{y} is the suspended length of the chain when it is raised up and first attached to the *unstretched* spring. The inequality in (5) is included to express the condition that the chain must stay in tension, since it cannot be in compression. Substituting (1)–(4) into (3.5.4) yields

$$\begin{aligned} \tilde{m}y(t) \frac{d^2y}{dt^2} &= \tilde{m} \frac{dy}{dt} \left(-\frac{dy}{dt} \right) - \tilde{m}y(t)g + k(\bar{y} - y(t)) \\ \text{or} \\ \tilde{m}y\ddot{y} + \tilde{m}\dot{y}^2 + \tilde{m}yg + ky &= k\bar{y} \quad \text{for } y < \bar{y} \end{aligned} \quad (5)$$

which is the desired equation of motion (EOM).

3.6 CHAPTER 3 EXERCISES

3.6.1 Exercise Location

All exercises may be conveniently viewed and downloaded at the following website: **www.wiley.com/go/palazzolo**. This new feature greatly reduces the length of the printed book, yielding a significant cost savings for the college student, and is updated.

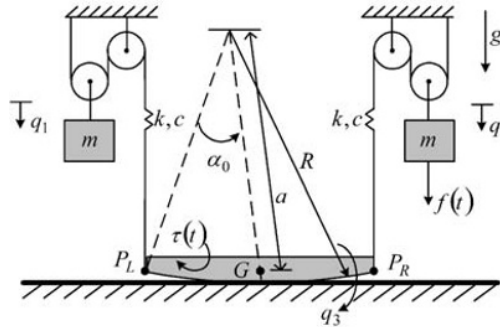
3.6.2 Exercise Goals

The goal of the exercises in Chapter 3 is to strengthen the student's understanding and related engineering problem-solving skills in the following areas:

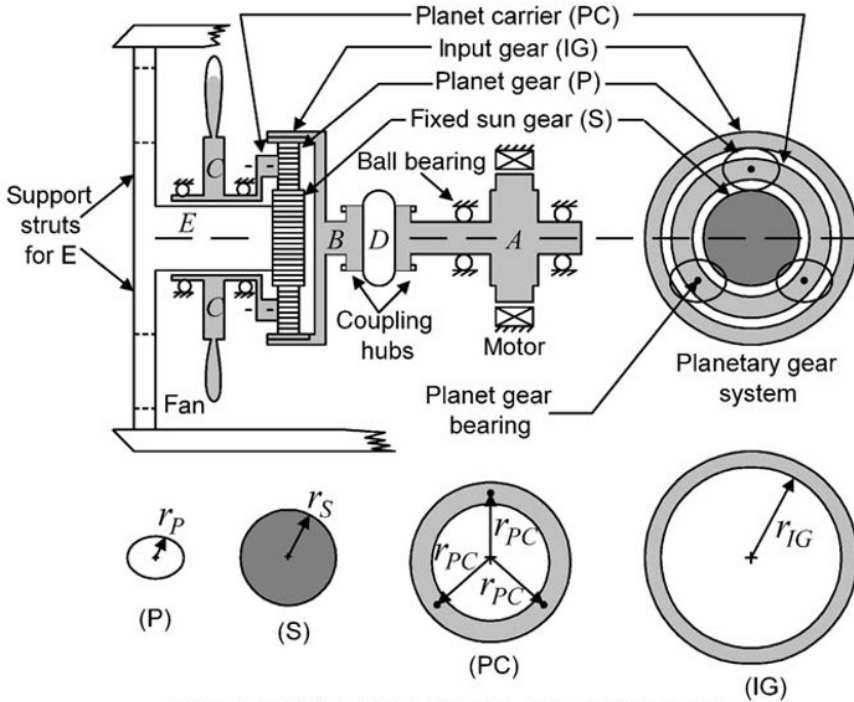
- (a) The governing differential equation(s) of equilibrium is not an end but instead an enabling device for system simulation which is a critical task for design and troubleshooting. Exercises task the students with obtaining numerically integrated responses using their derived governing equations.
- (b) Deriving governing differential equations using Newton's law for fairly complex systems. These systems include many kinematic constraints which fortunately were treated as an independent skill in Chapter 2.
- (c) Utilizing impulse–momentum theory in order to obtain initial conditions that are required to simulate the transient time response of a vibrating system.

3.6.3 Sample Exercises: 3.8 and 3.21

Exercise (3.8) requires use of both Newton's translational and rotational equations of motions and has some challenging kinematic constraint conditions. Exercise (3.21) has strong application appeal and requires kinematic constraint solving skills.



(3.8)



Forced draft fan driven through planetary gear box

(3.21)

REFERENCES

- BLAGOVESHCHENSKY, S. N., *Theory of Ship Motions*, Vol. 1, Dover Publications, New York, 1962.
 KIM, G. and SINGH, R., "A Study of Passive and Adaptive Hydraulic Engine Mount Systems with Emphasis on Non-Linear Characteristics," *Journal of Sound and Vibrations*, 1995, 179(3), 427-453.

Chapter 4

Equations of Motion by Energy Methods

4.1 INTRODUCTION

The use of an energy method-based approach may significantly simplify the derivation of the governing differential equations of motion (EOMs). To illustrate this, consider Example 3.3.1 which demonstrated how an EOM for a multimember rigid body (RB) system could be derived by applying Newton's law to each individual member. Figure E3.3.1(c) shows forces A, B, D, E that act equal and opposite on interconnected links and forces C and F that act between a link and ground. All six of these forces share something in common; they all perform zero work, where the work of a force is the integral of the product of its tangent component along a path times the differential of path length. Force A moves along a path and because of its directions performs negative work on m_1 and an equal and opposite amount of positive work on m_2 , so its net work equals zero. Similar conclusions hold for the forces at B, D, E . The forces at C and F do not move so their work is also zero. A significant effort was required to include these six forces on the free body diagrams, only to later eliminate them in the equations to obtain the system EOM. An advantage of energy-based methods for deriving the EOM is the elimination of this inefficient step of including zero work forces only to eliminate them at a later point. The derivation of expressions for these forces may be necessary if the forces are of interest for the design, but the forces may be neglected in obtaining the EOM. Some other advantages of energy-based EOM approaches include removal of the need to write expressions for accelerations and identify the numerical sign of forces that may be derived from potential functions. Most importantly, energy-based approaches provide a means to model flexible bodies with distributed mass by utilizing the assumed modes and finite element methods (FEM). The approaches presented in this chapter include (i) energy/power conservation and (ii) Lagrange's equations (LE). Derivations are provided to justify LE applications such as assumed modes that are presented without proof in other texts. A symbolic math code is demonstrated for reducing the workload and improving the accuracy in applying this EOM approach.

4.2 KINETIC ENERGY

4.2.1 Particle Motion

The "particle" model may also represent finite-sized bodies with negligible rotational inertia and flexibility effects. Consider the particle of mass m acted on by a set of forces with resultant \vec{F} as shown in Figure 4.2.1. This, for example, could represent a camera mounted on a wing, an antigalloping device fastened to a transmission line cable, or the vertical motion of a traffic light on a flexible support pole as shown in Figure 4.2.1.

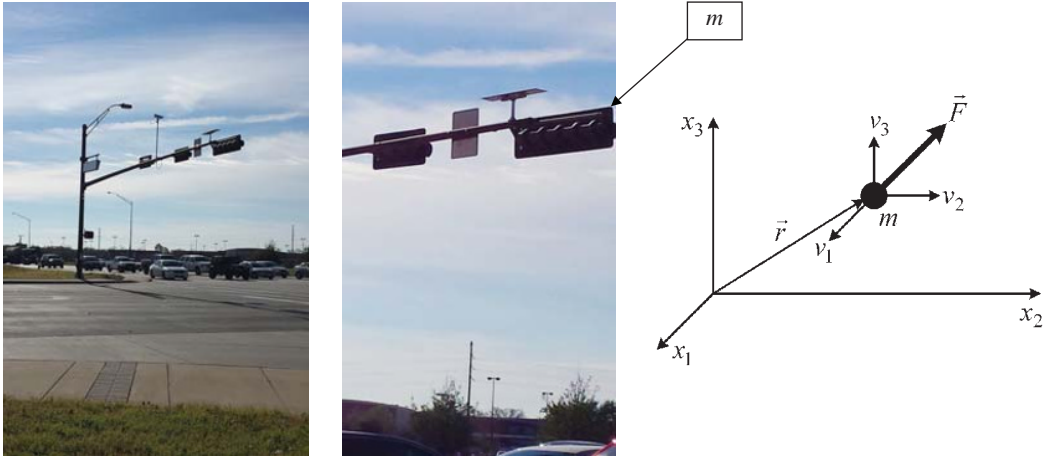


Figure 4.2.1 Particle model for kinetic energy equation

From this figure,

$$\vec{r} = x_1 \hat{e}_1 + x_2 \hat{e}_2 + x_3 \hat{e}_3, \quad \vec{v} = \frac{d}{dt} \vec{r} = v_1 \hat{e}_1 + v_2 \hat{e}_2 + v_3 \hat{e}_3, \quad \vec{F} = F_1 \hat{e}_1 + F_2 \hat{e}_2 + F_3 \hat{e}_3 \quad (4.2.1)$$

and

Particle Kinetic Energy

$$T = \frac{m}{2} \vec{v} \cdot \vec{v} = \frac{m}{2} (v_1^2 + v_2^2 + v_3^2) \quad (4.2.2)$$

4.2.2 Two-Dimensional Rigid Body Motion

Consider an RB which is free to translate and rotate in the x_1 - x_2 plane as shown in Figure 4.2.2.

The kinetic energy of the body is

$$T = \int \frac{|\vec{v}|^2}{2} dm = \int \vec{v} \cdot \vec{v} \frac{dm}{2} = \int \dot{\vec{R}} \cdot \dot{\vec{R}} \frac{dm}{2} \quad (4.2.3)$$

but

$$\vec{R} = \vec{R}_G + \vec{q} \quad (4.2.4)$$

so

$$T = \int \dot{\vec{R}}_G \cdot \dot{\vec{R}}_G \frac{dm}{2} + \int \dot{\vec{q}} \cdot \dot{\vec{q}} \frac{dm}{2} + \dot{\vec{R}}_G \cdot \int \dot{\vec{q}} dm \quad (4.2.5)$$

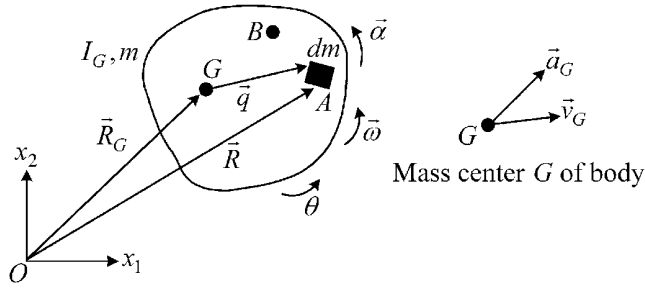


Figure 4.2.2 Rigid body in 2D motion

By the definition of the center of mass G ,

$$\int \bar{q} dm = 0 \quad (4.2.6)$$

$$\therefore \frac{d}{dt} \int \bar{q} dm = \int \dot{\bar{q}} dm = 0 \quad (4.2.7)$$

Also since $\dot{\bar{q}}$ is the velocity of A relative to G ,

$$\dot{\bar{q}} = \bar{\omega} \times \bar{q} \quad (4.2.8)$$

Use the vector identity

$$(\bar{A} \times \bar{B}) \cdot \bar{C} = \bar{A} \cdot (\bar{B} \times \bar{C}) \quad (4.2.9)$$

and (4.2.8) to obtain

$$\dot{\bar{q}} \cdot \dot{\bar{q}} = \bar{\omega} \times \bar{q} \cdot \bar{\omega} \times \bar{q} = \bar{\omega} \cdot \bar{q} \times (\bar{\omega} \times \bar{q}) \quad (4.2.10)$$

Apply the vector identity $\bar{A} \times (\bar{B} \times \bar{C}) = (\bar{A} \cdot \bar{C}) \bar{B} - (\bar{A} \cdot \bar{B}) \bar{C}$ to obtain

$$\dot{\bar{q}} \cdot \dot{\bar{q}} = \bar{\omega} \cdot [(\bar{q} \cdot \bar{q}) \bar{\omega} - (\bar{q} \cdot \bar{\omega}) \bar{q}] \quad (4.2.11)$$

Since \bar{q} and $\bar{\omega}$ are perpendicular, this simplifies to

$$\dot{\bar{q}} \cdot \dot{\bar{q}} = \omega^2 q^2 \quad (4.2.12)$$

Insert (4.2.7) and (4.2.12) into (4.2.5) to obtain

$$T = \frac{m}{2} \bar{v}_G \cdot \bar{v}_G + \frac{\omega^2}{2} \int q^2 dm \quad (4.2.13)$$

Kinetic Energy of Rigid Body with 2D Motion

$$T = \frac{m}{2} \bar{v}_G \cdot \bar{v}_G + \frac{I_G}{2} \omega^2 = \frac{m}{2} \bar{v}_G^2 + \frac{I_G}{2} \omega^2 \quad (4.2.14)$$

where

$$I_G = \int q^2 dm = \text{mass moment of inertia of the body about mass center } G \quad (4.2.15)$$

Note that if some point B on the body is fixed in the inertial frame n , then

$$\vec{v}_G = \vec{\omega} \times \vec{r}_{G/B} \quad (4.2.16)$$

Then by (4.2.8)–(4.2.12),

$$\vec{v}_G \cdot \vec{v}_G = (\vec{\omega} \times \vec{r}_{G/B}) \cdot (\vec{\omega} \times \vec{r}_{G/B}) = \omega^2 r_{G/B}^2 \quad (4.2.17)$$

Combining (4.2.14) and (4.2.17), and use of the parallel axis theorem (Appendix D), yields

Kinetic Energy of a Rigid Body with 2D Motion and a Fixed Point B

$$T = \frac{I_B}{2} \omega^2 \quad (4.2.18)$$

where

$$I_B = I_G + mr_{G/B}^2 = \text{the mass moment inertia of the body about point } B \quad (4.2.19)$$

4.2.3 Constrained 2D Rigid Body Motion

Kinetic energy should be written with only *independent* generalized coordinates. Constraint conditions such as in Example 2.11.1 must be imposed to eliminate dependent generalized coordinates. For example, consider the two-dimensional (2D) motion system in Figure 4.2.3.

The constraint conditions between bodies 1 and 2 are

$$x_{n1}^{G2} = x_{n1}^{G1} + l_1 \cos \theta_1 + l_2 \cos \theta_2, \quad x_{n2}^{G2} = x_{n2}^{G1} + l_1 \sin \theta_1 + l_2 \sin \theta_2 \quad (4.2.20)$$

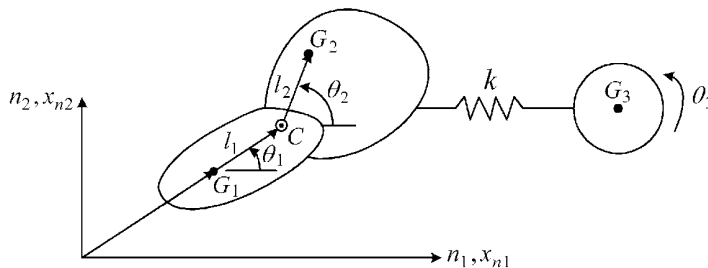


Figure 4.2.3 Planar rigid body motion model with interconnection constraint

Differentiating these expressions yields

$$\dot{x}_{n1}^{G2} = \dot{x}_{n1}^{G1} - l_1 \dot{\theta}_1 \sin \theta_1 - l_2 \dot{\theta}_2 \sin \theta_2, \quad \dot{x}_{n2}^{G2} = \dot{x}_{n2}^{G1} + l_1 \dot{\theta}_1 \cos \theta_1 + l_2 \dot{\theta}_2 \cos \theta_2 \quad (4.2.21)$$

Equations (4.2.20) and (4.2.21) eliminate two redundant *generalized coordinates* and their derivatives. The system kinetic energy is

$$T = \frac{m_1}{2} \left[(\dot{x}_{n1}^{G1})^2 + (\dot{x}_{n2}^{G1})^2 \right] + \frac{I_{G1}}{2} \dot{\theta}_1^2 + \frac{m_2}{2} \left[(\dot{x}_{n1}^{G2})^2 + (\dot{x}_{n2}^{G2})^2 \right] + \frac{I_{G2}}{2} \dot{\theta}_2^2 + \frac{m_3}{2} \left[(\dot{x}_{n1}^{G3})^2 + (\dot{x}_{n2}^{G3})^2 \right] + \frac{I_{G3}}{2} \dot{\theta}_3^2 \quad (4.2.22)$$

Define the generalized coordinates

$$q_1 = x_{n1}^{G1}, \quad q_2 = x_{n2}^{G1}, \quad q_3 = \theta_1, \quad q_4 = \theta_2, \quad q_5 = x_{n1}^{G3}, \quad q_6 = x_{n2}^{G3}, \quad q_7 = \theta_3 \quad (4.2.23)$$

Then using (4.2.20), (4.2.21), and (4.2.23) in (4.2.22) yields T in terms of the seven *independent generalized coordinates* instead of the original nine coordinates. The result is

$$T = \frac{m_1}{2} (\dot{q}_1^2 + \dot{q}_2^2) + \frac{I_{G1}}{2} \dot{q}_3^2 + \frac{m_2}{2} \left[(\dot{q}_1 - l_1 \dot{q}_3 \sin q_3 - l_2 \dot{q}_4 \sin q_4)^2 + (\dot{q}_2 + l_1 \dot{q}_3 \cos q_3 + l_2 \dot{q}_4 \cos q_4)^2 \right] + \frac{I_{G2}}{2} \dot{q}_4^2 + \frac{m_3}{2} (\dot{q}_5^2 + \dot{q}_6^2) + \frac{I_{G3}}{2} \dot{q}_7^2 \quad (4.2.24)$$

Therefore, T has the general form

$$T = T(q_1, q_2, \dots, q_n, \dot{q}_1, \dot{q}_2, \dots, \dot{q}_n) \quad (4.2.25)$$

where the generalized coordinates are the center of mass displacements and rotation angles for this example. Alternatively, constraints may be treated with Lagrange multipliers.

4.3 EXTERNAL AND INTERNAL WORK AND POTENTIAL ENERGY

The work performed by force \vec{F} in Figure 4.3.1 between times t_1 and t_2 is expressed by

$$W_{1 \rightarrow 2}^F = \int_{t_1}^{t_2} \vec{F} \cdot \frac{d\vec{R}_F}{dt} dt = \int_{\vec{R}_{F1}}^{\vec{R}_{F2}} \vec{F} \cdot d\vec{R}_F \quad (4.3.1)$$

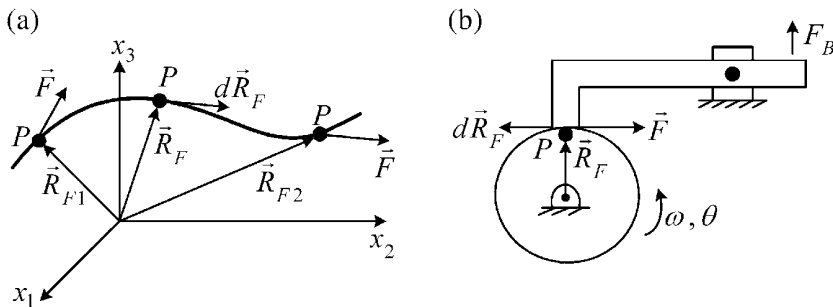


Figure 4.3.1 Work performed by force \vec{F} for (a) translational and (b) rotational motions

Figure 4.3.1(a) shows work being performed by a force on a single particle or body as it moves through space. An example of this would be the work of air friction as the space shuttle descends into the earth's atmosphere. Figure 4.3.1(b) shows work being performed by a force on many particles, each particle only experiencing the force \vec{F} for a short duration of time dt , over which time the particle moves a distance $d\vec{R}$. An example of this would be the flywheel braking mechanism shown. Note that since

$$dR_F = R_F d\theta \quad \text{and} \quad M_F = R_F F \quad (4.3.2)$$

the work performed by F becomes

$$W_{1 \rightarrow 2}^F = \int_{\vec{R}_{F1}}^{\vec{R}_{F2}} \vec{F} \cdot d\vec{R}_F = \int_{\theta_1}^{\theta_2} F R_F d\theta = \int_{\theta_1}^{\theta_2} M_F d\theta = \int_{t_1}^{t_2} M_F \omega dt \quad (4.3.3)$$

where M_F is the moment produced by F and ω is the angular velocity of the wheel. The torque M_F in (4.3.4) may also represent the resultant torque τ due to a distribution of forces, for example, in the case of the drag torque produced by lubricant friction in a bearing or the drive torque produced by a magnetic field on a motor armature. Discrete forces cannot be identified in these cases; instead, only the torque resultant of the distributed forces is sensed. Thus, a system of n_F forces and n_T torques acting on an RB perform the work

$$W_{1 \rightarrow 2} = \sum_{i=1}^{n_F} \int_{\vec{R}_{Fi}^{(1)}}^{\vec{R}_{Fi}^{(2)}} \vec{F}_i \cdot {}^n d\vec{R}_{Fi} + \int_{t_1}^{t_2} \left(\sum_{k=1}^{n_T} \vec{\tau}_k \right)^T \cdot \vec{\omega}^{b/n} dt \quad (4.3.4)$$

or in array notation

$$W_{1 \rightarrow 2} = \sum_{i=1}^{n_F} \int_{\vec{R}_{Fi}^{(1)}}^{\vec{R}_{Fi}^{(2)}} \underline{F}_i^T \cdot {}^n d\underline{R}_i + \int_{t_1}^{t_2} \left(\sum_{k=1}^{n_T} \underline{\tau}_k \right)^T \cdot \underline{\omega}^{b/n} dt \quad (4.3.5)$$

where

${}^n d\vec{R}_{Fi}$ = change in the position of the particle or point on the body at which the force

$$\vec{F} \text{ is applied, in time interval } dt, \text{ as sensed in inertial frame } n \quad (4.3.6)$$

$$\vec{\tau}_k = k\text{th torque due to a force distribution acting on the body} \quad (4.3.7)$$

$$\vec{\omega}^{b/n} = \text{angular velocity of the body relative to inertial frame } n \quad (4.3.8)$$

When using (4.3.4) or (4.3.5) to evaluate work, it is important to note the following:

- (a) \vec{R}_F locates a particle's position at the point of application of the force \vec{F}
- (b) The symbol $\vec{\tau}$ in the second work integral of (4.3.4) or (4.3.5) represents a torque due to a force distribution. Discrete force work contributions should be accounted for in either the first integral of (4.3.5) or in the expression

$$\int \vec{R}_F \times \vec{F} \cdot \vec{\omega}^{b/n} dt \quad (4.3.9)$$

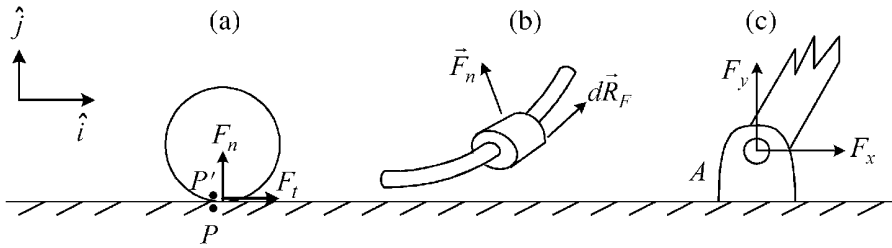


Figure 4.3.2 Examples of forces that do not perform work for (a) rolling contact, (b) a normal force in sliding, and (c) a zero rattle space pin joint

The work contribution of some forces is zero as illustrated in Figure 4.3.2.

The rolling contact forces in (a) are nonzero; however, $d\vec{R}_F$ is zero because of the no-slip condition between P and P' ; therefore,

$$W_{1 \rightarrow 2} = \int (F_t \hat{i} + F_n \hat{j}) \cdot d\vec{R}_F = 0 \quad (4.3.10)$$

In (b), the normal force \vec{F}_n on the frictionless sliding bead is perpendicular to $d\vec{R}_F$:

$$\vec{F}_n \cdot d\vec{R}_F = 0 \quad (4.3.11)$$

Finally, in (c), if the bearing at A is considered to be ideal, that is, frictionless rotation ($\vec{\tau}_{\text{friction}} = 0$) and no translational “rattle,” $d\vec{R}_F = 0$; therefore,

$$W_{1 \rightarrow 2} = \int (F_x \hat{i} + F_y \hat{j}) \cdot d\vec{R}_F + \int \vec{\tau}_{\text{friction}} \cdot \vec{\omega} dt = 0 \quad (4.3.12)$$

For the case of two or more bodies or particles, a contact force or force distribution between the bodies may contribute zero net work since Newton’s third law applies to the force(s) so the work on the two bodies cancel. This applies, for example, to the system depicted in Figure 4.2.3, and the next example.

EXAMPLE 4.3.1 Cable Tension Work in Pulley System

Statement: Cable and pulleys provide another means to couple the motions of two or more components. This example shows how a cable tension force contributes zero net work to the system shown in Figure E4.3.1(a).

Objective: Demonstrate that the net work performed by cable tension T is zero.

Solution:

Let l_2 and l_3 be the dimensions shown at static equilibrium, that is, $y_A = y_B = 0$; then

$$l^2 = l_1^2 + (l_2 - y_A)^2 \quad (1)$$

and since the cable is inextensible,

$$2l + b = 2l + (l_3 - y_B) = \text{constant} \quad (2)$$

Equations (1) and (2) imply

$$2l dl = -2(l_2 - y_A) dy_A \quad (3)$$

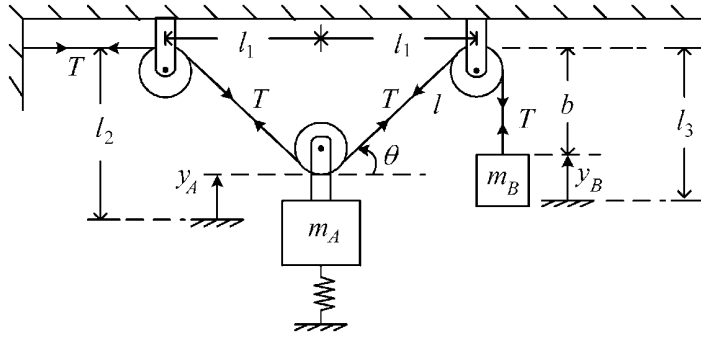


Figure E4.3.1(a) Two-mass system with inextensible cables and frictionless, massless pulleys

$$2dl - dy_B = 0 \quad (4)$$

or by eliminating dl

$$dy_B = \frac{-2(l_2 - y_A)}{l} dy_A = -2 \sin \theta dy_A \quad (5)$$

The work performed by T on mass m_A between times t_1 and t_2 is

$$W_{1 \rightarrow 2}^T|_A = \int_{y_{A1}}^{y_{A2}} 2\vec{T} \cdot d\vec{y}_A = \int_{y_{A1}}^{y_{A2}} 2T \sin \theta dy_A \quad (6)$$

Similarly, the work performed by T on mass m_B between times t_1 and t_2 is

$$W_{1 \rightarrow 2}^T|_B = \int \vec{T} \cdot d\vec{y}_B = \int_{y_{B1}}^{y_{B2}} T dy_B = \int_{y_{A1}}^{y_{A2}} T(-2 \sin \theta dy_A) \quad (7)$$

by Equation (5). Thus, the work performed by T on the entire system is

$$W_{1 \rightarrow 2}^T|_{\text{sys}} = W_{1 \rightarrow 2}^T|_A + W_{1 \rightarrow 2}^T|_B = 0 \quad (8)$$

Summary:

This example illustrated another force system that contributes zero net work.

4.3.1 External Work and Potential Energy

Some forces yield work expressions that only depend on the initial and final states of the system. This is true for the gravitational force in Figure 4.3.3(a) and the spring force in Figure 4.3.3(b). Consider the work performed by gravity as mass m moves from elevations y_1 to y_2 along path s :

$$W_{1 \rightarrow 2}^g = \int_{\vec{r}_1}^{\vec{r}_2} \vec{F}_g \cdot d\vec{r} = \int -mg\hat{j} \cdot (dx\hat{i} + dy\hat{j}) = \int_{y_1}^{y_2} -mgdy = mg(y_1 - y_2) \quad (4.3.13)$$

Next, consider the work performed by the deformation of a spring attached to mass m . The spring force on mass m is

$$\vec{F}_k = -k x \hat{i} \quad (4.3.14)$$

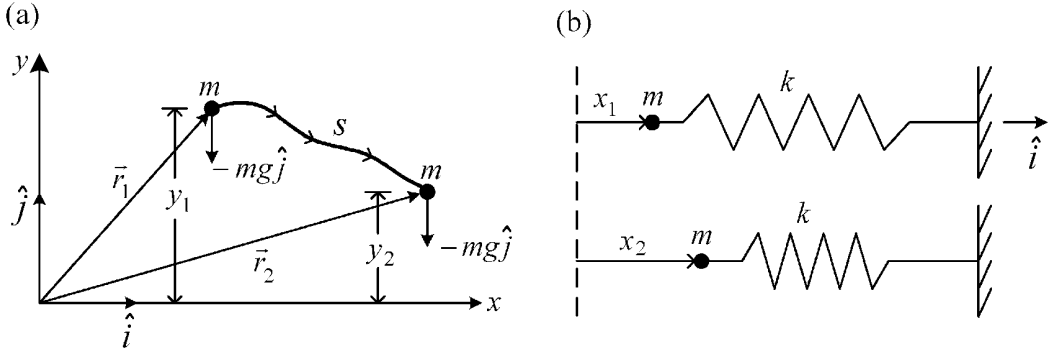


Figure 4.3.3 (a) Weight and (b) spring force examples for work dependent only on initial and final configurations

Therefore, the work done by k on the mass is

$$W_{1 \rightarrow 2}^k = \int_{x_1}^{x_2} (-k x \hat{i}) \cdot (dx \hat{i}) = \left. \frac{-kx^2}{2} \right|_{x_1}^{x_2} = \frac{-k}{2} (x_2^2 - x_1^2) \quad (4.3.15)$$

Note that in both cases $W_{1 \rightarrow 2}^g$ and $W_{1 \rightarrow 2}^k$, the work expressions are only dependent on the end point coordinates and not on the path traversed by the particle in going from 1 to 2. Thus, the work may be expressed in terms of the change in the value of a function that depends only on position variables (dofs). Equations (4.3.13) and (4.3.15) may then be written as

$$W_{1 \rightarrow 2}^g = - \left(U_g \Big|_{(2)} - U_g \Big|_{(1)} \right) = -\Delta U_g \quad (4.3.16)$$

$$W_{1 \rightarrow 2}^k = - \left(U_k \Big|_{(2)} - U_k \Big|_{(1)} \right) = -\Delta U_k \quad (4.3.17)$$

where

$$U_g = \text{gravity potential energy function} = mgy \quad (4.3.18)$$

$$U_k = \text{spring potential energy function} = \frac{k}{2} x^2 \quad (4.3.19)$$

Evaluating the work by calculating the change in a scalar function is certainly easier than performing the integral in (4.3.1). Note that in both cases, the forces may be expressed as the gradient of the potential energy function, that is,

$$\vec{F}_g = -\nabla U_g = -\frac{\partial}{\partial x} U_g \hat{i} - \frac{\partial}{\partial y} U_g \hat{j} = 0 \hat{i} - mg \hat{j} \quad (4.3.20)$$

$$\vec{F}_k = -\nabla U_k = -\frac{\partial}{\partial x} U_k \hat{i} = -kx \hat{i} \quad (4.3.21)$$

4.4 POWER AND WORK-ENERGY LAWS

4.4.1 Particles

Consider the particle of mass m acted on by a set of force with resultant \vec{F} as shown in Figure 4.4.1.

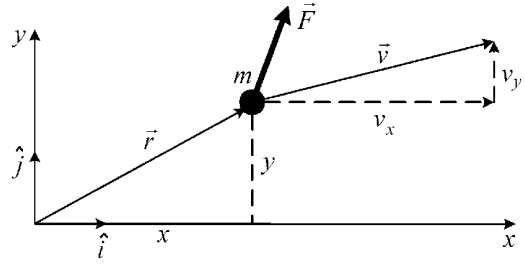


Figure 4.4.1 2D motion of a particle with force resultant \vec{F}

From this figure,

$$\vec{r} = x\hat{i} + y\hat{j}, \quad \vec{v} = \frac{d\vec{r}}{dt} = v_x\hat{i} + v_y\hat{j}, \quad \vec{F} = F_x\hat{i} + F_y\hat{j} \quad (4.4.1)$$

Define the kinetic energy of m to be

$$T = \frac{m}{2} |\vec{v}|^2 = \frac{m}{2} \vec{v} \cdot \vec{v} = \frac{m}{2} (v_x^2 + v_y^2) \quad (4.4.2)$$

Take the time derivative of T :

$$\frac{dT}{dt} = \frac{m}{2} \dot{\vec{v}} \cdot \vec{v} + \frac{m}{2} \vec{v} \cdot \dot{\vec{v}} = m\dot{\vec{v}} \cdot \vec{v} \quad (4.4.3)$$

Substitute (4.4.1) into (4.4.3) and integrate from t_1 to t_2

$$\int_{t_1}^{t_2} dT = \int_{t_1}^{t_2} m\dot{\vec{v}} \cdot \frac{d\vec{r}}{dt} dt = \int_{\vec{r}_1}^{\vec{r}_2} \vec{F} \cdot d\vec{r} \quad (4.4.4)$$

since by Newton's law

$$m\dot{\vec{v}} = m\vec{a} = \vec{F} \quad (4.4.5)$$

Then Equation (4.4.4) yields the result

Work–Energy Principle for a Particle

$$\Delta T = T(t_2) - T(t_1) = W_{1 \rightarrow 2} \quad (4.4.6)$$

where

$$W_{1 \rightarrow 2} = \int_{\vec{r}_1}^{\vec{r}_2} \vec{F} \cdot d\vec{r} = \text{work performed by } \vec{F} \text{ on } m \text{ between } t_1 \leq t \leq t_2$$

$$T = \frac{m}{2} |\vec{v}|^2 = \frac{m}{2} (v_x^2 + v_y^2) \quad (4.4.7)$$

Substitute (4.4.5) into (4.4.3) to obtain

Conservation of Power Principle for a Particle

$$\frac{dT}{dt} = \vec{F} \cdot \vec{v} \quad (4.4.8)$$

where

$$\vec{F} \cdot \vec{v} = \text{power contributed by force resultant } \vec{F}$$

Equations (4.3.16) and (4.3.17) showed that the work performed by some forces could be expressed by changes in a potential energy function U . Then (4.4.6)–(4.4.7) may be expressed as

Work–Energy Principle for a Particle with Conservative and Nonconservative Forces

$$\Delta E = E(t_2) - E(t_1) = W_{1 \rightarrow 2}^{\text{NC}} \quad (4.4.9)$$

where

$$E = T + U = \text{particle's total energy} \quad (4.4.10)$$

$$W_{1 \rightarrow 2}^{\text{NC}} = \int_{\vec{r}_1}^{\vec{r}_2} \vec{F}^{\text{NC}} \cdot d\vec{r} = \text{work of resultant } \vec{F}^{\text{NC}} \text{ of all nonconservative forces} \quad (4.4.11)$$

4.4.2 Rigid Body with 2D Motion

Recall from (4.2.14) that the kinetic energy for the RB planar motion depicted in Figure 4.4.2 is

$$T = \frac{m}{2} \vec{v}_G \cdot \vec{v}_G + \frac{I_G}{2} \omega^2 \quad (4.4.12)$$

Then

$$\frac{dT}{dt} = \frac{m}{2} \vec{v}_G \cdot \dot{\vec{v}}_G + \frac{m}{2} \dot{\vec{v}}_G \cdot \vec{v}_G + I_G \omega \dot{\omega} = m \vec{a}_G \cdot \vec{v}_G + I_G \alpha \omega = m \vec{a}_G \cdot \frac{d\vec{r}_G}{dt} + I_G \alpha \frac{d\theta}{dt} \quad (4.4.13)$$

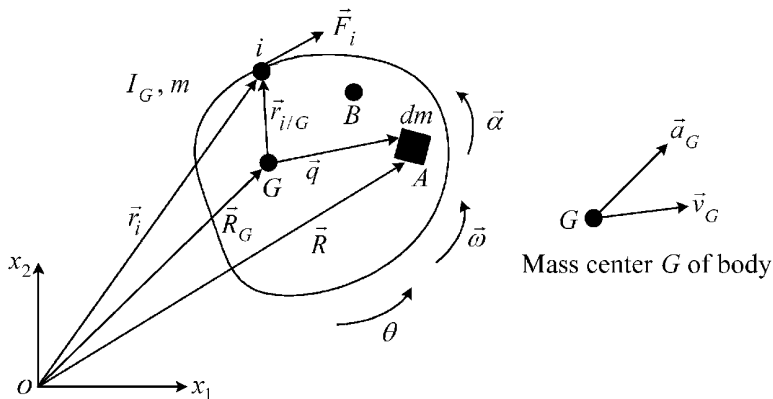


Figure 4.4.2 Rigid body with 2D motion and external forces

Substitute (3.3.5) and (3.3.39), with A at G , to obtain

$$dT = \vec{F}_{\text{ext}} \cdot d\vec{r}_G + \Gamma_G d\theta \quad (4.4.14)$$

Then by integrating from t_1 to t_2

Work–Energy Principle for a Rigid Body (RB) with Planar Motion in Terms of Resultant Force and Moment

$$\Delta T = T(t_2) - T(t_1) = W_{1 \rightarrow 2} \quad (4.4.15)$$

where

$$W_{1 \rightarrow 2} = \int_{\vec{r}_{G1}}^{\vec{r}_{G2}} \vec{F}_{\text{ext}} \cdot d\vec{r}_G + \int_{\theta_1}^{\theta_2} \Gamma_G d\theta \quad (4.4.16)$$

$$\vec{F}_{\text{ext}} = \text{resultant of all external forces acting on the RB} \quad (4.4.17)$$

$$\Gamma_G = \text{resultant moment of all forces about mass center } G \text{ plus pure torques acting on the RB} \quad (4.4.18)$$

Note that \vec{F}_{ext} is the *resultant* force vector on the body

$$\vec{F}_{\text{ext}} = \sum_{i=1}^n \vec{F}_i \quad (4.4.19)$$

and $\vec{\Gamma}_G$ is the resultant torque vector acting on the body, that is,

$$\vec{\Gamma}_G = \sum_{i=1}^n \vec{r}_{i/G} \times \vec{F}_i + \vec{\tau} \quad (4.4.20)$$

where $\vec{\tau}$ is the resultant of all pure torques acting on the body. Insert (4.4.19) and (4.4.20) into (4.4.14) to obtain

$$\frac{dT}{dt} = \sum_{i=1}^n \vec{F}_i \cdot \vec{v}_G + \sum_{i=1}^n (\vec{r}_{i/G} \times \vec{F}_i) \cdot \vec{\omega} + \vec{\tau} \cdot \vec{\omega} \quad (4.4.21)$$

Use the vector identity

$$\vec{a} \times \vec{b} \cdot \vec{c} = (\vec{c} \times \vec{a}) \cdot \vec{b} \quad (4.4.22)$$

and the kinematical relation $\vec{v}_i = (\vec{v}_G + \vec{\omega} \times \vec{r}_{i/G})$ to write (4.4.21) as

$$\begin{aligned} \frac{dT}{dt} &= \vec{v}_G \cdot \sum_{i=1}^n \vec{F}_i + \sum_{i=1}^n \vec{\omega} \times \vec{r}_{i/G} \cdot \vec{F}_i + \vec{\tau} \cdot \vec{\omega} = \sum_{i=1}^n (\vec{v}_G + \vec{\omega} \times \vec{r}_{i/G}) \cdot \vec{F}_i + \vec{\tau} \cdot \vec{\omega} \\ &= \sum_{i=1}^n \vec{F}_i \cdot \vec{v}_i + \vec{\tau} \cdot \vec{\omega} \end{aligned} \quad (4.4.23)$$

Utilize

$$\vec{v}_i = \frac{d\vec{R}_i}{dt}, \quad \vec{\omega} = \frac{d\vec{\theta}}{dt} \quad (4.4.24)$$

and integrate (4.4.23) to obtain

Work–Energy Principle for a Rigid Body (RB) with Planar Motion in Terms of Individual External Forces and Pure Torques

$$\Delta T = T(t_2) - T(t_1) = W_{1 \rightarrow 2}^F + W_{1 \rightarrow 2}^\tau \quad (4.4.25)$$

where

$$T = \frac{m}{2} v_G^2 + \frac{I_G}{2} \omega^2 \quad (4.4.26)$$

$$W_{1 \rightarrow 2}^F = \sum_{i=1}^{n_F} \int_{\vec{r}_{i1}}^{\vec{r}_{i2}} \vec{F}_i \cdot d\vec{r} = \text{work done by external forces acting on the body RB} \quad (4.4.27)$$

$$W_{1 \rightarrow 2}^\tau = \int_{\theta_1}^{\theta_2} \tau d\theta = \text{work done by all pure torques acting on the RB} \quad (4.4.28)$$

$$\vec{F}_i = \text{ith external force acting on the RB } (i = 1, 2, \dots, n_F) \quad (4.4.29)$$

$$\tau = \text{resultant (sum) of all external pure torques acting on the RB} \quad (4.4.30)$$

(The term τ does not include any $\vec{r} \times \vec{F}$ type moment terms.)

Equation (4.4.23) directly yields the power relationship

Conservation of Power Principle for an RB with Planar Motion in Terms of Individual External Forces and Pure Torques

$$\frac{dT}{dt} = P_F + P_\tau \quad (4.4.31)$$

where T is defined by (4.4.26) and

$$P_F = \sum_{i=1}^{n_F} \vec{F}_i \cdot \vec{v}_i = \text{power exchange due to external forces}$$

$$P_\tau = \tau \omega = \text{power exchange due to pure torques}$$

τ = resultant of all pure torques acting on the rigid body. This excludes $\vec{r} \times \vec{F}$ all moments

$$\vec{F}_i = \text{ith external force acting on the rigid body } (i = 1, 2, \dots, n_F)$$

$$\vec{v}_i = \text{velocity of point on rigid body where force } \vec{F}_i \text{ is applied}$$

EXAMPLE 4.4.1 *Resonant Vibrator for Compound Potting (Example 3.3.1 by Energy Approach)*

Description: Reference Figure E3.3.1(a)

Objective:

Derive the equation of motion for this system by the power conservation approach.
Determine an expression for the power required to drive this mechanism.

Assumptions:

Small angular motions, Rods AB and DE , remain horizontal. All joints are ideal (zero rattle space), and Rods AB and DE are light in weight, so $m_2 = m_4 = 0$.

At static equilibrium,

$$x_A = \theta_3 = \theta_5 = 0 \quad (1)$$

Solution:

Stiffness Transformations

From Example 3.3.1, it was shown that the stiffness forces at B and D could be represented by

$$F_{Bx}^k = F_{Dx}^k = kx \quad \text{and} \quad F_{By}^k = F_{Dy}^k = 0 \quad (2)$$

Free Body Diagram

The free body diagram in Figure E3.3.1(c) is nearly not required for the energy approach.

Kinematic Constraints

As discussed in Example 3.3.1, motion coordinates are related by the following equations:

$$\Rightarrow \theta_3 = \frac{2x}{L_3}, \quad \theta_5 = \frac{x}{L_{5b}}, \quad \delta_H = L_5 \theta_5 = \frac{L_5}{L_{5b}} x \quad (3)$$

Newton/Euler Approach

The equation of motion obtained from the Newton approach in Example 3.3.1 is given by

$$M_{\text{eq}} \ddot{\delta}_H + C_{\text{eq}} \dot{\delta}_H + K_{\text{eq}} \delta_H = F_{\text{eq}}$$

where $M_{\text{eq}} = \frac{I_{F5Q}}{L_5^2} + \frac{L_{5b}^2}{L_5^2} \left(m_1 + \frac{4}{L_3^2} I_{G3} \right)$, $C_{\text{eq}} = \frac{c_{TF}}{L_5^2} + \frac{L_{5b}^2}{L_5^2} \left(c_A + \frac{4c_{TC}}{L_3^2} \right)$, $K_{\text{eq}} = 2k \frac{L_{5b}^2}{L_5^2} - \frac{(L_{5a} + L_{5b})}{L_5^2} (W_5 + m_{Qg})$, $F_{\text{eq}} = \frac{L_{5b}}{L_5} f_p$ (4)

Power Conservation Approach

The total kinetic energy is obtained from Figure E3.3.1(a) and (3) as

$$T = \frac{1}{2} m_1 \dot{x}^2 + \frac{1}{2} I_{G3} \dot{\theta}_3^2 + \frac{1}{2} I_{F5Q} \dot{\theta}_5^2 = \left(\frac{m_1 L_{5b}^2}{2 L_5^2} + \frac{I_{G3} 4 L_{5b}^2}{2 L_3^2 L_5^2} + \frac{I_{F5Q} 1}{2 L_5^2} \right) \dot{\delta}_H^2 \quad (5)$$

The power terms are

$$P_{ow} = f_p \dot{x} - F_{Bx}^k \dot{x} - F_{Dx}^k \dot{x} - (w_5 + m_Q g) \dot{y}_{G5Q} - c_A \dot{x} \dot{x} - c_{TC} \dot{\theta}_3 \dot{\theta}_3 - c_{TF} \dot{\theta}_5 \dot{\theta}_5 \quad (6)$$

Unlike Newton's law, the force terms at the interconnections and connections to ground are ignored since they perform zero net work (and consequently zero net power). Note that by using a two-term Taylor series expansion (2.4.1) of the cosine function,

$$y_{G5Q} = -(L_{5a} + L_{5b})(1 - \cos \theta_5) \approx -(L_{5a} + L_{5b}) \left(\frac{\theta_5^2}{2} \right) \quad (7)$$

Therefore

$$\dot{y}_{G5Q} \approx -(L_{5a} + L_{5b}) \theta_5 \dot{\theta}_5 = - \left(\frac{L_{5a} + L_{5b}}{L_5^2} \right) \delta_H \dot{\delta}_H \quad (8)$$

Then by (3) and (6),

$$P_{ow} = \frac{L_{5b}}{L_5} f_p \dot{\delta}_H - \frac{L_{5b}}{L_5} \dot{\delta}_H \left(2k \frac{L_{5b}}{L_5} \delta_H \right) - (w_5 + m_Q g) \left[- \frac{(L_{5a} + L_{5b})}{L_5^2} \delta_H \dot{\delta}_H \right] \\ - c_A \frac{L_{5b}^2}{L_5^2} \dot{\delta}_H^2 - c_{TC} \frac{4}{L_3^2} \frac{L_{5b}^2}{L_5^2} \dot{\delta}_H^2 - \frac{c_{TF}}{L_5^2} \dot{\delta}_H^2 \quad (9)$$

Differentiate T and equate the result to P_{ow} and cancel $\dot{\delta}_H$ to obtain

$$M_{eq} \ddot{\delta}_H + C_{eq} \dot{\delta}_H + K_{eq} \delta_H = F_{eq} \quad (10)$$

where M_{eq} , C_{eq} , K_{eq} , and F_{eq} are Newton's law (4).

Summary:

The power approach is simpler than the Newton approach in the following ways:

- (a) Internal forces were allowed to be ignored.
- (b) The free body diagram is less detailed and important.
- (c) The spring force directions are not required.

4.5 LAGRANGE EQUATION FOR PARTICLES AND RIGID BODIES

The Lagrange approach is widely used to obtain the EOM of a rigid or flexible body model. Some reasons for this include:

- (a) Acceleration vectors of mass centers are not required.
- (b) Force vectors that contribute zero net work are not required.
- (c) Sign determination for forces derived from derivatives of scalar potential functions is not required.
- (d) Easily applied to flexible, such as assumed modes and finite elements, as well as rigid and hybrid body models.

4.5.1 Derivation of the Lagrange Equation

The “ R ” Identities Kinetic energy of the system always has the general form

$$T = T(q_1, q_2, \dots, q_n, \dot{q}_1, \dot{q}_2, \dots, \dot{q}_n) \quad (4.5.1)$$

as illustrated by (4.2.25), where q_i are independent generalized coordinates. These may represent translations or angles of an RB, assumed modes coordinates as in (2.11.28), or finite element node translations or rotations as in (2.11.36). A body or system of bodies can be considered to be a collection of an infinite number of differential masses dm 's, that is,

$$m = \sum_{i=1}^{N_\infty} m_i \quad (4.5.2)$$

in the limit as $N_\infty \rightarrow \infty$ and $m_i \rightarrow 0$. The position vector of mass m_i is \vec{R}_i , so that

$$\vec{R}_i = \vec{R}_i(q_1 \ q_2 \ \dots \ q_n, \ t) \quad (4.5.3)$$

and

$$\dot{\vec{R}}_i = \dot{\vec{R}}_i(q_1 \ q_2 \ \dots \ q_n, \ \dot{q}_1 \ \dot{q}_2 \ \dots \ \dot{q}_n, \ t) \quad (4.5.4)$$

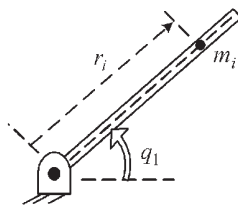
For example, Figure 4.5.1 shows a long, slender pendulum modeled as a RB. The motions of all particles comprising this body can be expressed in terms of a single generalized coordinate, the angle q_1 .

Two special derivative relationships between \vec{R}_i , $\dot{\vec{R}}_i$, q_j , and \dot{q}_j are required to derive the LE. These will be derived utilizing the chain rule of differentiation (Hildebrand, 1976) on the function $f(q_1, q_2, \dots, q_n, t)$, yielding

$$\frac{\tilde{n}df}{dt} = \frac{\partial f}{\partial t} + \sum_{k=1}^n \frac{\partial f}{\partial q_k} \frac{\tilde{n}dq_k}{dt} = \frac{\partial f}{\partial t} + \sum_{k=1}^n \frac{\partial f}{\partial q_k} \dot{q}_k \quad (4.5.5)$$

where the first term on the RHS accounts for the explicit presence of t in the definition of f and the left superscript \tilde{n} indicates that the time derivative is taken by an observer in the inertial (nonaccelerating) frame of reference n . First, apply Equation (4.5.5) to the components of the vector \vec{R}_i , which from (4.5.3) yields

$$\dot{\vec{R}}_i = \frac{\tilde{n}d}{dt} \vec{R}_i(q_1 \ q_2 \ \dots \ q_n \ t) = \frac{\partial \vec{R}_i}{\partial t} + \sum_{k=1}^n \frac{\partial \vec{R}_i}{\partial q_k} \frac{\partial q_k}{\partial t} \quad (4.5.6)$$



$$\begin{aligned} \vec{R}_i(q_1) &= r_i \cos(q_1) \hat{i} + r_i \sin(q_1) \hat{j} \\ \dot{\vec{R}}_i(q_1, \dot{q}_1) &= -r_i \dot{q}_1 \sin(q_1) \hat{i} + r_i \dot{q}_1 \cos(q_1) \hat{j} = \dot{\vec{R}}_i \end{aligned}$$

Figure 4.5.1 Rigid body model of pendulum with one generalized coordinate q_1

but since q_k is an “independent” generalized coordinate, it is only a function of t and not a function of $(q_j, j \neq k)$ so

$$\frac{\partial q_k}{\partial t} = \frac{\tilde{d}q_k}{dt} = \dot{q}_k \quad (4.5.7)$$

The last step should be kept in mind since it explains why the generalized coordinates must be independent. Insert (4.5.7) into (4.5.6):

$$\dot{\vec{R}}_i = \frac{\partial \vec{R}_i}{\partial t} + \sum_{k=1}^n \frac{\partial \vec{R}_i}{\partial q_k} \dot{q}_k \quad (4.5.8)$$

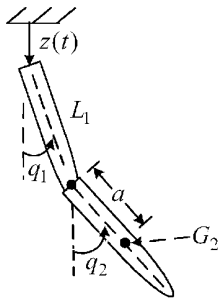
Note that by (4.5.3), \vec{R}_i and $\partial \vec{R}_i / \partial q_k$ are not functions of \dot{q}_k . Likewise, the partial derivative of \vec{R}_i with respect to t in (4.5.8) treats q_k as constants, so $\partial \vec{R}_i / \partial t$ is also not a function of \dot{q}_k . Therefore, taking the partial derivative of (4.5.8) with respect to \dot{q}_j yields the first “ \vec{R} ” identity:

$$\frac{\partial \dot{\vec{R}}_i}{\partial \dot{q}_j} = \frac{\partial \vec{R}_i}{\partial q_j} \quad (4.5.9)$$

This identity is illustrated by the double pendulum example in Figure 4.5.2. This figure shows the derivatives of the position and velocity vectors of the mass enter of link 2, with respect to the two generalized coordinates and their time derivatives. Equation (4.5.9) is shown to hold for the example.

The chain rule was applied to \vec{R}_i to derive the identity in (4.5.9). A second identity is obtained by applying the chain rule to $\partial \vec{R}_i / \partial q_j$. Note that by (4.5.3), $\partial \vec{R}_i / \partial q_j$ is only an explicit function of $(q_1, q_2, \dots, q_n, t)$ and not of $(\dot{q}_1, \dot{q}_2, \dot{q}_3, \dots, \dot{q}_n)$. Therefore, by the chain rule,

$$\frac{\tilde{d}}{dt} \left(\frac{\partial \vec{R}_i}{\partial q_j} \right) = \frac{\partial}{\partial t} \left(\frac{\partial \vec{R}_i}{\partial q_j} \right) + \sum_{k=1}^n \frac{\partial}{\partial q_k} \left(\frac{\partial \vec{R}_i}{\partial q_j} \right) \dot{q}_k = \frac{\partial^2 \vec{R}_i}{\partial t \partial q_j} + \sum_{k=1}^n \frac{\partial^2 \vec{R}_i}{\partial q_k \partial q_j} \dot{q}_k = \frac{\partial}{\partial q_j} \left(\frac{\partial \vec{R}_i}{\partial t} + \sum_{k=1}^n \frac{\partial \vec{R}_i}{\partial q_k} \dot{q}_k \right) \quad (4.5.10)$$



$$\vec{R}_{G_2} = [L_1 \sin(q_1) + a \sin(q_2)] \hat{i} + [-z(t) - L_1 \cos(q_1) - a \cos(q_2)] \hat{j}$$

$$\vec{V}_{G_2} = \dot{\vec{R}}_{G_2} = [L_1 \dot{q}_1 \cos(q_1) + a \dot{q}_2 \cos(q_2)] \hat{i} + [-\dot{z}(t) + L_1 \dot{q}_1 \sin(q_1) + a \dot{q}_2 \sin(q_2)] \hat{j}$$

$$\frac{\partial \vec{R}_{G_2}}{\partial q_1} = [L_1 \cos(q_1)] \hat{i} + [L_1 \sin(q_1)] \hat{j} = \frac{\partial \dot{\vec{R}}_{G_2}}{\partial \dot{q}_1}$$

$$\frac{\partial \vec{R}_{G_2}}{\partial q_2} = [a \cos(q_2)] \hat{i} + [a \sin(q_2)] \hat{j} = \frac{\partial \dot{\vec{R}}_{G_2}}{\partial \dot{q}_2}$$

Figure 4.5.2 Double pendulum example of first \vec{R} identity (4.5.9)

The term in brackets in (4.5.10) is $\dot{\vec{R}}_i$ from (4.5.8). Therefore, (4.5.10) yields the *second “ \vec{R} ” identity*:

$$\frac{\partial}{\partial q_j} \left(\frac{\tilde{n}d}{dt} \left(\vec{R}_i \right) \right) = \frac{\partial \dot{\vec{R}}_i}{\partial q_j} = \frac{\tilde{n}d}{dt} \left(\frac{\partial \vec{R}_i}{\partial q_j} \right) \quad (4.5.11)$$

4.5.2 System of Particles

The kinetic energy of a mass contained in volume V is defined by

$$T = \frac{1}{2} \int_V \frac{\tilde{n}d}{dt} \left(\vec{R} \right) \cdot \frac{\tilde{n}d}{dt} \left(\vec{R} \right) dm = T(q_1 \ q_2 \ \cdots \ q_n, \ \dot{q}_1 \ \dot{q}_2 \ \cdots \ \dot{q}_n, \ t) \quad (4.5.12a)$$

or by (4.5.1) as

$$\begin{aligned} T &= \frac{1}{2} \sum_{i=1}^{N_\infty} \left(\frac{\tilde{n}d}{dt} \vec{R}_i \right) \cdot \left(\frac{\tilde{n}d}{dt} \vec{R}_i \right) m_i \\ &= \frac{1}{2} \sum_{i=1}^{N_\infty} \dot{\vec{R}}_i(q_1 \ q_2 \ \cdots \ q_n, \ \dot{q}_1 \ \dot{q}_2 \ \cdots \ \dot{q}_n, \ t) \cdot \dot{\vec{R}}_i(q_1 \ q_2 \ \cdots \ q_n, \ \dot{q}_1 \ \dot{q}_2 \ \cdots \ \dot{q}_n, \ t) m_i \end{aligned} \quad (4.5.12b)$$

where the left superscript indicates that the time derivative is sensed in inertial frame \tilde{n} . Then it follows that

$$\frac{dT}{dq_j} = \sum_{i=1}^{N_\infty} \frac{1}{2} \left(\frac{\partial \dot{\vec{R}}_i}{\partial q_j} \cdot \dot{\vec{R}}_i + \dot{\vec{R}}_i \cdot \frac{\partial \dot{\vec{R}}_i}{\partial q_j} \right) m_i = \sum_{i=1}^{N_\infty} \dot{\vec{R}}_i \cdot \frac{\partial \dot{\vec{R}}_i}{\partial q_j} m_i \quad (4.5.13)$$

for all independent generalized coordinates $j = 1, 2, \dots, n$. Substitute (4.5.10) into (4.5.13) to obtain

$$\frac{dT}{dq_j} = \sum_{i=1}^{N_\infty} m_i \dot{\vec{R}}_i \cdot \left(\frac{\tilde{n}d}{dt} \frac{\partial \vec{R}_i}{\partial q_j} \right) \quad (4.5.14)$$

Similarly, from (4.5.12b),

$$\frac{dT}{d\dot{q}_j} = \sum_{i=1}^{N_\infty} m_i \dot{\vec{R}}_i \cdot \frac{\partial \dot{\vec{R}}_i}{\partial \dot{q}_j} \quad (4.5.15)$$

for all independent generalized coordinates $j = 1, 2, \dots, n$. Substitute the first \vec{R}_i identity (4.5.9) into (4.5.15):

$$\frac{dT}{d\dot{q}_j} = \sum_{i=1}^{N_\infty} m_i \dot{\vec{R}}_i \cdot \frac{\partial \vec{R}_i}{\partial \dot{q}_j} \quad (4.5.16)$$

Next, take the time derivative of (4.5.16):

$$\frac{\tilde{n}d}{dt} \left(\frac{dT}{d\dot{q}_j} \right) = \sum_{i=1}^{N_\infty} \left[\left(m_i \ddot{\vec{R}}_i \right) \cdot \frac{\partial \vec{R}_i}{\partial q_j} + m_i \dot{\vec{R}}_i \cdot \frac{\tilde{n}d}{dt} \left(\frac{\partial \vec{R}_i}{\partial q_j} \right) \right] \quad (4.5.17)$$

Substitute (4.5.14) into (4.5.17) to obtain

$$\frac{\tilde{n}d}{dt} \left(\frac{\partial T}{\partial \dot{q}_j} \right) - \frac{\partial T}{\partial q_j} = \sum_{i=1}^{N_\infty} \left(m_i \ddot{\vec{R}}_i \right) \cdot \frac{\partial \vec{R}_i}{\partial q_j} \quad (4.5.18)$$

Newton's second law states that

$$m_i \ddot{\vec{R}}_i = \vec{F}_i = \vec{F}_i^{\text{app}} + \vec{F}_i^{\text{int}} \quad (4.5.19)$$

where

\vec{F}_i^{app} = the sum (resultant) of all applied forces acting on differential mass m_i

\vec{F}_i^{int} = the sum (resultant) of all interaction forces acting on differential mass m_i due to its neighboring differential masses

Thus, (4.5.18) may be written as

$$\frac{n d}{dt} \left(\frac{\partial T}{\partial \dot{q}_j} \right) - \frac{\partial T}{\partial q_j} = \sum_{i=1}^{N_\infty} \left(\vec{F}_i^{\text{app}} + \vec{F}_i^{\text{int}} \right) \cdot \frac{\partial \vec{R}_i}{\partial q_j} \quad (4.5.20)$$

Apply Newton's third law (equal and opposite reactions) and assume that the interaction forces only exist between neighboring m_i that are separated by an infinitesimally small distance. This will cancel terms like

$$\vec{F}_i^{\text{int}} \cdot \frac{\partial \vec{R}_i}{\partial q_j} + \vec{F}_{i+1}^{\text{int}} \cdot \frac{\partial \vec{R}_{i+1}}{\partial q_j} = \vec{F}_i^{\text{int}} \cdot \frac{\partial \vec{R}_i}{\partial q_j} - \vec{F}_i^{\text{int}} \cdot \frac{\partial \vec{R}_i}{\partial q_j} = 0 \quad (4.5.21)$$

where m_i and m_{i+1} represent neighboring masses. In Equation (4.5.21), it is assumed that neighboring particles i and $i+1$ are separated by an infinitesimal distance and have identical motions. This is true if these particles are embedded in a continuous structural member, but may not be true if they represent particles at a contact point between two bodies that have relative sliding motion. The contact forces should be considered to be applied forces (\vec{F}_i^{app}) for this case. Collecting these results in (4.5.18) yields

$$\frac{\tilde{n}d}{dt} \left(\frac{\partial T}{\partial \dot{q}_j} \right) - \frac{\partial T}{\partial q_j} = \sum_{i=1}^{N_\infty} \vec{F}_i^{\text{app}} \cdot \frac{\partial \vec{R}_i}{\partial q_j} \quad (4.5.22)$$

Note that applied forces only occur at a finite number (n_F) of locations in the system; therefore, (4.5.22) becomes

Lagrange's Equations for a System of Particles

$$\tilde{n}d \left(\frac{\partial T}{\partial \dot{q}_j} \right) - \frac{\partial T}{\partial q_j} = Q_j \quad (4.5.23)$$

$j = 1, 2, \dots, n$ independent generalized coordinates (q_1, q_2, \dots, q_n)

T = sum of all kinetic energies in the system

$$Q_j = j\text{th "generalized force"} = \sum_{i=1}^{n_F} \bar{F}_i^{\text{app}} \cdot \frac{\tilde{n}\partial \bar{R}_i}{\partial q_j} = \sum_{i=1}^{n_F} \bar{F}_i^{\text{app}} \cdot \frac{\tilde{n}\partial \bar{v}_i}{\partial \dot{q}_j} \quad (4.5.24)$$

where the second equality holds if (4.5.9) is satisfied.

\bar{F}_i^{app} = i th applied force in the system

n_F = total number of applied forces acting in the system, including equal and opposite forces at connections of members

\bar{R}_i = position vector to the point of application for \bar{F}_i^{app}

\bar{v}_i = velocity of the point of application for \bar{F}_i^{app}

This result provides a full set of n EOM to solve for the n generalized coordinate q_i . The preceding derivation demonstrated that if the system is in dynamic equilibrium (all masses move in accordance with Newton's law (4.5.19)), then LE will be satisfied, that is, satisfaction of LE is a necessary condition for equilibrium. The proof that the solution of LE is a sufficient condition for dynamic equilibrium, that is, that the EOM obtained by solving LE are identical to those obtained by solving Newton's laws, may be shown utilizing the principle of virtual work and D'Alembert's principle.

4.5.3 Collection of Rigid Bodies

Consider the RB model depicted in Figure 4.5.3. The position vector \bar{R}_i to the point of application of force \bar{F}_i^{app} is

$$\bar{R}_i = \bar{R}_A + \bar{R}_{i/A} \quad (4.5.25)$$

Thus, the corresponding velocity relation is

$${}^n\bar{v}_i = {}^n\bar{v}_A + {}^n\bar{v}_{i/A} \quad (4.5.26)$$

where A is a point about which moments are taken.

From (4.5.24),

$$\begin{aligned} Q_j &= \sum_{i=1}^{n_F} \bar{F}_i^{\text{app}} \cdot \frac{{}^n\partial \bar{R}_i}{\partial q_j} = \left(\sum_{i=1}^{n_F} \bar{F}_i^{\text{app}} \right) \cdot \frac{{}^n\partial \bar{R}_A}{\partial q_j} + \sum_{i=1}^{n_F} \bar{F}_i^{\text{app}} \cdot \frac{{}^n\partial \bar{R}_{i/A}}{\partial q_j} \\ &= \bar{F}_{\text{tot}}^{\text{app}} \cdot \frac{{}^n\partial \bar{R}_A}{\partial q_j} + \sum_{i=1}^{n_F} \left(\bar{F}_i^{\text{app}} \cdot \frac{{}^n\partial \bar{R}_{i/A}}{\partial q_j} \right) \end{aligned} \quad (4.5.27)$$

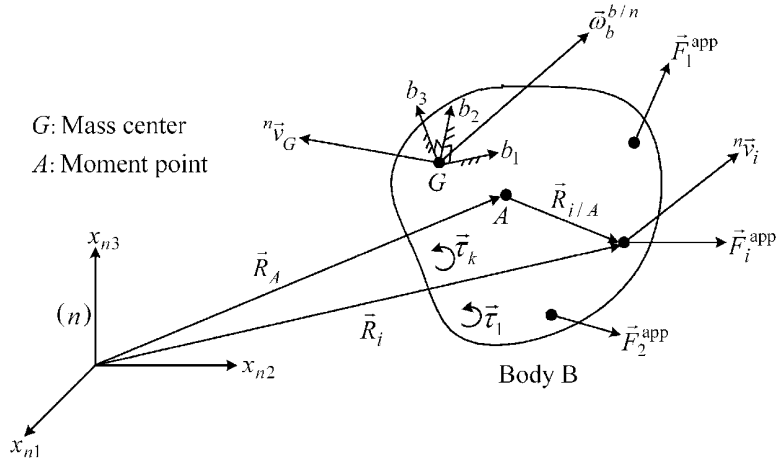


Figure 4.5.3 Rigid body with applied forces and moment point A

where

$$\vec{F}_{\text{tot}}^{\text{app}} = \text{resultant of all applied forces acting on the rigid body} = \sum_{i=1}^{n_F} \vec{F}_i^{\text{app}} \quad (4.5.28)$$

By the chain rule (4.5.4),

$$\frac{{}^n d \vec{R}_{i/A}}{dt} = \frac{\partial \vec{R}_{i/A}}{\partial t} + \sum_{k=1}^n \frac{\partial \vec{R}_{i/A}}{\partial q_k} \dot{q}_k \quad (4.5.29)$$

For reasons similar to the derivation of (4.5.9), taking the partial derivative of (4.5.29) with respect to \dot{q}_k yields

$$\frac{\partial \dot{\vec{R}}_{i/A}}{\partial \dot{q}_k} = \frac{\partial \vec{R}_{i/A}}{\partial q_k} \quad (4.5.30)$$

Then (4.5.27) becomes

$$Q_j = \vec{F}_{\text{tot}}^{\text{app}} \cdot \frac{{}^n \partial \vec{R}_A}{\partial q_j} + \sum_{i=1}^{n_F} \left(\vec{F}_i^{\text{app}} \cdot \frac{{}^n \partial \dot{\vec{R}}_{i/A}}{\partial \dot{q}_j} \right) \quad (4.5.31)$$

Utilize the transport theorem (2.11.27) on the term $\dot{\vec{R}}_{i/A}$:

$$\frac{{}^n d}{dt} (\vec{R}_{i/A}) = \dot{\vec{R}}_{i/A} = \frac{{}^b d}{dt} (\vec{R}_{i/A}) + \vec{\omega}_b^{-b/n} \times \vec{R}_{i/A} \quad (4.5.32)$$

The first term on the RHS of (4.5.32) is zero by the RB approximation. Substitute (4.5.32) into (4.5.31):

$$Q_j = \vec{F}_{\text{tot}}^{\text{app}} \cdot \frac{{}^n \partial \vec{R}_A}{\partial q_j} + \sum_{i=1}^{n_F} \left(\vec{F}_i^{\text{app}} \cdot \frac{\partial (\vec{\omega}_b^{-b/n} \times \vec{R}_{i/A})}{\partial \dot{q}_j} \right) \quad (4.5.33)$$

The vector $\vec{R}_{i/A}$ is independent of \dot{q}_j so (4.5.33) becomes

$$Q_j = \vec{F}_{\text{tot}}^{\text{app}} \cdot \frac{{}^n \partial \vec{R}_A}{\partial q_j} + \sum_{i=1}^{n_F} \vec{F}_i^{\text{app}} \cdot \left(-\vec{R}_{i/A} \times \frac{\partial \vec{\omega}_b^{b/n}}{\partial \dot{q}_j} \right) \quad (4.5.34)$$

Utilize the triple product formula

$$\vec{a} \cdot (\vec{b} \times \vec{c}) = (\vec{a} \times \vec{b}) \cdot \vec{c} \quad (4.5.35)$$

to obtain

$$Q_j = \vec{F}_{\text{tot}}^{\text{app}} \cdot \frac{{}^n \partial \vec{R}_A}{\partial q_j} + \sum_{i=1}^{n_F} -\vec{F}_i^{\text{app}} \times \vec{R}_{i/A} \cdot \frac{\partial \vec{\omega}_b^{b/n}}{\partial \dot{q}_j} = \vec{F}_{\text{tot}}^{\text{app}} \cdot \frac{{}^n \partial \vec{R}_A}{\partial q_j} + \left(\sum_{i=1}^{n_F} \vec{R}_{i/A} \times \vec{F}_i^{\text{app}} \right) \cdot \frac{\partial \vec{\omega}_b^{b/n}}{\partial \dot{q}_j} \quad (4.5.36)$$

The resultant moment of the applied forces taken about point A is

$$\vec{\Gamma}_{\text{tot}}^{\text{app}} = \sum_{i=1}^{n_F} \vec{R}_{i/A} \times \vec{F}_i^{\text{app}} \quad (4.5.37)$$

Point forces are idealized representations of actual force distributions. For instance, most forces are applied over a finite area over which they exert a pressure or more generally a traction. Some force distributions are unknown except for the resultant force and *pure torque* (τ) which they produce. Some examples are the magnetic field in a motor, the hydrodynamic force in an oil film bearing, or the aerodynamic force in a fan or turbine. Some devices such as an oil film bearing produce resultant forces (to support a spinning shaft) plus a pure torque τ_D (drag torque due to oil friction). Thus, Equation (4.5.37) may be extended to include a resultant of pure (distributed) torques and a resultant moment about A of concentrated forces. Then (4.5.36) can assume a more general form that accounts for the existence of pure torques. These results are summarized below with the use of (4.5.9) for generalization.

Generalized Forces Q_j for a Single Rigid Body in Terms of Force, Moment, and Torque Resultants

$$\begin{aligned} Q_j &= \vec{F}_{\text{tot}} \cdot \frac{{}^n \partial \vec{R}_A}{\partial q_j} + \left(\vec{\Gamma}_{\text{tot},A} + \vec{\tau}_{\text{tot}} \right) \cdot \frac{{}^n \partial \vec{\omega}_b^{b/n}}{\partial \dot{q}_j} \\ &= \vec{F}_{\text{tot}} \cdot \frac{\partial {}^n \vec{v}_A}{\partial \dot{q}_j} + \left(\vec{\Gamma}_{\text{tot},A} + \vec{\tau}_{\text{tot}} \right) \cdot \frac{{}^n \partial \vec{\omega}_b^{b/n}}{\partial \dot{q}_j} \end{aligned} \quad (4.5.38)$$

where

A = an arbitrary point about which moments are taken, which is fixed in body-fixed frame b (Figure 4.5.3)

q_j = j th generalized coordinates for $j = 1, 2, \dots, n$

$\vec{F}_{\text{tot}} = \sum_{i=1}^{n_F} \vec{F}_i^{\text{app}}$ = resultant of all applied forces acting on the rigid body

$\vec{R}_A = \vec{R}_A(q_1, q_2, \dots, q_n, t)$ = position vector for point A

$$\vec{\Gamma}_{\text{tot},A} = \sum_{i=1}^{n_F} \vec{R}_{i/A} \times \vec{F}_i^{\text{app}} = \text{resultant moment about point A of all applied forces acting on the rigid body} \quad (4.5.39)$$

$$\vec{\tau}_{\text{tot}} = \sum_{i=1}^{n_F} \vec{\tau}_k = \text{resultant of all pure torques acting on the rigid body}$$

${}^n\vec{\omega}_b^{b/n}$ = angular velocity of body-fixed frame b , relative to inertial frame n , with components in b

${}^n\vec{v}_A$ = velocity of point A, as sensed in inertia frame n

The second equality in (4.5.38) holds if ${}^n\partial\vec{R}_A/\partial q_j = \partial^n\vec{v}_A/\partial\dot{q}_j$

Sometimes, it is preferable to use only the individual forces instead of their resultants for evaluating the generalized forces Q_j . This avoids evaluation of $\vec{\Gamma}_{\text{tot},A}$ and ${}^n\vec{v}_A$. Recall from (4.5.24) that

$$Q_j = \sum_{i=1}^{n_{FF}} \vec{F}_i^{\text{app}} \cdot \frac{{}^n\partial\vec{R}_i}{\partial q_j} + \sum_{i=1}^{n_{F\tau}} \vec{F}_i^{\text{app}} \cdot \frac{{}^n\partial\vec{R}_i}{\partial q_j} \quad (4.5.40)$$

The second sum in this expression is taken over all force distributions that produce pure torques, and the first sum is over all remaining forces and force distributions. The former include differential forces acting over differential areas, combining to form a torque. Force distributions that produce pure torques may also produce nonzero force resultants. These force resultants are accounted for in the first sum of (4.5.40). Consideration of (4.5.38) shows that the second sum in (4.5.40) is

$$\sum_{i=1}^{n_{F\tau}} \vec{F}_i^{\text{app}} \cdot \frac{{}^n\partial\vec{R}_i}{\partial q_j} = \vec{\tau}_{\text{tot}} \cdot \frac{{}^n\partial\vec{\omega}_b^{b/n}}{\partial\dot{q}_j} \quad (4.5.41)$$

Therefore, Q_j in (4.5.40) may be written as

Generalized Forces Q_j for a Single Rigid Body with Component Forces and a Resultant Torque

$$Q_j = \sum_{i=1}^{n_F} \left(\vec{F}_i^{\text{app}} \cdot \frac{{}^n\partial\vec{R}_i}{\partial q_j} \right) + \vec{\tau}_{\text{tot}} \cdot \frac{{}^n\partial\vec{\omega}_b^{b/n}}{\partial\dot{q}_j} = \sum_{i=1}^{n_F} \left(\vec{F}_i^{\text{app}} \cdot \frac{{}^n\partial\vec{v}_i}{\partial\dot{q}_j} \right) + \vec{\tau}_{\text{tot}} \cdot \frac{{}^n\partial\vec{\omega}_b^{b/n}}{\partial\dot{q}_j} \quad (4.5.42)$$

where

n_F = total number of applied forces acting on the rigid body

\vec{R}_i = position vector for point of application of \vec{F}_i^{app} , in Figure 4.5.3 (4.5.43)

\vec{F}_i^{app} = i th applied force on body B . These include resultants of force distributions which may or may not produce torques $\vec{\tau}$

The second equality in (4.5.42) holds if ${}^n\partial\vec{R}_i/\partial q_j = \partial^n\vec{v}_i/\partial\dot{q}_j$

Recall from (4.5.23) that LE apply to the *total* system. Thus, for a collection of RB, T is the sum of the kinetic energies of all the RB expressed in terms of generalized coordinates $(q_1, q_2, \dots, q_n, \dot{q}_1, \dot{q}_2, \dots, \dot{q}_n)$. Also, \bar{F}_i^{app} include all forces acting on the RB with equal and opposite interconnection forces included independently. Therefore, from (4.5.9) and (4.5.24),

$$Q_j = \left(\sum_{i=1}^{n_{FE}} \bar{F}_{iE}^{\text{app}} \cdot \frac{\partial \bar{R}_i}{\partial q_j} + \sum_{i=1}^{n_{FI}} \bar{F}_{iI}^{\text{app}} \cdot \frac{\partial \bar{R}_i}{\partial q_j} \right)_{\text{rigid body 1}} + \left(\sum_{i=1}^{n_{FE}} \bar{F}_{iE}^{\text{app}} \cdot \frac{\partial \bar{R}_i}{\partial q_j} + \sum_{i=1}^{n_{FI}} \bar{F}_{iI}^{\text{app}} \cdot \frac{\partial \bar{R}_i}{\partial q_j} \right)_{\text{rigid body 2}} + \dots + \left(\sum_{i=1}^{n_{FE}} \bar{F}_{iE}^{\text{app}} \cdot \frac{\partial \bar{R}_i}{\partial q_j} + \sum_{i=1}^{n_{FI}} \bar{F}_{iI}^{\text{app}} \cdot \frac{\partial \bar{R}_i}{\partial q_j} \right)_{\text{rigid body } N_B} \quad (4.5.44)$$

or by using (4.5.9)

$$Q_j = \left(\sum_{i=1}^{n_{FE}} \bar{F}_{iE}^{\text{app}} \cdot \frac{\partial^n \bar{v}_i}{\partial q_j^n} + \sum_{i=1}^{n_{FI}} \bar{F}_{iI}^{\text{app}} \cdot \frac{\partial^n \bar{v}_i}{\partial q_j^n} \right)_{\text{rigid body 1}} + \left(\sum_{i=1}^{n_{FE}} \bar{F}_{iE}^{\text{app}} \cdot \frac{\partial^n \bar{v}_i}{\partial q_j^n} + \sum_{i=1}^{n_{FI}} \bar{F}_{iI}^{\text{app}} \cdot \frac{\partial^n \bar{v}_i}{\partial q_j^n} \right)_{\text{rigid body 2}} + \dots + \left(\sum_{i=1}^{n_{FE}} \bar{F}_{iE}^{\text{app}} \cdot \frac{\partial^n \bar{v}_i}{\partial q_j^n} + \sum_{i=1}^{n_{FI}} \bar{F}_{iI}^{\text{app}} \cdot \frac{\partial^n \bar{v}_i}{\partial q_j^n} \right)_{\text{rigid body } N_B} \quad (4.5.45)$$

The first sum in all terms of (4.5.44) or (4.5.45) accounts for external (E) forces acting on the bodies, and the second sum accounts for the interaction (I) forces between bodies. Some of the interaction forces are distributed in nature. These local force distributions may be replaced by force resultants and friction torques. The definition of Q_j as a sum in (4.5.44) or (4.5.45) permits net contributions from bodies joined at an interconnection to simplify or sum to zero. For example, let body (1) and body (2) be joined at an “ideal joint” (*zero rattle space*). Then the joint reaction’s contribution to Q_j in (4.5.45) is

$$\bar{F}_{iI}^{\text{app}} \cdot \frac{\partial^n \bar{v}_{i1}}{\partial q_j^n} + \left(-\bar{F}_{iI}^{\text{app}} \right) \cdot \frac{\partial^n \bar{v}_{i2}}{\partial q_j^n} = \bar{F}_{iI}^{\text{app}} \cdot \frac{\partial^n \bar{v}_{i1/i2}}{\partial q_j^n} \equiv 0 \quad (4.5.46)$$

since the relative velocities ${}^n \bar{v}_{i1/i2}$ between bodies (1) and (2) at an ideal joint is zero. The expression in (4.5.46) will also be zero for the same reason if:

- One of the bodies is ground (fixed in inertial space), that is, ${}^n \bar{v}_{i1} = {}^n \bar{v}_{i2} = 0$.
- The two bodies are connected by a rolling contact interface, since the relative velocity ${}^n \bar{v}_{i1/i2}$ of the two bodies at the rolling contact point is zero.

The first sum in (4.5.44) or (4.5.45) may be expressed in the forms of (4.5.38) or (4.5.42) for each body. The result for a collection of RB is summarized below.

Generalized Forces Q_j for (N_B) Multiple Rigid Bodies with Component or Resultant Forces and Resultant Torque

$$Q_j = \sum_{l=1}^{N_B} Q_{jl} \quad (4.5.47)$$

$$Q_{jl} = Q_{Fjl} + \vec{\tau}_{\text{tot},l} \cdot \frac{{}^n \partial \vec{\omega}_{bl}^{bl/n}}{\partial \dot{q}_j} \quad (4.5.48)$$

where any of the following forms can be used for Q_{Fjl} :

(a) Use force resultant on each body:

$$\vec{F}_{\text{tot}}^l \cdot \frac{{}^n \partial \vec{R}_{Al}}{\partial q_j} + \vec{\Gamma}_{\text{tot},A}^l \cdot \frac{{}^n \partial \vec{\omega}_{bl}^{bl/n}}{\partial \dot{q}_j} \quad (4.5.49)$$

(b) Use force resultant on each body:

$$\vec{F}_{\text{tot}}^l \cdot \frac{\partial {}^n \vec{v}_{Al}}{\partial \dot{q}_j} + \vec{\Gamma}_{\text{tot},A}^l \cdot \frac{{}^n \partial \vec{\omega}_{bl}^{bl/n}}{\partial \dot{q}_j} \quad (4.5.50)$$

(Same as (a) but with (4.5.9).)

(c) Use individual forces on each body:

$$\sum_{i=1}^{n_{Fl}} \vec{F}_{il} \cdot \frac{{}^n \partial \vec{R}_{il}}{\partial q_j} \quad (4.5.51)$$

(d) Use individual forces on each body:

$$\sum_{i=1}^{n_{Fl}} \vec{F}_{il} \cdot \frac{\partial {}^n \vec{v}_{il}}{\partial \dot{q}_j} \quad (4.5.52)$$

and the remaining terms are defined by

$$\vec{F}_{\text{tot}}^l = \sum_{i=1}^{n_{Fl}} \vec{F}_{il} = \text{resultant of all } \vec{F}_{il} \text{ acting on rigid body } l$$

$$\vec{\Gamma}_{\text{tot},A}^l = \sum_{i=1}^{n_{Fl}} \vec{R}_{il/A_l} \times \vec{F}_{il} = \text{resultant moment about point } A \text{ of all forces acting on rigid body } l$$

$q_j = j$ th independent generalized coordinate of the system

$\vec{\tau}_{\text{tot},l}$ = vector sum of all pure torques acting on rigid body l , including external and interconnection (drag or friction) pure torques

$\vec{\omega}_{bl}^{bl/n}$ = angular velocity vector of rigid body l with respect to the inertial frame n , with components in b_l (reference frame fixed to body l)

\vec{F}_{il} = i th force acting on body l , excluding all reaction forces at interconnections between bodies with Q_{Fjl} contributions that cancel when the system is considered as a whole (see (4.5.46) and related discussion). (The number of these forces on body l is n_{Fl} .)

A_l = an arbitrary point that is fixed on body l and about which moments of forces acting on body l are taken

$$\vec{R}_{Al} = \text{position vector of } A_l, \text{ as sensed in inertial frame } n \quad (4.5.53)$$

\vec{R}_{il} = position vector of the point of application for \vec{F}_{il}

\vec{R}_{il/A_l} = position vector of point of application of force \vec{F}_{il} relative to moment point A_l , that is, $\vec{R}_{il/A_l} = \vec{R}_{il} - \vec{R}_{Al}$

$${}^n\vec{v}_{Al} = \frac{d}{dt} \vec{R}_{Al} = \text{velocity of point } A_l, \text{ as sensed in inertial frame } n$$

$${}^n\vec{v}_{il} = \frac{d}{dt} \vec{R}_{il} = \text{velocity of point of application for } \vec{F}_{il}, \text{ as sensed in inertial frame } n$$

4.5.4 Potential, Circulation, and Dissipation Functions

Implementation of LE is simplified by replacing forces and torques in the generalized force formulas (4.5.47)–(4.5.52) with gradients of scalar functions. Recall from Section 4.3 that conservative forces can be represented as gradients of *potential functions*. Viscous damping and circulatory forces may also be expressed in a similar manner. To illustrate this, consider the intentionally general system of interconnected RBs shown in Figure 4.5.4.

4.5.4.1 Weight Loads (w_i)

Recall from (4.3.18) that the potential energy function for the weight w_i of RB i is

$$U_{wi} = w_i x_{n3}^{Gi} \quad (4.5.54)$$

The contribution of w_i to Q_j is from (4.5.51)

$$Q_j^{wi} = -w_i n_3 \cdot \frac{\partial \vec{R}_{Gi}}{\partial q_j} = \left(-\frac{\partial U_{wi}}{\partial x_{n3}^{Gi}} n_3 \right) \cdot \left(\frac{\partial x_{n1}^{Gi}}{\partial q_j} n_1 + \frac{\partial x_{n2}^{Gi}}{\partial q_j} n_2 + \frac{\partial x_{n3}^{Gi}}{\partial q_j} n_3 \right) = -\frac{\partial U_{wi}}{\partial x_{n3}^{Gi}} \frac{\partial x_{n3}^{Gi}}{\partial q_j} = -\frac{\partial U_{wi}}{\partial q_j} \quad (4.5.55)$$

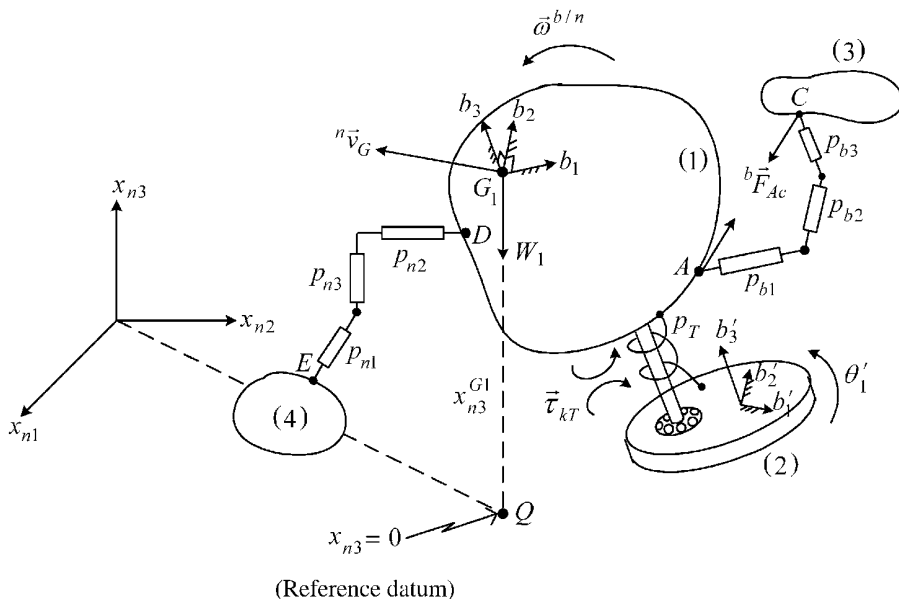


Figure 4.5.4 System of rigid bodies with motion-dependent forces

Summarizing, if

$$\vec{F}^{wi} = -w_i n_3 \quad (4.5.56)$$

the potential energy U_{wi} is

$$U_{wi} = w_i x_{n3}^{Gi} \quad (4.5.57)$$

and the contribution of w_i to the generalized force Q_j becomes

$$Q_j^{wi} = -\frac{\partial U_{wi}}{\partial q_j} \quad (4.5.58)$$

4.5.4.2 Translational Stiffness Defined in the Inertial Frame: Symmetric Stiffness Matrix

Consider the case where the p force elements in Figure 4.5.4 represent a general stiffness connection between D and E , that is,

$$\underline{F}_{KDE} = -\underline{K}_{DE}(\underline{R}_D - \underline{R}_E) - \underline{K}_{DE}(\underline{R}_{D0} - \underline{R}_{E0}) = -\underline{K}_{DE}\underline{R}_{D/E} - \underline{K}_{DE}\underline{R}_{D/E}^0 \quad (4.5.59)$$

where \underline{K}_{DE} is a symmetric matrix and $\underline{R}_{D/E}^0$ is a vector of prestretch displacements of the stiffness element. A special case occurs if \underline{K}_{DE} is diagonal and $\underline{R}_{D/E}^0$ equals zero which implies

$$\underline{F}_{KDE} = -k_{n1}\Delta x_{n1}n_1 - k_{n2}\Delta x_{n2}n_2 - k_{n3}\Delta x_{n3}n_3 \quad (4.5.60)$$

where

$$\Delta x_{n1} = x_{n1D} - x_{n1E}, \quad \Delta x_{n2} = x_{n2D} - x_{n2E}, \quad \Delta x_{n3} = x_{n3D} - x_{n3E} \quad (4.5.61)$$

This, for instance, could be the force representation for the vehicle suspension leaf spring in Figure 4.5.5.

Define the scalar potential function

$$U_{KDE} = \frac{1}{2} \underline{R}_{D/E}^T \underline{K}_{DE} \underline{R}_{D/E} + \underline{R}_{D/E}^T \underline{K}_{DE} \underline{R}_{D/E}^0 \quad (4.5.62)$$

Note that since \underline{K}_{DE} is a constant, symmetric matrix and by using (4.5.59)

$$\begin{aligned} -\frac{\partial U_{KDE}}{\partial q_j} &= -\frac{1}{2} \frac{\partial \left(\underline{R}_{D/E}^T \right)}{\partial q_j} \underline{K}_{DE} \underline{R}_{D/E} - \frac{1}{2} \underline{R}_{D/E}^T \underline{K}_{DE} \frac{\partial \underline{R}_{D/E}}{\partial q_j} - \frac{\partial \left(\underline{R}_{D/E}^T \right)}{\partial q_j} \underline{K}_{DE} \underline{R}_{D/E}^0 \\ &= -\frac{\partial \left(\underline{R}_{D/E}^T \right)}{\partial q_j} \underline{K}_{DE} \left(\underline{R}_{D/E} + \underline{R}_{D/E}^0 \right) = \underline{F}_{KDE} \frac{\partial \underline{R}_{D/E}}{\partial q_j} = \vec{F}_{KDE} \cdot \frac{\partial \vec{R}_D}{\partial q_j} - \vec{F}_{KDE} \cdot \frac{\partial \vec{R}_E}{\partial q_j} \end{aligned} \quad (4.5.63)$$



Figure 4.5.5 Vehicle suspension with translational springs and dampers

The stiffness force is applied at both D and E in the system, and this force is equal and opposite at D and E . This and a comparison of (4.5.63) with (4.5.51) show

Summarizing, if

$$\underline{F}_{KDE} = -\underline{K}_{DE} \{ (\underline{R}_D - \underline{R}_E) + (\underline{R}_{D0} - \underline{R}_{E0}) \} = -\underline{K}_{DE} \begin{pmatrix} \underline{R}_{D/E} + \underline{R}_{D/E}^0 \\ \underline{R}_{D/E} + \underline{R}_{D/E}^0 \end{pmatrix} \quad (4.5.64)$$

where $\underline{K}_{DE}^T = \underline{K}_{DE}$ and $\underline{R}_{D/E}^0$ contains the prestretch deflections of the stiffness element and the scalar potential function is defined by

$$U_{KDE} = \frac{1}{2} \underline{R}_{D/E}^T \underline{K}_{DE} \underline{R}_{D/E} + \underline{R}_{D/E}^T \underline{K}_{DE} \underline{R}_{D/E}^0 \quad (4.5.65)$$

then the contribution of \underline{F}_{KDE} to the generalized force Q_j in (4.5.47) becomes

$$Q_j^{KDE} = -\frac{\partial U_{KDE}}{\partial q_j} \quad (4.5.66)$$

Equations (4.5.64)–(4.5.66) apply if D and E are on two separate bodies or if E or D is fixed or is given some prescribed displacements in the inertial frame n .

EXAMPLE 4.5.1 *Generalized Force for a Symmetric Stiffness Matrix with Prestretch and 1D Spring*

Objective: Show that the generalized force expression (4.5.66) utilizing potential energy yields the same result as the general expression (4.5.51) for a 1-dimensional spring with prestretch (Figure E4.5.1(a)).

For this example,

$$\underline{R}_{D/E} = x_D - x_E, \quad \underline{R}_{D/E}^0 = x_{D0} - x_{E0}, \quad \underline{K}_{DE} = k \quad (1)$$

$$F_D = -k[x_{D0} + x_D - (x_{E0} + x_E)] = -k(x_D - x_E + x_{D0} - x_{E0}) \quad (2)$$

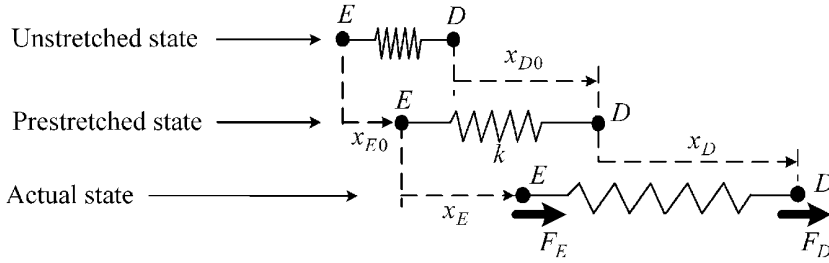


Figure E4.5.1(a) Prestretched spring in its unstretched, prestretched, and actual states

$$F_E = -F_D = k(x_D - x_E + x_{D0} - x_{E0}) \quad (3)$$

From (4.5.65),

$$\begin{aligned} U_{kDE} &= \frac{1}{2}(x_D - x_E)k(x_D - x_E) + (x_D - x_E)k(x_{D0} - x_{E0}) \\ &= \frac{k}{2}(x_D - x_E)^2 + k(x_D - x_E)(x_{D0} - x_{E0}) \end{aligned} \quad (4)$$

From (4.5.47) and (4.5.51), the generalized forces are

$$Q_E = \vec{F}_E \cdot \frac{\partial \vec{R}_E}{\partial q_E} = F_E \frac{\partial x_E}{\partial x_E} = F_E, \quad Q_D = \vec{F}_D \cdot \frac{\partial \vec{R}_D}{\partial q_D} = F_D \frac{\partial x_D}{\partial x_D} = F_D \quad (5)$$

From (4.5.66),

$$\begin{aligned} Q_E &= -\frac{\partial U_{kDE}}{\partial q_E} = \frac{\partial U_{kDE}}{\partial x_E} = k(x_D - x_E) + k(x_{D0} - x_{E0}) \\ Q_D &= -\frac{\partial U_{kDE}}{\partial q_D} = -\frac{\partial U_{kDE}}{\partial x_D} = -k(x_D - x_E) - k(x_{D0} - x_{E0}) \end{aligned} \quad (6)$$

Either the force (5) or potential (6) approach produces the same results by (2) and (3).

4.5.4.3 Translational Stiffness Defined in the Inertial Frame: Unsymmetric Stiffness Matrix

Displacement-dependent forces arise in rotating machinery due to circulation of fluids in tight clearance components such as the fluid film bearing shown in Figure 4.5.6.

These forces are caused by deformation of the fluids by the vibrating shaft and may be described by a nonsymmetric stiffness matrix. The direct stiffness terms are analogous to structural stiffnesses, but the off-diagonal terms are nonsymmetric. A reason for this can be seen from Figure 4.5.7, which is the end view of a shaft, spinning within a fluid film bearing or liquid seal. The observer at A sees fluid circulating in the $+y$ direction, but the observer at B sees the fluid circulating in the $-x$ direction. The shaft is centered and the bearing is axisymmetric; therefore, by symmetry, a force applied on the shaft in the $+x$ direction produces displacements in the $+x$ and $+y$ directions, and the same force



Figure 4.5.6 Five-pad tilting pad journal bearing for supporting a high-speed compressor shaft

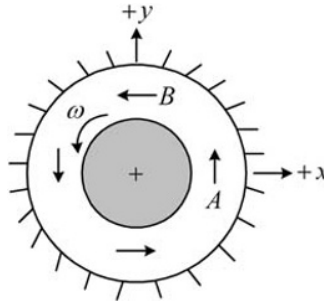


Figure 4.5.7 End view of a component (bearing or seal) with annular clearance and a spinning shaft

applied in the $+y$ direction will cause displacements in the $+y$ and $-x$ direction. This yields an antisymmetric stiffness matrix with equal and opposite off-diagonal terms.

Excellent discussions of this topic may be found in many references including Venkataraman and Palazzolo (1997), Moore and Palazzolo (1999), Suh and Palazzolo (2014), Vance (1987), and Childs (1993). Let \underline{K}_{DE} be nonsymmetric in (4.5.59), that is,

$$\underline{K}_{DE} = \underline{K}_{DE}^{NS} \quad (4.5.67)$$

and define the circulatory scalar function

$$\mathfrak{S}_{DE}^c = \frac{\partial \left(\underline{R}_{D/E}^T \right)}{\partial t} \underline{K}_{DE}^{NS} \underline{R}_{D/E} = \underline{\dot{R}}_{D/E}^T \underline{K}_{DE}^{NS} \underline{R}_{D/E} \quad (4.5.68)$$

$\begin{matrix} 1 \times 3 & 3 \times 3 & 1 \times 3 \end{matrix}$

Note that

$$\frac{-\partial \mathfrak{S}_{DE}^c}{\partial \dot{q}_j} = \frac{-\partial \left(\underline{\dot{R}}_{DE}^T \right)}{\partial \dot{q}_j} \underline{K}_{DE}^{NS} \underline{R}_{D/E} - \underline{\dot{R}}_{D/E}^T \underline{K}_{DE}^{NS} \frac{\partial \left(\underline{R}_{D/E} \right)}{\partial \dot{q}_j} = \frac{-\partial \left(\underline{\dot{R}}_{DE}^T \right)}{\partial \dot{q}_j} \underline{K}_{DE}^{NS} \underline{R}_{D/E} \quad (4.5.69)$$

since $\underline{R}_{D/E}$ is not a function \dot{q}_j . Recall from (4.5.59) that

$$\underline{F}_{KDE}^{NS} = -\underline{K}_{DE}^{NS} \underline{R}_{D/E} \quad (4.5.70)$$

so that

$$\frac{-\partial \mathfrak{S}_{DE}^c}{\partial \dot{q}_j} = (\underline{F}_{KDE}^{\text{NS}})^T \frac{\partial (\underline{\dot{R}}_{D/E})}{\partial \dot{q}_j} \quad (4.5.71)$$

or in vector notation

$$\frac{-\partial \mathfrak{S}_{DE}^c}{\partial \dot{q}_j} = \bar{F}_{KDE}^{\text{NS}} \cdot \frac{\partial ({}^n \vec{v}_{D/E})}{\partial \dot{q}_j} = \bar{F}_{KDE}^{\text{NS}} \cdot \frac{\partial {}^n \vec{v}_D}{\partial \dot{q}_j} - \bar{F}_{KDE}^{\text{NS}} \cdot \frac{\partial {}^n \vec{v}_E}{\partial \dot{q}_j} \quad (4.5.72)$$

The circulatory force is applied at both D and E in the system, and this force is equal and opposite at D and E . This and a comparison of (4.5.72) with (4.5.52) show

If

$$\underline{F}_{KDE} = -\underline{K}_{DE}(\underline{R}_D - \underline{R}_E) = -\underline{K}_{DE} \underline{R}_{D/E} \quad \text{for } \underline{K}_{DE} \text{ general} \quad (4.5.73)$$

and the circulatory scalar function is defined by

$$\mathfrak{S}_{DE}^c = \underline{\dot{R}}_{D/E}^T \underline{K}_{DE} \underline{R}_{D/E} \quad (4.5.74)$$

the contribution of \underline{F}_{KDE} to the generalized force Q_j in (4.5.47) becomes

$$Q_j^{KDE} = -\frac{\partial \mathfrak{S}_{DE}^c}{\partial \dot{q}_j} \quad (4.5.75)$$

Equations (4.5.73)–(4.5.75) apply if D and E are on two separate bodies or if E or D is fixed or is given some prescribed displacements in the inertial frame n .

EXAMPLE 4.5.2 Generalized Force for an Unsymmetric Stiffness Matrix

Objective: Show that the generalized force expression (4.5.75) utilizing the circulatory scalar function yields the same result as the general expression (4.5.52) for an unsymmetric stiffness matrix (Figure E4.5.2(a)).

For this example,

$$\underline{R}_{D/E} = \begin{Bmatrix} x_D - x_E \\ y_D - y_E \end{Bmatrix}, \quad \underline{K}_{DE} = \begin{bmatrix} k_{xx} & k_{xy} \\ k_{yx} & k_{yy} \end{bmatrix}, \quad \underline{\dot{R}}_{D/E} = \begin{Bmatrix} \dot{x}_D - \dot{x}_E \\ \dot{y}_D - \dot{y}_E \end{Bmatrix} \quad (1)$$

$$F_{xD} = -F_{xE} = -k_{xx}(x_D - x_E) - k_{xy}(y_D - y_E) \quad (2)$$

$$F_{yD} = -F_{yE} = -k_{yx}(x_D - x_E) - k_{yy}(y_D - y_E) \quad (3)$$

From (4.5.47) and (4.5.51), the generalized forces are

$$Q_{xD} = \bar{F}_{xD} \cdot \frac{\partial \bar{R}_{xD}}{\partial q_{xD}} = F_{xD} \frac{\partial x_D}{\partial x_D} = F_{xD} \quad (4)$$

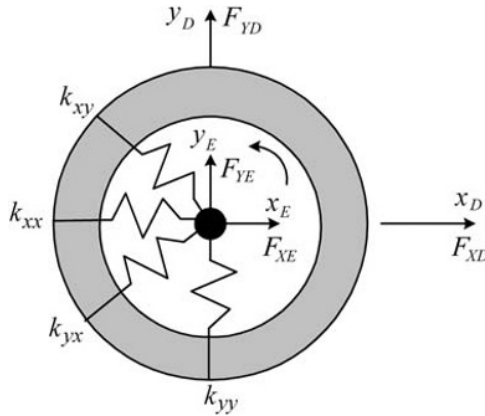


Figure E4.5.2(a) Spinning shaft in seal or bearing yielding an unsymmetric stiffness matrix

Similarly,

$$Q_{yD} = F_{yD}, \quad Q_{xE} = F_{xE}, \quad Q_{yE} = F_{yE} \quad (5)$$

From (4.5.74) and (1),

$$\begin{aligned} \mathfrak{S}_{DE}^c &= \dot{\underline{R}}_{D/E}^T \underline{K}_{DE} \underline{R}_{D/E} \\ &= (\dot{x}_D - \dot{x}_E) [k_{xx}(x_D - x_E) + k_{xy}(y_D - y_E)] + (\dot{y}_D - \dot{y}_E) [k_{yx}(x_D - x_E) + k_{yy}(y_D - y_E)] \end{aligned} \quad (6)$$

From (4.5.75), (2), (3), and (6),

$$Q_{xD} = \frac{\partial \mathfrak{S}_{DE}^c}{\partial \dot{x}_D} = -k_{xx}(x_D - x_E) - k_{xy}(y_D - y_E) = F_{xD} \quad (7)$$

Similar results follow for Q_{yD} , Q_{xE} , and Q_{yE} . The force (4) or potential (7) produces the same result for the generalized forces (Q 's).

4.5.4.4 Translational Damping Force Defined in the Inertial Frame

Damping may result from the intrinsic internal energy dissipation in a deformable component or may result from a specialized damping device as shown by the dampers in Figure 4.5.8.

Consider the case when the p force element in Figure 4.5.4 represents a general, translational damping connection between D and E , that is,

$$\underline{F}_{CDE} = -\underline{C}_{DE} (\dot{\underline{R}}_D - \dot{\underline{R}}_E) = -\underline{C}_{DE} {}^n \underline{v}_{D/E} \quad (4.5.76)$$

where \underline{C}_{DE} is symmetric. A special case occurs if \underline{C}_{DE} is diagonal which implies

$$\bar{F}_{CDE} = -c_{n1} \Delta \dot{x}_{n1} n_1 - c_{n2} \Delta \dot{x}_{n2} n_2 - c_{n3} \Delta \dot{x}_{n3} n_3 \quad (4.5.77)$$

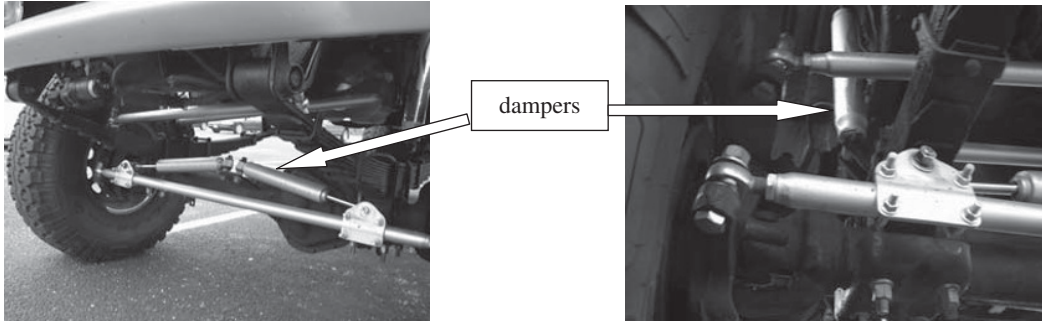


Figure 4.5.8 Translational damper on a vehicle

Define the scalar “Rayleigh dissipation function”

$$\mathfrak{F}_{DE}^d = \frac{1}{2} {}^n \underline{v}_{D/E}^T \underline{C}_{DE} {}^n \underline{v}_{D/E} \quad (4.5.78)$$

Note that since \underline{C}_{DE} is a constant, symmetric matrix and by using (4.5.76)

$$\frac{-\partial \mathfrak{F}_{DE}^d}{\partial \dot{q}_j} = \frac{-\partial ({}^n \underline{v}_{D/E})}{\partial \dot{q}_j} \underline{C}_{DE} {}^n \underline{v}_{D/E} = \underline{F}_{CDE}^T \cdot \frac{\partial {}^n \underline{v}_{D/E}}{\partial \dot{q}_j} = \underline{F}_{CDE}^T \cdot \frac{\partial {}^n \underline{v}_D}{\partial \dot{q}_j} - \underline{F}_{CDE} \cdot \frac{\partial {}^n \underline{v}_E}{\partial \dot{q}_j} \quad (4.5.79)$$

The damping force is applied at both D and E in the system, and this force is equal and opposite at D and E . This and a comparison of (4.5.52) and (4.5.79) show

If

$$\underline{F}_{CDE} = -\underline{C}_{DE} (\dot{\underline{R}}_D - \dot{\underline{R}}_E) = -\underline{C}_{DE} {}^n \underline{v}_{DE} \quad \text{for } \underline{C}_{DE}^T = \underline{C}_{DE} \quad (4.5.80)$$

and the scalar Rayleigh dissipation function is defined by

$$\mathfrak{F}_{DE}^d = \frac{1}{2} {}^n \underline{v}_{D/E}^T \underline{C}_{DE} {}^n \underline{v}_{D/E} \quad (4.5.81)$$

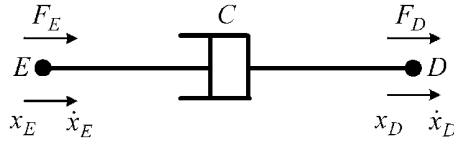
the contribution of \underline{F}_{CDE} to the generalized force Q_j in (4.5.47) becomes

$$Q_j^{CDE} = -\frac{\partial \mathfrak{F}_{DE}^d}{\partial \dot{q}_j} \quad (4.5.82)$$

Equations (4.5.80)–(4.5.82) apply if D and E are on two separate bodies or if E or D is fixed or is given some prescribed motion in the inertial frame n .

EXAMPLE 4.5.3 Generalized Force for a Symmetric Translational Damping Matrix

Objective: Show that the generalized force expression (4.5.82) utilizing the Rayleigh dissipation function yields the same result as the general expression (4.5.52) for a symmetric damping matrix (Figure E4.5.3(a)).

Figure E4.5.3(a) Damping element connecting points D and E

For this example,

$$\underline{V}_{DE} = v_D - v_E = \dot{x}_D - \dot{x}_E, \quad \underline{C}_{DE} = c \quad (1)$$

$$F_D = -c(\dot{x}_D - \dot{x}_E), \quad F_E = c(\dot{x}_D - \dot{x}_E) \quad (2)$$

By (4.5.47) and (4.5.52),

$$Q_D = \bar{F}_D \cdot \frac{\partial \bar{V}_D}{\partial \dot{q}_D} = F_D \frac{\partial \dot{x}_D}{\partial \dot{x}_D} = F_D \quad (3)$$

$$Q_E = \bar{F}_E \cdot \frac{\partial \bar{V}_E}{\partial \dot{q}_E} = F_E \frac{\partial \dot{x}_E}{\partial \dot{x}_E} = F_E \quad (4)$$

From (4.5.81),

$$\mathfrak{S}_{DE}^d = \frac{1}{2}(\dot{x}_D - \dot{x}_E)c(\dot{x}_D - \dot{x}_E) = \frac{c}{2}(\dot{x}_D - \dot{x}_E)^2 \quad (5)$$

By (4.5.82) and (2),

$$Q_D = -\frac{\partial \mathfrak{S}_{DE}^d}{\partial \dot{q}_D} = -\frac{\partial \mathfrak{S}_{DE}^d}{\partial \dot{x}_D} = -c(\dot{x}_D - \dot{x}_E) = F_D \quad (6)$$

$$Q_E = -\frac{\partial \mathfrak{S}_{DE}^d}{\partial \dot{q}_E} = -\frac{\partial \mathfrak{S}_{DE}^d}{\partial \dot{x}_E} = c(\dot{x}_D - \dot{x}_E) = F_E \quad (7)$$

Both force and potential approaches yield the same result for the generalized forces (Q 's).

4.5.4.5 Rotational Stiffness

The relative rotation between two objects produces a restoring torque in a torsional spring connecting the objects. Figure 4.5.9 shows a high-strength commercial torsional spring. Other familiar examples include self-closing door hinges or torsion bars on the front suspension of a vehicle. Torsional stiffness-related vibration problems often occur in structural members, for example, drillstrings, that deflect torsionally due to drive and load (typically cutting or friction) torques.

The torsional spring k_T connects RB (1) and (2) in Figure 4.5.4. These bodies have a relative angular velocity

$$\bar{\omega}_{b'}^{2/1} = \dot{\theta}'_1 b'_3 \quad (4.5.83)$$

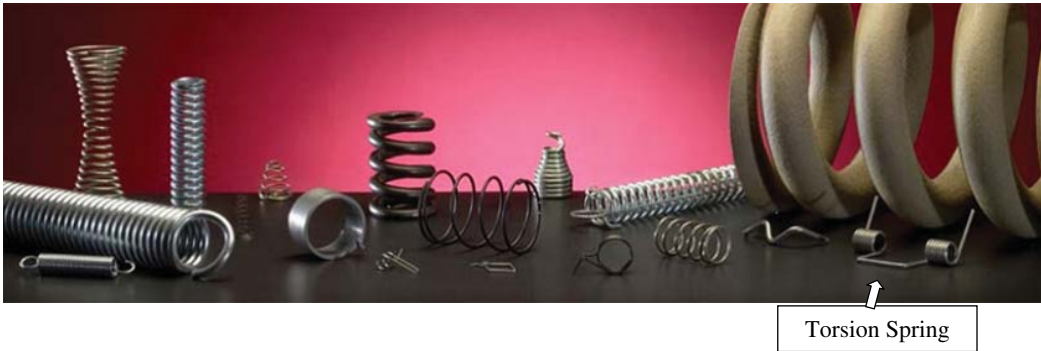


Figure 4.5.9 Rotational (torsional) spring. Reproduced with permission from Murphy & Read Spring Manufacturing Co.

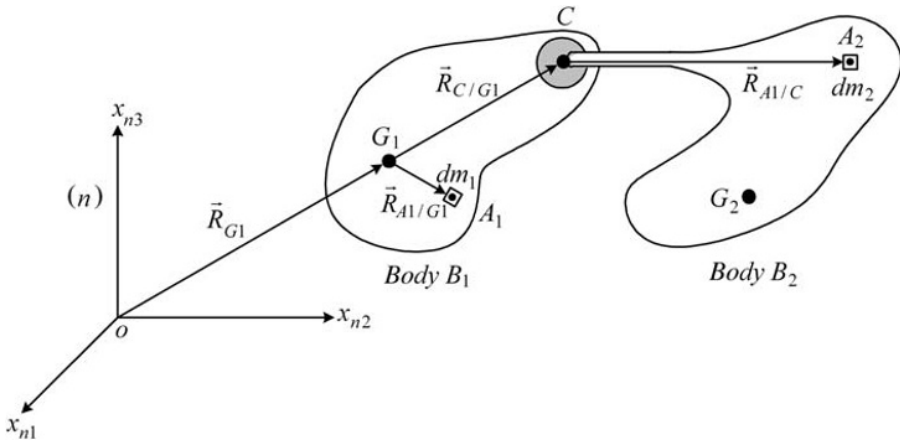


Figure 4.5.10 Ball and socket joint with a three internal rotational spring stiffness

Let $\vec{\tau}_{KT}$ represent the torque provided by the spring, that is,

$$\vec{\tau}_{KT} = -k_T \theta'_1 b'_3 \quad (4.5.84)$$

This description of the torsional spring torque could be generalized by considering up to three Euler angles (Section 2.7) at the joint connecting bodies (1) and (2) as illustrated by the ball and socket joint in Figure 4.5.10. With reference to Figure 4.5.11, the joint torque may appear as

$$\vec{\tau}_{KT} = -k_{T1} \theta_1 b'_3 - k_{T2} \theta_2 b''_2 - k_{T3} \theta_3 b'''_1 \quad (4.5.85)$$

The stiffness torque in (4.5.85) may be generalized to the form

$$\underline{\tau}_{KT} = -\underline{K}_T \underline{\Theta} - \underline{K}_T \underline{\Theta}_0 \quad (4.5.86)$$

where \underline{K}_T is symmetric, $\underline{\Theta}_0$ are initial angular deflections, and

$$\underline{\Theta} = (\theta_1 \ \theta_2 \ \theta_3)^T \quad (4.5.87)$$

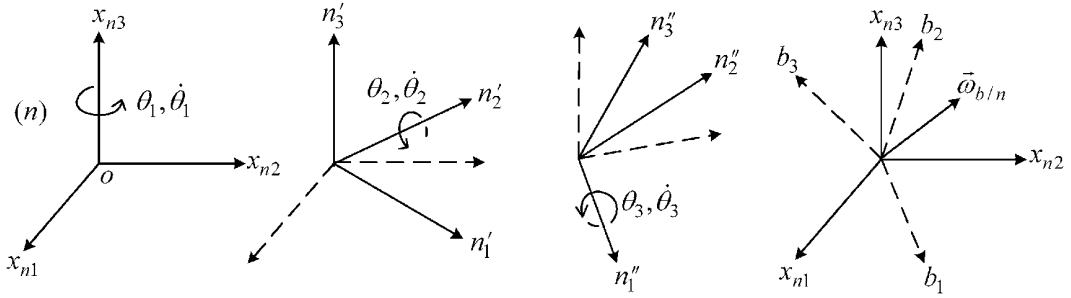


Figure 4.5.11 Successive (3–2–1) Euler angle rotations from frame “n” to frame “b” and angular velocity vector $\bar{\omega}$

Note the first, second, and third rows in $\bar{\tau}_{KT}$, \underline{K}_T , or $\underline{\Theta}$ correspond to the directions b'_3 , b''_2 , and b'''_1 , respectively. Define the scalar potential function

$$U_{KT} = \frac{1}{2} \underline{\Theta}^T \underline{K}_T \underline{\Theta} + \underline{\Theta}^T \underline{K}_T \underline{\Theta}_0 \quad (4.5.88)$$

Then

$$\begin{aligned} -\frac{\partial U_{KT}}{\partial q_j} &= -\frac{1}{2} \frac{\partial}{\partial q_j} \underline{\Theta}^T \underline{K}_T \underline{\Theta} - \frac{1}{2} \underline{\Theta}^T \underline{K}_T \frac{\partial}{\partial q_j} \underline{\Theta} - \frac{\partial}{\partial q_j} \underline{\Theta}^T \underline{K}_T \underline{\Theta}_0 \\ &= \left(-\frac{\partial}{\partial q_j} \underline{\Theta}^T \right) (\underline{K}_T \underline{\Theta} + \underline{K}_T \underline{\Theta}_0) \end{aligned} \quad (4.5.89)$$

which by (4.5.9) implies

$$-\frac{\partial U_{KT}}{\partial q_j} = -\frac{\partial}{\partial q_j} \left(\dot{\underline{\Theta}}^T \right) (\underline{K}_T \underline{\Theta} + \underline{K}_T \underline{\Theta}_0) \quad (4.5.90)$$

The relative angular velocity between bodies (1) and (2) is

$$\bar{\omega}^{-2/1} = \dot{\theta}_1 b'_3 + \dot{\theta}_2 b''_2 + \dot{\theta}_3 b'''_1 \quad (4.5.91)$$

The unit vectors b'_3 , b''_2 , and b'''_1 are functions of the q_j via the direction cosine transformation matrices (DCTM) (2.7.6) which relate them to the inertial frame unit vectors n_1 , n_2 , and n_3 .

They are, however, not functions of \dot{q}_j since \dot{q}_j does not appear in the DCTM. Hence,

$$\frac{\partial \bar{\omega}^{-2/1}}{\partial \dot{q}_j} = \frac{\partial \dot{\theta}_1}{\partial \dot{q}_j} b'_3 + \frac{\partial \dot{\theta}_2}{\partial \dot{q}_j} b''_2 + \frac{\partial \dot{\theta}_3}{\partial \dot{q}_j} b'''_1 \quad (4.5.92)$$

or

$$\frac{\partial}{\partial \dot{q}_j} \bar{\omega}^{-2/1} = \frac{\partial}{\partial \dot{q}_j} \dot{\underline{\Theta}} \quad (4.5.93)$$

Substitute (4.5.86) and (4.5.93) into (4.5.90) to obtain

$$-\frac{\partial U_{KT}}{\partial q_j} = \left(\frac{\partial}{\partial \dot{q}_j} \omega^{2/1} \right)^T \underline{\tau}_{KT} = \underline{\tau}_{KT}^T \frac{\partial}{\partial \dot{q}_j} (\omega^{2/1}) = \underline{\tau}_{KT}^T \frac{\partial}{\partial \dot{q}_j} \omega^{2/n} - \underline{\tau}_{KT} \frac{\partial}{\partial \dot{q}_j} \omega^{1/n} \quad (4.5.94)$$

The stiffness torque is applied to both bodies 1 and 2 in the system and is equal and opposite on the bodies. This and a comparison of (4.5.48) with (4.5.94) shows:

If

$$\underline{\tau}_{KT} = -\underline{K}_T \underline{\Theta} - \underline{K}_T \underline{\Theta}_0 \quad (4.5.95)$$

$\begin{matrix} 3 \times 1 & & 3 \times 3 & 3 \times 1 & 3 \times 3 & 3 \times 1 \end{matrix}$

for \underline{K}_T symmetric, $\underline{\theta}_0$ the pretwist of the stiffness element, and

$$\underline{\tau}_{KT} = \begin{cases} \text{stiffness torque between the bodies, taken about } b'_3 \\ \text{stiffness torque between the bodies, taken about } b''_2 \\ \text{stiffness torque between the bodies, taken about } b'''_1 \end{cases} \quad (4.5.96)$$

$$\underline{\Theta} = \begin{cases} \theta_1 \\ \theta_2 \\ \theta_3 \end{cases} = \begin{cases} \text{relative rotation between the bodies, about } b'_3 \\ \text{relative rotation between the bodies, about } b''_2 \\ \text{relative rotation between the bodies, about } b'''_1 \end{cases} \quad (4.5.97)$$

and the scalar potential function is defined by

$$U_{KT} = \frac{1}{2} \underline{\Theta}^T \underline{K}_T \underline{\Theta} + \underline{\Theta}^T \underline{K}_T \underline{\Theta}_0 \quad (4.5.98)$$

$\begin{matrix} 1 & & 1 \times 3 & 3 \times 3 & 3 \times 1 & & 1 \times 3 & 3 \times 3 & 3 \times 1 \end{matrix}$

The contribution of $\underline{\tau}_{KT}$ to the generalized force Q_j in (4.5.47) becomes

$$Q_j^{KT} = -\frac{\partial U_{KT}}{\partial q_j} \quad (4.5.99)$$

EXAMPLE 4.5.4 Generalized Force for a Symmetric Torsional Stiffness Matrix

Objective: Show that the generalized force expression (4.5.99) utilizing the potential energy function (4.5.98) yields the same result as the general expression (4.5.48) for a symmetric torsional stiffness matrix (Figure E4.5.4(a)).

For this example,

$$\underline{\theta} = \theta_D - \theta_E, \quad \underline{\theta}_0 = \theta_D^0 - \theta_E^0, \quad \underline{K}_T = k_T \quad (1)$$

Torque on body D :

$$\tau_D = -k_T [(\theta_D^0 + \theta_D) - (\theta_E^0 + \theta_E)] = -\tau_E \quad (2)$$

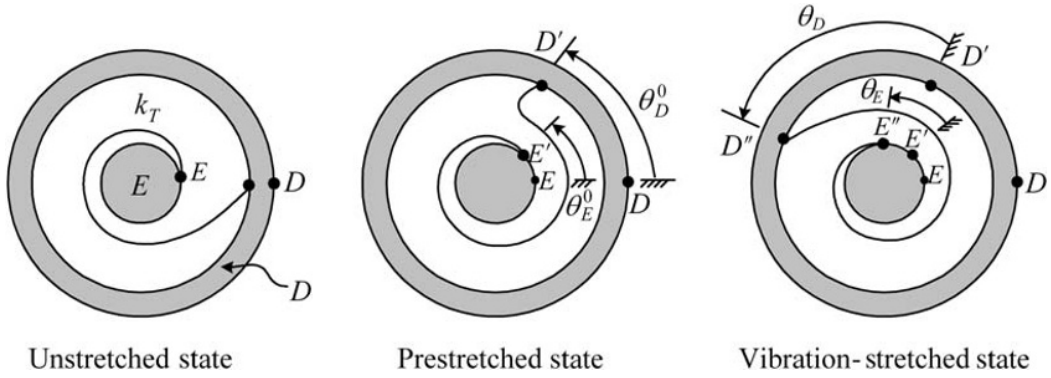


Figure E4.5.4(a) Torque developed by relative rotations and torsional spring

From (4.5.48), the generalized forces are

$$Q_{\theta_D} = \vec{\tau}_D \cdot \frac{\partial \vec{\omega}_D}{\partial \dot{\theta}_D} = \tau_D \frac{\partial \dot{\theta}_D}{\partial \dot{\theta}_D} = \tau_D, \quad Q_{\theta_E} = \vec{\tau}_E \cdot \frac{\partial \vec{\omega}_E}{\partial \dot{\theta}_E} = \tau_E \frac{\partial \dot{\theta}_E}{\partial \dot{\theta}_E} = \tau_E \quad (3)$$

From (4.5.98),

$$\begin{aligned} U_{KT} &= \frac{1}{2}(\theta_D - \theta_E)k_T(\theta_D - \theta_E) - (\theta_D - \theta_E)k_T(\theta_D^0 - \theta_E^0) \\ &= \frac{k_T}{2}(\theta_D - \theta_E)^2 + k_T(\theta_D - \theta_E)(\theta_D^0 - \theta_E^0) \end{aligned} \quad (4)$$

From (4.5.99),

$$\begin{aligned} Q_{\theta_D} &= -\frac{\partial U_{KT}}{\partial q_{\theta_D}} = -\frac{\partial U_{KT}}{\partial \theta_D} = -k_T(\theta_D - \theta_E) - k_T(\theta_D^0 - \theta_E^0) \\ Q_{\theta_E} &= -\frac{\partial U_{KT}}{\partial q_{\theta_E}} = -\frac{\partial U_{KT}}{\partial \theta_E} = k_T(\theta_D - \theta_E) + k_T(\theta_D^0 - \theta_E^0) \end{aligned} \quad (5)$$

Comparison of (2), (3), and (5) shows that the generalized forces are identical from the force approach (3) or potential approach (e).

4.5.4.6 Rotational Damping

Suppose that the torque discussed in the preceding section was caused by viscous drag instead of stiffness, that is,

$$\underline{\tau}_{CT} = -\underline{C}_T \underline{\dot{\theta}} \quad (4.5.100)$$

instead of (4.5.86). Conducting a derivation similar to (4.5.87)–(4.5.94) would yield

Rotational, Symmetric Damping Matrix Connection between Two Bodies*

If

$$\underline{\tau}_{CT} = -\underline{C}_T \underline{\dot{\theta}} \quad (4.5.101)$$

for \underline{C}_T symmetric, and

$$\underline{\tau}_{CT} = \left\{ \begin{array}{l} \text{damping torque between the bodies, taken about } b'_3 \\ \text{damping torque between the bodies, taken about } b''_2 \\ \text{damping torque between the bodies, taken about } b'''_1 \end{array} \right\} \quad (4.5.102)$$

$$\underline{\dot{\theta}} = \left\{ \begin{array}{l} \dot{\theta}_1 \\ \dot{\theta}_2 \\ \dot{\theta}_3 \end{array} \right\} = \left\{ \begin{array}{l} \text{relative angular velocity between the bodies, about } b'_3 \\ \text{relative angular velocity between the bodies, about } b''_2 \\ \text{relative angular velocity between the bodies, about } b'''_1 \end{array} \right\} \quad (4.5.103)$$

and the scalar dissipation function is defined by

$$\mathfrak{F}_{CT}^d = \frac{1}{2} \underline{\dot{\theta}}^T \underline{C}_T \underline{\dot{\theta}} \quad (4.5.104)$$

The contribution of $\underline{\tau}_{CT}$ to the generalized force Q_j in (4.5.47) becomes

$$Q_j = -\frac{\partial \mathfrak{F}_{CT}^d}{\partial \dot{q}_j} \quad (4.5.105)$$

EXAMPLE 4.5.5 *Generalized Force for an Symmetric Torsional Damping Matrix*

Objective: Show that the generalized force expression (4.5.105) utilizing the Rayleigh dissipation function (4.5.104) yields the same result as the general expression (4.5.48) for a symmetric torsional damping matrix (Figure E4.5.5(a)).

For this example,

$$\underline{\theta} = \theta_D - \theta_E, \quad \underline{\dot{\theta}} = \dot{\theta}_D - \dot{\theta}_E \quad (1)$$

Torque on body D :

$$\tau_D = -c_T (\dot{\theta}_D - \dot{\theta}_E) = -\tau_E \quad (2)$$

From (4.5.48), the generalized forces are

$$Q_{\theta_D} = \vec{\tau}_D \cdot \frac{\partial \vec{\omega}_D}{\partial \dot{\theta}_D} = \tau_D \hat{k} \cdot \frac{\partial \dot{\theta}_D \hat{k}}{\partial \dot{\theta}_D} = \tau_D, \quad Q_{\theta_E} = \vec{\tau}_E \cdot \frac{\partial \vec{\omega}_E}{\partial \dot{\theta}_E} = \tau_E \hat{k} \cdot \frac{\partial \dot{\theta}_E \hat{k}}{\partial \dot{\theta}_E} = \tau_E \quad (3)$$

*The above formula applies if one of the bodies is fixed or is given some prescribed angular velocities in the inertial frame.

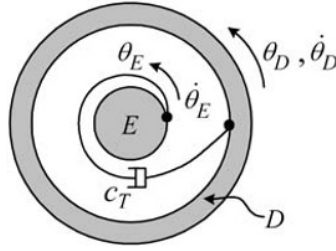


Figure E4.5.5(a) Torque developed by relative rotations and torsional damper

From (4.5.104), the Rayleigh dissipation function is

$$\mathfrak{F}_{CT}^D = \frac{1}{2} (\dot{\theta}_D - \dot{\theta}_E) c_T (\dot{\theta}_D - \dot{\theta}_E) = \frac{c_T}{2} (\dot{\theta}_D - \dot{\theta}_E)^2 \quad (4)$$

From (4.5.105),

$$Q_{\theta_D} = -\frac{\partial \mathfrak{F}_{CT}^D}{\partial \dot{q}_{\theta_D}} = -\frac{\partial \mathfrak{F}_{CT}^D}{\partial \dot{\theta}_D} = -c_T (\dot{\theta}_D - \dot{\theta}_E) \quad (5)$$

$$Q_{\theta_E} = -\frac{\partial \mathfrak{F}_{CT}^E}{\partial \dot{q}_{\theta_E}} = -\frac{\partial \mathfrak{F}_{CT}^E}{\partial \dot{\theta}_E} = c_T (\dot{\theta}_D - \dot{\theta}_E)$$

Comparison of (2), (3), and (5) shows that the generalized forces are identical from the force approach (3) or potential approach (e).

4.5.5 Summary for Lagrange Equation

Consideration of the previous discussion and examples about obtaining generalized forces from derivatives of scalar functions, along with the basic LE (4.5.23) and generalized force summation (4.5.47), yields

Lagrange's Equations of Motion: N_B Rigid Bodies and Scalar Potentials

$$\frac{d}{dt} \left(\frac{\partial T}{\partial \dot{q}_j} \right) - \frac{\partial T}{\partial q_j} = Q_j - \frac{\partial U}{\partial q_j} - \frac{\partial (\mathfrak{F}^c + \mathfrak{F}^d)}{\partial \dot{q}_j} \quad (4.5.106a)$$

$j = 1, 2, 3, \dots, n$ (the number of independent generalized coordinates (q_1, q_2, \dots, q_n))

This equation may be expressed in vector form by utilizing the vector differentiation notation in (2.6.42a), which yields

$$\frac{d}{dt} \left(\frac{\partial T}{\partial \underline{\dot{q}}} \right) - \frac{\partial T}{\partial \underline{q}} = \underline{Q} - \frac{\partial U}{\partial \underline{q}} - \frac{\partial (\mathfrak{F}^c + \mathfrak{F}^d)}{\partial \underline{\dot{q}}} \quad (4.5.106b)$$

The kinetic energy is

$$T = \sum_{i=1}^{N_B} \left(\frac{1}{2} m_i^n \underline{v}_{Gi}^T \underline{v}_{Gi} + \frac{1}{2} \left(\underline{\omega}_{bi}^{bi/n} \right)^T \underline{I}_{Gi}^{Bi/bi} \underline{\omega}_{bi}^{bi/n} \right) \quad (4.5.107)$$

U = sum of all scalar potential functions in the entire system. Some special cases include

- U_w in (4.5.57)
- U_{KDE} in (4.5.65) (4.5.108)
- U_{KT} in (4.5.98)

\mathfrak{F}^c = sum of all circulatory scalar functions in the entire system, that is,

- \mathfrak{F}_{DE}^c in (4.5.74) (4.5.109)

\mathfrak{F}^d = sum of all Rayleigh dissipation scalar functions in the entire system, that is,

- \mathfrak{F}_{DE}^c in (4.5.78) (4.5.110)
- \mathfrak{F}_{CT}^c in (4.5.104)

Q_j = j th generalized force determined from only the forces which are not described by U , \mathfrak{F}^c , or \mathfrak{F}^d type functions.

See Equations (4.5.47)–(4.5.53) for the related Q_j definitions. (4.5.111)

Another common form of LE is obtained from (4.5.106a) as

Lagrange's Equations of Motion: Lagrangian Function

Note that in general

$$\frac{\partial U}{\partial \dot{q}_j} = 0 \quad (4.5.112)$$

and also define the “Lagrangian function”

$$L = T - U \quad (4.5.113)$$

then (4.5.106a) becomes

$$\frac{d}{dt} \left(\frac{\partial L}{\partial \dot{q}_j} \right) - \frac{\partial L}{\partial q_j} = Q_j - \frac{\partial (\mathfrak{F}^c + \mathfrak{F}^d)}{\partial \dot{q}_j} \quad (4.5.114)$$

4.5.6 Nonconservative Generalized Forces and Virtual Work

Some vibration texts utilize Hamilton's variational principle

$$\delta(T + U) = \delta W_{nc} \quad (4.5.115)$$

to derive the LE, where the variational operator δ represents an infinitesimally small change in a function or variable. The independent generalized coordinates q_j are given variations δq_j which cause the points of application of applied nonconservative forces to displace. Let the i th nonconservative force on body l be designated by \vec{F}_{il} and its point of application be the position vector \vec{R}_{il} , which changes by the infinitesimal amount $\delta\vec{R}_{il}(\delta q_1, \delta q_2, \dots, \delta q_n)$ due to the variations δq_j of the generalized coordinates. The “virtual work” performed by \vec{F}_{il} moving through the virtual displacement $\delta\vec{R}_{il}$ is given by

$$\delta W_{il} = \delta\vec{R}_{il} \cdot \vec{F}_{il} = \left(\sum_{j=1}^n \frac{\partial \vec{R}_{il}}{\partial q_j} \delta q_j \right) \cdot \vec{F}_{il} \quad (4.5.116)$$

where the total differential of \vec{R}_{il} has been used. The virtual work performed by all nonconservative forces on body l becomes

$$\delta W_l = \sum_{i=1}^{n_{Fl}} \delta W_{il} = \delta\vec{R}_{il} \cdot \vec{F}_{il} = \sum_{i=1}^{n_{Fl}} \left(\left(\sum_{j=1}^n \frac{\partial \vec{R}_{il}}{\partial q_j} \delta q_j \right) \cdot \vec{F}_{il} \right) \quad (4.5.117)$$

A rearrangement of terms yields

$$\delta W_l = \sum_{j=1}^n Q_{jl} \delta q_j \quad (4.5.118)$$

where

$$Q_{jl} = \sum_{i=1}^{n_{Fl}} \vec{F}_{il} \cdot \frac{\partial \vec{R}_{il}}{\partial q_j} \quad (4.5.119)$$

for

$$l = 1, 2, \dots, N_B$$

Operations on the left-hand side of (4.5.115) similar to the derivation of (4.5.23) and consideration of all N_B in the system yield

$$\sum_{j=1}^n \left(\frac{d}{dt} \left(\frac{\partial T}{\partial \dot{q}_j} \right) - \frac{\partial T}{\partial q_j} + \frac{\partial U}{\partial q_j} \right) \delta q_j = \sum_{l=1}^{N_B} \delta W_l = \left(\sum_{l=1}^{N_B} Q_{jl} \right) \delta q_j \quad (4.5.120)$$

The virtual displacements are independent and totally arbitrary, so from (4.5.120), it follows that

$$\frac{d}{dt} \left(\frac{\partial T}{\partial \dot{q}_j} \right) - \frac{\partial T}{\partial q_j} + \frac{\partial U}{\partial q_j} = Q_j \quad (4.5.121)$$

where

$$Q_j = \sum_{l=1}^{N_B} Q_{jl} \quad (4.5.122)$$

Equation (4.5.121) is LE, and (4.5.119) and (4.5.122) are identical to the originally derived generalized force expressions (4.5.47) and (4.5.51). The preceding analysis shows

the relation between generalized forces and virtual work. Specifically, (4.5.118) provides the interpretation of the j th generalized force Q_j as being the force which moves through the j th generalized coordinate's virtual displacement δq_j to contribute the virtual work.

EXAMPLE 4.5.6 Wind Tunnel Mounted Wing Vibration

Description: The model below depicts an airfoil mounted on a support structure in a wind tunnel. The θ and x coordinates define the pitch and heave motions (Figure 2.6.1), respectively. The forces and moments that act on this rigid body model of the airfoil include the attachment stiffnesses for heave (k) and pitch (k_R) motions, aerodynamic pressure ($f_p(t)$ and $m_p(t)$), aerodynamic drag ($c\dot{x}$ and $c_R\dot{\theta}$), and an engine-related, rotating mass imbalance force $F_E(t)$. A static equilibrium position (SEP) reference is utilized for coordinates x and θ ; therefore, the weight and initial spring deflections due to “static sag” may be ignored. Small-angle approximations are assumed for the following analysis.

Objective: Derive the EOMs for the wing model shown in Figure E4.5.6(a) utilizing Lagrange's equations. The two generalized coordinates are $q_1 = x$ for heave motion and $q_2 = \theta$ for pitch motion (ref. Figure 2.6.1).

Solution:

(a) The kinetic energy of the system is expressed as (4.2.14)

$$T(q_1, q_2, \dot{q}_1, \dot{q}_2) = \frac{m}{2}(\dot{q}_1 - e\dot{q}_2)^2 + \frac{I_G}{2}\dot{q}_2^2 \quad (1)$$

(b) Sum all contributions to the scalar potential function in (4.5.108). The weight contribution is ignored since the coordinates in Figure E4.5.6(a) are SEP referenced:

- For k_R , (4.5.98) becomes

$$U_{KR} = \frac{1}{2}\theta k_R \theta = \frac{k_R}{2}\theta^2 \quad (2)$$

- For k , (4.5.65) becomes

$$U_K = \frac{1}{2}x k x = \frac{k}{2}x^2 \quad (3)$$

Therefore

$$U = U_{KR} + U_K = \frac{k_R}{2}\theta^2 + \frac{k}{2}x^2 = \frac{k_R}{2}q_2^2 + \frac{k}{2}q_1^2 \quad (4)$$

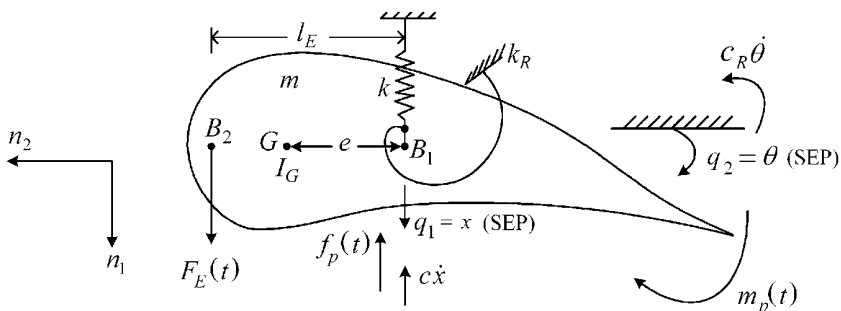


Figure E4.5.6(a) Simplified airfoil model with attachment stiffnesses and aerodynamic forces

(c) Sum all contributions to the scalar dissipation functions in (4.5.110):

- For c_R , (4.5.104) becomes

$$\mathfrak{F}_{c_R}^d = \frac{1}{2} \dot{\theta} c_R \dot{\theta} = \frac{c_R}{2} \dot{\theta}^2 \quad (5)$$

- For c , (4.5.81) becomes

$$\mathfrak{F}_c^d = \frac{1}{2} \dot{x} c \dot{x} = \frac{c}{2} \dot{x}^2 \quad (6)$$

Therefore

$$\mathfrak{F}^d = \mathfrak{F}_{c_R}^d + \mathfrak{F}_c^d = \frac{c_R}{2} \dot{\theta}^2 + \frac{c}{2} \dot{x}^2 = \frac{c_R}{2} \dot{q}_2^2 + \frac{c}{2} \dot{q}_1^2 \quad (7)$$

(d) Sum all generalized force contributions for forces that cannot be expressed with U , \mathfrak{F}^d , or \mathfrak{F}^c . Note that $l = I$ in Equation (4.5.47) since there is only one rigid body in the body. Therefore, by (4.5.47) and (4.5.48),

$$Q_j = Q_{j1} = Q_{Fj1} + \bar{\tau}_{\text{tot},1} \cdot \frac{{}^n \partial \bar{\omega}_{b1}^{b1/n}}{\partial \dot{q}_j} \quad (8)$$

where from (4.5.52)

$$Q_{Fj1} = \sum_{i=1}^{n_{F1}} \bar{F}_{i1} \cdot \frac{\partial^n \bar{v}_{i1}}{\partial \dot{q}_j} \quad (9)$$

The resultant of all of the pure external torques acting on body 1 is

$$\bar{\tau}_{\text{tot},1} = (m_p(t)) n_3 \quad (10)$$

where n_3 is the unit vector perpendicular to the plane of the paper. Note that

$$\frac{{}^n \partial \bar{\omega}_{b1}^{b1/n}}{\partial \dot{q}_1} = \frac{\partial(\dot{q}_2 n_3)}{\partial \dot{q}_1} = 0 n_3, \quad \frac{{}^n \partial \bar{\omega}_{b1}^{b1/n}}{\partial \dot{q}_2} = \frac{\partial(\dot{q}_2 n_3)}{\partial \dot{q}_2} = n_3 \quad (11)$$

Therefore, from (8),

$$Q_{1\tau}|_{l=1} = \bar{\tau}_{\text{tot},1} \cdot \frac{\partial \bar{\omega}_{b1}^{b1/n}}{\partial \dot{q}_1} = 0, \quad Q_{2\tau}|_{l=1} = \left(\bar{\tau}_{\text{tot},1} \cdot \frac{\partial \bar{\omega}_{b1}^{b1/n}}{\partial \dot{q}_2} \right) = m_p(t) \quad (12)$$

The external force applied at B_1 is $f_p(t)$. Therefore, from (9),

$$Q_{jB1} = \bar{F}_{11} \cdot \frac{\partial^n \bar{v}_{11}}{\partial \dot{q}_j} = -f_p(t) n_1 \cdot \frac{\partial^n \bar{v}_{11}}{\partial \dot{q}_j} \quad (13)$$

where since $f_p(t)$ is applied at B_1

$${}^n \bar{v}_{11} = \dot{q}_1 n_1 \Rightarrow \frac{\partial^n \bar{v}_{11}}{\partial \dot{q}_1} = \frac{\partial(\dot{q}_1 n_1)}{\partial \dot{q}_1} = n_1 \Rightarrow \frac{\partial^n \bar{v}_{11}}{\partial \dot{q}_2} = \frac{\partial(\dot{q}_1 n_1)}{\partial \dot{q}_2} = 0 n_1 \quad (14)$$

Combining (13) and (14) yields

$$Q_{1B1} = \bar{F}_{11} \cdot \frac{\partial^n \bar{v}_{11}}{\partial \dot{q}_1} = -f_p(t), \quad Q_{2B1} = \bar{F}_{11} \cdot \frac{\partial^n \bar{v}_{11}}{\partial \dot{q}_2} = 0 \quad (15)$$

The external force applied at B_2 is $F_E(t)$. Therefore, from (9),

$$Q_{jB2} = \bar{F}_{21} \cdot \frac{\partial^n \bar{v}_{21}}{\partial \dot{q}_j} = F_E(t) n_1 \cdot \frac{\partial^n \bar{v}_{21}}{\partial \dot{q}_j} \quad (16)$$

where since $F_E(t)$ is applied at B_2

$$\begin{aligned} {}^n \bar{v}_{21} &= (\dot{q}_1 - l_E \dot{q}_2) n_1 \Rightarrow \frac{\partial^n \bar{v}_{21}}{\partial \dot{q}_1} = \frac{\partial((\dot{q}_1 - l_E \dot{q}_2) n_1)}{\partial \dot{q}_1} = n_1 \\ &\Rightarrow \frac{\partial^n \bar{v}_{21}}{\partial \dot{q}_2} = \frac{\partial((\dot{q}_1 - l_E \dot{q}_2) n_1)}{\partial \dot{q}_2} = -l_E n_1 \end{aligned} \quad (17)$$

Combining (16) and (17) yields

$$Q_{1B2} = \bar{F}_{21} \cdot \frac{\partial^n \bar{v}_{21}}{\partial \dot{q}_1} = F_E(t), \quad Q_{2B2} = \bar{F}_{21} \cdot \frac{\partial^n \bar{v}_{21}}{\partial \dot{q}_2} = -l_E F_E(t) \quad (18)$$

Combining the results of Equations (12), (15), and (18) into (8) yields

$$Q_1 = Q_{1\tau} + Q_{1B1} + Q_{1B2} = -f_p(t) + F_E, \quad Q_2 = Q_{2\tau} + Q_{2B1} + Q_{2B2} = m_p(t) - l_E F_E(t) \quad (19)$$

(e) Substitute the expressions for T (Eq. 1), U (Eq. 4), \mathfrak{S}^d (Eq. 7), and Equation (19) into the Lagrange equations (4.5.106a) yields

$$\frac{{}^n d}{dt} \left(\frac{\partial T}{\partial \dot{q}_j} \right) - \frac{\partial T}{\partial q_j} = Q_j - \frac{\partial U}{\partial q_j} - \frac{\partial(\mathfrak{S}^c + \mathfrak{S}^d)}{\partial \dot{q}_j} \quad (20)$$

$$\begin{aligned} &\frac{{}^n d}{dt} \left\{ \frac{\partial}{\partial \dot{q}_j} \left(\frac{m}{2} (\dot{q}_1 - e \dot{q}_2)^2 + \frac{I_G}{2} \dot{q}_2^2 \right) \right\} \\ &= \begin{cases} -f_p(t) + F_E(t), & \text{for } j=1 \\ -l_E F_E(t) + m_p(t), & \text{for } j=2 \end{cases} - \frac{\partial}{\partial q_j} \left(\frac{k_R}{2} q_2^2 + \frac{k}{2} q_1^2 \right) - \frac{\partial}{\partial \dot{q}_j} \left(\frac{c_R}{2} \dot{q}_2^2 + \frac{c}{2} \dot{q}_1^2 \right) \end{aligned} \quad (21)$$

EOM for $q_1 = x$, from Equation (21):

$$\frac{d}{dt} (m(\dot{q}_1 - e \dot{q}_2)) = m \ddot{q}_1 - m e \ddot{q}_2 = -f_p(t) + F_E(t) - k q_1 - c \dot{q}_1 \quad (22)$$

EOM for $q_2 = \theta$, from Equation (21):

$$\begin{aligned} \frac{d}{dt} (m(\dot{q}_1 - e \dot{q}_2)(-e) + I_G \dot{q}_2) &= -m e \ddot{q}_1 + (I_G + m e^2) \ddot{q}_2 \\ &= -l_E F_E(t) + m_p(t) - k_R q_2 - c_R \dot{q}_2 \end{aligned} \quad (23)$$

Equations (22) and (23) may be written in matrix form as

$$\begin{bmatrix} m & -me \\ -me & I_G + me^2 \end{bmatrix} \begin{Bmatrix} \ddot{q}_1 \\ \ddot{q}_2 \end{Bmatrix} + \begin{bmatrix} c & 0 \\ 0 & c_R \end{bmatrix} \begin{Bmatrix} \dot{q}_1 \\ \dot{q}_2 \end{Bmatrix} + \begin{bmatrix} k & 0 \\ 0 & k_R \end{bmatrix} \begin{Bmatrix} q_1 \\ q_2 \end{Bmatrix} = \begin{Bmatrix} F_E(t) - f_p(t) \\ m_p(t) - I_E F_E(t) \end{Bmatrix} \quad (24)$$

This result has the general form for the matrix governing differential equation of a linear vibrating system:

$$\underline{M}\ddot{\underline{q}} + \underline{C}\dot{\underline{q}} + \underline{K}\underline{q} = \underline{F}(t) \quad (25)$$

The Lagrange equations' advantages over Newton's law for this example include acceleration expressions or stiffness and damping force sign identifications were not required.

EXAMPLE 4.5.7 Resonant Vibrator for Compound Potting (Examples 3.3.1 and 4.4.1 Revisited)

Background: This example was presented in Example 3.3.1 (Newton's law) and Example 4.4.1 (conservation of power).

Objective: Derive the EOMs utilizing the Lagrange approach in (4.5.106a) with the single generalized coordinate $q_1 = \delta_H$.

Solution:

Figure E4.5.7(a) shows the vibrator mechanism with the equivalent spring stiffness, follower weight, and bearing drag moments.

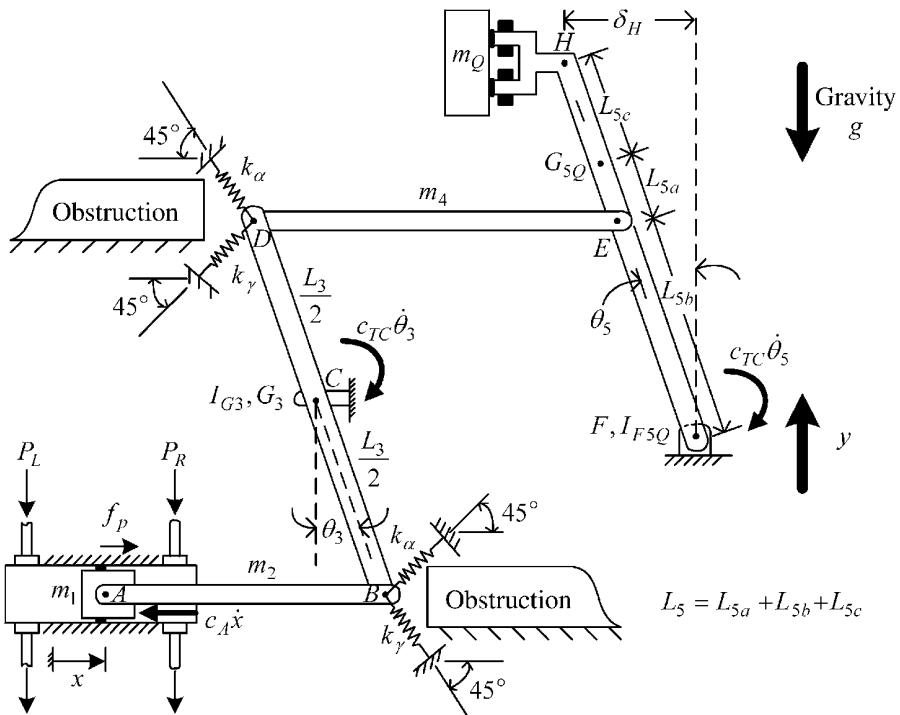


Figure E4.5.7(a) Resonant vibrator mechanism

The following constraints were identified in Example 4.4.1 with $q_1 = \delta_H$:

$$\begin{aligned}\theta_3 &= \frac{2 L_{5b}}{L_3 L_5} q_1 \Rightarrow \dot{\theta}_3 = \frac{2 L_{5b}}{L_3 L_5} \dot{q}_1, & \theta_5 &= \frac{1}{L_5} q_1 \Rightarrow \dot{\theta}_5 = \frac{1}{L_5} \dot{q}_1 \\ x &= \frac{L_{5b}}{L_5} q_1 \Rightarrow \dot{x} = \frac{L_{5b}}{L_5} \dot{q}_1, & y_{G5Q} &= -\frac{L_{5a} + L_{5b}}{2L_5^2} q_1^2, & \dot{y}_{G5Q} &= -\frac{L_{5a} + L_{5b}}{L_5^2} q_1 \dot{q}_1\end{aligned}\quad (1)$$

and the kinetic energy was identified in Example 4.4.1 as

$$T = \frac{Meq}{2} \dot{\delta}_H^2 = \frac{Meq}{2} \dot{q}_1^2 \quad (2)$$

where

$$Meq = \frac{I_{F5Q}}{L_5^2} + \frac{L_{5b}^2}{L_5^2} \left(m_1 + \frac{4}{L_3^2} I_{G3} \right) \quad (3)$$

- Sum all contributions to the scalar potential function in (4.5.108). The weight contribution ($w_5 + m_Q g$) *cannot* be ignored since it is not balanced by an initial spring deflection:
 - For k at B , (4.5.65) becomes

$$U_{kB} = \frac{1}{2} x k x = \frac{k}{2} x^2 = \frac{k L_{5b}^2}{2 L_5^2} q_1^2 \quad (4)$$

- For k at D , (4.5.65) becomes

$$U_{kD} = \frac{1}{2} x k x = \frac{k}{2} x^2 = \frac{k L_{5b}^2}{2 L_5^2} q_1^2 \quad (5)$$

- For $(w_5 + m_Q g)$ at G_5 , Equation (4.5.57) becomes

$$U_{w5G} = (w_5 + m_Q g) y_{G5Q} = -(w_5 + m_Q g) \frac{(L_{5a} + L_{5b})}{2L_5^2} q_1^2 \quad (6)$$

Therefore, the potential energy function for the entire system becomes

$$\therefore U = U_{kB} + U_{kD} + U_{w5G} = \frac{1}{2L_5^2} [2kL_{5b}^2 - (w_5 + m_Q g)(L_{5a} + L_{5b})] q_1^2 \quad (7)$$

- Sum all contributions to the scalar dissipation function in Equation (4.5.110):
 - For c_{TF} at F , Equation (4.5.104) becomes

$$\mathfrak{F}_F^d = \frac{1}{2} \dot{\theta}_5 c_{TF} \dot{\theta}_5 = \frac{c_{TF}}{2} \frac{1}{L_5^2} \dot{q}_1^2 \quad (8)$$

- For c_{TC} at C , (4.5.104) becomes

$$\mathfrak{F}_C^d = \frac{1}{2} \dot{\theta}_3 c_{TC} \dot{\theta}_3 = \frac{c_{TC}}{2} \frac{4 L_{5b}^2}{L_3^2 L_5^2} \dot{q}_1^2 \quad (9)$$

- For c_A at A , (4.5.81) becomes

$$\mathfrak{F}_A^d = \frac{1}{2} \dot{x} c_A \dot{x} = \frac{c_A L_{5b}^2}{2 L_5^2} \dot{q}_1^2 \quad (10)$$

Therefore, the Rayleigh dissipation function for the entire system becomes

$$\mathfrak{F}^d = \mathfrak{F}_F^d + \mathfrak{F}_C^d + \mathfrak{F}_A^d = \frac{1}{2L_5^2} \left(c_{TF} + c_A L_{5b}^2 + 4c_{TC} \frac{L_{5b}^2}{L_3^2} \right) \dot{q}_1^2 \quad (11)$$

- Sum all generalized force contributions for forces and moments that cannot be expressed with U , \mathfrak{F}^d , or \mathfrak{F}^c . The only force or moment that satisfies this requirement is the pressure force $f_p(t)$. Recall from (4.5.47), (4.5.48), and (4.5.52) that

$$Q_j = \sum_{l=1}^{N_B} Q_{jl}, \quad Q_{jl} = Q_{Fjl} + \vec{\tau}_{\text{tot},l} \cdot \frac{{}^n \partial \vec{\omega}_{bl}^{bl/n}}{\partial \dot{q}_j}, \quad Q_{Fjl} = \sum_{i=1}^{n_{Fl}} \vec{F}_{il} \cdot \frac{\partial {}^n \vec{v}_{il}}{\partial \dot{q}_j} \quad (12)$$

Therefore, by (1) and (12),

$$Q_{\delta_H} = Q_{q_1} = Q_1 = (f_p \hat{i}) \cdot \frac{\partial (\dot{x} \hat{i})}{\partial \delta_H} = f_p(t) \frac{L_{5b}}{L_5} \quad (13)$$

- Substitute the expressions for T (Eq. 2), U (Eq. 7), \mathfrak{F}^d (Eq. 11), and Q_{δ_H} (Eq. 13) into the Lagrange equation (Eq. (4.5.106a))

$$\frac{{}^n d}{dt} \left(\frac{\partial T}{\partial \dot{q}_j} \right) - \frac{\partial T}{\partial q_j} = Q_j - \frac{\partial U}{\partial q_j} - \frac{\partial (\mathfrak{F}^c + \mathfrak{F}^d)}{\partial \dot{q}_j} \quad (14)$$

to obtain

$$\frac{{}^n d}{dt} \left(\frac{\partial}{\partial \dot{q}_1} \left(\frac{M_{\text{eq}}}{2} \dot{q}_1^2 \right) \right) = \frac{L_{5b}}{L_5} f_p(t) - \frac{\partial}{\partial q_1} \left(\frac{K_{\text{eq}}}{2} q_1^2 \right) - \frac{\partial}{\partial \dot{q}_1} \left(\frac{C_{\text{eq}}}{2} \dot{q}_1^2 \right) \quad (15)$$

$$\Rightarrow M_{\text{eq}} \ddot{q}_1 + C_{\text{eq}} \dot{q}_1 + K_{\text{eq}} q_1 = F_{\text{eq}}(t) \quad (16)$$

where

$$C_{\text{eq}} = \frac{c_{TF}}{L_5^2} + \frac{L_{5b}^2}{L_5^2} \left(c_A + \frac{4c_{TC}}{L_3^2} \right), \quad K_{\text{eq}} = 2k \frac{L_{5b}^2}{L_5^2} - \frac{(L_{5a} + L_{5b})}{L_5^2} (W_5 + m_{QG}) \quad (17)$$

$$M_{\text{eq}} = \frac{I_{F5Q}}{L_5^2} + \frac{L_{5b}^2}{L_5^2} \left(m_1 + \frac{4}{L_3} I_{G3} \right), \quad F_{\text{eq}} = \frac{L_{5b}}{L_5} f_p \quad (18)$$

Summary: The Lagrange approach is seen to be simpler in execution than the Newton approach (Example 3.3.1) since it does not require free body diagrams, expressions for accelerations, or ideal joint reaction forces (due to (4.5.46)). The Lagrange approach is seen to be as simple to apply as the conservation of power approach (Example 4.4.1) and will also provide all EOMs for a multi-DOF model.

EXAMPLE 4.5.8 *Labeling Mechanism (Example 3.3.2 Revised)*

Description: The system shown in Figure E4.5.8(a) is part of a mechanism employed to attach labels in a manufacturing process. Vibration of the system results from actuator forces $f_1(t)$ and $f_2(t)$ and torque $\tau_1(t)$.

Objective: Derive the two equations of motion for coordinates q_1 and q_2 utilizing Lagrange's approach.

Assumptions: q_1 and q_2 are small motions.

Recall from Example 3.3.2 that the change in length of the k_1 - c_1 impedance was approximated as a two-term Taylor series expansion:

$$\Delta D = D - D' \approx \frac{2a}{\sqrt{a^2 + b^2}} q_1 \quad (1)$$

The kinetic energy of the system is (4.2.14)

$$T = \frac{1}{2} I_A \dot{q}_2^2 + \frac{1}{2} m_1 \dot{q}_1^2 + \frac{1}{2} I_B \dot{\theta}^2 = \frac{1}{2} I_A \dot{q}_2^2 + \frac{1}{2} \left(m_1 + \frac{I_B}{r^2} \right) \dot{q}_1^2 \quad (2)$$

The potential energy is obtained from Figure E4.5.8(b) and (4.5.57), (4.5.65), (4.5.98) as

$$U = -m_2 g L_1 (1 - \cos q_2) + \frac{k_3}{2} q_2^2 + \frac{k_2}{2} (q_1 + L_2 q_2)^2 + \frac{k_1}{2} \Delta D^2 \quad (3)$$

where ΔD is given by (1) and via a two-term Taylor series expansion

$$\cos q_2 \approx 1 - \frac{q_2^2}{2} \quad (4)$$

for small motions. The dissipation function is (4.5.81) (4.5.104)

$$\mathfrak{F}^d = \frac{c_3}{2} \dot{q}_2^2 + \frac{c_2}{2} (\dot{q}_1 + L_2 \dot{q}_2)^2 + \frac{c_1}{2} \Delta \dot{D}^2 \quad (5)$$

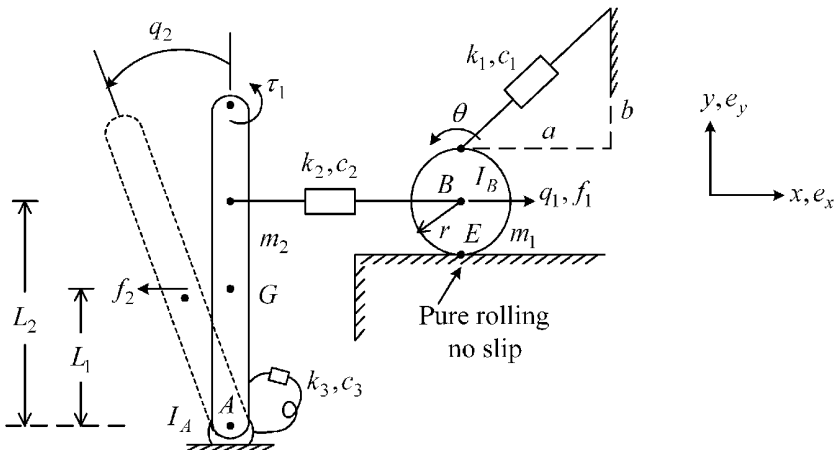


Figure E4.5.8(a) Vibrating mechanical system with two dofs and three excitations

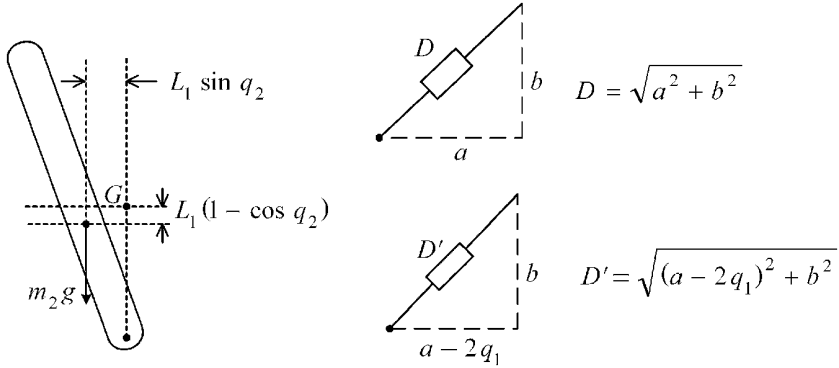


Figure E4.5.8(b) Inverted pendulum and k_1 - c_1 impedance geometries

where from (1), for small motion

$$\Delta \dot{D} = \frac{2a}{\sqrt{a^2 + b^2}} \dot{q}_1 \quad (6)$$

The generalized forces are given by (4.5.47), (4.5.48), and (4.5.52)

$$Q_j = \sum_{l=1}^{N_B} Q_{jl}, \quad Q_{jl} = Q_{Fjl} + \bar{\tau}_{\text{tot},l} \cdot \frac{\partial \bar{\omega}_{bl}^{-bl/n}}{\partial \dot{q}_j}, \quad Q_{Fjl} = \sum_{i=1}^{n_{Fl}} \bar{F}_{il} \cdot \frac{\partial \bar{v}_{il}}{\partial \dot{q}_j} \quad (7)$$

as

$$Q_j = \tau_1 e_z \cdot \frac{\partial (\dot{q}_2 e_z)}{\partial \dot{q}_j} + f_1 e_x \cdot \frac{\partial (\dot{q}_1 e_x)}{\partial \dot{q}_j} - f_2 e_x \cdot \frac{\partial (-L_1 \dot{q}_2 e_x)}{\partial \dot{q}_j} = \tau_1 \frac{\partial \dot{q}_2}{\partial \dot{q}_j} + f_1 \frac{\partial \dot{q}_1}{\partial \dot{q}_j} + f_2 L_1 \frac{\partial \dot{q}_2}{\partial \dot{q}_j} \quad (8)$$

Therefore,

$$Q_1 = f_1, \quad Q_2 = \tau_1 + L_1 f_2 \quad (9)$$

The Lagrange equation (4.5.106a)

$$\frac{d}{dt} \left(\frac{\partial T}{\partial \dot{q}_j} \right) - \frac{\partial T}{\partial q_j} = Q_j - \frac{\partial U}{\partial q_j} - \frac{\partial \mathfrak{S}^d}{\partial \dot{q}_j} \quad (10)$$

yields for $j=1$

$$\left(m_1 + \frac{I_B}{r^2} \right) \ddot{q}_1 = f_1 - k_2(q_1 + L_2 q_2) - k_1 \frac{4a^2}{a^2 + b^2} q_1 - c_2(\dot{q}_1 + L_2 \dot{q}_2) - c_1 \frac{4a^2}{a^2 + b^2} \dot{q}_1 \quad (11)$$

and for $j=2$

$$I_A \ddot{q}_2 = \tau_1 + L_1 f_2 + m_2 g L_1 q_2 - k_3 q_2 - k_2(q_1 + L_2 q_2) L_2 - c_3 \dot{q}_2 - c_2(\dot{q}_1 + L_2 \dot{q}_2) L_2 \quad (12)$$

Equations (11) and (12) are identical to the Newton's laws results as obtained in Example 3.3.2.

EXAMPLE 4.5.9 *Industrial Screening Machine*

Description: Figure E4.5.9(a) depicts an industrial screening machine utilized for separating minerals. Two stages of screening are shown with each stage containing two screens. A scotch yoke mechanism provides a harmonic input motion $z(t)$ which is assisted by a hydraulic force $f(t)$ and torque $\tau(t)$. Assume that the vibration angle q_5 of bar AD is much smaller than its orientation angle γ .

Objective: Determine the equations of motion utilizing the Lagrange method.

Kinematics

The reaction forces at A and D are functions of the horizontal displacements of A and D , respectively. The generalized force contribution at C is determined from the horizontal velocity at C . These motions are determined in the following manner:

$$+ \Rightarrow \Delta A_x = \frac{L}{2} \sin(\gamma + q_5) - \frac{L}{2} \sin(\gamma) \quad (1)$$

The two-term Taylor series (Section 2.4) for $\sin(\gamma + q_5)$ is

$$\sin(\gamma + q_5) \approx \sin \gamma + \left. \frac{\partial \sin(\gamma + q_5)}{\partial q_5} \right|_{q_5=0} * q_5 = \sin \gamma + \cos \gamma * q_5 \quad (2)$$

Combining (1) and (2) yields

$$+ \Rightarrow \Delta A_x \approx \frac{L}{2} \cos(\gamma) q_5 \quad (3)$$

Similarly,

$$+ \Leftarrow \Delta C_x \approx \frac{L}{4} \cos(\gamma) q_5, \quad + \Leftarrow \Delta D_x = \frac{L}{2} \cos(\gamma) q_5 \quad (4)$$

Energy and Dissipation Functions

From (4.2.14),

$$T = \frac{m_1}{2} \dot{q}_1^2 + \frac{m_2}{2} \dot{q}_2^2 + \frac{m_3}{2} \dot{q}_3^2 + \frac{m_4}{2} \dot{q}_4^2 + \frac{I_G}{2} \dot{q}_5^2 \quad (5)$$

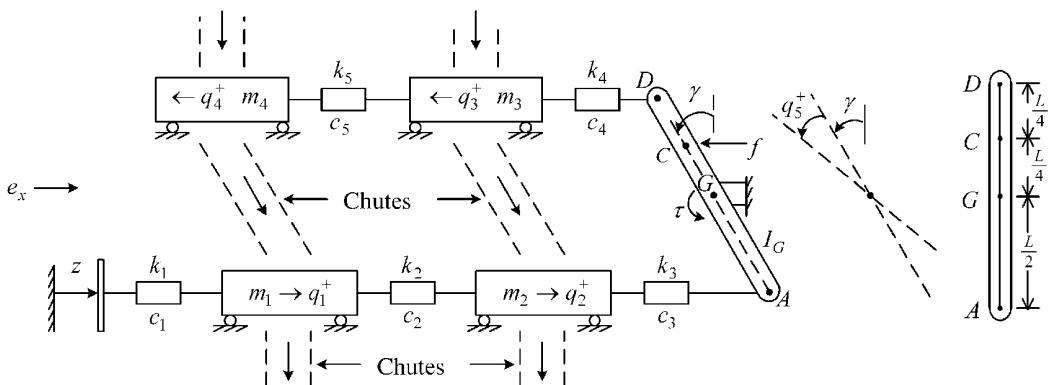


Figure E4.5.9(a) Five-degree of freedom (dof) lumped inertia model of an industrial screening machine

From (4.5.65),

$$U = \frac{k_1}{2}(q_1 - z)^2 + \frac{k_2}{2}(q_2 - q_1)^2 + \frac{k_3}{2}(\Delta A_x - q_2)^2 + \frac{k_4}{2}(q_3 - \Delta D_x)^2 + \frac{k_5}{2}(q_4 - q_3)^2 \quad (6)$$

From (4.5.81),

$$\mathfrak{S}^d = \frac{c_1}{2}(\dot{q}_1 - \dot{z})^2 + \frac{c_2}{2}(\dot{q}_2 - \dot{q}_1)^2 + \frac{c_3}{2}(\Delta \dot{A}_x - \dot{q}_2)^2 + \frac{c_4}{2}(\dot{q}_3 - \Delta \dot{D}_x)^2 + \frac{c_5}{2}(\dot{q}_4 - \dot{q}_3)^2 \quad (7)$$

Generalized Forces

From (4) and (4.5.47), (4.5.48), and (4.5.52),

$$Q_j = \sum_{l=1}^{N_B} Q_{jl}, \quad Q_{jl} = Q_{Fjl} + \bar{\tau}_{\text{tot},l} \cdot \frac{n \partial \bar{\omega}_{bl}^{bl/n}}{\partial \dot{q}_j}, \quad Q_{Fjl} = \sum_{i=1}^{n_{Fl}} \bar{F}_{il} \cdot \frac{\partial^n \bar{v}_{il}}{\partial \dot{q}_j} \quad (8)$$

it results that

$$Q_j = -f e_x \cdot \frac{\partial}{\partial \dot{q}_j} (-\Delta \dot{C}_x e_x) + \tau e_z \cdot \frac{\partial}{\partial \dot{q}_j} (\dot{q}_5 e_z) = f \frac{\partial}{\partial \dot{q}_j} \left(\frac{L}{4} \cos(\gamma) \dot{q}_5 \right) + \tau \frac{\partial}{\partial \dot{q}_j} (\dot{q}_5) \quad (9)$$

Therefore,

$$Q_1 = Q_2 = Q_3 = Q_4 = 0, \quad Q_5 = f \frac{L}{4} \cos(\gamma) + \tau \quad (10)$$

Lagrange's Equations

The Lagrange equation (4.5.106a)

$$\frac{d}{dt} \left(\frac{\partial T}{\partial \dot{q}_j} \right) - \frac{\partial T}{\partial q_j} = Q_j - \frac{\partial U}{\partial q_j} - \frac{\partial \mathfrak{S}^d}{\partial \dot{q}_j} \quad (11)$$

yields

$$j=1: \quad m_1 \ddot{q}_1 + c_1(\dot{q}_1 - \dot{z}) - c_2(\dot{q}_2 - \dot{q}_1) + k_1(q_1 - z) - k_2(q_2 - q_1) = 0 \quad (12)$$

$$j=2: \quad m_2 \ddot{q}_2 + c_2(\dot{q}_2 - \dot{q}_1) - c_3 \left(\frac{L}{2} \cos(\gamma) \dot{q}_5 - \dot{q}_2 \right) + k_2(q_2 - q_1) - k_3 \left(\frac{L}{2} \cos(\gamma) q_5 - q_2 \right) = 0 \quad (13)$$

$$j=3: \quad m_3 \ddot{q}_3 + c_4 \left(\dot{q}_3 - \frac{L}{2} \cos \gamma * \dot{q}_5 \right) - c_5(\dot{q}_4 - \dot{q}_3) + k_4 \left(q_3 - \frac{L}{2} \cos \gamma * q_5 \right) - k_5(q_4 - q_3) = 0 \quad (14)$$

$$j=4: \quad m_4 \ddot{q}_4 + c_5(\dot{q}_4 - \dot{q}_3) + k_5(q_4 - q_3) = 0 \quad (15)$$

$$j=5: \quad I_G \ddot{q}_5 + c_3 \left(\frac{L}{2} \cos \gamma * \dot{q}_5 - \dot{q}_2 \right) \frac{L}{2} \cos \gamma - c_4 \left(\dot{q}_3 - \frac{L}{2} \cos \gamma * \dot{q}_5 \right) \frac{L}{2} \cos \gamma + k_3 \left(\frac{L}{2} \cos \gamma * q_5 - q_2 \right) \frac{L}{2} \cos \gamma - k_4 \left(q_3 - \frac{L}{2} \cos \gamma * q_5 \right) \frac{L}{2} \cos \gamma = f \frac{L}{4} \cos \gamma + \tau \quad (16)$$

Expressing these in matrix–vector form yields

$$\underline{M}\ddot{\underline{q}} + \underline{C}\dot{\underline{q}} + \underline{K}\underline{q} = \underline{F} \quad (17)$$

$$\underline{q} = (q_1 \ q_2 \ q_3 \ q_4 \ q_5)^T \quad (5 \times 1) \quad (18)$$

$$\underline{M} = \underline{\text{diag}}(m_1 \ m_2 \ m_3 \ m_4 \ I_G)^T \quad (5 \times 5) \quad (19)$$

$$\underline{F} = \begin{Bmatrix} c_1\dot{z} + k_1z \\ 0 \\ 0 \\ 0 \\ \frac{L}{4}\cos(\gamma)*f(t) + \tau(t) \end{Bmatrix} \quad (20)$$

$$\underline{K} = \begin{bmatrix} k_1 + k_2 & -k_2 & 0 & 0 & 0 \\ -k_2 & k_2 + k_3 & 0 & 0 & -\alpha k_3 \\ 0 & 0 & k_4 + k_5 & -k_5 & -\alpha k_4 \\ 0 & 0 & -k_5 & k_5 & 0 \\ 0 & -\alpha k_3 & -\alpha k_4 & 0 & \alpha^2(k_3 + k_4) \end{bmatrix} \quad (21)$$

$$\underline{C} = \begin{bmatrix} c_1 + c_2 & -c_2 & 0 & 0 & 0 \\ -c_2 & c_2 + c_3 & 0 & 0 & -\alpha c_3 \\ 0 & 0 & c_4 + c_5 & -c_5 & -\alpha c_4 \\ 0 & 0 & -c_5 & c_5 & 0 \\ 0 & -\alpha c_3 & -\alpha c_4 & 0 & \alpha^2(c_3 + c_4) \end{bmatrix} \quad (22)$$

where

$$\alpha = \frac{L}{2}\cos\gamma \quad (23)$$

4.5.7 Effects of Gravity for the Lagrange Approach

The gravity force (weight) and initial static deflection may be neglected in some, but not all models (ref. Example 3.3.3). The coordinates are referenced to the static equilibrium state SEP in these models.

EXAMPLE 4.5.10 Linear Spring Mass

Consider the linear spring mass system shown in Figure E4.5.10(a).

Let Δ be the static deflection due to gravity, that is,

$$k\Delta = mg \quad (1)$$

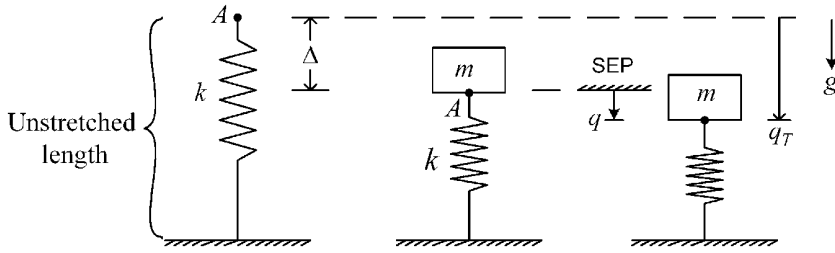


Figure E4.5.10(a) Unloaded, static equilibrium, and dynamically deflected states of simple single-mass oscillator

q_T : total deflection of the spring

q : spring deflection relative to SEP

Consider the Lagrange equation contribution $\partial U/\partial q$ if U is evaluated by:

(a) Including gravity g and utilizing the total spring deflection coordinate q_T :

$$U_a = \frac{k}{2}q_T^2 - mgq_T = \frac{k}{2}(q + \Delta)^2 - mg(q + \Delta) \quad (2)$$

$$\frac{\partial U_a}{\partial q_T} = kq_T - mg = k(q + \Delta) - mg = kq \quad (3)$$

where (1) has been used.

(b) Neglecting g and utilizing the SEP referenced coordinate q :

$$U_b = \frac{k}{2}q^2 \text{ (neglect gravity)} \quad (4)$$

$$\frac{\partial U_b}{\partial q} = kq \quad (5)$$

Therefore,

$$\frac{\partial U_a}{\partial q_T} = \frac{\partial U_b}{\partial q} \quad (6)$$

and either approach yields the same contribution to the Lagrange equation. Note that the gravity force must be ignored if the coordinate is referenced to SEP, that is,

$$U = \frac{k}{2}q^2 - mgq \quad (7)$$

is incorrect and will result in an incorrect equation of motion (EOM).

EXAMPLE 4.5.11 *Linearized System with a Nonlinear Spring*

This system is the same as the previous example; however, the spring is a cubic hardening spring:

$$F_k = -kq_T^3 \quad (1)$$

The gradient of the corresponding potential energy function U_k will equal $-F_k$ if U_k is defined as

$$U_k = - \int_0^{q_T} (-kq_T^3) dq_T = \frac{kq_T^4}{4} \quad (2)$$

Static equilibrium ($\sum \text{forces} = 0$) is satisfied if

$$mg = k\Delta^3 \quad (3)$$

(a) Method I: Include gravity and utilize q_T :

$$U_a = \frac{kq_T^4}{4} - mgq_T \quad (4)$$

$$\frac{\partial U_a}{\partial q_T} = kq_T^3 - mg \quad (5)$$

A two-term Taylor series linearization about the SEP ($q_T = \Delta$) then yields

$$q_T^3 \approx q_T^3 \Big|_{q_T=\Delta} + 3q_T^2 \Big|_{q_T=\Delta} * (q_T - \Delta) \quad (6)$$

$$\therefore \frac{\partial U_a}{\partial q_T} \Big|_{\text{lin}} = k(\Delta^3 + 3\Delta^2 * q) - mg \quad (7)$$

Substitute (3) into (7) and cancel terms to obtain

$$\frac{\partial U_a}{\partial q_T} \Big|_{\text{lin}} = 3\Delta^2 * q * k \quad (8)$$

where by (3) $\Delta = \left(\frac{mg}{k}\right)^{1/3}$.

(b) Method II: Utilize q , ignore gravity, and ignore Δ (static deflection):

$$U_b = \frac{k}{4}q^4 \quad (9)$$

$$\frac{\partial U_b}{\partial q} = kq^3 \quad (10)$$

Performing a two-term Taylor series linearization about the SEP ($q=0$) yields

$$\frac{\partial U_b}{\partial q} \Big|_{\text{lin}} \approx kq^3 \Big|_{q=0} + 3kq^2 \Big|_{q=0}q = 0 \quad (11)$$

Thus, for the nonlinear spring system, the potential energy U should be expressed in terms of the total deflection coordinate q_T and include the gravity force (weight) as shown in Equation (4), since (11) is incorrect (force = 0 when $q \neq 0$).

EXAMPLE 4.5.12 *Linear Spring with Geometric Nonlinearity and Small Motion Assumption*

Consider the inclined, inverted pendulum shown in Figure E4.5.12(a).
Let

$$\Delta = \text{static deflection of the spring} \approx L(\sin \gamma_s - \sin \gamma_0) \quad (1)$$

Take moments about A for static equilibrium:

$$+ \curvearrowright \quad F_k L \cos \gamma_s = k \Delta L \cos \gamma_s = mg \frac{L}{2} \sin \gamma_s \quad (2)$$

The total deflection of the spring is the sum of the static and dynamic deflections:

$$x_{KT} = \Delta + L(\sin \gamma - \sin \gamma_s) \quad (3)$$

The vertical deflection of G is

$$Y_G = -\frac{L}{2}(\cos \gamma_0 - \cos \gamma) \quad (4)$$

Therefore, the potential energy evaluated relative to the undeformed configuration is

$$U_a = -mg \frac{L}{2}(\cos \gamma_0 - \cos \gamma) + \frac{k}{2}[\Delta + L(\sin \gamma - \sin \gamma_s)]^2 \quad (5)$$

The angular deflection relative to the undeformed state is

$$\begin{aligned} \beta &= \gamma - \gamma_0 \\ \Rightarrow \frac{\partial}{\partial \beta} &= \frac{\partial}{\partial \gamma} \frac{\partial \gamma}{\partial \beta} = \frac{\partial}{\partial \gamma} \end{aligned} \quad (6)$$

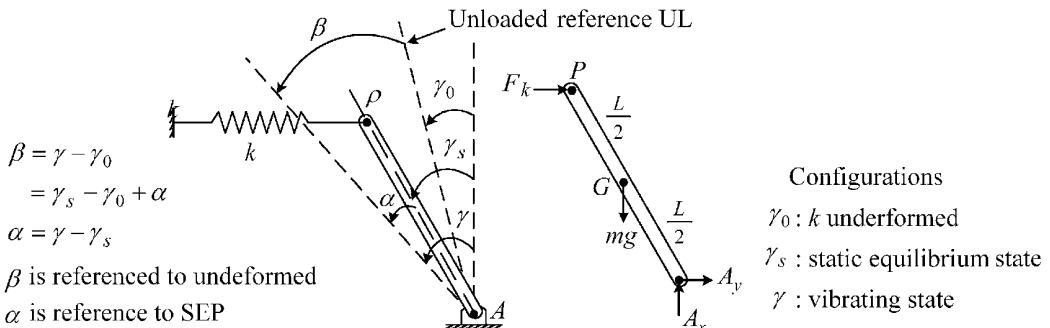


Figure E4.5.12(a) Inclined, inverted pendulum with a horizontal spring

The potential energy term in Lagrange's equation becomes

$$\frac{\partial U_a}{\partial \beta} = \frac{\partial U_a}{\partial \gamma} = -mg\frac{L}{2}\sin\gamma + k(\Delta + L\sin\gamma - L\sin\gamma_s)L\cos\gamma \quad (7)$$

where the total angle coordinate β is utilized and the gravitational force (weight) is included.

Note that

$$\gamma = \gamma_s + \alpha \quad (8)$$

where α is a small perturbation angle referenced to the static equilibrium state ($\gamma = \gamma_s$).

Consider the Taylor series representations utilizing (8)

$$\sin\gamma \approx \sin\gamma_s + \cos\gamma_s\alpha \quad (9)$$

$$\cos\gamma \approx \cos\gamma_s - \sin\gamma_s\alpha \quad (10)$$

$$\sin\gamma\cos\gamma \approx \sin\gamma_s\cos\gamma_s + (\cos^2\gamma_s - \sin^2\gamma_s)\alpha - \sin\gamma_s\cos\gamma_s\alpha^2 \quad (11)$$

Neglect the α^2 term in (11), since α is a small quantity, and insert (9)–(11) into (7):

$$\begin{aligned} \Rightarrow \frac{\partial U_a}{\partial \beta} \cong & -mg\frac{L}{2}\sin\gamma_s - mg\frac{L}{2}\cos\gamma_s\alpha + k\Delta L\cos\gamma_s - k\Delta L\sin\gamma_s\alpha \\ & + kL^2[\sin\gamma_s\cos\gamma_s + (\cos^2\gamma_s - \sin^2\gamma_s)\alpha] + kL^2[-\sin\gamma_s\cos\gamma_s + \sin^2\gamma_s\alpha] \end{aligned} \quad (12)$$

Substitute the static equilibrium condition (2) into (12) and cancel terms to obtain

$$\frac{\partial U_a}{\partial \beta} \cong kL^2\cos^2\gamma_s\alpha - k\Delta L\sin\gamma_s\alpha - mg\frac{L}{2}\cos\gamma_s\alpha \quad (13)$$

Substitute (1) into (13) to obtain

$$\frac{\partial U_a}{\partial \beta} \cong kL^2(\cos^2\gamma_s - \sin^2\gamma_s + \sin\gamma_s\sin\gamma_0)\alpha - mg\frac{L}{2}(\cos\gamma_s)\alpha \quad (14)$$

Static Equilibrium Position (SEP) Reference

Next, consider evaluating the potential energy relative to the SEP (neglecting gravity effects):

$$U_b = \frac{k}{2}[L\sin(\gamma_s + \alpha) - L\sin(\gamma_s)]^2 \quad (15)$$

$$\frac{\partial U_b}{\partial \alpha} = k[L\sin(\gamma_s + \alpha) - L\sin\gamma_s]L\cos(\gamma_s + \alpha) \quad (16)$$

Substitute (11) and (12) into (16) to obtain

$$\frac{\partial U_b}{\partial \alpha} = kL^2\cos^2\gamma_s\alpha \quad (17)$$

Equations (14) and (17) are not identical, so in a strict sense, evaluation of U should utilize U_a and not U_b . Consider a “stiff spring” approximation, that is, the static deflection is approximately zero:

$$\Rightarrow \gamma_s = \gamma_0 \quad (18)$$

Then, (14) becomes

$$\frac{\partial U_a}{\partial \beta} \cong kL^2 \cos^2 \gamma_s \alpha - mg \frac{L}{2} \cos \gamma_s \alpha \quad (19)$$

For (18) to be true, k must be a large number so that it is reasonable to assume that

$$mg \frac{L}{2} \ll kL^2 \cos \gamma_s \quad (20)$$

Therefore, (19) becomes

$$\frac{\partial U_a}{\partial \beta} \approx kL^2 \cos^2 \gamma_s \alpha \quad (21)$$

which is identical to the SEP referenced results (17). The EOM is obtained from (4.5.106a) with the total deflection coordinate β :

$$\frac{d}{dt} \left(\frac{\partial T}{\partial \dot{\beta}} \right) - \frac{\partial T}{\partial \beta} + \frac{\partial U_a}{\partial \beta} = 0 \quad (22)$$

where since $\dot{\beta} = \dot{\alpha}$

$$T = \frac{I_A}{2} \dot{\beta}^2 = \frac{I_A}{2} \dot{\alpha}^2 \quad (23)$$

and $\frac{\partial U_a}{\partial \beta} \approx kL^2 \cos^2 \gamma_s \alpha$ is defined in (13). Equation (22) yields

$$\therefore I_A \ddot{\alpha} + k_{\text{eq}} \alpha = 0 \quad (24)$$

where

$$\begin{aligned} k_{\text{eq}} &= kL^2 (\cos^2 \gamma_s - \sin^2 \gamma_s + \sin \gamma_s \sin \gamma_0) - mg \frac{L}{2} \cos \gamma_s \\ &= kL^2 \cos^2 \gamma_s - kL \Delta \sin \gamma_s - mg \frac{L}{2} \cos \gamma_s \\ &\approx kL^2 \cos^2 \gamma_s \end{aligned} \quad (25)$$

for the stiff spring approximation and $\Delta \ll L$.

EXAMPLE 4.5.13 Vertical, Inverted Pendulum with Horizontal Spring

Consider the inverted pendulum with side spring shown in Figure E4.5.13(a).

The potential energy is

$$U = \frac{k}{2} (L\theta)^2 - mg \frac{L}{2} (1 - \cos \theta) \quad (1)$$

$$\frac{\partial U}{\partial \theta} = kL^2 \theta - mg \frac{L}{2} \sin \theta \quad (2)$$

$$\sin \theta \approx \sin(0) + \cos(0) * \theta = \theta \quad (3)$$

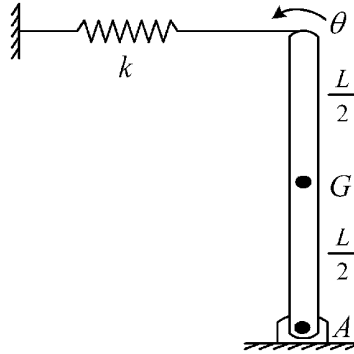


Figure E4.5.13(a) Vertical, inverted pendulum with horizontal spring

$$\frac{\partial U}{\partial \theta} = \left(kL^2 - mg\frac{L}{2} \right) \theta \quad (4)$$

The gravity term must be included here since the physical system's motion requires a moment to cause the pendulum to drop if $k \rightarrow 0$. The gravity term may be ignored for $kL \gg mg$.

4.5.8 “Automating” the Derivation of the LE Approach

Obtaining a full set of EOM via (4.5.106) or (4.5.114) may become very tedious and error prone when conducted manually on large-order, nonlinear systems. Maple, Mathematica, MATLAB, or other symbolic math codes can be employed to somewhat automate this process. Following this approach may provide more accurate results or at least a good “second opinion” on your by-hand calculations. Example 3.3.4 illustrates this approach utilizing the Newton's law method.

EXAMPLE 4.5.14 EOMs for Pipe Transport Elevator

Description: The Figure E4.5.14(a) depicts an elevator of mass m_C that transports circular pipe of various radii r . The mass and moment of inertia of a single pipe are m_P and I_P , respectively. The carriage has a circular inner profile with center point O and radius R . The cables that support C are flexible with stiffness k and are pulled vertically with support motion $z(t)$. The guide bearings for C cause a vertical drag force $-b\dot{y}$. The carriage motor causes a vertical force $F(t)$.

Objective: The objective here is to derive the two EOMs with the Lagrange equations utilizing the symbolic math software Maple.

Assumptions: Rolling (no-slip) contact between the pipe and carriage.

Solution:

(a) Figure E4.5.14(b) shows a velocity vector diagram for the mass center G_P of pipe m_P . The velocity of the mass center is given by

$$\vec{V}_{G_P} = \vec{V}_O + \vec{V}_{G_P/O} = v_{yC}\hat{j} + [R\omega \cos(\theta)\hat{i} + R\omega \sin(\theta)\hat{j}] \quad (1)$$

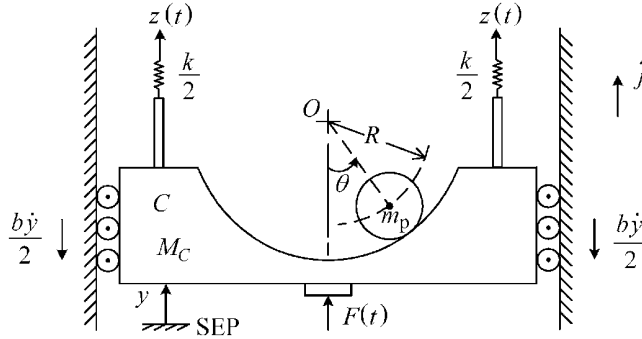
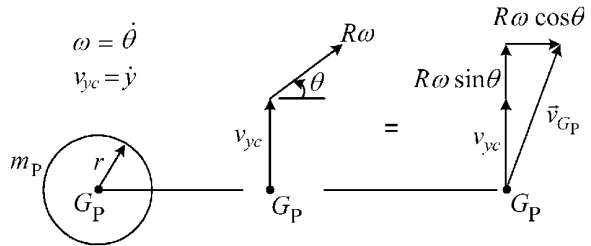


Figure E4.5.14(a) Pipe transport elevator with support motion carriage C

Figure E4.5.14(b) Velocity diagram for the pipe's mass center G_P 

where $\omega = \dot{\theta}$.

- (b) Figure E4.5.14(c) shows an angular velocity diagram for pipe P . The arc length $\overline{AA'}$ can be expressed as viewed in a reference frame attached to the carriage, that is, $\overline{AA'} = (R+r)\theta$ or in a rotating reference frame that is attached to line $\overline{OG_P}$, that is, $\overline{AA'} = r\phi$. Equating these expressions yields

$$\phi = -\frac{R+r}{r}\theta = -\left(1 + \frac{R}{r}\right)\theta \quad (2)$$

where the minus sign is included since θ is positive in the counterclockwise sense and ϕ is positive in the clockwise sense.

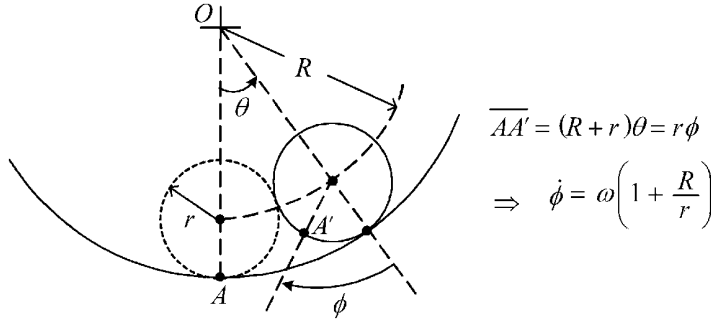
The kinetic energy due to rotation is given by $\frac{1}{2}I_P\Omega^2$ where Ω is the total angular velocity of the pipe, that is,

$\Omega =$ angular velocity of reference frame $\overline{OG_P}$ plus the angular velocity $\dot{\phi}$ as sensed in frame $\overline{OG_P}$

$$= \dot{\theta} + \dot{\phi} = \dot{\theta} - \left(1 + \frac{R}{r}\right)\dot{\theta} = -\frac{R}{r}\dot{\theta} = -\frac{R}{r}\omega \quad (3)$$

- (c) The kinetic energy of this system is obtained from (4.2.14) and Figures E4.5.14(a), E4.5.14(b), and E4.5.14(c) as

$$\begin{aligned} T &= \frac{m_C}{2}v_{yc}^2 + \frac{m_P}{2}v_{G_P}^2 + \frac{I_P}{2}\Omega^2 \\ &= \frac{m_C}{2}v_{yc}^2 + \frac{m_P}{2}\left[R^2\omega^2\cos^2\theta + (v_{yc} + R\omega\sin\theta)^2\right] + \frac{I_P R^2}{2r^2}\omega^2 \end{aligned} \quad (4)$$

Figure E4.5.14(c) Angular velocity diagram for pipe P

This simplifies to

$$\begin{aligned}
 T &= \frac{(m_C + m_P)}{2} v_{yc}^2 + \frac{m_P}{2} R^2 \omega^2 + R\omega v_{yc} m_P \sin \theta + \frac{I_P R^2}{2 r^2} \omega^2 \\
 &= \frac{m_{\text{tot}}}{2} v_{yc}^2 + \frac{I_{\text{eq}}}{2} \omega^2 + R m_P \omega v_{yc} \sin \theta
 \end{aligned} \quad (5)$$

where

$$m_{\text{tot}} = m_C + m_P \quad (6)$$

$$I_{\text{eq}} = I_P \frac{R^2}{r^2} + m_P R^2 \quad (7)$$

- (d) The potential energy of this system has contributions from the elevation change $(R - R \cos \theta)$ of G_P (ref. Eq. (4.5.57)) and from the deformation of the cables (springs) (ref. Eq. (4.5.65)):

$$U = m_P g R (1 - \cos \theta) + \frac{k}{2} (z - y)^2 \quad (8)$$

The weight potential energy of m_C is not included due to employing the SEP reference.

- (e) The Rayleigh dissipation function is given by Equation (4.5.81) and Figure E4.5.14(a) as

$$\mathfrak{F}^d = \frac{1}{2} b v_{yc}^2 \quad (9)$$

where b is the damping constant.

- (f) The generalized forces due to the motor force $F(t)$ are obtained from (4.5.47), (4.5.48), and (4.5.52) as

$$Q_y = F \hat{j} \cdot \frac{\partial v_{yc} \hat{j}}{\partial v_{yc}} = F, \quad Q_\theta = F \hat{j} \cdot \frac{\partial v_{yc} \hat{j}}{\partial \omega} = 0 \quad (10)$$

- (g) The Lagrange equations are then formed from (4.5.106a):

$$\frac{d}{dt} \left(\frac{\partial L}{\partial \dot{q}_j} \right) - \frac{\partial L}{\partial q_j} = Q_j - \frac{\partial \mathfrak{F}^d}{\partial \dot{q}_j} \quad (11)$$

$$j=1, \quad q_j=y, \quad \dot{q}_j=v_{yc} \quad (12)$$

$$j=2, \quad q_j=\theta, \quad \dot{q}_j=\omega \quad (13)$$

(h) The MAPLE code shown below performs the operations in Equation (11) to obtain the two EOMs shown below:

$$y: \quad m_{\text{tot}}\ddot{y} + Rm_p\ddot{\theta} \sin\theta + Rm_p\dot{\theta}^2 \cos\theta + b\dot{y} + ky = kz + F(t) \quad (14)$$

$$\theta: \quad I_{\text{eq}}\ddot{\theta} + Rm_p\ddot{y} \sin\theta + Rm_pg \sin\theta = 0 \quad (15)$$

Summary: Automation of the EOM process of Lagrange by utilizing MAPLE or another symbolic math code may greatly facilitate the process or provide a reliable “second opinion” if the process is also performed manually:

```
># Example 4.5.14 EOM's for Pipe Transport Elevator
>restart;
># Define Auxiliary Variables
>thetadot(t) := diff(theta(t), t); ydot(t) := diff(y(t), t);
thetadot(t) := d/dt theta(t) ydot(t) := d/dt y(t)
># Kinetic Energy
>T := Mtot/2*Vyc^2 + Ieq/2*omega^2
      + R*Mp*omega*Vyc*sin(theta);
T := 1/2*Mtot Vyc^2 + 1/2*Ieq omega^2 + R Mp omega Vyccsin(theta)
># Potential Energy
>U := Mp*g*R*(1-cos(theta)) + k/2*(z-y)^2;
U := Mp g R(1-cos(theta)) + 1/2*k(z-y)^2
># Rayleigh Dissipation Function
>Fd := b/2*Vyc^2;
Fd := 1/2*b Vyc^2
># Circulatory Forces
>Fc := 0;
Fc := 0
># Generalized Forces
>Qy := F; Qtheta := 0;
Qy:F Qtheta:=0
*****
># ***** Lagrange Equation For j=1 (q=y, qdot=vy) *****
># See eq. 4.5.114
*****
># Lagrangian Function L (See eq 4.5.113)
>L := T - U;
L := 1/2*Mtot Vyc^2 + 1/2*Ieq omega^2 + R Mp omega Vyccsin(theta) - Mp g R(1-cos(theta))
      - 1/2*k(z-y)^2
```

```

# Partial derivative of L with respect to y dot
>dLdVyc:= diff (L, Vyc) ;
dLdVyc:= Mtot Vyc + R Mp ω sin(θ)
dLdVyc:= subs (Vyc=Vyc (t) , omega=omega (t) , y=y (t) ,
               theta=theta (t) , dLdVyc) ;
dLdVyc:= Mtot Vyc(t) + R Mp ω(t) sin(θ(t))
# Time derivative of ( Partial derivative of L with
respect to y dot)
>d_dLdVyc_dt (t) := diff (dLdVyc, t) ;
d_dLdVyc_dt(t) := Mtot  $\left(\frac{d}{dt}Vyc(t)\right) + R Mp \left(\frac{d}{dt}\omega(t)\right) \sin(\theta(t))$ 
               + R Mp ω(t) cos(θ(t))  $\left(\frac{d}{dt}\theta(t)\right)$ 
LEQa := subs (omega (t) = thetadot (t) , Vyc (t) = ydot (t) ,
              d_dLdVyc_dt (t) ) ;
LEQa := Mtot  $\left(\frac{d^2}{dt^2}y(t)\right) + R Mp \left(\frac{d^2}{dt^2}\theta(t)\right) \sin(\theta(t))$ 
        + R Mp  $\left(\frac{d}{dt}\theta(t)\right)^2 \cos(\theta(t))$ 
# Partial derivative of L with respect to y
>LEQb := diff (L, y) ;
LEQb := k(z-y)
LEQb := subs (Vyc=Vyc (t) , omega=omega (t) , y=y (t) , theta=
theta (t) , LEQb) ;
LEQb := k(z-y(t))
>LEQb := subs (omega (t) = thetadot (t) , Vyc (t) = ydot (t) , LEQb) ;
LEQb := k(z-y(t))
# y generalized force
>LEQc := Qy ;
LEQc := F
# Partial derivative of dissipation function with respect
to y dot
>LEQd := diff (Fd, Vyc) ;
LEQd := b Vyc
>LEQd := subs (Vyc=ydot (t) , LEQd) ;
LEQd := b  $\left(\frac{d}{dt}y(t)\right)$ 
# Partial derivative of the circulatory function with
respect to y dot
>LEQe := diff (Fc, Vyc) ;
LEQe := 0
># The y EOM is the equation (LEQ1 = 0)
>LEQ1 := LEQa + LEQd - LEQb + LEQe - LEQc ;
LEQ1 := Mtot  $\left(\frac{d^2}{dt^2}y(t)\right) + R Mp \left(\frac{d^2}{dt^2}\theta(t)\right) \sin(\theta(t))$ 
        + R Mp  $\left(\frac{d}{dt}\theta(t)\right)^2 \cos(\theta(t)) + b \left(\frac{d}{dt}y(t)\right) - k(z-y(t)) - F$ 

```

```

*****
># ***** Lagrange Equation For j=2 (q=theta , qdot=omega)
># See eq. 4.5.114
> *****
>dLdomega:= diff (L, omega) ;
dLdomega:= Ieq ω + R Mp Vycsin(θ)
dLdomega:= subs (Vyc=Vyc (t) , omega=omega (t) ,
y=y (t) , theta=theta (t) , dLdomega) ;
dLdomega:= Ieq ω(t) + R Mp Vyc(t)sin(θ(t))

>d_dLdomega_dt (t) := diff (dLdomega, t) ;
d_dLdomega_dt(t) := Ieq  $\left(\frac{d}{dt}\omega(t)\right) + R Mp \left(\frac{d}{dt}Vyc(t)\right) \sin(\theta(t))$ 
+ R Mp Vyc(t)cos(θ(t))  $\left(\frac{d}{dt}\theta(t)\right)$ 
LEQa:= subs (omega (t) =thetadot (t) , Vyc (t) =ydot (t) ,
d_dLdomega_dt (t) ) ;
LEQa:= Ieq  $\left(\frac{d^2}{dt^2}\theta(t)\right) + R Mp \left(\frac{d^2}{dt^2}y(t)\right) \sin(\theta(t))$ 
+ R Mp  $\left(\frac{d}{dt}y(t)\right) \cos(\theta(t)) \left(\frac{d}{dt}\theta(t)\right)$ 
>LEQb := diff (L, theta) ;
LEQb:= R Mp ω Vyc cos(θ) - Mp g R sin(θ)
LEQb:= subs (Vyc=Vyc (t) , omega=omega (t) , y=y (t) ,
theta=theta (t) , LEQb) ;
LEQb:= R Mp ω(t) Vyc(t)cos(θ(t)) - Mp g R sin(θ(t))
>LEQb := subs (omega (t) =thetadot (t) , Vyc (t) =ydot (t) , LEQb) ;
LEQb:= R Mp  $\left(\frac{d}{dt}y(t)\right) \cos(\theta(t)) \left(\frac{d}{dt}\theta(t)\right) - Mp g R \sin(\theta(t))$ 
>LEQc := Qtheta ;
LEQc:= 0
>LEQd := diff (Fd, omega) ;
LEQd:= 0
>LEQd:= subs (omega=thetadot (t) , LEQd) ;
LEQd:= 0
>LEQe := diff (Fc, omega) ;
LEQe:= 0
># The theta EOM is the equation (LEQ2 = 0)
>LEQ2:=LEQa+LEQd-LEQb+LEQe-LEQc ;
LEQ2:= Ieq  $\left(\frac{d^2}{dt^2}\theta(t)\right) + R Mp \left(\frac{d^2}{dt^2}y(t)\right) \sin(\theta(t)) + Mp g R \sin(\theta(t))$ 

```

EXAMPLE 4.5.15 Industrial Louver System for a Large Air Duct

Description: The model in Figure E4.5.15(a) depicts a door that is used to control airflow through a large air duct in an industrial process. The inverted pendulum-type louver is opened by retraction of a holding latch during certain stages in the operation. The upstream

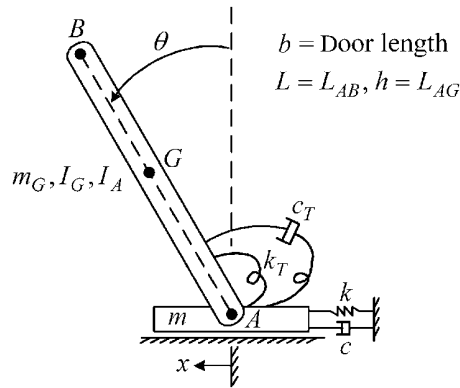


Figure E4.5.15(a) Model of louver for airflow control in industrial ductwork

air pressure forces the unlatched door open causing it to swing downward and oscillate. The equations of motion are to be derived in order to develop a simulation model to assist in designing the bearings and other components of the device. The base mass m is allowed to slide to accommodate thermal expansion concerns and is compliantly mounted to help absorb sudden pressure fluctuations in the air supply. The louver has a rotational return spring and damper.

Objective: Write the equations by both the Newton and Lagrange approaches and compare results. Assume large motions to derive the nonlinear equations of motion and then linearize the equations about the closed state $x = \theta = 0$.

Assumptions: The louver (door) is subjected to a constant, uniform pressure p at all times. A near-frictionless restraint constrains the mass m from rotating.

(a) Kinematic Relationships

$$x_G = x + h \sin \theta, \quad \dot{x}_G = \dot{x} + h \cos \theta \dot{\theta}, \quad \ddot{x}_G = \ddot{x} + h \cos \theta \ddot{\theta} - h \sin \theta \dot{\theta}^2 \quad (1)$$

$$y_G = h \cos \theta, \quad \dot{y}_G = -h \sin \theta \dot{\theta} \quad (2)$$

$$\vec{r}_{G/A} = h \sin \theta \hat{i} + h \cos \theta \hat{j} \quad (3)$$

$$\vec{a}_A = \ddot{x} \hat{i} \quad (4)$$

(b) Newton's Law Approach

From Figures E4.5.15(b) and E4.5.15(c), the resultant pressure forces and moment are

$$F_x = \int_0^L p b dz \cos \theta = p b L \cos \theta \quad (5)$$

$$F_y = - \int_0^L p b dz \sin \theta = -p b L \sin \theta \quad (6)$$

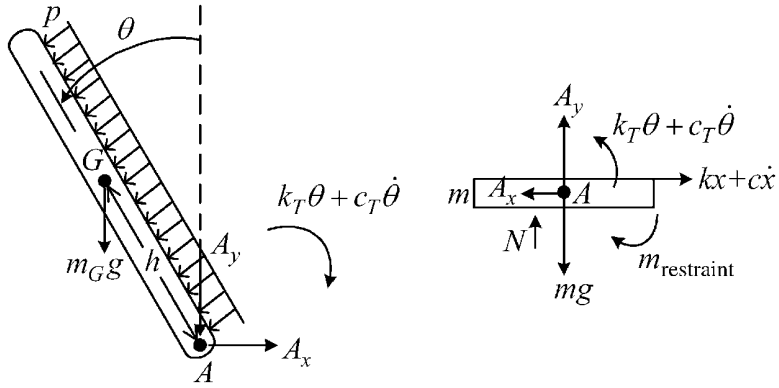


Figure E4.5.15(b) Free body diagram for Newton law-based derivation

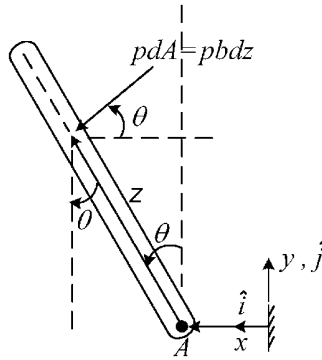


Figure E4.5.15(c) Diagram for analysis of pressure-induced forces and moments

Using the right-hand rule about the \hat{k} unit vector (directed into the page),

$$M_A = - \int_0^L z p b dz = - p b \frac{L^2}{2} \quad (7)$$

The translational equations of motion (EOMs) are

$$m\ddot{x} = A_x - kx - c\dot{x} \quad (8)$$

$$m_G\ddot{x}_G = m_G(\ddot{x} + h\cos\theta\ddot{\theta} - h\sin\theta\dot{\theta}^2) = F_x - A_x = p b L \cos\theta - A_x \quad (9)$$

From (7) and (3.3.26), $[I_A \bar{\alpha} + \vec{r}_{G/A} \times m_G \bar{a}_A = \vec{\Gamma}_A]$, and using the right-hand rule about \hat{k} yields

$$I_A(-\ddot{\theta})\hat{k} + (h\sin\theta\hat{i} + h\cos\theta\hat{j}) \times m_G\ddot{x}\hat{i} = \left(-pb\frac{L^2}{2} + k_T\theta - m_Ggh\sin\theta\right)\hat{k} + c_T\dot{\theta} \quad (10)$$

$$(I_G + m_Gh^2)\ddot{\theta} + m_Gh\cos\theta\ddot{x} = \frac{pbL^2}{2} - k_T\theta - m_Ggh\sin\theta - c_T\dot{\theta} \quad (11)$$

Sum Equations (8) and (9) to eliminate A_x :

$$(m + m_G)\ddot{x} + m_G(h\cos\theta\ddot{\theta} - h\sin\theta\dot{\theta}^2) = -kx - c\dot{x} + pbL\cos\theta \quad (12)$$

(c) Lagrange Approach

Kinetic energy:

$$T = \frac{m}{2}\dot{x}^2 + \frac{m_G}{2}(\dot{x}_G^2 + \dot{y}_G^2) + \frac{I_G}{2}\dot{\theta}^2 \quad (13)$$

$$T = \frac{m}{2}\dot{x}^2 + \frac{m_G}{2}\left[(\dot{x} + h\cos\theta\dot{\theta})^2 + (h\sin\theta\dot{\theta})^2\right] + \frac{I_G}{2}\dot{\theta}^2$$

Potential energy:

$$U = \frac{k}{2}x^2 + \frac{k_T}{2}\theta^2 + m_Ggh\cos\theta \quad (14)$$

Dissipation function:

$$\mathfrak{F}^d = \frac{c}{2}\dot{x}^2 + \frac{c_T}{2}\dot{\theta}^2 \quad (15)$$

Lagrange's equation (4.6.52):

$$\frac{d}{dt}\left(\frac{\partial T}{\partial \dot{q}_j}\right) - \frac{\partial T}{\partial q_j} = Q_j - \frac{\partial U}{\partial q_j} - \frac{\partial \mathfrak{F}^d}{\partial \dot{q}_j} \quad (16)$$

$$\frac{\partial T}{\partial x} = 0 \quad (17)$$

$$\frac{\partial T}{\partial \theta} = m_G[(\dot{x} + h\cos\theta\dot{\theta})(-h\sin\theta\dot{\theta}) + (h\sin\theta\dot{\theta})(h\cos\theta\dot{\theta})] = m_G(-h\dot{x}\sin\theta\dot{\theta}) \quad (18)$$

$$\frac{\partial T}{\partial \dot{x}} = m\dot{x} + m_G(\dot{x} + h\cos\theta\dot{\theta}) \quad (19)$$

$$\frac{\partial T}{\partial \dot{\theta}} = m_G[(\dot{x} + h\cos\theta\dot{\theta})(h\cos\theta) + (h\sin\theta\dot{\theta})(h\sin\theta)] + I_G\dot{\theta} = m_G(\dot{x}h\cos\theta + h^2\dot{\theta}) + I_G\dot{\theta} \quad (20)$$

$$\frac{d}{dt}\left(\frac{\partial T}{\partial \dot{x}}\right) = m\ddot{x} + m_G\ddot{x} + m_Gh\cos\theta\ddot{\theta} - m_Gh\dot{\theta}^2\sin\theta \quad (21)$$

$$\frac{d}{dt}\left(\frac{\partial T}{\partial \dot{\theta}}\right) = I_G\ddot{\theta} + m_Gh^2\ddot{\theta} + m_Gh(\ddot{x}\cos\theta - \dot{x}\dot{\theta}\sin\theta) \quad (22)$$

$$\frac{\partial U}{\partial x} = kx, \quad \frac{\partial U}{\partial \theta} = k_T\theta - m_Ggh\sin\theta \quad (23)$$

$$\frac{\partial \mathfrak{F}^d}{\partial \dot{x}} = c\dot{x}, \quad \frac{\partial \mathfrak{F}^d}{\partial \dot{\theta}} = c_T\dot{\theta} \quad (24)$$

Generalized forces for applied pressure (ref. 4.5.51):

$$d\vec{F} = p dA(\cos\theta\hat{i} - \sin\theta\hat{j}) \quad (25)$$

$$\vec{R}_F = \vec{R}_B = (x + y \sin \theta) \hat{i} + y \cos \theta \hat{j} \quad (26)$$

$$Q_x = \int_0^L d\vec{F} \cdot \frac{\partial \vec{F}_R}{\partial x} = \int_0^L p b d y (\cos \theta \hat{i} - \sin \theta \hat{j}) \cdot \hat{i} = \int_0^L p b d z \cos \theta = p b L \cos \theta \quad (27)$$

$$\begin{aligned} Q_\theta &= \int_0^L d\vec{F} \cdot \frac{\partial \vec{F}_R}{\partial \theta} = \int_0^L p b d z (\cos \theta \hat{i} - \sin \theta \hat{j}) \cdot (z \cos \theta \hat{i} - y \sin \theta \hat{j}) \\ &= \int_0^L p b (\cos^2 \theta z + \sin^2 \theta z) d z = p b \frac{L^2}{2} \end{aligned} \quad (28)$$

Substituting the above results into Lagrange's equations (16) yields
x EOM:

$$(m + m_G) \ddot{x} + m_G h \cos \theta \ddot{\theta} - m_G h \dot{\theta}^2 \sin \theta = p b L \cos \theta - k x - c \dot{x} \quad (29)$$

θ EOM:

$$\begin{aligned} &(I_G + m_G h^2) \ddot{\theta} + m_G h (\ddot{x} \cos \theta - \dot{x} \dot{\theta} \sin \theta) + m_G h \dot{x} \sin \theta \dot{\theta} \\ &= p b \frac{L^2}{2} - k_T \theta + m_G g h \sin \theta - c_T \dot{\theta} \end{aligned} \quad (30)$$

(d) Comparison

The Lagrange approach results (Equations (29), (30)) are identical to the Newton approach results (Equations (11), (12)).

(e) Linearized EOM

Linearization is performed with the Taylor series approach shown in Equations (2.4.3)–(2.4.7). The equilibrium state (ES) is defined by

$$x = \dot{x} = \ddot{x} = \theta = \dot{\theta} = \ddot{\theta} = 0 \quad (31)$$

The pressure is considered to be zero at $t=0$ and suddenly jump to p at $t=0^+$ (when the louver is unlatched):

x EOM (Equations (12) or (29)):

$$\begin{aligned} f_1 &= \cos \theta \ddot{\theta} \\ &\approx f_1|_{\text{ES}} + \left. \frac{\partial f_1}{\partial \theta} \right|_{\text{ES}} \theta + \left. \frac{\partial f_1}{\partial \ddot{\theta}} \right|_{\text{ES}} \ddot{\theta} = \cos \theta|_{\text{ES}} + (-\sin \theta \ddot{\theta})|_{\text{ES}} \theta + \cos \theta|_{\text{ES}} \ddot{\theta} = \ddot{\theta} \end{aligned} \quad (32)$$

$$\begin{aligned} f_2 &= \dot{\theta}^2 \sin \theta \\ &\approx f_2|_{\text{ES}} + \left. \frac{\partial f_2}{\partial \dot{\theta}} \right|_{\text{ES}} \dot{\theta} + \left. \frac{\partial f_2}{\partial \theta} \right|_{\text{ES}} \theta = \dot{\theta}^2 \sin \theta|_{\text{ES}} + 2\dot{\theta} \sin \theta|_{\text{ES}} \dot{\theta} + \dot{\theta}^2 \cos \theta|_{\text{ES}} \theta = 0 + 0 + 0 = 0 \end{aligned} \quad (33)$$

$$f_3 = \cos \theta \approx f_3|_{\text{ES}} + \left. \frac{\partial f_3}{\partial \theta} \right|_{\text{ES}} \theta = \cos \theta|_{\text{ES}} - \sin \theta|_{\text{ES}} \theta = 1 - 0 = 1 \quad (34)$$

θ EOM (Equations (11) or (30)):

$$f_4 = \ddot{x} \cos \theta \approx \ddot{x} \text{ (similar to (32))} \quad (35)$$

$$f_5 = \dot{x}\dot{\theta}\sin\theta \approx f_5|_{ES} + \left.\frac{\partial f_5}{\partial \dot{x}}\right|_{ES} \dot{x} + \left.\frac{\partial f_5}{\partial \dot{\theta}}\right|_{ES} \dot{\theta} + \left.\frac{\partial f_5}{\partial \theta}\right|_{ES} \theta$$

$$= \dot{x}\dot{\theta}\sin\theta|_{ES} + \dot{\theta}\sin\theta|_{ES}\dot{x} + \dot{x}\sin\theta|_{ES}\dot{\theta} + \dot{x}\dot{\theta}\cos\theta|_{ES}\theta = 0 + 0 + 0 + 0 = 0$$

$$f_6 = \sin\theta \approx f_6|_{ES} + \left.\frac{\partial f_6}{\partial \theta}\right|_{ES} \theta = \sin\theta|_{ES} + \cos\theta|_{ES}\theta = 0 + \theta = \theta$$

Substituting the linearized forms into (29) and (30) yields
 x EOM (linearized about ES):

$$(m + m_G)\ddot{x} + m_G h \ddot{\theta} = pbL - kx - c\dot{x} \quad (38)$$

θ EOM (linearized about ES):

$$(I_G + m_G h^2)\ddot{\theta} + m_G h \ddot{x} = pb\frac{L^2}{2} - k_T\theta + m_G g h \theta - c_T \dot{\theta} \quad (39)$$

or

$$\begin{bmatrix} m + m_G & m_G h \\ m_G h & I_G + m_G h^2 \end{bmatrix} \begin{Bmatrix} \ddot{x} \\ \ddot{\theta} \end{Bmatrix} + \begin{bmatrix} c & 0 \\ 0 & c_T \end{bmatrix} \begin{Bmatrix} \dot{x} \\ \dot{\theta} \end{Bmatrix} + \begin{bmatrix} k & 0 \\ 0 & k_T - m_G g h \end{bmatrix} \begin{Bmatrix} x \\ \theta \end{Bmatrix} = \begin{Bmatrix} pbL \\ pbL^2/2 \end{Bmatrix} \quad (40)$$

4.6 LE FOR FLEXIBLE, DISTRIBUTED MASS BODIES: ASSUMED MODES APPROACH

Section 4.5 provided a derivation of the fundamental form of LE (4.5.23) for a system of particles. These results were then specialized (4.5.106) for RB which are connected to ground or to each other via stiffness, damping, etc. and had forces obtainable from scalar potential, circulation, and dissipation functions. This section extends the use of (4.5.106) to include the forces and kinetic energy internal to a flexible body with distributed inertia. The importance of considering flexible structure vibrations is illustrated by the failure of a NASA prototype Helios solar-powered aircraft shown in Figure 4.6.1.



Figure 4.6.1 Prototype solar–electric aircraft shortly before and after failure due to vibration. Reproduced with permission from NASA

The displacements in a flexible component are approximated by a weighted sum of known displacement functions using the assumed modes method (2.11.28). The resulting form of LE enables vibration modeling of flexible bodies by using assumed modes.

4.6.1 Assumed Modes Kinetic Energy and Mass Matrix Expressions

From Figure 4.6.2 and Equation (4.2.3), the most general expression for the kinetic energy is

$$T = \frac{1}{2} \int_V \frac{n d}{dt} (\vec{R}) \cdot \frac{n d}{dt} (\vec{R}) dm \quad (4.6.1)$$

where the left superscript n indicates that the time derivatives are taken as sensed in the inertial reference frame n . The assumed modes approximation to the velocities in (4.6.1) is by (2.11.35):

$$\begin{aligned} \dot{\vec{R}} &= \dot{u}_1 n_1 + \dot{u}_2 n_2 + \dot{u}_3 n_3 \\ &= \left(\sum_{i=1}^{N_1} \dot{q}_{i1} \phi_{i1}(x_1, x_2, x_3) \right) n_1 + \left(\sum_{i=1}^{N_2} \dot{q}_{i2} \phi_{i2}(x_1, x_2, x_3) \right) n_2 + \left(\sum_{i=1}^{N_3} \dot{q}_{i3} \phi_{i3}(x_1, x_2, x_3) \right) n_3 \end{aligned} \quad (4.6.2)$$

where n_i are unit vectors along x_{ni} in Figure 4.6.2 and where the global shape functions $\phi_{ij}(x_1, x_2, x_3)$ are known functions of the spatial coordinates x_1, x_2, x_3 . The shape functions must satisfy the actual displacement boundary conditions of the problem. This property is referred to as “kinematic admissibility” and is discussed in the text following (2.11.34).

Substitution of (4.6.2) into (4.6.1) yields the kinetic energy

$$\begin{aligned} T &= \frac{1}{2} \int_V \left[\left(\sum_{i=1}^{N_1} \dot{q}_{i1} \phi_{i1} \right) \left(\sum_{k=1}^{N_1} \dot{q}_{k1} \phi_{k1} \right) + \left(\sum_{i=1}^{N_2} \dot{q}_{i2} \phi_{i2} \right) \left(\sum_{k=1}^{N_2} \dot{q}_{k2} \phi_{k2} \right) + \left(\sum_{i=1}^{N_3} \dot{q}_{i3} \phi_{i3} \right) \left(\sum_{k=1}^{N_3} \dot{q}_{k3} \phi_{k3} \right) \right] \\ &= \frac{1}{2} \sum_{i=1}^{N_1} \sum_{k=1}^{N_1} \tilde{m}_{ik1} \dot{q}_{i1}(t) \dot{q}_{k1}(t) + \frac{1}{2} \sum_{i=1}^{N_2} \sum_{k=1}^{N_2} \tilde{m}_{ik2} \dot{q}_{i2}(t) \dot{q}_{k2}(t) + \frac{1}{2} \sum_{i=1}^{N_3} \sum_{k=1}^{N_3} \tilde{m}_{ik3} \dot{q}_{i3}(t) \dot{q}_{k3}(t) \end{aligned} \quad (4.6.3)$$

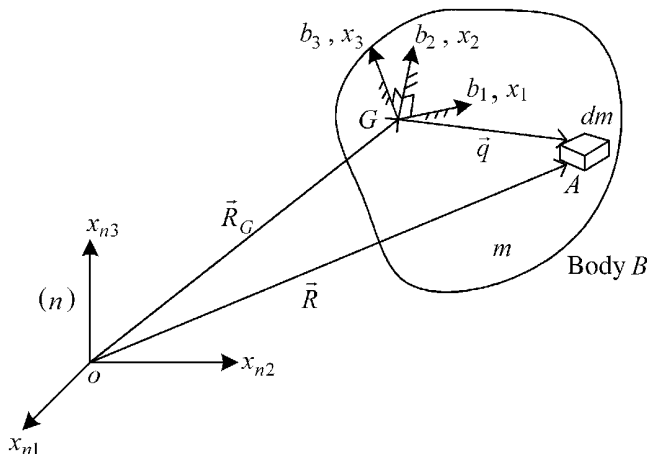


Figure 4.6.2 Diagram for kinetic energy derivation of a flexible body

where

$$\tilde{m}_{ikj} = \int_V \phi_{ij} \phi_{kj} dm = \int_V \phi_{ij}(x_1, x_2, x_3) \phi_{kj}(x_1, x_2, x_3) \rho dV \begin{cases} j=1, 2, 3 \\ i=1, N_j \\ k=1, N_j \end{cases} \quad (4.6.4)$$

and ρ is the mass density of the material. The \tilde{m}_{ikj} are symmetric since

$$\tilde{m}_{ikj} = \int_V \phi_{ij} \phi_{kj} \rho dV = \int_V \phi_{kj} \phi_{ij} \rho dV = \tilde{m}_{kij} \quad (4.6.5)$$

Thus, the total number of independent \tilde{m}_{ikj} is reduced to

$$\frac{N_1(N_1 + 1)}{2} + \frac{N_2(N_2 + 1)}{2} + \frac{N_3(N_3 + 1)}{2} \quad (4.6.6)$$

The total number of independent \tilde{m}_{ikj} can be further reduced to

$$N_1 + N_2 + N_3 \quad (4.6.7)$$

if the density ρ is constant and ϕ_{ij} are selected to be orthogonal functions (2.11.29), that is,

$$\tilde{m}_{ikj} = \rho \int_V \phi_{ij} \phi_{kj} dV = \begin{cases} 0, & i \neq k \\ m_{ii}, & i = k \end{cases}, \quad j=1, 2, 3, \quad i=1, N_j, \quad k=1, N_j \quad (4.6.8)$$

In general, the kinetic energy in (4.6.3) may be expressed as the quadratic form

$$T = \frac{1}{2} \underline{\dot{q}}^T \underline{\tilde{m}} \underline{\dot{q}} \quad (1 \times 1) \quad (4.6.9)$$

where

$$\underline{\dot{q}} = \begin{Bmatrix} \dot{q}_1 \\ \dot{q}_2 \\ \dot{q}_3 \end{Bmatrix} = \begin{Bmatrix} N_1 \times 1 \\ N_2 \times 1 \\ N_3 \times 1 \end{Bmatrix} = N \times 1 \text{ vector of independent generalized coordinate velocities} \quad (4.6.10)$$

$$N = N_1 + N_2 + N_3 = \text{number of independent generalized coordinates} \quad (4.6.11)$$

$$\underline{q}_1 = \begin{Bmatrix} q_{11} \\ q_{21} \\ \vdots \\ q_{N_1 1} \end{Bmatrix}, \quad \underline{q}_2 = \begin{Bmatrix} q_{12} \\ q_{22} \\ \vdots \\ q_{N_2 2} \end{Bmatrix}, \quad \underline{q}_3 = \begin{Bmatrix} q_{13} \\ q_{23} \\ \vdots \\ q_{N_3 3} \end{Bmatrix} \quad (4.6.12)$$

and the “generalized coordinate mass matrix” is

$$\underline{\tilde{m}} = \begin{bmatrix} \tilde{m}_1 & \underline{0} & \underline{0} \\ (N_1 \times N_1) & (N_1 \times N_2) & (N_1 \times N_3) \\ \underline{0} & \tilde{m}_2 & \underline{0} \\ (N_2 \times N_1) & (N_2 \times N_2) & (N_2 \times N_3) \\ \underline{0} & \underline{0} & \tilde{m}_3 \\ (N_3 \times N_1) & (N_3 \times N_2) & (N_3 \times N_3) \end{bmatrix} \quad (4.6.13)$$

where

$$\begin{aligned}(\underline{\tilde{m}}_1)_{ik} &= \tilde{m}_{ik1}, \quad i = 1, N_1, \quad k = 1, N_1 \\(\underline{\tilde{m}}_2)_{ik} &= \tilde{m}_{ik2}, \quad i = 1, N_2, \quad k = 1, N_2 \\(\underline{\tilde{m}}_3)_{ik} &= \tilde{m}_{ik3}, \quad i = 1, N_3, \quad k = 1, N_3\end{aligned}\quad (4.6.14)$$

EXAMPLE 4.6.1 Assumed Modes Generalized Mass Matrix for Cantilever Beam

Objective: To demonstrate the evaluation of an assumed modes matrix for the simple cantilever beam shown in Figure 2.11.8.

Solution: From (2.11.30) to (2.11.32), the only deflection is in the x_2 direction:

$$u_2(x_1, t) = q_1(t)\phi_{12}(x_1) + q_2(t)\phi_{22}(x_1) \quad (1)$$

$$N_1 + N_3 = 0, \quad N_2 = 2 \quad (2)$$

Equation (4.6.5) yields

$$\begin{aligned}\tilde{m}_{112} &= \int_0^L \phi_{12}\phi_{12}dm = \int_0^L \phi_{12}(x_1)\phi_{12}(x_1)\rho(x_1)A(x_1)dx_1 \\ \tilde{m}_{122} = \tilde{m}_{212} &= \int_0^L \phi_{12}\phi_{22}dm = \int_0^L \phi_{12}(x_1)\phi_{22}(x_1)\rho(x_1)A(x_1)dx_1 \\ \tilde{m}_{222} &= \int_0^L \phi_{22}\phi_{22}dm = \int_0^L \phi_{22}(x_1)\phi_{22}(x_1)\rho(x_1)A(x_1)dx_1\end{aligned}\quad (3)$$

where

$$\phi_{12}(x_1) = \frac{3x_1^2}{L^2} - \frac{2x_1^3}{L^3}, \quad \phi_{22}(x_1) = \frac{-x_1^2}{L} - \frac{x_1^3}{L^2} \quad (4)$$

$$\begin{aligned}A(x_1) &= \text{cross-sectional area of beam which may vary with } x_1 \\ \rho(x_1) &= \text{mass density of beam material which may vary with } x_1\end{aligned}\quad (5)$$

The shape functions in (4) are kinematically admissible since they satisfy the zero slope and deflection boundary conditions of the cantilevered beam at $x_1=0$ in Figure 2.11.8. The \tilde{m}_{112} , \tilde{m}_{122} , and \tilde{m}_{222} are constants since all function in (4) and (5) are known and the integrals in (3) may then be evaluated. The kinetic energy for this example is from (4.6.9):

$$T = \frac{1}{2}(\dot{q}_1 \quad \dot{q}_2) \begin{bmatrix} \tilde{m}_{112} & \tilde{m}_{122} \\ \tilde{m}_{122} & \tilde{m}_{222} \end{bmatrix} \begin{Bmatrix} \dot{q}_1 \\ \dot{q}_2 \end{Bmatrix} \quad (6)$$

The following MAPLE code performs the integrals in (3) for constant ρ and A , yielding

$$\tilde{m}_{112} = \rho A \frac{13L}{35}, \quad \tilde{m}_{122} = -\rho A \frac{11L^2}{210}, \quad \tilde{m}_{222} = \rho A \frac{L^3}{105} \quad (7)$$

Maple Code for Assumed Mode Mass Matrix

```

>restart;
>phi1 := 3*x^2/L^2-2*x^3/L^3 :
>phi2 := -x^2/L+x^3/L^2 :
>int(phi1*phi1 , x=0..L) ;
13
---L
35
>int(phi1*phi2 , x=0..L) ;
-11
---L^2
210
>int(phi2*phi2 , x=0..L) ;
1
---L^3
105

```

Summary: This example provides a simple illustration for evaluating an assumed modes generalized mass matrix. The mass matrix will become an essential part of the assumed modes coordinate, dynamic equilibrium equations obtained via Lagrange's equation.

4.6.2 Rotating Structures

The assumed modes approach is often applied to model the deflections of a structural member that is most effectively modeled as vibrating in a rotating reference from b . Some examples of this include blade on wind turbines, steam turbines, fans or compressors, and solar arrays on spinning satellites. Figure 4.6.3 shows a steam turbine bladed disk and a wind turbine for illustration.

For these cases, Figure 4.6.2 and the transport theorem (2.11.27) imply

$$\frac{{}^n d\vec{R}}{dt} = \dot{\vec{R}} = \frac{{}^n d\vec{R}_G}{dt} + \frac{{}^b d\vec{q}}{dt} + \vec{\omega}_b^{b/n} \times \vec{q} \quad (4.6.15)$$

where b represent the RB on which the flexible structural member is attached and

$$\frac{{}^b d\vec{q}}{dt} = \text{velocity of point A on the flexible structural member, as sensed in frame } b. \quad (4.6.16)$$



Figure 4.6.3 Wind turbine and industrial turbine examples for vibration in a rotating frame. Wind turbine photos reproduced with permission from Center for Wind Energy, University of Massachusetts Lowell. Industrial turbine photo reproduced with permission from JETMAX Feinmechanik

The assumed modes approximation is applied to the velocities and displacement as sensed in the rotating frame, that is, the term ${}^b d\bar{q}/dt$ is from (4.6.2),

$$\frac{{}^b d\bar{q}}{dt} = \left(\sum_{i=1}^{N_1} \dot{q}_{i1} \phi_{i1}(x_{1b}, x_{2b}, x_{3b}) \right) b_1 + \left(\sum_{i=1}^{N_2} \dot{q}_{i2} \phi_{i2}(x_{1b}, x_{2b}, x_{3b}) \right) b_2 + \left(\sum_{i=1}^{N_3} \dot{q}_{i3} \phi_{i3}(x_{1b}, x_{2b}, x_{3b}) \right) b_3 \quad (4.6.17)$$

4.6.3 Internal Forces and Strain Energy of an Elastic Object

Previous energy expressions U as in (4.5.65) or (4.5.98) were derived for ideal, concentrated stiffness models. The following development instead focuses on obtaining a potential energy expression for components with distributed stiffness and mass. Wings and blades may come to mind; however, the majority of all machine and structural components behave with distributed stiffness and response. Figure 4.6.4 illustrates this by the sand pattern nodal lines of a violin body when it is shaken at a resonance state. The sand indicates near-zero vibration, whereas all other locations have vibrations strong enough to repel the loose sand.

The following analysis demonstrates that the internal stiffness-related generalized forces in the flexible body can be accounted for in LE (4.5.106) utilizing a potential energy function, an approach similar to the concentrated stiffness case.

Equation (A.6.11) shows that the strain energy stored in a linear elastic solid is given by

$$U_1 = \frac{1}{2} \int_{V_i} \underline{\underline{\epsilon}}^T \underline{\underline{E}} \underline{\underline{\epsilon}} dV \quad (4.6.18)$$

The volume of the entire deformable body is represented by the integration domain symbol V in this formula. Represent the displacements in the (x_1, x_2, x_3) directions in V



Figure 4.6.4 Distributed deflection response of a violin shaken at resonance. Reproduced with permission from Renaud Carpentier and Emmanuel Bossy, University of New South Wales

by (u_1, u_2, u_3) , respectively. The corresponding small displacement strains are given by Equation (A.3.18) as

$$\underline{\varepsilon} = \begin{Bmatrix} \varepsilon_{11} \\ \varepsilon_{22} \\ \varepsilon_{33} \\ \gamma_{23} \\ \gamma_{13} \\ \gamma_{12} \end{Bmatrix} = \begin{Bmatrix} \varepsilon_{11} \\ \varepsilon_{22} \\ \varepsilon_{33} \\ 2\varepsilon_{23} \\ 2\varepsilon_{13} \\ 2\varepsilon_{12} \end{Bmatrix} = \begin{bmatrix} \partial_{x1} & 0 & 0 \\ 0 & \partial_{x2} & 0 \\ 0 & 0 & \partial_{x3} \\ 0 & \partial_{x3} & \partial_{x2} \\ \partial_{x3} & 0 & \partial_{x1} \\ \partial_{x2} & \partial_{x1} & 0 \end{bmatrix} \begin{Bmatrix} u_1 \\ u_2 \\ u_3 \end{Bmatrix} \quad (4.6.19)$$

and the material (constitutive) matrix \underline{E} is defined in the isotropic stress–strain relation (A.4.3):

$$\begin{Bmatrix} \sigma_{11} \\ \sigma_{22} \\ \sigma_{33} \\ \sigma_{23} \\ \sigma_{13} \\ \sigma_{12} \end{Bmatrix} = \frac{E}{(1+\nu)(1-2\nu)} \begin{bmatrix} 1-\nu & \nu & \nu & 0 & 0 & 0 \\ \nu & 1-\nu & \nu & 0 & 0 & 0 \\ \nu & \nu & 1-\nu & 0 & 0 & 0 \\ 0 & 0 & 0 & \frac{(1-2\nu)}{2} & 0 & 0 \\ 0 & 0 & 0 & 0 & \frac{(1-2\nu)}{2} & 0 \\ 0 & 0 & 0 & 0 & 0 & \frac{(1-2\nu)}{2} \end{bmatrix} \begin{Bmatrix} \varepsilon_{11} \\ \varepsilon_{22} \\ \varepsilon_{33} \\ 2\varepsilon_{23} \\ 2\varepsilon_{13} \\ 2\varepsilon_{12} \end{Bmatrix} \quad (4.6.20)$$

or

$$\underline{\sigma} = \underline{E} \underline{\varepsilon} \quad (4.6.21)$$

where

ν = Poisson's ratio and E = Young's modulus.

For small deflection, the integration domain in Equation (4.6.18) is approximately invariant with deformation; therefore,

$$-\frac{\partial U_I}{\partial q_j} = -\frac{1}{2} \frac{\partial}{\partial q_j} \int_V \underline{\varepsilon}^T \underline{E} \underline{\varepsilon} dV = -\frac{1}{2} \int_V \left(\frac{\partial \underline{\varepsilon}^T}{\partial q_j} \underline{E} \underline{\varepsilon} + \underline{\varepsilon}^T \underline{E} \frac{\partial \underline{\varepsilon}}{\partial q_j} \right) dV = -\int_V \frac{\partial \underline{\varepsilon}^T}{\partial q_j} \underline{E} \underline{\varepsilon} dV \quad (4.6.22a)$$

since the transpose of a scalar equals itself and since \underline{E} is assumed to be symmetric. Substitute (4.6.21) into (4.6.22a) to obtain

$$\begin{aligned} -\frac{\partial U_I}{\partial q_j} &= -\int_V \underline{\sigma}^T \frac{\partial \underline{\varepsilon}}{\partial q_j} dV \\ &= -\int_V \left(\sigma_{11} \frac{\partial \varepsilon_{11}}{\partial q_j} + \sigma_{22} \frac{\partial \varepsilon_{22}}{\partial q_j} + \sigma_{33} \frac{\partial \varepsilon_{33}}{\partial q_j} + \sigma_{21} \frac{\partial \gamma_{21}}{\partial q_j} + \sigma_{13} \frac{\partial \gamma_{13}}{\partial q_j} + \sigma_{32} \frac{\partial \gamma_{32}}{\partial q_j} \right) dx_1 dx_2 dx_3 \\ &= -\int_V \left(\sigma_{11} dx_2 dx_3 * \frac{\partial \varepsilon_{11}}{\partial q_j} dx_1 + \sigma_{22} dx_1 dx_3 * \frac{\partial \varepsilon_{22}}{\partial q_j} dx_2 + \sigma_{33} dx_1 dx_2 * \frac{\partial \varepsilon_{33}}{\partial q_j} dx_3 \right. \\ &\quad \left. + \sigma_{21} dx_1 dx_3 * \frac{\partial \gamma_{21}}{\partial q_j} dx_2 + \sigma_{13} dx_2 dx_3 * \frac{\partial \gamma_{13}}{\partial q_j} dx_1 + \sigma_{32} dx_1 dx_2 * \frac{\partial \gamma_{32}}{\partial q_j} dx_3 \right) \end{aligned}$$

$$\begin{aligned}
&= - \int_V \left\{ \sigma_{11} dx_2 dx_3 \left[\frac{\partial}{\partial q_j} (u_1 + \varepsilon_{11} dx_1) - \frac{\partial u_1}{\partial q_j} \right] + \sigma_{22} dx_1 dx_3 \left[\frac{\partial}{\partial q_j} (u_2 + \varepsilon_{22} dx_2) - \frac{\partial u_2}{\partial q_j} \right] \right. \\
&\quad + \sigma_{33} dx_1 dx_2 \left[\frac{\partial}{\partial q_j} (u_3 + \varepsilon_{33} dx_3) - \frac{\partial u_3}{\partial q_j} \right] + \sigma_{21} dx_1 dx_3 \left[\frac{\partial}{\partial q_j} (u_1 + \gamma_{21} dx_2) - \frac{\partial u_1}{\partial q_j} \right] \\
&\quad \left. + \sigma_{13} dx_2 dx_3 \left[\frac{\partial}{\partial q_j} (u_3 + \gamma_{13} dx_1) - \frac{\partial u_3}{\partial q_j} \right] + \sigma_{32} dx_1 dx_2 \left[\frac{\partial}{\partial q_j} (u_2 + \gamma_{32} dx_3) - \frac{\partial u_2}{\partial q_j} \right] \right\} \quad (4.6.22b)
\end{aligned}$$

Representing the volume integral as the limit of a sum over differential volumes, recognizing that $\sigma^* dA$ type terms produce stress resultants represented by F_{ik} , and finally by adding the identity $(\partial u_i / \partial q_j - \partial u_i / \partial q_j = 0)$ to individual terms yield

$$\begin{aligned}
-\frac{\partial U_I}{\partial q_j} &= - \int_V \underline{\sigma}^T \frac{\partial \underline{\varepsilon}}{\partial q_j} dV \\
&= \lim_{\Delta V \rightarrow 0} \sum_{\text{entire body}} \left\{ \left[F_{11} \frac{\partial}{\partial q_j} (u_1 + \varepsilon_{11} dx_1) - F_{11} \frac{\partial u_1}{\partial q_j} \right] + \left[F_{22} \frac{\partial}{\partial q_j} (u_2 + \varepsilon_{22} dx_2) - F_{22} \frac{\partial u_2}{\partial q_j} \right] \right. \\
&\quad + \left[F_{33} \frac{\partial}{\partial q_j} (u_3 + \varepsilon_{33} dx_3) - F_{33} \frac{\partial u_3}{\partial q_j} \right] + \left[F_{21} \frac{\partial}{\partial q_j} (u_1 + \gamma_{21} dx_2) - F_{21} \frac{\partial u_1}{\partial q_j} \right] \\
&\quad \left. + \left[F_{13} \frac{\partial}{\partial q_j} (u_3 + \gamma_{13} dx_1) - F_{13} \frac{\partial u_3}{\partial q_j} \right] + \left[F_{32} \frac{\partial}{\partial q_j} (u_2 + \gamma_{32} dx_3) - F_{32} \frac{\partial u_2}{\partial q_j} \right] \right\} \quad (4.6.23)
\end{aligned}$$

Recall from (4.5.51) that

$$Q_j = \sum \bar{F} \cdot \frac{\partial \bar{R}}{\partial q_j} \quad (4.6.24)$$

which by comparison with Figure A.6.1 and Equation (4.6.23) yields

Generalized Force for Internal Forces of a Deformable, Linear, Elastic Body

$$Q_j^I = - \frac{\partial U_I}{\partial q_j} \quad (4.6.25)$$

where

$$U_I = \frac{1}{2} \int_V \underline{\varepsilon}^T \underline{E} \underline{\varepsilon} dV = \frac{1}{2} \int_V \underline{\sigma}^T \underline{\varepsilon} dV \quad (4.6.26)$$

From (4.6.21) and (4.6.25)

$$Q_j^I = - \int_V \frac{\partial \underline{\varepsilon}^T}{\partial q_j} \underline{E} \underline{\varepsilon} dV \quad (4.6.27)$$

4.6.4 The Assumed Modes Approximation

Recall from (2.11.28) that the deflections of a deformable body (in three dimensions) can be approximated by

$$\underline{u} = \begin{Bmatrix} u_1 \\ u_2 \\ u_3 \end{Bmatrix} = \begin{Bmatrix} \sum_{i=1}^{n_1} q_{i1}(t) * \phi_{i1}(x_1, x_2, x_3) \\ \sum_{i=1}^{n_2} q_{i2}(t) * \phi_{i2}(x_1, x_2, x_3) \\ \sum_{i=1}^{n_3} q_{i3}(t) * \phi_{i3}(x_1, x_2, x_3) \end{Bmatrix}$$

$$= \begin{bmatrix} \phi_{11} & \phi_{21} & \cdots & \phi_{n_1 1} & \mathbf{0}_{1 \times n_2} & \mathbf{0}_{1 \times n_3} \\ & \mathbf{0}_{1 \times n_1} & & \phi_{12} & \phi_{22} & \cdots & \phi_{n_2 2} & \mathbf{0}_{1 \times n_3} \\ & \mathbf{0}_{1 \times n_1} & & \mathbf{0}_{1 \times n_2} & & & \phi_{13} & \phi_{23} & \cdots & \phi_{n_3 3} \end{bmatrix} \begin{Bmatrix} q_{11} \\ q_{21} \\ \vdots \\ q_{n_1 1} \\ q_{12} \\ q_{22} \\ \vdots \\ q_{n_2 2} \\ q_{13} \\ q_{23} \\ \vdots \\ q_{n_3 3} \end{Bmatrix} \quad (4.6.28)$$

or

$$\underline{u}(x_1, x_2, x_3, t) = \underline{\Phi}(x_1, x_2, x_3) \underline{q}(t) \quad (4.6.29)$$

$\begin{matrix} 3 \times 1 & & 3 \times n & & n \times 1 \end{matrix}$

where

$$n = n_1 + n_2 + n_3 = \text{total number of generalized coordinates} \quad (4.6.30)$$

Note from Equation (A.3.19), the strain–displacement relationship can be expressed as

$$\underline{\varepsilon} = \underline{D} \underline{u} \quad (4.6.31)$$

$\begin{matrix} 6 \times 1 & & 6 \times 33 \times 1 \end{matrix}$

where \underline{D} is a spatial derivative operator matrix (Eq. (A.3.18)). The assumed modes strains may then be expressed by combining (4.6.29) and (4.6.31):

$$\underline{\varepsilon} = \left(\underline{D} \underline{\Phi} \right) \underline{q}(t) \quad (4.6.32)$$

$\begin{matrix} 6 \times 1 & & \left(\begin{matrix} 6 \times 3 & 3 \times n \end{matrix} \right) & & n \times 1 \end{matrix}$

or

$$\underline{\varepsilon}_{6 \times 1} = \underline{B}_{6 \times n}(x_1, x_2, x_3) \underline{q}_{n \times 1}(t) \quad (4.6.33)$$

where

$$\underline{B}_{6 \times n} = [\underline{B}_1 \quad \underline{B}_2 \quad \cdots \quad \underline{B}_n] = \underline{D}_{6 \times 3} \underline{\Phi}_{3 \times n} \quad (4.6.34)$$

$$\underline{B}_j = j\text{th column of } \underline{B}_{6 \times 1} \quad (4.6.35)$$

Note that $\underline{\varepsilon}$ may be represented from (4.6.33) as

$$\underline{\varepsilon} = \sum_{i=1}^n q_i \underline{B}_i \quad (4.6.36)$$

so

$$\frac{\partial \underline{\varepsilon}}{\partial q_j} = \underline{B}_j \quad (4.6.37)$$

Substitution of (4.6.33) and (4.6.37) into (4.6.27) yields

$$Q_j^I = - \int_V \underline{B}_j^T \underline{E} \underline{B}_j \underline{q} dV \quad (4.6.38)$$

The vector of all internal force-related generalized forces becomes

$$\underline{Q}_{n \times 1}^I = \begin{Bmatrix} Q_1^I \\ Q_2^I \\ \vdots \\ Q_n^I \end{Bmatrix} = - \int_V \begin{bmatrix} \underline{B}_1^T \\ \underline{B}_2^T \\ \vdots \\ \underline{B}_n^T \end{bmatrix} \underline{E} \underline{B} \underline{q} dV \quad (4.6.39)$$

Note that \underline{q} is only a function of t so it may come out of the integral and that the first matrix of the integrand is \underline{B}^T . Summarizing these results yields

Generalized Force Vector of Internal Forces for Assumed Modes Model

$$\underline{Q}_{n \times 1}^I(t) = \begin{Bmatrix} Q_1^I \\ Q_2^I \\ \vdots \\ Q_n^I \end{Bmatrix} = - \underline{K}_{n \times n} \underline{q}_{n \times 1}(t) \quad (4.6.40)$$

where

$$\underline{K}_{n \times n} = \int_V \underline{B}^T \underline{E} \underline{B} dV = \text{assumed modes stiffness matrix} \quad (4.6.41)$$

$$\frac{\underline{B}}{6 \times n} = \frac{\underline{D}}{6 \times 33 \times n} \underline{\Phi} \quad (4.6.42)$$

$$\underline{U} = \frac{\underline{\Phi}}{3 \times 1} \frac{\underline{q}}{3 \times n \times 1} \quad (4.6.43)$$

$$\underline{\varepsilon} = \frac{\underline{D}}{6 \times 1} \frac{\underline{u}}{6 \times 33 \times 1} \quad (4.6.44)$$

4.6.5 Generalized Force for *External Loads Acting on a Deformable Body*

Differentiate the external work expression W^E in (A.6.12) with respect to q_j while assuming that the integration domain and the force $\underline{\bar{F}}_{EV}$ and $\underline{\bar{F}}_{ES}$ are independent of q_j :

$$\frac{\partial W^E}{\partial q_j} = \int_V \underline{\bar{F}}_{EV}^T \frac{\partial u}{\partial q_j} dV + \int_S \underline{\bar{F}}_{ES}^T \frac{\partial u}{\partial q_j} u dS \quad (4.6.45)$$

Consideration of the integrals in (4.6.45) as limits of sums over particles and recalling that by (4.5.43)

$$Q_j = \sum_{i=1}^{\infty} \underline{\bar{F}}_i \cdot \frac{\partial \underline{\bar{R}}_i}{\partial q_j} = \sum_{i=1}^{\infty} \underline{\bar{F}}_i^T \cdot \frac{\partial \underline{\bar{R}}_i}{\partial q_j} \quad (4.6.46)$$

shows that

Generalized Force for External Forces Acting on a Deformable Body

$$Q_j = \frac{\partial W^E}{\partial q_j} = \int_V \underline{\bar{F}}_{EV}^T \frac{\partial u}{\partial q_j} dV + \int_S \underline{\bar{F}}_{ES}^T \frac{\partial u}{\partial q_j} dS \quad (4.6.47)$$

4.6.6 Assumed Modes Model Generalized Forces for External Load Acting on a Deformable Body

Recall from (2.11.28) that for the assumed modes approach, the displacement fields are approximated by

$$u_1 = \sum_{i=1}^{n_1} q_i(t) \phi_i(x_1, x_2, x_3), \quad u_2 = \sum_{i=n_1+1}^{n_1+n_2} q_i(t) \phi_i(x_1, x_2, x_3), \quad u_3 = \sum_{i=n_1+n_2+1}^n q_i(t) \phi_i(x_1, x_2, x_3) \quad (4.6.48)$$

where

$$n = n_1 + n_2 + n_3 \quad (4.6.49)$$

All $\phi_i(x_1, x_2, x_3)$ are known (given) functions of position. Substitute (4.6.48) into (4.6.47), noting that

$$\frac{\partial q_i}{\partial q_j} = \begin{cases} 0, & i \neq j \\ 1, & i = j \end{cases} \quad (4.6.50)$$

to obtain

Generalized Force Vector of External Forces for Assumed Modes Model

$$Q_j = \frac{\partial W^E}{\partial q_j} = \begin{cases} \int_V \bar{F}_{EV1} \phi_j dV + \int_S \bar{F}_{ES1} \phi_j dS, & j \leq n_1 \\ \int_V \bar{F}_{EV2} \phi_j dV + \int_S \bar{F}_{ES2} \phi_j dS, & n_1 < j \leq n_1 + n_2 \\ \int_V \bar{F}_{EV3} \phi_j dV + \int_S \bar{F}_{ES3} \phi_j dS, & n_1 + n_2 < j \leq n \end{cases} \quad (4.6.51)$$

EXAMPLE 4.6.2 *Assumed Modes Generalized Forces for Cantilever Beam*

Objective: To demonstrate the evaluation of assumed modes generalized forces for the simple cantilever beam shown in Figure 2.11.8. The mass matrix for this example was derived in Example 4.6.1.

Solution:

From (2.11.30) to (2.11.32), the only deflection is in the x_2 direction:

$$u_2(x_1, t) = q_1(t)\phi_{12}(x_1) + q_2(t)\phi_{22}(x_1) \quad (1)$$

$$N_1 = N_3 = 0, \quad N_2 = 2 \quad (2)$$

The externally applied forces ($\bar{F}_{EVk}, \bar{F}_{ESk}$) and global shape functions (ϕ_j) are known (given) functions of position (x_1, x_2, x_3) within volume V and/or on bounding surfaces S . Hence, the Q_j may be evaluated per the integrations in (4.6.51).

For the model in Figure E4.6.2(a), the shape functions are selected as

$$\phi_{12}(x_1) = \frac{3x_1^2}{L^2} - \frac{2x_1^3}{L^3} \quad (3)$$

$$\phi_{22}(x_1) = \frac{-x_1^2}{L} - \frac{2x_1^3}{L^2} \quad (4)$$

and $F_2(x)$ is a force per unit length applied in the x_2 direction. In this case, (4.6.51) gives

$$Q_j = \int_0^L F_2(x)\phi_{j2}(x)dx \quad j=1,2 \quad (5)$$

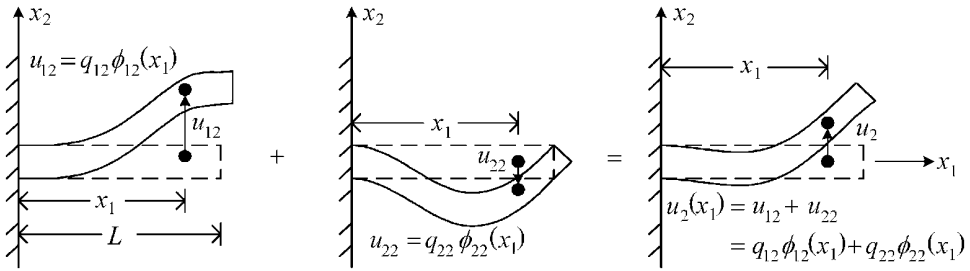


Figure E4.6.2(a) Two shape functions for the assumed modes solution

4.6.7 LE for a System of Rigid and Deformable Bodies

The preceding results show that the form of the LE (4.5.106) is still valid for systems composed of flexible and rigid bodies along with additional conservative, nonconservative, dissipative, and circulatory forces. The following is a summary of the LE for a combination of flexible and rigid bodies that are interconnected by force elements such as springs and dampers. The flexible bodies are modeled by either finite elements or assumed modes approximations.

Lagrange's Equations of Motion for a Combination of N_{RB} Rigid and N_{FB} Flexible Bodies

Lagrange's Equations

From (4.5.106),

$$\frac{d}{dt} \left(\frac{\partial T}{\partial \dot{q}_j} \right) - \frac{\partial T}{\partial q_j} = Q_j - \frac{\partial U}{\partial q_j} - \frac{\partial (\mathfrak{F}^c + \mathfrak{F}^d)}{\partial \dot{q}_j} \quad (4.6.52)$$

$j = 1, 2, \dots, n$ independent generalized coordinates (q_1, q_2, \dots, q_n)

Kinetic Energy

A general expression for the total system's kinetic energy is

$$T = \text{total system kinetic energy} = T_{RB} + T_{FB} \quad (4.6.53)$$

where from (4.5.107) for rigid bodies

$$T_{RB} = \frac{1}{2} \sum_{i=1}^{N_{RB}} \left(m_i {}^n \underline{v}_{Gi}^T {}^n \underline{v}_{Gi} + \left(\underline{\omega}_{bi}^{bi/n} \right)^T I_{Gi}^{Bi/bi} \underline{\omega}_{bi}^{bi/n} \right) \quad (4.6.54)$$

and from (4.6.1) for flexible bodies

$$T_{\text{FB}} = \frac{1}{2} \sum_{l=1}^{N_{\text{FB}}} \int_{V_R} \frac{nd}{dt}(\bar{R}) \cdot \frac{nd}{dt}(\bar{R}) dm \quad (4.6.55)$$

(a) Kinetic Energy for Assumed Modes Model of a Flexible Body

Assume the following form for the displacement field for a flexible body:

$$\bar{R} = u_1 n_1 + u_2 n_2 + u_3 n_3 = \left(\sum_{i=1}^{N_1} q_{i1} \phi_{i1} \right) n_1 + \left(\sum_{i=1}^{N_2} q_{i2} \phi_{i2} \right) n_2 + \left(\sum_{i=1}^{N_3} q_{i3} \phi_{i3} \right) n_3 \quad (4.6.56)$$

where $q_{ij}(t)$ are generalized coordinates to be solved for and $\phi_{ij}(x_1, x_2, x_3)$ are known shape functions. Then from (4.6.9)

$$T_{\text{FB}} = \frac{1}{2} \underline{\dot{q}}^T \underline{\tilde{m}} \underline{\dot{q}} \quad (4.6.57)$$

The Lagrange equation (4.6.52) derivatives of this kinetic energy component become

$$\frac{\partial T_{\text{FB}}}{\partial \underline{\dot{q}}} = \underline{\tilde{m}} \underline{\dot{q}} \quad (4.6.58)$$

$$\frac{d}{dt} \left(\frac{\partial T_{\text{FB}}}{\partial \underline{\dot{q}}} \right) = \underline{\tilde{m}} \underline{\ddot{q}} \quad (4.6.59)$$

where from (4.6.10) to (4.6.12)

$$N = N_1 + N_2 + N_3 = \text{number of independent generalized coordinates} \quad (4.6.60)$$

$$\underline{\dot{q}} = \left\{ \begin{array}{l} \underline{\dot{q}}_1 \\ \underline{\dot{q}}_2 \\ \underline{\dot{q}}_3 \end{array} \right\} = N \times 1 \text{ vector of independent generalized coordinate velocities} \quad (4.6.61)$$

$$\underline{q}_1 = \begin{Bmatrix} q_{11} \\ q_{21} \\ \vdots \\ q_{N_1 1} \end{Bmatrix}, \quad \underline{q}_2 = \begin{Bmatrix} q_{12} \\ q_{22} \\ \vdots \\ q_{N_2 2} \end{Bmatrix}, \quad \underline{q}_3 = \begin{Bmatrix} q_{13} \\ q_{23} \\ \vdots \\ q_{N_3 3} \end{Bmatrix} \quad (4.6.62)$$

and the “generalized coordinate mass matrix” is given by (4.6.13)

$$\tilde{\underline{m}} = \begin{bmatrix} \tilde{\underline{m}}_1 & \underline{0} & \underline{0} \\ (N_1 \times N_1) & (N_1 \times N_2) & (N_1 \times N_3) \\ \underline{0} & \tilde{\underline{m}}_2 & \underline{0} \\ (N_2 \times N_1) & (N_2 \times N_2) & (N_2 \times N_3) \\ \underline{0} & \underline{0} & \tilde{\underline{m}}_3 \\ (N_3 \times N_1) & (N_3 \times N_2) & (N_3 \times N_3) \end{bmatrix} \quad (4.6.63)$$

$$(\tilde{\underline{m}}_1)_{ik} = \tilde{m}_{ik1}, \quad i = 1, N_1, \quad k = 1, N_1$$

$$(\tilde{\underline{m}}_2)_{ik} = \tilde{m}_{ik2}, \quad i = 1, N_2, \quad k = 1, N_2 \quad (4.6.64)$$

$$(\tilde{\underline{m}}_3)_{ik} = \tilde{m}_{ik3}, \quad i = 1, N_3, \quad k = 1, N_3$$

where from (4.6.5)

$$m_{ikj} = m_{kij} = \int_V \phi_{ij} \phi_{kj} dm = \int_V \phi_{ij}(x_1, x_2, x_3) \phi_{kj}(x_1, x_2, x_3) \rho dV \quad \begin{cases} j = 1, 2, 3 \\ i = 1, N_j \\ k = 1, N_j \end{cases} \quad (4.6.65)$$

(b) Potential Energy of a Flexible Body

A general expression for the system's potential energy is given by

$$U = \text{total system potential energy} = U_S + U_W + U^I \quad (4.6.66)$$

- External Sources

U_S = sum of all potential energy contributions due to discrete stiffness in the model, reference

$$U_{KDE} \text{ in (4.5.65) or } U_{KT} \text{ in (4.5.88)} \quad (4.6.67)$$

U_W = sum of all potential energy contributions due to rigid body weights (reference (4.5.57))

- Internal Sources:

$$U_I = \frac{1}{2} \sum_{i=1}^{N_{FB}} \int_{V_i} \underline{\epsilon}^T \underline{E} \underline{\epsilon} dV$$

= sum of all potential energy contributions from internal forces and strain in all flexible bodies (reference (4.6.18)) and the associated generalized forces are (4.6.27)

$$(4.6.68)$$

$$Q_j^I = -\frac{\partial U^I}{\partial q_j} = -\int_V \frac{\partial \underline{\epsilon}^T}{\partial q_j} \underline{E} \underline{\epsilon} dV \quad (4.6.69)$$

- (c) Potential Energy for an Assumed Modes Model of a Flexible Body
If the deflections of a flexible body are approximated by (4.6.28)–(4.6.29)

$$\underline{u} = \begin{Bmatrix} u_1 \\ u_2 \\ u_3 \end{Bmatrix} = \begin{Bmatrix} \sum_{i=1}^{n_1} q_{i1}(t) \phi_{i1}(x_1, x_2, x_3) \\ \sum_{i=1}^{n_2} q_{i2}(t) \phi_{i2}(x_1, x_2, x_3) \\ \sum_{i=1}^{n_3} q_{i3}(t) \phi_{i3}(x_1, x_2, x_3) \end{Bmatrix}$$

$$= \begin{bmatrix} \phi_{11} & \phi_{21} & \cdots & \phi_{n_1 1} & \underline{0}_{1 \times n_2} & \underline{0}_{1 \times n_3} \\ \underline{0}_{1 \times n_1} & \phi_{12} & \phi_{22} & \cdots & \phi_{n_2 2} & \underline{0}_{1 \times n_3} \\ \underline{0}_{1 \times n_1} & \underline{0}_{1 \times n_2} & \phi_{13} & \phi_{23} & \cdots & \phi_{n_3 3} \end{bmatrix} \begin{Bmatrix} q_{11} \\ q_{21} \\ \vdots \\ q_{n_1 1} \\ q_{12} \\ q_{22} \\ \vdots \\ q_{n_2 2} \\ q_{13} \\ q_{23} \\ \vdots \\ q_{n_3 3} \end{Bmatrix} \quad (4.6.70)$$

or

$$\underline{u}(x_1, x_2, x_3, t) = \underline{\Phi}(x_1, x_2, x_3) \underline{q}(t) \quad (4.6.71)$$

where

$$n = n_1 + n_2 + n_3 = \text{total number of generalized coordinates} \quad (4.6.72)$$

and the strains and displacements are related by (4.6.31)

$$\underline{\varepsilon} = \underline{D} \underline{u} \quad (4.6.73)$$

Then for that body

$$U = \frac{1}{2} \int_V \underline{\varepsilon}^T \underline{E} \underline{\varepsilon} \, dV = \frac{1}{2} \underline{q}^T \underline{K} \underline{q} \quad (4.6.74)$$

where by (4.6.41) and (4.6.42)

$$\underline{K}_{n \times n} = \int_V \underline{B}_{n \times 6}^T \underline{E}_{6 \times 6} \underline{B}_{6 \times n} dV = \text{assumed modes stiffness matrix} \quad (4.6.75)$$

$$\underline{B}_{6 \times n} = \underline{D}_{6 \times 3} \underline{\Phi}_{3 \times n} \quad (4.6.76)$$

The corresponding generalized forces are from (4.6.40):

$$\underline{Q}_{n \times 1}^I(t) = - \frac{\partial U^I}{\partial \underline{q}} = \begin{Bmatrix} Q_1^I \\ Q_2^I \\ \vdots \\ Q_n^I \end{Bmatrix}_{n \times 1} = - \underline{K}_{n \times n} \underline{q}_{n \times 1}(t) \quad (4.6.77)$$

(d) Circulatory and Dissipation Functions

$$\mathfrak{F}^c = \text{sum of all circulatory scalar functions in the entire system} \quad (4.6.78)$$

(e.g., \mathfrak{F}_{DE}^c in (4.5.74))

$$\mathfrak{F}^d = \text{sum of all Rayleigh dissipation, scalar functions in the entire system} \quad (4.6.79)$$

(e.g., \mathfrak{F}_{DE}^d in (4.5.78) or \mathfrak{F}_{CT}^d in (4.5.104))

(e) All Remaining Forces

$$\begin{aligned} Q_j &= Q_{jRB} + Q_{jFB} \\ &= \text{sum of all generalized force contributions from forces} \\ &\quad \text{not described by } U, \mathfrak{F}^c, \text{ and } \mathfrak{F}^d \text{ terms} \end{aligned} \quad (4.6.80)$$

$$\begin{aligned} Q_{jRB} &= Q_j \text{ terms for forces and "pure torques"} \\ &\quad \text{acting on rigid bodies (ref. (4.5.47)–(4.5.53))} \end{aligned} \quad (4.6.81)$$

$$\begin{aligned} Q_{jFB} &= Q_j \text{ terms for flexible bodies (ref. 4.6.47)} \\ &= \sum_{i=1}^{N_{FB}} \left(\int_{V_i} \underline{\bar{F}}_{EV}^T \frac{\partial u}{\partial q_j} dV_i + \int_{S_i} \underline{\bar{F}}_{ES}^T \frac{\partial u}{\partial q_j} dS_i \right) \end{aligned} \quad (4.6.82)$$

where from (A.6.13) to (A.6.14)

$$\begin{aligned} \underline{\bar{F}}_{EV} &= \begin{Bmatrix} \bar{F}_{EV1}(x_1, x_2, x_3) \\ \bar{F}_{EV2}(x_1, x_2, x_3) \\ \bar{F}_{EV3}(x_1, x_2, x_3) \end{Bmatrix} \\ &= \text{applied distributed body force acting inside the body (force per unit volume)} \end{aligned} \quad (4.6.83)$$

$$\underline{\bar{F}}_{ES} = \begin{Bmatrix} \bar{F}_{ES1}(x_1, x_2, x_3) \\ \bar{F}_{ES2}(x_1, x_2, x_3) \\ \bar{F}_{ES3}(x_1, x_2, x_3) \end{Bmatrix}$$

= distributed surface traction acting on the surface of the body (force per unit area) (4.6.84)

$$\underline{u} = \begin{Bmatrix} u_1(x_1, x_2, x_3) \\ u_2(x_1, x_2, x_3) \\ u_3(x_1, x_2, x_3) \end{Bmatrix} \quad (4.6.85)$$

= displacements of body in regions of application of either $\underline{\bar{F}}_{EV}$ or $\underline{\bar{F}}_{ES}$

(f) Generalized Forces for External Loading in an Assumed Modes Model of a Flexible Body Given the assumed modes deflection (4.6.70), Equation (4.6.51) provides

$$Q_j = \frac{\partial W^E}{\partial q_j} = \begin{Bmatrix} \int_V \bar{F}_{EV1} \phi_j dV + \int_S \bar{F}_{ES1} \phi_j dS, & j \leq n_1 \\ \int_V \bar{F}_{EV2} \phi_j dV + \int_S \bar{F}_{ES2} \phi_j dS, & n_1 < j \leq n_1 + n_2 \\ \int_V \bar{F}_{EV3} \phi_j dV + \int_S \bar{F}_{ES3} \phi_j dS, & n_1 + n_2 < j \leq n \end{Bmatrix} \quad (4.6.86)$$

where \bar{F}_{EVj} is the external force per unit volume (gravity, magnetic, etc.) in the x_j direction and \bar{F}_{ESj} is the external force per unit are (pressure, traction, etc.) in the x_j direction

The scalar form of the LE (4.6.52) can be written in vector form by using the notation of (2.6.42), yielding

$$\frac{d}{dt} \left(\frac{\partial T}{\partial \dot{\underline{q}}} \right) - \frac{\partial T}{\partial \underline{q}} + \frac{\partial U}{\partial \underline{q}} + \frac{\partial \mathfrak{S}^d}{\partial \dot{\underline{q}}} = \underline{Q} \quad (4.6.87)$$

The standard forms for the kinetic energy, potential energy, and dissipation function are typically quadratic forms and inner products, that is,

$$T = \sum_i \frac{1}{2} \dot{\underline{q}}^T \underline{M}_i \dot{\underline{q}} \quad (4.6.88)$$

$$U = \sum_j \left(\frac{1}{2} \underline{q}^T \underline{K}_j \underline{q} - \underline{q}^T \underline{S}_j \right) \quad (4.6.89)$$

$$\mathfrak{S}^d = \sum_k \frac{1}{2} \dot{\underline{q}}^T \underline{C}_k \dot{\underline{q}} \quad (4.6.90)$$

where the summations extend over all sources of kinetic and potential energy and dissipation functions. Substitute (4.6.88)–(4.6.90) into (4.6.87) and utilize the vector differentiation formulas (2.6.42) and (2.6.49) to obtain

$$\left(\sum_i \underline{M}_i \right)_{n \times n} \ddot{\underline{q}} + \left(\sum_k \underline{C}_k \right)_{n \times n} \dot{\underline{q}} + \left(\sum_j \underline{K}_j \right)_{n \times n} \underline{q} = \underline{Q} + \sum_j \underline{S}_j \quad (4.6.91)$$

which is in the standard form for linear system vibration analysis.

EXAMPLE 4.6.3 Vortex-Driven Vibration of a Thermocouple Probe

Statement: A thermocouple probe protrudes into the discharge line of a gas compressor. A high-temperature elastomeric plug supports the probe while dampening the probe's vibration, as depicted in Figure E4.6.3(a). The properties of the two components are listed below (Table E4.6.3(a)).

The exhaust flow about the probe creates vortices which force the probe in a direction transverse to the flow (Blevins, 1977). A simplified model of the force is given by the force per unit length

$$f(x,t) = \begin{cases} 0, & x < \frac{L}{3} \\ \gamma \left(\frac{3x}{2L} - \frac{1}{2} \right) \sin \omega_s t, & x \geq \frac{L}{3} \end{cases} \quad (1)$$

The constant γ is experimentally determined and the forcing frequency is given by

$$\omega_s = 2\pi f_s \text{ (rad/s)}, \quad f_s = \frac{SV}{D} \text{ (Hz)} \quad (2)$$

where

S = Strouhal Number ≈ 0.2
 (for circular cross sections of diameter D and Reynolds numbers
 (VD/ν) in the range 100–100,000)

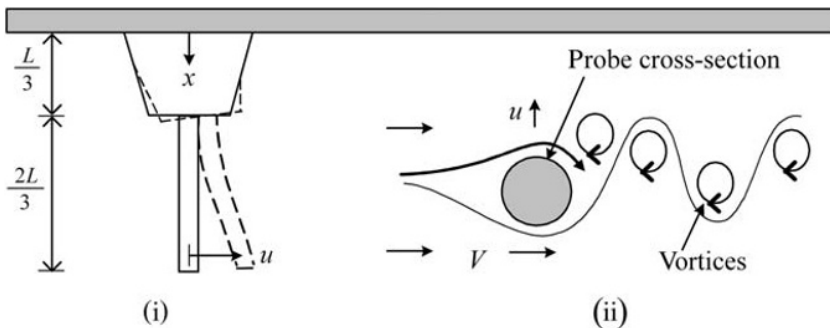
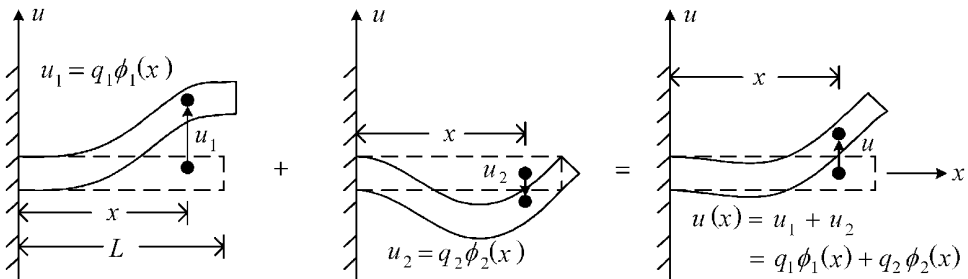


Figure E4.6.3(a) Bending motion (i) of thermocouple due to vortex shedding (ii)

Table E4.6.3(a) Properties of thermocouple probe system

	Plug	Probe
Density	ρ	$\alpha_1\rho$
Length	$L/3$	$2L/3$
Modulus	E	α_2E
Area inertia	$I_0\left(1-0.6\frac{x}{L}\right)^2$	α_3I_0
Area	$A_0\left(1-0.6\frac{x}{L}\right)$	α_4A_0

**Figure E4.6.3(b)** Two shape functions for the assumed modes solution

V = flow velocity in meters/second

D = diameters in meters (3)

Objective: Derive the equations of motion for this system utilizing the assumed modes method with the following two shape functions which are depicted in Figure E4.6.3(b):

$$\phi_1(x) = \frac{3x^2}{L^2} - \frac{2x^3}{L^3}, \quad \phi_2(x) = \frac{-x^2}{L^2} + \frac{x^3}{L^3} \quad (4)$$

These shape functions are kinematically admissible (Section 2.11) since they satisfy the zero slope and deflection boundary conditions at $x=0$.

Assumptions:

- Small motions (linear strain–displacement and stress–strain relations hold)
- Both components deflect as beams in bending.

Solution:

- (a) In this example, there are $n=2$ generalized coordinates (q_1, q_2) where the lateral deflection of the probe assembly is approximated by the assumed modes model (4.6.56):

$$u(x, t) = q_1(t)\phi_1(x) + q_2(t)\phi_2(x) \quad (5)$$

- (b) The kinetic energy derivative terms in Lagrange's equations are given by (4.6.59)

$$\frac{d}{dt} \left(\frac{\partial T}{\partial \dot{\underline{q}}} \right) = \left\{ \begin{array}{l} \frac{d}{dt} \left(\frac{\partial T}{\partial \dot{q}_1} \right) \\ \frac{d}{dt} \left(\frac{\partial T}{\partial \dot{q}_2} \right) \end{array} \right\} = \underline{M} \ddot{\underline{q}} = \begin{bmatrix} m_{11} & m_{12} \\ m_{21} & m_{22} \end{bmatrix} \left\{ \begin{array}{l} \ddot{q}_1 \\ \ddot{q}_2 \end{array} \right\} \quad (6)$$

and also

$$\frac{\partial T}{\partial \underline{q}} = \left\{ \begin{array}{l} \frac{\partial T}{\partial q_1} \\ \frac{\partial T}{\partial q_2} \end{array} \right\} = \left\{ \begin{array}{l} 0 \\ 0 \end{array} \right\} \quad (7)$$

The generalized mass coefficients are determined from (4) and (4.6.65):

$$\begin{aligned} m_{11} &= \int_V \phi_1 \phi_1 dm = \int_V \phi_1^2 \rho dV = \int_0^L \phi_1(x) \phi_1(x) \rho(x) A(x) dx \\ &= \int_0^{\frac{L}{3}} \phi_1(x) \phi_1(x) \rho A_0 \left(1 - 0.6 \frac{x}{L}\right) dx + \int_{\frac{L}{3}}^L \phi_1(x) \phi_1(x) \alpha_1 \rho \alpha_4 A_0 dx \\ &= c_1 \int_0^{\frac{L}{3}} \phi_1 \phi_1 g dx + c_2 \int_{\frac{L}{3}}^L \phi_1 \phi_1 dx \end{aligned} \quad (8)$$

where

$$c_1 = \rho A_0, \quad c_2 = \alpha_1 \alpha_4 \rho A_0, \quad g(x) = \left(1 - 0.6 \frac{x}{L}\right) \quad (9)$$

Similarly,

$$\begin{aligned} m_{12} &= m_{21} = \int_V \phi_1 \phi_2 dm = \int_V \phi_1 \phi_2 \rho dV = \int_0^L \phi_1(x) \phi_2(x) \rho(x) A(x) dx \\ &= \int_0^{\frac{L}{3}} \phi_1(x) \phi_2(x) \rho A_0 g(x) dx + \int_{\frac{L}{3}}^L \phi_1(x) \phi_2(x) \alpha_1 \rho \alpha_4 A_0 dx \\ &= c_1 \int_0^{\frac{L}{3}} \phi_1(x) \phi_2(x) g(x) dx + c_2 \int_{\frac{L}{3}}^L \phi_1(x) \phi_2(x) dx \end{aligned} \quad (10)$$

$$m_{22} = c_1 \int_0^{\frac{L}{3}} \phi_2(x) \phi_2(x) g(x) dx + c_2 \int_{\frac{L}{3}}^L \phi_2(x) \phi_2(x) dx \quad (11)$$

Summarizing,

$$\underline{M} = \begin{bmatrix} m_{11} & m_{12} \\ m_{21} & m_{22} \end{bmatrix} = c_1 \int_0^{\frac{L}{3}} \begin{bmatrix} \phi_1 \phi_1 g & \phi_1 \phi_2 g \\ \phi_1 \phi_2 g & \phi_2 \phi_2 g \end{bmatrix} dx + c_2 \int_{\frac{L}{3}}^L \begin{bmatrix} \phi_1 \phi_1 & \phi_1 \phi_2 \\ \phi_1 \phi_2 & \phi_2 \phi_2 \end{bmatrix} dx \quad (12)$$

The integrals in (12) are evaluated with Maple as shown below, yielding

$$\underline{M} = c_1 L \begin{bmatrix} 0.00411 & -0.00122 \\ -0.00122 & 0.000361 \end{bmatrix} + c_2 L \begin{bmatrix} 0.3665 & -0.051 \\ -0.051 & 0.0091 \end{bmatrix} \quad (13)$$

Maple Code for Mass Matrix in Equation (12)

```

phi1:= 3*x^2/L^2 - 2*x^3/L^3;
phi2:= -x^2/L^2 + x^3/L^3;
g:= 1-0.6*x/L;
A:= linalg[matrix](2,2, [phi1*phi1*g, phi1*phi2*
g, phi1*phi2*g, phi2*phi2*g]);
B:= linalg[matrix](2,2, [phi1*phi1, phi1*phi2, phi1*phi2,
phi2*phi2]);

c1*map(int, A, x=0..L/3) + c2*map(int, B, x=L/3..L);

```

- (c) The potential energy of the beams is evaluated assuming Euler–Bernoulli beam theory holds. The bending strain varies linearly over a cross section of a beam and is zero at the neutral axis as shown in Figure E4.6.3(c).

From elementary strength of materials, the bending strain (curvature formula) is

$$\epsilon_B = -y \frac{\partial^2 u}{\partial x^2} \quad (14)$$

However, by (4.6.73), $\underline{\epsilon} = \underline{D}u$; therefore,

$$\underline{D} = D = -y \frac{\partial^2 (\)}{\partial x^2} \quad (15)$$

The shape function matrix for this 1-dimensional example is given by (4.6.71)

$$\underline{\Phi} = [\phi_1(x) \ \phi_2(x)] \quad (16)$$

and from (4.6.76)

$$\underline{B} = \underline{D} \underline{\Phi} = -y \frac{d^2}{dx^2} [\phi_1(x) \ \phi_2(x)] = -y [\phi_1'' \ \phi_2''] \quad (17)$$

where from (4)

$$\phi_1'' = \frac{6}{L^2} - \frac{12x}{L^3}, \quad \phi_2'' = -\frac{2}{L^2} + \frac{6x}{L^3} \quad (18)$$

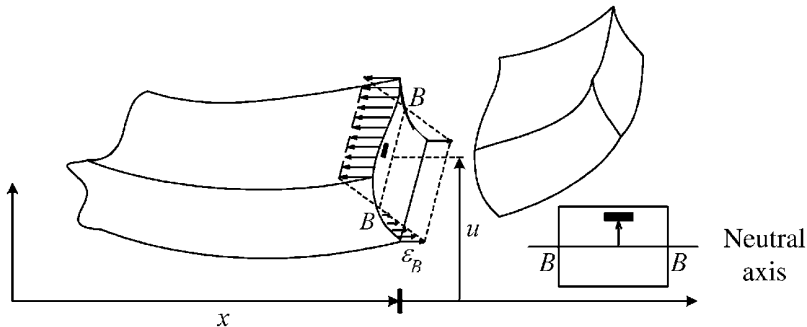


Figure E4.6.3(c) Bending strain over cross section of beam

The generalized forces corresponding to the strains and internal forces are from (4.6.75) and (4.6.77):

$$\frac{\underline{Q}^I(t)}{2 \times 1} = - \frac{\underline{K}}{2 \times 2} \frac{q(t)}{2 \times 1} \quad (19)$$

where

$$\underline{K} = \int_V \underline{B}^T \underline{E} \underline{B} dV = \int_V E \begin{bmatrix} \phi_1'' \\ \phi_2'' \end{bmatrix} [\phi_1'' \ \phi_2''] y^2 dA dx \quad (20)$$

Recalling that

$$I = \int_A y^2 dA \quad (21)$$

and perform the “inner” integral over dA in (21) to obtain

$$\begin{aligned} \underline{K} &= \int_0^L E(x) I(x) \begin{bmatrix} \phi_1'' \phi_1'' & \phi_1'' \phi_2'' \\ \phi_1'' \phi_2'' & \phi_2'' \phi_2'' \end{bmatrix} dx \\ &= \int_0^{\frac{L}{3}} EI_0 \left(1 - 0.6 \frac{x}{L}\right)^2 \begin{bmatrix} \phi_1'' \phi_1'' & \phi_1'' \phi_2'' \\ \phi_1'' \phi_2'' & \phi_2'' \phi_2'' \end{bmatrix} dx + \int_{\frac{L}{3}}^L \alpha_2 E \alpha_3 I_0 \begin{bmatrix} \phi_1'' \phi_1'' & \phi_1'' \phi_2'' \\ \phi_1'' \phi_2'' & \phi_2'' \phi_2'' \end{bmatrix} dx \\ &= c_3 \int_0^{\frac{L}{3}} g^2 \begin{bmatrix} \phi_1'' \phi_1'' & \phi_1'' \phi_2'' \\ \phi_1'' \phi_2'' & \phi_2'' \phi_2'' \end{bmatrix} dx + c_4 \int_{\frac{L}{3}}^L \begin{bmatrix} \phi_1'' \phi_1'' & \phi_1'' \phi_2'' \\ \phi_1'' \phi_2'' & \phi_2'' \phi_2'' \end{bmatrix} dx \end{aligned} \quad (22)$$

where

$$c_3 = EI_0, \quad c_4 = \alpha_2 \alpha_3 EI_0 \quad (23)$$

The MAPLE code shown below evaluates (22) to obtain

$$\underline{K} = \frac{c_3}{L^3} \begin{bmatrix} 5.020 & -1.386 \\ -1.386 & 0.402 \end{bmatrix} + \frac{c_4}{L^3} \begin{bmatrix} 6.222 & -4.444 \\ -4.444 & 3.556 \end{bmatrix} \quad (24)$$

Maple Code for Stiffness Matrix in Equation (22)

```
with(linalg);
philpp:= 6/L^2 - 12*x/L^3;
phi2pp:= -2/L^2 + 6*x/L^3;
g:= 1-0.6*x/L;
A:= linalg[matrix] (2,2, [g^2*philpp*philpp,
g^2*philpp*phi2pp, g^2*philpp*phi2pp, g^2*phi2pp*phi2pp]);
B:= linalg[matrix] (2,2, [philpp*philpp, philpp*phi2pp,
philpp*phi2pp, phi2pp*phi2pp]);
c3*map(int, A, x=0..L/3) + c4*map(int, B, x=L/3..L);
```

- (d) The generalized forces contributed by the vortex-generated disturbances are obtained from (4.6.86) and (1):

$$\begin{Bmatrix} Q_1 \\ Q_2 \end{Bmatrix} = \begin{Bmatrix} \int_0^L f(x,t)\phi_1(x)dx \\ \int_0^L f(x,t)\phi_2(x)dx \end{Bmatrix} = \begin{Bmatrix} \gamma \sin \omega_s t \int_{L/3}^L \left(\frac{3x}{2L} - \frac{1}{2}\right) \phi_1(x)dx \\ \gamma \sin \omega_s t \int_{L/3}^L \left(\frac{3x}{2L} - \frac{1}{2}\right) \phi_2(x)dx \end{Bmatrix} \quad (25)$$

where ϕ_1 and ϕ_2 are defined in Equation (4). Integration of (25) with the MAPLE code shown below yields

$$Q_1 = 0.279L\gamma \sin \omega_s t, \quad Q_2 = -0.03457L\gamma \sin \omega_s t \quad (26)$$

Maple Code for External Generalized Force Vector of Equation (25)

```
h := 1.5*x/L - 0.5;
phi1 := 3*x^2/L^2 - 2*x^3/L^3;
phi2 := -x^2/L^2 + x^3/L^3;

int(phi1*h, x=L/3..L)
int(phi2*h, x=L/3..L)
```

- (e) The system equations of motion for the generalized coordinates are obtained by combining the above results into Lagrange's equations. Substitute (6), (7), (19), and (25) into ((4.6.52), (4.6.91)) to obtain

$$\underline{\tilde{M}}\ddot{\underline{q}} - \underline{0} = \begin{Bmatrix} Q_1 \\ Q_2 \end{Bmatrix} - \underline{K}\underline{q} \quad (27)$$

Substitution of (13), (24), and (26) into (27) yields:
Thermocouple Probe/Plug EOMs

$$\begin{aligned} n=2, \quad \phi_1 &= \frac{3x^2}{L^2} - \frac{2x^3}{L^3}, \quad \phi_2 = \frac{-x^2}{L^2} + \frac{x^3}{L^3} \\ &\left(c_1 L \begin{bmatrix} 0.00411 & -0.00122 \\ -0.00122 & 0.000361 \end{bmatrix} + c_2 L \begin{bmatrix} 0.3665 & -0.051 \\ -0.051 & 0.0091 \end{bmatrix} \right) \begin{Bmatrix} \ddot{q}_1 \\ \ddot{q}_2 \end{Bmatrix} \\ &+ \left(\frac{c_3}{L^3} \begin{bmatrix} 5.020 & -1.386 \\ -1.386 & 0.402 \end{bmatrix} + \frac{c_4}{L^3} \begin{bmatrix} 6.222 & -4.444 \\ -4.444 & 3.556 \end{bmatrix} \right) \begin{Bmatrix} q_1 \\ q_2 \end{Bmatrix} \\ &= \gamma \sin \omega_s t \begin{Bmatrix} 0.279L \\ -0.03457L \end{Bmatrix} \end{aligned} \quad (28)$$

where

$$c_1 = \rho A_0, \quad c_2 = \alpha_1 \alpha_4 \rho A_0, \quad c_3 = EI_0, \quad c_4 = \alpha_2 \alpha_3 EI_0 \quad (29)$$

Equation (28) may be solved by analytic or numerical means for the generalized coordinate $q_1(t)$ and $q_2(t)$ as a function of time as will be demonstrated in Chapters 5, 6, and 7.

(f) The displacement field may then be obtained by recalling from (4) and (5) that

$$u(x, t) = q_1(t)\phi_1(x) + q_2(t)\phi_2(x) \quad (30)$$

where

$$\phi_1(x) = \frac{3x^2}{L^2} - \frac{2x^3}{L^3}, \quad \phi_2(x) = \frac{-x^2}{L^2} + \frac{x^3}{L^3} \quad (31)$$

Therefore, if $q_1(t)$ and $q_2(t)$ are obtained from integrating (28), then $u(x, t)$ may be obtained from (30).

Summary: This example has demonstrated the use of two shape functions and generalized coordinates for estimating the response of a thermocouple probe assembly to vortex-induced forces. The results were two coupled ordinary differential equations (ODEs) for the generalized coordinates $q_1(t)$ and $q_2(t)$. These equations (28) may be integrated to obtain $q_1(t)$ and $q_2(t)$ for given initial conditions (ICs):

$$q_1(0), q_2(0), \dot{q}_1(0), \dot{q}_2(0) \quad (32)$$

The displacements $u(x, t)$ may then be obtained from (30). Note that a limitation of the assumed modes approach is that simulations cannot be performed for arbitrary initial displacements and velocity distributions ($u(x, 0), \dot{u}(x, 0)$). Instead, the ICs are restricted to lie in the subspace (Section 2.6) spanned by ϕ_1 and ϕ_2 , namely, only those u 's and \dot{u} 's obtainable from (30). Quite often, only the steady-state solution of (28) is desired in which case the ICs are not required, and they can be set to zero. Stresses may be estimated for purposes of fatigue life evaluation via (14) and (30):

$$\begin{aligned} \sigma &= E\varepsilon = -yE \frac{\partial^2 u}{\partial x^2} = -yE(q_1(t)\phi_1'' + q_2(t)\phi_2'') \\ &= -yE \left[q_1(t) \left(\frac{6}{L^2} - \frac{12x}{L^3} \right) + q_2(t) \left(-\frac{2}{L^2} + \frac{6x}{L^3} \right) \right] \end{aligned} \quad (33)$$

EXAMPLE 4.6.4 *Machine Mounted on a Platform with Flexible Flooring*

Statement: Many machines in industrial processes are mounted on platforms to locate auxiliary equipment beneath the platform. Figure E4.6.4(a) depicts a machine that is mounted on a platform with flexible flooring and with support columns modeled as concentrated stiffness and damping components. The machine's mass \bar{m} and force F are localized at $x = d$, and the platform supports are localized at $x = 0$ and $x = L$. The modulus of the platform's flooring is E , and it is modeled as a tapered beam with planar motion in the vertical direction. Coordinates are referenced to the static equilibrium (sagged) state; hence, gravity loading and

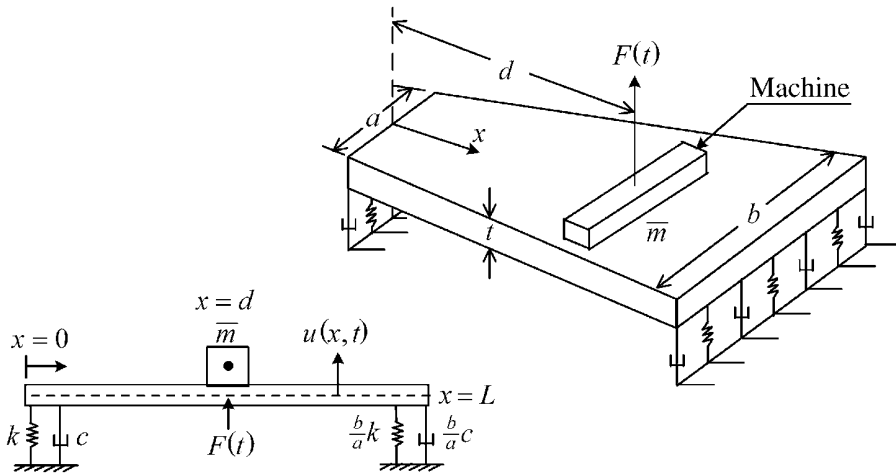


Figure E4.6.4(a) Planar vibration model of flexible platform supporting a machine

initial deflections due to gravity are ignored. The flooring's rectangular cross-sectional area and bending inertia vary along its length as

$$\begin{aligned} A &= \alpha_1 x + \alpha_2 \\ I &= \alpha_3 x + \alpha_4 \end{aligned} \quad (1)$$

$$\alpha_1 = \frac{(b-a)t}{L}, \quad \alpha_2 = at, \quad \alpha_3 = \frac{(b-a)t^3}{12L}, \quad \alpha_4 = \frac{at^3}{12} \quad (2)$$

Objective: Derive the equations of motion for this system utilizing a six generalized coordinate assumed modes model for the flexible flooring of the platform:

$$u(x,t) = \sum_{i=1}^6 q_i(t) \phi_i(x) = \underline{\Phi} \underline{q} = [\phi_1 \quad \phi_2 \quad \phi_3 \quad \phi_4 \quad \phi_5 \quad \phi_6] \begin{Bmatrix} q_1 \\ q_2 \\ \vdots \\ q_6 \end{Bmatrix} \quad (3)$$

The corresponding six shape functions are

$$\begin{aligned} \phi_1(x) &= 1, & \phi_2(x) &= \frac{x}{L}, \\ \phi_3(x) &= \sin\left(\frac{\pi x}{L}\right), & \phi_4(x) &= \sin\left(\frac{2\pi x}{L}\right), \\ \phi_5(x) &= \sin\left(\frac{3\pi x}{L}\right), & \phi_6(x) &= \sin\left(\frac{4\pi x}{L}\right) \end{aligned} \quad (4)$$

The first two shape functions produce rigid body translation and rotational motions of the platform flooring; the last four produce its flexible motion. There are no essential boundary conditions (fixed points) that the shape functions must satisfy to be “kinematically admissible” in this problem.

Assumptions:

- Small motions (linear strain–displacement and stress–strain relations hold).
- Platform behaves as beam in bending, that is, it is constrained against torsion, axial motion, and axial motions and out-of-plane bending.

Solution:**(a) Kinetic Energy and Mass Matrix**

The kinetic energy includes contributions from the platform flooring's mass and from the machinery's mass, that is, from (4.6.57),

$$T = T_p + T_m = \frac{1}{2} \underline{\dot{q}}^T \underline{M}_p \underline{\dot{q}} + \frac{1}{2} \bar{m} \dot{u}^2(x=d) = \frac{1}{2} \underline{\dot{q}}^T \underline{M}_p \underline{\dot{q}} + \frac{1}{2} \bar{m} \left(\sum_{i=1}^6 \dot{q}_i \phi_i(d) \right)^2 \quad (5)$$

Note that

$$\frac{d}{dt} \left(\frac{\partial T_m}{\partial \dot{q}_j} \right) = \bar{m} \phi_j(d) \sum_{i=1}^6 (\ddot{q}_i \phi_i(d)) \quad (6)$$

or

$$\frac{d}{dt} \left(\frac{\partial T_m}{\partial \underline{\dot{q}}} \right) = \underline{M}_m \underline{\ddot{q}} \quad (7)$$

where

$$(\underline{M}_m)_{ij} = \bar{m} \phi_i(d) \phi_j(d)$$

and

$$\frac{\partial(\quad)}{\partial \underline{\dot{q}}} = \left(\frac{\partial(\quad)}{\partial \dot{q}_1} \quad \frac{\partial(\quad)}{\partial \dot{q}_2} \quad \frac{\partial(\quad)}{\partial \dot{q}_3} \quad \frac{\partial(\quad)}{\partial \dot{q}_4} \quad \frac{\partial(\quad)}{\partial \dot{q}_5} \quad \frac{\partial(\quad)}{\partial \dot{q}_6} \right)^T \quad (8)$$

Also from (4.6.59),

$$\frac{d}{dt} \left(\frac{\partial T_p}{\partial \underline{\dot{q}}} \right) = \underline{M}_p \underline{\ddot{q}} \quad (9)$$

where from (4.6.65)

$$(\underline{M}_p)_{ij} = \int_V \phi_i \phi_j dm = \int_0^L \phi_i(x) \phi_j(x) \rho A(x) dx = \rho \int_0^L (\alpha_1 x + \alpha_2) \phi_i(x) \phi_j(x) dx \quad (10)$$

The \underline{M}_p matrix is evaluated with the following MAPLE code:

Maple Code for Obtaining the Platform Generalized Mass Matrix in Equation (11)

```
with(linalg);
piv := 3.141592654;
gg := alp1*x + alp2;
phi(1) := 1;
phi(2) := x/L;
phi(3) := sin(piv*x/L);
phi(4) := sin(2*piv*x/L);
phi(5) := sin(3*piv*x/L);
phi(6) := sin(4*piv*x/L);

for i from 1 by 1 while i<7 do
for j from 1 by 1 while j<7 do
f(i,j) := gg*phi(i) *phi(j);
end do;
end do;

A := matrix(6,6,f);
MP := rho*map(int, A, x=0..L);
```

The Maple code result is

$$\underline{M}_p = \alpha_1 L^2 \rho \begin{bmatrix} 0.5 & 0.3333 & 0.3183 & -0.1592 & 0.1061 & -0.0796 \\ & 0.2500 & 0.1893 & -0.1592 & 0.10113 & -0.0796 \\ & & 0.2500 & -0.0901 & 0 & -0.0072 \\ & & & 0.2500 & -0.0973 & 0 \\ & \text{symmetric} & & & 0.2500 & -0.0993 \\ & & & & & 0.2500 \end{bmatrix} \quad (11)$$

$$+ \alpha_2 L \rho \begin{bmatrix} 1 & 0.500 & 0.6366 & 0 & 0.2122 & 0 \\ & 0.3333 & 0.3183 & -0.1592 & 0.1061 & -0.0796 \\ & & 0.500 & 0 & 0 & 0 \\ & & & 0.500 & 0 & 0 \\ & \text{symmetric} & & & 0.5000 & 0 \\ & & & & & 0.5000 \end{bmatrix}$$

From (2.6.46), (2.6.47), and (5) and (7), the mass matrix due to the machine is obtained by evaluating the following matrix at $x=d$:

$$\underline{M}_m = \bar{m} \begin{bmatrix} \phi_1\phi_1 & \phi_1\phi_2 & \phi_1\phi_3 & \phi_1\phi_4 & \phi_1\phi_5 & \phi_1\phi_6 \\ & \phi_2\phi_2 & \phi_2\phi_3 & \phi_2\phi_4 & \phi_2\phi_5 & \phi_2\phi_6 \\ & & \phi_3\phi_3 & \phi_3\phi_4 & \phi_3\phi_5 & \phi_3\phi_6 \\ & & & \phi_4\phi_4 & \phi_4\phi_5 & \phi_4\phi_6 \\ \text{symmetric} & & & & \phi_5\phi_5 & \phi_5\phi_6 \\ & & & & & \phi_6\phi_6 \end{bmatrix}_{|x=d} \quad (12)$$

The total mass matrix becomes

$$\underline{M} = \underline{M}_m + \underline{M}_p \quad (13)$$

(b) Potential Energy and Stiffness Matrix

From Figure E4.6.4(a), the potential energy due to the support springs is (4.5.65)

$$U_s = \frac{1}{2}ku^2(0) + \frac{1}{2}k\frac{b}{a}u^2(L) = \frac{k}{2} \left(\sum_{i=1}^6 q_i\phi_i(0) \right)^2 + \frac{kb}{2a} \left(\sum_{i=1}^6 q_i\phi_i(L) \right)^2 \quad (14)$$

The corresponding generalized forces are obtained from (4.5.66) or (2.6.46) and (2.6.47) as

$$\begin{aligned} \underline{Q}_s &= \frac{\partial U_s}{\partial \underline{q}} = \left(-\frac{\partial U_s}{\partial q_1} \quad -\frac{\partial U_s}{\partial q_2} \quad \dots \quad -\frac{\partial U_s}{\partial q_6} \right)^T \\ &= -\underline{K}_s|_{x=0}\underline{q} - \frac{b}{a}\underline{K}_s|_{x=L}\underline{q} = -\left(\underline{K}_s|_{x=0} + \frac{b}{a}\underline{K}_s|_{x=L} \right)\underline{q} \end{aligned}$$

where

$$\underline{K}_s = k \begin{bmatrix} \phi_1\phi_1 & \phi_1\phi_2 & \phi_1\phi_3 & \phi_1\phi_4 & \phi_1\phi_5 & \phi_1\phi_6 \\ & \phi_2\phi_2 & \phi_2\phi_3 & \phi_2\phi_4 & \phi_2\phi_5 & \phi_2\phi_6 \\ & & \phi_3\phi_3 & \phi_3\phi_4 & \phi_3\phi_5 & \phi_3\phi_6 \\ & & & \phi_4\phi_4 & \phi_4\phi_5 & \phi_4\phi_6 \\ \text{symmetric} & & & & \phi_5\phi_5 & \phi_5\phi_6 \\ & & & & & \phi_6\phi_6 \end{bmatrix} \quad (15)$$

which must be evaluated at $x=0$ and $x=L$ in (15). The generalized forces corresponding to beam-type bending of the platform's flooring are obtained from (4.6.77) as

$$\underline{Q}^I(t) = -\frac{\partial U^I}{\partial \underline{q}} = \begin{Bmatrix} Q_1^I \\ Q_2^I \\ \vdots \\ Q_n^I \end{Bmatrix}_{n \times 1} = -\frac{\underline{K}_B}{n \times n} \underline{q}(t)_{n \times 1} \quad (16)$$

where from (4.6.75)

$$\underline{K}_B = \int_V \underline{B}_B^T \underline{E}_B \underline{B}_B dV = \text{assumed modes stiffness matrix} \quad (17)$$

and from (4.6.76) and Equations (15)–(17) of Example 4.6.3

$$\underline{B} = -y \frac{d^2}{dx^2} [\phi_1 \ \phi_2 \ \phi_3 \ \phi_4 \ \phi_5 \ \phi_6] = -y [\phi_1'' \ \phi_2'' \ \phi_3'' \ \phi_4'' \ \phi_5'' \ \phi_6''] \quad (18)$$

where from (4)

$$\begin{aligned} \phi_1'' &= 0, & \phi_2'' &= 0, \\ \phi_3'' &= -\left(\frac{\pi}{L}\right)^2 \sin\left(\frac{\pi x}{L}\right), & \phi_4'' &= -\left(\frac{2\pi}{L}\right)^2 \sin\left(\frac{2\pi x}{L}\right) \\ \phi_5'' &= -\left(\frac{3\pi}{L}\right)^2 \sin\left(\frac{3\pi x}{L}\right), & \phi_6'' &= -\left(\frac{4\pi}{L}\right)^2 \sin\left(\frac{4\pi x}{L}\right) \end{aligned} \quad (19)$$

Similar to Equations (20)–(22) of Example 4.6.3, Equation (16) becomes

$$\underline{Q}_B^I = -\underline{K}_B \underline{q} \quad (20)$$

where

$$\underline{K}_B = \int_V \underline{B}^T \underline{E} \underline{B} dV = \int_0^L EI(x) \begin{bmatrix} \phi_1'' \phi_1'' & \phi_1'' \phi_2'' & \phi_1'' \phi_3'' & \phi_1'' \phi_4'' & \phi_1'' \phi_5'' & \phi_1'' \phi_6'' \\ & \phi_2'' \phi_2'' & \phi_2'' \phi_3'' & \phi_2'' \phi_4'' & \phi_2'' \phi_5'' & \phi_2'' \phi_6'' \\ & & \phi_3'' \phi_3'' & \phi_3'' \phi_4'' & \phi_3'' \phi_5'' & \phi_3'' \phi_6'' \\ & & & \phi_4'' \phi_4'' & \phi_4'' \phi_5'' & \phi_4'' \phi_6'' \\ & \text{symmetric} & & & \phi_5'' \phi_5'' & \phi_5'' \phi_6'' \\ & & & & & \phi_6'' \phi_6'' \end{bmatrix} dx \quad (21)$$

where from (1)

$$I(x) = \alpha_3 x + \alpha_4 \quad (22)$$

The integral in (21) is performed is performed utilizing the following MAPLE code

Maple Code for Obtaining the Platform Flooring Generalized Stiffness Matrix
Due to Bending in Equation (22)

```
with(linalg);
Ib := alp3*x + alp4;
piv := 3.141592654;
phidd(1) := 0;
phidd(2) := 0;
phidd(3) := -(piv/L)^2*sin(piv*x/L);
phidd(4) := -(2*piv/L)^2*sin(2*piv*x/L);
phidd(5) := -(3*piv/L)^2*sin(3*piv*x/L);
phidd(6) := -(4*piv/L)^2*sin(4*piv*x/L);

for i from 1 by 1 while i<7 do
for j from 1 by 1 while j<7 do
f(i,j) := Ib*phidd(i)*phidd(j);
end do
end do

A := matrix(6,6,f);
KB := E*map(int, A, x=0..L);
```

This produces the following results:

$$\underline{K}_B = \alpha_3 \frac{E}{L^2} \begin{bmatrix} 0 & 0 & 0 & 0 & 0 & 0 \\ 0 & 0 & 0 & 0 & 0 & 0 \\ & & 24.35 & -35.10 & 0 & -11.23 \\ & & & 389.64 & -341.1 & 0 \\ & \text{symmetric} & & & 1972.5 & -1392.2 \\ & & & & & 6234.2 \end{bmatrix} \quad (23)$$

$$+ \alpha_4 \frac{E}{L^3} \begin{bmatrix} 0 & 0 & 0 & 0 & 0 & 0 \\ 0 & 0 & 0 & 0 & 0 & 0 \\ & & 48.70 & 0 & 0 & 0 \\ & & & 779.27 & 0 & 0 \\ & \text{symmetric} & & & 3945.1 & 0 \\ & & & & & 12468.4 \end{bmatrix}$$

which is the stiffness matrix for the flooring represented by the assumed modes generalized coordinate model given by (3) and (4). The generalized stiffness matrix for the total platform model including the spring-modeled support columns and the beam-modeled flooring is given by

$$K = \underline{K}_s|_{x=0} + \frac{b}{a} \underline{K}_s|_{x=L} + \underline{K}_B \quad (24)$$

where $\underline{K}_s|_{x=0}$, $\underline{K}_s|_{x=L}$, and \underline{K}_B are obtained from (15) and (23) and the associated generalized force vector is

$$\underline{Q}_U = -\underline{K}\underline{q} \quad (25)$$

(c) Rayleigh Dissipation Function and Damping Matrix

From Figure E4.6.4(a), the Rayleigh dissipation function due to the support dampers is (4.5.81)

$$\mathfrak{S}^d = \frac{1}{2} c \dot{u}^2(0) + \frac{1}{2} c \frac{b}{a} \dot{u}^2(L) = \frac{c}{2} \left(\sum_{i=1}^6 \dot{q}_i \phi_i(0) \right)^2 + \frac{cb}{2a} \left(\sum_{i=1}^6 \dot{q}_i \phi_i(L) \right)^2 \quad (26)$$

The corresponding generalized forces are obtained from (4.5.82), (2.6.46), and (2.6.47) as

$$\underline{Q}_d = -\frac{\partial \mathfrak{S}^d}{\partial \underline{\dot{q}}} = \left(-\frac{\partial \mathfrak{S}^d}{\partial \dot{q}_1} - \frac{\partial \mathfrak{S}^d}{\partial \dot{q}_2} - \frac{\partial \mathfrak{S}^d}{\partial \dot{q}_3} - \frac{\partial \mathfrak{S}^d}{\partial \dot{q}_4} - \frac{\partial \mathfrak{S}^d}{\partial \dot{q}_5} - \frac{\partial \mathfrak{S}^d}{\partial \dot{q}_6} \right) \quad (27)$$

$$= -\underline{C}_d|_{x=0} \underline{\dot{q}} - \frac{b}{a} \underline{C}_d|_{x=L} \underline{\dot{q}} = -\left(\underline{C}_d|_{x=0} + \frac{b}{a} \underline{C}_d|_{x=L} \right) \underline{\dot{q}} = -\underline{C}\underline{\dot{q}}$$

where

$$\underline{C}_d = c \begin{bmatrix} \phi_1\phi_1 & \phi_1\phi_2 & \phi_1\phi_3 & \phi_1\phi_4 & \phi_1\phi_5 & \phi_1\phi_6 \\ & \phi_2\phi_2 & \phi_2\phi_3 & \phi_2\phi_4 & \phi_2\phi_5 & \phi_2\phi_6 \\ & & \phi_3\phi_3 & \phi_3\phi_4 & \phi_3\phi_5 & \phi_3\phi_6 \\ & & & \phi_4\phi_4 & \phi_4\phi_5 & \phi_4\phi_6 \\ \text{symmetric} & & & & \phi_5\phi_5 & \phi_5\phi_6 \\ & & & & & \phi_6\phi_6 \end{bmatrix} \quad (28)$$

which must be evaluated at $x=0$ and $x=L$ in (28).

(d) External Force Terms

The machinery force $F(t)$ in Figure E4.6.4(a) is a concentrated point load so its force/length expression is a Dirac delta function (ref. Section 2.12):

$$\bar{F}_{ES} = F(t)\delta(x-d) \quad (29)$$

The generalized force expression for the external force $F(t)$ is given by (4.6.86), that is,

$$\underline{Q}_F = \int_0^L F_{ES} \begin{Bmatrix} \phi_1 \\ \phi_2 \\ \phi_3 \\ \phi_4 \\ \phi_5 \\ \phi_6 \end{Bmatrix} dx = \int_0^L F(t)\delta(x-d) \begin{Bmatrix} \phi_1 \\ \phi_2 \\ \phi_3 \\ \phi_4 \\ \phi_5 \\ \phi_6 \end{Bmatrix} dx = F(t) \begin{Bmatrix} \phi_1 \\ \phi_2 \\ \phi_3 \\ \phi_4 \\ \phi_5 \\ \phi_6 \end{Bmatrix} \Big|_d \quad (30)$$

(e) Lagrange's Equations for the Platform Model

The terms required in (4.6.52) are

(i) From (7) and (9),

$$\frac{d}{dt} \left(\frac{\partial T}{\partial \dot{q}} \right) = \underline{M}\ddot{q} = (\underline{M}_m + \underline{M}_p)\ddot{q} \quad (31)$$

(ii) \underline{Q}_F from (30)

(iii) From (14), (16), (24), and (25),

$$-\frac{\partial U}{\partial q} = -\underline{K}q \quad (32)$$

(iv) From (28),

$$-\frac{\partial \mathcal{S}^d}{\partial \dot{q}} = \underline{C}\dot{q} \quad (33)$$

Combining the results yields the following EOMs for the generalized coordinates:

Machinery/Platform Flooring EOMs: Summary

The vertical displacements of the flooring are assumed to have the form

$$u(x,t) = \sum_{i=1}^6 q_i(t)\phi_i(x) = \underline{\Phi} \underline{q} = [\phi_1 \ \phi_2 \ \phi_3 \ \phi_4 \ \phi_5 \ \phi_6] \begin{Bmatrix} q_1 \\ q_2 \\ \vdots \\ q_6 \end{Bmatrix} \quad (34)$$

where $n=6$ generalized coordinates

$$\begin{aligned} \phi_1(x) &= 1, & \phi_2(x) &= \frac{x}{L}, & \phi_3(x) &= \sin\left(\frac{\pi x}{L}\right) \\ \phi_4(x) &= \sin\left(\frac{2\pi x}{L}\right), & \phi_5(x) &= \sin\left(\frac{3\pi x}{L}\right), & \phi_6(x) &= \sin\left(\frac{4\pi x}{L}\right) \end{aligned} \quad (35)$$

The generalized coordinates $q_j(t)$ are obtained by solving

$$\underline{M}\ddot{\underline{q}} + \underline{C}\dot{\underline{q}} + \underline{K}\underline{q} = \underline{Q}_F \quad (36)$$

where

$$\alpha_1 = \frac{(b-a)t}{L}, \quad \alpha_2 = at, \quad \alpha_3 = \frac{(b-a)t^3}{12L}, \quad \alpha_4 = \frac{at^3}{12} \quad (37)$$

$$\underline{M} = \underline{M}_m + \underline{M}_p \quad (38)$$

$$\underline{M}_m = \bar{m} \begin{bmatrix} \phi_1\phi_1 & \phi_1\phi_2 & \phi_1\phi_3 & \phi_1\phi_4 & \phi_1\phi_5 & \phi_1\phi_6 \\ & \phi_2\phi_2 & \phi_2\phi_3 & \phi_2\phi_4 & \phi_2\phi_5 & \phi_2\phi_6 \\ & & \phi_3\phi_3 & \phi_3\phi_4 & \phi_3\phi_5 & \phi_3\phi_6 \\ & & & \phi_4\phi_4 & \phi_4\phi_5 & \phi_4\phi_6 \\ \text{symmetric} & & & & \phi_5\phi_5 & \phi_5\phi_6 \\ & & & & & \phi_6\phi_6 \end{bmatrix}_{|x=d} \quad (39)$$

$$\underline{M}_p = \alpha_1 L^2 \rho \begin{bmatrix} 0.5 & 0.3333 & 0.3183 & -0.1592 & 0.1061 & -0.0796 \\ & 0.2500 & 0.1893 & -0.1592 & 0.1013 & -0.0796 \\ & & 0.2500 & -0.0901 & 0 & -0.0072 \\ & & & 0.2500 & -0.0973 & 0 \\ & \text{sym} & & & 0.2500 & -0.0993 \\ & & & & & 0.2500 \end{bmatrix} \quad (40)$$

$$+ \alpha_2 L \rho \begin{bmatrix} 1 & 0.500 & 0.6366 & 0 & 0.2122 & 0 \\ & 0.3333 & 0.3183 & -0.1592 & 0.1061 & -0.0796 \\ & & 0.500 & 0 & 0 & 0 \\ & & & 0.500 & 0 & 0 \\ & \text{sym} & & & 0.5000 & .0 \\ & & & & & 0.5000 \end{bmatrix}$$

$$K = \underline{K}_s \Big|_{x=0} + \frac{b}{a} \underline{K}_s \Big|_{x=L} + \underline{K}_B \quad (41)$$

$$\underline{K}_s = k \begin{bmatrix} \phi_1 \phi_1 & \phi_1 \phi_2 & \phi_1 \phi_3 & \phi_1 \phi_4 & \phi_1 \phi_5 & \phi_1 \phi_6 \\ & \phi_2 \phi_2 & \phi_2 \phi_3 & \phi_2 \phi_4 & \phi_2 \phi_5 & \phi_2 \phi_6 \\ & & \phi_3 \phi_3 & \phi_3 \phi_4 & \phi_3 \phi_5 & \phi_3 \phi_6 \\ & & & \phi_4 \phi_4 & \phi_4 \phi_5 & \phi_4 \phi_6 \\ & \text{sym} & & & \phi_5 \phi_5 & \phi_5 \phi_6 \\ & & & & & \phi_6 \phi_6 \end{bmatrix} \quad (42)$$

$$\underline{K}_B = \alpha_3 \frac{E}{L^2} \begin{bmatrix} 0 & 0 & 0 & 0 & 0 & 0 \\ & 0 & 0 & 0 & 0 & 0 \\ & & 24.35 & -35.10 & 0 & -11.23 \\ & & & 389.64 & -341.1 & 0 \\ & \text{sym} & & & 1972.5 & -1392.2 \\ & & & & & 6234.2 \end{bmatrix} \quad (43)$$

$$+ \alpha_4 \frac{E}{L^3} \begin{bmatrix} 0 & 0 & 0 & 0 & 0 & 0 \\ & 0 & 0 & 0 & 0 & 0 \\ & & 48.70 & 0 & 0 & 0 \\ & & & 779.27 & 0 & 0 \\ & \text{sym} & & & 3945.1 & 0 \\ & & & & & 12468.4 \end{bmatrix}$$

$$\underline{Q}_F = F(t) \begin{Bmatrix} \phi_1(d) \\ \phi_2(d) \\ \phi_3(d) \\ \phi_4(d) \\ \phi_5(d) \\ \phi_6(d) \end{Bmatrix} \quad (44)$$

Summary: This example illustrated how to obtain EOMs for a flexible structure with concentrated mass and stiffnesses via the assumed modes approach. The first two rows and columns of the beam stiffness matrix \underline{K}_B are zeros since strain energy cannot be stored in the rigid body modes:

$$\phi_1(x) = 1, \quad \phi_2(x) = \frac{x}{L} \quad (45)$$

EXAMPLE 4.6.5 *Vibration of a Rotating Beam with Tip Mass, Damping, and Aero-excitation*

Statement: Rotating machinery blades become stiffer in bending vibration as their rotational speed increase. The results from centrifugal force tending to straighten the beam back to its undeflected state. This increased stiffness in the transverse direction raises the transverse deflection natural frequencies as the rotating speed increases. A simplified rotating blade model consists of a uniform flexible beam as shown in Figure E4.6.5(a). The disk on which the blade is attached rotates with a constant angular velocity ω .

The blade has a tip mass and experiences a damping force proportional to its vibration velocity. A distributed aerodynamic force per unit area (f) causes the beam to vibrate. The beam width in the \hat{j} direction is $b(x)$, its cross-sectional area is $A(x)$, and its projected area in the \hat{k} direction is $a(x)$.

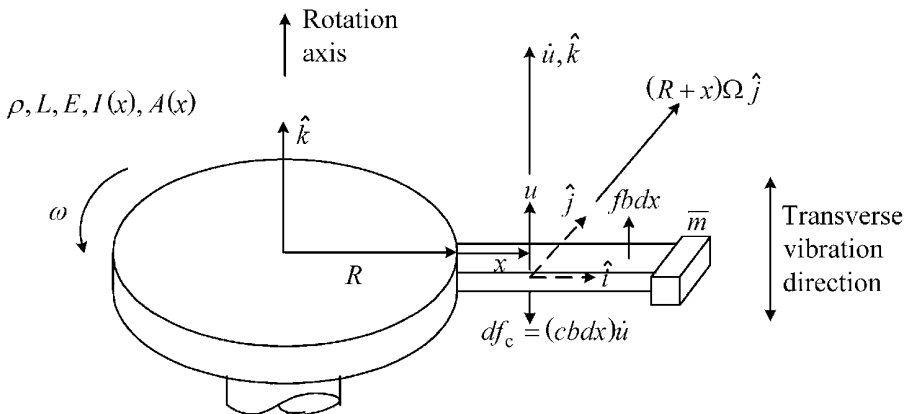


Figure E4.6.5(a) Vibrating blade attached to a spinning disk

Objective: Derive the EOMs using the assumed modes approach with the variable properties:

$$b = b(x), \quad A = A(x), \quad E = E(x), \quad I = I(x) \quad (1)$$

Assumptions: Small vibratory motion however includes a second-order strain term to investigate the stress stiffening phenomena.

Solution:

(a) Two ($n = 2$) generalized coordinates are utilized to approximate the transverse vibration of the beam. Thus, from (4.6.56),

$$u(x, t) = \sum_{i=1}^2 q_i(t) \phi_i(x) \quad (2)$$

The kinetic energy includes both rotational and transverse components and is derived with (4.6.54) and (4.6.55) as

$$\begin{aligned} T_B &= \frac{1}{2} \int_0^L \left[(R+x)^2 \Omega^2 + \dot{u}^2 \right] (\rho A(x) dx) + \frac{\bar{m}}{2} \left[(R+L)^2 \omega^2 + \dot{u}^2(L, t) \right] \\ &= \frac{\rho}{2} \int_0^L (R+x)^2 \Omega^2 A(x) dx + \frac{\bar{m}}{2} (R+L)^2 \omega^2 + \frac{\rho}{2} \int_0^L \dot{u}^2 A(x) dx + \frac{\bar{m}}{2} \dot{u}^2(L, t) \\ &= \frac{\rho}{2} \int_0^L (R+x)^2 \Omega^2 A(x) dx + \frac{\bar{m}}{2} (R+L)^2 \omega^2 \\ &\quad + \frac{\rho}{2} \int_0^L A(x) (\dot{q}_1 \phi_1 + \dot{q}_2 \phi_2)^2 dx + \frac{\bar{m}}{2} (\dot{q}_1 \phi_1(L) + \dot{q}_2 \phi_2(L))^2 \end{aligned} \quad (3)$$

Therefore,

$$\frac{\partial T}{\partial q_1} = \frac{\partial T}{\partial q_2} = 0 \quad (4)$$

$$\left\{ \begin{array}{l} \frac{d}{dt} \left(\frac{\partial T}{\partial \dot{q}_1} \right) \\ \frac{d}{dt} \left(\frac{\partial T}{\partial \dot{q}_2} \right) \end{array} \right\} = \left\{ \begin{array}{l} \rho \int_0^L A(x) (\ddot{q}_1 \phi_1 + \ddot{q}_2 \phi_2) \phi_1 dx + \bar{m} (\ddot{q}_1 \phi_1(L) + \ddot{q}_2 \phi_2(L)) \phi_1(L) \\ \rho \int_0^L A(x) (\ddot{q}_1 \phi_1 + \ddot{q}_2 \phi_2) \phi_2 dx + \bar{m} (\ddot{q}_1 \phi_1(L) + \ddot{q}_2 \phi_2(L)) \phi_2(L) \end{array} \right\} = \underline{M} \ddot{\underline{q}} \quad (5)$$

where

$$\underline{M} = \left\{ \begin{array}{l} \int_0^L \rho A(x) \phi_1 \phi_1 dx + \bar{m} \phi_1(L) \phi_1(L) \quad \left| \quad \int_0^L \rho A(x) \phi_1 \phi_2 dx + \bar{m} \phi_1(L) \phi_2(L) \right. \\ \hline \int_0^L \rho A(x) \phi_1 \phi_2 dx + \bar{m} \phi_1(L) \phi_2(L) \quad \left| \quad \int_0^L \rho A(x) \phi_2 \phi_2 dx + \bar{m} \phi_2(L) \phi_2(L) \right. \end{array} \right\} \quad (6)$$

$$\underline{\ddot{q}} = \left\{ \begin{array}{l} \ddot{q}_1 \\ \ddot{q}_2 \end{array} \right\} \quad (7)$$

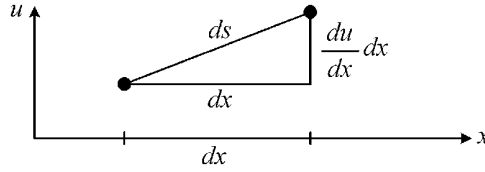


Figure E4.6.5(b) Differential length of beam in pure bending

- (b) The potential energy of the vibrating, rotating beam has two contributions. The first arises from the transverse bending deflection of the beam as in the case of a nonrotating cantilevered beam. The second source results from the tendency of the centrifugal force to restore the deflected beam to its original, undeflected shape along the x axis. This effect is analogous to a pendulum being pulled toward its vertical equilibrium state by gravity. Thus, additional work is performed by the centrifugal radial force. Figure E4.6.5(b) shows a differential length along the beam before (dx) and after (ds) deformation.

The strain is given by the change in length per initial length:

$$\varepsilon = \frac{ds - dx}{dx} = \frac{\sqrt{\left(\frac{du}{dx} dx\right)^2 + dx^2} - dx}{dx} = \sqrt{\left(\frac{du}{dx}\right)^2 + 1} - 1 \quad (8)$$

A two-term Taylor series expansion of the first term yields

$$\varepsilon(x) \cong \left(1 + \frac{1}{2} \left(\frac{du}{dx}\right)^2\right) - 1 = \frac{1}{2} \left(\frac{du}{dx}\right)^2 \quad (9)$$

This represents a higher-order strain that is nonzero on the neutral axis of the cross section (Cook et al., 1989). The centrifugal force acting at the location of $\varepsilon(x)$ is given by

$$F(x) = \sigma(x)A(x) = \int_x^L \omega^2 (R + \xi) \rho A(\xi) d\xi + \bar{m}(L + R)\omega^2 \quad (10)$$

where ξ is a dummy integration variable. For example, if A is constant,

$$\begin{aligned} F(x) &= \sigma(x)A = \rho A \omega^2 \left(R\xi + \frac{\xi^2}{2} \right) \Big|_x^L + \bar{m}(L + R)\omega^2 \\ &= \rho A \omega^2 \left(RL + \frac{L^2}{2} - Rx - \frac{x^2}{2} \right) + \bar{m}(L + R)\omega^2 \end{aligned} \quad (11)$$

The internal work performed to counteract this force is given by (A.6.8)

$$W_1^C = - \int_V \int_0^\varepsilon \underline{\sigma} \, d\underline{\varepsilon} \, dV \quad (12)$$

Note that σ in (10) is independent of ε in (9); therefore, the inner integral in (12) may be performed, yielding

$$W_I^C = - \int_V \sigma \varepsilon dV = - \int_0^L \frac{F(x)}{A(x)} \frac{1}{2} \left(\frac{du}{dx} \right)^2 A(x) dx = - \frac{1}{2} \int_0^L F(x) \left(\frac{du}{dx} \right)^2 dx \quad (13)$$

The potential energy contribution due to the centrifugal force is by (A.6.11) and (10):

$$\begin{aligned} U_I^C = -W_I^C &= \frac{1}{2} \int_0^L \left(\int_x^L \omega^2 (R + \xi) \rho A(\xi) d\xi + \bar{m}(L+R)\omega^2 \right) \left(\frac{du}{dx} \right)^2 dx \\ &= \frac{1}{2} \int_0^L \left(\rho \omega^2 \int_x^L (R + \xi) A(\xi) d\xi + \bar{m}(L+R)\omega^2 \right) (q_1 \phi_1' + q_2 \phi_2')^2 dx \end{aligned} \quad (14)$$

The corresponding generalized forces are given by (4.6.25)

$$\begin{aligned} \underline{Q}^C &= \begin{Bmatrix} Q_1^C \\ Q_2^C \end{Bmatrix} = \begin{Bmatrix} -\frac{\partial U_I^C}{\partial q_1} \\ -\frac{\partial U_I^C}{\partial q_2} \end{Bmatrix} \\ &= \begin{Bmatrix} - \int_0^L \left(\rho \omega^2 \int_x^L (R + \xi) A(\xi) d\xi + \bar{m}(L+R)\omega^2 \right) \phi_1' (q_1 \phi_1' + q_2 \phi_2') dx \\ - \int_0^L \left(\rho \omega^2 \int_x^L (R + \xi) A(\xi) d\xi + \bar{m}(L+R)\omega^2 \right) \phi_2' (q_1 \phi_1' + q_2 \phi_2') dx \end{Bmatrix} \\ &= - \begin{bmatrix} K_{11}^C & K_{12}^C \\ K_{21}^C & K_{22}^C \end{bmatrix} \begin{Bmatrix} q_1 \\ q_2 \end{Bmatrix} = -\underline{K}^C \underline{q} \end{aligned} \quad (15)$$

where

$$\begin{aligned} \underline{K}^C &= \rho \omega^2 \begin{bmatrix} \int_0^L \left(\int_x^L (R + \xi) A(\xi) d\xi \right) \phi_1' \phi_1' dx & \int_0^L \left(\int_x^L (R + \xi) A(\xi) d\xi \right) \phi_1' \phi_2' dx \\ \int_0^L \left(\int_x^L (R + \xi) A(\xi) d\xi \right) \phi_1' \phi_2' dx & \int_0^L \left(\int_x^L (R + \xi) A(\xi) d\xi \right) \phi_2' \phi_2' dx \end{bmatrix} \\ &+ \bar{m}(L+R)\omega^2 \begin{bmatrix} \int_0^L \phi_1' \phi_1' dx & \int_0^L \phi_1' \phi_2' dx \\ \int_0^L \phi_1' \phi_2' dx & \int_0^L \phi_2' \phi_2' dx \end{bmatrix} \end{aligned} \quad (16)$$

and

$$\phi_j'(x) = \frac{d\phi_j}{dx} \quad (17)$$

- (c) The generalized forces due to centrifugal force were considered in (b). This accounted for the tendency of a deflected blade to return to the equilibrium state ($u=0$) due to its spin. In addition, there is also a tendency of the blade to return to the equilibrium state due to the bending strain potential energy. The corresponding generalized forces were obtained in Equations (19) and (22) of Example 4.6.3 as

$$\underline{Q}_B = \begin{Bmatrix} Q_1^B \\ Q_2^B \end{Bmatrix} = -\underline{K}^B \underline{q} \quad (18)$$

where

$$\underline{K}^B = \int_0^L E(x)I(x) \begin{bmatrix} \phi_1''\phi_1'' & \phi_1''\phi_2'' \\ \phi_1''\phi_2'' & \phi_2''\phi_2'' \end{bmatrix} dx \quad (19)$$

- (d) The distributed damping force is shown in Figure E4.6.5(a) as

$$df_c = -(c\dot{u})da = -c\dot{u}b dx \quad (20)$$

where $c\dot{u}$ is a force per unit area and b is the width of the beam in the \hat{j} direction. The Rayleigh dissipation function for df_c is given by (4.5.81) as

$$d\mathfrak{S}_c^d = \frac{1}{2}\dot{u}(cb dx)\dot{u} \quad (21)$$

Therefore,

$$\mathfrak{S}_c^d = \frac{c}{2} \int_0^L b(x)\dot{u}^2(x) dx = \frac{c}{2} \int_0^L b(x)(\dot{q}_1\phi_1 + \dot{q}_2\phi_2)^2 dx \quad (22)$$

The generalized forces are obtained from (4.5.82) as

$$\underline{Q}_D = \begin{Bmatrix} Q_1^D \\ Q_2^D \end{Bmatrix} = \begin{Bmatrix} \frac{\partial \mathfrak{S}_c^d}{\partial \dot{q}_1} \\ \frac{\partial \mathfrak{S}_c^d}{\partial \dot{q}_2} \end{Bmatrix} = \begin{Bmatrix} -c \int_0^L b(x)\phi_1(\dot{q}_1\phi_1 + \dot{q}_2\phi_2) dx \\ -c \int_0^L b(x)\phi_2(\dot{q}_1\phi_1 + \dot{q}_2\phi_2) dx \end{Bmatrix} = -\underline{C}\underline{\dot{q}} \quad (23)$$

where

$$\underline{C} = \begin{bmatrix} c \int_0^L b(x)\phi_1\phi_1 dx & c \int_0^L b(x)\phi_1\phi_2 dx \\ c \int_0^L b(x)\phi_1\phi_2 dx & c \int_0^L b(x)\phi_2\phi_2 dx \end{bmatrix} \quad (24)$$

- (e) A distributed aerodynamic force per unit area $f(x, t)$ is shown acting on the blade in Figure E4.6.5(a). The corresponding generalized forces are given by (4.6.51) as

$$\underline{Q}_f = \begin{Bmatrix} Q_1^f \\ Q_2^f \end{Bmatrix} = \begin{Bmatrix} \int_a^L f(x, t)\phi_1 da \\ \int_a^L f(x, t)\phi_2 da \end{Bmatrix} = \begin{Bmatrix} \int_0^L f(x, t)\phi_1(x)b(x) dx \\ \int_0^L f(x, t)\phi_2(x)b(x) dx \end{Bmatrix} \quad (25)$$

(f) Gathering terms into (4.6.52)

$$\frac{d}{dt} \left(\frac{\partial T}{\partial \dot{q}_j} \right) - \frac{\partial T}{\partial q_j} = \underline{Q}_j - \frac{\partial U}{\partial q_j} - \frac{\partial (\mathfrak{S}^c + \mathfrak{S}^d)}{\partial \dot{q}_j} \quad (26)$$

yields

$$\underline{M} \underline{\ddot{q}} = \underline{Q}_f - (\underline{K}^C + \underline{K}^B) \underline{q} - \underline{C} \underline{\dot{q}} \quad (27)$$

EOMs for a Damped Rotating Blade with Tip Mass and Aero Force

The transverse deflection field for the rotating, vibrating beam blade model is given by

$$u(x, t) = \sum_{i=1}^n q_i(t) \phi_i(x) \quad (28)$$

where the generalized coordinates are obtained by solving

$$\underline{M} \underline{\ddot{q}} + \underline{C} \underline{\dot{q}} + (\underline{K}^C + \underline{K}^B) \underline{q} = \underline{Q}_f \quad (29)$$

(with the initial conditions $q_i(0)$) for

$$\underline{q} = \begin{Bmatrix} q_1 \\ q_2 \end{Bmatrix} \quad (30)$$

where

$$(\underline{M})_{ij} = \rho \int_0^L A(x) \phi_i(x) \phi_j(x) dx + \bar{m} \phi_i(L) \phi_j(L) \quad (31)$$

$$(\underline{C})_{ij} = c \int_0^L b(x) \phi_i(x) \phi_j(x) dx \quad (32)$$

$$(\underline{K}^C)_{ij} = \rho \omega^2 \int_0^L \left(\int_x^L (R + \xi) A(\xi) d\xi \right) \phi_i'(x) \phi_j'(x) dx + \bar{m} (L + R) \omega^2 \int_0^L \phi_i' \phi_j' dx \quad (33)$$

$$(\underline{K}^B)_{ij} = \int_0^L E(x) I(x) \phi_i''(x) \phi_j''(x) dx \quad (34)$$

where

$$\phi' = \frac{d\phi}{dx}, \quad \phi'' = \frac{d^2\phi}{dx^2}, \quad (35)$$

and

$$\left(\underline{Q}_f \right)_i = \int_0^L f(x, t) \phi_i(x) b(x) dx \quad (36)$$

(g) To illustrate a seminumerical evaluation of the EOMs, consider the following example:

$$\begin{aligned}\phi_1(x) &= \left(\frac{x}{L}\right)^3 - 3\left(\frac{x}{L}\right)^2, \quad \phi_2(x) = \left(\frac{x}{L}\right)^4 - \left(\frac{x}{L}\right)^2, \quad \phi_1(L) = -2, \quad \phi_2(L) = 0 \\ A(x) &= A_0\left(1 - 0.5\frac{x}{L}\right), \quad b(x) = b_0\left(1 - 0.5\frac{x}{L}\right), \quad E(x) = E_0 \\ I(x) &= I_0\left(1 - 0.5\frac{x}{L}\right)^2, \quad f(x, t) = \beta\left(\frac{x}{L}\right)\sin(\omega_f t)\end{aligned}\quad (37)$$

The integrals in (31)–(36) are performed in the following MAPLE code yielding

- The mass matrix in (29) and (31):

$$\underline{M} = \begin{bmatrix} 0.5589\rho A_0 L + 4\bar{m} & 0.0831\rho A_0 L \\ 0.0831\rho A_0 L & 0.01706\rho A_0 L \end{bmatrix}\quad (38)$$

- The damping matrix in (29) and (32):

$$\underline{C} = cLb_0 \begin{bmatrix} 0.5589 & 0.0831 \\ 0.0831 & 0.0176 \end{bmatrix}\quad (39)$$

- The centrifugal stiffness matrix in (29) and (33):

$$\underline{K}^C = \rho\omega^2 A_0 \begin{bmatrix} 0.688L + 0.921R & 0.077L + 0.1286R \\ 0.077L + 0.1286R & 0.0381L + 0.054R \end{bmatrix} + \bar{m}\frac{(R+L)}{L}\omega^2 \begin{bmatrix} 4.8 & -0.3 \\ -0.3 & 0.42 \end{bmatrix}\quad (40)$$

- The bending stiffness matrix in (29) and (34):

$$\underline{K}_B = \frac{E_0 I_0}{L^3} \begin{bmatrix} 9.3 & 1.25 \\ 1.25 & 5.876 \end{bmatrix}\quad (41)$$

- The generalized aero force vector in (29) and (36):

$$\underline{Q}_f = \beta b_0 L \sin(\omega_f t) \begin{Bmatrix} -0.3333 \\ -0.05476 \end{Bmatrix}\quad (42)$$

Substitution of these results into (29) yields

Summary for Model Defined by (37)

$$\underline{M}\ddot{\underline{q}} + \underline{C}\dot{\underline{q}} + (\underline{K}^C + \underline{K}^B)\underline{q} = \underline{Q}_f\quad (43)$$

or

$$\begin{aligned}
& \begin{bmatrix} 0.5589\rho A_0 L + 4\bar{m} & 0.0831\rho A_0 L \\ 0.0831\rho A_0 L & 0.01706\rho A_0 L \end{bmatrix} \begin{Bmatrix} \ddot{q}_1 \\ \ddot{q}_2 \end{Bmatrix} + cLb_0 \begin{bmatrix} 0.5589 & 0.0831 \\ 0.0831 & 0.0176 \end{bmatrix} \begin{Bmatrix} \dot{q}_1 \\ \dot{q}_2 \end{Bmatrix} \\
& + \left\{ \rho\omega^2 A_0 \begin{bmatrix} 0.688L + 0.921R & 0.077L + 0.1286R \\ 0.077L + 0.1286R & 0.0381L + 0.054R \end{bmatrix} \right. \\
& \left. + \bar{m} \frac{(R+L)}{L} \omega^2 \begin{bmatrix} 4.8 & -0.3 \\ -0.3 & 0.42 \end{bmatrix} + \frac{E_0 I_0}{L^3} \begin{bmatrix} 9.3 & 1.25 \\ 1.25 & 5.876 \end{bmatrix} \right\} \begin{Bmatrix} q_1 \\ q_2 \end{Bmatrix} \\
& = \beta b_0 L \sin(\omega_f t) \begin{Bmatrix} -0.3333 \\ -0.05476 \end{Bmatrix}
\end{aligned} \tag{44}$$

The transverse deflection field for the rotating, vibrating beam blade model is given by

$$u(x,t) = \sum_{i=1}^2 q_i(t) \phi_i(x) \tag{45}$$

where the generalized coordinates are obtained by solving (43) with the initial conditions $q_i(0)$.

Maple Code for Obtaining the Blades Matrices in Example 4.6.5

```

with(linalg);
# maple 7 code for obtaining the blade matrices
phi1 := (x/L)^3 - 3*(x/L)^2;
phi2 := (x/L)^4 - (x/L)^2;
phi1d := diff(phi1,x);
phi2d := diff(phi2,x);
phi1dd := diff(phi1d,x);
phi2dd := diff(phi2d,x);
g := (1-0.5*x/L);
A := A0*g;
b := b0*g;
IA := I0*g^2;

# evaluate mass matrix
f(1,1) := rho*A*phi1*phi1;
f(1,2) := rho*A*phi1*phi2;
f(2,1) := rho*A*phi2*phi1;
f(2,2) := rho*A*phi2*phi2;
AAA := matrix(2,2,f);
MMAT := map(int, AAA, x=0..L);

```

```

# evaluate damping matrix
f(1,1) := c*b*phi1*phi1;
f(1,2) := c*b*phi1*phi2;
f(2,1) := c*b*phi2*phi1;
f(2,2) := c*b*phi2*phi2;
AAA := matrix(2,2,f);
CMAT := map(int, AAA, x=0..L);

# evaluate centrifugal stiffness matrix
force_centrif := int((R+zeta) *A0*(1-0.5*zeta/L),
zeta=0..L);
f(1,1) := (rho*omega^2*force_centrif+mbar(L+R)*omega^2)
*phi1d*phi1d;
f(1,2) := (rho*omega^2*force_centrif+mbar(L+R)*omega^2)
*phi1d*phi2d;
f(2,1) := (rho*omega^2*force_centrif+mbar(L+R)*omega^2)
*phi2d*phi1d;
f(2,2) := (rho*omega^2*force_centrif+mbar(L+R)*omega^2)
*phi2d*phi2d;
AAA := matrix(2,2,f);
KCMAT := simplify(map(int, AAA, x=0..L), symbolic);

# evaluate bending stiffness matrix
f(1,1) := E0*IA*phi1dd*phi1dd;
f(1,2) := E0*IA*phi1dd*phi2dd;
f(2,1) := E0*IA*phi2dd*phi1dd;
f(2,2) := E0*IA*phi2dd*phi2dd;
AAA := matrix(2,2,f);
KBMAT := simplify(map(int, AAA, x=0..L), symbolic);

# generalizedaeroforce vector
f_aero := beta*x/L*sin(omegaf*t);
f(1,1) := f_aero*phi1*b;
f(2,1) := f_aero*phi2*b;
AAA := matrix(2,1,f);
fvect := simplify(map(int, AAA, x=0..L), symbolic);

```

Summary: This example illustrates how to derive the assumed modes EOMs for centrifugal stiffening, damping, tip mass, aerodynamic force, and disk radius effects. The centrifugal stiffness matrix in (33) adds to the bending stiffness matrix, that is, it becomes a hardening spring as ω increases. Therefore, the natural frequencies vary with centrifugal load and thus with speed as illustrated by the *Campbell diagram* in Figure E4.6.5(c). Similar results may be found with any structural member under axial load as discussed in (Cook et al., 1989). Examples of this include guitar strings, loaded columns and long vertical pump shafts with end suction impellers, etc. The general phenomenon is referred to as “stress stiffening” in finite element books and commercial software.

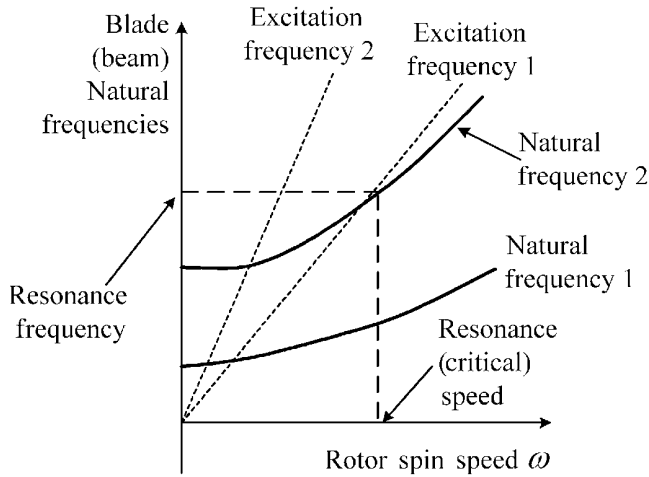


Figure E4.6.5(c) Interference or Campbell diagram

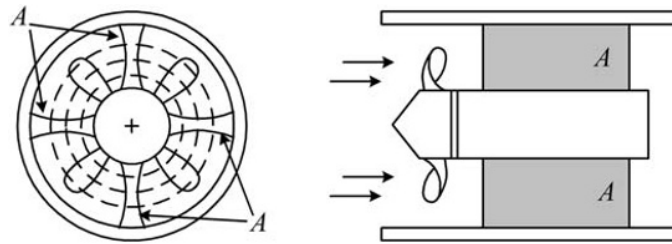


Figure E4.6.6(a) In-line fan and support plates

EXAMPLE 4.6.6 Vibration of Plate-Type Support Struts for an In-Line Fan System

Statement: Figure E4.6.6(a) depicts an in-line fan supported by four plates attached to the fan body and inner diameter of a circular pipe. The plates have experienced high-cycle fatigue failure due to vibration. Engineers at the vendor company seek to develop a simulation model of the plate to predict its response and to simulate thickness distribution modifications for eliminating the failure.

Objective: Derive the plate EOMs using the assumed modes approach.

Assumptions: Vibration measurements on the fan body indicate very little motion compared to that measured on the plates, and the plate vibration is mainly in the out-of-plane direction (x_3 in Figure E4.6.6(b)). This justifies use of fixed (zero deflections, zero slope) boundary conditions at $x_2 = \pm b$ which represents the pipe inner diameter and fan body outer surface. The plate is fairly thin which justifies utilizing a plane stress model. The material law (Appendix A.4) becomes (Dym and Shames, 1973)

$$\frac{\sigma}{3 \times 1} = \frac{E}{3 \times 33 \times 1} \frac{\epsilon}{1} \quad (1)$$

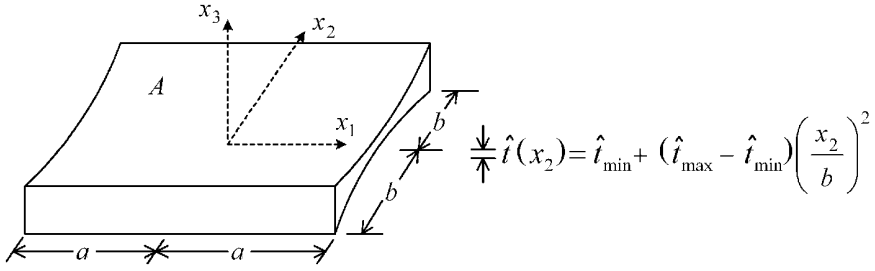


Figure E4.6.6(b) Support plate geometry

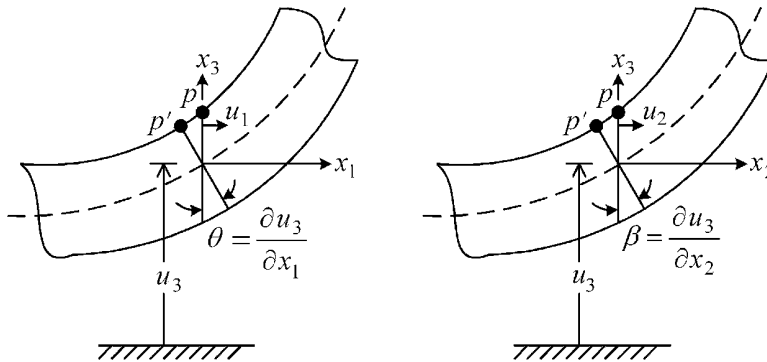


Figure E4.6.6(c) Small out-of-plane deflection of a thin plate

where

$$\underline{\sigma} = \begin{Bmatrix} \sigma_{11} \\ \sigma_{22} \\ \sigma_{12} \end{Bmatrix}, \underline{\varepsilon} = \begin{Bmatrix} \varepsilon_{11} \\ \varepsilon_{22} \\ 2\varepsilon_{12} \end{Bmatrix}, \underline{E} = \frac{E}{1-\nu^2} \begin{bmatrix} 1 & \nu & 0 \\ \nu & 1 & 0 \\ 0 & 0 & \frac{1-\nu}{2} \end{bmatrix} = \frac{E}{1-\nu^2} \hat{E} \quad (2)$$

and due to the plane stress assumption

$$\sigma_{13} = \sigma_{23} = \sigma_{33} = 0 \quad (3)$$

The deformation assumption for thin plates is similar to that of a Euler beam (plane sections remain plane and perpendicular to the neutral axis) and is illustrated in Figure E4.6.6(c).

From this figure, it is seen that

$$u_1 = -x_3 \frac{\partial u_3}{\partial x_1}, \quad u_2 = -x_3 \frac{\partial u_3}{\partial x_2} \quad (4)$$

From Appendix (A.3.21) and Equation (4),

$$\varepsilon_{11} = \frac{\partial u_1}{\partial x_1} = -x_3 \frac{\partial^2 u_3}{\partial x_1^2}, \quad \varepsilon_{22} = \frac{\partial u_2}{\partial x_2} = -x_3 \frac{\partial^2 u_3}{\partial x_2^2}, \quad \varepsilon_{12} = \frac{1}{2} \left(\frac{\partial u_1}{\partial x_2} + \frac{\partial u_2}{\partial x_1} \right) = -x_3 \frac{\partial^2 u_3}{\partial x_1 \partial x_2} \quad (5)$$

Equations (5) may be written in the form of (4.6.73):

$$\underline{\varepsilon} = \underline{D} \underline{u} \quad (6)$$

$3 \times 1 \quad 3 \times 11 \times 1$

where

$$\underline{u} = u_3 \quad (7)$$

and

$$\underline{D} = -x_3 \begin{bmatrix} \frac{\partial^2}{\partial x_1^2} \\ \text{-----} \\ \frac{\partial^2}{\partial x_2^2} \\ \text{-----} \\ \frac{2\partial}{\partial x_1 \partial x_2} \end{bmatrix} \quad (8)$$

Solution:

(a) The shape functions for this problem must satisfy

$$u_3(x_2 = \pm b) = \frac{\partial u_3}{\partial x_2}(x_2 = \pm b) = 0 \quad (9)$$

to be kinematically admissible (see discussion of Eq. (2.11.34)). Any functions

$$\phi_j = \phi_{jx1}(x_1) \phi_{jx2}(x_2) \quad (10)$$

satisfies (14) if $\phi_{jx2}(x_2)$ has the form

$$\phi_{jx2}(x_2) = \phi_{jx2}^I(x_2) \phi_{jx2}^{II}(x_2) \quad (11)$$

where

$$\phi_{jx2}^I(x_2 = -b) = \frac{\partial \phi_{jx2}^I}{\partial x_2}(x_2 = -b) = 0, \quad \phi_{jx2}^{II}(x_2 = b) = \frac{\partial \phi_{jx2}^{II}}{\partial x_2}(x_2 = b) = 0 \quad (12)$$

This follows since

$$\phi_j(x_2 = \pm b) = \phi_{jx1}(x_1) \phi_{jx2}^I(x_2 = \pm b) \phi_{jx2}^{II}(x_2 = \pm b) = 0 \quad (13)$$

and

$$\frac{\partial \phi_j}{\partial x_2}(x_2 = \pm b) = \phi_{jx1}(x_1) \left(\phi_{jx2}^{II} \frac{\partial \phi_{jx2}^I}{\partial x_2} \right)_{\pm b} + \phi_{jx1}(x_1) \left(\phi_{jx2}^I \frac{\partial \phi_{jx2}^{II}}{\partial x_2} \right)_{\pm b} = 0 \quad (14)$$

For example, a set of admissible shape functions may be generated from

$$\phi^{(m,n)}(x_1, x_2) = \phi_{x_1}^{(m)}(x_1) \phi_{x_2}^{I(n)}(x_2) \phi_{x_2}^{II(n)}(x_2) \quad (15)$$

where

$$\phi_{x_1}^{(m)}(x_1) = \sin \left[m\pi \left(\frac{1}{2} + \frac{x_1}{2a} \right) \right] \quad \text{or} \quad \cos \left[m\pi \left(\frac{1}{2} + \frac{x_1}{2a} \right) \right] \quad (16)$$

$$\phi_{x_2}^{I(n)}(x_2) = \left(1 + \frac{x_2}{b} \right)^2 \sin \left[n\pi \left(\frac{1}{2} + \frac{x_2}{2b} \right) \right], \quad \phi_{x_2}^{II(n)}(x_2) = \left(1 - \frac{x_2}{b} \right)^2 \quad (17)$$

The shape functions in (21) are plotted in Figure E4.6.6(d) for the sin option in (16) with $(m, n) = (1, 1), (1, 2), (2, 1),$ and $(2, 2)$.

The assumed modes deflection interpolation is given by (4.6.71)

$$u_3(x_1, x_2, t) = \underset{1 \times 1}{\Phi}(x_1, x_2) \underset{1 \times 4}{q}(t) \underset{4 \times 1}{\quad} \quad (18)$$

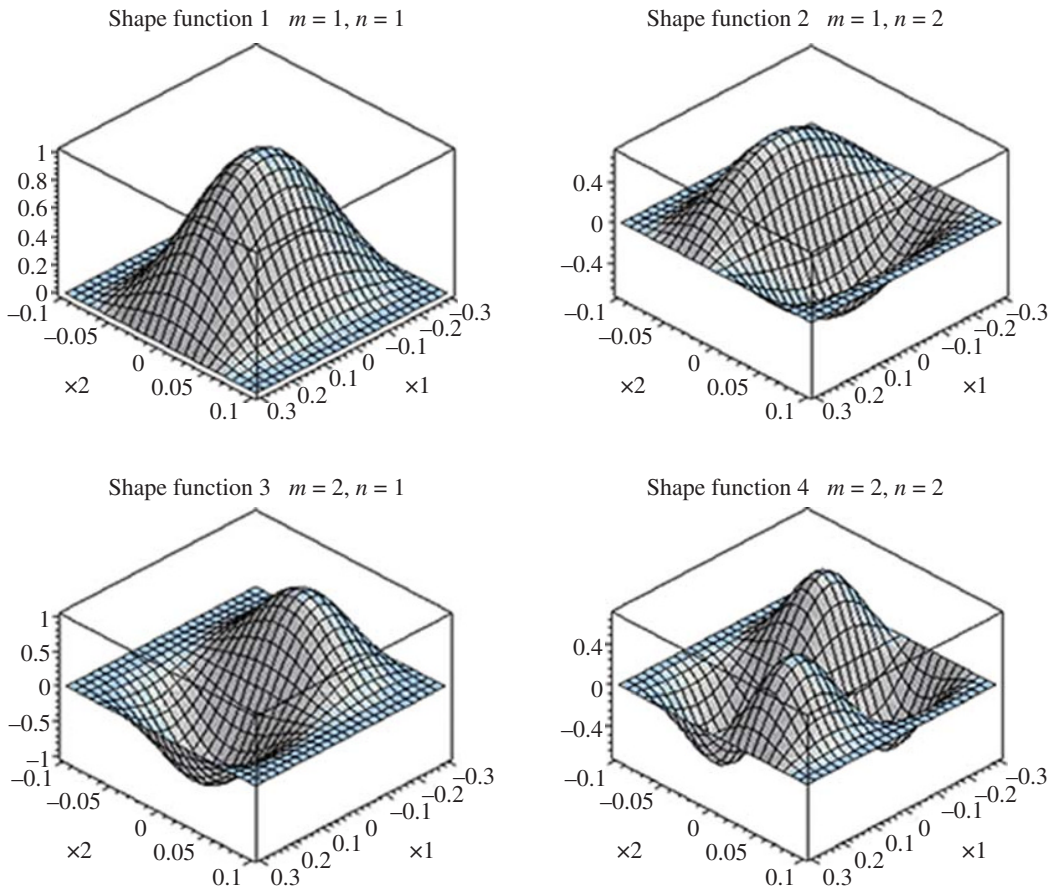


Figure E4.6.6(d) Lowest four shape functions

where

$$\underline{q}(t) = (q_1(t) \ q_2(t) \ q_3(t) \ q_4(t))^T \quad (19)$$

and

$$\begin{aligned} \underline{\Phi}(x_1, x_2) &= (\phi_1(x_1, x_2) \ \phi_2(x_1, x_2) \ \phi_3(x_1, x_2) \ \phi_4(x_1, x_2)) \\ &= (\phi^{(1,1)} \ \phi^{(1,2)} \ \phi^{(2,1)} \ \phi^{(2,2)}) \end{aligned} \quad (20)$$

- (b) The \underline{K} matrix in (4.6.75) first requires evaluation of the \underline{B} matrix in (4.6.76), that is, from (8) and (20):

$$\begin{aligned} \underline{B} &= \underline{D} \underline{\Phi} = -x_3 \begin{bmatrix} \partial^2 / \partial x_1^2 \\ \partial^2 / \partial x_2^2 \\ 2\partial^2 / \partial x_1 \partial x_2 \end{bmatrix} (\phi_1 \ \phi_2 \ \phi_3 \ \phi_4) \\ &= -x_3 \begin{bmatrix} \phi_{1,11} & \phi_{2,11} & \phi_{3,11} & \phi_{4,11} \\ \phi_{1,22} & \phi_{2,22} & \phi_{3,22} & \phi_{4,22} \\ 2\phi_{1,12} & 2\phi_{2,12} & 2\phi_{3,12} & 2\phi_{4,12} \end{bmatrix} = -x_3 \hat{\underline{\Phi}}(x_1, x_2) \end{aligned} \quad (21)$$

where

$$\phi_{i,jl} = \frac{\partial^2 \phi_i}{\partial x_j \partial x_l} \quad (22)$$

The $\tilde{\underline{K}}$ matrix of (4.6.75) becomes

$$\begin{aligned} \tilde{\underline{K}} &= \int_V \underline{B}^T \underline{E} \underline{B} dV = \frac{E}{1-\nu^2} \int_{-a-b-t/2}^a \int_{-a-b-t/2}^b \int_{-a-b-t/2}^{t/2} x_3^2 \hat{\underline{\Phi}}^T \hat{\underline{E}} \hat{\underline{\Phi}} dx_3 dx_2 dx_1 \\ &= \frac{E}{1-\nu^2} \int_{-a-b}^a \int_{-a-b}^b \frac{\hat{t}^3(x_2)}{12} \hat{\underline{\Phi}}^T(x_1, x_2) \hat{\underline{E}} \hat{\underline{\Phi}}(x_1, x_2) dx_2 dx_1 \end{aligned} \quad (23)$$

where the integration over x_3 is performed, and from Figure E4.6.6(b), the plate thickness function is

$$\hat{t}(x_2) = \hat{t}_{\min} + (\hat{t}_{\max} - \hat{t}_{\min}) \left(\frac{x_2}{b} \right)^2 \quad (24)$$

The stiffness matrix $\tilde{\underline{K}}$ in (23) was evaluated by MAPLE code below for the parameter values $E = 2.0 \times 10^{11}$ N/m², $\nu = 0.3$ dim, $\hat{t}_{\min} = 0.002$ m, $\hat{t}_{\max} = 0.003$ m, $a = 0.3$ m, and $b = 0.1$ m. The result is

$$\tilde{\underline{K}} = 10^7 \begin{bmatrix} 0.2081 & 0 & 0 & 0 \\ & 0.7629 & 0 & 0 \\ & & \text{symmetric} & 0.2360 \\ & & & & 0.8130 \end{bmatrix} \text{N/m} \quad (25)$$

(c) The mass matrix for the plate is obtained from (4.6.65) as

$$\begin{aligned}\tilde{\underline{M}} &= \int_V \underline{\Phi}^T \underline{\Phi} dm = \int_V \underline{\Phi}^T \underline{\Phi} \rho dV = \int_{-a-b-t/2}^a \int_{-a-b-t/2}^b \int_{-a-b-t/2}^{t/2} \underline{\Phi}^T \underline{\Phi} \rho dx_3 dx_2 dx_1 \\ &= \int_{-a-b}^a \int_{-a-b}^b \rho t(x_2) \underline{\Phi}^T \underline{\Phi} dx_2 dx_1\end{aligned}\quad (26)$$

This matrix is evaluated in the MAPLE code below with $\rho = 7700 \text{ kg/m}^3$. The result is

$$\tilde{\underline{M}} = \begin{bmatrix} 0.31528 & 0 & 0 & 0 \\ & 0.17971 & 0 & 0 \\ & \text{symmetric} & 0.31528 & 0 \\ & & & 0.17971 \end{bmatrix} \text{ kg} \quad (27)$$

(d) The governing differential equation for the generalized coordinates $q_1(t) \cdots q_4(t)$ becomes

$$\tilde{\underline{M}} \ddot{\underline{q}} + \tilde{\underline{K}} \underline{q} = \underline{0} \quad (4 \times 1) \quad (28)$$

where $\tilde{\underline{M}}$ and $\tilde{\underline{K}}$ are defined in (27) and (25), respectively,

$$\underline{q} = \begin{Bmatrix} q_1 \\ q_2 \\ q_3 \\ q_4 \end{Bmatrix} \quad (29)$$

and the transverse deflection is given by (18)

$$u_3(x_1, x_2, t) = \sum_{i=1}^4 q_i(t) \phi_i(x_1, x_2) \quad (30)$$

where the ϕ_i are defined in (15)–(17) and (20):

Maple Code for Obtaining the Plate Matrices

```
>restart;
>with(linalg):
>a:=.3 : b:=.1 : tmin:=.002 : tmax:=.003 : nu:=.3 : Pie :=
=3.14159265:
>E:=2e+11 : rho:=7700:
>fun:=evalf(sin(m*Pie*(1/2+x1/2/a))*(1+x2/b)^2*(1-x2/b)
^2*sin(n*Pie*(1/2+x2/2/b))):
```

```

>phi(1) := subs(m=1,n=1,fun) :   phi(2) := subs(m=1,n=2,fun) :
phi(3) := subs(m=2,n=1,fun) :   phi(4) := subs(m=2,n=2,fun) :
>
>plot3d(phi(1), x1=-a..a, x2=-b..b, axes=BOXED,
lightmodel=light3,
color=gray,title="SHAPE FUNCTION 1  m=1 , n=1" );
>
>plot3d(phi(2), x1=-a..a, x2=-b..b, axes=BOXED,
lightmodel=light3,
color=gray,title="SHAPE FUNCTION 2  m=1 , n=2" );
>
>plot3d(phi(3), x1=-a..a, x2=-b..b, axes=BOXED,
lightmodel=light3,
color=gray,title="SHAPE FUNCTION 3  m=2 , n=1" );

>plot3d(phi(4), x1=-a..a, x2=-b..b, axes=BOXED,
lightmodel=light3,
color=gray,title="SHAPE FUNCTION 4  m=2 , n=2" );

>Phi:=matrix(1,4,[phi(1),phi(2),phi(3),phi(4)]);
Φ := [sin(1.570796325 + 5.235987748x1)(1 + 10.x2)2(1 - 10.x2)2
      sin(1.570796325 + 15.70796325x2),
      sin(1.570796325 + 5.235987748x1)
      (1 + 10.x2)2(1 - 10.x2)2 sin(3.141592650 + 31.41592650x2),
      sin(3.141592650 + 10.47197550x1)(1 + 10.x2)2(1 - 10.x2)2
      sin(1.570796325 + 15.70796325x2),
      sin(3.141592650 + 10.47197550x1)
      (1 + 10.x2)2(1 - 10.x2)2 sin(3.141592650 + 31.41592650x2)]
>
>Phihatrow1:=simplify(map(diff,Phi,x1,x1)):
>Phihatrow2:=simplify(map(diff,Phi,x2,x2)):
>Phihatrow3:=simplify(map(diff,Phi,x1,x2)):
>Phihat:=stackmatrix(Phihatrow1,Phihatrow2,2*Phihatrow3):
>Phihat:=matrix(3,4,Phihat):
>Ehat:=matrix(3,3,[1,nu,0,nu,1,0,0,0,(1-nu)/2]):
>thk:= tmin + (tmax - tmin) * (x2/b) ^2 :
>
># Evaluate Stiffness Matrix
>Kmat := simplify(evalm(E/12/(1-nu^2)*thk^3*transpose
(Phihat)&*Ehat&*Phihat)):
>Kmat := simplify(map(int,evalm(Kmat),x1=-a..a)):
>
>Kmat:= simplify(map(int,evalm(Kmat),x2=-b..b));

```

$$Kmat := \begin{bmatrix} 0.2080690074 \cdot 10^7 & 0.002945363596 & 0.0002867800424 & 0.5000809593 \\ 0.002945363623 & 0.7629397779 \cdot 10^7 & 0.5000809737 \cdot 10^{-12} & 0.0005288867360 \\ 0.0002867800424 & 0.5000809737 \cdot 10^{-12} & 0.2359860115 \cdot 10^7 & 0.003438333736 \\ 0.5000809667 \cdot 10^{-12} & 0.0005288867360 & 0.003438333736 & 0.8130102610 \end{bmatrix}$$

```

># Evaluate Mass Matrix
>Mmat := simplify( evalm( rho*thk*transpose( Phi ) &*Phi ) ):
>Mmat := simplify( map( int, evalm( Mmat ), x1=-a..a ) ):
>Mmat := simplify( map( int, evalm( Mmat ), x2=-b..b ) );

```

$$Mmat := \begin{bmatrix} 0.3152796693, 0.6289456068 \cdot 10^{-9}, -0.4094541153 \cdot 10^{-18}, -0.8168124791 \cdot 10^{-27} \\ 0.6289456068 \cdot 10^{-9}, 0.1797055656, -0.8168124791 \cdot 10^{-27}, -0.2333838511 \cdot 10^{-18} \\ -0.4094541153 \cdot 10^{-18}, -0.8168124791 \cdot 10^{-27}, 0.3152796691, 0.6289456160 \cdot 10^{-9} \\ -0.8168124791 \cdot 10^{-27}, -0.2333838511 \cdot 10^{-18}, 0.6289456160 \cdot 10^{-9}, 0.1797055655 \end{bmatrix}$$

EXAMPLE 4.6.7 Longitudinal Vibration of a Mixed Rigid–Flexible Body System with Concentrated and Distributed Mass, Stiffness, and Damping

Description: The triangular bar shown in Figure E4.6.7(a) vibrates in its longitudinal (x) direction. The bar has a distributed external damping $\tilde{c}(x)$ (per unit length) and an internal, viscoelastic, strain-rate damping $\gamma EA \frac{\partial \dot{u}}{\partial x}$. The triangular bar is subjected to a force per unit length \tilde{f}_0 along its entire length and to a concentrated force \bar{f} applied at $x=L/4$. The forcing functions \tilde{f}_0 and \bar{f} vary with time but not with x .

Objective: Derive an approximate set of differential equations for the assumed modes generalized coordinates.

Assumptions: Assume that $\gamma, \tilde{c}, E, A_0$, and ρ are constants.

The cross-sectional area of the bar varies with x according to

$$A(x) = A_0 \left(1 - \frac{x}{L} \right) \quad (1)$$

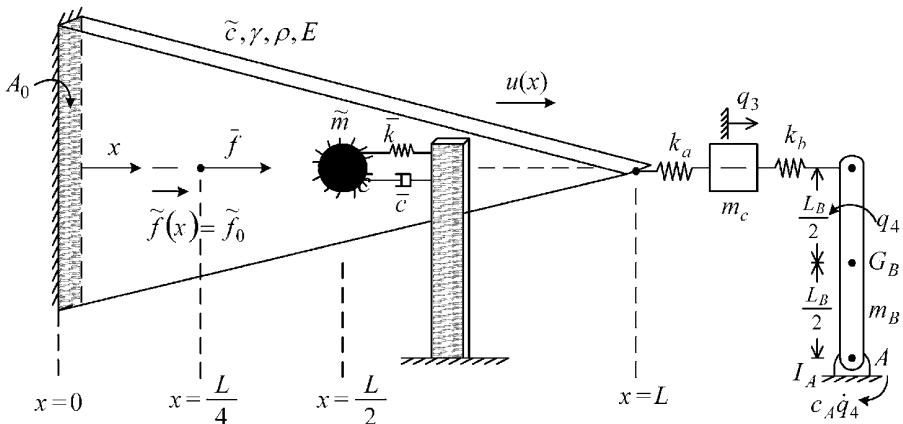


Figure E4.6.7(a) Axial vibration model for a triangular bar–mass–pendulum system

The concentrated mass \tilde{m} is welded to the triangular bar in the above figure. The assumed modes deflection interpolation expression for this example is

$$u \approx q_1(t)\phi_1(x) + q_2(t)\phi_2(x) \quad (2)$$

where

$$\phi_1(x) = \sin\left(\frac{\pi x}{2L}\right), \quad \phi_2(x) = \sin\left(\frac{3\pi x}{2L}\right) \quad (3)$$

Note that both ϕ_1 and ϕ_2 are kinematically admissible since

$$\phi_1(x=0) = \phi_2(x=0) = 0 \quad (4)$$

that is, they satisfy the deflection boundary conditions.

(a) Begin by deriving the EOMs for only the isolated triangular bar system with the attached concentrated mass \tilde{m} . This will be coupled with the remaining components in step (b).

Obtain the mass matrix coefficients from (4.6.65) with $A(x)$ from (1), $\rho = \text{constant}$, a point mass \tilde{m} at $x=L/2$ and $\phi_l(x)$ from (3)

$$\tilde{m}_{jk} = \rho \int_0^L A_0 \left(1 - \frac{x}{L}\right) \phi_j(x) \phi_k(x) dx + \tilde{m} \phi_j\left(\frac{L}{2}\right) \phi_k\left(\frac{L}{2}\right) \quad (5)$$

with

$$\phi_1\left(\frac{L}{2}\right) = \frac{\sqrt{2}}{2}, \quad \phi_2\left(\frac{L}{2}\right) = \frac{\sqrt{2}}{2} \quad (6)$$

The second term in (5) results from the kinetic energy contribution from \tilde{m} and can be derived with formulas (2.6.46) and (2.6.47):

$$\begin{aligned} \frac{d}{dt} \left(\frac{\partial T_{\tilde{m}}}{\partial \dot{q}_j} \right) &= \frac{d}{dt} \left(\frac{\partial}{\partial \dot{q}_j} \left(\frac{\tilde{m}}{2} \dot{u} \left(\frac{L}{2}, t \right)^2 \right) \right) = \frac{d}{dt} \left(\frac{\partial}{\partial \dot{q}_j} \left(\frac{\tilde{m}}{2} \left(\sum_{i=1}^2 \dot{q}_i \phi_i \left(\frac{L}{2} \right) \right)^2 \right) \right) \\ &= \tilde{m} \phi_j \left(\frac{L}{2} \right) \left(\ddot{q}_1 \phi_1 \left(\frac{L}{2} \right) + \ddot{q}_2 \phi_2 \left(\frac{L}{2} \right) \right) \end{aligned} \quad (7)$$

Evaluation of the integrals in (5) yields

$$\begin{aligned} \tilde{m}_{11} &= \frac{\rho A_0 L}{4} \left(1 - \frac{4}{\pi^2} \right) + \frac{\tilde{m}}{2} \\ \tilde{m}_{12} = \tilde{m}_{21} &= \frac{\rho A_0 L}{\pi^2} + \frac{\tilde{m}}{2} \\ \tilde{m}_{22} &= \frac{\rho A_0 L}{4} \left(1 - \frac{4}{9\pi^2} \right) + \frac{\tilde{m}}{2} \end{aligned} \quad (8)$$

Obtain the stiffness coefficients from (4.6.73) to (4.6.76):

$$\underline{\varepsilon} = \underline{D} \underline{u} \Rightarrow \underline{B} = \underline{D} \underline{\Phi} \Rightarrow \underline{K} = \int_V \underline{B}^T \underline{E} \underline{B} dV \quad (9)$$

The strain–displacement relation for simple uniaxial deformation of the bar is

$$\varepsilon = \frac{\partial u}{\partial x} \Rightarrow D = \frac{\partial}{\partial x} \quad (10)$$

Therefore, the \underline{B} matrix becomes

$$\underline{B} = \underline{D} \underline{\Phi} = \frac{\partial}{\partial x} [\phi_1 \quad \phi_2] = \left[\frac{d\phi_1}{dx} \quad \frac{d\phi_2}{dx} \right] \quad (11)$$

Substitute this form of \underline{B} along with the volume differential expression $dV = A(x)dx$ into the above formula for \underline{K} to obtain

$$\tilde{k}_{jk} = EA_0 \int_0^L \left(1 - \frac{x}{L}\right) \frac{d\phi_j}{dx} \frac{d\phi_k}{dx} dx + \bar{k} \phi_j \left(\frac{L}{2}\right) \phi_k \left(\frac{L}{2}\right) \quad (12)$$

From (3),

$$\frac{d\phi_1}{dx} = \frac{\pi}{2L} \cos\left(\frac{\pi x}{2L}\right), \quad \frac{d\phi_2}{dx} = \frac{3\pi}{2L} \cos\left(\frac{3\pi x}{2L}\right) \quad (13)$$

Therefore, (12) yields

$$\tilde{k}_{11} = \frac{EA_0}{4L} \left(1 - \frac{\pi^2}{4}\right) + \frac{\bar{k}}{2}, \quad \tilde{k}_{12} = \tilde{k}_{21} = \frac{3EA_0}{4L} + \frac{\bar{k}}{2}, \quad \tilde{k}_{22} = \frac{EA_0}{4L} \left(1 + \frac{9\pi^2}{4}\right) + \frac{\bar{k}}{2} \quad (14)$$

The second term in (12) results from the potential energy stored in the “spring to ground” \bar{k} and can be derived with the generalized force (4.6.25) and the formulas (2.6.46) and (2.6.47):

$$\begin{aligned} Q_j^{\bar{k}} &= - \left(\frac{\partial U}{\partial q_j} \right) = \frac{\partial}{\partial q_j} \left(\frac{\bar{k}}{2} u \left(\frac{L}{2}, t \right)^2 \right) \\ &= \frac{\partial}{\partial q_j} \left(\frac{\bar{k}}{2} \left(\sum_{i=1}^2 q_i \phi_i \left(\frac{L}{2} \right) \right)^2 \right) = \bar{k} \phi_j \left(\frac{L}{2} \right) \left(q_1 \phi_1 \left(\frac{L}{2} \right) + q_2 \phi_2 \left(\frac{L}{2} \right) \right) \end{aligned} \quad (15)$$

Obtain the damping coefficients from the Rayleigh dissipation function \mathfrak{S}^d for this system (4.5.81):

$$\mathfrak{S}^d = \int_0^L \left(\frac{\tilde{c}}{2} \dot{u}^2 + \frac{\gamma EA}{2} \left(\frac{\partial \dot{u}}{\partial x} \right)^2 \right) dx + \frac{\bar{c}}{2} \dot{u} \left(\frac{L}{2}, t \right)^2 \quad (16)$$

Therefore, the generalized force due to damping is (4.5.82):

$$Q_j^c = - \frac{\partial \mathfrak{S}^d}{\partial \dot{q}_j} = - \int_0^L \left(\tilde{c} \dot{u} \frac{\partial \dot{u}}{\partial q_j} + \gamma EA \frac{\partial \dot{u}}{\partial x} \frac{\partial}{\partial \dot{q}_j} \left(\frac{\partial \dot{u}}{\partial x} \right) \right) dx - \bar{c} \dot{u} \left(\frac{L}{2}, t \right) \frac{\partial}{\partial \dot{q}_j} \left(\dot{u} \left(\frac{L}{2}, t \right) \right) \quad (17)$$

where

$$u(x, t) = q_1(t) \phi_1(x) + q_2(t) \phi_2(x) \quad (18)$$

Substitution of (18) into Q_j^c yields

$$Q_j^c = -c_{j1}\dot{q}_1 - c_{j2}\dot{q}_2 \quad (19)$$

where

$$\tilde{c}_{jk} = \tilde{c} \int_0^L \phi_j \phi_k dx + \gamma EA_0 \int_0^L \left(1 - \frac{x}{L}\right) \frac{d\phi_j}{dx} \frac{d\phi_k}{dx} dx + \bar{c} \phi_j \left(\frac{L}{2}\right) \phi_k \left(\frac{L}{2}\right) \quad (20)$$

$$\begin{aligned} \tilde{c}_{11} &= \tilde{c} \int_0^L \sin\left(\frac{\pi x}{2L}\right) \sin\left(\frac{\pi x}{2L}\right) dx + \gamma EA_0 \int_0^L \left(1 - \frac{x}{L}\right) \frac{\pi}{2L} \frac{\pi}{2L} \cos\left(\frac{\pi x}{2L}\right)^2 dx + \frac{\bar{c}}{2} \\ &= \tilde{c} \frac{L}{2} + \frac{\gamma EA_0}{4L} \left(1 + \frac{\pi^2}{4}\right) + \frac{\bar{c}}{2} \end{aligned} \quad (21)$$

and

$$\begin{aligned} \tilde{c}_{12} &= \tilde{c}_{21} \\ &= \tilde{c} \int_0^L \sin\left(\frac{\pi x}{2L}\right) \sin\left(\frac{3\pi x}{2L}\right) dx + \gamma EA_0 \int_0^L \left(1 - \frac{x}{L}\right) \frac{\pi}{2L} \frac{3\pi}{2L} \cos\left(\frac{\pi x}{2L}\right) \cos\left(\frac{3\pi x}{2L}\right) dx + \frac{\bar{c}}{2} \\ &= \frac{3\gamma EA_0}{4L} + \frac{\bar{c}}{2} \end{aligned} \quad (22)$$

$$\begin{aligned} \tilde{c}_{22} &= \tilde{c} \int_0^L \sin\left(\frac{3\pi x}{2L}\right) \sin\left(\frac{3\pi x}{2L}\right) dx \\ &\quad + \gamma EA_0 \int_0^L \left(1 - \frac{x}{L}\right) \frac{3\pi}{2L} \frac{3\pi}{2L} \cos\left(\frac{3\pi x}{2L}\right) \cos\left(\frac{3\pi x}{2L}\right) dx + \frac{\bar{c}}{2} \\ &= \tilde{c} \frac{L}{2} + \frac{\gamma EA_0}{4L} \left(1 + \frac{9\pi^2}{4}\right) + \frac{\bar{c}}{2} \end{aligned} \quad (23)$$

The concentrated force \bar{f} is treated as a Dirac delta-type force distribution as explained in Section 2.12, and the distributed force \bar{f}_0 only varies with time; therefore, (4.6.86) yields

$$\tilde{Q}_1 = \tilde{f}_0 \int_0^L \phi_1 dx + \bar{f} \phi_1 \left(\frac{L}{4}\right) = \frac{2L}{\pi} \tilde{f}_0 + 0.383 \bar{f}(t) \quad (24)$$

$$\tilde{Q}_2 = f_0 \int_0^L \phi_2 dx + \bar{f} \phi_2 \left(\frac{L}{4}\right) = \frac{2L}{3\pi} f_0 + 0.942 \bar{f}(t) \quad (25)$$

System Equations

The system EOMs are obtained with the mass, stiffness, damping, and generalized force terms derived above as

$$\begin{bmatrix} \tilde{m}_{11} & \tilde{m}_{12} \\ \tilde{m}_{21} & \tilde{m}_{22} \end{bmatrix} \begin{Bmatrix} \ddot{q}_1 \\ \ddot{q}_2 \end{Bmatrix} + \begin{bmatrix} \tilde{c}_{11} & \tilde{c}_{12} \\ \tilde{c}_{21} & \tilde{c}_{22} \end{bmatrix} \begin{Bmatrix} \dot{q}_1 \\ \dot{q}_2 \end{Bmatrix} + \begin{bmatrix} \tilde{k}_{11} & \tilde{k}_{12} \\ \tilde{k}_{21} & \tilde{k}_{22} \end{bmatrix} \begin{Bmatrix} q_1 \\ q_2 \end{Bmatrix} = \begin{Bmatrix} \tilde{Q}_1 \\ \tilde{Q}_2 \end{Bmatrix} \quad (26)$$

Equation (26) may be solved for $q_1(t)$ and $q_2(t)$ by numerical or numerical integration means. The axial displacement u at any location (x) along the length of the bar is then obtained from (2) as

$$u(x,t) = \phi_1(x)q_1(t) + \phi_2(x)q_2(t) \quad (27)$$

where $\phi_1(x)$ and $\phi_2(x)$ are defined in (3).

(b) Next, consider the entire system including the plate, attached concentrated mass \tilde{m} , sprung mass m_c , and the inverted pendulum m_B .

- The additional kinetic energy from the mass and pendulum is (Figure E4.6.7 (a), (4.2.14))

$$T_A = \frac{m_c}{2} \dot{q}_3^2 + \frac{I_A}{2} \dot{q}_4^2 \quad (28)$$

The related terms in Lagrange's equations are

$$\frac{\partial T_A}{\partial q_j} = 0 \quad (29)$$

$$\frac{d}{dt} \left(\frac{\partial T_A}{\partial \dot{q}_j} \right) = \begin{cases} 0, & j=1 \\ 0, & j=2 \\ m_c \ddot{q}_3, & j=3 \\ I_A \ddot{q}_4, & j=4 \end{cases} \quad (30)$$

- The additional generalized force terms are

$$Q_{jA} = \sum \bar{F}_l \cdot \frac{\partial \bar{v}_l}{\partial \dot{q}_j} = 0 \cdot \frac{\partial \bar{v}_l}{\partial \dot{q}_j} = 0 \quad (31)$$

that is, no additional generalized forces result since the velocities of the points of applications of \bar{f} and \bar{f} are independent of \dot{q}_3 and \dot{q}_4 .

- The additional Rayleigh dissipation function term (4.5.78) is

$$\mathfrak{S}_A^d = \frac{c_A}{2} \dot{q}_4^2 \quad (32)$$

The new terms in Lagrange's equations are

$$\frac{\partial \mathfrak{S}_A^d}{\partial \dot{q}_j} = \begin{cases} 0, & j=1 \\ 0, & j=2 \\ 0, & j=3 \\ c_A \dot{q}_4, & j=4 \end{cases} \quad (33)$$

- The additional potential energy terms (4.5.57), (4.5.65) are

$$U_A = \frac{k_a}{2} (q_3 - u(L,t))^2 + \frac{k_b}{2} (q_3 + L_B q_4)^2 - m_B g \frac{L_B}{2} (1 - \cos q_4) \quad (34)$$

where $\cos(q_4) \approx 1 - q_4^2/2$ for small angles q_4 , and from (2) and (3),

$$u(L, t) = \phi_1(L)q_1 + \phi_2(L)q_2 = q_1 - q_2 \quad (35)$$

Therefore,

$$U_A \approx \frac{k_a}{2}(q_3 - q_1 + q_2)^2 + \frac{k_b}{2}(q_3 + L_B q_4)^2 - m_B g \frac{L_B}{2} q_4^2 \quad (36)$$

The new potential energy terms in Lagrange's equations are

$$\frac{\partial U_A}{\partial q_j} = \begin{cases} -k_a(q_3 - q_1 + q_2), & j=1 \\ k_a(q_3 - q_1 + q_2), & j=2 \\ k_a(q_3 - q_1 + q_2) + k_b(q_3 + L_B q_4), & j=3 \\ k_b(q_3 + L_B q_4)L_B - m_B g \frac{L_B}{2} q_4^2, & j=4 \end{cases} \quad (37)$$

Combining these additional terms for Lagrange's equations with those from part (a) yields the total system EOM:

$$\underset{4 \times 4}{\underline{M}} \underset{4 \times 1}{\ddot{q}} + \underset{4 \times 4}{\underline{C}} \underset{4 \times 1}{\dot{q}} + \underset{4 \times 4}{\underline{K}} \underset{4 \times 1}{q} = \underset{4 \times 1}{\underline{Q}(t)} \quad (38)$$

where

$$\underset{4 \times 4}{\underline{M}} = \begin{bmatrix} \tilde{m}_{11} & \tilde{m}_{12} & 0 & 0 \\ \tilde{m}_{12} & \tilde{m}_{22} & 0 & 0 \\ 0 & 0 & m_c & 0 \\ 0 & 0 & 0 & I_A \end{bmatrix}, \quad \underset{4 \times 4}{\underline{C}} = \begin{bmatrix} \tilde{c}_{11} & \tilde{c}_{12} & 0 & 0 \\ \tilde{c}_{12} & \tilde{c}_{22} & 0 & 0 \\ 0 & 0 & 0 & 0 \\ 0 & 0 & 0 & c_A \end{bmatrix} \quad (39)$$

$$\underset{4 \times 4}{\underline{K}} = \begin{bmatrix} \tilde{k}_{11} + k_a & \tilde{k}_{12} - k_a & -k_a & 0 \\ \tilde{k}_{12} - k_a & \tilde{k}_{22} + k_a & k_a & 0 \\ -k_a & k_a & k_a + k_b & k_B L_B \\ 0 & 0 & k_b L_B & k_B L_B^2 - m_B \frac{g L_B}{2} \end{bmatrix} \quad (40)$$

The force vector in (39) is given by (24), (25), and (31) as

$$\underline{Q} = \begin{Bmatrix} \tilde{Q}_1 \\ \tilde{Q}_2 \\ 0 \\ 0 \end{Bmatrix} = \begin{Bmatrix} \frac{2L}{\pi} \tilde{f}_0(t) + 0.383 \tilde{f}(t) \\ \frac{2L}{3\pi} \tilde{f}_0(t) + 0.924 \tilde{f}(t) \\ 0 \\ 0 \end{Bmatrix} \quad (41)$$

Equation (38) may be solved for $q_1(t)$, $q_2(t)$, $q_3(t)$, and $q_4(t)$ by analytical or numerical integration means. The axial displacement u at any location (x) along the length of the bar is then obtained from (2):

$$u(x, t) = \phi_1(x)q_1(t) + \phi_2(x)q_2(t) \quad (42)$$

where by (3)

$$\phi_1(x) = \sin\left(\frac{\pi x}{2L}\right), \quad \phi_2(x) = \sin\left(\frac{3\pi x}{2L}\right) \quad (43)$$

4.7 LE FOR FLEXIBLE, DISTRIBUTED MASS BODIES: FINITE ELEMENT APPROACH—GENERAL FORMULATION

This section provides the framework for obtaining the finite element-based EOMs for any linear finite element model. An 8-node, 3-degree of freedom (dof) per node element is utilized to illustrate the theory component of this framework. The theory applies to any element with an arbitrary number of nodes and dofs per node. The theory will be utilized for truss elements in Section 4.8, beam elements with 2 nodes and 6 dof per node in Chapter 9, plane stress–strain elements with 4 nodes and 2 dof per node, in Chapter 10, and 3D solid elements with 8 nodes and 3 dof per node in Chapter 11.

4.7.1 Element Kinetic Energy and Mass Matrix

Recall from Figure 2.11.10 and Equation (4.2.3) that the most general expression for kinetic energy is

$$T = \frac{1}{2} \int_V \frac{^n d}{dt}(\vec{R}) \cdot \frac{^n d}{dt}(\vec{R}) dm \quad (4.7.1)$$

For the FEM, the domain V is subdivided into subdomains called elements, as depicted in Figure 2.11.10. Consequently, T may be written as

$$T = \sum_{e=1}^{N_e} T_e \quad (4.7.2)$$

where

$$T_e = \frac{1}{2} \int_{V_e} \frac{^n d}{dt}(\vec{R}) \cdot \frac{^n d}{dt}(\vec{R}) \rho dV \quad (4.7.3)$$

N_e : number of elements in the model

T_e : kinetic energy contributed to the system kinetic energy by element e (4.7.4)

V_e : domain of element e

The deflections within V_e are given, for example, in an 8-node element by (2.11.36)

$$u_j^e(x_1^e, x_2^e, x_3^e, t) = \sum_{k=1}^8 u_{jk}^e(t) N_k^e(x_1^e, x_2^e, x_3^e) \quad j=1,2,3 \quad (4.7.5)$$

The velocity shape functions are called “consistent” if they are the same as those used for the displacement interpolation, that is,

$${}^n v_j^e(x_1^e, x_2^e, x_3^e, t) = \frac{{}^n d}{dt} u_j^e(x_1^e, x_2^e, x_3^e, t) = \sum_{k=1}^8 \dot{u}_{jk}^e(t) N_k^e(x_1^e, x_2^e, x_3^e) \quad (4.7.6)$$

where $\dot{u}_{jk}^e(t)$ is the velocity of mode k of element e , in direction j , as sensed in frame n .

Therefore,

$$\frac{{}^n d}{dt} \underline{\underline{R}} = {}^n v_1^e n_1 + {}^n v_2^e n_2 + {}^n v_3^e n_3 \quad (4.7.7)$$

and from (4.7.3),

$$\begin{aligned} T_e &= \frac{1}{2} \int_{V_e} \left[({}^n v_1^e)^2 + ({}^n v_2^e)^2 + ({}^n v_3^e)^2 \right] \rho dV \\ &= \frac{1}{2} \int_{V_e} \sum_{i=1}^8 \sum_{k=1}^8 (\dot{u}_{1k}^e \dot{u}_{1i}^e N_k^e N_i^e + \dot{u}_{2k}^e \dot{u}_{2i}^e N_k^e N_i^e + \dot{u}_{3k}^e \dot{u}_{3i}^e N_k^e N_i^e) \rho dV \\ &= \frac{1}{2} \sum_{i=1}^8 \sum_{k=1}^8 \left(\dot{u}_{1k}^e \dot{u}_{1i}^e \int_{V_e} N_k^e N_i^e \rho dV + \dot{u}_{2k}^e \dot{u}_{2i}^e \int_{V_e} N_k^e N_i^e \rho dV + \dot{u}_{3k}^e \dot{u}_{3i}^e \int_{V_e} N_k^e N_i^e \rho dV \right) \\ &= \frac{1}{2} (\underline{\underline{U}}_{e1}^T \underline{\underline{m}}_e \underline{\underline{U}}_{e1} + \underline{\underline{U}}_{e2}^T \underline{\underline{m}}_e \underline{\underline{U}}_{e2} + \underline{\underline{U}}_{e3}^T \underline{\underline{m}}_e \underline{\underline{U}}_{e3}) \end{aligned} \quad (4.7.8)$$

where

$$\underline{\underline{U}}_{e1} = (\dot{u}_{11}^e \quad \dot{u}_{12}^e \quad \cdots \quad \dot{u}_{18}^e)^T = \text{eight nodal velocities in direction } n_1 \quad (8 \times 1)$$

$$\underline{\underline{U}}_{e2} = (\dot{u}_{21}^e \quad \dot{u}_{22}^e \quad \cdots \quad \dot{u}_{28}^e)^T = \text{eight nodal velocities in direction } n_2 \quad (8 \times 1) \quad (4.7.9)$$

$$\underline{\underline{U}}_{e3} = (\dot{u}_{31}^e \quad \dot{u}_{32}^e \quad \cdots \quad \dot{u}_{38}^e)^T = \text{eight nodal velocities in direction } n_3 \quad (8 \times 1)$$

$$(\underline{\underline{m}}_e)_{ki} = \int_{V_e} N_k^e N_i^e \rho dV \quad (4.7.10)$$

Define the vector of generalized coordinates as the nodal displacements:

$$\begin{aligned} \underline{\underline{q}}_e &= \begin{Bmatrix} \underline{\underline{U}}_{e1} \\ \underline{\underline{U}}_{e2} \\ \underline{\underline{U}}_{e3} \end{Bmatrix} = (u_{11}^e \quad u_{12}^e \quad \cdots \quad u_{18}^e \quad u_{21}^e \quad u_{22}^e \quad \cdots \quad u_{28}^e \quad u_{31}^e \quad u_{32}^e \quad \cdots \quad u_{38}^e)^T \\ &= (q_1 \quad q_2 \quad q_3 \quad \cdots \quad q_{24})^T \\ &= \text{element } e\text{'s nodal displacements that occur at its 8 nodes in the } n_1, n_2, \\ &\quad \text{and } n_3 \text{ directions} \end{aligned} \quad (4.7.11)$$

The kinetic energy in (4.7.8) then becomes

$$T_e = T_e(\dot{q}_1 \quad \dot{q}_2 \quad \dot{q}_3 \quad \cdots \quad \dot{q}_{24}) = \frac{1}{2} \underline{\underline{\dot{q}}}_e^T \underset{(1 \times n)}{\underline{\underline{M}}_e} \underset{(n \times 1)}{\underline{\underline{\dot{q}}}_e} \quad (1 \times 1) \quad (4.7.12)$$

where

$$n = 24 = \text{number of independent generalized coordinates} \quad (4.7.13)$$

$$\underline{M}_e = \text{“consistent” mass matrix of element } e = \begin{bmatrix} \underline{\tilde{m}}_e & \underline{0} & \underline{0} \\ \underline{0} & \underline{\tilde{m}}_e & \underline{0} \\ \underline{0} & \underline{0} & \underline{\tilde{m}}_e \end{bmatrix} \quad (4.7.14)$$

\underline{M}_e $\begin{matrix} (n \times n) \\ (8 \times 8) \end{matrix}$ $\begin{matrix} (8 \times 8) \\ (8 \times 8) \\ (8 \times 8) \end{matrix}$

$\underline{\tilde{m}}_e$ is defined in (4.7.10), and the term “consistent” refers to the velocity and displacement shape functions being identical. Note that as in the RB or assumed modes approximations, the finite element approximation yields a kinetic energy expression (4.7.12) of the form

$$T = T(\dot{q}_1 \quad \dot{q}_2 \quad \dot{q}_3 \quad \cdots \quad \dot{q}_{24}) \quad (4.7.15)$$

where q_i are the *generalized coordinates*.

4.7.2 Element Stiffness Matrix

From (2.11.36) and Figure 2.11.10, the displacements within an 8-node brick element (e) are interpolated from the nodal displacements according to

$$\underline{u} = \begin{Bmatrix} u_1^e(x_1, x_2, x_3, t) \\ u_2^e(x_1, x_2, x_3, t) \\ u_3^e(x_1, x_2, x_3, t) \end{Bmatrix} = \begin{Bmatrix} \sum_{k=1}^8 u_{1k}^e(t) N_k^e(x_1, x_2, x_3) \\ \sum_{k=1}^8 u_{2k}^e(t) N_k^e(x_1, x_2, x_3) \\ \sum_{k=1}^8 u_{3k}^e(t) N_k^e(x_1, x_2, x_3) \end{Bmatrix} \quad (4.7.16)$$

$$= \begin{bmatrix} N_1^e & N_2^e & \cdots & N_8^e & \underline{0} & \underline{0} \\ \underline{0} & \underline{0} & \cdots & \underline{0} & N_1^e & N_2^e & \cdots & N_8^e & \underline{0} \\ \underline{0} & \underline{0} & \cdots & \underline{0} & \underline{0} & \underline{0} & \cdots & \underline{0} & N_1^e & N_2^e & \cdots & N_8^e \end{bmatrix} \begin{Bmatrix} u_{11}^e \\ u_{12}^e \\ \vdots \\ u_{18}^e \\ u_{21}^e \\ u_{22}^e \\ \vdots \\ u_{28}^e \\ u_{31}^e \\ u_{32}^e \\ \vdots \\ u_{38}^e \end{Bmatrix}$$

or

$$\underline{u}^e(x_1, x_2, x_3, t) = \underline{N}^e(x_1, x_2, x_3) \underline{q}_e(t) \quad (4.7.17)$$

$3 \times 1 \qquad \qquad \qquad 3 \times 24 \qquad \qquad \qquad 24 \times 1$

where

$$\underline{q}_e = (u_{11}^e \cdots u_{18}^e \ u_{21}^e \cdots u_{28}^e \ u_{31}^e \cdots u_{38}^e)^T = (q_{1e} \cdots q_{24e})^T \quad (4.7.18)$$

$u_{jk}^e(t)$ = deflection of node k of element e , in the j th direction

$e = 1, n_E$ (number of elements in model)

$j = 1, 2, 3$

$k = 1, 2, \dots, 8$

$$(4.7.19)$$

and

$$N_k^e = k\text{th shape function (given) of element } e \quad (4.7.20)$$

Substitution of (4.7.17) into (A.3.19) yields

$$\underline{\varepsilon}_e = \left(\begin{array}{c} D \\ \hline 6 \times 3 \quad 3 \times 24 \end{array} \right) \underline{q}_e \quad (4.7.21)$$

$6 \times 1 \qquad \qquad \qquad 24 \times 1$

or

$$\underline{\varepsilon}_e = \underline{B}_e \underline{q}_e \quad (4.7.22)$$

$6 \times 1 \quad 6 \times 24 \quad 24 \times 1$

where

$$\underline{B}_e = [\underline{B}_{1e} \ \underline{B}_{2e} \ \cdots \ \underline{B}_{24e}] = \underline{D} \ \underline{N}^e \quad (4.7.23)$$

$6 \times 24 \qquad \qquad \qquad 6 \times 24 \qquad \qquad \qquad 6 \times 3 \quad 3 \times 24$

$$\underline{B}_{je} = j\text{th column of } \underline{B}_e \quad (4.7.24)$$

6×1

Note that from (4.7.21) and (4.7.23)

$$\underline{\varepsilon} = \sum_{i=1}^{24} q_i \underline{B}_{ie} \quad (4.7.25)$$

Then

$$\frac{\partial \varepsilon}{\partial q_j} = \underline{B}_{je} \quad (4.7.26)$$

Substitute (4.7.22) and (4.7.23) into (4.6.27) to obtain

$$Q_j^{le} = - \int_{V_e} \underline{B}_{je}^T \underline{E}_e \underline{B}_e \underline{q}_e \, dV \quad (4.7.27)$$

$1 \times 6 \quad 6 \times 6 \quad 6 \times 24 \quad 24 \times 1$

The vector of all internal force-related generalized forces becomes

$$\underline{Q}^{le} = \begin{Bmatrix} Q_1^{le} \\ Q_2^{le} \\ \vdots \\ Q_{24}^{le} \end{Bmatrix}_{24 \times 1} = - \int_{V_e} \begin{bmatrix} \underline{B}_{1e}^T \\ \underline{B}_{2e}^T \\ \vdots \\ \underline{B}_{24e}^T \end{bmatrix}_{24 \times 6} \underline{E}_e \underline{B}_e dV \underline{q}_e \quad (4.7.28)$$

Summarizing these results yields

Generalized Force Vector of Internal Forces for a Finite Element (8-Node Brick)

$$\underline{Q}^{le}(t) = \begin{Bmatrix} Q_1^{le} \\ Q_2^{le} \\ \vdots \\ Q_{24}^{le} \end{Bmatrix}_{24 \times 1} = - \underline{K}_e \underline{q}_e(t) \quad (4.7.29)$$

where

$$\underline{K}_e = \int_{V_e} \underline{B}_e^T \underline{E}_e \underline{B}_e dV = \text{element stiffness matrix} \quad (4.7.30)$$

$$\underline{B}_e = \underline{D} \underline{N}^e \quad (4.7.31)$$

$$\underline{u}^e = \underline{N}^e \underline{q}_e \quad (4.7.32)$$

$$\underline{\varepsilon}_e = \underline{D} \underline{u}^e \quad (4.7.33)$$

$$V_e = \text{volume of element } e \quad (4.7.34)$$

Note that

$$\underline{u}^e = \underline{N}^e \underline{q}_e(t) = \sum_{i=1}^{24} \underline{N}_i^e q_i^e \quad (4.7.35)$$

where \underline{N}_i^e is the i th column of \underline{N}^e . Therefore,

$$\frac{\partial \underline{u}^e}{\partial q_i^e} = \underline{N}_i^e \quad (4.7.36)$$

Substitute (4.7.36) into (4.6.47) to obtain

$$\underline{Q}_j^e = \int_{V_e} \underline{\bar{F}}_{EV}^T \underline{N}_j^e dV_e + \int_{S_e} \underline{\bar{F}}_{ES}^T \underline{N}_j^e dS_e \quad (4.7.37)$$

where dV_e is the element's differential volume and S_e is the portion of the element's surface where external tractions are applied. Utilize (4.7.16) and (4.7.37) to obtain

Generalized Force Vector of External Forces for an 8-Node Brick-Type Finite Element

$$\begin{aligned} Q_j^e &= \int_{V_e} \bar{F}_{EV1} N_j^e dV_e + \int_{S_e} \bar{F}_{ES1} N_j^e dS_e \\ Q_{j+8}^e &= \int_{V_e} \bar{F}_{EV2} N_j^e dV_e + \int_{S_e} \bar{F}_{ES2} N_j^e dS_e \\ Q_{j+16}^e &= \int_{V_e} \bar{F}_{EV3} N_j^e dV_e + \int_{S_e} \bar{F}_{ES3} N_j^e dS_e \\ &\text{for } j = 1, 2, \dots, 8 \end{aligned} \quad (4.7.38)$$

The externally applied forces (\bar{F}_{EVk} , \bar{F}_{ESk}) and element shape functions are known (given) functions of position (x_1, x_2, x_3) in element volume V_e or on the element bounding surface S_e . Hence, the Q_j may be evaluated per the integrations in (4.7.38).

4.7.3 Summary

The following provides a summary of the general formulation for finite elements. An 8-node, 3-degree of freedom (dof) per node element is treated for illustration. Similar formulations apply for elements with arbitrary number of nodes and dofs per node.

Finite Element Kinetic Energy and Mass Matrix

This displacement within element e are interpolated as

$$u_j^e(x_1^e, x_2^e, x_3^e, t) = \sum_{k=1}^8 u_{jk}^e(t) N_k^e(x_1^e, x_2^e, x_3^e) \quad j = 1, 2, 3 \quad (4.7.39)$$

in the element volume V_e where the $u_{jk}^e(t)$ are nodal displacements and $N_k^e(x_1^e, x_2^e, x_3^e)$ are given shape functions. The kinetic energy of element e is

$$T_e = T_e(\dot{q}_1 \quad \dot{q}_2 \quad \dot{q}_3 \quad \dots \quad \dot{q}_{24}) = \frac{1}{2} \underline{\dot{q}}_e^T \underset{(1 \times n)}{\underline{M}_e} \underset{(n \times 1)}{\underline{\dot{q}}_e} \quad (1 \times 1) \quad (4.7.40)$$

and the corresponding Lagrange equation derivatives are

$$\frac{\partial T_e}{\partial \underline{\dot{q}}_e} = \underline{M}_e \underline{\dot{q}}_e \quad (4.7.41)$$

$$\frac{d}{dt} \left(\frac{\partial T_e}{\partial \underline{\dot{q}}_e} \right) = \underline{M}_e \underline{\ddot{q}}_e \quad (4.7.42)$$

$$\frac{\partial T_e}{\partial \underline{q}_e} = \underline{0} \quad (4.7.43)$$

$$\begin{aligned} \underline{q}_e &= \begin{Bmatrix} \underline{U}_{e1} \\ \underline{U}_{e2} \\ \underline{U}_{e3} \end{Bmatrix} = (u_{11}^e \ u_{12}^e \ \cdots \ u_{18}^e \ u_{21}^e \ u_{22}^e \ \cdots \ u_{28}^e \ u_{31}^e \ u_{32}^e \ \cdots \ u_{38}^e)^T \\ &= (q_1 \ q_2 \ q_3 \ \cdots \ q_{24})^T \\ &= \text{element } e\text{'s nodal displacements that occur at its 8 nodes in the } n_1, n_2, \\ &\quad \text{and } n_3 \text{ directions} \end{aligned} \quad (4.7.44)$$

$$n = 24 = \text{number of independent generalized coordinates} \quad (4.7.45)$$

$$\underline{M}_e = \text{“consistent” mass matrix of element } e = \begin{bmatrix} \underline{\tilde{m}}_e & \underline{0} & \underline{0} \\ \underline{0} & \underline{\tilde{m}}_e & \underline{0} \\ \underline{0} & \underline{0} & \underline{\tilde{m}}_e \end{bmatrix} \quad (4.7.46)$$

$(\underline{\tilde{m}}_e)_{ki} = \int_{V_e} N_k^e N_i^e \rho dV \quad (4.7.47)$

Potential Energy for a Finite Element Model of a Flexible Body

The deflection within an 8-node brick element is approximated by

$$\underline{u} = \begin{Bmatrix} u_1^e(x_1, x_2, x_3, t) \\ u_2^e(x_1, x_2, x_3, t) \\ u_3^e(x_1, x_2, x_3, t) \end{Bmatrix} = \begin{Bmatrix} \sum_{k=1}^8 u_{1k}^e(t) N_k^e(x_1, x_2, x_3) \\ \sum_{k=1}^8 u_{2k}^e(t) N_k^e(x_1, x_2, x_3) \\ \sum_{k=1}^8 u_{3k}^e(t) N_k^e(x_1, x_2, x_3) \end{Bmatrix} \quad (4.7.48)$$

$$= \begin{bmatrix} N_1^e & N_2^e & \cdots & N_8^e & \underline{0} & \underline{0} \\ \underline{0} & \underline{0} & \cdots & \underline{0} & N_1^e & N_2^e & \cdots & N_8^e & \underline{0} \\ \underline{0} & \underline{0} & \cdots & \underline{0} & \underline{0} & \underline{0} & \cdots & \underline{0} & N_1^e & N_2^e & \cdots & N_8^e \end{bmatrix} \begin{Bmatrix} u_{11}^e \\ u_{12}^e \\ \vdots \\ u_{18}^e \\ u_{21}^e \\ u_{22}^e \\ \vdots \\ u_{28}^e \\ u_{31}^e \\ u_{32}^e \\ \vdots \\ u_{38}^e \end{Bmatrix}$$

or

$$\underline{u}^e(x_1, x_2, x_3, t) = \underline{N}^e(x_1, x_2, x_3) \underline{q}_e(t) \quad (4.7.49)$$

$3 \times 1 \qquad \qquad \qquad 3 \times 24 \qquad \qquad \qquad 24 \times 1$

where

$$\underline{q}_e = (u_{11}^e \ \cdots \ u_{18}^e \ u_{21}^e \ \cdots \ u_{28}^e \ u_{31}^e \ \cdots \ u_{38}^e)^T = (q_{1e} \ \cdots \ u_{24e})^T \quad (4.7.50)$$

$u_{jk}^e(t)$ = deflection of node k of element e , in the j th direction

$e = 1, n_E$ (number of elements in model)

$j = 1, 2, 3$

$k = 1, 2, \dots, 8$

$$(4.7.51)$$

and

$$N_k^e = k\text{th shape function (given) of element } e \quad (4.7.52)$$

and the strains and displacements are related by

$$\underline{\varepsilon} = \underline{D} \underline{u}^e \quad (4.7.53)$$

Then the strain potential energy of this element is

$$U = \frac{1}{2} \int_{V_e} \underline{\varepsilon}^T \underline{E}_e \underline{\varepsilon} \, dV_e = \frac{1}{2} \underline{q}_e^T \underline{k}_e \underline{q}_e \quad (4.7.54)$$

where

$$\underline{K}_e = \int_{V_e} \underline{B}_e^T \underline{E}_e \underline{B}_e \, dV = \text{element stiffness matrix} \quad (4.7.55)$$

$24 \times 24 \qquad \int_{V_e} \underline{B}_e^T \underline{E}_e \underline{B}_e \, dV \qquad 24 \times 66 \times 66 \times 24$

$$\underline{B}_e = \underline{D} \underline{N}^e \quad (4.7.56)$$

$6 \times 24 \qquad \qquad \qquad 6 \times 33 \times 24$

and from (A.4.4) the constitutive matrix is defined from

$$\underline{\sigma} = \underline{E} \underline{\varepsilon} \quad (4.7.57)$$

The corresponding generalized forces are

$$\underline{Q}_{24 \times 1}^{1e}(t) = - \frac{\partial U}{\partial \underline{q}_e} = \left\{ \begin{array}{c} Q_1^{1e} \\ Q_2^{1e} \\ \vdots \\ Q_{24}^{1e} \end{array} \right\} = - \underline{K}_e \underline{q}_e(t) \quad (4.7.58)$$

$24 \times 24 \qquad 24 \times 1$

Generalized Forces for External Loading in a Finite Element (8-Node Brick Element) Model of a Flexible Body

$$\begin{aligned}
 Q_j^e &= \int_{V_e} \bar{F}_{EV1} N_j^e dV_e + \int_{S_e} \bar{F}_{ES1} N_j^e dS_e \\
 Q_{j+8}^e &= \int_{V_e} \bar{F}_{EV2} N_j^e dV_e + \int_{S_e} \bar{F}_{ES2} N_j^e dS_e \\
 Q_{j+16}^e &= \int_{V_e} \bar{F}_{EV3} N_j^e dV_e + \int_{S_e} \bar{F}_{ES3} N_j^e dS_e
 \end{aligned} \tag{4.7.59}$$

for $j = 1, 2, \dots, 8$

Element Degree of Freedom (DOF) Equation of Motion (EOM)

From (4.5.106b),

$$\frac{d}{dt} \left(\frac{\partial T}{\partial \dot{q}_j} \right) - \frac{\partial T}{\partial q_j} = Q_j - \frac{\partial U}{\partial q_j} - \frac{\partial (\mathfrak{S}^c + \mathfrak{S}^d)}{\partial \dot{q}_j} \tag{4.7.60}$$

Substitution of (4.7.42) and (4.7.58) into this equation yields the element dof EOM

$$\underline{M}_e \ddot{\underline{q}}_e + \underline{K}_e \underline{q}_e = \underline{Q}_e - \frac{\partial (\mathfrak{S}^c + \mathfrak{S}^d)}{\partial \dot{\underline{q}}} \tag{4.7.61}$$

4.8 LE FOR FLEXIBLE, DISTRIBUTED MASS BODIES: FINITE ELEMENT APPROACH—BAR/TRUSS MODES

4.8.1 Introduction

The FEM provides a means to model highly complicated structural and machinery components for vibration response simulation. The FEM can model complex shapes, material property variations, boundary conditions, and loading patterns with relative ease. This is accomplished in a building block approach by considering the relationships between force and displacement variables within a small part, or element, of the model. The displacement field is approximated within an element by interpolating it between user-specified “node” points typically arranged in a regular geometric pattern within the element in its physical or mathematically transformed form. The element building blocks are then assembled into a system model typically defined by mass, stiffness, and damping matrices and a force vector. The assembly is automated by utilizing connectivity arrays which are bookkeeping devices that relate local (element) nodes and degrees of freedom to their system-level counterparts. Boundary conditions are applied to the system model, and then natural frequencies, mode shapes, eigenvalues, or displacements at the node points are solved for. Displacements

throughout each element may then be obtained along with the associated strains, stresses, and forces. The FEM is the approach of preference in most industrial and research and development environments. Acquiring a good grasp of the corresponding theory will assist the person utilizing commercial finite element software to respect its assumptions and limitations and properly apply it in solving real-world vibration problems.

4.8.2 1D Truss/Bar Element

The simplest structural finite element is a bar element which can deform only along its longitudinal axis. The bar element (e) shown in Figure 4.8.1 has 2 nodes located at the end point, with 1 degree of freedom per node (deflections q_1 and q_2) and with distributed force/length $\bar{f}(x, t)$, density ρ , Young's modulus E , cross-sectional area A , length L , end actions (forces) a_j , and deflection $u(x, t)$.

4.8.3 1D Truss/Bar Element: Element Stiffness Matrix

The uniaxial strain–displacement relation for this element is given by

$$\varepsilon_{xx} = \frac{\partial u}{\partial x} \quad (4.8.1)$$

Thus, the strain–displacement operator matrix in (4.7.35) is

$$D = \frac{\partial}{\partial x} \quad (4.8.2)$$

The displacement interpolation within the element is (4.7.48)–(4.7.50):

$$u(x, t) = q_1(t)N_1(x) + q_2(t)N_2(x) = \underset{1 \times 2}{N^e(x)} \underset{2 \times 1}{q_e(t)} \quad (4.8.3)$$

where

$$\underline{N}^e = [N_1(x) \ N_2(x)] = \left[1 - \frac{x}{L} \quad \frac{x}{L} \right], \quad \underline{q}_e = (q_1 \ q_2)^T \quad (4.8.4)$$

The shape functions in (4.8.4) satisfy the consistency conditions in (2.11.37). From (4.7.56),

$$\underset{1 \times 2}{B}_e = \underset{1 \times 1}{D} \underset{1 \times 1 \times 2}{N^e} = \frac{\partial}{\partial x} [N_1(x) \ N_2(x)] = [N_1' \ N_2'] \quad (4.8.5)$$

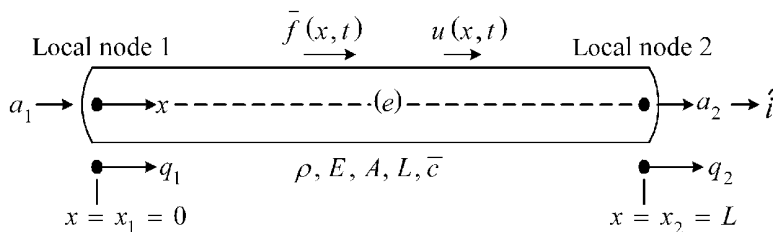


Figure 4.8.1 One-dimensional bar element

The material (constitutive) relation for this element is given by (A.4.4)

$$\underline{\sigma} = \underline{E} \underline{\varepsilon} = E \varepsilon_{xx} \quad (4.8.6)$$

Thus,

$$\underline{E} = E \quad (4.8.7)$$

The element stiffness matrix is obtained from (4.7.55), (4.8.5), and (4.8.7) as

$$\begin{aligned} \underline{K}_{2 \times 2}^{(e)} &= \begin{bmatrix} K_{11}^{(e)} & K_{12}^{(e)} \\ K_{21}^{(e)} & K_{22}^{(e)} \end{bmatrix} = \int_{V_e} \underline{B}_e^T \underline{E}_e \underline{B}_e dV_e \\ &= \int_0^L \begin{Bmatrix} N_1' \\ N_2' \end{Bmatrix} E [N_1' \quad N_2'] A dx = \int_0^L E(x) A(x) \begin{bmatrix} N_1' N_1' & N_1' N_2' \\ N_2' N_1' & N_2' N_2' \end{bmatrix} dx \end{aligned} \quad (4.8.8)$$

4.8.4 1D Truss/Bar Element: Element Mass Matrix

The element mass matrix is obtained from (4.7.46) and (4.7.47):

$$\underline{M}^{(e)} = \begin{bmatrix} M_{11}^{(e)} & M_{12}^{(e)} \\ M_{21}^{(e)} & M_{22}^{(e)} \end{bmatrix} = \int_0^L \rho(x) A(x) \begin{bmatrix} N_1 N_1 & N_1 N_2 \\ N_2 N_1 & N_2 N_2 \end{bmatrix} dx \quad (4.8.9)$$

4.8.5 1D Truss/Bar Element: Element Damping Matrix

Let $\tilde{c}(x)$ be the damping per unit length exerted on the bar by its surrounding medium. The Rayleigh dissipation function (4.5.81) for the bar element becomes

$$\mathfrak{S}^d = \frac{1}{2} \int_0^L \dot{u}^2 \tilde{c} dx \quad (4.8.10)$$

where from (4.8.3)

$$\dot{u}(x, t) = \dot{q}_1(t) N_1(x) + \dot{q}_2(t) N_2(x) = \underline{N}^e(x) \underline{\dot{q}}_e(t) \quad (4.8.11)$$

Substitution of (4.8.11) into (4.8.10) yields

$$\mathfrak{S}^d = \frac{1}{2} \int_0^L \dot{u}^2 \tilde{c} dx = \frac{1}{2} \underline{\dot{q}}^T \underline{C}^{(e)} \underline{\dot{q}} \quad (4.8.12)$$

where the element damping matrix becomes

$$\underline{C}^{(e)} = \begin{bmatrix} C_{11}^{(e)} & C_{12}^{(e)} \\ C_{21}^{(e)} & C_{22}^{(e)} \end{bmatrix} = \int_0^L \tilde{c}(x) \begin{bmatrix} N_1 N_1 & N_1 N_2 \\ N_2 N_1 & N_2 N_2 \end{bmatrix} dx \quad (4.8.13)$$

4.8.6 1D Truss/Bar Element: Generalized Force Vector

The bar's generalized forces are given by (4.5.7) and (4.5.52):

$$Q_j = a_1 \hat{i} \cdot \frac{\partial \hat{q}_1 \hat{i}}{\partial \hat{q}_j} + a_2 \hat{i} \cdot \frac{\partial \hat{q}_2 \hat{i}}{\partial \hat{q}_j} + \int_0^L (\bar{f} dx \hat{i}) \cdot \frac{\partial \hat{i} \hat{i}}{\partial \hat{q}_j} \quad (4.8.14)$$

This simplifies to

$$\underline{Q} = \begin{Bmatrix} Q_1 \\ Q_2 \end{Bmatrix} = \begin{Bmatrix} a_1 \\ a_2 \end{Bmatrix} + \begin{Bmatrix} f_1 \\ f_2 \end{Bmatrix} = \underline{a}^{(e)} + \underline{f}^{(e)} \quad (4.8.15)$$

where

$$\underline{f}^{(e)} = \begin{Bmatrix} f_1 \\ f_2 \end{Bmatrix} = \int_0^L \bar{f} \begin{Bmatrix} N_1 \\ N_2 \end{Bmatrix} dx \quad (4.8.16)$$

For constant $\bar{f}_e, \rho_e, A_e, E_e$, Equations (4.8.4), (4.8.8), and (4.8.9) yield

$$\underline{K}^{(e)} = E_e A_e \int_0^{L_e} \begin{bmatrix} N_1' N_1' & N_1' N_2' \\ N_2' N_1' & N_2' N_2' \end{bmatrix} dx = E_e A_e \int_0^{L_e} \begin{bmatrix} 1/L_e^2 & -1/L_e^2 \\ -1/L_e^2 & 1/L_e^2 \end{bmatrix} dx = \frac{E_e A_e}{L_e} \begin{bmatrix} 1 & -1 \\ -1 & 1 \end{bmatrix} \quad (4.8.17)$$

$$\underline{M}^{(e)} = \rho_e A_e \int_0^{L_e} \begin{bmatrix} N_1 N_1 & N_1 N_2 \\ N_2 N_1 & N_2 N_2 \end{bmatrix} dx = \rho_e A_e L_e \begin{bmatrix} 1/3 & 1/6 \\ 1/6 & 1/3 \end{bmatrix} \quad (4.8.18)$$

$$\underline{C}^{(e)} = \int_0^L \tilde{c}(x) \begin{bmatrix} N_1 N_1 & N_1 N_2 \\ N_2 N_1 & N_2 N_2 \end{bmatrix} dx = \tilde{c}_e \begin{bmatrix} 1/3 & 1/6 \\ 1/6 & 1/3 \end{bmatrix} \quad (4.8.19)$$

$$\underline{f}^{(e)} = \bar{f}_e \int_0^{L_e} \begin{Bmatrix} N_1 \\ N_2 \end{Bmatrix} dx = \bar{f}_e \frac{L}{2} \begin{Bmatrix} 1 \\ 1 \end{Bmatrix} \quad (4.8.20)$$

Application of LE (4.7.61) to the bar element yields the element dof EOM:

$$\underline{M}^{(e)} \ddot{\underline{q}} + \underline{C}^{(e)} \dot{\underline{q}} + \underline{K}^{(e)} \underline{q} = \underline{a}^{(e)} + \underline{f}^{(e)} \quad (2 \times 1) \quad (4.8.21)$$

The motions ($\underline{q}, \dot{\underline{q}}, \ddot{\underline{q}}$) may be obtained by solving (4.8.17), for example, by numerical integration (ref. Example 2.3.1). Then the end actions (forces) may be determined from (4.8.17), written as

$$\underline{a}^{(e)} = \underline{M}^{(e)} \ddot{\underline{q}} + \underline{C}^{(e)} \dot{\underline{q}} + \underline{K}^{(e)} \underline{q} - \underline{f}^{(e)} \quad (4.8.22)$$

utilizing the calculated motions. The end (nodal) actions $\underline{a}^{(e)}$ are typically very important quantities since stresses may be determined from the end actions. Most fatigue-related theories of failure are based on the levels of stress as discussed in Section 1.4.

4.8.7 1D Truss/Bar Element: Nodal Connectivity Array

Figure 4.8.2 represents a mathematical model, consisting of E bar elements, which is employed to predict the longitudinal vibration of a machine or structural system. The displacement and internal action (force) at local node i of element e are denoted by $q_i^{(e)}$ and $a_i^{(e)}$, respectively.

Connected elements share nodes which cause a redundancy in the displacement and action labeling system shown in Figure 4.8.2. For example, note that local node 2 of element 1 is local node 1 of elements 2, 3, and 4. Therefore,

$$q_2^{(1)} = q_1^{(2)} = q_1^{(3)} = q_1^{(4)} \tag{4.8.23}$$

and by Newton’s third law, the internal forces (actions) at the nodes are

$$a_2^{(1)} = -\left(a_1^{(2)} + a_1^{(3)} + a_1^{(4)}\right) \tag{4.8.24}$$

Equation (4.8.23) is an interelement displacement compatibility condition, and Equation (4.8.24) is an interelement equilibrium condition. The redundancy in “local” displacements is removed by defining a “global” node system as illustrated in Figure 4.8.3.

Note that the nodes may be shared by adjacent elements and that there are a total of N_N independent nodes. For example,

Global node 1 = local node 2 of element 1 = local node 1 of element 2

The “nodal” connectivity array (NCA) provides a systematic means to relate local nodes of connected elements to unique global node numbers. This aids “assembly” of

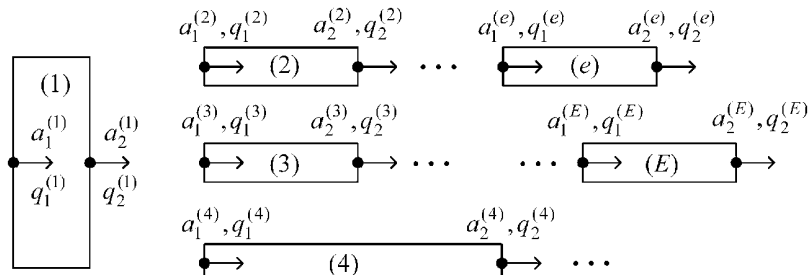


Figure 4.8.2 Local (element) node numbering for a system of bar elements

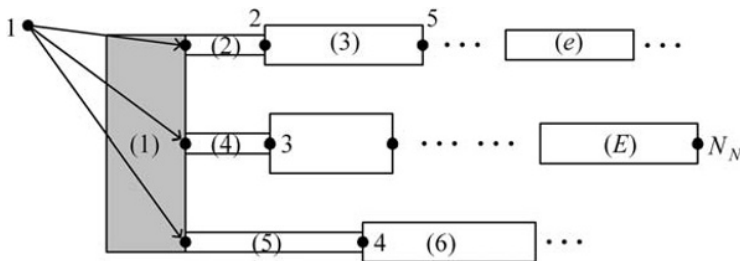


Figure 4.8.3 Global node numbering of structural model with system of bar elements

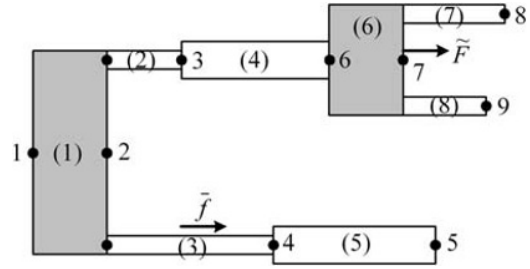


Figure 4.8.4 A bar-type structural model with 8 elements and 9 nodes

Table 4.8.1 Nodal connectivity array \underline{B} for the model in Figure 4.8.4

Element no. e	Local node 1 B_{e1}	Local node 2 B_{e2}
1	1	2
2	2	3
3	2	4
4	3	6
5	4	5
6	6	7
7	7	8
8	7	9

the element matrices into the system matrices in an automated (programmable) manner. To illustrate this, consider the 8-element model shown in Figure 4.8.4.

The nodal connectivity for this model is contained in the \underline{B} array in Table 4.8.1.

Formally, the “NCA” is defined as

$$\underline{B}_{ej} = \text{NCA} = \text{“global” node number for local node } j \text{ of element } e$$

$$e = 1, 2, \dots, E, \quad j = 1, 2 \quad (4.8.25)$$

where for the model in Figure 4.8.4, $E = 8$ and $N_N = 9$.

4.8.8 System of 1D Bar Elements: Matrix Assembly

Each element is in a state of dynamic equilibrium, that is, from (4.8.17),

$$\underline{M}^{(1)} \ddot{\underline{q}}^{(1)} + \underline{C}^{(1)} \dot{\underline{q}}^{(1)} + \underline{K}^{(1)} \underline{q}^{(1)} = \underline{a}^{(1)} + \underline{f}^{(1)} \quad (4.8.26)$$

⋮

$$\underline{M}^{(e)} \ddot{\underline{q}}^{(e)} + \underline{C}^{(e)} \dot{\underline{q}}^{(e)} + \underline{K}^{(e)} \underline{q}^{(e)} = \underline{a}^{(e)} + \underline{f}^{(e)} \quad (4.8.27)$$

⋮

$$\underline{M}^{(E)} \ddot{\underline{q}}^{(E)} + \underline{C}^{(E)} \dot{\underline{q}}^{(E)} + \underline{K}^{(E)} \underline{q}^{(E)} = \underline{a}^{(E)} + \underline{f}^{(E)} \quad (4.8.28)$$

where E is the total number of elements in the system model. The dynamic equilibrium equation for the entire structure is “assembled” from these element equations. Redundancies are eliminated in the process by enforcing:

- Interelement compatibility
- Interelement equilibrium

and by expressing local node displacements in terms of global node displacements utilizing the NCA \underline{B} . The final result of this *assembly procedure* is a systematic, programmable algorithm for obtaining the dynamic equilibrium equations

$$\underline{M}\ddot{\underline{q}} + \underline{C}\dot{\underline{q}} + \underline{K}\underline{q} = \underline{f} \quad (N_N \times 1) \quad (4.8.29)$$

of the total system from the element $\underline{M}^{(e)}, \underline{C}^{(e)}, \underline{K}^{(e)}$ matrices and $\underline{f}^{(e)}$ vectors. Note that the interelement actions $\underline{a}^{(e)}$ do not appear in (4.8.29) since they cancel by Newton’s third law in the assembly process. The assembly procedure is summarized by the following steps:

(a) Let \underline{G} represent $\underline{M}, \underline{C}$, or \underline{K} and $\underline{G}^{(e)}$ represent $\underline{M}^{(e)}, \underline{C}^{(e)}$, or $\underline{K}^{(e)}$. (4.8.30a)

(b) Then \underline{G} is formed by initializing $\underline{G} = \underline{0}$ (4.8.30b)

and then adding the row r , column s entry of $\underline{G}^{(e)}$, that is, $(\underline{G}^{(e)})_{rs}$, into the (row B_{er} , column B_{es}) position of \underline{G} for all elements ($e = 1, 2, \dots, E$) and all rows and columns ($r = 1, 2, s = 1, 2$) of each element matrix $\underline{G}^{(e)}$. This is illustrated in Figure 4.8.5.

(c) The excitation vector \underline{f} is formed by initializing $\underline{f} = \underline{0}$ (4.8.30c)

and then by adding the r th entry of $\underline{f}^{(e)}$, that is, $(\underline{f}^{(e)})_r$, into the row B_{er} position of \underline{f} for all elements ($e = 1, 2, \dots, E$) and all rows of each element force vector $\underline{f}^{(e)}$. This is illustrated in Figure 4.8.6.

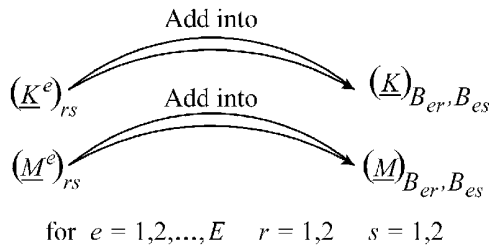


Figure 4.8.5 Assembly of the \underline{M} and \underline{K} matrices

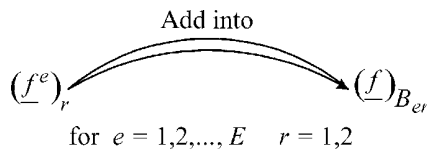


Figure 4.8.6 Assembly of the \underline{f} vector

The result of this assembly procedure is the system \underline{M} , \underline{C} , and \underline{K} matrices and the \underline{f} vector for the unconstrained system. This procedure is applicable to any type of element but will first need to be extended to accommodate constrained (fixed) degrees of freedom and elements with multiple degrees of freedom per node.

EXAMPLE 4.8.1 *Matrix Assembly for Model in Figure 4.8.4 and Table 4.8.1*

Description: The model in Figure 4.8.4 consists of 8 bar elements and 9 nodes. Element 3 has a distributed force \bar{f} , and node 7 has a concentrated force \tilde{F} . From Table 4.8.1, the nodal connectivity matrix is

$$\underline{B} = \begin{array}{cc} \begin{array}{c} \text{local} \\ \text{node} \\ 1 \end{array} & \begin{array}{c} \text{local} \\ \text{node} \\ 2 \end{array} \\ \left[\begin{array}{cc} 1 & 2 \\ 2 & 3 \\ 2 & 4 \\ 3 & 6 \\ 4 & 5 \\ 6 & 7 \\ 7 & 8 \\ 7 & 9 \end{array} \right] & \begin{array}{l} \leftarrow \text{element 1} \\ \leftarrow \text{element 2} \\ \leftarrow \text{element 3} \\ \leftarrow \text{element 4} \\ \leftarrow \text{element 5} \\ \leftarrow \text{element 6} \\ \leftarrow \text{element 7} \\ \leftarrow \text{element 8} \end{array} \end{array} \quad (1)$$

Application of the algorithm illustrated in Figure 4.8.5 to this model yields the results in Table E4.8.1(a) for assembling the element stiffness \underline{K}^e and mass \underline{M}^e matrices of elements 1, 2, and 8 into the system or “global” stiffness \underline{K} and mass \underline{M} matrices, respectively.

According with (4.8.16), the distributed force \bar{f} acting on element 3 creates the element force vector

$$\underline{f}^{(3)} = \begin{Bmatrix} f_1^3 \\ f_2^3 \end{Bmatrix} = \int_0^{L_3} \bar{f} \begin{Bmatrix} N_1 \\ N_2 \end{Bmatrix} dx \quad (2)$$

According with Figure 4.8.6, the element 3 force vector components add into the global force vector as follows:

$$f_1^3 \Rightarrow e = 3, r = 1 \text{ and from Equation (1) } B_{er} = B_{31} = 2 \Rightarrow \text{so add } f_1^3 \text{ into row 2 of } \underline{f} \quad (3)$$

Likewise,

$$f_2^3 \Rightarrow e = 3, r = 2 \text{ and from Equation (1) } B_{er} = B_{32} = 4 \Rightarrow \text{so add } f_2^3 \text{ into row 4 of } \underline{f} \quad (4)$$

Table E4.8.1(a) Assembly of elements 1, 2, and 8 into the global stiffness and mass matrices

Element (e)	r	s	B_{er}	B_{es}	Add $(\underline{K}^e)_{rs}$ into $(\underline{K})_{B_{er}B_{es}}$	Add $(\underline{M}^e)_{rs}$ into $(\underline{M})_{B_{er}B_{es}}$
1	1	1	1	1	\underline{K}_{11}	\underline{M}_{11}
	1	2	1	2	\underline{K}_{12}	\underline{M}_{12}
	2	1	2	1	\underline{K}_{21}	\underline{M}_{21}
	2	2	2	2	\underline{K}_{22}	\underline{M}_{22}
2	1	1	2	2	\underline{K}_{22}	\underline{M}_{22}
	1	2	2	3	\underline{K}_{23}	\underline{M}_{23}
	2	1	3	2	\underline{K}_{32}	\underline{M}_{32}
	2	2	3	3	\underline{K}_{33}	\underline{M}_{33}
8	1	1	7	7	\underline{K}_{77}	\underline{M}_{77}
	1	2	7	9	\underline{K}_{79}	\underline{M}_{79}
	2	1	9	7	\underline{K}_{97}	\underline{M}_{97}
	2	2	9	9	\underline{K}_{99}	\underline{M}_{99}

The generalized forces corresponding to the concentrated force \tilde{F} at node 7 are given by (4.5.51) as

$$Q_j = \sum_{i=1}^{n_{FI}} \tilde{F}_i \cdot \frac{\partial \tilde{R}_i}{\partial q_j} = \tilde{F}_i \cdot \frac{\partial q_7}{\partial q_j} = \tilde{F} \frac{\partial q_7}{\partial q_j} = \begin{cases} 0, & \text{if } j \neq 7 \\ \tilde{F} & \text{if } j = 7 \end{cases} \quad (5)$$

Consideration of (2)–(5) shows that the global force vector equals

$$\underline{f} = (0 \ f_1^3 \ 0 \ f_2^3 \ 0 \ 0 \ \tilde{F} \ 0 \ 0)^T \quad (6)$$

EXAMPLE 4.8.2 *Pile Impact Simulation*

Description: Piles are pounded into the soil by repeated drops of a ram onto a cap block. This example utilizes a simplified model of the soil, pile, and driver to illustrate the usage of bar-type finite elements.

Objective: Determine the vibration response of the pile due to a ram strike event.

Assumptions:

- Soil drag is modeled by a coulomb dry friction force.
- The dry friction force, density, cross-sectional area, and Young's modulus are assumed constant within each element.
- $A_e, \rho_e, \bar{f}_e, E_e$ are constant within an element (e).
- Gravity effect neglected.

Model: The model consists of 10 in-line bar elements plus two lumped masses, m_r and m_c , and soil friction forces, \bar{f}_j , as shown in Figure E4.8.2(a).

The pile element properties are:

- Nominal area = $A = 0.01 \text{ m}^2$, nominal Young's modulus = $E = 2 \times 10^{11} \text{ N/m}^2$
- Nominal density = $\rho = 7000 \text{ kg/m}^3$, nominal element length = $L = 1 \text{ m}$
- Nominal friction force per length = $|\bar{f}| = \mu p C = 50 \mu$
- $A_e = A, L_e = L$ for all e , except $L_1 = L/2$

The nodal connectivity and element properties are shown in Table E4.8.2(a) based on Figure E4.8.2(a).

Solution:

(a) Assemble \underline{M} and \underline{K} in (4.8.29) as explained in (4.8.30a) and (4.8.30b) and shown in Figure 4.8.5. The lumped masses must also be added into the system mass matrix as follows:

$$(\underline{M})_{11} = (\underline{M})_{1,1} + m_r, \quad (\underline{M})_{2,2} = (\underline{M})_{2,2} + m_c \quad (1)$$

to account for the ram and pile cap masses at node 1 and 2.

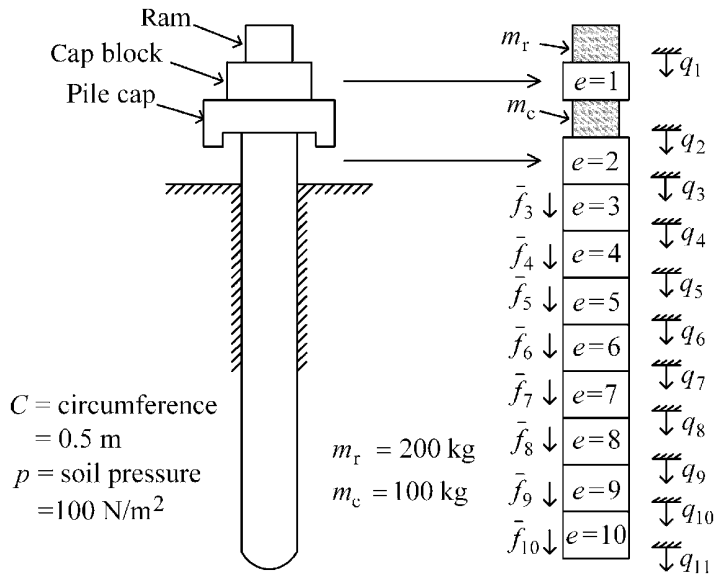


Figure E4.8.2(a) Finite element model of pile with soil forces

Table E4.8.2(a) Nodal connectivity array and element properties $E = 10$ elements
 $N_N = 11$ nodes, $\mu = 0.5$

e	1	2	3	4	5	6	7	8	9	10
B_{e1}	1	2	3	4	5	6	7	8	9	10
B_{e2}	2	3	4	5	6	7	8	9	10	11
E_e	$E/5$	E								
ρ_e	$\rho/5$	ρ								
$ \bar{f}_e $	0	0	$ \bar{f} $	$2 \bar{f} $	$3 \bar{f} $	$4 \bar{f} $	$5 \bar{f} $	$6 \bar{f} $	$7 \bar{f} $	$10 \bar{f} $

(b) From (4.8.16),

$$\underline{f}^e = \begin{Bmatrix} f_1^e \\ f_2^e \end{Bmatrix} = \begin{Bmatrix} \bar{f}_e(L/2) \\ \bar{f}_e(L/2) \end{Bmatrix} = \frac{L_e}{2} \begin{Bmatrix} |\bar{f}_e| * (-\text{sgn}(\dot{q}_1^e)) \\ |\bar{f}_e| * (-\text{sgn}(\dot{q}_2^e)) \end{Bmatrix} \quad (2)$$

where the friction force direction is made opposite to the direction of the velocity by utilizing the sgn function:

$$\text{sgn}(x) = \begin{cases} -1, & x < 0 \\ 0, & x = 0 \\ 1, & x > 0 \end{cases} \quad (3)$$

Assemble \underline{f} in (4.8.29) as explained in (4.8.30c) and illustrated in Figure 4.8.6.

(c) Solve for the system's transient response utilizing the MATLAB ODE 45 numerical integration solver as illustrated in Example 2.3.1. By (4.8.29),

$$\underline{\dot{V}} = -\underline{M}^{-1}\underline{C}\underline{V} - \underline{M}^{-1}\underline{K}\underline{q} + \underline{M}^{-1}\underline{f} = -\underline{M}^{-1}\underline{K}\underline{q} + \underline{M}^{-1}\underline{f}, \quad \underline{\dot{q}} = \underline{V}, \quad \underline{\dot{x}} = \underline{\hat{A}}\underline{x} + \underline{\hat{f}} \quad (4)$$

where

$$\underline{\hat{A}} = \begin{bmatrix} \underline{0} & -\underline{M}^{-1}\underline{K} \\ \underline{I} & \underline{0} \end{bmatrix}, \quad \underline{\hat{f}} = \begin{Bmatrix} \underline{M}^{-1}\underline{f} \\ \underline{0} \end{Bmatrix}, \quad \underline{x} = \begin{Bmatrix} \underline{V} \\ \underline{q} \end{Bmatrix} \quad (5)$$

The ram strike is modeled by imposing an initial velocity on degree of freedom 1 per the discussion of impulse and momentum in Section 3.4. The initial conditions are

$$\begin{aligned} \underline{q}_0 &= \underline{0} \\ V_{10} &= 1 \text{ m/s}, \quad V_{j0} = 0, \quad j \neq 1 \end{aligned} \quad (6)$$

Figure E4.8.2(b) shows the movement of degree of freedom q_{11} in response to a ram strike.

4.8.9 Incorporation of Displacement Constraint

The previous section provided an assembly procedure for a free (unconstrained) structure, for which the total number of dofs N_d equals the number of free dofs N_f . In many instances, a structure will possess *displacement constraints* applied at one or more nodes in the model in order to eliminate rigid body motions or to prestretch or precompress the structure. These constraints require an additional “bookkeeping” array for the system model assembly procedure. For illustration, consider the model shown in Figure 4.8.7 undergoing longitudinal (axial) vibration. The element numbers are indicated in parentheses.

The shaded regions are considered rigid and therefore represent a single node. This structure has four constrained (zero displacement) nodes:

$$i_c \in (1 \ 4 \ 7 \ 17) \quad (4.8.31)$$

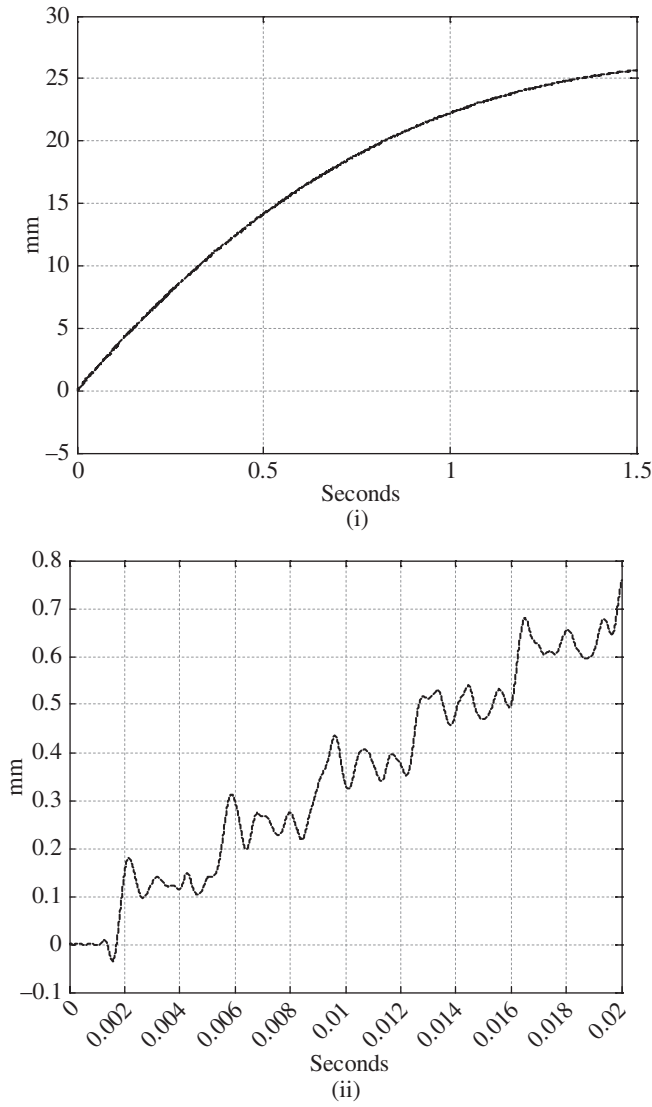


Figure E4.8.2(b) (i) Displacement q_{11} for $0 \leq t \leq 1.5$ seconds and (ii) displacement q_{11} for $0 \leq t \leq 0.02$ seconds

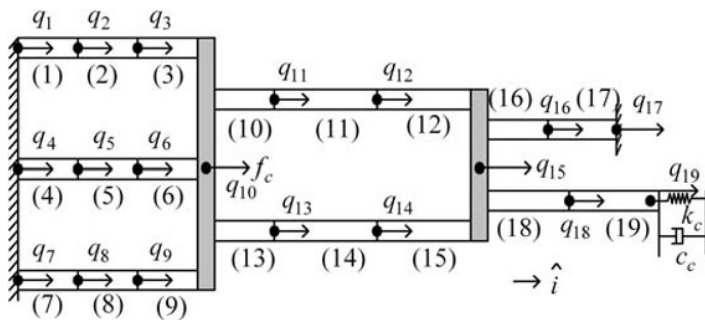


Figure 4.8.7 Structural model with displacement constraints

Therefore, only 15 nodes are free (f) to move, that is,

$$\begin{aligned} \underline{q}_f &= (q_1^f \ q_2^f \ q_3^f \ q_4^f \ q_5^f \ q_6^f \ q_7^f \ q_8^f \ q_9^f \ q_{10}^f \ q_{11}^f \ q_{12}^f \ q_{13}^f \ q_{14}^f \ q_{15}^f)^T \\ &= (q_2 \ q_3 \ q_5 \ q_6 \ q_8 \ q_9 \ q_{10} \ q_{11} \ q_{12} \ q_{13} \ q_{14} \ q_{15} \ q_{16} \ q_{18} \ q_{19})^T \end{aligned} \quad (4.8.32)$$

where for this example

$$N_f = \text{number of free dofs} = 15 \quad (4.8.33)$$

Define the j array as containing the dof numbers for the free (unconstrained) nodes:

$$\tilde{J} = (j_1 \ j_2 \ \cdots \ j_{15}) = (2 \ 3 \ 5 \ 6 \ 8 \ 9 \ 10 \ 11 \ 12 \ 13 \ 14 \ 15 \ 16 \ 18 \ 19) \quad (4.8.34)$$

Define the l array which indicates the locations of each free (unconstrained) node in the vector \underline{q}_f of only free (unconstrained) node displacements:

$$\begin{aligned} \tilde{L} &= (l_1 \ l_2 \ \cdots \ l_{19}) \\ &= \begin{pmatrix} 0 & 1 & 2 & 0 & 3 & 4 & 0 & 5 & 6 & 7 & 8 & 9 & 10 & 11 & 12 & 13 & 0 & 14 & 15 \\ 1 & 2 & 3 & 4 & 5 & 6 & 7 & 8 & 9 & 10 & 11 & 12 & 13 & 14 & 15 & 16 & 17 & 18 & 19 \end{pmatrix} \end{aligned} \quad (4.8.35)$$

For reference, the positions of these entries are indicated by the index numbers shown beneath the array in (4.8.35). Note that l_i is set equal to zero if node i is fixed. Imposing the zero-displacement constraint conditions yields the following “condensed” dynamic equilibrium equation for the constrained structure:

$$\underline{M}_f \ddot{\underline{q}}_f + \underline{C}_f \dot{\underline{q}}_f + \underline{K}_f \underline{q}_f = \underline{F}_f \quad (4.8.36)$$

$N_f \times N_f$ $N_f \times 1$ $N_f \times N_f$ $N_f \times 1$ $N_f \times N_f$ $N_f \times 1$ $N_f \times 1$

The nodal connectivity \underline{B} and free node assignment l arrays are employed to assemble \underline{M}_f , \underline{K}_f , and \underline{F}_f as summarized by the following steps:

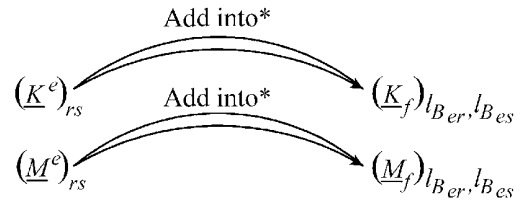
(a) Let \underline{G}_f represent \underline{M}_f , \underline{C}_f , or \underline{K}_f and $\underline{G}^{(e)}$ represent $\underline{M}^{(e)}$, $\underline{C}^{(e)}$, or $\underline{K}^{(e)}$. (4.8.37a)

(b) Then \underline{G}_f is formed by initializing $\underline{G}_f = \underline{0}$ (4.8.37b)

and then adding the row r , column s entry of $\underline{G}^{(e)}$, that is, $(\underline{G}^{(e)})_{rs}$, into the (row $l_{B_{er}}$, column $l_{B_{es}}$) position of \underline{G}_f for all elements ($e = 1, 2, \dots, E$) and for all rows and columns ($r = 1, 2, \quad s = 1, 2$) of each element matrix $\underline{G}^{(e)}$. The addition operation is performed if and only if $l_{B_{er}} \neq 0$ and $l_{B_{es}} \neq 0$. This procedure is illustrated in Figure 4.8.8.

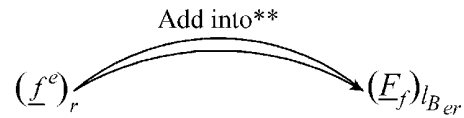
(c) The excitation vector \underline{F}_f is formed by initializing $\underline{F}_f = \underline{0}$ (4.8.37c)

then adding the r th entry of $\underline{f}^{(e)}$, that is, $(\underline{f}^{(e)})_r$, into the row $l_{B_{er}}$ position of \underline{F}_f for all elements ($e = 1, 2, \dots, E$) and all rows ($r = 1, 2$) of each of each element force vector $\underline{f}^{(e)}$. The addition operation is performed if and only if $l_{B_{er}} \neq 0$. This procedure is illustrated in Figure 4.8.8.



for $e = 1, 2, \dots, E$ (no. of elements)
 $r = 1, 2$ (no. of nodes per element)
 $s = 1, 2$ (no. of nodes per element)

*Add into if and only if $l_{B_{er}} \neq 0$ and $l_{B_{es}} \neq 0$



for $e = 1, 2, \dots, E$ $r = 1, 2$

**Add into if and only if $l_{B_{er}} \neq 0$

Figure 4.8.8 Assembly of the free dof system \underline{M}_f and \underline{K}_f matrices and \underline{F}_f vector for a constrained system

The result of this assembly procedure is the system \underline{M}_f , \underline{C}_f , and \underline{K}_f matrices and the \underline{F}_f vector for the constrained system. The concentrated force f_c at node 10 in Figure 4.8.7 contributes the following generalized forces (4.5.28) to LE:

$$Q_j = \hat{f}_c \hat{i} \cdot \frac{\partial \hat{q}_{10} \hat{i}}{\partial \hat{q}_j} = \begin{cases} f_c, & j = 10 \\ 0, & j \neq 10 \end{cases} \quad (4.8.38)$$

However, node 10 in the unconstrained system is the l_{10} free node. Then by Equation (4.8.35), $l_{10} = 7$, the concentrated force f_c modifies \underline{F}_f in the following manner:

$$\left(\underline{F}_f \right)_7 = \left(\underline{F}_f \right)_7 + f_c \quad (4.8.39)$$

The concentrated damper c_c in Figure 4.8.7 has the dissipation function

$$\mathfrak{S}^d = \frac{c_c}{2} \dot{q}_{19}^2 \quad (4.8.40)$$

Therefore, its contributions to the LE are

$$\frac{\partial \mathfrak{S}^d}{\partial \dot{q}_j} = \begin{cases} 0, & j \neq 19 \\ c_c \dot{q}_{19}, & j = 19 \end{cases} \quad (4.8.41)$$

However, node 19 in the unconstrained system is the l_{19} free node. Then by Equation (4.8.35), $l_{19} = 15$, so the concentrated damper c_c modifies \underline{C}_f in the following manner:

$$\left(\underline{C}_f \right)_{15,15} = \left(\underline{C}_f \right)_{15,15} + c_c \quad (4.8.42)$$

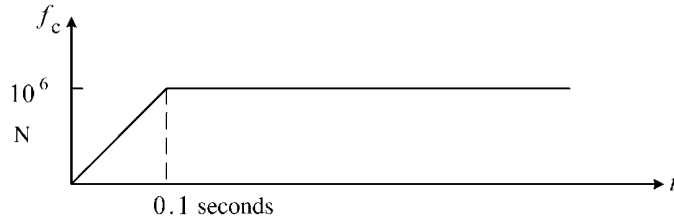


Figure 4.8.9 Applied force (f_c) time history

Likewise, k_c has the effect

$$\left(\underline{K}_f\right)_{15,15} = \left(\underline{K}_f\right)_{15,15} + k_c \quad (4.8.43)$$

For sake of illustration, let

$$A_e = 0.01 \text{ m}^2, \quad E_e = 2 \times 10^{11} \text{ N/m}^2, \quad \rho_e = 7000 \text{ kg/m}^3, \quad L_e = 1 \text{ m}$$

for all elements e . Furthermore, let

$$k_c = 2 \times 10^8 \text{ N/m}, \quad c_c = 10000 \text{ Ns/m}$$

Figure 4.8.9 shows the time history of the dynamic force applied at degree of freedom q_{10} in Figure 4.8.7.

The response of the q_{10} degree of freedom in Figure 4.8.7 is shown in Figure 4.8.10. This is obtained by MATLAB ODE 45 numerical integration (ref. Example 2.3.1).

4.8.10 Modeling of 2D Trusses

The preceding discussion of bar elements was for models with nodal displacements in a single direction. 2D truss models allow nodal deflections to occur in two orthogonal directions (x_1 and x_2). Consider a structure consisting of bars that are connected by hinges as illustrated by the trusses shown in Figure 4.8.11.

The standard rules employed for static truss analysis are often stated as:

- The internal forces (actions) at the ends of a truss member are collinear.
- If three truss members are joined at a node that is free from external loads, and two of the members are collinear, then the third member has a zero action.

These rules are invalid for vibration of trusses due to the presence of inertial forces. The main assumption of 2D truss analysis for vibrations is that the strain energy is dominated by axial deformation so that bending (transverse deflection) is negligible. This assumption is not imposed for modeling of frames with Euler–Bernoulli or Timoshenko beams (Chapter 9). Consider the truss member shown in Figure 4.8.12. Note that there are 2 nodes per element with 2 degrees of freedom (displacements) per node. The actions are the internal reaction forces that occur at a node shared between two or more elements.

The local and global coordinates are related by the following coordinate transformations (2.7.1):

$$\tilde{\underline{q}}_e = \underline{T}_{Te} \underline{q}_e, \quad \tilde{\underline{a}}_e = \underline{T}_{Te} \underline{a}_e, \quad \tilde{\underline{f}}_e = \underline{T}_{Te} \underline{f}_e \quad (4.8.44)$$

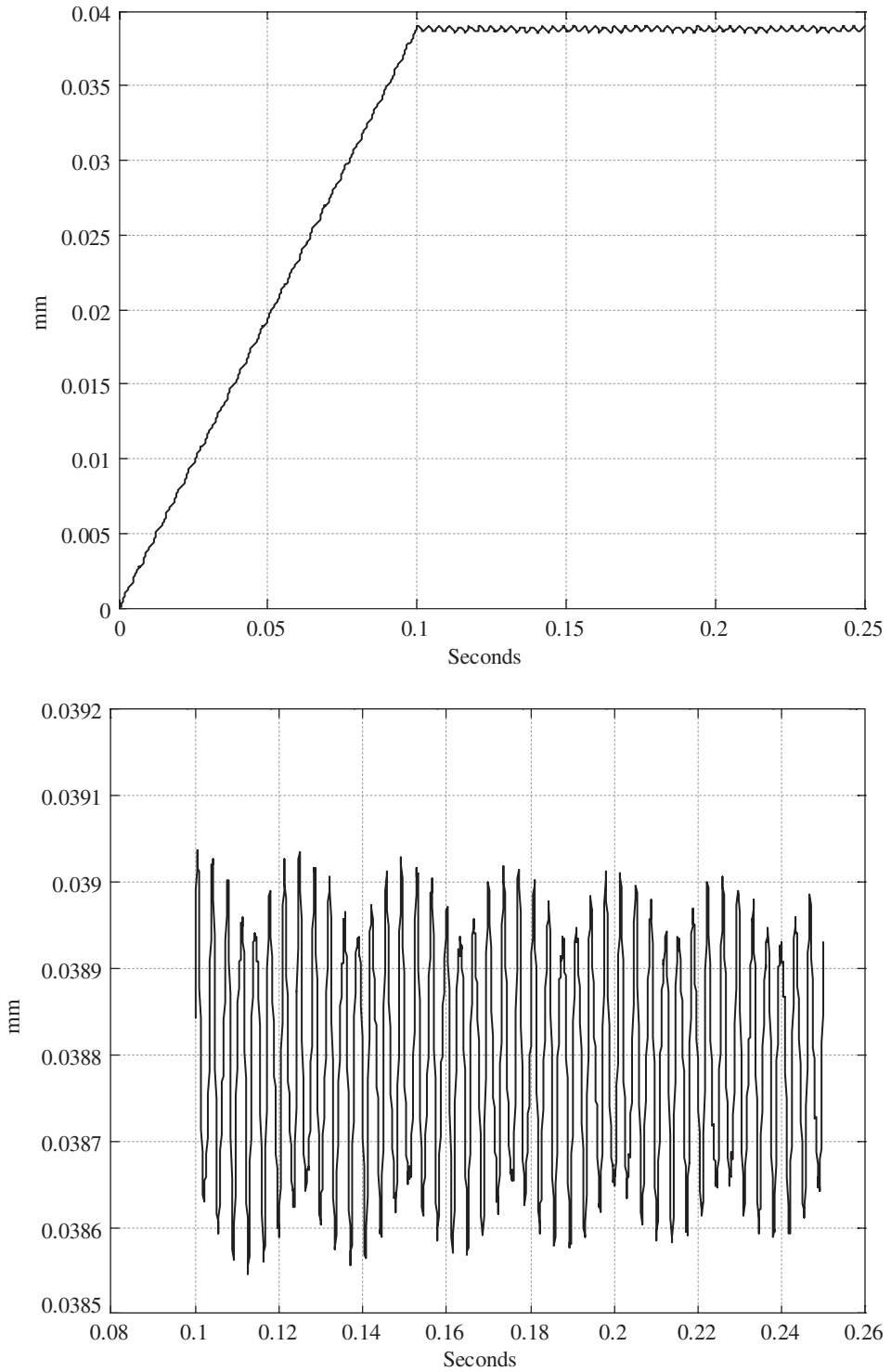


Figure 4.8.10 Displacement q_{10} versus t for bar structure over (a) full simulation time and (b) over time from 0.1 to 0.25 seconds

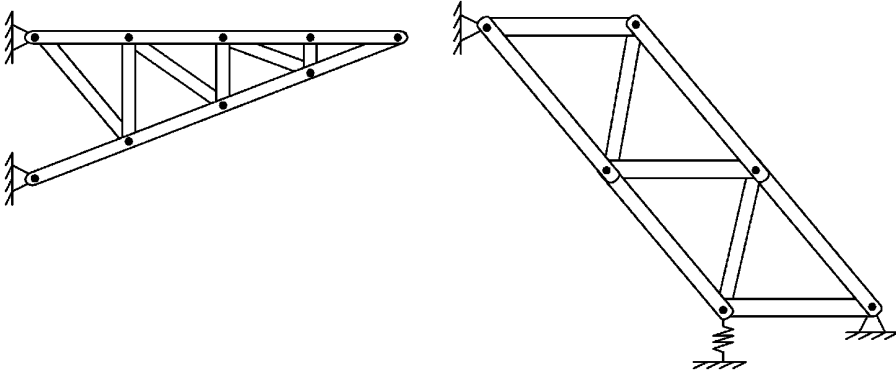
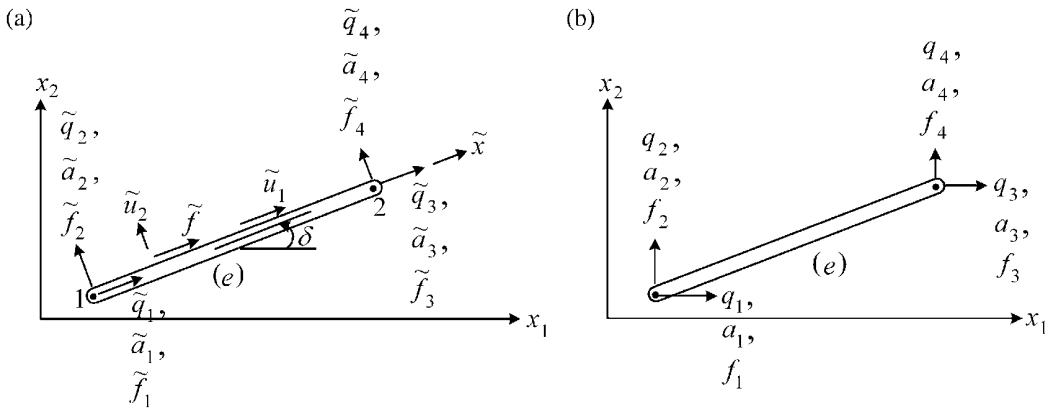


Figure 4.8.11 Typical 2D trusses

Figure 4.8.12 Truss element (e) shown with local (a) and global (b) nodal displacements (q), internal actions (a), and applied (external) forces (f)

where

$$\underline{q}_e = (q_{1e} \ q_{2e} \ q_{3e} \ q_{4e})^T, \quad \tilde{\underline{q}}_e = (\tilde{q}_{1e} \ \tilde{q}_{2e} \ \tilde{q}_{3e} \ \tilde{q}_{4e})^T \quad (4.8.45)$$

$$\underline{a}_e = (a_{1e} \ a_{2e} \ a_{3e} \ a_{4e})^T, \quad \tilde{\underline{a}}_e = (\tilde{a}_{1e} \ \tilde{a}_{2e} \ \tilde{a}_{3e} \ \tilde{a}_{4e})^T \quad (4.8.46)$$

$$\underline{f}_e = (f_{1e} \ f_{2e} \ f_{3e} \ f_{4e})^T, \quad \tilde{\underline{f}}_e = (\tilde{f}_{1e} \ \tilde{f}_{2e} \ \tilde{f}_{3e} \ \tilde{f}_{4e})^T \quad (4.8.47)$$

and

$$\underline{T}_{T_e} = \begin{bmatrix} \underline{C}_e & \underline{0} \\ \underline{0} & \underline{C}_e \end{bmatrix} \quad (4.8.48)$$

where

$$\underline{C}_e = \begin{bmatrix} \cos \delta_e & \sin \delta_e \\ -\sin \delta_e & \cos \delta_e \end{bmatrix} \quad (4.8.49)$$

4.8.11 2D Truss/Bar Element: Element Stiffness Matrix

The element stiffness matrix corresponding to the local coordinates shown in Figure 4.8.12 (a) may be easily inferred from the 1D bar element case in Figure 4.8.1 and Equation (4.8.8) or (4.8.17):

$$\frac{\tilde{\mathbf{K}}_e}{4 \times 4} = \begin{bmatrix} \tilde{K}_{11} & 0 & \tilde{K}_{13} & 0 \\ 0 & 0 & 0 & 0 \\ \tilde{K}_{31} & 0 & \tilde{K}_{33} & 0 \\ 0 & 0 & 0 & 0 \end{bmatrix} \quad (4.8.50)$$

where the odd number rows and columns correspond to the axial direction, and even number rows and columns correspond to the transverse direction in Figure 4.8.12, and

$$\begin{aligned} \tilde{K}_{11} &= \int_0^{L_e} E_e(\tilde{x}) A_e(\tilde{x}) N'_{1e} N'_{1e} d\tilde{x} \\ \tilde{K}_{13} = \tilde{K}_{31} &= \int_0^{L_e} E_e(\tilde{x}) A_e(\tilde{x}) N'_{1e} N'_{2e} d\tilde{x} \\ \tilde{K}_{33} &= \int_0^{L_e} E_e(\tilde{x}) A_e(\tilde{x}) N'_{2e} N'_{2e} d\tilde{x} \end{aligned} \quad (4.8.51)$$

$$N_{1e} = 1 - \frac{\tilde{x}}{L_e}, \quad N_{2e} = \frac{\tilde{x}}{L_e} \quad (4.8.52)$$

The potential energy (4.7.54) in the truss element is the same whether evaluated in the local coordinates of Figure 4.8.12(a) or the global (system) coordinates of Figure 4.8.12(b). The potential energy expressed in local coordinates (Figure 4.8.12(a)) is (4.7.54)

$$\tilde{U}_e = \frac{1}{2} \tilde{\mathbf{q}}_e^T \tilde{\mathbf{K}}_e \tilde{\mathbf{q}}_e \quad (4.8.53)$$

Substitution of (4.8.44) into (4.8.53) yields

$$\tilde{U}_e = \frac{1}{2} \mathbf{q}_e^T (\mathbf{T}_{Te}^T \tilde{\mathbf{K}}_e \mathbf{T}_{Te}) \mathbf{q}_e \quad (4.8.54)$$

The potential energy has the following form in global coordinates:

$$U_e = \frac{1}{2} \mathbf{q}_e^T \mathbf{K}_e \mathbf{q}_e \quad (4.8.55)$$

The element stiffness matrix in global coordinates is obtained by equating (4.8.54) and (4.8.55), which yields

$$\Rightarrow \mathbf{K}_e = \mathbf{T}_{Te}^T \tilde{\mathbf{K}}_e \mathbf{T}_{Te} \quad (4.8.56)$$

For the special case, when E_e and A_e are independent of \tilde{x} , Equations (4.8.48)–(4.8.52) and (4.8.56) yield

$$\frac{\mathbf{K}_e}{4 \times 4} = \frac{E_e A_e}{L_e} \begin{bmatrix} \underline{\Lambda}_e & -\underline{\Lambda}_e \\ -\underline{\Lambda}_e & \underline{\Lambda}_e \end{bmatrix} \quad (4.8.57)$$

$$\underline{\Lambda}_e = \begin{bmatrix} \cos^2 \delta_e & \sin \delta_e \cos \delta_e \\ \sin \delta_e \cos \delta_e & \sin^2 \delta_e \end{bmatrix} \quad (4.8.58)$$

4.8.12 2D Truss/Bar Element: Element Mass Matrix

The axial (parallel to \tilde{x}) and transverse (perpendicular to \tilde{x}) displacements of the bar in Figure 4.8.12(a) are interpolated with the same shape functions:

$$\tilde{u}_1 = \tilde{q}_1 N_1 + \tilde{q}_3 N_2 \quad (4.8.59)$$

$$\tilde{u}_2 = \tilde{q}_2 N_1 + \tilde{q}_4 N_2 \quad (4.8.60)$$

This does not violate the zero bending assumption since N_1 and N_2 are linear in \tilde{x} , so that \tilde{u}_2 represents rigid body (no bending) displacements in the transverse direction. The kinetic energy is then given by (4.7.1)

$$\begin{aligned} \tilde{T}_e &= \frac{1}{2} \int_0^{L_e} (\dot{\tilde{u}}_1^2 + \dot{\tilde{u}}_2^2) \rho_e A_e d\tilde{x} = \frac{1}{2} \int_0^{L_e} \left[(\dot{\tilde{q}}_1 N_1 + \dot{\tilde{q}}_3 N_2)^2 + (\dot{\tilde{q}}_2 N_1 + \dot{\tilde{q}}_4 N_2)^2 \right] d\tilde{x} \\ &= \frac{1}{2} \underline{\dot{\tilde{q}}}_e^T \underline{\tilde{M}}_e \underline{\dot{\tilde{q}}}_e \end{aligned} \quad (4.8.61)$$

where

$$\underline{\tilde{M}}_e = \begin{bmatrix} \tilde{M}_{11} & 0 & \tilde{M}_{13} & 0 \\ 0 & \tilde{M}_{22} & 0 & \tilde{M}_{24} \\ \tilde{M}_{31} & 0 & \tilde{M}_{33} & 0 \\ 0 & \tilde{M}_{42} & 0 & \tilde{M}_{44} \end{bmatrix} \quad (4.8.62)$$

$$\begin{aligned} \tilde{M}_{11} = \tilde{M}_{22} &= \int_0^{L_e} \rho_e(\tilde{x}) A_e(\tilde{x}) N_1 N_1 d\tilde{x} \\ \tilde{M}_{33} = \tilde{M}_{44} &= \int_0^{L_e} \rho_e(\tilde{x}) A_e(\tilde{x}) N_2 N_2 d\tilde{x} \\ \tilde{M}_{13} = \tilde{M}_{24} = \tilde{M}_{31} = \tilde{M}_{42} &= \int_0^{L_e} \rho_e(\tilde{x}) A_e(\tilde{x}) N_1 N_2 d\tilde{x} \end{aligned} \quad (4.8.63)$$

The kinetic energy expressed in local coordinates (Figure 4.8.12(a)) is (4.7.12)

$$\tilde{T}_e = \frac{1}{2} \underline{\dot{\tilde{q}}}_e^T \underline{\tilde{M}}_e \underline{\dot{\tilde{q}}}_e \quad (4.8.64)$$

Substitution of (4.8.44) into (4.8.64) yields

$$\tilde{T}_e = \frac{1}{2} \underline{\dot{\tilde{q}}}_e^T (\underline{T}_{Te}^T \underline{\tilde{M}}_e \underline{T}_{Te}) \underline{\dot{q}}_e \quad (4.8.65)$$

The kinetic energy expressed in global coordinates (Figure 4.8.12(b)) is (4.7.12)

$$T_e = \frac{1}{2} \underline{\dot{q}}_e^T \underline{M}_e \underline{\dot{q}}_e \quad (4.8.66)$$

The element mass matrix in global coordinates is obtained by equating (4.8.65) and (4.8.66), which yields

$$\underline{M}_e = \underline{T}_{Te}^T \tilde{\underline{M}}_e \underline{T}_{Te} \quad (4.8.67)$$

For the special case, when ρ_e and A_e are independent of \tilde{x} , Equations (4.8.4), (4.8.18), (4.8.62), and (4.8.63) yield

$$\tilde{\underline{M}}_e = \rho_e A_e L_e \begin{bmatrix} 1/3 & 0 & 1/6 & 0 \\ 0 & 1/3 & 0 & 1/6 \\ 1/6 & 0 & 1/3 & 0 \\ 0 & 1/6 & 0 & 1/3 \end{bmatrix} \quad (4.8.68)$$

Substitution of (4.8.48), (4.8.49), and (4.8.68) into (4.8.67) provides the result

$$\underline{M}_e = \tilde{\underline{M}}_e \quad (4.8.69)$$

4.8.13 2D Truss/Bar Element: Element Damping Matrix

Consider a distributed viscous damping (per length) $\tilde{c}(\tilde{x})$ which acts both in the transverse and axial directions with respect to the bar element. The corresponding dissipation function (4.5.81) is

$$\mathfrak{S}^d = \frac{1}{2} \int_0^{L_e} \tilde{c}(\tilde{x}) (\dot{u}_1^2 + \dot{u}_2^2) d\tilde{x} \quad (4.8.70)$$

By comparing (4.8.61) with (4.8.70) and considering the corresponding LE terms (4.7.60),

$$\text{Mass matrix generation from: } \frac{n d}{dt} \left(\frac{\partial T}{\partial \dot{q}_j} \right) \quad (4.8.71)$$

$$\text{Damping matrix generation from: } \frac{\partial \mathfrak{S}^d}{\partial \dot{q}_j}$$

it results that the mass and damping matrices have identical forms. Thus, from (4.8.62) and (4.8.63), the element damping matrix becomes

$$\tilde{\underline{C}}_e = \begin{bmatrix} \tilde{C}_{11} & 0 & \tilde{C}_{13} & 0 \\ 0 & \tilde{C}_{22} & 0 & \tilde{C}_{24} \\ \tilde{C}_{31} & 0 & \tilde{C}_{33} & 0 \\ 0 & \tilde{C}_{42} & 0 & \tilde{C}_{44} \end{bmatrix} \quad (4.8.72)$$

$$\tilde{C}_{11} = \tilde{C}_{22} = \int_0^{L_e} \tilde{c}(\tilde{x}) N_1 N_1 d\tilde{x}$$

$$\tilde{C}_{33} = \tilde{C}_{44} = \int_0^{L_e} \tilde{c}(\tilde{x}) N_2 N_2 d\tilde{x} \quad (4.8.73)$$

$$\tilde{C}_{13} = \tilde{C}_{24} = \tilde{C}_{31} = \tilde{C}_{42} = \int_0^{L_e} \tilde{c}(\tilde{x}) N_1 N_2 d\tilde{x}$$

The element damping matrix in global coordinates (Figure 4.8.12(b)) is

$$\underline{C}_e = \underline{T}_{Te}^T \tilde{C}_e \underline{T}_{Te} \quad (4.8.74)$$

For the special case when \tilde{c} is independent of \tilde{x} , Equations (4.8.72)–(4.8.74) yield

$$\underline{C}_e = \tilde{C}_e = \tilde{c}_e L_e \begin{bmatrix} 1/3 & 0 & 1/6 & 0 \\ 0 & 1/3 & 0 & 1/6 \\ 1/6 & 0 & 1/3 & 0 \\ 0 & 1/6 & 0 & 1/3 \end{bmatrix} \quad (4.8.75)$$

4.8.14 2D Truss/Bar Element: Element Force Vector

From (4.8.16) and Figure 4.8.12(a), the element force vector in local coordinates is

$$\tilde{\underline{f}}_e = \int_0^{L_e} \tilde{f}_e(\tilde{x}) \begin{Bmatrix} N_1 \\ 0 \\ N_2 \\ 0 \end{Bmatrix} d\tilde{x} \quad (4.8.76)$$

The coordinate transformation matrix \underline{T}_{Te} defined in (4.8.48) and (4.8.49) is orthogonal:

$$\underline{T}_{Te}^T = \underline{T}_{Te}^{-1} \quad (4.8.77)$$

Thus, (4.8.44) provides the global coordinate element force vector as

$$\underline{f}_e = \underline{T}_{Te}^T \tilde{\underline{f}}_e \quad (4.8.78)$$

Substitution of (4.8.48), (4.8.49), and (4.8.76) yields

$$\underline{f}_e = \int_0^{L_e} \bar{f}_e(\tilde{x}) \begin{Bmatrix} N_1 \cos \delta_e \\ N_1 \sin \delta_e \\ N_2 \cos \delta_e \\ N_2 \sin \delta_e \end{Bmatrix} d\tilde{x} \quad (4.8.79)$$

where δ_e is the element orientation angle in Figure 4.8.12. For constant $\tilde{f}_e(\tilde{x}) = \bar{f}_e$, (4.8.79) becomes

$$\underline{f}_e = \bar{f}_e \frac{L_e}{2} \begin{Bmatrix} \cos \delta_e \\ \sin \delta_e \\ \cos \delta_e \\ \sin \delta_e \end{Bmatrix} \quad (4.8.80)$$

4.8.15 2D Truss/Bar Element: Element Action Vector

The actions transform in the same manner as (4.8.78), yielding

$$\underline{a}_e = \underline{T}_{Te}^T \tilde{\underline{a}}_e = \begin{Bmatrix} \cos(\delta_e) \tilde{a}_{1e} - \sin(\delta_e) \tilde{a}_{2e} \\ \sin(\delta_e) \tilde{a}_{1e} + \cos(\delta_e) \tilde{a}_{2e} \\ \cos(\delta_e) \tilde{a}_{3e} - \sin(\delta_e) \tilde{a}_{4e} \\ \sin(\delta_e) \tilde{a}_{3e} + \cos(\delta_e) \tilde{a}_{4e} \end{Bmatrix} \quad (4.8.81)$$

The dynamic equilibrium equation for element e is (4.7.61):

$$\underline{M}_e \ddot{\underline{q}}_e + \underline{C}_e \dot{\underline{q}}_e + \underline{K}_e \underline{q}_e = \underline{a}_e + \underline{f}_e \quad (4.8.82)$$

The actions can be obtained if \underline{q}_e , $\dot{\underline{q}}_e$, and $\ddot{\underline{q}}_e$ are known, that is, from (4.8.78),

$$\underline{a}_e = \underline{M}_e \ddot{\underline{q}}_e + \underline{C}_e \dot{\underline{q}}_e + \underline{K}_e \underline{q}_e - \underline{f}_e \quad (4.8.83)$$

Then from (4.8.44), the actions in local coordinates become

$$\tilde{\underline{a}}_e = \underline{T}_{Te} \underline{a}_e = (\tilde{a}_{1e} \quad \tilde{a}_{2e} \quad \tilde{a}_{3e} \quad \tilde{a}_{4e})^T \quad (4.8.84)$$

The local coordinate actions are used to determine element stresses, for example,

$$\sigma_{e1}(t) = \frac{\tilde{a}_{1e}(t)}{A_e(\tilde{x}=0)} \quad (4.8.85)$$

$$\sigma_{e2}(t) = \frac{\tilde{a}_{3e}(t)}{A_e(\tilde{x}=L_e)} \quad (4.8.86)$$

which can be employed to evaluate the fatigue life of each element (e) as discussed in Section 1.4.

4.8.16 2D Truss/Bar Element: Degree of Freedom Connectivity Array and Matrix Assembly

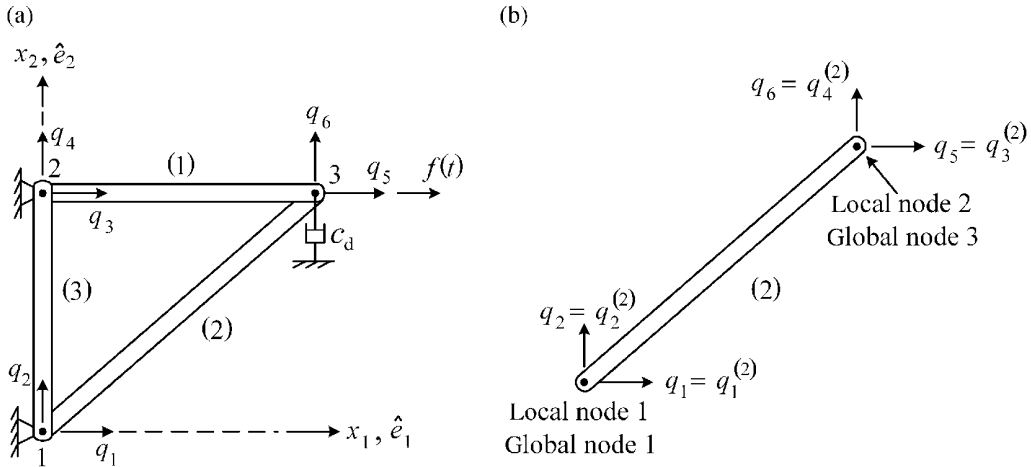
The 1D bar model had a single degree of freedom (dof) at each node, which allowed all dof information to be stored in the NCA (4.8.21). The 2D truss model has 2 *dof at each node*; therefore, a new array is needed to store the local degrees of freedom information for assembling the global (system) matrices. This is referred to as the “*degree of freedom*” connectivity array (DFCA). For the 4 dof, 2D, 2-node bar element,

$$\hat{B}_{ei} = \text{global dof corresponding to the local dof } i \text{ of element } e \quad (4.8.87)$$

$$e = 1, 2, \dots, E, \quad i = 1, 2, 3, 4$$

The DFCA \hat{B}_{ei} can be defined by simple coding that utilizes:

- (i) The nodal connectivity array NCA B_{ei}
- (ii) A convention for numbering the global dofs.



Element 1	Element 2	Element 3
$L_1 = L, \quad A_1 = A$	$L_2 = \sqrt{2}L, \quad A_2 = A$	$L_3 = L, \quad A_3 = 3A$
$E_1 = E, \quad \rho_1 = 2\rho$	$E_2 = 2E, \quad \rho_2 = \rho$	$E_3 = E, \quad \rho_3 = \rho$

Figure 4.8.13 Three-member truss model to illustrate constrained system assembly showing (a) entire truss and (b) isolated element (2)

The degree of freedom and matrix assembly method is illustrated by the following example.

The convention in (ii) is illustrated in Figure 4.8.13(a) which shows that the x_1 and x_2 dofs at node j are numbered as

$$\begin{aligned} x_1 \text{ dof at global node } j &\Rightarrow q_{2j-1} \\ x_2 \text{ dof at global node } j &\Rightarrow q_{2j} \end{aligned} \quad (4.8.88)$$

The nodal connectivity \underline{B} and dof connectivity $\hat{\underline{B}}$ array entries for element 2 are shown in Figure 4.8.13(a) as

$$\begin{aligned} B_{21} = 1, \quad B_{22} = 3 \\ \hat{B}_{21} = 1, \quad \hat{B}_{22} = 2, \quad \hat{B}_{23} = 5, \quad \hat{B}_{24} = 6 \end{aligned} \quad (4.8.89)$$

The nodal and degree of freedom (dof) connectivity arrays for the entire structure are

$$\underline{B}_{3 \times 2} = \begin{bmatrix} 2 & 3 \\ 1 & 3 \\ 1 & 2 \end{bmatrix}, \quad \hat{\underline{B}}_{3 \times 4} = \begin{bmatrix} 3 & 4 & 5 & 6 \\ 1 & 2 & 5 & 6 \\ 1 & 2 & 3 & 4 \end{bmatrix} \quad (4.8.90)$$

The DFCA \hat{B} may be obtained from the NCA B utilizing the numbering convention in (4.8.88) and the following “for” loops:

```

for  $e = 1 : 1 : E$       element index
  for  $i = 1 : 1 : 2$     local node index
    for  $k = 1 : 1 : 2$   local dof index at a node
       $\alpha = 2 * (i - 1) + k$   local dof index in element
       $\hat{B}_{ea} = 2(B_{ei} - 1) + k$ 
    end
  end
end
end

```

The l and j constraint arrays are also defined in terms of degree of freedom instead of node numbers. The $jarray$ contains the free degree of freedoms, that is, from Figure 4.8.13(a):

$$\tilde{J} = (j_1 \ j_2) = (5 \ 6) \quad (4.8.91)$$

$$N_f = 2 \text{ free dofs} \quad (4.8.92)$$

Then the position of each of the six system degrees of freedom in the free dof displacement vector

$$\underline{q}_f = (q_1^f \ q_2^f)^T = (q_{j_1} \ q_{j_2})^T = (q_5 \ q_6)^T \quad (4.8.93)$$

is given by the $larray$:

$$\tilde{L} = (l_1 \ l_2 \ \dots \ l_6) = (0 \ 0 \ 0 \ 0 \ 1 \ 2) \ (N_d \times 1) \quad (4.8.94)$$

$$N_d = \text{number of system dofs} = 2 \times N_N = 2 \times 3 = 6 \quad (4.8.95)$$

Note that l_i is zero if the system dof i is fixed. The dynamic equilibrium equation for the free dofs of the constrained structure has the general form

$$\underline{M}_f \ddot{\underline{q}}_f + \underline{C}_f \dot{\underline{q}}_f + \underline{K}_f \underline{q}_f = \underline{F}_f \quad (4.8.96)$$

$N_f \times N_f \ N_f \times 1$ $N_f \times N_f \ N_f \times 1$ $N_f \times N_f \ N_f \times 1$ $N_f \times 1$

The \hat{B} (dof connectivity) and \tilde{L} (free node assignment) arrays are employed to assemble \underline{M}_f , \underline{K}_f , and \underline{F}_f as summarized by the following steps:

(a) Let \underline{G}_f represent \underline{M}_f , \underline{C}_f , or \underline{K}_f and $\underline{G}^{(e)}$ represent element matrices $\underline{M}^{(e)}$, $\underline{C}^{(e)}$, or $\underline{K}^{(e)}$. (4.8.97a)

(b) Initialize $\underline{G}_f = \underline{0}$ and $\underline{F}_f = \underline{0}$.

(c) Then \underline{G}_f is formed by adding the row r , column s entry of $\underline{G}^{(e)}$, (4.8.97b)

that is, $(\underline{G}^{(e)})_{rs}$, into the (row $l_{\hat{B}_{er}}$, column $l_{\hat{B}_{es}}$) position of \underline{G}_f for all elements ($e = 1, 2, \dots, E$) and all rows and columns ($r = 1, 4$, $s = 1, 4$) of each element matrix $\underline{G}^{(e)}$. The addition operation is performed if and only if $l_{\hat{B}_{er}} \neq 0$ and $l_{\hat{B}_{es}} \neq 0$.

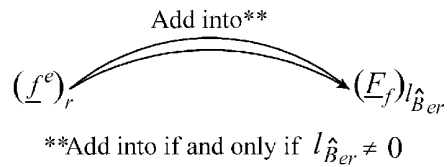
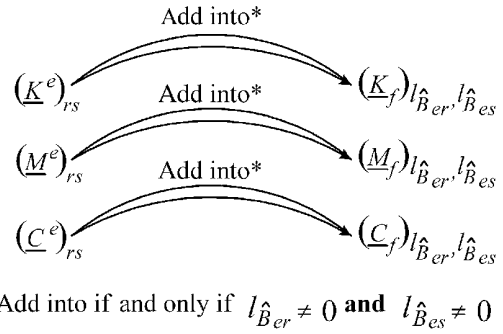


Figure 4.8.14 Assembly of free dof system matrices and force vector for a constrained system

(d) The excitation vector \underline{F}_f is formed by adding the r th entry of $\underline{f}^{(e)}$, (4.8.97c)

that is, $(\underline{f}^{(e)})_r$ into the row $l_{\hat{B}_{er}}$ position of \underline{F}_f for all elements ($e = 1, 2, \dots, E$) and all rows ($r = 1, 4$) of each of each element force vector $\underline{f}^{(e)}$. The addition operation is performed if and only if $l_{\hat{B}_{er}} \neq 0$.

This procedure is illustrated in Figure 4.8.14.

Repeat the above “assembly” step for all E elements in the model and for all four local degrees of freedom, that is,

$$\begin{aligned} e &= 1, 2, \dots, E \\ r &= 1, \dots, 4 \\ s &= 1, \dots, 4 \end{aligned} \quad (4.8.98)$$

Table 4.8.2 provides the arrays required to assemble the global (system) matrices from the element matrices for the three-member truss example shown in Figure 4.8.13.

By inspection of the last columns in Table 4.8.2, the matrix assembly criterion, $l_{\hat{B}_{er}} \neq 0$ and $l_{\hat{B}_{es}} \neq 0$, in (4.8.97b) is satisfied only for the entries shown in Table 4.8.3.

The last two columns of Table 4.8.3 are the row and column numbers in the free dof matrices $(\underline{M}_f, \underline{C}_f,$ and $\underline{K}_f)$. Therefore, Table 4.8.3, along with the assembly diagram in Figure 4.8.14, yields the free dof mass and stiffness matrices as

$$\underline{K}_f = \begin{bmatrix} k_{33}^1 + k_{33}^2 & k_{34}^1 + k_{34}^2 \\ k_{43}^1 + k_{43}^2 & k_{44}^1 + k_{44}^2 \end{bmatrix}, \quad \underline{M}_f = \begin{bmatrix} m_{33}^1 + m_{33}^2 & m_{34}^1 + m_{34}^2 \\ m_{43}^1 + m_{43}^2 & m_{44}^1 + m_{44}^2 \end{bmatrix} \quad (4.8.99)$$

Figure 4.8.13 shows a damper is attached in the x_2 direction at node 3. The dissipation function (4.5.81) for this damper is

$$\mathfrak{D}^d = \frac{c_d}{2} \dot{q}_6^2 = \frac{c_d}{2} (\dot{q}_2^f)^2 \quad (4.8.100)$$

Table 4.8.2 Dof Connectivity and constraint arrays for the model in Figure 4.8.13

e	r	s	\hat{B}_{er}	\hat{B}_{es}	$l_{\hat{B}_{er}}$	$l_{\hat{B}_{es}}$
1	1	1	3	3	0	0
1	1	2	3	4	0	0
1	1	3	3	5	0	1
1	1	4	3	6	0	2
1	2	1	4	3	0	0
1	2	2	4	4	0	0
1	2	3	4	5	0	1
1	2	4	4	6	0	2
1	3	1	5	3	1	0
1	3	2	5	4	1	0
1	3	3	5	5	1	1
1	3	4	5	6	1	2
1	4	1	6	3	2	0
1	4	2	6	4	2	0
1	4	3	6	5	2	1
1	4	4	6	6	2	2
2	1	1	1	1	0	0
2	1	2	1	2	0	0
2	1	3	1	5	0	1
2	1	4	1	6	0	2
2	2	1	2	1	0	0
2	2	2	2	2	0	0
2	2	3	2	5	0	1
2	2	4	2	6	0	2
2	3	1	5	1	1	0
2	3	2	5	2	1	0
2	3	3	5	5	1	1
2	3	4	5	6	1	2
2	4	1	6	1	2	0
2	4	2	6	2	2	0
2	4	3	6	5	2	1
2	4	4	6	6	2	2
3	1	1	1	1	0	0
3	1	2	1	2	0	0
3	1	3	1	3	0	0
3	1	4	1	4	0	0
3	2	1	2	1	0	0
3	2	2	2	2	0	0
3	2	3	2	3	0	0
3	2	4	2	4	0	0
3	3	1	3	1	0	0
3	3	2	3	2	0	0
3	3	3	3	3	0	0
3	3	4	3	4	0	0
3	4	1	4	1	0	0
3	4	2	4	2	0	0
3	4	3	4	3	0	0
3	4	4	4	4	0	0

Table 4.8.3 Entries in Table 4.8.2 that assemble into the system matrices

e	r	s	$l_{\hat{B}_{er}}$	$l_{\hat{B}_{es}}$
1	3	3	1	1
1	3	4	1	2
1	4	3	2	1
1	4	4	2	2
2	3	3	1	1
2	3	4	1	2
2	4	3	2	1
2	4	4	2	2

Therefore, the contribution of c_d to the constrained system EOM (4.8.96) is from (4.5.82):

$$\begin{Bmatrix} \partial \mathfrak{S}^d / \partial \dot{q}_1^f \\ \partial \mathfrak{S}^d / \partial \dot{q}_2^f \end{Bmatrix} = \begin{Bmatrix} 0 \\ c_d \dot{q}_2^f \end{Bmatrix} = \begin{bmatrix} 0 & 0 \\ 0 & c_d \end{bmatrix} \begin{Bmatrix} \dot{q}_1^f \\ \dot{q}_2^f \end{Bmatrix} \quad (4.8.101)$$

Therefore, since c_d is the only damper in the system,

$$\underline{C}_f = \begin{bmatrix} 0 & 0 \\ 0 & c_d \end{bmatrix} \quad (4.8.102)$$

in (4.8.96). Figure 4.8.13 shows a force in the x_1 direction at node 3. The corresponding generalized forces are obtained utilizing $q_1^f = q_5$ and $q_2^f = q_6$ and the generalized force definition (4.5.52) as

$$Q_1 = f \hat{e}_1 \cdot \frac{\partial(\dot{q}_5 \hat{e}_1 + \dot{q}_6 \hat{e}_2)}{\partial \dot{q}_1^f} = f \frac{\partial \dot{q}_1^f}{\partial \dot{q}_1^f} = f \quad (4.8.103)$$

$$Q_2 = f \hat{e}_1 \cdot \frac{\partial(\dot{q}_5 \hat{e}_1 + \dot{q}_6 \hat{e}_2)}{\partial \dot{q}_2^f} = f \frac{\partial \dot{q}_1^f}{\partial \dot{q}_2^f} = f \cdot 0 = 0 \quad (4.8.104)$$

Therefore, the constrained system force vector in (4.8.96) is

$$\underline{F}_f = \begin{Bmatrix} Q_1 \\ Q_2 \end{Bmatrix} = \begin{Bmatrix} f \\ 0 \end{Bmatrix} \quad (4.8.105)$$

The constrained system EOM (4.8.96) for the free dofs is obtained from (4.8.99), (4.8.102), and (4.8.105) as

$$\begin{bmatrix} m_{33}^1 + m_{33}^2 & m_{34}^1 + m_{34}^2 \\ m_{43}^1 + m_{43}^2 & m_{44}^1 + m_{44}^2 \end{bmatrix} \begin{Bmatrix} \ddot{q}_1^f \\ \ddot{q}_2^f \end{Bmatrix} + \begin{bmatrix} 0 & 0 \\ 0 & c_d \end{bmatrix} \begin{Bmatrix} \dot{q}_1^f \\ \dot{q}_2^f \end{Bmatrix} + \begin{bmatrix} k_{33}^1 + k_{33}^2 & k_{34}^1 + k_{34}^2 \\ k_{43}^1 + k_{43}^2 & k_{44}^1 + k_{44}^2 \end{bmatrix} \begin{Bmatrix} q_1^f \\ q_2^f \end{Bmatrix} = \begin{Bmatrix} f(t) \\ 0 \end{Bmatrix} \quad (4.8.106)$$

where

$$q_1^f = q_5, \quad q_2^f = q_6 \quad (4.8.107)$$

The absence of “3” as a superscript in (4.8.106) indicates that element 3 does not contribute to the constrained system EOMs. This results since both of its nodes are fixed as shown in Figure 4.8.13. The mass and stiffness matrix entries in (4.8.106) are obtained from (4.8.57), (4.8.58), (4.8.68), and (4.8.69) for $e=1$ and $e=2$ in the following manner.

4.8.16.1 Element Mass Matrix Entries

Let

$$\underline{R}_m = \begin{bmatrix} 1/3 & 0 & 1/6 & 0 \\ 0 & 1/3 & 0 & 1/6 \\ 1/6 & 0 & 1/3 & 0 \\ 0 & 1/6 & 0 & 1/3 \end{bmatrix} \quad (4.8.108)$$

Then by (4.8.57) and (4.8.58) and the information provided in Figure 4.8.13,

$$\begin{aligned} \underline{M}_1 &= 2\rho AL\underline{R}_m = 2m\underline{R}_m \\ \underline{M}_2 &= \sqrt{2}\rho AL\underline{R}_m = \sqrt{2}m\underline{R}_m \\ \underline{M}_3 &= 3\rho AL\underline{R}_m = 3m\underline{R}_m \end{aligned} \quad (4.8.109)$$

where

$$m = \rho AL = \text{mass of elements 1 or 3} \quad (4.8.110)$$

4.8.16.2 Element Stiffness Matrix Entries

Recall from (4.8.57) and (4.8.58) that

$$\underline{K}_e = \frac{E_e A_e}{L_e} \begin{bmatrix} \underline{\Lambda}_e & -\underline{\Lambda}_e \\ -\underline{\Lambda}_e & \underline{\Lambda}_e \end{bmatrix} \quad (4.8.111)$$

$$\underline{\Lambda}_e = \begin{bmatrix} \cos^2 \delta_e & \sin \delta_e \cos \delta_e \\ \sin \delta_e \cos \delta_e & \sin^2 \delta_e \end{bmatrix} \quad (4.8.112)$$

Then from Figure 4.8.13 and the nodal ordering in \underline{B} (4.8.90),

$$\underline{e}=1 \quad \delta_1=0, \quad \underline{\Lambda}_1 = \begin{bmatrix} 1 & 0 \\ 0 & 0 \end{bmatrix} \quad (4.8.113)$$

$$\underline{K}_1 = \frac{EA}{L} * \begin{bmatrix} 1 & 0 & -1 & 0 \\ 0 & 0 & 0 & 0 \\ -1 & 0 & 1 & 0 \\ 0 & 0 & 0 & 0 \end{bmatrix} \quad (4.8.114)$$

$$\underline{e}=2 \quad \delta_2=45^\circ, \quad \underline{\Lambda}_2=\begin{bmatrix} 1/2 & 1/2 \\ 1/2 & 1/2 \end{bmatrix} \quad (4.8.115)$$

$$\underline{K}_2=\frac{1}{2}\frac{2EA}{\sqrt{2}L}*\begin{bmatrix} 1 & 1 & -1 & -1 \\ 1 & 1 & -1 & -1 \\ -1 & -1 & 1 & 1 \\ -1 & -1 & 1 & 1 \end{bmatrix} \quad (4.8.116)$$

$$\underline{e}=3 \quad \delta_3=90^\circ, \quad \underline{\Lambda}_3=\begin{bmatrix} 0 & 0 \\ 0 & 1 \end{bmatrix} \quad (4.8.117)$$

$$\underline{K}_3=\frac{3EA}{L}*\begin{bmatrix} 0 & 0 & 0 & 0 \\ 0 & 1 & 0 & -1 \\ 0 & 0 & 0 & 0 \\ 0 & -1 & 0 & 1 \end{bmatrix} \quad (4.8.118)$$

Substituting (4.8.109), (4.8.114), (4.8.116), and (4.8.118) into (4.8.106) yields the system equilibrium equation

$$m\begin{bmatrix} \frac{2}{3}+\frac{\sqrt{2}}{3} & 0 \\ 0 & \frac{2}{3}+\frac{\sqrt{2}}{3} \end{bmatrix}\begin{Bmatrix} \ddot{q}_1^f \\ \ddot{q}_2^f \end{Bmatrix}+\begin{bmatrix} 0 & 0 \\ 0 & c_d \end{bmatrix}\begin{Bmatrix} \dot{q}_1^f \\ \dot{q}_2^f \end{Bmatrix}+\frac{EA}{L}\begin{bmatrix} 1+\frac{1}{\sqrt{2}} & \frac{1}{\sqrt{2}} \\ \frac{1}{\sqrt{2}} & \frac{1}{\sqrt{2}} \end{bmatrix}\begin{Bmatrix} q_1^f \\ q_2^f \end{Bmatrix}=\begin{Bmatrix} f(t) \\ 0 \end{Bmatrix} \quad (4.8.119)$$

where

$$\begin{Bmatrix} q_1^f \\ q_2^f \end{Bmatrix}=\begin{Bmatrix} q_5 \\ q_6 \end{Bmatrix} \quad (4.8.120)$$

4.8.17 2D Truss/Bar Element: Rigid Region Modeling for 2D Trusses

Truss- and frame-type structures often support machinery or equipment that are very rigid and geometrically complex relative to the truss or frame. One finite element modeling approach is to “cover” the rigid area with truss members that are assigned artificially high stiffness (Young’s modulus, cross-sectional area, etc.) and attach the inertia of the rigid component near to its actual center of mass. The somewhat salient penalty for this approach is that numerical solutions greatly increase in time if there is a large separation in the max and min values in the stiffness matrix (ill conditioning). Thus, inserting elements of artificially high stiffness may cause excessively long simulation times. An approach that circumvents that problem is to incorporate the kinematic conditions that accompany rigid components into the deformations of the elements that are attached to the rigid components.

Consider an RB with mass m_R and centroidal mass moment of inertia I_{GR} as shown in Figure 4.8.15. The body undergoes small rotations and translations in planar motion.

The velocity at D may be expressed in terms of that at G as (2.11.19)

$$\vec{v}_D=\vec{v}_G+\dot{\theta}_R\hat{e}_3\times\vec{r}_{D/G} \quad (4.8.121)$$

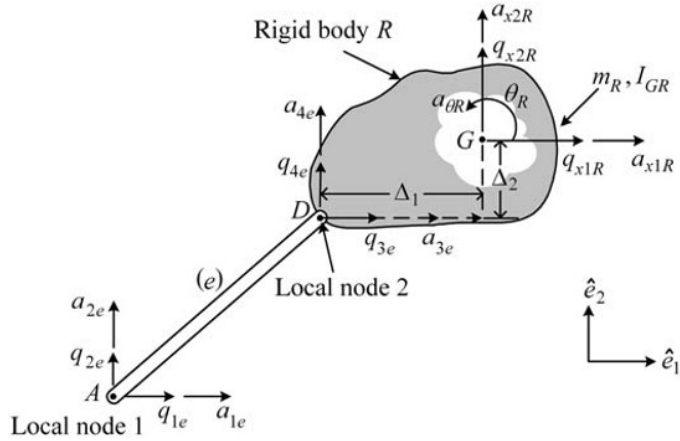


Figure 4.8.15 Rigid body attached to a 2D truss

or

$$\dot{q}_{3e}\hat{e}_1 + \dot{q}_{4e}\hat{e}_2 = \dot{q}_{x1R}\hat{e}_1 + \dot{q}_{x2R}\hat{e}_2 + \dot{\theta}_R\hat{e}_3 \times (-\Delta_1\hat{e}_1 - \Delta_2\hat{e}_2) \quad (4.8.122)$$

$$\dot{q}_{3e} = \dot{q}_{x1R} + \Delta_2\dot{\theta}_R \quad (4.8.123)$$

$$\dot{q}_{4e} = \dot{q}_{x2R} - \Delta_1\dot{\theta}_R \quad (4.8.124)$$

Thus, for small motions,

$$q_{3e} \approx q_{x1R} + \Delta_2\theta_R \quad (4.8.125)$$

$$q_{4e} \approx q_{x2R} - \Delta_1\theta_R \quad (4.8.126)$$

The displacement vector for element e may then be written as

$$\underline{q}_e = \begin{Bmatrix} q_{1e} \\ q_{2e} \\ q_{3e} \\ q_{4e} \end{Bmatrix} = \begin{bmatrix} 1 & 0 & 0 & 0 & 0 \\ 0 & 1 & 0 & 0 & 0 \\ 0 & 0 & 1 & 0 & \Delta_2 \\ 0 & 0 & 0 & 1 & -\Delta_1 \end{bmatrix} \begin{Bmatrix} q_{1e} \\ q_{2e} \\ q_{x1R} \\ q_{x2R} \\ \theta_R \end{Bmatrix} \quad (4.8.127)$$

or

$$\underline{q}_e = \underline{\Gamma}_e \underline{q}_{Re} \quad (4.8.128)$$

The actions (internal forces) at local node 2 of each element attached to the rigid body R contribute to the resultant forces and moment acting on R . Let N_{cR} be the number of elements connected to rigid body R . Then the resultant forces and moment exerted on R due to the truss actions are

$$\begin{Bmatrix} a_{x1R} \\ a_{x2R} \\ a_{\theta R} \end{Bmatrix} = \sum_e^{N_c} \begin{bmatrix} 0 & 0 & 1 & 0 \\ 0 & 0 & 0 & 1 \\ 0 & 0 & \Delta_{2e} & -\Delta_{1e} \end{bmatrix} \begin{Bmatrix} a_{1e} \\ a_{2e} \\ a_{3e} \\ a_{4e} \end{Bmatrix} = \sum_e^{N_c} \underline{\beta}_{-e} * \underline{a}_{-e} \quad (4.8.129)$$

where $\underline{\beta}_e$ is the matrix in (4.8.129). The sum in (4.8.129) includes only elements that are attached to the rigid body R . Recall from (4.8.83) that

$$\underline{a}_e = \underline{M}_e \ddot{\underline{q}}_e + \underline{K}_e \underline{q}_e \quad (4.8.130)$$

Substitute (4.8.130) into (4.8.129) to obtain

$$\begin{Bmatrix} a_{x1R} \\ a_{x2R} \\ a_{\theta R} \end{Bmatrix} = \sum_{e^*}^{N_c} \underline{\beta}_e \left(\underline{M}_e \ddot{\underline{q}}_e + \underline{K}_e \underline{q}_e \right) \quad (4.8.131)$$

Inserting (4.8.128) yields

$$\begin{Bmatrix} a_{x1R} \\ a_{x2R} \\ a_{\theta R} \end{Bmatrix} = \sum_{e^*}^{N_c} \left(\underline{M}_{Re} \ddot{\underline{q}}_{Re} + \underline{K}_{Re} \underline{q}_{Re} \right) \quad (4.8.132)$$

where

$$\underline{M}_{Re} = \underline{\beta}_e \underline{M}_e \underline{\Gamma}_e \quad (4.8.133)$$

$3 \times 5 \quad 3 \times 4 \quad 4 \times 4 \quad 4 \times 5$

$$\underline{K}_{Re} = \underline{\beta}_e \underline{K}_e \underline{\Gamma}_e \quad (4.8.134)$$

$3 \times 5 \quad 3 \times 4 \quad 4 \times 4 \quad 4 \times 5$

Unlike the 2D elements that are not attached to R and have 4 dofs, there are 5 degrees of freedom for the element (truss member + R) that extends from local node 1 of element e to the mass center G of the rigid body, that is,

$$\underline{q}_{Re} = \begin{Bmatrix} q_{1e} \\ q_{2e} \\ q_{x1R} \\ q_{x2R} \\ \theta_R \end{Bmatrix} \quad (4.8.135)$$

Therefore, the size of the element stiffness matrix is 5×5 with the bottom three rows given by (4.8.132), that is,

$$\begin{Bmatrix} a_{1e} \\ a_{2e} \\ a_{x1R} \\ q_{x2R} \\ a_{\theta R} \end{Bmatrix} = \begin{bmatrix} ? \\ \text{---} \\ \underline{M}_{Re} \end{bmatrix} \left\{ \ddot{\underline{q}}_{Re} \right\} + \begin{bmatrix} ? \\ \text{---} \\ \underline{K}_{Re} \end{bmatrix} \left\{ \underline{q}_{Re} \right\} \quad (4.8.136)$$

where the summation in (4.8.132) is implicitly performed by assembling the matrices in (4.8.136) into the total system mass and stiffness matrices for all elements with local node 2 on R . The top row partitions in (4.8.136) are obtained by recalling that

$$\begin{Bmatrix} a_{1e} \\ a_{2e} \\ a_{3e} \\ a_{4e} \end{Bmatrix} = \underline{M}_e \ddot{\underline{q}}_e + \underline{K}_e \underline{q}_e = \begin{bmatrix} \underline{M}_{11e} & \underline{M}_{12e} \\ \underline{M}_{21e} & \underline{M}_{22e} \end{bmatrix} \left\{ \ddot{\underline{q}}_e \right\} + \begin{bmatrix} \underline{K}_{11e} & \underline{K}_{12e} \\ \underline{K}_{21e} & \underline{K}_{22e} \end{bmatrix} \left\{ \underline{q}_e \right\} \quad (4.8.137)$$

Therefore,

$$\begin{Bmatrix} a_{1e} \\ a_{2e} \end{Bmatrix} = \begin{bmatrix} \underline{M}_{11e} & \underline{M}_{12e} \\ \underline{M}_{21e} & \underline{M}_{22e} \end{bmatrix} \ddot{\underline{q}}_e + \begin{bmatrix} \underline{K}_{11e} & \underline{K}_{12e} \\ \underline{K}_{21e} & \underline{K}_{22e} \end{bmatrix} \underline{q}_e \quad (4.8.138)$$

Substitute (4.8.128) into (4.8.138):

$$\begin{Bmatrix} a_{1e} \\ a_{2e} \end{Bmatrix} = \hat{\underline{M}}_{Re} \ddot{\underline{q}}_{Re} + \hat{\underline{K}}_{Re} \underline{q}_{Re} \quad (4.8.139)$$

where

$$\hat{\underline{M}}_{Re} = \begin{bmatrix} \underline{M}_{11e} & \underline{M}_{12e} \\ \underline{M}_{21e} & \underline{M}_{22e} \end{bmatrix} \underline{\Gamma}_e \quad (2 \times 5) \quad (4.8.140)$$

$$\hat{\underline{K}}_{Re} = \begin{bmatrix} \underline{K}_{11e} & \underline{K}_{12e} \\ \underline{K}_{21e} & \underline{K}_{22e} \end{bmatrix} \underline{\Gamma}_e \quad (2 \times 5) \quad (4.8.141)$$

Therefore, from (4.8.136) and (4.8.139), the final form for the element mass and stiffness matrices, for elements with their node 2 on R , are

$$\underline{M}'_e = \begin{bmatrix} \hat{\underline{M}}_{Re} \\ \underline{M}_{Re} \end{bmatrix}, \quad \underline{K}'_e = \begin{bmatrix} \hat{\underline{K}}_{Re} \\ \underline{K}_{Re} \end{bmatrix} \quad (4.8.142)$$

Elements without nodes attached to R have the standard 4×4 matrices which are assembled as discussed previously. The mass m_R and inertia I_{GR} of the rigid body are added into the diagonal entries of the system mass matrix corresponding to dofs q_{x1R} , q_{x2R} , and θ_R .

Example 5.4.2 illustrates the usage of kinematic constraint conditions to model a rigid component embedded in a flexible finite element model for natural frequencies and mode shapes.

4.9 CHAPTER 4 EXERCISES

4.9.1 Exercise Location

All exercises may be conveniently viewed and downloaded at the following website: www.wiley.com/go/palazzolo. This new feature greatly reduces the length of the printed book, yielding a significant cost savings for the college student, and is updated.

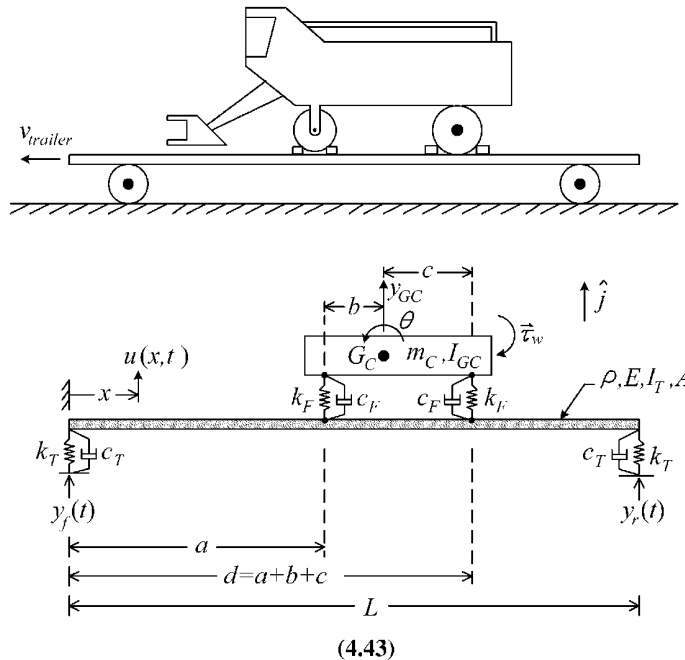
4.9.2 Exercise Goals

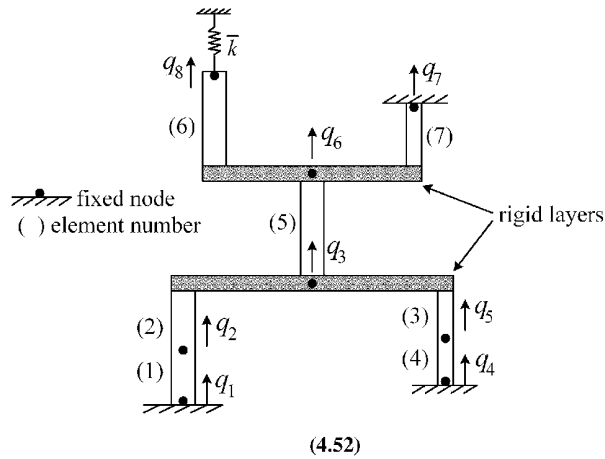
The goal of the exercises in Chapter 4 is to strengthen the student's understanding and related engineering problem-solving skills in the following areas:

- Deriving governing equations of motion utilizing energy methods: power conservation and Lagrange's equations.
- Recognizing and implementing the advantages of using energy methods over Newton's laws: Ignoring forces that contribute zero net work, only determining velocity and not acceleration, and the capability to model flexible body problems with distributed stiffness and inertia.
- Deriving expressions for kinetic energy, potential energy, dissipation, and generalized forces.
- Deriving equations of motion for systems comprised of both rigid and flexible bodies.
- Deriving equations of motion for finite element-derived models.

4.9.3 Sample Exercises: 4.43 and 4.52

These challenging exercises treat systems with both flexible and rigid bodies. Exercises (4.43) and (4.52) utilize the assumed modes and finite element methods, respectively.





REFERENCES

- BLEVINS, R. *Flow Induced Vibrations*. Van Nostrand Reinhold, 1977.
- CHILDS, D. *Turbomachinery Rotordynamics*. John Wiley & Sons, 1993.
- COOK, R. D., MALKUS, D. S. and PLESHA, M. E. *Concepts and Applications of Finite Element Analysis*, 3rd ed. John Wiley & Sons, 1989.
- DYM, C. and SHAMES, I. *Solid Mechanics: A Variational Approach*. McGraw-Hill, 1973.
- HILDEBRAND, F. B. *Advanced Calculus for Applications*, 2nd ed. Prentice Hall, 1976.
- MOORE, J. J. and PALAZZOLO, A. B. "CFD Comparison to 3D Laser Anemometer and Rotordynamic Force Measurements for Grooved Liquid Annular Seals". *ASME J. Tribol.*, Vol. **121**, 306–314, April 1999.
- SUH, J. and PALAZZOLO, A. B. "Three Dimensional Thermohydrodynamic Morton Effect Analysis—Part I: Theoretical Model". *ASME J. Tribol.*, Vol. **136**, Issue 3, 031706, July 2014.
- VANCE, J. *Rotordynamics of Turbomachinery*. John Wiley & Sons, 1987.
- VENKATARAMAN, B. and PALAZZOLO, A. "Thermohydrodynamic Analysis of Eccentric Annular Seals Using Cubic Spline Interpolation". *STLE Trans.*, Vol. **40**, Issue 1, 183–194, 1997.

Chapter 5

Free Vibration Response

5.1 INTRODUCTION

This chapter examines the free (unforced) vibration response and associated properties for various types of linear vibration system models. The free vibration analysis of a system typically consists of determining *natural frequencies*, *damping ratios*, *mode shapes*, and the vibration due to imposing *initial conditions* (ICs) on displacements and velocities. The major topics covered in this chapter include natural frequencies, damping, mode shapes, modal orthogonality, IC response, and stability. The material covered progresses from a simple single-degree-of-freedom (SDOF) model to an infinite degree-of-freedom (dof) continuous system model. Rotating systems with circulatory and gyroscopic moments are considered along with the more common nonrotating system models. Self-excited unstable systems are common in nature (communication cable whipping) and in industrial applications (machine tool chatter, fluid film bearing instability) and are discussed near the end of the chapter. Results from this chapter will be utilized extensively in succeeding chapters in transient response, steady-state harmonic response, modal synthesis, modal identification, and other areas. The mode shapes provide excellent basis vectors to reduce the number of variables required to predict the responses as discussed in Section 2.6.

The carillon bells in Figure 5.1.1 illustrate a system with widely separated natural frequencies. The bell oscillates at a very low natural frequency in a pendulum-type SDOF mode. The bell simultaneously oscillates (rings) at a much higher natural frequency in a flexible structure-type multi-dof mode. The lower mode frequency is typically near 1 Hz, and the higher frequency ringing occurs at 100s of Hz. A lack of damping is desired for both natural frequencies, in the low-frequency case to sustain clanging and in the high-frequency case to sustain the tone of the bell. A vibrating bell rings with many frequencies of sound, each produced by a separate vibrational mode shape. These natural frequencies are tuned by removing metal in annular rings, usually from the inside.

5.2 SINGLE DEGREE OF FREEDOM SYSTEMS

The equilibrium equation for an unforced SDOF linear system has the general form

$$m\ddot{q} + c\dot{q} + kq = 0 \quad (5.2.1)$$

The solution of this equation may be obtained by solving the complex variable differential equation (DE) (Section 2.5)

$$m\ddot{z} + c\dot{z} + kz = 0 \quad (5.2.2)$$

where

$$z(t) = z_R + iz_I \quad (5.2.3)$$



Figure 5.1.1 A vibrating system with very low and very high natural frequencies. Wallace Memorial Carillon. Reproduced by permission from Christ Church Cranbrook

and then obtaining $q(t)$ from

$$q(t) = \text{Real}(z(t)) \quad (5.2.4)$$

This is proven by substituting (5.2.3) into (5.2.2) to obtain

$$m(\ddot{z}_R + i\ddot{z}_I) + c(\dot{z}_R + i\dot{z}_I) + k(z_R + iz_I) = 0 \quad (5.2.5)$$

which is equivalent to the two real variable equations

$$m\ddot{z}_R + c\dot{z}_R + kz_R = 0 \quad (5.2.6)$$

$$m\ddot{z}_I + c\dot{z}_I + kz_I = 0 \quad (5.2.7)$$

Comparison of (5.2.6) to (5.2.1) shows that q and z_R must be equivalent since they have the same governing equation so (5.2.4) is proven. To solve (5.2.2), substitute

$$z(t) = \psi e^{\lambda t} \quad (5.2.8)$$

into (5.2.2), where ψ and λ are in general complex constants, to obtain

$$(m\lambda^2 + c\lambda + k)\psi = 0 \quad (5.2.9)$$

5.2.1 SDOF Eigenvalues (Characteristic Roots)

Note that by (5.2.8) vibrations will not occur, for all time t , if $\psi = 0$. This contradicts experience since a system will vibrate if given ICs and released; therefore, for the equality in (5.2.9) to hold, it must be true that

$$m\lambda^2 + c\lambda + k = 0 \quad (5.2.10)$$

which is the “characteristic equation” of (5.2.1). Divide by m and define the variables

$$\omega_n = \left(\frac{k}{m}\right)^{1/2} = \text{undamped natural frequency} \quad (5.2.11)$$

and

$$\xi = \frac{c}{2m\omega_n} = \text{damping ratio} \quad (5.2.12)$$

to obtain the characteristic equation

$$\lambda^2 + 2\xi\omega_n\lambda + \omega_n^2 = 0 \quad (5.2.13)$$

The roots of this equation are readily solved with the quadratic formula or via the Maple code:

Maple Code for Quadratic Formula

```
sdoREQ := lambda^2 + 2*zeta*omegan*lambda + omegan^2=0;
solve(sdoREQ, lambda);
```

This yields the “proper or characteristic roots” or in German “eigenvalues”

$$\lambda = -\xi\omega_n \pm i\omega_n\sqrt{1-\xi^2} = -\xi\omega_n \pm i\omega_d \quad (5.2.14)$$

where

$$\omega_d = \omega_n\sqrt{1-\xi^2} = \text{damped natural frequency} \quad (5.2.15)$$

“Natural” describes the ability of the system to oscillate at this frequency, independent of any external excitation. Some common examples include bells, tuning forks, light posts, and car antennas. Less familiar examples include turbine blades, rotating shafts, vehicle, offshore platforms, buildings, bridges, and so on. Equation (5.2.14) shows

$$\lambda_2 = \bar{\lambda}_1 \quad (5.2.16)$$

where $\bar{(\)}$ denotes “complex conjugate.” This is consistent with taking the complex conjugate of (5.2.13), yielding

$$\bar{\lambda}^2 + 2\xi\omega_n\bar{\lambda} + \omega_n^2 = 0 \quad (5.2.17)$$

which shows that if a complex number λ satisfies (5.2.13), then it must also be true that $\bar{\lambda}$ and $\bar{\psi}$ also satisfy (5.2.13). This property will hold independent of the number of dofs in the model as will be demonstrated in the later sections of this chapter.

5.2.2 SDOF Initial Condition Response

Equation (5.2.2) is a linear DE; hence, its complete solution is the linear superposition of all linearly independent solutions. From (5.2.8),

$$z(t) = \psi e^{\lambda t} + \bar{\psi} e^{\bar{\lambda} t} \quad (5.2.18)$$

where

$$\lambda = -\xi\omega_n + i\omega_d, \quad \bar{\lambda} = -\xi\omega_n - i\omega_d \quad (5.2.19)$$

Use of Euler's identity (Example 2.4.3) yields

$$\begin{aligned}\text{Conj}(e^{\lambda t}) &= \text{Conj}(e^{-\xi\omega_n t + i\omega_d t}) = \text{Conj}(e^{-\xi\omega_n t} e^{i\omega_d t}) \\ &= e^{-\xi\omega_n t} (\cos \omega_d t - i \sin \omega_d t) \\ &= e^{-\xi\omega_n t} e^{-i\omega_d t} \\ &= e^{(-\xi\omega_n - i\omega_d)t} = e^{\bar{\lambda}t}\end{aligned}\quad (5.2.20)$$

Therefore, (5.2.18) becomes

$$\begin{aligned}z(t) &= \psi e^{\lambda t} + \overline{(\psi e^{\lambda t})} = 2\text{Re}(\psi e^{\lambda t}) = 2\text{Re}((\psi_R + i\psi_I)e^{-\xi\omega_n t} e^{i\omega_d t}) \\ &= 2e^{-\xi\omega_n t} (\psi_R \cos \omega_d t - \psi_I \sin \omega_d t)\end{aligned}\quad (5.2.21)$$

Finally, from (5.2.4),

$$q(t) = 2e^{-\xi\omega_n t} (\psi_R \cos \omega_d t - \psi_I \sin \omega_d t) \quad (5.2.22)$$

Thus

$$\dot{q}(t) = 2e^{-\xi\omega_n t} [(\omega_d)(-\psi_R \sin \omega_d t - \psi_I \cos \omega_d t) - \xi\omega_n (\psi_R \cos \omega_d t - \psi_I \sin \omega_d t)] \quad (5.2.23)$$

It follows that

$$q(0) = 2\psi_R \quad (5.2.24)$$

$$\dot{q}(0) = 2(-\omega_d \psi_I - \xi\omega_n \psi_R) \quad (5.2.25)$$

or

$$\psi_R = \frac{q(0)}{2} \quad (5.2.26)$$

$$\psi_I = -\frac{\left(\frac{\dot{q}(0)}{2} + \xi\omega_n \frac{q(0)}{2}\right)}{\omega_d} \quad (5.2.27)$$

Substituting (5.2.26) and (5.2.27) into (5.2.22) yields

$$q(t) = e^{-\xi\omega_n t} \left(q(0) \cos \omega_d t + \frac{\dot{q}(0) + \xi\omega_n q(0)}{\omega_d} \sin \omega_d t \right) \quad (5.2.28)$$

This result may be rewritten using the trigonometric identity

$$A \cos x + B \sin x = \sqrt{A^2 + B^2} \cos \left(x - \tan^{-1} \left(\frac{B}{A} \right) \right) \quad (5.2.29)$$

to obtain the *IC displacement response* from (5.2.29) as

$$q(t) = e^{-\xi\omega_n t} |q| \cos(\omega_d t - \angle q) \quad (5.2.30)$$

where

$$|q| = \sqrt{q^2(0) + \left(\frac{\dot{q}(0) + \xi\omega_n q(0)}{\omega_d} \right)^2}, \quad \angle q = \tan^{-1} \left(\frac{\dot{q}(0) + \xi\omega_n q(0)}{q(0)\omega_d} \right) \quad (5.2.31)$$

This response is illustrated in Figure 5.2.1.

Differentiate (5.2.30) to obtain the *IC velocity response*

$$\begin{aligned}v &= e^{-\xi\omega_n t} |q| (-\xi\omega_n \cos(\omega_d t - \angle q) - \omega_d \sin(\omega_d t - \angle q)) \\ &= e^{-\xi\omega_n t} |v| \cos(\omega_d t - \angle v)\end{aligned}\quad (5.2.32)$$

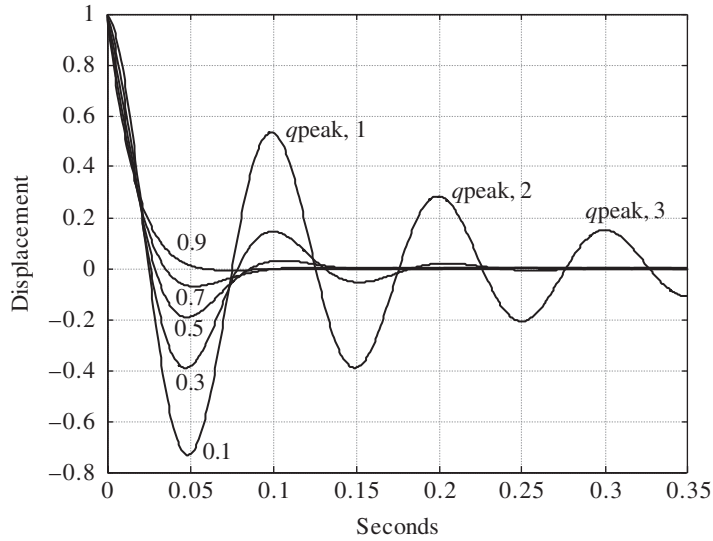


Figure 5.2.1 Initial displacement response for five values of damping ratio ξ (shown)

where

$$|v| = |q|\omega_n, \quad \angle v = \angle q + \tan^{-1} \left(\frac{-\sqrt{1-\xi^2}}{-\xi} \right) \quad (5.2.33)$$

Similarly, the *IC acceleration response* is

$$a(t) = e^{-\xi\omega_n t} |a| \cos(\omega_d t - \angle a) \quad (5.2.34)$$

where

$$|a| = \omega_n |v| = \omega_n^2 |q|, \quad \angle a = \angle v + \tan^{-1} \left(\frac{-\sqrt{1-\xi^2}}{-\xi} \right) = \angle q + 2 \tan^{-1} \left(\frac{-\sqrt{1-\xi^2}}{-\xi} \right) \quad (5.2.35)$$

The *IC jerk response* is given by

$$J = \dot{a} = \ddot{q}(t) = e^{-\xi\omega_n t} |J| \cos(\omega_d t - \angle J) \quad (5.2.36)$$

where

$$|J| = \omega_n |a| = \omega_n^3 |q|, \quad \angle J = \angle a + \tan^{-1} \left(\frac{-\sqrt{1-\xi^2}}{-\xi} \right) = \angle q + 3 \tan^{-1} \left(\frac{-\sqrt{1-\xi^2}}{-\xi} \right) \quad (5.2.37)$$

5.2.3 Log Decrement: A Measure of Damping—Displacement-Based Measurement

Damping limits vibration amplitude at resonance, reduces overshoot, and helps stabilize self-excited vibrations. It is important to measure damping for obtaining an accurate simulation model and for determining how prone a machine is to damaging vibrations. The following describes a commonly utilized approach for experimentally measuring damping.

A plot of displacement versus time (q vs. t) will show positive peaks whenever the velocity v equals zero, that is, from (5.2.32) when

$$\omega_d t_j - \angle v = \frac{\pi}{2} + 2\pi j \Rightarrow t_j = \frac{\pi/2 + 2\pi j + \angle v}{\omega_d} = \frac{\pi/2 + 2\pi j + \angle q + \gamma}{\omega_d} \quad (5.2.38)$$

where

$$j = 0, 1, 2, \dots \quad \text{and} \quad \gamma = \tan^{-1} \left(\frac{-\sqrt{1-\xi^2}}{-\xi} \right) \quad (5.2.39)$$

Insert t_j from (5.2.38) into (5.2.30) to obtain the peak displacement amplitudes shown in Figure 5.2.1:

$$q_{\text{peak},j} = e^{-\xi\omega_n t_j} |q| \cos(\omega_d t_j - \angle q) = e^{-\xi\omega_n t_j} |q| \cos\left(\frac{\pi}{2} + 2\pi j + \gamma\right) = -e^{-\xi\omega_n t_j} |q| \sin(\gamma) \quad (5.2.40)$$

The $\sin(\gamma)$ term may be expressed in terms of ξ by considering Figure 5.2.2, from which

$$\sin \gamma = -\sqrt{1-\xi^2} \quad (5.2.41)$$

Therefore, (5.2.40) becomes

$$q_{\text{peak},j} = |q| \sqrt{1-\xi^2} e^{-\xi\omega_n t_j} \quad (5.2.42)$$

The ratio of successive peak displacement amplitudes in Figure 5.2.1 is

$$\left(\frac{q_{\text{peak},j}}{q_{\text{peak},j+1}} \right) = e^{-\xi\omega_n (t_j - t_{j+1})} \quad (5.2.43)$$

Let

$$r_{qj} = \left(\frac{q_{\text{peak},j}}{q_{\text{peak},j+1}} \right) \quad (5.2.44)$$

and define the *displacement log decrement* as

$$\delta_q = \ln(r_{qj}) = -\xi\omega_n (t_j - t_{j+1}) \quad (5.2.45)$$

Substitute t_j from (5.2.38) into (5.2.45) to obtain

$$\delta_q = \frac{-\xi\omega_n}{\omega_d} [2\pi j - 2\pi(j+1)] = \frac{2\pi\xi}{\sqrt{1-\xi^2}} \quad (5.2.46)$$

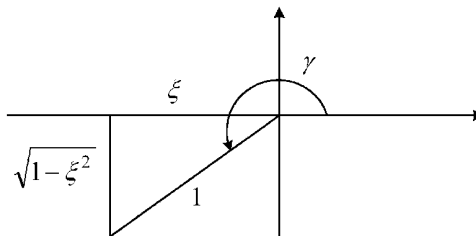


Figure 5.2.2 Damping angle (γ)

This may be solved for ξ yielding

$$\xi = \frac{\delta_q}{\sqrt{\delta_q^2 + 4\pi^2}} \quad (5.2.47)$$

Note that

$$\frac{q_{\text{peak},j}}{q_{\text{peak},j+n}} = \frac{q_{\text{peak},j}}{q_{\text{peak},j+1}} \frac{q_{\text{peak},j+1}}{q_{\text{peak},j+2}} \cdots \frac{q_{\text{peak},j+n-1}}{q_{\text{peak},j+n}} = r_j * r_{j+1} * \cdots * r_{j+n-1} \quad (5.2.48)$$

Then

$$\ln\left(\frac{q_{\text{peak},j}}{q_{\text{peak},j+n}}\right) = \ln(r_j) + \ln(r_{j+1}) + \cdots + \ln(r_{j+n-1}) = \delta_q + \delta_q + \cdots + \delta_q = n\delta_q \quad (5.2.49)$$

or

$$\delta_q = \frac{1}{n} \ln\left(\frac{q_{\text{peak},j}}{q_{\text{peak},j+n}}\right) \quad (5.2.50)$$

5.2.4 Log Decrement: A Measure of Damping—Acceleration-Based Measurement

Peaks in the acceleration (5.2.34) occur when J is zero in (5.2.36), that is,

$$\omega_d t_{ja} - \angle a - \gamma = \frac{\pi}{2} + 2\pi j, \quad j = 0, 1, 2, \dots \quad (5.2.51)$$

therefore when

$$t_{ja} = \frac{\pi/2 + 2\pi j + \gamma + \angle a}{\omega_d} \quad (5.2.52)$$

Substitute (5.2.52) into (5.2.34) to obtain

$$a_{\text{peak},j} = e^{-\xi\omega_n t_{ja}} |a| \cos\left(\frac{\pi}{2} + 2\pi j + \gamma\right) = -\sin\gamma |a| e^{-\xi\omega_n t_{ja}} = \sqrt{1-\xi^2} |a| e^{-\xi\omega_n t_{ja}} \quad (5.2.53)$$

The ratio of successive peak acceleration amplitudes is

$$\frac{a_{\text{peak},j}}{a_{\text{peak},j+1}} = e^{-\xi\omega_n (t_{ja} - t_{j+1,a})} \quad (5.2.54)$$

Substitute (5.2.52) to obtain

$$\delta_a = \ln\left(\frac{a_{\text{peak},j}}{a_{\text{peak},j+1}}\right) = -\frac{\xi\omega_n}{\omega_d} [2\pi j - 2\pi(j+1)] = \frac{2\pi\xi\omega_n}{\omega_d} = \frac{2\pi\xi}{\sqrt{1-\xi^2}} = \delta_q \quad (5.2.55)$$

which shows that measurement of log decrement for the SDOF system produces the same results if either an acceleration or displacement sensor is utilized. Summarizing these results yields:

Underdamped SDOF Free Vibration Summary

In the case that $\xi < 1$ the damped SDOF EOM

$$m\ddot{q} + c\dot{q} + kq = 0 \quad (5.2.56)$$

has the *initial condition response*

$$q(t) = e^{-\xi\omega_n t} Q \cos(\omega_d t - \angle q) \quad (5.2.57)$$

$$v(t) = \dot{q}(t) = e^{-\xi\omega_n t} \omega_n Q \cos(\omega_d t - \angle q - \gamma) \quad (5.2.58)$$

$$a(t) = \ddot{q}(t) = e^{-\xi\omega_n t} \omega_n^2 Q \cos(\omega_d t - \angle q - 2\gamma) \quad (5.2.59)$$

where

$$\omega_n = \left(\frac{k}{m}\right)^{1/2}, \quad \xi = \frac{c}{c_{cr}}, \quad c_{cr} = 2m\omega_n \quad (5.2.60)$$

$$\omega_d = \omega_n \sqrt{1 - \xi^2} \quad (5.2.61)$$

$$\gamma = \tan^{-1} \left(\frac{-\sqrt{1 - \xi^2}}{-\xi} \right) \quad (5.2.62)$$

Underdamped case : $\xi < 1 \Rightarrow \omega_d > 0$ (Oscillation occurs)

Critical damped case : $\xi = 1 \Rightarrow \omega_d = 0$ (No oscillation) (5.2.63)

Overdamped case : $\xi > 1$ (No oscillation)

For the underdamped case

$$Q = \left[q^2(0) + \left(\frac{\dot{q}(0) + \xi\omega_n q(0)}{\omega_d} \right)^2 \right]^{1/2} \quad (5.2.64)$$

$$\angle q = \tan^{-1} \left(\frac{\dot{q}(0) + \xi\omega_n q(0)}{q(0)\omega_d} \right) \quad (5.2.65)$$

Peak Times

- Displacement : $t_{qj} = \frac{(\pi/2 + 2\pi j + \angle q + \gamma)}{\omega_d}$
- Velocity : $t_{vj} = \frac{(\pi/2 + 2\pi j + \angle q + 2\gamma)}{\omega_d}$ (5.2.66)
- Acceleration : $t_{aj} = \frac{(\pi/2 + 2\pi j + \angle q + 3\gamma)}{\omega_d}$ for $j=0, 1, 2, \dots$

Peak Amplitudes

- Displacement : $q_{\text{peak},j} = Q \sqrt{1 - \xi^2} e^{-\xi\omega_n t_{aj}}$
- Velocity : $v_{\text{peak},j} = \omega_n Q \sqrt{1 - \xi^2} e^{-\xi\omega_n t_{vj}}$ (5.2.67)
- Acceleration : $a_{\text{peak},j} = \omega_n^2 Q \sqrt{1 - \xi^2} e^{-\xi\omega_n t_{aj}}$

Logarithmic Decrement

$$\delta = \ln \left(\frac{q_{\text{peak},j}}{q_{\text{peak},j+1}} \right) = \ln \left(\frac{v_{\text{peak},j}}{v_{\text{peak},j+1}} \right) = \ln \left(\frac{a_{\text{peak},j}}{a_{\text{peak},j+1}} \right) \quad (5.2.68)$$

or

$$\delta = \frac{1}{N} \ln \left(\frac{q_{\text{peak},j}}{q_{\text{peak},j+N}} \right) = \frac{1}{N} \ln \left(\frac{v_{\text{peak},j}}{v_{\text{peak},j+N}} \right) = \frac{1}{N} \ln \left(\frac{a_{\text{peak},j}}{a_{\text{peak},j+N}} \right) \quad (5.2.69)$$

Damping Ratio

$$\xi = \frac{\delta}{\sqrt{\delta^2 + 4\pi^2}} \approx \frac{\delta}{2\pi} \quad \text{for } \xi \ll 1 \quad (5.2.70)$$

Damping

$$c = \xi c_{cr} = 2m\omega_n \xi = 2\sqrt{mk}\xi \quad (5.2.71)$$

Note from Equation (5.2.57) that the response will exponentially grow toward infinity if $\xi < 0$. This form of vibration is typically referred to as unstable or self-excited and occurs in many real engineering systems such as the flutter of airplane wings and turbine blades, the chatter of machine tools and valves, and the fish tailing of trailers at high speeds. This subject will be discussed in detail in Section 5.6.

EXAMPLE 5.2.1 *Slicing Mechanism*

Statement: Figure E5.2.1(a) illustrates a cutting mechanism utilized as part of a manufacturing process. The motor torque Γ_m rotates drum 1 which rotates drum 2 through rolling contact (no slip) at point A. The chopper B is attached to drum 2 and cuts part C which is translated along table D in a direction normal to the plane of the drawing. The motor torque is turned off at the end of the cutting stroke ($\theta_2 = \theta_2(0) = \theta_{20}$), and the return spring k pulls the chopper back toward its starting position ($\theta_2 = 0$).

Objective: Derive the equation of motion (EOM) for this SDOF model and then solve for its initial condition (IC) response during the return stroke.

Assumptions:

(a) Assume a no-slip interface at contact point A, so the kinematic constraint (Section 2.11) is

$$r_1\theta_1 = r_2\theta_2 \quad (1)$$

(b) Only consider the return cycle.

Solution:

(a) Derive the EOM by the Lagrange method. From (4.2.14), (4.5.88), and (4.5.104),

$$T = \frac{1}{2}I_{G1}\dot{\theta}_1^2 + \frac{1}{2}I_{G2}\dot{\theta}_2^2 = \frac{1}{2}I_{EQ}\dot{\theta}_2^2 \quad (2)$$

where the equivalent SDOF inertia is

$$I_{eq} = \left(\frac{r_2}{r_1}\right)^2 I_{G1} + I_{G2} \quad (3)$$

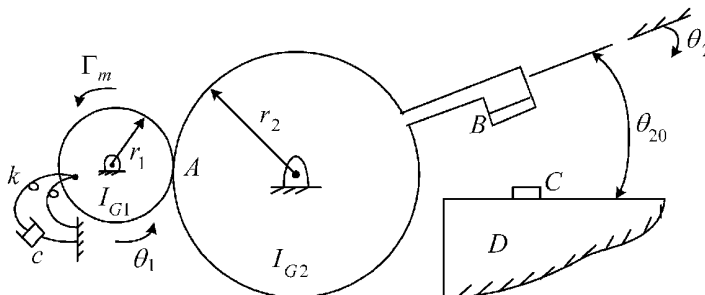


Figure E5.2.1(a) Industrial slicing mechanism

$$U = \frac{1}{2}k\theta_1^2 = \frac{k}{2}\left(\frac{r_2}{r_1}\right)^2\theta_2^2 \quad (4)$$

$$\mathfrak{F}_c^d = \frac{1}{2}c\dot{\theta}_1^2 = \frac{c}{2}\left(\frac{r_2}{r_1}\right)^2\dot{\theta}_2^2 \quad (5)$$

Substitute the above into the Lagrange equation (4.5.106a)

$$\frac{d}{dt}\left(\frac{\partial T}{\partial \dot{\theta}_2}\right) - \frac{\partial T}{\partial \theta_2} = Q - \frac{\partial U}{\partial \theta_2} - \frac{\partial(\mathfrak{F}^d + \mathfrak{F}^c)}{\partial \dot{\theta}_2} \quad (6)$$

to obtain the EOM

$$I_{\text{eq}}\ddot{\theta}_2 = -k\left(\frac{r_2}{r_1}\right)^2\theta_2 - c\left(\frac{r_2}{r_1}\right)^2\dot{\theta}_2 \quad (7)$$

or

$$I_{\text{eq}}\ddot{\theta}_2 + C_{\text{eq}}\dot{\theta}_2 + K_{\text{eq}}\theta_2 = 0 \quad (8)$$

where the equivalent SDOF damping and stiffness are

$$C_{\text{eq}} = c\left(\frac{r_2}{r_1}\right)^2 \quad (9)$$

$$K_{\text{eq}} = k\left(\frac{r_2}{r_1}\right)^2 \quad (10)$$

(b) Comparison of (8) to (5.2.56), and (5.2.60)–(5.2.62) yields

$$\omega_n = \sqrt{\frac{K_{\text{eq}}}{I_{\text{eq}}}}, \quad C_{\text{cr}} = 2I_{\text{eq}}\omega_n, \quad \xi = \frac{C_{\text{eq}}}{C_{\text{cr}}}, \quad \omega_d = \omega_n\sqrt{1-\xi^2} \quad (11)$$

(c) The ICs for the return stroke are

$$\theta_2(0) = \theta_{20}, \quad \dot{\theta}_2(0) = 0 \quad (12)$$

so that from (5.2.64) and (5.2.65)

$$Q = \theta_{20}\left(1 + \frac{\xi^2\omega_n^2}{\omega_d^2}\right)^{1/2} = \theta_{20}\left(1 + \frac{\xi^2}{1-\xi^2}\right)^{1/2} = \frac{\theta_{20}}{\sqrt{1-\xi^2}} \quad (13)$$

$$\angle q = \tan^{-1}\left(\frac{\xi\omega_n}{\omega_d}\right) = \tan^{-1}\left(\frac{\xi}{\sqrt{1-\xi^2}}\right) \quad (14)$$

Substitution of (13) and (14) into (5.2.57) yields

$$q(t) = e^{-\xi\omega_n t} \frac{\theta_{20}}{\sqrt{1-\xi^2}} \cos\left(\omega_d t - \tan^{-1}\left(\frac{\xi}{\sqrt{1-\xi^2}}\right)\right) \quad (15)$$

5.3 TWO-DEGREE-OF-FREEDOM SYSTEMS

Free vibration analysis of a system typically consists of determining natural frequencies, damping ratios, mode shapes, and the vibration due to imposing ICs on displacements and velocities. Systems that have a two-degree-of-freedom (2dof) model also have solutions for free vibration response characteristics that can often be obtained in closed form. This is generally untrue for systems with more than 2dofs which require a numerical solution. A 2dof system has the general unforced form

$$\underline{M}\ddot{\underline{q}} + (\underline{C} + \underline{G})\dot{\underline{q}} + (\underline{K} + \underline{K}_C)\underline{q} = \underline{0} \quad (2 \times 1) \quad (5.3.1)$$

where

$$\begin{aligned} \underline{M} &= \begin{bmatrix} m_{11} & m_{12} \\ m_{12} & m_{22} \end{bmatrix} = \text{mass matrix,} \\ \underline{C} &= \begin{bmatrix} c_{11} & c_{12} \\ c_{12} & c_{22} \end{bmatrix} = \text{damping matrix,} \\ \underline{G} &= \begin{bmatrix} 0 & g_{12} \\ -g_{12} & 0 \end{bmatrix} = \text{gyroscopic matrix,} \\ \underline{K} &= \begin{bmatrix} k_{11} & k_{12} \\ k_{12} & k_{22} \end{bmatrix} = \text{stiffness matrix,} \\ \underline{K}_C &= \begin{bmatrix} 0 & k_{c12} \\ -k_{c12} & 0 \end{bmatrix} = \text{circulatory matrix.} \end{aligned} \quad (5.3.2)$$

The complex variable (Section 2.5) form of Equation (5.3.1) is

$$\underline{M}\ddot{\underline{z}} + (\underline{C} + \underline{G})\dot{\underline{z}} + (\underline{K} + \underline{K}_C)\underline{z} = \underline{0} \quad (5.3.3)$$

where

$$\underline{z} = \underline{z}_R + i\underline{z}_I \quad (5.3.4)$$

Then the real part of \underline{z} , that is, \underline{z}_R , satisfies

$$\underline{M}\ddot{\underline{z}}_R + (\underline{C} + \underline{G})\dot{\underline{z}}_R + (\underline{K} + \underline{K}_C)\underline{z}_R = \underline{0} \quad (5.3.5)$$

which has the identical form of (5.3.1), so it follows that

$$\underline{q}(t) = \underline{z}_R(t) = \text{Real}(\underline{z}(t)) \quad (5.3.6)$$

Substitute

$$\underline{z} = \underline{\psi}e^{\lambda t} \quad (5.3.7)$$

into (5.3.5) to obtain

$$[\lambda^2 \underline{M} + \lambda(\underline{C} + \underline{G}) + (\underline{K} + \underline{K}_C)]\underline{\psi} = \underline{0} \quad (5.3.8)$$

The displacement vector $\underline{\psi}$ is identically zero (null vector) if the coefficient matrix

$$\underline{A}(\lambda) = \lambda^2 \underline{M} + \lambda(\underline{C} + \underline{G}) + (\underline{K} + \underline{K}_C) \quad (5.3.9)$$

is invertible (nonsingular) and (5.3.8) is satisfied. However, from (5.3.7), this would imply that the system does not vibrate after being released with some ICs, which contradicts our

experience. Therefore, the coefficient matrix must be noninvertible, that is, singular, which from a mathematical standpoint requires that

$$\det(\underline{A}(\lambda)) = \det \begin{bmatrix} \lambda^2 m_{11} + \lambda c_{11} + k_{11} & \lambda^2 m_{12} + \lambda(c_{12} + g_{12}) + k_{12} + k_{c12} \\ \lambda^2 m_{12} + \lambda(c_{12} - g_{12}) + k_{12} - k_{c12} & \lambda^2 m_{22} + \lambda c_{22} + k_{22} \end{bmatrix} = 0 \quad (5.3.10)$$

Equation (5.3.10) is the 2dof “characteristic equation.” The determinant is expanded with the following symbolic math code:

Maple Code for Symbolic Determinant Evaluation

```
f(1,1) := lambda^2*m11+lambda*c11+k11;
f(1,2) := lambda^2*m12+lambda*(c12+g12)+k12+k_c12;
f(2,1) := lambda^2*m12+lambda*(c12-g12)+k12-k_c12;
f(2,2) := lambda^2*m22+lambda*c22+k22;
with(LinearAlgebra);
A:=Matrix([[f(1,1), f(1,2)], [f(2,1), f(2,2)]]);
Simplify(Determinant(A));
```

The results are

$$\begin{aligned} & \lambda^4 (m_{11}m_{22} - m_{12}^2) + \lambda^3 [m_{11}c_{22} + m_{22}c_{11} - m_{12}(2c_{12})] \\ & + \lambda^2 [m_{11}k_{22} + c_{11}c_{22} + k_{11}m_{22} - m_{12}(2k_{12}) + (-c_{12}^2 + g_{12}^2)] \\ & + \lambda(c_{11}k_{22} + c_{22}k_{11} - 2c_{12}k_{12} + 2g_{12}k_{c12}) + (k_{11}k_{22} - k_{12}^2 + k_{c12}^2) = 0 \end{aligned} \quad (5.3.11)$$

or

$$\lambda^4 + c_3\lambda^3 + c_2\lambda^2 + c_1\lambda + c_0 = 0 \quad (5.3.12)$$

where

$$\begin{aligned} c_0 &= \frac{k_{11}k_{22} - k_{12}^2 + k_{c12}^2}{m_{11}m_{22} - m_{12}^2}, \\ c_1 &= \frac{c_{11}k_{22} + c_{22}k_{11} - 2c_{12}k_{12} + 2g_{12}k_{c12}}{m_{11}m_{22} - m_{12}^2}, \\ c_2 &= \frac{m_{11}k_{22} + m_{22}k_{11} + c_{11}c_{22} - 2m_{12}k_{12} + g_{12}^2 - c_{12}^2}{m_{11}m_{22} - m_{12}^2}, \\ c_3 &= \frac{m_{11}c_{22} + m_{22}c_{11} - 2m_{12}c_{12}}{m_{11}m_{22} - m_{12}^2} \end{aligned} \quad (5.3.13)$$

A closed-form solution of (5.3.12) is possible if c_1 and c_3 are zero, that is, if the system is undamped and if either

$$\begin{aligned} & \text{(i) } g_{12} = 0 \text{ (no gyroscopic terms) or} \\ & \text{(ii) } k_{c12} = 0 \text{ (no circulatory force term)} \end{aligned} \quad (5.3.14)$$

Equations (5.3.12) and (5.3.13) simplify for these cases to the following form:

$$\lambda^4 + \alpha_2\lambda^2 + \alpha_0 = 0 \quad (5.3.15)$$

where

$$\Delta = m_{11}m_{22} - m_{12}^2, \quad \alpha_0 = \frac{k_{11}k_{22} - k_{12}^2 + k_{c12}^2}{\Delta}, \quad \alpha_2 = \frac{m_{11}k_{22} + m_{22}k_{11} - 2m_{12}k_{12} + g_{12}^2}{\Delta} \quad (5.3.16)$$

By (5.3.6), (5.3.7), and (5.3.15) and linear superposition, the total solution for $\underline{q}(t)$ is

$$\underline{q}(t) = \text{Real} \left(\beta_1 \underline{\psi}_1 e^{\lambda_1 t} + \beta_2 \underline{\psi}_2 e^{\lambda_2 t} + \beta_3 \underline{\psi}_3 e^{\lambda_3 t} + \beta_4 \underline{\psi}_4 e^{\lambda_4 t} \right) \quad (5.3.17)$$

where λ_j has the form

$$\lambda_j = d_j + i\omega_j \quad (5.3.18)$$

Euler's identity (Example 2.4.3) shows that

$$e^{\lambda_j t} = e^{d_j t} e^{i\omega_j t} = e^{d_j t} (\cos \omega_j t + i \sin \omega_j t) \quad (5.3.19)$$

For physical reasons, the free response of undamped systems with positive direct stiffness and without circulatory forces will neither dampen to zero nor grow to infinity. From (5.3.19), this is expressed mathematically as

$$d_j = 0 \quad (5.3.20)$$

so that the eigenvalues are pure imaginary:

$$\lambda_j = i\omega_j \quad (5.3.21)$$

Then the characteristic equation (5.3.15) becomes

$$\omega_j^4 - \alpha_2 \omega_j^2 + \alpha_0 = 0 \quad (5.3.22)$$

This equation has the roots

$$\begin{aligned} \omega_1 = + \left(\frac{\alpha_2}{2} - \frac{1}{2} \sqrt{\alpha_2^2 - 4\alpha_0} \right)^{1/2}, \quad \omega_2 = + \left(\frac{\alpha_2}{2} + \frac{1}{2} \sqrt{\alpha_2^2 - 4\alpha_0} \right)^{1/2} \\ \omega_3 = - \left(\frac{\alpha_2}{2} - \frac{1}{2} \sqrt{\alpha_2^2 - 4\alpha_0} \right)^{1/2}, \quad \omega_4 = - \left(\frac{\alpha_2}{2} + \frac{1}{2} \sqrt{\alpha_2^2 - 4\alpha_0} \right)^{1/2} \end{aligned} \quad (5.3.23)$$

Taking the conjugate of (5.3.8) yields

$$\left[\bar{\lambda}^2 \underline{M} + \bar{\lambda} (\underline{C} + \underline{G}) + (\underline{K} + \underline{K}_C) \right] \bar{\underline{\psi}} = \bar{\underline{0}} = \underline{0} \quad (5.3.24)$$

which shows that if λ and $\underline{\psi}$ solve (5.3.8), then $\bar{\lambda}$ and $\bar{\underline{\psi}}$ will also solve (5.3.8). Note that this results because the conjugates of the real matrices in (5.3.24) are the matrices themselves, so by (5.3.23)

$$\lambda_1 = i\omega_1, \quad \lambda_2 = i\omega_2, \quad \lambda_3 = i\omega_3 = -i\omega_1 = \bar{\lambda}_1, \quad \lambda_4 = i\omega_4 = -i\omega_2 = \bar{\lambda}_2 \quad (5.3.25)$$

and

$$\underline{\psi}_3 = \bar{\underline{\psi}}_1, \quad \underline{\psi}_4 = \bar{\underline{\psi}}_2 \quad (5.3.26)$$

Finally, by (5.3.17),

$$\underline{q}(t) = \text{Real} \left(\beta_1 \underline{\psi}_1 e^{i\omega_1 t} + \beta_2 \underline{\psi}_2 e^{i\omega_2 t} + \beta_3 \bar{\underline{\psi}}_1 e^{-i\omega_1 t} + \beta_4 \bar{\underline{\psi}}_2 e^{-i\omega_2 t} \right) \quad (5.3.27)$$

5.3.1 Special Case I ($\underline{C} = \underline{G} = \underline{K}_C = \underline{0}$) (Undamped, Nongyroscopic, and Noncirculatory Case)

For this case, (5.3.8) becomes

$$(\lambda^2 \underline{M} + \underline{K}) \underline{\psi} = \underline{0} \quad (5.3.28)$$

or by (5.3.25)

$$(-\omega^2 \underline{M} + \underline{K}) \underline{\psi} = \underline{0} \quad (5.3.29)$$

Row-wise equation (5.3.29) may be written as

$$(-\omega^2 m_{11} + k_{11}) \psi_1 + (-\omega^2 m_{12} + k_{12}) \psi_2 = 0 \quad (5.3.30)$$

$$(-\omega^2 m_{12} + k_{12}) \psi_1 + (-\omega^2 m_{22} + k_{22}) \psi_2 = 0 \quad (5.3.31)$$

Divide these equations by ψ_1 to obtain

$$(-\omega^2 \underline{M} + \underline{K}) \left\{ \begin{matrix} 1 \\ \tilde{\psi} \end{matrix} \right\} = 0 \quad (5.3.32)$$

where

$$\tilde{\psi} = \frac{\psi_2}{\psi_1} \quad (5.3.33)$$

Therefore, without loss of generality, $\underline{\psi}$ can be expressed in the form

$$\underline{\psi} = \left\{ \begin{matrix} 1 \\ \tilde{\psi} \end{matrix} \right\} \quad (5.3.34)$$

where by (5.3.30) and (5.3.33)

$$\tilde{\psi} = \frac{\omega^2 m_{11} - k_{11}}{-\omega^2 m_{12} + k_{12}} \quad (5.3.35)$$

Note that since all terms in (5.3.35) are real $\tilde{\psi}$ and $\underline{\psi}$ are real and therefore

$$\underline{\psi} = \underline{\bar{\psi}} \quad (5.3.36)$$

so from (5.3.27)

$$\underline{q}(t) = \text{Real} \left((\beta_1 e^{i\omega_1 t} + \beta_3 e^{-i\omega_1 t}) \underline{\psi}_1 + (\beta_2 e^{i\omega_2 t} + \beta_4 e^{-i\omega_2 t}) \underline{\psi}_2 \right) \quad (5.3.37)$$

In general, β_j are complex, so

$$\beta_j = \beta_{jR} + i\beta_{jI}, \quad j = 1, 2, 3, 4 \quad (5.3.38)$$

and (5.3.37) become

$$\begin{aligned} \underline{q}(t) = & [(\beta_{1R} \cos \omega_1 t - \beta_{1I} \sin \omega_1 t) + (\beta_{3R} \cos \omega_1 t + \beta_{3I} \sin \omega_1 t)] \underline{\psi}_1 \\ & + [(\beta_{2R} \cos \omega_2 t - \beta_{2I} \sin \omega_2 t) + (\beta_{4R} \cos \omega_2 t + \beta_{4I} \sin \omega_2 t)] \underline{\psi}_2 \end{aligned} \quad (5.3.39)$$

The β_{jR} and β_{jI} are arbitrary real constants, so by collecting terms (5.3.39) may be written as

$$\underline{q}(t) = (\alpha_{1c} \cos \omega_1 t + \alpha_{1s} \sin \omega_1 t) \underline{\psi}_1 + (\alpha_{2c} \cos \omega_2 t + \alpha_{2s} \sin \omega_2 t) \underline{\psi}_2 \quad (5.3.40)$$

Differentiation yields

$$\dot{\underline{q}}(t) = (-\omega_1 \alpha_{1c} \sin \omega_1 t + \omega_1 \alpha_{1s} \cos \omega_1 t) \underline{\psi}_1 + (-\omega_2 \alpha_{2c} \sin \omega_2 t + \omega_2 \alpha_{2s} \cos \omega_2 t) \underline{\psi}_2 \quad (5.3.41)$$

where the α 's are arbitrary real constants. At the initial time ($t=0$), these equations become

$$\underline{q}(0) = \begin{Bmatrix} q_{10} \\ q_{20} \end{Bmatrix} = \alpha_{1c} \underline{\psi}_1 + \alpha_{2c} \underline{\psi}_2, \quad \dot{\underline{q}}(0) = \begin{Bmatrix} \dot{q}_{10} \\ \dot{q}_{20} \end{Bmatrix} = \alpha_{1s} \omega_1 \underline{\psi}_1 + \alpha_{2s} \omega_2 \underline{\psi}_2 \quad (5.3.42)$$

which implies

$$\begin{bmatrix} \underline{\psi}_1 & \underline{\psi}_2 \end{bmatrix} \begin{Bmatrix} \alpha_{1c} \\ \alpha_{2c} \end{Bmatrix} = \begin{Bmatrix} q_{10} \\ q_{20} \end{Bmatrix}, \quad \begin{bmatrix} \omega_1 \underline{\psi}_1 & \omega_2 \underline{\psi}_2 \end{bmatrix} \begin{Bmatrix} \alpha_{1s} \\ \alpha_{2s} \end{Bmatrix} = \begin{Bmatrix} \dot{q}_{10} \\ \dot{q}_{20} \end{Bmatrix} \quad (5.3.43)$$

or since

$$\underline{\psi}_1 = \begin{Bmatrix} \psi_{11} \\ \psi_{21} \end{Bmatrix}, \quad \underline{\psi}_2 = \begin{Bmatrix} \psi_{12} \\ \psi_{22} \end{Bmatrix} \quad (5.3.44)$$

then

$$\begin{bmatrix} \psi_{11} & \psi_{12} \\ \psi_{21} & \psi_{22} \end{bmatrix} \begin{Bmatrix} \alpha_{1c} \\ \alpha_{2c} \end{Bmatrix} = \begin{Bmatrix} q_{10} \\ q_{20} \end{Bmatrix}, \quad \begin{bmatrix} \omega_1 \psi_{11} & \omega_2 \psi_{12} \\ \omega_1 \psi_{21} & \omega_2 \psi_{22} \end{bmatrix} \begin{Bmatrix} \alpha_{1s} \\ \alpha_{2s} \end{Bmatrix} = \begin{Bmatrix} \dot{q}_{10} \\ \dot{q}_{20} \end{Bmatrix} \quad (5.3.45)$$

which has the solutions

$$\alpha_{1c} = \frac{q_{10} \psi_{22} - q_{20} \psi_{12}}{\Delta}, \quad \alpha_{2c} = \frac{q_{20} \psi_{11} - q_{10} \psi_{21}}{\Delta} \quad (5.3.46)$$

$$\alpha_{1s} = \frac{\dot{q}_{10} \psi_{22} - \dot{q}_{20} \psi_{12}}{\omega_1 \Delta}, \quad \alpha_{2s} = \frac{\dot{q}_{20} \psi_{11} - \dot{q}_{10} \psi_{21}}{\omega_2 \Delta}$$

where

$$\Delta = \psi_{11} \psi_{22} - \psi_{12} \psi_{21} \quad (5.3.47)$$

Summarizing these results yields:

Two Dof System without Damping, Gyroscopics or Circulatory Forces

$$\underline{C} = \underline{G} = \underline{K}_C = 0 \quad (5.3.48)$$

From (5.3.16) define

$$\alpha_0 = \frac{k_{11} k_{22} - k_{12}^2}{m_{11} m_{22} - m_{12}^2} \quad \text{and} \quad \alpha_2 = \frac{m_{11} k_{22} + m_{22} k_{11} - 2 m_{12} k_{12}}{m_{11} m_{22} - m_{12}^2} \quad (5.3.49)$$

From (5.3.23), the two natural frequencies¹ are

$$\omega_1 = \sqrt{\frac{\alpha_2}{2} - \frac{1}{2} \sqrt{\alpha_2^2 - 4\alpha_0}}, \quad \omega_2 = \sqrt{\frac{\alpha_2}{2} + \frac{1}{2} \sqrt{\alpha_2^2 - 4\alpha_0}} \quad (5.3.50)$$

¹ The expression "natural frequencies" indicates that the oscillations in (5.3.54) occur at these frequencies due to the initial conditions and to the nature of the system's mass and stiffness parameters and not to any external excitation.

From (5.3.33) and (5.3.34), the two mode shapes are

$$\underline{\psi}_1 = \begin{Bmatrix} 1 \\ \tilde{\psi}_1 \end{Bmatrix}, \quad \underline{\psi}_2 = \begin{Bmatrix} 1 \\ \tilde{\psi}_2 \end{Bmatrix} \quad (5.3.51)$$

and from (5.3.35)

$$\tilde{\psi}_j = \frac{\omega_j^2 m_{11} - k_{11}}{-\omega_j^2 m_{12} + k_{12}} \quad j = 1, 2 \quad (5.3.52)$$

Given the initial conditions

$$\underline{q}(0) = \begin{Bmatrix} q_{10} \\ q_{20} \end{Bmatrix}, \quad \underline{\dot{q}}(0) = \begin{Bmatrix} \dot{q}_{10} \\ \dot{q}_{20} \end{Bmatrix} \quad (5.3.53)$$

the free vibration, initial condition response is given by (5.3.40)

$$\underline{q}(t) = \begin{Bmatrix} q_1(t) \\ q_2(t) \end{Bmatrix} = (\alpha_{1c} \cos \omega_1 t + \alpha_{1s} \sin \omega_1 t) \underline{\psi}_1 + (\alpha_{2c} \cos \omega_2 t + \alpha_{2s} \sin \omega_2 t) \underline{\psi}_2 \quad (5.3.54)$$

where from (5.3.34), (5.3.46), and (5.3.47)

$$\alpha_{1c} = \frac{q_{10} \tilde{\psi}_2 - q_{20}}{\Delta}, \quad \alpha_{2c} = \frac{q_{20} - q_{10} \tilde{\psi}_1}{\Delta}, \quad \alpha_{1s} = \frac{\dot{q}_{10} \tilde{\psi}_2 - \dot{q}_{20}}{\omega_1 \Delta}, \quad \alpha_{2s} = \frac{\dot{q}_{20} - \dot{q}_{10} \tilde{\psi}_1}{\omega_2 \Delta} \quad (5.3.55)$$

where

$$\Delta = \tilde{\psi}_2 - \tilde{\psi}_1 \quad (5.3.56)$$

EXAMPLE 5.3.1 Gravel Loading Station Vibration

Statement: A structure used for crushing rocks (1) into gravel (2) and loading it into trucks (3) is depicted below. A large quantity of gravel is quickly deposited (dropped) into arriving trucks via the hatch (4). The container and its contents have mass $2m$ just prior to loading the truck and m just after loading, and the mass of the rock crusher is m . A highly simplified model for vibration simulation is shown in Figure E5.3.1(a). The top spring represents the stiffness of the support columns (beams) beneath the container, the middle spring represents the stiffness of the columns between the container and crusher, and the uppermost spring represents the stiffness of the side brace beams.

Objective: Determine the free vibration responses (x_1, x_2) of the crusher and container following the dumping of a load of gravel from the container into the truck.

Assumptions: The mass of the container and its contents changes from $2m$ to m instantaneously in a gravel dump (truck loading) event.

Solution:

- (a) At $t = 0^-$, the static equilibrium positions (SEPs) are at $SEP1^-$ and $SEP2^-$, corresponding to weights $W_1 = mg$ and $W_2 = 2mg$. At $t = 0^+$, the SEPs change to $SEP1^+$ and $SEP2^+$, corresponding to weights $W_1 = mg$ and $W_2 = mg$. The SEP changes are determined by considering the force balances in Figure E5.3.1(b) which show absolute deflections (relative to the unloaded spring state).

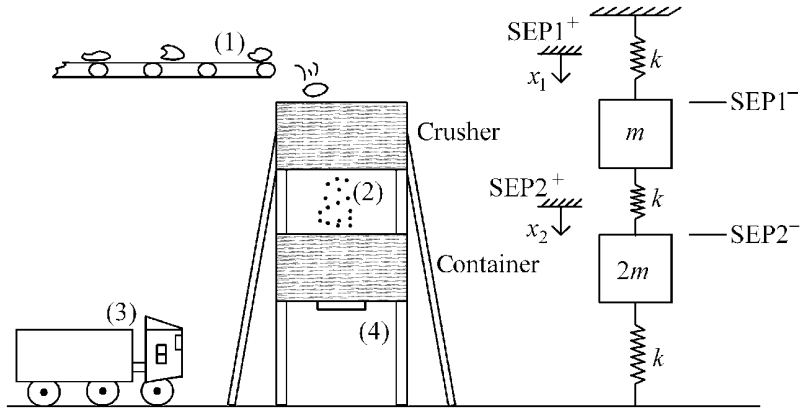


Figure E5.3.1(a) Gravel loading station and corresponding vibration model

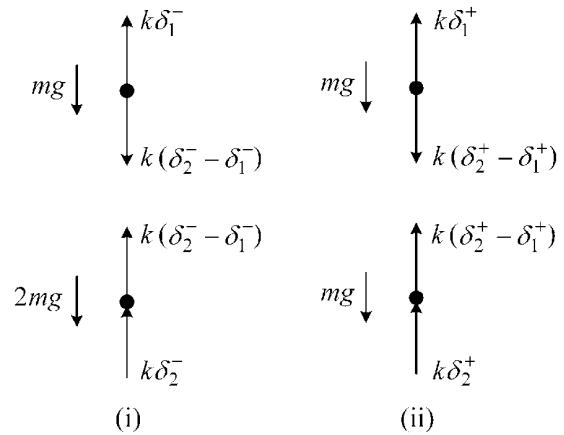


Figure E5.3.1(b) Free body diagrams for SEP change determination. (i) Before drop. (ii) After drop

The static equilibrium equations for the two states are:

1. Before drop ($t=0^-$):

$$\begin{bmatrix} k+k & -k \\ -k & k+k \end{bmatrix} \begin{Bmatrix} \delta_1^- \\ \delta_2^- \end{Bmatrix} = \begin{Bmatrix} mg \\ 2mg \end{Bmatrix} \quad (1)$$

2. After drop ($t=0^+$):

$$\begin{bmatrix} 2k & -k \\ -k & 2k \end{bmatrix} \begin{Bmatrix} \delta_1^+ \\ \delta_2^+ \end{Bmatrix} = \begin{Bmatrix} mg \\ mg \end{Bmatrix} \quad (2)$$

Subtract Equation (2) from (1) to obtain

$$\begin{bmatrix} 2k & -k \\ -k & 2k \end{bmatrix} \begin{Bmatrix} \delta_1^- - \delta_1^+ \\ \delta_2^- - \delta_2^+ \end{Bmatrix} = \begin{Bmatrix} 0 \\ mg \end{Bmatrix} \quad (3)$$

Solving this equation yields

$$\delta_1^- - \delta_1^+ = \frac{mgk}{3k^2} = \frac{mg}{3k}, \quad \delta_2^- - \delta_2^+ = \frac{2kmg}{3k^2} = \frac{2mg}{3k} \quad (4)$$

Equation (4) provides the positions of the masses before the gravel is dropped (SEP1⁻ and SEP2⁻) relative to the static positions of the masses after the gravel is dropped (SEP1⁺ and SEP2⁺). Therefore, the gravel dumping operation may be viewed as an initial condition response problem. With reference to the coordinates (SEP1⁺ and SEP2⁺) in Figure E5.3.1(a), the initial conditions become (4)

$$x_1(0) = \frac{mg}{3k}, \quad x_2(0) = \frac{2mg}{3k} \quad (5)$$

(b) The equations of motion for $t > 0$ are obtained by applying Newton's law (3.3.5) to masses 1 and 2 in Figure E5.3.1(b):

$$+ \downarrow \quad m\ddot{x}_1 = -kx_1 + k(x_2 - x_1) \quad (6)$$

$$+ \downarrow \quad m\ddot{x}_2 = -kx_2 - k(x_2 - x_1) \quad (7)$$

or in matrix form

$$\underline{M}\ddot{\underline{X}} + \underline{K}\underline{X} = \underline{0} \quad (8)$$

where

$$\underline{M} = \begin{bmatrix} m_{11} & m_{12} \\ m_{12} & m_{22} \end{bmatrix} = \begin{bmatrix} m & 0 \\ 0 & m \end{bmatrix}, \quad \underline{K} = \begin{bmatrix} k_{11} & k_{12} \\ k_{12} & k_{22} \end{bmatrix} = \begin{bmatrix} 2k & -k \\ -k & 2k \end{bmatrix}, \quad \underline{X} = \begin{Bmatrix} x_1 \\ x_2 \end{Bmatrix} \quad (9)$$

(c) The natural frequencies are determined by substituting (9) into (5.3.49)–(5.3.50):

$$\alpha_0 = \frac{3k^2}{m^2}, \quad \alpha_2 = \frac{4mk}{m^2} \quad (10)$$

$$\therefore \omega_1 = \sqrt{\frac{4k}{2m} - \frac{1}{2}\sqrt{\frac{16k^2}{m^2} - \frac{12k^2}{m^2}}} = \sqrt{\frac{k}{m}}, \quad f_1 = \frac{\omega_1}{2\pi} = \frac{1}{2\pi}\sqrt{\frac{k}{m}} \quad (\text{Hz}), \quad (11)$$

$$\omega_2 = \sqrt{\frac{2k}{m} + \frac{k}{m}} = \sqrt{\frac{3k}{m}}, \quad f_2 = \frac{\omega_2}{2\pi} = \frac{1}{2\pi}\sqrt{\frac{3k}{m}} \quad (\text{Hz}) \quad (12)$$

(d) The corresponding mode shapes are obtained from (11), (12), (5.3.51), and (5.3.52) as

$$\tilde{\psi}_1 = \frac{\omega_1^2 m - 2k}{-\omega_1^2 \cdot 0 - k} = \frac{k - 2k}{-k} = 1, \quad \tilde{\psi}_2 = \frac{\omega_2^2 m - 2k}{-\omega_2^2 \cdot 0 - k} = \frac{k}{-k} = -1 \quad (13)$$

$$\therefore \underline{\psi}_1 = \begin{Bmatrix} 1 \\ 1 \end{Bmatrix}, \quad \underline{\psi}_2 = \begin{Bmatrix} 1 \\ -1 \end{Bmatrix} \quad (14)$$

(e) The free vibration responses of the crusher (x_1) and container (x_2) to the given initial conditions (5)

$$\underline{q}(0) = \begin{Bmatrix} q_{10} \\ q_{20} \end{Bmatrix} = \begin{Bmatrix} x_{10} \\ x_{20} \end{Bmatrix} = \frac{mg}{k} \begin{Bmatrix} \frac{1}{3} \\ \frac{2}{3} \end{Bmatrix}, \quad \dot{\underline{q}}(0) = \begin{Bmatrix} \dot{q}_{10} \\ \dot{q}_{20} \end{Bmatrix} = \begin{Bmatrix} \dot{x}_{10} \\ \dot{x}_{20} \end{Bmatrix} = \begin{Bmatrix} 0 \\ 0 \end{Bmatrix} \quad (15)$$

are obtained from (5.3.53)–(5.3.56) as

$$\alpha_{1c} = \frac{\frac{mg}{3k}(-1) - \frac{2mg}{3k}}{-2} = \frac{mg}{2k}, \quad (16)$$

$$\alpha_{2c} = \frac{\frac{2mg}{3k} - \frac{mg}{3k}}{-2} = -\frac{mg}{6k}, \quad (17)$$

$$\alpha_{1s} = \alpha_{2s} = 0 \quad (18)$$

$$\underline{X}(t) = \begin{Bmatrix} x_1(t) \\ x_2(t) \end{Bmatrix} = \alpha_{1c} \cos(\omega_1 t) \underline{\psi}_1 + \alpha_{2c} \cos(\omega_2 t) \underline{\psi}_2 \quad (19)$$

$$\underline{X}(t) = \frac{mg}{2k} \cos\left(\sqrt{\frac{k}{m}}t\right) \begin{Bmatrix} 1 \\ 1 \end{Bmatrix} - \frac{mg}{6k} \cos\left(\sqrt{\frac{3k}{m}}t\right) \begin{Bmatrix} 1 \\ -1 \end{Bmatrix} \quad (20)$$

Summary:

- The results show that the first mode component of the response involves in-phase motion of the crusher and container and is three times larger in amplitude than the second mode component which involves out-of-phase motion of the crusher and container.
- The responses of the undamped model do not diminish with time t due to an absence of damping in the model.
- The use of SEP coordinates allowed the weight loading (mg) to be ignored in writing the dynamic equations of motion in (6) and (7). This approach may be explained alternatively by writing the equations of motion with absolute coordinates (referenced to the unloaded spring state) and including the applied weight loading, that is,

$$\underline{M} \ddot{\underline{X}} + \underline{K} \underline{X} = \underline{M} \begin{Bmatrix} \ddot{\bar{x}}_1 \\ \ddot{\bar{x}}_2 \end{Bmatrix} + \underline{K} \begin{Bmatrix} \bar{x}_1 \\ \bar{x}_2 \end{Bmatrix} = \underline{M} \begin{Bmatrix} \ddot{x}_1 + \ddot{\delta}_1^+ \\ \ddot{x}_2 + \ddot{\delta}_2^+ \end{Bmatrix} + \underline{K} \begin{Bmatrix} x_1 + \delta_1^+ \\ x_2 + \delta_2^+ \end{Bmatrix} = \begin{Bmatrix} mg \\ mg \end{Bmatrix} \quad (21)$$

Substitution of (2) into (21) and noting that $\ddot{\delta}_i^+ = 0$ yield the same result as the SEP referenced equation (8) which ignores the mg weight loading.

EXAMPLE 5.3.2 Desktop Oscillating Curio with Beat Phenomenon

Introduction: Desktop curios that execute high-frequency oscillation modulated by low-frequency amplitude variation are objects of fascination and delight. The flow of energy between components of the devices is readily apparent and demonstrates how kinetic energy can be transferred between components of a system, yet remain conserved.

Statement: An entrepreneur seeks to develop and sell a curio consisting of two oscillating clowns and an ornate lightweight rod connecting the clowns (Figure E5.3.2(a)). The clowns can freely oscillate about their hinged attachment points (A, B) to the rod. The same points are suspended from the support arch via strings between A and C and B and D . The clown figures are constructed from a thin plastic sheet and have a pendulum mass attached at their

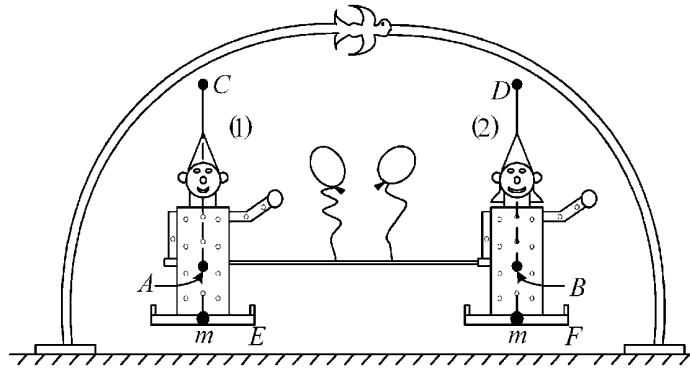


Figure E5.3.2(a) Clown desk curio

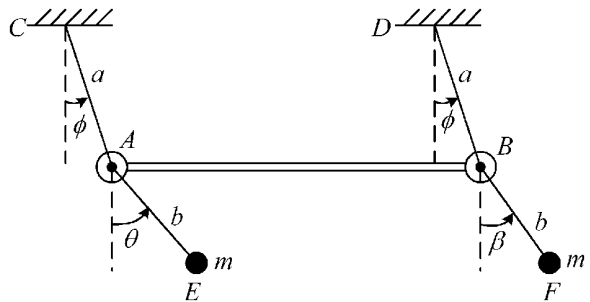


Figure E5.3.2(b) Equivalent system model for clown desk curio

feet. The fascinating motions displayed by this apparatus are responses that occur after the LHS clown's foot mass m is displaced to the right and then released. The responses include the following:

- (a) Clown 1's rocking amplitude increases then decreases as clown 2's rocking amplitude does the opposite, that is, decreases then increases. These amplitudes modulate the rocking motion of the clowns.
- (b) The connecting rod AB simultaneously sways at a single frequency which is lower than the clown rocking frequency. The rod's sway amplitude is constant with time.

Objective: Derive equations relating the natural frequencies of the curio to its dimensional parameters. Select lengths a and b in Figure E5.3.2(b) such that the desired behaviors of the curio in (a) and (b) actually occur.

Assumptions:

- (a) Small-angle motion.
- (b) All masses are negligible except for the two pendulum masses (m).

Solution:

- (a) A simplified model for analyzing the motion of the clown desk curio is shown in Figure E5.3.2(b).

The corresponding free body diagrams are shown in Figure E5.3.2(c).

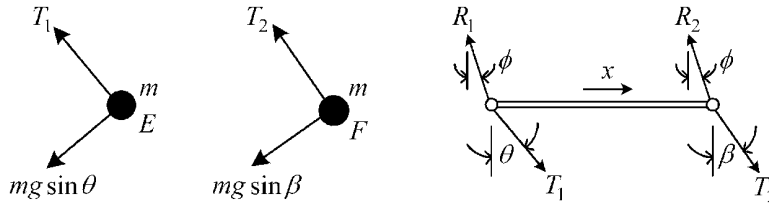


Figure E5.3.2(c) Free body diagram of model in Figure E5.3.2(b)

- (b) The horizontal connecting rod has negligible mass, so its horizontal equation of motion (EOM) becomes (3.3.5)

$$0 \approx m_{cR}\ddot{x} = T_1 \sin \theta + T_2 \sin \beta - R_1 \sin \phi - R_2 \sin \phi \quad (1)$$

which for small angles implies

$$T_1 \theta + T_2 \beta - (R_1 + R_2) \phi = 0 \quad (2)$$

Assuming small angles and utilizing symmetry, the cable forces only change slightly from their values at equilibrium ($\theta = \beta = \phi = 0$). Therefore

$$R_1 \approx R_2 \approx T_1 \approx T_2 \approx mg \quad (3)$$

Substitution of (3) into (2) yields the kinematic constraint condition

$$\phi = \frac{\theta + \beta}{2} \quad (4)$$

- (c) Next write the EOMs for both m 's. Take moments about point A treating AE as a massless rigid link with all of its mass (m) concentrated at its mass center E . The rotational EOM (3.3.39) yields

$$I_G \ddot{\theta} + b m a_E \ddot{\theta} = -b m g \sin \theta \quad (5)$$

where for small angles

$$a_E \approx a \ddot{\phi} + b \ddot{\theta}, \quad \sin \theta \approx \theta \quad (6)$$

and since m is concentrated at E , that is, m is a point mass

$$I_G \approx 0 \quad (7)$$

Therefore, (5) becomes

$$b m (a \ddot{\phi} + b \ddot{\theta}) = -b m g \theta$$

or by using (4)

$$\left(b + \frac{a}{2}\right) \ddot{\theta} + \frac{a}{2} \ddot{\beta} + g \theta = 0 \quad (8)$$

Similarly, for the mass at F ,

$$\frac{a}{2} \ddot{\theta} + \left(b + \frac{a}{2}\right) \ddot{\beta} + g \beta = 0 \quad (9)$$

or in matrix form

$$\underline{M}\ddot{\underline{X}} + \underline{K}\underline{X} = \underline{0} \quad (2 \times 1) \quad (10)$$

where

$$\underline{M} = \begin{bmatrix} b + \frac{a}{2} & \frac{a}{2} \\ \frac{a}{2} & b + \frac{a}{2} \end{bmatrix}, \quad \underline{K} = \begin{bmatrix} g & 0 \\ 0 & g \end{bmatrix}, \quad \underline{X} = \begin{Bmatrix} \theta \\ \beta \end{Bmatrix} \quad (11)$$

(d) Determine the natural frequencies for the system. From (11), (5.3.49), and (5.3.50),

$$\alpha_0 = \frac{g^2 - 0}{\left(b + \frac{a}{2}\right)^2 - \frac{a^2}{4}} = \frac{g^2}{b^2 + ab}, \quad \alpha_2 = \frac{2g\left(b + \frac{a}{2}\right)}{b^2 + ab} \quad (12)$$

$$\omega_{1,2} = \sqrt{\frac{g\left(b + \frac{a}{2}\right)}{b(a+b)} \mp \sqrt{\frac{g^2\left(b + \frac{a}{2}\right)^2}{b^2(a+b)^2} - \frac{g^2}{b(a+b)}}} = \sqrt{\frac{g\left(b + \frac{a}{2}\right)}{b(a+b)} \mp \frac{g\frac{a}{2}}{b(a+b)}} \quad (13)$$

$$\omega_1 = \sqrt{\frac{g}{a+b}}, \quad \omega_2 = \sqrt{\frac{g}{b}}$$

(e) Determine the mode shapes of the system. From (13), (5.3.51), and (5.3.52),

$$\tilde{\psi}_1 = \frac{\frac{g}{a+b}\left(b + \frac{a}{2}\right) - g}{\frac{-g}{a+b} \frac{a}{2}} = 1, \quad \tilde{\psi}_2 = \frac{\frac{g}{b}\left(b + \frac{a}{2}\right) - g}{\frac{-g}{b} \frac{a}{2}} = -1 \quad (14)$$

Therefore

$$\underline{\psi}_1 = \begin{Bmatrix} 1 \\ 1 \end{Bmatrix}, \quad \underline{\psi}_2 = \begin{Bmatrix} 1 \\ -1 \end{Bmatrix} \quad (15)$$

(f) From Figure E5.3.2(a), the foot of clown 1 is displaced to the right to start the rocking sequence. This action exerts a horizontal force on the connecting rod which also displaces to the right. Clown 2 is free to pivot about B so its angle β does not change. Therefore, by (4),

$$\theta(0) = \theta_0, \quad \beta(0) = 0, \quad \phi(0) = \frac{\theta_0}{2}, \quad \dot{\theta}(0) = \dot{\beta}(0) = 0 \quad (16)$$

From (15), (16), and (5.3.55),

$$\alpha_{1c} = \frac{\theta_0(-1) - 0}{-2} = \frac{\theta_0}{2}, \quad \alpha_{2c} = \frac{\theta_0}{2}, \quad \alpha_{1s} = \alpha_{2s} = 0 \quad (17)$$

The initial condition response is obtained from (15), (17), and (5.3.54) as

$$\begin{Bmatrix} \theta(t) \\ \beta(t) \end{Bmatrix} = \frac{\theta_0}{2} \cos(\omega_1 t) \begin{Bmatrix} 1 \\ 1 \end{Bmatrix} + \frac{\theta_0}{2} \cos(\omega_2 t) \begin{Bmatrix} 1 \\ -1 \end{Bmatrix} \quad (18)$$

The motion of the lightweight connecting rod is from (4) and (18)

$$\phi = \theta_0 \cos \omega_1 t \quad (19)$$

This clearly demonstrates that behavior (b) in the Problem Statement will occur, that is, the connecting rod rocks with a single frequency (the lower one) and constant amplitude. Use the trig identities

$$\begin{aligned}\cos x + \cos y &= 2 \cos\left(\frac{x-y}{2}\right) \cos\left(\frac{x+y}{2}\right), \\ \cos x - \cos y &= -2 \sin\left(\frac{x-y}{2}\right) \sin\left(\frac{x+y}{2}\right)\end{aligned}\quad (20)$$

to write (18) as

$$\theta(t) = \Theta_c(t) \cos\left(\frac{\omega_1 + \omega_2}{2}t\right), \quad \beta(t) = \Theta_s(t) \sin\left(\frac{\omega_1 + \omega_2}{2}t\right) \quad (21)$$

where

$$\Theta_c(t) = \theta_0 \cos\left(\frac{\omega_2 - \omega_1}{2}t\right), \quad \Theta_s(t) = \theta_0 \sin\left(\frac{\omega_2 - \omega_1}{2}t\right) = \theta_0 \cos\left(\frac{\omega_2 - \omega_1}{2}t - 90^\circ\right) \quad (22)$$

Thus, it is seen that

- Both clowns rock at the same frequency $(\omega_1 + \omega_2)/2$.
- If $a \ll b$, then $\omega_1 \approx \omega_2$, and the rocking amplitudes of both clowns are modulated by a low-frequency $(\omega_2 - \omega_1)$ oscillation. This amplitude modulation (AM) is often referred to as the “beat” phenomenon.
- Since the time-varying modulation amplitudes, $\Theta_c(t)$ and $\Theta_s(t)$, are phase shifted by 90° , it will appear that clown 1’s waving will increase as clown 2’s waving decreases, and vice versa, so behavior (a) in the Problem Statement will occur.

Figure E5.3.2(d) shows the initial condition responses in (18) and (19) for $\theta_0 = 10^\circ$, $a = 5.0\text{cm}$, and $b = 20.0\text{cm}$.

Summary: This example has illustrated the phenomena of *beats* for free vibration. Forced vibration-induced beats are much more common as exemplified by the following examples:

- (i) Tuning of musical instruments, that is, when $\omega_1 = \omega_2$ the instruments are tuned to each other. From (22), the beat period

$$T = \frac{2\pi}{(\omega_2 - \omega_1)/2} \quad (23)$$

goes to infinity, when the instruments are tuned so tuning has been accomplished when beats, that is, sound amplitude oscillations, are no longer audible.

- (ii) The beating sound of engines with slightly different speeds on a small commuter prop plane or fans with slightly different speeds on a cooling tower.

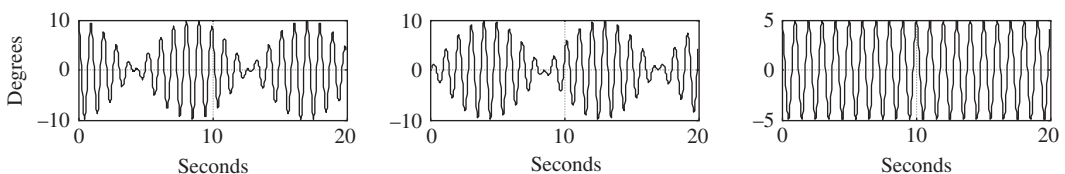


Figure E5.3.2(d) Left clown (top), right clown (middle), and connecting rod (bottom) angles

EXAMPLE 5.3.3 *Finite Element: Three-Member Truss Model*

Introduction: The 6-dof truss in Figure 4.8.13 was condensed to a 2 “free” dof model represented by Equation (4.8.119)

$$m \begin{bmatrix} \frac{2}{3} + \frac{\sqrt{2}}{3} & 0 \\ 0 & \frac{2}{3} + \frac{\sqrt{2}}{3} \end{bmatrix} \begin{Bmatrix} \ddot{q}_1^f \\ \ddot{q}_2^f \end{Bmatrix} + \begin{bmatrix} 0 & 0 \\ 0 & c_d \end{bmatrix} \begin{Bmatrix} \dot{q}_1^f \\ \dot{q}_2^f \end{Bmatrix} + \frac{EA}{L} \begin{bmatrix} 1 + \frac{1}{\sqrt{2}} & \frac{1}{\sqrt{2}} \\ \frac{1}{\sqrt{2}} & \frac{1}{\sqrt{2}} \end{bmatrix} \begin{Bmatrix} q_1^f \\ q_2^f \end{Bmatrix} = \begin{Bmatrix} f(t) \\ 0 \end{Bmatrix} \quad (1)$$

Objective: Determine the natural frequencies of this three-member truss for the following parameter values:

$$E = 5 \times 10^{11} \text{ N/m}^2, \quad \rho = 5000 \text{ kg/m}^3, \quad A = 0.005 \text{ m}^2, \quad L = 3 \text{ m}, \quad c_d = 0 \quad (2)$$

and where

$$m = \rho AL = \text{mass of elements 1 or 3} \quad (3)$$

Solution: Use of (5.3.50) yields

$$\begin{aligned} \omega_1 &= 1825 \text{ rad/s}, \quad f_1 = \frac{\omega_1}{2\pi} = 290 \text{ Hz}, \quad \underline{\psi}_1 = \begin{bmatrix} 1 \\ -1.93 \end{bmatrix} \\ \omega_2 &= 4500 \text{ rad/s}, \quad f_2 = \frac{\omega_2}{2\pi} = 716 \text{ Hz}, \quad \underline{\psi}_2 = \begin{bmatrix} 1 \\ 0.52 \end{bmatrix} \end{aligned} \quad (4)$$

5.3.2 Special Case II $\underline{C} = \underline{K}_C = \underline{0}$ (Undamped, Gyroscopic, and Noncirculatory Case)

For this case, (5.3.8) becomes

$$(\lambda^2 \underline{M} + \lambda \underline{G} + \underline{K}) \underline{\psi} = \underline{0} \quad (5.3.57)$$

or by (5.3.25)

$$(-\omega^2 \underline{M} + i\omega \underline{G} + \underline{K}) \underline{\psi} = \underline{0} \quad (5.3.58)$$

Substitution of (5.3.2) into (5.3.58) yields

$$\begin{bmatrix} -\omega^2 m_{11} + k_{11} & -\omega^2 m_{12} + i\omega g_{12} + k_{12} \\ -\omega^2 m_{12} - i\omega g_{12} + k_{12} & -\omega^2 m_{22} + k_{22} \end{bmatrix} \begin{Bmatrix} \psi_1 \\ \psi_2 \end{Bmatrix} = \begin{Bmatrix} 0 \\ 0 \end{Bmatrix} \quad (5.3.59)$$

Divide the first row of this equation by ψ_1 and define

$$\tilde{\psi}_j = \frac{\psi_{2j}}{\psi_{1j}} \quad j = 1, 2 \quad (5.3.60)$$

to obtain

$$\tilde{\psi}_j = \frac{\omega_j^2 m_{11} - k_{11}}{-\omega_j^2 m_{12} + i\omega_j g_{12} + k_{12}} \quad (5.3.61)$$

Without loss of generality, the mode shapes may then be expressed as

$$\underline{\psi}_1 = \begin{Bmatrix} 1 \\ \tilde{\psi}_1 \end{Bmatrix}, \quad \underline{\psi}_2 = \begin{Bmatrix} 1 \\ \tilde{\psi}_2 \end{Bmatrix} \quad (5.3.62)$$

corresponding to the natural frequencies ω_1 and ω_2 . In the event that

$$m_{12} = k_{12} = 0 \quad (5.3.63)$$

Equation (5.3.61) simplifies to

$$\tilde{\psi}_j = i\gamma_j \quad (5.3.64)$$

where

$$\gamma_j = \frac{k_{11} - \omega_j^2 m_{11}}{\omega_j g_{12}} \quad (5.3.65)$$

The mode shapes for this case become

$$\underline{\psi}_j = \left\{ \begin{array}{c} 1 \\ i\gamma_j \end{array} \right\} \quad j=1,2 \quad (5.3.66)$$

Consider the expression

$$\begin{aligned} \text{Real}(\beta_a \underline{\psi} e^{i\omega t} + \beta_b \bar{\underline{\psi}} e^{-i\omega t}) &= \text{Real}((\beta_{aR} + i\beta_{aI})(\underline{\psi}_R + i\underline{\psi}_I)(\cos \omega t + i \sin \omega t) \\ &\quad + (\beta_{bR} + i\beta_{bI})(\underline{\psi}_R - i\underline{\psi}_I)(\cos \omega t - i \sin \omega t)) \\ &= \text{Real}((\beta_{aR} + i\beta_{aI})[(\underline{\psi}_R \cos \omega t - \underline{\psi}_I \sin \omega t) + i(\underline{\psi}_R \sin \omega t + \underline{\psi}_I \cos \omega t)] \\ &\quad + (\beta_{bR} + i\beta_{bI})[(\underline{\psi}_R \cos \omega t - \underline{\psi}_I \sin \omega t) + i(-\underline{\psi}_R \sin \omega t - \underline{\psi}_I \cos \omega t)]) \\ &= (\beta_{aR} + \beta_{bR})(\underline{\psi}_R \cos \omega t - \underline{\psi}_I \sin \omega t) + (-\beta_{aI} + \beta_{bI})(\underline{\psi}_R \sin \omega t + \underline{\psi}_I \cos \omega t) \end{aligned} \quad (5.3.67)$$

and apply (5.3.67) to (5.3.27) to obtain

$$\begin{aligned} \underline{q}(t) &= (\beta_{1R} + \beta_{3R})(\underline{\psi}_{1R} \cos \omega_1 t - \underline{\psi}_{1I} \sin \omega_1 t) \\ &\quad + (-\beta_{1I} + \beta_{3I})(\underline{\psi}_{1R} \sin \omega_1 t + \underline{\psi}_{1I} \cos \omega_1 t) \\ &\quad + (\beta_{2R} + \beta_{4R})(\underline{\psi}_{2R} \cos \omega_2 t - \underline{\psi}_{2I} \sin \omega_2 t) \\ &\quad + (-\beta_{2I} + \beta_{4I})(\underline{\psi}_{2R} \sin \omega_2 t + \underline{\psi}_{2I} \cos \omega_2 t) \end{aligned} \quad (5.3.68)$$

The β are arbitrary constants so (5.3.68) may be written as

$$\begin{aligned} \underline{q}(t) &= a_1(\underline{\psi}_{1R} \cos \omega_1 t - \underline{\psi}_{1I} \sin \omega_1 t) + a_2(\underline{\psi}_{1R} \sin \omega_1 t + \underline{\psi}_{1I} \cos \omega_1 t) \\ &\quad + a_3(\underline{\psi}_{2R} \cos \omega_2 t - \underline{\psi}_{2I} \sin \omega_2 t) + a_4(\underline{\psi}_{2R} \sin \omega_2 t + \underline{\psi}_{2I} \cos \omega_2 t) \end{aligned} \quad (5.3.69)$$

where the a_i are also arbitrary constants. Therefore, considering initial positions and velocities

$$\left[\begin{array}{c|c|c|c} \underline{\psi}_{1R} & \underline{\psi}_{1I} & \underline{\psi}_{2R} & \underline{\psi}_{2I} \\ \hline -\omega_1 \underline{\psi}_{1I} & \omega_1 \underline{\psi}_{1R} & -\omega_2 \underline{\psi}_{2I} & \omega_2 \underline{\psi}_{2R} \end{array} \right] \left\{ \begin{array}{c} a_1 \\ a_2 \\ a_3 \\ a_4 \end{array} \right\} = \left\{ \begin{array}{c} q_{10} \\ q_{20} \\ \dot{q}_{10} \\ \dot{q}_{20} \end{array} \right\} \quad (5.3.70)$$

Substitute (5.3.66) into (5.3.70) to obtain

$$\begin{bmatrix} 1 & 0 & 1 & 0 \\ 0 & \gamma_1 & 0 & \gamma_2 \\ 0 & \omega_1 & 0 & \omega_2 \\ -\omega_1\gamma_1 & 0 & -\omega_2\gamma_2 & 0 \end{bmatrix} \begin{Bmatrix} a_1 \\ a_2 \\ a_3 \\ a_4 \end{Bmatrix} = \begin{Bmatrix} q_{10} \\ q_{20} \\ \dot{q}_{10} \\ \dot{q}_{20} \end{Bmatrix} \quad (5.3.71)$$

or by switching rows 3 and 4

$$\begin{bmatrix} 1 & 0 & 1 & 0 \\ 0 & \gamma_1 & 0 & \gamma_2 \\ -\omega_1\gamma_1 & 0 & -\omega_2\gamma_2 & 0 \\ 0 & \omega_1 & 0 & \omega_2 \end{bmatrix} \begin{Bmatrix} a_1 \\ a_2 \\ a_3 \\ a_4 \end{Bmatrix} = \begin{Bmatrix} q_{10} \\ q_{20} \\ \dot{q}_{20} \\ \dot{q}_{10} \end{Bmatrix} \quad (5.3.72)$$

Apply Gauss elimination between rows 1 and 3 and 2 and 4 to obtain

$$\begin{bmatrix} 1 & 0 & 1 & 0 \\ 0 & \gamma_1 & 0 & \gamma_2 \\ 0 & 0 & \omega_1\gamma_1 - \omega_2\gamma_2 & 0 \\ 0 & 0 & 0 & -\omega_1(\gamma_2/\gamma_1) + \omega_2 \end{bmatrix} \begin{Bmatrix} a_1 \\ a_2 \\ a_3 \\ a_4 \end{Bmatrix} = \begin{Bmatrix} q_{10} \\ q_{20} \\ \dot{q}_{20} + \omega_1\gamma_1 q_{10} \\ \dot{q}_{10} - (\omega_1/\gamma_1)q_{20} \end{Bmatrix} \quad (5.3.73)$$

The a_i may be easily obtained from (5.3.73) by back substitution. Then, from (5.3.69),

$$\begin{aligned} \underline{q}(t) = & \left(a_1 \underline{\psi}_{1R} + a_2 \underline{\psi}_{1I} \right) \cos \omega_1 t + \left(-a_1 \underline{\psi}_{1I} + a_2 \underline{\psi}_{1R} \right) \sin \omega_1 t \\ & + \left(a_3 \underline{\psi}_{2R} + a_4 \underline{\psi}_{2I} \right) \cos \omega_2 t + \left(-a_3 \underline{\psi}_{2I} + a_4 \underline{\psi}_{2R} \right) \sin \omega_2 t \end{aligned} \quad (5.3.74)$$

Note from (5.3.66)

$$\underline{\psi}_{jR} = \begin{Bmatrix} 1 \\ 0 \end{Bmatrix}, \quad \underline{\psi}_{jI} = \begin{Bmatrix} 0 \\ \gamma_j \end{Bmatrix} \quad (5.3.75)$$

So (5.3.74) may be written as

$$\underline{q}(t) = \begin{Bmatrix} a_1 \\ a_2\gamma_1 \end{Bmatrix} \cos \omega_1 t + \begin{Bmatrix} a_2 \\ -a_1\gamma_1 \end{Bmatrix} \sin \omega_1 t + \begin{Bmatrix} a_3 \\ a_4\gamma_2 \end{Bmatrix} \cos \omega_2 t + \begin{Bmatrix} a_4 \\ -a_3\gamma_2 \end{Bmatrix} \sin \omega_2 t \quad (5.3.76)$$

Summarizing results yields:

Two Dof Gyroscopic System without Damping or Circulatory Forces

For

$$\underline{C} = \underline{K}_C = \underline{0} \quad (5.3.77)$$

and with

$$m_{12} = k_{12} = 0 \quad (5.3.78)$$

define from (5.3.16)

$$\alpha_0 = \frac{k_{11}}{m_{11}} \frac{k_{22}}{m_{22}}, \quad \alpha_2 = \frac{k_{11}}{m_{11}} + \frac{k_{22}}{m_{22}} + \frac{g_{12}^2}{m_{11}m_{22}} \quad (5.3.79)$$

Then from (5.3.23) the two natural frequencies are

$$\omega_1 = \sqrt{\frac{\alpha_2}{2} - \frac{1}{2}\sqrt{\alpha_2^2 - 4\alpha_0}}, \quad \omega_2 = \sqrt{\frac{\alpha_2}{2} + \frac{1}{2}\sqrt{\alpha_2^2 - 4\alpha_0}} \quad (5.3.80)$$

and from (5.3.65) and (5.3.66) the corresponding mode shapes are

$$\underline{\psi}_1 = \begin{Bmatrix} 1 \\ i\gamma_1 \end{Bmatrix}, \quad \underline{\psi}_2 = \begin{Bmatrix} 1 \\ i\gamma_2 \end{Bmatrix} \quad (5.3.81)$$

where

$$\gamma_j = \frac{k_{11} - \omega_j^2 m_{11}}{\omega_j g_{12}} \quad (5.3.82)$$

Given the initial conditions

$$\underline{q}(0) = \begin{Bmatrix} q_{10} \\ q_{20} \end{Bmatrix}, \quad \underline{\dot{q}}(0) = \begin{Bmatrix} \dot{q}_{10} \\ \dot{q}_{20} \end{Bmatrix} \quad (5.3.83)$$

the free vibration response is given by (5.3.76)

$$\underline{q}(t) = \begin{Bmatrix} q_1(t) \\ q_2(t) \end{Bmatrix} = \begin{Bmatrix} a_1 \\ a_2\gamma_1 \end{Bmatrix} \cos \omega_1 t + \begin{Bmatrix} a_2 \\ -a_1\gamma_1 \end{Bmatrix} \sin \omega_1 t + \begin{Bmatrix} a_3 \\ a_4\gamma_2 \end{Bmatrix} \cos \omega_2 t + \begin{Bmatrix} a_4 \\ -a_3\gamma_2 \end{Bmatrix} \sin \omega_2 t \quad (5.3.84)$$

where from (5.3.73)

$$a_4 = \frac{\gamma_1 \dot{q}_{10} - \omega_1 q_{20}}{\omega_2 \gamma_1 - \omega_1 \gamma_2}, \quad a_3 = \frac{\dot{q}_{20} + \omega_1 \gamma_1 q_{10}}{\omega_1 \gamma_1 - \omega_2 \gamma_2}, \quad a_2 = \frac{q_{20} - \gamma_2 a_4}{\gamma_1}, \quad a_1 = q_{10} - a_3 \quad (5.3.85)$$

5.3.2.1 Small Vibration: Gyroscopic Systems

Figure 5.3.1 shows a rigid cylinder which is spinning and vibrating with small motions, has transverse I_T and polar I_P moments of inertia, and has mass center G .

The small angular displacements of the cylinder about the y and z axes are θ_y and θ_z , respectively. Figure 5.3.2 shows the projections of the cylinder's motion in the xz and yz planes.

This depiction assumes that the H_x component dominates the other components of the angular momentum vector \vec{H} . It follows that the change in \vec{H} is

$$\Delta \vec{H}_g = \Delta \vec{H}_{gy} + \Delta \vec{H}_{gz} = I_P \omega \theta_z \hat{j} - I_P \omega \theta_y \hat{k} \quad (5.3.86)$$

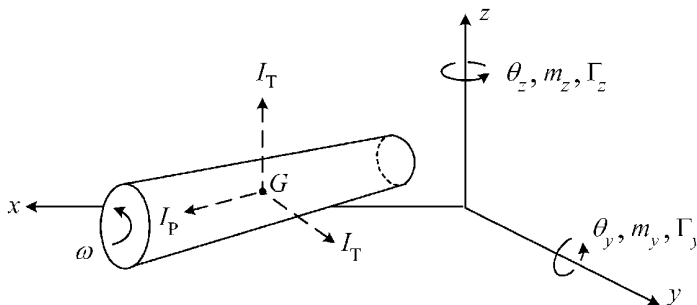


Figure 5.3.1 Spinning rigid cylinder

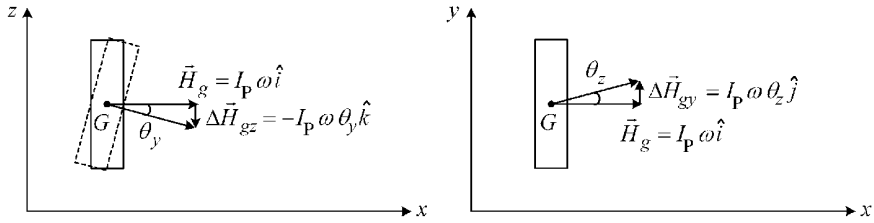


Figure 5.3.2 Approximate changes in the angular momentum vector \vec{H}

Then, for constant ω ,

$$\frac{d}{dt}\vec{H}_g = I_P\omega\dot{\theta}_z\hat{j} - I_P\omega\dot{\theta}_y\hat{k} \quad (5.3.87)$$

The standard planar motion components of angular momentum are due to rotary inertia and are expressed by

$$\vec{H}_1 = I_T\dot{\theta}_y\hat{j} + I_T\dot{\theta}_z\hat{k} \quad (5.3.88)$$

$$\therefore \frac{d}{dt}\vec{H}_1 = I_T\ddot{\theta}_y\hat{j} + I_T\ddot{\theta}_z\hat{k} \quad (5.3.89)$$

Newton's rotational equation of motion (EOM) (3.3.25) may be stated in general terms as

$$\frac{d}{dt}\vec{H} = \vec{\Gamma} \quad (5.3.90)$$

where $\vec{\Gamma}$ equals the resultant torque vector relative to the cylinder's mass center G .

Combining the gyroscopic and rotary inertia terms yields

$$\frac{d}{dt}\vec{H} = \frac{d}{dt}\vec{H}_g + \frac{d}{dt}\vec{H}_1 = (I_T\ddot{\theta}_y + I_P\omega\dot{\theta}_z)\hat{j} + (I_T\ddot{\theta}_z - I_P\omega\dot{\theta}_y)\hat{k} = \Gamma_y\hat{j} + \Gamma_z\hat{k} \quad (5.3.91)$$

$$\therefore I_T\ddot{\theta}_y + I_P\omega\dot{\theta}_z = \Gamma_y \quad (5.3.92)$$

$$I_T\ddot{\theta}_z - I_P\omega\dot{\theta}_y = \Gamma_z \quad (5.3.93)$$

The rotational EOMs in (5.3.92) and (5.3.93) and the translational EOMs (TEOM)

$$m\ddot{y}_G = F_y \quad (5.3.94)$$

$$m\ddot{z}_G = F_z \quad (5.3.95)$$

form the full set of EOMs for transverse motions. The terms F_y , F_z , Γ_y , and Γ_z mainly arise from elastic or damping restraint forces on the disk as shown in Figure 5.3.3.

EXAMPLE 5.3.4 Industrial Exhaust Fan Vibrations

Statement: A fan manufacturer produces a unit with a large diameter wheel (impeller) to increase airflow rate when driven by a low-speed motor, as depicted in Figure E5.3.4(a).

The shaft (1) and bearing (2) are assumed to be rigid and the shaft spin rate Ω is constant. The fan wheel is attached to the shaft via a flexible internal plate diaphragm (4) and a bolted flange (5). The mass center (G) of the impeller coincides with the end of the rigid shaft. This unit experienced large vibrations during several months of operation and then failed catastrophically by complete separation of the wheel from the diaphragm. Inspection of the 360° crack around the diaphragm revealed signs of high-cycle fatigue. It is known that if the spin frequency Ω is near ($\pm 15\%$) to any natural frequency, large vibrations will

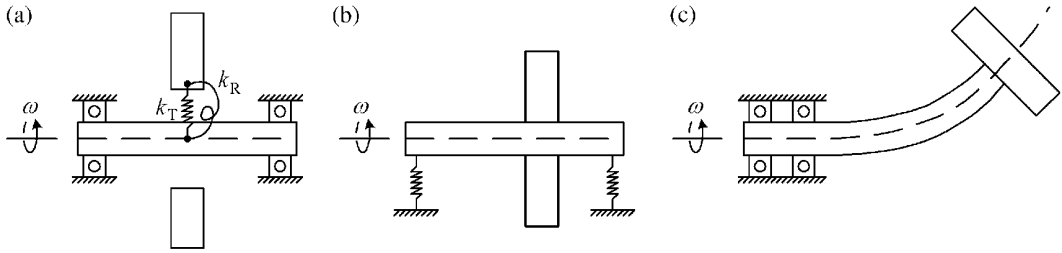


Figure 5.3.3 Elastic restraints on a spinning disk (a) rigid shaft and bearing and flexible disk attachment, (b) rigid shaft and flexible bearings, and (c) rigid bearings and flexible shaft

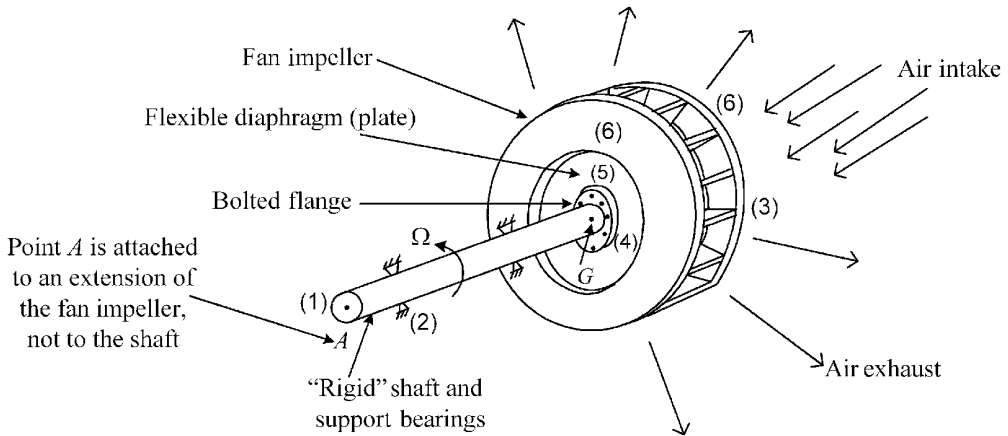


Figure E5.3.4(a) Industrial fan impeller with a flexible diaphragm attachment

result so calculation of these frequencies is an important part of a post-failure investigation conducted by the machinery user and vendor.

Objective: Determine the natural frequencies, mode shapes, and initial condition response of the impeller wheel.

Assumptions:

- (a) Small-angle oscillations of the wheel.
- (b) The diaphragm is very stiff in the radial direction so the impeller's mass center G does not move radially (perpendicular to the shaft axis). The impeller only tilts and does not translate.
- (c) Axial vibration of the impeller is uncoupled from its bending vibration so the two problems may be treated independently.
- (d) The large majority of the impeller's mass is in its axisymmetric shroud plates (6) so that its inertia matrix is axisymmetric and can be expressed as

$$I_G = \begin{bmatrix} I_P & 0 & 0 \\ 0 & I_T & 0 \\ 0 & 0 & I_T \end{bmatrix} \quad (1)$$

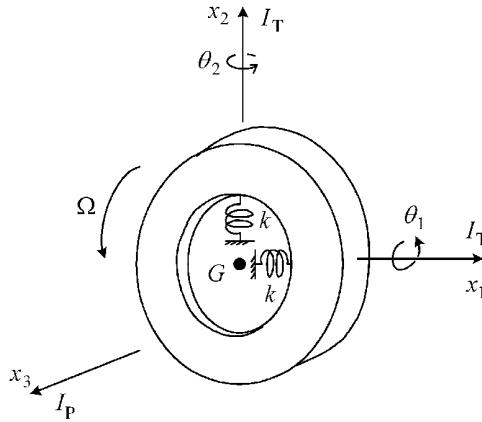


Figure E5.3.4(b) Equivalent inertia–stiffness representation for fan impeller vibration model

where I_P is the polar moment of inertia of the wheel and I_T is the transverse moment of inertia of the wheel about an axis passing through mass center G .

Solution:

- (a) An equivalent model of the fan impeller and its flexible diaphragm support is shown in Figure E5.3.4(b) which is similar to case (a) in Figure 5.3.3.

The torsional springs k represent the flexible diaphragm which is connected to ground via the rigidly supported rigid shaft. The rotational stiffness (k) of the diaphragm is typically determined by (i) experiment, (ii) by the finite element model, or (iii) by a handbook formula, such as Roark and Young (1975):

$$k = \frac{Et^3}{\alpha}$$

where E and t are Young's modulus and the thickness of the diaphragm and α is a constant that depends on the ratio of the flange's bolt circle diameter to the diaphragm's outer diameter.

- (b) The equations of motion for the disk are obtained from Equations (5.3.92) and (5.3.93) and from the rotational spring torques implied in Figure E5.3.4(b):

$$I_T \ddot{\theta}_1 + I_P \Omega \dot{\theta}_2 = -k\theta_1, \quad I_T \ddot{\theta}_2 - I_P \Omega \dot{\theta}_1 = -k\theta_2 \quad (2)$$

or in matrix–vector form

$$\underline{M}\ddot{\underline{q}} + \underline{G}\dot{\underline{q}} + \underline{K}\underline{q} = \underline{0}$$

where

$$\begin{aligned} \underline{M} &= \begin{bmatrix} m_{11} & m_{12} \\ m_{12} & m_{22} \end{bmatrix} = \begin{bmatrix} I_T & 0 \\ 0 & I_T \end{bmatrix}, \\ \underline{G} &= \begin{bmatrix} 0 & g_{12} \\ -g_{12} & 0 \end{bmatrix} = \begin{bmatrix} 0 & I_P \Omega \\ -I_P \Omega & 0 \end{bmatrix}, \\ \underline{K} &= \begin{bmatrix} k_{11} & k_{12} \\ k_{12} & k_{22} \end{bmatrix} = \begin{bmatrix} k & 0 \\ 0 & k \end{bmatrix}, \quad \underline{q} = \begin{Bmatrix} \theta_1 \\ \theta_2 \end{Bmatrix} \end{aligned} \quad (3)$$

- (c) To obtain expressions for the natural frequencies, substitute (3) into (5.3.79) and (5.3.80):

$$\alpha_0 = \frac{k^2}{I_T^2}, \quad \alpha_2 = \frac{2k}{I_T} + \frac{I_P^2 \Omega^2}{I_T^2} \quad (4)$$

$$\begin{aligned} \omega_{1,2} &= \sqrt{\frac{k}{I_T} + \frac{I_P^2 \Omega^2}{2I_T^2} \mp \sqrt{\frac{I_P^4 \Omega^4}{4I_T^4} + \frac{k}{I_T} \frac{I_P^2 \Omega^2}{I_T^2}}} \\ &= \sqrt{\frac{k}{I_T} + \frac{I_P^2 \Omega^2}{2I_T^2} \mp \frac{I_P \Omega}{I_T} \sqrt{\frac{k}{I_T} + \frac{I_P^2 \Omega^2}{4I_T^2}}} = \sqrt{\left(\frac{I_P \Omega}{2I_T} \mp \sqrt{\frac{k}{I_T} + \left(\frac{I_P \Omega}{2I_T} \right)^2} \right)^2} \end{aligned} \quad (5)$$

Therefore

$$\omega_1 = \left| \frac{I_P \Omega}{2I_T} - \sqrt{\frac{k}{I_T} + \left(\frac{I_P \Omega}{2I_T} \right)^2} \right| = \sqrt{\frac{k}{I_T} + \left(\frac{I_P \Omega}{2I_T} \right)^2} - \frac{I_P \Omega}{2I_T}, \quad \omega_2 = \frac{I_P \Omega}{2I_T} + \sqrt{\frac{k}{I_T} + \left(\frac{I_P \Omega}{2I_T} \right)^2} \quad (6)$$

Note that these natural frequencies depend on the shaft's spin rate Ω and that

$$\lim_{\Omega \rightarrow \infty} \omega_1 = 0, \quad \lim_{\Omega \rightarrow \infty} \omega_2 = \infty \quad (7)$$

- (d) The mode shapes are obtained by first substituting (6) into (5.3.82):

$$\gamma_j = \frac{k - I_T \omega_j^2}{\omega_j I_P \Omega} = \frac{\frac{k}{I_T} - \omega_j^2}{\frac{I_P}{I_T} \Omega \omega_j} \quad (8)$$

where

$$\omega_{\frac{1}{2}}^2 = \frac{k}{I_T} + \frac{I_P^2 \Omega^2}{2I_T^2} \mp \frac{I_P \Omega}{I_T} \sqrt{\frac{k}{I_T} + \left(\frac{I_P \Omega}{2I_T} \right)^2}$$

Therefore, from (5.3.82),

$$\gamma_{\frac{1}{2}} = \frac{-\frac{I_P \Omega}{2I_T} \pm \sqrt{\frac{k}{I_T} + \left(\frac{I_P \Omega}{2I_T} \right)^2}}{\omega_j} \quad (9)$$

Substitution of (6) into (9) yields

$$\gamma_1 = 1, \quad \gamma_2 = -1 \quad (10)$$

Then, by (5.3.25), (5.3.26), and (5.3.81),

$$\underline{\psi}_1 = \begin{Bmatrix} 1 \\ i \end{Bmatrix}, \quad \underline{\psi}_2 = \begin{Bmatrix} 1 \\ -i \end{Bmatrix}, \quad \underline{\psi}_3 = \bar{\underline{\psi}}_1 = \begin{Bmatrix} 1 \\ -i \end{Bmatrix}, \quad \underline{\psi}_4 = \bar{\underline{\psi}}_2 = \begin{Bmatrix} 1 \\ i \end{Bmatrix} \quad (11)$$

where

$$\omega_3 = -\omega_1, \quad \omega_4 = -\omega_2 \quad (12)$$

Mode 1 Visualization. From (5.3.17), the contribution of \underline{y}_1 to the response is

$$\begin{Bmatrix} \theta_{1,1} \\ \theta_{2,1} \end{Bmatrix} = \text{Real}(\underline{y}_1 e^{i\omega_1 t}) = \text{Real}\left(\begin{Bmatrix} 1 \\ i \end{Bmatrix} (\cos \omega_1 t + i \sin \omega_1 t)\right) = \begin{Bmatrix} \cos \omega_1 t \\ -\sin \omega_1 t \end{Bmatrix} \quad (13)$$

Let point A lie on an imaginary extension of the wheel in Figure E5.3.4(a) such that A is located on the x_3 axis at a distance L from G if $\theta_1 = \theta_2 = 0$. For small angles, the position coordinates of Point A in Figures E5.3.4(a) and E5.3.4(b) are

$$x_{1A} = L\theta_{2,1}, \quad x_{2A} = -L\theta_{1,1} \quad (14)$$

The coordinates of A are shown in Figure E5.3.4(c).

Since

$$\phi = \tan^{-1}\left(\frac{x_{2A}}{x_{1A}}\right) \quad (15)$$

it follows that

$$\dot{\phi} = \frac{1}{1 + \left(\frac{x_{2A}}{x_{1A}}\right)^2} \frac{d}{dt} \left(\frac{x_{2A}}{x_{1A}}\right) = \frac{1}{x_{1A}^2 + x_{2A}^2} (x_{1A}\dot{x}_{2A} - x_{2A}\dot{x}_{1A}) \quad (16)$$

or

$$\text{sgn}(\dot{\phi}) = \text{sgn}(x_{1A}\dot{x}_{2A} - x_{2A}\dot{x}_{1A}) \quad (17)$$

Insert (13) and (14) into (17) to obtain

$$\text{sgn}(\dot{\phi}) = \text{sgn}((-\sin \omega_1 t)(\omega_1 \sin \omega_1 t) - (-\cos \omega_1 t)(-\omega_1 \cos \omega_1 t)) = \text{sgn}(-\omega_1) = -1 \quad (18)$$

Hence, since $\dot{\phi}$ is negative, mode 1 with natural frequency

$$\omega_1 = \frac{-I_p \Omega}{2I_T} + \sqrt{\frac{k}{I_T} + \left(\frac{I_p \Omega}{2I_T}\right)^2} \quad (19)$$

corresponds to a natural “whirling” of the fan impeller in a direction opposite to its spin rate (Ω) (ref. Figure E5.3.4(c)). Thus, \underline{y}_3 is referred to as a “backward precession mode,” or simply “backward whirl mode,” in the vernacular of rotordynamics.

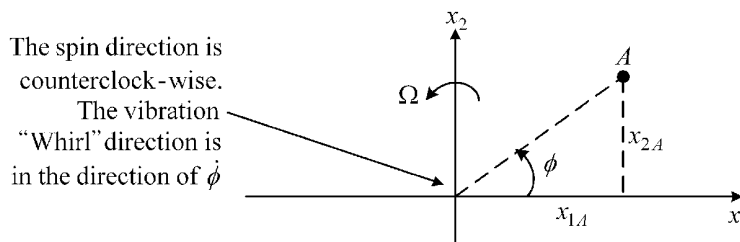


Figure E5.3.4(c) Coordinates of point A attached to an imaginary extension of the impeller

Mode 2 Visualization. From (5.3.17), the contribution of \underline{y}_2 to the response is

$$\begin{Bmatrix} \theta_{1,2} \\ \theta_{2,2} \end{Bmatrix} = \text{Real}(\underline{y}_2 e^{i\omega_2 t}) = \text{Real}\left(\begin{Bmatrix} 1 \\ -i \end{Bmatrix} (\cos \omega_2 t + i \sin \omega_2 t)\right) = \begin{Bmatrix} \cos \omega_2 t \\ \sin \omega_2 t \end{Bmatrix} \quad (20)$$

or by (14)

$$\begin{Bmatrix} x_{1A} \\ x_{2A} \end{Bmatrix} = L \begin{Bmatrix} \theta_{2,2} \\ -\theta_{1,2} \end{Bmatrix} = L \begin{Bmatrix} \sin \omega_2 t \\ -\cos \omega_2 t \end{Bmatrix}$$

The whirl direction is again given by (17)

$$\text{sgn}(\dot{\phi}) = \text{sgn}((\sin \omega_2 t)(\omega_2 \sin \omega_2 t) - (-\cos \omega_2 t)(\omega_2 \cos \omega_2 t)) = \text{sgn}(\omega_2) = +1 \quad (21)$$

Hence, mode 2 with natural frequency

$$\omega_2 = \frac{I_P \Omega}{2I_T} + \sqrt{\frac{k}{I_T} + \left(\frac{I_P \Omega}{2I_T}\right)^2} \quad (22)$$

corresponds to a natural “whirling” of the fan impeller in the direction of the spin rate (Ω). This mode is referred to as a “forward whirl mode.” If the spin speed Ω is high enough, that is,

$$\left(\frac{I_P \Omega}{2I_T}\right)^2 \gg \frac{k}{I_T}$$

the following asymptotic form is valid for ω_2 :

$$\omega_2 \approx \frac{I_P}{I_T} \Omega \quad (23)$$

which shows that the forward mode natural frequency is proportional to the rotor spin frequency, with proportionality constant (I_P/I_T), for high spin speeds.

(e) Determine the response of the impeller to the following initial conditions:

$$\dot{\theta}_1(0) = \theta_2(0) = 0, \quad \theta_1(0) = 0.01, \quad \dot{\theta}_2(0) = 1 \quad (24)$$

From (10),

$$\gamma_1 = -\gamma_2 = 1$$

then the a_i in (5.3.85) become

$$\begin{aligned} a_4 &= \frac{\gamma_1 \dot{\theta}_1(0) - \omega_1 \theta_2(0)}{\omega_2 \gamma_1 - \omega_1 \gamma_2} = 0, & a_3 &= \frac{\dot{\theta}_2(0) + \omega_1 \gamma_1 \theta_1(0)}{\omega_1 \gamma_1 - \omega_2 \gamma_2} = \frac{1 + \omega_1(+1)(0.01)}{\omega_1 + \omega_2} \\ a_2 &= \frac{\theta_2(0) - \gamma_2 a_4}{\gamma_1} = 0, & a_1 &= \theta_1(0) - a_3 = \frac{0.01\omega_2 - 1}{\omega_1 + \omega_2} \end{aligned} \quad (25)$$

and the response from (5.3.84) becomes

$$\underline{q}(t) = \begin{Bmatrix} \theta_1(t) \\ \theta_2(t) \end{Bmatrix} = \begin{Bmatrix} a_1 \\ 0 \end{Bmatrix} \cos \omega_1 t + \begin{Bmatrix} 0 \\ -a_1 \end{Bmatrix} \sin \omega_1 t + \begin{Bmatrix} a_3 \\ 0 \end{Bmatrix} \cos \omega_2 t + \begin{Bmatrix} 0 \\ a_3 \end{Bmatrix} \sin \omega_2 t$$

or

$$\begin{aligned}\theta_1(t) &= \frac{(0.01\omega_2 - 1)\cos\omega_1 t + (1 + 0.01\omega_1)\cos\omega_2 t}{\omega_1 + \omega_2} \\ \theta_2(t) &= \frac{(1 - 0.01\omega_2)\sin\omega_1 t + (1 + 0.01\omega_1)\sin\omega_2 t}{\omega_1 + \omega_2}\end{aligned}\quad (26)$$

Summary: This example demonstrated how to determine the free vibration characteristics of a rotating gyroscopic system. This type of system will always possess a non-null skew-symmetric \underline{G} matrix (3) and yield speed-dependent natural frequencies (6). The first natural frequency diminishes as fan speed Ω increases and has a mode that provides a backward whirl motion relative to the spin direction. The second natural frequency increases as Ω increases and has a mode that provides a forward whirl motion component. The initial conditions for the example

$$\dot{\theta}_1(0) = \theta_2(0) = 0, \quad \theta_1(0) = 0.01, \quad \dot{\theta}_2(0) = 1 \quad (27)$$

impart an initial forward whirl motion to the impeller since by (14) and (17)

$$\text{sgn}(\dot{\phi}) = \text{sgn}(-\theta_2\dot{\theta}_1 + \theta_1\dot{\theta}_2) = \text{sgn}(0*0 + 0.01*1) = +1 \quad (28)$$

Although this initial condition was forward, Equation (26) shows that the impeller responds with both forward (ω_2) and backward (ω_1) components of motion.

5.3.3 Special Case III $\underline{C} = \underline{G} = \underline{0}$ (Undamped, Nongyroscopic, and Circulatory Case)

For this case, (5.3.8) becomes

$$(\lambda^2 \underline{M} + \underline{K} + \underline{K}_C) \underline{\psi} = \underline{0} \quad (5.3.96)$$

or by using (5.3.2) with

$$m_{12} = k_{12} = 0, \quad m_{11} = m_{22} = I_T, \quad k_{11} = k_{22} = k \quad (5.3.97)$$

it results

$$\begin{bmatrix} I_T \lambda^2 + k & k_C \\ -k_C & I_T \lambda^2 + k \end{bmatrix} \underline{\psi} = \underline{0} \quad (5.3.98)$$

where k_C is the *circulatory stiffness*. As discussed previously, the coefficient matrix in (5.3.98) must be singular if the system has free vibrations. This implies that its determinant must equal zero, yielding

$$\lambda^4 + \alpha_2 \lambda^2 + \alpha_0 = 0 \quad (5.3.99)$$

where

$$\alpha_0 = \frac{k^2 + k_C^2}{I_T^2}, \quad \alpha_2 = \frac{2k}{I_T}$$

The following MAPLE code is utilized to solve for the roots of (5.3.99):

Maple Code for Root Determination

```
a2 := 2*k/IT;
a0 := (k^2+kC^2)/IT^2;
solve(lambda^4+a2*lambda^2+a0=0, lambda);
```

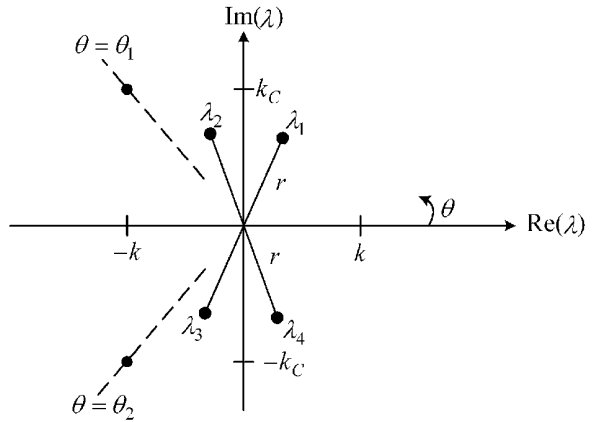


Figure 5.3.4 Eigenvalue locations for pure circulatory system

The results are

$$\begin{aligned}\lambda_1 &= \sqrt{\frac{-k + ik_C}{I_T}} = \frac{1}{I_T} \sqrt{k^2 + k_C^2} \left(\cos \frac{\theta_1}{2} + i \sin \frac{\theta_1}{2} \right) \quad \text{where } \theta_1 = \tan^{-1} \left(\frac{k_C}{-k} \right) \\ \lambda_2 &= \frac{1}{I_T} \sqrt{k^2 + k_C^2} \left(\cos \frac{\theta_2}{2} + i \sin \frac{\theta_2}{2} \right) \quad \text{where } \theta_2 = \tan^{-1} \left(\frac{-k_C}{-k} \right) \\ \lambda_3 &= -\lambda_1, \quad \lambda_4 = -\lambda_2\end{aligned}\tag{5.3.100}$$

The locations of the four roots in the complex (λ) plane are illustrated in Figure 5.3.4, where

$$r = \frac{1}{I_T} \sqrt{k^2 + k_C^2}\tag{5.3.101}$$

Roots 1 and 4 occur in the right half plane so that their real parts satisfy

$$\lambda_{1R} > 0, \quad \lambda_{4R} > 0\tag{5.3.102}$$

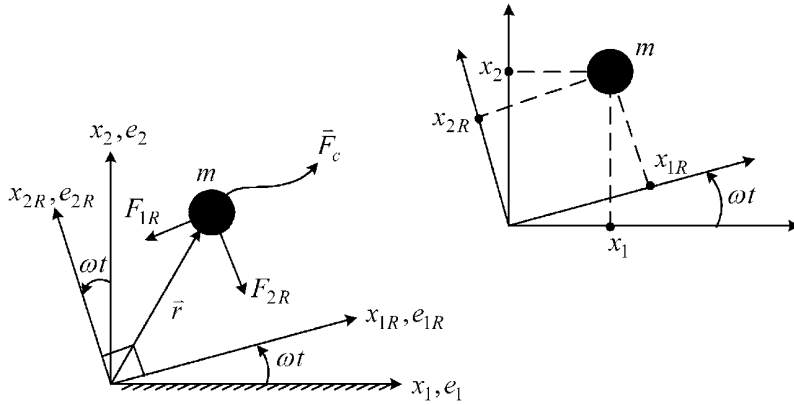
The contributions of these roots to the free vibration response are given by (5.3.17), that is,

$$\beta_1 \underline{\psi}_1 e^{\lambda_1 t} = \beta_1 \underline{\psi}_1 e^{\lambda_{1R} t} e^{i \lambda_{1I} t} = \beta_1 \underline{\psi}_1 e^{\lambda_{1R} t} (\cos \lambda_{1I} t + i \sin \lambda_{1I} t)\tag{5.3.103}$$

Hence, as $t \rightarrow \infty$, the response also goes to infinity, since $e^{\lambda_{1R} t}$ increases monotonically with time. This illustrates the “destabilizing” effects of the circulatory force term. Generally, the circulatory forces arise in the bearings and seals of centrifugal (rotary) pumps and compressors and increase with speed and with discharge pressures. These machines may become unstable, experiencing large, destructive vibrations if the circulatory forces exceed the positive damping forces.

EXAMPLE 5.3.5 Damping in the Rotating Frame of a Turntable

Consider a mass (m) that is attached by springs and dampers to a table that is rotating with constant spin rate ω as shown in Figure E5.3.5(a). For example, the mass might represent the impeller and the stiffness and damping represent the forces resulting from the in-plane deflection of the flexible diaphragm in Figure E5.3.4(a).

Figure E5.3.5(a) Motion of concentrated mass m in a rotating frame

Let

x_1, x_2 : fixed frame (inertial frame) coordinates

x_{1R}, x_{2R} : rotating frame coordinates

Then

$$F_{1R} = -k_R x_{1R} - c_R v_{1R}, \quad F_{2R} = -k_R x_{2R} - c_R v_{2R} \quad (1)$$

where

$$\vec{r}_R = x_{1R} e_{1R} + x_{2R} e_{2R} = x_1 e_1 + x_2 e_2 = \vec{r} = \text{position of } m \quad (2)$$

$$\begin{aligned} \vec{v}_R &= v_{1R} e_{1R} + v_{2R} e_{2R} = \text{velocity of } m \text{ as sensed in the rotating frame} \\ &= \vec{v} - \vec{\omega} \times \vec{r}_R = \vec{v} - \vec{\omega} \times \vec{r} \end{aligned} \quad (3)$$

since by the transport theorem (2.11.27)

$$\frac{d(\vec{r})}{dt} = \frac{{}^R d(\vec{r})}{dt} + \vec{\omega} \times (\vec{r}) \quad (4)$$

and

$$\vec{v} = \text{velocity of } m \text{ as sensed in the fixed frame} \quad (5)$$

Let

$$\vec{F}_E = -c \vec{v} = \text{external damping force} \quad (6)$$

Then

$$m \vec{a} = -k_R \vec{r} - c_R \vec{v}_R - c \vec{v} = -k_R \vec{r} - (c + c_R) \vec{v} + c_R \vec{\omega} \times \vec{r} \quad (7)$$

$$\Rightarrow m(\ddot{x}_1 e_1 + \ddot{x}_2 e_2) = -k_R(x_1 e_1 + x_2 e_2) - (c + c_R)(\dot{x}_1 e_1 + \dot{x}_2 e_2) + c_R \omega e_3 \times (x_1 e_1 + x_2 e_2) \quad (8)$$

Separate the e_1 and e_2 terms to obtain

$$\Rightarrow \begin{bmatrix} m & 0 \\ 0 & m \end{bmatrix} \begin{Bmatrix} \ddot{x}_1 \\ \ddot{x}_2 \end{Bmatrix} + \begin{bmatrix} c + c_R & 0 \\ 0 & c + c_R \end{bmatrix} \begin{Bmatrix} \dot{x}_1 \\ \dot{x}_2 \end{Bmatrix} + \left\{ \begin{array}{cc} \underbrace{\begin{bmatrix} k_R & 0 \\ 0 & k_R \end{bmatrix}}_{\text{direct stiffness matrix}} & + \underbrace{\begin{bmatrix} 0 & c_R \omega \\ -c_R \omega & 0 \end{bmatrix}}_{\text{circulatory stiffness matrix}} \end{array} \right\} \begin{Bmatrix} x_1 \\ x_2 \end{Bmatrix} = \begin{Bmatrix} 0 \\ 0 \end{Bmatrix} \quad (9)$$

The \underline{K} matrix in (9) is shown to consist of a symmetric and a skew-symmetric part. The skew-symmetric part is the “circulatory” stiffness matrix (5.3.2)

$$\underline{K}_C = \begin{bmatrix} 0 & k_{c12} \\ -k_{c12} & 0 \end{bmatrix} = \underbrace{\begin{bmatrix} 0 & c_R \omega \\ -c_R \omega & 0 \end{bmatrix}}_{\text{circulatory stiffness matrix}}$$

Consider the free vibration solution of (9) by setting

$$\begin{Bmatrix} x_1 \\ x_2 \end{Bmatrix} = \underline{\psi} e^{\lambda t} \quad (10)$$

This yields

$$\begin{bmatrix} \lambda^2 m + (c + c_R)\lambda + k_R & c_R \omega \\ -c_R \omega & \lambda^2 m + (c + c_R)\lambda + k_R \end{bmatrix} \underline{\psi} = \underline{0} \quad (11)$$

The eigenvector $\underline{\psi}$ cannot be $\underline{0}$ or free vibration would not exist; thus, the coefficient matrix must be noninvertible, that is, its determinant is zero:

$$m^2 \lambda^4 + \lambda^3 [2m(c + c_R)] + \lambda^2 [2mk_R + (c + c_R)^2] + \lambda [2k_R(c + c_R)] + k_R^2 + c_R^2 \omega^2 = 0 \quad (12)$$

Divide by m^2 and define

$$\omega_n^2 = \frac{k_R}{m}, \quad \xi_R = \frac{c_R}{2m\omega_n}, \quad \xi = \frac{c}{2m\omega_n} \quad (13)$$

Equation (12) becomes

$$\lambda^4 + \lambda^3 [4\omega_n(\xi + \xi_R)] + \lambda^2 [2 + 4(\xi + \xi_R)^2] \omega_n^2 + \lambda [4\omega_n^3(\xi + \xi_R)] + \omega_n^4 + 4\xi_R^2 \omega^2 \omega_n^2 = 0 \quad (14)$$

Consider an example with

$$\xi_R = 0.03, \quad \xi = 0.05, \quad \omega_n = 100 \text{ rad/s} \quad (15)$$

Figure E5.3.5(b) shows that the real part of the second eigenvalue becomes positive as the spin speed (ω) of the rotating frame exceeds 260 rad/s. Thus, the system will become unstable so damping in the rotating frame is shown to be counterproductive for suppressing vibration. The instability frequency is nearly equal to the undamped natural frequency. The instability onset frequency ratio is

$$\text{Instability onset frequency ratio} = \frac{\text{unstable mode frequency}}{\text{spin frequency}} = \frac{100 \text{ rad/s}}{260 \text{ rad/s}} = 0.385$$

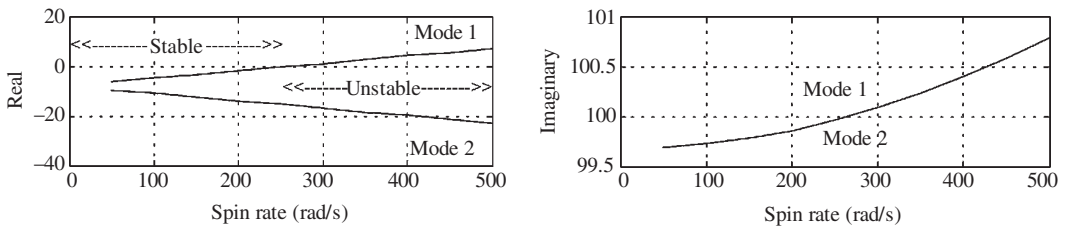


Figure E5.3.5(b) Real and imaginary parts of eigenvalues (in rad/s) versus spin rate

5.4 *N*-DEGREE-OF-FREEDOM SYSTEMS

5.4.1 General Identities

An *N*-degree-of-freedom (*N*dof), unforced linear system has the general mathematical form

$$\underline{M} \frac{d^2 \underline{q}}{dt^2} + \left(\underline{C} + \underline{G} \right) \frac{d \underline{q}}{dt} + \left(\underline{K} + \underline{K}_C \right) \underline{q} = \underline{0} \quad (5.4.1)$$

The characteristics of the IC response of the *N*dof system are very dependent on which matrices are present in (5.4.1).

5.4.2 Undamped, Nongyroscopic, and Noncirculatory Systems—Description

The equilibrium equation becomes

$$\underline{M} \ddot{\underline{q}} + \underline{K} \underline{q} = \underline{0} \quad (5.4.2)$$

Similar to (5.3.3)–(5.3.7), let

$$\underline{q}(t) = \text{Real} \left(e^{\lambda t} \underline{\psi} \right) \quad (5.4.3)$$

so that (5.4.2) becomes

$$(\lambda^2 \underline{M} + \underline{K}) \underline{\psi} = \underline{0} \quad (5.4.4)$$

Premultiply (5.4.4) by $\underline{\bar{\psi}}^T$ (conjugate transpose of $\underline{\psi}$) to obtain

$$\lambda^2 \hat{m} + \hat{k} = 0 \quad (5.4.5)$$

where by (2.6.29) and since \underline{M} and \underline{K} are symmetric

$$\hat{m} = \underline{\bar{\psi}}^T \underline{M} \underline{\psi} = \text{real constant}, \quad \hat{k} = \underline{\bar{\psi}}^T \underline{K} \underline{\psi} = \text{real constant} \quad (5.4.6)$$

Recall from Equations (4.7.40) and (4.7.54) that in general the kinetic energy has the form

$$T = \frac{1}{2} \dot{\underline{q}}^T \underline{M} \dot{\underline{q}} \quad (5.4.7)$$

and the strain energy has the form

$$U = \frac{1}{2} \underline{q}^T \underline{K} \underline{q} \quad (5.4.8)$$

Therefore, it must be true that

$$\underline{x}^T \underline{M} \underline{x} \geq 0 \quad \text{for all } \underline{x}, \quad \underline{x}^T \underline{K} \underline{x} \geq 0 \quad \text{for all } \underline{x} \quad (5.4.9)$$

where the stiffness matrix equality in (5.4.9) indicates motion in a zero strain state, that is, rigid body motion. Matrices that satisfy (5.4.9) are called positive semidefinite (positive definite if the equality never holds (2.6.22)). Considering the above results, it follows that if \underline{M} is positive definite,

$$\lambda^2 = -\frac{\hat{k}}{\hat{m}} \quad (5.4.10)$$

is negative real or zero. Consequently,

$$\lambda_j = \pm i\omega_j, \quad \text{where } \omega_j = \sqrt{\frac{\hat{k}_j}{\hat{m}_j}} \quad (5.4.11)$$

Although Equation (5.4.11) proves that all eigenvalues (λ) of this system type are pure imaginary, it does not provide a means to calculate them since it presupposes that $\underline{\psi}$ is available to form \hat{m} and \hat{k} . Many solution algorithms exist to determine the eigenvalues (λ) and eigenvectors ($\underline{\psi}$) of (5.4.4), and a summary of these may be found in Palazzolo and Pilkey (1987). Substitution of (5.4.11) into (5.4.4) yields

$$\left(-\omega_j^2 \underline{M} + \underline{K}\right) \underline{\psi}_j = \underline{0} \quad (5.4.12)$$

By (5.4.12), the eigenvector $\underline{\psi}$ would be zero if the coefficient matrix $\left(-\omega_j^2 \underline{M} + \underline{K}\right)$ is invertible. By (5.4.3), this would imply that the flexible structure modeled by \underline{M} and \underline{K} would never freely vibrate. Hence, it must be the case that for a certain set of ω_j , the coefficient matrix is singular, that is,

$$\det\left(-\omega_j^2 \underline{M} + \underline{K}\right) = 0 \quad (5.4.13)$$

Although the ω_j must satisfy (5.4.13), this condition is rarely used to obtain the ω_j because of its numerical inefficiency. The $\underline{\psi}_j$ are real vectors since the coefficient matrix in (5.4.12) is real. The $\underline{\psi}_j$ are unique only to within a multiplicative constant since if $\underline{\psi}_j$ satisfies (5.4.12), so does $\gamma \underline{\psi}_j$ where γ is a constant.

5.4.3 Undamped, Nongyroscopic, and Noncirculatory Systems—Solution Form

Many commercially available math software packages can readily solve (5.4.12), that is, see the example for MATLAB in Section 2.2 or the example for MAPLE in Section 2.3. These codes can operate with either of the two general forms

$$\underline{A} \underline{X} = \alpha \underline{B} \underline{X} \quad (5.4.14)$$

or

$$\underline{A} \underline{X} = \alpha \underline{X} \quad (5.4.15)$$

For the first form,

$$\underline{X} = \underline{\psi}, \quad \underline{A} = \underline{K}, \quad \underline{B} = \underline{M}, \quad \alpha = \omega^2 \Rightarrow \omega_j = \sqrt{\alpha_j} \quad (5.4.16)$$

There exist several common approaches to transform (5.4.12) into the second form (5.4.15):

(a) The first approach is simply to multiply (5.4.12) by \underline{M}^{-1} , if it exists, yielding

$$\underline{A} \underline{X} = \alpha \underline{X} \quad (5.4.17)$$

where

$$\underline{X} = \underline{\psi}, \quad \underline{A} = \underline{M}^{-1} \underline{K}, \quad \alpha = \omega^2 \Rightarrow \omega_j = \sqrt{\alpha_j}$$

- (b) The second approach is to multiply (5.4.12) by \underline{K}^{-1} , if it exists, yielding

$$\underline{A}\underline{X} = \alpha\underline{X} \quad (5.4.18)$$

where

$$\underline{X} = \underline{\psi}, \quad \underline{A} = \underline{K}^{-1}\underline{M}, \quad \alpha = \frac{1}{\omega^2} \Rightarrow \omega_j = \frac{1}{\sqrt{\alpha_j}}$$

Both approaches (a) and (b) form an unsymmetric matrix \underline{A} from two symmetric matrices \underline{M} and \underline{K} . The numerical solution for the eigenvalues and eigenvectors of an unsymmetric matrix may require considerably more computation time than for an equally dimensioned symmetric matrix. Therefore, the following approaches form a symmetric \underline{A} matrix.

- (c) If \underline{M} is diagonal with nonzero diagonal entries, which occurs for lumped mass models,

$$\underline{M} = \underline{\text{diag}}(m_{ii}) \quad N \times N \quad (5.4.19)$$

then define

$$\underline{M}^{1/2} = \underline{\text{diag}}(m_{ii}^{1/2}) \quad N \times N \quad (5.4.20)$$

Introduce the transformation

$$\underline{\psi} = \underline{M}^{-1/2}\underline{\chi} \quad (5.4.21)$$

into (5.4.12) to obtain $\underline{K}\underline{M}^{-1/2}\underline{\chi} = \omega_j^2\underline{M}\underline{M}^{-1/2}\underline{\chi}$

Premultiply this equation by $\underline{M}^{-1/2}$ to obtain

$$\underline{A}\underline{X} = \alpha\underline{X} \quad (5.4.22)$$

where

$$\underline{X} = \underline{\chi}, \quad \underline{A} = \underline{M}^{-1/2}\underline{K}\underline{M}^{-1/2}, \quad \alpha = \omega^2 \Rightarrow \omega_j = \sqrt{\alpha_j}$$

The coefficient matrix in (5.4.22) is symmetric since

$$\left(\underline{M}^{-1/2}\underline{K}\underline{M}^{-1/2}\right)^T = \underline{M}^{-1/2}\underline{K}\underline{M}^{-1/2} \quad (5.4.23)$$

- (d) In general, the assumed modes and finite element modeling approaches yield a nondiagonal “consistent” mass \underline{M} matrix, unless the mass is lumped at the node locations. This renders approach (c) unusable, so a different transformation is employed. If \underline{K} and \underline{M} are positive definite, they may be expressed by the following Cholesky factorizations from (Franklin, 1968):

$$\underline{K} = \underline{T}_K \underline{T}_K^T \quad (5.4.24)$$

$$\underline{M} = \underline{T}_M \underline{T}_M^T \quad (5.4.25)$$

where \underline{T}_K and \underline{T}_M are lower triangular matrices. Define the transformation

$$\underline{\psi} = \left(\underline{T}_K^{-1}\right)^T \underline{\chi} = \underline{T}_K^{-T} \underline{\chi} \quad (5.4.26)$$

Substitute (5.4.24) and (5.4.26) into (5.4.12) and then premultiply by \underline{T}_K^{-1} to obtain

$$\underline{A}\underline{X} = \alpha\underline{X} \quad (5.4.27)$$

where

$$\underline{X} = \underline{\chi}, \quad \underline{A} = \underline{T}_K^{-1} \underline{M} \underline{T}_K^{-T}, \quad \alpha = \frac{1}{\omega^2} \Rightarrow \omega_j = \frac{1}{\sqrt{\alpha_j}}$$

Alternatively, define the transformation

$$\underline{\psi} = (\underline{T}_M^{-1})^T \underline{\chi} = \underline{T}_M^{-T} \underline{\chi} \quad (5.4.28)$$

Substitute (5.4.25) and (5.4.28) into (5.4.12) and then premultiply by \underline{T}_M^{-1} to obtain

$$\underline{A}\underline{X} = \alpha\underline{X} \quad (5.4.29)$$

where

$$\underline{X} = \underline{\chi}, \quad \underline{A} = \underline{T}_M^{-1} \underline{M} \underline{T}_M^{-T}, \quad \alpha = \omega^2 \Rightarrow \omega_j = \sqrt{\alpha_j}$$

The benefit of having both options (5.4.27) and (5.4.29) is derived from the possibility that one of the matrices \underline{M} or \underline{K} may not be positive definite so that its factorization, (5.4.24) or (5.4.25), may not exist.

5.4.4 Undamped, Nongyroscopic, and Noncirculatory Systems—Orthogonality

The solutions of (5.4.12) have an interesting and useful property of being orthogonal. This “orthogonality condition” may be derived as follows. Write (5.4.12) for two distinct solutions i and j

$$-\omega_i^2 \underline{M}\underline{\psi}_i + \underline{K}\underline{\psi}_i = \underline{0} \quad (5.4.30)$$

$$-\omega_j^2 \underline{M}\underline{\psi}_j + \underline{K}\underline{\psi}_j = \underline{0} \quad (5.4.31)$$

Premultiply (5.4.30) by $\underline{\psi}_j^T$ and (5.4.31) by $\underline{\psi}_i^T$

$$-\omega_i^2 \underline{\psi}_j^T \underline{M}\underline{\psi}_i + \underline{\psi}_j^T \underline{K}\underline{\psi}_i = 0 \quad (5.4.32)$$

$$-\omega_j^2 \underline{\psi}_i^T \underline{M}\underline{\psi}_j + \underline{\psi}_i^T \underline{K}\underline{\psi}_j = 0 \quad (5.4.33)$$

Transpose (5.4.33) and then subtract the results from (5.4.32) to obtain

$$\left(\omega_j^2 - \omega_i^2\right) \underline{\psi}_j^T \underline{M}\underline{\psi}_i = 0 \quad (5.4.34)$$

since $\underline{M} = \underline{M}^T$ and $\underline{K} = \underline{K}^T$. This implies that

$$\underline{\psi}_j^T \underline{M}\underline{\psi}_i = 0 \quad i \neq j \quad (5.4.35)$$

since $\omega_i \neq \omega_j$ for distinct natural frequencies. For $i = j$, the quadratic form in (5.4.35) is called the “modal mass” \tilde{m}_i , so

$$\tilde{m}_i = \underline{\psi}_i^T \underline{M}\underline{\psi}_i \quad (5.4.36)$$

The orthogonality condition becomes

$$\underline{\psi}_i^T \underline{M} \underline{\psi}_j = \begin{cases} 0, & i \neq j \\ \tilde{m}_i, & i = j \end{cases} = \delta_{ij} \tilde{m}_i \quad (5.4.37)$$

where the Kronecker delta δ_{ij} equals 0 for $i \neq j$ and 1 for $i = j$. The mode $\underline{\psi}$ is unique only to within a multiplicative constant, since

$$\underline{\psi} \Rightarrow \gamma \underline{\psi} \quad (5.4.38)$$

satisfies (5.4.12) for any real or complex constant γ , if $\underline{\psi}$ satisfies (5.4.12). The choice of the constant γ is referred to as the mode normalization convention. Suppose $\underline{\psi}_i$ is obtained from a commercial code and the corresponding modal mass \tilde{m}_i is obtained from (5.4.36). Surely by (5.4.38)

$$\tilde{\underline{\psi}}_i = \frac{\underline{\psi}_i}{\sqrt{\tilde{m}_i}} \quad (5.4.39)$$

also satisfies (5.4.12) so it also is a valid mode corresponding to ω_i . Its modal mass is from (5.4.36)

$$\frac{\tilde{\underline{\psi}}_i^T}{\sqrt{\tilde{m}_i}} \underline{M} \frac{\tilde{\underline{\psi}}_i}{\sqrt{\tilde{m}_i}} = \frac{\tilde{m}_i}{\tilde{m}_i} = 1 \quad (5.4.40)$$

The orthogonality condition becomes

$$\tilde{\underline{\psi}}_i^T \underline{M} \tilde{\underline{\psi}}_j = \begin{cases} 0, & i \neq j \\ 1, & i = j \end{cases} \quad (5.4.41)$$

The modes in (5.4.39) are said to be “mass orthonormalized.”

Define a “modal matrix” as

$$\underline{\Psi} = \begin{pmatrix} \underline{\psi}_1 & \underline{\psi}_2 & \dots & \underline{\psi}_m \end{pmatrix} \quad N \times m \quad (5.4.42)$$

where $m < N$ and the modes form columns of $\underline{\Psi}$. Then, by (5.4.37), (2.6.31), and (2.6.32)

$$(\underline{\Psi}^T \underline{M} \underline{\Psi})_{ij} = \underline{\psi}_i^T \underline{M} \underline{\psi}_j = \begin{cases} 0, & i \neq j \\ \tilde{m}_i, & i = j \end{cases} \quad (5.4.43)$$

Therefore

$$\frac{\underline{\Psi}^T}{m \times N} \underline{M} \frac{\underline{\Psi}}{N \times N \times m} = \text{Diag} \left(\frac{\tilde{m}_i}{m \times m} \right) \quad (5.4.44)$$

Substitute (5.4.37) into (5.4.33) to obtain

$$\underline{\psi}_i^T \underline{K} \underline{\psi}_j = \begin{cases} 0, & i \neq j \\ \tilde{m}_i \omega_i^2, & i = j \end{cases} \quad (5.4.45)$$

So that similar to (5.4.44)

$$\frac{\underline{\Psi}^T}{m \times N} \underline{K} \frac{\underline{\Psi}}{N \times N \times m} = \text{Diag} \left(\frac{\tilde{m}_i \omega_i^2}{m \times m} \right) \quad (5.4.46)$$

The above formulas relate the property matrices ($\underline{M}, \underline{K}$) of a system to its modes and natural frequencies.

5.4.5 Undamped, Nongyroscopic, and Noncirculatory Systems—IC Response

Equations (5.4.4) and (5.4.11) show that the λ_j for this problem occur in N pairs, that is, $\pm i\omega_j$, and that the eigenvectors $\underline{\psi}$ are real. Therefore, the analysis for the 2dof case (5.3.36)–(5.3.45) applies, yielding

$$\underline{q}(t) = \sum_{j=1}^N (\alpha_{jc} \cos \omega_j t + \alpha_{js} \sin \omega_j t) \underline{\psi}_j \quad (5.4.47)$$

So that at $t=0$

$$\underline{\Psi} \underline{\alpha}_c = \underline{q}_0, \quad \underline{\Psi} \underline{\beta}_s = \underline{\dot{q}}_0 \quad (5.4.48)$$

where \underline{q}_0 and $\underline{\dot{q}}_0$ are the given initial displacements and velocities, $\underline{\Psi}$ is the modal matrix defined in (5.4.42) and

$$\underline{\alpha}_c = \begin{Bmatrix} \alpha_{1c} \\ \alpha_{2c} \\ \vdots \\ \alpha_{Nc} \end{Bmatrix}, \quad \underline{\beta}_s = \begin{Bmatrix} \beta_{1s} \\ \beta_{2s} \\ \vdots \\ \beta_{Ns} \end{Bmatrix} = \begin{Bmatrix} \omega_1 \alpha_{1s} \\ \omega_2 \alpha_{2s} \\ \vdots \\ \omega_N \alpha_{Ns} \end{Bmatrix} \quad (5.4.49)$$

Equation (5.4.48) is solved for the α_{jc} and β_{js} in $\underline{\alpha}_c$ and $\underline{\beta}_s$, and then the α_{js} are obtained from (5.4.49)

$$\alpha_{js} = \frac{\beta_{js}}{\omega_j} \quad (5.4.50)$$

The time history of the displacements may then be obtained by substituting the calculated α_{jc} and α_{js} into (5.4.47). The solution of (5.4.48) may be facilitated by premultiplying these equations with $\underline{\Psi}^T \underline{M}$ and then using the orthogonality condition (5.4.44)

$$\underline{\text{Diag}}(\tilde{m}_i) \underline{\alpha}_c = \underline{\Psi}^T \underline{M} \underline{q}_0 \Rightarrow \underline{\alpha}_c = \underline{\text{Diag}}\left(\frac{1}{\tilde{m}_i}\right) \underline{\Psi}^T \underline{M} \underline{q}_0 \quad (5.4.51)$$

Similarly

$$\Rightarrow \underline{\alpha}_s = \begin{Bmatrix} \alpha_{1s} \\ \alpha_{2s} \\ \vdots \\ \alpha_{Ns} \end{Bmatrix} = \underline{\text{Diag}}\left(\frac{1}{\omega_i}\right) \underline{\beta}_s = \underline{\text{Diag}}\left(\frac{1}{\tilde{m}_i \omega_i}\right) \underline{\Psi}^T \underline{M} \underline{\dot{q}}_0 \quad (5.4.52)$$

Equations (5.4.51) and (5.4.52) may still be employed if the number of modes is incomplete ($m < N$). It should be noted however that the vectors

$$\underline{\tilde{q}}_0 = \underline{\Psi} \underline{\alpha}_c = \sum_{j=1}^m \alpha_{jc} \underline{\psi}_j, \quad \underline{\tilde{\dot{q}}}_0 = \underline{\Psi} \underline{\beta}_s = \sum_{j=1}^m \omega_j \alpha_{js} \underline{\psi}_j \quad (5.4.53)$$

are only approximations of \underline{q}_0 and $\underline{\dot{q}}_0$ since the subspace (Section 2.6) that they are obtained from is spanned by only m of the $\underline{\psi}_j$ basis vectors instead of the full set of N .

5.4.6 Undamped, Nongyroscopic, and Noncirculatory Systems—Rigid Body Modes

Some structures or structural components such as airplanes or rotating shafts operate with one or more of their six rigid body motions unconstrained. This means that the objects are capable of undergoing rigid body motions in the absence of applied forces so that for a linear model

$$\underline{M}\ddot{\underline{q}}_{\text{rig}} = \underline{0} \quad (5.4.54)$$

Therefore by (5.4.2)

$$\underline{K}\underline{q}_{\text{rig}} = \underline{0} \quad (5.4.55)$$

The result (5.4.55) also follows from requiring that rigid body motions have zero strain energy:

$$U_I = \frac{1}{2}\underline{q}_{\text{rig}}^T \underline{K}\underline{q}_{\text{rig}} \quad (5.4.56)$$

Substitute (5.4.55) into (5.4.12) to obtain

$$\omega_{\text{rig},j}^2 \underline{M}\underline{\psi}_{\text{rig},j} = \underline{K}\underline{\psi}_{\text{rig},j} = \underline{0} \quad (5.4.57)$$

Therefore, the natural frequencies $\omega_{\text{rig},j}$ corresponding to the rigid body modes are zero. Conversely, the modes corresponding to zero natural frequencies obtained from the output of an eigensolution solver are rigid body modes. In a mathematical sense, from (5.4.57), the rigid body modes are the basis vectors (Section 2.6) that span the null space of \underline{K} , and if the number of these modes is n_{rig} , then the rank of \underline{K} is $N - n_{\text{rig}}$. The solution of (5.4.54) has the general form

$$\underline{q}_{\text{rig}} = \sum_{l=1}^{n_{\text{rig}}} \left(\alpha_{\text{rig}0,l} \underline{\psi}_{\text{rig},l} + \alpha_{\text{rig}1,l} t \underline{\psi}_{\text{rig},l} \right) \quad (5.4.58)$$

Combining (5.4.47) and (5.4.58), the total IC response of the flexible structure with rigid body motion capability becomes

$$\underline{q}(t) = \sum_{l=1}^{n_{\text{rig}}} \left(\alpha_{\text{rig}0,l} \underline{\psi}_{\text{rig},l} + \alpha_{\text{rig}1,l} t \underline{\psi}_{\text{rig},l} \right) + \sum_{j=1}^{N-n_{\text{rig}}} \left(\alpha_{jc} \cos \omega_j t + \alpha_{js} \sin \omega_j t \right) \underline{\psi}_j \quad (5.4.59)$$

The α 's in (5.4.59) may be solved for by imposing the ICs

$$\underline{q}(0) = \sum_{l=1}^{n_{\text{rig}}} \alpha_{\text{rig}0,l} \underline{\psi}_{\text{rig},l} + \sum_{j=1}^{N-n_{\text{rig}}} \alpha_{jc} \underline{\psi}_j \quad (5.4.60)$$

$$\dot{\underline{q}}(0) = \sum_{l=1}^{n_{\text{rig}}} \alpha_{\text{rig}1,l} \underline{\psi}_{\text{rig},l} + \sum_{j=1}^{N-n_{\text{rig}}} \alpha_{js} \omega_j \underline{\psi}_j \quad (5.4.61)$$

5.4.7 Summary

The following provides a summary for the nongyroscopic, noncirculatory system case.

Initial Condition Response of Undamped, Nongyroscopic, Noncirculatory Systems

- Equilibrium equation (5.4.2):

$$\underline{M}\ddot{\underline{q}} + \underline{K}\underline{q} = \underline{0} \quad N \times 1 \quad (5.4.62)$$

- Eigensolution problem (5.4.12):

$$(-\omega^2 \underline{M} + \underline{K})\underline{\psi} = \underline{0} \quad (5.4.63)$$

- Eigensolution forms (5.4.14)–(5.4.29)

- (i) Equilibrium equation form $\underline{A}\underline{X} = \alpha \underline{B}\underline{X}$

$$\underline{X} = \underline{\psi}, \quad \underline{A} = \underline{K}, \quad \underline{B} = \underline{M}, \quad \alpha = \omega^2 \Rightarrow \omega_j = \sqrt{\alpha_j} \quad (5.4.64)$$

$$\underline{X} = \underline{\psi}, \quad \underline{A} = \underline{M}, \quad \underline{B} = \underline{K}, \quad \alpha = \frac{1}{\omega^2} \Rightarrow \omega_j = \frac{1}{\sqrt{\alpha_j}} \quad (5.4.65)$$

- (ii) Equilibrium equation form $\underline{A}\underline{X} = \alpha \underline{X}$

If \underline{M}^{-1} exists

$$\underline{X} = \underline{\psi}, \quad \underline{A} = \underline{M}^{-1}\underline{K}, \quad \alpha = \omega^2 \Rightarrow \omega_j = \sqrt{\alpha_j} \quad (5.4.66)$$

If \underline{K}^{-1} exists

$$\underline{X} = \underline{\psi}, \quad \underline{A} = \underline{K}^{-1}\underline{M}, \quad \alpha = \frac{1}{\omega^2} \Rightarrow \omega_j = \frac{1}{\sqrt{\alpha_j}} \quad (5.4.67)$$

If \underline{M} is diagonal and \underline{M}^{-1} exists

$$\underline{X} = \underline{M}^{1/2}\underline{\psi}, \quad \underline{A} = \underline{A}^T = \underline{M}^{-1/2}\underline{K}\underline{M}^{-1/2}, \quad \alpha = \omega^2 \Rightarrow \omega_j = \sqrt{\alpha_j} \quad (5.4.68)$$

If the Cholesky factorization matrix \underline{T}_K exists, where $(\underline{K} = \underline{T}_K \underline{T}_K^T)$

$$\underline{X} = \underline{T}_K^T \underline{\psi}, \quad \underline{A} = \underline{A}^T = \underline{T}_K^{-1} \underline{M} \underline{T}_K^{-T}, \quad \alpha = \frac{1}{\omega^2} \Rightarrow \omega_j = \frac{1}{\sqrt{\alpha_j}} \quad (5.4.69)$$

If the Choleski factorization matrix \underline{T}_M exists, where $(\underline{M} = \underline{T}_M \underline{T}_M^T)$

$$\underline{X} = \underline{T}_K^T \underline{\psi}, \quad \underline{A} = \underline{A}^T = \underline{T}_M^{-1} \underline{K} \underline{T}_M^{-T}, \quad \alpha = \omega^2 \Rightarrow \omega_j = \sqrt{\alpha_j} \quad (5.4.70)$$

- Orthogonality

$$\delta_{ij} = \text{Kronecker delta} = \begin{cases} 0, & i \neq j \\ 1, & i = j \end{cases} \quad (5.4.71)$$

From (5.4.37) the mass orthogonality condition is

$$\underline{\psi}_i^T \underline{M} \underline{\psi}_j = \tilde{m}_i \delta_{ij} \quad (5.4.72)$$

From (5.4.41) for mass orthonormalized modes

$$\tilde{\underline{\psi}}_i^T \underline{M} \tilde{\underline{\psi}}_j = \delta_{ij} \quad (5.4.73)$$

From (5.4.42) the modal matrix is defined by

$$\underline{\Psi} = \left(\underline{\psi}_1 \quad \underline{\psi}_2 \quad \dots \quad \underline{\psi}_m \right) \quad N \times m \quad (5.4.74)$$

From (5.4.44) the mass orthogonality condition is

$$\frac{\underline{\Psi}^T}{m \times N} \underline{M} \frac{\underline{\Psi}}{N \times N \times m} = \underline{\text{Diag}}(\tilde{m}_i) \quad m \times m \quad (5.4.75)$$

From (5.4.45) the stiffness orthogonality condition is

$$\underline{\psi}_i^T \underline{K} \underline{\psi}_j = \delta_{ij} \tilde{m}_i \omega_i^2 \quad (5.4.76)$$

From (5.4.46) the stiffness orthogonality condition is

$$\frac{\underline{\Psi}^T}{m \times N} \underline{K} \frac{\underline{\Psi}}{N \times N \times m} = \underline{\text{Diag}}(\tilde{m}_i \omega_i^2) \quad m \times m \quad (5.4.77)$$

- Initial condition response

From (5.4.47), for a structure *constrained against rigid body motion*

$$\underline{q}(t) = \sum_{j=1}^N (\alpha_{jc} \cos \omega_j t + \alpha_{js} \sin \omega_j t) \underline{\psi}_j \quad (5.4.78)$$

where from (5.4.51) and (5.4.52)

$$\underline{\alpha}_c = \begin{Bmatrix} \alpha_{1c} \\ \alpha_{2c} \\ \vdots \\ \alpha_{Nc} \end{Bmatrix} = \underline{\text{Diag}}\left(\frac{1}{\tilde{m}_i}\right) \underline{\Psi}^T \underline{M} \underline{q}_0, \quad \underline{\alpha}_s = \begin{Bmatrix} \alpha_{1s} \\ \alpha_{2s} \\ \vdots \\ \alpha_{Ns} \end{Bmatrix} = \underline{\text{Diag}}\left(\frac{1}{\tilde{m}_i \omega_i}\right) \underline{\Psi}^T \underline{M}_0 \dot{\underline{q}}_0 \quad (5.4.79)$$

- For a structure that is *capable of undergoing one or more rigid body motions*, the rigid body natural frequencies are zero $\omega_{\text{rig},j} = 0$, and from (5.4.57)

$$\underline{K} \underline{\psi}_{\text{rig},j} = \underline{0} \quad (5.4.80)$$

has n_{rig} nontrivial solution vectors $\underline{\psi}_{\text{rig},j}$ where n_{rig} is the number of unconstrained, linearly independent, rigid body motions that the model ($n_{\text{rig}} \leq 6$) is capable of undergoing. From (5.4.59)

$$\underline{q}(t) = \sum_{l=1}^{n_{\text{rig}}} \left(\alpha_{\text{rig}0,l} \underline{\psi}_{\text{rig},l} + \alpha_{\text{rig}1,l} t \underline{\psi}_{\text{rig},l} \right) + \sum_{j=1}^{N-n_{\text{rig}}} (\alpha_{jc} \cos \omega_j t + \alpha_{js} \sin \omega_j t) \underline{\psi}_j \quad (5.4.81)$$

where the α 's may be obtained from (5.4.60) and (5.4.61) as

$$\begin{Bmatrix} \vdots \\ \alpha_{\text{rig}0,l} \\ \vdots \\ \alpha_{jc} \\ \vdots \end{Bmatrix} = \left(\begin{bmatrix} \overbrace{\psi_{\text{rig},l}}^{n_{\text{rig}} \text{ columns}} & \overbrace{\psi_j}^{N-n_{\text{rig}} \text{ columns}} \\ \vdots & \vdots \end{bmatrix} \right)^{-1} \underline{q}_0 \quad (5.4.82)$$

$$\begin{Bmatrix} \vdots \\ \alpha_{\text{rig}1,l} \\ \vdots \\ \alpha_{js} \\ \vdots \end{Bmatrix} = \left(\begin{bmatrix} \overbrace{\psi_{\text{rig},l}}^{n_{\text{rig}} \text{ columns}} & \overbrace{\omega_j \psi_j}^{N-n_{\text{rig}} \text{ columns}} \\ \vdots & \vdots \end{bmatrix} \right)^{-1} \underline{\dot{q}}_0 \quad (5.4.83)$$

EXAMPLE 5.4.1 Platform Bracing Mishap Vibration

Statement: A vertical brace is installed at the left end of a platform raising it slightly as shown in Figure E5.4.1(a). The brace accidentally snaps and falls away causing the platform and its attached piping to vibrate due to the initial displacement distribution shown in Figure E5.4.1(b). A stress simulation of the piping is required as part of a plant safety review of the mishap. The initial condition response of the platform is a necessary step in the piping stress simulation.

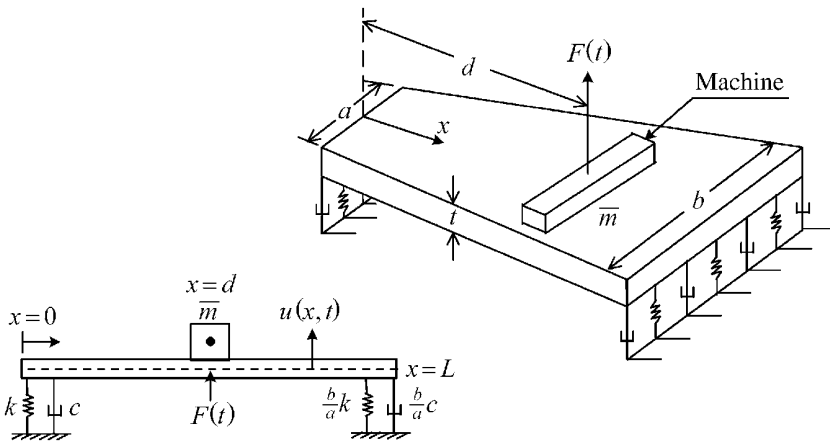


Figure E5.4.1(a) Planar vibration model of platform mounted machine



Figure E5.4.1(b) Initial deflection of the platform relative to its static equilibrium (Sag) state

The physical parameter values for the platform are

$$\begin{aligned}
 a &= 4\text{m}, \quad b = 6\text{m}, \quad t = 0.25\text{m}, \quad L = 20\text{m}, \quad \rho = 4000 \text{ kg/m}^3, \\
 \bar{m} &= 1 \times 10^4 \text{ kg}, \quad E = 1 \times 10^{11} \text{ N/m}^2, \quad k = 2 \times 10^7 \text{ N/m}, \quad d = 12\text{m}, \\
 \alpha_1 &= \frac{(b-a)t}{L} = 0.025 \text{ m}, \quad \alpha_2 = at = 1 \text{ m}^2, \\
 \alpha_3 &= \frac{(b-a)t^3}{12L} = 1.3 \times 10^{-4} \text{ m}^3, \quad \alpha_4 = \frac{at^3}{12} = 5.21 \times 10^{-3} \text{ m}^3
 \end{aligned} \tag{1}$$

Objective: Solve for the initial condition response of the platform using Equations(5.4.78) and (5.4.79) and the six generalized coordinates model in Example 4.6.4 and compare the results to a direct integration solution of the equilibrium Equation (5.4.2):

$$\underline{M}\ddot{\underline{q}} + \underline{K}\underline{q} = \underline{0} \tag{2}$$

Assumptions: Same as in Example 4.6.4.

Solution:

(a) Recall from Equation (4) of Example 4.6.4 that the six shape functions for this model are

$$\begin{aligned}
 \phi_1(x) &= 1, \quad \phi_2(x) = \frac{x}{L}, \quad \phi_3(x) = \sin\left(\frac{\pi x}{L}\right), \quad \phi_4(x) = \sin\left(\frac{2\pi x}{L}\right), \\
 \phi_5(x) &= \sin\left(\frac{3\pi x}{L}\right), \quad \phi_6(x) = \sin\left(\frac{4\pi x}{L}\right)
 \end{aligned} \tag{3}$$

The physical deflection of the platform is approximated by Equation (3) of Example 4.6.4 as

$$u(x,t) = \sum_{l=1}^6 q_l(t)\phi_l(x) \tag{4}$$

Figure E5.4.1(b) shows that at $t=0$

$$u(x,0) = 0.1 \left(1 - \frac{x}{L}\right) \text{ m} = \sum_{l=1}^6 q_l(0)\phi_l(x) = 0.1\phi_1 - 0.1\phi_2 + 0\phi_3 + 0\phi_4 + 0\phi_5 + 0\phi_6 \tag{5}$$

Therefore, the ICs for this example are

$$\begin{aligned}
 \underline{q}_0 &= (q_{10} \quad q_{20} \quad q_{30} \quad q_{40} \quad q_{50} \quad q_{60})^T = (0.1 \quad -0.1 \quad 0 \quad 0 \quad 0 \quad 0)^T \\
 \underline{\dot{q}}_0 &= \underline{0} \quad 6 \times 1
 \end{aligned} \tag{6}$$

- (b) The mass matrix for this model is obtained from Equation (38) of Example 4.6.4, which for the parameters given above becomes

$$\begin{aligned}
 \underline{M} &= \underline{M}_p + \underline{M}_m \\
 &= \alpha_1 L^2 \rho \begin{bmatrix} 0.5 & 0.3333 & 0.3183 & -0.1592 & 0.1061 & -0.0796 \\ & 0.2500 & 0.1893 & -0.1592 & 0.1013 & -0.0796 \\ & & 0.2500 & -0.0901 & 0 & -0.0072 \\ & \text{symmetric} & & 0.2500 & -0.0973 & 0 \\ & & & & 0.2500 & -0.0993 \\ & & & & & 0.2500 \end{bmatrix} \\
 &+ \alpha_2 L \rho \begin{bmatrix} 1 & 0.500 & 0.6366 & 0 & 0.2122 & 0 \\ & 0.3333 & 0.3183 & -0.1592 & 0.1061 & -0.0796 \\ & & 0.500 & 0 & 0 & 0 \\ & \text{symmetric} & & 0.500 & 0 & 0 \\ & & & & 0.5000 & 0 \\ & & & & & 0.5000 \end{bmatrix} \\
 &+ \bar{m} \begin{bmatrix} \phi_1\phi_1 & \phi_1\phi_2 & \phi_1\phi_3 & \phi_1\phi_4 & \phi_1\phi_5 & \phi_1\phi_6 \\ & \phi_2\phi_2 & \phi_2\phi_3 & \phi_2\phi_4 & \phi_2\phi_5 & \phi_2\phi_6 \\ & & \phi_3\phi_3 & \phi_3\phi_4 & \phi_3\phi_5 & \phi_3\phi_6 \\ & & & \phi_4\phi_4 & \phi_4\phi_5 & \phi_4\phi_6 \\ & \text{symmetric} & & & \phi_5\phi_5 & \phi_5\phi_6 \\ & & & & & \phi_6\phi_6 \end{bmatrix} \Big|_{x=d} \\
 &= \begin{bmatrix} 110000.0 & 59333.3 & 73172.5 & -12244.1 & 15342.8 & 6327.5 \\ & 40267.0 & 38743.0 & -22625.0 & 9015.0 & -3843.0 \\ & & 59045.0 & -9193.0 & -5590.0 & 8757.0 \\ & & & 53455.0 & -436.0 & -5590.0 \\ & \text{symmetric} & & & 53455.0 & -9560.0 \\ & & & & & 59045.0 \end{bmatrix}
 \end{aligned} \tag{7}$$

in units of kg. The system stiffness matrix is obtained from Equation (41) of Example 4.6.4 as

$$K = \underline{K}_s \Big|_{x=0} + \frac{b}{a} \underline{K}_s \Big|_{x=L} + \underline{K}_B \tag{8}$$

where

$$\begin{aligned}
 \underline{K}_s &= k \begin{bmatrix} \phi_1\phi_1 & \phi_1\phi_2 & \phi_1\phi_3 & \phi_1\phi_4 & \phi_1\phi_5 & \phi_1\phi_6 \\ & \phi_2\phi_2 & \phi_2\phi_3 & \phi_2\phi_4 & \phi_2\phi_5 & \phi_2\phi_6 \\ & & \phi_3\phi_3 & \phi_3\phi_4 & \phi_3\phi_5 & \phi_3\phi_6 \\ & & & \phi_4\phi_4 & \phi_4\phi_5 & \phi_4\phi_6 \\ & \text{symmetric} & & & \phi_5\phi_5 & \phi_5\phi_6 \\ & & & & & \phi_6\phi_6 \end{bmatrix} \\
 \underline{K}_B &= \alpha_3 \frac{E}{L^2} \begin{bmatrix} 0 & 0 & 0 & 0 & 0 \\ 0 & 0 & 0 & 0 & 0 \\ & 24.4 & -35.1 & 0 & -11.2 \\ & & 389.6 & -341 & 0 \\ & \text{symmetric} & & 1972 & -1392 \\ & & & & 6234 \end{bmatrix} + \alpha_4 \frac{E}{L^3} \begin{bmatrix} 0 & 0 & 0 & 0 & 0 \\ 0 & 0 & 0 & 0 & 0 \\ & 48.7 & 0 & 0 & 0 \\ & & 779.3 & 0 & 0 \\ & \text{symmetric} & & 3945 & 0 \\ & & & & 12468 \end{bmatrix} \tag{9}
 \end{aligned}$$

Therefore

$$\underline{K} = 10^8 * \begin{bmatrix} 0.5 & 0.3 & 0 & 0 & 0 & 0 \\ & 0.3 & 0 & 0 & 0 & 0 \\ & & 0.0396 & -0.01142 & 0 & -0.00366 \\ & & & 0.6342 & -0.111 & 0 \\ \text{symmetric} & & & & 3.21 & -0.4532 \\ & & & & & 10.15 \end{bmatrix} \quad (10)$$

in units of N/m. The undamped natural frequencies of the model are obtained from (5.4.66), that is, $\underline{A}\underline{X} = \alpha\underline{X}$, since \underline{M}^{-1} exists

$$\underline{X}_j = \underline{\psi}_j, \quad \underline{A} = \underline{M}^{-1}\underline{K}, \quad \alpha_j = \omega_j^2, \quad \omega_j = \sqrt{\alpha_j}, \quad f_j = \frac{\omega_j}{2\pi}$$

The MATLAB commands for obtaining the eigenvalues α_j and eigenvectors \underline{X}_j are explained below:

```
>> help eig
EIG Eigenvalues and eigenvectors.
[V,D] = EIG(A) produces a diagonal matrix D of generalized eigenvalues ( $\alpha_j$ )
and a full matrix V whose columns are the corresponding eigenvectors
( $\underline{X}_j$ ) so that  $A*V = V*D$ 
```

The results are

$$f = \frac{\omega}{2\pi} = (1.23 \ 4.34 \ 7.56 \ 11.54 \ 19.64 \ 29.42) \text{ Hz} \quad (11)$$

with the corresponding modal matrix

$$\underline{\Psi} = \begin{bmatrix} 0.118 & 0.585 & -0.8168 & 0.582 & -0.788 & -0.554 \\ -0.030 & -1.000 & 0.037 & -1.000 & 0.049 & 1.000 \\ 1.000 & -0.004 & 1.000 & -0.137 & 1.000 & 0.043 \\ 0.009 & 0.494 & 0.017 & -0.395 & 0.009 & 0.349 \\ -0.000 & 0.019 & -0.198 & -0.005 & 0.533 & 0.054 \\ 0.001 & 0.004 & 0.004 & 0.064 & 0.005 & 0.320 \end{bmatrix} \quad (12)$$

The orthogonality check of (5.4.75) yields

$$\begin{aligned} \underline{\Psi}^T \underline{M} \underline{\Psi} &= \underline{\text{Diag}}(\tilde{m}_i) \\ &= \underline{\text{Diag}}(75036 \ 36919 \ 21416 \ 4946 \ 8141 \ 3588) \end{aligned} \quad (13)$$

and that of (5.4.77) yields

$$\begin{aligned} \underline{\Psi}^T \underline{K} \underline{\Psi} &= \underline{\text{Diag}}(\tilde{m}_i \omega_i^2) \\ &= 10^8 \underline{\text{diag}}(0.0446 \ 0.275 \ 0.482 \ 0.26 \ 1.24 \ 1.23) \end{aligned} \quad (14)$$

Recall from (5.4.78) that the generalized coordinate response is given by

$$\underline{q}(t) = \sum_{j=1}^6 (\alpha_{jc} \cos \omega_j t + \alpha_{js} \sin \omega_j t) \underline{\psi}_j \quad (15)$$

and from (4) the actual vertical displacement vibration response is given by

$$u(x, t) = \sum_{l=1}^6 q_l(t) \phi_l(x) = \underline{\Phi}^T \underline{q} \quad (16)$$

where

$$\underline{\Phi} = \begin{Bmatrix} \phi_1 \\ \phi_2 \\ \phi_3 \\ \phi_4 \\ \phi_5 \\ \phi_6 \end{Bmatrix} = \begin{Bmatrix} 1 \\ x/L \\ \sin(\pi x/L) \\ \sin(2\pi x/L) \\ \sin(3\pi x/L) \\ \sin(4\pi x/L) \end{Bmatrix} \quad (17)$$

and

$$\underline{q}^T = (q_1 \quad q_2 \quad q_3 \quad q_4 \quad q_5 \quad q_6)$$

Combining these equations yields

$$u(x, t) = \sum_{j=1}^6 (\alpha_{jc} \cos \omega_j t + \alpha_{js} \sin \omega_j t) u_j(x) \quad (18)$$

where

$$u_j(x) = \underline{\Phi}^T \underline{\psi}_j = \sum_{i=1}^6 \phi_i(x) \psi_{ij} \quad (19)$$

Note the $u_j(x)$ are the mode shapes for the actual vertical displacement distribution, whereas the $\underline{\psi}_j$ are the mode shapes for the generalized coordinates. For example, from the third column of $\underline{\Psi}$ in (12) and from (17) and (19),

$$\begin{aligned} u_3(x) &= \psi_{13} \phi_1(x) + \psi_{23} \phi_2(x) + \psi_{33} \phi_3(x) + \psi_{43} \phi_4(x) + \psi_{53} \phi_5(x) + \psi_{63} \phi_6(x) \\ &= -0.8168 * 1 + 0.037 * \frac{x}{L} + 1 * \sin\left(\frac{\pi x}{L}\right) + 0.017 * \sin\left(\frac{2\pi x}{L}\right) \\ &\quad - 0.198 * \sin\left(\frac{3\pi x}{L}\right) + 0.004 * \sin\left(\frac{4\pi x}{L}\right) \end{aligned} \quad (20)$$

The actual vertical displacement mode shapes $u_j(x)$ are shown in Figure E5.4.1(c).

The initial conditions (6) on the generalized coordinates are substituted into (5.4.79) to obtain $\underline{\alpha}_c = \underline{0}$ and

$$\underline{\alpha}_c = \underline{\text{Diag}}(\tilde{m}_i^{-1}) \underline{\Psi}^T \underline{M} \underline{q}_0 \quad (21)$$

where \underline{q}_0 is defined in (6) and $\underline{\text{Diag}}(\tilde{m}_i^{-1})$ is defined in (13). This yields

$$\underline{\alpha}_c = (0.0533 \quad 0.0426 \quad -0.0338 \quad 0.0448 \quad -0.0127 \quad -0.0091)^T \quad (22)$$

Then, from (18) and (21),

$$u(x, t) = \sum_{j=1}^6 \alpha_{jc} \cos(\omega_j t) u_j(x) \quad (23)$$

The responses $u(x=0, t)$, $u(x=d, t)$, and $u(x=L, t)$ are shown in Figure E5.4.1(d).

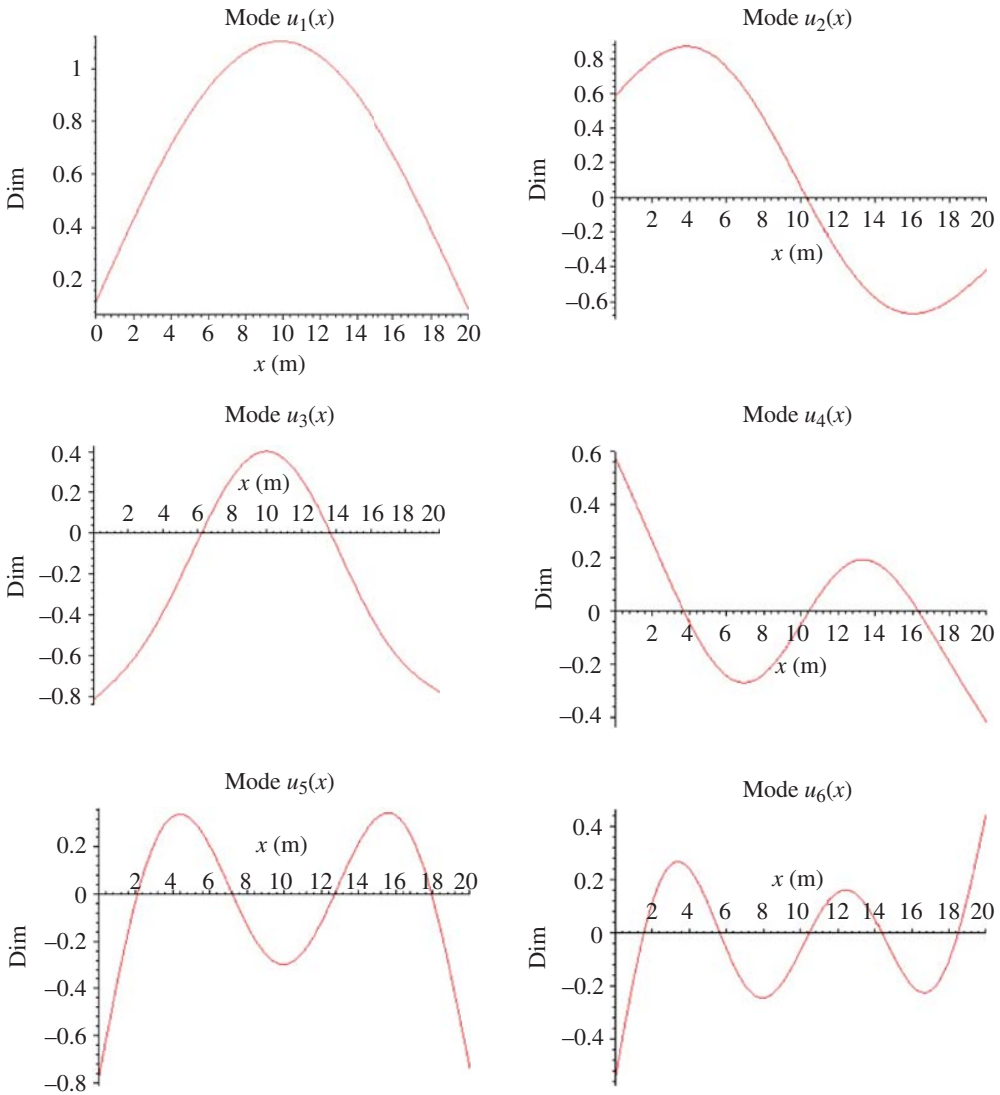


Figure E5.4.1(c) Vertical displacement modes shapes $u_i(x)$ for the platform system

This approach to obtain the initial condition response does not require analytical or numerical integration and only requires evaluation of (23) for selected x and t . This is a benefit of the orthogonality properties (5.4.73) and (5.4.76). Alternatively, the response of the platform may also be determined by direct numerical integration of the EOMs (5.4.2) written in the first-order (state) form

$$\dot{\underline{v}} = -\underline{M}^{-1}\underline{K}\underline{q} \quad (6 \times 1), \quad \dot{\underline{q}} = \underline{v} \quad (6 \times 1) \quad (24)$$

where \underline{M} and \underline{K} are defined in (7) and (10) and with the initial conditions defined in (6). The numerical integration solution of the above initial value problem is similar to Example 2.3.1 and yields the time histories of the generalized coordinates. The response of the physical coordinates $u(x, t)$ is then obtained from the selected shape functions $\phi_i(x)$ and (16). The results of the direct numerical integration solution (Figure E5.4.1(e)) are the same as the modal solution results (Figure E5.4.1(d)).

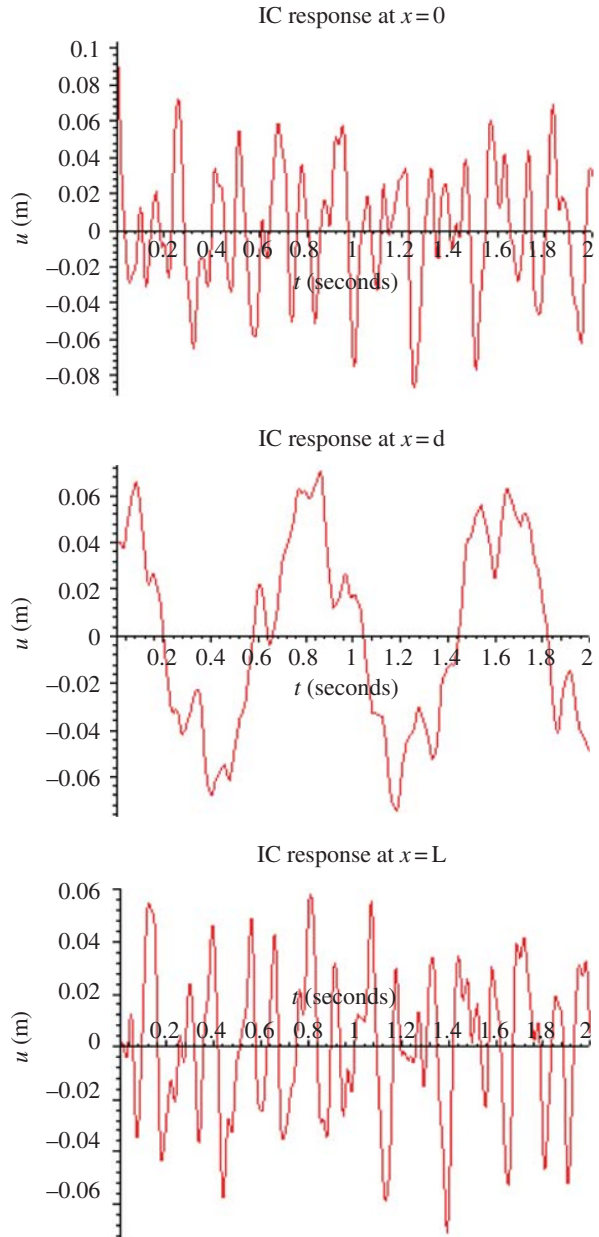


Figure E5.4.1(d) Vertical displacement responses at $x=0$, d , and L

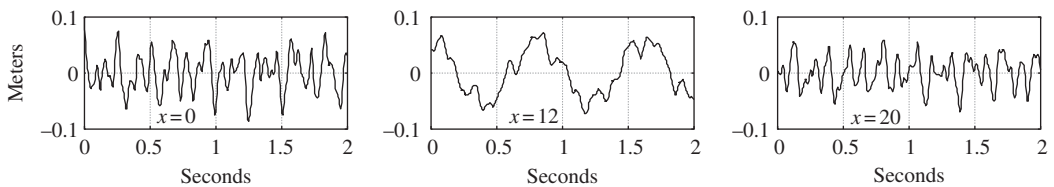


Figure E5.4.1(e) Displacements from direct integration of Equation (24)

EXAMPLE 5.4.2 *Truss Tower with Rigid Section Model*

Description: Figure 4.8.15 and the accompanying analysis treated the modeling of a rigid component in a flexible structure. This example models a 35-node truss tower with an embedded rigid plate. The plate might represent an idealized model of a section of the tower with auxiliary equipment that is attached to the tower by a heavy plate. This entire assembly is then modeled as a single rigid body attached to the tower at certain truss members. To simplify the example, the plate’s center of mass G_p is located at the center of the plate. The truss member elements E , A , and ρ and the plate’s mass m_p and inertia I_{G_p} are shown in Figure E5.4.2(a). The rigid body mass m_{rig} and $I_{G_{rig}}$ are equal to the corresponding plate terms plus the contributions of the elements that lie entirely on the plate (49, 50, 54, 55, 62, and 63); thus

$$m_{rig} = 4000\text{kg}, \quad I_{G_{rig}} = 58133\text{kg}\cdot\text{m}^2$$

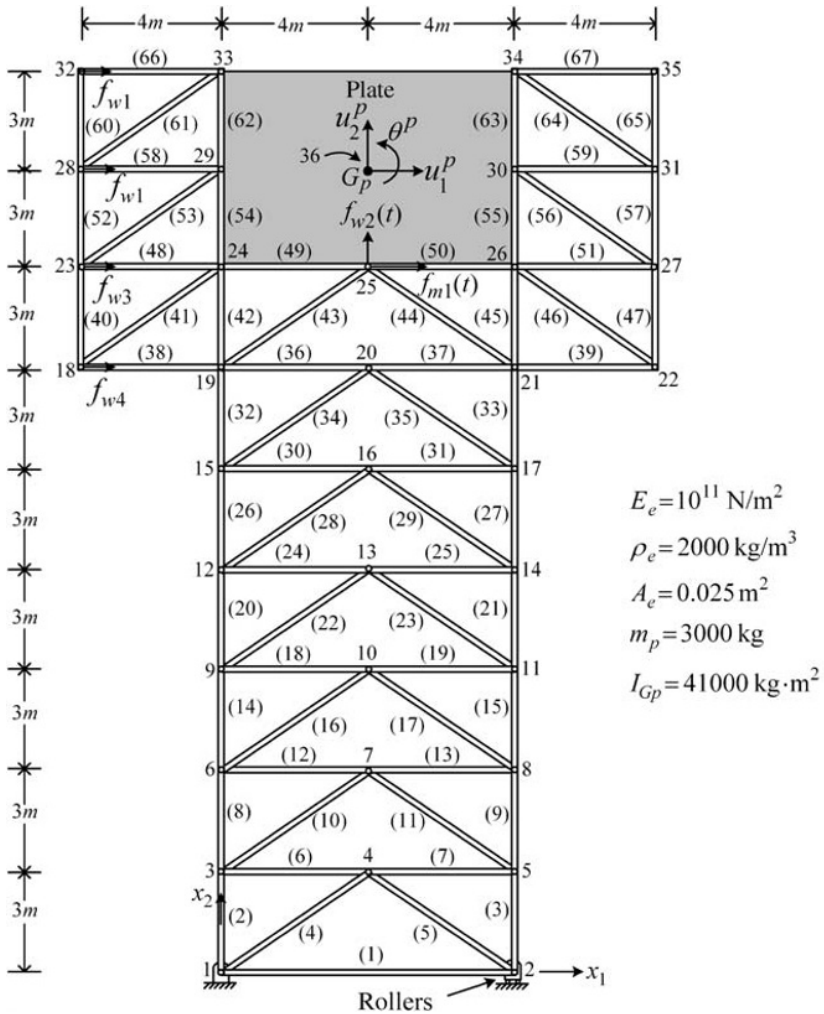


Figure E5.4.2(a) Truss tower with rigid plate

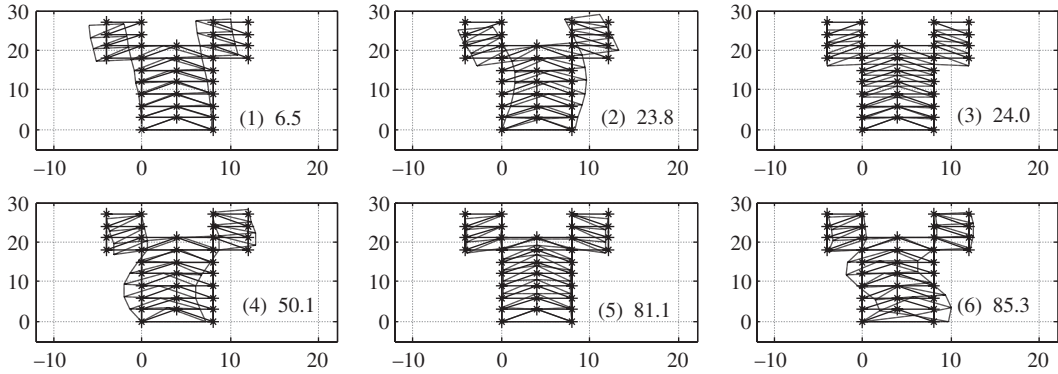


Figure E5.4.2(b) Mode shapes 1–6 and natural frequencies (Hz) for the truss tower example

Objective: Determine the six lowest natural frequencies and mode shapes for the truss tower.

Solution: Utilize (4.8.142) to form the element stiffness and mass element matrices for all elements with a local node 2 attached to the rigid plate, that is, elements 41, 42, 43, 44, 45, 46, 48, 51, 53, 56, 58, 59, 61, 64, 66, and 67. The results are shown in Figure E5.4.2(b).

5.4.8 Undamped, Nongyroscopic, and Noncirculatory Systems—Response to an IC Modal Displacement Distribution

From Equation (5.4.47), it is seen

$$\underline{q}_0 = \sum_{j=1}^N \alpha_{jc} \underline{\psi}_j \quad (5.4.84)$$

If the structure is given the initial displacement

$$\underline{q}_0 = \gamma \underline{\psi}_k \quad (5.4.85)$$

(5.4.85) becomes

$$\gamma \underline{\psi}_k = \sum_{j=1}^N \alpha_{jc} \underline{\psi}_j \quad (5.4.86)$$

Premultiplication by $\underline{\psi}_l^T \underline{M}$ and use of the orthogonality condition (5.4.37) yield

$$\gamma \delta_{kl} \tilde{m}_k = \sum_{j=1}^N \alpha_{jc} \delta_{lj} \tilde{m}_l = \alpha_{lc} \tilde{m}_l \Rightarrow \alpha_{lc} = \begin{cases} 0, & l \neq k \\ \gamma, & l = k \end{cases} \quad (5.4.87)$$

where δ is the Kronecker delta. Therefore, from (5.4.47) and (5.4.48),

$$\text{If } \dot{\underline{q}}_0 = \underline{0} \text{ and } \underline{q}_0 = \gamma \underline{\psi}_k \text{ then } \underline{q}(t) = \gamma \cos(\omega_k t) \underline{\psi}_k \quad (5.4.88)$$

This shows that if the structure is released from rest, with initial displacements $\gamma \underline{\psi}_k$, it will vibrate with the single frequency ω_k and in the single mode $\underline{\psi}_k$ for all ensuing time.

5.4.9 Orthogonally Damped, Nongyroscopic, and Noncirculatory Systems—Description

Suppose that a multi-dof structure is initially deflected into the pattern of its i th mode shape, released from rest

$$\underline{q}_0 = \gamma \underline{\psi}_i, \quad \dot{\underline{q}}_0 = \underline{0} \quad (5.4.89)$$

and that its ensuing response at any dof had the same general form as a SDOF system (Eq. 5.2.30). This implies that all dof respond with a single frequency ω_{di} , where

$$\omega_{di} = \omega_i \sqrt{1 - \xi_i^2} \quad (5.4.90)$$

and with a general damped time history of the form

$$\underline{q}(t) = \frac{\gamma}{\sqrt{1 - \xi_i^2}} \underline{\psi}_i e^{-\xi_i \omega_i t} \cos(\omega_{di} t - \angle \chi_i) \quad (5.4.91)$$

This behavior is quite common for nonrotating, lightly damped structures or structural components, that is, towers, frames, wings, bridges, and so on. Here, we seek the form of the damping matrix \underline{C}_0 that will produce this response behavior. As will be demonstrated, the requirement is that \underline{C}_0 satisfies the additional orthogonality condition

$$\underline{\Psi}^T \underline{C}_0 \underline{\Psi} = \underline{\text{Diag}}(\tilde{c}_i) \quad (5.4.92)$$

or in scalar form

$$\underline{\psi}_i^T \underline{C}_0 \underline{\psi}_k = \tilde{c}_i \delta_{ik} \quad (5.4.93)$$

The proof begins with the equilibrium condition

$$\underline{M}\ddot{\underline{q}} + \underline{C}_0\dot{\underline{q}} + \underline{K}\underline{q} = \underline{0} \quad (5.4.94)$$

Substitute the change in basis vectors (Section 2.6)

$$\underline{q} = \underline{\Psi}\underline{\chi} \quad (5.4.95)$$

premultiply by $\underline{\Psi}^T$, and utilize the orthogonality conditions (5.4.75), (5.4.77), and (5.4.92) to obtain

$$\underline{\text{Diag}}(\tilde{m}_i)\ddot{\underline{\chi}} + \underline{\text{Diag}}(\tilde{c}_i)\dot{\underline{\chi}} + \underline{\text{Diag}}(\tilde{m}_i\omega_i^2)\underline{\chi} = \underline{0} \quad (5.4.96)$$

Equation (5.4.96) is a set of N -uncoupled second-order DE

$$\tilde{m}_i\ddot{\chi}_i + \tilde{c}_i\dot{\chi}_i + \tilde{k}_i\chi_i = 0 \quad (5.4.97)$$

where from (5.4.77)

$$\tilde{k}_i = \tilde{m}_i\omega_i^2 \quad (5.4.98)$$

Equation (5.4.97) has a form identical with (5.2.1), so its solution is given by (5.2.30)

$$\chi_i(t) = e^{-\xi_i \omega_i t} |\chi_i| \cos(\omega_{di} t - \angle \chi_i) \quad (5.4.99)$$

where from (5.2.12) and (5.2.31)

$$\xi_i = \frac{\tilde{c}_i}{2\tilde{m}_i\omega_i} \Rightarrow \tilde{c}_i = 2\tilde{m}_i\omega_i\xi_i \quad (5.4.100)$$

$$|\chi_i| = \sqrt{\chi_i^2(0) + \left(\frac{\dot{\chi}_i(0) + \xi_i \omega_i \chi_i(0)}{\omega_{di}}\right)^2}, \quad \angle \chi_i = \tan^{-1} \left(\frac{\dot{\chi}_i(0) + \xi_i \omega_i \chi_i(0)}{\chi_i(0) \omega_{di}} \right) \quad (5.4.101)$$

Substitute the ICs from (5.4.89) into the transformation (5.4.95) and use the orthogonality condition (5.4.75) to obtain

$$\dot{\underline{\chi}}(0) = \underline{\Psi}^{-1} \dot{\underline{q}}(0) = \underline{0} \quad (5.4.102)$$

$$\underline{\Psi}^T \underline{M} \underline{q}_0 = \underline{\Psi}^T \underline{M} (\gamma \underline{\psi}_i) = \underline{\Psi}^T \underline{M} \underline{\Psi} \underline{\chi}(0) \Rightarrow \underline{\text{Diag}}(\tilde{m}_i) \underline{\chi}(0) = \gamma \left\{ \begin{array}{c} 0 \\ 0 \\ \vdots \\ \tilde{m}_i \\ \vdots \\ 0 \end{array} \right\} \leftarrow i\text{th row}$$

$$\Rightarrow \chi_j(0) = \begin{cases} 0, & j \neq i \\ \gamma, & j = i \end{cases} \quad (5.4.103)$$

Substituting (5.4.102) and (5.4.103) into (5.4.95) and substituting these results into (5.4.99)–(5.4.101) yields,

$$\underline{q}(t) = \chi_i(t) \underline{\psi}_i \quad (5.4.104)$$

where

$$\chi_i(t) = \frac{\gamma}{\sqrt{1 - \xi_i^2}} e^{-\xi_i \omega_i t} \cos(\omega_{di} t - \angle \chi_i) \quad (5.4.105)$$

This is identical to (5.4.91) which shows that if the undamped system eigenvectors are orthogonal with respect to \underline{C}_0 , that is, (5.4.92), (5.4.93) holds, and the system is released from rest in the form of the i th mode shape (5.4.89), and the resulting response at all dofs in the structure will have the same form as an SDOF system response (5.2.30), with the same frequency and damping ratio:

$$\xi_i = \frac{\tilde{c}_i}{2\tilde{m}_i \omega_i} \quad (5.4.106)$$

5.4.10 Orthogonally Damped, Nongyroscopic, and Noncirculatory Systems—Eigenvalues and Eigenvectors

The eigenvalues of this system type are readily obtained by substituting

$$\underline{q} = e^{\lambda t} \underline{\Delta} \quad (5.4.107)$$

into (5.4.94), yielding

$$(\lambda^2 \underline{M} + \lambda \underline{C}_0 + \underline{K}) \underline{\Delta} = \underline{0} \quad (5.4.108)$$

Let

$$\underline{\Delta} = \underline{\Psi} \underline{\Gamma} \quad (5.4.109)$$

where $\underline{\Psi}$ is the modal matrix containing the undamped system eigenvectors (modes) arranged as columns. Substitute (5.4.109) into (5.4.108), premultiply the result by $\underline{\Psi}^T$, and utilize the orthogonality conditions (5.4.75), (5.4.77), and (5.4.92) to obtain

$$\underline{\text{Diag}}\left(\lambda^2\tilde{m}_i + \lambda\tilde{c}_i + \tilde{k}_i\right)\underline{\Gamma} = \underline{0} \quad (5.4.110)$$

The determinant of the coefficient matrix must be zero, or $\underline{\Gamma}, \underline{\Delta}$ (5.4.109), and \underline{q} (5.4.107) will be zero for all time t , that is, no vibration. Therefore, the determinant is

$$\prod_{i=1}^N \left(\lambda^2\tilde{m}_i + \lambda\tilde{c}_i + \tilde{k}_i\right) = 0 \quad (5.4.111)$$

which has the roots

$$\lambda_j = \frac{-\tilde{c}_j}{2\tilde{m}_j} \pm i\sqrt{\frac{\tilde{k}_j}{\tilde{m}_j} - \left(\frac{\tilde{c}_j}{2\tilde{m}_j}\right)^2}$$

which simplifies utilizing (5.4.98) and (5.4.100) to

$$\lambda_j = -\xi_j\omega_j \pm i\omega_j\sqrt{1-\xi_j^2} \quad (5.4.112)$$

This form is identical to the SDOF case (5.2.14), except in the multi-dof case where there are N eigenvalues instead of only one. Consider (5.4.110) for $\lambda = \lambda_i$, in which case the i th term on the diagonal is zero and the other diagonal terms are nonzero. This indicates that

$$\Gamma_j = \begin{cases} 0, & j \neq i \\ 1, & j = i \end{cases} \quad (5.4.113)$$

or by (5.4.109) and (5.4.113)

$$\underline{\Delta}_i = \underline{\psi}_i \quad (5.4.114)$$

This shows that the eigenvectors (mode shapes) of the orthogonally damped system are identical to those of the undamped system.

5.4.11 Orthogonally Damped, Nongyroscopic, and Noncirculatory Systems—IC Response

The response of this system type to zero initial velocities and a modal distribution of initial displacements was given by (5.4.104) and (5.4.105). The response to general initial conditions is given by the linear superposition of all possible solutions of the form (5.4.107). Utilizing (5.4.114) with (5.4.107) yields

$$\underline{q}(t) = \text{Real} \left(\sum_{k=1}^N \beta_k e^{\lambda_k t} \underline{\psi}_k + \beta_{kc} e^{\bar{\lambda}_k t} \bar{\underline{\psi}}_k \right) \quad (5.4.115)$$

where $\underline{\psi}_k$ are the real eigenvectors of the undamped system so that $\underline{\bar{\psi}}_k = \underline{\psi}_k$. Substitution of (5.4.112) yields

$$\begin{aligned} \underline{q}(t) &= \text{Real} \left(\sum_{k=1}^N e^{-\xi_k \omega_k t} (\beta_k e^{i\omega_{dk} t} + \beta_{kc} e^{-i\omega_{dk} t}) \underline{\psi}_k \right) \\ &= \sum_{k=1}^N e^{-\xi_k \omega_k t} (\beta_{kR} \cos \omega_{dk} t - \beta_{kI} \sin \omega_{dk} t + \beta_{kcR} \cos \omega_{dk} t + \beta_{kcI} \sin \omega_{dk} t) \underline{\psi}_k \end{aligned}$$

Since the β are arbitrary real constants, $\underline{q}(t)$ may be written as

$$\underline{q}(t) = \sum_{k=1}^N e^{-\xi_k \omega_k t} (\alpha_{kc} \cos \omega_{dk} t + \alpha_{ks} \sin \omega_{dk} t) \underline{\psi}_k \quad (5.4.116)$$

where the α are arbitrary real constants determined by the initial conditions. From (5.4.116) at $t=0$,

$$\underline{q}(0) = \underline{q}_0 = \sum_{k=1}^N \alpha_{kc} \underline{\psi}_k, \quad \dot{\underline{q}}(0) = \dot{\underline{q}}_0 = \sum_{k=1}^N (\omega_{dk} \alpha_{ks} - \xi_k \omega_k \alpha_{kc}) \underline{\psi}_k \quad (5.4.117)$$

To solve for the α_{kc} and α_{ks} , multiply (5.4.117) by $\underline{\psi}_l^T \underline{M}$ and use the orthogonality relation (5.4.72) to obtain

$$\alpha_{lc} = \frac{1}{\tilde{m}_l} \underline{\psi}_l^T \underline{M} \underline{q}_0 \quad (5.4.118)$$

$$\underline{\psi}_l^T \underline{M} \dot{\underline{q}}_0 = \omega_{dl} \alpha_{ls} \tilde{m}_l - \xi_l \omega_l \alpha_{lc} \tilde{m}_l \Rightarrow \alpha_{ls} = \frac{\underline{\psi}_l^T \underline{M} (\dot{\underline{q}}_0 + \xi_l \omega_l \underline{q}_0)}{\omega_{dl} \tilde{m}_l} \quad (5.4.119)$$

5.4.12 Orthogonally Damped, Nongyroscopic, and Noncirculatory Systems—Determination of \underline{C}_0

This model type is commonly used when modeling structures and structural components which do not involve very strong, localized sources of damping such as fluid film bearings and liquid or gas seals in rotating machinery, and dampers, isolators, snubbers, absorbers, and dashpots in machinery, mechanism, and structural system models. These strong sources of localized damping can also be combined with the \underline{C}_0 matrix to represent the total system damping.

Methods 1–4 below demonstrate how to form an “orthogonal damping matrix” \underline{C}_0 given some lower natural frequencies and their respective damping ratios ξ_i from measurement or estimation. The orthogonal damping matrix \underline{C}_0 is required for simulations where a modal equation solution (5.4.116) is impractical or invalid and a direct numerical integration (Section 2.3) of the EOMs is utilized. This may be the case when a lightly damped structural system or component that is accurately modeled with \underline{C}_0 is modified to include concentrated damping, circulatory, gyroscopic, or nonlinear terms. Examples of this include a shaft supported by oil film or magnetic bearings or a nuclear power plant piping system with shock absorbers (dampers). The matrix \underline{C}_0 accounts for the light structural damping internal to the structure which may be very important for dampening high-frequency modes in actively controlled vehicles, structures, or machines. *Method 5* yields approximate damping ratios ξ_i given the model’s damping matrix \underline{C} . This is useful for converting the actual model into

a simplified, but approximate, orthogonal damping model for ease of solution. Caution should be exercised in employing this method due to the possibility of significant inaccuracy in certain applications.

5.4.12.1 Method 1

The matrix \underline{C}_0 will automatically satisfy (5.4.92) for certain definitions of \underline{C}_0 . For example, if \underline{C}_0 has the form

$$\underline{C}_0 = \mu_m \underline{M} + \mu_k \underline{K} \quad (5.4.120)$$

for arbitrary real constants μ_m and μ_k , it follows from (5.4.75), (5.4.77), and (5.4.100) that

$$\begin{aligned} \underline{\Psi}^T \underline{C}_0 \underline{\Psi} &= \mu_m \underline{\Psi}^T \underline{M} \underline{\Psi} + \mu_k \underline{\Psi}^T \underline{K} \underline{\Psi} = \underline{\text{Diag}}(\tilde{m}_i(\mu_m + \mu_k \omega_i^2)) \\ &= \underline{\text{Diag}}(\tilde{c}_i) = \underline{\text{Diag}}(2\tilde{m}_i \omega_i \xi_i) \end{aligned} \quad (5.4.121)$$

Thus, if \underline{C}_0 is proportional to a linear combination of \underline{M} and \underline{K} , it automatically satisfies the orthogonality condition (5.4.92), and its corresponding damping ratios are given by

$$\xi_i = \frac{\mu_m}{2\omega_i} + \frac{\mu_k}{2} \omega_i \quad (5.4.122)$$

Equation (5.4.120) is the reason that \underline{C}_0 is referred to as a “proportional damping” matrix or “Rayleigh damping” after its discoverer John William Strutt (Baron Rayleigh). The constants μ_m and μ_k may be determined if two natural frequencies ω_i and ω_j and their corresponding damping ratios ξ_i and ξ_j have been measured, that is, (by (5.4.122))

$$\begin{Bmatrix} \xi_i \\ \xi_j \end{Bmatrix} = \begin{bmatrix} \frac{1}{2\omega_i} & \frac{\omega_i}{2} \\ \frac{1}{2\omega_j} & \frac{\omega_j}{2} \end{bmatrix} \begin{Bmatrix} \mu_m \\ \mu_k \end{Bmatrix} \Rightarrow \mu_m = \frac{\left(\xi_i \frac{\omega_j}{2} - \xi_j \frac{\omega_i}{2}\right)}{\Delta}, \quad \mu_k = \frac{\left(\frac{\xi_j}{2\omega_i} - \frac{\xi_i}{2\omega_j}\right)}{\Delta} \quad (5.4.123)$$

where

$$\Delta = \frac{\omega_j^2 - \omega_i^2}{4\omega_i \omega_j}$$

The damping ratios ξ_l of the other modes in the model are constrained to satisfy

$$\xi_l = \frac{\mu_m}{2\omega_l} + \frac{\mu_k}{2} \omega_l \quad (5.4.124)$$

with μ_m and μ_k determined from (5.4.123) for modes i and j , which may yield results conflicting with the experimentally measured ξ_l for $l \neq i$. Commercially available finite elements software for vibration simulation such as ANSYS and NASTRAN have options to enter the constants μ_m and μ_k .

5.4.12.2 Method 2

A \underline{C}_0 matrix that can reproduce more than two measured damping ratios may be obtained by including more terms in the relation (5.4.120) as presented in Clough and Penzien (1975) or Craig (1981). Recall that the undamped modes satisfy (5.4.30)

$$-\omega_i^2 \underline{M} \underline{\psi}_i + \underline{K} \underline{\psi}_i = \underline{0} \quad (5.4.125)$$

Premultiply this equation by $\underline{\psi}_j^T \underline{K} \underline{M}^{-1}$ and use the orthogonality relation (5.4.45) to obtain

$$-\omega_i^2 \delta_{ij} \tilde{m}_i \omega_i^2 + \underline{\psi}_j^T \underline{K} \underline{M}^{-1} \underline{K} \underline{\psi}_i = 0 \Rightarrow \underline{\psi}_j^T (\underline{K} \underline{M}^{-1} \underline{K}) \underline{\psi}_i = \begin{cases} 0, & i \neq j \\ \tilde{m}_i \omega_i^4, & i = j \end{cases} \quad (5.4.126)$$

Next, premultiply (5.4.125) by $\underline{\psi}_j^T (\underline{K} \underline{M}^{-1}) (\underline{K} \underline{M}^{-1})$ and utilize (5.4.126) to obtain

$$\underline{\psi}_j^T (\underline{K} \underline{M}^{-1})^2 \underline{K} \underline{\psi}_i = \omega_i^2 \delta_{ij} \tilde{m}_i \omega_i^4 \quad (5.4.127)$$

where the Kronecker delta δ_{ij} equals 0 for $i \neq j$ and 1 for $i = j$. Continuation of this process yields the first extended orthogonality relation

$$\underline{\psi}_j^T (\underline{K} \underline{M}^{-1})^r \underline{K} \underline{\psi}_i = \omega_i^{2(r+1)} \delta_{ij} \tilde{m}_i \quad r = 0, 1, 2, \dots \quad (5.4.128)$$

Note that for $r = -1$, premultiply (5.4.125) by $\underline{\psi}_j^T (\underline{K} \underline{M}^{-1})^{-1} = \underline{\psi}_j^T \underline{M} \underline{K}^{-1}$ to obtain

$$\underline{\psi}_j^T \underline{M} \underline{\psi}_i = \omega_i^2 \underline{\psi}_j^T \underline{M} \underline{K}^{-1} \underline{M} \underline{\psi}_i \quad \text{or} \quad \underline{\psi}_j^T \underline{M} \underline{K}^{-1} \underline{M} \underline{\psi}_i = \frac{\tilde{m}_i}{\omega_i^2} \delta_{ij} \quad (5.4.129)$$

For $r = -2$, premultiply (5.4.125) by

$$\underline{\psi}_j^T (\underline{K} \underline{M}^{-1})^{-2} = \underline{\psi}_j^T (\underline{K} \underline{M}^{-1})^{-1} \underline{M} \underline{K}^{-1}$$

and use (5.4.129) to obtain

$$\begin{aligned} \underline{\psi}_j^T (\underline{K} \underline{M}^{-1})^{-1} \underline{M} \underline{\psi}_i &= \omega_i^2 \underline{\psi}_j^T (\underline{K} \underline{M}^{-1})^{-1} \underline{M} \underline{K}^{-1} \underline{M} \underline{\psi}_i \\ \Rightarrow \frac{\tilde{m}_i \delta_{ij}}{\omega_i^2} &= \omega_i^2 \underline{\psi}_j^T (\underline{K} \underline{M}^{-1})^{-2} \underline{M} \underline{\psi}_i \quad \text{or} \quad \underline{\psi}_j^T (\underline{K} \underline{M}^{-1})^{-2} \underline{M} \underline{\psi}_i = \frac{\tilde{m}_i \delta_{ij}}{\omega_i^4} \end{aligned} \quad (5.4.130)$$

Continuation of this process yields the second extended orthogonality relation

$$\underline{\psi}_j^T (\underline{K} \underline{M}^{-1})^{-r} \underline{M} \underline{\psi}_i = \frac{\tilde{m}_i \delta_{ij}}{\omega_i^{2r}} \quad r = 0, 1, 2, \dots \quad (5.4.131)$$

where the Kronecker delta δ_{ij} equals 0 for $i \neq j$ and 1 for $i = j$. Thus, \underline{C}_0 may have a more general form than (5.4.120) and still satisfy the orthogonality condition (5.4.92). The more general form for \underline{C}_0 is obtained by using (5.4.128) and (5.4.131) yielding

$$\underline{C}_0 = \sum_{r=-\infty}^{+\infty} \mu_{r+1} (\underline{K} \underline{M}^{-1})^r \underline{K} \quad (5.4.132)$$

To illustrate the utility of this formula, consider a three-term ($r = -1, 0, 1$) example

$$\underline{C}_0 = \mu_1 \underline{M} + \mu_2 \underline{K} + \mu_3 \underline{K} \underline{M}^{-1} \underline{K} \quad (5.4.133)$$

Then, by (5.4.37), (5.4.45), and (5.4.128),

$$\underline{\psi}_i^T \underline{C}_0 \underline{\psi}_j = (\mu_1 \tilde{m}_i + \mu_2 \tilde{m}_i \omega_i^2 + \mu_3 \tilde{m}_i \omega_i^4) \delta_{ij} = \tilde{c}_i \delta_{ij} = 2 \tilde{m}_i \omega_i \xi_i \delta_{ij} \quad (5.4.134)$$

So that if three natural frequencies and their damping ratios are known, it results

$$\xi_1 = \frac{\mu_1}{2\omega_1} + \frac{\mu_2}{2}\omega_1 + \frac{\mu_3}{2}\omega_1^3, \quad \xi_2 = \frac{\mu_1}{2\omega_2} + \frac{\mu_2}{2}\omega_2 + \frac{\mu_3}{2}\omega_2^3, \quad \xi_3 = \frac{\mu_1}{2\omega_3} + \frac{\mu_2}{2}\omega_3 + \frac{\mu_3}{2}\omega_3^3 \quad (5.4.135)$$

These three equations may be solved for μ_1, μ_2 , and μ_3 to form the matrix \underline{C}_0 in (5.4.133), which produces damping ratios ξ_1 at ω_1 , ξ_2 at ω_2 , and ξ_3 at ω_3 .

5.4.12.3 Method 3

The third approach, as discussed in Craig (1981), defines

$$\underline{C}_0 = \sum_{l=1}^N \frac{2\xi_l \omega_l}{\tilde{m}_l} \underline{M} \underline{\psi}_l \underline{\psi}_l^T \underline{M} \quad (5.4.136)$$

where ξ_l are the desired damping ratios. Note that \underline{C}_0 is orthogonal with respect to $\underline{\psi}_l$ since

$$\begin{aligned} \underline{\psi}_i^T \underline{C}_0 \underline{\psi}_j &= \sum_{l=1}^N \frac{2\xi_l \omega_l}{\tilde{m}_l} (\underline{\psi}_i^T \underline{M} \underline{\psi}_l) (\underline{\psi}_l^T \underline{M} \underline{\psi}_j) \\ &= \sum_{l=1}^N \frac{2\xi_l \omega_l}{\tilde{m}_l} \tilde{m}_i \delta_{il} \tilde{m}_j \delta_{jl} = \delta_{ij} \tilde{m}_i 2\xi_i \omega_i \end{aligned} \quad (5.4.137)$$

which is the desired result by (5.4.121). Use of (5.4.136) to specify the damping in as many modes as desired is quite simple and does not require solution of sets of linear equations as in Equation (5.4.123) or (5.4.135). Consider the usual case where only a small set (m) of undamped system modes is available for use in Equation (5.4.136):

$$\underline{C}_0 = \sum_{l=1}^m \frac{2\xi_l \omega_l}{\tilde{m}_l} \underline{M} \underline{\psi}_l \underline{\psi}_l^T \underline{M} \quad (5.4.138)$$

Then

$$\underline{\psi}_i^T \underline{C}_0 \underline{\psi}_j = \tilde{m}_i 2\xi_i \omega_i = 0 \quad \text{for } i > m \quad (5.4.139)$$

since $\underline{\psi}_i$ does not appear in (5.4.138). Thus, the damping ξ_i is zero for $i > m$, which is an undesired result since the higher modes need damping to suppress their oscillations in a simulation.

5.4.12.4 Method 4

To insure that the modes $i(i > m)$ possess damping, it is necessary to modify (5.4.136) into the form (Craig, 1981)

$$\underline{C}_0 = \mu_1 \underline{K} + \sum_{l=1}^{m-1} \frac{2\kappa_l \omega_l}{\tilde{m}_l} \underline{M} \underline{\psi}_l \underline{\psi}_l^T \underline{M} \quad (5.4.140)$$

where m is the number of modes with prescribed damping values and the μ_1 and κ_i are constants to be solved for so that \underline{C}_0 gives the desired modal damping ratios ξ_i^d . Consider the m th mode case using (5.4.140)

$$\underline{\psi}_m^T \underline{C}_0 \underline{\psi}_m = \mu_1 \underline{\psi}_m^T \underline{K} \underline{\psi}_m + 0 = \mu_1 \tilde{m}_m \omega_m^2 \quad (5.4.141)$$

since $m > m-1$ and by using the orthogonality relations (5.4.37) and (5.4.45). Then, from (5.4.93), (5.4.106), and (5.4.141)

$$\underline{\psi}_m^T \underline{C}_0 \underline{\psi}_m = \tilde{c}_m = 2\xi_m^d \tilde{m}_m \omega_m = \mu_1 \tilde{m}_m \omega_m^2 \Rightarrow \mu_1 = \frac{2\xi_m^d}{\omega_m} \quad (5.4.142)$$

Thus, μ_1 is selected so that \underline{C}_0 provides the desired damping ratio ξ_m^d for mode m . Let κ_i represent the values utilized in forming (5.4.140) and ξ_i^d the desired damping ratio for mode i . The κ_i must be solved for and then inserted into (5.4.140) to determine \underline{C}_0 . Note that by (5.4.93), (5.4.106), and (5.4.142),

$$\underline{\psi}_i^T \underline{C}_0 \underline{\psi}_j = \delta_{ij} 2\xi_i^d \tilde{m}_i \omega_i = \frac{2\xi_m^d}{\omega_m} \delta_{ij} \tilde{m}_i \omega_i^2 + \sum_{l=1}^{m-1} \frac{2\kappa_l \omega_l}{\tilde{m}_l} \delta_{il} \delta_{jl} \tilde{m}_i \tilde{m}_j \quad (5.4.143)$$

where the Kronecker delta δ_{ij} equals 0 for $i \neq j$ and 1 for $i = j$. This shows that \underline{C}_0 as defined by (5.4.140) remains orthogonal to all undamped system eigenvectors $\underline{\psi}_i$ with distinct ω_i since by (5.4.143)

$$\underline{\psi}_i^T \underline{C}_0 \underline{\psi}_j = 0, \quad i \neq j \quad (5.4.144)$$

Consider (5.4.143) for the following three cases:

$$2\xi_i^d \tilde{m}_i \omega_i = \begin{cases} \frac{2\xi_m^d}{\omega_m} \tilde{m}_i \omega_i^2 + 2\kappa_i \omega_i \tilde{m}_i, & i \leq m-1 \\ \frac{2\xi_m^d}{\omega_m} \tilde{m}_m \omega_m^2, & i = m \\ \frac{2\xi_m^d}{\omega_m} \tilde{m}_i \omega_i^2, & i > m \end{cases} \quad (5.4.145)$$

This shows that for modes $l \leq m-1$, the κ_l used to form \underline{C}_0 in (5.4.140) should be calculated from

$$\kappa_l = \frac{1}{2\omega_l \tilde{m}_l} \left(2\xi_l^d \tilde{m}_l \omega_l - \frac{2\xi_m^d \tilde{m}_l \omega_l^2}{\omega_m} \right)$$

which simplifies to

$$\kappa_l = \xi_l^d - \xi_m^d \frac{\omega_l}{\omega_m} \quad (5.4.146)$$

For mode m , the damping ratio will be its desired value ξ_m^d , and for mode $l > m$, the damping ratio will automatically become

$$\xi_l = \xi_m^d \frac{\omega_l}{\omega_m} > \xi_m^d \quad (5.4.147)$$

Thus, all modes numbered greater than m have damping ratios that are greater than the value for the m th mode and increase linearly with frequency.

5.4.12.5 Method 5

Assume that the EOMs for a spring–mass–damper model with 2 or more dofs have been derived and are available. The damping matrix \underline{C} contains the damping constants that appear in the system model along with lengths and possibly other constants. In general, there is no reason to expect that the \underline{C} matrix will satisfy the orthogonality relation (5.4.92), (5.4.93) with the undamped system modes. So in general, the matrix $\tilde{\underline{C}}$ formed from

$$\tilde{\underline{C}} = \underline{\Psi}^T \underline{C} \underline{\Psi} \neq \underline{\text{Diag}}(2\tilde{m}_i \omega_i \xi_i) \quad (5.4.148)$$

will not be diagonal. Method 5 ignores the off-diagonal coupling terms in $\tilde{\underline{C}}$ and forms the damping ratios from the diagonal terms, that is, from (5.4.106),

$$\xi_i = \frac{\tilde{C}_{ii}}{2\tilde{m}_i\omega_i} \quad (5.4.149)$$

Summarizing, methods 1–4 all provide an orthogonal damping matrix \underline{C}_0 given measured damping ratios ξ_i , and method 5 yields approximate damping ratios ξ_i given the model's damping matrix \underline{C} .

EXAMPLE 5.4.3 Platform Leveling Mishap Vibration with an Orthogonal Damping Model

Statement: This example adds an orthogonal damping model to the same system and parameter values as in Example 5.4.1. Assume that the damping ratios for the four lowest modes were measured and are listed in Table E5.4.3(a). It is desired for the damping matrix \underline{C}_0 to reproduce these same damping ratios.

Objective: Determine the following:

- Evaluate the \underline{C}_0 matrix which will produce the ξ_l^d shown in Table E5.4.3(a) and provide damping to modes 5 and 6. Utilize the formulas in (5.4.140) with κ_l defined in (5.4.146).
- Determine the system eigenvalues and from these the actual damping ratios of all six modes in the model. Compare these with the specified ξ_l^d in Table E5.4.3(a).
- Determine the damped system's response to the initial conditions defined in Figure E5.4.1(b) and compare to the undamped system model responses in Figure E5.4.1(d) or Figure E5.4.1(e).

Table E5.4.3(a) Desired damping ratios for lowest four modes

Mode (l)	Undamped natural frequency (Hz) (f_l from Eq. (11) of Example 5.4.1) $f = \frac{\omega}{2\pi}$	ξ_l^d
1	1.23	0.05
2	4.34	0.10
3	7.56	0.075
4	11.54	0.14

Solution:

- Recall that the response of this system model is given by the assumed modes formula Equation (4) of Example 5.4.1:

$$u(x, t) = \sum_{l=1}^6 q_l(t)\phi_l(x) = \underline{\Phi}^T(x)\underline{q}(t) \quad (1)$$

where from Equation (17) of Example 5.4.1

$$\underline{\Phi} = (\phi_1 \ \phi_2 \ \phi_3 \ \phi_4 \ \phi_5 \ \phi_6) = \left(1 \ \frac{x}{L} \ \sin\left(\frac{\pi x}{L}\right) \ \sin\left(\frac{2\pi x}{L}\right) \ \sin\left(\frac{3\pi x}{L}\right) \ \sin\left(\frac{4\pi x}{L}\right) \right) \quad (2)$$

and $\underline{q}(t)$ is obtained by solving (5.4.94) with the initial conditions given by Equation (6) of Example 5.4.1, that is,

$$\underline{M}\ddot{\underline{q}} + \underline{C}_0\dot{\underline{q}} + \underline{K}\underline{q} = \underline{0}, \quad \underline{q}_0 = (0.1 \quad -0.1 \quad 0 \quad 0 \quad 0 \quad 0)^T, \quad \dot{\underline{q}}_0 = \underline{0} \quad 6 \times 1 \quad (3)$$

The modal-based solution for \underline{q} is given by (5.4.116)

$$\underline{q}(t) = \sum_{k=1}^6 e^{-\hat{\xi}_k \omega_k t} (\alpha_{kc} \cos \omega_{dk} t + \alpha_{ks} \sin \omega_{dk} t) \underline{\psi}_k \quad (4)$$

Substitution of (4) into (1) yields

$$u(x, t) = \sum_{k=1}^6 e^{-\hat{\xi}_k \omega_k t} (\alpha_{kc} \cos \omega_{dk} t + \alpha_{ks} \sin \omega_{dk} t) u_k(x) \quad (5)$$

where

$$u_k(x) = l\text{th mode shape} = \underline{\Phi}\underline{\psi}_k \quad (6)$$

(b) The form selected for \underline{C}_0 is (5.4.140) with $m=4$, and utilize (5.4.142) to obtain

$$\begin{aligned} \underline{C}_0 &= \mu_1 \underline{K} + \sum_{l=1}^{m-1} \frac{2\kappa_l \omega_l}{\tilde{m}_l} \underline{M}\underline{\psi}_l \underline{\psi}_l^T \underline{M} \\ \Rightarrow \underline{C}_0 &= \frac{2\xi_4^d}{\omega_4} \underline{K} + \sum_{l=1}^3 \frac{2\kappa_l \omega_l}{\tilde{m}_l} \underline{M}\underline{\psi}_l \underline{\psi}_l^T \underline{M} \end{aligned} \quad (7)$$

where from (5.4.146) and Table E5.4.3(a)

$$\begin{aligned} \kappa_1 &= \xi_1^d - \xi_4^d \frac{\omega_1}{\omega_4} = 0.05 - 0.14 \left(\frac{1.23}{11.54} \right) = 0.0351 \\ \kappa_2 &= \xi_2^d - \xi_4^d \frac{\omega_2}{\omega_4} = 0.10 - 0.14 \left(\frac{4.34}{11.54} \right) = 0.0473 \\ \kappa_3 &= \xi_3^d - \xi_4^d \frac{\omega_3}{\omega_4} = 0.075 - 0.14 \left(\frac{7.56}{11.54} \right) = -0.0167 \\ \kappa_4 &= \xi_m^d = 0.14 \end{aligned} \quad (8)$$

Combining (7) and (8) and utilizing the modes and modal masses from Equations (12) and (13) of Example 5.4.1 yield

$$\underline{C}_0 = 1 \times 10^6 \begin{bmatrix} 0.2213 & 0.1304 & 0.0428 & -0.0075 & -0.0398 & 0.0127 \\ & 0.1416 & 0.0235 & -0.0513 & -0.0241 & 0.0017 \\ & & 0.0471 & -0.0114 & 0.0016 & 0.0023 \\ & & & 0.3682 & -0.0384 & 0.0130 \\ & \text{symmetric} & & & 1.1800 & -0.1635 \\ & & & & & 3.9196 \end{bmatrix} \quad (9)$$

(c) An orthogonality check on \underline{C}_0 yields

$$\underline{\Psi}^T \underline{C}_0 \underline{\Psi} = \text{Diag}(\tilde{c}_i) = \text{Diag}(2\xi_i \omega_i \tilde{m}_i) \Rightarrow \xi_i = \frac{\tilde{c}_i}{2\omega_i \tilde{m}_i}$$

yielding

Mode i	1	2	3	4	5	6
\tilde{c}_i	57 880	200 950	152 390	100 480	477 350	473 750
ξ_i	0.050	0.10	0.075	0.14	0.238	0.357

This demonstrates that the desired ξ_i^d in Table E5.4.3(a) will occur in the model. The results for ξ_5 and ξ_6 are also in agreement with the theory (5.4.147)

$$\xi_l = \xi_m^d \frac{\omega_l}{\omega_m} > \xi_m^d \text{ for } l > m$$

(d) The eigenvalues of the system have the form

$$\lambda_j = -\xi_j \omega_j \pm i \omega_j \sqrt{1 - \xi_j^2} \Rightarrow |\lambda_j| = \omega_j \Rightarrow \xi_j = \frac{-\text{Re}(\lambda_j)}{|\lambda_j|} \quad (10)$$

To obtain the eigenvalues, set

$$\underline{q} = e^{\lambda t} \underline{\Lambda} \quad (11)$$

in (3), yielding

$$(\lambda^2 \underline{M} + \lambda \underline{C}_0 + \underline{K}) \underline{\Lambda} = \underline{0} \quad (12)$$

Combine this and the identity

$$\lambda \underline{M} \underline{\Lambda} = \lambda \underline{M} \underline{\Lambda} \quad (13)$$

to obtain the first-order form

$$\lambda \underline{E} \underline{\Gamma} = \underline{H} \underline{\Gamma} \quad (14)$$

where

$$\underline{E} = \begin{bmatrix} \underline{0} & \underline{M} \\ \underline{M} & \underline{C}_0 \end{bmatrix}, \quad \underline{H} = \begin{bmatrix} \underline{M} & \underline{0} \\ \underline{0} & -\underline{K} \end{bmatrix}, \quad \underline{\Gamma} = \begin{Bmatrix} \lambda \underline{\Lambda} \\ \underline{\Lambda} \end{Bmatrix} \quad (15)$$

MATLAB can extract the eigenvalues and eigenvectors of (14) as

```
>> help eig
EIG    Eigenvalues and eigenvectors.
[V,D] = EIG(H,E) produces a diagonal matrix D of generalized eigenvalues
        and a full matrix V whose columns are the corresponding eigenvectors
        so that H*V = E*V*D
```

The results are from (10)

i	λ	ξ
1	$-0.39 \pm i7.7$	0.051
2	$-2.7 \pm i27.13$	0.100
3	$-3.55 \pm i47.32$	0.075
4	$-10.14 \pm i71.77$	0.140
5	$-29.4 \pm i119.8$	0.238
6	$-65.9 \pm i172.6$	0.357

which shows excellent agreement with Table E5.4.3(a) for the desired damping ratios.

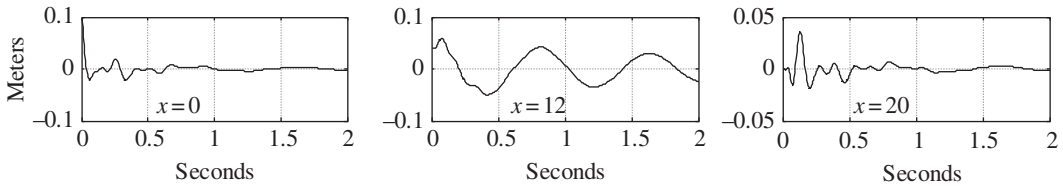


Figure E5.4.3(a) Platform initial condition response including damping

- (e) A numerical integration solution of (3) yields the time histories of the generalized coordinates $q_i(t)$. The response of the physical coordinates $u(x, t)$ is then obtained from the selected shape functions $\phi_i(x)$, the generalized coordinates $q_i(t)$, and Equation (1). The responses at three locations along the platform are shown in Figure E5.4.3(a). The effect of damping is clearly seen by comparing Figure E5.4.1(d) or E5.4.1(e) with Figure E5.4.3(a).

EXAMPLE 5.4.4 Instrumentation Tower Impact Investigation

Statement: An instrumentation module is supported by a multilayered structure consisting of “floor” masses with an interconnecting frame. The tower is accidentally struck by materials overhung on a passing truck, as depicted in Figure E5.4.4(a). The approximate impact force of duration τ is also shown. A simplified N mass model of the pole is shown in Figure E5.4.4(b), where k_i represents the horizontal frame stiffness between mass i and mass $i-1$. The model is formed as part of an effort to evaluate acceleration-induced damage to the instrumentation. The present example only considers the mode shapes and natural frequencies of the tower model. Examples 6.3.1 and 6.4.2 treat its transient response due to impact.

The physical parameters in this model are

$$\begin{aligned} N &= 20, \quad H = 20\text{m}, \quad k_j = 50000\text{N/m}, \quad m_j = 20\text{kg} \\ h_i &= i * \frac{H}{N}, \quad m_s = 50\text{kg}, \quad F_I = 500\text{N}, \quad \tau = \text{variable} \end{aligned} \quad (1)$$

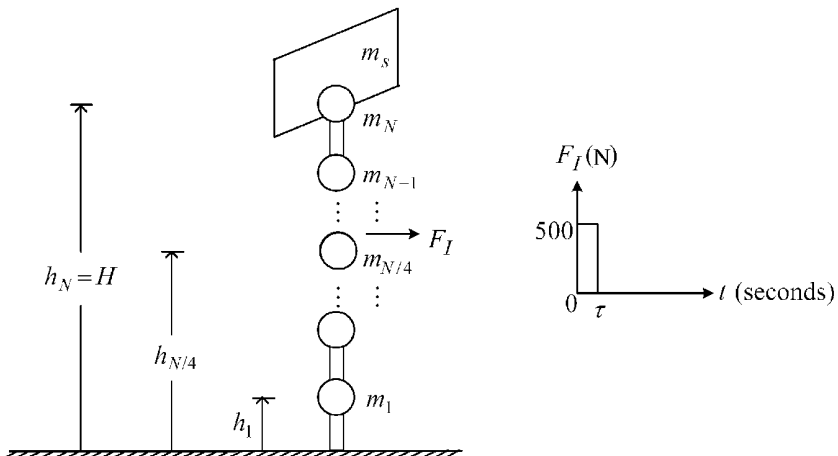


Figure E5.4.4(a) Tower model with sudden impact loading

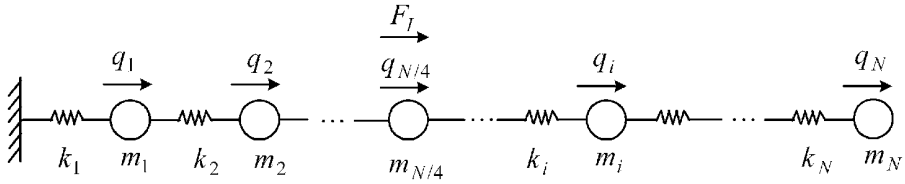


Figure E5.4.4(b) Simplified tower model diagram

Objective: Determine the natural frequencies, mode shapes, and orthogonal damping matrix for this system.

Assumption: Utilize an orthogonal damping matrix based on (5.4.140) with $m = 5$ and the following desired damping ratios:

$$\xi_1^d = 0.02, \quad \xi_2^d = 0.02, \quad \xi_3^d = \xi_4^d = 0.025, \quad \xi_5^d = 0.03 \quad (2)$$

Procedure:

(a) Form the \underline{M} , \underline{K} , and \underline{C}_0 matrices.

(b) The potential energy expression for the model is

$$U = \frac{1}{2} [k_1 q_1^2 + k_2 (q_2 - q_1)^2 + k_3 (q_3 - q_2)^2 + \cdots + k_N (q_N - q_{N-1})^2] \quad (3)$$

Then

$$\frac{\partial U}{\partial q_j} = \begin{cases} (k_1 + k_2)q_1 - k_2 q_2, & j = 1 \\ (k_j + k_{j+1})q_j - k_j q_{j-1} - k_{j+1} q_{j+1}, & j \neq 1, j \neq N \\ k_N q_N - k_N q_{N-1}, & j = N \end{cases} \quad (4)$$

or

$$\frac{\partial U}{\partial \underline{q}} = \underline{K} \underline{q} = \begin{bmatrix} k_1 + k_2 & -k_2 & 0 & 0 & \cdots & 0 \\ & k_2 + k_3 & -k_3 & 0 & \cdots & 0 \\ & & k_3 + k_4 & -k_4 & \cdots & 0 \\ & & & & \ddots & \\ & & & & & -k_N \\ & & & & & k_N \end{bmatrix} \begin{Bmatrix} q_1 \\ q_2 \\ \vdots \\ q_N \end{Bmatrix} \quad (5)$$

The kinetic energy expression for the model is

$$T = \frac{1}{2} [m_1 \dot{q}_1^2 + m_2 \dot{q}_2^2 + \cdots + (m_N + m_s) \dot{q}_N^2] \quad (6)$$

Then

$$\frac{d}{dt} \left(\frac{\partial T}{\partial \dot{q}_j} \right) = \begin{cases} m_j \ddot{q}_j, & j \neq N \\ (m_j + m_s) \ddot{q}_j, & j = N \end{cases} \quad \text{or} \quad \frac{d}{dt} \left(\frac{\partial T}{\partial \dot{\underline{q}}} \right) = \underline{\text{Diag}}(m_j^*) \ddot{\underline{q}} \quad (7)$$

where

$$m_j^* = \begin{cases} m_j, & j \neq N \\ m_N + m_s, & j = N \end{cases} \quad (8)$$

From (5.4.140), (5.4.142), and (5.4.146), the damping matrix is obtained from

$$\underline{C}_0 = \mu_1 \underline{K} + \sum_{l=1}^4 \frac{2\kappa_l \omega_l}{\tilde{m}_l} \underline{M} \underline{\psi}_l \underline{\psi}_l^T \underline{M}, \quad \mu_1 = \frac{2\xi_5^d}{\omega_5}, \quad \kappa_l = \xi_l^d - \xi_5^d \frac{\omega_l}{\omega_5} \quad (9)$$

where ω_l and $\underline{\psi}_l$ are the l th natural frequency and mode shape of the undamped system.

Solution:

- (a) The undamped natural frequencies of the model are obtained from (5.4.66), that is, $\underline{A}\underline{X} = \alpha\underline{X}$, since \underline{M}^{-1} exists

$$\underline{X}_j = \underline{\psi}_j, \quad \underline{A} = \underline{M}^{-1} \underline{K}, \quad \alpha_j = \omega_j^2, \quad \omega_j = \sqrt{\alpha_j}, \quad f_j = \frac{\omega_j}{2\pi} \quad (10)$$

The MATLAB commands for obtaining the eigenvalues α_j and eigenvectors \underline{X}_j are

```
>> help eig
EIG Eigenvalues and eigenvectors.
[V,D] = EIG(A) produces a diagonal matrix D of eigenvalues ( $\alpha_j$ ) and a full matrix
V whose columns are the corresponding eigenvectors ( $\underline{X}_j$ ) so that
A*V = V*D.
```

The natural frequencies are

$$f_n \in (0.54 \ 1.65 \ 2.79 \ 3.94 \ 5.09 \ 6.23 \ 7.33 \ 8.40 \ 9.43 \ 10.40 \\ 11.3 \ 12.14 \ 12.90 \ 13.59 \ 14.20 \ 14.71 \ 15.14 \ 15.48 \ 15.72 \ 15.89) \text{ Hz} \quad (11)$$

The modes are mass orthonormalized, yielding unity as the value for all modal masses \tilde{m}_i . The \underline{C}_0 matrix defined in (9) is orthogonal with respect to $\underline{\Psi}$ and the relationship in (5.4.137) yields

$$\xi_n \in (0.02 \ 0.02 \ 0.025 \ 0.025 \ 0.03 \ 0.037 \ 0.043 \ 0.050 \ 0.056 \ 0.061 \\ 0.067 \ 0.072 \ 0.076 \ 0.080 \ 0.084 \ 0.087 \ 0.089 \ 0.091 \ 0.093 \ 0.094)$$

which agrees with (2) and (5.4.147). The lowest five modes are shown in Figure E5.4.4(c).

5.4.13 Nonorthogonally Damped System with Symmetric Mass, Stiffness, and Damping Matrices

The system EOMs

$$\underline{M}\ddot{\underline{q}} + \underline{C}\dot{\underline{q}} + \underline{K}\underline{q} = \underline{F} \quad (5.4.150)$$

are augmented with the identity

$$\underline{K}\underline{\dot{q}} - \underline{K}\underline{\dot{q}} = \underline{0} \quad (5.4.151)$$

and definition

$$\underline{v} = \underline{\dot{q}} \quad (5.4.152)$$

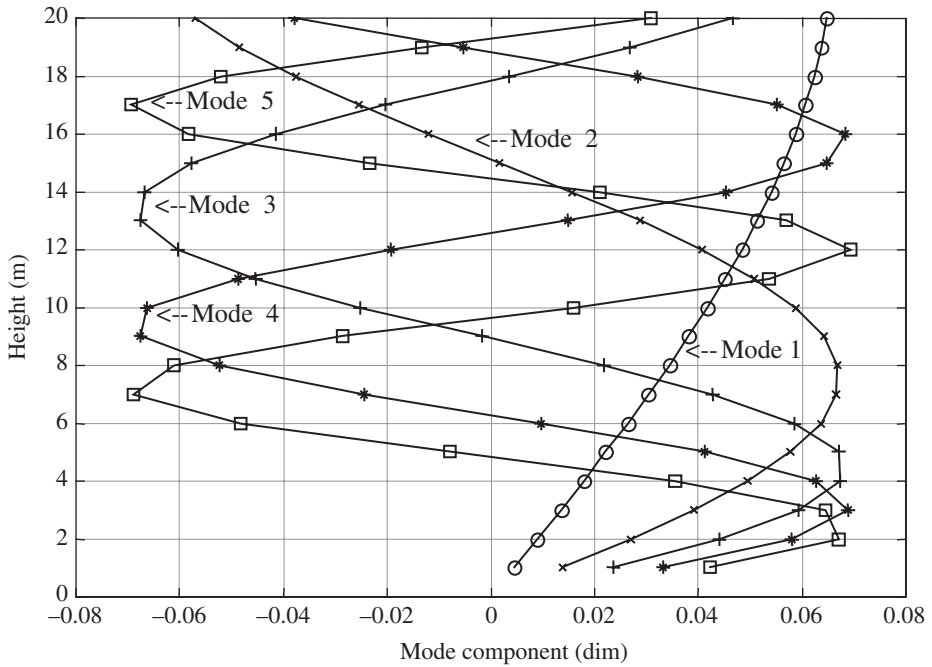


Figure E5.4.4(c) Five lowest mode shapes of the tower model

to form the first-order (state) equations

$$\begin{bmatrix} -\underline{K} & \underline{0} \\ \underline{0} & \underline{M} \end{bmatrix} \begin{Bmatrix} \dot{\underline{q}} \\ \dot{\underline{v}} \end{Bmatrix} - \begin{bmatrix} \underline{0} & -\underline{K} \\ -\underline{K} & -\underline{C} \end{bmatrix} \begin{Bmatrix} \underline{q} \\ \underline{v} \end{Bmatrix} = \begin{Bmatrix} \underline{0} \\ \underline{F} \end{Bmatrix} \quad (5.4.153)$$

which may be written as

$$\underline{A} \dot{\underline{X}} - \underline{B} \underline{X} = \hat{\underline{F}} \quad (5.4.154)$$

For free vibrations, (5.4.154) becomes

$$\underline{A} \dot{\underline{X}} - \underline{B} \underline{X} = \underline{0} \quad (5.4.155)$$

Let

$$\underline{X} = \underline{\Lambda} e^{\lambda t} \quad (5.4.156)$$

Then, for modes i and j ,

$$\lambda_i \underline{A} \underline{\Lambda}_i - \underline{B} \underline{\Lambda}_i = \underline{0} \quad (5.4.157)$$

$$\lambda_j \underline{A} \underline{\Lambda}_j - \underline{B} \underline{\Lambda}_j = \underline{0} \quad (5.4.158)$$

Premultiply (5.4.157) by $\underline{\Lambda}_j^T$ and (5.4.158) by $\underline{\Lambda}_i^T$ to obtain

$$\lambda_i \left(\underline{\Lambda}_j^T \underline{A} \underline{\Lambda}_i \right) - \left(\underline{\Lambda}_j^T \underline{B} \underline{\Lambda}_i \right) = 0 \quad (5.4.159)$$

$$\lambda_j \left(\underline{\Lambda}_i^T \underline{A} \underline{\Lambda}_j \right) - \left(\underline{\Lambda}_i^T \underline{B} \underline{\Lambda}_j \right) = 0 \quad (5.4.160)$$

From (5.4.153) and (5.4.154), it follows that if \underline{M} , \underline{K} , and \underline{C} are symmetric, then both \underline{A} and \underline{B} are also symmetric matrices. Therefore, transposing (5.4.159) yields

$$\lambda_i \left(\underline{\Lambda}_i^T \underline{A} \underline{\Lambda}_j \right) - \left(\underline{\Lambda}_i^T \underline{B} \underline{\Lambda}_j \right) = 0 \quad (5.4.161)$$

Subtract (5.4.159) from (5.4.160) to obtain

$$(\lambda_j - \lambda_i) \left(\underline{\Lambda}_i^T \underline{A} \underline{\Lambda}_j \right) = 0 \quad (5.4.162)$$

Therefore, if λ_i and λ_j are distinct eigenvalues, it follows from (5.4.162) that

$$\underline{\Lambda}_i^T \underline{A} \underline{\Lambda}_j = 0 \quad i \neq j \quad (5.4.163)$$

Substitution of (5.4.163) into (5.4.161) yields

$$\underline{\Lambda}_i^T \underline{B} \underline{\Lambda}_j = 0 \quad i \neq j \quad (5.4.164)$$

Consideration of (5.4.161), (5.4.163), and (5.4.164) yields the orthogonality conditions

$$\underline{\Lambda}_i^T \underline{A} \underline{\Lambda}_j = \nu_i \delta_{ij}, \quad \underline{\Lambda}_i^T \underline{B} \underline{\Lambda}_j = \nu_i \lambda_i \delta_{ij} \quad (5.4.165)$$

where the Kronecker delta δ_{ij} equals 0 for $i \neq j$ and 1 for $i = j$, and the generalized modal mass is defined by

$$\nu_i = \underline{\Lambda}_i^T \underline{A} \underline{\Lambda}_i \quad (5.4.166)$$

5.4.14 Undamped, Gyroscopic, and Noncirculatory Systems—Description

Example 5.3.3 illustrated that gyroscopic torques in linear models with small motions result in a skew-symmetric matrix proportional to the speed (Ω) of a spinning structure or structural component in the model, that is,

$$\underline{G} = \Omega \hat{\underline{G}} = -\underline{G}^T \quad (5.4.167)$$

Some models contain several components rotating at different speeds, that is, a helicopter gear box has a high-speed input shaft from a gas turbine engine and a low-speed (high torque) output shaft that drives the main rotor. These shafts are not directly coupled by gyroscopic or inertia terms, that is, in this case, \underline{G} will be the block diagonal form

$$\underline{G} = \Omega_1 \begin{bmatrix} \underline{0} & \underline{0} & \underline{0} & \underline{0} & \underline{0} \\ 0 & \hat{\underline{G}}_1 & 0 & 0 & 0 \\ \hline 0 & 0 & \cdot & 0 & 0 \\ 0 & 0 & 0 & r \hat{\underline{G}}_2 & 0 \\ 0 & 0 & 0 & 0 & 0 \end{bmatrix} \quad (5.4.168)$$

where $r = \Omega_2 / \Omega_1$, and the $\underline{0}$ main diagonal blocks account for nonspinning components in the model. Note that the form (5.4.167) still applies to (5.4.168).

5.4.15 Undamped, Gyroscopic, and Noncirculatory Systems—Eigenvalues and Eigenvectors

The equilibrium equation for this model type is given by

$$\underline{M}\ddot{\underline{q}} + \underline{G}\dot{\underline{q}} + \underline{K}\underline{q} = \underline{0} \quad (5.4.169)$$

where

$$\underline{M}(\text{positive definite}), \quad \underline{K}(\text{positive semidefinite}), \quad \underline{G}^T = -\underline{G} \quad (5.4.170)$$

Substitution of

$$\underline{q} = e^{\lambda t} \underline{\psi}_G \quad (5.4.171)$$

into (5.4.169) yields

$$(\lambda^2 \underline{M} + \lambda \underline{G} + \underline{K}) \underline{\psi}_G = \underline{0} \quad (5.4.172)$$

Recall that an overbar indicates a “conjugate” operation, and multiply (5.4.172) by $\overline{\underline{\psi}}_G^T$ to obtain

$$a\lambda^2 + b\lambda + c = 0 \quad (5.4.173)$$

where

$$a = \overline{\underline{\psi}}_G^T \underline{M} \underline{\psi}_G, \quad b = \overline{\underline{\psi}}_G^T \underline{G} \underline{\psi}_G, \quad c = \overline{\underline{\psi}}_G^T \underline{K} \underline{\psi}_G$$

The matrices M and K are symmetric so that (2.6.29) indicates that the constants a and c are pure real. The matrix G is skew-symmetric so that (2.6.27) indicates that the constant b is pure imaginary, that is,

$$b = ib_1$$

The solutions of (5.4.173) are

$$\lambda = -\frac{ib_1}{2a} \pm \sqrt{\frac{-b_1^2}{4a^2} - \frac{c}{a}} = i \left(\frac{b_1}{2a} \pm \sqrt{\left(\frac{b_1}{2a}\right)^2 + \frac{c}{a}} \right) = i\omega_{G1}, i\omega_{G2} \quad (5.4.174)$$

which shows that the eigenvalues of an undamped gyroscopic system are pure imaginary.

EXAMPLE 5.4.5 Natural Frequencies of a Rigid Rotor on Flexible, Undamped Supports

Description: Figure E5.4.5(a) depicts a rigid spinning shaft on flexible support. The rotating assembly which includes the shaft and two disks is assumed to be rigid with inertia properties I_T , m , and I_P referenced to the mass center G . The free body diagram for this model is shown in Figure E5.4.5(b).

The reaction forces and torques due to the bearings are

$$F_y = -F_{ya} - F_{yb}, \quad F_z = -F_{za} - F_{zb}, \quad \Gamma_y = aF_{za} - bF_{zb}, \quad \Gamma_z = -aF_{ya} + bF_{yb} \quad (1)$$

where F_{ya} , F_{yb} , Γ_{za} , and Γ_{zb} are shown in Figure E5.4.5(b). Substitution of (1) into (5.3.92)–(5.3.95) yields

$$\underline{M}\ddot{\underline{q}} + (\underline{C}_D + \underline{C}_g)\dot{\underline{q}} + \underline{K}\underline{q} = \underline{0} \quad (2)$$

where

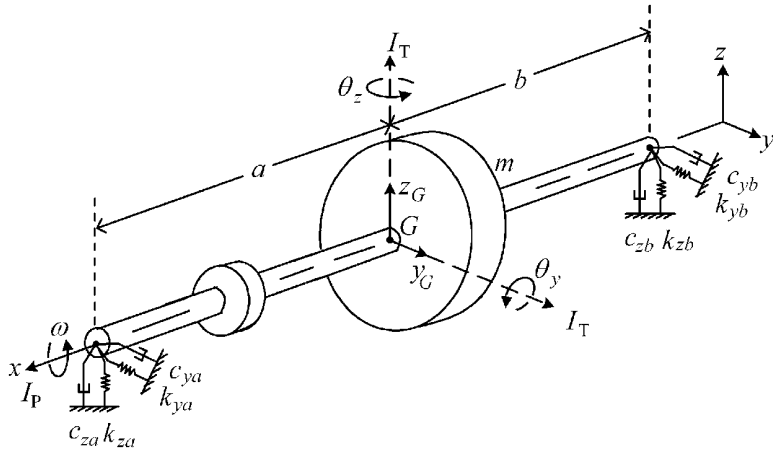


Figure E5.4.5(a) Rigid rotor on flexible supports

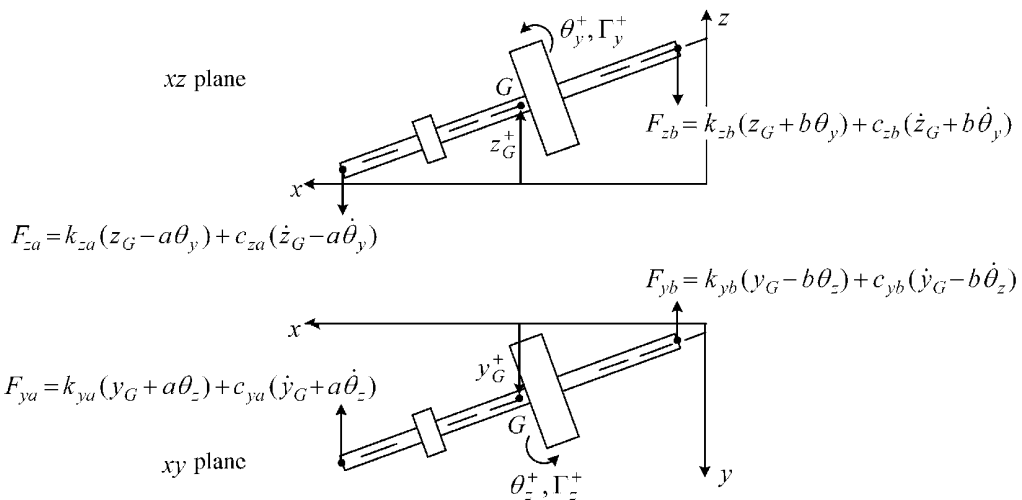


Figure E5.4.5(b) Free body diagram for rigid rotor on flexible supports

$$\underline{q} = \begin{Bmatrix} y_G \\ z_G \\ \theta_y \\ \theta_z \end{Bmatrix}, \quad \underline{M} = \begin{bmatrix} m & 0 & 0 & 0 \\ 0 & m & 0 & 0 \\ 0 & 0 & I_T & 0 \\ 0 & 0 & 0 & I_T \end{bmatrix}, \quad \underline{C}_g = \begin{bmatrix} 0 & 0 & 0 & 0 \\ 0 & 0 & 0 & 0 \\ 0 & 0 & 0 & I_P \omega \\ 0 & 0 & -I_P \omega & 0 \end{bmatrix}$$

$$\underline{K} = \begin{bmatrix} k_{ya} + k_{yb} & 0 & 0 & ak_{ya} - bk_{yb} \\ k_{za} + k_{zb} & -ak_{za} + bk_{zb} & 0 & 0 \\ \text{symmetric} & +a^2k_{za} + b^2k_{zb} & 0 & 0 \\ & & a^2k_{ya} + b^2k_{yb} & \end{bmatrix} \quad (3)$$

and \underline{C}_D has an identical form to \underline{K} with k replaced by c . Consider the undamped case with

$$a = b = \frac{L}{2}, \quad k_{ya} = k_{za} = k_{yb} = k_{zb} = k \quad (4)$$

to illustrate the effects of only the gyroscopic moment terms. Set

$$\underline{q} = e^{\lambda t} \underline{\psi} \quad (5)$$

in (5) to obtain

$$\left(\lambda^2 \begin{bmatrix} m & 0 & 0 & 0 \\ 0 & m & 0 & 0 \\ 0 & 0 & I_T & 0 \\ 0 & 0 & 0 & I_T \end{bmatrix} + \lambda \begin{bmatrix} 0 & 0 & 0 & 0 \\ 0 & 0 & 0 & 0 \\ 0 & 0 & 0 & I_P \omega \\ 0 & 0 & -I_P \omega & 0 \end{bmatrix} + \begin{bmatrix} 2k & 0 & 0 & 0 \\ 0 & 2k & 0 & 0 \\ 0 & 0 & kL^2/2 & 0 \\ 0 & 0 & 0 & kL^2/2 \end{bmatrix} \right) \begin{Bmatrix} \psi_y \\ \psi_z \\ \psi_{\theta y} \\ \psi_{\theta z} \end{Bmatrix} = \underline{0} \quad (6)$$

The determinant of the coefficient matrix in (6) must be zero for $\underline{\psi}$ to be nonzero, that is, for vibrations to exist. This implies

$$(\lambda^2 m + 2k)^2 \left[\left(\lambda^2 I_T + \frac{kL^2}{2} \right)^2 + \lambda^2 \omega^2 I_P^2 \right] = 0 \quad (7)$$

which has the roots

$$\lambda_1 = i\Omega_1 = i\sqrt{\frac{2k}{m}} \quad (8)$$

$$\lambda_2 = i\Omega_2 = i\Omega_T \left(\frac{I_P}{2I_T} \frac{\omega}{\Omega_T} + \sqrt{1 + \left(\frac{I_P}{2I_T} \frac{\omega}{\Omega_T} \right)^2} \right) \quad (9)$$

$$\lambda_3 = i\Omega_3 = i\Omega_T \left(\frac{-I_P}{2I_T} \frac{\omega}{\Omega_T} + \sqrt{1 + \left(\frac{I_P}{2I_T} \frac{\omega}{\Omega_T} \right)^2} \right) \quad (10)$$

$$\lambda_4 = \bar{\lambda}_1, \quad \lambda_5 = \bar{\lambda}_2, \quad \lambda_6 = \bar{\lambda}_3 \quad (11)$$

and where

$$\Omega_T = \lim_{\omega \rightarrow 0} \Omega_2 = \lim_{\omega \rightarrow 0} \Omega_3 = \sqrt{\frac{kL^2}{2I_T}} \quad (12)$$

The form of (8) shows that mode 1 is a simple “bounce mode” where the shaft whirls in a cylindrical shape with $\theta_y = \theta_z = 0$. Equations (9) and (10) show that the second and third natural frequencies are identical at 0 rpm; however, they diverge (bifurcate) with an increasing spin speed ω and for large spin rates

$$\Omega_2 \approx \frac{I_P}{I_T} \omega \quad \left(\text{for } \omega \gg \frac{2I_T}{I_P} \Omega_T \right) \quad (13)$$

$$\Omega_3 = 0 \quad \left(\text{for } \omega \gg \frac{2I_T}{I_P} \Omega_T \right) \quad (14)$$

Thus, for $(I_P/I_T) > 1$, the second mode’s natural frequency always exceeds the spin frequency. The rotating assembly’s shape is like a disk for $(I_P/I_T) > 1$ as shown in Figure E5.4.5(c). For a uniform, solid cylinder,

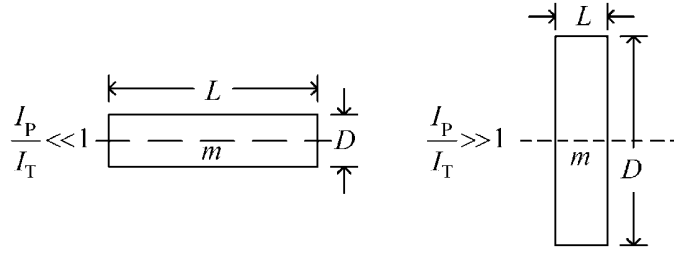


Figure E5.4.5(c) Effect of I_P/I_T ratio on rotor shape

$$I_P = \frac{mD^2}{8}, \quad I_T = \frac{m}{12} \left(L^2 + \frac{3D^2}{4} \right) \quad (15)$$

Therefore

$$\frac{I_P}{I_T} > 1 \Rightarrow D > 1.16L \quad (16)$$

Figure E5.4.5(d) shows plots of (Ω_2/Ω_T) and (Ω_3/Ω_T) versus (ω/Ω_T) for various (I_P/I_T) ratios. The dashed straight line represents $\Omega_2 = \omega$ and $\Omega_3 = \omega$. Imbalance causes a force on the rotor which has the same frequency as the spin speed ω . Figure E5.4.5(d) then shows that an imbalance-induced resonance of mode 2 will only occur if $(I_P/I_T) \leq 1$.

As a mode normalization step, set

$$\psi_{\theta_y} = 1 \quad (17)$$

in the third row of (6). This equation becomes

$$\lambda^2 I_T + \lambda I_P \omega \psi_{\theta_z} + \frac{kL^2}{2} = 0 \quad (18)$$

$$\Rightarrow \psi_{\theta_{z,j}} = \frac{-(\lambda^2 I_T + kL^2/2)}{\lambda I_P \omega} = \frac{i(-\Omega_j^2 I_T + kL^2/2)}{\Omega_j I_P \omega} \quad j=2,3 \quad (19)$$

Substitution of Ω_2 from (9) into (19) yields

$$\psi_{\theta_{z,2}} = -i = e^{-i\pi/2} \quad (20)$$

The actual physical motion in mode 2 becomes

$$\theta_{y,2}(t) = \text{Re}(\psi_{\theta_{y,2}} e^{\lambda_2 t}) = \text{Re}(1 * e^{i\Omega_2 t}) = \cos(\Omega_2 t) \quad (21)$$

and

$$\theta_{z,2}(t) = \text{Re}(\psi_{\theta_{z,2}} e^{\lambda_2 t}) = \text{Re}(e^{-i\pi/2} e^{i\Omega_2 t}) = \cos\left(\Omega_2 t - \frac{\pi}{2}\right) = \sin(\Omega_2 t) \quad (22)$$

This demonstrates that θ_z lags θ_y by 90° ; hence, the end of the shaft in Figure E5.4.5(a) will execute the motion shown on the left side of Figure E5.4.5(e) while whirling in a “pure” mode 2 motion.

Therefore, mode 2 is a conically shaped ($y_G = z_G = 0$, $\theta_y \neq 0$, $\theta_z \neq 0$) mode in which the shaft whirls in the same direction as the spin direction; hence, this is called a “forward whirl mode.” Substitution of Ω_3 from (10) into (19) yields

$$\psi_{\theta_{z,3}} = i = e^{i\pi/2} \quad (23)$$

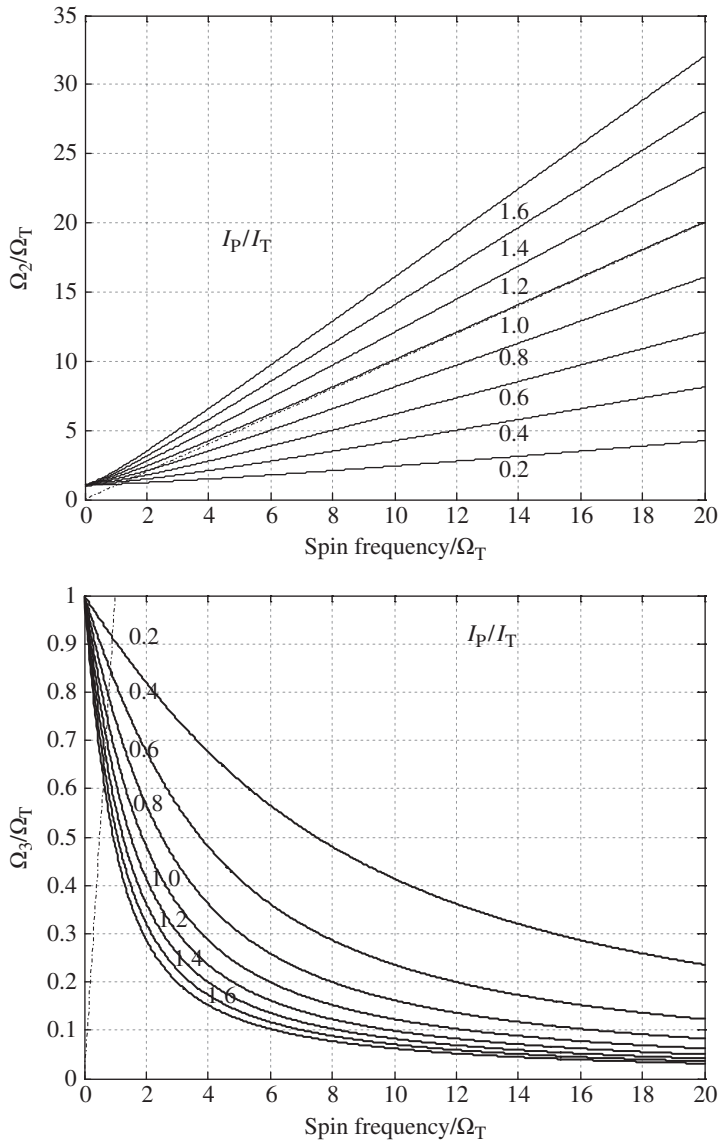


Figure E5.4.5(d) Second and third natural frequencies versus spin frequency

The actual physical motion in mode 3 becomes

$$\theta_{y,3}(t) = \text{Re}(\psi_{\theta_{y,3}} e^{\lambda_3 t}) = \text{Re}(1 * e^{i\Omega_3 t}) = \cos(\Omega_3 t) \quad (24)$$

and

$$\theta_{z,3}(t) = \text{Re}(\psi_{\theta_{z,3}} e^{\lambda_3 t}) = \text{Re}\left(e^{i\pi/2} e^{i\Omega_3 t}\right) = \cos\left(\Omega_3 t + \frac{\pi}{2}\right) = -\sin(\Omega_3 t) \quad (25)$$

The resulting whirl direction is counter to the spin direction as shown on the right side of Figure E5.4.5(e); hence, mode 3 is referred to as a “backward whirl mode.”

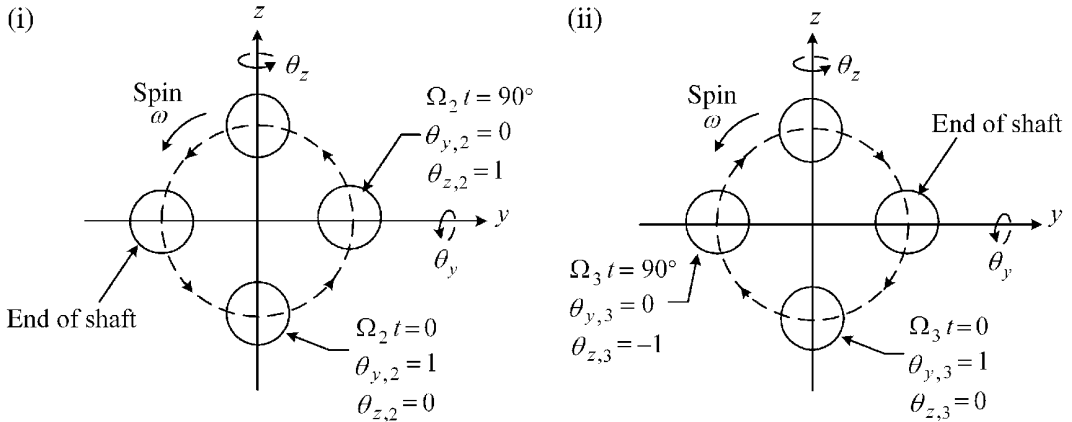


Figure E5.4.5(e) (i) Forward conical motion in mode 2. (ii) Backward conical motion in mode 1

5.4.16 Undamped, Gyroscopic, and Noncirculatory Systems—Biorthogonality

Unlike the undamped and orthogonally damped system models, the \underline{G} matrix does not form an orthogonality relation with respect to the undamped, nongyroscopic modes $\underline{\psi}$, that is,

$$\underline{\psi}_i^T \underline{G} \underline{\psi}_j \neq 0 \text{ for } i \neq j \tag{5.4.175}$$

Alternate orthogonality conditions will be derived beginning with (5.4.169), written in first-order form as

$$\begin{bmatrix} \underline{0} & \underline{M} \\ \underline{M} & \underline{G} \end{bmatrix} \begin{Bmatrix} \dot{\underline{V}} \\ \underline{\dot{q}} \end{Bmatrix} = \begin{bmatrix} \underline{M} & \underline{0} \\ \underline{0} & -\underline{K} \end{bmatrix} \begin{Bmatrix} \underline{V} \\ \underline{q} \end{Bmatrix} \tag{5.4.176}$$

where

$$\underline{V} = \underline{\dot{q}} \quad (N \times 1)$$

Equation (5.4.176) is expressed as

$$\underline{E} \underline{\dot{X}} = \underline{H} \underline{X} \tag{5.4.177}$$

or

$$\underline{\dot{X}} = \underline{A} \underline{X} \tag{5.4.178}$$

where

$$\underline{A} = \underline{E}^{-1} \underline{H} = \begin{bmatrix} -\underline{M}^{-1} \underline{G} \underline{M}^{-1} & \underline{M}^{-1} \\ \underline{M}^{-1} & \underline{0} \end{bmatrix} \begin{bmatrix} \underline{M} & \underline{0} \\ \underline{0} & -\underline{K} \end{bmatrix} = \begin{bmatrix} -\underline{M}^{-1} \underline{G} & -\underline{M}^{-1} \underline{K} \\ \underline{I}_N & \underline{0} \end{bmatrix} \tag{5.4.179}$$

Let

$$\underline{X} = e^{\lambda t} \underline{\Gamma} \tag{5.4.180}$$

where since \underline{X} has the form

$$\underline{X} = \begin{Bmatrix} \underline{V} \\ \underline{q} \end{Bmatrix} = \begin{Bmatrix} \dot{\underline{q}} \\ \underline{q} \end{Bmatrix} \quad (5.4.181)$$

it follows that the “right” eigenvector $\underline{\Gamma}$ must have the form

$$\underline{\Gamma} = \begin{Bmatrix} \lambda \underline{\psi}_G \\ \underline{\psi}_G \end{Bmatrix} \quad (5.4.182)$$

Substitute (5.4.180) into (5.4.177) and consider for the i th eigensolution pair $(\lambda_i, \underline{\Gamma}_i)$

$$\lambda_i \underline{E} \underline{\Gamma}_i = \underline{H} \underline{\Gamma}_i \quad (5.4.183)$$

The “adjoint” or “left” eigensolution problem is obtained by considering Equation (5.4.172) with $(\underline{M}, \underline{G}, \underline{K})$ replaced by $(\underline{M}^T, \underline{G}^T, \underline{K}^T)$, that is,

$$\left(\lambda^2 \underline{M}^T + \lambda \underline{G}^T + \underline{K}^T \right) \underline{\theta} = \underline{0} \quad (5.4.184)$$

Augment this with the identity

$$\alpha \underline{M}^T \underline{\theta} = \alpha \underline{M}^T \underline{\theta}$$

to form the equations

$$\alpha \begin{bmatrix} \underline{0} & \underline{M}^T \\ \underline{M}^T & \underline{G}^T \end{bmatrix} \begin{Bmatrix} \alpha \underline{\theta} \\ \underline{\theta} \end{Bmatrix} = \begin{bmatrix} \underline{M}^T & \underline{0} \\ \underline{0} & -\underline{K}^T \end{bmatrix} \begin{Bmatrix} \alpha \underline{\theta} \\ \underline{\theta} \end{Bmatrix} \quad (5.4.185)$$

or by comparison with (5.4.176) and (5.4.177)

$$\alpha \underline{E}^T \underline{\beta} = \underline{H}^T \underline{\beta} \quad (5.4.186)$$

From (5.4.183), the eigenvalues λ are determined from

$$\det(\lambda \underline{E} - \underline{H}) = 0 \quad (5.4.187)$$

From (5.4.186), the eigenvalues α are determined from

$$\det(\alpha \underline{E}^T - \underline{H}^T) = 0 \quad (5.4.188)$$

The determinant of the transpose of a matrix equals the determinant of the matrix itself so from (5.4.188)

$$\det(\alpha \underline{E} - \underline{H}) = 0 \quad (5.4.189)$$

Thus, the condition for determining α is the same as the condition for determining λ in (5.4.187) so

$$\alpha = \lambda \quad (5.4.190)$$

Equation (5.4.186) may then be written as

$$\lambda_j \underline{E}^T \underline{\beta}_j = \underline{H}^T \underline{\beta}_j \quad (5.4.191)$$

where

$$\underline{\beta}_j = \begin{Bmatrix} \lambda_j \underline{\theta}_j \\ \underline{\theta}_j \end{Bmatrix} \quad (5.4.192)$$

Premultiply (5.4.183) by $\underline{\beta}_j^T$ and (5.4.191) by $\underline{\Gamma}_i^T$ to obtain

$$\lambda_i \underline{\beta}_j^T \underline{E} \underline{\Gamma}_i = \underline{\beta}_j^T \underline{H} \underline{\Gamma}_i, \quad \lambda_j \underline{\Gamma}_i^T \underline{E}^T \underline{\beta}_j = \underline{\Gamma}_i^T \underline{H}^T \underline{\beta}_j \quad (5.4.193)$$

Transpose the latter equation and subtract it from the former to obtain

$$(\lambda_i - \lambda_j) \underline{\beta}_j^T \underline{E} \underline{\Gamma}_i = 0 \quad (5.4.194)$$

Thus, if λ_i and λ_j are distinct,

$$\underline{\beta}_j^T \underline{E} \underline{\Gamma}_i = \tilde{e}_i \delta_{ij} \quad (5.4.195)$$

where δ_{ij} is a Kronecker delta and $\tilde{e}_i = \underline{\beta}_i^T \underline{E} \underline{\Gamma}_i$

Substitution of (5.4.195) into (5.4.193) yields

$$\underline{\beta}_j^T \underline{H} \underline{\Gamma}_i = \lambda_i \tilde{e}_i \delta_{ij} \quad (5.4.196)$$

Equations (5.4.195) and (5.4.196) are the two *biorthogonality* relations for the system.

The above results are valid for general (unsymmetric) \underline{M} , \underline{G} , and \underline{K} matrices. Consider the special case of symmetric \underline{M} and \underline{K} matrices and a skew-symmetric (gyroscopic) \underline{G} matrix.

Since $\alpha = \lambda$ by (5.4.190) and $\underline{M}^T = \underline{M}$, $\underline{K}^T = \underline{K}$, $\underline{G}^T = -\underline{G}$ for a pure gyroscopic system, Equation (5.4.184) becomes

$$(\lambda^2 \underline{M} - \lambda \underline{G} + \underline{K}) \underline{\theta} = \underline{0} \quad (5.4.197)$$

Also recall that from (5.4.172)

$$(\lambda^2 \underline{M} + \lambda \underline{G} + \underline{K}) \underline{\psi}_G = \underline{0} \quad (5.4.198)$$

From (5.4.174), $\lambda = i\omega_G$ for pure gyroscopic system so (5.4.197) and (5.4.198) may be written as

$$(-\omega_G^2 \underline{M} - i\omega_G \underline{G} + \underline{K}) \underline{\theta} = \underline{0} \quad (5.4.199)$$

$$(-\omega_G^2 \underline{M} + i\omega_G \underline{G} + \underline{K}) \underline{\psi}_G = \underline{0} \quad (5.4.200)$$

Take the conjugate of (5.4.199) to obtain

$$(-\omega_G^2 \underline{M} + i\omega_G \underline{G} + \underline{K}) \bar{\underline{\theta}} = \underline{0} \quad (5.4.201)$$

Comparison of (5.4.200) and (5.4.201) shows

$$\underline{\theta} = \bar{\underline{\psi}}_G \quad (5.4.202)$$

This demonstrates that if the “right” eigenvector

$$\underline{\Gamma}_i = \left\{ \begin{array}{c} \lambda_i \underline{\psi}_G \\ \underline{\psi}_G \end{array} \right\} \quad (5.4.203)$$

is determined by solving (5.4.183), the “left” eigenvector may be obtained by (5.4.192) and (5.4.202) as

$$\underline{\beta}_{-j} = \begin{Bmatrix} \lambda_j \underline{\theta}_j \\ \underline{\theta}_j \end{Bmatrix} = \begin{Bmatrix} \lambda_j \underline{\bar{\psi}}_{-Gj} \\ \underline{\bar{\psi}}_{-Gj} \end{Bmatrix} \quad (5.4.204)$$

Finally, using these results, the “generalized modal mass” (\tilde{e}_i) in (5.4.195) may be written as

$$\begin{aligned} \tilde{e}_i &= \underline{\beta}_{-i}^T \underline{E} \underline{\Gamma}_i = \begin{pmatrix} \lambda_i \underline{\bar{\psi}}_{-Gi}^T & \underline{\bar{\psi}}_{-Gi}^T \end{pmatrix} \begin{bmatrix} \underline{Q} & \underline{M} \\ \underline{M} & \underline{G} \end{bmatrix} \begin{Bmatrix} \lambda_i \underline{\psi}_{-Gi} \\ \underline{\psi}_{-Gi} \end{Bmatrix} \\ &= \lambda_i \underline{\bar{\psi}}_{-Gi}^T \underline{M} \underline{\psi}_{-Gi} + \underline{\bar{\psi}}_{-Gi}^T (\lambda_i \underline{M} + \underline{G}) \underline{\psi}_{-Gi} = \underline{\bar{\psi}}_{-Gi}^T (2\lambda_i \underline{M} + \underline{G}) \underline{\psi}_{-Gi} \end{aligned} \quad (5.4.205)$$

which is a pure imaginary number by (2.6.27), (2.6.29), and (5.4.174).

5.4.17 General Linear Systems—Description

A general form for the linear free vibration problem is given by

$$\underline{M} \underline{\ddot{q}} + (\underline{C} + \underline{G}) \underline{\dot{q}} + (\underline{K} + \underline{K}_C) \underline{q} = \underline{0} \quad (5.4.206)$$

where

$$\begin{aligned} \underline{M} &\geq 0 \text{ (positive semidefinite, symmetric)} \\ \underline{C} &\text{ (symmetric), } \underline{K} \text{ (symmetric)} \\ \underline{G} &\text{ (skew-symmetric), } \underline{K}_C \text{ (skew-symmetric)} \end{aligned} \quad (5.4.207)$$

In general, \underline{C} will have the form

$$\underline{C} = \underline{C}_0 + \hat{\underline{C}} \quad (5.4.208)$$

where \underline{C}_0 is an orthogonal damping matrix and $\hat{\underline{C}}$ typically contains concentrated passive or active dampers. Note that the forms of the coefficient matrices for $\underline{\dot{q}}$ and \underline{q} in (5.4.206) are very general since any matrix may be decomposed into the sum of a symmetric and skew-symmetric matrix, that is,

$$\underline{Q} = \underline{Q}_{\text{sym}} + \underline{Q}_{\text{skew}} \quad (5.4.209)$$

where

$$\underline{Q}_{\text{sym}} = \frac{1}{2} (\underline{Q} + \underline{Q}^T), \quad \underline{Q}_{\text{skew}} = \frac{1}{2} (\underline{Q} - \underline{Q}^T) \quad (5.4.210)$$

that is,

$$\underline{Q}_{\text{sym}}^T = \underline{Q}_{\text{sym}}, \quad \underline{Q}_{\text{skew}}^T = -\underline{Q}_{\text{skew}} \quad (5.4.211)$$

A common application area for the general form of (5.4.206) is in rotating machinery vibration modeling in which case linearized representations of seal and bearing forces result in significant concentrated damping terms, unsymmetric stiffness and damping terms, and unsymmetric gyroscopic terms. Structures or structural components with concentrated dampers or with active vibration control systems also require the general form in (5.4.206) for more accurate modeling.

5.4.18 General Linear Systems—Biorthogonality

The biorthogonality results of (5.4.195) and (5.4.196) are directly applicable to this case with the following substitutions:

$$\underline{G} \Rightarrow \underline{C} + \underline{G}, \quad \underline{K} \Rightarrow \underline{K} + \underline{K}_C \quad (5.4.212)$$

This is valid since the derivations of (5.4.195) and (5.4.196) were independent of the symmetry of \underline{G} and \underline{K} . Therefore, the following equations are valid for the general case of (5.4.206) and (5.4.207).

From (5.4.171), (5.4.172), *Quadratic Eigen-Problem*

$$\underline{q} = e^{\lambda t} \underline{\Lambda} \quad (N \times 1) \quad (5.4.213)$$

$$[\lambda^2 \underline{M} + \lambda(\underline{C} + \underline{G}) + (\underline{K} + \underline{K}_C)] \underline{\Lambda} = \underline{0} \quad (N \times 1) \quad (5.4.214)$$

From (5.4.176) and (5.4.177), *First-Order Generalized Form*

$$\underline{E} \dot{\underline{X}} = \underline{H} \underline{X} \quad (5.4.215)$$

$$\underline{E}_{(2N \times 2N)} = \begin{bmatrix} \underline{0} & \underline{M} \\ \underline{M} & \underline{G} + \underline{C} \end{bmatrix}, \quad \underline{H}_{(2N \times 2N)} = \begin{bmatrix} \underline{M} & \underline{0} \\ \underline{0} & -(\underline{K} + \underline{K}_C) \end{bmatrix} \quad (5.4.216)$$

$$\underline{X}_{(2N \times 1)} = \begin{Bmatrix} \underline{V} \\ \underline{q} \end{Bmatrix}, \quad \underline{V}_{(N \times 1)} = \underline{\dot{q}} \quad (5.4.217)$$

From (5.4.178) and (5.4.179), *First-Order Standard Form*

$$\dot{\underline{X}} = \underline{A} \underline{X} \quad (2N \times 1) \quad (5.4.218)$$

$$\underline{A} = \underline{E}^{-1} \underline{H} = \begin{bmatrix} -\underline{M}^{-1}(\underline{G} + \underline{C}) & -\underline{M}^{-1}(\underline{K} + \underline{K}_C) \\ \underline{I}_N & \underline{0} \end{bmatrix} \quad (2N \times 2N) \quad (5.4.219)$$

From (5.4.182) and (5.4.183), *the Right Eigenvector Problem*

$$\lambda_i \underline{E} \underline{\Gamma}_i = \underline{H} \underline{\Gamma}_i \quad (2N \times 1) \quad (5.4.220)$$

$$\underline{\Gamma}_i = \begin{Bmatrix} \lambda_i \underline{\Lambda}_i \\ \underline{\Lambda}_i \end{Bmatrix} \quad (2N \times 1) \quad (5.4.221)$$

From (5.4.191), *the Left (Adjoint) Eigenvector Problem*

$$\lambda_j \underline{E}^T \underline{\beta}_j = \underline{H}^T \underline{\beta}_j \quad (5.4.222)$$

From (5.4.195) and (5.4.196), *the Bi-Orthogonality Relations for Distinct Eigenvalues in Scalar Form*

$$\underline{\beta}_j^T \underline{E} \underline{\Gamma}_i = \tilde{e}_i \delta_{ij} \quad (1 \times 1) \quad (5.4.223)$$

$$\underline{\beta}_j^T \underline{H} \underline{\Gamma}_i = \lambda_i \tilde{e}_i \delta_{ij} \quad (1 \times 1) \quad (5.4.224)$$

$$\tilde{e}_i = \underline{\beta}_i^T \underline{E} \underline{\Gamma}_i \quad (1 \times 1) \quad (5.4.225)$$

$$\delta_{ij} = \begin{cases} 0, & i \neq j \\ 1, & i = j \end{cases} \quad (5.4.226)$$

Bi-Orthogonality Relations for Distinct Eigenvalues in Matrix Form (follows from (2.6.52), (5.4.223) and (5.4.224))

$$\underline{\Gamma} = [\underline{\Gamma}_1 \quad \underline{\Gamma}_2 \quad \cdots \quad \underline{\Gamma}_{2N}] \quad (2N \times 2N) \quad (5.4.227)$$

$$\underline{\beta} = [\underline{\beta}_1 \quad \underline{\beta}_2 \quad \cdots \quad \underline{\beta}_{2N}] \quad (2N \times 2N) \quad (5.4.228)$$

$$\underline{\beta}^T \underline{E} \underline{\Gamma} = \underline{\text{Diag}}(\tilde{e}_i) \quad (2N \times 2N) \quad (5.4.229)$$

$$\underline{\beta}^T \underline{H} \underline{\Gamma} = \underline{\text{Diag}}(\lambda_i \tilde{e}_i) \quad (2N \times 2N) \quad (5.4.230)$$

5.5 INFINITE DOF CONTINUOUS MEMBER SYSTEMS

5.5.1 Introduction

In reality, all points on a body may move independently of all other points. Thus, the rigid body, assumed modes, and finite element approaches artificially constrain relative motions on a body to produce a simulation model with a finite number of dofs that may be solved for motions. Infinite dof models are free of these constraints and are typically derived by considering equilibrium requirements for a differential mass within the domain of the structural member. This yields a partial differential equation (PDE) for the displacements at any point on the body and for any time. Solutions of PDE are possible only for simple geometries and boundary conditions (BC) and homogeneous materials. The following sections illustrate the infinite dof (PDE) approach for some simple problems.

5.5.2 Transverse Vibration of Strings and Cables

Figure 5.5.1 shows the model of a string or cable undergoing transverse vibration and a portion of its free body diagram.

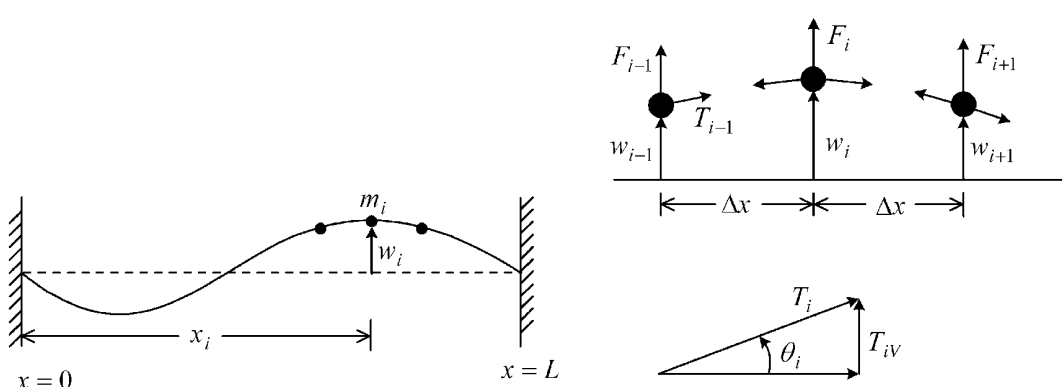


Figure 5.5.1 Continuous model of vibrating string

Let T represent the internal tension force, F the external applied force, w the lateral displacement, and m_i a differential mass at location. From the FBD and the geometry,

$$T_{iV} = T_i \sin \theta_i \approx T_i \frac{\Delta w}{\Delta x} = T_i \left(\frac{w_{i+1} - w_i}{\Delta x} \right)$$

Then by the Newton TEOM (3.3.5) applied to m_i

$$m_i \ddot{w}_i = F_i - T_{i-1} \frac{w_i - w_{i-1}}{\Delta x} + T_i \frac{w_{i+1} - w_i}{\Delta x} \quad i = 1, 2, \dots, n \quad (5.5.1)$$

Let

$$\Delta w_i = w_{i+1} - w_i \quad (5.5.2)$$

Then Equation (5.5.1) becomes

$$m_i \ddot{w}_i = F_i - T_{i-1} \frac{\Delta w_{i-1}}{\Delta x} + T_i \frac{\Delta w_i}{\Delta x} \quad (5.5.3)$$

or

$$m_i \frac{\partial^2 w_i}{\partial t^2} = F_i + \Delta \left(T_i \frac{\Delta w_i}{\Delta x} \right) \quad (5.5.4)$$

or

$$\left(\frac{m_i}{\Delta x} \right) \frac{\partial^2 w_i}{\partial t^2} = \left(\frac{F_i}{\Delta x} \right) + \frac{\Delta \left(T_i \frac{\Delta w_i}{\Delta x} \right)}{\Delta x} \quad (5.5.5)$$

Consider the limit as $\Delta x \rightarrow 0$, which yields

$$f(x, t) = \text{force per unit length} = \lim_{\Delta x \rightarrow 0} \left(\frac{F_i}{\Delta x} \right) \quad (5.5.6)$$

$$\bar{m} = \text{mass per unit length} = \lim_{\Delta x \rightarrow 0} \left(\frac{m_i}{\Delta x} \right) = \frac{\text{total mass}}{L}$$

and

$$\bar{m} \frac{\partial^2 w}{\partial t^2} = f(x, t) + \frac{\partial}{\partial x} \left(T \frac{\partial w}{\partial x} \right) \quad (5.5.7)$$

The string is initially pretensioned with a constant value τ , and the total tension also has a time-varying component τ^* . It is assumed that $\tau^* \ll \tau$ so that the total tension is assumed to be the constant τ . Equation (5.5.7) then becomes

$$\frac{\partial^2 w}{\partial t^2} = \frac{f(x, t)}{\bar{m}} + c^2 \frac{\partial^2 w}{\partial x^2} \quad (5.5.8)$$

where

$$c^2 = \frac{\tau}{\bar{m}} \quad (5.5.9)$$

For unforced vibrations, (5.5.8) becomes

$$\frac{\partial^2 w}{\partial t^2} = c^2 \frac{\partial^2 w}{\partial x^2} \quad (5.5.10)$$

The solution of this PDE is obtained using separation of variables method, that is, let

$$w(x, t) = X(x)T(t) \quad (5.5.11)$$

Then Equation (5.5.10) becomes

$$X\ddot{T} = c^2TX'' \quad (5.5.12)$$

where $(\dot{})$ indicates time derivative and (\prime) indicates x derivative. Rearranging this equation yields

$$\frac{1}{c^2T}\ddot{T} = \frac{X''}{X} = \text{Constant} = -\sigma^2 \quad (5.5.13)$$

The expressions in (5.5.13) must be the constant shown since a function of independent variable t can equal a function of independent variable x , only if both functions equal the same constant. The special form of the constant shown produces an oscillatory temporal part (T) of the solution, consistent with nature. First, consider the spatial DE

$$X'' + \sigma^2X = 0 \quad (5.5.14)$$

which has solutions of the form

$$X(x) = a_1 \sin(\sigma x) + a_2 \cos(\sigma x) \quad (5.5.15)$$

The BC for a cable or string fixed at both ends are

$$X(0) = 0 = a_2, \quad X(L) = 0 = a_1 \sin(\sigma L) \quad (5.5.16)$$

This condition is satisfied if $a_1 = 0$ or $\sin(\sigma L) = 0$. The former condition would imply that the system never vibrates which is analogous to setting $\underline{\psi}$ to zero in (5.4.12). The other possibility is

$$\sin(\sigma L) = 0 \quad (5.5.17)$$

Equation (5.5.17) is the “characteristic equation” for this continuous mass member problem, which yields a set of special values of σ , that is,

$$\sigma_n = \frac{n\pi}{L} \quad n = 1, 2, 3, \dots \quad (5.5.18)$$

just like $\det(-\omega^2 \underline{M} + \underline{K}) = 0$ yielded special values (eigenvalues or natural frequencies) for ω^2 in (5.4.13). In addition, recall that once ω was determined from (5.4.13), it was substituted back into

$$(-\omega^2 \underline{M} + \underline{K})\underline{\psi} = \underline{0} \quad (5.5.19)$$

to solve for $\underline{\psi}$ (the eigenvector or mode shape). Similarly, the solutions to σ in (5.5.18) are substituted into (5.5.15) to obtain the mode shapes or “eigenfunctions”:

$$X_n(x) = a_n \sin\left(\frac{n\pi}{L}x\right) \quad (5.5.20)$$

Note that as in the case of the $\underline{\psi}$, $X_n(x)$ is unique only to within a multiplication constant, that is, a_n can be arbitrary and $X_n(x)$ will still satisfy (5.5.14). The temporal DE in (5.5.13) is

$$\ddot{T} + \sigma_n^2 c^2 T = 0 \quad (5.5.21)$$

which has solutions

$$T_n(t) = A_n \sin(\sigma_n ct) + B_n \cos(\sigma_n ct) \quad (5.5.22)$$

Thus, from (5.5.9), (5.5.18), and (5.5.22), the natural frequencies are

$$\omega_n = \sigma_n c = \frac{n\pi}{L} c = \frac{n\pi}{L} \sqrt{\frac{\tau}{\bar{m}}} \quad (5.5.23)$$

Note that the BC on the mode shape were essential in determining the natural frequencies since the σ_n are determined from the BC (5.5.16). The total solution for w is obtained from (5.5.11), (5.5.20), and (5.5.22) as

$$w_n(x, t) = X_n(x)T_n(t) = c_n \sin(\sigma_n x) \sin(\sigma_n ct) + d_n \sin(\sigma_n x) \cos(\sigma_n ct) \quad (5.5.24)$$

where c_n and d_n are constants to be determined and σ_n is given by (5.5.18). All solutions of the form (5.5.24) satisfy the PDE (5.5.10) and the BC (5.5.16); therefore, the total solution is the superposition of all $w_n(x, t)$:

$$w(x, t) = \sum_{i=1}^{\infty} w_n(x, t) = \sum_{i=1}^{\infty} [c_n \sin(\sigma_n x) \sin(c\sigma_n t) + d_n \sin(\sigma_n x) \cos(c\sigma_n t)] \quad (5.5.25)$$

The c_n and d_n are determined from the ICs using the orthogonality of the sine and cosine functions, that is,

$$\int_0^L \sin(\sigma_n x) \sin(\sigma_m x) dx = \int_0^L \sin\left(\frac{n\pi x}{L}\right) \sin\left(\frac{m\pi x}{L}\right) dx = \begin{cases} 0, & n \neq m \\ \frac{L}{2}, & n = m \end{cases} \quad (5.5.26)$$

Let the IC on displacement be

$$w(x, t=0) = w_0(x) = \sum_{i=1}^{\infty} d_n \sin(\sigma_n x) \quad (5.5.27)$$

which follows from (5.5.25), evaluated at $t = 0$. Multiply (5.5.27) by $\sin(\sigma_m x)$ and integrate from 0 to L using (5.5.26) to obtain

$$\int_0^L w_0(x) \sin(\sigma_m x) dx = d_1 \int_0^L \sin(\sigma_1 x) \sin(\sigma_m x) dx + d_2 \int_0^L \sin(\sigma_2 x) \sin(\sigma_m x) dx + \dots = d_m \frac{L}{2} \quad (5.5.28)$$

Therefore,

$$d_m = \frac{2}{L} \int_0^L w_0(x) \sin(\sigma_m x) dx \quad (5.5.29)$$

Let the IC on velocity be

$$\dot{w}(x, t=0) = \dot{w}_0(x) = \sum_{i=1}^{\infty} c_n c \sigma_n \sin(\sigma_n x) \quad (5.5.30)$$

which follows from (5.5.25), evaluated at $t = 0$. Multiply (5.5.30) by $\sin(\sigma_m x)$ and integrate from 0 to L using (5.5.26) to obtain

$$\int_0^L \dot{w}_0(x) \sin(\sigma_m x) dx = c c_m \sigma_m \frac{L}{2}$$

$$\Rightarrow c_m = \frac{2}{c \sigma_m L} \int_0^L \dot{w}_0(x) \sin(\sigma_m x) dx \quad (5.5.31)$$

Summarizing:

For a string or cable that is fixed at both ends has constant tension τ and mass per unit length \bar{m}

- The wave velocity is (5.5.9)

$$c = \sqrt{\frac{\tau}{\bar{m}}} \quad (5.5.32)$$

- The natural frequencies are (5.5.23)

$$\omega_n = c \sigma_n = \frac{n \pi c}{L} = n \frac{\pi}{L} \sqrt{\frac{\tau}{\bar{m}}}, \quad n = 0, 1, 2, \dots, \infty \quad (5.5.33)$$

- The mode shapes are (5.5.20)

$$X_n(x) = \sin\left(\frac{n \pi}{L} x\right) \quad (5.5.34)$$

- Initial Condition Response from (5.5.25), (5.5.29), and (5.5.31)

$$w(x, t) = \sum_{i=1}^{\infty} [c_n \sin(\sigma_n x) \sin(c \sigma_n t) + d_n \sin(\sigma_n x) \cos(c \sigma_n t)] \quad (5.5.35)$$

$$c_n = \frac{2}{c \sigma_n L} \int_0^L \dot{w}_0(x) \sin(\sigma_n x) dx, \quad d_n = \frac{2}{L} \int_0^L w_0(x) \sin(\sigma_n x) dx$$

5.5.3 Axial Vibration of a Uniform Bar

Figure 5.5.2 shows the model of a uniform bar with axial vibration and its free body diagram.

The above free body diagram and Newton's law (3.3.5) yield

$$F + dF - F = dm \frac{\partial^2 w}{\partial t^2} = \rho A dx \frac{\partial^2 w}{\partial t^2} \quad (5.5.36)$$

Equations (A.3.16) and (A.4.4) give

$$F = \sigma A = E \epsilon A = EA \frac{\partial w}{\partial x} \quad (5.5.37)$$

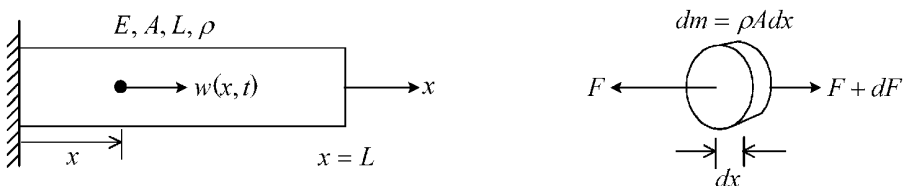


Figure 5.5.2 Continuous mass model of a vibrating bar

which implies

$$dF = \frac{\partial}{\partial x} \left(EA \frac{\partial w}{\partial x} \right) dx \quad (5.5.38)$$

Substitute (5.5.38) into (5.5.36) to obtain

$$\frac{\partial^2 w}{\partial t^2} = c^2 \frac{\partial^2 w}{\partial x^2} \quad (5.5.39)$$

where

$$c = \sqrt{\frac{E}{\rho}} \quad (5.5.40)$$

Equation (5.5.39) has an identical form with (5.5.10); therefore, the general form of the solution for $w(x, t)$ follows from (5.5.11), (5.5.15), and (5.5.22) as

$$w(x, t) = \sum_{n=1}^{\infty} X_n(x) T_n(t) \quad (5.5.41)$$

where

$$X_n(x) = a_{1n} \sin(\sigma_n x) + a_{2n} \cos(\sigma_n x) \quad (5.5.42)$$

$$T_n(t) = A_n \sin(c\sigma_n t) + B_n \cos(c\sigma_n t) \quad (5.5.43)$$

For the BC shown in Figure 5.5.2, the left end is fixed so

$$X_n(0) = 0 = a_{2n} \quad (5.5.44)$$

and there is zero internal force at the free end, $x = L$, so from (5.5.37)

$$\begin{aligned} \Rightarrow \text{at } x=L, \quad F = EA \frac{\partial w}{\partial x} = 0 &\Rightarrow \frac{dX_n}{dx} = 0 \Rightarrow \frac{d}{dx}(a_{1n} \sin(\sigma_n x)) = 0 \\ &\Rightarrow a_{1n} \sigma_n \cos(\sigma_n x) = 0 \end{aligned} \quad (5.5.45)$$

The constant a_{1n} cannot be zero, since if it was then there would be no vibration by (5.5.41)–(5.5.44). Thus, (5.5.45) requires that

$$\Rightarrow \sigma_n = \frac{2n-1}{L} \frac{\pi}{2}, \quad n = 1, 2, 3, \dots, \infty \quad (5.5.46)$$

Equations (5.5.42), (5.5.44), and (5.5.46) show that the mode shapes $X_n(x)$ have the form

$$X_n(x) = a_{1n} \sin\left((2n-1) \frac{\pi x}{2L}\right) \quad (5.5.47)$$

From (5.5.40), (5.5.43), and (5.5.46), the corresponding natural frequencies are

$$\omega_n = c\sigma_n = \sqrt{\frac{E}{\rho}} \frac{(2n-1)\pi}{L} \frac{\pi}{2}, \quad n = 1, 2, 3, \dots, \infty \quad (5.5.48)$$

The above development shows how the BC on the mode shape were essential in determining the natural frequencies. The general form of the response is from (5.5.41), (5.5.43), and (5.5.47)

$$w(x, t) = \sum_{i=1}^{\infty} (c_n \sin(\sigma_n x) \sin(c\sigma_n t) + d_n \sin(\sigma_n x) \cos(c\sigma_n t)) \quad (5.5.49)$$

This form is identical to Equation (5.5.25) for the vibrating string. Therefore, by imposing the ICs

$$w_0(x) = w(x, t=0) \quad (5.5.50)$$

$$\dot{w}_0(x) = \dot{w}(x, t=0) \quad (5.5.51)$$

on (5.5.49) and by using the orthogonality condition (5.5.26), the results found in (5.5.29) and (5.5.31) are found to be applicable for the bar, that is,

$$c_n = \frac{2}{c\sigma_n L} \int_0^L \dot{w}_0(x) \sin(\sigma_n x) dx, \quad d_n = \frac{2}{L} \int_0^L w_0(x) \sin(\sigma_n x) dx \quad (5.5.52)$$

EXAMPLE 5.5.1 *Impact of Translating Bar*

Statement: Consider the bar that is translating to the right with constant velocity $\dot{w}_0(x) = v_0$ and hits and sticks to a barrier as shown in Figure E5.5.1(a).

Objective: Find the initial condition response $w(x, t)$.

Solution: Utilize the fixed-free modes of the model in Figure 5.5.2. Since $w_0(x) = 0$, Equation (5.5.52) implies $d_n = 0$, and substituting $\dot{w}_0(x) = v_0$ into (5.5.52) yields

$$c_n = \frac{2}{c\sigma_n L} v_0 \int_0^L \sin(\sigma_n x) dx = \frac{2v_0}{c\sigma_n L} \left(\frac{-1}{\sigma_n} \right) \cos(\sigma_n x) \Big|_0^L = \frac{-2v_0}{cL\sigma_n^2} (\cos(\sigma_n L) - 1) \quad (1)$$

Collecting results into (5.5.49) yields the initial condition response for this example:

$$w(x, t) = \frac{-2v_0}{cL} \sum_{n=1}^{\infty} \frac{(\cos(\sigma_n L) - 1)}{\sigma_n^2} \sin(\sigma_n x) \sin(\omega_n t) \quad (2)$$

where

$$c = \sqrt{\frac{E}{\rho}}, \quad \sigma_n = \frac{(2n-1)\pi}{L}, \quad n = 1, 2, 3 \quad (3)$$

5.5.4 Torsion of Bars

Consider the bar shown in Figure 5.5.3

The internal torque is denoted by T and the external torque (per unit length) is τ . The balance between torque and integrated shear stress, combined with the material law, yields the standard strength of materials formula

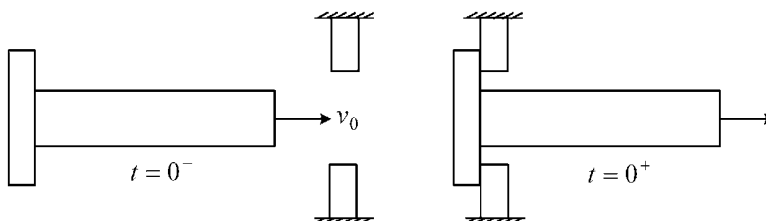


Figure E5.5.1(a) Axial vibration of bar with initial velocity v_0

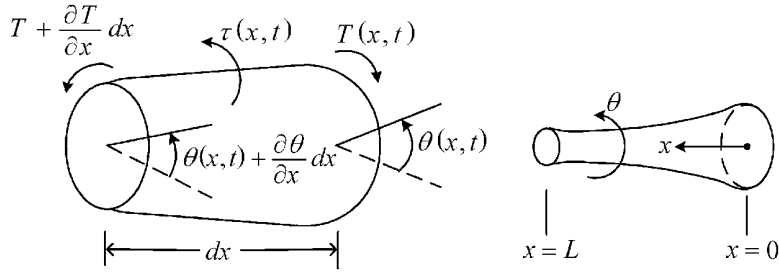


Figure 5.5.3 Bar undergoing pure torsional vibration

$$\frac{\partial \theta}{\partial x} = \frac{T}{J(x)G(x)} \quad (5.5.53)$$

where G is the shear modulus of elasticity and $J(x)$ is the torsion function which depends on the cross-sectional geometry. The simplest cross-sectional geometry is an annulus with outer diameter $d_o(x)$ and inner diameter $d_i(x)$ for which

$$J(x) = \frac{\pi}{32} (d_o^4(x) - d_i^4(x)) \quad (5.5.54)$$

The “torsion constant” in a structural member handbook should be utilized for other geometries such as I beam, channels, box beams, and so on, since for noncircular geometries

$$J(x) \neq I_x + I_y \quad (5.5.55)$$

Application of Newton’s rotational EOM (3.3.46) to the differential bar length in Figure 5.5.3 yields

$$(\tilde{I}_G dx) \frac{\partial^2 \theta}{\partial t^2} = T + \frac{\partial T}{\partial x} dx - T + \tau dx \quad (5.5.56)$$

$$\Rightarrow \tilde{I}_G \frac{\partial^2 \theta}{\partial t^2} = \frac{\partial T}{\partial x} + \tau \quad (5.5.57)$$

where $\tilde{I}_G(x)$ is the mass moment of inertia per unit length, evaluated about the x axis. Substitute T from (5.5.53) into (5.5.57) to obtain

$$\tilde{I}_G \frac{\partial^2 \theta}{\partial t^2} = \frac{\partial}{\partial x} \left(JG \frac{\partial \theta}{\partial x} \right) + \tau(x,t) \quad (5.5.58)$$

For a uniform bar \tilde{I}_G , J and G are constants so that (5.5.58) simplifies to

$$\frac{\partial^2 \theta}{\partial t^2} = \frac{JG}{\tilde{I}_G} \frac{\partial^2 \theta}{\partial x^2} + \frac{\tau(x,t)}{\tilde{I}_G} \quad (5.5.59)$$

Consider the free vibration case ($\tau = 0$) and substitute the separation of variable solution

$$\theta = X(x)T(t) \quad (5.5.60)$$

to obtain

$$\frac{1}{T} \frac{d^2 T}{dt^2} = \frac{JG}{\tilde{I}_G X} \frac{d^2 X}{dx^2} \quad (5.5.61)$$

The LHS of this equation is a function only of t and the RHS is a function only of x ; therefore, both sides must equal to the same constant, say, $-\omega^2$. The separation yields

$$\Rightarrow \frac{d^2 T}{dt^2} + \omega^2 T = 0 \quad (5.5.62)$$

$$\frac{d^2 X}{dx^2} + \frac{\omega^2 \tilde{I}_G}{JG} X = 0 \quad (5.5.63)$$

The solutions to these two ordinary DE are

$$T(t) = \tilde{A} \cos(\omega t) + \tilde{B} \sin(\omega t) \quad (5.5.64)$$

$$X(x) = \tilde{C} \cos\left(\gamma \frac{x}{L}\right) + \tilde{D} \sin\left(\gamma \frac{x}{L}\right) \quad (5.5.65)$$

where

$$\gamma = \omega L \sqrt{\frac{\tilde{I}_G}{JG}} \quad (5.5.66)$$

The natural frequencies ω_i are determined by imposing BC on the solution for $X(x)$ in (5.5.65). For example, consider the fixed-free bar in Figure 5.5.4.

Angle $\theta = 0$ at $x = 0$ for all time t : therefore, from (5.5.60),

$$X(0) = 0 \quad (5.5.67)$$

Torque $T = 0$ at $x = L$ for all time t : therefore, from (5.5.53) and (5.5.60),

$$\left. \frac{dX}{dx} \right|_{x=L} = 0 \quad (5.5.68)$$

Apply (5.5.67) to (5.5.65) to obtain

$$\tilde{C} = 0 \quad (5.5.69)$$

Apply (5.5.68) and (5.5.69) to (5.5.65) to obtain

$$\tilde{D} \frac{\gamma}{L} \cos \gamma = 0 \quad (5.5.70)$$

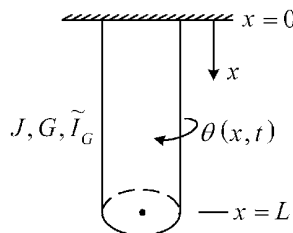


Figure 5.5.4 Fixed-free bar undergoing torsional vibration

If $\tilde{D}=0$, then $X(x)=0$ for all x and t ; however, this implies $\theta(x,t)=0$ for all x and t . This contradicts free vibration (initial condition response) behavior, so it must be true that

$$\cos \gamma = 0 \quad (5.5.71)$$

$$\Rightarrow \gamma_i = \left(i - \frac{1}{2}\right)\pi \quad i = 1, 2, \dots \quad (5.5.72)$$

Therefore, from (5.5.66), the i th natural frequency becomes

$$\omega_i = \left(i - \frac{1}{2}\right)\frac{\pi}{L}\sqrt{\frac{JG}{I_G}}, \quad i = 1, 2, \dots \quad (5.5.73)$$

Note that the BC on the mode shape were instrumental in determining the natural frequencies. From (5.5.65), (5.5.69), and (5.5.72), the i th mode shape is

$$\psi_i(x) = X_i(x) = \sin\left(\gamma_i \frac{x}{L}\right) = \sin\left(\pi\left(i - \frac{1}{2}\right)\frac{x}{L}\right) \quad (5.5.74)$$

Finally, by superposition of (5.5.60), (5.5.64), and (5.5.74), the free vibration response has the form

$$\theta(x,t) = \sum_{i=1}^{\infty} \sin\left(\pi\left(i - \frac{1}{2}\right)\frac{x}{L}\right) (A_i \cos(\omega_i t) + B_i \sin(\omega_i t)) \quad (5.5.75)$$

where ω_i is defined in (5.5.73). The constants in this equation are obtained by considering the ICs

$$\theta(x,0) = \Theta_0(x) = \sum_{i=1}^{\infty} A_i \sin\left(\pi\left(i - \frac{1}{2}\right)\frac{x}{L}\right) \quad (5.5.76)$$

$$\dot{\theta}(x,0) = \Omega_0(x) = \sum_{i=1}^{\infty} B_i \omega_i \sin\left(\pi\left(i - \frac{1}{2}\right)\frac{x}{L}\right) \quad (5.5.77)$$

where $\Theta_0(x)$ and $\Omega_0(x)$ are the known (given) initial angular deflection and angular velocity functions, respectively. Multiply (5.5.76) and (5.5.77) by

$$\sin\left(\pi\left(j - \frac{1}{2}\right)\frac{x}{L}\right) \quad (5.5.78)$$

integrate from 0 to L , and utilize the orthogonality condition

$$\int_0^L \sin\left(\pi\left(j - \frac{1}{2}\right)\frac{x}{L}\right) \sin\left(\pi\left(i - \frac{1}{2}\right)\frac{x}{L}\right) dx = \begin{cases} 0, & i \neq j \\ \frac{L}{2}, & i = j \end{cases} \quad (5.5.79)$$

to obtain

$$A_i = \frac{2}{L} \int_0^L \sin\left(\pi\left(i - \frac{1}{2}\right)\frac{x}{L}\right) * \Theta_0(x) dx \quad (5.5.80)$$

$$B_i = \frac{2}{L\omega_i} \int_0^L \sin\left(\pi\left(i-\frac{1}{2}\right)\frac{x}{L}\right) * \Omega_0(x) dx \quad (5.5.81)$$

5.5.5 Euler–Bernoulli (Classical) Beam Theory

It is assumed that plane sections remain plane (no warping) and perpendicular to the neutral axis, before and after deformation in Figure 5.5.5.

Figure 5.5.6 shows a free body diagram for a differential length (dx) of the beam.

The translational EOM is given by (3.3.5) and Figure (5.5.6) as

$$\rho A dx \frac{\partial^2 w}{\partial t^2} = \tilde{f} dx + V + \frac{\partial V}{\partial x} dx - V = \tilde{f} dx + \frac{\partial V}{\partial x} dx \quad (5.5.82)$$

$$\Rightarrow \rho A \frac{\partial^2 w}{\partial t^2} = \tilde{f} + \frac{\partial V}{\partial x} \quad (5.5.83)$$

where ρ is the mass density of the beam material and

$$\tilde{f}(x, t) = \text{applied load per unit length} \quad (5.5.84)$$

The length of the differential segment in Figure 5.5.6 is infinitesimally short, although its height is finite as shown in Figure 5.5.7.

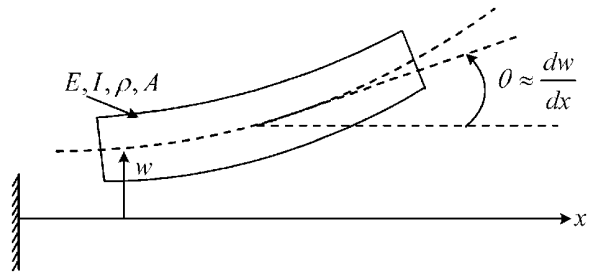


Figure 5.5.5 Euler–Bernoulli beam segment

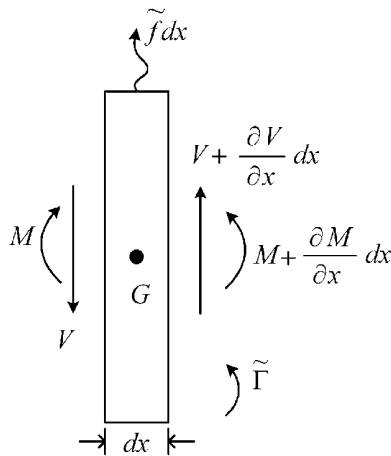


Figure 5.5.6 Free body diagram of differential length of beam

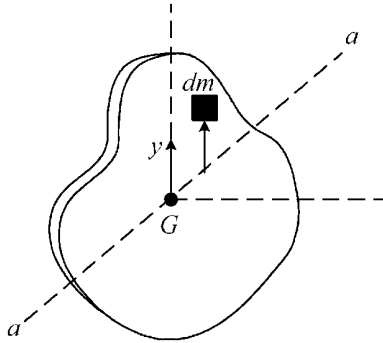


Figure 5.5.7 Differential beam segment

Hence

$$I_G \cong \int y^2 dm = \int y^2 \rho dA dx = \int \rho \left(\int y^2 dA \right) dx = \int \rho I dx = \rho dx I \quad (5.5.85)$$

where I is the area moment of inertia about axis $a-a$ passing through G . Newton's rotational EOM (3.3.46) for Figure 5.5.6 becomes

$$+ \curvearrowleft (\rho dx I) \frac{\partial^2 \theta}{\partial t^2} = \rho dx I \frac{\partial^2}{\partial t^2} \left(\frac{\partial w}{\partial x} \right) = M + \frac{\partial M}{\partial x} dx - M + \frac{dx}{2} \left(V + \frac{\partial V}{\partial x} dx + V \right) + \tilde{\Gamma} dx \quad (5.5.86)$$

where

$$\tilde{\Gamma}(x, t) = \text{applied moment per unit length} \quad (5.5.87)$$

Cancellations and neglect of the dx^2 term in (5.5.86) yield

$$\rho I \frac{\partial^3 w}{\partial t^2 \partial x} = \frac{\partial M}{\partial x} + V + \tilde{\Gamma} \quad (5.5.88)$$

Differentiate (5.5.88) with respect to x to obtain

$$\frac{\partial V}{\partial x} = \rho I \frac{\partial^4 w}{\partial x^2 \partial t^2} - \frac{\partial^2 M}{\partial x^2} - \frac{\partial \tilde{\Gamma}}{\partial x} \quad (5.5.89)$$

Substitution of (5.5.83) into (5.5.89) yields

$$\rho A \frac{\partial^2 w}{\partial t^2} = \rho I \frac{\partial^4 w}{\partial x^2 \partial t^2} - \frac{\partial^2 M}{\partial x^2} - \frac{\partial \tilde{\Gamma}}{\partial x} + \tilde{f} \quad (5.5.90)$$

Recall from the "strength of materials" that the formula for bending strain is

$$\epsilon_B = -y \frac{\partial}{\partial x} \left(\frac{\partial w}{\partial x} \right) \quad (5.5.91)$$

and that integration of differential moments due to the bending stress

$$\sigma_B = E \epsilon_B \quad (5.5.92)$$

over the cross section yields the stress resultant moment

$$M = EI \frac{\partial \theta}{\partial x} = EI \frac{\partial^2 w}{\partial x^2} \quad (5.5.93)$$

Substitution of (5.5.93) into (5.5.90) yields

$$\rho A \frac{\partial^2 w}{\partial t^2} = \rho I \frac{\partial^4 w}{\partial x^2 \partial t^2} - \frac{\partial^2}{\partial x^2} \left(EI \frac{\partial^2 w}{\partial x^2} \right) - \frac{\partial \tilde{\Gamma}}{\partial x} + \tilde{f} \quad (5.5.94)$$

Consider the case of free vibration ($\tilde{f} = \tilde{\Gamma} = 0$) and negligible rotary inertia ($I_G \approx 0$). Then (5.5.94) simplifies to

$$\rho A \frac{\partial^2 w}{\partial t^2} + \frac{\partial^2}{\partial x^2} \left(EI \frac{\partial^2 w}{\partial x^2} \right) = 0 \quad (5.5.95)$$

Further simplification results by assuming a uniform (constant) cross section, yielding

$$\frac{\rho A}{EI} \frac{\partial^2 w}{\partial t^2} + \frac{\partial^4 w}{\partial x^4} = 0 \quad (5.5.96)$$

Utilize separation of variables

$$w = X(x)T(t) \quad (5.5.97)$$

to obtain

$$\frac{\rho A}{EI} X \ddot{T} + X'''' T = 0 \quad (5.5.98)$$

$$\Rightarrow \frac{\rho A}{EI} \frac{\ddot{T}}{T} = - \frac{X''''}{X} \quad (5.5.99)$$

The LHS is a function of t and the RHS is a function of x . This can be true only if both sides equal the same constant:

$$\Rightarrow \frac{-X''''}{X} = -\sigma^4 \quad (5.5.100)$$

$$\frac{\rho A}{EI} \frac{\ddot{T}}{T} = -\sigma^4 \quad (5.5.101)$$

From (5.5.100),

$$X'''' - \sigma^4 X = 0 \quad (5.5.102)$$

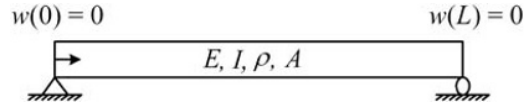
which has the solution

$$X(x) = a \cosh(\sigma x) + b \sinh(\sigma x) + c \cos(\sigma x) + d \sin(\sigma x) \quad (5.5.103)$$

Equation (5.5.101) has the solution form

$$T(t) = e \sin(\omega t) + f \cos(\omega t) \quad (5.5.104)$$

Figure 5.5.8 Simply supported Euler–Bernoulli beam



where

$$\omega = \sigma^2 \sqrt{\frac{EI}{\rho A}} \quad (5.5.105)$$

For illustration, consider the free vibration of the uniform, simply supported beam in Figure 5.5.8.

The deflection and moment are zero at both ends of the beam so from (5.5.97) and (5.5.103)

$$X(0) = a + c = 0 \quad (5.5.106)$$

$$X(L) = a \cosh(\sigma L) + b \sinh(\sigma L) + c \cos(\sigma L) + d \sin(\sigma L) = 0 \quad (5.5.107)$$

$$X''(0) = \sigma^2 a - \sigma^2 c = 0 \quad (5.5.108)$$

$$X''(L) = (a \cosh(\sigma L) + b \sinh(\sigma L) - c \cos(\sigma L) - d \sin(\sigma L))\sigma^2 = 0 \quad (5.5.109)$$

From (5.5.106) and (5.5.108),

$$a = c = 0 \quad (5.5.110)$$

From (5.5.107), (5.5.109), and (5.5.110),

$$b \sinh(\sigma L) = 0 \Rightarrow b = 0 \quad (5.5.111)$$

since \sinh is never zero.

Substitute (5.5.110) and (5.5.111) into (5.5.109) to obtain

$$d \sin(\sigma L) = 0 \quad (5.5.112)$$

$$\Rightarrow \sigma L = n\pi, \quad n = 1, 2, \dots, \infty \quad (5.5.113)$$

Then, from (5.5.105) and (5.5.113), the natural frequencies are

$$\omega_n = \left(\frac{n\pi}{L}\right)^2 \sqrt{\frac{EI}{\rho A}} \quad (5.5.114)$$

Note that the BC on the mode shape were instrumental in determining the natural frequencies. The corresponding mode shapes are obtained from (5.5.103) with $a = b = c = 0$:

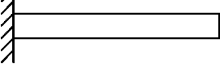
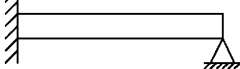
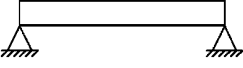
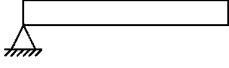
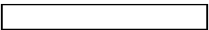
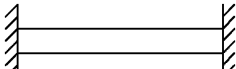
$$X_n(x) = d_n \sin\left(n\pi \frac{x}{L}\right) \quad (5.5.115)$$

The total response is given by

$$w(x, t) = \sum_{n=1}^{\infty} X_n(x) T_n(t) = \sum_{n=1}^{\infty} \sin\left(n\pi \frac{x}{L}\right) * (\alpha_n \sin(\omega_n t) + \beta_n \cos(\omega_n t)) \quad (5.5.116)$$

Table 5.5.1 Beam natural frequencies for common support conditions:

$$\omega_n = \left((\alpha_n L)^2 / L^2 \right) \sqrt{(EI)/(\rho A)}$$

Cantilever 	$(\alpha_1 L)^2 = 3.52$ $(\alpha_2 L)^2 = 22.2$ $(\alpha_3 L)^2 = 61.7$	Clamped-Hinge 	$(\alpha_1 L)^2 = 15.4$ $(\alpha_2 L)^2 = 50$ $(\alpha_3 L)^2 = 104$
Simple Supports 	$(\alpha_1 L)^2 = 9.87$ $(\alpha_2 L)^2 = 39.5$ $(\alpha_3 L)^2 = 88.9$	Hinged-Free 	$(\alpha_1 L)^2 = 0$ $(\alpha_2 L)^2 = 15.4$ $(\alpha_3 L)^2 = 50$
Free-Free 	$(\alpha_1 L)^2 = 22.4$ $(\alpha_2 L)^2 = 61.7$ $(\alpha_3 L)^2 = 121$	Clamped-Clamped 	$(\alpha_1 L)^2 = 22.4$ $(\alpha_2 L)^2 = 61.7$ $(\alpha_3 L)^2 = 121$

where the constants α_n and β_n are determined from the ICs $w(x,0), \partial w / \partial t(x,0)$.

Table 5.5.1 provides natural frequencies and mode shapes for the constant cross section, Euler–Bernoulli beam neglecting rotary inertia, with various support conditions. The free–free beam of course has two zero frequency rigid body modes (5.4.57) along with those shown.

5.5.6 Timoshenko Beam Theory

Classical (Euler–Bernoulli) beam theory imposes the kinematic constraints:

- Plane sections remain plane (no warping).
- Plane sections remain perpendicular to the neutral axis before and after deformation.

Timoshenko developed a beam theory that removes constraint (b).

The slope angle for classical beam theory is $(\partial w / \partial x)$, and the corresponding bending strain is

$$\epsilon_B = -y \frac{\partial}{\partial x} \left(\frac{\partial w}{\partial x} \right) \quad (5.5.117)$$

The plane section actually rotates through a smaller angle

$$\theta < \frac{\partial w}{\partial x} \quad (5.5.118)$$

due to shearing as shown in Figure 5.5.9. Hence, (5.5.117) becomes

$$\epsilon_B = -y \frac{\partial \theta}{\partial x} \quad (5.5.119)$$

It can be shown that γ in Figure 5.5.9 is the shear strain (Appendix A, (A.3.16)), and from this figure

$$\gamma = \frac{\partial w}{\partial x} - \theta \quad (5.5.120)$$

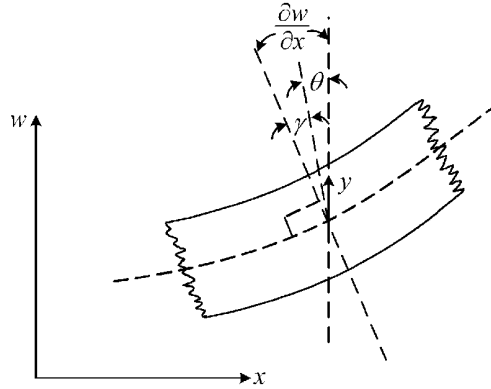
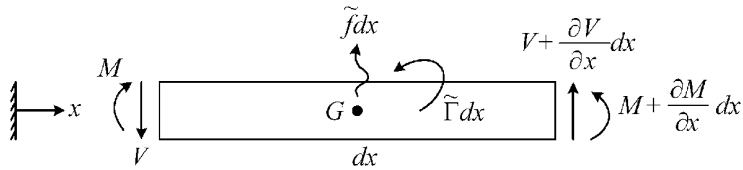


Figure 5.5.9 Timoshenko beam kinematics

Figure 5.5.10 Free body diagram of differential beam segment of length dx

A second alteration of the classical beam theory is the shear stress that is reduced from the average shear stress $\tau_{\text{ave}} = (V/A)$ to a modified, average shear stress

$$\tau_{\text{shear}} = \frac{1}{k} \left(\frac{V}{A} \right) \quad (5.5.121)$$

where k is called a shear form factor and is analytically derived to match strain energies between the approximate model (5.5.121) and a more exact model. For instance, for a circular cross section,

$$k = \frac{6(1+\nu)}{7+6\nu} \quad (5.5.122)$$

where ν is the material's Poisson ratio. The factor k is a standard input for beam elements in commercial finite element codes and is discussed more extensively in Chapter 9. Integration of the moment that results from bending stress ($\sigma_B = E\epsilon_B$) over the cross section yields

$$M = EI \frac{\partial \theta}{\partial x} \quad (5.5.123)$$

where M is shown in Figure 5.5.10.

Newton's translational equation (3.3.5) applied to Figure 5.5.10 yields

$$dm \frac{\partial^2 w}{\partial t^2} = (\rho A(x) dx) \frac{\partial^2 w}{\partial t^2} = V + \frac{\partial V}{\partial x} dx - V + \tilde{f} dx \quad (5.5.124)$$

$$\Rightarrow \rho A(x) \frac{\partial^2 w}{\partial t^2} = \frac{\partial V}{\partial x} + \tilde{f} \quad (5.5.125)$$

where ρ is the mass density of the beam material and

$$\tilde{f} = \text{load per unit length} \quad (5.5.126)$$

Note from (5.5.120) and (5.5.121)

$$V = kA\tau_{\text{shear}} = kA(G\gamma_{\text{shear}}) = kAG\gamma = kAG\left(\frac{\partial w}{\partial x} - \theta\right) \quad (5.5.127)$$

Substitute (5.5.127) into (5.5.125) to obtain

$$\rho A(x) \frac{\partial^2 w}{\partial t^2} = \frac{\partial}{\partial x} \left(kAG \left(\frac{\partial w}{\partial x} - \theta \right) \right) + \tilde{f} \quad (5.5.128)$$

From (5.5.85) and Figure 5.5.10, the Newton's rotational EOM (3.3.46) is

$$\rho \, dx \, I \frac{\partial^2 \theta}{\partial t^2} = M + \frac{\partial M}{\partial x} dx - M + \tilde{\Gamma} dx + \frac{dx}{2} \left(V + \frac{\partial V}{\partial x} dx \right) + \frac{dx}{2} V \quad (5.5.129)$$

where $\tilde{\Gamma}(x, t)$ is an externally applied moment per unit length. Simplification of (5.5.129) by cancelling dx and ignoring second-order (dx^2) terms yields

$$\rho I \frac{\partial^2 \theta}{\partial t^2} = \frac{\partial M}{\partial x} + \tilde{\Gamma} + V \quad (5.5.130)$$

The two coupled PDE for the Timoshenko beam are obtained from (5.5.128) and substitution of (5.5.123) and (5.5.127) into (5.5.130):

$$\rho I \frac{\partial^2 \theta}{\partial t^2} = \frac{\partial}{\partial x} \left(EI \frac{\partial \theta}{\partial x} \right) + kAG \left(\frac{\partial w}{\partial x} - \theta \right) + \Gamma(x, t) \quad (5.5.131)$$

$$\rho A \frac{\partial^2 w}{\partial t^2} = \frac{\partial}{\partial x} \left(kAG \left(\frac{\partial w}{\partial x} - \theta \right) \right) + \tilde{f} \quad (5.5.132)$$

Equations (5.5.131) and (5.5.132) provide two coupled PDE for the unknown rotation angle θ of the cross section and transverse deflection w of the neutral axis.

For free vibration of a uniform beam (constant E , I , A , and G), Equations (5.5.131) and (5.5.132) simplify to

$$\rho I \frac{\partial^2 \theta}{\partial t^2} = EI \frac{\partial^2 \theta}{\partial x^2} + kAG \left(\frac{\partial w}{\partial x} - \theta \right) \quad (5.5.133)$$

$$\rho A \frac{\partial^2 w}{\partial t^2} = kAG \left(\frac{\partial^2 w}{\partial x^2} - \frac{\partial \theta}{\partial x} \right) \quad (5.5.134)$$

These two second-order DE in w and θ may be combined into a single fourth-order DE in w by eliminating θ in Equation (5.5.133). From Equation (5.5.134),

$$\frac{\partial \theta}{\partial x} = \frac{-\rho}{kG} \frac{\partial^2 w}{\partial t^2} + \frac{\partial^2 w}{\partial x^2} \quad (5.5.135)$$

Differentiation of (5.5.133) with respect to x yields

$$\rho I \frac{\partial^2}{\partial t^2} \left(\frac{\partial \theta}{\partial x} \right) = EI \frac{\partial^2}{\partial x^2} \left(\frac{\partial \theta}{\partial x} \right) + kAG \left(\frac{\partial^2 w}{\partial x^2} - \frac{\partial \theta}{\partial x} \right) \quad (5.5.136)$$

Substitution of (5.5.135) into (5.5.136) yields

$$\rho I \frac{\partial^4 w}{\partial t^2 \partial x^2} - \frac{\rho^2 I}{kG} \frac{\partial^4 w}{\partial t^4} = EI \frac{\partial^4 w}{\partial x^4} - \frac{EI \rho}{kG} \frac{\partial^4 w}{\partial x^2 \partial t^2} + kAG \frac{\partial^2 w}{\partial x^2} + \frac{kAG \rho}{kG} \frac{\partial^2 w}{\partial t^2} - kAG \frac{\partial^2 w}{\partial x^2} \quad (5.5.137)$$

$$\Rightarrow EI \frac{\partial^4 w}{\partial x^4} + \frac{\rho^2 I}{kG} \frac{\partial^4 w}{\partial t^4} + \rho I \left(-1 - \frac{E}{kG} \right) \frac{\partial^4 w}{\partial x^2 \partial t^2} + A \rho \frac{\partial^2 w}{\partial t^2} = 0 \quad (5.5.138)$$

Equation (5.5.138) is the desired fourth-order PDE for $w(x, t)$. For illustration, consider the free vibrations of the simply supported beam in Figure 5.5.8. The trial solution

$$w(x, t) = C \sin\left(\frac{n\pi x}{L}\right) \cos(\omega_n t) \quad (5.5.139)$$

satisfies the BC

$$w(0) = w(L) = 0 \quad (5.5.140)$$

for

$$n = 1, 2, 3, \dots, \infty \quad (5.5.141)$$

Substitute (5.5.139) into (5.5.138) to obtain

$$EI \left(\frac{n\pi}{L}\right)^4 + \frac{\rho^2 I}{kG} \omega_n^4 + \rho I \left(-1 - \frac{E}{kG}\right) \omega_n^2 \left(\frac{n\pi}{L}\right)^2 - A \rho \omega_n^2 = 0 \quad (5.5.142)$$

The second term and the first part of the third term on the left-hand side of (5.5.142) are due to the inertial torque caused by bending rotation of the beam and are referred to as rotary inertia terms. Equation (5.5.142) simplifies to the following form if “rotary inertia” is neglected:

$$EI \left(\frac{n\pi}{L}\right)^4 - \frac{\rho IE}{kG} \omega_n^2 \left(\frac{n\pi}{L}\right)^2 - A \rho \omega_n^2 = 0 \quad (5.5.143)$$

$$\Rightarrow \omega_n = \sqrt{\frac{EI \left(\frac{n\pi}{L}\right)^4}{\frac{\rho IE}{kG} \left(\frac{n\pi}{L}\right)^2 + A \rho}} = \sqrt{\frac{\frac{EI}{\rho A} n^4 \pi^4}{L^4 \left(1 + \frac{I E n^2 \pi^2}{A kG L^2}\right)}} \quad (5.5.144)$$

From (5.5.114) and (5.5.144), it results that

$$\frac{\omega_n^2|_{\text{Timoshenko}}}{\omega_n^2|_{\text{Euler}}} = \frac{\frac{EI n^4 \pi^4}{\rho A L^4} / \left(1 + \frac{I E n^2 \pi^2}{A kG L^2}\right)}{\frac{EI n^4 \pi^4}{\rho A L^4}} = \frac{1}{1 + \frac{I E n^2 \pi^2}{A kG L^2}} \quad (5.5.145)$$

which shows that shear deformation becomes important for short beams and for higher-order modes and that the Timoshenko prediction of the n th natural frequency is always less than its Euler–Bernoulli counterpart.

5.6 UNSTABLE FREE VIBRATIONS

The vibration of a structure or machinery component affects, and is affected by, its surrounding medium. The former is illustrated by the sound created by musical instruments, and the latter is illustrated by the dampening effect of oil on the vibrations of a submerged component. In contrast to dissipating energy, vibrations of a structure, structural member, or machinery component in a moving gas or liquid, or in contact with a sliding friction surface, may actually cause the component to absorb energy, thereby increasing its vibration. These “self-excited” or “unstable” vibrations are of growing concerns to designers as structures and machinery become lighter weight and pushed to extreme performance levels to improve efficiency and reduce cost. Some examples include fluid film bearing and seal-induced instabilities in rotating machinery, galloping of power lines, machine tool chatter, whip of pipes transferring high-velocity fluids, airplane wing and turbomachinery blade flutter, wheel shimmy, brake squeal, valve-induced pipe chatter, drillstring stick slip or bit bounce vibration, and so on. The importance of controlling “self-excited,” or unstable, vibrations is clearly recognized by considering that at a certain speed the wings of an aircraft or the body of a vehicle will vibrate violently leading to its destruction. This effect is exacerbated by lighter-weight, more fuel efficient designs. The same holds true for high-speed rotating machinery which we depend on for the production of gasoline, plastics, chemicals, electricity, paper, pharmaceuticals, and so on. Linear system instability is mathematically identified by the presence of one or more system eigenvalues located in the right-hand complex plane, that is, with positive real part. The response of the unstable linear system model approaches infinity as time approaches infinity; however, nonlinear forces will arise in the real system that will restrain the vibrations to a finite amplitude limit cycle, or the system will fracture and fail.

EXAMPLE 5.6.1 *Valve Vibration*

Description: Severe oscillatory vibration of household piping (plumbing) occurs often and is caused by bath, sink, or toilet valves. This is a direct result of flow leaking around a compliantly mounted valve plug as it is gradually opened or closed. To better understand this, consider the flow of a viscous fluid through the small clearance surrounding a compliantly mounted mass as shown in Figure E5.6.1(a).

The cylindrically shaped valve plug mass m is suspended by a compliant material of stiffness k and damping c . The other parameters include:

- D : inner diameter of the pipe,
- Q : volumetric flow rate,
- H : length of gap along m ,
- h : radial clearance ($\ll D$, i.e., thin film),
- μ : absolute viscosity of the fluid,
- P_e : plug perimeter,
- ρ : fluid density,
- u_p : pipe velocity,
- u_m : vertical velocity of m .

Objective: Write the equation of motion for the plug’s vertical displacement (x) assuming laminar leakage flow, and determine an instability onset condition.

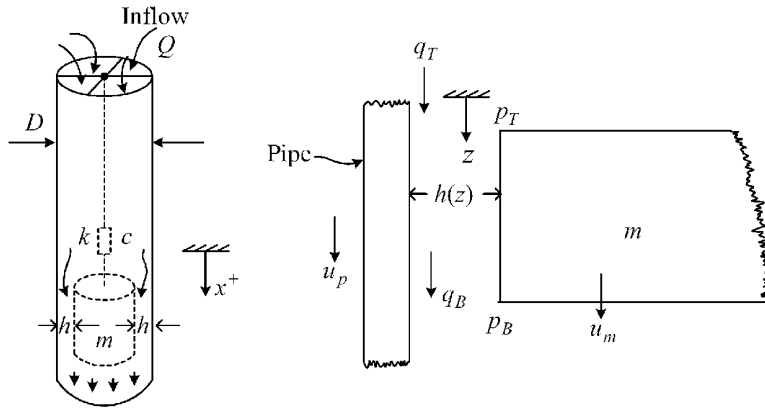


Figure E5.6.1(a) Flow around a valve plug

Solution: Reynolds equation is a statement of mass conservation for the fluid in a thin film (passage), expressed in terms of pressure by utilizing the momentum equation. It is commonly used to determine the pressure distribution in thin lubricant films. The incompressible laminar flow version of Reynolds equation is

$$\frac{\partial}{\partial z} \left(\frac{\rho h^3}{12\mu} \frac{\partial p}{\partial z} \right) = \frac{\partial}{\partial z} (\rho h \bar{u}) + \frac{d}{dt} (\rho h) \quad (1)$$

and its companion flow equation is

$$q = \frac{\rho Q}{P_e} = \rho h \left(-\bar{u} - \frac{h^2}{12\mu} \frac{\partial p}{\partial z} \right) \quad (2)$$

where

$$\bar{u} = \frac{u_p + u_m}{2} = \frac{u_m}{2} = \frac{\dot{x}}{2} \quad (3)$$

since the pipe's velocity is assumed to equal zero. For a constant thickness film,

$$\frac{dh}{dt} = \frac{dh}{dz} = 0 \quad (4)$$

so (1) becomes

$$\frac{d^2 p}{dz^2} = 0 \quad (5)$$

$$\Rightarrow p = az + b \quad (6)$$

where a and b are constants in z . At $z = 0$ (top of mass m),

$$p(0) = p_T \quad (7)$$

$$\Rightarrow p = az + p_T \quad (8)$$

Insert (3) and (8) into (2) to obtain

$$\frac{\rho Q}{P_e} = \rho h \left(-\frac{\dot{x}}{2} - \frac{h^2}{12\mu} a \right) \quad (9)$$

$$\Rightarrow a = -\frac{12\mu}{h^2} \left(\frac{Q}{P_e h} + \frac{\dot{x}}{2} \right) \quad (10)$$

Evaluate (8) at $z=H$ (bottom of m):

$$p_B = aH + p_T \quad (11)$$

$$\Rightarrow \Delta p = p_T - p_B = -aH = \frac{12\mu H}{h^2} \left(\frac{Q}{P_e h} + \frac{\dot{x}}{2} \right) \quad (12)$$

Let x be referenced to the SEP and then Newton's law applied to m yields

$$+ \downarrow m\ddot{x} = -c\dot{x} - kx + \Delta p * \text{Area} \quad (13)$$

$$\Rightarrow m\ddot{x} + c\dot{x} + kx = \frac{\pi D^2}{4} \frac{12\mu H}{h^2} \left(\frac{Q}{P_e h} + \frac{\dot{x}}{2} \right) \quad (14)$$

or

$$m\ddot{x} + \tilde{c}\dot{x} + kx = \frac{3\pi D^2 \mu H Q}{P_e h^3} = \frac{3D^2 \mu H Q}{h^3} \quad (15)$$

where

$$\tilde{c} = c - \frac{3}{2} \pi D^2 \frac{\mu H}{h^2} \quad (16)$$

The damping ratio is

$$\xi = \frac{\tilde{c}}{2m\omega_n} \quad (17)$$

Thus, instability will occur if the damping ratio becomes negative:

$$\xi < 0 \quad (18)$$

$$\Rightarrow c < \frac{3}{2} \pi D^2 \frac{\mu H}{h^2} \quad (19)$$

Or conversely the system will be stable if

$$c > \frac{3}{2} \pi D^2 \frac{\mu H}{h^2} \quad (19)$$

Note that the damping c of the valve plug support part must be large enough to overcome the negative damping effect in order to prevent instability. A design objective may be to keep the right-hand side of (19) small. Thus, a large value of h is desirable so that this instability may be temporarily suppressed by increasing the opening of the valve.

5.6.1 Oil Film Bearing-Induced Instability

The petrochemical and power utility industries utilize thousands of rotating machines with high rpm shafts supported by fluid film bearings. Consider a highly simplified model of the spinning shaft of a turbomachine supported symmetrically by two oil film bearings as depicted in Figure 5.6.1.

The viscosity of the oil causes it to be dragged by the shaft into the converging clearance creating a lift pressure that supports the shaft as shown in Figure 5.6.2.

The oil loses energy in going from the converging to the diverging side due to shear losses. Thus, the pressure in the oil film is not symmetric about the line connecting the centers of the bearing and the shaft. The higher pressure on the converging side produces a force with a component along the line of centers (lift force F_L) and with a component F_D perpendicular to the line of centers in the direction of shaft spin. The latter is the source of the so-called “destabilizing” component of bearing force. The shaft center is displaced away from the bearing center due to static loading, which arises from the shaft weight, gear forces, hydraulic side loads, and so on that act on the shaft. The statically displaced position of the shaft center is called the equilibrium position. Vibrations of the shaft occur about the equilibrium position and are due to mass imbalance, bearing and seal forces, misalignment, flow forces, and so on. For example, the shaft center B may whirl in a nearly circular orbit about the equilibrium position A' as depicted in Figure 5.6.3 and described by the equations

$$x = a \cos \Omega t, \quad y = a \sin \Omega t \quad (5.6.1)$$

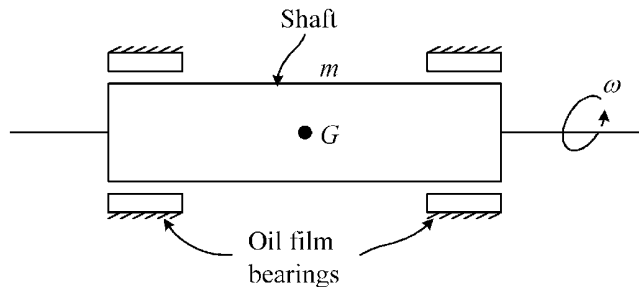


Figure 5.6.1 Spinning shaft supported by two identical oil film bearings

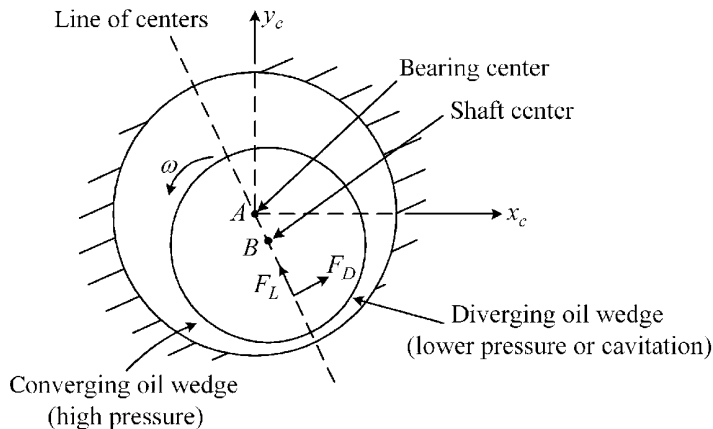


Figure 5.6.2 Spinning shaft supported by oil film bearing

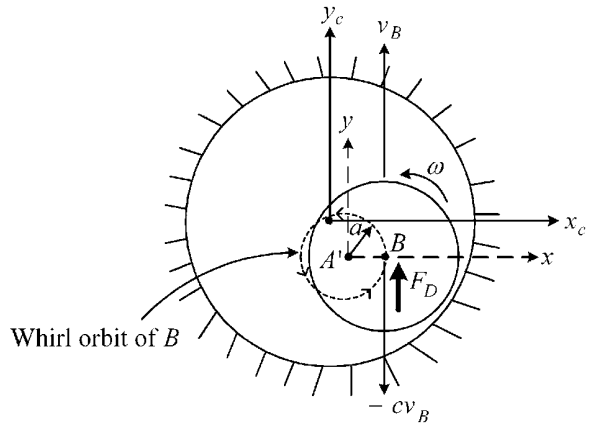


Figure 5.6.3 Circular whirl vibration of a shaft in a fluid film bearing

where B “whirls” with frequency Ω and radius a .

Figure 5.6.3 shows that if the shaft center is along the x axis, the “destabilizing force component” is in the y direction, that is, in the direction of v_B , while the damping force ($-cv_B$) is in the opposite direction. This explains the name “destabilizing force component” since it opposes the damping force.

Researchers solve the fluid dynamic equations (momentum, continuity) to obtain the stiffness and damping coefficients of fluid film bearings. These coefficients represent a linearization of the actual nonlinear forces exerted by the lubricant film on the shaft for small motions about the shaft’s equilibrium position. The clearance distribution changes in the bearing as a result of the vibration of the shaft. The clearance distribution changes the oil film pressure distribution, which changes the forces, as represented in terms of the stiffness and damping coefficients. Oil film bearing stiffness and damping coefficients are provided by design catalogs (Someya, 2014) and commercially available software (Texas A&M Turbomachinery Lab, University of Virginia ROMAC, Dyrobes, and others) for many types of bearings. The data is typically presented versus a nondimensional number called the Sommerfeld number S :

$$S = \frac{\mu N_s L D}{W_B} \left(\frac{R}{c_B} \right)^2 \quad (5.6.2)$$

where

μ = absolute viscosity,

N_s = shaft speed in revolutions/second,

L = bearing length,

D = bearing diameter,

W_B = weight supported by the bearing,

R = shaft radius,

c_B = bearing radial clearance (bearing internal radius–shaft outer radius)

The linearized model reaction force exerted on the shaft by the bearing is composed of a static component that reacts against the static weight and/or machinery steady force loading and a dynamic component expressed by

$$\begin{aligned} F_x &= -k_{xx}x - k_{xy}y - c_{xx}\dot{x} - c_{xy}\dot{y}, \\ F_y &= -k_{yx}x - k_{yy}y - c_{yx}\dot{x} - c_{yy}\dot{y} \end{aligned} \quad (5.6.3)$$

The nondimensional stiffness (\bar{k}_{ij}) and damping (\bar{c}_{ij}) coefficients provided by the catalogs or software are related to the actual stiffness (k_{ij}) and damping (c_{ij}) through the relations

$$k_{xx} = \frac{W_B}{c_B} \bar{k}_{xx}, \quad k_{xy} = \frac{W_B}{c_B} \bar{k}_{xy}, \quad k_{yx} = \frac{W_B}{c_B} \bar{k}_{yx}, \quad k_{yy} = \frac{W_B}{c_B} \bar{k}_{yy} \quad (5.6.4)$$

$$c_{xx} = \frac{W_B}{\omega c_B} \bar{c}_{xx}, \quad c_{xy} = \frac{W_B}{\omega c_B} \bar{c}_{xy}, \quad c_{yx} = \frac{W_B}{\omega c_B} \bar{c}_{yx}, \quad c_{yy} = \frac{W_B}{\omega c_B} \bar{c}_{yy} \quad (5.6.5)$$

EXAMPLE 5.6.2 Rigid Rotor on Fluid Film Bearings

Let the rotor weight in Figure 5.6.1 be

$$W = 100 \text{ lbs} \quad (1)$$

Then the static load on each bearing becomes

$$W_B = \frac{100}{2} = 50 \text{ lbs} \quad (2)$$

The bearing parameter values are

$$\mu = 3.0 \times 10^{-6} \text{ lb.s/in.}^2, \quad L = 3.0 \text{ in.}, \quad D = 4.0 \text{ in.}, \quad R = \frac{D}{2} = 2.0 \text{ in.}, \quad c_B = 0.007 \text{ in.} \quad (3)$$

Consider the five shaft speeds

$$60 * N_s \in (330 \text{ rpm}, 814 \text{ rpm}, 2113 \text{ rpm}, 4522 \text{ rpm}, 6084 \text{ rpm}) \quad (4)$$

The Sommerfeld numbers for these shaft speeds are obtained from (5.6.2) and (2)–(4) as

$$S \in (0.323, 0.789, 2.07, 4.43, 5.96) \quad (5)$$

The nondimensional stiffness and damping constants for the two-groove cylindrical oil film bearing depicted in Figure E5.6.2(a) are listed in Table E5.6.2(a). This table also provides the SEP eccentricity ratio

$$\epsilon = \frac{\text{static offset of shaft from its centered position}}{c_B} \quad (6)$$

and the SEP attitude angle

$$\phi = \text{angle between the line of centers and the load direction} \quad (7)$$

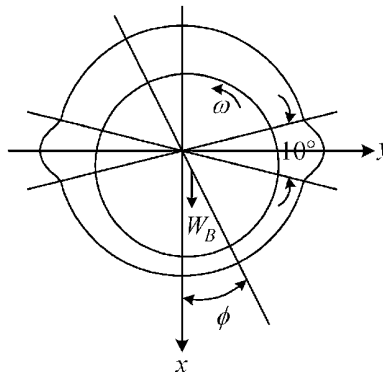
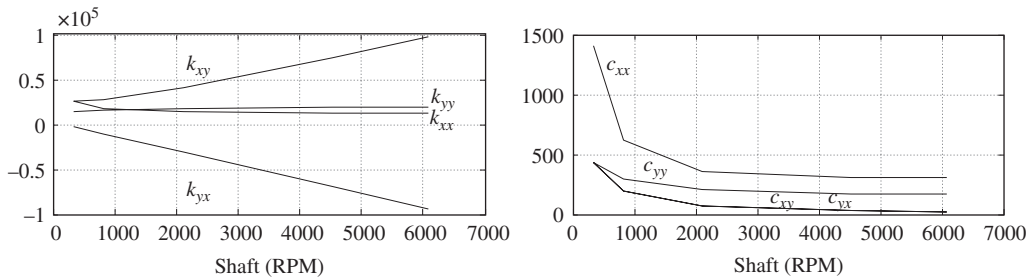
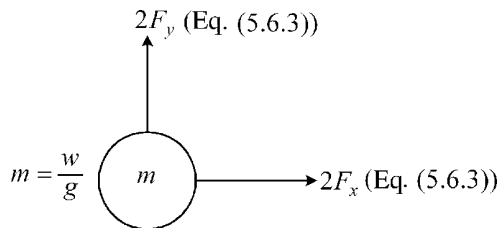


Figure E5.6.2(a) Two-groove cylindrical oil film bearing

Table E5.6.2(a) Bearing coefficients for the example bearing

S	Eccentricity and attitude angle		Stiffness coefficient				Damping coefficients			
	ϵ	ϕ	\bar{k}_{xx}	\bar{k}_{xy}	\bar{k}_{yx}	\bar{k}_{yy}	\bar{c}_{xx}	\bar{c}_{xy}	\bar{c}_{yx}	\bar{c}_{yy}
5.96	0.0750	82.6	1.77	13.6	-13.1	2.72	27.2	2.06	2.06	14.9
4.43	0.100	80.4	1.75	10.3	-9.66	2.70	20.6	2.08	2.08	11.4
2.07	0.200	71.6	1.88	5.63	-4.41	2.56	11.2	2.22	2.22	6.43
0.798	0.400	57.5	2.39	3.75	-1.57	2.17	7.32	2.24	2.24	3.50
0.373	0.600	44.7	3.65	3.62	-0.427	1.92	6.81	2.08	2.08	2.06

**Figure E5.6.2(b)** Bearing stiffness (lb/in.) and damping (lb.s/in.) versus shaft speed. Values are for each bearing**Figure E5.6.2(c)** FBD of shaft with oil film bearings

Equation (5.6.2) and Table E5.6.2(a) show that S becomes smaller and ϵ becomes larger as the static load W_B on the shaft increases.

Figure E5.6.2(b) shows the dimensional stiffness and damping from Table E5.6.2(a) and Equations (5.6.4) and (5.6.5). Note that the cross-coupled stiffnesses (k_{xy} , k_{yx}) are of opposite sign and increase with shaft rpm. From the discussion of circulatory stiffness matrices (reference: Figure 5.3.4), it will be recognized that this behavior of the cross-coupled stiffness coefficients will increase the likelihood for unstable eigenvalues as the speed increases. This propensity toward instability is exacerbated by the decrease in damping with increased speed shown in Figure E5.6.2(b).

The free body diagram for the shaft in Figure 5.6.1 is shown in Figure E5.6.2(c). Note that both bearings contribute to the forces and that the model is valid only for the cylindrical (bounce) rotor mode vibration in which both ends of the rotor have identical motions.

From this figure,

$$\begin{bmatrix} m & 0 \\ 0 & m \end{bmatrix} \begin{Bmatrix} \ddot{x} \\ \ddot{y} \end{Bmatrix} + \begin{bmatrix} 2c_{xx} & 2c_{xy} \\ 2c_{yx} & 2c_{yy} \end{bmatrix} \begin{Bmatrix} \dot{x} \\ \dot{y} \end{Bmatrix} + \begin{bmatrix} 2k_{xx} & 2k_{xy} \\ 2k_{yx} & 2k_{yy} \end{bmatrix} \begin{Bmatrix} x \\ y \end{Bmatrix} = \begin{Bmatrix} 0 \\ 0 \end{Bmatrix} \quad (8)$$

Let

$$\begin{Bmatrix} x \\ y \end{Bmatrix} = \begin{Bmatrix} \hat{x} \\ \hat{y} \end{Bmatrix} e^{\lambda t} \quad (9)$$

In general, λ may be complex, that is,

$$\lambda = a + i\omega_d \quad (10)$$

Then, from (9),

$$x = \hat{x}e^{\lambda t} = \hat{x}e^{(a+i\omega_d)t} = \hat{x}e^{at}e^{i\omega_d t} \quad (11)$$

Note from (11) that the real part of the eigenvalue

$$a = \text{Real}(\lambda) \quad (12)$$

determines stability, that is,

$$\text{if } a < 0, \quad e^{at} \rightarrow 0 \quad \text{as } t \rightarrow \infty \quad (\text{stable}) \quad (13)$$

$$\text{if } a > 0, \quad e^{at} \rightarrow \infty \quad \text{as } t \rightarrow \infty \quad (\text{unstable}) \quad (14)$$

Note also from (11) that the imaginary part of the eigenvalue

$$\omega_d = \text{imaginary}(\lambda) \quad (15)$$

determines the damped natural frequency, that is, from (11),

$$e^{i\omega_d t} = \cos(\omega_d t) + i \sin(\omega_d t) \quad (16)$$

To obtain the λ 's in (9), insert (9) into (8):

$$\begin{bmatrix} \lambda^2 m + 2c_{xx}\lambda + 2k_{xx} & 2c_{xy}\lambda + 2k_{xy} \\ 2c_{yx}\lambda + 2k_{yx} & \lambda^2 m + 2c_{yy}\lambda + 2k_{yy} \end{bmatrix} \begin{Bmatrix} \hat{x} \\ \hat{y} \end{Bmatrix} = \begin{Bmatrix} 0 \\ 0 \end{Bmatrix} \quad (17)$$

In order for the system to vibrate, the determinant of the matrix in (17) must be zero. This yields the system characteristic equation

$$\text{CE} \Rightarrow \text{Det} \begin{bmatrix} \lambda^2 m + 2c_{xx}\lambda + 2k_{xx} & 2c_{xy}\lambda + 2k_{xy} \\ 2c_{yx}\lambda + 2k_{yx} & \lambda^2 m + 2c_{yy}\lambda + 2k_{yy} \end{bmatrix} = 0 \quad (18)$$

$$\begin{aligned} \Rightarrow & \lambda^4 (m^2) + \lambda^3 [2m(c_{xx} + c_{yy})] + \lambda^2 [2m(k_{xx} + k_{yy}) + 4(c_{xx}c_{yy} - c_{xy}c_{yx})] \\ & + \lambda [4(c_{xx}k_{yy} + c_{yy}k_{xx} - c_{xy}k_{yx} - c_{yx}k_{xy})] + [4(k_{xx}k_{yy} - k_{xy}k_{yx})] = 0 \end{aligned} \quad (19)$$

Equation (19) is of the form

$$b_4 \lambda^4 + b_3 \lambda^3 + b_2 \lambda^2 + b_1 \lambda + b_0 = 0 \quad (20)$$

where the b_i are real numbers. Take the complex conjugate of (20), noting that the conjugate of a real number, that is,

$$\bar{b}_2 = \overline{b_2 + i0} = b_2 - i0 = b_2 \quad (21)$$

is the real number itself. Therefore,

$$b_4\bar{\lambda}^4 + b_3\bar{\lambda}^3 + b_2\bar{\lambda}^2 + b_1\bar{\lambda} + b_0 = 0 \quad (22)$$

Comparison of (20) and (22) shows that

If λ solves the CE, then $\bar{\lambda}$ also does, where $\bar{\lambda} = \overline{a + i\omega_d} = a - i\omega_d$.

For the example with stiffness and damping constants in Table E5.6.2(a), there exist two negative real eigenvalues, λ_1 and λ_2 , that are stable by Equation (13). The two remaining eigenvalues are a complex conjugate pair:

$$\lambda_4 = \bar{\lambda}_3 \quad (23)$$

Figure E5.6.2(d) shows the real and imaginary parts of λ_3 versus the five shaft speeds considered in (4) and Table E5.6.2(a). The real part of λ_3 crosses from negative (stable system) to positive (unstable system) values at about 5200 rpm, at which speed the third mode natural frequency is about 57 Hz (3420 cycles per minute (cpm)).

Equation (8) may be written in state space form as

$$\dot{v}_x = \frac{1}{m} (-2k_{xx}x - 2k_{xy}y - 2c_{xx}v_x - 2c_{xy}v_y) \quad (24)$$

$$\dot{v}_y = \frac{1}{m} (-2k_{yx}x - 2k_{yy}y - 2c_{yx}v_x - 2c_{yy}v_y) \quad (25)$$

$$\dot{x} = v_x, \quad \dot{y} = v_y \quad (26)$$

Equations (24)–(26) are numerically integrated with the initial conditions

$$v_x(0) = v_y(0) = 0, \quad x(0) = y(0) = 0.0001 \text{ in.} \quad (27)$$

Figure E5.6.2(e): (i) shows x versus t at a speed of 4522 rpm. Since this speed is less than the instability onset speed (5200 rpm), the motion is stable (decays toward zero). Figure E5.6.2(e): (ii) shows x versus t at 6084 rpm, that is, above the instability onset speed (5200 rpm). Now the motion is clearly unstable (diverging toward infinity as time increases). The period of the motion is seen to be about 0.0159 seconds which corresponds to a frequency of 63 Hz. This is very close to the damped natural frequency, at 6084 rpm, as shown in Figure E5.6.2(d). The motion in the actual machine would be bounded by a limit cycle due to nonlinear forces in the bearings as the motion increases.

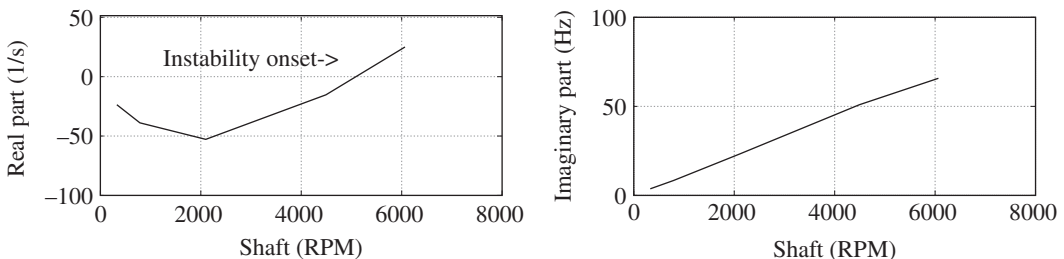


Figure E5.6.2(d) Real and imaginary parts of the third eigenvalue versus shaft RPM

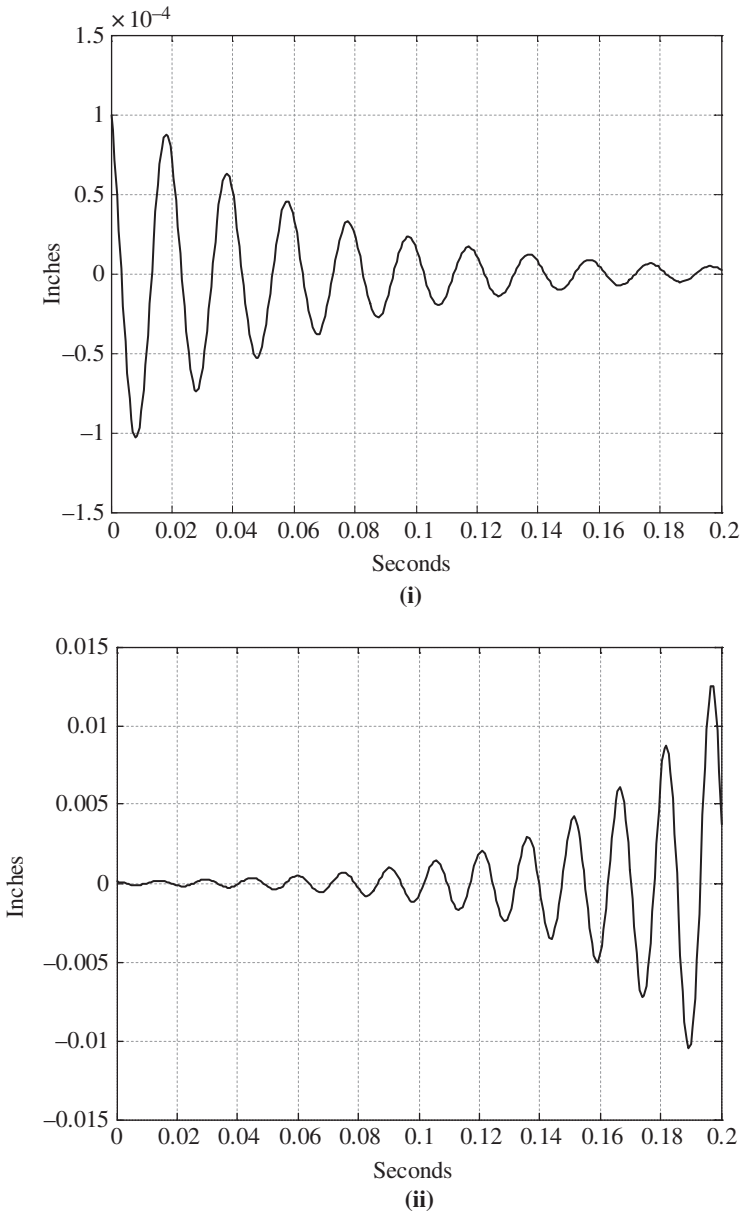


Figure E5.6.2(e) X versus time at (i) 4522 rpm and (ii) 6084 rpm

Some summary points from this example are as follows:

- Unlike “resonance,” unstable (self-excited) vibrations do not require external forces to sustain the unstable vibrations.
- In practice, operation above an instability onset speed is nearly always impossible, that is, the machine will wreck.
- Stability/instability may be determined solely by the real part of the eigenvalues, that is,
 - if negative \rightarrow stable system, if positive \rightarrow unstable system

- Instability is a system design problem, that is, to correct it some mechanical or operations related parameters must be altered. In general, the reduction of external forces will not correct an instability.
-

5.7 SUMMARY

The topics covered in Chapter 5 should provide the reader with an understanding and working knowledge of:

- (a) Free vibration analysis for linear 1, 2, N , and ∞ dof systems
- (b) Solution for natural frequencies, mode shapes, and damping ratios given the linear EOMs
- (c) Solution for initial condition responses of linear system
- (d) Understanding of the beat phenomena and gyroscopic torque effects on natural frequencies
- (e) Formation of a damping matrix that “produces” desired modal damping ratios
- (f) Understanding of orthogonality and biorthogonality relationships between modes
- (g) A capability to solve continuous system models for providing examples to benchmark finite element models against
- (h) Understanding of unstable vibrations and related mathematical modeling approach

5.8 CHAPTER 5 EXERCISES

5.8.1 Exercise Location

All exercises may be conveniently viewed and downloaded at the following web site: **www.wiley.com/go/palazzolo**. This new feature greatly reduces the length of the printed book, yielding a significant cost savings for the college student, and is updated.

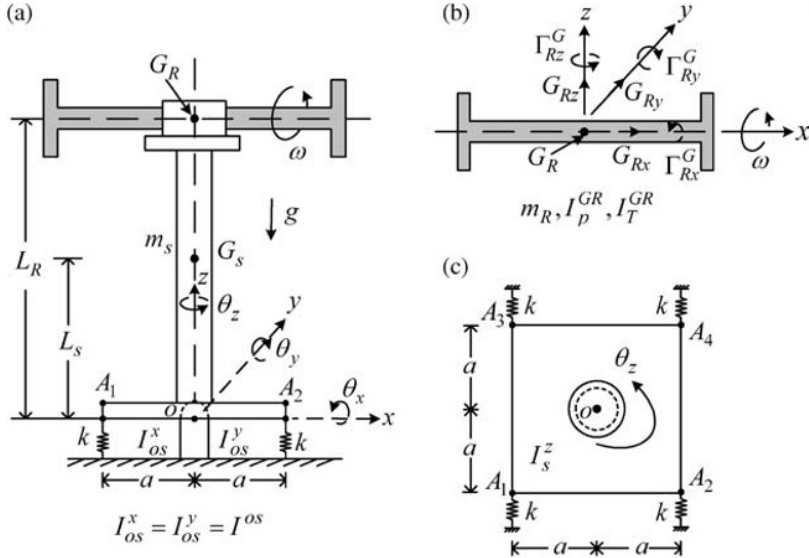
5.8.2 Exercise Goals

The goal of the exercises in Chapter 5 is to strengthen the student’s understanding and related engineering problem-solving skills in the following areas:

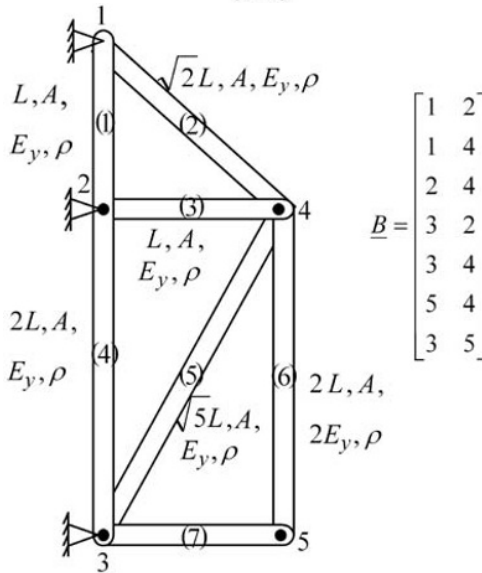
- (a) The mathematical aspects of free vibration, including eigenvalues, eigenvectors, orthogonality, biorthogonality, modal coordinates, and so on
- (b) Determination of natural frequencies, damping ratios (log decrements), and modes shapes from the governing DE
- (c) Calculation of free vibration response due to initial conditions
- (d) Determination of free vibration parameters for both rigid body and flexible body systems (derived by assumed modes, finite elements, or continuous member modeling)
- (e) Calculation of orthogonal damping matrices given a subset of damping ratios and natural frequencies
- (f) Understand the nature of unstable vibratory systems and to obtain conditions for instability in term of system constant values

5.8.3 Sample Exercises: 5.25 and 5.35

These challenging exercises task the student with obtaining speed-dependent natural frequencies of a high-speed grinder and the natural frequencies and mode shapes of a finite element truss model.



(5.25)



(5.35)

REFERENCES

CLOUGH, R. W. and PENZIEN, J. *Dynamics of Structures*, McGraw Hill, New York, 1975.
 CRAIG, R. *Structural Dynamics*, John Wiley & Sons, Inc., New York, 1981.

420 Vibration Theory and Applications with Finite Elements and Active Vibration Control

FRANKLIN, J. N. *Matrix Theory*, Prentice Hall, Englewood Cliffs, NJ, 1968.

PALAZZOLO, A. and PILKEY, W. "Eigensolution Extraction Methods," Ch. 1, Section 1.2, *Finite Element Handbook*, Part 4, McGraw Hill, New York, 1987, pp. 4.36–4.54.

ROARK, R. and YOUNG, W. *Formulas for Stress and Strain*, 5th ed., McGraw Hill, New York, 1975, pp. 368.

SOMEYA, T. *Journal Bearing Databook*, Springer Verlag, Berlin, 2014.

Chapter 6

Vibration Response Due to Transient Loading

6.1 INTRODUCTION

Structural or mechanical systems are often subjected to forces that may be aperiodic. Examples of these include step, ramp, impulse, random, or any other form of *nonperiodic loading*. It is often necessary to determine the displacement, velocity, acceleration, or stress responses to these loads as part of the design process, troubleshooting, or accident reconstruction. This chapter presents concepts and methodology for predicting the response of structural systems to aperiodic, that is, transient and external, forces. The emphasis will be on determining the system's total transient response due to initial conditions (ICs), applied external forces, and/or support motion. Both single and multiple (N) degree of freedom systems are considered. Methods of solution include both analytical (closed-form) and numerical integration (NI)-based approaches. Condensation techniques are provided to reduce the dimensionality of the problem in order to provide faster computer simulations.

6.2 SINGLE DEGREE OF FREEDOM TRANSIENT RESPONSE

This type of system is treated as a special case of N dof systems because closed-form solutions are possible. It is also worth examining closely since the orthogonality or biorthogonality conditions of modes discussed in Chapter 5 may be used to transform N dof problems into a set of uncoupled single degree of freedom (SDOF) modal coordinate equations, as discussed in Section 6.3.

In general, the solution of a linear ordinary differential equation (ODE) consists of a homogeneous part x_h and particular part x_p , that is, if

$$L(x) = f \quad (6.2.1)$$

where L is a linear differential operator, then

$$x = x_h + x_p \quad (6.2.2)$$

where

$$L(x_p) = f \quad (6.2.3)$$

$$L(x_h) = 0 \quad (6.2.4)$$

The proof of this follows from the linearity of L , that is,

$$L(y+z) = L(y) + L(z) \quad (6.2.5)$$

Therefore, if one determines functions x_p and x_h that satisfy (6.2.3) and (6.2.4) and then defines the total solution as

$$x = x_h + x_p \quad (6.2.6)$$

it follows that

$$L(x) = L(x_h + x_p) = L(x_h) + L(x_p) = 0 + f = f \quad (6.2.7)$$

Therefore, x as defined in (6.2.6) is the solution of the original ODE (6.2.1).

6.2.1 Direct Analytical Solution Method

This approach relies on the availability of solutions to standard forms of differential equations. The steps include the following:

- (a) Find a solution (x_h) of the homogeneous ODE including unknown integration constants $L(x_h) = 0$.
- (b) Find a solution (x_p) of the particular ODE $L(x_p) = f$.
- (c) Define the total solution as $x = x_h + x_p$.
- (d) Impose ICs on the total solution x to determine the unknown integration constants.

EXAMPLE 6.2.1 *Pressure Relief Valve Blowout on Natural Gas Meter*

Statement: Figure E6.2.1(a) depicts the rupture of a pressure relief valve on a gas meter supported by a vertical pipe.

The stream of the outflowing gas has a velocity v_g , and the resulting side force acting on the meter is approximately

$$F_p = \rho A v_g^2 = cp \quad (1)$$

where c is a constant that depends on ρ , A and the orifice constant for the PRV.

Objective: Determine the motion $u_m(t)$ and the stress at the base of the pipe for the three pressure histories

$$p(t) = p_0 \text{ (step), } \tilde{p}_0 t \text{ (ramp), } p_0 e^{-\gamma t} \text{ (exponential)} \quad (2)$$

Assumptions:

- (a) Small motions.
- (b) The mass of the pipe is negligible compared to mass of the meter.
- (c) The meter is treated as a point mass.
- (d) Both u_m and \dot{u}_m are zero at $t = 0$.

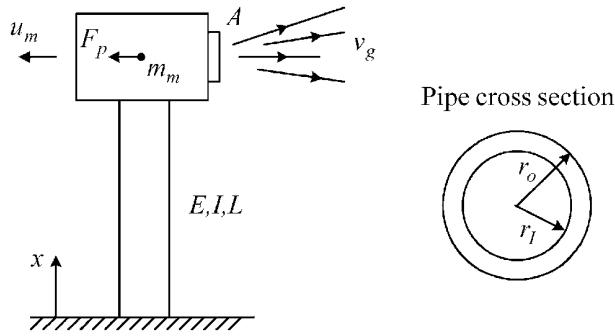


Figure E6.2.1(a) Pressure release valve (PRV) event occurring on gas meter

Solution:

- (a) From the strength of materials, the horizontal force and horizontal deflection at the top of the pipe are related by $F_{\text{pipe}} = ku_m$ where the lateral stiffness of the pipe is

$$k = \frac{3EI}{L^3} \quad (3)$$

so Newton's law (3.3.5) for the meter provides

$$m_m \ddot{u}_m + ku_m = F_p(t) = cp(t) \quad (4)$$

- (b) The solution to the homogeneous ($p = 0$) form of (3) is

$$u_{\text{mh}} = A \cos \omega_n t + B \sin \omega_n t \quad (5)$$

where $\omega_n = (k/m_m)^{1/2}$ is the undamped natural frequency and A and B are the arbitrary constants of integration.

- (c) The particular solutions are selected to have the same form as the right-hand side (RHS) of the ODE, that is, f in (6.2.1):

Case 1: Find the particular solution for $p = p_0 = \text{constant}$.

From (4),

$$m_m \ddot{u}_{mp} + ku_{mp} = cp_0 \quad (6)$$

Since cp_0 is a constant, let

$$u_{mp} = \text{constant} = u_0 \Rightarrow m_m * 0 + ku_0 = cp_0 \Rightarrow u_{mp} = u_0 = \frac{cp_0}{k} \quad (7)$$

Case 2: Find the particular solution for $p = \tilde{p}_0 t$.

From (4),

$$m_m \ddot{u}_{mp} + ku_{mp} = c\tilde{p}_0 t \quad (8)$$

Since $c\tilde{p}_0 t$ is a linear function of t , let

$$u_{mp} = a_0 + a_1 t \Rightarrow m_m * 0 + k(a_0 + a_1 t) = c\tilde{p}_0 t$$

Equating coefficients of like powers of t yields

$$a_0k=0, \text{ and } ka_1=cp_0 \Rightarrow u_{mp}(t)=\frac{c\tilde{p}_0}{k}t \quad (9)$$

Case 3: Find the particular solution for $p=p_0e^{-\gamma t}$.

From (4),

$$m_m\ddot{u}_{mp}+ku_{mp}=cp_0e^{-\gamma t} \quad (10)$$

Since $cp_0e^{-\gamma t}$ is an exponential function of time, let

$$\begin{aligned} u_{mp} &= \beta e^{-\gamma t} \Rightarrow m_m\beta\gamma^2 e^{-\gamma t} + k\beta e^{-\gamma t} = cp_0e^{-\gamma t} \\ &\Rightarrow \beta = \frac{cp_0}{m_m\gamma^2 + k} \Rightarrow u_{mp} = \frac{cp_0e^{-\gamma t}}{m_m\gamma^2 + k} \end{aligned} \quad (11)$$

(d) The total solution is the sum of the homogeneous and particular solutions ($u_m = u_{mh} + u_{mp}$):

Case 1 ($p = p_0$):

$$u_m(t) = A \cos \omega_n t + B \sin \omega_n t + \frac{cp_0}{k} \quad (12)$$

Case 2 ($p = \tilde{p}_0 t$):

$$u_m(t) = A \cos \omega_n t + B \sin \omega_n t + \frac{c\tilde{p}_0}{k}t \quad (13)$$

Case 3 ($p = p_0e^{-\gamma t}$):

$$u_m(t) = A \cos \omega_n t + B \sin \omega_n t + \frac{cp_0e^{-\gamma t}}{m_m\gamma^2 + k} \quad (14)$$

(e) The ICs

$$u_m(0) = \dot{u}_m(0) = 0 \quad (15)$$

are applied to each case to yield the final form of the responses:

Case 1: $p = p_0$.

From (12),

$$\begin{aligned} u_m(0) = 0 &\Rightarrow A = \frac{-cp_0}{k} \\ \dot{u}_m(0) = 0 &\Rightarrow \omega_n B = 0 \Rightarrow B = 0 \Rightarrow u_m(t) = \frac{cp_0}{k}(1 - \cos \omega_n t) \end{aligned} \quad (16)$$

Case 2: $p = \tilde{p}_0 t$.

From (13),

$$\begin{aligned} u_m(0) = 0 &\Rightarrow A = 0 \\ \dot{u}_m(0) = 0 &\Rightarrow B\omega_n + \frac{c\tilde{p}_0}{k} = 0 \Rightarrow B = \frac{-c\tilde{p}_0}{k\omega_n} \\ &\Rightarrow u_m(t) = \frac{c\tilde{p}_0}{k} \left(t - \frac{1}{\omega_n} \sin \omega_n t \right) \end{aligned} \quad (17)$$

Case 3: $p = p_0 e^{-\gamma t}$.

Let $\alpha = cp_0 / (m_m \gamma^2 + k)$, and then from (14),

$$u_m(0) = A + \alpha = 0 \Rightarrow A = -\alpha$$

$$\dot{u}_m(0) = B\omega_n - \gamma\alpha = 0 \Rightarrow B = \frac{\gamma\alpha}{\omega_n}$$

$$\Rightarrow u_m(t) = \frac{cp_0}{m_m \gamma^2 + k} \left(e^{-\gamma t} - \cos \omega_n t + \frac{\gamma}{\omega_n} \sin \omega_n t \right) \quad (18)$$

- (f) The preceding cases all involved undamped systems. Consider the effects of damping by including the damping force $c_m \dot{u}_m$ in (4):

$$m_m \ddot{u}_m + c_m \dot{u}_m + k u_m = F_p(t) = cp(t) \quad (19)$$

Dividing by m_m yields

$$\ddot{u}_m + 2\xi\omega_n \dot{u}_m + \omega_n^2 u_m = \frac{F_p(t)}{m_m} = \frac{cp(t)}{m_m} \quad (20)$$

The solution to the homogeneous form ($F = p = 0$) of (20) is

$$u_{mh}(t) = e^{-\xi\omega_n t} (A \cos(\omega_d t) + B \sin(\omega_d t)) \quad (21)$$

where A and B are integration constants determined from the ICs.

For illustration, consider the case 2 loading $p = \tilde{p}_0 t$ so that (20) becomes

$$\ddot{u}_m + 2\xi\omega_n \dot{u}_m + \omega_n^2 u_m = \frac{c\tilde{p}_0 t}{m_m} \quad (22)$$

Since $c\tilde{p}_0 t / m_m$ is a linear function of t , let

$$u_{mp} = a_0 + a_1 t \quad (23)$$

Substitute (23) into (22) to obtain

$$0 + 2\xi\omega_n a_1 + \omega_n^2 (a_0 + a_1 t) = \frac{c\tilde{p}_0 t}{m_m} \quad (24)$$

Equating coefficients of like powers of t yields

$$2\xi\omega_n a_1 + \omega_n^2 a_0 = 0 \quad \text{and} \quad \omega_n^2 a_1 = \frac{c\tilde{p}_0}{m_m} \quad (25)$$

This results in

$$a_1 = \frac{c\tilde{p}_0}{m_m \omega_n^2} \quad \text{and} \quad a_0 = -2\xi \frac{c\tilde{p}_0}{m_m \omega_n^3} \quad (26)$$

Therefore, the particular solution in (23) becomes

$$u_{mp}(t) = -2\xi \frac{c\tilde{p}_0}{m_m \omega_n^3} + \frac{c\tilde{p}_0}{m_m \omega_n^2} t \quad (27)$$

The total solution becomes

$$u_m(t) = u_{mh}(t) + u_{mp}(t) = e^{-\xi\omega_n t} (A \cos(\omega_d t) + B \sin(\omega_d t)) - 2\xi \frac{c\tilde{p}_0}{m_m \omega_n^3} + \frac{c\tilde{p}_0}{m_m \omega_n^2} t \quad (28)$$

Apply the IC for zero displacement in (15)–(28):

$$0 = A - 2\xi \frac{c\tilde{p}_0}{m_m \omega_n^3} \Rightarrow A = 2\xi \frac{c\tilde{p}_0}{m_m \omega_n^3} \quad (29)$$

Apply the IC for zero velocity in (15)–(28):

$$\begin{aligned} \dot{u}_m(t) &= e^{-\xi\omega_n t} [-\xi\omega_n (A \cos(\omega_d t) + B \sin(\omega_d t)) + \omega_d (-A \sin(\omega_d t) + B \cos(\omega_d t))] + \frac{c\tilde{p}_0}{m_m \omega_n^2} \\ \dot{u}_m(0) &= -\xi\omega_n A + \omega_d B + \frac{c\tilde{p}_0}{m_m \omega_n^2} = 0 \\ \Rightarrow B &= \frac{\xi\omega_n A - \frac{c\tilde{p}_0}{m_m \omega_n^2}}{\omega_d} = \frac{\xi\omega_n 2\xi \frac{c\tilde{p}_0}{m_m \omega_n^3} - \frac{c\tilde{p}_0}{m_m \omega_n^2}}{\omega_d} = \frac{c\tilde{p}_0}{m_m \omega_n^2} \frac{(2\xi^2 - 1)}{\omega_d} \end{aligned} \quad (30)$$

Substitution of A and B from (29) and (30) into (28) yields the final form for the total solution of (22) which also satisfies the ICs (15).

- (g) The outer fiber bending stress at the base of the pipe may be obtained for all pressure cases using the solutions for $u_m(t)$ derived above and the strength of materials formula:

$$\sigma_{mo}(t) = \frac{\text{Moment at base}}{I} r_o = \frac{F_{\text{pipe}} L}{I} r_o = \frac{k u_m(t) L}{\pi (r_o^4 - r_i^4) / 4} r_o \quad (31)$$

where r_o is the outer radius of the pipe.

This stress could be employed to evaluate the possibility of fatigue-related failure as described in Chapter 1, Section 1.4.

Summary: This example illustrates how to obtain analytical solutions for a 1 dof problem. An alternative approach is to use the Maple code shown below.

Maple Code for Solving Example 6.2.1

```
> #Example 6.2.1
> # Form 1st derivative
> ud := diff (u (t) , t) ;

ud :=  $\frac{d}{dt}u(t)$ 

> # Form 2nd derivative
> udd := diff (u (t) , t , t) ;

udd :=  $\frac{d^2}{dt^2}u(t)$ 

> ode1 := m * udd + k * u (t) = c * p0 ;

ode1 :=  $m \left( \frac{d^2}{dt^2}u(t) \right) + ku(t) = cp0$ 
```

```

> simplify(dsolve({ode1,u(0)=0,D(u)(0)=0},{u(t)}));

$$u(t) = -\frac{cp0 \left( \cos\left(\frac{\sqrt{kt}}{\sqrt{m}}\right) - 1 \right)}{k}$$

> # This result agrees with (16)
> ode2 := m*udd+k*u(t) = c*p0tilda*t;
ode2 := m\left(\frac{d^2}{dt^2}u(t)\right) + ku(t) = cp0tilda t
> simplify(dsolve({ode2,u(0)=0,D(u)(0)=0},{u(t)}));
>

$$u(t) = \left( \frac{cp0tilda \left( -\sin\left(\frac{\sqrt{kt}}{\sqrt{m}}\right) \sqrt{m} + \sqrt{kt} \right)}{k^{(3/2)}} \right)$$

> # This result agrees with (17)
> ode3 := m*udd+k*u(t) = c*p0*exp(-gamma*t);
ode3 := m\left(\frac{d^2}{dt^2}u(t)\right) + ku(t) = cp0e^{(-\gamma t)}
> simplify(dsolve({ode3,u(0)=0,D(u)(0)=0},{u(t)}));

$$u(t) = \frac{cp0 \left( \sin\left(\frac{\sqrt{kt}}{\sqrt{m}}\right) \gamma \sqrt{m} - \cos\left(\frac{\sqrt{kt}}{\sqrt{m}}\right) \sqrt{k} + e^{(-\gamma t)} \sqrt{k} \right)}{\sqrt{k}(k + m\gamma^2)}$$

> # This result agrees with (18)
> assume(0 < zeta, zeta < 1); # zeta is positive and less than 1
>
> ode4 := udd + 2*zeta*omega[n]*ud + omega[n]^2*u(t) -
c*p_tilda_0*t/Mm = 0;
ode4 := \left(\frac{d^2}{dt^2}u(t)\right) + 2\zeta \sim \omega_n \left(\frac{d}{dt}u(t)\right) + \omega_n^2 u(t) - \frac{cp\_tilda\_0 t}{Mm} = 0
> SOL1:=simplify(evalc(dsolve({ode4,u(0)=0,D(u)(0)=0},
{u(t)})));
SOL1 := u(t) = cp_tilda_0 \left( 2e^{(-\omega_n \zeta \sim)} \cos\left(\sqrt{-\zeta \sim^2 + 1} \omega_n t\right) \zeta \sim^3
- 2e^{(-\omega_n \zeta \sim)} \cos\left(\sqrt{-\zeta \sim^2 + 1} \omega_n t\right) \zeta \sim
- 2e^{(-\omega_n \zeta \sim)} \sin\left(\sqrt{-\zeta \sim^2 + 1} \omega_n t\right) \sqrt{-\zeta \sim^2 + 1} \zeta \sim^2
+ e^{(-\omega_n \zeta \sim)} \sin\left(\sqrt{-\zeta \sim^2 + 1} \omega_n t\right) \sqrt{-\zeta \sim^2 + 1} - 2\zeta \sim^3 + 2\zeta \sim + t\omega_n \zeta \sim^2 - t\omega_n \right)
/(\omega_n^3 Mm(\zeta \sim^2 - 1))
> SOL2:=collect(SOL1,exp(-t*omega[n]*zeta)):
> SOL3:=collect(SOL2,cos((1-zeta^2)^(1/2)*omega[n]*t)):
> SOL4:=collect(SOL3,sin((1-zeta^2)^(1/2)*omega[n]*t)):
> SOL5:=collect(SOL4,exp(-t*omega[n]*zeta)):
> SOL6:=collect(SOL5,p_tilda_0):

```

```

> SOL7:=collect (SOL6, c) :
> SOL8:=collect (SOL7, 1/Mm) :
>SOL9:=collect (SOL8, 1/omega [n] ^3) ;

```

$$\begin{aligned}
SOL9 := u(t) &= \frac{(t\zeta^2 - t)p_{\text{tilda}}_0 c}{(\zeta^2 - 1)Mm\omega_n^2} \\
&+ \left(\left(\frac{(-2\sqrt{1-\zeta^2}\zeta^2 + \sqrt{1-\zeta^2}) \sin(\sqrt{1-\zeta^2}\omega_n t)}{\zeta^2 - t} \right. \right. \\
&+ \left. \left. \frac{(2\zeta^3 - 2\zeta) \cos(\sqrt{1-\zeta^2}\omega_n t)}{\zeta^2 - 1} \right) e^{(-t\omega_n \zeta)} \right. \\
&+ \left. \frac{-2\zeta^3 + 2\zeta}{\zeta^2 - 1} \right) p_{\text{tilda}}_0 c / (Mm\omega_n^3)
\end{aligned}$$

$$\begin{aligned}
SOL9 := u(t) &= \frac{(t\zeta^2 - t)p_{\text{tilda}}_0 c}{(\zeta^2 - 1)Mm\omega_n^2} \\
&+ \left(\left(\frac{(-2\sqrt{-\zeta^2 + 1}\zeta^2 + \sqrt{-\zeta^2 + 1}) \sin(\sqrt{-\zeta^2 + 1}\omega_n t)}{\zeta^2 - t} \right. \right. \\
&+ \left. \left. \frac{(2\zeta^3 - 2\zeta) \cos(\sqrt{-\zeta^2 + 1}\omega_n t)}{\zeta^2 - 1} \right) e^{(-t\omega_n \zeta)} \right. \\
&+ \left. \frac{-2\zeta^3 + 2\zeta}{\zeta^2 - 1} \right) p_{\text{tilda}}_0 c / (Mm\omega_n^3)
\end{aligned}$$

The computer code-generated solutions above could have also been obtained utilizing MATLAB SYMBOLIC as shown for case 2 with the t forcing term in (8) and (17), as shown next:

```

clear all
syms u(t) m k c p0tilda
Du = diff(u) ;
assume(k>0 & m>0)
u(t) = dsolve(m*diff(u, t, t)+k*u(t) == c*p0tilda*t, u(0) == 0,
Du(0) == 0) ;
u(t) = simplify(u)

```

OUTPUT

```

u(t) = (c*p0tilda*t)/k - (c*m^(1/2)*p0tilda*sin((k^(1/2)*t)/
m^(1/2)))/k^(3/2)

```

6.2.2 Laplace Transform Method

The definition of the Laplace transform (LT), its usage, a related list of identities, and a table of common LTs are discussed in Section 2.10. The following procedure is employed to solve the governing differential equations of vibration problems:

- (a) Take the LT of the given differential equation.
 (b) Algebraically solve for the LT of the dependent variable.
 (c) Decompose the expression obtained in (b) into terms that appear in Table 2.10.1, that is, $\bar{F}_i(s)$.
 (d) Use Table 2.10.1 to identify the functions of time corresponding to $\bar{F}_i(s)$ and assemble these to form the total solution of the differential equation.

EXAMPLE 6.2.2 Pressure Relief Valve Blowout Analysis with Laplace Transforms

Statement: This example treats Example 6.2.1 with the LT solution method.

Objective: Determine the motion $u_m(t)$ and the stress at the base of the pipe for $p(t) = p_0$ (step), $\tilde{p}_0 t$ (ramp), $p_0 e^{-\gamma t}$ (exponential).

Solution:

- (a) The system differential equation is provided by Equation (4) of Example 6.2.1:

$$m_m \ddot{u}_m + k u_m = c p(t) \quad (1)$$

Take the Laplace transform using (2.10.6)–(2.10.9) to obtain

$$m_m (s^2 U_m(s) - \dot{u}_m(0) - s u_m(0)) + k U_m(s) = c P(s) \quad (2)$$

Imposing the ICs yields

$$U_m(s) = \frac{c P(s)}{m_m s^2 + k} \quad (3)$$

- (b) Consider the three pressure cases given in Example 6.2.1 (Table E6.2.2).

Therefore, from this table and Equation (3), the LT of the meter displacement u_m is:

Case 1:

$$U_m(s) = c p_0 \frac{1}{s(m_m s^2 + k)} = \frac{c p_0}{m_m} \frac{1}{s(s^2 + \omega_n^2)} \quad (4)$$

Case 2:

$$U_m(s) = c \tilde{p}_0 \frac{1}{s^2(m_m s^2 + k)} = \frac{c \tilde{p}_0}{m_m} \frac{1}{s^2(s^2 + \omega_n^2)} \quad (5)$$

Case 3:

$$U_m(s) = \frac{c p_0}{m_m} \frac{1}{(s + \gamma)(s^2 + \omega_n^2)} \quad (6)$$

- (c) The unknown response $u_m(t)$ may be determined by matching the time function in Table 2.10.1 (left column) with the LT of $u_m(t)$, that is, $U_m(s)$ in case 1, case 2, and case 3. The results are:

Case 1 (Eq. (4) and Table 2.10.1, entry 10):

$$u_m(t) = \frac{c p_0}{m_m} \frac{1}{\omega_n^2} (1 - \cos \omega_n t) = \frac{c p_0}{k} (1 - \cos \omega_n t) \quad (7)$$

Case 2 (Eq. (5) and Table 2.10.1, entry 11):

$$u_m(t) = \frac{c \tilde{p}_0}{m_m} \frac{1}{\omega_n^3} (\omega_n t - \sin \omega_n t) = \frac{c \tilde{p}_0}{k} \left(t - \frac{1}{\omega_n} \sin \omega_n t \right) \quad (8)$$

Table E6.2.2 Laplace transforms for pressure time histories

Case	$P(t)$	$P(s)$ from Table 2.101
1	p_0	$p_0 \frac{1}{s}$ (entry 9)
2	$\tilde{p}_0 t$	$\tilde{p}_0 \frac{1}{s^2}$ (entry 2)
3	$p_0 e^{-\gamma t}$	$p_0 \frac{1}{s + \gamma}$ (entry 1)

Case 3 (Eq. (6) and Table 2.10.1, entry 12):

$$\begin{aligned}
 u_m(t) &= \frac{cp_0}{m_m} \left[\frac{e^{-\gamma t}}{\gamma^2 + \omega_n^2} + \frac{\gamma \sin \omega_n t}{\omega_n (\gamma^2 + \omega_n^2)} - \frac{\cos \omega_n t}{\gamma^2 + \omega_n^2} \right] \\
 &= \frac{cp_0}{m_m \gamma^2 + k} \left(e^{-\gamma t} + \frac{\gamma}{\omega_n} \sin \omega_n t - \cos \omega_n t \right)
 \end{aligned} \tag{9}$$

Summary: The procedure of taking the Laplace transform of $p(t)$ and the “inverse” Laplace transform of $U_m(s)$ can be readily performed via the following Maple code. The results are in agreement with Example 6.2.1 as expected. This example begs the question “why transform the EOM to the s domain if solutions are readily available in the t domain.” One reason is the occurrence of forces that are frequency dependent and are measured in the s domain as illustrated by Example 6.2.3.

Maple Code for Example 6.2.2

```

> #Example E6.2.2
> restart;
> with(inttrans):
> #Do LT of p(t)
> ps1 := laplace(p0, t, s);

ps1 :=  $\frac{p0}{s}$ 

> ps2 := laplace(p0tilda*t, t, s);

ps2 :=  $\frac{p0tilda}{s^2}$ 

> ps3 := laplace(p0*exp(-gamma*t), t, s);

ps3 :=  $\frac{p0}{s+\gamma}$ 

> ubar := c/m/(s^2+omega^2);

ubar :=  $\frac{c}{m(s^2+\omega^2)}$ 

> #Form U(s) and its Inverse LT
> Um1 := ubar*ps1;

Um1 :=  $\frac{cp0}{m(s^2+\omega^2)s}$ 

```

```
> um1 := invlaplace (Um1, s, t);
```

$$um1 := \frac{cp0(-\cos(\omega t) + 1)}{m\omega^2}$$

```
> Um2 := ubar * ps2;
```

$$Um2 := \frac{cp0\tilde{t}}{m(s^2 + \omega^2)s^2}$$

```
> um2 := invlaplace (Um2, s, t);
```

$$um2 := \frac{cp0\tilde{t}}{m} \left(-\frac{\sin(\omega t)}{\omega^3} + \frac{t}{\omega^2} \right)$$

```
> Um3 := ubar * ps3;
```

$$Um3 := \frac{cp0}{m(s^2 + \omega^2)(s + \gamma)}$$

```
> um3 := invlaplace (Um3, s, t);
```

$$um3 := \frac{cp0 \left(\frac{-\cos(\omega t) + \frac{\gamma \sin(\omega t)}{\omega}}{\gamma^2 + \omega^2} + \frac{e^{(-\gamma t)}}{\gamma^2 + \omega^2} \right)}{m}$$

The computer code-generated solutions above could have also been obtained utilizing MATLAB SYMBOLIC as shown for case 2 with the “ t ” forcing term in (5) and (8), as shown next:

```
clear all
syms t sp0tilde Um2 c m omega
laplace(p0tilde*t, t, s)
Um2 = c/m/(s^2+omega^2)*p0tilde/s^2;
ilaplace(Um2, s, t)
```

OUTPUT

```
ans =
p0tilde/s^2
ans =
(c*p0tilde*t)/(m*omega^2) - (c*p0tilde*sin(omega*t))/(m*omega^3)
```

EXAMPLE 6.2.3 *Rocket Launch Pad Vibration Response*

Statement: A rocket launch facility consists of a concrete block resting on compliant soil as shown in Figure E6.2.3(a). The *transfer function* of the soil beneath the pad is measured to be

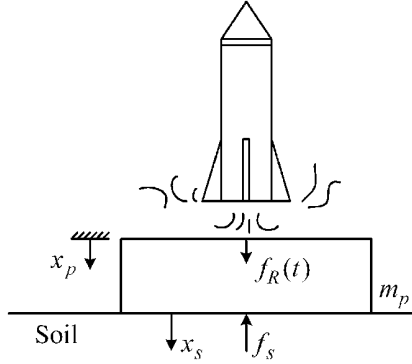


Figure E6.2.3(a) Launch pad vibration model

$$G(s) = \frac{X_s(s)}{F_s(s)} = \frac{L(x_s)}{L(f_s)} = \frac{\alpha}{(s^2 + 2\xi_s \omega_s s + \omega_s^2)} = \frac{\text{soil vertical displacement}}{\text{applied vertical force on soil}} \quad (1)$$

where α , ξ_s , and ω_s^2 are experimentally determined constants.

Objective: Determine the response (x_p) of the launch pad m_p to the rocket force

$$f_R(t) = F_0 e^{-t/\tau} \quad (2)$$

Assumption: The mass of the rocket is much less than m_p so the change in static equilibrium position (SEP) before and after liftoff can be neglected.

Solution:

(a) The EOM for the launch pad is

$$m_p \ddot{x}_p = f_R(t) - f_s(t) \quad (3)$$

(b) Take the LT of (3) by utilizing (2.10.9) with zero ICs

$$m_p s^2 X_p(s) = F_R(s) - F_s(s) \quad (4)$$

Use Table 2.10.1, entry 1, and (1) to obtain

$$m_p s^2 X_p(s) = \frac{F_0}{s + \beta} - \frac{1}{\alpha} (s^2 + 2\xi_s \omega_s s + \omega_s^2) X_p(s) \quad (5)$$

$$\Rightarrow X_p(s) \left[\left(m_p + \frac{1}{\alpha} \right) s^2 + \frac{1}{\alpha} 2\xi_s \omega_s s + \frac{\omega_s^2}{\alpha} \right] = \frac{F_0}{s + \beta} \quad (6)$$

$$\Rightarrow X_p(s) = \frac{F_0}{\gamma(s + \beta)(s^2 + 2\hat{\xi}_s \hat{\omega}_s s + \hat{\omega}_s^2)} \quad (7)$$

where

$$\beta = \frac{1}{\tau}, \quad \gamma = \left(m_p + \frac{1}{\alpha} \right), \quad \hat{\omega}_s^2 = \frac{\omega_s^2}{1 + \alpha m_p}, \quad \hat{\xi}_s = \frac{\xi_s}{\sqrt{1 + \alpha m_p}}, \quad \hat{\omega}_{sd} = \hat{\omega}_s \sqrt{1 - \hat{\xi}_s^2}$$

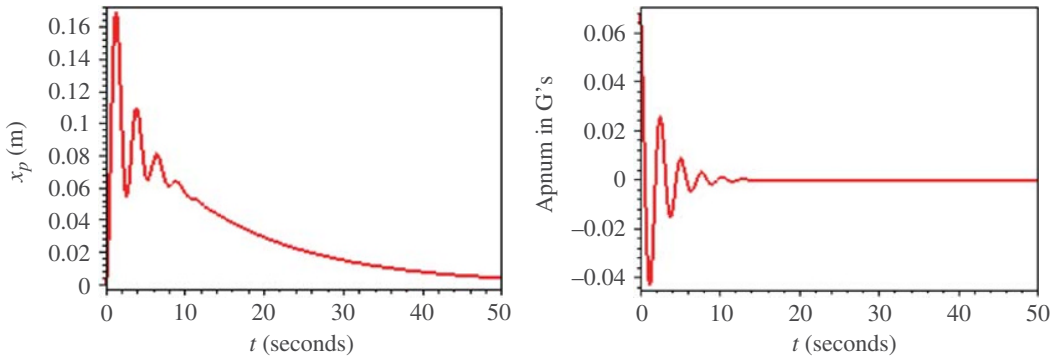


Figure E6.2.3(b) Launch pad displacement and acceleration responses to rocket thrust force

(c) Take the inverse Laplace transform of $X_p(s)$ to $x_p(t)$. This is programmed in the Maple code in the following, where $x_p(t)$ is coded as xp .

(d) Utilize the following numerical values in the simulation:

$$F_0 = 10^5 \text{ N}, \quad \tau = 15 \text{ s}, \quad \alpha = 10^{-5} \text{ kg}^{-1}, \quad \xi_s = 0.20, \quad \omega_s = 3 \text{ rad/s}, \quad m_p = 50000 \text{ kg} \quad (8)$$

Therefore, from (7),

$$\beta = \frac{1}{\tau} = 0.067 \text{ s}^{-1}, \quad \gamma = m_p + \frac{1}{\alpha} = 150000 \text{ kg}, \quad \hat{\omega}_s = 2.45 \text{ rad/s}, \quad \hat{\xi}_s = 0.163 \text{ (dim)} \quad (9)$$

The Maple code yields the following results for these parameters:

$$x_p(t) = 0.11198 * e^{-0.067t} - e^{-0.3994t} [0.11198 * \cos(2.417t) + 0.0154 * \sin(2.417t)] \quad (10)$$

The response of the pad to the rocket thrust force is shown in Figures E6.2.3(b).

Summary: This example illustrated the usefulness of the Laplace transform approach when a force in the model is given in terms of a transfer function (1). The form of this transfer function is

$$\frac{1}{m_{\text{soil}}s^2 + c_{\text{soil}}s + k_{\text{soil}}} \quad (11)$$

so that by comparison with (1),

$$k_{\text{soil}} = \frac{\omega_s^2}{\alpha} = \frac{(3 \text{ s}^{-1})^2}{10^{-5} \text{ kg}^{-1}} = 900000 \text{ N/M} \quad (12)$$

The static deflection due to the full thrust force is

$$\delta_{\text{stat}} = \frac{F_0}{k_{\text{soil}}} = \frac{100000 \text{ N}}{900000 \text{ N/M}} = 0.11 \text{ m} \quad (13)$$

Figure E6.2.3(b) shows that the dynamic response overshoots the static response by $[100 * (0.17 - 0.11)] / 0.11 = 83\%$. This illustrates that a static response simulation may be inadequate and it is very important to perform a dynamic simulation to estimate peak stresses in the piping attached between the pad and ground.

Although the following code is in Maple, MATLAB symbolic could also be utilized.

```

> #Example 6.2.3 Rocket Launch Pad Vibration Response
> restart ;
> with(inttrans) ;
> # Determine xp(t)
> xp:=simplify(invlaplace(F0/gamma/(s+beta)/(s^2
+2*zshat*omshat*s+omshat^2),s,t));
xp:=F0(e^(-beta*t)*sqrt(omshat^2(zshat^2-1))e^(-t*zshat*omshat)
cosh(t*sqrt(omshat^2(zshat^2-1)))*sqrt(omshat^2(zshat^2-1))
+sinh(t*sqrt(omshat^2(zshat^2-1)))*e^(-t*zshat*omshat)*beta
-sinh(t*sqrt(omshat^2(zshat^2-1)))*e^(-t*zshat*omshat)*zshat*omshat)/
((beta^2-2*zshat*omshat*beta+omshat^2)*gamma*sqrt(omshat^2(zshat^2-1)))
>xpnum:=simplify(subs(zshat=0.163,omshat=2.45,beta=.067,
F0=100000.,gamma=150000.,evalm(xp)));
xpnum:=0.1119793974e^(-0.06700000000t)
-0.1119793974e^(-0.3993500000t)cos(2.417233869t)
-0.01539625653sin(2.417233869t)e^(-0.3993500000t)
> #evaluate complex exponential quantities
> xpnumplot:=evalc(xpnum);
xpnumplot:=0.1119793974e^(-0.06700000000t)
-0.1119793974e^(-0.3993500000t)cos(2.417233869t)
-0.01539625653sin(2.417233869t)e^(-0.3993500000t)
> plot(xpnumplot,t=0..50,title="",labels=["t in seconds","xp
in meters"],thickness=2,axes=BOXED);
> apnum:=diff(xpnumplot,t,t)/9.8;
apnum:=0.00005129341987e^(-0.06700000000t)
+0.06797591738e^(-0.3993500000t)cos(2.417233869t)
-0.01313134716sin(2.417233869t)e^(-0.3993500000t)
> plot(apnum,t=0..50,title="",labels=["t in seconds","apnum
in G's"],thickness=2,axes=BOXED);

```

6.2.3 Convolution Integral

Consider the simple SDOF damped oscillator shown in Figure 6.2.1.

The solution $q(t)$ to its equilibrium equation

$$m\ddot{q} + c\dot{q} + kq = f(t) \quad (6.2.8)$$

for the case that

$$f(t) = \delta(t - \tau) = \text{Dirac Delta (impulse) Function (Section 2.12)} \quad (6.2.9)$$

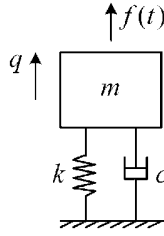


Figure 6.2.1 Simple SDOF damped oscillator

is called a *Green's function* or *fundamental solution* of the differential equation. Thus, the *Green's function* $G(t, \tau)$ satisfies

$$m\ddot{G} + c\dot{G} + kG = \delta(t - \tau) \quad (6.2.10)$$

The solution to (6.2.10) may be obtained via the LT approach (ref. Table 2.10.1, entry 8) yielding

$$G(t, \tau) = \frac{e^{-\xi\omega_n(t-\tau)}}{m\omega_d} \sin(\omega_d(t-\tau))h(t-\tau) \quad (6.2.11)$$

where h is the Heaviside function (Section 2.12)

$$h(t-\tau) = \begin{cases} 1, & t > \tau \\ 0, & t < \tau \end{cases} \quad (6.2.12)$$

Multiply (6.2.10) by $f(\tau)$ and integrate from

$$0 < \tau < \infty \quad (6.2.13)$$

$$m \int_0^{\infty} \frac{d^2}{dt^2} (G(t, \tau)) f(\tau) d\tau + c \int_0^{\infty} \frac{d}{dt} (G(t, \tau)) f(\tau) d\tau + k \int_0^{\infty} G(t, \tau) f(\tau) d\tau = \int_0^{\infty} f(\tau) \delta(t - \tau) d\tau \quad (6.2.14)$$

The differentiation and integration operations may be interchanged since the integration limits are independent of t , yielding

$$m\ddot{r} + c\dot{r} + kr = \int_0^{\infty} f(\tau) \delta(t - \tau) d\tau \quad (6.2.15)$$

where

$$r(t) = \int_0^{\infty} G(t, \tau) f(\tau) d\tau \quad (6.2.16)$$

The Dirac delta (Section 2.12) satisfies

$$\int_0^{\infty} f(\tau) \delta(t - \tau) d\tau = f(t) \quad (6.2.17)$$

Therefore, (6.2.15) becomes

$$m\ddot{r} + c\dot{r} + kr = f(t) \quad (6.2.18)$$

Comparison of (6.2.8) and (6.2.18) shows that r satisfies the same differential equation as q :

$$\therefore q(t) = r(t) = \int_0^{\infty} G(t, \tau) f(\tau) d\tau \quad (6.2.19)$$

Thus, the solution to (6.2.8) reduces to the evaluation of the integral in (6.2.19). An alternative derivation of (6.2.19) reasons that the excitation $f(t)$ may be interpreted as a succession of impulses on mass m . Each impulse has the form $f(t)\Delta t$ which by the impulse and momentum theory (3.4.2) causes a change in velocity of m :

$$m\Delta v = f\Delta\tau \quad (6.2.20)$$

$$\Delta\dot{q} = \frac{f\Delta\tau}{m} \quad (6.2.21)$$

The displacement response following an imposed velocity change was determined in the free vibration response equation (5.2.28). If the impulse (or velocity change) is imposed at time τ , the change in response becomes

$$\Delta q = \frac{\Delta(\dot{q})}{\omega_d} e^{-\xi\omega_n(t-\tau)} \sin(\omega_d(t-\tau)) \quad (6.2.22)$$

Substitute (6.2.21) into (6.2.22)

$$\Delta q = \frac{f(\tau)\Delta\tau}{m\omega_d} e^{-\xi\omega_n(t-\tau)} \sin(\omega_d(t-\tau)) \quad (6.2.23)$$

By linear superposition, the total response is the sum of responses due to each impulse acting independently. Let

$$q = \sum \Delta q = \sum \frac{f(\tau)}{m\omega_d} e^{-\xi\omega_n(t-\tau)} \sin(\omega_d(t-\tau)) \Delta\tau \quad (6.2.24)$$

Let $\Delta\tau \rightarrow 0$ and the sum becomes an integral, and then

$$q(t) = \int_0^{\infty} \frac{f(\tau)}{m\omega_d} e^{-\xi\omega_n(t-\tau)} \sin(\omega_d(t-\tau)) d\tau \quad (6.2.25)$$

which is the same form as (6.2.19) with (6.2.11) inserted.

Due to causality arguments, $f(\tau)$ cannot influence $q(t)$ if $\tau > t$; therefore, the integration limit in (6.2.25) must be t , that is,

$$q(t) = \int_0^t \frac{f(\tau)}{m\omega_d} e^{-\xi\omega_n(t-\tau)} \sin(\omega_d(t-\tau)) d\tau \quad (6.2.26)$$

An alternative form results from the change in integration variable

$$\gamma = t - \tau \quad (6.2.27)$$

Since t is treated as a constant in the integral in (6.2.26), it results that

$$d\gamma = -d\tau, \quad \tau=0 \Rightarrow \gamma=t, \quad \text{and} \quad \tau=t \Rightarrow \gamma=0 \quad (6.2.28)$$

Then (6.2.26) becomes

$$q(t) = \int_0^t \frac{f(t-\gamma)}{m\omega_d} e^{-\xi\omega_n\gamma} \sin(\omega_d\gamma) d\gamma \quad (6.2.29)$$

EXAMPLE 6.2.4 Undamped Oscillator Response to Finite Length Step Input

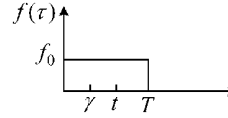
Statement: Utilize the convolution integral approach to obtain the displacement response for the system depicted in Figure E6.2.4(a).

Given:

$$q(0) = \dot{q}(0) = 0, \quad \xi = \frac{c}{2m\omega_n} = 0, \quad \omega_d = \omega_n = \frac{k}{m} \quad (1)$$

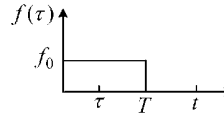
Solution:

- For $0 < t < T$, Equation (6.2.29) becomes



$$q(t) = \frac{1}{m\omega_n} \int_0^t f_0 \sin(\omega_n\gamma) d\gamma = \frac{f_0}{m\omega_n} \left[-\frac{\cos(\omega_n\gamma)}{\omega_n} \right]_0^t = \frac{f_0}{k} (1 - \cos(\omega_n t)) \quad (2)$$

- For $t > T$, Equation (6.2.26) becomes



$$q(t) = \int_0^T \frac{f(\tau)}{m\omega_n} \sin(\omega_n(t-\tau)) d\tau \quad (3)$$

where the upper integration limit extends only to T since $f(\tau) = 0$ for $t > T$. Let

$$u = t - \tau, \quad du = -d\tau \quad (4)$$

then (3) becomes

$$q(t) = \frac{f_0}{m\omega_n} \int_{t-T}^t \sin(\omega_n u) du = \frac{f_0}{k} [\cos(\omega_n(t-T)) - \cos(\omega_n t)]$$

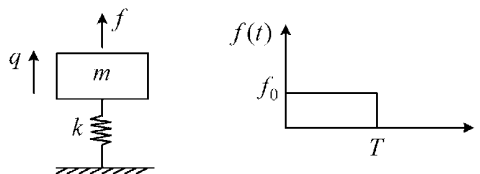


Figure E6.2.4(a) Undamped oscillator with finite length step input

6.2.4 Response to Successive Disturbances

Consider the initial value problem

$$m\ddot{q} + c\dot{q} + kq = f(t) \quad (6.2.30)$$

$$q(0) = q_0, \quad \dot{q}(0) = \dot{q}_0 \quad (6.2.31)$$

Divide (6.2.30) by m to obtain

$$\ddot{q} + 2\xi\omega_n\dot{q} + \omega_n^2q = \frac{f(t)}{m} \quad (6.2.32)$$

Take the LT of (6.2.32) to obtain

$$(s^2\hat{q} - sq_0 - \dot{q}_0) + 2\xi\omega_n(s\hat{q} - q_0) + \omega_n^2\hat{q} = \frac{\hat{f}}{m} \quad (6.2.33)$$

where

$$\hat{q}(s) = L(q) = \int_0^{\infty} e^{-st} q(t) dt \quad (6.2.34)$$

$$\hat{f}(s) = L(f) = \int_0^{\infty} e^{-st} f(t) dt \quad (6.2.35)$$

$$L(\cdot) = \text{Laplace Transform of } (\cdot) \quad (6.2.36)$$

Solve (6.2.33) for $\hat{q}(s)$:

$$\hat{q} = \frac{\hat{f}(s)}{m\Delta(s)} + \frac{q_0(s + 2\xi\omega_n) + \dot{q}_0}{\Delta(s)} \quad (6.2.37)$$

where

$$\Delta(s) = s^2 + 2\xi\omega_n s + \omega_n^2 \quad (6.2.38)$$

The solution for $q(t)$ is obtained by taking the inverse LT of Equation (6.2.37):

$$q(t) = L^{-1}(\hat{q}(s)) = \frac{1}{m} L^{-1}\left(\frac{\hat{f}}{\Delta(s)}\right) + L^{-1}\left(\frac{q_0(s + 2\xi\omega_n) + \dot{q}_0}{\Delta(s)}\right) \quad (6.2.39)$$

Let the ICs be zero so that (6.2.39) simplifies to the form (6.2.41)

$$q_0 = \dot{q}_0 = 0 \quad (6.2.40)$$

$$q(t) = \frac{1}{m} L^{-1}\left(\frac{\hat{f}(s)}{\Delta(s)}\right) \quad (6.2.41)$$

The Heaviside function (Section 2.12) is illustrated in Figure 6.2.2 and defined by

$$h(t-a) = \begin{cases} 1, & t > a \\ 0, & t < a \end{cases} \quad (6.2.42)$$

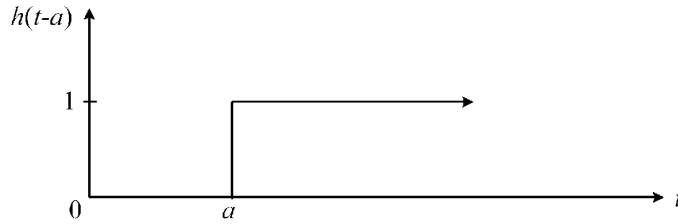


Figure 6.2.2 Heaviside function

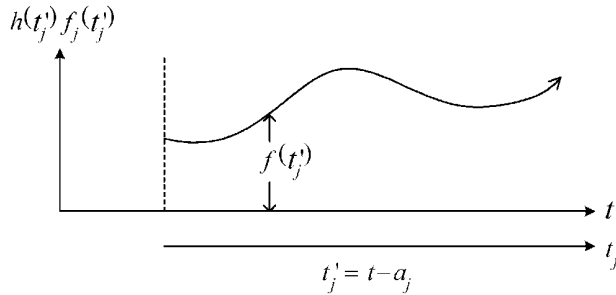


Figure 6.2.3 Delayed force term in Equation (6.2.26)

Let the excitation have the general form of a summation of delayed input forces

$$f(t) = \sum_{j=1}^{n_E} h(t-a_j) f_j(t-a_j) \quad (6.2.43)$$

where a typical f_j term is shown in Figure 6.2.3.

Thus, the effect of the Heaviside function is to turn on the force segment $f_j(t-a_j)$ at time $t=a_j$. The LT of (6.2.43) is given by (Spiegel, 1998)

$$\hat{f}(s) = L(f) = \sum_{j=1}^{n_E} e^{-a_j s} \hat{f}_j(s) \quad (6.2.44)$$

where

$$\hat{f}_j(s) = L(f_j(t)) \quad (6.2.45)$$

Therefore, from (6.2.41),

$$q(t) = \frac{1}{m} L^{-1} \left(\sum_{j=1}^{n_E} \frac{e^{-a_j s} \hat{f}_j(s)}{\Delta(s)} \right) = \frac{1}{m} \sum_{j=1}^{n_E} L^{-1} \left(e^{-a_j s} \frac{\hat{f}_j(s)}{\Delta(s)} \right) \quad (6.2.46)$$

Let

$$q_j(t) = \frac{1}{m} L^{-1} \left(\frac{\hat{f}_j(s)}{\Delta(s)} \right) \quad (6.2.47)$$

and from the LT theory

$$\frac{1}{m}L^{-1}\left(e^{-a_j s}\frac{\hat{f}_j(s)}{\Delta(s)}\right) = \begin{cases} 0, & t < a_j \\ q_j(t-a_j), & t > a_j \end{cases} = h(t-a_j)q_j(t'_j) \quad (6.2.48)$$

where

$$t'_j = t - a_j \quad (6.2.49)$$

Then (6.2.46) becomes

$$q(t) = \sum_{j=1}^{n_E} h(t'_j) * q_j(t'_j) = \sum_{j=1}^{n_E} h(t-a_j) * q_j(t-a_j) \quad (6.2.50)$$

Equation (6.2.50) expresses the result that if the excitation is a sum of time-delayed forces, as given by (6.2.43), then the response is the sum of time-delayed responses. These time-delayed responses have the same form as the responses to the non time-delayed excitations, with the exception that t is replaced by the shifted time $t' = t - a_j$.

Summarizing, if the governing differential equation of the SDOF model is

$$\ddot{q} + 2\xi\omega_n\dot{q} + \omega_n^2q = \frac{f(t)}{m} \quad (6.2.51)$$

and the external force has the form of a sum of time-delayed forces

$$f(t) = \sum_{j=1}^{n_E} h(t-a_j)f_j(t-a_j) \quad (6.2.52)$$

then the response has the form of a sum of time-delayed responses

$$q(t) = \sum_{j=1}^{n_E} h(t'_j) * q_j(t'_j) = \sum_{j=1}^{n_E} h(t-a_j) * q_j(t-a_j) \quad (6.2.53)$$

where $q_j(t)$ satisfies

$$q_j(t) = \frac{1}{m}L^{-1}\left(\frac{\hat{f}_j(s)}{\Delta(s)}\right) \quad (6.2.54)$$

Equation (6.2.53) provides the total solutions (particular + homogeneous) for the zero IC case.

6.2.5 Pulsed Excitations

A pulse-type excitation is applied over some time interval and is then removed, as illustrated in Figure 6.2.4.

Pulse excitations may be expressed with Heaviside functions as

$$f(t) = f(t)(h(t) - h(t-a)) = \begin{cases} f(t) & 0 < t < a \\ 0 & t > a \end{cases} \quad (6.2.55)$$

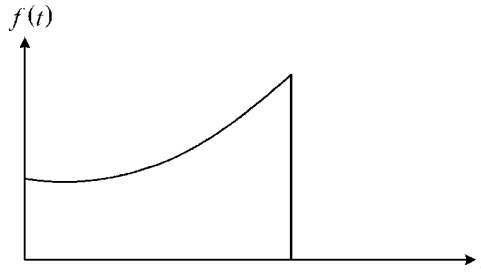


Figure 6.2.4 Pulse-type excitation

Note that (6.2.55) does not have the required form of (6.2.52) since

$$f(t)h(t-a) \quad (6.2.56)$$

appears instead of the required form

$$f(t-a)h(t-a) \quad (6.2.57)$$

This may be remedied in some cases by transforming the form in (6.2.56) to the form required in (6.2.57). Consider, for example,

$$\begin{aligned} f(t) &= A \sin(\omega t) = A \sin(\omega(t-a+a)) \\ &= A \cos(\omega a) \sin(\omega(t-a)) + A \sin(\omega a) \cos(\omega(t-a)) \end{aligned} \quad (6.2.58)$$

where

$$a = \frac{\pi}{\omega} \quad (6.2.59)$$

Insert (6.2.59) into (6.2.58)

$$f(t) = -A \sin(\omega(t-a)) \quad (6.2.60)$$

Then Equation (6.2.55) becomes

$$\begin{aligned} f(t) &= f(t)[h(t) - h(t-a)] \\ &= f_1(t)h(t) - f_2(t-a)h(t-a) \\ &= \underbrace{A \sin(\omega t)}_{f_1} h(t) + \underbrace{A \sin(\omega(t-a))}_{f_2} h(t-a) \end{aligned} \quad (6.2.61)$$

Equation (6.2.61) has the required form of (6.2.52).

EXAMPLE 6.2.5 Example for Pulsed Excitation: Rocket

Description: An instrument is soft mounted inside of a rocket as depicted in Figure E6.2.5(a). The rocket has a known acceleration $\ddot{y} = at^2$ for $t < t_0$ and $\ddot{y} = 0$ for $t > t_0$. The actual acceleration $-g$ of the rocket after the pulsed acceleration is considered negligible relative to its peak, imposed pulsed acceleration, for determining peak response.

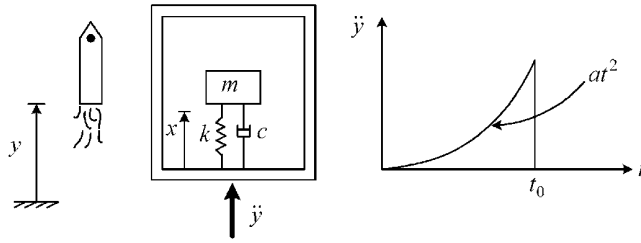


Figure E6.2.5(a) Instrument package in launched rocket

Objective: Determine the relative motion $x(t)$ of the instrument m with respect to the rocket. Compare analytically and numerically derived solutions.

Assumption: Neglect the weight (mg) force for determining the relative motion.

Given: The solutions to the differential equations

$$\ddot{q}_i + 2\xi\omega_n\dot{q}_i + \omega_n^2q_i = \begin{cases} \alpha, & i=0 \\ \beta t, & i=1 \\ \gamma t^2, & i=2 \end{cases} \quad (1)$$

with the ICs

$$q(0) = \dot{q}(0) = 0 \quad (2)$$

are

$$q_0(t) = \frac{\alpha}{\omega_n^2} + \alpha e^{-\xi\omega_n t} \left[\frac{\xi\sqrt{1-\xi^2}}{\omega_n^2(\xi^2-1)} \sin(\omega_d t) - \frac{1}{\omega_n^2} \cos(\omega_d t) \right] \quad (3)$$

$$q_1(t) = \frac{\beta}{\omega_n^3} (-2\xi + \omega_n t) + \beta e^{-\xi\omega_n t} \left[\frac{(2\xi^2-1)\sqrt{1-\xi^2}}{\omega_n^3(\xi^2-1)} \sin(\omega_d t) + \frac{2\xi}{\omega_n^3} \cos(\omega_d t) \right] \quad (4)$$

$$q_2(t) = \frac{\gamma}{\omega_n^4} (-2 + 8\xi^2 - 4\xi\omega_n t + \omega_n^2 t^2) + \gamma e^{-\xi\omega_n t} \left[\frac{-2\xi(-3+4\xi^2)}{\omega_n^3} \frac{1}{\omega_d} \sin(\omega_d t) - \frac{2}{\omega_n^4} (-1+4\xi^2) \cos(\omega_d t) \right] \quad (5)$$

respectively, where $\omega_d = \omega_n \sqrt{1-\xi^2}$.

Solution: First, write the equation of motion for the instrument mass m in terms of the relative motion coordinate $x(t)$, \ddot{y} and the system constants. By Newton's law,

$$m \frac{d^2}{dt^2}(y+x) = -kx - c\dot{x} \quad (6)$$

or

$$\ddot{x} + \frac{c}{m}\dot{x} + \frac{k}{m}x = -\ddot{y} \quad (7)$$

which becomes

$$\ddot{x} + 2\xi\omega_n\dot{x} + \omega_n^2x = -\ddot{y} \quad (8)$$

since

$$\omega_n^2 = \frac{k}{m}, \quad \frac{c}{m} = 2\xi\omega_n \quad (9)$$

From the figure,

$$\ddot{y} = at^2[h(t) - h(t-t_0)] \quad (10)$$

where

$$at^2 = a(t-t_0+t_0)^2 = a[(t-t_0)^2 + 2t_0(t-t_0) + t_0^2] \quad (11)$$

Therefore,

$$\ddot{y} = at^2h(t) - a[(t-t_0)^2 + 2t_0(t-t_0) + t_0^2]h(t-t_0) \quad (12)$$

Substitute (12) into (8) to obtain

$$\ddot{x} + 2\xi\omega_n\dot{x} + \omega_n^2x = f_1(t)h(t) + f_2(t-t_0)h(t-t_0) \quad (13)$$

where

$$f_1(t) = -at^2, \quad f_2(t-t_0) = a[(t-t_0)^2 + 2t_0(t-t_0) + t_0^2] \quad (14)$$

The next task is to write the solution for $x(t)$ in (13), in terms of Heaviside functions, q_0 , q_1 , q_2 , t_0 , and a . Recall from (6.2.51)–(6.2.53) that if

$$\ddot{q} + 2\xi\omega_n\dot{q} + \omega_n^2q = \frac{1}{m} \sum_{j=1}^{n_E} h(t-a_j)\hat{f}_j(t-a_j) \quad (15)$$

then

$$q(t) = \sum_{j=1}^{n_E} h(t-a_j) * q_j(t-a_j) \quad (16)$$

where $q_j(t)$ is the solution of

$$\ddot{q}_j + 2\xi\omega_n\dot{q}_j + \omega_n^2q_j = \frac{1}{m}\hat{f}_j(t) \quad (17)$$

From (13) and (14), $x_1(t)$ satisfies

$$\ddot{x}_1 + 2\xi\omega_n\dot{x}_1 + \omega_n^2x_1 = -at^2 \quad (18)$$

The solution for

$$\ddot{q}_2 + 2\xi\omega_n\dot{q}_2 + \omega_n^2q_2 = \gamma t^2 \quad (19)$$

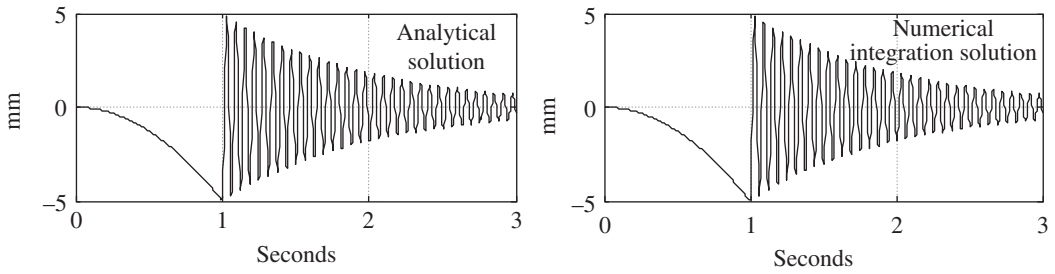


Figure E6.2.5(b) Relative displacement $x(t)$ of instrument during launch

is given in (1) and (5). Therefore,

$$x_1(t) = q_2(t)|_{\gamma=-a} \quad (20)$$

From (14) and (17), $x_2(t)$ satisfies

$$\ddot{x}_2 + 2\xi\omega_n\dot{x}_2 + \omega_n^2x_2 = a(t^2 + 2t_0t + t_0^2) \quad (21)$$

and from (1) to (5)

$$\ddot{q}_i + 2\xi\omega_n\dot{q}_i + \omega_n^2q_i = \begin{cases} \alpha, & i=0 \\ \beta t, & i=1 \\ \gamma t^2, & i=2 \end{cases} \quad (22)$$

therefore,

$$x_2(t) = q_2(t)|_{\gamma=a} + q_1(t)|_{\beta=2at_0} + q_0(t)|_{\alpha=at_0^2} \quad (23)$$

Then

$$x_2(t-t_0) = q_2(t-t_0)|_{\gamma=a} + q_1(t-t_0)|_{\beta=2at_0} + q_0(t-t_0)|_{\alpha=at_0^2} \quad (24)$$

The total, analytically derived solution is given by (16), (20), and (24) as

$$x(t) = q_2(t)|_{\gamma=-a} * h(t) + \left(q_2(t-t_0)|_{\gamma=a} + q_1(t-t_0)|_{\beta=2at_0} + q_0(t-t_0)|_{\alpha=at_0^2} \right) h(t-t_0) \quad (25)$$

Consider this solution for the following parameters and time range:

$$m = 5 \text{ kg}, \quad k = 50000 \text{ N/m}, \quad c = 10 \text{ Ns/m}, \quad a = 50, \quad t_0 = 1 \text{ second}, \quad 0 < t < 3 \text{ seconds}$$

The analytical and numerical integration (see Example 2.3.1) solutions are plotted in Figure E6.2.5(b). Both results are nearly identical.

6.2.6 Response Spectrum

The same loading history may be impressed on many different objects, for example, many different structures are subjected to the same ground excitation during an earthquake. The response spectrum approach provides a quick means to evaluate the peak responses for a

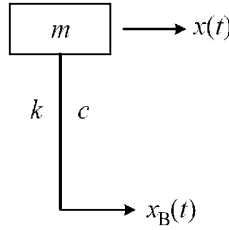


Figure 6.2.5 Vibration of mass m due to base excitation $x_B(t)$

large class of structures, all subjected to the same loading history. This section treats this problem only for SDOF systems, and the analysis is extended to multidegree of freedom systems in the following section (ref. Figure 6.3.1). Consider the system subjected to base motion excitation as depicted in Figure 6.2.5.

The relative motion between $x(t)$ and $x_B(t)$ typically causes damage due to fracture, yielding, or fatigue. The relative motion is represented by

$$x_R(t) = x(t) - x_B(t) \quad (6.2.62)$$

This implies that

$$x(t) = x_B(t) + x_R(t), \quad \dot{x}(t) = \dot{x}_B(t) + \dot{x}_R(t), \quad \ddot{x}(t) = \ddot{x}_B(t) + \ddot{x}_R(t) \quad (6.2.63)$$

The translational equilibrium equation for this system is

$$m\ddot{x} + c\dot{x}_R + kx_R = 0 \quad (6.2.64)$$

Substitution of (6.2.63) into (6.2.64) yields

$$m\ddot{x}_R + c\dot{x}_R + kx_R = -m\ddot{x}_B \quad (6.2.65)$$

and dividing by m yields

$$\ddot{x}_R + 2\xi\omega_n\dot{x}_R + \omega_n^2x_R = -\ddot{x}_B \quad (6.2.66)$$

The solution to (6.2.65) is given by the convolution integral approach (6.2.26) as

$$x_R(t) = \int_0^t \frac{-m\ddot{x}_B(\tau)}{m\omega_d} e^{-\xi\omega_n(t-\tau)} \sin(\omega_d(t-\tau)) d\tau = \frac{-1}{\omega_d} \int_0^t \ddot{x}_B(\tau) e^{-\xi\omega_n(t-\tau)} \sin(\omega_d(t-\tau)) d\tau \quad (6.2.67)$$

The displacement response spectrum corresponding to a given base excitation history $\ddot{x}_B(t)$ is defined as

$$x_R^{SD}(\omega_n, \xi) = \max(x_R(t)) \quad 0 < t < \infty \quad (6.2.68)$$

Similarly, the velocity and acceleration response spectra are defined as

$$x_R^{SV}(\omega_n, \xi) = \max(\dot{x}_R(t)) \quad 0 < t < \infty \quad (6.2.69)$$

$$x_R^{SA}(\omega_n, \xi) = \max(\ddot{x}_R(t) + \ddot{x}_B(t)) = \max(\ddot{x}(t)) \quad 0 < t < \infty \quad (6.2.70)$$

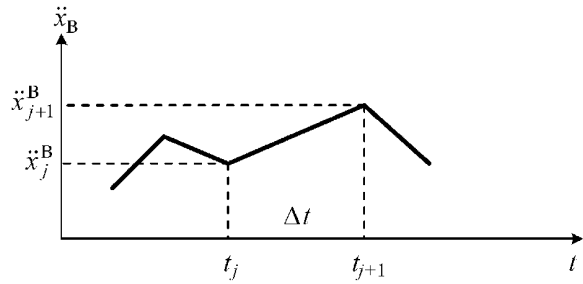


Figure 6.2.6 Base excitation record described by discrete data points

The objective is to evaluate the peak response for a large class of structures subjected to the same base motion loading $\ddot{x}_B(t)$. Therefore, x_R^{SD} , x_R^{SV} , and x^{SA} are determined for wide ranges of ω_n and ξ utilizing the same $\ddot{x}_B(t)$ for all cases. The response spectra are then plotted versus ω_n and ξ . The base acceleration is often available in digital form as recorded at discrete times as shown in Figure 6.2.6.

The base acceleration is linearly interpolated between consecutive data points j and $j+1$ yielding

$$\ddot{x}_B = \ddot{x}_j^B + \frac{(\ddot{x}_{j+1}^B - \ddot{x}_j^B)}{\Delta t} (t - t_j) \quad (6.2.71)$$

Combining (6.2.66) and (6.2.71) yields

$$\ddot{x}_R + 2\xi\omega_n\dot{x}_R + \omega_n^2 x_R = -\ddot{x}_j^B - \frac{\ddot{x}_{j+1}^B - \ddot{x}_j^B}{\Delta t} (t - t_j), \quad t_j < t < t_{j+1} \quad (6.2.72)$$

with the ICs

$$x_R(t = t_j) = x_j^R, \quad \dot{x}_R(t = t_j) = \dot{x}_j^R \quad (6.2.73)$$

The solution of this initial value problem can be obtained by any of the methods presented in this section and is given by

$$x_R(t) = e^{-\xi\omega_n(t-t_j)} [A \cos(\omega_d(t-t_j)) + B \sin(\omega_d(t-t_j))] + \alpha + \beta(t-t_j) \quad (6.2.74)$$

where

$$\begin{aligned} \Delta t = t_{j+1} - t_j, \quad a = -\ddot{x}_j^B, \quad b = -\frac{(\ddot{x}_{j+1}^B - \ddot{x}_j^B)}{\Delta t} \\ \alpha = \frac{a}{\omega_n^2} - \frac{2\xi b}{\omega_n^3}, \quad \beta = \frac{b}{\omega_n^2}, \quad A = x_j^R - \alpha, \quad B = \frac{1}{\omega_d} (\dot{x}_j^R - \beta + A\xi\omega_n) \end{aligned} \quad (6.2.75)$$

EXAMPLE 6.2.6 Response Spectrum for Northridge California Earthquake

Description: The ground acceleration during the Northridge California earthquake of January 17, 1994, was recorded and is readily available in the literature.

Objective: Determine the displacement response spectrum for this earthquake.

Solution: Figure E6.2.6(a) shows an approximate, N–S ground motion acceleration record $\ddot{x}_B(t)$ for the Northridge California earthquake. The acceleration axis is in units of g 's ($1g = 386 \text{ in./s}^2$).

The record consists of 67 piecewise linear segments like shown in Figure 6.2.6. The resulting displacements are solved utilizing (6.2.74) for each segment. The final conditions of segment i become the ICs for segment $i + 1$. Figure E6.2.6(b) shows the predicted displacement and velocity time responses for $\xi = 0.05$ and $T_n = (1/f_n) = (2\pi/\omega_n) = 3$ seconds. The maximum displacement is approximately 9.5 in. for $\xi = 0.05$ and $T_n = (1/f_n) = (2\pi/\omega_n) = 3$ seconds.

The displacement response spectrum for the Northridge earthquake is shown in Figure E6.2.6(c). This provides the peak displacement response versus system natural period and damping ratio. Buildings with light damping and natural period between 2.5 and 3.0 seconds are seen to be most susceptible to large, internal relative motions for the given record of ground motion. This is a plot of

$$x_R^{SD}(\omega_n, \xi) = \max(x_R(t)) \quad 0 < t < \infty \quad (1)$$

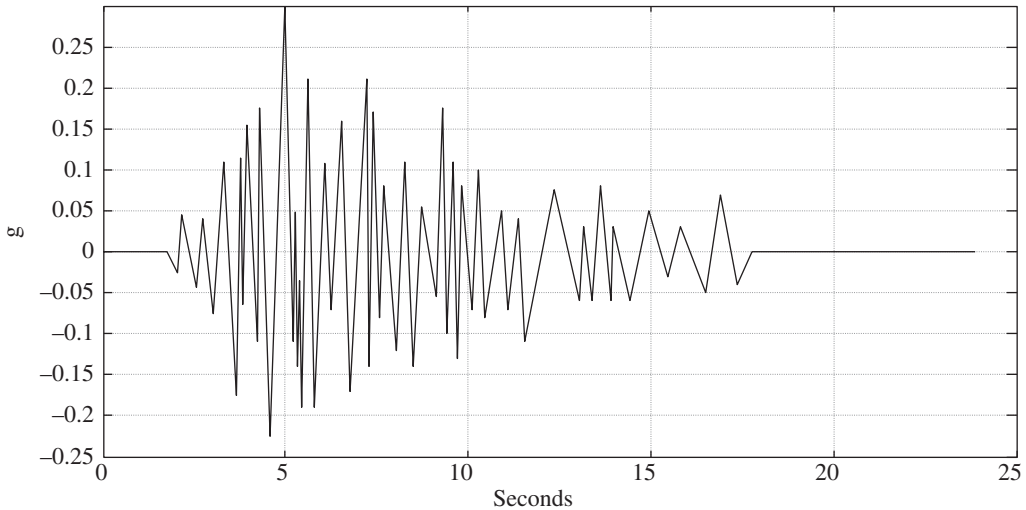


Figure E6.2.6(a) Approximate acceleration record $\ddot{x}_B(t)$ of N-S ground motion for the Northridge California earthquake of January 17, 1994

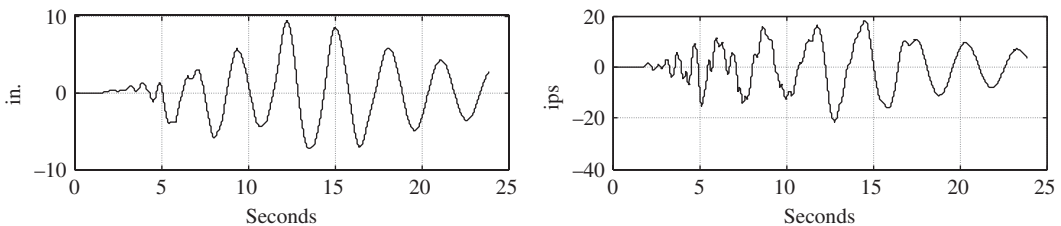


Figure E6.2.6(b) Predicted relative displacement x_R (in.) and velocity \dot{x}_R (in./s) for Northridge earthquake with $\xi = 0.05$ and $T_n = 1/f_n = (2\pi)/\omega_n = 3.0$ seconds

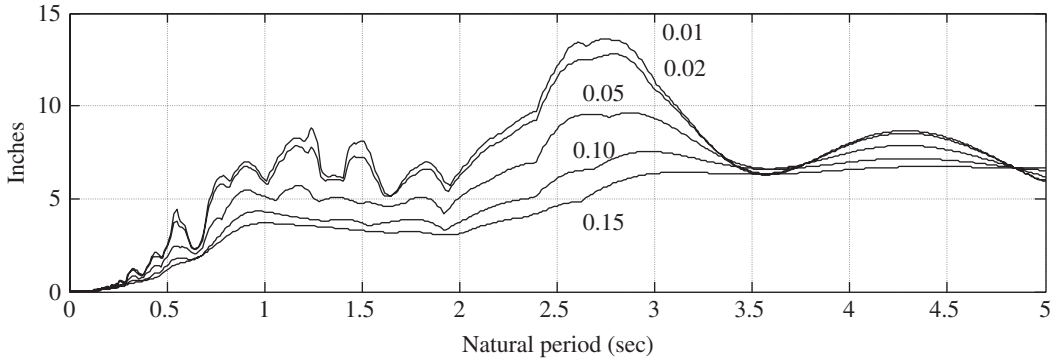


Figure E6.2.6(c) Displacement response spectrum for the Northridge California earthquake N-S excitation for five values of ξ

The MATLAB code for this example is listed below.

```
clear
Zeta_plot = 0.05; Tn_plot = 3.0;
N_S_Northridge_t = [0 0.8 0.95 1 1.18 1.27 1.4 1.52 1.68 1.74 1.77 ...
    1.81 1.95 1.97 2.1 2.3 2.4 2.43 2.45 2.49 2.52 ...
    2.6 2.67 2.8 2.88 3.0 3.12 3.33 3.36 3.42 ...
    3.5 3.55 3.7 3.82 3.92 4.02 4.21 4.3 4.34 ...
    4.43 4.46 4.53 4.66 4.75 4.82 5.02 5.1 5.25 ...
    5.33 5.7 6.0 6.06 6.17 6.28 6.4 6.44 6.65 6.89 ...
    7.13 7.3 7.6 7.8 8.0 8.2 9 10 11].*2.17;
N_S_Northridge_g = [0 0 -.25 .45 -.43 .4 -.75 1.1 -1.75 1.15 -.65 ...
    1.55 -1.1 1.75 -2.25 3.0 -1.1 0.49 -1.4 -.35 ...
    -1.9 2.1 -1.9 1.08 -.7 1.6 -1.7 2.1 -1.4 1.7 ...
    -.8 .8 -1.2 1.1 -1.4 0.55 -.55 1.75 -1 1.1 -1.3 ...
    .8 -.7 1 -.8 .5 -.7 .4 -1.1 .75 -.6 .3 -.6 .8 ...
    -.6 .3 -.6 .5 -.3 .3 -.5 .7 -.4 0 0 0 0]*0.1;
N_S_Northridge_inches_per_s2 = N_S_Northridge_g*386.;
plot(N_S_Northridge_t, N_S_Northridge_g)
grid on
title('Approximate N-S Ground Acceleration. Northridge
California Earthquake Jan. 17, 1994')
xlabel('Time in Seconds')
ylabel('Acceleration in g')
pause
close

nseg= size(N_S_Northridge_t,2) -1
zeta = [0.015 0.02 0.05 0.10 0.15] ;
for ij=1:1:5 % zeta loop
for k = 1:1:500 % Natural Period Loop
```

```

k
XMAX(ij,k)=0;
XdMAX(ij,k)=0;
Natural_Period(k) = 0.01*k;
omegan = 2*pi/Natural_Period(k);
omegad = omegan*sqrt(1-zeta(ij)^2);
x0 = 0;  xd0 = 0;

for j=1:1:nseg
if j==1
xRj = x0 ;  xRdj = xd0;
else
xRj = xR(101) ;  xRdj = xRd(101);
end
tj = N_S_Northridge_t(1,j);
tjpl= N_S_Northridge_t(1,j+1);
deltat = tjpl - tj;
xddbJ=N_S_Northridge_inches_per_s2(1,j);
xddbJpl = N_S_Northridge_inches_per_s2(1,j+1);
b= -(xddbJpl - xddbJ)/deltat;
a = -xddbJ;
alpha = a/omegan^2 - 2*zeta(ij)*b/omegan^3;
beta = b/omegan^2;
A = xRj - alpha;
B= 1/omegad*( xRdj - beta +A*zeta(ij)*omegan);
deltadeltat = deltat/100;
for i=1:1:101
  t(i) = tj + (i-1)*deltadeltat;
  xR(i)=exp(-zeta(ij)*omegan*(t(i)-tj))* (A*cos(omegad*
(t(i)-tj))+ B*sin(omegad*(t(i)-tj))) + alpha + beta*
(t(i)-tj);
  xRd(i)=-zeta(ij)*omegan*exp(-zeta(ij)*omegan*(t(i)-tj))*
(A*cos(omegad*(t(i)-tj))+ B*sin(omegad*(t(i)-tj))) + ...
  exp(-zeta(ij)*omegan*(t(i)-tj))* (-A*omegad*sin(omegad*
(t(i)-tj))+ B*omegad*cos(omegad*(t(i)-tj))) + beta;

  ABSx = abs(xR(i));
  ABSxd = abs(xRd(i));
  if ABSx>XMAX(ij,k)
    XMAX(ij,k)=ABSx;
  end
  if ABSxd>XdMAX(ij,k)
    XdMAX(ij,k)=ABSxd;
  end
  t_tot(i+(j-1)*101) = t(i);
  xR_tot(i+(j-1)*101) = xR(i);
  xRd_tot(i+(j-1)*101) = xRd(i);
end % i
end % j

```

```

if zeta(ij)==Zeta_plot
    if Natural_Period(k)==Tn_plot
        subplot(2,1,1)
        plot(t_tot,xR_tot)
        title('Relative Displacement. Northridge California
Earthquake Jan. 17, 1994')
        xlabel('Time in Seconds')
        ylabel('Displacement in inches')
        grid on
        msg = sprintf('Zeta = %0.2f  Natural Period= %1.2f',Zeta_plot,
Tn_plot);
        gtext(msg);

        subplot(2,1,2)
        plot(t_tot,xRd_tot)
        title('Relative Velocity. Northridge California Earthquake
Jan. 17, 1994')
        xlabel('Time in Seconds')
        ylabel('Velocity in inches/second')
        grid on
        msg = sprintf('Zeta = %1.2f  Natural Period= %1.2f',Zeta_plot,
Tn_plot);
        gtext(msg);
        pause
        close
    end
end
end %k
end % ij

for ij=1:1:5
    plot(Natural_Period,XMAX(ij,:))
    grid on
    hold on
end
title('Displacement Response Spectra. Northridge California
Earthquake Jan. 17, 1994')
xlabel('Natural Period in Seconds')
ylabel('Displacement in inches')
for ij=1:1:5
    msg=sprintf('zeta= %1.2f',zeta(ij));
    gtext(msg)
end
pause
close

for ij=1:1:3
    plot(Natural_Period,XdMAX(ij,:))
    grid on

```

```

hold on
end
title('Velocity Response Spectra. Northridge California
Earthquake Jan. 17, 1994')
xlabel('Natural Period in Seconds')
ylabel('Velocity in inches/second')
for ij=1:1:5
msg=sprintf('zeta= %1.2f', zeta(ij));
gtext(msg)
end
pause
close

```

6.3 MODAL CONDENSATION OF NDOF: TRANSIENT FORCED VIBRATING SYSTEMS

The discussion of the determination of transient vibration response for arbitrary order vibrating systems begins with the general form of the linear model equilibrium equation

$$\underline{M}\ddot{\underline{q}} + \underline{C}_T\dot{\underline{q}} + \underline{K}_T\underline{q} = \underline{f}(t) + \underline{g}(\underline{q}, \dot{\underline{q}}, t) \quad (N \times 1) \quad (6.3.1)$$

where (5.3.1), (5.4.212):

\underline{M} = system mass matrix ($N \times N$)

$\underline{C}_T = \underline{C} + \underline{G}$ = total rate matrix ($N \times N$)

$\underline{K}_T = \underline{K} + \underline{K}_c$ = total stiffness matrix ($N \times N$)

$\underline{f}(t)$ = external forces that depend only on t ($N \times 1$)

$\underline{g}(\underline{q}, \dot{\underline{q}}, t)$ = external or nonlinear internal forces that depend on \underline{q} , $\dot{\underline{q}}$, and t ($N \times 1$)

$$(6.3.2)$$

A first-order form for Equation (6.3.1) may be derived by defining the velocity states \underline{V} as

$$\dot{\underline{q}} = \underline{V} \quad (N \times 1) \quad (6.3.3)$$

and utilizing the identity

$$\underline{M}\dot{\underline{q}} = \underline{M}\dot{\underline{V}} \quad (N \times 1) \quad (6.3.4)$$

to obtain

$$\begin{bmatrix} \underline{0} & \underline{M} \\ \underline{M} & \underline{C}_T \end{bmatrix} \begin{Bmatrix} \underline{\dot{V}} \\ \underline{\dot{q}} \end{Bmatrix} = \begin{bmatrix} \underline{M} & \underline{0} \\ \underline{0} & -\underline{K}_T \end{bmatrix} \begin{Bmatrix} \underline{V} \\ \underline{q} \end{Bmatrix} + \begin{Bmatrix} \underline{0} \\ \underline{f} + \underline{g} \end{Bmatrix} \quad (6.3.5)$$

or similar with (5.4.215)

$$\underline{E} \underline{\dot{X}} = \underline{H} \underline{X} + \underline{\hat{f}} \quad (6.3.6)$$

$2N \times 2N$ $2N \times 1$ $2N \times 2N$ $2N \times 1$ $2N \times 1$

Premultiplying by \underline{E}^{-1} yields

$$\underline{\dot{X}} = \underline{A} \underline{X} + \underline{F}(t, \underline{X}, \underline{\dot{X}}) \quad (6.3.7)$$

where (5.4.219)

$$\underline{X} = \begin{Bmatrix} \underline{V} \\ \underline{q} \end{Bmatrix}, \quad \underline{A} = \begin{bmatrix} -\underline{M}^{-1} \underline{C}_T & -\underline{M}^{-1} \underline{K}_T \\ \hline \underline{I}_N & \underline{0} \end{bmatrix} \quad (6.3.8)$$

$$\underline{F} = \underline{E}^{-1} \underline{\hat{f}} = \begin{Bmatrix} \underline{M}^{-1} (\underline{f} + \underline{g}) \\ \hline \underline{0} \end{Bmatrix} \quad (2N \times 1) \quad (6.3.9)$$

6.3.1 Undamped and Orthogonally Damped Nongyroscopic, Noncirculatory Systems

For this case, (6.3.1) may be written as

$$\underline{M} \underline{\ddot{q}} + \underline{C}_0 \underline{\dot{q}} + \underline{K} \underline{q} = \underline{f}(t) + \underline{g}(\underline{\dot{q}}, \underline{q}, t) \quad (6.3.10)$$

Let's assume the response is restricted to a subspace (see Section 2.6) spanned by some of the lower modes of the undamped system. As discussed in Section 2.6,

$$\underline{q}(t) = \underline{\Psi} \underline{\chi} = \sum_{i=1}^m \chi_i(t) \underline{\psi}_i \quad (6.3.11)$$

$N \times 1$ $N \times m$ $m \times 1$ $i=1$ m

where $\underline{\Psi}$ is the truncated modal matrix containing m undamped system mode shapes

$$\underline{\Psi} = [\underline{\Psi}_1 \quad \underline{\Psi}_2 \quad \cdots \quad \underline{\Psi}_m] \quad (N \times M) \quad (6.3.12)$$

and

$$\underline{\psi}_i = \text{ith normal mode} \quad (N \times 1) \quad (6.3.13)$$

where “normal” refers to an undamped, nongyroscopic, noncirculatory system. Substitute (6.3.10) into (6.3.11), premultiply by $\underline{\Psi}^T$, and use the orthogonality relations (5.4.44), (5.4.46), (5.4.92), and (5.4.100) to obtain

$$\underline{\text{diag}}(\tilde{m}_i) \underline{\ddot{\chi}} + \underline{\text{diag}}(2\xi_i \omega_i \tilde{m}_i) \underline{\dot{\chi}} + \underline{\text{diag}}(\tilde{m}_i \omega_i^2) \underline{\chi} = \underline{r}(t, \underline{q}, \underline{\dot{q}}) = \underline{\Psi}^T (\underline{f}(t) + \underline{g}(t, \underline{q}, \underline{\dot{q}})) \quad (6.3.14)$$

The i th row of this equation states

$$\ddot{\chi}_i + 2\xi_i \omega_i \dot{\chi}_i + \omega_i^2 \chi_i = \frac{r_i}{\tilde{m}_i} \quad i = 1, 2, \dots, m \quad (6.3.15)$$

where

$$r_i = i\text{th modal force} = \underline{\psi}_i^T f(t) + \underline{\psi}_i^T g(t, \underline{q}, \underline{\dot{q}}) \quad (6.3.16)$$

Equation (6.3.15) is a second-order, real, uncoupled ODE so it may be solved by using any approach discussed in Section 6.2. The ICs on the $r_i(t)$ are obtained by considering (6.3.11) at $t=0$, that is,

$$\underline{q}(0) \cong \underline{\Psi}^T \underline{\chi}(0) = \sum_{i=1}^m \chi_i(0) \underline{\psi}_i \quad (6.3.17)$$

Premultiply (6.3.17) by $\underline{\psi}_j^T \underline{M}$ and use orthogonality (5.4.75) to obtain

$$\chi_i(0) = \frac{1}{m_i} \underline{\psi}_i^T \underline{M} \underline{q}(0) \quad (6.3.18)$$

In a similar manner,

$$\dot{\chi}_i(0) = \frac{1}{m_i} \underline{\psi}_i^T \underline{M} \dot{\underline{q}}(0) \quad (6.3.19)$$

It should be noted that although Equations (6.3.18) and (6.3.19) provide formulas for $\chi_i(0)$ and $\dot{\chi}_i(0)$, the vectors formed from

$$\sum_{i=1}^m \chi_i(0) \underline{\psi}_i, \quad \sum_{i=1}^m \dot{\chi}_i(0) \underline{\psi}_i \quad (6.3.20)$$

will not in general be equal to $\underline{q}(0)$ and $\dot{\underline{q}}(0)$, respectively, since $m < N$. This should be readily apparent by considering the $m=1$ case, that is,

$$\underline{q}(0) = \chi_1(0) \underline{\psi}_1 \quad (6.3.21)$$

where $\underline{q}(0)$ may have a totally arbitrary shape and $\underline{\psi}_1$ is limited to the first mode shape. Equations (6.3.18)–(6.3.20) provide an approximation for $\underline{q}(0)$ and $\dot{\underline{q}}(0)$ that is consistent with orthogonality of the modes and that exist in the same subspace as $\underline{q}(t)$ and $\dot{\underline{q}}(t)$. The approximation for $\underline{q}(0)$, $\dot{\underline{q}}(0)$, $\underline{q}(t)$, and $\dot{\underline{q}}(t)$ will improve as the number of basis vectors ($\underline{\psi}_i$) spanning the solution subspace increases. Table 6.3.1 provides an outline for the modal-based solution procedure.

The utility of modal condensation can be appreciated by considering that finite element structural models typically contain 1000s, 10 000s, or even 100 000s of degrees of freedom. Thus, solution of the noncondensed EOMs would require integrating very many *coupled* ODEs. The modally condensed system may include only about 5–10% of the modes, requiring solution of only m *uncoupled* ordinary differential equations (6.3.15).

6.3.1.1 Mode Acceleration Approach

The number of modes required to obtain convergence of the response results may be reduced by using the *mode acceleration* (MA) approach. The preceding section described the standard approach of solving for $\underline{\chi}(t)$ in (6.3.14) and then recovering the $\underline{q}(t)$ from (6.3.11). The MA approach instead recovers \underline{q} using the equilibrium equation (6.3.10)

Table 6.3.1 Steps for modal condensation of the EOMs for orthogonally damped systems

1. Compute the undamped natural frequencies and mode shapes $(\omega_i \text{ and } \underline{\psi}_i)$ for $i = 1, \dots, m$. The number of modes m is typically selected based on the experience of the analyst and may be checked by considering if \underline{q} has converged with the m modes
2. Use measurements or experience to assign a damping ratio ξ_i to each of the modes
3. Determine the modal force (r_i) from (6.3.16) for each mode
4. Solve for the ICs on $(\chi_i(0), \dot{\chi}_i(0))$ from (6.3.18) and (6.3.19)
5. Solve the m uncoupled, single dof equations given by (6.3.15) for $\chi_i(t)$. Any analytical or numerical integration-type methods may be used for this purpose
6. Solve for $\underline{q}(t)$ and $\underline{\dot{q}}(t)$ using $\chi_i(t)$ and (6.3.11)

$$\underline{q}(t) = \sum_{i=1}^m \chi_i(t) \underline{\psi}_i$$

$$\underline{q} = \underline{K}^{-1} \left(\underline{f}(t) + \underline{g}(t, \underline{q}, \underline{\dot{q}}) - \underline{M}\underline{\dot{q}} - \underline{C}_0\underline{\dot{q}} \right) \quad (6.3.22)$$

where $\underline{\ddot{q}}$ and $\underline{\dot{q}}$ are expressed in terms of the modal coordinate vector $\underline{\chi}(t)$ in (6.3.11) yielding

$$\underline{q} \approx \underline{K}^{-1} \left(\underline{f}(t) + \underline{g}(t, \underline{q}, \underline{\dot{q}}) \right) - \underline{K}^{-1} \underline{M} \underline{\Psi} \underline{\ddot{\chi}} - \underline{K}^{-1} \underline{C}_0 \underline{\Psi} \underline{\dot{\chi}} \quad (6.3.23)$$

From (5.4.92) and (5.4.100), the orthogonally damped \underline{C}_0 matrix satisfies

$$\underline{\Psi}^T \underline{C}_0 \underline{\Psi} = \underline{\text{diag}}(2\tilde{m}_i \xi_i \omega_i) \quad (6.3.24)$$

and from (5.4.75),

$$\underline{\Psi}^T \underline{M} \underline{\Psi} = \underline{\text{diag}}(\tilde{m}_i) \quad (6.3.25)$$

and from (5.4.77),

$$\underline{\Psi}^T \underline{K} \underline{\Psi} = \underline{\text{diag}}(\tilde{m}_i \omega_i^2) \Rightarrow \underline{\Psi}^{-1} \underline{K}^{-1} \underline{\Psi}^{-T} = \underline{\text{diag}}\left(\frac{1}{\tilde{m}_i \omega_i^2}\right) \quad (6.3.26)$$

Premultiplication of (6.3.24) and (6.3.25) by (6.3.26) yields

$$\underline{\Psi}^{-1} \underline{K}^{-1} \underline{C}_0 \underline{\Psi} = \underline{\text{diag}}\left(\frac{2\xi_i \omega_i}{\omega_i^2}\right) \quad (6.3.27)$$

and

$$\underline{\Psi}^{-1} \underline{K}^{-1} \underline{M} \underline{\Psi} = \underline{\text{diag}}\left(\frac{1}{\omega_i^2}\right) \quad (6.3.28)$$

or

$$\underline{K}^{-1} \underline{C}_0 \underline{\Psi} = \underline{\Psi} \underline{\text{diag}}\left(\frac{2\xi_i \omega_i}{\omega_i^2}\right) \quad (6.3.29)$$

and

$$\underline{K}^{-1} \underline{M} \underline{\Psi} = \underline{\Psi} \underline{\text{diag}} \left(\frac{1}{\omega_i^2} \right) \quad (6.3.30)$$

Substitution of (6.3.29) and (6.3.30) into (6.3.23) yields

$$\underline{q} \approx \underline{K}^{-1} \left(\underline{f}(t) + \underline{g}(t, \underline{q}, \underline{\dot{q}}) \right) - \underline{\Psi} \underline{\text{diag}} \left(\frac{1}{\omega_i^2} \right) \left(\underline{\ddot{\chi}} + \underline{\text{diag}}(2\xi_i \omega_i) \underline{\dot{\chi}} \right) \quad (6.3.31)$$

The term $\underline{g}(t, \underline{q}, \underline{\dot{q}})$ may be evaluated at the preceding time step in an NI-type solution of (6.3.14), and the bracketed terms in (6.3.31) may be evaluated from (6.3.14) as

$$\underline{\ddot{\chi}} + \underline{\text{diag}}(2\xi_i \omega_i) \underline{\dot{\chi}} = \underline{\text{diag}} \left(\frac{1}{\tilde{m}_i} \right) \underline{r}(t, \underline{q}, \underline{\dot{q}}) - \underline{\text{diag}}(\omega_i^2) \underline{\chi} \quad (6.3.32)$$

The $1/\omega_i^2$ term in (6.3.31) is credited with accelerating convergence since it becomes very small for higher modes. Combining (6.3.31) and (6.3.32) with the definition of $\underline{r}(t)$ in (6.3.14) yields

$$\underline{q}_{N \times 1} = \underline{\Psi}_{N \times m} \underline{\chi}_{m \times 1} + \underline{\beta}_{N \times 1} \left[\underline{f}(t) + \underline{g}(t, \underline{q}, \underline{\dot{q}}) \right]_{N \times 1} \quad (6.3.33)$$

where

$$\underline{\beta}_{N \times N} = \underline{K}^{-1}_{N \times N} - \underline{\Psi}_{N \times m} \underline{\text{diag}} \left(\frac{1}{\tilde{m}_i \omega_i^2} \right)_{m \times m} \underline{\Psi}^T_{m \times N} \quad (6.3.34)$$

Thus, it is seen that modal acceleration equation (6.3.33) for recovering \underline{q} is identical to the standard modal condensation equation (6.3.11) except for the second term on the RHS of (6.3.33). If a full set of modes is employed, ($m = N$) $\underline{\Psi}$ is square and invertible, in which case (6.3.26) implies

$$\underline{K}^{-1} = \underline{\Psi} \underline{\text{diag}} \left(\frac{1}{\tilde{m}_i \omega_i^2} \right) \underline{\Psi}^T \quad (6.3.35)$$

Thus, if a full set of modes is used, then $\underline{\beta}_{N \times N}$ in (6.3.34) is zero and the MA and standard modal condensation approaches are identical.

EXAMPLE 6.3.1 Instrumentation Tower Impact Investigation (Ex. 5.4.4 cont.)

Statement: An instrumentation module is supported by a multilayered structure consisting of “floor” masses with an interconnecting frame. The tower is accidentally struck by materials overhung on a passing truck, as depicted in Figure E6.3.1(a). The approximate impact force of duration τ is also shown. A simplified N mass model of the pole is shown in Figure E6.3.1(b), where k_i represents the horizontal frame stiffness between mass i and mass $i-1$. The model is formed as part of an effort to evaluate acceleration-induced damage to the instrumentation.

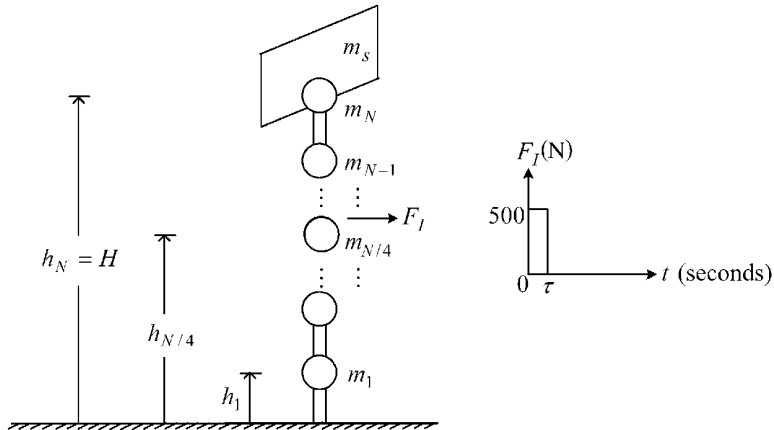


Figure E6.3.1(a) Tower model and impact loading

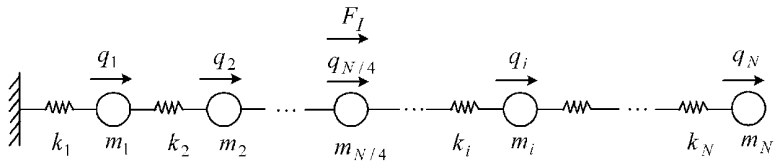


Figure E6.3.1(b) Simplified tower model diagram

The physical parameters in this model are

$$\begin{aligned} N = 20, \quad H = 20\text{m}, \quad k_j = 50000\text{N/m}, \quad m_j = 20\text{kg} \\ h_i = i * H / N, \quad m_s = 50\text{kg}, \quad F_I = 500\text{N}, \quad \tau = \text{variable} \end{aligned} \quad (1)$$

Damping:

$$\xi_1^d = 0.02, \quad \xi_2^d = 0.02, \quad \xi_3^d = \xi_4^d = 0.025, \quad \xi_5^d = 0.03 \quad (2)$$

Objectives:

- Solve for the transient forced response of the tower subjected to the impact load.
- Compare response results between numerical integration of the full set of 20 coupled, physical coordinate equations of motion and numerical integration of a partial set of modal coordinate equations of motion, with and without MA.
- Determine the dependence of the peak response on the impact duration τ .

Assumption: Assume that the system is at rest and undeflected prior to impact.

Procedure:

- Form the \underline{M} , \underline{K} , and \underline{C}_0 matrices and $\underline{f}(t)$ vector.

The potential energy expression for the model is

$$U = \frac{1}{2} \left[k_1 q_1^2 + k_2 (q_2 - q_1)^2 + k_3 (q_3 - q_2)^2 + \cdots + k_N (q_N - q_{N-1})^2 \right] \quad (3)$$

then

$$\frac{\partial U}{\partial q_j} = \begin{cases} (k_1 + k_2)q_1 - k_2q_2, & j=1 \\ (k_j + k_{j+1})q_j - k_jq_{j-1} - k_{j+1}q_{j+1}, & j \neq 1, j \neq N \\ k_Nq_N - k_Nq_{N-1}, & j=N \end{cases} \quad (4)$$

or

$$\frac{\partial U}{\partial \underline{q}} = \underline{K}\underline{q} = \begin{bmatrix} k_1 + k_2 & -k_2 & 0 & 0 & \cdots & 0 \\ & k_2 + k_3 & -k_3 & 0 & \cdots & 0 \\ & & k_3 + k_4 & -k_4 & \cdots & 0 \\ & & & & & \vdots \\ \text{symmetric} & & & & & -k_N \\ & & & & & k_N \end{bmatrix} \begin{Bmatrix} q_1 \\ q_2 \\ \vdots \\ q_N \end{Bmatrix} \quad (5)$$

The kinetic energy expression for the model is

$$T = \frac{1}{2} [m_1\dot{q}_1^2 + m_2\dot{q}_2^2 + \cdots + (m_N + m_s)\dot{q}_N^2] \quad (6)$$

then

$$\frac{d}{dt} \left(\frac{\partial T}{\partial \dot{q}_j} \right) = \begin{cases} m_j\ddot{q}_j, & j \neq N \\ (m_j + m_s)\ddot{q}_j, & j = N \end{cases} \quad (7)$$

or

$$\frac{d}{dt} \left(\frac{\partial T}{\partial \dot{\underline{q}}} \right) = \underline{\text{diag}}(m_j^*) \ddot{\underline{q}} \quad (8)$$

where

$$m_j^* = \begin{cases} m_j, & j \neq N \\ m_N + m_s, & j = N \end{cases} \quad (9)$$

An orthogonal damping matrix is required for comparing the solution of the physical coordinate model to the modal coordinate model. From (5.4.140), (5.4.142), and (5.4.146), the damping matrix may be written as

$$\underline{C}_0 = \mu_1 \underline{K} + \sum_{l=1}^4 \frac{2\kappa_l \omega_l}{\tilde{m}_l} \underline{M} \underline{\psi}_l \underline{\psi}_l^T \underline{M} \quad (10)$$

where

$$\mu_1 = \frac{2\xi_5^d}{\omega_5} \quad \text{and} \quad \kappa_l = \xi_l^d - \xi_5^d \frac{\omega_l}{\omega_5}, \quad l = 1, 2, 3, 4 \quad (11)$$

and ω_l and $\underline{\psi}_l$ are the l th natural frequency and mode shape of the undamped system.

The force vector is obtained from the generalized force expression (4.5.52) and noting that the force is applied at dof 5

$$Q_j = \delta_{j5} F_1 \hat{i} \cdot \frac{\partial \bar{v}_5}{\partial \hat{q}_j} = \delta_{j5} F_1 \hat{i} \cdot \frac{\partial \hat{q}_5}{\partial \hat{q}_j} \hat{i} = \begin{cases} 0, & j \neq 5 \\ F_1, & j = 5 \end{cases} \quad (12)$$

where δ_{j5} is a Kronecker delta. From (12),

$$\underline{f}(t) = \underline{Q} = (0 \ 0 \ 0 \ 0 \ F_1 \ 0 \ \dots \ 0)^T \quad 20 \times 1 \quad (13)$$

(b) Equations of motion:

The equations of motion are obtained from Lagrange's equation in the form (4.7.61)

$$\frac{d}{dt} \left(\frac{\partial T}{\partial \underline{\dot{q}}} \right) = \underline{Q} - \frac{\partial U}{\partial \underline{q}} - \underline{C}_0 \underline{\dot{q}} \quad (14)$$

$$\Rightarrow \underline{M} \underline{\ddot{q}} + \underline{C}_0 \underline{\dot{q}} + \underline{K} \underline{q} = \underline{f}(t) \quad (N \times 1) \quad (15)$$

(c) Write code for solving the equations of motion with numerical integration of the physical coordinate equations using MATLAB's ODE45 Runge–Kutta numerical integration routine (see Example 2.3.1). Let

$$\underline{v} = \underline{\dot{q}} \quad (16)$$

then (15) is equivalent to the $2N$ first-order differential equations

$$\underline{\dot{q}} = \underline{V} \quad (17)$$

$$\underline{\dot{V}} = \underline{M}^{-1} \left(\underline{f}(t) - \underline{C}_0 \underline{V} - \underline{K} \underline{q} \right) \quad (18)$$

with the IC vectors

$$\underline{q}(0) = \underline{V}(0) = \underline{0} \quad (19)$$

(d) Modal coordinate-based solution:

Use the MATLAB ODE45 routine (see Example 2.3.1) to numerically integrate the modal EOMs from (6.3.32)

$$\underline{\dot{\chi}} = \underline{V} \underline{\chi} \quad (20)$$

$$\underline{\dot{V}} \underline{\chi} = \text{diag} \left(\frac{1}{\underline{m}_i} \right) \underline{\Psi}^T \underline{f}(t) - \text{diag} (2\underline{\xi}_i \omega_i) \underline{V} \underline{\chi} - \text{diag} (\omega_i^2) \underline{\chi} \quad (21)$$

where $\underline{\Psi}$ is the modal matrix and m is the number of modes ($m \ll N$) utilized. The solution $\underline{\chi}(t)$ of (20) and (21) is substituted into (6.3.11) to obtain the actual physical coordinate displacements

$$\underline{q}(t) = \underline{\Psi} \underline{\chi}(t) \quad (22)$$

(e) Modal coordinate-based solution including modal acceleration:

Same solution procedure as (d); however, use (6.3.33) instead of (22) to obtain the physical coordinate displacements, that is,

$$\underline{q} = \underline{\Psi} \underline{\chi} + \underline{\beta}_c \underline{f}(t) \quad (23)$$

$N \times 1 \quad N \times m \quad m \times 1 \quad N \times N \quad N \times 1$

where $\underline{\beta}_c$ is defined in (6.3.34).

Solution:

(a) This problem is solved with the MATLAB code provided at the end of this example. The natural frequencies for $N=20$ are

$$\underline{f}_n \in (0.54 \ 1.65 \ 2.79 \ 3.94 \ 5.09 \ 6.23 \ 7.33 \ 8.40 \ 9.43 \ 10.40 \ 11.3 \ 12.14 \ 12.90 \ 13.59 \ 14.20 \ 14.71 \ 15.14 \ 15.48 \ 15.72 \ 15.89) \text{ Hz} \quad (24)$$

The modes are mass orthonormalized (5.4.39) yielding unity (5.4.41) as the value for all modal masses \tilde{m}_i . The \underline{C}_0 matrix defined in (10) and (11) and the modal matrix $\underline{\Psi}$ form an orthogonality relation (5.4.121) yielding

$$\underline{\xi}_n \in (0.02 \ 0.02 \ 0.025 \ 0.025 \ 0.03 \ 0.037 \ 0.043 \ 0.050 \ 0.056 \ 0.061 \ 0.067 \ 0.072 \ 0.076 \ 0.080 \ 0.084 \ 0.087 \ 0.089 \ 0.091 \ 0.093 \ 0.094) \quad (25)$$

which agrees with (2). The lowest five mode shapes are shown in Figure E5.4.4(c).

(b) *Physical coordinate solution:*

Figure E6.3.1(c) shows the response of the pole at four locations (mass nos. 1, $N/4$, $N/2$, and N) with an impulse duration of $\tau = 1$ second. The MATLAB ODE45 integrator (ref. Example 2.3.1) is employed to solve (17) and (18) for the ICs given by (19).

(c) *Modal coordinate solution:*

The responses are also obtained by numerically integrating the modal coordinate EOMs given in (20) and (21) with $\underline{\chi} = \underline{\dot{\chi}} = \underline{0}$ at $t=0$. The MATLAB numerical integration option ODE45 (ref. Example 2.3.1) is utilized for this purpose. Figure E6.3.1(d) shows the responses when 10% ($m=2$) and 15% ($m=3$) of the modes, respectively, are utilized in the standard physical coordinate recovery formula (22).

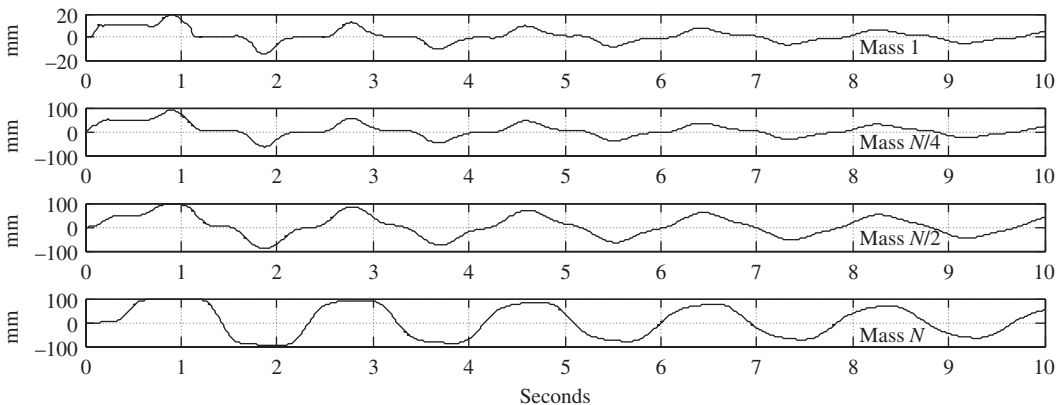


Figure E6.3.1(c) Displacements from direct integration of the physical coordinate EOMs for $\tau = 1$ second

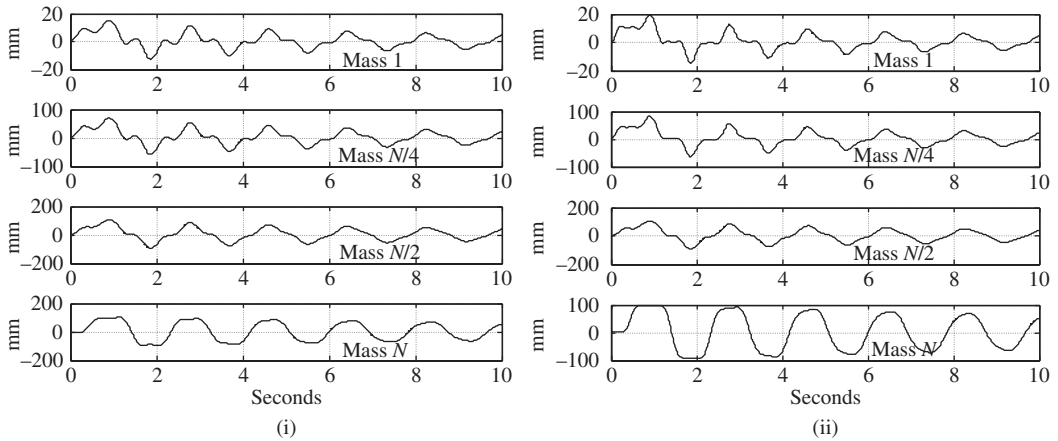


Figure E6.3.1(d) Displacements by integration of modal coordinate EOMs with (i) $m=2$ modes and (ii) $m=3$ modes

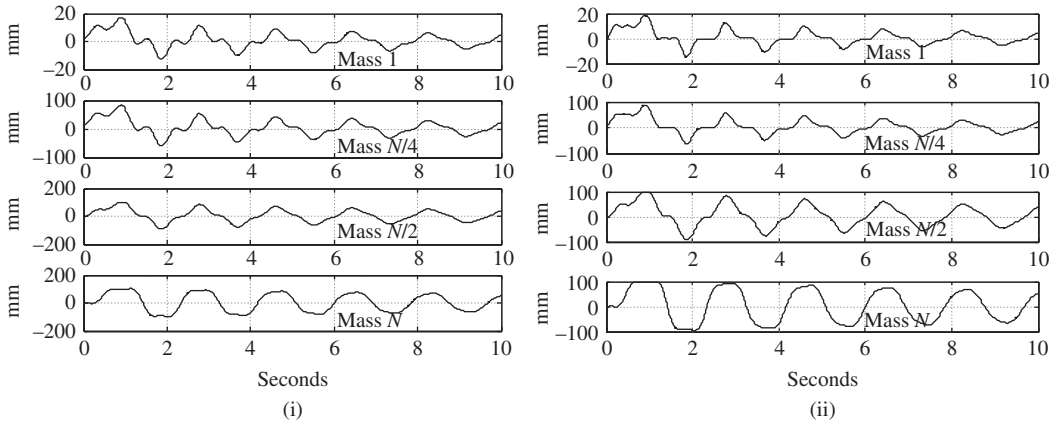


Figure E6.3.1(e) Modal acceleration displacements with (i) $m=2$ modes and (ii) $m=3$ modes

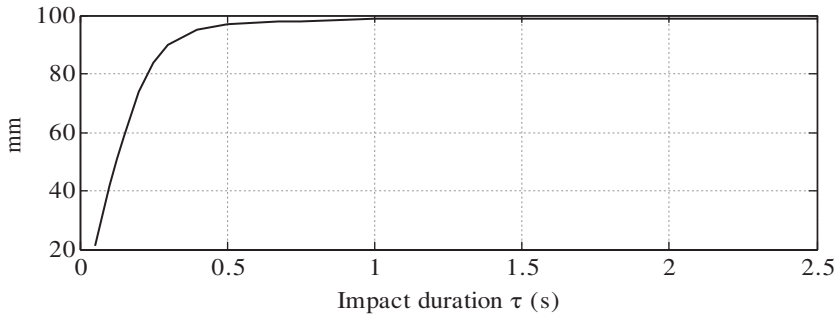
(d) Modal coordinate solution with modal acceleration:

Figure E6.3.1(e) shows the responses when the modal coordinate EOMs are solved with $m=2$ and $m=3$ modes and the physical coordinates are obtained using the modal acceleration method (6.3.33).

Summary: This example provided a comparison between numerical integration of the physical coordinate EOMs and the modal coordinate EOMs for 10 and 15% of the modes. The latter approach is applied with and without modal acceleration for the determination of the physical coordinate responses from the modal coordinate responses. Table E6.3.1(a) summarizes the peak response predications for the various cases. The results show an improvement resulting from application of the modal acceleration approach to the modal condensation solution. The numbers in parentheses are the actual wall clock, elapsed times (in seconds) for performing the integrations. The improved accuracy demonstrates an advantage of using the modal condensation/acceleration approach. Figure E6.3.1(f) shows the peak response over the entire model versus impact duration time τ in Figure E6.3.1(a). The peak increases significantly up to $\tau=0.5$ seconds and then remains constant at approximately 99 mm for longer impact durations. The corresponding static response of masses

Table E6.3.1(a) Peak response summary (wall clock computation time in second)

No. of modes	Physical coordinate integration	Modal coordinate integration	
		Without mode acceleration	With mode acceleration
—	98.56 (4.56)	—	—
2	—	108.89 (1.32)	104.0 (1.65)
3	—	101.40 (1.98)	99.16 (2.31)

**Figure E6.3.1(f)** Peak displacement response of the system versus impact duration (τ)

5 through 20 to the 500 N force at mass 5 is $\delta = F/k_{eq} = F/(k_j/5) = 500/10000 = 50$ mm. This illustrates the importance of performing a dynamic simulation since the vibration overshoot response is twice as large as the static response to the same force.

The preceding results were determined from the following MATLAB code.

```
clear
global N M K Co H height MINV mmod RedModMat diag2zetom omsqmat
iopt tau
% NOTE THAT N MUST BE A MULTIPLE OF 4 FOR PLOTTING PURPOSES AND
% IORDER MUST BE CHANGED IF N IS CHANGED
N=20 ; H = 20 ; k=50000 ; m=20 ; h = H/N ; ms = 50. ;
zetadesired = [.02 .02 .025 .025 .03] ; % desired damping ratios
for modes 1-5
height = h*linspace(1,N,N)
iopt = 2 ; % =0 for direct integration , =1 for modal solution
%           =2 for modal solution with modal acceleration
mmod = 3 ; % No. of modes used in the modal solution
tau = 1.0 % impact duration
% Form mass matrix and its inverse
M = m*eye(N) ; M(N,N) = M(N,N) + ms ; MINV = inv(M) ;
% Form Stiffness Matrix
K = zeros(N,N) ;
kel = k*[1 -1 ; -1 1] ;
for i=1:1:N-1
    K(i:i+1,i:i+1) = K(i:i+1,i:i+1) + kel ;
end
K(1,1) = K(1,1) + k ;
```

```

% Determine the undamped system's natural frequencies and mode
shapes
[modalmatrix, otemp] = eig(K,M) ;
omegasquared = diag(otemp) ;
omega =sqrt(omegasquared) ;
natfreq = omega/2/pi;
% In general, the natural frequencies may not be arranged in
ascending order
% in omegasquared , omega and natfreq . For this example the
ordering is
iorder= [1 2 3 4 5 6 7 8 9 10 11 12 13 14 15 16 17 18 19 20];
% Reorder mode shapes and natural frequencies in ascending order
as follows
for i=1:1:N
    orderomega(iorder(i)) = omega(i) ;
    ordernatfreq(iorder(i)) = natfreq(i) ;
    ordermodmat(1:N,iorder(i)) = modalmatrix(1:N,i) ;
end
orderomega
ordernatfreq

% Determine the Modal Masses of the original modes (Use of diag
here insures % that no off diagonal terms in modalmassmatrix are
negative which will cause % there sqrt to be complex below)
modalmass = diag(ordermodmat'*M*ordermodmat);
modalmassmatrix=diag(modalmass) ;
% Rescale the modeshapes so that all the modal masses equal one.
ordermodmat=ordermodmat*inv(sqrt(modalmassmatrix)) ;
% Determine the Modal Masses of the "mass orthonormalized" mode
shapes
modalmass = ordermodmat'*M*ordermodmat;
% The modal masses are now all unity and the modalmass matrix is
the identity % matrix
% Plot 5 lowest modes
iplt=0
if iplt==1
plot(ordermodmat(1:N,1),height,'ok-',ordermodmat(1:N,2),
height,'xk-',...
ordermodmat(1:N,3),height,'+k-',ordermodmat(1:N,4),
height,'*k-',...
ordermodmat(1:N,5),height,'sk-')
grid on
xlabel('mode component (dim)');
ylabel('height in meters');
for i=1:1:5
    msg=sprintf('<<<mode %2.f ',i);
    gtext(msg)
end
pause
end % iplt

```

```

% Form the orthogonal damping matrix in eqs.10 and 11
mul = 2*zetadesired(5)/orderomega(5) ;
dum=zeros(N,N);
for i=1:1:4
    zeta = zetadesired(i) - zetadesired(5)*orderomega(i) /
orderomega(5);
    dum = dum+2*zeta*orderomega(i)*ordermodmat(1:N,i)
*ordermodmat(1:N,i)';
end
Co = mul*K + M*dum*M ;
% Check if Co is orthogonal and if the desired zetas are obtained
ZETACHECK = 0.5*ordermodmat'*Co*ordermodmat*inv(diag
(orderomega));

% Begin Direct Numerical Integration Solution With Matlab ODE45
Option
tfin = 10 ; % integrate response for 10 seconds
tspan=linspace(0,tfin,800) ; % Times for plotting
if iopt == 0 % Use Matlab ODE45 for direct integration of the EOM's
Qinitial = zeros(2*N,1) ; % Zero initial deflections and
velocities
[t,Q] = ode45('CodeE6_3_1sub',tspan,Qinitial);

else % Do Modal Based Solution
    % Form the reduced modal matrix with only the lowest mmod modes as
columns
    RedModMat=ordermodmat(1:N,1:mmod) ;
    % Form the reduced 2*zeta*omega matrix
    diag2zetom = RedModMat'*Co*RedModMat ;
    % Form The omega^2 matrix
    omsqmat = zeros(mmod,mmod) ;
    for i=1:1:mmod
        omsqmat(i,i) = orderomega(i)^2 ;
    end
    Qinitial = zeros(2*mmod,1) ; % Zero initial modal coordinate
deflections
                                % and velocities
    [t,Q] = ode45('CodeE6_3_1sub',tspan,Qinitial);
    % Determine the physical coordinate responses from the modal
coordinate
% responses
for i =1:1:800
    Q(i,1:N)=Q(i,1:mmod)*RedModMat' ;
end

if iopt==2 % Use mode acceleration method
    betac = inv(K) - RedModMat*inv(omsqmat)*RedModMat'
    for i=1:1:800
        f = zeros(N,1) ;
        if i<81

```



```

        f(N/4,1) = 500 ;
    end
    Q(i,1:N) = Q(i,1:N) + f'*betac' ;
end
end
end % if iopt

maxresp= max(max(abs(1000*Q(1:800,1:N))))

subplot(4,1,1);
plot(t',1000*Q(1:800,1));
grid on
ylabel('q mm')
msg = sprintf('Mass 1 ');
gtext(msg);
if iopt>0
msg=sprintf('The maximum response= %2.f in mm',maxresp);
end
if iopt==0
msg=sprintf('The maximum response= %2.f in mm', maxresp);
end
gtext(msg);
pause
subplot(4,1,2);
plot(t',1000*Q(1:800,N/4));
grid on
ylabel('q mm')
msg = sprintf('Mass N/4 ');
gtext(msg);
pause
subplot(4,1,3);
plot(t',1000*Q(1:800,N/2));
grid on
ylabel('q mm')
msg = sprintf('Mass N/2 ');
gtext(msg);
pause
subplot(4,1,4);
plot(t',1000*Q(1:800,N));
grid on
ylabel('q mm')
msg = sprintf('Mass N ');
gtext(msg);xlabel('time in sec');
pause
close

% Plot maximum response values vs. tau
tauvec=[.05 .1 .125 .15 .2 .25 .3 .4 .5 .675 .75 .875 1.0 1.25 1.5
2.0 2.5];
mxresvec= [21 42 51 59 74 84 90 95 97 98 98 98.4 99 99 99 99 99 ];
```

```

plot(tauvec, mxresvec, 'k-' );
grid on
xlabel('Impact duration tau in sec. ');
ylabel('Disp mm');

subfunction for Example 6.3.1
function Qdot = CodeE9_3_1sub(t,Q)
global N M K Co H height MINV mmod RedModMat diag2zetom omsqmat
iopt tau
f = zeros(N,1);
if t<tau
    f(N/4,1) = 500;
end
if iopt == 0 % Directly integrate EOM's with Matlab ODE45
Qdot = zeros(2*N,1);
Qdot(1:N,1) = Q(N+1:2*N,1);
Qdot(N+1:2*N,1) = MINV*( f - Co*Q(N+1:2*N,1) - K*Q(1:N,1) );
else % Integrate the modal EOM's
    Qdot = zeros(2*mmod,1);
    Qdot(1:mmod,1) = Q(mmod+1:2*mmod,1);
    Qdot(mmod+1:2*mmod,1) = RedModMat'*f - diag2zetom*Q(mmod
+1:2*mmod,1) - ...
    omsqmat*Q(1:mmod,1);
end

```

6.3.2 Unconstrained Structures

An unconstrained structure or machinery component such as an airplane, satellite, or rotating shaft can be displaced as a rigid body mode without applying external loads or reactions. Therefore, from (5.4.54), (5.4.55), (5.4.57), and (5.4.58),

$$\underline{K}\underline{q}_{\text{rig}} = \underline{0} \quad (N \times 1) \quad (6.3.36)$$

$$\underline{M}\underline{\ddot{q}}_{\text{rig}} = \underline{0} \quad (N \times 1) \quad (6.3.37)$$

$$\underline{q}_{\text{rig}} = \sum_{l=1}^{n_{\text{rig}}} \left(\alpha_{\text{rig}0,l} \underline{\psi}_{\text{rig},l} + \alpha_{\text{rig}1,l} t * \underline{\psi}_{\text{rig},l} \right) \quad (6.3.38)$$

$$\Rightarrow \omega_{\text{rig},l} = 0 \quad l = 1, 2, \dots, n_{\text{rig}} \text{ (no. of rigid body modes)} \quad (6.3.39)$$

The rigid body modes are obtained by solving (6.3.36) where \underline{K} is singular. The $\underline{\psi}_{\text{rig},l}$ therefore are the basis vectors that span the null space of \underline{K} (see Section 2.6). The $\alpha_{\text{rig}0,l}$ and $\alpha_{\text{rig}1,l}$ in (6.3.38) are obtained by considering ICs as in ((5.4.60) and (5.4.61)). Partition the modal matrix into two groups (rigid body and elastic body modes):

$$\underline{\Psi} = \left[\underline{\psi}_{\text{R}1} \quad \dots \quad \underline{\psi}_{\text{R}n_{\text{rig}}} \quad \underline{\psi}_{\text{e}1} \quad \dots \quad \underline{\psi}_{\text{e}n_{\text{e}}} \right] = \left[\underline{\Psi}_{\text{R}} \quad \underline{\Psi}_{\text{e}} \right] \quad (6.3.40)$$

where

$$\underline{\psi}_{Rj} = j\text{th rigid body mode, } \underline{\psi}_{el} = l\text{th elastic (flexible) body mode} \quad (6.3.41)$$

Then by (2.6.31) and (6.3.36),

$$\underline{K}\underline{\Psi}_R = \begin{bmatrix} \underline{K}\underline{\psi}_{R1} & \underline{K}\underline{\psi}_{R2} & \cdots & \underline{K}\underline{\psi}_{Rn_{\text{rig}}} \end{bmatrix} = \underline{0} \quad (6.3.42)$$

Consider an undamped system represented by the equilibrium equation

$$\underline{M}\ddot{\underline{q}} + \underline{K}\underline{q} = \underline{f}(t) \quad (N \times 1) \quad (6.3.43)$$

Utilize (2.6.30) to transform coordinates according to

$$\underline{q}(t) = \sum_{l=1}^{n_{\text{rig}}} \eta_{Rl}(t) \underline{\psi}_{Rl} + \sum_{j=1}^{n_e} \eta_{ej}(t) \underline{\psi}_{ej} = \underline{\Psi}_R * \eta_{\underline{R}}(t) + \underline{\Psi}_e * \eta_{\underline{e}}(t) = \underline{q}_R(t) + \underline{q}_e(t) \quad (6.3.44)$$

where η_{Ri} and η_{ej} are the rigid and elastic body modal coordinates. Substitute (6.3.44) into (6.3.43):

$$\underline{M}\underline{\Psi}_R \ddot{\eta}_{\underline{R}} + \underline{M}\underline{\Psi}_e \ddot{\eta}_{\underline{e}} + \underline{K}\underline{\Psi}_R \eta_{\underline{R}} + \underline{K}\underline{\Psi}_e \eta_{\underline{e}} = \underline{f}(t) \quad (6.3.45)$$

The third term in (6.3.45) is zero by (6.3.42). Premultiply (6.3.45) by $\underline{\Psi}_R^T$ and utilize the orthogonality conditions (5.4.35) and (5.4.45)

$$\underline{\Psi}_R^T \underline{M} \underline{\Psi}_e = \underline{0} \quad (6.3.46)$$

$$\underline{\Psi}_R^T \underline{K} \underline{\Psi}_e = \underline{0} \quad (6.3.47)$$

which results since the elastic modes have distinct natural frequencies from the rigid body modes to obtain

$$\underline{\Psi}_R^T \underline{M} \underline{\Psi}_R \ddot{\eta}_{\underline{R}} = \underline{\Psi}_R^T \underline{f}(t) \quad (6.3.48)$$

$$\ddot{\eta}_{\underline{R}} = \tilde{\underline{M}}_R^{-1} \underline{\Psi}_R^T \underline{f}(t) \quad (n_{\text{rig}} \times 1) \quad (6.3.49)$$

where the rigid body mode modal mass matrix is

$$\tilde{\underline{M}}_R = \underline{\Psi}_R^T \underline{M} \underline{\Psi}_R = \tilde{\underline{M}}_R^T \quad (n_{\text{rig}} \times n_{\text{rig}}) \quad (6.3.50)$$

Equation (6.3.49) may be solved for the rigid body modal coordinates $\eta_{Ri}(t)$, that is, the first-order form

$$\dot{\underline{V}}_{\eta R} = \tilde{\underline{M}}_R^{-1} \underline{\Psi}_R^T \underline{f}(t) \quad (6.3.51)$$

$$\dot{\underline{\eta}}_R = \underline{V}_{\eta R} \quad (6.3.52)$$

can be numerically integrated (Section 6.4). Multiply (6.3.45) by $\underline{\Psi}_e^T$ and utilize the transposed form of the orthogonality conditions (6.3.46) and (6.3.47)

$$\underline{\Psi}_e^T \underline{M} \underline{\Psi}_R = \underline{0}^T = \underline{0}, \quad \underline{\Psi}_e^T \underline{K} \underline{\Psi}_R = \underline{0}^T = \underline{0} \quad (6.3.53)$$

to obtain the governing equation for the elastic modal coordinates

$$\underline{\text{diag}}(\tilde{m}_{ei})\ddot{\underline{\eta}}_e + \underline{\text{diag}}(\tilde{m}_{ei}\omega_{ei}^2)\underline{\eta}_e = \underline{\Psi}_e^T f(t) \quad (6.3.54)$$

where \tilde{m}_{ei} and ω_{ei} are the elastic mode modal masses and natural frequencies, respectively. Equation (6.3.54) yields the following uncoupled ODEs for the elastic mode modal coordinates

$$\ddot{\eta}_{ej} + \omega_{ej}^2 \eta_{ej} = \frac{1}{\tilde{m}_{ej}} \underline{\psi}_{ej}^T f(t) = \frac{\tilde{f}_{ej}}{\tilde{m}_{ej}} \quad (6.3.55)$$

where

$$\tilde{f}_{ej} = \underline{\psi}_{ej}^T f(t) = j\text{th elastic mode's modal force} \quad (6.3.56)$$

$$\tilde{m}_{ej} = \underline{\psi}_{ej}^T \underline{M} \underline{\psi}_{ej} = j\text{th elastic mode's modal force} \quad (6.3.57)$$

6.3.2.1 Separation of Elastic Body Motion Component

Substitute (6.3.49) into (6.3.45)

$$\underline{M} \underline{\Psi}_e \ddot{\underline{\eta}}_e + \underline{K} \underline{\Psi}_e \underline{\eta}_e = \underline{f}(t) - \underline{M} \underline{\Psi}_R \ddot{\underline{\eta}}_R = \left(\underline{I} - \underline{M} \underline{\Psi}_R \tilde{\underline{M}}_R^{-1} \underline{\Psi}_R^T \right) \underline{f}(t) \quad (6.3.58)$$

Define

$$\underline{H} = \underline{I} - \underline{\Psi}_R \tilde{\underline{M}}_R^{-1} \underline{\Psi}_R^T \underline{M} \quad (6.3.59)$$

or

$$\underline{H}^T = \underline{I} - \underline{M}^T \underline{\Psi}_R \tilde{\underline{M}}_R^{-T} \underline{\Psi}_R^T = \underline{I} - \underline{M} \underline{\Psi}_R \tilde{\underline{M}}_R^{-1} \underline{\Psi}_R^T \quad (6.3.60)$$

since \underline{M} and $\tilde{\underline{M}}_R$ are symmetric. Then (6.3.58) may be written as

$$\underline{M} \underline{\Psi}_e \ddot{\underline{\eta}}_e + \underline{K} \underline{\Psi}_e \underline{\eta}_e = \underline{H}^T \underline{f}(t) \quad (6.3.61)$$

Some special properties of the \underline{H} matrix are derived as follows. Multiply (6.3.61) by $\underline{\Psi}_R^T$ and employ orthogonality (6.3.46 and 6.3.47) to obtain

$$\underline{\Psi}_R^T \underline{H}^T \underline{f}(t) = \underline{0} \quad (n_{rig} \times 1) \quad (6.3.62)$$

which implies by (6.3.40) that

$$\underline{\psi}_{Rj}^T \underline{H}^T \underline{f}(t) = \underline{0} \quad (6.3.63)$$

Thus, $\underline{H}^T \underline{f}(t)$ is orthogonal with respect to the rigid body modes $\underline{\psi}_{Rj}^T$, for all time t .

From (6.3.50) and (6.3.59),

$$\underline{H} \underline{\Psi}_R = \underline{\Psi}_R - \underline{\Psi}_R \tilde{\underline{M}}_R^{-1} \underline{\Psi}_R^T \underline{M} \underline{\Psi}_R = \underline{\Psi}_R - \underline{\Psi}_R \tilde{\underline{M}}_R^{-1} \tilde{\underline{M}}_R = \underline{0} \quad (6.3.64)$$

From (6.3.46) and (6.3.59),

$$\underline{H} \underline{\Psi}_e = \underline{\Psi}_e - \underline{\Psi}_e \tilde{\underline{M}}_R^{-1} \underline{\Psi}_R^T \underline{M} \underline{\Psi}_e = \underline{\Psi}_e \quad (6.3.65)$$

The elastic body motion component of the total response vector $\underline{q}(t)$ may be separated out from the total response by considering (6.3.44), (6.3.64), and (6.3.65):

$$\begin{aligned}\underline{H}\underline{q}(t) &= \underline{H}\underline{\Psi}_R\underline{\eta}_R(t) + \underline{H}\underline{\Psi}_e\underline{\eta}_e(t) = \underline{\Psi}_e\underline{\eta}_e(t) = \underline{q}_e(t) \\ &= \text{elastic body component of the total response, by (6.3.44)}\end{aligned}\quad (6.3.66)$$

Thus, the \underline{H} may be viewed as a “filter” matrix which produces only the elastic component of the response when it premultiplies the total (rigid + elastic) response vector.

EXAMPLE 6.3.2 *Free Fall of a Crate with Flexibly Mounted Contents*

Description: The crate shown in Figure E6.3.2(a) contains two instruments which are packaged with a compliant material. The package is ejected out of the cargo hold of an aircraft.

Objective: Determine the relative motions of the packages with respect to the crate for a short period of time (T), after ejection of the crate and prior to parachute deployment.

Assumptions:

- (a) The crate does not rotate from $0 \leq t \leq T$.
- (b) The wind force f_w acts like a short ramp and then a step from $0 \leq t \leq T$.
- (c) The packages do not rotate in the crate.

Solution: The solution begins by considering the initial deflections of the masses in the crate in the translating nonaccelerating frame attached to the plane (Figure E6.3.2(b)). These are listed in the following table and may be calculated as follows:

$$k_v\Delta_6 + k_v(\Delta_6 - \Delta_4) = m_2g, \quad k_v\Delta_4 - k_v(\Delta_6 - \Delta_4) = m_1g \quad (1)$$

$$\Rightarrow \Delta_4 = \frac{(2m_1 + m_2)g}{3k_v}, \quad \Delta_6 = \frac{(2m_2 + m_1)g}{3k_v} \quad (2)$$

	q_1	q_2	q_3	q_4	q_5	q_6
Displacements	0	0	0	$-\Delta_4$	0	$-\Delta_6$
Velocities	0	0	0	0	0	0

The free body diagrams for the three masses are shown in Figure E6.3.2(c). The spring forces are

$$\begin{aligned}f_{Hc1} &= 2k_H(q_3 - q_1), \quad f_{Hc2} = 2k_H(q_5 - q_1), \\ f_{vc1} &= k_v(q_4 - q_2), \quad f_{vc2} = k_v(q_2 - q_6), \quad f_{12} = k_v(q_6 - q_4)\end{aligned}\quad (3)$$

Applying Newton's law yields

$$m_c\ddot{q}_1 = f_{Hc1} + f_{Hc2} + f_w = -4k_Hq_1 + 2k_Hq_3 + 2k_Hq_5 + f_w \quad (4)$$

$$m_c\ddot{q}_2 = f_{vc1} - f_{vc2} - m_cg = -2k_vq_2 + k_vq_4 + k_vq_6 - m_cg \quad (5)$$

$$m_1\ddot{q}_3 = -f_{Hc1} = -2k_Hq_3 + 2k_Hq_1 \quad (6)$$

$$m_1\ddot{q}_4 = f_{12} - f_{vc1} - m_1g = k_v(q_6 - q_4) - k_v(q_4 - q_2) - m_1g \quad (7)$$

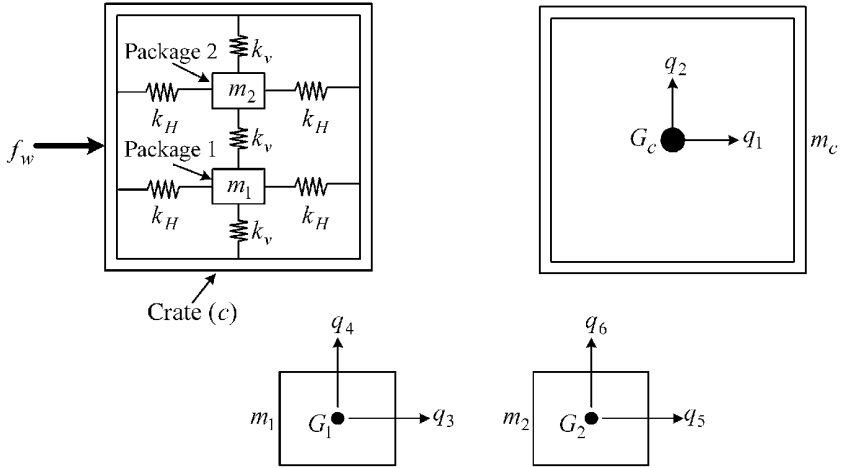


Figure E6.3.2(a) Crate with elastically mounted components

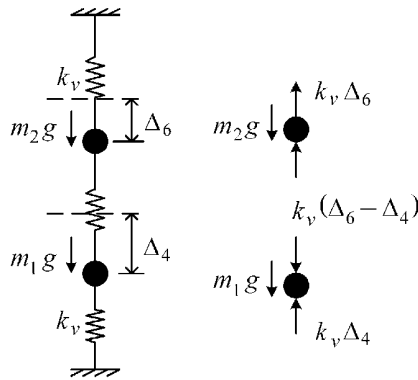


Figure E6.3.2(b) Initial static deflections for packages

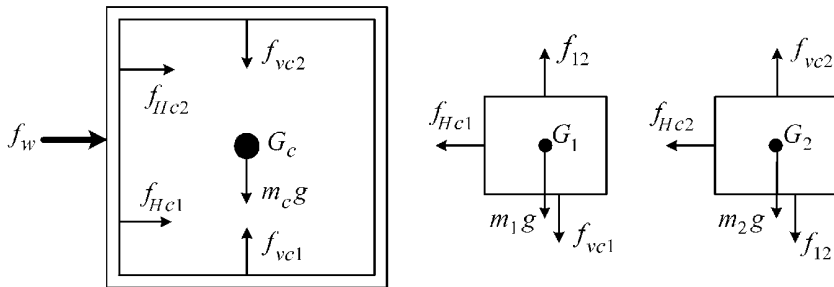


Figure E6.3.2(c) Free body diagrams for crate and packages

$$m_2 \ddot{q}_5 = -f_{Hc2} = -2k_H q_5 + 2k_H q_1 \quad (8)$$

$$m_2 \ddot{q}_6 = f_{vc2} - f_{12} - m_2 g = k_v(q_2 - q_6) - k_v(q_6 - q_4) - m_2 g \quad (9)$$

The matrix–vector form of these equations is

$$\underline{M}\ddot{\underline{q}} + \underline{K}\underline{q} = \underline{f}(t) \quad (6 \times 1) \quad (10)$$

where

$$\underline{M}_{6 \times 6} = \underline{\text{diag}}(m_c \quad m_c \quad m_1 \quad m_1 \quad m_2 \quad m_2) \quad (11)$$

$$\underline{K}_{6 \times 6} = \begin{bmatrix} 4k_H & 0 & -2k_H & 0 & -2k_H & 0 \\ 0 & 2k_v & 0 & -k_v & 0 & -k_v \\ -2k_H & 0 & 2k_H & 0 & 0 & 0 \\ 0 & -k_v & 0 & 2k_v & 0 & -k_v \\ -2k_H & 0 & 0 & 0 & 2k_H & 0 \\ 0 & -k_v & 0 & -k_v & 0 & 2k_v \end{bmatrix} \quad (12)$$

$$\underline{f}_{6 \times 1} = (f_w \quad -m_c g \quad 0 \quad -m_1 g \quad 0 \quad -m_2 g)^T \quad (13)$$

The horizontal wind force has the form shown in Figure E6.3.2(d). Therefore,

$$f_w(t) = \begin{cases} 1000 * t, & t < 0.5 \text{ second (Newtons)} \\ 500, & 1 \leq t \leq 3 \text{ seconds} \end{cases} \quad (14)$$

The mass and stiffness values are

$$m_c = 100\text{kg}, \quad m_1 = 25\text{kg}, \quad m_2 = 20\text{kg}, \quad k_H = 1500\text{N/m}, \quad k_v = 2000\text{N/m} \quad (15)$$

The natural frequencies (ω_i) and mode shapes ($\underline{\psi}_i$) are obtained by solving

$$\omega_i^2 \underline{M}\underline{\psi}_i = \underline{K}\underline{\psi}_i \quad (16)$$

$$\Rightarrow \lambda \underline{\psi}_i = \underline{A}\underline{\psi}_i, \quad \lambda = \omega_i^2, \quad \underline{A} = \underline{M}^{-1} \underline{K} \quad (17)$$

Modes 1 and 2 in Figure E6.3.2(e) are rigid body modes and are not unique since any linear combination of these modes is also a valid rigid body mode. Rigid body modes may also be selected by inspection. For example, both

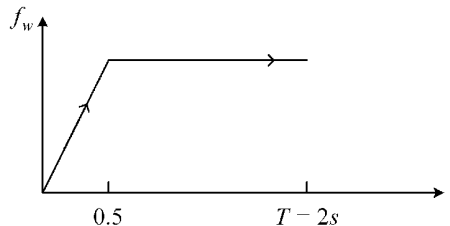


Figure E6.3.2(d) Wind force time history

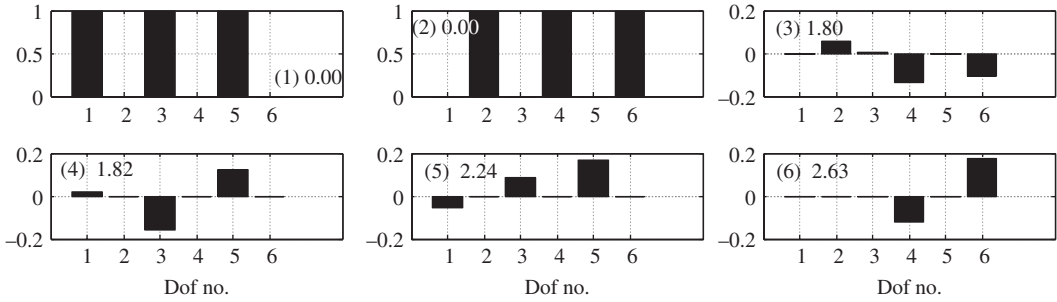


Figure E6.3.2(e) Natural frequencies (Hz) and mode shape components versus degree of freedom number for the crate and packages

$$\underline{\psi}_{\text{rig, horizontal}} = (1 \ 0 \ 1 \ 0 \ 1 \ 0)^T, \quad \underline{\psi}_{\text{rig, vertical}} = (0 \ 1 \ 0 \ 1 \ 0 \ 1)^T \quad (18)$$

satisfy the rigid body mode condition

$$\underline{K}\underline{\psi}_{\text{rig}} = \underline{0} \quad (19)$$

for \underline{K} defined in (12). The rigid body modes are not orthogonal with respect to each other (because $\omega=0$ is a *repeated* eigenvalue); however, the rigid body and elastic modes are orthogonal, and the elastic modes are orthogonal with respect to each other. The transient response may be obtained by numerically integrating (Section 6.4) Equation (10) in its first-order form

$$\underline{\dot{V}} = -\underline{M}^{-1}\underline{K}\underline{q} + \underline{M}^{-1}\underline{f}(t) \quad (6 \times 1) \quad (20)$$

$$\underline{\dot{q}} = \underline{V} \quad (6 \times 1) \quad (21)$$

or

$$\underline{\dot{X}} = \underline{\hat{A}}\underline{X} + \underline{\hat{f}} \quad (12 \times 1) \quad (22)$$

$$\underline{\dot{X}} = \left\{ \begin{array}{c} \underline{V} \\ \underline{q} \end{array} \right\}, \quad \underline{\hat{A}} = \begin{bmatrix} \underline{0} & -\underline{M}^{-1}\underline{K} \\ \underline{I} & \underline{0} \end{bmatrix}, \quad \underline{\hat{f}} = \left\{ \begin{array}{c} \underline{M}^{-1}\underline{f} \\ \underline{0} \end{array} \right\} \quad (23)$$

The elastic displacements are then obtained by applying the “filter” equation (6.3.66)

$$\underline{q}_e(t) = \underline{H}\underline{q}(t) \quad (24)$$

Figure E6.3.2(f) shows the total displacements, and Figure E6.3.2(g) shows the elastic displacements obtained by this approach. The elastic part of the transient response may also be obtained by integrating the elastic mode modal coordinate differential equations (6.3.54)

$$\ddot{\eta}_{ej} + \omega_{ej}^2 \eta_{ej} = \frac{1}{\tilde{m}_{ej}} \underline{\Psi}_{ej}^T \underline{f}(t) \quad (25)$$

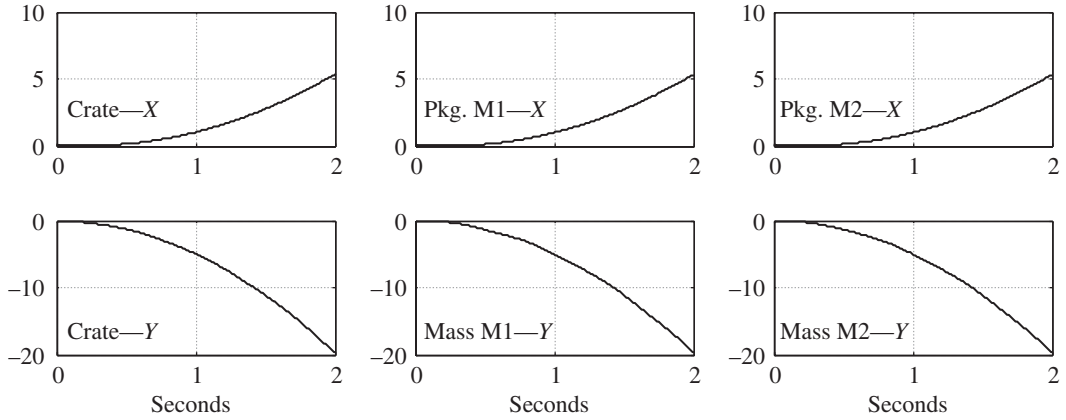


Figure E6.3.2(f) Total displacements in meters for $0 \leq t \leq 2$ seconds utilizing numerical integration of physical coordinate

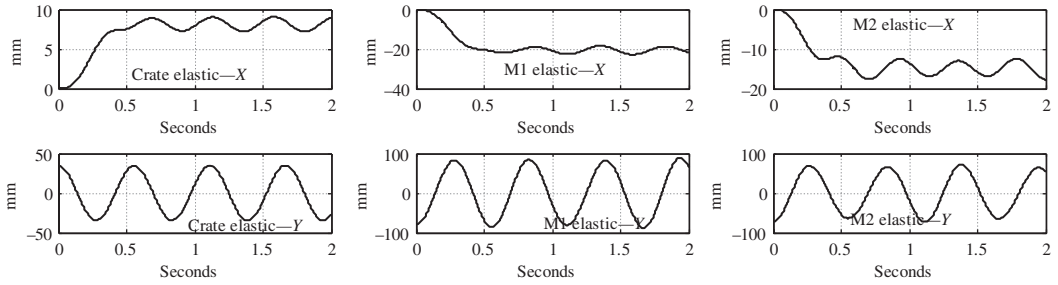


Figure E6.3.2(g) Elastic displacements (mm) for $0 \leq t \leq 2$ seconds by physical coordinate integration with elastic response filter in Equation (24)

with ICs obtained from

$$\begin{Bmatrix} \eta_R(0) \\ \eta_e(0) \end{Bmatrix} = [\underline{\Psi}_R \quad \underline{\Psi}_e]^{-1} \underline{q}(0), \quad \begin{Bmatrix} \dot{\eta}_R(0) \\ \dot{\eta}_e(0) \end{Bmatrix} = [\underline{\Psi}_R \quad \underline{\Psi}_e]^{-1} \dot{\underline{q}}(0) \quad (26)$$

Another approach for obtaining the modal coordinate ICs utilizes orthogonality, that is, from (6.3.44),

$$\underline{\psi}_{ek}^T \underline{M} \underline{q}(0) = \sum \eta_{Ri}(0) (\underline{\psi}_{ek}^T \underline{M} \underline{\psi}_{Ri}) + \sum \eta_{ej}(0) \underline{\psi}_{ek}^T \underline{M} \underline{\psi}_{ej} = \eta_{ek}(0) \tilde{m}_{ek} \quad (27)$$

$$\Rightarrow \eta_{ek}(0) = \frac{1}{\tilde{m}_{ek}} \underline{\psi}_{ek}^T \underline{M} \underline{q}(0) \quad (28)$$

Similarly,

$$\dot{\eta}_{ek}(0) = \frac{1}{\tilde{m}_{ek}} \underline{\psi}_{ek}^T \underline{M} \dot{\underline{q}}(0) \quad (29)$$

The elastic response is then obtained using (6.3.44)

$$\underline{q}_e(t) = \underline{\Psi}_e \underline{\eta}_e(t) \quad (30)$$

The numerical integration utility MATLAB ODE45 of Section 2.3 requires first-order differential equations (Example 2.3.1) so (25) is written as

$$\dot{v}_{\eta_{ej}} = -\omega_{ej}^2 \eta_{ej} + \frac{1}{\tilde{m}_{ej}} \Psi_{ej}^T f(t), \quad \dot{\eta}_{ej} = v_{\eta_{ej}} \quad (31)$$

where $j=1,2,3,4$ for the four elastic modes. The state vector integrated by MATLAB ODE45 (ref. Example 2.3.1) for this approach has the form

$$\underline{X}_{\text{modal}} = (v_{\eta_{e1}} \ v_{\eta_{e2}} \ v_{\eta_{e3}} \ v_{\eta_{e4}} \ \eta_{e1} \ \eta_{e2} \ \eta_{e3} \ \eta_{e4})^T \quad (32)$$

Figure E6.3.2(e) illustrates the two rigid body and four elastic mode shapes. The rigid body modes (1 and 2) have zero (0) natural frequencies. Figure E6.3.2(f) shows the total displacements for all six coordinates, where the maximum total displacement is shown to be 20 m. Clearly, the rigid body modes dominate this response. There is an elastic mode (vibration) component of the response as shown in Figure E6.3.2(g) for $0 \leq t \leq 2$ seconds. This plot is made utilizing the elastic response filter Equation (24) and MATLAB ODE45 integration of the physical coordinate equations. Figure E6.3.2(h) shows the elastic displacements for $0 \leq t \leq 2$ seconds utilizing Equation (30) and MATLAB ODE45 numerical integration of modal coordinates. Figure E6.3.2(i) shows the total displacements for $0 \leq t \leq 6$ seconds with a maximum displacement of 180 m. Figure E6.3.2(j) was made with the same conditions (elastic response filter, Eq. 24, approach) as Figure E6.3.2(g) however

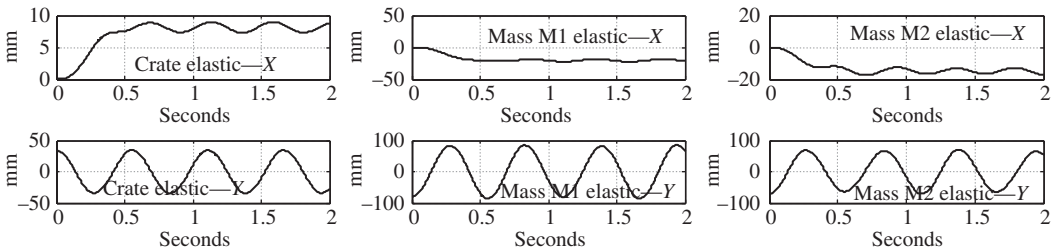


Figure E6.3.2(h) Elastic displacements (mm) for $0 \leq t \leq 2$ seconds by modal coordinate integration

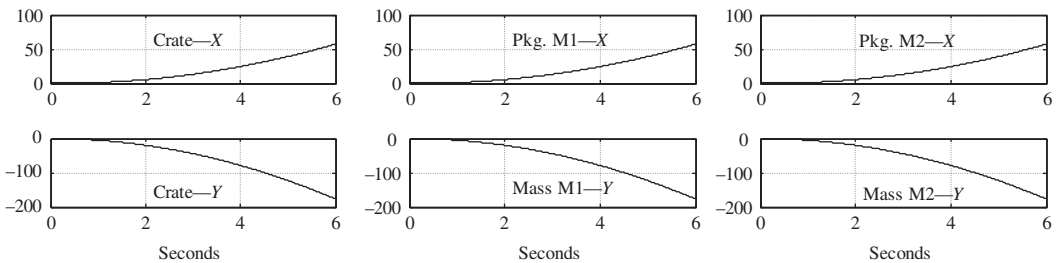


Figure E6.3.2(i) Total displacements (m) for $0 \leq t \leq 6$ seconds

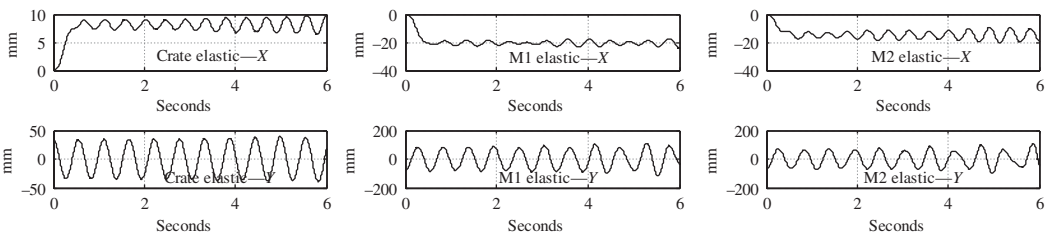


Figure E6.3.2(j) Elastic displacements for $0 \leq t \leq 6$ seconds by physical coordinate integration

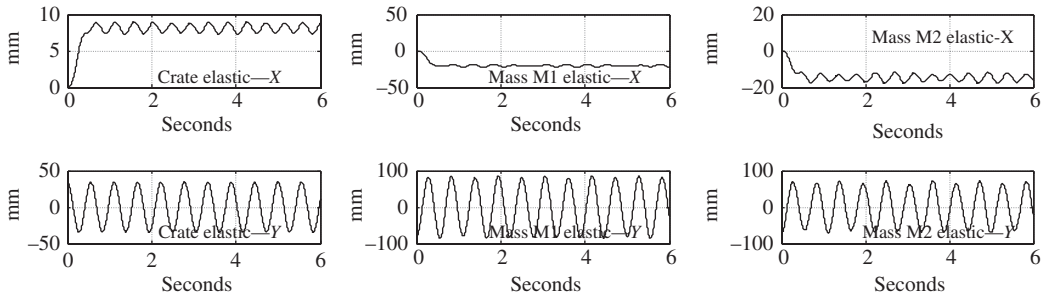


Figure E6.3.2(k) Elastic displacements for $0 \leq t \leq 6$ seconds by modal coordinate integration

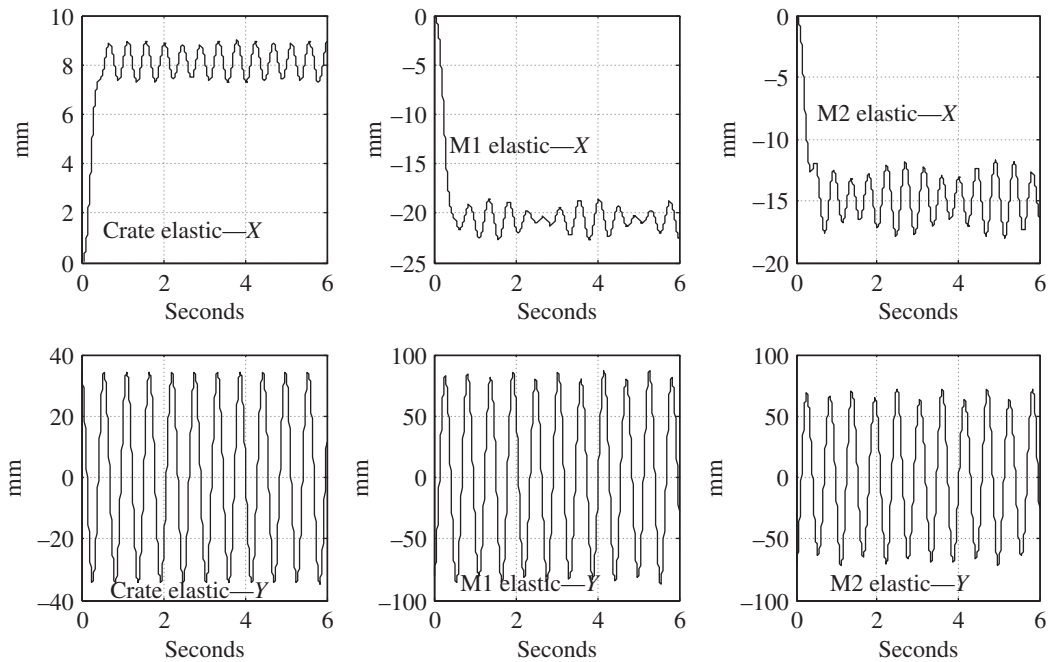


Figure E6.3.2(l) Elastic displacements for $0 \leq t \leq 6$ seconds by physical coordinate integration and using $\text{RelTol} = 10^{-4}$ in MATLAB ODE45 numerical integration

for $0 \leq t \leq 6$ seconds. Note the divergence in the Crate Elastic x amplitudes due to a numerical instability. There is no physical reason for unstable response (Section 5.6), so it must be a numerical integration-induced instability. This type of divergence may result when spring forces are obtained using the difference between very large displacements to obtain the very small relative displacements. Figure E6.3.2(k) has the same conditions as Figure E6.3.2(j); however, the integration of the modal coordinates yields numerically stable results.

NI Tolerance

This example illustrates the limitations encountered when implementing some numerical solutions. The numerical instability shown in the Crate Elastic x and m_2 Elastic x plots in Figure E6.3.2(j) renders the results unreliable. Fortunately, MATLAB is a very versatile code and offers the user a quick fix simply by lowering an integration error tolerance.

The default absolute error tolerance is $\text{AbsTol} = 10^{-6}$, and the default relative error tolerance $\text{RelTol} = 10^{-3}$. These tolerances may be lowered with the following MATLAB commands:

```
REL TOL=1.0e-04; ABSTOL = 1.0e-06;
options = odeset('RelTol',REL TOL,'AbsTol',ABSTOL);
[t,x] = ode45('CodeE_6_3_2_sub',tspan,InitialConditions,
options);
```

The displacement responses are shown in Figure E6.3.2(l). Clearly, by comparison with Figure E6.3.2(j), the numerical instability has been removed by lowering the relative error tolerance from 10^{-3} to 10^{-4} .

6.3.3 Base Excitation

The analysis in Equations (6.2.62)–(6.2.75) provided a systematic approach for obtaining the peak response of a single dof model to arbitrary base excitation, as a function of natural frequency or damping ratio. This methodology can be extended to general N degree of freedom models by utilizing uncoupled modal coordinates. Consider a system subjected to base excitation $x_B(t)$ only in the X direction as depicted in Figure 6.3.1. The frame-type model has two translational and one rotational degree of freedom at each node.

The system displacement vector is expressed in terms of absolute and relative coordinates as follows:

$$\underline{X} = \begin{Bmatrix} x_1 \\ x_2 \\ x_3 \\ x_4 \\ x_5 \\ x_6 \\ \vdots \\ x_{N-2} \\ x_{N-1} \\ x_N \end{Bmatrix} = \begin{Bmatrix} x_B + x_{R1} \\ x_{R2} \\ x_{R3} \\ x_B + x_{R4} \\ x_{R5} \\ x_{R6} \\ \vdots \\ x_B + x_{R,N-2} \\ x_{R,N-1} \\ x_{R,N} \end{Bmatrix} = \begin{Bmatrix} x_{R1} \\ x_{R2} \\ x_{R3} \\ x_{R4} \\ x_{R5} \\ x_{R6} \\ \vdots \\ x_{R,N-2} \\ x_{R,N-1} \\ x_{R,N} \end{Bmatrix} + \begin{Bmatrix} 1 \\ 0 \\ 0 \\ 1 \\ 0 \\ 0 \\ \vdots \\ 1 \\ 0 \\ 0 \end{Bmatrix} * x_B(t) = \underline{X}_R + \underline{H}x_B(t) \quad (6.3.67)$$

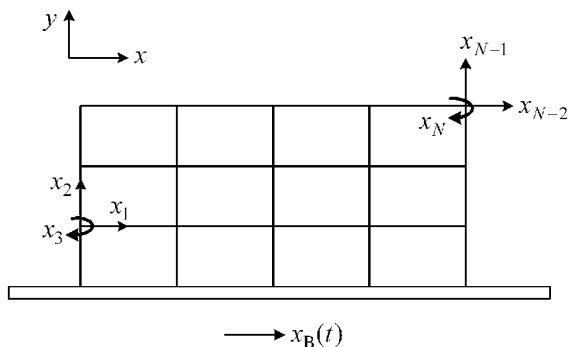


Figure 6.3.1 Multidegree of freedom, two-dimensional model with base excitation

The equilibrium equation for the entire (linear) system has the standard form

$$\underline{M}\ddot{\underline{X}} + \underline{C}\dot{\underline{X}}_R + \underline{K}\underline{X}_R = \underline{F}(t) \quad (6.3.68)$$

where the stiffness-related forces are caused by the relative displacements and the damping-related forces are caused by the relative velocities within the system. Substitution of (6.3.67) into (6.3.68) yields

$$\underline{M}\ddot{\underline{X}}_R + \underline{C}\dot{\underline{X}}_R + \underline{K}\underline{X}_R = -\underline{M}\underline{H}\ddot{x}_B(t) \quad (6.3.69)$$

Similar with (6.3.11), transform the relative displacement vector into modal coordinates

$$\underline{X}_R(t) = \underline{\Psi} \underline{\chi} = \sum_{i=1}^m \chi_i(t) \underline{\psi}_i \quad (6.3.70)$$

where $\underline{\Psi}$ is the truncated modal matrix containing m undamped system mode shapes

$$\underline{\Psi} = [\underline{\Psi}_1 \quad \underline{\Psi}_2 \quad \cdots \quad \underline{\Psi}_m] \quad (N \times M) \quad (6.3.71)$$

and

$$\underline{\psi}_i = i\text{th normal mode} \quad (N \times 1) \quad (6.3.72)$$

where “normal” refers to an undamped, nongyroscopic, noncirculatory system. Substitute (6.3.70) into (6.3.69), premultiply by $\underline{\Psi}^T$, assume \underline{C} is an orthogonal damping matrix, and use the orthogonality relations (5.4.44), (5.4.46), and (5.4.121) to obtain

$$\underline{\text{diag}}(\tilde{m}_i)\ddot{\underline{\chi}} + \underline{\text{diag}}(2\xi_i\omega_i\tilde{m}_i)\dot{\underline{\chi}} + \underline{\text{diag}}(\tilde{m}_i\omega_i^2)\underline{\chi} = \underline{r}(t, \underline{q}, \dot{\underline{q}}) = -\underline{\Psi}^T \underline{M} \underline{H} \ddot{x}_B(t) \quad (6.3.73)$$

Considering this equation row-wise yields

$$\ddot{\chi}_i + 2\xi_i\omega_i\dot{\chi}_i + \omega_i^2\chi_i = -\Lambda_i\ddot{x}_B(t) \quad i = 1, 2, \dots, m \quad (6.3.74)$$

where

$$\Lambda_i = \frac{\underline{\psi}_i^T \underline{M} \underline{H}}{\tilde{m}_i} = i\text{th modal participation factor} \quad (6.3.75)$$

and ξ_i , ω_i , and \tilde{m}_i are the i th mode damping ratio, undamped natural frequency, and modal mass, respectively.

The only difference between the forms of (6.3.74) and the single degree of freedom base-excited system described by (6.2.66) is that the source (RHS) term is multiplied by the modal participation factor Λ_i in Equation (6.3.74). Thus, the i th modal coordinate response may be written as

$$\chi_i(t) = \Lambda_i w_i(t) \quad (6.3.76)$$

where $w_i(t)$ is the response of the single degree of freedom system with damping ratio ξ_i , natural frequency ω_i , and mass \tilde{m}_i to the base excitation $x_B(t)$, that is, from (6.2.67)

$$w_i(t) = \frac{-1}{\omega_{di}} \int_0^t \ddot{x}_B(\tau) e^{-\xi_i\omega_i(t-\tau)} \sin(\omega_{di}(t-\tau)) d\tau \quad (6.3.77)$$

The total response of the N degree of freedom model is given by (6.3.70) and (6.3.76) as

$$\underline{X}_R(t) = \underline{\Psi} \underline{\chi} = \sum_{i=1}^m \chi_i(t) \underline{\psi}_i = \sum_{i=1}^m \Lambda_i w_i(t) \underline{\psi}_i \quad (6.3.78)$$

This may be written as

$$\underline{X}_R(t) = \sum_{i=1}^m \underline{X}_{Ri}(t) \quad (6.3.79)$$

where

$$\underline{X}_{Ri}(t) = \Lambda_i w_i(t) \underline{\psi}_i \quad (6.3.80)$$

The maximum relative displacement response for the i th mode contribution is expressed in terms of (6.3.80) and the displacement response spectrum (6.2.68)

$$\max(\underline{X}_{Ri}(t)) = \Lambda_i \underline{\psi}_i w_i^{\text{SD}}(\omega_i, \xi_i) \quad (6.3.81)$$

where $w_i^{\text{SD}}(\omega_n, \xi)$ is the single degree of freedom displacement response spectrum which, for the sake of illustration, is given for the N-S component of the 1994 Northridge California earthquake in Figure E6.2.6(c).

From (6.3.79) and (6.3.81), a very conservative estimate of the maximum total relative displacements may be obtained from

$$\max(\underline{X}_R(t)) \approx \sum_{i=1}^m |\max(\underline{X}_{Ri}(t))| \approx \sum_{i=1}^m \left| \Lambda_i \underline{\psi}_i w_i^{\text{SD}}(\omega_i, \xi_i) \right| \quad (6.3.82)$$

This assumes that all of the maximum modal contributions occur at the same time, which is unlikely. More accurate (less conservative) estimates may be obtained by treating the problem in a statistical sense which is discussed in earthquake engineering texts (Tedesco et al., 1999; Villaverde, 2009).

6.3.4 Participation Factor and Modal Effective Mass

Imposed ground, support, or base motion excitation has wide-ranging applications including earthquake excitation and satellite orientation control. Here, we are interested in determining which modes dominate in the response of a flexible body to support excitation. This has the practical use of selecting which modes to retain in a transient simulation utilizing a modal condensation approach ((6.3.11) and (6.3.33)). The response is divided into rigid body displacements that result from the support motion being applied quasistatically plus the elastic response component representing the relative motions with respect to the support motions. The relative importance of the individual modes in the relative motion of the structure with respect to the imposed base motion is ranked by using the modal participation factor or effective model mass as derived in the following analysis.

Let $(x_{Ri}, i = 1, 2, \dots, N_R)$ be the imposed support displacements that cause the body being modeled to move as a rigid body, if the x_{Ri} were imposed quasistatically. These are initially identified with a mass matrix in the following analysis. This mass matrix is eventually ignored since the x_{Ri} are imposed (known) so there is no need to solve for them. The x_{Ri}

must be selected so that the body is constrained against all rigid body motions if the x_{Ri} are held fixed $x_{Ri} = 0, i = 1, 2, \dots, N_R$. Setting $x_{Ri} = 1$ and $x_{Rj} = 0$ for $j \neq i$ causes the entire body to undergo a rigid body motion in the x_{Ri} direction.

Let

$$\underline{x}_R = (x_{R1} \ x_{R2} \ \cdots \ x_{RN_R})^T \quad N_R \times 1 \quad (6.3.83)$$

and

$$\underline{x}_e = \text{vector of all remaining displacements} \quad N_e \times 1 \quad (6.3.84)$$

The total system displacement vector then becomes

$$\underline{X} = \begin{Bmatrix} \underline{x}_R \\ \underline{x}_e \end{Bmatrix} \quad N \times 1, \quad N = N_R + N_e \quad (6.3.85)$$

The equations of motion are

$$\underline{M} \ddot{\underline{X}} + \underline{K} \underline{X} = \underline{F} \quad (6.3.86)$$

or in partitioned matrix form

$$\begin{bmatrix} \underline{M}_{RR} & \underline{M}_{Re} \\ \underline{M}_{eR} & \underline{M}_{ee} \end{bmatrix} \begin{Bmatrix} \ddot{\underline{x}}_R \\ \ddot{\underline{x}}_e \end{Bmatrix} + \begin{bmatrix} \underline{K}_{RR} & \underline{K}_{Re} \\ \underline{K}_{eR} & \underline{K}_{ee} \end{bmatrix} \begin{Bmatrix} \underline{x}_R \\ \underline{x}_e \end{Bmatrix} = \begin{Bmatrix} \underline{F}_R \\ \underline{F}_e \end{Bmatrix} \quad (6.3.87)$$

Suppose that the system is moved quasistatically through a rigid body motion by prescribing displacements in \underline{x}_R while being in an external force-free state. In this case, (6.3.87) becomes

$$\begin{bmatrix} \underline{K}_{RR} & \underline{K}_{Re} \\ \underline{K}_{eR} & \underline{K}_{ee} \end{bmatrix} \begin{Bmatrix} \underline{x}_R \\ \underline{x}_e \end{Bmatrix} = \begin{Bmatrix} \underline{0} \\ \underline{0} \end{Bmatrix} \quad (6.3.88)$$

The bottom row implies that

$$\underline{x}_e = -\underline{K}_{ee}^{-1} \underline{K}_{eR} \underline{x}_R \quad (6.3.89)$$

The inverse in (6.3.89) will exist if the \underline{x}_R are selected so that the body is constrained against all rigid body motions if $\underline{x}_R = \underline{0}$. The \underline{x}_e in (6.3.88) then are the resulting rigid body motions of all degrees of freedom, excluding those in \underline{x}_R . The total system motion in this rigid body (base motion) mode is

$$\underline{X} = \begin{Bmatrix} \underline{x}_R \\ \underline{x}_e \end{Bmatrix} = \underline{T} \underline{x}_R \quad (6.3.90)$$

where

$$\underline{T} = [\underline{T}_1 \ \underline{T}_2 \ \cdots \ \underline{T}_{N_R}] = \begin{bmatrix} \underline{I} \\ -\underline{K}_{ee}^{-1} \underline{K}_{eR} \end{bmatrix} \quad N \times N_R \quad (6.3.91)$$

The degrees of freedom in \underline{x}_e also undergo elastic motion which may be viewed as the motion of the degrees of freedom relative to the imposed base motions. This component will be represented as the sum of the flexible body mode shapes corresponding to a fixed $\underline{x}_R = \underline{0}$ boundary condition. The free vibration equation in this case is obtained from (6.3.87) as

$$\underline{M}_{ee}\ddot{\underline{x}}_e + \underline{K}_{ee}\underline{x}_e = \underline{0} \quad (6.3.92)$$

Let

$$\underline{x}_e = \underline{\psi}_l e^{i\omega_l t} \quad (6.3.93)$$

$$\Rightarrow (-\omega_l^2 \underline{M}_{ee} + \underline{K}_{ee})\underline{\psi}_l = \underline{0} \quad (6.3.94)$$

from which the fixed (\underline{x}_R) boundary modes $\underline{\psi}_l$ and natural frequencies ω_l are extracted. Define the modal matrix as

$$\underline{\Psi}_e = [\underline{\psi}_1 \quad \underline{\psi}_2 \quad \cdots \quad \underline{\psi}_{N_e}] \quad N_e \times N_e \quad (6.3.95)$$

The flexible (relative motion) component of the total system motion may then be expressed by

$$\underline{X} = \begin{Bmatrix} \underline{x}_R \\ \underline{x}_e \end{Bmatrix} = \underline{\Psi}_e \underline{\beta} \quad (6.3.96)$$

where

$$\underline{\Psi} = [\underline{\Psi}_1 \quad \underline{\Psi}_2 \quad \cdots \quad \underline{\Psi}_{N_e}] = \begin{Bmatrix} \underline{0} \\ \underline{\Psi}_e \end{Bmatrix} \quad N \times N_e \quad (6.3.97)$$

and $\underline{\beta}$ is a $N_e \times 1$ vector of *modal coordinates*. The complete motion of the system from (6.3.90) and (6.3.96) may then be expressed as

$$\underline{X} = \begin{Bmatrix} \underline{x}_R \\ \underline{x}_e \end{Bmatrix} = \underline{\Gamma} \underline{\bar{X}} \quad N \times 1 \quad (6.3.98)$$

where

$$\underline{\Gamma} = [\underline{T} \quad \underline{\Psi}] \quad N \times N \quad (6.3.99)$$

and

$$\underline{\bar{X}} = \begin{Bmatrix} \underline{x}_R \\ \underline{\beta} \end{Bmatrix} \quad (6.3.100)$$

Substitute (6.3.98) into (6.3.86) to obtain

$$\underline{\tilde{M}} \underline{\ddot{\bar{X}}} + \underline{\tilde{K}} \underline{\bar{X}} = \underline{\tilde{F}} \quad (6.3.101)$$

where

$$\tilde{\underline{M}} = \underline{\Gamma}^T \underline{M} \underline{\Gamma} = \begin{bmatrix} \underline{T}^T \\ \underline{\Psi}^T \end{bmatrix} \underline{M} \begin{bmatrix} \underline{T} \\ \underline{\Psi} \end{bmatrix} = \begin{bmatrix} \underline{T}^T \underline{M} \underline{T} & \underline{T}^T \underline{M} \underline{\Psi} \\ \underline{\Psi}^T \underline{M} \underline{T} & \underline{\Psi}^T \underline{M} \underline{\Psi} \end{bmatrix} = \begin{bmatrix} \underline{M}_{BB} & \underline{M}_{BF} \\ \underline{M}_{FB} & \underline{M}_{FF} \end{bmatrix} \quad (6.3.102)$$

and

$$\tilde{\underline{K}} = \underline{\Gamma}^T \underline{K} \underline{\Gamma} = \begin{bmatrix} \underline{T}^T \underline{K} \underline{T} & \underline{T}^T \underline{K} \underline{\Psi} \\ \underline{\Psi}^T \underline{K} \underline{T} & \underline{\Psi}^T \underline{K} \underline{\Psi} \end{bmatrix} = \begin{bmatrix} \underline{K}_{BB} & \underline{K}_{BF} \\ \underline{K}_{FB} & \underline{K}_{FF} \end{bmatrix} \quad (6.3.103)$$

Mass Matrix

Consider the individual terms in (6.3.102):

$$(\underline{M}_{BB})_{ij} = (\underline{T}^T \underline{M} \underline{T})_{ij} = \underline{T}_i^T \underline{M} \underline{T}_j \quad (6.3.104)$$

and \underline{T}_i is a vector containing the displacements of all degrees of freedom corresponding with

$$(\underline{x}_R)_i = 1 \quad \text{and all other } (\underline{x}_R)_j = 0 \quad (6.3.105)$$

For example, for a 2D truss (Figure 4.8.11), each node has an x and a y displacement, so for this case,

$$\underline{T}_1 = (1 \ 0 \ 1 \ 0 \ 1 \ 0 \ \dots \ 0)^T \quad (6.3.106)$$

$$\underline{T}_2 = (0 \ 1 \ 0 \ 1 \ 0 \ 1 \ \dots \ 1)^T \quad (6.3.107)$$

$$N_R = 2 \quad (6.3.108)$$

For a lumped mass matrix,

$$\underline{M} = \begin{bmatrix} m_1 & & & & & & \\ & m_1 & & \underline{0} & & & \\ & & \ddots & & & & \\ & & & & & & \\ & \underline{0} & & & m_{N/2} & & \\ & & & & & & m_{N/2} \end{bmatrix} \quad (6.3.109)$$

$$\underline{T}_1^T \underline{M} \underline{T}_1 = \underline{T}_2^T \underline{M} \underline{T}_2 = \sum_{i=1}^{N/2} m_i = m_{\text{total}} \quad (6.3.110)$$

$$\underline{T}_1^T \underline{M} \underline{T}_2 = \underline{T}_2^T \underline{M} \underline{T}_1 = 0 \quad (6.3.111)$$

Therefore, for this case,

$$\underline{M}_{BB} = \underline{T}^T \underline{M} \underline{T} = \begin{bmatrix} m_{\text{total}} & 0 \\ 0 & m_{\text{total}} \end{bmatrix} \quad (6.3.112)$$

The diagonal entries in \underline{M}_{BB} are seen to be the total mass of the model. Thus, designate

$$\underline{M}_{\text{total}} = \underline{M}_{BB} = \underline{T}^T \underline{M} \underline{T} \quad (6.3.113)$$

Next, consider the \underline{M}_{FF} term in (6.3.102), utilizing (6.3.87) and (6.3.99):

$$\underline{M}_{FF} = \underline{\Psi}^T \underline{M} \underline{\Psi} = \begin{bmatrix} \underline{0} & \underline{\Psi}_e^T \end{bmatrix} \begin{bmatrix} \underline{M}_{RR} & \underline{M}_{Re} \\ \underline{M}_{eR} & \underline{M}_{ee} \end{bmatrix} \begin{bmatrix} \underline{0} \\ \underline{\Psi}_e \end{bmatrix} = \underline{\Psi}_e^T \underline{M}_{ee} \underline{\Psi}_e = \text{diag}(\tilde{m}_i) \quad (6.3.114)$$

where \tilde{m}_i are the fixed \underline{x}_R system modal masses.

Next, consider

$$\underline{\Lambda} = \underline{M}_{FB} = \underline{\Psi}^T \underline{M} \underline{T} = \underline{M}_{BF}^T \quad (6.3.115)$$

Thus,

$$\Lambda_{ij} = \underline{\Psi}_i^T \underline{M} \underline{T}_j \quad (6.3.116)$$

By comparison with (6.3.75), the Λ_{ij} are modal participation factors between the i th flexible mode and j th rigid body (base motion) mode, which relate the coupling of the rigid base motion modes $\underline{\Gamma}_j$ to the elastic, fixed \underline{x}_R modes ($\underline{\Psi}_i$).

Collecting results in (6.3.102) yields

$$\tilde{\underline{M}} = \begin{bmatrix} \underline{M}_{BB} & \underline{M}_{BF} \\ \underline{M}_{FB} & \underline{M}_{FF} \end{bmatrix} = \begin{bmatrix} \underline{M}_{\text{total}} & \underline{\Lambda}^T \\ \underline{\Lambda} & \text{diag}(\tilde{m}_i) \end{bmatrix} \quad (6.3.117)$$

Stiffness Matrix

Consider the following term in (6.3.103): $\underline{K}_{BB} = \underline{T}^T \underline{K} \underline{T}$.

Note that

$$\underline{K} \underline{T} = \begin{bmatrix} \underline{K} \underline{T}_1 & \underline{K} \underline{T}_2 & \cdots & \underline{K} \underline{T}_{N_R} \end{bmatrix} = \underline{0} \quad (6.3.118)$$

since \underline{T}_j are rigid body motions that are the solutions to (6.3.88).

Next, consider the \underline{K}_{FF} term in (6.3.103):

$$\underline{K}_{FF} = \underline{\Psi}^T \underline{K} \underline{\Psi} = \begin{bmatrix} \underline{0} & \underline{\Psi}_e^T \end{bmatrix} \begin{bmatrix} \underline{K}_{RR} & \underline{K}_{Re} \\ \underline{K}_{eR} & \underline{K}_{ee} \end{bmatrix} \begin{bmatrix} \underline{0} \\ \underline{\Psi}_e \end{bmatrix} = \underline{\Psi}_e^T \underline{K}_{ee} \underline{\Psi}_e = \text{diag}(\tilde{m}_i \omega_i^2) \quad (6.3.119)$$

Next, consider

$$\underline{K}_{FB} = \underline{\Psi}^T \underline{K} \underline{T} = \underline{K}_{BF}^T \quad (6.3.120)$$

From (6.3.87), (6.3.91), and (6.3.97),

$$\underline{K}_{FB} = \begin{bmatrix} \underline{0} & \underline{\Psi}_e^T \end{bmatrix} \begin{bmatrix} \underline{K}_{RR} & \underline{K}_{Re} \\ \underline{K}_{eR} & \underline{K}_{ee} \end{bmatrix} \begin{bmatrix} \underline{I} \\ -\underline{K}_{ee}^{-1} \underline{K}_{eR} \end{bmatrix} = \underline{\Psi}_e^T (\underline{K}_{eR} - \underline{K}_{ee} \underline{K}_{ee}^{-1} \underline{K}_{eR}) = \underline{0} \quad (6.3.121)$$

Collecting results in (6.3.103),

$$\tilde{\underline{K}} = \begin{bmatrix} \underline{K}_{BB} & \underline{K}_{BF} \\ \underline{K}_{FB} & \underline{K}_{FF} \end{bmatrix} = \begin{bmatrix} \underline{0} & \underline{0} \\ \underline{0} & \text{diag}(\tilde{m}_i \omega_i^2) \end{bmatrix} \quad (6.3.122)$$

Consider the case when there are no external forces and the input is the base or ground motion $\underline{x}_R(t)$. Equation (6.3.101) becomes

$$\tilde{\underline{M}} \ddot{\underline{X}} + \tilde{\underline{K}} \underline{X} = \underline{0} \quad N \times 1 \quad (6.3.123)$$

$$\begin{bmatrix} \underline{M}_{\text{total}} & \underline{\Delta}^T \\ \underline{\Delta} & \text{diag}(\tilde{m}_i) \end{bmatrix} \begin{Bmatrix} \ddot{\underline{x}}_R \\ \underline{\beta} \end{Bmatrix} + \begin{bmatrix} \underline{0} & \underline{0} \\ \underline{0} & \text{diag}(\tilde{m}_i \omega_i^2) \end{bmatrix} \begin{Bmatrix} \underline{x}_R \\ \underline{\beta} \end{Bmatrix} = \begin{Bmatrix} \underline{0} \\ \underline{0} \end{Bmatrix} \quad (6.3.124)$$

The bottom row shows

$$\text{diag}(\tilde{m}_i) \underline{\beta} + \text{diag}(\tilde{m}_i \omega_i^2) \underline{\beta} = -\underline{\Delta} \ddot{\underline{x}}_R \quad (6.3.125)$$

Or in scalar form using (6.3.97) and (6.3.115),

$$\ddot{\beta}_i + \omega_i^2 \beta_i = -\frac{1}{\tilde{m}_i} \underline{\Delta}_i \ddot{\underline{x}}_R \quad (6.3.126)$$

where

$$\underline{\Delta}_i = \underline{\Psi}_i^T \underline{M} \underline{T}_j \quad 1 \times N_R \quad (6.3.127)$$

Equation (6.3.126) may be further simplified by assuming the modes ($\underline{\psi}_i$ in (6.3.94)) are mass orthonormalized (5.4.40), that is, $\tilde{m}_i = 1$. Then (6.3.126) becomes

$$\ddot{\beta}_i + \omega_i^2 \beta_i = -\underline{\Delta}_i \ddot{\underline{x}}_R = -(\Lambda_{i1} \quad \Lambda_{i2} \quad \cdots \quad \Lambda_{iN_R}) \begin{Bmatrix} \ddot{x}_{R1} \\ \ddot{x}_{R2} \\ \vdots \\ \ddot{x}_{RN_R} \end{Bmatrix} \quad (6.3.128)$$

Equation (6.3.128) shows that modes with large modal participation factors Λ_{ij} will be more strongly excited than modes with small Λ_{ij} . There is a modal participation factor Λ_{ij} between mode ($\underline{\psi}_i, \omega_i$) and each imposed base motion x_{Rj} ($j = 1, 2, \dots, N_R$). These factors are obtained from (6.3.91) and (6.3.127) as

$$\begin{aligned} \Lambda_{ij} &= \underline{\Psi}_i^T \underline{M} \underline{T}_j \\ &= (\textit{ith total system flexible mode}) \times (\textit{total system mass matrix}) \\ &\quad \times (\textit{jth total system rigid body (base motion) displacement vector}) \end{aligned} \quad (6.3.129)$$

In application, the mass associated with the \underline{x}_R degrees of freedom is ignored since the support motion $\underline{x}_R(t)$ is the given excitation. Therefore, the modal participation vectors simplify to the form (6.3.127)

$$\underline{\Delta}_i^e = \underline{\Psi}_i^T \underline{M}_{ee} \underline{G} \quad 1 \times N_R \quad (6.3.130)$$

where from (6.3.93), $\underline{\psi}_i$ is the i th mass-orthonormalized mode of the boundary constrained structure, that is, ($\underline{x}_R = 0$), and from (6.3.91),

$$\underline{G} = -\underline{K}_{ee}^{-1} \underline{K}_{eR} \quad N_e \times N_R \quad (6.3.131)$$

Define the i th mode's "modal effective mass" matrix as

$$\underline{M}_i^E = (\underline{\Lambda}_i^e)^T \underline{\Lambda}_i^e \quad N_R \times N_R \quad (6.3.132)$$

Consider the following sum:

$$\sum_{i=1}^{N_E} \underline{M}_i^E = \sum_{i=1}^{N_E} (\underline{\Lambda}_i^e)^T \underline{\Lambda}_i^e = \sum_{i=1}^{N_E} \underline{G}^T \underline{M}_{ee} \underline{\psi}_i \underline{\psi}_i^T \underline{M}_{ee} \underline{G} = \underline{G}^T \underline{M}_{ee} \left(\sum_{i=1}^{N_E} \underline{\psi}_i \underline{\psi}_i^T \right) \underline{M}_{ee} \underline{G} \quad (6.3.133)$$

From the identity in (2.6.35) and the definition in (6.3.95),

$$\sum \underline{\psi}_i \underline{\psi}_i^T = \underline{\Psi}_e \underline{\Psi}_e^T \quad (6.3.134)$$

Therefore,

$$\sum_{i=1}^{N_E} \underline{M}_i^E = \underline{G}^T \underline{M}_{ee} \underline{\Psi}_e \underline{\Psi}_e^T \underline{M}_{ee} \underline{G} \quad (6.3.135)$$

Note from (6.3.114)

$$\underline{\Psi}_e^T \underline{M}_{ee} \underline{\Psi}_e = \underline{I} \quad (6.3.136)$$

since the modes are mass orthonormalized.

From (6.3.136),

$$\begin{aligned} \underline{\Psi}_e^{-1} \underline{M}_{ee}^{-1} (\underline{\Psi}_e^T)^{-1} &= \underline{I} \\ \Rightarrow \underline{M}_{ee}^{-1} &= \underline{\Psi}_e \underline{\Psi}_e^T \end{aligned} \quad (6.3.137)$$

Substitution of (6.3.137) into (6.3.135) yields

$$\sum_{i=1}^{N_E} \underline{M}_i^E = \underline{G}^T \underline{M}_{ee} \underline{G} \quad (6.3.138)$$

The RHS of (6.3.138) has the same physical interpretation as $\underline{M}_{\text{total}}$ in (6.3.113) with the masses limited to just the masses associated with the degrees of freedom in \underline{x}_e (and not in \underline{x}_R). Let $\underline{M}_{\text{total}}^e$ be the matrix of sums of the physical masses for only the degrees of freedom in \underline{x}_e . Therefore, from (6.3.132) and (6.3.138),

$$\sum_{i=1}^{N_E} \underline{M}_i^E = \sum_{i=1}^{N_E} (\underline{\Lambda}_i^e)^T \underline{\Lambda}_i^e = \underline{G}^T \underline{M}_{ee} \underline{G} = \underline{M}_{\text{total}}^e \quad N_R \times N_R \quad (6.3.139)$$

The larger the modal effective mass, the larger the modal participation vector $\underline{\Lambda}_i^e$ and from the previous discussion the stronger the base excitation in mode i . Modes that have large modal effective masses are typically retained for transient response simulations using modal condensation (6.3.15). This is not the sole criteria though since modes with natural frequencies near excitation frequencies should always be retained.

EXAMPLE 6.3.3 *Modal Effective Mass of a Building with Vertical Ground Motion*

Description: Figure E6.3.3(a) illustrates a 20-story building model that is subjected to ground motion $x_1(t)$. The floor masses are connected by springs which represent the inter-floor beams. The masses and stiffnesses of the model are

$$m_1 \text{ (ground mass : ignored in model since } x_1(t) \text{ is given)}$$

$$m_2 - m_6 : 100000 \text{ kg, } m_7 - m_{11} : 75000 \text{ kg, } m_{12} - m_{21} : 50000 \text{ kg}$$

$$\text{Total mass : } 1375000 \text{ kg}$$

$$\text{Stiffness : } k_1 - k_8 = 1.0 \times 10^8 \text{ N/m, } k_9 - k_{20} = 0.5 \times 10^8 \text{ N/m}$$

Objective: Determine the mode participation factors $\underline{\Delta}_i^e$ and modal effective masses $\underline{M}_i^E = (\underline{\Delta}_i^e)^T \underline{\Delta}_i^e$ and their corresponding percentages of the total system mass.

Solution: The mass \underline{M}_{ee} and stiffness \underline{K}_{ee} matrices for this problem are assembled in the same manner as explained in Example 6.3.1. The dimensions for this problem are $N_e = 20$ and $N_R = 1$. The ground motion $x_1(t)$ is assumed fixed for determining the elastic structure modes $\underline{\psi}_i$, $i=1,2,\dots,20$. The corresponding 20 natural frequencies are

$$f_i = [0.4575 \quad 1.1200 \quad 1.8899 \quad 2.6481 \quad 3.3636 \quad 4.0543 \quad 4.7771 \\ 5.3340 \quad 6.0947 \quad 6.6006 \quad 7.0505 \quad 7.6655 \quad 8.1081 \quad 8.4747 \\ 9.0210 \quad 9.1496 \quad 9.6497 \quad 9.7303 \quad 9.9610 \quad 10.8607] \text{ Hz} \quad (1)$$

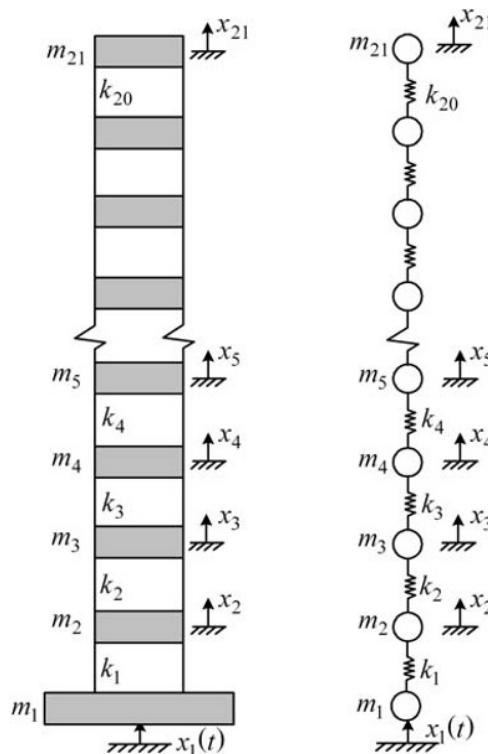


Figure E6.3.3(a) Twenty-story building and spring mass model

Figure E6.3.3(b) shows the five lowest mode shapes of the fixed x_1 system. The unconstrained system stiffness matrix is needed to form the submatrix

$$\underline{K}_{eR} = (-k_1 \ 0 \ 0 \ 0 \ 0 \ 0 \ 0 \ 0 \ 0 \ 0 \ 0 \ 0 \ 0 \ 0 \ 0 \ 0 \ 0 \ 0 \ 0 \ 0)^T, \quad (2)$$

$$N_e \times N_R, \quad 20 \times 1$$

The rigid body displacement vector is calculated to be

$$\underline{G} = -\underline{K}_{ee}^{-1} \underline{K}_{eR} = (1 \ 1 \ 1 \ 1 \ 1 \ 1 \ 1 \ 1 \ 1 \ 1 \ 1 \ 1 \ 1 \ 1 \ 1 \ 1 \ 1 \ 1 \ 1 \ 1)^T, \quad (3)$$

$$N_e \times N_R, \quad 20 \times 1$$

where \underline{K}_{ee} is the system stiffness matrix with degree of freedom $x_1(t)$ fixed. All modes are mass orthonormalized ($\tilde{m}_i = 1$), and the modal participation factors are

$$\underline{\Delta}_i^e = \underline{\Psi}_i^T \underline{M}_{ee} \underline{G} \quad 1 \times N_R, \quad i = 1, N_e$$

$$\begin{bmatrix} 987.5401 & -499.6575 & -240.4308 & 172.1812 & 147.9946 & 98.6365 \\ -106.1830 & 66.2951 & -58.7555 & 66.5341 & -46.6226 & 20.0387 & -54.3975 \\ 9.1615 & 35.9444 & 6.3925 & -2.0853 & 22.7432 & 0.1481 & -0.7252 \end{bmatrix} \quad (4)$$

where \underline{M}_{ee} is the system mass matrix with degree of freedom $x_1(t)$ fixed. The modal effective masses for the $N_e = 20$ modes are

$$\underline{M}_i^E = (\underline{\Delta}_i^e)^T \underline{\Delta}_i^e \quad N_R \times N_R, \quad i = 1, N_e$$

$$1.0e+005 * \begin{bmatrix} 9.7524 & 2.4966 & 0.5781 & 0.2965 & 0.2190 & 0.0973 & 0.1127 & 0.0440 \\ 0.0345 & 0.0443 & 0.0217 & 0.0040 & 0.0296 & 0.0008 & 0.0129 & 0.0004 \\ 0.0000 & 0.0052 & 0.0000 & 0.0000 \end{bmatrix} \text{ kg} \quad (5)$$

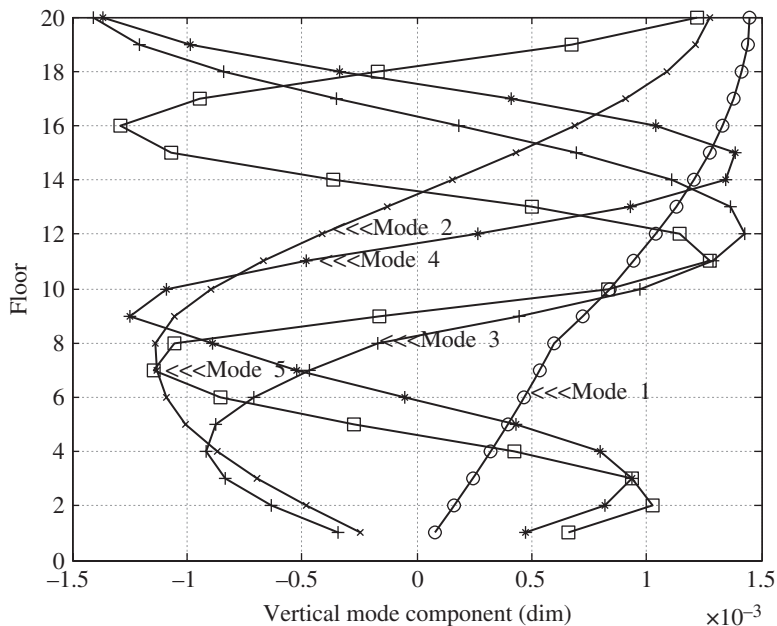
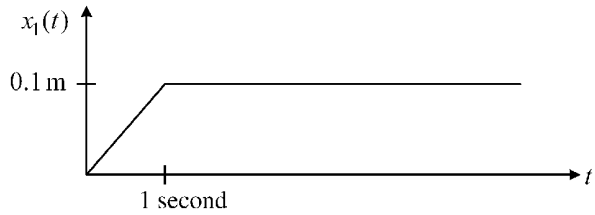


Figure E6.3.3(b) Five lowest mode shapes of the fixed x_1 system

Figure E6.3.3(c) Imposed ground motion $x_1(t)$



The sum of the modal effective masses equals 1 375 000 kg which is the total physical mass of the system. The percentages of total system mass for the modal effective masses are

$$\begin{bmatrix} 70.9262 & 18.1569 & 4.2041 & 2.1561 & 1.5929 & 0.7076 & 0.8200 & 0.3196 \\ 0.2511 & 0.3219 & 0.1581 & 0.0292 & 0.2152 & 0.0061 & 0.0940 & 0.0030 \\ 0.0003 & 0.0376 & 0.0000 & 0.0000 & & & & \end{bmatrix} \% \quad (6)$$

The modal effective masses of the lowest five modes account for 97% of the total system's physical mass. Consider the transient response case when the vertical ground motion has the time history shown in Figure E6.3.3(c).

The fixed boundary condition model may still be employed for the transient response simulation with the inclusion of an upward force $k_1 * x_1(t)$ applied on m_2 . An orthogonal damping matrix is included in the transient response model. From (5.4.140), (5.4.142), and (5.4.146), the damping matrix may be written as

$$\underline{C}_0 = \mu_1 \underline{K} + \sum_{l=1}^4 \frac{2\kappa_l \omega_l}{\tilde{m}_l} \underline{M} \underline{\psi}_l \underline{\psi}_l^T \underline{M} \quad (7)$$

where

$$\mu_1 = \frac{2\xi_5^d}{\omega_5} \quad \text{and} \quad \kappa_l = \xi_l^d - \xi_5^d \frac{\omega_l}{\omega_5}, \quad l = 1, 2, 3, 4 \quad (8)$$

ω_l and $\underline{\psi}_l$ are the l th natural frequency and mode shape of the undamped system.

Damping:

$$\xi_1^d = 0.02, \quad \xi_2^d = 0.02, \quad \xi_3^d = \xi_4^d = 0.025, \quad \xi_5^d = 0.03 \quad (9)$$

Figure E6.3.3(d) shows the responses obtained from numerically integrating the physical coordinate differential equations for the entire system. The maximum displacement is 0.197 m.

Figure E6.3.3(e) shows the responses obtained from numerically integrating the modal coordinate differential equations for the five lowest modes. The maximum displacement is 0.205 m, a 4% difference with the full system integration. Figure E6.3.3(f) shows the responses obtained from numerically integrating the modal coordinate differential equations for the five lowest modes with modal acceleration (6.3.33). The maximum displacement is again 0.205 m, a 4% difference with the full system, physical coordinate integration.

The modal approach solutions using the 5 lowest modes are seen to provide response predictions that are very close to the physical coordinate integration, excluding the motion of m_2 , which requires about 13 modes to closely agree. The modal effective masses of the lowest five modes account for 97% of the total system's physical mass.

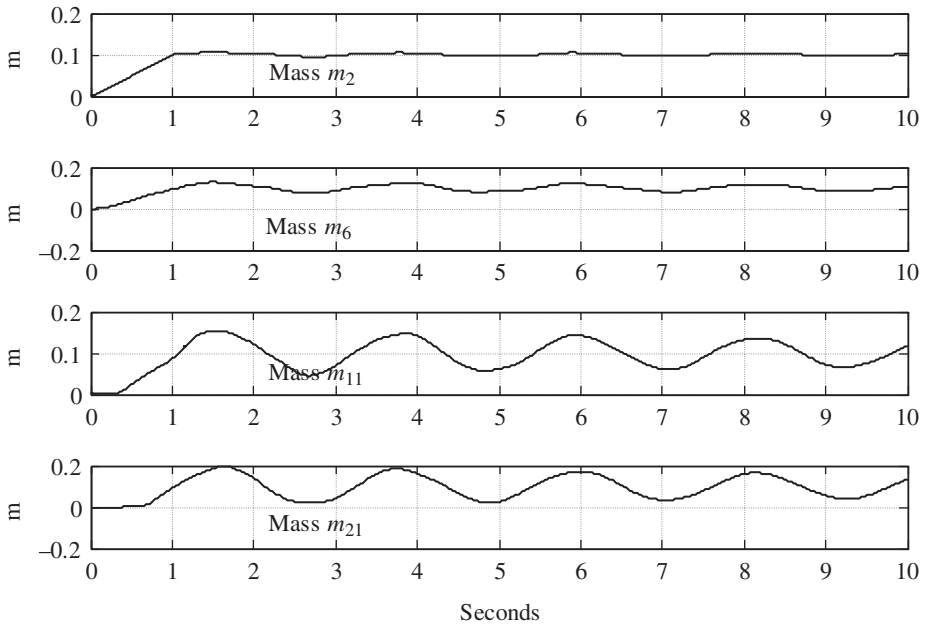


Figure E6.3.3(d) Response from direct numerical integration of entire system equations

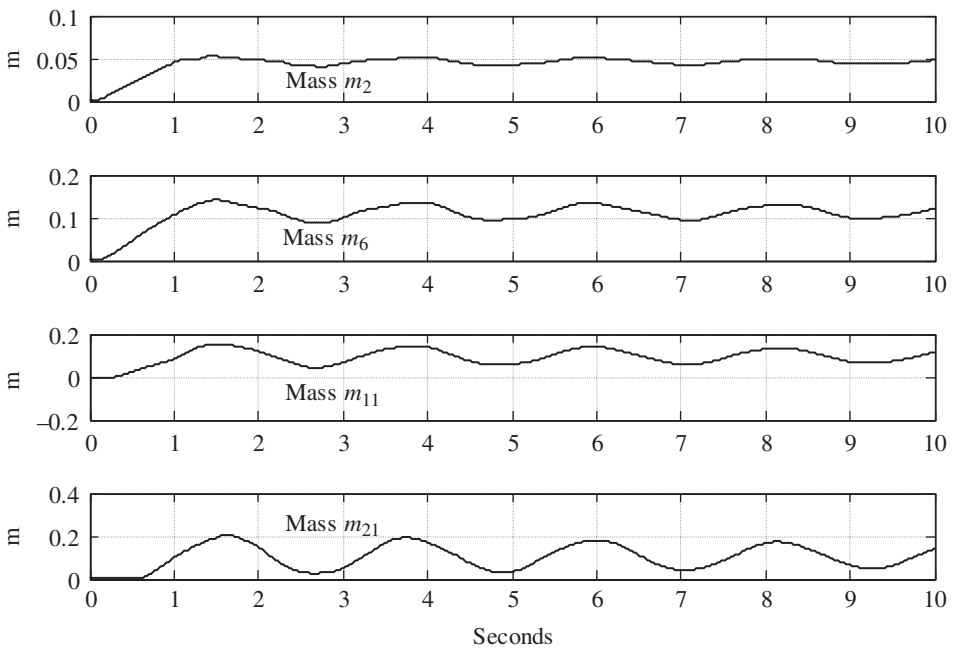


Figure E6.3.3(e) Response from numerical integration of lowest five modal differential equations

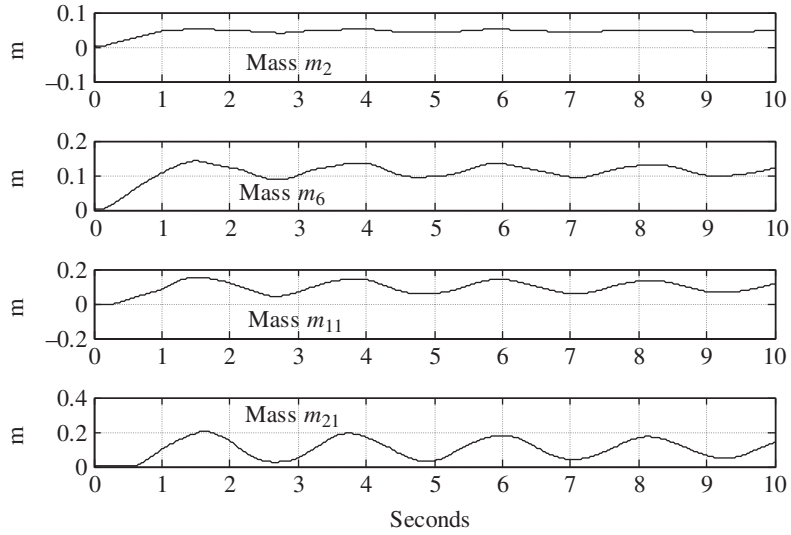


Figure E6.3.3(f) Response from numerical integration of lowest five modal differential equations and usage of modal acceleration

6.3.5 General Nonsymmetric, Nonorthogonal Damping Models

The starting point for this system condensation is the first-order form of the EOMs, that is, by (6.3.5) and (6.3.6)

$$\underline{E} \underline{\dot{X}} = \underline{H} \underline{X} + \underline{\hat{f}}(t, \underline{q}, \underline{\dot{q}}) \quad (6.3.140)$$

$2N \times 2N$ $2N \times 1$ $2N \times 2N$ $2N \times 1$ $2N \times 1$

where

$$\underline{E} = \begin{bmatrix} \underline{0} & \underline{M} \\ \underline{M} & \underline{C}_T \end{bmatrix}, \quad \underline{H} = \begin{bmatrix} \underline{M} & \underline{0} \\ \underline{0} & -\underline{K}_T \end{bmatrix}, \quad \underline{X} = \begin{Bmatrix} \underline{V} \\ \underline{q} \end{Bmatrix} \quad (6.3.141)$$

$$\underline{\hat{f}} = \begin{Bmatrix} \underline{0} \\ \underline{f} + \underline{g} \end{Bmatrix}, \quad \underline{f} = \underline{f}(t), \quad \underline{g} = \underline{g}(\underline{q}, \underline{\dot{q}}, t) \quad (6.3.142)$$

Recall from Equations (5.4.213)–(5.4.230) that the corresponding right and left eigenvectors had the form

$$\underline{\Gamma}_j = \begin{Bmatrix} \lambda_j \underline{\Delta}_j \\ \underline{\Delta}_j \end{Bmatrix}, \quad \underline{\beta}_j = \begin{Bmatrix} \lambda_j \underline{\theta}_j \\ \underline{\theta}_j \end{Bmatrix} \quad (6.3.143)$$

$2N \times 1$ $N \times 1$ $N \times 1$ $2N \times 1$ $N \times 1$ $N \times 1$

where

$$\lambda_j \underline{E} \underline{\Gamma}_j = \underline{H} \underline{\Gamma}_j, \quad \lambda_j \underline{E}^T \underline{\beta}_j = \underline{H}^T \underline{\beta}_j$$

$$\left(\lambda_j^2 \underline{M} + \lambda_j \underline{C}_T + \underline{K}_T \right) \underline{\Delta}_j = \underline{0}, \quad \left(\lambda_j^2 \underline{M}^T + \lambda_j \underline{C}_T^T + \underline{K}_T^T \right) \underline{\theta}_j = \underline{0} \quad (6.3.144)$$

and the right and left modal matrices are

$$\underline{\Gamma} = [\underline{\Gamma}_1 \quad \underline{\Gamma}_2 \quad \cdots \quad \underline{\Gamma}_m], \quad \underline{\beta} = [\underline{\beta}_1 \quad \underline{\beta}_2 \quad \cdots \quad \underline{\beta}_m]$$

Consider the approximation

$$\underline{X}(t) = \sum_{j=1}^m w_j(t) \underline{\Gamma}_j = \underset{2N \times m}{\underline{\Gamma}} \underset{m \times 1}{\underline{W}} \quad (6.3.145)$$

where $m < 2N$. This approximation restricts the system response (state) vector \underline{X} to the m -dimensional subspace spanned by the modal basis vectors $\underline{\Gamma}_j, j = 1, \dots, m$. This approximation is typically very good and provides a significant increase in computational efficiency for m/N in the range 0.1–0.2. Premultiply (6.3.140) by $\underline{\beta}^T$ and use the biorthogonality relations in (5.4.229) and (5.4.230) to obtain

$$\underline{\text{diag}}(\tilde{e}_j) \dot{\underline{W}} - \underline{\text{diag}}(\lambda_j \tilde{e}_j) \underline{W} = \underline{R}(t, \underline{q}, \dot{\underline{q}}) \quad (6.3.146)$$

Considering this equation row-wise yields

$$\dot{w}_j - \lambda_j w_j = \frac{R_j(t, \underline{q}, \dot{\underline{q}})}{\tilde{e}_j} \quad (6.3.147)$$

where the *modal force* is

$$R_j = \underline{\beta}_{-j}^T \hat{\underline{f}} = \left\{ \begin{array}{c} \lambda_s \underline{\theta}_j \\ \underline{\theta}_j \end{array} \right\}^T \left\{ \begin{array}{c} \underline{0} \\ \underline{f} + \underline{g} \end{array} \right\} = \underline{\theta}_j^T [\underline{f}(t) + \underline{g}(t, \underline{q}, \dot{\underline{q}})] \quad (6.3.148)$$

and from (5.4.225), the *generalized modal mass* is

$$\tilde{e}_j = \underline{\beta}_{-j}^T \underline{E} \underline{\Gamma}_j = \left\{ \begin{array}{c} \lambda_s \underline{\theta}_j \\ \underline{\theta}_j \end{array} \right\}^T \left[\begin{array}{c|c} \underline{0} & \underline{M} \\ \hline \underline{M} & \underline{C}_T \end{array} \right] \left\{ \begin{array}{c} \lambda_j \underline{\Delta}_j \\ \underline{\Delta}_j \end{array} \right\} = \underline{\theta}_j^T (2\lambda_j \underline{M} + \underline{C}_T) \underline{\Delta}_j \quad (6.3.149)$$

The initial conditions on the $w_j(t)$ are obtained by premultiplying (6.3.145) evaluated at $t=0$, by $(\underline{\beta}_{-j}^T \underline{E})$, yielding

$$\sum_{j=1}^m w_j(0) \underline{\beta}_{-j}^T \underline{E} \underline{\Gamma}_j = \underline{\beta}_{-j}^T \underline{E} \underline{X}(0) \quad (6.3.150)$$

The biorthogonality condition (5.4.223) simplifies this, yielding

$$\begin{aligned} \Rightarrow w_l(0) &= \frac{1}{\tilde{e}_l} \underline{\beta}_{-l}^T \underline{E} \underline{X}(0) = \frac{1}{\tilde{e}_l} \left\{ \begin{array}{c} \lambda_l \underline{\theta}_l \\ \underline{\theta}_l \end{array} \right\}^T \left[\begin{array}{c|c} \underline{0} & \underline{M} \\ \hline \underline{M} & \underline{C}_T \end{array} \right] \left\{ \begin{array}{c} \underline{V}(0) \\ \underline{q}(0) \end{array} \right\} \\ &= \frac{1}{\tilde{e}_l} \left[\underline{\theta}_l^T (\lambda_l \underline{M} + \underline{C}_T) \underline{q}(0) + \underline{\theta}_l^T \underline{M} \underline{V}(0) \right] \end{aligned} \quad (6.3.151)$$

which relates the modal coordinate w_l and physical coordinate ICs. Consider the following two cases of contributions $(w_j(t) \underline{\Gamma}_j)$ to $\underline{X}(t)$ in (6.3.145).

Case 1 (λ_j is real):

In this case, both $\underline{\Gamma}_j$ and $\underline{\beta}_j$ are real vectors since λ_j , \underline{E} , and \underline{H} are real in

$$(\lambda_j \underline{E} - \underline{H}) \underline{\Gamma}_j = \underline{0}, \quad (\lambda_j \underline{E}^T - \underline{H}^T) \underline{\beta}_j = \underline{0} \quad (6.3.152)$$

It follows from (6.3.148), (6.3.149), and (6.3.151) that R_j , \tilde{e}_j , and $w_j(0)$ are also real numbers. Then the coefficients, RHS, and ICs of (6.3.147) are real, so $w_j(t)$ is a real variable. The contribution, $w_j(t) \underline{\Gamma}_j$, of mode j to the total response $\underline{X}(t)$ in (6.3.145) is also real since both $w_j(t)$ and $\underline{\Gamma}_j$ are real.

Case 2 (λ_j is complex):

Note that if λ_j , $\underline{\Gamma}_j$ are the eigensolutions of

$$\lambda_j \underline{E} \underline{\Gamma}_j = \underline{H} \underline{\Gamma}_j \quad (6.3.153)$$

and by conjugating this equation and noting that \underline{E} and \underline{H} are real matrices, it follows that

$$\bar{\lambda}_j \underline{E} \bar{\underline{\Gamma}}_j = \underline{H} \bar{\underline{\Gamma}}_j \quad (6.3.154)$$

Comparison of (6.3.153) and (6.3.154) shows that $\bar{\lambda}_j$ and $\bar{\underline{\Gamma}}_j$ also solve (6.3.153). In a similar manner, if λ_j and $\underline{\beta}_j$ satisfy

$$\lambda_j \underline{E}^T \underline{\beta}_j = \underline{H}^T \underline{\beta}_j \quad (6.3.155)$$

then conjugating this equation

$$\bar{\lambda}_j \underline{E}^T \bar{\underline{\beta}}_j = \underline{H}^T \bar{\underline{\beta}}_j \quad (6.3.156)$$

shows that $\bar{\lambda}_j$ and $\bar{\underline{\beta}}_j$ also solve (6.3.155).

Hence, if λ_j is complex, the eigenvalues and eigenvectors can be arranged as follows:

$$\begin{aligned} j: & \quad \lambda_j, \underline{\Gamma}_j, \underline{\beta}_j \\ j+1: & \quad \bar{\lambda}_j, \bar{\underline{\Gamma}}_j, \bar{\underline{\beta}}_j \end{aligned} \quad (6.3.157)$$

It follows from (6.3.149) and (6.3.157) that

$$\tilde{e}_{j+1} = \underline{\beta}_{j+1}^T \underline{E} \underline{\Gamma}_{j+1} = \bar{\underline{\beta}}_j^T \underline{E} \bar{\underline{\Gamma}}_j = \bar{\tilde{e}}_j \quad (6.3.158)$$

Similarly, from (6.3.148) and (6.3.157),

$$R_{j+1} = \underline{\beta}_{j+1}^T \hat{f} = \bar{\underline{\beta}}_j^T \hat{f} = \bar{R}_j \quad (6.3.159)$$

and from (6.3.151) and (6.3.157),

$$w_{j+1}(0) = \frac{1}{\tilde{e}_{j+1}} \underline{\beta}_{j+1}^T \underline{E} \underline{X}(0) = \frac{1}{\bar{\tilde{e}}_j} \bar{\underline{\beta}}_j^T \underline{E} \underline{X}(0) = \bar{w}_j(0) \quad (6.3.160)$$

Therefore, the $j+1$ term for $(\lambda, \underline{\Gamma}, \underline{\beta}, \tilde{e}, R, w(0))$ is always the conjugate of the j term. Consider the EOM for w_{j+1} for (6.3.147), that is,

$$\dot{w}_{j+1} - \lambda_{j+1} w_{j+1} = \frac{R_{j+1}}{\tilde{e}_{j+1}} \quad (6.3.161)$$

Substitute the results of (6.3.157)–(6.3.159) into (6.3.161) to obtain

$$\dot{w}_{j+1} - \bar{\lambda}_j w_{j+1} = \frac{\bar{R}_j}{\bar{e}_j} \quad (6.3.162)$$

Taking the conjugate of this equation yields

$$\dot{\bar{w}}_{j+1} - \lambda_j \bar{w}_{j+1} = \frac{\bar{R}_j}{\bar{e}_j} \quad (6.3.163)$$

with the accompanying IC from (6.3.160)

$$\bar{w}_{j+1}(0) = w_j(0) \quad (6.3.164)$$

Thus, by comparing (6.3.147) to (6.3.163), it is seen that \bar{w}_{j+1} satisfies the same ODE and IC as w_j . Therefore,

$$\bar{w}_{j+1} = w_j \Rightarrow w_{j+1}(t) = \bar{w}_j(t) \text{ for all time } t \quad (6.3.165)$$

The contribution of the j and $j+1$ terms to the summation for obtaining $\underline{X}(t)$ in (6.3.145) becomes

$$w_j(t)\underline{\Gamma}_j + w_{j+1}(t)\underline{\Gamma}_{j+1} = w_j(t)\underline{\Gamma}_j + \bar{w}_j(t)\bar{\underline{\Gamma}}_j = 2\text{Real}\left(w_j(t)\underline{\Gamma}_j\right) \quad (6.3.166)$$

which is a real vector. Consideration of the two cases (λ real and λ complex) has shown that $\underline{X}(t)$ as determined by the modal summation in (6.3.145) is a real vector, as it should be since it produces real physical displacements and velocities:

$$\underline{X}(t) = \begin{Bmatrix} \underline{V}(t) \\ \underline{q}(t) \end{Bmatrix} = \begin{Bmatrix} \underline{\dot{q}}(t) \\ \underline{q}(t) \end{Bmatrix} \quad 2N \times 1 \quad (6.3.167)$$

6.3.5.1 Real Variable Form of Modal Equations

Equation (6.3.147) is a differential equation that involves a complex response, a complex source, and complex constants and therefore becomes difficult if not impossible to integrate with some computer-aided math solvers. Thus, it is beneficial to convert this equation into real variable form. Write (6.3.147) in terms of real and imaginary parts

$$\frac{d}{dt}(w_{jR} + iw_{jI}) - (\lambda_{jR} + i\lambda_{jI})(w_{jR} + iw_{jI}) = (R_{jR} + iR_{jI}) \frac{(\tilde{e}_{jR} - i\tilde{e}_{jI})}{|\tilde{e}_j|^2} \quad (6.3.168)$$

Separate the real and imaginary parts of Equation (6.3.168)

$$\frac{d}{dt} \begin{Bmatrix} w_{jR} \\ w_{jI} \end{Bmatrix} = \begin{bmatrix} \lambda_{jR} & -\lambda_{jI} \\ \lambda_{jI} & \lambda_{jR} \end{bmatrix} \begin{Bmatrix} w_{jR} \\ w_{jI} \end{Bmatrix} + \frac{1}{|\tilde{e}_j|^2} \begin{Bmatrix} R_{jR} \tilde{e}_{jR} + R_{jI} \tilde{e}_{jI} \\ R_{jI} \tilde{e}_{jR} - R_{jR} \tilde{e}_{jI} \end{Bmatrix} \quad (6.3.169)$$

It has been shown that if λ_j is real, then the following imaginary parts are zero:

$$\lambda_{jI} = R_{jI} = \tilde{e}_{jI} = w_{jI}(0) = 0$$

which simplifies Equation (6.3.169) to

$$w_{jI}(t) = 0 \quad (6.3.170)$$

and

$$\dot{w}_{jR} = \lambda_j w_{jR} + \frac{R_j}{\tilde{e}_j} \quad (6.3.171)$$

where λ_j , \tilde{e}_j , and R_j are real numbers. Next, consider the more general case where λ_j is complex. The ICs on the real and imaginary parts of w_j are obtained from (6.3.151) as follows:

$$\begin{aligned} w_{jR}(0) + iw_{jI}(0) &= \frac{(\tilde{e}_{jR} - i\tilde{e}_{jI})}{|\tilde{e}_j|^2} \left(\underline{\beta}_{jR}^T + i\underline{\beta}_{jI}^T \right) \underline{E} \underline{X}(0) \\ \Rightarrow w_{jR}(0) &= \frac{1}{|\tilde{e}_j|^2} \left(\tilde{e}_{jR} \underline{\beta}_{jR}^T + \tilde{e}_{jI} \underline{\beta}_{jI}^T \right) \underline{E} \underline{X}(0) \\ w_{jI}(0) &= \frac{1}{|\tilde{e}_j|^2} \left(\tilde{e}_{jR} \underline{\beta}_{jI}^T - \tilde{e}_{jI} \underline{\beta}_{jR}^T \right) \underline{E} \underline{X}(0) \end{aligned} \quad (6.3.172)$$

Note that both $w_{jR}(0)$ and $w_{jI}(0)$ are real variables as defined by (6.3.172). Thus, the real variable differential equations in (6.3.169) have the real variable ICs given by (6.3.172). The modal solution procedure for this general system type is summarized in the following.

Steps for Modal Condensation of EOMs for General System

1. Use Equations (6.3.144) and (6.3.149) to compute λ_i , $\underline{\Gamma}_i$, $\underline{\beta}_i$, and \tilde{e}_i for $i = 1, 2, \dots, m$.
2. Use (6.3.148) to evaluate modal forces R_j .
3. Use (6.3.172) to evaluate the modal coordinate ICs

$$w_{jR}(0) = \frac{1}{|\tilde{e}_j|^2} \left(\tilde{e}_{jR} \underline{\beta}_{jR}^T + \tilde{e}_{jI} \underline{\beta}_{jI}^T \right) \underline{E} \underline{X}(0)$$

$$w_{jI}(0) = \frac{1}{|\tilde{e}_j|^2} \left(\tilde{e}_{jR} \underline{\beta}_{jI}^T - \tilde{e}_{jI} \underline{\beta}_{jR}^T \right) \underline{E} \underline{X}(0)$$

4. Numerically or analytically integrate the real differential equations (6.3.169)

$$\frac{d}{dt} \begin{Bmatrix} w_{jR} \\ w_{jI} \end{Bmatrix} = \begin{bmatrix} \lambda_{jR} & -\lambda_{jI} \\ \lambda_{jI} & \lambda_{jR} \end{bmatrix} \begin{Bmatrix} w_{jR} \\ w_{jI} \end{Bmatrix} + \frac{1}{|\tilde{e}_j|^2} \begin{Bmatrix} R_{jR} \tilde{e}_{jR} + R_{jI} \tilde{e}_{jI} \\ R_{jI} \tilde{e}_{jR} - R_{jR} \tilde{e}_{jI} \end{Bmatrix}$$

5. Obtain the displacement and velocity state vector $\underline{X}(t)$ from (6.3.145)

$$\underline{X}(t) = \sum_{j=1}^{m_1} w_j(t) \underline{\Gamma}_j + 2 * \text{Real} \left(\sum_{j=1}^{m_2} w_j(t) \underline{\Gamma}_j \right)$$

$$m = m_1 + m_2$$

where the first sum extends over all modes with real eigenvalues λ_j and the second sum includes all modes with complex eigenvalues λ_j . The second sum implicitly includes the contributions of the conjugate eigensolutions, and therefore, they are not included in the m_2 terms.

6.4 NUMERICAL INTEGRATION OF MDOF TRANSIENT VIBRATION RESPONSE

Some forms of the governing differential equations of equilibrium encountered thus far include:

Form (a): Physical coordinates and second-order form (6.3.1)

$$\underline{M}\ddot{\underline{q}} + \underline{C}_T\dot{\underline{q}} + \underline{K}_T\underline{q} = \underline{f}(t) + \underline{g}(\underline{q}, \dot{\underline{q}}, t) \quad (N \times 1) \quad (6.4.1)$$

Form (b): Physical coordinates and first-order form (6.3.6)

$$\begin{matrix} \underline{E} & \dot{\underline{X}} \\ 2N \times 2N & 2N \times 1 \end{matrix} = \begin{matrix} \underline{H} & \underline{X} \\ 2N \times 2N & 2N \times 1 \end{matrix} + \begin{matrix} \hat{f} \\ 2N \times 1 \end{matrix} \quad (2N \times 1) \quad (6.4.2)$$

Form (c): Modal coordinates and orthogonally damped, nongyroscopic, noncirculatory systems (6.3.15)

$$\ddot{\chi}_i + 2\xi_i\omega_i\dot{\chi}_i + \omega_i^2\chi_i = r_i(t, \underline{q}, \dot{\underline{q}}) \quad (1 \times 1) \quad (6.4.3)$$

Form (d): Modal coordinates and general systems (6.3.168)

$$\frac{d}{dt}(w_{jR} + iw_{jI}) - (\lambda_{jR} + i\lambda_{jI})(w_{jR} + iw_{jI}) = (R_{jR} + iR_{jI}) \frac{(\tilde{e}_{jR} - i\tilde{e}_{jI})}{|\tilde{e}_j|^2} \quad (6.4.4)$$

or by considering real and imaginary parts of Equation (6.3.169):

$$\frac{d}{dt} \begin{Bmatrix} w_{jR} \\ w_{jI} \end{Bmatrix} = \begin{bmatrix} \lambda_{jR} & -\lambda_{jI} \\ \lambda_{jI} & \lambda_{jR} \end{bmatrix} \begin{Bmatrix} w_{jR} \\ w_{jI} \end{Bmatrix} + \frac{1}{|\tilde{e}_j|^2} \begin{Bmatrix} R_{jR}\tilde{e}_{jR} + R_{jI}\tilde{e}_{jI} \\ R_{jI}\tilde{e}_{jR} - R_{jR}\tilde{e}_{jI} \end{Bmatrix} \quad (6.4.5)$$

Section 6.3 showed that if λ was real, the following imaginary parts were zero:

$$\lambda_{jI} = R_{jI} = \tilde{e}_{jI} = w_{jI}(0) = 0$$

which simplifies Equation (6.4.5) to

$$w_{jI}(t) = 0 \quad (6.4.6)$$

and

$$\dot{w}_{jR} = \lambda_j w_{jR} + \frac{R_j}{\tilde{e}_j} \quad (6.4.7)$$

where λ_j , \tilde{e}_j , and R_j are real numbers.

Forms (a), (b), (c), and (d) of the governing EOMs may be numerically integrated given the following ICs:

Form (a):

$$\underline{q}(0), \underline{\dot{q}}(0) \quad (6.4.8)$$

Form (b):

$$\underline{X}(0) = \begin{Bmatrix} \underline{\dot{q}}(0) \\ \underline{q}(0) \end{Bmatrix} \quad (6.4.9)$$

Form (c): From (6.3.18) and (6.3.19),

$$\chi_i(0) = \frac{1}{\tilde{m}_i} \underline{\psi}_i^T \underline{M} \underline{q}(0), \quad \dot{\chi}_i(0) = \frac{1}{\tilde{m}_i} \underline{\psi}_i^T \underline{M} \underline{\dot{q}}(0) \quad (6.4.10)$$

Form (d): From (6.3.172),

$$\begin{aligned} \Rightarrow w_{jR}(0) &= \frac{1}{|\tilde{e}_j|^2} \left(\tilde{e}_{jR} \beta_{jR}^T + \tilde{e}_{jI} \beta_{jI}^T \right) \underline{E} \underline{X}(0) \\ w_{jI}(0) &= \frac{1}{|\tilde{e}_j|^2} \left(\tilde{e}_{jR} \beta_{jI}^T - \tilde{e}_{jI} \beta_{jR}^T \right) \underline{E} \underline{X}(0) \end{aligned} \quad (6.4.11)$$

All of the above forms of the system equilibrium conditions may be numerically integrated forward in time to obtain the displacement and velocity responses to arbitrary forcing functions.

The basic idea of NI is to divide the time domain into a series of discrete steps and to impose simplifying approximations on the acceleration and velocity variations between these times. In this manner, the NI algorithm carries the displacements, velocities, and accelerations forward from time t_i to time t_{i+1} as depicted in Figure 6.4.1.

Although this figure depicts a constant Δt , an adaptive predictor–corrector approach may adapt Δt with t to quicken the required computation (CPU) time and/or improve NI accuracy. NI algorithms have been developed for both the first (Eqs. 6.4.2 and 6.4.5) and second (Eqs. 6.4.1 and 6.4.3) order forms of the governing EOMs.

6.4.1 Second-Order System NI Algorithms

There are many NI approaches (Bathe, 1982) for second-order systems, and two are presented in the following for illustration.

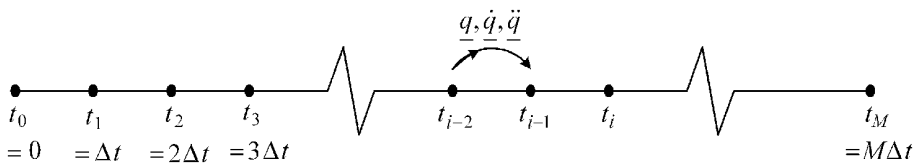


Figure 6.4.1 Discrete time axis for the application of NI algorithm

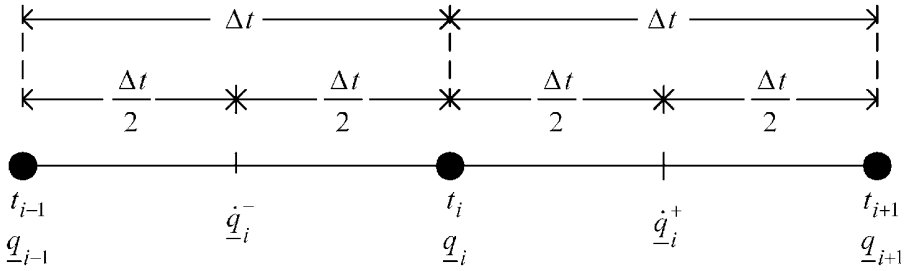


Figure 6.4.2 Discretized time and response variables for central difference NI

6.4.1.1 Central Difference Method

Consider the two consecutive time steps shown in Figure 6.4.2.

Define

$$\dot{q}_i^- = \frac{q_i - q_{i-1}}{\Delta t}, \quad \dot{q}_i^+ = \frac{q_{i+1} - q_i}{\Delta t} \quad (6.4.12)$$

Then make the approximation

$$\dot{q}_i = \frac{\dot{q}_i^- + \dot{q}_i^+}{2} = \frac{q_{i+1} - q_{i-1}}{2\Delta t} \quad (6.4.13)$$

Assume also that

$$\ddot{q}_i = \frac{\dot{q}_i^+ - \dot{q}_i^-}{\Delta t} = \frac{q_{i+1} - 2q_i + q_{i-1}}{\Delta t^2} \quad (6.4.14)$$

The system equilibrium equation is given at time i by (6.4.1)

$$\underline{M}\ddot{q}_i + \underline{C}_T\dot{q}_i + \underline{K}q_i = \underline{f}_i + \underline{g}_{i-1} \quad (6.4.15)$$

Note that the nonlinear force term \underline{g} is evaluated at the previous time step so that it is assumed to be known at time t_i

$$\underline{g}_{i-1} = \underline{g}(t_i, q_{i-1}, \dot{q}_{i-1}) \quad (6.4.16)$$

The reason for this is that \underline{g} is a function of \underline{q} and $\dot{\underline{q}}$ which are not yet known at time t_i .

Substitute (6.4.13) and (6.4.14) into (6.4.15) to obtain

$$\left(\frac{1}{\Delta t^2} \underline{M} + \frac{1}{2\Delta t} \underline{C}_T \right) q_{i+1} = \underline{f}_i + \underline{g}_{i-1} + \left(\frac{2}{\Delta t^2} \underline{M} - \underline{K} \right) q_i + \left(\frac{-1}{\Delta t^2} \underline{M} + \frac{1}{2\Delta t} \underline{C}_T \right) q_{i-1} \quad (6.4.17)$$

If Δt is a constant, the coefficient matrix $((1/\Delta t^2)\underline{M} + (1/2\Delta t)\underline{C}_T)$ need only be triangularized once, and therefore, each iteration only requires a back substitution procedure to obtain q_{i+1} from (6.4.17). Start the NI by solving for \ddot{q}_0 from (6.4.15), that is,

$$\ddot{q}_0 = \underline{M}^{-1} \left(\underline{f}(0) + \underline{g}(0, q_0, \dot{q}_0) - \underline{C}_T \dot{q}_0 - \underline{K} q_0 \right) \quad (6.4.18)$$

where \underline{q}_0 and $\underline{\dot{q}}_0$ are given. Consider (6.4.13) and (6.4.14) at $t=0$:

$$\underline{\dot{q}}_0 = \frac{q_1 - q_{-1}}{2\Delta t} \quad (6.4.19)$$

$$\underline{\ddot{q}}_0 = \frac{q_1 - 2q_0 + q_{-1}}{\Delta t^2} \quad (6.4.20)$$

Solve (6.4.19) for q_1 :

$$q_1 = 2\Delta t \underline{\dot{q}}_0 + q_{-1} \quad (6.4.21)$$

Substitute (6.4.21) into (6.4.20):

$$\underline{\ddot{q}}_0 = \frac{2q_{-1} + 2\Delta t \underline{\dot{q}}_0 - 2q_0}{\Delta t^2} \quad (6.4.22)$$

Solve this equation for q_{-1} :

$$q_{-1} = \frac{\Delta t^2}{2} \underline{\ddot{q}}_0 - \Delta t \underline{\dot{q}}_0 + q_0 \quad (6.4.23)$$

Summary of Central Difference NI Algorithm

Given the initial displacements and velocities q_0 and $\underline{\dot{q}}_0$.

1. Determine the initial accelerations $\underline{\ddot{q}}_0$ from (6.4.18).
2. Determine q_{-1} from (6.4.23).
3. Use (6.4.17) to solve for q_{i+1} , $i=0, 1, 2, \dots, m$.
4. Note that, if desired, the velocities or accelerations may be obtained at any time step from (6.4.13) and (6.4.14): $\underline{\dot{q}}_i = (q_{i+1} - q_{i-1}) / (2\Delta t)$, $\underline{\ddot{q}}_i = (q_{i+1} - 2q_i + q_{i-1}) / \Delta t^2$.
5. Continue the NI process until the final simulation time is reached.

6.4.1.2 Newmark Beta Method

This method has gained considerable popularity among vibration analysts and assumes that the acceleration is approximately constant within any time step (Figure 6.4.3).

A reasonable assumption for the variation of $\underline{\ddot{q}}$ between t_i and t_{i+1} is that it is the constant vector:

$$\underline{\ddot{q}}(t) = \frac{\underline{\ddot{q}}_i + \underline{\ddot{q}}_{i+1}}{2} \quad (6.4.24)$$

Newmark generalized this expression into the form

$$\underline{\ddot{q}} = (1-\delta)\underline{\ddot{q}}_i + \delta\underline{\ddot{q}}_{i+1}, \quad t_i < t < t_{i+1} \quad (6.4.25)$$

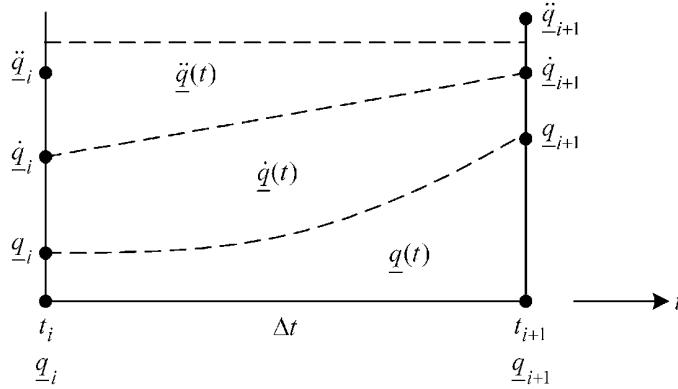


Figure 6.4.3 Discretized time and response variables for Newmark beta method

Note that (6.4.25) reduces to (6.4.24) if $\delta = 1/2$. Integration of (6.4.25) yields

$$\underline{\dot{q}}_{i+1} = \underline{\dot{q}}_i + \left[(1-\delta)\underline{\dot{q}}_i + \delta\underline{\dot{q}}_{i+1} \right] \Delta t \quad (6.4.26)$$

Integrating again yields

$$\underline{q}_{i+1} = \underline{q}_i + \underline{\dot{q}}_i \Delta t + \frac{\Delta t^2}{2} \left[(1-\delta)\underline{\ddot{q}}_i + \delta\underline{\ddot{q}}_{i+1} \right] \quad (6.4.27)$$

Newmark generalized this result by replacing $\delta/2$ by a constant α independent of δ . Newmark's approximations for \underline{q} , $\underline{\dot{q}}$, and $\underline{\ddot{q}}$ within the Δt interval then become

$$\begin{aligned} \underline{\ddot{q}} &= (1-\delta)\underline{\ddot{q}}_i + \delta\underline{\ddot{q}}_{i+1}, \quad t_i < t < t_{i+1} \\ \underline{\dot{q}}_{i+1} &= \underline{\dot{q}}_i + \left[(1-\delta)\underline{\dot{q}}_i + \delta\underline{\dot{q}}_{i+1} \right] \Delta t \\ \underline{q}_{i+1} &= \underline{q}_i + \underline{\dot{q}}_i \Delta t + \left[\left(\frac{1}{2} - \alpha \right) \underline{\ddot{q}}_i + \alpha \underline{\ddot{q}}_{i+1} \right] \Delta t^2 \end{aligned} \quad (6.4.28)$$

The recommended values for δ and α are

$$\delta = \frac{1}{2}, \quad \alpha = \frac{1}{4} \quad (6.4.29)$$

for which Equation (6.4.28) becomes

$$\underline{\dot{q}}_{i+1} = \underline{\dot{q}}_i + \left(\underline{\ddot{q}}_i + \underline{\ddot{q}}_{i+1} \right) \frac{\Delta t}{2}, \quad \underline{q}_{i+1} = \underline{q}_i + \underline{\dot{q}}_i \Delta t + \left(\underline{\ddot{q}}_i + \underline{\ddot{q}}_{i+1} \right) \frac{\Delta t^2}{4} \quad (6.4.30)$$

Consider the system equilibrium equation (6.4.1) at time t_{i+1} , that is,

$$\underline{M}\underline{\ddot{q}}_{i+1} + \underline{C}_T \underline{\dot{q}}_{i+1} + \underline{K}_T \underline{q}_{i+1} = \underline{f}(t_{i+1}) + \underline{g}(t_{i+1}, \underline{q}_i, \underline{\dot{q}}_i) \quad (6.4.31)$$

This equation has three unknowns $(\underline{q}_{i+1}, \underline{\dot{q}}_{i+1}, \underline{\ddot{q}}_{i+1})$ at time t_{i+1} . Assume that these quantities are known at time t_i and use (6.4.28) to eliminate $\underline{\dot{q}}_{i+1}$ and $\underline{\ddot{q}}_{i+1}$ from Equation (6.4.31). From the third equation in (6.4.28),

$$\ddot{q}_{i+1} = \frac{1}{\alpha\Delta t^2}q_{i+1} - \frac{1}{\alpha\Delta t^2}q_i - \frac{1}{\alpha\Delta t}\dot{q}_i + \left(1 - \frac{1}{2\alpha}\right)\ddot{q}_i \quad (6.4.32)$$

Substitute this result into the second equation in (6.4.28):

$$\dot{q}_{i+1} = -\frac{\delta}{\alpha\Delta t}q_i + \left(-\frac{\delta\Delta t}{2\alpha} + \Delta t\right)\ddot{q}_i + \frac{\delta}{\alpha\Delta t}q_{i+1} + \left(1 - \frac{\delta}{\alpha}\right)\dot{q}_i \quad (6.4.33)$$

Substitute (6.4.32) and (6.4.33) into (6.4.31) to eliminate the \dot{q}_{i+1} and \ddot{q}_{i+1} terms and solve for q_{i+1} to obtain

$$\begin{aligned} \left(\frac{1}{\alpha\Delta t^2}\underline{M} + \frac{\delta}{\alpha\Delta t}\underline{C}_T + \underline{K}_T\right)q_{i+1} = & f_{i+1} + \underline{g}(t_{i+1}, q_i, \dot{q}_i) + \underline{M}\left[\frac{1}{\alpha\Delta t^2}q_i + \frac{1}{\alpha\Delta t}\dot{q}_i + \left(\frac{1}{2\alpha} - 1\right)\ddot{q}_i\right] \\ & + \underline{C}_T\left[\frac{\delta}{\alpha\Delta t}q_i + \left(\frac{\delta}{\alpha} - 1\right)\dot{q}_i + \left(\frac{\delta\Delta t}{2\alpha} - \Delta t\right)\ddot{q}_i\right] \end{aligned} \quad (6.4.34)$$

Some notable points about this formula are:

1. The coefficient matrix $\left(\frac{1}{\alpha\Delta t^2}\right)\underline{M} + \left(\frac{\delta}{\alpha\Delta t}\right)\underline{C}_T + \underline{K}_T$ of q_{i+1} is triangularized only once, unless \underline{M} , \underline{C}_T , \underline{K}_T , or Δt changes during the duration of the NI. Thus, unless these terms change, the solution for q_{i+1} will only require a back substitution operation for each iteration.
2. The velocity (\dot{q}_{i+1}) and acceleration (\ddot{q}_{i+1}) vectors must be calculated for each iteration. This is accomplished by substituting q_{i+1} from the solution of (6.4.34) into (6.4.32) to obtain \ddot{q}_{i+1} . Then \ddot{q}_{i+1} is substituted into the second of equation (6.4.28), that is, to obtain \dot{q}_{i+1} .

Summary of the Newmark Beta Method

Given the initial displacements and velocities q_0 and \dot{q}_0 :

1. Solve for the initial accelerations \ddot{q}_0 from (6.4.31):

$$\ddot{q}_0 = \underline{M}^{-1}\left[f(0) + \underline{g}(0, q_0, \dot{q}_0) - \underline{C}_T\dot{q}_0 - \underline{K}_Tq_0\right] \quad (6.4.35)$$

2. Select δ and α values. Typically, $\delta = 1/2$, $\alpha = 1/4$.
3. Form the matrices

$$\begin{aligned} \underline{A} &= \left(\frac{1}{\alpha\Delta t^2}\underline{M} + \frac{\delta}{\alpha\Delta t}\underline{C}_T + \underline{K}_T\right), \quad \underline{B} = \frac{1}{\alpha\Delta t}\left(\frac{1}{\Delta t}\underline{M} + \delta\underline{C}_T\right) \\ \underline{D} &= \frac{1}{\alpha\Delta t}\underline{M} + \left(\frac{\delta}{\alpha} - 1\right)\underline{C}_T, \quad \underline{E} = \left(\frac{1}{2\alpha} - 1\right)\underline{M} + \left(\frac{\delta\Delta t}{2\alpha} - \Delta t\right)\underline{C}_T \end{aligned} \quad (6.4.36)$$

4. Triangularize (or invert) \underline{A} and store.
5. Solve (6.4.34) for q_{i+1} in the form

$$\underline{A}q_{i+1} = f_{i+1} + \underline{g}(t_{i+1}, q_i, \dot{q}_i) + \underline{B}q_i + \underline{D}\dot{q}_i + \underline{E}\ddot{q}_i \quad (6.4.37)$$

This will require only a back substitution operation if \underline{A} has been triangularized or a multiplication by \underline{A}^{-1} if \underline{A} has been inverted.

6. Update the velocity and acceleration vectors, that is, from (6.4.32)

$$\ddot{\underline{q}}_{i+1} = \frac{1}{\alpha\Delta t^2}\underline{q}_{i+1} - \frac{1}{\alpha\Delta t^2}\underline{q}_i - \frac{1}{\alpha\Delta t}\dot{\underline{q}}_i + \left(1 - \frac{1}{2\alpha}\right)\ddot{\underline{q}}_i \quad (6.4.38)$$

and from the second of Equation (6.4.28)

$$\dot{\underline{q}}_{i+1} = \dot{\underline{q}}_i + \left[(1-\delta)\ddot{\underline{q}}_i + \delta\ddot{\underline{q}}_{i+1} \right] \Delta t \quad (6.4.39)$$

7. Repeat (6) and (7) until the final time for the simulation is reached or until Δt is changed, which may occur if an adaptive time step algorithm is employed. Repeat step (5) whenever Δt or \underline{M} , \underline{K}_T , or \underline{C}_T change.

The Newmark beta algorithm can be applied directly to the uncoupled modal coordinate differential equations in (6.3.15):

$$\ddot{\chi}_j + 2\xi_j\omega_j\dot{\chi}_j + \omega_j^2\chi_j = \frac{r_j}{\tilde{m}_j} \quad (6.4.40)$$

where

$$r_j = \underline{\psi}_j^T \underline{f}(t) + \underline{\psi}_j^T \underline{g}(t, \underline{q}, \dot{\underline{q}}) \quad j = 1, 2, \dots, m \text{ (number of modal coordinates } \chi)$$

From (6.4.35)–(6.4.40), the Newmark beta algorithm becomes

$$1. \quad \ddot{\chi}_j(0) = \frac{r_j(0)}{\tilde{m}_j} - 2\xi_j\omega_j\dot{\chi}_j(0) + \omega_j^2\chi_j(0) \quad (6.4.41)$$

$$2. \quad a_j = \frac{1}{\alpha\Delta t^2} + \frac{\delta}{\alpha\Delta t} 2\xi_j\omega_j + \omega_j^2, \quad b_j = \frac{1}{\alpha\Delta t^2} + \frac{\delta}{\alpha\Delta t} 2\xi_j\omega_j$$

$$d_j = \frac{1}{\alpha\Delta t} + \left(\frac{\delta}{\alpha} - 1\right) 2\xi_j\omega_j, \quad e_j = \left(\frac{1}{2\alpha} - 1\right) + \left(\frac{\delta\Delta t}{2\alpha} - \Delta t\right) 2\xi_j\omega_j \quad (6.4.42)$$

$$3. \quad \chi_j|_{i+1} = \frac{1}{a_j} \left(\frac{1}{\tilde{m}_j} r_j|_{i+1} + b_j \chi_j|_i + d_j \dot{\chi}_j|_i + e_j \ddot{\chi}_j|_i \right)$$

$$\text{where } r_j|_{i+1} = \underline{\psi}_j^T \left(\underline{f}(t_{i+1}) + \underline{g}(t_{i+1}, \underline{q}_i, \dot{\underline{q}}_i) \right) \quad (6.4.43)$$

$$4. \quad \ddot{\chi}_j|_{i+1} = \frac{1}{\alpha\Delta t^2} (\chi_j|_{i+1} - \chi_j|_i) - \frac{1}{\alpha\Delta t} \dot{\chi}_j|_i + \left(1 - \frac{1}{2\alpha}\right) \ddot{\chi}_j|_i \quad (6.4.44)$$

$$5. \quad \dot{\chi}_j|_{i+1} = \dot{\chi}_j|_i + \left[(1-\delta)\ddot{\chi}_j|_i + \delta\ddot{\chi}_j|_{i+1} \right] \Delta t \quad (6.4.45)$$

To implement the algorithm for the j th modal coordinate:

(a) Obtain $\chi_j(0)$ and $\dot{\chi}_j(0)$ from (6.3.18) and (6.3.19):

$$\chi_j(0) = \frac{1}{\bar{m}_j} \underline{\psi}_j^T \underline{M} \underline{q}(0), \quad \dot{\chi}_j(0) = \frac{1}{\bar{m}_j} \underline{\psi}_j^T \underline{M} \underline{\dot{q}}(0) \quad (6.4.46)$$

and substitute the results into (1) to obtain $\ddot{\chi}_j(0)$.

(b) Evaluate a_j , b_j , d_j , and e_j from (6.4.42).

(c) Repeat steps (3)–(5) for $i = 1, \dots, N_{\text{steps}}$ where N_{steps} is the total number of time steps. The term \underline{g} in (6.4.40) is a nonlinear function of the physical coordinate displacements (\underline{q}) and velocities ($\underline{\dot{q}}$). Therefore, if \underline{g} exist, the “physical coordinate” vectors \underline{q}_i and $\underline{\dot{q}}_i$ will need to be evaluated at each time step, that is,

$$\underline{q}_i = \underline{\Psi} \underline{\chi}_i, \quad \underline{\dot{q}}_i = \underline{\Psi} \underline{\dot{\chi}}_i \quad (6.4.47)$$

6.4.2 First-Order System NI Algorithms

The first-order form for the governing equilibrium equations is given by (6.3.7)–(6.3.9)

$$\underline{\dot{X}}_{2N \times 1} = \underline{A}_{2N \times 2N} \underline{X}_{2N \times 1} + \underline{F}(t)_{2N \times 1} + \underline{G}_{2N \times 1}(t, \underline{q}, \underline{\dot{q}}) \quad (6.4.48)$$

where

$$\underline{X} = \begin{Bmatrix} \underline{V} \\ \underline{q} \end{Bmatrix}, \quad \underline{A} = \begin{bmatrix} -\underline{M}^{-1} \underline{C}_T & -\underline{M}^{-1} \underline{K}_T \\ \underline{I}_N & \underline{0} \end{bmatrix},$$

$$\underline{V} = \underline{\dot{q}}, \quad \underline{F}(t) = \begin{Bmatrix} \underline{M}^{-1} \underline{f}(t) \\ \underline{0} \end{Bmatrix}, \quad \underline{G} = \begin{Bmatrix} \underline{M}^{-1} \underline{g}(t, \underline{q}, \underline{\dot{q}}) \\ \underline{0} \end{Bmatrix} \quad (6.4.49)$$

The force term G is a nonlinear function of positions and velocities to account for nonlinear forces in the model. Define the augmented state vector \underline{X}' and state matrix \underline{A}' as

$$\underline{X}' = \begin{Bmatrix} \underline{X} \\ \underline{1} \end{Bmatrix}, \quad \underline{A}' = \begin{bmatrix} \underline{A} & \underline{F} + \underline{G} \\ \underline{0} & \underline{0} \end{bmatrix} \quad (6.4.50)$$

Note that the force terms now appear in the matrix term \underline{A}' of the equilibrium equation, which implies that \underline{A}' in general varies with time. Then (6.4.48) may be written as

$$\underline{\dot{X}}' = \underline{A}'(t, \underline{q}, \underline{\dot{q}}) \underline{X}' \quad (6.4.51)$$

$(2N+1) \times 1$ $(2N+1) \times (2N+1)$ $(2N+1) \times 1$

Equation (6.4.51) will be used as the starting point to illustrate several first-order NI algorithms. The matrix \underline{A}' varies with t because of $\underline{F}(t)$ and with \underline{q} and $\underline{\dot{q}}$ because of the non-linear terms in \underline{G} . This only affects the last column of \underline{A}' .

6.4.2.1 Euler Numerical Integration

The Euler numerical integration (ENI) algorithm utilizes a two-term Taylor series expansion for \underline{X}' about $t = t_i$, that is,

$$\underline{X}'_{-i+1} = \underline{X}'_{-i} + \left. \frac{d}{dt} \underline{X}' \right|_{t_i} \Delta t \quad (6.4.52)$$

Substitute (6.4.51) into (6.4.52) to obtain

$$\underline{X}'_{-i+1} = \underline{X}'_{-i} + \underline{A}'_{-i} \underline{X}'_{-i} \Delta t = \left(\underline{I} + \Delta t \underline{A}'_{-i} \right) \underline{X}'_{-i} \quad (6.4.53)$$

Assume that the integration begins at $t = 0$, that is, when

$$\underline{X}'_{-0} = \begin{Bmatrix} \underline{\dot{q}}_0 \\ \underline{q}_0 \\ 1 \end{Bmatrix} \quad (6.4.54)$$

Then after n_{steps} time increments,

$$\underline{X}'_{-n_{\text{steps}}} = \underline{B}_{-n_{\text{steps}}} \underline{X}'_{-0} \quad (6.4.55)$$

where

$$\underline{B}_{-n_{\text{steps}}} = \underline{b}_{-n_{\text{steps}}} \underline{b}_{-n_{\text{steps}}-1} \cdots \underline{b}_{-0} = \prod_{i=1}^{n_{\text{steps}}} \underline{b}_{-i}$$

$$\underline{b}_{-i} = \underline{I} + \Delta t \underline{A}'_{-i}, \quad \underline{A}'_{-i} = \underline{A}'(t_i, \underline{q}_{-i}, \underline{\dot{q}}_{-i}) \quad (6.4.56)$$

The displacements and velocities can be obtained from \underline{X}' at any time step since by (6.4.49) and (6.4.50),

$$\underline{X}' = \begin{Bmatrix} \underline{\dot{q}} \\ \underline{q} \\ 1 \end{Bmatrix} \quad (6.4.57)$$

6.4.2.2 Improved ENI

Suppose that the ENI provided an estimate of \underline{X}'_{-i+1} according to (6.4.53). Let's call this "predictor step" estimate

$$\underline{\tilde{X}}'_{i+1} = \underline{X}'_i + \underline{A}'_i \underline{X}'_i \Delta t \quad (6.4.58)$$

Then an estimate of $\underline{\dot{X}}'_{i+1}$ is obtained from (6.4.51) and (6.4.55) as

$$\underline{\dot{X}}'_{i+1} = \underline{A}'_{i+1} \underline{\tilde{X}}'_{i+1} \quad (6.4.59)$$

An average value of $\underline{\dot{X}}'_i$ between t_i and t_{i+1} is obtained from (6.4.58) and (6.4.59) as

$$\underline{\dot{X}}'_i \Big|_{\text{ave}} = \frac{1}{2} \left(\underline{A}'_i \underline{X}'_i + \underline{A}'_{i+1} \underline{\tilde{X}}'_{i+1} \right) \quad (6.4.60)$$

and therefore, a “corrector step” estimate of \underline{X}'_{i+1} is

$$\underline{X}'_{i+1} = \underline{X}'_i + \Delta t \underline{\dot{X}}'_i \Big|_{\text{ave}} \quad (6.4.61)$$

Insert (6.4.58) into (6.4.60) and the results into (6.4.61) to obtain

$$\begin{aligned} \underline{X}'_{i+1} &= \underline{X}'_i + \frac{\Delta t}{2} \left(\underline{A}'_i \underline{X}'_i + \underline{A}'_{i+1} \underline{\tilde{X}}'_{i+1} \right) \\ &= \underline{X}'_i + \frac{\Delta t}{2} \left(\underline{A}'_i \underline{X}'_i + \underline{A}'_{i+1} \underline{X}'_i + \Delta t \underline{A}'_{i+1} \underline{A}'_i \underline{X}'_i \right) \\ &= \left[\underline{I} + \frac{\Delta t}{2} \left(\underline{A}'_i + \underline{A}'_{i+1} + \Delta t \underline{A}'_{i+1} \underline{A}'_i \right) \right] \underline{X}'_i \end{aligned} \quad (6.4.62)$$

Then after n_{steps} time increments,

$$\underline{X}'_{n_{\text{steps}}} = \underline{B}_{n_{\text{steps}}} \underline{X}'_0 \quad (6.4.63)$$

where

$$\begin{aligned} \underline{B}_{n_{\text{steps}}} &= \underline{b}_{n_{\text{steps}}} \underline{b}_{n_{\text{steps}}-1} \cdots \underline{b}_0 = \prod_{i=1}^{n_{\text{steps}}} \underline{b}_i \\ \underline{b}_i &= \underline{I} + \frac{\Delta t}{2} \left(\underline{A}'_i + \underline{A}'_{i+1} + \Delta t \underline{A}'_{i+1} \underline{A}'_i \right) \\ \underline{A}'_i &= \underline{A}'(t_i, \underline{q}_i, \underline{\dot{q}}_i), \quad \underline{A}'_{i+1} = \underline{A}'(t_{i+1}, \underline{\tilde{q}}_{i+1}, \underline{\dot{\tilde{q}}}_{i+1}) \end{aligned} \quad (6.4.64)$$

The displacements and velocities can be obtained from \underline{X}' at any time step since by (6.4.49) and (6.4.50),

$$\underline{X}' = \begin{Bmatrix} \underline{\dot{q}} \\ \underline{q} \\ 1 \end{Bmatrix} \quad (6.4.65)$$

The estimated displacements $\underline{\tilde{q}}_i$ and velocities $\underline{\dot{\tilde{q}}}_i$ in \underline{A}'_{i+1} are obtained from $\underline{\tilde{X}}'_{i+1}$ in (6.4.58), that is,

$$\underline{\tilde{X}}'_{i+1} = \begin{Bmatrix} \underline{\dot{\tilde{q}}}_{i+1} \\ \underline{\tilde{q}}_{i+1} \\ 1 \end{Bmatrix} \quad (6.4.66)$$

6.4.2.3 Fourth-Order Runge–Kutta NI

A general discussion of the Runge–Kutta algorithm may be found in Isaacson and Keller (1966) or Davis and Rabinowitz (1984). The following presents one approach for the implementation of fourth-order Runge–Kutta NI (RK4NI). From (6.4.51),

$$\frac{d}{dt}\underline{X}' = \underline{A}'(t, \underline{q}, \underline{\dot{q}})\underline{X}' = L(t, \underline{X}') \quad (6.4.67)$$

Let

$$\underline{A}'_i = \underline{A}'(t_i), \quad \underline{A}'_{(i+\frac{1}{2})} = \underline{A}'\left(t_i + \frac{\Delta t}{2}\right), \quad \underline{A}'_{i+1} = \underline{A}'(t_i + \Delta t)$$

and define

$$(a) \quad \underline{\alpha}'_i = \Delta t \underline{L}\left(t_i, \underline{X}'_i\right) = \Delta t \underline{A}'_i \underline{X}'_i = \underline{\alpha}'_i \underline{X}'_i \Rightarrow \underline{\alpha}'_i = \Delta t \underline{A}'_i \quad (6.4.68)$$

$$(b) \quad \underline{\beta}'_i = \Delta t \underline{L}\left(t_i + \frac{\Delta t}{2}, \underline{X}'_i + \frac{\underline{\alpha}'_i}{2}\right) = \Delta t \underline{A}'_{(i+\frac{1}{2})} * \left(\underline{X}'_i + \frac{1}{2} \underline{\alpha}'_i \underline{X}'_i\right) = \underline{\beta}'_i \underline{X}'_i \\ \Rightarrow \underline{\beta}'_i = \Delta t \underline{A}'_{(i+\frac{1}{2})} + \frac{\Delta t}{2} \underline{A}'_{(i+\frac{1}{2})} \underline{\alpha}'_i \quad (6.4.69)$$

$$(c) \quad \underline{\gamma}'_i = \Delta t \underline{L}\left(t_i + \frac{\Delta t}{2}, \underline{X}'_i + \frac{\underline{\beta}'_i}{2}\right) = \Delta t \underline{A}'_{(i+\frac{1}{2})} * \left(\underline{X}'_i + \frac{1}{2} \underline{\beta}'_i \underline{X}'_i\right) = \underline{\gamma}'_i \underline{X}'_i \\ \Rightarrow \underline{\gamma}'_i = \Delta t \underline{A}'_{(i+\frac{1}{2})} + \frac{\Delta t}{2} \underline{A}'_{(i+\frac{1}{2})} \underline{\beta}'_i \quad (6.4.70)$$

$$(d) \quad \underline{\delta}'_i = \Delta t \underline{L}\left(t_{i+1}, \underline{X}'_i + \underline{\gamma}'_i\right) = \Delta t \underline{A}'_{i+1} \left(\underline{X}'_i + \underline{\gamma}'_i \underline{X}'_i\right) = \underline{\delta}'_i \underline{X}'_i \\ \Rightarrow \underline{\delta}'_i = \Delta t \underline{A}'_{i+1} + \Delta t \underline{A}'_{i+1} \underline{\gamma}'_i \quad (6.4.71)$$

The transfer of \underline{X}'_i to \underline{X}'_{i+1} then becomes

$$\underline{X}'_{i+1} = \underline{X}'_i + \frac{1}{6} \left(\underline{\alpha}'_i + 2\underline{\beta}'_i + 2\underline{\gamma}'_i + \underline{\delta}'_i\right) = \underline{X}'_i + \frac{1}{6} \left(\underline{\alpha}'_i + 2\underline{\beta}'_i + 2\underline{\gamma}'_i + \underline{\delta}'_i\right) \underline{X}'_i \quad (6.4.72)$$

or

$$\underline{X}'_{i+1} = \underline{b}_i \underline{X}'_i \quad (6.4.73)$$

where

$$\underline{b}_i = \underline{I} + \frac{1}{6} \left(\underline{\alpha}'_i + 2\underline{\beta}'_i + 2\underline{\gamma}'_i + \underline{\delta}'_i\right) \quad (6.4.74)$$

Then

$$\underline{X}'_{n_{\text{steps}}} = \underline{B}_{n_{\text{steps}}} \underline{X}'_0 \quad (6.4.75)$$

where

$$\underline{B}_{n_{\text{steps}}} = \underline{b}_{n_{\text{steps}}} \underline{b}_{n_{\text{steps}}-1} \cdots \underline{b}_0 = \prod_{i=1}^{n_{\text{steps}}} \underline{b}_i \quad (6.4.76)$$

The velocities and displacements can be obtained from \underline{X}' at any time step since by (6.4.49) and (6.4.50),

$$\underline{X}' = \begin{Bmatrix} \underline{\dot{q}} \\ \underline{q} \\ 1 \end{Bmatrix} \quad (6.4.77)$$

Examples

The following examples illustrate the use of NI algorithms to determine transient vibration response.

EXAMPLE 6.4.1 *Blade Loss in Rotating Machinery*

Statement: Loss of a blade from a turbine, fan, or compressor wheel can lead to catastrophic failure of a jet engine or turbine-generator set. This may cause injury, loss of life, and/or loss of critical machinery. Mitigation of blade loss effects is an area of active R&D in both government and industry.

Objective: Determine the peak bearing force during a blade loss event for several bearing stiffness values. This type of parametric study provides guidance in the design of the machine to reduce the possibility of bearing failure during a blade loss event.

Assumptions:

- (a) Small angle motion.
- (b) Linear bearing forces.
- (c) No internal rubs in the machine, that is, no blade rubs against seals.
- (d) The mass of the disc is significantly larger than the mass of the shaft so the mass center of the rotor plus disc is approximately at the mass center of the disc.

Solution: The model shown in Figure E6.4.1(a) may represent a single-stage turbine supported by flexibly mounted ball bearings. The x_2 – x_3 plane is referred to as the “radial” plane.

- (a) Apply the gyroscopic moment analysis in ((5.3.92)–(5.3.95)) and Figures 5.3.1 and 5.3.2 to obtain the equations of motion:

$$\underline{M}\underline{\ddot{q}} + (\underline{C}_B + \underline{G})\underline{\dot{q}} + (\underline{K}_B + \underline{K}_f)\underline{q} = \underline{F}_{BL}(t) \quad (1)$$

where

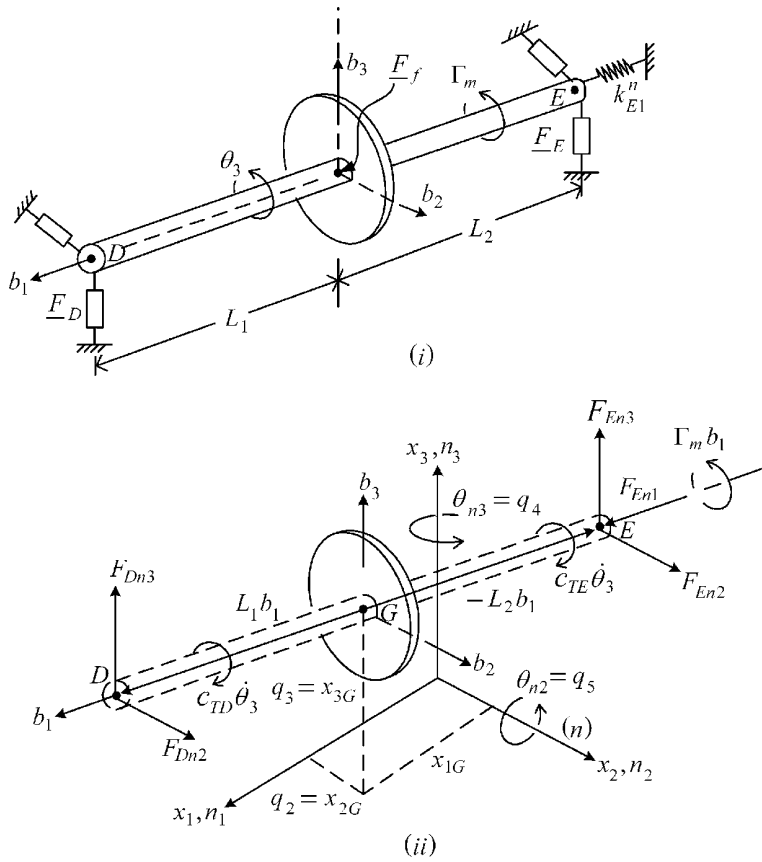


Figure E6.4.1(a) (i) Rotor geometry and (ii) free body diagram of rotor-bearing system

$$\underline{M} = \text{radial vibration mass matrix} = \begin{matrix} & q_2 & q_3 & q_4 & q_5 \\ \begin{matrix} q_2 \\ q_3 \\ q_4 \\ q_5 \end{matrix} & \begin{bmatrix} m & 0 & 0 & 0 \\ 0 & m & 0 & 0 \\ 0 & 0 & I_1 & 0 \\ 0 & 0 & 0 & I_T \end{bmatrix} \end{matrix} \quad (2)$$

$\underline{C}_B =$ bearing damping matrix

$$= \begin{matrix} & q_2 & q_3 & q_4 & q_5 \\ \begin{matrix} q_2 \\ q_3 \\ q_4 \\ q_5 \end{matrix} & \begin{bmatrix} c_{22}^D + c_{22}^E & 0 & L_1 c_{22}^D - L_2 c_{22}^E & 0 \\ 0 & c_{33}^D + c_{33}^E & 0 & -L_1 c_{33}^D + L_2 c_{33}^E \\ L_1 c_{22}^D - L_2 c_{22}^E & 0 & L_1^2 c_{22}^D + L_2^2 c_{22}^E & 0 \\ 0 & -L_1 c_{33}^D + L_2 c_{33}^E & 0 & L_1^2 c_{33}^D + L_2^2 c_{33}^E \end{bmatrix} \end{matrix} \quad (3)$$

$$\underline{G} = \text{gyroscopic matrix} = \begin{matrix} & q_2 & q_3 & q_4 & q_5 \\ \begin{matrix} q_2 \\ q_3 \\ q_4 \\ q_5 \end{matrix} & \begin{bmatrix} 0 & 0 & 0 & 0 \\ 0 & 0 & 0 & 0 \\ 0 & 0 & 0 & -I_p\omega \\ 0 & 0 & I_p\omega & 0 \end{bmatrix} \end{matrix} \quad (4)$$

\underline{K}_B = bearing stiffness matrix

$$= \begin{matrix} & q_2 & q_3 & q_4 & q_5 \\ \begin{matrix} q_2 \\ q_3 \\ q_4 \\ q_5 \end{matrix} & \begin{bmatrix} k_{22}^D + k_{22}^E & 0 & L_1 k_{22}^D - L_2 k_{22}^E & 0 \\ 0 & k_{33}^D + k_{33}^E & 0 & -L_1 k_{33}^D + L_2 k_{33}^E \\ L_1 k_{22}^D - L_2 k_{22}^E & 0 & L_1^2 k_{22}^D + L_2^2 k_{22}^E & 0 \\ 0 & -L_1 k_{33}^D + L_2 k_{33}^E & 0 & L_1^2 k_{33}^D + L_2^2 k_{33}^E \end{bmatrix} \end{matrix} \quad (5)$$

$$\underline{K}_f = \text{circulatory stiffness matrix due to seal leakage flow} = \begin{matrix} & q_2 & q_3 & q_4 & q_5 \\ \begin{matrix} q_2 \\ q_3 \\ q_4 \\ q_5 \end{matrix} & \begin{bmatrix} 0 & k_f & 0 & 0 \\ -k_f & 0 & 0 & 0 \\ 0 & 0 & 0 & 0 \\ 0 & 0 & 0 & 0 \end{bmatrix} \end{matrix} \quad (6)$$

$$\underline{q} = \begin{Bmatrix} q_2 \\ q_3 \\ q_4 \\ q_5 \end{Bmatrix} = \begin{Bmatrix} x_{2G} \\ x_{3G} \\ \theta_{n3} \\ \theta_{n2} \end{Bmatrix} \quad \text{and} \quad \underline{F}_{BL}(t) = \begin{Bmatrix} \bar{m}e\omega^2 \cos t \\ \bar{m}e\omega^2 \sin t \\ 0 \\ 0 \end{Bmatrix} \quad (7)$$

where \bar{m} equals the mass of the blade or portion of the blade which is lost, e is the radius from the shaft center to the blade location, and ω is the constant spin speed of the rotor. The destabilizing effect of the circulatory stiffness matrix was demonstrated in Figure 5.3.4. Gas or liquid leakage through the thin annular passages of a shaft seal is known to cause this type of stiffness. The bearing reaction forces are

$$\begin{aligned} F_{Dn2} &= -k_{22}^D x_2^D - c_{22}^D \dot{x}_2^D, & F_{Dn3} &= -k_{33}^D x_3^D - c_{33}^D \dot{x}_3^D, & F_{En2} &= -k_{22}^E x_2^E - c_{22}^E \dot{x}_2^E \\ F_{En3} &= -k_{33}^E x_3^E - c_{33}^E \dot{x}_3^E, & F_{Dn} &= \sqrt{F_{Dn2}^2 + F_{Dn3}^2}, & F_{En} &= \sqrt{F_{En2}^2 + F_{En3}^2} \end{aligned} \quad (8)$$

where

$$\begin{aligned} x_2^D &= q_2 + L_1 q_4, & \dot{x}_2^D &= \dot{q}_2 + L_1 \dot{q}_4, & x_3^D &= q_3 - L_1 q_5, & \dot{x}_3^D &= \dot{q}_3 - L_1 \dot{q}_5 \\ x_2^E &= q_2 - L_2 q_4, & \dot{x}_2^E &= \dot{q}_2 - L_2 \dot{q}_4, & x_3^E &= q_3 + L_2 q_5, & \dot{x}_3^E &= \dot{q}_3 + L_2 \dot{q}_5 \end{aligned} \quad (9)$$

(b) The numerical values utilized in the model are

$$\begin{aligned} L_1 &= 0.35 \text{ m}, L_2 = 0.65 \text{ m}, e = 0.15 \text{ m}, m = 100 \text{ kg}, \bar{m} = 0.2 \text{ kg}, I_p = 2.2 \text{ kgm}^2, \\ I_T &= 2 \text{ kgm}^2, \omega = 1570 \text{ rad/s (15000 rpm)}, \underline{q}_0 = \underline{\dot{q}}_0 = (0 \ 0 \ 0 \ 0)^T, \\ c_{22}^D &= c_{22}^E = 6000 \text{ Ns/m}, c_{33}^D = c_{33}^E = 10000 \text{ Ns/m}, k_{22}^D = k_{22}^E = 20 \times 10^6 \text{ N/m}, \\ k_{33}^D &= k_{33}^E = 25 \times 10^6 \text{ N/m}, k_f = 1 \times 10^6 \text{ N/m} \end{aligned} \quad (10)$$

(c) Newmark beta solution:

The Newmark beta NI solution for this problem follows the steps shown in Equations (6.4.35)–(6.4.39) and is option 1 in the companion MATLAB code. The integration parameter values are

$$\alpha = \frac{1}{4}, \quad \delta = \frac{1}{2} \quad (11)$$

and the integration time step is $\Delta t = 1 \times 10^{-5}$ seconds. Figure E6.4.1(b) shows the responses for the mass center deflection in the x_2 direction, bearing E deflection in the x_2 direction, and the resultant forces at bearings D and E . The figure shows responses for the (i) full bearing stiffness and (ii) with the bearing stiffness reduced by 50%. The results show a significant reduction in bearing forces with little change in the overall vibration levels. Figure E6.4.1(c) shows the responses at the 50% stiffness level and $\Delta t = 10^{-4}$. Clearly, the time step is too large to yield accurate results.

(d) Runge–Kutta solution:

The coding for the Runge–Kutta solution is shown as option 2 in the companion code. The coding follows Equations (6.4.67)–(6.4.77) with $(i + 1)$ as the “current” time, $(i + 1/2)$ as $\Delta t/2$ earlier, and (i) as Δt earlier. Figure E6.4.1(d) shows the response with the 50% stiffness model. Note that the RK solution shows accurate results at the time step (i) $\Delta t = 10^{-4}$ but not at the larger time step (ii) $\Delta t = 10^{-3}$.

(e) MATLAB ODE45 solution:

The MATLAB ODE45 numerical integration solution for the 50% reduced bearing stiffness case is shown in Figure E6.4.1(e). As expected, MATLAB ODE45 executes considerably faster than the other approaches, being a highly optimized algorithm and code.

Summary: This example illustrated an approach for simulating a blade loss event of a shaft with a rigid rotor model. The results show nearly identical predicted responses using the Newmark beta algorithm Equations (6.4.35)–(6.4.39) or the Runge–Kutta algorithm (6.4.67)–(6.4.77).

Reduction of the nominal bearing stiffnesses by 50% yielded a similar level of reduction in bearing forces. This level is about 19.0% of the rigid bearing force level of approximately $(1/2)\bar{m}e\omega^2 = (37000 \text{ N})$, which results from the force isolation effect of the soft bearing supports. The vibration level (0.3 mm peak at steady state) would be considered excessive in most machinery so additional steps for mitigating the vibrations would be required. The responses of this system could be quite different at other speeds depending on the proximity of the speed with a natural frequency (f_n). Two of the four natural frequencies vary significantly with speed due to the gyroscopic moments as shown in the Campbell diagram in Figure E6.4.1(f), which corresponds to 50% bearing stiffness. Resonance may occur at spin speeds near to the natural frequencies as indicated by triangles.

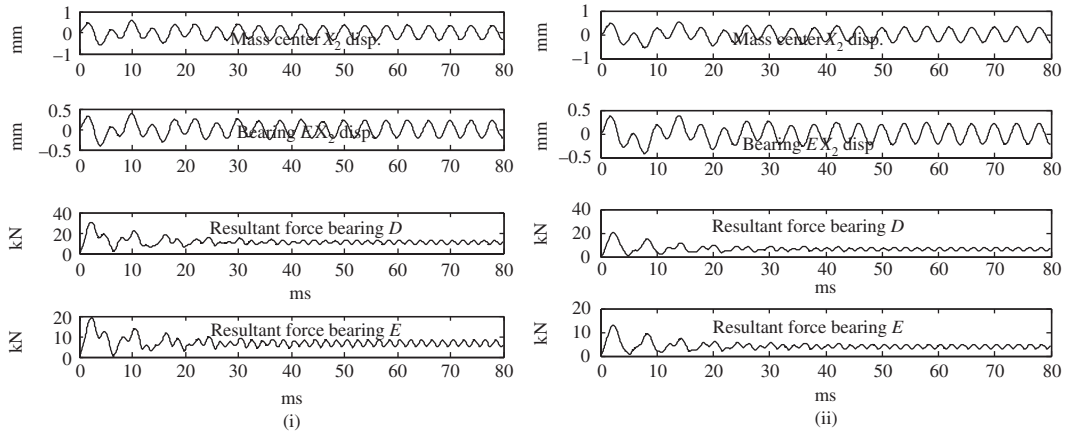


Figure E6.4.1(b) Blade loss in rotating machinery—Newmark beta solution with $\Delta t = 10^{-5}$ second for (i) full and (ii) 50% reduced bearing stiffnesses

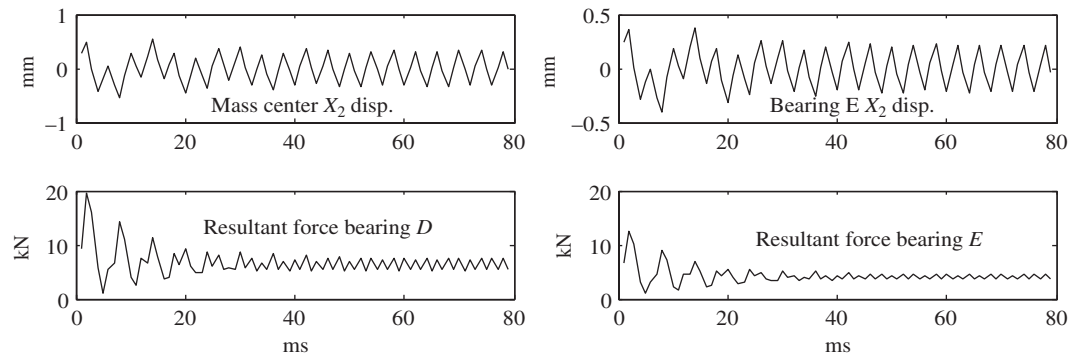


Figure E6.4.1(c) Blade loss in rotating machinery—Newmark beta solution with large Δt (10^{-4} second) value

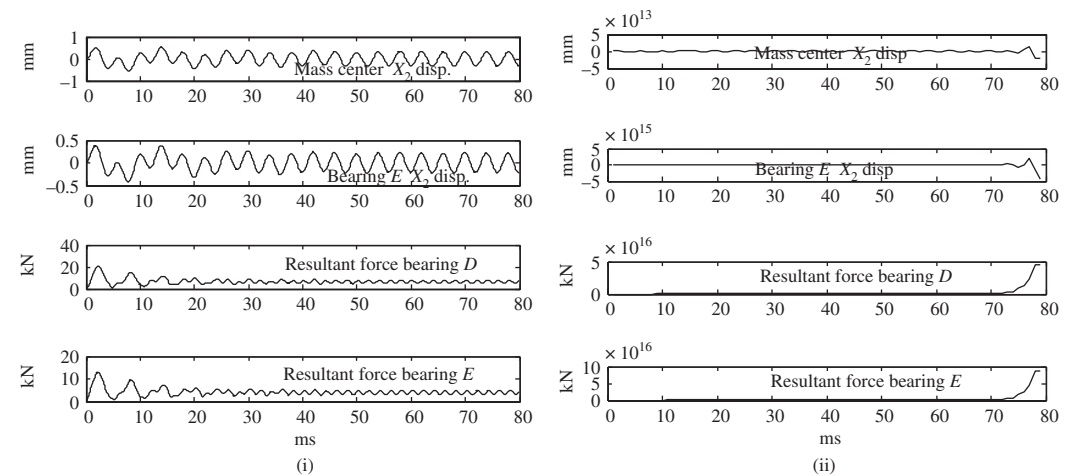


Figure E6.4.1(d) Blade loss in rotating machinery—Runge-Kutta with (i) ($\Delta t = 10^{-4}$ second) and with (ii) ($\Delta t = 10^{-3}$ second)

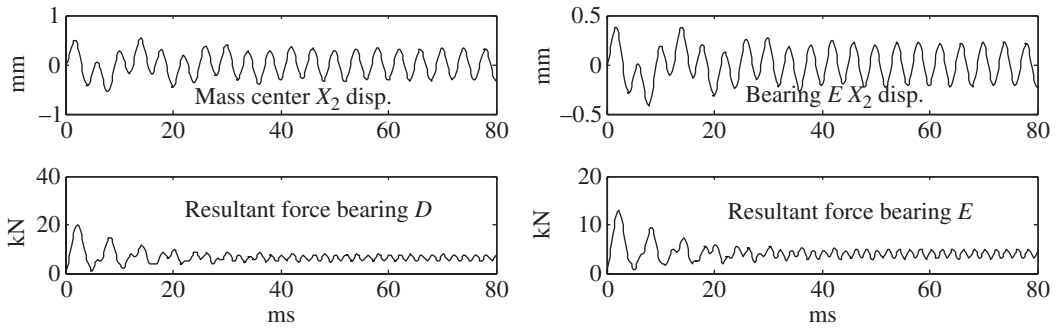


Figure E6.4.1(e) Blade loss in rotating machinery—MATLAB ODE45

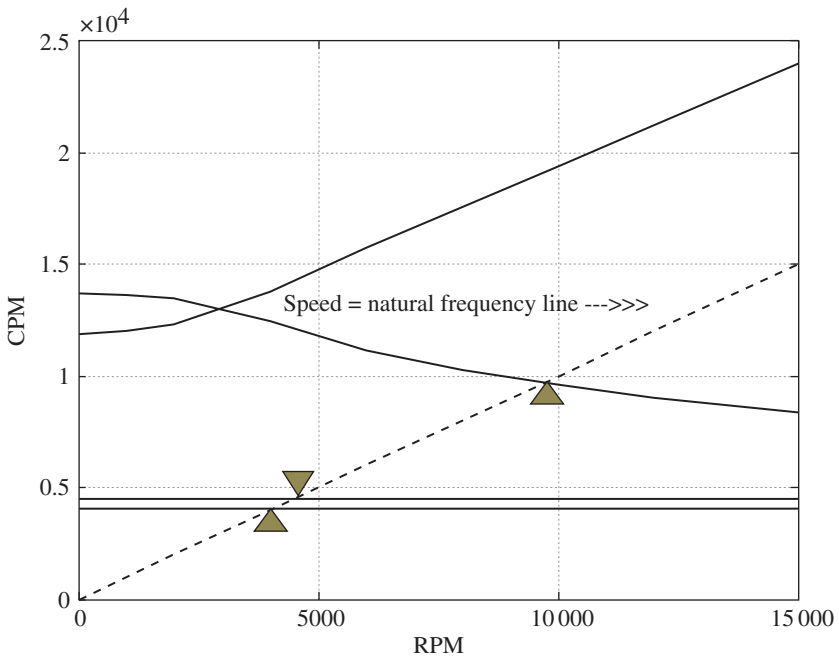


Figure E6.4.1(f) Natural frequencies versus shaft speed for 50% bearing stiffness

The response would also be quite different if the circulatory force term k_p was large, that is, if k_p is increased to 10^7 lb/in. and with 50% bearing stiffness. The system eigenvalues (5.4.220) become

$$(\lambda_1 = -180 + i457, \lambda_2 = +31 + i460, \lambda_3 = -539 + i874, \lambda_4 = -1652 + i2513)$$

The second eigenvalue has a positive real part indicating an unstable system (Section 5.6) so that the resulting response in Figure E6.4.1(g) diverges with increasing time.

510 Vibration Theory and Applications with Finite Elements and Active Vibration Control

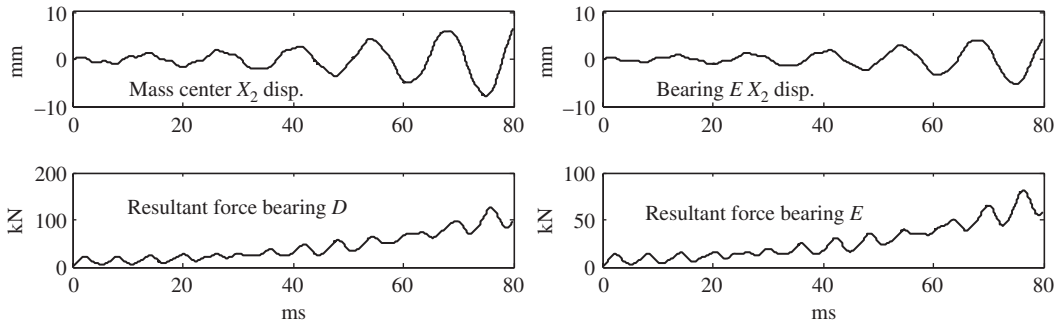


Figure E6.4.1(g) Blade loss in rotating machinery: $k_f = 1.0 \times 10^7$ N/m, Newmark beta, $\Delta t = 1.0 \times 10^{-5}$ second

Example 6.4.1 MATLAB Code

```

Clear
global AMAT mbar e omega M
ioption = 1
% If ioption = 1 (Newmark) , = 2 (Runge Kutta) , = 3 (Matlab ODE45)
L1 = .35; L2 = .65;
m = 100 ; IT = 2.0 ; IP = 2.2 ;
rpm = 15000 ; omega = 2*pi*rpm/60
C2 = 6000.0 ; C3 = 10000. ;
K2 = 20.e+06/2 ; K3 = 25.e+06/2 ; kf = 10000000.0 ;
mbar = 0.20 ; e = 0.15 ;
qzero = zeros(4,1) ; qdotzero = zeros(4,1) ;
delta = .50 ; alpha = .25 ; del = 1.0e-05 ;
M = zeros(4,4) ;
M(1,1) = m ; M(2,2) = m ; M(3,3) = IT ; M(4,4) = IT ;
C = zeros(4,4) ;
C(1,1) = 2*C2 ; C(2,2) = 2*C3 ; C(3,3) = C2*(L1^2+L2^2) ; C(4,4) = C3*
(L1^2+L2^2) ;
C(1,3) = C2*(L1-L2) ; C(3,1) = C2*(L1-L2) ; C(2,4) = C3*(L2-L1) ;
C(4,2) = C2*(L2-L1) ;
K = zeros(4,4) ;
K(1,1) = 2*K2 ; K(2,2) = 2*K3 ; K(3,3) = K2*(L1^2+L2^2) ; K(4,4) = K3*
(L1^2+L2^2) ;
K(1,3) = K2*(L1-L2) ; K(3,1) = K2*(L1-L2) ; K(2,4) = K3*(L2-L1) ; K
(4,2) = K2*(L2-L1) ;
G = zeros(4,4) ;
G(3,4) = -IP*omega ; G(4,3) = IP*omega ;
Kf = zeros(4,4) ;
Kf(1,2) = kf ; Kf(2,1) = -kf ;
KT = K + Kf ;
CT = C + G ;
AMAT(1:4,1:4) = -inv(M)*CT ;
AMAT(1:4,5:8) = -inv(M)*KT ;
AMAT(5:8,1:4) = eye(4,4) ;

```

```

AMAT(5:8,5:8) = zeros(4,4);
%Compute System Eigenvalues
rpm
lamb = eig(AMAT)
natfreqcps = 60*imag(lamb)/2/pi
pause
% Determine the number of iterations
nrev = 20;
freq = omega/2/pi ;
period = 1/freq ;
Integration_time = nrev*period ;
number_iter = fix(Integration_time/del) ;% the fix command
rounds down
icount = 0 ; iplt = 0 ;

if ioption == 1 % Newmark Beta Method
FBL_at_t0 = [mbar*e*omega^2 0 0 0 ]' ;
% Determine the acceleration vector at t = 0 using eq. 6.4.35
qddi = inv(M)*( FBL_at_t0 - CT*qdotzero - KT*qzero )
% Initialize the velocity and displacement vectors
qdi = qdotzero
qi = qzero

% Form Newmark Beta matrices from eq. 6.4.36
A = M/alpha/del^2 + CT*delta/alpha/del + KT ;
B = M/alpha/del^2 + CT*delta/alpha/del ;
D = M/alpha/del + ( delta/alpha - 1 )*CT ;
E = (1/2/alpha -1)*M + (delta*del/2/alpha -del)*CT ;
Ainv = inv(A) ;

%Begin integrating
for i = 1:number_iter
t = i*del ;
fiplus1 = mbar*e*omega^2*[cos(omega*t) sin(omega*t) 0 0 ]' ;
%Update Displacements (eq. 6.4.37)
qiplus1 = Ainv*( fiplus1 + B*qi + D*qdi + E*qddi) ;
%Update Accelerations (eq.6.4.38)
qddiplus1=(qiplus1-qi)/alpha/del^2-qdi/alpha/del+(1-1/2/
alpha)*qddi ;
%Update Velocities (eq.6.4.39)
qdiplus1 = qdi + ((1-delta)*qddi + delta*qddiplus1)*del ;
qi = qiplus1; qdi = qdiplus1; qddi = qddiplus1 ;
icount = icount + 1 ;
if icount == 10
icount = 0 ;
t
x2D = qi(1,1)+L1*qi(3,1) ; x2Ddot = qdi(1,1)+L1*qdi(3,1) ;
x3D = qi(2,1)-L1*qi(4,1) ; x3Ddot = qdi(2,1)-L1*qdi(4,1) ;
x2E = qi(1,1)-L2*qi(3,1) ; x2Edot = qdi(1,1)-L2*qdi(3,1) ;

```



```

    x3E = qi(2,1)+L2*qi(4,1) ; x3Edot = qdi(2,1)+L2*qdi(4,1) ;

    F2D=-K2*x2D-C2*x2Ddot ; F3D=-K3*x3D-C3*x3Ddot ; FD=sqrt
(F2D^2+F3D^2) ;
    F2E=-K2*x2E-C2*x2Edot ; F3E=-K3*x3E-C3*x3Edot ; FE=sqrt
(F2E^2+F3E^2) ;
    iplt = iplt + 1 ;
    tplot(1,iplt) = t ;
    plotq2(1,iplt) = qi(1,1) ; plotx2E(1,iplt) = x2E ;
    plotFD(1,iplt) = FD ;    plotFE(1,iplt) = FE ;
end
end
end % End Newmark Option

if ioption==2 % Runge Kutta Option
    AMATpr = zeros(9,9) ;
    AMATpr(1:8,1:8) = AMAT ;
    Xpri = zeros(9,1) ; % Initial Conditions on positions and
velocities
    Xpri(9,1) = 1 ;
%Begin integrating
for i = 1:1:number_iter
    til = i*del ; tionehalf = i*del-del/2 ; ti=i*del-del ;
    fil=mbar*e*omega^2*[cos(omega*til) sin(omega*til) 0 0]';
    fionehalf=mbar*e*omega^2*[cos(omega*tionehalf)
sin(omega*tionehalf) 0 0]';
    fi=mbar*e*omega^2*[cos(omega*ti) sin(omega*ti) 0 0]';
    AMATpr(1:4,9) = inv(M)*fil ;
    AMATpril = AMATpr ;
    AMATpr(1:4,9) = inv(M)*fionehalf ;
    AMATprionehalf = AMATpr ;
    AMATpr(1:4,9) = inv(M)*fi ;
    AMATpri = AMATpr ;
    alphapr = del*AMATpri ;
    betapr = del*AMATprionehalf + .5*del*AMATprionehalf*alphapr ;
    gammapr = del*AMATprionehalf + .5*del*AMATprionehalf*betapr ;
    deltapr = del*AMATpril + del*AMATpril*gammapr ;
    bi = eye(9,9) + (alphapr + 2*betapr + 2*gammapr + deltapr)/6 ;
    Xpri = bi*Xpri ;
    qi = Xpri(5:8,1) ; qdi = Xpri(1:4,1) ;
    icount = icount + 1 ;
    if icount == 1
        icount = 0 ;
        til
        x2D = qi(1,1)+L1*qi(3,1) ; x2Ddot = qdi(1,1)+L1*qdi(3,1) ;
        x3D = qi(2,1)-L1*qi(4,1) ; x3Ddot = qdi(2,1)-L1*qdi(4,1) ;
        x2E = qi(1,1)-L2*qi(3,1) ; x2Edot = qdi(1,1)-L2*qdi(3,1) ;
        x3E = qi(2,1)+L2*qi(4,1) ; x3Edot = qdi(2,1)+L2*qdi(4,1) ;

```

```

    F2D=-K2*x2D-C2*x2Ddot ; F3D=-K3*x3D-C3*x3Ddot ; FD=sqrt
(F2D^2+F3D^2) ;
    F2E=-K2*x2E-C2*x2Edot ; F3E=-K3*x3E-C3*x3Edot ; FE=sqrt
(F2E^2+F3E^2) ;
    iplt = iplt + 1 ;
    tplot(1,iplt) = t11 ;
    plotq2(1,iplt) = qi(1,1) ; plotx2E(1,iplt) = x2E ;
    plotFD(1,iplt) = FD ;    plotFE(1,iplt) = FE ;
end
end
end % End Runge

if ioption == 3 %(Matlab ODE 45 )
tfin = Integration_time;
tspan=linspace(0,tfin,400);
Qinitial = zeros(8,1);
%Use ODE45 (Runge Kutta) to numerically integrate the first
Order EOM's
[t,Q] = ode45('CodeE6_4_1_a_sub',tspan,Qinitial);

    x2D = Q(1:400,5)'+L1*Q(1:400,7)'; x2Ddot = Q(1:400,1)'+L1*Q
(1:400,3)';
    x3D = Q(1:400,6)'+L1*Q(1:400,8)'; x3Ddot = Q(1:400,2)'+
L1*Q(1:400,4)';
    x2E = Q(1:400,5)'+L2*Q(1:400,7)'; x2Edot = Q(1:400,1)'+L2*Q
(1:400,3)';
    x3E = Q(1:400,6)'+L2*Q(1:400,8)'; x3Edot = Q(1:400,2)'+L2*Q
(1:400,4)';
    F2D=-K2*x2D-C2*x2Ddot;F3D=-K3*x3D-C3*x3Ddot;FD=sqrt(F2D.
*F2D+F3D.*F3D) ;
    F2E=-K2*x2E-C2*x2Edot;F3E=-K3*x3E-C3*x3Edot;FE=sqrt(F2E.
*F2E+F3E.*F3E) ;
    tplot = t';
    plotq2 = Q(1:400,5)'; plotx2E = x2E ;
    plotFD = FD ;    plotFE = FE ;
    whos
    pause
end

subplot(4,1,1);
plot(tplot*1000,plotq2*1000);
ylabel('Disp mm');
msg=sprintf('Mass Center X2 Direction');
gtext(msg);
pause
subplot(4,1,2);
plot(tplot*1000,plotx2E*1000);
ylabel('Disp mm');
msg=sprintf('Bearing E X2 Direction');

```

```

gtext(msg);
pause
subplot(4,1,3);
plot(tplot*1000,plotFD/1000);
ylabel('Force kN');
msg=sprintf('Resultant Force Bearing D');
gtext(msg);
pause
subplot(4,1,4)
plot(tplot*1000,plotFE/1000);
ylabel('Force kN');
msg=sprintf('Resultant Force Bearing E');
gtext(msg);
xlabel('time msec');
pause
close
%Plot Natural Frequencies vs. Speed at 50% Bearing
Stiffness Level
SPD = [0 1000 2000 4000 6000 8000 10000 12000 15000];
N1 = [4044 4044 4044 4044 4044 4044 4044 4044 4044];
N2 = [4513 4513 4513 4513 4513 4513 4513 4513 4513];
N3 = [11900 12000 12318 13812 15786 17615 19415 21230 24000];
N4 = [13725 13664 13464 12427 11173 10284 9598 9035 8340];
plot(SPD,N1,'k',SPD,N2,'k',SPD,N3,'k',SPD,N4,'k',SPD,
SPD,'k--');
axis([0 15000 0 25000]);
xlabel('Shaft Speed in RPM');
ylabel('Frequency in CPM');
msg=sprintf('Speed = Natural Frequency Line --->>>');
gtext(msg);
grid on

subfunction file for Ex. 6.4.1
function Qdot = CodeE6_4_1_a_sub(t,Q)
global AMAT mbar e omega M
tee=t
Qdot =zeros(8,1);
F = zeros(8,1);
f = mbar*e*omega^2*[cos(omega*t) sin(omega*t) 0 0]';
F(1:4,1) = inv(M)*f;
Qdot = AMAT*Q + F;

```

EXAMPLE 6.4.2 *Instrumentation Tower Impact Investigation via the Runge–Kutta and Newmark Beta Numerical Integration (Examples 5.4.4 and 6.3.1 Continued)*

Statement: The description of the physical problem and the related parameter values are identical to those given in Examples 5.4.4 and 6.3.1.

Objective: The objective of this example is to illustrate the use of the Newmark beta (NB) (6.4.35)–(6.4.39) and Runge–Kutta (RK) (6.4.67)–(6.4.77) numerical integration algorithms as applied to the physical coordinate EOMs of Example 6.3.1. The simulation is for a duration τ of impact equal to 1.0 seconds. The effects of varying time step size are also investigated.

Results: Figure E6.4.2(a) shows the results for numerically integrating the physical coordinate EOMs using the NB method with time steps ($\Delta t = \text{del}$) of 10^{-1} , 10^{-2} , and 10^{-3} second. The NB response results for $\Delta t = 10^{-2}$ and 10^{-3} are very similar to those obtained with MATLAB ODE45 from comparison with Figure E6.3.1(c).

Figure E6.4.2(b) shows the responses from the RK approach at the same locations. This again illustrates the effect of setting Δt too small, which results in a numerical integration

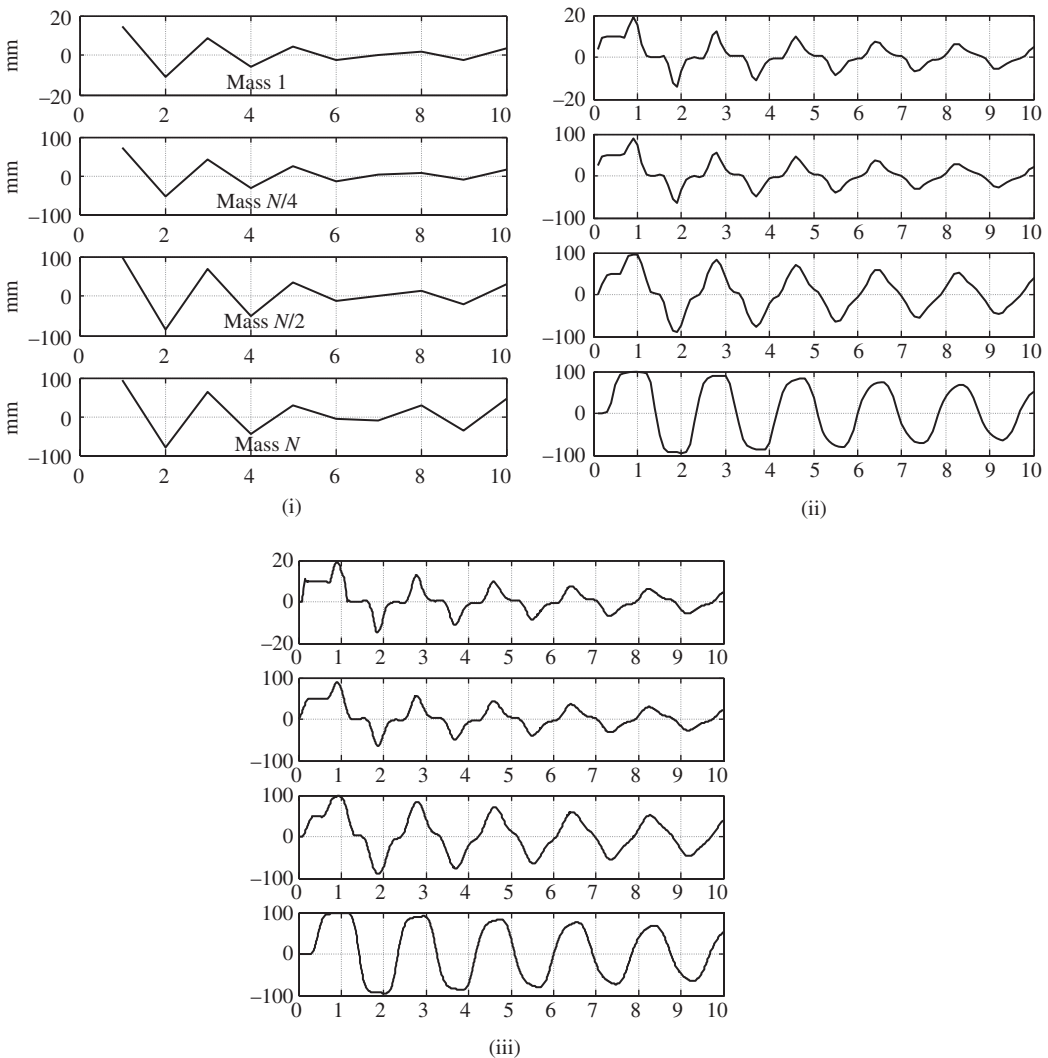


Figure E6.4.2(a) Tower deflections versus time (seconds) by NB integration with (i) $\Delta t = 10^{-1}$, (ii) $\Delta t = 10^{-2}$, and (iii) $\Delta t = 10^{-3}$ second

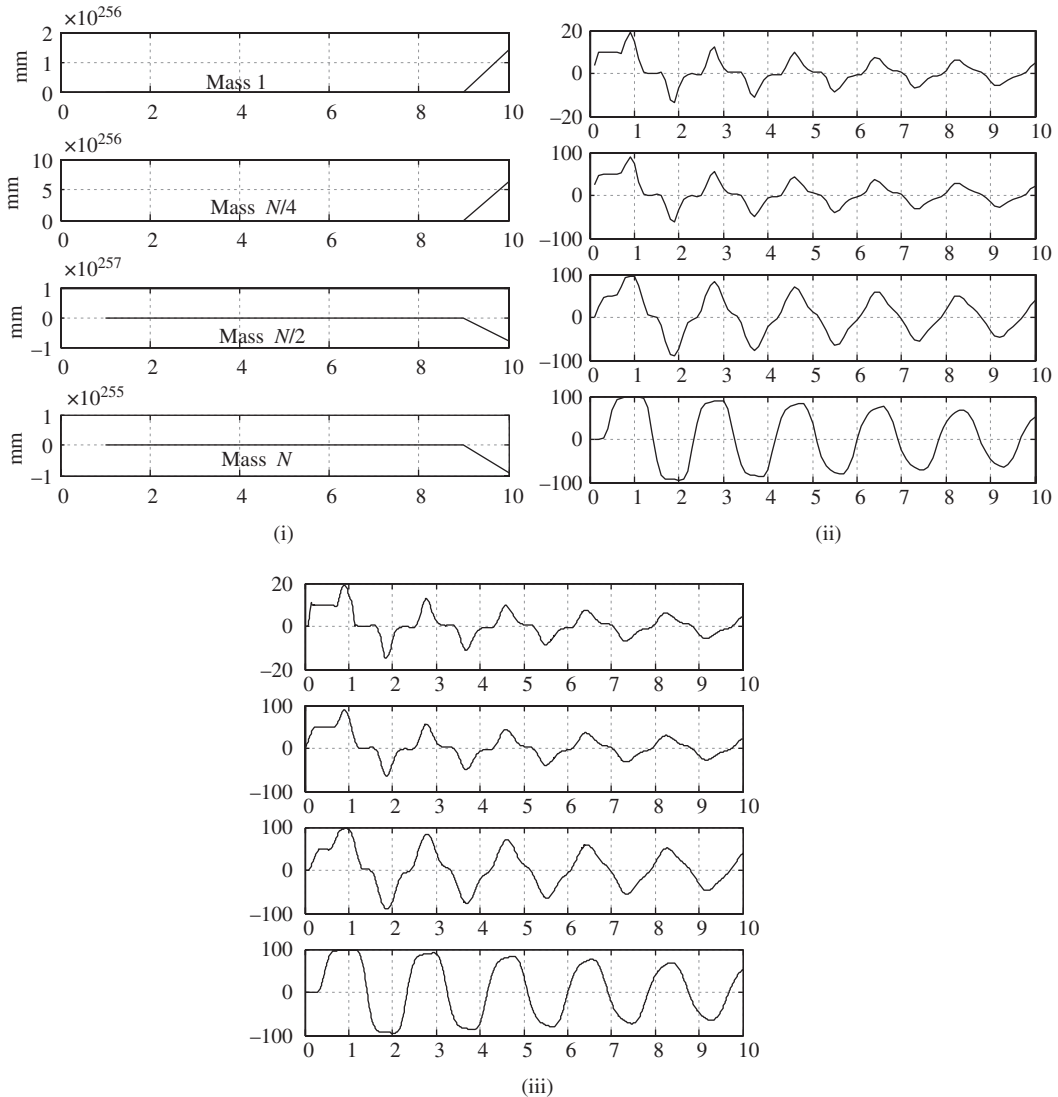


Figure E6.4.2(b) Tower deflections versus time (seconds) by RK integration with (i) $\Delta t = 10^{-1}$, (ii) $\Delta t = 10^{-2}$, and (iii) $\Delta t = 10^{-3}$ second

instability (Bathe, 1982). From Figure E6.3.1(c), the responses for $\Delta t = 10^{-2}$ or 10^{-3} are very similar with those obtained by using MATLAB's built-in RK integrator ODE45.

Table E6.4.2 shows a comparison of predicted peak response and wall clock computation times for the RK and NB methods. For this example, the adaptive time step approach utilized in the MATLAB ODE45 RK solver is much faster than the fixed time step RK approach presented and is moderately more efficient compared to the NB method. The MATLAB's ODE45 RK integrator is exceptionally fast as is to be expected considering its highly mature and optimized coding and algorithms.

Table E6.4.2 Peak responses and wall clock elapsed times for the RK and NB approaches

Δt (second)	Runge-Kutta (RK)		Newmark beta (NB)	
	Peak response (mm)	Computation time (seconds)	Peak response (mm)	Computation time (seconds)
ODE45 ^a	98.56	4.56	—	—
0.1	10 ²⁵⁷	1.15	94.60	0.05
0.01	98.30	10.65	98.24	0.61
0.001	98.56	110.7	98.56	6.55

^a Δt is variable (adaptive) in ODE45.

```

clear
% Parameter Values
% NOTE THAT N MUST BE A MULTIPLE OF 4 FOR PLOTTING PURPOSES AND
% IORDER MUST BE CHANGED IF N IS CHANGED
N=20 ; H = 20 ; k=50000 ; m=20 ; h = H/N ; ms = 50. ;
zetadesired = [.02 .02 .025 .025 .03 ] ; %desired damping ratios
for modes 1-5
height = h*linspace(1,N,N)
ioption = 2
% If ioption = 1 (Newmark) , = 2 (Runge Kutta)
tau = 1.0 % impact duration
tfin = 10 ; % final time for simulation
qzero = zeros (N,1) ; qdotzero = zeros (N,1) ; % Initial positions
and velocities
delta = .50 ; alpha = .25 ; % Newmark Beta parameters
del = 1.0e-03 ; % Time step in seconds
number_iter =tfin/del ;
icount = 0 ; iplt = 0 ;

% Form mass matrix and its inverse
M= m*eye (N) ; M (N,N) = M (N,N) + ms ; MINV = inv (M) ;
% Form Stiffness Matrix
K= zeros (N,N) ;
kel = k*[1 -1 ; -1 1] ;
for i=1:1:N-1
    K(i:i+1,i:i+1) = K(i:i+1,i:i+1) + kel ;
end
K(1,1) = K(1,1) + k ; KT = K ;
% Determine the undamped system's natural frequencies and mode
shapes
[modalmatrix, otemp] = eig (K,M) ;
omegasquared = diag (otemp) ;
omega =sqrt (omegasquared) ;
natfreq = omega/2/pi ;
% Note that the natural frequencies are generally not arranged
% in ascending order in omegasquared , omega and natfreq . For
N=20 the mode

```

```

% ordering is
iorder= [1 2 3 4 5 6 7 8 9 10 11 12 13 14 15 16 17 18 19 20 ];
% Reorder mode shapes and natural frequencies in ascending order
as follows
for i=1:1:N
    orderomega(iorder(i)) = omega(i) ;
    ordernatfreq(iorder(i)) = natfreq(i) ;
    ordermodmat(1:N,iorder(i)) = modalmatrix(1:N,i) ;
end
orderomega
ordernatfreq
% Determine the Modal Masses of the original modes (Use of diag
here insures % that no off diagonal terms in modalmassmatrix are
negative which will cause % there sqrt to be complex below)
modalmass = diag(ordermodmat'*M*ordermodmat);
modalmassmatrix=diag(modalmass);
% Rescale the modeshapes so that all the modal masses equal one.
ordermodmat=ordermodmat*inv(sqrt(modalmassmatrix));
% Form the orthogonal damping matrix in eqs.10 and 11 of Ex. 6.3.1
mul = 2*zetadesired(5)/orderomega(5) ;
dum=zeros(N,N);
for i=1:1:4
    zeta = zetadesired(i) - zetadesired(5)*orderomega(i) /
orderomega(5);
    dum = dum+2*zeta*orderomega(i)*ordermodmat(1:N,i)
*ordermodmat(1:N,i)';
end
Co = mul*K + M*dum*M ; CT = Co ;

AMAT(1:N,1:N)=-inv(M)*CT ;
AMAT(1:N,N+1:2*N)=-inv(M)*KT ;
AMAT(N+1:2*N,1:N)=eye(N,N) ;
AMAT(N+1:2*N,N+1:2*N) = zeros(N,N) ;

% *****
if ioption == 1 % Newmark Beta Method
    % *****
F_at_t0 = zeros(N,1); % Initial Force Vector
F_at_t0(N/4,1) = 500. ;
% Determine the acceleration vector at t = 0 using eq. 6.4.35
qddi = inv(M)*( F_at_t0 - CT*qdotzero - KT*qzero );
% Initialize the velocity and displacement vectors
qdi = qdotzero;
qi = qzero;

% Form Newmark Beta matrices from eq. 6.4.36
A = M/alpha/del^2 + CT*delta/alpha/del + KT ;
B = M/alpha/del^2 + CT*delta/alpha/del ;
D = M/alpha/del + ( delta/alpha - 1)*CT ;

```

```

E = (1/2/alpha -1)*M + (delta*del/2/alpha -del)*CT ;
Ainv = inv(A) ;

%Begin integrating
for i = 1:1:number_iter
    t = i*del ;
    fiplus1 = zeros(N,1) ;
    if t<tau
        fiplus1(N/4,1) = 500 ;
    end
    %Update Displacements (eq. 6.4.37)
    qiplus1 = Ainv*( fiplus1 + B*qi + D*qdi + E*qddi) ;
    %Update Accelerations (eq. 6.4.38)
    qddiplus1=(qiplus1-qi)/alpha/del^2-qdi/alpha/del+(1-1/2/
alpha)*qddi ;
    %Update Velocities (eq. 6.4.39)
    qdiplus1 = qdi + ((1-delta)*qddi + delta*qddiplus1)*del ;
    qi = qiplus1;    qdi = qdiplus1;    qddi = qddiplus1 ;
    icount = icount + 1 ;    % Plot every 10th point in time
    if icount == 10
        icount = 0 ;
        t;
        iplt = iplt + 1 ;
        x1(iplt,1) = qi(1,1) ;
        xN4(iplt,1) = qi(N/4,1) ;
        xN2(iplt,1) = qi(N/2,1) ;
        xN(iplt,1) = qi(N,1) ;
        tplot(iplt,1) = t ;
    end
end
maxresp = max(abs(xN)) *1000
end % End Newmark Option

% *****
if ioption==2 % Runge Kutta Option
% *****
% Form the A prime and initial X prime terms in (6.4.50)
AMATpr = zeros(2*N+1,2*N+1) ;
AMATpr(1:2*N,1:2*N) = AMAT ;
Xpri = zeros(2*N+1,1) ; % Initial Conditions on positions and
velocities
Xpri(2*N+1,1) = 1 ;

%Begin integrating
for i = 1:1:number_iter
    til = i*del ; tionehalf = i*del-del/2; ti=i*del-del;
    fil = zeros(N,1) ; fiandonehalf = zeros(N,1) ; fi = zeros(N,1) ;
    if til<tau %
        fil(N/4,1) = 500; % evaluate force at time ti + deltat

```



```

end
  if tionehalf<tau %
    fionehalf(N/4,1) = 500; % evaluate force at time ti + deltat/2
  end
  if ti<tau %
    fi(N/4,1) = 500;% evaluate force at time ti
  end

% Form A_prime in 6.4.50 at ti , ti+deltat/2 and ti+deltat
AMATpr(1:N,2*N+1) = inv(M)*fil ;
AMATpril = AMATpr;
AMATpr(1:N,2*N+1) = inv(M)*fionehalf ;
AMATprionehalf = AMATpr;
AMATpr(1:N,2*N+1) = inv(M)*fi ;
AMATpri = AMATpr;

alphapr = del*AMATpri; % alpha_i_prime 6.4.68
betapr = del*AMATprionehalf + .5*del*AMATprionehalf*alphapr ;
% beta_i_prime in 6.4.69
gammapr = del*AMATprionehalf + .5*del*AMATprionehalf*betapr ;
% gamma_i_prime in 6.4.70
deltapr = del*AMATpri1 + del*AMATpril*gammapr ; % delta_i_prime
in 6.4.71
bi = eye(2*N+1,2*N+1) + (alphapr + 2*betapr + 2*gammapr +
deltapr)/6 ; % ref. eq . 6.4.74
Xpri = bi*Xpri ; % eq. 6.4.73
qi = Xpri(N+1:2*N,1) ; qdi = Xpri(1:N,1) ; % ref. 6.4.65
  icount = icount + 1 ; % Plot every 10th point in time
  if icount == 10
    icount = 0 ;
    til
    iplt = iplt + 1 ;
    x1(iplt,1) = qi(1,1) ;
    xN4(iplt,1) = qi(N/4,1) ;
    xN2(iplt,1) = qi(N/2,1) ;
    xN(iplt,1) = qi(N,1) ;
    tplot(iplt,1) = til ;
  end
end
maxresp = max(abs(xN)) *1000
end % End Runge

subplot(4,1,1);
plot(tplot,1000*x1);
grid on
ylabel('q mm')
msg = sprintf('Mass 1 ');

```

```

gtext(msg);
msg=sprintf('Maximum response=%2.f in mm',maxresp);
gtext(msg);
pause
subplot(4,1,2);
plot(tplot,1000*xN4);
grid on
ylabel('q mm')
msg = sprintf('Mass N/4');
gtext(msg);
pause
subplot(4,1,3);
plot(tplot,1000*xN2);
grid on
ylabel('q mm')
msg = sprintf('Mass N/2');
gtext(msg);
pause
subplot(4,1,4);
plot(tplot,1000*xN);
grid on
ylabel('q mm')
msg = sprintf('Mass N ');
gtext(msg);xlabel('time in sec');
pause
close
whos

```

6.5 SUMMARY

The topics in Chapter 6 should provide the reader with an understanding and working knowledge of:

- (a) Transient response of 1 dof and N dof linear systems to step, ramp, sinusoidal, exponential, and other types of disturbances
- (b) Direct analytical, LT, convolution integral, and NI approaches for obtaining the transient response given ICs and force time histories
- (c) Modal-based subspace condensation approaches for reducing problem size prior to transient response solution of undamped, orthogonally damped, and general systems
- (d) Selecting of modes to employ in a modal condensation-based NI solution using modal effective masses
- (e) First derivative (state) and second derivative system NI techniques

6.6 CHAPTER 6 EXERCISES

6.6.1 Exercise Location

All exercises may be conveniently viewed and downloaded at the following website: www.wiley.com/go/palazzolo. This new feature greatly reduces the length of the printed book, yielding a significant cost savings for the college student, and is updated.

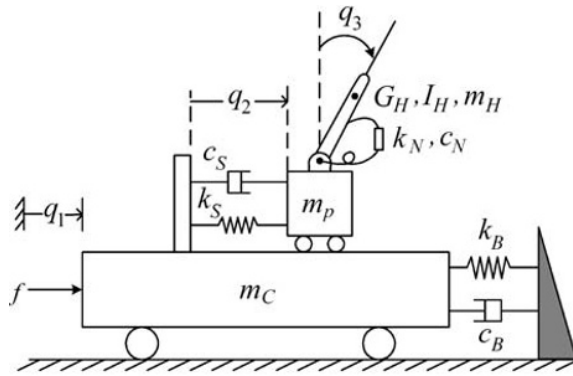
6.6.2 Exercise Goals

The goal of the Exercises in Chapter 6 is to strengthen the student's understanding and related engineering problem solving skills in the following areas:

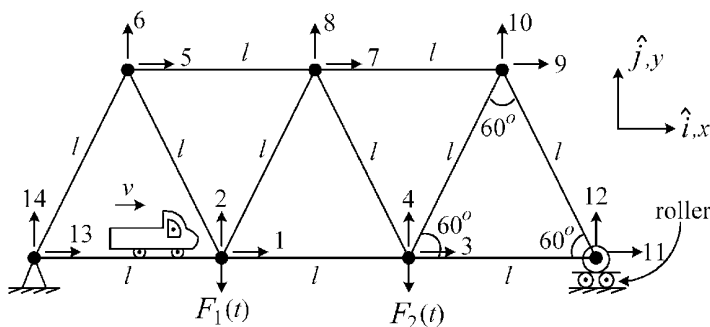
- (a) Obtaining closed-form solutions for time transient vibration responses when they exist
- (b) Treatment of vibrating systems subjected to successive disturbances
- (c) Usage of modal coordinates to accelerate the simulation time for transient vibration response of large-order systems
- (d) Methodology and implementation of numerical integration for obtaining transient vibration response predictions

6.6.3 Sample Exercises: 6.18 and 6.21

Exercise 6.18 represents a simplified model of a moving vehicle with passenger, as subjected to either a quick acceleration of the vehicle or the vehicle crashing into a fixed barrier. The objective of the study is to determine the moment that is exerted on the passenger's head with the two loading scenarios. Exercise 6.21 represents a model of a bridge subjected to the transient loading of a passing truck. The bridge is represented by 2D finite element truss members, and the predicted responses must be determined by numerical integration of physical coordinates and also of modal coordinates.



(6.18)



(6.21)

REFERENCES

- BATHE, K., *Finite Element Procedures in Engineering Analysis*, 1st ed. Prentice Hall, Englewood Cliffs, NJ, 1982.
- DAVIS, P. and RABINOWITZ, P., *Methods of Numerical Integration*, Academic Press, New York, 1984.
- ISAACSON, E. and KELLER, H., *Analysis of Numerical Methods*, John Wiley & Sons, Inc., New York, 1966.
- SPIEGEL, M., *Schaum's Mathematical Handbook of Formulas and Tables*, McGraw-Hill, New York, 1998.
- TEDESCO, J. W., MCDUGAL, W. G. and ROSS, C. A., *Structural Dynamics: Theory and Applications*, Addison-Wesley, Reading, 1999.
- VILLAVERDE, R., *Fundamental Concepts of Earthquake Engineering*, CRC Press, New York, 2009.

Chapter 7

Steady-State Vibration Response to Periodic Loading

7.1 INTRODUCTION

Many vibrating systems are subjected to periodic forces and consequently exhibit periodic responses. Some examples include gas forces in piston/cylinder applications, waves, internal vortex shedding in gas piping systems or external shedding on structures, imbalanced spinning shafts, jack hammers, pile drivers, and so on. Although most of these forces are not sinusoidal, they may be expressed in terms of sinusoids via their Fourier series (Section 2.9) representation. Consequently, the majority of the chapter treats responses due to sinusoidal input. Some common topics related to steady-state harmonic response (SSHR) include resonance, damping, Q (amplification) factor, impedances, receptances, and modal-based identification. The order of the chapter is as follows:

- Background
- Single dof systems
- 2 dof systems
- N dof systems
- Continuous systems

In mathematical terms, steady-state harmonic vibration represents the “particular part” (Section 6.2) of the solution to the governing equations of motion (EOMs) with only sinusoidal forces. The homogeneous part is assumed to be damped out so the transient response has diminished to zero. It is important to note that an unstable system (Section 5.6) does not possess an SSHR so the homogeneous part of the solution must always be considered first. For example, see Figure E6.4.1(g) for which the rotor system is harmonically forced with an imbalance force but is also unstable, and consequently the homogeneous part of the response diverges to infinity.

7.2 COMPLEX PHASOR APPROACH

Figure 1.2.1 illustrates the sinusoidal response of a structure or component. The peak positive or negative amplitudes or zero crossings for the different responses occur at different times; hence, it is said that they differ in phase angle. The description of a time delay (lag) or lead in terms of phase angle requires a forcing period T where $T = 2\pi/\omega$. Then phase lead or lag represents time lead or lag since 360° of angle change

$$0 \leq \omega t \leq (360^\circ = \omega T) \quad (7.2.1)$$

represents one forcing period T . The phase angle of any response may be measured with respect to a once per forcing cycle event marker that establishes $\omega t = 0, 2\pi, 4\pi$, and so on. This is indicated in Figure 1.2.1 as arrowheads and the accompanying discussion. Physical events that correspond to this marker include a once per revolution mark on a shaft or the “top dead center” position of a piston within a cylinder. Phase may also be expressed as the relative phase angle between two responses, which is the difference in time between their positive peak events multiplied by ω . Measurement of phase leads or lags is very useful in identifying mode shapes or damping, for balancing shafts, and for diagnosing vibration problems. The sinusoidal forces in a structural simulation model may be written in a general vector form as

$$\underline{\underline{f}}_{N \times 1}(t) = \begin{Bmatrix} A_{f1} \cos(\omega t + \phi_{f1}) \\ A_{f2} \cos(\omega t + \phi_{f2}) \\ \vdots \\ A_{fN} \cos(\omega t + \phi_{fN}) \end{Bmatrix} \quad (7.2.2)$$

Euler’s identity (Example 2.4.3)

$$e^{i(\omega t + \phi)} = \cos(\omega t + \phi) + i \sin(\omega t + \phi) \quad (7.2.3)$$

is utilized to express $\underline{\underline{f}}$ in complex variable form as

$$\underline{\underline{f}}(t) = \text{Real}(\underline{\underline{\tilde{F}}} e^{i\omega t}) \quad N \times 1 \quad (7.2.4)$$

where

$$\underline{\underline{\tilde{F}}} = \begin{Bmatrix} A_{f1} e^{i\phi_{f1}} \\ A_{f2} e^{i\phi_{f2}} \\ \vdots \\ A_{fN} e^{i\phi_{fN}} \end{Bmatrix} = \begin{Bmatrix} \tilde{F}_1 \\ \tilde{F}_2 \\ \vdots \\ \tilde{F}_N \end{Bmatrix} \quad (7.2.5)$$

where \tilde{F}_j is the j th force phasor representation (ref. Eq. (2.5.2)). This suggests replacing the real form of the governing EOMs with a complex form since it is much easier to differentiate an exponential than a cosine or sine. Consider the real equation of motion

$$\underline{\underline{M}}\underline{\underline{\ddot{q}}} + \underline{\underline{C}}_T\underline{\underline{\dot{q}}} + \underline{\underline{K}}_T\underline{\underline{q}} = \underline{\underline{f}}(t) \quad (7.2.6)$$

and its complex variable counterpart

$$\underline{\underline{M}}\underline{\underline{\ddot{Q}}} + \underline{\underline{C}}_T\underline{\underline{\dot{Q}}} + \underline{\underline{K}}_T\underline{\underline{Q}} = \underline{\underline{\tilde{F}}} e^{i\omega t} \quad (7.2.7)$$

where $\underline{\underline{Q}}$ and $\underline{\underline{F}}$ are, in general, complex vectors. Therefore,

$$\underline{\underline{M}}(\underline{\underline{\ddot{Q}}}_R + i\underline{\underline{\ddot{Q}}}_I) + \underline{\underline{C}}_T(\underline{\underline{\dot{Q}}}_R + i\underline{\underline{\dot{Q}}}_I) + \underline{\underline{K}}_T(\underline{\underline{Q}}_R + i\underline{\underline{Q}}_I) = \text{Re}(\underline{\underline{\tilde{F}}} e^{i\omega t}) + i\text{Im}(\underline{\underline{\tilde{F}}} e^{i\omega t}) \quad (7.2.8)$$

Consider the real part of this equation

$$\underline{\underline{M}}\underline{\underline{\ddot{Q}}}_R + \underline{\underline{C}}_T\underline{\underline{\dot{Q}}}_R + \underline{\underline{K}}_T\underline{\underline{Q}}_R = \text{Re}(\underline{\underline{\tilde{F}}} e^{i\omega t}) \quad (7.2.9)$$

By comparing (7.2.6) and (7.2.9) and using (7.2.4), it is seen that the desired real response $\underline{q}(t)$ has the same differential equation as \underline{Q}_R ; thus,

$$\underline{q}(t) = \underline{Q}_R = \text{Real}(\underline{Q}) \quad (7.2.10)$$

This suggests using the following complex variable-based solution procedure:

- (a) For any given sinusoidally forced structure, form the $\underline{\tilde{F}}$ vector in (7.2.5). Note that

$$\sin(\omega t + \alpha) = \cos(\omega t + \alpha - 90^\circ) \quad (7.2.11)$$

Therefore, if a force has a $\sin(\omega t + \alpha)$ factor, the phase angle to use in (7.2.5) is

$$\phi = \alpha - 90^\circ \quad (7.2.12)$$

It may also be more convenient to work with (7.2.5) in rectangular form as provided by Euler's identity, that is,

$$\underline{\tilde{F}} = \begin{Bmatrix} A_{f1} \cos \phi_{f1} + iA_{f1} \sin \phi_{f1} \\ A_{f2} \cos \phi_{f2} + iA_{f2} \sin \phi_{f2} \\ \vdots \\ A_{fN} \cos \phi_{fN} + iA_{fN} \sin \phi_{fN} \end{Bmatrix} \quad (7.2.13)$$

- (b) Obtain the steady-state (particular) solution of the complex EOMs (7.2.7) for $\underline{Q}(t)$ with the $e^{i\omega t}$ -type force term.
(c) Obtain the actual physical response vector from

$$\underline{q}(t) = \underline{Q}_R(t) = \text{Real}(\underline{Q}(t)) \quad (7.2.14)$$

This approach will be employed in the following sections.

7.3 SINGLE DEGREE OF FREEDOM MODELS

The single degree of freedom (SDOF) model provides a simple means to illustrate damping, resonance, isolation, and force transmissibility and has many practical applications. A resonance that most have enjoyed is the simple swing set as shown in Figure 7.3.1(a). Figure 7.3.1(b) illustrates a means for attenuating forces transmitted from a machine to the work environment.

Figure 7.3.2 shows a generic model of an SDOF system with a harmonic force. This may represent a complex system of links that have a sufficient number of kinematic constraints to eliminate all but one dof, such as in Figure E3.3.1(a). In these cases, m , c , k , and f may be regarded as being the "equivalent" mass, damping, stiffness, and force, respectively, of the complex system.

Newton's law (3.3.5) for this model is

$$m\ddot{q} = f(t) - F_T(t) \quad (7.3.1)$$

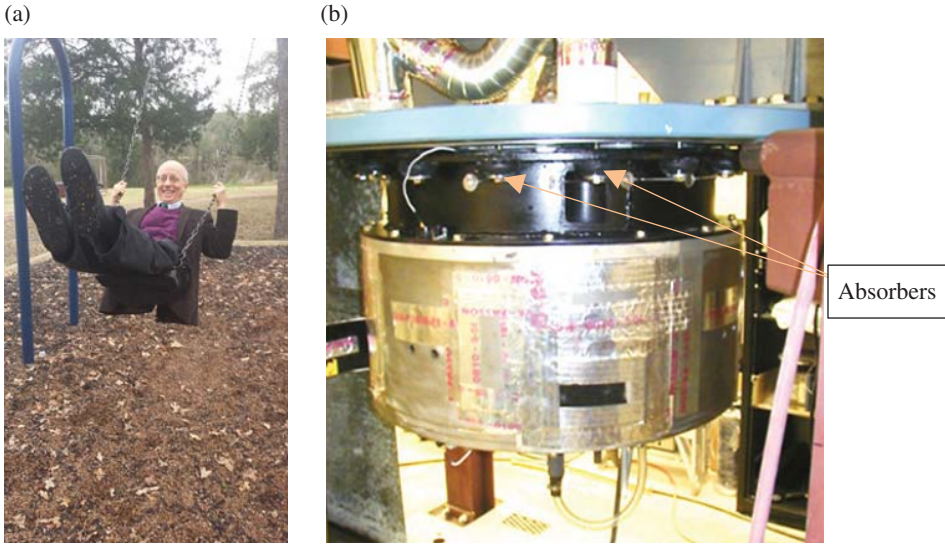


Figure 7.3.1 (a) Resonant swing and (b) elastomeric absorbers for reducing transmitted forces

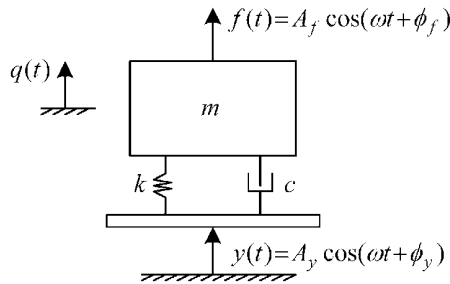


Figure 7.3.2 Equivalent system—SDOF model for steady-state harmonic response analysis

where

$$F_T(t) = c(\dot{q} - \dot{y}) + k(q - y) \quad (7.3.2)$$

$$f(t) = A_f \cos(\omega t + \phi_f) \quad (7.3.3)$$

$$y(t) = A_y \cos(\omega t + \phi_y) \quad (7.3.4)$$

$$\Rightarrow m\ddot{q} + c\dot{q} + kq = f(t) + ky + c\dot{y} \quad (7.3.5)$$

The four application areas that will be modeled with (7.3.5) are summarized in Table 7.3.1.

The complex variable solution of Equation (7.3.5) proceeds via Equations (7.2.1)–(7.2.7). The real external forces are replaced by their complex counterparts as in (7.2.5):

$$\begin{aligned} f(t) &= A_f \cos(\omega t + \phi_f) \Rightarrow A_f e^{i\phi_f} e^{i\omega t} \\ y(t) &= A_y \cos(\omega t + \phi_y) \Rightarrow A_y e^{i\phi_y} e^{i\omega t} \\ \dot{y}(t) &\Rightarrow A_y e^{i\phi_y} i\omega e^{i\omega t} \end{aligned} \quad (7.3.6)$$

Table 7.3.1 Application areas for steady-state harmonic analysis

Condition	Typical objective	$ f $	$ y $
Constant amplitude excitation	Control resonance	A_f	0
Force transmission	$ F_T \approx 0$	A_f	0
Vibration isolation	$ q \approx 0$	0	A_y
Rotating imbalance	Control resonance	$\omega^2 \hat{A}_f$	0

The real response $q(t)$ is replaced by its complex counterpart so (7.3.5) becomes

$$m\ddot{Q} + c\dot{Q} + kQ = [A_f e^{i\phi_f} + A_y e^{i\phi_y} (k + ic\omega)] e^{i\omega t} \quad (7.3.7)$$

As in (2.5.13), substitute

$$Q = \tilde{Q} e^{i\omega t} \quad (7.3.8)$$

and solve for the displacement phasor \tilde{Q} (Section 2.5), yielding

$$\tilde{Q} = \frac{A_f e^{i\phi_f}}{(k - m\omega^2) + ic\omega} + \frac{A_y e^{i\phi_y} (k + ic\omega)}{(k - m\omega^2) + ic\omega} \quad (7.3.9)$$

The conditions in Table 7.3.1 are divided into two cases as discussed next.

7.3.1 Class I ($f(t) \neq 0, y(t) = 0$): No Support Excitation—Only External Forcing

Set $A_y = 0$ in (7.3.9) and express the complex constant \tilde{Q} in polar form

$$\tilde{Q} = |\tilde{Q}| e^{i\phi_Q} \quad (7.3.10)$$

where using the identities in Section 2.5

$$|\tilde{Q}| = \frac{|A_f e^{i\phi_f}|}{|(k - m\omega^2) + ic\omega|} = \frac{A_f}{\sqrt{(k - m\omega^2)^2 + (c\omega)^2}} \quad (7.3.11)$$

$$\phi_Q = \angle A_f e^{i\phi_f} - \angle((k - m\omega^2) + ic\omega) = \phi_f - \tan^{-1} \frac{c\omega}{k - m\omega^2}$$

Substitute

$$\frac{m}{k} = \frac{1}{\omega_n^2}, \quad \frac{c\omega}{k} = \frac{2m\omega_n \xi \omega}{k} = 2\xi \frac{\omega}{\omega_n}, \quad r = \frac{\omega}{\omega_n} \quad (7.3.12)$$

to obtain

$$|\tilde{Q}| = \frac{A_f/k}{\sqrt{(1-r^2)^2 + (2\xi r)^2}}, \quad \phi_Q = \phi_f - \tan^{-1} \frac{2\xi r}{1-r^2} \quad (7.3.13)$$

Recall from (7.2.10), (7.3.8), and (7.3.10) that

$$q(t) = \text{Re}(Q(t)) = \text{Re}\left(\tilde{Q}e^{i\omega t}\right) = \text{Re}\left(|\tilde{Q}|e^{i\phi_Q}e^{i\omega t}\right) = \text{Re}\left(|\tilde{Q}|e^{i(\omega t + \phi_Q)}\right) = |\tilde{Q}|\cos(\omega t + \phi_Q) \quad (7.3.14)$$

From (7.3.2), the transmitted force is

$$\begin{aligned} F_T(t) &= kq + c\dot{q} = k\text{Re}(Q) + c\frac{d}{dt}\text{Re}(Q) = k\text{Re}(Q) + c\text{Re}(\dot{Q}) \\ &= \text{Re}(kQ + c\dot{Q}) = \text{Re}\left((k\tilde{Q} + ci\omega\tilde{Q})e^{i\omega t}\right) = \text{Re}\left((k + ic\omega)\tilde{Q}e^{i\omega t}\right) \end{aligned} \quad (7.3.15)$$

From (7.3.9), Equation (7.3.15) may be written as

$$F_T(t) = \text{Re}(G(\omega)A_f e^{i\phi_f} e^{i\omega t}) \quad (7.3.16)$$

where

$$G(\omega) = \frac{k + ic\omega}{(k - m\omega^2) + ic\omega} = \frac{1 + i2\xi r}{(1 - r^2) + i2\xi r} \quad (7.3.17)$$

and with the identities of Section 2.5

$$G(\omega) = |G|e^{i\phi_G}, \quad |G| = \sqrt{\frac{1 + (2\xi r)^2}{(1 - r^2)^2 + (2\xi r)^2}} \quad (7.3.18)$$

$$\phi_G = \angle(1 + i2\xi r) - \angle((1 - r^2) + i2\xi r) = \tan^{-1}(2\xi r) - \tan^{-1}\left(\frac{2\xi r}{1 - r^2}\right)$$

Equation (7.3.16) becomes

$$F_T(t) = \text{Re}\left(|G|A_f e^{i\phi_f} e^{i\phi_G} e^{i\omega t}\right) = A_f |G| \cos(\omega t + \phi_f + \phi_G) \quad (7.3.19)$$

Therefore,

$$|F_T| = A_f |G| \quad (7.3.20)$$

$$\angle F_T = \phi_f + \phi_G \quad (7.3.21)$$

Define the force transmissibility ratio (TR) magnitude as

$$\text{TR} = \frac{|F_T|}{|f|} = \frac{|F_T|}{A_f} = |G(\omega)| = \sqrt{\frac{1 + (2\xi r)^2}{(1 - r^2)^2 + (2\xi r)^2}} \quad (7.3.22)$$

which is the ratio of transmitted force to applied force. Figure 7.3.3 shows the TR's (a) amplitude and (b) phase angle versus frequency ratio (r) and damping ratio (ξ). Figure 7.3.3 shows that the transmitted forces can become very large for values of r near r_{\max} . Avoiding this condition of "resonance" is commonly the reason for integrating vibration analysis into the design process for high-performance machinery and structures.

The TR magnitude in (7.3.22) equals 1 at $r = \sqrt{2}$, independent of the value of ξ . Figure 7.3.3 and Equation (7.3.22) clearly show that the frequency ratio ($r = \omega/\omega_n$) must exceed $\sqrt{2}$ to reduce the transmitted force F_T . This suggests soft mounting a machine, which

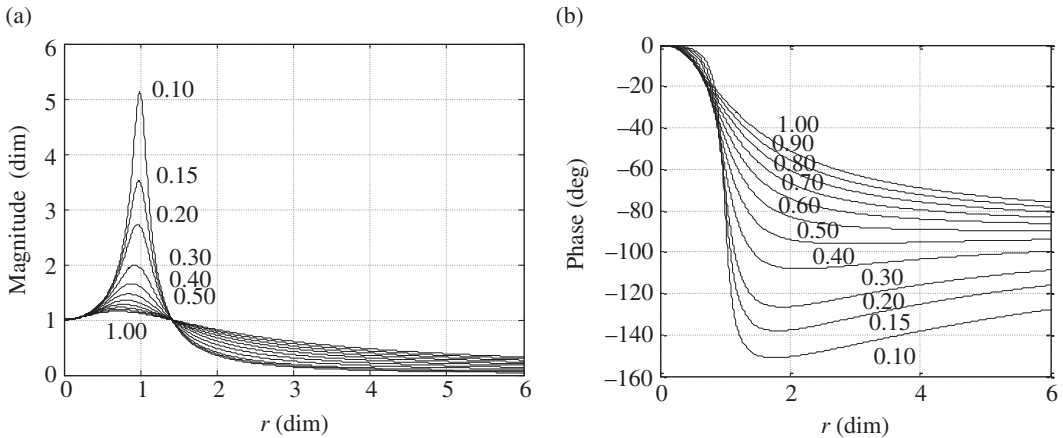


Figure 7.3.3 (a) Magnitude and (b) phase angle of G versus $r = \omega/\omega_n$ and ξ

has the effect of making ω_n small relative to the forcing frequency range. Light damping (ξ) is also seen to be desirable for lowering $|G|$ for $r > \sqrt{2}$. Some active damping approaches increase damping as the forcing frequency passes through resonance and lower damping when operating with $r > \sqrt{2}$.

Figure 7.3.3(b) shows the variation of ϕ_G in (7.3.18) versus frequency ratio (r) and damping ratio (ξ). The effect of increasing ξ is to decrease the phase lag of the response relative to the force. Equation (7.3.18) shows that ϕ_G approaches -90° as r approaches ∞ for all $\xi > 0$. The peaks in the $|G|$ curves of Figure 7.3.3(a) occur at different values of r , depending on the value of ξ , that is,

$$r_{\max} = \text{value of } r \text{ at } \max(|G|) = r_{\max}(\xi) \quad (7.3.23)$$

The value of r_{\max} is determined by solving for the r that satisfies

$$\frac{d|G|}{dr} = 0 \quad (7.3.24)$$

The r that satisfies this equation is r_{\max} and is substituted into $|G(r)|$ to determine the peak amplitude of G . The following Maple code performs these calculations with its symbolic calculus capabilities:

```
> restart;
> f:= sqrt( (1+(2*zeta*r)^2) / ( (1-r^2)^2 + (2*zeta*r)^2 ) );
> y:= diff(f,r);
> rmaxv :=solve(y=0,r);
> rmax := rmaxv[2];
> plot(rmax,zeta=.01..3.0,title="",labels=["Damping Ratio
(dim)", "r at G Peak"],thickness=2);
> f:= sqrt( (1+(2*zeta*rmax)^2) / ( (1-rmax^2)^2 + (2*zeta*rmax)^2
) );
> plot(f,zeta=.05..1.0,title="",labels=["DampingRatio
(dim)", "G peak"],thickness=2);
```

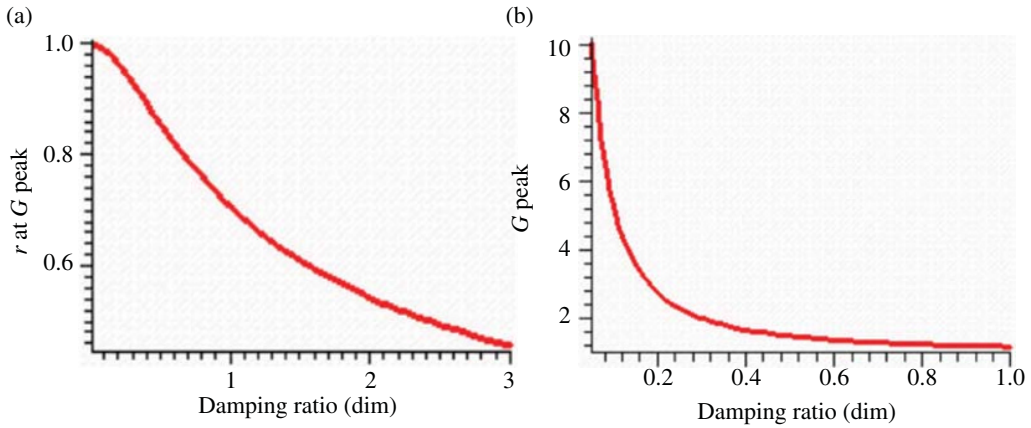


Figure 7.3.4 (a) Frequency ratio r at peak $|G|$ and (b) peak $|G|$ versus ξ

This code provides the formula for the r value at the peak $|G|$:

$$r_{\max}(\xi) = \frac{1}{2} \frac{\sqrt{-1 + \sqrt{1 + 8\xi^2}}}{\xi} \quad (7.3.25)$$

and the peak value of $|G|$:

$$|G|_{\text{peak}} = |G(r_{\max})| = \frac{\sqrt{1 + 8\xi^2}}{\left(1 - \frac{1 - 1 + \sqrt{1 + 8\xi^2}}{4\xi^2}\right)^2 - 1 + \sqrt{1 + 8\xi^2}} \quad (7.3.26)$$

Figure 7.3.4(a) and (b) shows plots of r_{\max} versus ξ and $\max(|G|)$ versus ξ , respectively.

The displacement $q(t)$ of the effective mass m in Figure 7.3.2 is given by Equations (7.3.13) and (7.3.14) as

$$q(t) = \frac{A_f}{k} |G_f| \cos(\omega t + \phi_f + \phi_{Gf}) \quad (7.3.27)$$

where

$$|G_f| = \frac{1}{\sqrt{(1-r^2)^2 + (2\xi r)^2}} \quad (7.3.28)$$

$$\phi_{Gf} = -\tan^{-1}\left(\frac{2\xi r}{1-r^2}\right) \quad (7.3.29)$$

Figure 7.3.5 shows plots of $|G_f|$ and ϕ_{Gf} versus r and ξ .

The pronounced peak in the displacement versus frequency ratio curve represents a resonance condition. Note that $|G_f| \rightarrow 0$ as $r \rightarrow \infty$, which from (7.3.27) indicates that the displacement amplitude will approach zero at frequencies well above the resonance frequencies. Figure 7.3.6 shows the peak displacement values of r and the peak value of $|G_f|$

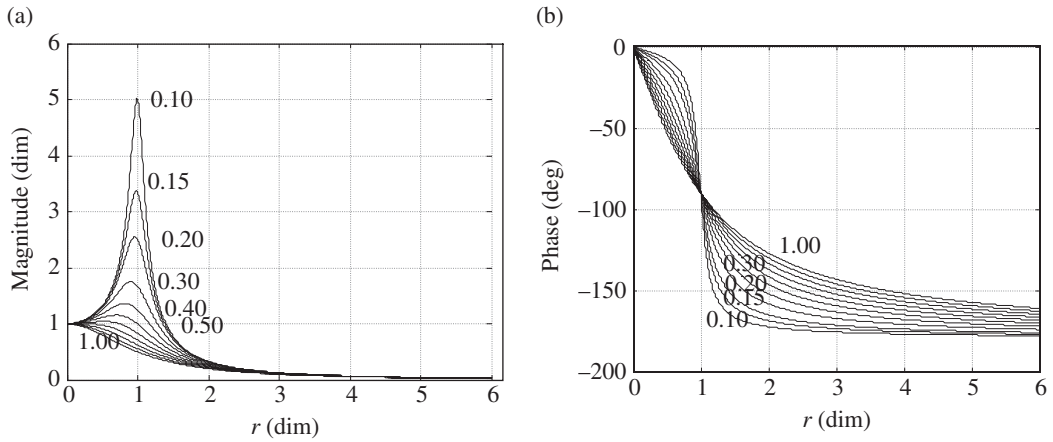


Figure 7.3.5 (a) Magnitude and (b) phase angle of G_f versus $r = \omega/\omega_n$ and ξ values

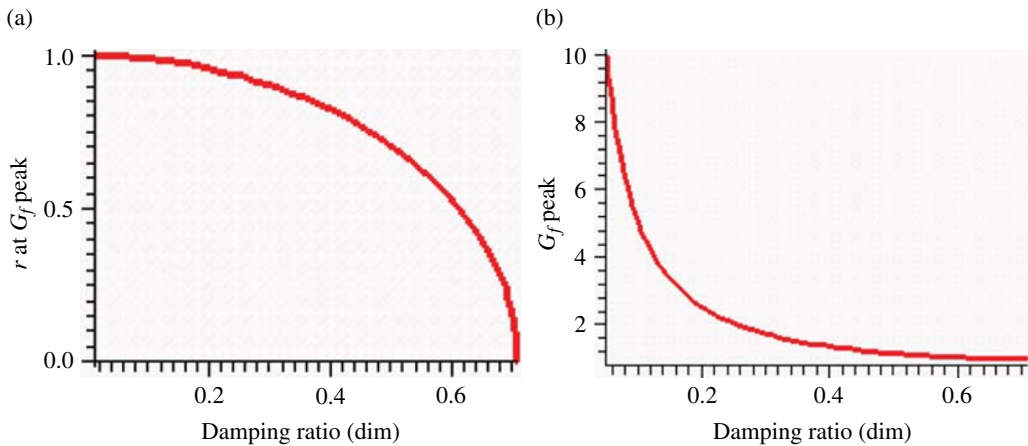


Figure 7.3.6 Frequency ratio (r) for (a) Max $|G_f|$ and (b) maximum amplitude of $|G_f|$ versus ξ

versus ξ . The amplitude must decrease to zero as $r \rightarrow \infty$; otherwise, the required input power ($|f * \dot{x}| = |f|\omega|x|$) would become infinite.

The value of r at which the peak displacement in Figure 7.3.5 occurs is determined utilizing a Maple code. The result is

$$r_{\text{peak}} = \sqrt{1 - 2\xi^2}, \quad 0 \leq \xi \leq \frac{1}{\sqrt{2}} (=0.707) \quad (7.3.30)$$

In a similar manner, the peak value of $|G_f|$ is determined to be

$$|G_f|_{\text{peak}} = |G_f(r_{\text{peak}})| = \frac{1}{2\xi} \sqrt{1 - \xi^2}, \quad 0 \leq \xi \leq \frac{1}{\sqrt{2}} \quad (7.3.31)$$

The static displacement amplitude of q is given by setting $r=0$ in (7.3.27) and (7.3.28) yielding

$$|q_{\text{static}}| = \frac{A_f}{k} \quad (7.3.32)$$

combining these results in (7.3.27) shows that the peak displacement amplitude is given by

$$|q_{\text{peak}}| = \frac{A_f}{k} |G_f|_{\text{peak}} = |q_{\text{static}}| * \frac{1}{2\xi} \sqrt{1-\xi^2}, \quad 0 \leq \xi \leq \frac{1}{\sqrt{2}} \quad (7.3.33)$$

which illustrates the potentially dangerous risk of utilizing a static response estimate for a dynamic system's response, for lightly damped systems near resonance.

The following Maple code performs these calculations with its symbolic calculus capabilities:

```
> restart;
> f:= sqrt( 1 / ( (1-r^2)^2 + (2*zeta*r)^2 ) );
> y:= diff(f,r);
> rmaxv :=solve(y=0,r);
> rmax := rmaxv[2];
> plot(rmax, zeta=.01..(.7071), title="", labels=["Damping Ratio (dim)", "r at Gf Peak"], thickness=2);
> f:= sqrt( 1 / ( (1-rmax^2)^2 + (2*zeta*rmax)^2 ) );
> plot(f, zeta=.05..(.7071), title="", labels=["Damping Ratio (dim)", "Gf peak"], thickness=2);
```

The fourth case in Table 7.3.1 corresponds with A_f being proportional to ω^2 , that is,

$$A_f = \hat{A}_f \omega^2 \quad (7.3.34)$$

This form of the harmonic force amplitude always applies to rotating machines with mass unbalance on the rotating component of the machine. The unbalance results from the impossibility of originally machining or maintaining a rotating part that has its mass center precisely on its spin axis. From (7.3.27) and (7.3.34),

$$|q| = \frac{\hat{A}_f}{k} |G_f| \omega^2 = \frac{\hat{A}_f}{k/\omega_n^2} |G_{f\omega}| = \frac{\hat{A}_f}{m} |G_{f\omega}| \quad (7.3.35)$$

where

$$|G_{f\omega}| = |G_f| r^2 = \frac{r^2}{\sqrt{(1-r^2)^2 + (2\xi r)^2}} \quad (7.3.36)$$

Figure 7.3.7 shows plots of the peak displacement values of r and the peak value of $|G_{f\omega}|$ versus ξ . The value of r at which the peak occurs is determined by a Maple code to be

$$r_{\text{peak}} = \frac{1}{\sqrt{1-2\xi^2}} \quad (7.3.37)$$

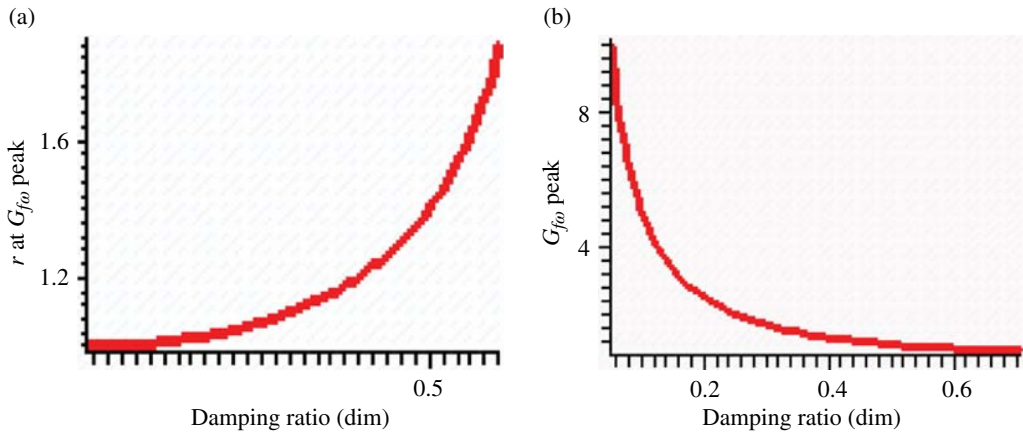


Figure 7.3.7 (a) Frequency ratio (r) for Max $|G_{f\omega}|$ and (b) maximum amplitude of $|G_{f\omega}|$ versus ξ

The corresponding peak value is given by

$$|q_{\text{peak}}| = \frac{\hat{A}_f}{m} |G_{f\omega}(r_{\text{peak}})| = \frac{\hat{A}_f/m}{2\xi\sqrt{1-\xi^2}} \quad (7.3.38)$$

The Maple code employed to generate the results in Figure 7.3.7 is as follows:

```
> restart;
> f:= r^2 / sqrt( (1-r^2)^2 + (2*zeta*r)^2 );
> y:= diff(f,r);
> rmaxv :=solve(y=0,r);
> rmax := rmaxv[3];
> plot(rmax, zeta=.01..(.6), title="", labels=["Damping Ratio
(dim)", "r at Gf_omega Peak"], thickness=2);
> f:= rmax^2 / sqrt( (1-rmax^2)^2 + (2*zeta*rmax)^2 );
> plot(f, zeta=.05..(.7071), title="", labels=["Damping Ratio
(dim)", "Gf_omega Peak"], thickness=2);
```

Figure 7.3.8 shows plots of $|G_{f\omega}|$ versus r for various values of ξ . Note that the peaks of $|G_{f\omega}|$ increase in frequency as ξ increases in contrast to $|G_f|$ in Figure 7.3.5.

7.3.2 Class II ($f(t) = 0, y(t) \neq 0$): Only Support Excitation—No External Forcing

To analyze this case, set $A_f = 0$ in (7.3.9) yielding

$$\tilde{Q} = \frac{A_y e^{i\phi_y} (k + ic\omega)}{(k - m\omega^2) + ic\omega} = A_y e^{i\phi_y} G(\omega) \quad (7.3.39)$$

where $G(\omega)$ is defined in (7.3.17). Note that from (7.3.6),

$$|y| = A_y = \text{amplitude of the support motion} \quad (7.3.40)$$

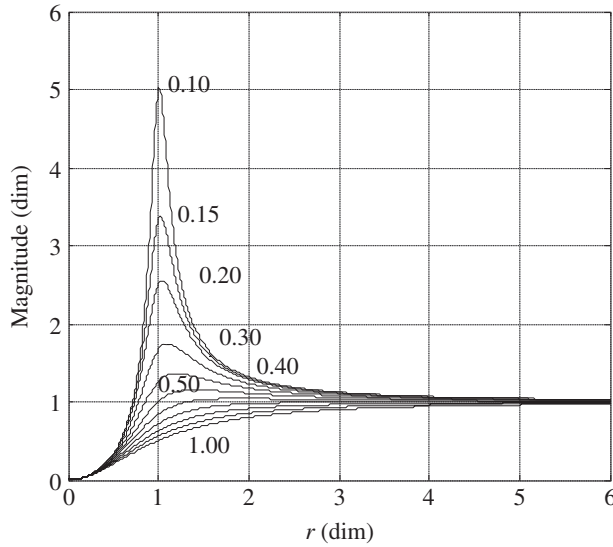


Figure 7.3.8 $|G_{f\omega}|$ versus frequency ratio $r = \omega/\omega_n$ and damping ratio ξ values

so (7.3.39) implies that the isolation ratio (mass displacement/support displacement) becomes

$$\frac{|q|}{|y|} = \frac{|\tilde{Q}|}{A_y} = |G(\omega)| \quad (7.3.41)$$

Thus, the force transmissibility (F_T/f) and the displacement isolation (q/y) ratios have identical dependences on ξ and r , as expressed by $|G(\omega)|$ in Equation (7.3.18). Thus, Figures 7.3.3 and 7.3.4 are applicable either to the vibration isolation problem or to the force transmissibility problem. Figure 7.3.3 shows that soft mounting an object ($r = (\omega/\omega_n) \gg 1$) provides a good means to isolate its motion from the support motion. This is the basis for soft mounting precision optical devices.

EXAMPLE 7.3.1 *Microgravity Experiment on the International Space Station*

Statement: The International Space Station (ISS) provides an excellent environment for developing new and improved medicines, crystals, and manufacturing processes and for performing unique fluid mechanics, biology, astrophysics and physiology experiments. This results from the absence of the strong gravitational force present at the earth's surface. The micro-g environment can be compromised by ISS-borne vibration sources such as crew movements, machinery, and space shuttle docking. Very effective and innovative approaches have been developed by NASA scientists and their contractors to isolate the micro-g experiments from support motion-induced disturbances. The two configurations for experiments requiring micro-g environments include a multiple experiment rack, which is itself isolated from the ISS, and a single experiment approach, which is housed in a glove box to prevent contamination. One innovative method developed to isolate the experiment is to use electromagnetic forces to support its container. This "active suspension" directs position and acceleration sensor outputs to a controller that adjusts currents in a set of electromagnetic

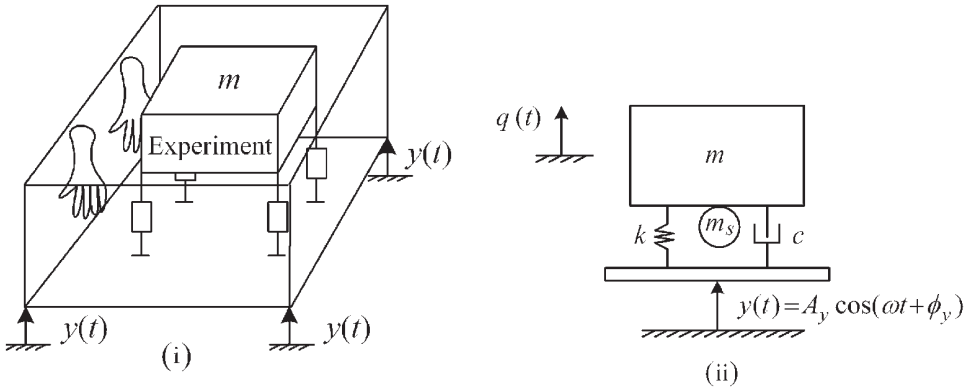


Figure E7.3.1(a) (i) Micro-g experiment with support motion disturbance and (ii) the simulation model

actuators. The forces produced have the effect of providing “active” stiffness (k), mass (m_s), and damping (c) as depicted in Figure E7.3.1(a).

Objective: A crystal growth experiment weighs 50 N and is supported by a vibration isolation system in a glove box. The deck of the station in the vicinity of the experiment undergoes periodic vibration caused by an air-conditioning compressor located on the ISS. The deck motion at the glove box is sinusoidal with the amplitude of 0.01 mm and frequency 50 Hz. This is equivalent to about 0.1 g(o-peak) acceleration of the deck. Identify the support design requirements for achieving *micro-g* (10^{-6} g) isolation of the experiment.

Assumptions: Small unidirectional motions in the (y, q) dofs only.

Solution: As shown in Equations (7.3.18) and (7.3.35), the isolation ratio of the experiment container motion amplitude to the glove box amplitude is

$$\frac{|q|}{|y|} = |G(\omega)| = \sqrt{\frac{1 + (2\xi r)^2}{(1-r^2)^2 + (2\xi r)^2}} \quad (1)$$

Since it is assumed that y consists of only one frequency, it follows that

$$\frac{|a_E|}{|a_D|} = \frac{\text{experiment acceleration}}{\text{deck acceleration}} = \frac{\omega^2 |q|}{\omega^2 |y|} = |G(\omega)| \quad (2)$$

The design objective is to achieve

$$|a_E| = |a_D| |G(\omega)| = \omega^2 |y| |G(\omega)| = 10^{-6} \text{ g} \quad (3)$$

$$\Rightarrow |G(\omega)| = \frac{10^{-6} \text{ g}}{\omega^2 |y|} = \frac{(10^{-6})(9.8 \text{ m/s}^2)}{(2\pi 50 \text{ s}^{-1})^2 (10^{-5} \text{ m})} = 10^{-5} \quad (4)$$

From Figure 7.3.3, it is seen that a very high frequency ratio and very low damping ratio are required to achieve (4). From (1) and (4),

$$10^{-10} \left[(1-r^2)^2 + (2\xi r)^2 \right] - 1 - (2\xi r)^2 = 0 \quad (5)$$

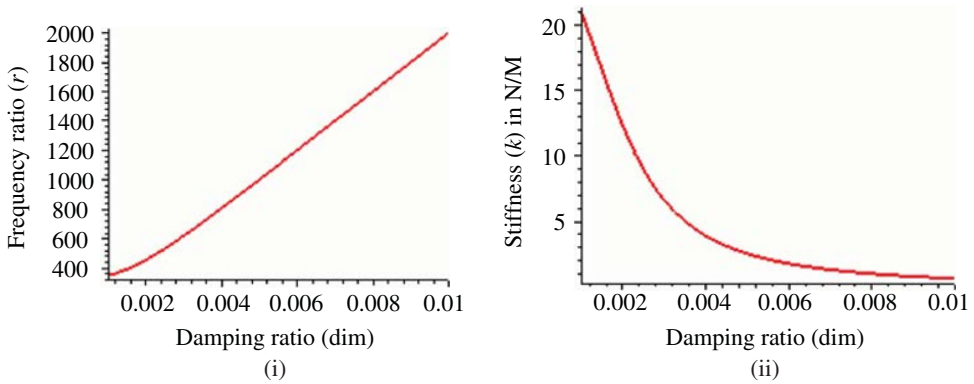


Figure E7.3.1(b) (i) Frequency ratio and (ii) stiffness required for micro-g isolation versus ζ

The solution of this equation is obtained from a MAPLE code as

$$r = \sqrt{1.0 + 0.2 \times 10^{11} \zeta^2 + 10^5 \sqrt{1.0 + 4.0 \zeta^2 + 0.4 \times 10^{11} \zeta^4}} \quad (6)$$

and is plotted versus ξ in Figure E7.3.1(b)-(i). Recall

$$r = \frac{\omega}{\omega_n} = \frac{\omega}{\sqrt{k/(m+m_s)}} \Rightarrow k = \frac{\omega^2}{r^2} (m+m_s) \quad (7)$$

The required stiffness is plotted versus ξ in Figure E7.3.1(b)-(ii) for $\omega = 2\pi * 50$, $m = 5.10\text{kg}$, and $m_s = 0$.

7.3.3 Half Power Point Damping Identification

Let R represent the amplitude of the SSHR of an SDOF system. The velocity and acceleration are the first and second time derivatives of displacement $q(t)$; therefore, Equations (7.3.27), (7.3.28), (7.3.35), and (7.3.36) yield

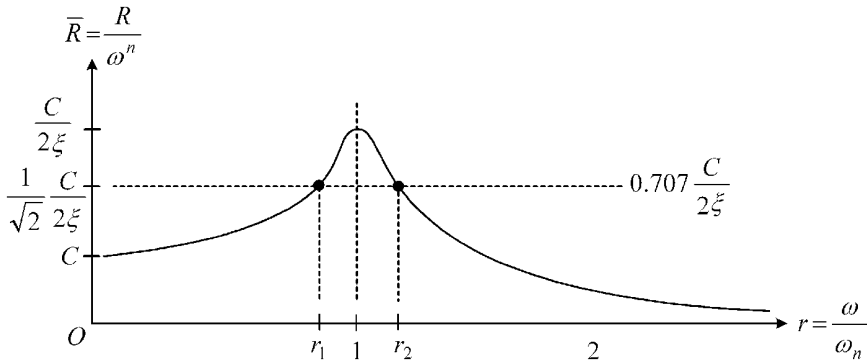
$$R = \frac{C\omega^n}{\sqrt{(1-r^2)^2 + (2\xi r)^2}} \quad (7.3.42)$$

where C and n are shown in Table 7.3.2.

The response amplitude R may be experimentally measured with a displacement, velocity, or acceleration sensor. The frequency ω is specified (known) if a shaker is used for “resonance testing” and is measured with a tachometer for rotating machinery imbalance-induced vibration ($\omega = \text{shaft spin rate}$). The quantity (R/ω^n) may then be plotted versus $(r = \omega/\omega_n)$. The value of ω_n used to evaluate the r values for this plot may be approximated by the frequency at the peak response. This practice is acceptable for damping ratios

Table 7.3.2 Response amplitude parameters for Equation (7.3.42)

Response amplitude (R)	Force amplitude	C	n
Displacement (q)	Constant	A_f/k	0
Velocity (v)	Constant	A_f/k	1
Acceleration (a)	Constant	A_f/k	2
Displacement (q)	Proportional to ω^2 (rotating imbalance)	$\hat{A}_f/(m\omega_n^2)$	2
Velocity (v)	Proportional to ω^2 (rotating imbalance)	$\hat{A}_f/(m\omega_n^2)$	3
Acceleration (a)	Proportional to ω^2 (rotating imbalance)	$\hat{A}_f/(m\omega_n^2)$	4

**Figure 7.3.9** Plot of frequency normalized response amplitude versus frequency ratio

less than 0.20 as can be seen from Figures 7.3.3, 7.3.4, 7.3.5, 7.3.6, 7.3.7, and 7.3.8. The theoretical value of (R/ω^n) is given by Equations (7.3.28) and (7.3.42) as

$$\bar{R} = \frac{R}{\omega^n} = \frac{C}{\sqrt{(1-r^2)^2 + (2\xi r)^2}} = C|G_f| \quad (7.3.43)$$

From Figure 7.3.5, the general shape of this plot will resemble Figure 7.3.9. The peak in this figure is given by (7.3.43) as

$$\bar{R}_{\text{peak}} = \frac{R}{\omega^n} \Big|_{\text{peak}} \approx \frac{R}{\omega^n} \Big|_{r=1} = \frac{C}{2\xi} \quad (7.3.44)$$

The frequency ratios r_1 and r_2 are determined experimentally as the two values of r at which

$$\bar{R}_{1/2} = \frac{\bar{R}_{\text{peak}}}{\sqrt{2}} \approx 0.707\bar{R}_{\text{peak}} \quad (7.3.45)$$

These are referred to as the “half power point” frequency ratios. From (7.3.43) and (7.3.44),

$$\bar{R}_{1/2} = \frac{1}{\sqrt{2}} \frac{C}{2\xi} = \frac{C}{\sqrt{(1-r^2)^2 + (2\xi r)^2}} \quad (7.3.46)$$

The results shown below are applicable to all response and force types shown in Table 7.3.2 since C cancels in (7.3.46). The values of r that satisfy (7.3.46) are shown in Figure 7.3.9 to be r_1 and r_2 . Equation (7.3.46) is rewritten as

$$(1-r^2)^2 + 4\xi^2 r^2 = 8\xi^2 \quad (7.3.47)$$

or

$$r^4 + (4\xi^2 - 2)r^2 + (1 - 8\xi^2) = 0 \quad (7.3.48)$$

The roots of this equation are

$$r_1^2 = (1 - 2\xi^2) - 2\xi\sqrt{1 + \xi^2}, \quad r_2^2 = (1 - 2\xi^2) + 2\xi\sqrt{1 + \xi^2} \quad (7.3.49)$$

Note that for $\xi \leq 0.2$, the expressions $(1 - 2\xi^2)$ and $(1 + \xi^2)$ are both approximately equal to 1. Therefore,

$$r_1^2 \approx 1 - 2\xi, \quad r_2^2 \approx 1 + 2\xi \quad (7.3.50)$$

and then

$$\xi \approx \frac{r_2^2 - r_1^2}{4} \quad (7.3.51)$$

A commonly used simplified version of (7.3.51) for the damping ratio is

$$\xi = \frac{(r_2 - r_1)(r_2 + r_1)}{4} \approx \frac{(r_2 - r_1)(1 + 1)}{4} = \frac{r_2 - r_1}{2} \quad (7.3.52)$$

The damping ratio ξ may then be experimentally measured by measuring r_1 and r_2 as shown in Figure 7.3.9 and then using Equation (7.3.52). The ratio of the peak value of \bar{R} to its value at $\omega = 0$ is given by (7.3.43) and (7.3.44) as

$$Q = \text{quality factor} = \text{amplification factor} = \frac{\bar{R}_{\text{peak}}}{\bar{R}_{\omega=0}} = \frac{C/2\xi}{C} = \frac{1}{2\xi} \quad (7.3.53)$$

which from Equation (7.3.52) becomes

$$Q = \frac{1}{2\xi} = \frac{1}{r_2 - r_1} \quad (7.3.54)$$

Measurement of \bar{R}_{peak} and $\bar{R}_{\omega=0}$ provides yet another means to estimate ξ via Equation (7.3.53). For lightly damped systems, Figures 7.3.5 and 7.3.8 show that $r_2 \approx r_1$ so that Q becomes very large by (7.3.54). Some machinery acceptance standards are specified in terms of maximum allowable Q . Turbines and compressors in the petrochemical industry must traverse a resonance to reach their operating speed range. Continuous operation in this speed range may extend from days to months and even a year or longer. Imbalance may accumulate on turbine or compressor wheels and blades from wear and deposits over this period. This may cause excessive vibration and damage while traversing the resonance frequency during spin-down of the machine if Q is too high. Consequently, machinery designers carefully select bearings and seals to provide adequate damping. Recommended allowable values of Q for general-purpose turbines are discussed in the

American Petroleum Institute standard API Std 617 (R2009). The author's experience would indicate that Q should be between 3 and 5; however, the standards should be consulted in an actual machinery application.

7.3.4 Phase Slope Damping Identification

Commercially available phase meters can accurately measure, store, and display phase angle relative to some reference, that is, a once per revolution marker on a rotating shaft. From Equations (7.3.27)–(7.3.29), the measured phase angles of the response quantities are:

Displacement:

$$\angle q = \phi_{m/f} + \phi_f - \tan^{-1} \left(\frac{2\xi r}{1-r^2} \right) \quad (7.3.55)$$

Velocity:

$$\angle v = \phi_{m/f} + \phi_f - \tan^{-1} \left(\frac{2\xi r}{1-r^2} \right) + 90^\circ \quad (7.3.56)$$

Acceleration:

$$\angle a = \phi_{m/f} + \phi_f - \tan^{-1} \left(\frac{2\xi r}{1-r^2} \right) + 180^\circ \quad (7.3.57)$$

where $\phi_{m/f}$ is the relative phase angle between the reference marker and the force. The phase of any of the above responses may be measured and plotted versus $r (= \omega/\omega_n)$. The slope of the phases of any of these responses at $r = 1$, that is, at $\omega = \omega_n$, is

$$\begin{aligned} \left. \frac{d}{dr} (\angle q \text{ or } \angle v \text{ or } \angle a) \right|_{r=1} &= \left. \frac{d}{dr} \left(-\tan^{-1} \left(\frac{2\xi r}{1-r^2} \right) \right) \right|_{r=1} \\ &= \left. \frac{-1}{1 + [(2\xi r)/(1-r^2)]^2} * \frac{2\xi(1-r^2) - 2\xi r(-2r)}{(1-r^2)^2} \right|_{r=1} = \frac{1}{\xi} \end{aligned} \quad (7.3.58)$$

Thus, the damping ratio may also be estimated by

$$\xi = \frac{1}{\text{slope of plot of } (\angle q \text{ or } \angle v \text{ or } \angle a) \text{ vs. } r \text{ at } r = 1} \quad (7.3.59)$$

7.3.5 Accurate Measurement of ω_n

The half power point and phase slope methods of determining ξ required a value of ω_n to determine the frequency ratio $r (= \omega/\omega_n)$. The undamped natural frequency was assumed to equal the peak response frequency, that is, from (7.3.30),

$$\omega_n \approx \omega_{\text{peak}} = \omega_n \sqrt{1-2\xi^2} \quad 0 \leq \xi \leq \frac{1}{\sqrt{2}} \quad (7.3.60)$$

which is fairly accurate for $\xi \leq 0.2$, at which value the above approximation becomes

$$\omega_{\text{peak}} \approx \omega_n(0.959) \quad (7.3.61)$$

The response phasor is given for external force excitation by (7.3.8), (7.3.9), and (7.3.12) as

$$\tilde{Q} = \frac{(A_f/k)e^{i\phi_f}}{(1-r^2) + i2\xi r} \quad (7.3.62)$$

The phase angle of the response relative to the phase angle of the force becomes:

Displacement response:

$$\angle q_{rf} = \phi_q - \phi_f = \tan^{-1} \left(\frac{-2\xi r}{1-r^2} \right) \quad (7.3.63)$$

Velocity response:

$$\angle v_{rf} = \phi_v - \phi_f = \angle i\omega + \angle \left(\frac{e^{i\phi_f}}{(1-r^2) + i2\xi r} \right) - \phi_f = 90^\circ + \tan^{-1} \left(\frac{-2\xi r}{1-r^2} \right) \quad (7.3.64)$$

Acceleration response:

$$\angle a_{rf} = \phi_a - \phi_f = \angle -1 + \angle \left(\frac{e^{i\phi_f}}{(1-r^2) + i2\xi r} \right) - \phi_f = 180^\circ + \tan^{-1} \left(\frac{-2\xi r}{1-r^2} \right) \quad (7.3.65)$$

The undamped natural frequency is then identified as the forcing frequency for which the relative phase angles have the following values:

Displacement:

$$\angle q_{rf} = \phi_q - \phi_f = -90^\circ \quad (7.3.66)$$

Velocity response:

$$\angle v_{rf} = \phi_v - \phi_f = 0^\circ \quad (7.3.67)$$

Acceleration response:

$$\angle a_{rf} = \phi_a - \phi_f = 90^\circ \quad (7.3.68)$$

These results are obtained by assigning $r = 1$, that is, $\omega = \omega_n$, in Equations (7.3.63), (7.3.64), and (7.3.65). An approach to resonance testing employs a feedback loop to vary the forcing frequency until the relative phase angle has the value given by the appropriate equation ((7.3.66), (7.3.67), or (7.3.68)). The resulting frequency ω is then assumed to equal the undamped natural frequency ω_n . Another approach utilizes a plot of the receptance (\hat{R}), that is, the ratio of the measured response phasor to the measured force phasor. For example, for displacement response (7.3.62) and (7.3.63), the polar form of \hat{R} is

$$\hat{R} = \frac{\tilde{Q}}{\tilde{F}} = \frac{\tilde{Q}}{A_f e^{i\phi_f}} = |\hat{R}| e^{i\phi_{\hat{R}}} = \frac{1/k}{\sqrt{(1-r^2)^2 + (2\xi r)^2}} \angle \tan^{-1} \left(\frac{-2\xi r}{1-r^2} \right) \quad (7.3.69)$$

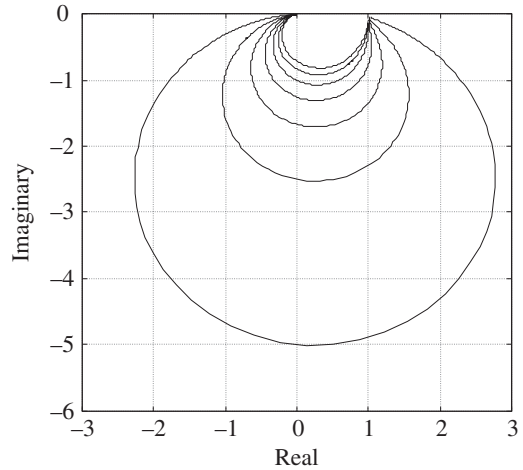


Figure 7.3.10 Polar plot of receptance \hat{R} versus frequency with damping of $\xi = 0.1, 0.2, 0.3, 0.4, 0.5, 0.6, \text{ and } 0.7$

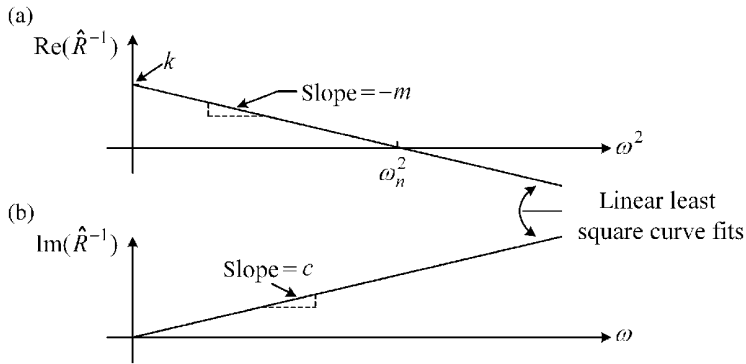


Figure 7.3.11 (a) Real and (b) imaginary parts of the dynamic stiffness

A polar plot of this quantity in the complex plane is shown in Figure 7.3.10 for various values of damping ratio zeta ξ . The phase angle decreases from 0 to -90° to -180° as r increases from 0 to ∞ . The forcing frequency ω equals the undamped natural frequency ω_n when the locus crosses from the right-hand to the left-hand planes ($\phi = -90^\circ$). The positive peak of the response lags the positive peak of the force by 90° at this frequency.

7.3.6 Experimental Parameter Identification: Receptances

From (7.3.12) and (7.3.69),

$$\hat{R}^{-1} = k[(1-r^2) + i2\xi r] = (k-m\omega^2) + i(c\omega) = \text{dynamic stiffness} \quad (7.3.70)$$

Plots of the real and imaginary parts of \hat{R}^{-1} are shown in Figure 7.3.11.

The upper plot shows $\text{Re}(\hat{R}^{-1})$ versus ω^2 and from (7.3.70) provides the effective mass m as the negative of its slope and effective stiffness k as its intercept. The lower plot shows $\text{Im}(\hat{R}^{-1})$ versus ω and from (7.3.70) provides the effective damping as its slope.

EXAMPLE 7.3.2 *Identification of Effective m, k, and c from Experimental Data*

Objective: This example illustrates how to identify the effective mass, stiffness, and damping of an SDOF system given measured response amplitude and phase angle. The term “effective” is used to indicate that the system may include many stiffnesses, masses, and dampers; however, the system is kinematically constrained so that it behaves as an SDOF. This is illustrated by the “Resonant Vibrator for Compound Potting” mechanism in Example 3.3.1.

Solution: Assume that a system is shaken by an excitation force with

$$A_f = 100\text{N}, \quad \phi_f = 30^\circ = \frac{\pi}{6}\text{rad} \quad (1)$$

$$\Rightarrow A_f e^{i\phi_f} = 100 \left(\cos \frac{\pi}{6} + i \sin \frac{\pi}{6} \right) = 86.6 + i50 \quad (2)$$

The displacement response is given by

$$q(t) = |\tilde{Q}| \cos(\omega t + \angle\tilde{Q}) \quad (3)$$

“Measured” response amplitudes and phase angles are given in Table E7.3.2(a). The complex number (phasor) form of the response is given by

$$\tilde{Q} = |\tilde{Q}| e^{i\angle\tilde{Q}} = |\tilde{Q}| \left(\cos \angle\tilde{Q} + i \sin \angle\tilde{Q} \right) \quad (4)$$

and is listed in Table E7.3.2(b). The dynamic stiffness is the inverse of the receptance and is listed in Table E7.3.2(c).

This data is also plotted in Figure E7.3.2(a). By comparison of Figures 7.3.11 and E7.3.2(a), the intercepts and slope in the upper plot yield

$$k = 5000\text{N/m}, \quad \omega_n^2 = 2500(\text{rad/s})^2, \quad m = 2\text{kg}$$

and the slope in the lower plot yields $c = 20\text{Ns/m}$.

Table E7.3.2(a) “Measured” amplitudes and phase angles

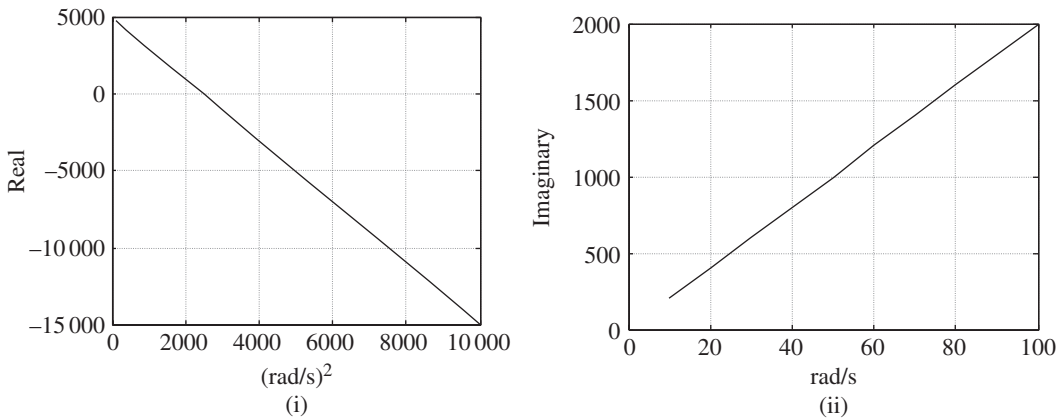
ω (rad/s)	$ \tilde{Q} $ (m)	$\angle\tilde{Q}$ (rad)
10	0.021	0.48
20	0.024	0.43
30	0.031	0.34
40	0.051	0.11
50	0.10	-1.05
60	0.04	-2.11
70	0.02	-2.33
80	0.013	-2.42
90	0.009	-2.46
100	0.007	-2.49

Table E7.3.2(b) “Measured” displacement phasors

$\omega(\text{rad/s})$	\tilde{Q}	$\omega(\text{rad/s})$	\tilde{Q}
10	$0.018 + i0.0096$	60	$-0.021 - i0.034$
20	$0.021 + i0.0099$	70	$-0.014 - i0.014$
30	$0.029 + i0.010$	80	$-0.009 - i0.008$
40	$0.051 + i0.005$	90	$-0.007 - i0.006$
50	$0.05 - i0.087$	100	$-0.005 - i0.004$

Table E7.3.2(c) Inverse receptances

$\omega(\text{rad/s})$	$\text{Re}(\hat{R}^{-1})$	$\text{Im}(\hat{R}^{-1})$	$\omega(\text{rad/s})$	$\text{Re}(\hat{R}^{-1})$	$\text{Im}(\hat{R}^{-1})$
10	4 800	200	60	-2 200	1 200
20	4 200	400	70	-4 800	1 400
30	3 200	600	80	-7 800	1 600
40	1 800	800	90	-11 200	1 800
50	0	1 000	100	-15 000	2 000

**Figure E7.3.2(a)** (i) Real and (ii) imaginary parts of the inverse receptance \hat{R}^{-1} versus ω^2 and ω , respectively

7.3.7 Steady-State Harmonic Response of a Jeffcott Rotor and Rotor Balancing

Figure 7.3.12 shows a spinning shaft/disk system with flexibility of the shaft or of the supporting bearings. This is a simplified model of a class of rotating machines (turbines, fans, motors, and so on), which in most cases have several disks, stepped or tapered shafts, seals, and so on. Therefore, the model in Figure 7.3.12 is presented only to explain some general aspects of rotating machinery vibration response and balancing.

Figure 7.3.12(a) depicts the rigid bearing–shaft bending case where for a uniform shaft that is simply supported the midpoint transverse stiffness is

$$k = \frac{48EI}{L^3} \quad (7.3.71)$$

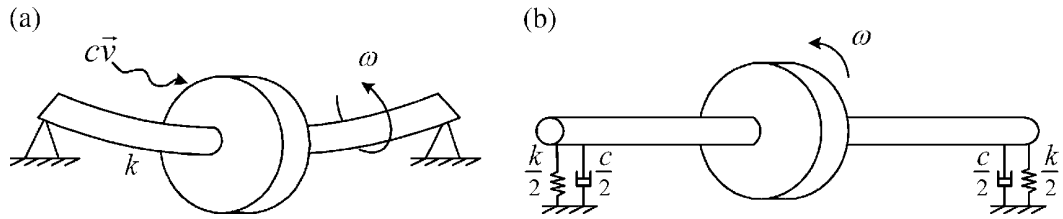


Figure 7.3.12 Simplified “Jeffcott” model of rotating shaft/disk assembly. (a) Flexible shaft and rigid bearings. (b) Flexible bearings and rigid shaft

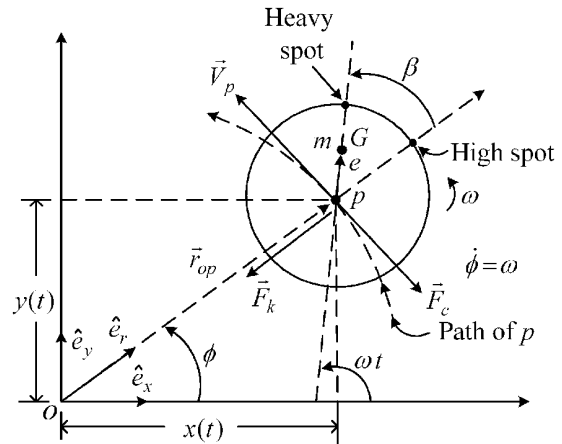


Figure 7.3.13 Free body diagram of the rotor disk

The $c\dot{v}$ term represents a damping force due to vibration of the disk in the surrounding medium.

Figure 7.3.12(b) depicts the case when the bearing supports are considerably softer than the shaft, in which case the rotating element behaves like a rigid body supported on springs and dampers. Figure 7.3.13 shows a free body diagram of the disk for either case in Figure 7.3.12. The spin frequency ω of the shaft is assumed to be constant. The mass center G is shifted away from the spin (geometric) center C by the imbalance eccentricity distance e .

By Newton's law (3.3.5) applied to Figure 7.3.13,

$$m(\ddot{r}_{Op} + \ddot{r}_{Gp}) = \vec{F}_k + \vec{F}_c \quad (7.3.72)$$

or

$$m \left[\ddot{x}\hat{e}_x + \ddot{y}\hat{e}_y + \frac{d^2}{dt^2} (e \cos(\omega t)\hat{e}_x + e \sin(\omega t)\hat{e}_y) \right] = -k\vec{r}_{Op} - c\dot{\vec{r}}_{Op} = -k(x\hat{e}_x + y\hat{e}_y) - c(\dot{x}\hat{e}_x + \dot{y}\hat{e}_y) \quad (7.3.73)$$

The component form of (7.3.73) is

$$m\ddot{x} + c\dot{x} + kx = me\omega^2 \cos(\omega t) \quad (7.3.74)$$

$$m\ddot{y} + c\dot{y} + ky = me\omega^2 \sin(\omega t) \quad (7.3.75)$$

Both (7.3.74) and (7.3.75) have the standard form for an SDOF harmonically excited system

$$m\ddot{q} + c\dot{q} + kq = A_f \cos(\omega t + \phi_f) \quad (7.3.76)$$

where

$$A_f = \omega^2 \hat{A}_f, \quad \hat{A}_f = me, \quad \phi_f = \begin{cases} 0, & x \text{ motion} \\ -\frac{\pi}{2}, & y \text{ motion} \end{cases} \quad (7.3.77)$$

Therefore, the solution in Equations (7.3.34)–(7.3.38) is applicable, that is,

$$|x| = |y| = e \frac{r^2}{\sqrt{(1-r^2)^2 + (2\xi r)^2}} = e |G_{f\omega}| \quad (7.3.78)$$

$$\angle x = -\tan^{-1} \left(\frac{2\xi r}{1-r^2} \right) = \phi_{Gf} \quad (7.3.79)$$

$$\angle y = \angle x - \frac{\pi}{2} = \phi_{Gf} - \frac{\pi}{2} \quad (7.3.80)$$

where $|G_{f\omega}|$ was defined in (7.3.36) and plotted versus ω for various ξ s in Figure 7.3.8 and ϕ_{Gf} was defined in (7.3.29) and plotted versus ω for various ξ s in Figure 7.3.5, and

$$r = \frac{\omega}{\omega_n}, \quad \omega_n = \sqrt{\frac{k}{m}}, \quad \xi = \frac{c}{2m\omega_n} \quad (7.3.81)$$

$$x = |x| \cos(\omega t + \angle x) = e |G_{f\omega}| \cos(\omega t + \phi_{Gf}) \quad (7.3.82)$$

$$y = |y| \cos(\omega t + \angle y) = e |G_{f\omega}| \cos\left(\omega t + \phi_{Gf} - \frac{\pi}{2}\right) \quad (7.3.83)$$

Note from Figure 7.3.13 and Equations (7.3.82) and (7.3.83)

$$|r_{Op}| = \sqrt{x^2 + y^2} = e |G_{f\omega}| \sqrt{\cos^2(\omega t + \phi_{Gf}) + \sin^2(\omega t + \phi_{Gf})} = e |G_{f\omega}| \quad (7.3.84)$$

which shows that the “whirl” or “orbit” radius of point p in Figure 7.3.13 is constant, so that the orbit of p is a circle about its undeflected position O . The orbit radius is

$$|r_{Op}| = (\text{imbalance eccentricity distance}) * (\text{factor plotted in Figure 7.3.8}) \quad (7.3.85)$$

Asymptotic values of the amplitude and phase angle are given in Table 7.3.3 based on (7.3.78)–(7.3.85).

The “amplification” or “quality” factor Q (7.3.54) may be experimentally measured from (7.3.78) as

$$AF = Q = \frac{1}{2\xi} = \frac{|x|_{\omega=\omega_n}}{|x|_{\omega=\infty}} = \frac{|y|_{\omega=\omega_n}}{|y|_{\omega=\infty}} \quad (7.3.86)$$

Table 7.3.3 Asymptotic values of rotor amplitude and phase angle

$\lim_{\omega \rightarrow (\cdot)}$	$ x , y , r_{Op} $	$\angle x$	$\angle y$
0	0	0	-90°
∞	e	-180°	-270°
ω_n	$e/(2\xi)$	-90°	-180°

Table 7.3.4 Asymptotic values of heavy spot angle β

$\lim_{\omega \rightarrow 0}$	β
0	0
ω_n	90°
∞	180°

API standards specify restrictions on AF in terms of separation margins between operating speed ranges and natural frequencies (resonances). The whirl rate of point p along its circular orbit is obtained from Figure 7.3.13 by

$$\begin{aligned}
 \dot{\phi} &= \frac{d}{dt} \left(\tan^{-1} \left(\frac{y}{x} \right) \right) = \frac{1}{1 + (y/x)^2} \frac{d}{dt} \left(\frac{y}{x} \right) = \frac{1}{1 + y^2/x^2} \frac{x\dot{y} - y\dot{x}}{x^2} \\
 &= \frac{1}{x^2 + y^2} (x\dot{y} - y\dot{x}) = \frac{1}{r_{Op}^2} (x\dot{y} - y\dot{x}) \\
 &= \frac{1}{e^2 |G_{f\omega}|^2} e^2 |G_{f\omega}|^2 [\cos(\omega t + \phi_{Gf}) \omega \cos(\omega t + \phi_{Gf}) \\
 &\quad + \omega \sin(\omega t + \phi_{Gf}) \sin(\omega t + \phi_{Gf})] \\
 &= \omega
 \end{aligned} \tag{7.3.87}$$

Therefore, the whirl direction is positive (ccw), and the whirl (vibration) frequency is equal to the shaft spinning frequency. This type of vibration motion is referred to as “forward, circular, synchronous” whirl of the shaft/disk assembly. Note from Figure 7.3.13 and Equations (7.3.82), (7.3.83), and (7.3.29)

$$\begin{aligned}
 \beta &= \omega t - \phi = \omega t - \tan^{-1} \left(\frac{y}{x} \right) = \omega t - \tan^{-1} \left(\frac{e |G_{f\omega}| \sin(\omega t + \phi_{Gf})}{e |G_{f\omega}| \cos(\omega t + \phi_{Gf})} \right) \\
 &= \omega t - (\omega t + \phi_{Gf}) = -\phi_{Gf} = \tan^{-1} \left(\frac{2\xi r}{1 - r^2} \right)
 \end{aligned} \tag{7.3.88}$$

The angle β is constant in time and is the angle that the heavy spot leads (in the direction of rotation) the high spot in Figure 7.3.13. Limiting values of β are shown in Table 7.3.4.

The high spot location can be identified (although for safety reasons this is not recommended) by carefully advancing a piece of chalk into the spinning disk in the radial direction, so that it lightly contacts it. The resulting white mark is the high spot location.

By Table 7.3.4 for $\omega \ll \omega_n$, the heavy spot will also be near the white mark so place a balance weight opposite the white chalk mark on the disk. By Table 7.3.4 for $\omega \gg \omega_n$, the heavy spot will be opposite the white mark so place a balance weight on the white mark. Note from (7.3.78)

$$e = |x|_{\omega \rightarrow \infty} \quad (7.3.89)$$

The correction mass m_C required to balance e perfectly in Figure 7.3.13 must satisfy

$$m_C R_C = me \quad (7.3.90)$$

where R_C is its attachment point radius.

7.3.8 Single Plane Influence Coefficient Balancing

The preceding balancing method utilizes the knowledge of the asymptotic relations for the angle between the high spot and heavy spot. A more effective approach that only assumes linearity and does not require the knowledge of phase angle asymptotic relationships is referred to in industry as “influence coefficient” balancing. As the name implies, the strategy is to first determine the influence of attaching a known imbalance (trial weight) on the vibration and then to utilize that information to calculate “correction” weights that act to zero or minimize the vibration at specific sensors and speeds. To analyze this approach, first consider attaching a “trial” mass m_T at an angle ψ_T from some arbitrary reference direction on the disk, as shown in Figure 7.3.14.

The new location of the mass center is

$$\vec{r}_{G,\text{new}} = \frac{m\vec{r}_{GP} + m_T\vec{r}_{TP}}{m_T + m} + \vec{r}_{Op} \quad (7.3.91)$$

Newton’s law (3.3.5) in the x direction is

$$(m_T + m) \frac{d^2}{dt^2} \left(x + \frac{m}{m_T + m} e \cos(\omega t + \psi_G) + \frac{m_T}{m_T + m} R_T \cos(\omega t + \psi_G) \right) = -kx - c\dot{x} \quad (7.3.92)$$

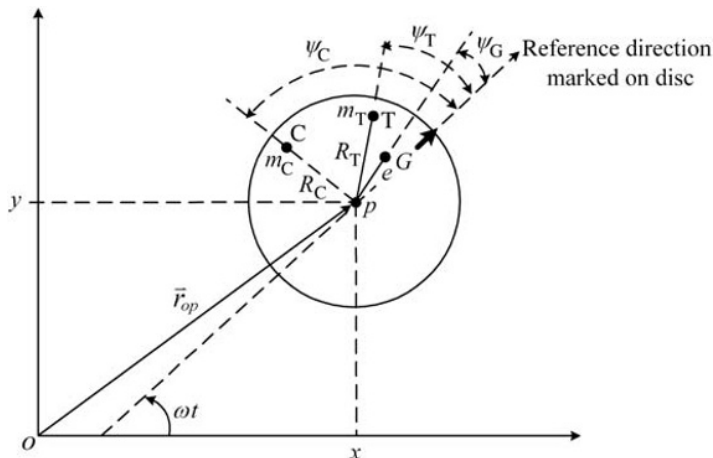


Figure 7.3.14 Disk with trial weight “T” attached

Assume

$$m_T \ll m \quad (7.3.93)$$

Equation (7.3.92) then becomes

$$m\ddot{x} + c\dot{x} + kx = me\omega^2 \cos(\omega t + \psi_G) + m_T R_T \omega^2 \cos(\omega t + \psi_T) \quad (7.3.94)$$

Following the complex variable approach (Section 7.2), make the following substitutions:

$$x \Rightarrow \tilde{x}_T e^{i\omega t} \quad (7.3.95)$$

$$\cos(\omega t + \psi) \Rightarrow e^{i(\omega t + \psi)} = e^{i\omega t} e^{i\psi} \quad (7.3.96)$$

so that Equation (7.3.94) yields

$$\tilde{x}_T = \alpha (me e^{i\psi_G} + m_T R_T e^{i\psi_T}) \quad (7.3.97)$$

where

$$\alpha = \text{“influence coefficient”} = \frac{\omega^2}{k - m\omega^2 + ic\omega} \quad (7.3.98)$$

The phasor response before the trial weight was attached is obtained by setting $m_T = 0$ in (7.3.97):

$$\tilde{x}_B = \alpha me e^{i\psi_G} \quad (7.3.99)$$

Then the influence coefficient can be experimentally measured from (7.3.97) and (7.3.99):

$$\alpha = \frac{\tilde{x}_T - \tilde{x}_B}{m_T R_T e^{i\psi_T}} \quad (7.3.100)$$

The experimental procedure is to record the trial weight location (R_T, ψ_T) and mass m_T and then to measure the amplitudes and phase angles before and after adding the trial weight, that is,

$$\tilde{x}_B = |\tilde{x}_B| e^{i\phi_{BX}}, \quad \tilde{x}_T = |\tilde{x}_T| e^{i\phi_{TX}} \quad (7.3.101)$$

Finally, α is calculated from (7.3.100). The complex response due to removing the trial weight and adding the correction weight is obtained from (7.3.97) by replacing “T” by “C”:

$$\tilde{x}_C = \alpha (me e^{i\psi_G} + m_C R_C e^{i\psi_C}) \quad (7.3.102)$$

Substitution of (7.3.99) into (7.3.102) yields

$$\tilde{x}_C = \tilde{x}_B + \alpha m_C R_C e^{i\psi_C} \quad (7.3.103)$$

The balance condition is to make the vibration become zero due to the correction weight

$$\tilde{x}_C = 0 \quad (7.3.104)$$

from which the correction weight mass and angle are determined

$$m_C R_C e^{i\psi_C} = -\frac{\tilde{x}_B}{\alpha} \quad (7.3.105)$$

therefore,

$$m_C R_C = \left| \frac{\tilde{x}_B}{\alpha} \right| = \text{correction imbalance magnitude} \quad (7.3.106)$$

$$\psi_C = \angle \left(-\frac{\tilde{x}_B}{\alpha} \right) = \text{correction imbalance phase angle}$$

The influence coefficient balancing method does not require values for m , k , c or the value of spin speed ω relative to ω_n as in Table 7.3.4. The only requirements are that the system acts linearly, the trial mass m_T is relatively small, and the responses (\tilde{x}_B, \tilde{x}_T) need to be measured. The interested reader will find an excellent discussion of influence coefficient and other rotor balancing methods in Barlow (1989).

7.3.9 Related American Petroleum Institute Standards for Balancing

The physics, math, and logic of vibration studies are intellectually rewarding and have very practical applications. An example of the latter benefit is illustrated by vibration standards. The following contains some examples related to balancing in the API standards. *The latest versions of the standards should always be consulted for use in actual applications, since they are updated as related knowledge improves.*

7.3.9.1 Allowable Imbalance

- All disks should be balanced as isolated components prior to assembly on the shaft.
- The fully assembled shaft should be multiplane balanced, and the maximum allowable final correction weights should be less than

$$U_{\max} = \beta * W \quad (7.3.107)$$

where W is journal bearing static weight in lb (typically the total weight of the rotor) and β is a small number (specified in the standard) that decreases with rotor speed.

- During the shop test of the machine...the peak-to-peak amplitude of unfiltered vibration in any plane, measured on the shaft adjacent and relative to each radial bearing, shall not exceed the following value or 0.002 in. (2 mils), whichever is less

$$A = \sqrt{\frac{12000}{\text{RPM}}} \text{ mils, peak to peak} \quad (7.3.108)$$

where one mil equals 25.4×10^{-6} m.

7.3.9.2 Damped Imbalance Response Simulation

The API standards also provide recommendations for the amounts, locations, and relative phase angles of unbalances included in dynamic response simulations of the rotor-bearing

systems. These are conservative (large) values of unbalance for which the simulated (predicted) responses must be less than specified requirements.

7.3.10 Response of an SDOF Oscillator to Nonsinusoidal, Periodic Excitation

Nature and industrial machinery provide many examples of vibrating system that are excited periodically in a nonsinusoidal manner, such as:

- A jack hammer pounding pavement
- Pile driver installing a pile rod
- Waves impinging on an offshore structure
- A rotating turbine blade striking jets of gas or steam flowing through a row of stator vanes
- Discharge pressure from a reciprocating compressor impinging on elbows and valves along the attached piping
- A drum skin during a “roll”
- Equipment with indexing mechanisms
- Bearing reactions in a reciprocating internal combustion engine
- Flooring in an aerobics (exercise) room
- A vehicle traversing expansion joint slats along a highway
- Gears meshing
- And so on

The response of the related systems is obtained by expressing the nonsinusoidal, periodic excitation as a sum of sinusoidal terms via the theory of Fourier series (Section 2.9). This approach represents the periodic excitation as an infinite (in practice truncated with a finite number of terms) sum of sinusoidal excitations with frequencies at integer harmonics (multiples) of a fundamental frequency. Destructive resonance may occur if any harmonic frequency coincides with a natural frequency, especially when the damping is low and if the amplitude of the excitation harmonic is large. The Fourier series approach provides the amplitude of each harmonic. The author is familiar from his industrial work experience with an incident of repeated high-cycle fatigue failure of piping connected to a gas compressor on an offshore platform. The fundamental frequency was the crankshaft rotation frequency and resonance resulted from coincidence of the 32nd harmonic and a piping system natural frequency. Pressure pulsations occurring in the piping system at this harmonic were strong enough to eventually crack the piping, resulting in the very dangerous situation of leaking high-pressure, explosive gas.

Consider an SDOF system that is subjected to a periodic, nonsinusoidal excitation:

$$m\ddot{q} + c\dot{q} + kq = \sum_{j=1}^{\infty} f_j(t) \quad (7.3.109)$$

where

$$f_0 = \frac{A_0}{2} \quad (7.3.110)$$

$$f_j = C_j \cos(j\omega t - \phi_j), \quad j = 1, 2, \dots, \infty \quad (7.3.111)$$

Let q_j be the response to f_j for $j = 1, 2, \dots, \infty$, that is,

$$m\ddot{q}_j + c\dot{q}_j + kq_j = f_j \quad (7.3.112)$$

Sum equation (7.3.112) over all j

$$\sum_{j=0}^{\infty} (m\ddot{q}_j + c\dot{q}_j + kq_j) = \sum_{j=0}^{\infty} f_j \quad (7.3.113)$$

$$\Rightarrow m \left(\sum_{j=0}^{\infty} \ddot{q}_j \right) + c \left(\sum_{j=0}^{\infty} \dot{q}_j \right) + k \left(\sum_{j=0}^{\infty} q_j \right) = \sum_{j=0}^{\infty} f_j \quad (7.3.114)$$

Comparison of (7.3.109) and (7.3.114) shows that if q_j is defined in (7.3.112), that is, if q_j is the response to f_j , then the total response q equals

$$q = \sum_{j=0}^{\infty} q_j(t) \quad (7.3.115)$$

since both q and $\sum_{j=0}^{\infty} q_j$ satisfy the same governing differential equation. This is known as the superposition principle, and it applies to all linear systems. Substitute (7.3.111) into (7.3.112):

$$m\ddot{q}_j + c\dot{q}_j + kq_j = C_j \cos(j\omega t - \phi_j) \quad (7.3.116)$$

where ω is the fundamental forcing frequency. It has been previously shown (7.3.11)–(7.3.14) that the steady-state response for this equation is

$$q_j(t) = \frac{C_j/k}{\sqrt{(1-r_j^2)^2 + (2\xi r_j)^2}} \cos(j\omega t - \phi_j - \beta_j) \quad (7.3.117)$$

where

$$r_j = \frac{j\omega}{\omega_n}, \quad \beta_j = \tan^{-1} \left(\frac{2\xi r_j}{1-r_j^2} \right), \quad \omega_n = \sqrt{\frac{k}{m}}, \quad \xi = \frac{c}{2m\omega_n} \quad (7.3.118)$$

By (7.3.115), the total SSHR becomes

$$q(t) \Big|_{\text{steady state}} = \frac{A_0}{2k} + \frac{1}{k} \sum_{j=1}^{\infty} \frac{C_j \cos(j\omega t - \phi_j - \beta_j)}{\sqrt{(1-r_j^2)^2 + (2\xi r_j)^2}} \quad (7.3.119)$$

Note from (7.3.119) that for lightly damped systems, resonance will occur if any harmonic $j\omega$ of the fundamental frequency ω equals ω_n since

$$r_j = 1 \Rightarrow j\omega = \omega_n \Rightarrow \omega = \frac{\omega_n}{j} \quad (7.3.120)$$

EXAMPLE 7.3.3 *Single Degree of Freedom Oscillator with Sawtooth Pattern Force*

Objective: The objective of this example is to illustrate the use of Fourier series to derive the response of a SDOF system to a periodic, nonsinusoidal excitation and then to show how resonance can occur due to coincidence between the natural frequency and a higher harmonic of the fundamental frequency. Figure E7.3.3(a) depicts an equivalent $m-k-c$ system with a periodic “sawtooth” excitation.

For this example, it is helpful to utilize the alternative form of the Fourier series formulas

$$f(t) = \frac{A_0}{2} + \sum_{n=1}^{\infty} A_n \cos\left(\frac{n2\pi t}{T}\right) + B_n \sin\left(\frac{n2\pi t}{T}\right) = \frac{A_0}{2} + \sum_{n=1}^{\infty} C_n \cos\left(\frac{n2\pi t}{T} - \phi_n\right) \quad (1)$$

$$C_n = \sqrt{A_n^2 + B_n^2}, \quad \phi_n = \tan^{-1}\left(\frac{B_n}{A_n}\right) \quad (2)$$

$$A_0 = \frac{2}{T} \int_{-T/2}^{T/2} f(t) dt, \quad A_n = \frac{2}{T} \int_{-T/2}^{T/2} f(t) \cos\left(\frac{2n\pi t}{T}\right) dt, \quad B_n = \frac{2}{T} \int_{-T/2}^{T/2} f(t) \sin\left(\frac{2n\pi t}{T}\right) dt \quad (3)$$

For this example,

$$f(t) = 2F \frac{t}{T}, \quad -\frac{T}{2} < t < \frac{T}{2} \quad (4)$$

Consideration of the area under the curve for $f(t)$ shows

$$A_0 = 0 \quad (5)$$

The remaining integrals become

$$A_n = \frac{2}{T} \int_{-T/2}^{T/2} 2F \frac{t}{T} \cos\left(\frac{2n\pi t}{T}\right) dt = \frac{4F}{T^2} \left[\left(\frac{T}{2n\pi}\right)^2 \cos\left(\frac{2n\pi t}{T}\right) + \left(\frac{T}{2n\pi}\right) t \sin\left(\frac{2n\pi t}{T}\right) \right]_{-T/2}^{T/2} = 0 \quad (6)$$

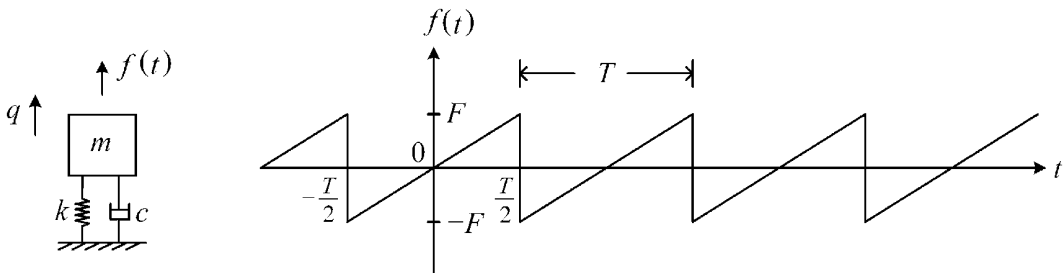


Figure E7.3.3(a) Damped single degree of freedom oscillator and external force $f(t)$

$$\begin{aligned}
 B_n &= \frac{2}{T} \int_{-T/2}^{T/2} 2F \frac{t}{T} \sin\left(\frac{2n\pi t}{T}\right) dt = \frac{4F}{T^2} \left[\left(\frac{T}{2n\pi}\right)^2 \sin\left(\frac{2n\pi t}{T}\right) - t \left(\frac{T}{2n\pi}\right) \cos\left(\frac{2n\pi t}{T}\right) \right]_{-T/2}^{T/2} \\
 &= \frac{4F}{T^2} \left(\frac{-T^2}{4n\pi}\right) (\cos n\pi + \sin(-n\pi)) = \frac{-F}{n\pi} 2 \cos n\pi = -\frac{2F}{n\pi} (-1)^n = \frac{2F}{n\pi} (-1)^{n+1}
 \end{aligned} \tag{7}$$

Substituting (7) into (1) yields

$$f(t) = \frac{2F}{\pi} \sum_{n=1}^{\infty} \frac{(-1)^{n+1}}{n} \sin\left(\frac{2n\pi t}{T}\right) \tag{8}$$

From (2), (6), and (7),

$$C_n = \sqrt{0^2 + \left[\frac{2F}{n\pi} (-1)^{n+1}\right]^2} = \frac{2F}{n\pi}, \quad \phi_n = \tan^{-1}\left(\frac{\frac{2F}{n\pi} (-1)^{n+1}}{0}\right) = \begin{cases} 90^\circ, & n \text{ odd} \\ -90^\circ, & n \text{ even} \end{cases}, \quad A_0 = 0 \tag{9}$$

The steady-state response as obtained from (7.3.119) and (9) is

$$q(t) \Big|_{\text{state}}^{\text{steady}} = \frac{1}{k} * \frac{2F}{\pi} * \sum_{j=1}^{\infty} \frac{\cos(j\omega t - \phi_j - \beta_j)}{j * \sqrt{(1-r_j^2)^2 + (2\xi r_j)^2}} \tag{10}$$

where

$$\frac{F}{k} = \delta_{sT} = \text{static deflection}, \quad r_j = \frac{j\omega}{\omega_n} = jr, \quad \phi_j = \begin{cases} 90^\circ, & j \text{ odd} \\ -90^\circ, & j \text{ even} \end{cases}, \quad \beta_j = \tan^{-1}\left(\frac{2\xi r_j}{1-r_j^2}\right) \tag{11}$$

and

$$\omega = \frac{2\pi}{T} \Rightarrow r_j = \frac{j2\pi}{\omega_n T} \quad \text{and} \quad \omega t = \frac{2\pi}{T} t \tag{12}$$

Consider plots of the response for the condition $\xi = 0.05$, $F = 1$, and $k = 1$.

The fundamental (first) harmonic frequency of the excitation is first set to 10 times the natural frequency

$$\omega_n T = \frac{2\pi}{T_n} T = 0.2\pi \Rightarrow T = \frac{1}{10} T_n \Rightarrow \omega = 10\omega_n, \quad r = 10 \tag{13}$$

Figure E7.3.3(b)-(i) shows that the mass motion is dominated by the first harmonic response since ω is much higher than ω_n . From (10), the first harmonic response amplitude is

$$\text{First harmonic response} = \frac{2F/(k\pi)}{\sqrt{(1-r^2)^2 + (2\xi r)^2}} = 0.0064 \tag{14}$$

This amplitude is very small since $\omega \gg \omega_n$ and the response in (10) is converged with only eight harmonics. The fundamental (first) harmonic frequency of the excitation is next set equal to the natural frequency

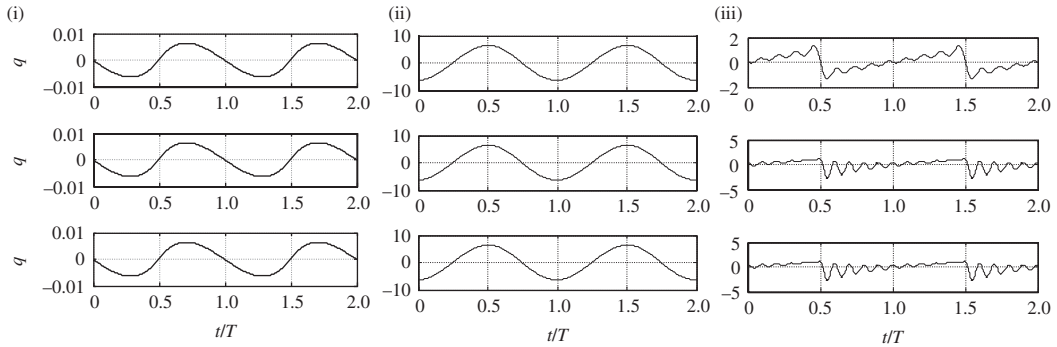


Figure E7.3.3(b) Displacement of mass m versus t/T , utilizing 8 (top), 16 (middle), and 32 (bottom) harmonics for (i) $\omega = 10\omega_n$, (ii) $\omega = \omega_n$, and (iii) $\omega = \omega_n/10$

$$\omega_n T = 2\pi \Rightarrow T = T_n \Rightarrow \omega = \omega_n, \quad r = 1 \quad (15)$$

Referring to Figure E7.3.3(b)-(ii), the first harmonic, which has the largest force amplitude by (9), is at resonance ($\omega = \omega_n$) so the amplitude is very large and dominated by the first harmonic. From (10) and (14), the first harmonic response amplitude is 6.36. The response in (10) is converged with only eight harmonics. The fundamental (first) harmonic frequency of the excitation is finally equal to 1/10 of the natural frequency

$$\omega_n T = 20\pi \Rightarrow T = 10T_n \Rightarrow \omega = \frac{\omega_n}{10}, \quad r = \frac{1}{10} \quad (16)$$

From (10) and (14), the first harmonic response amplitude is 0.643. The response in (10) is converged with only 16 harmonics. Referring to Figure E7.3.3(b)-(iii), the 10th harmonic is at resonance ($10 * \omega = \omega_n$) so the 10th harmonic dominates the response.

7.3.11 Forced Harmonic Response with Elastomeric Stiffness and Damping

Elastomeric damping devices are typically inserted in machinery and structures to suppress vibration under resonance conditions. For example, a spinning shaft may be supported by ball bearings, which are themselves mounted on elastomeric O rings. Measured damping in elastomerics is typically expressed in terms of a “loss factor,” γ , which is defined in the following manner.

Consider an SDOF oscillator with sinusoidal excitation

$$m\ddot{q} + c\dot{q} + kq = F_0 \cos(\omega t) \quad (7.3.121)$$

The real part of

$$m\ddot{z} + c\dot{z} + kz = F_0 e^{i\omega t} \quad (7.3.122)$$

is identical to Equation (7.3.121) with

$$z = q + iy \quad (7.3.123)$$

so (7.3.121) may be solved by solving (7.3.122) for z and obtaining $q(t)$ from

$$q(t) = \text{Re}(z(t)) \quad (7.3.124)$$

To solve (7.3.122), let

$$z = \tilde{z}e^{i\omega t} \quad (7.3.125)$$

then (7.3.122) becomes

$$(-\omega^2 m + i\omega c + k)\tilde{z} = F_0 \quad (7.3.126)$$

or

$$(-\omega^2 m + k(1 + i\gamma))\tilde{z} = F_0 \quad (7.3.127)$$

where

$$\gamma = \frac{\omega c}{k} \quad (7.3.128)$$

is referred to as a loss factor. From (7.3.12),

$$\xi = \frac{c\omega_n}{2k} = \frac{\gamma\omega_n}{2\omega} \quad (7.3.129)$$

This shows that the loss factor is proportional to the damping ratio, and at resonance

$$\xi = \frac{\gamma}{2}, \quad \text{for } \omega = \omega_n \quad (7.3.130)$$

The response amplitude is obtained by substituting (7.3.128) into (7.3.11):

$$|q| = \frac{F_0}{\sqrt{(k - m\omega^2)^2 + (k\gamma)^2}} \quad (7.3.131)$$

The stiffness and loss factor are vibration frequency dependent as shown for a particular *O* ring in Figure 7.3.15, which is obtained from Darlow et al. (1979). The particular *O* ring has the following properties:

Material, Viton-70; cross-sectional diameter, 1/8 in. (0.353 cm); temperature, 25°C; stretch, 5%; amplitude of motion, 7.62×10^{-6} m; groove width, 135%; and squeeze, 15%.

The figure is a plot of the experimentally determined regression curve fits

$$\begin{aligned} k_{\text{O ring}} &= a_1 (2\pi f_{\text{Hz}})^{b_1} \text{ N/m} \\ \gamma_{\text{O ring}} &= a_2 (2\pi f_{\text{Hz}})^{b_2} \text{ (dim)} \end{aligned} \quad (7.3.132)$$

where for the plots in Figure 7.3.15

$$a_1 = 3.8 \times 10^5, \quad b_1 = 0.400 \quad (7.3.133)$$

$$a_2 = 0.329, \quad b_2 = 0.144 \quad (7.3.134)$$

For illustration, (7.3.132) yields the results in Table 7.3.5 at 100 and 800 Hz.

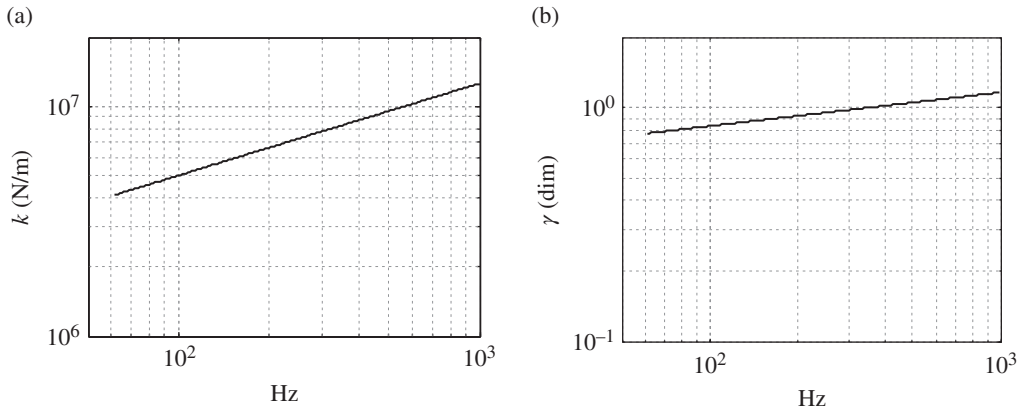


Figure 7.3.15 (a) *O* ring stiffness in N/m and (b) loss factor (dim) versus excitation frequency (Hz)

Table 7.3.5 *O* ring stiffness and loss factor at 10 and 800 Hz

f (Hz)	k (N/m)	γ	ξ at resonance = $\gamma/2$
100	5×10^6	0.83	0.42
800	11.5×10^6	1.12	0.56

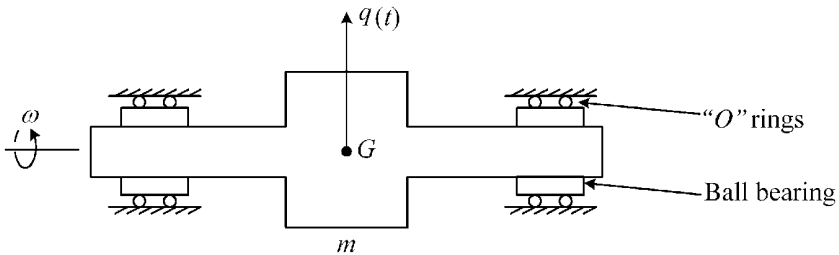


Figure E7.3.4(a) Rigid rotor supported on *O* rings and executing parallel motion

EXAMPLE 7.3.4 Rigid Spinning Shaft Mounted on Two Ball Bearings with *O* Rings

Objective: Determine the resonance frequency with a frequency-dependent *O* ring stiffness support.

Description: The shaft shown in Figure E7.3.4(a) has two bearings mounted on four elastomeric *O* rings. The shaft is assumed to be rigid and only to oscillate in a parallel (both ends have same amplitude and phase) manner for the frequency range considered.

The equilibrium equation for translational motion is

$$m\ddot{x} + 4c\dot{x} + 4kx = me\omega^2 \cos(\omega t) \quad (1)$$

where e is the eccentricity of the shaft's mass center from its geometric (spin) center.

Resonance occurs when $\omega \approx \omega_n$, where

$$\omega_n^2 = \frac{4k(\omega)}{m} \quad (2)$$

Therefore, from (7.3.132) and (2), resonance will occur if

$$\omega^2 \approx \frac{4k(\omega)}{m} = \frac{4}{m} a_1 \omega^{b_1} \quad (3)$$

$$\Rightarrow \omega = \left(\frac{4a_1}{m} \right)^{\frac{1}{2-b_1}} \quad (4)$$

The resonance rpm (critical speed) is approximately

$$\text{Resonance RPM} \approx 60 \frac{\omega_{\text{res}}}{2\pi} = \frac{60}{2\pi} \left(\frac{4a_1}{m} \right)^{\frac{1}{2-b_1}} \quad (5)$$

To illustrate, let

$$\begin{aligned} m &= 200 \text{ kg}, \quad a_1 = 3.8 \times 10^5, \quad b_1 = 0.40 \\ \Rightarrow \text{Resonance RPM} &= 2500 \text{ rpm} (= 42 \text{ Hz}) \end{aligned} \quad (6)$$

This resonance will be well damped since by (7.3.130)

$$\xi = \frac{\gamma}{2} = \frac{1}{2} a_2 (2\pi f)^{b_2} = \frac{1}{2} (0.329)(2\pi * 42)^{0.144} = 0.37 \text{ (at resonance)} \quad (7)$$

which should provide a “smooth” traversal of the critical speed.

7.4 TWO DEGREE OF FREEDOM RESPONSE

Similar with free vibration response, analytic solutions are obtainable for 2 degree of freedom (2dof), steady-state forced harmonic response problems. A generic 2dof harmonically forced system is described by

$$\underline{M}\ddot{\underline{q}} + \underline{C}_T\dot{\underline{q}} + \underline{K}_T\underline{q} = \underline{f}(t) \quad 2 \times 1 \quad (7.4.1)$$

where

$$\begin{aligned} \underline{M} &= \begin{bmatrix} m_{11} & m_{12} \\ m_{21} & m_{22} \end{bmatrix}, \quad \underline{C}_T = \begin{bmatrix} c_{11} & c_{12} \\ c_{21} & c_{22} \end{bmatrix}, \quad \underline{K}_T = \begin{bmatrix} k_{11} & k_{12} \\ k_{21} & k_{22} \end{bmatrix} \\ \underline{q} &= \begin{Bmatrix} q_1 \\ q_2 \end{Bmatrix}, \quad \underline{f}(t) = \begin{Bmatrix} A_{f1} \cos(\omega t + \phi_{f1}) \\ A_{f2} \cos(\omega t + \phi_{f2}) \end{Bmatrix} \end{aligned} \quad (7.4.2)$$

The complex variable representation of this system is from (7.2.7):

$$\underline{M}\ddot{\underline{Q}} + \underline{C}_T\dot{\underline{Q}} + \underline{K}_T\underline{Q} = \tilde{\underline{F}}e^{i\omega t} \quad (7.4.3)$$

where from (7.2.5),

$$\tilde{\underline{F}} = \begin{Bmatrix} A_{f1}e^{i\phi_{f1}} \\ A_{f2}e^{i\phi_{f2}} \end{Bmatrix} \quad (7.4.4)$$

Let

$$\underline{\underline{Q}}(t) = \underline{\underline{Q}}e^{i\omega t} \quad (7.4.5)$$

to obtain

$$\begin{bmatrix} -\omega^2 m_{11} + i\omega c_{11} + k_{11} & -\omega^2 m_{12} + i\omega c_{12} + k_{12} \\ -\omega^2 m_{21} + i\omega c_{21} + k_{21} & -\omega^2 m_{22} + i\omega c_{22} + k_{22} \end{bmatrix} \begin{Bmatrix} \tilde{Q}_1 \\ \tilde{Q}_2 \end{Bmatrix} = \begin{Bmatrix} A_{f1}e^{i\phi_{f1}} \\ A_{f2}e^{i\phi_{f2}} \end{Bmatrix} \quad (7.4.6)$$

Define $\Delta(\omega)$ as being the determinant of the coefficient matrix in (7.4.6), and then by Cramer's rule

$$\begin{aligned} \tilde{Q}_1 &= \frac{[A_{f1}e^{i\phi_{f1}}(-\omega^2 m_{22} + i\omega c_{22} + k_{22}) - A_{f2}e^{i\phi_{f2}}(-\omega^2 m_{12} + i\omega c_{12} + k_{12})]}{\Delta} \\ \tilde{Q}_2 &= \frac{[-A_{f1}e^{i\phi_{f1}}(-\omega^2 m_{21} + i\omega c_{21} + k_{21}) + A_{f2}e^{i\phi_{f2}}(-\omega^2 m_{11} + i\omega c_{11} + k_{11})]}{\Delta} \end{aligned} \quad (7.4.7)$$

The actual steady-state solution is given by (7.2.14) as

$$q_j(t) = \text{real}(Q_j(t)) = \text{real}\left(|\tilde{Q}_j|e^{i\phi_{qj}}e^{i\omega t}\right) = |\tilde{Q}_j|\cos(\omega t + \phi_{qj}) \quad \text{for } j = 1, 2 \quad (7.4.8)$$

7.4.1 Vibration Absorber: Principles

Vibration absorbers employ an appendage mass to absorb the vibratory energy and thus reduce the vibration of the primary mass, which is typically a machine or stationary, or rotating, structure. Suppose that a “vibration absorber” mass m_{22} is attached to the primary mass m_{11} causing its motion $q_1(t)$ to become zero, which by (7.4.8) will occur if $|\tilde{Q}_1| = 0$. Since there is no external force ($A_{f2} = 0$) on the absorber mass, Equation (7.4.7) simplifies to

$$|\tilde{Q}_1| = \frac{|A_{f1}||-\omega^2 m_{22} + i\omega c_{22} + k_{22}|}{|\Delta|} = 0 \quad (7.4.9)$$

Thus, $|\tilde{Q}_1| = 0$ if

$$(k_{22} - \omega^2 m_{22})^2 + (\omega c_{22})^2 = 0 \quad (7.4.10)$$

and then the upper row in (7.4.6) yields

$$\tilde{Q}_2 = \frac{A_{f1}e^{i\phi_{f1}}}{-\omega^2 m_{12} + i\omega c_{12} + k_{12}} \quad (7.4.11)$$

or

$$|\tilde{Q}_2| = \frac{A_{f1}}{\sqrt{(k_{12} - \omega^2 m_{12})^2 + (\omega c_{12})^2}} \quad (7.4.12)$$

Equations (7.4.10) and (7.4.12) provide two equations to design the absorber's mass and stiffness based on (i) stopping the vibration of the primary mass and (ii) limiting the vibration amplitude of the absorber mass to the value $|\tilde{Q}_2|$ specified (7.4.12), at a specific forcing frequency ω .

EXAMPLE 7.4.1 Pump Vibration Control via Vibration Absorber

Statement: The vibration level is measured on a bearing housing of a pump (m_1) to be 2 mm/s 0-peak velocity. Further testing indicates that although the balance of the shaft is acceptable, the shaft speed is near a natural frequency. This phenomenon is referred to as a critical speed resonance and presents a significant challenge for designers of rotating machinery. It is decided to weld a beam (k_2) and end mass (m_2) to the pump to act as a vibration absorber. The imbalance force amplitude (A_{f1}) equals 10 N at the pump spin rate of 3000 rpm.

Objective: Determine the beam stiffness (k_2) and end mass (m_2) values that will stop the pump's vibration and will limit the absorber's amplitude to 0.05 mm when the pump operates at 3000 rpm.

Assumptions:

- (a) The damping of the beam and mass is negligible.
- (b) The pump housing undergoes only pure translational motion.

Solution:

- (a) The model of the pump is shown in Figure E7.4.1(a).
- (b) Newton's law yields the following matrices for this model:

$$\underline{M} = \begin{bmatrix} m_1 & 0 \\ 0 & m_2 \end{bmatrix}, \quad \underline{C}_T = \begin{bmatrix} c_1 & 0 \\ 0 & 0 \end{bmatrix}, \quad \underline{K}_T = \begin{bmatrix} k_1 + k_2 & -k_2 \\ -k_2 & k_2 \end{bmatrix} \quad (1)$$

$$\underline{q} = \begin{Bmatrix} q_1 \\ q_2 \end{Bmatrix}, \quad \underline{f}(t) = \begin{Bmatrix} f_1(t) \\ f_2(t) \end{Bmatrix} = \begin{Bmatrix} A_{f1} \cos(\omega t) \\ 0 \end{Bmatrix}$$

comparison of (7.4.2) and (1) shows that

$$\begin{aligned} m_{11} &= m_1, & m_{22} &= m_2, & m_{12} &= 0 \\ k_{11} &= k_1 + k_2, & k_{12} &= k_{21} = -k_2, & k_{22} &= k_2 \\ c_{11} &= c_1, & c_{12} &= c_{21} = 0, & c_{22} &= 0 \\ \phi_{f1} &= \phi_{f2} = 0, & A_{f2} &= 0 \end{aligned} \quad (2)$$

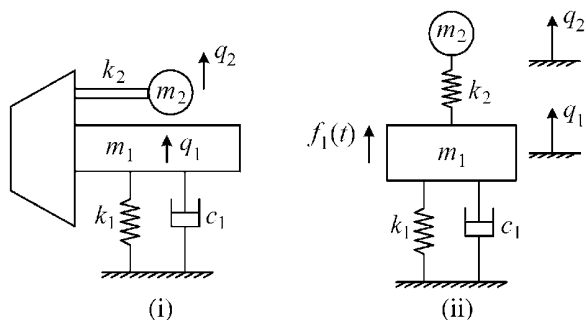


Figure E7.4.1(a) Pump with vibration absorber (i) and equivalent system model (ii)

(c) The equations for selecting m_2 and k_2 , that is, (7.4.10) and (7.4.12), then become

$$k_2 - \omega^2 m_2 = 0 \quad (3)$$

and

$$|q_2| = |\tilde{Q}_2| = \frac{A_{f1}}{k_2} \quad (4)$$

The equations for determining m_2 and k_2 become

$$k_2 = \frac{A_{f1}}{|q_2|}, \quad m_2 = \frac{k_2}{\omega^2} \quad (5)$$

(d) The numerical values for this problem are as follows:

$$A_{f1} = 10\text{N}, \quad |q_2| = 0.05 \times 10^{-3}\text{m}, \quad \omega = 2\pi f = 2\pi \frac{3000}{60} = 314\text{rad/s} \quad (6)$$

(e) Solving for the required beam stiffness and absorber mass from (5) yields

$$k_2 = \frac{10\text{N}}{0.05 \times 10^{-3}\text{m}} = 200000\text{N/m}, \quad m_2 = \frac{200000\text{N/m}}{(314\text{s}^{-1})^2} = 2.03\text{kg} \quad (7)$$

(f) The vibration response versus pump speed is obtained from Equations (7.4.6) and (7.4.7) as

$$\tilde{Q}_1 = \frac{A_{f1}(-\Omega^2 m_2 + k_2)(\Omega/\omega)^2}{(-\Omega^2 m_1 + i\Omega c_1 + k_1 + k_2)(-\Omega^2 m_2 + k_2) - k_2^2} \quad (8)$$

where Ω is the varying speed of the pump shaft and ω is the shaft speed at 3000 rpm, that is, ($\omega = 314\text{rad/s}$). The “speed squared” dependence of the imbalance force is accounted for in the term $(\Omega/\omega)^2$. The pump mass and support stiffness are $m_1 = 100\text{kg}$ and $k_1 = 11.5 \times 10^6\text{N/m}$. Therefore, the natural frequency before adding the absorber is $\omega_{11} = \sqrt{k_1/m_1} = 339.1\text{rad/s}$, $f_{11} = 54\text{Hz}$, and $N_{11} = 3240\text{cpm}$. The magnitude of the pump’s vibration velocity before adding the absorber is given by (7.3.27) and (7.3.28) as

$$v_0 = \frac{A_f}{k_1} \frac{\omega}{\sqrt{(1-r^2)^2 + (2\xi_1 r)^2}} \quad (9)$$

where

$$r = \frac{\omega}{\omega_{11}} = \frac{3000}{3240} = 0.93$$

Equation (9) is solved for ξ_1 given the values

$$v_0 = 0.002\text{m/s}, \quad A_f = 10\text{N}, \quad k_1 = 11.5 \times 10^6\text{N/m}, \quad \omega = 314\text{rad/s}, \quad r = 0.93$$

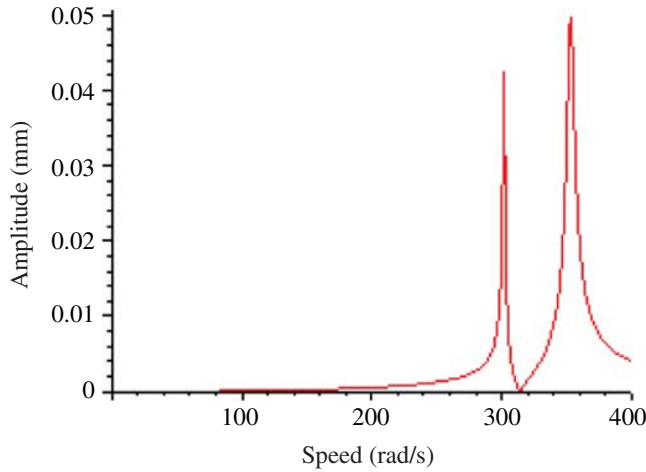


Figure E7.4.1(b) Pump vibration versus speed with the absorber attached

This yields $\xi_1 = 0.0106$ and therefore

$$c_1 = 2m_1\omega_{11}\xi_1 = (2)(100\text{kg})(339.1\text{s}^{-1})(0.0106) = 719\text{Ns/m}$$

The response of the pump with the absorber mass attached is

$$|q_1| = |\tilde{Q}_1|$$

where $|\tilde{Q}_1|$ is obtained from (8) and plotted versus the spin speed in Figure E7.4.1(b).

Summary: This example has illustrated how to calculate the stiffness and mass properties of an absorber to force the vibration of the primary mass (pump) to become zero at a single frequency, that is, the constant operating speed of the pump (314 rad/s) in Figure E7.4.1(b).

7.4.2 Vibration Absorber: Mass Ratio Effect

Assume that damping is negligible, the mass matrix is diagonal, and the external force on the absorber mass (m_{22}) is zero:

$$c_{11} = c_{12} = c_{21} = c_{22} = 0, \quad m_{12} = m_{21} = 0, \quad A_{f_2} = 0 \quad (7.4.13)$$

Then (7.4.6)–(7.4.12) become

$$\begin{bmatrix} -\omega^2 m_{11} + k_{11} & k_{12} \\ k_{12} & -\omega^2 m_{22} + k_{22} \end{bmatrix} \begin{Bmatrix} \tilde{Q}_1 \\ \tilde{Q}_2 \end{Bmatrix} = \begin{Bmatrix} A_{f_1} e^{i\phi_{f_1}} \\ 0 \end{Bmatrix} \quad (7.4.14)$$

Setting the vibration amplitude of the primary mass to zero, $|\tilde{Q}_1| = 0$, at frequency ω_0 , yields

$$k_{22} - \omega_0^2 m_{22} = 0 \quad (7.4.15)$$

and

$$|\tilde{Q}_2| = \frac{A_{f_1}}{k_{12}} \quad (7.4.16)$$

The coupled system has two resonant frequencies, as illustrated by Figure E7.4.1(b), and is the roots of

$$\Delta(\Omega) = (k_{11} - \Omega^2 m_{11})(k_{22} - \Omega^2 m_{22}) - k_{12}^2 = 0 \quad (7.4.17)$$

where Δ is the determinant of the coefficient matrix in (7.4.14). A simple spring–mass model for this type of system is shown in Figure 7.4.1.

The stiffness and mass matrices for this model are

$$\begin{bmatrix} k_{11} & k_{12} \\ k_{12} & k_{22} \end{bmatrix} = \begin{bmatrix} k_1 + k_2 & -k_2 \\ -k_2 & k_2 \end{bmatrix}, \quad \begin{bmatrix} m_{11} & m_{12} \\ m_{21} & m_{22} \end{bmatrix} = \begin{bmatrix} m_1 & 0 \\ 0 & m_2 \end{bmatrix} \quad (7.4.18)$$

Substitute (7.4.18) into (7.4.17) to obtain the characteristic equation

$$(k_1 + k_2 - \Omega^2 m_1)(k_2 - \Omega^2 m_2) - k_2^2 = 0 \quad (7.4.19)$$

which simplifies to

$$\Omega^4 m_1 m_2 + \Omega^2 (-k_2 m_1 - k_1 m_2 - k_2 m_2) + k_1 k_2 = 0 \quad (7.4.20)$$

Define

$$\alpha = \frac{\omega_0}{\omega_{11}} = \frac{\text{zero amplitude frequency}}{\text{primary system natural frequency}} \quad (7.4.21)$$

where

$$\omega_{11} = \sqrt{\frac{k_1}{m_1}} \quad (7.4.22)$$

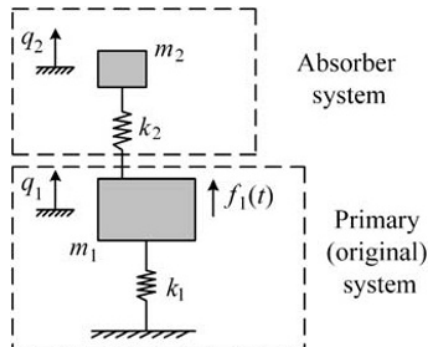


Figure 7.4.1 Primary mass with attached absorber mass

Divide (7.4.20) by $(k_1 * k_2)$ and utilize (7.4.15), (7.4.21), and (7.4.22) to obtain

$$\frac{\Omega^4}{(\omega_0^2/\alpha^2)\omega_0^2} + \Omega^2 \left(-\frac{\alpha^2}{\omega_0^2} - \frac{1}{\omega_0^2} - \mu \frac{\alpha^2}{\omega_0^2} \right) + 1 = 0 \quad (7.4.23)$$

where

$$\mu = \frac{m_2}{m_1} = \frac{\text{absorber mass}}{\text{primary mass}} \quad (7.4.24)$$

Define

$$\beta = \frac{\Omega}{\omega_0} = \frac{\text{coupled system natural frequency}}{\text{zero amplitude frequency}} \quad (7.4.25)$$

Then (7.4.23) becomes

$$\beta^4 + \beta^2 \left(1 - \mu - \frac{1}{\alpha^2} \right) + \frac{1}{\alpha^2} = 0 \quad (7.4.26)$$

The roots of this equation are plotted versus μ and α in Figure 7.4.2. Assume that ω_0 (the zero amplitude frequency for the coupled system) is held constant. This requires that the ratio k_2/m_2 be held constant, which implies that changes in m_2 are accompanied by proportional changes in k_2 since by (7.4.15)

$$\omega_0 = \sqrt{\frac{k_2}{m_2}} \quad (7.4.27)$$

The figure shows that the natural frequencies diverge away from ω_0 as m_2 increases. This is good since it will reduce the vibration amplitude for forcing frequencies near to, but not exactly coincident with the zero vibration frequency ω_0 . Note that decreasing

$$\alpha = \frac{\omega_0}{\omega_{11}} = \omega_0 \sqrt{\frac{m_1}{k_1}} \quad (7.4.28)$$

also increases the separation between the two natural frequencies of the coupled system.

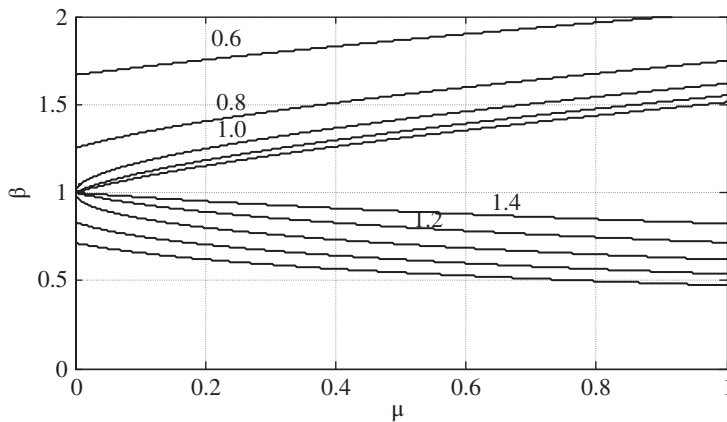


Figure 7.4.2 Nondimensional natural frequencies $\beta = \Omega/\omega_0$ of the coupled system versus mass ratio $\mu = m_2/m_1$. Values of $\alpha = \omega_0/\omega_{11}$ are shown on the curves

7.5 N DEGREE OF FREEDOM STEADY-STATE HARMONIC RESPONSE

7.5.1 Direct Approach

Equations (7.2.6) and (7.2.7) are general forms for the N dof equilibrium equation and its complex variable counterpart

$$\underline{M}\ddot{\underline{q}} + \underline{C}_T\dot{\underline{q}} + \underline{K}_T\underline{q} = \underline{f}(t) \quad (N \times 1) \quad (7.5.1)$$

and

$$\underline{M}\ddot{\underline{Q}} + \underline{C}_T\dot{\underline{Q}} + \underline{K}_T\underline{Q} = \underline{\tilde{F}}e^{i\omega t} \quad (N \times 1) \quad (7.5.2)$$

where

$$\underline{f}(t) = \begin{Bmatrix} A_{f1} \cos(\omega t + \phi_{f1}) \\ A_{f2} \cos(\omega t + \phi_{f2}) \\ \vdots \\ A_{fN} \cos(\omega t + \phi_{fN}) \end{Bmatrix}, \quad \underline{\tilde{F}} = \begin{Bmatrix} A_{f1} e^{i\phi_{f1}} \\ A_{f2} e^{i\phi_{f2}} \\ \vdots \\ A_{fN} e^{i\phi_{fN}} \end{Bmatrix} \quad (7.5.3)$$

Substitute

$$\underline{Q} = \underline{\tilde{Q}}e^{i\omega t} \quad (7.5.4)$$

into (7.5.2) to obtain

$$\left(-\omega^2 \underline{M} + i\omega \underline{C}_T + \underline{K}_T \right) \underline{\tilde{Q}} = \underline{\tilde{F}} \quad (7.5.5)$$

This set of N linear, complex, algebraic equations for the N unknown \tilde{Q}_j may be easily solved for any forcing frequency using available math software. The steady-state response is obtained by converting \tilde{Q}_j into polar form

$$\tilde{Q}_j = |\tilde{Q}_j| e^{i\phi_{Qj}} \quad (7.5.6)$$

where

$$|\tilde{Q}_j| = \sqrt{(\text{Re}(\tilde{Q}_j))^2 + (\text{Im}(\tilde{Q}_j))^2} \quad \text{and} \quad \phi_{Qj} = \tan^{-1} \left(\frac{\text{Im}(\tilde{Q}_j)}{\text{Re}(\tilde{Q}_j)} \right) \quad (7.5.7)$$

and then from (7.2.10)

$$\begin{aligned} q_j(t) &= \text{Re}(Q_j(t)) = \text{Re}(\tilde{Q}_j e^{i\omega t}) = \text{Re}(|\tilde{Q}_j| e^{i\phi_{Qj}} e^{i\omega t}) \\ &= \text{Re}(|\tilde{Q}_j| e^{i(\omega t + \phi_{Qj})}) = |\tilde{Q}_j| \cos(\omega t + \phi_{Qj}) \quad j=1, 2, \dots, N \end{aligned} \quad (7.5.8)$$

EXAMPLE 7.5.1 *Steady-State Imbalance Response of Rotating Machinery*

Statement: The system formerly used to illustrate transient response methods in Example 6.4.1 here illustrates SSHR determination. The rotor-bearing system is shown in Figure E6.4.1(a). The parameter values for this simulation are

$$\begin{aligned} L_1 &= 0.35 \text{ m}, \quad L_2 = 0.65 \text{ m}, \quad e = 0.15 \text{ m}, \quad m = 100 \text{ kg}, \quad \bar{m} = 0.2 \text{ kg}, \\ I_p &= 2.2 \text{ kg m}^2, \quad I_T = 2 \text{ kg m}^2, \quad \omega = 1570 \text{ rad/s (15000 rpm)}, \\ \underline{q}_0 = \dot{\underline{q}}_0 &= (0 \ 0 \ 0 \ 0)^T, \quad c_{22}^D = c_{22}^E = 6000 \text{ N s/m}, \quad c_{33}^D = c_{33}^E = 10000 \text{ N s/m}, \\ k_{22}^D = k_{22}^E &= 10 \times 10^6 \text{ N/m}, \quad k_{33}^D = k_{33}^E = 12.50 \times 10^6 \text{ N/m}, \quad k_f = 1.0 \times 10^6 \text{ N/m} \end{aligned}$$

Solution: From Example 6.4.1, Equation (1), the system equilibrium equation is (7.5.1) with

$$\underline{C}_T = \underline{C}_B + \underline{G}, \quad \underline{K}_T = \underline{K}_B + \underline{K}_f, \quad \underline{f}(t) = \underline{F}_{BL}(t) \quad (1)$$

The mass, stiffness, circulatory stiffness, damping, and gyroscopic matrices are provided in Example 6.4.1, Equations (2)–(6). The displacement and imbalance force vectors are

$$\underline{q} = \begin{Bmatrix} q_2 \\ q_3 \\ q_4 \\ q_5 \end{Bmatrix} = \begin{Bmatrix} x_{2G} \\ x_{3G} \\ \theta_{n3} \\ \theta_{n2} \end{Bmatrix}, \quad \underline{F}_{BL}(t) = \begin{Bmatrix} \bar{m}\omega^2 \cos \omega t \\ \bar{m}\omega^2 \sin \omega t \\ 0 \\ 0 \end{Bmatrix} \quad (2)$$

Comparison of (2) and (7.5.3) shows

$$\tilde{\underline{F}} = \begin{Bmatrix} A_{f1} e^{i\phi_{f1}} \\ A_{f2} e^{i\phi_{f2}} \\ A_{f3} e^{i\phi_{f3}} \\ A_{f4} e^{i\phi_{f4}} \end{Bmatrix} = \begin{Bmatrix} \bar{m}\omega^2 e^{i0^\circ} \\ \bar{m}\omega^2 e^{-i90^\circ} \\ 0 \\ 0 \end{Bmatrix} = \begin{Bmatrix} \bar{m}\omega^2 \\ -i\bar{m}\omega^2 \\ 0 \\ 0 \end{Bmatrix} \quad (3)$$

Since \underline{G} varies with spin speed ω , Equation (7.5.5) has the more general form

$$[-\omega^2 \underline{M} + i\omega(\underline{C}_B + \underline{G}(\omega)) + \underline{K}_T] \tilde{\underline{Q}} = \tilde{\underline{F}}(\omega) \quad (4)$$

This equation is solved for each ω , and $|q_j|$ and ϕ_{Q_j} are determined via Equations (7.5.7) and (7.5.8). The x_{2G} amplitude and phase angle are plotted versus rotor speed from 0 to 20 000 rpm in Figure E7.5.1(a). *The amplitude at 15000 rpm (≈ 0.35 mm, 0–p) is in agreement with the transient results as $t \rightarrow \infty$ in Figure E6.4.1(b).*

The resonance peak in Figure E7.5.1(a) is called a “critical speed” and occurs at approximately 4200 rpm. This corresponds with the intersection of the spin speed and natural frequency curves in Figure E6.4.1(f).

EXAMPLE 7.5.2 *Wind Turbine Tower with Rotating Mass Imbalance*

Statement: A frame/tower structure is used to support a wind turbine as shown along with its simplified, transverse vibration model in Figure E7.5.2(a). Mass imbalance in the rotor

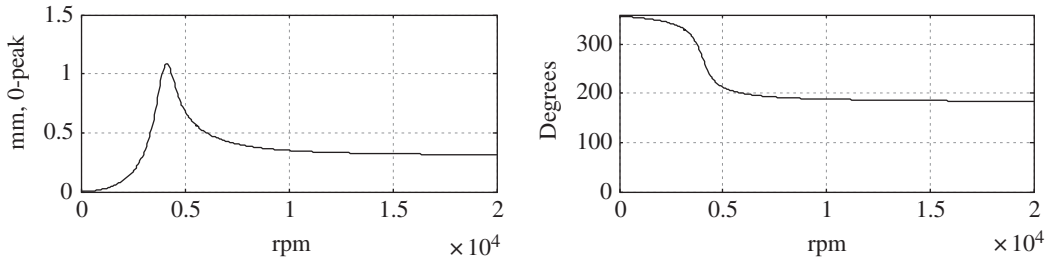


Figure E7.5.1(a) Amplitude and phase angle of displacement x_{2G} at mass center

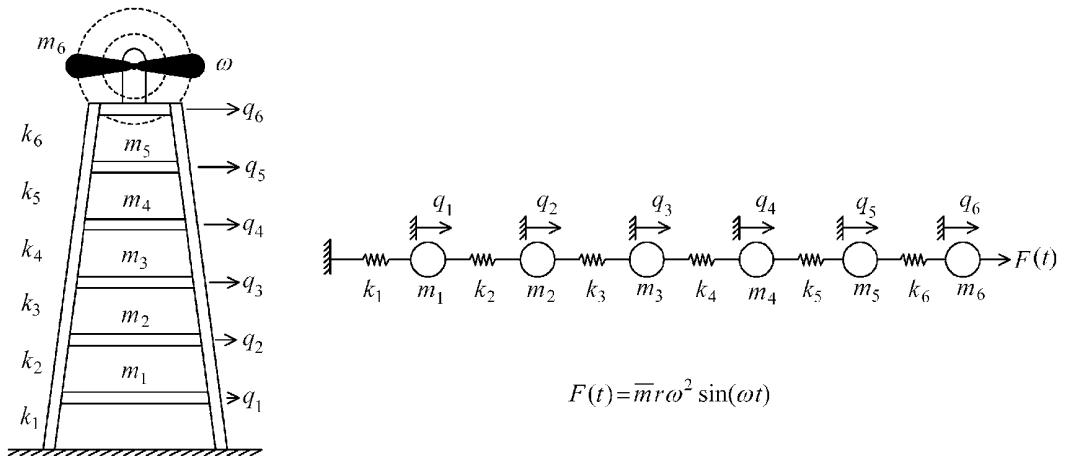


Figure E7.5.2(a) Wind turbine tower and simplified model

blades has been found to cause excessive vibration of the tower and subsequent premature wear of the bearings in several installed units. The model is developed to investigate modifications that will lower the sensitivity of the structure and bearings to blade imbalance.

Objective:

- (a) Plot the SSHR amplitudes and phase angles of q_2 , q_4 , and q_6 versus rotational frequency ω over the range

$$0 \leq f \leq 100 \text{ Hz} \quad \text{where } f = \frac{\omega}{2\pi} \quad (1)$$

- (b) Compare steady-state and transient response amplitudes as $t \rightarrow \infty$ at $f = 25 \text{ Hz}$.

Parameter Values:

$$\begin{aligned} m_1 &= 50 \text{ kg}, \quad m_2 = 45 \text{ kg}, \quad m_3 = 40 \text{ kg}, \quad m_4 = 35 \text{ kg}, \quad m_5 = 30 \text{ kg}, \quad m_6 = 50 \text{ kg}, \quad \bar{m} = 0.05 \text{ kg}, \\ k_1 &= 10^6 \text{ N/m}, \quad k_2 = 0.9 \times 10^6 \text{ N/m}, \quad k_3 = 0.80 \times 10^6 \text{ N/m}, \quad k_4 = 0.70 \times 10^6 \text{ N/m}, \\ k_5 &= 0.6 \times 10^6 \text{ N/m}, \quad k_6 = 0.5 \times 10^6 \text{ N/m}, \quad \xi_1^d = 0.05, \quad \xi_2^d = 0.07, \quad \xi_3^d = 0.10, \quad r = 1 \text{ m} \end{aligned}$$

Assumptions: Use the orthogonal damping matrix formula (5.4.140) with $m = 3$ modes with prescribed damping values.

Solution: The equations of motion may be obtained directly following the same procedure as in Example 6.3.1. This yields

$$\underline{M}\ddot{\underline{q}} + \underline{C}_0\dot{\underline{q}} + \underline{K}\underline{q} = \underline{f}(t) \quad (6 \times 1) \quad (2)$$

$$\underline{K} = \begin{bmatrix} k_1 + k_2 & -k_2 & 0 & 0 & 0 & 0 \\ & k_2 + k_3 & -k_3 & 0 & 0 & 0 \\ & & k_3 + k_4 & -k_4 & 0 & 0 \\ & & & k_4 + k_5 & -k_5 & 0 \\ & & & & k_5 + k_6 & -k_6 \\ & & & & & k_6 \end{bmatrix}, \quad \underline{M} = \text{diag}(m_i) \quad (6 \times 6) \quad (3)$$

symmetric

$$\underline{C}_0 = \mu_1 \underline{K} + \sum_{l=1}^2 \frac{2\xi_l \omega_l}{\bar{m}_l} \underline{M} \underline{\psi}_l \underline{\psi}_l^T \underline{M}, \quad \mu_1 = \frac{2\xi_3^d}{\omega_3}, \quad \xi_l = \xi_l^d - \xi_3^d \frac{\omega_l}{\omega_3} \quad l = 1, 2 \quad (4)$$

The quantities ω_l and $\underline{\psi}_l$ are the l th, undamped system natural frequency and mode shape, respectively. The force vector is obtained from (4.5.52) in scalar or vector form as

$$f_j = F(t) \hat{i} \cdot \frac{\partial \hat{q}_6 \hat{i}}{\partial \hat{q}_j} = \begin{cases} 0, & j \neq 6 \\ F(t), & j = 6 \end{cases} \quad (5)$$

$$\underline{f}(t) = \begin{pmatrix} 0 \\ 0 \\ 0 \\ 0 \\ 0 \\ F(t) \end{pmatrix} = \begin{pmatrix} 0 \\ 0 \\ 0 \\ 0 \\ 0 \\ u \sin(\omega t) \end{pmatrix} = \begin{pmatrix} 0 \\ 0 \\ 0 \\ 0 \\ 0 \\ u \cos(\omega t - 90) \end{pmatrix} = \text{Re} \left(\begin{pmatrix} 0 \\ 0 \\ 0 \\ 0 \\ 0 \\ u e^{i(\omega t - 90)} \end{pmatrix} \right) = \text{Re} \left(\begin{pmatrix} 0 \\ 0 \\ 0 \\ 0 \\ 0 \\ -iu \end{pmatrix} e^{i\omega t} \right) \quad (6)$$

where $u = \bar{m} r \omega^2$ is the magnitude of the imbalance force. Comparison with Equation (7.5.3) yields

$$\underline{\tilde{F}} = (0 \ 0 \ 0 \ 0 \ 0 \ -iu)^T \quad (7)$$

The complex displacement phasors are then obtained from (7.5.5) as

$$\underline{\tilde{Q}} = (-\omega^2 \underline{M} + i\omega \underline{C}_0 + \underline{K})^{-1} \underline{\tilde{F}} \quad (8)$$

Finally, the steady-state displacements are obtained from (7.5.8) as

$$q_j(t) = |\tilde{Q}_j| \cos(\omega t + \phi_{Q_j}) \quad j = 1, \dots, 6, \quad \text{where } \phi_{Q_j} = \angle \tilde{Q}_j \quad (9)$$

The natural frequencies and damping ratios of this model are (5.5, 14.2, 23.3, 31.6, 38.0 and 42.2) Hz and (0.05, 0.07, 0.1, 0.074, 0.045 and 0.018), respectively.

The amplitudes and phase angles at dofs 2, 4, and 6 are shown in Figure E7.5.2(b).

The asymptotic ($\omega \rightarrow \infty$) results in this figure agree with the asymptotic ($\omega \rightarrow \infty$) form of (8)

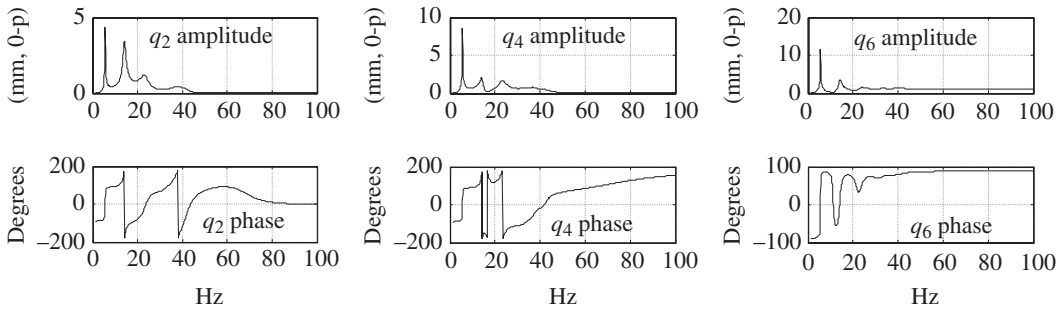


Figure E7.5.2(b) Amplitudes and phase angles of q_2 , q_4 , and q_6 versus spin frequency

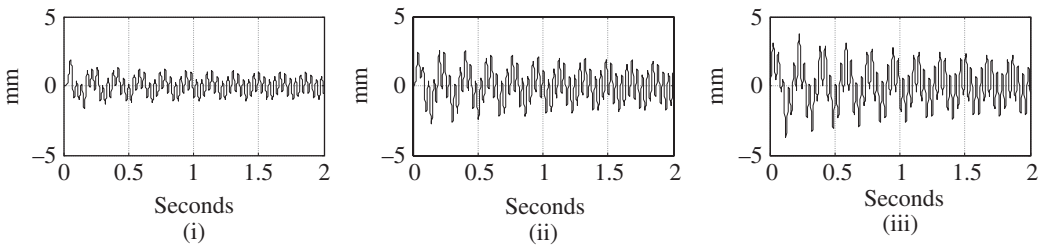


Figure E7.5.2(c) Transient response of (i) q_2 , (ii) q_4 , and (iii) q_6

Table E7.5.2(a) Comparison of steady-state and transient response predictions at 25 Hz

	q_2 amplitude	q_4 amplitude	q_6 amplitude
SSHR	0.598	1.06	1.37
Transient	0.582	1.01	1.34

$$\tilde{\underline{Q}} = \frac{-1}{\omega^2} \underline{M}^{-1} \tilde{\underline{F}} = \begin{pmatrix} 0 & 0 & 0 & 0 & 0 & \frac{i\bar{m}r}{m_6} \end{pmatrix}^T = \begin{pmatrix} 0 & 0 & 0 & 0 & 0 & \frac{10^{-3}}{\angle 90^\circ} \end{pmatrix}^T \quad (10)$$

The transient response of dofs q_2 , q_4 , and q_6 at a 25 Hz rotational frequency is shown in Figure E7.5.2(c).

Table E7.5.2(a) compares the results of these figures using the MATLAB zoom plotting feature at 25 Hz. The transient response amplitude is evaluated near $t = 2$ seconds.

Summary: This example illustrated how to predict the SSHR of a six-level windmill tower model with (7.5.5). A transient response simulation was utilized to confirm the accuracy of the approach.

7.5.2 Modal Approach

The first-order form for the complex variable equilibrium was given in Equations (6.3.140)–(6.3.142) as

$$\underline{E} \underline{\dot{X}} = \underline{H} \underline{X} + \hat{\underline{f}}(t) \quad (7.5.9)$$

$\begin{matrix} 2N \times 2N & 2N \times 1 \\ 2N \times 2N & 2N \times 1 \\ 2N \times 1 & \end{matrix}$

where

$$\underline{E} = \begin{bmatrix} \underline{0} & \underline{M} \\ \underline{M} & \underline{C}_T \end{bmatrix}, \quad \underline{H} = \begin{bmatrix} \underline{M} & \underline{0} \\ \underline{0} & -\underline{K}_T \end{bmatrix}, \quad \underline{X} = \begin{Bmatrix} \underline{\dot{Q}} \\ \underline{Q} \end{Bmatrix}, \quad \underline{\hat{f}} = \begin{Bmatrix} \underline{0} \\ \underline{\tilde{F}} e^{i\omega t} \end{Bmatrix} \quad (7.5.10)$$

The corresponding right and left eigenvectors had the form (6.3.143)

$$\underline{\Gamma}_j = \begin{Bmatrix} \lambda_j \underline{\Lambda}_j \\ \underline{\Lambda}_j \end{Bmatrix}_{2N \times 1}, \quad \underline{\beta}_j = \begin{Bmatrix} \lambda_j \underline{\theta}_j \\ \underline{\theta}_j \end{Bmatrix}_{2N \times 1} \quad (7.5.11)$$

where by (6.3.144)

$$\begin{aligned} \lambda_j \underline{E} \underline{\Gamma}_j &= \underline{H} \underline{\Gamma}_j, & \lambda_j \underline{E}^T \underline{\beta}_j &= \underline{H}^T \underline{\beta}_j \\ (\lambda_j^2 \underline{M} + \lambda_j \underline{C}_T + \underline{K}_T) \underline{\Lambda}_j &= \underline{0}, & (\lambda_j^2 \underline{M}^T + \lambda_j \underline{C}_T^T + \underline{K}_T^T) \underline{\theta}_j &= \underline{0} \\ \underline{\Gamma} &= [\underline{\Gamma}_1 \quad \underline{\Gamma}_2 \quad \cdots \quad \underline{\Gamma}_m], & \underline{\beta} &= [\underline{\beta}_1 \quad \underline{\beta}_2 \quad \cdots \quad \underline{\beta}_m] \end{aligned} \quad (7.5.12)$$

As in (6.3.145), let

$$\underline{X}(t) = \sum_{j=1}^m w_j(t) \underline{\Gamma}_j = \underline{\Gamma} \underline{W} \quad (7.5.13)$$

premultiply (7.5.9) by $\underline{\beta}^T$ and use the biorthogonality relations in (5.4.229) and (5.4.230) to obtain

$$\underline{\text{diag}}(\tilde{e}_j) \underline{\dot{W}} - \underline{\text{diag}}(\lambda_j \tilde{e}_j) \underline{W} = \underline{R}(t) \quad (7.5.14)$$

Considering this equation row-wise yields

$$\dot{w}_j - \lambda_j w_j = \frac{R_j(t)}{\tilde{e}_j} \quad (7.5.15)$$

where the modal force is

$$R_j = \underline{\beta}_j^T \underline{\hat{f}} = \begin{Bmatrix} \lambda_j \underline{\theta}_j \\ \underline{\theta}_j \end{Bmatrix}^T \begin{Bmatrix} \underline{0} \\ \underline{\tilde{F}} e^{i\omega t} \end{Bmatrix} = \underline{\theta}_j^T \underline{\tilde{F}} e^{i\omega t} \quad (7.5.16)$$

and from (5.4.225) the generalized modal mass is

$$\tilde{e}_j = \underline{\beta}_j^T \underline{E} \underline{\Gamma}_j = \begin{Bmatrix} \lambda_j \underline{\theta}_j \\ \underline{\theta}_j \end{Bmatrix}^T \begin{bmatrix} \underline{0} & \underline{M} \\ \underline{M} & \underline{C}_T \end{bmatrix} \begin{Bmatrix} \lambda_j \underline{\Lambda}_j \\ \underline{\Lambda}_j \end{Bmatrix} = \underline{\theta}_j^T (2\lambda_j \underline{M} + \underline{C}_T) \underline{\Lambda}_j \quad (7.5.17)$$

Substitute (7.5.16) into (7.5.15) to obtain the modal coordinate equation

$$\dot{w}_j - \lambda_j w_j = \frac{\tilde{F}^T \underline{\theta}_j e^{i\omega t}}{\tilde{e}_j} \quad (7.5.18)$$

Assume the steady-state solution

$$w_j(t) = \tilde{w}_j e^{i\omega t} \quad (7.5.19)$$

which transforms (7.5.18) into

$$\tilde{w}_j = \frac{\tilde{\underline{F}}^T \underline{\theta}_j}{\tilde{e}_j(i\omega - \lambda_j)} \quad (7.5.20)$$

Substitute (7.5.20) into (7.5.19) and the results into (7.5.13) to obtain

$$\underline{\underline{X}}(t) = \left\{ \begin{array}{c} \underline{\underline{\dot{Q}}} \\ \underline{\underline{Q}} \end{array} \right\} \approx \sum_{j=1}^m w_j(t) \underline{\Gamma}_j = \left(\sum_{j=1}^m \frac{\tilde{\underline{F}}^T \underline{\theta}_j \left\{ \begin{array}{c} \lambda_j \underline{\Delta}_j \\ \underline{\Delta}_j \end{array} \right\}}{\tilde{e}_j(i\omega - \lambda_j)} \right) e^{i\omega t} \quad (7.5.21)$$

The steady-state response becomes

$$\underline{\underline{q}}(t) = \text{Re}(\underline{\underline{Q}}(t)) \approx \text{Re} \left(\left(\sum_{j=1}^m \frac{\tilde{\underline{F}}^T \underline{\theta}_j \underline{\Delta}_j}{\tilde{e}_j(i\omega - \lambda_j)} \right) e^{i\omega t} \right) \quad (7.5.22)$$

or for the k th dof

$$q_k(t) \Big|_{\text{steady study}} \approx \text{Re} \left(\left(\sum_{j=1}^m \frac{\tilde{\underline{F}}^T \underline{\theta}_j \Lambda_{kj}}{\tilde{e}_j(i\omega - \lambda_j)} \right) e^{i\omega t} \right) \quad (7.5.23)$$

The j th eigenvalue has the general form

$$\lambda_j = -\xi_j \omega_{nj} + i\omega_{dj} \quad (7.5.24)$$

so that (7.5.23) becomes

$$q_k(t) \Big|_{\text{steady study}} \approx \text{Re} \left(\tilde{\underline{F}}^T \left(\sum_{j=1}^m \frac{\underline{\theta}_j \Lambda_{kj}}{\tilde{e}_j(i\omega + \xi_j \omega_{nj} - i\omega_{dj})} \right) e^{i\omega t} \right) \quad k = 1, 2, \dots, N \quad (7.5.25)$$

The denominator of the j th term in (7.5.25) will be zero if both

$$\omega = \omega_{dj} \text{ and damping } \xi_j = 0 \quad (7.5.26)$$

This yields an infinite response demonstrating that *even the most general linear system will experience resonance if the disturbance frequency ω is near to any natural frequency and the modal damping associated with this natural frequency is low*. Use of Equation (7.5.25) circumvents the requirement to solve the N complex equations in (7.5.5) for every value of ω , thus providing an efficient means to determine the SSHR.

7.5.3 Receptances

The complex variable responses may be obtained from (7.5.5) as

$$\underline{\underline{\tilde{Q}}} = \underline{\underline{R}}(\omega) \underline{\underline{\tilde{F}}} \quad (N \times 1) \quad (7.5.27)$$

where

$$\underline{R}(\omega) = \text{receptance matrix} = (-\omega^2 \underline{M} + i\omega \underline{C}_T + \underline{K}_T)^{-1} \quad (N \times N) \quad (7.5.28)$$

Note from (7.5.27) and (2.6.30)

$$\tilde{Q}_k = \sum_{l=1}^{n_F} (\underline{R})_{k_j l}(\omega) (\tilde{F})_{j_l} \quad (N \times 1) \quad (7.5.29)$$

where $j_1 \ j_2 \ \dots \ j_{n_F}$ are nonzero rows of \tilde{F} . Thus, it can be seen that evaluation of \tilde{Q}_k may require only a small subset of the total number (N^2) of receptances $R_{k_j l}$. Obtaining these receptances may be computationally demanding if Equation (7.5.28) is utilized for a large number of ω 's or when N is large. Thus, it would be helpful to evaluate isolated $R_{k_j l}$ without using the matrix inverse operation in (7.5.28). This may be accomplished if \underline{C}_T is zero or is an orthogonal damping matrix (5.4.92), and \underline{K}_T is symmetric so that the modes and undamped natural frequencies satisfy (5.4.63)

$$(-\omega_l^2 \underline{M} + \underline{K}_T) \underline{\psi}_l = 0 \quad (7.5.30)$$

and from (5.4.72), (5.4.75), (5.4.76), (5.4.77), (5.4.93), and (5.4.121)

$$\underline{\psi}_l^T \underline{C}_T \underline{\psi}_j = \delta_{ij} 2\xi_l \omega_l \tilde{m}_l, \quad \underline{\psi}_l^T \underline{M} \underline{\psi}_j = \delta_{ij} \tilde{m}_l, \quad \underline{\psi}_l^T \underline{K}_T \underline{\psi}_j = \delta_{ij} \tilde{m}_l \omega_l^2 \quad (7.5.31)$$

The receptance matrix for an orthogonally damped system is

$$\underline{R}(\omega) = (-\omega^2 \underline{M} + i\omega \underline{C}_0 + \underline{K})^{-1} \quad (7.5.32)$$

It follows that

$$\begin{aligned} \underline{\Psi}^T \underline{R}^{-1} \underline{\Psi} &= \underline{\text{diag}}(-\omega^2 \tilde{m}_i + i\omega 2\tilde{m}_i \xi_i \omega_i + \tilde{m}_i \omega_i^2) \\ \underline{\Psi}^{-1} \underline{R} \underline{\Psi}^{-T} &= \underline{\text{diag}}\left(\frac{1}{\tilde{m}_i(\omega_i^2 - \omega^2 + i2\xi_i \omega \omega_i)}\right) \end{aligned} \quad (7.5.33)$$

Finally, using (2.6.38) yields

$$\underline{R} = \underline{\Psi} \underline{\text{diag}}\left(\frac{1}{\tilde{m}_i(\omega_i^2 - \omega^2 + i2\xi_i \omega \omega_i)}\right) \underline{\Psi}^T = \sum_{l=1}^N \frac{\underline{\psi}_l \underline{\psi}_l^T}{\tilde{m}_l(\omega_l^2 - \omega^2 + i2\xi_l \omega \omega_l)} \quad (7.5.34)$$

or in scalar form

$$R_{ij}(\omega) = \sum_{l=1}^N \frac{\psi_{il} \psi_{jl}}{\tilde{m}_l(\omega_l^2 - \omega^2 + i2\xi_l \omega \omega_l)} \quad (7.5.35)$$

Equation (7.5.35) demonstrates that individual entries in $\underline{R}(\omega)$ may be obtained without performing the $N \times N$ matrix inverse in (7.5.28) for each excitation frequency ω . Convergence of the summations in (7.5.34) or (7.5.35) may be accelerated for a partial set of m modes ($m \ll N$) as follows. By (5.4.46),

$$\begin{aligned}\underline{\Psi}^T \underline{K} \underline{\Psi} &= \text{diag} \left(\tilde{m}_i \omega_i^2 \right) \\ \underline{\Psi}^{-1} \underline{K}^{-1} \underline{\Psi}^{-T} &= \text{diag} \left(\frac{1}{\tilde{m}_i \omega_i^2} \right) \\ \therefore \underline{K}^{-1} &= \underline{\Psi} \text{diag} \left(\frac{1}{\tilde{m}_i \omega_i^2} \right) \underline{\Psi}^T\end{aligned}\quad (7.5.36)$$

Furthermore, note that

$$\frac{1}{\omega_l^2 - \omega^2 + i2\xi_l \omega \omega_l} = \frac{1}{\omega_l^2} + \frac{\omega^2 \left(1 - i2\xi_l \frac{\omega_l}{\omega} \right)}{\omega_l^2 (\omega_l^2 - \omega^2 + i2\xi_l \omega \omega_l)} \quad (7.5.37)$$

Substituting (7.5.36) and (7.5.37) into (7.5.34) yields

$$\underline{R}(\omega) \approx \underline{K}^{-1} + \omega^2 \sum_{l=1}^m \frac{\left(1 - i2\xi_l \frac{\omega_l}{\omega} \right) \underline{\Psi}_l \underline{\Psi}_l^T}{\tilde{m}_l \omega_l^2 (\omega_l^2 - \omega^2 + i2\xi_l \omega \omega_l)} \quad (7.5.38)$$

The scalar form of this equation is

$$R_{kj}(\omega) = (\underline{K}^{-1})_{kj} + \omega^2 \sum_{l=1}^m \frac{\left(1 - i2\xi_l \frac{\omega_l}{\omega} \right) \psi_{kl} \psi_{jl}}{\tilde{m}_l \omega_l^2 (\omega_l^2 - \omega^2 + i2\xi_l \omega \omega_l)} \quad (7.5.39)$$

The convergence of $R(\omega)$ is “accelerated” by using (7.5.38) in place of (7.5.34) if a partial set of modes is utilized because of the attenuating effect of the ω_l^2 term in the denominator of (7.5.38). Undamped system receptances are obtained from (7.5.34), (7.5.35), (7.5.38), or (7.5.39) by setting all $\xi_l = 0$. Formulas (7.5.38) or (7.5.39) may only be used if \underline{K}^{-1} exists, that is, only for models that are constrained to prevent rigid body motion. Once the receptances required in (7.5.29) are obtained, the \tilde{Q}_k may be determined and the SSHRs become

$$q_k(t) = |\tilde{Q}_k| \cos(\omega t + \angle \tilde{Q}_k) \quad (7.5.40)$$

The receptances have an interesting physical interpretation derived from the form of Equation (7.5.27):

$$\tilde{Q}_k = \sum_{j=1}^N R_{kj} \tilde{F}_j = \sum_{j=1}^N \tilde{Q}_{kj} \quad (7.5.41)$$

where

$$\tilde{Q}_{kj} = \text{the part of } \tilde{Q}_k \text{ caused by the force } \tilde{F}_j, \text{ where } \tilde{Q}_{kj} = R_{kj} \tilde{F}_j \quad (7.5.42)$$

Thus, receptance R_{kj} is the ratio of the phasor displacement at dof k divided by the phasor force at dof j, with all other forces set to zero

$$R_{kj} = \frac{\tilde{Q}_{kj}}{\tilde{F}_j} \quad (7.5.43)$$

7.5.4 Receptance-Based Synthesis

The physical interpretation of receptances in (7.5.43) can be utilized to predict the response of coupled structures or structural components, given receptances of the individual uncoupled components as discussed in Beards (1981). To illustrate this, consider the two components connected by a stiffness k as shown in Figure 7.5.1. The objective is to predict the coupled system's SSHR at point d on body II due to the harmonic forces at c on body I. The given (available) quantities include the uncoupled system receptances, the forces at c , and the interconnection stiffness k . Apply Equation (7.5.41) to point a on component I treating \tilde{f}_k , \tilde{F}_{1c} , and \tilde{F}_{2c} as harmonic forces that are “external” to body I. This yields

$$\tilde{Q}_{1a} = R_{1a,1c}^I \tilde{F}_{1c} + R_{1a,2c}^I \tilde{F}_{2c} + R_{1a,1a}^I (-\tilde{f}_k) \quad (7.5.44)$$

Apply (7.5.42) to component II treating \tilde{f}_k as a harmonic force that is “external” to body II. This yields

$$\tilde{Q}_{1b} = R_{1b,1b}^{II} \tilde{f}_k \quad (7.5.45)$$

$$\tilde{Q}_{1d} = R_{1d,1b}^{II} \tilde{f}_k \quad (7.5.46)$$

Finally, express \tilde{f}_k in terms of the relative displacement of its end points

$$\tilde{f}_k = k(\tilde{Q}_{1a} - \tilde{Q}_{1b}) \quad (7.5.47)$$

Insert (7.5.44) and (7.5.45) into (7.5.47)

$$\begin{aligned} \tilde{f}_k &= k(R_{1a,1c}^I \tilde{F}_{1c} + R_{1a,2c}^I \tilde{F}_{2c} - R_{1a,1a}^I \tilde{f}_k) - kR_{1b,1b}^{II} \tilde{f}_k \\ \Rightarrow \tilde{f}_k &= \frac{k(R_{1a,1c}^I \tilde{F}_{1c} + R_{1a,2c}^I \tilde{F}_{2c})}{1 + k(R_{1a,1a}^I + R_{1b,1b}^{II})} \end{aligned} \quad (7.5.48)$$

Substitute (7.5.48) into (7.5.46) to obtain

$$\tilde{Q}_{1d} = \frac{kR_{1d,1b}^{II}(R_{1a,1c}^I \tilde{F}_{1c} + R_{1a,2c}^I \tilde{F}_{2c})}{1 + k(R_{1a,1a}^I + R_{1b,1b}^{II})} \quad (7.5.49)$$

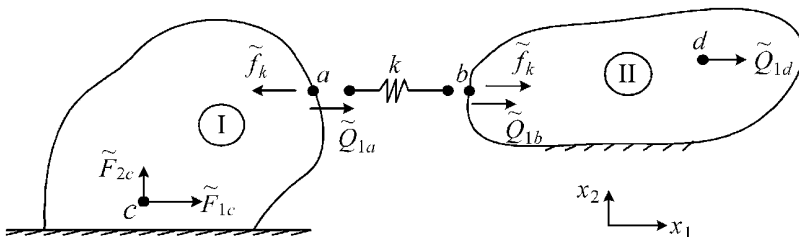


Figure 7.5.1 Two flexible structural components connected by stiffness k

A business utility of (7.5.49) is that it requires that only receptance descriptions be disclosed by the manufacturers of the individual components. Thus, the separate manufacturers of components I and II may protect proprietary, detailed information related to the design and construction of their products and still allow the end user or packaging company to predict the combined system response. An example of this might be a gas turbine engine manufacturer and an airplane manufacturer. The former manufactures the engine and the latter manufactures the airplane structure on which the engine is attached.

EXAMPLE 7.5.3 Space Lab Microgravity Experiment Isolation

Statement: An orbiting space lab may be composed of modules that are manufactured not only by different organizations but also in different countries. Receptance descriptions of the internal dynamics of each component would be beneficial for obtaining coupled system responses without disclosing proprietary design or manufacturing details. Consider a case of a two-module space lab that is connected by a tubular structure of longitudinal stiffness k . A heating, ventilation, and air-conditioning (HVAC) equipment skid in module I is isolated from transmitting vertical forces, but its soft mount arrangement still transmits significant longitudinal forces. Microgravity experiments (ME) are conducted in module II so it is important to estimate its response due to the module I HVAC forces. The two-module, stiffness-connected system model is illustrated in Figure E7.5.3(a).

Objective: To determine the SSHR at the ME location (q_3^{II}) in module II due to the HVAC force at position (q_2^{I}) in module I using the isolated component receptances.

Assumptions: Linear components

Numerical Values: Interconnection stiffness $k = 0.75 \times 10^8 \text{ N/m}$

Module I:

$$\begin{aligned} m_1^{\text{I}} &= 5000 \text{ kg}, & m_2^{\text{I}} &= 2000 \text{ kg}, & m_3^{\text{I}} &= 2000 \text{ kg}, & m_4^{\text{I}} &= 2000 \text{ kg}, & m_5^{\text{I}} &= 2000 \text{ kg} \\ k_1^{\text{I}} &= 2 \times 10^8 \text{ N/m}, & k_2^{\text{I}} &= 1 \times 10^8 \text{ N/m}, & k_3^{\text{I}} &= 1 \times 10^8 \text{ N/m}, & k_4^{\text{I}} &= 1 \times 10^8 \text{ N/m} \\ c_1^{\text{I}} &= 75000 \text{ Ns/m}, & c_2^{\text{I}} &= 75000 \text{ Ns/m}, & c_3^{\text{I}} &= 75000 \text{ Ns/m}, & c_4^{\text{I}} &= 75000 \text{ Ns/m} \\ f_{\text{HVAC}} &= 100 \text{ N} \end{aligned}$$

Module II:

$$\begin{aligned} m_1^{\text{II}} &= 1500 \text{ kg}, & m_2^{\text{II}} &= 1500 \text{ kg}, & m_3^{\text{II}} &= 1500 \text{ kg}, & m_4^{\text{II}} &= 1500 \text{ kg} \\ k_1^{\text{II}} &= 0.5 \times 10^8 \text{ N/m}, & k_2^{\text{II}} &= 0.5 \times 10^8 \text{ N/m}, & k_3^{\text{II}} &= 0.5 \times 10^8 \text{ N/m} \\ c_1^{\text{II}} &= 25000 \text{ Ns/m}, & c_2^{\text{II}} &= 25000 \text{ Ns/m}, & c_3^{\text{II}} &= 25000 \text{ Ns/m} \end{aligned}$$

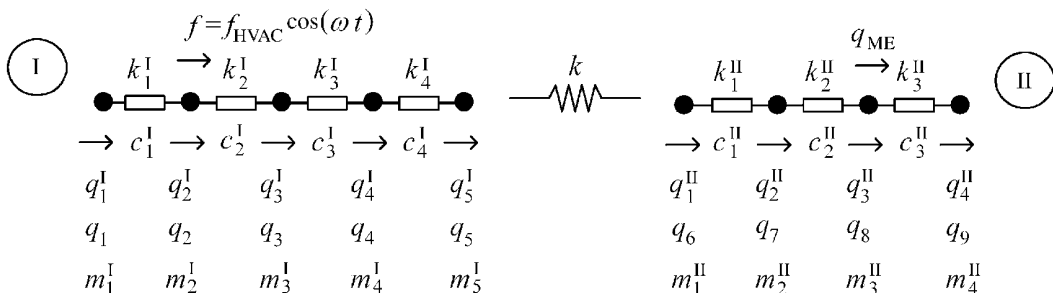


Figure E7.5.3(a) Space station model with two flexible modules and an interconnection stiffness

Solution:

(a) Form isolated module \underline{M} , \underline{K} , and \underline{C} matrices.

(b) Form isolated module receptance matrices. By (7.5.28),

$$\underline{R}_I(\omega) = (-\omega^2 \underline{M}_I + i\omega \underline{C}_{TI} + \underline{K}_{TI})^{-1}, \quad \underline{R}_{II}(\omega) = (-\omega^2 \underline{M}_{II} + i\omega \underline{C}_{TII} + \underline{K}_{TII})^{-1} \quad (1)$$

Note that by comparison of Figure 7.5.1 and (1),

$$\begin{aligned} a &= \text{node 5 of module I}, & b &= \text{node 1 of module II} \\ c &= \text{node 2 of module I}, & d &= \text{node 3 of module II} \end{aligned} \quad (2)$$

$$\tilde{F}_{1c} = f_{\text{HVAC}}, \quad \tilde{F}_{2c} = 0$$

Utilize the following receptances:

$$\begin{aligned} R_{1a,1a}^I &= (\underline{R}_I)_{5,5}, & R_{1a,1c}^I &= (\underline{R}_I)_{5,2} \\ R_{1b,1b}^{II} &= (\underline{R}_{II})_{1,1}, & R_{1d,1b}^{II} &= (\underline{R}_{II})_{3,1} \end{aligned} \quad (3)$$

in (7.5.49) to solve for the amplitude and phase angle of motion at node 8 in the coupled system

$$\tilde{Q}_{1d} = \tilde{Q}_8 = \frac{k(\underline{R}_{II})_{3,1}(\underline{R}_I)_{5,2}f_{\text{HVAC}}}{1 + k\left((\underline{R}_I)_{5,5} + (\underline{R}_{II})_{1,1}\right)} \quad (4)$$

$$|q_8(\omega)| = |\tilde{Q}_8(\omega)|, \quad \angle q_8(\omega) = \angle \tilde{Q}_8(\omega) \quad (5)$$

(c) The response at node 8 may also be obtained by solving the problem as a single coupled system. The solution is then given by (7.5.27) and (7.5.28) as

$$\tilde{\underline{Q}}_{9 \times 1} = \underline{R}(\omega) \tilde{\underline{F}}_{9 \times 9} \quad (6)$$

where

$$\begin{aligned} \underline{R} &= (-\omega^2 \underline{M} + i\omega \underline{C}_T + \underline{K}_T)^{-1} \\ \tilde{\underline{F}} &= (0 \ f_{\text{HVAC}} \ 0 \ 0 \ 0 \ 0 \ 0 \ 0 \ 0)^T \end{aligned} \quad (7)$$

This implies

$$\tilde{Q}_8 = (\underline{R})_{8,2} f_{\text{HVAC}} \quad (8)$$

Figure E7.5.3(b) shows that the q_8 amplitude frequency response as determined utilizing component receptances or by utilizing the coupled system receptances is identical.

Summary: This example has illustrated how to obtain the SSHR of a coupled system by using the receptances of its isolated components.

7.5.5 Dominance of a Single Mode in the Steady-State Harmonic Response

Recall from (7.5.27)

$$\tilde{\underline{Q}} = \underline{R}(\omega) \tilde{\underline{F}} \quad (N \times 1) \quad (7.5.50)$$

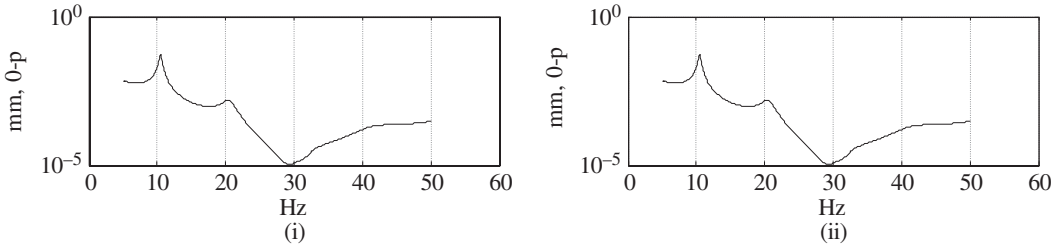


Figure E7.5.3(b) Displacement amplitude response at node 8 utilizing component (i) and system (ii) receptances

and from (7.5.34)

$$\underline{R} = \sum_{l=1}^N \frac{\underline{\psi}_l \underline{\psi}_l^T}{\tilde{m}_l (\omega_l^2 - \omega^2 + i2\xi_l \omega \omega_l)} \quad (7.5.51)$$

Therefore,

$$\tilde{\underline{Q}} = \sum_{l=1}^N \frac{(\underline{\psi}_l^T \tilde{\underline{F}})}{\tilde{m}_l (\omega_l^2 - \omega^2 + i2\xi_l \omega \omega_l)} \underline{\psi}_l \quad (7.5.52)$$

Suppose $\omega \approx \omega_p$, and ξ_p is very small, then the p th term in (7.5.52) may dominate the response, yielding

$$\tilde{\underline{Q}} \approx \frac{(\underline{\psi}_p^T \tilde{\underline{F}})}{\tilde{m}_p (\omega_p^2 - \omega^2 + i2\xi_p \omega \omega_p)} \underline{\psi}_p \approx \frac{(\underline{\psi}_p^T \tilde{\underline{F}})}{\tilde{m}_p (i2\xi_p \omega \omega_p)} \underline{\psi}_p \quad (7.5.53)$$

This shows that the relative amplitudes and phase angles between responses at different dofs will be approximately the same as the relative amplitudes and phase angles between the corresponding components of mode shape p .

7.5.6 Receptance-Based Modal Parameter Identification: Method I

The experimental identification of mode shape components, modal frequencies, and damping ratios is a very useful technique for validating simulation models and for determining structural modifications to increase modal, shift natural frequencies, or decrease sensitivity to external forces. Two basic approaches are considered here, and more advanced techniques may be found in books dedicated to that subject, such as Ewins (2001).

Consider an orthogonally damped system and assume that the undamped system modes have been mass orthonormalized so that all modal masses are unity $\tilde{m}_l = 1 = \underline{\psi}_l^T \underline{M} \underline{\psi}_l$. Then the receptance formula in (7.5.35) is

$$R_{kj}(\omega) = \sum_{l=1}^N \frac{\psi_{kl} \psi_{jl}}{\omega_l^2 - \omega^2 + i2\xi_l \omega \omega_l} \quad (7.5.54)$$

Assume that the system is lightly damped and that the forcing frequency is nearly equal to the p th natural frequency. The p th mode will predominate in (7.5.54) so that

$$R_{kj}(\omega) \approx \frac{\psi_{kp}\psi_{jp}}{\omega_p^2 - \omega^2 + i2\xi_p\omega\omega_p} \quad (7.5.55)$$

or

$$R_{kj}^{-1}(\omega) \approx \frac{\omega_p^2 - \omega^2}{\psi_{kp}\psi_{jp}} + i \frac{2\xi_p\omega\omega_p}{\psi_{kp}\psi_{jp}} \quad (7.5.56)$$

Therefore, ω_p may be identified as the value of ω where an experimentally determined plot of $\text{Real}(R_{kj}^{-1}(\omega))$ becomes zero as depicted in Figure 7.5.2.

The phase angle of $R_{kj}(\omega)$ is given by (7.5.55) as

$$\phi_{kj} = \angle R_{kj} \approx \tan^{-1} \left(\frac{\text{Im}(R_{kj})}{\text{Re}(R_{kj})} \right) = \tan^{-1} \left(\frac{-2\xi_p\omega\omega_p}{\omega_p^2 - \omega^2} \right) \quad (7.5.57)$$

Following similar logic as in (7.3.58), the slope of the ϕ_{kj} versus ω curve is

$$\begin{aligned} \frac{d\phi_{kj}}{d\omega} &\approx \frac{1}{1 + \left[(2\xi_p\omega\omega_p) / (\omega_p^2 - \omega^2) \right]^2} * \frac{(\omega_p^2 - \omega^2)(-2\xi_p\omega_p) + (2\xi_p\omega\omega_p)(-2\omega)}{(\omega_p^2 - \omega^2)^2} \\ &= \frac{2\xi_p * \omega_p (-2\omega^2 + \omega^2 - \omega_p^2)}{(\omega_p^2 - \omega^2)^2 + (2\xi_p\omega\omega_p)^2} \end{aligned} \quad (7.5.58)$$

Evaluate this slope at $\omega = \omega_p$:

$$\left. \frac{d\phi_{kj}}{d\omega} \right|_{\omega=\omega_p} \approx \frac{-4\xi_p\omega_p^3}{4\xi_p^2\omega_p^4} = \frac{-1}{\omega_p\xi_p} \Rightarrow \xi_p = \frac{-1}{\omega_p * \left. \frac{d\phi_{kj}}{d\omega} \right|_{\omega=\omega_p}} \quad (7.5.59)$$

Therefore, approximate values of ξ_p and ω_p may be obtained from Figure 7.5.2 and (7.5.59) with receptances that are experimentally measured according to the definition in (7.5.43). The damping ratio ξ_p can also be identified by the “half power point” method discussed for SDOF systems (ref. Figure 7.3.9), again assuming that the p th mode strongly dominates the response.

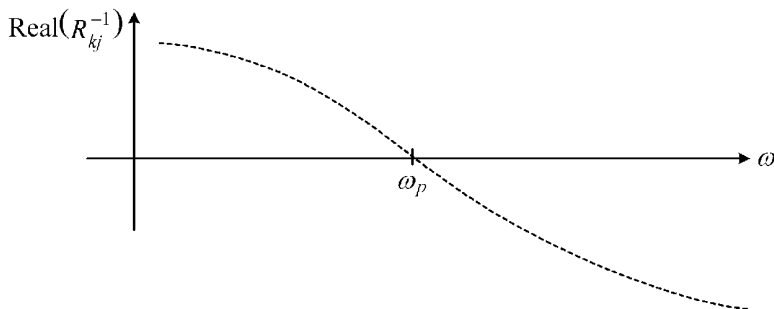


Figure 7.5.2 Real part of inverse receptance versus excitation frequency for mode p dominated response

In order to experimentally estimate the mode shape components at selected locations, assume that the receptances are measured at $\omega = \omega_p$ according with their definition (7.5.43) and that the p th mode strongly dominates the response. Equation (7.5.55) becomes

$$R_{kj}(\omega_p) = \text{phasor displacement at dof } k \text{ divided by phasor force at dof } j, \\ \text{with all other forces set to zero} \\ \approx \frac{\psi_{kp}\psi_{jp}}{i2\xi_p\omega_p^2} \Rightarrow \psi_{kp}\psi_{jp} \approx i2\xi_p\omega_p^2 R_{kj}(\omega_p) \quad (7.5.60)$$

Consider the special case when the displacement is measured at the force location ($k=j$). Then (7.5.60) yields

$$\psi_{jp} = \sqrt{i2\xi_p\omega_p^2 R_{jj}(\omega_p)} \quad (7.5.61)$$

From (7.5.55), R_{jj} is theoretically negative pure imaginary when $\omega = \omega_p$, so in practice (7.5.61) is replaced by

$$\psi_{jp} = \sqrt{2\xi_p\omega_p^2 |R_{jj}(\omega_p)|} \quad (7.5.62)$$

The selection of the positive root for ψ_{jp} in (7.5.61) and (7.5.62) does not violate the earlier condition that $\underline{\psi}_{-p}$ is mass orthonormalized since if

$$\underline{\psi}_{-p}^T \underline{M} \underline{\psi}_{-p} = 1 \quad (7.6.63)$$

it is also true that

$$\left(-\underline{\psi}_{-p}\right)^T \underline{M} \left(-\underline{\psi}_{-p}\right) = 1 \quad (7.5.64)$$

so either root may have been selected. To obtain the other components of the p th, mass-orthonormalized mode shape $\underline{\psi}_{-p}$, divide (7.5.60) by ψ_{jp}^2 where ψ_{jp} is given by (7.5.62)

$$\frac{\psi_{kp}}{\psi_{jp}} \cong \frac{i2\xi_p\omega_p^2 R_{kj}(\omega_p)}{2\xi_p\omega_p^2 |R_{jj}(\omega_p)|} \quad (7.5.65)$$

$$\Rightarrow \psi_{kp} = \psi_{jp} * \frac{iR_{kj}(\omega_p)}{|R_{jj}(\omega_p)|} \quad (7.5.66)$$

The i in (7.5.66) will multiply the i in $R_{kj}(\omega_p)$, which is theoretically pure imaginary by (7.5.60). In practice, $R_{kj}(\omega_p)$ may have a small real component so ψ_{kp} is determined from

$$\psi_{kp} \approx \text{sgn} * \psi_{jp} * \frac{|R_{kj}(\omega_p)|}{|R_{jj}(\omega_p)|} \quad (7.5.67)$$

where

$$\text{sgn} = \begin{cases} 1, & \text{if } \angle R_{kj}(\omega_p) - \angle R_{jj}(\omega_p) \approx 0^\circ \\ -1, & \text{if } \angle R_{kj}(\omega_p) - \angle R_{jj}(\omega_p) \approx \pm 180^\circ \end{cases}$$

This approach for identifying the mode shape $\underline{\psi}_p$ may lose its accuracy for large ξ_p and if other ω_l are close to ω_p .

EXAMPLE 7.5.4 Experimental Identification of Piping System Mode Shapes

Statement: A piping system is vibrating excessively and needs to be modified to reduce the possibility of high-cycle fatigue failure (Figure E7.5.4(a)). As a first step, mode shapes of the actual system are measured to verify the accuracy of the simulation model, which will be used to determine structural modifications to the piping system. The piping system consists of three branches and a common header, which is attached to a vessel through two bellows for accommodating thermal expansion. The bellows have a very low stiffness relative to the branch stiffness. The branches are connected by flanges at the opposite end to a second vessel.

Objective: Estimate the four mode shapes of the system from the given “measured” receptances.

The governing equations for the model are

$$\underline{M}\ddot{\underline{q}} + \underline{K}\underline{q} = \underline{f} \quad (1)$$

where

$$\underline{q} = (q_1 \ q_2 \ q_3 \ q_4)^T \quad (2)$$

$$\underline{M} = \begin{bmatrix} m_1 & 0 & 0 & 0 \\ 0 & m_2 & 0 & 0 \\ 0 & 0 & m_3 & 0 \\ 0 & 0 & 0 & m_4 \end{bmatrix}, \quad \underline{K} = \begin{bmatrix} k_1 + k_3 + k_5 & -k_1 & -k_3 & -k_5 \\ -k_1 & k_1 + k_2 & 0 & 0 \\ -k_3 & 0 & k_3 + k_4 & 0 \\ -k_5 & 0 & 0 & k_5 + k_6 \end{bmatrix} \quad (3)$$

The parameter values are provided in Table E7.5.4(a).

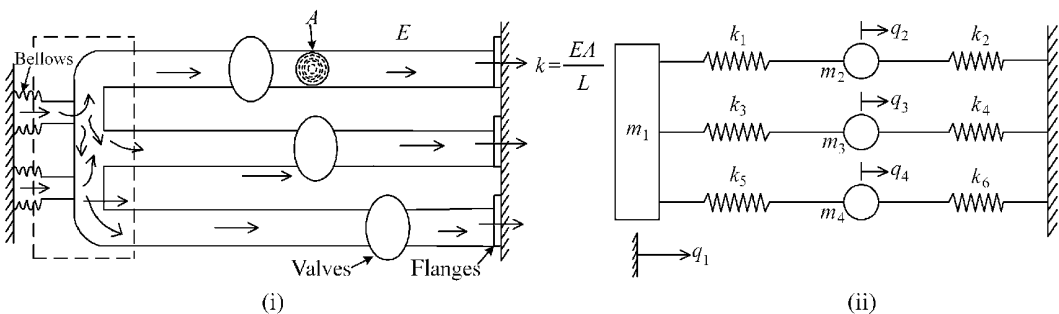


Figure E7.5.4(a) Piping system (i) and its simplified four-mass model (ii)

Table E7.5.4(a) Stiffness and mass values for the four-mass model

I	1	2	3	4	5	6
k_i (N/m)	10^9	0.5×10^9	2×10^9	0.75×10^9	3×10^9	5×10^9
m_i (kg)	500	200	300	150	—	—

The mass and stiffness properties are not required to identify the modal parameters and are provided only to describe the system. The modal parameters are instead identified from simulated “measured responses” to known input forces. For the sake of illustration, the simulated “measured responses” shown in Figure E7.5.4(b) were obtained by calculating the SSHR due to an excitation force applied at dof 3, that is,

$$\underline{f} = (0 \ 0 \ 100 \cos(\omega t) \ 0)^T \text{ N} \quad (4)$$

In actual practice, these amplitude and phase responses would be experimentally measured and the sinusoidal force would be applied with a shaker or impact hammer to the structure.

The undamped natural frequencies ω_i in Table E7.5.4(b) are estimated from the frequencies where peak amplitude occurs. The ξ_i are the damping ratios at the respective peaks as obtained by inserting the phase slope results shown in Figure E7.5.4(b) and the natural frequencies in Table E7.5.4(b) into Equation (7.5.59).

The “measured” receptances are determined from (7.5.50)

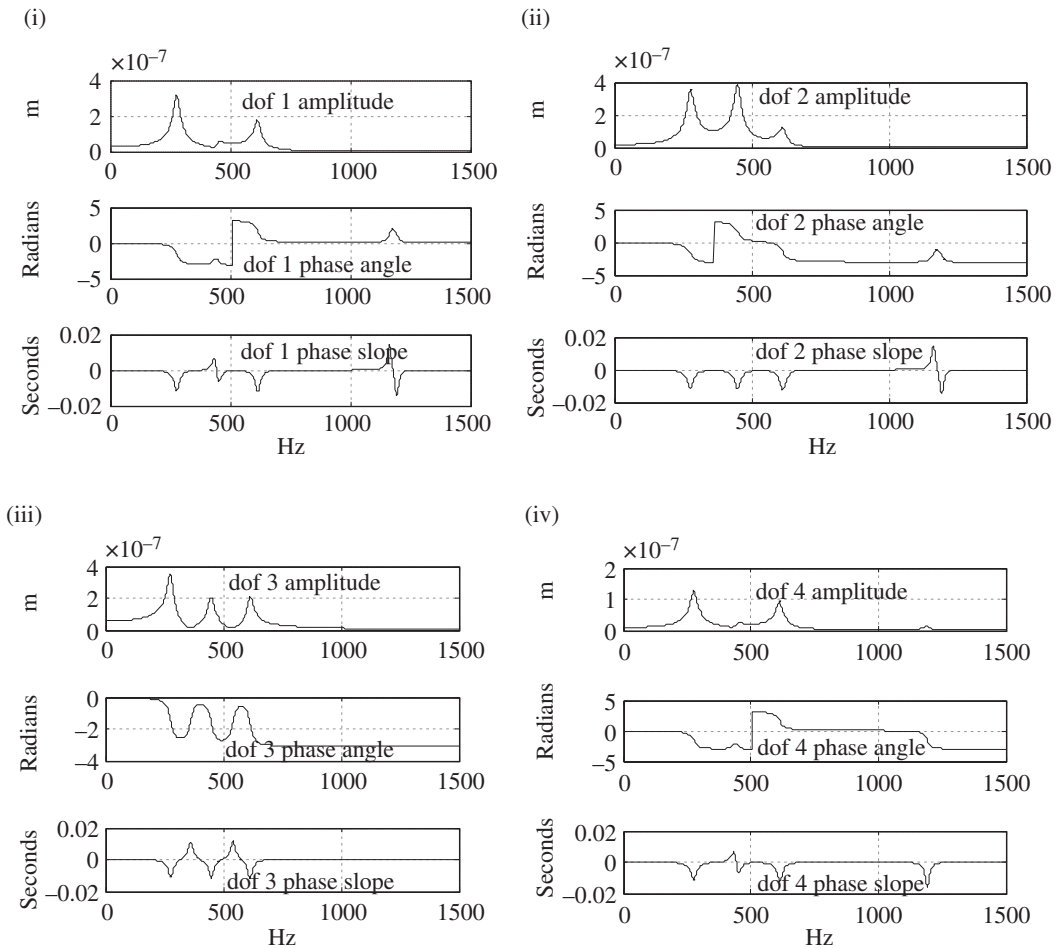


Figure E7.5.4(b) Displacement amplitude, phase angle ϕ , and phase slope ($d\phi/d\omega$) at (i) q_1 , (ii) q_2 , (iii) q_3 , and (iv) q_4 , due to a 100 N amplitude force at q_3

Table E7.5.4(b) Undamped natural frequencies and damping ratios

I	1	2	3	4
ω_i (rad/s)	$2\pi*277$	$2\pi*449$	$2\pi*613$	$2\pi*1192$
ξ_i (dim)	0.05	0.0298	0.0211	0.0083

Table E7.5.4(c) Receptances determined from the amplitude and phase angle responses in Figure E7.5.4(b).

R column 3 at ω_1	R column 3 at ω_2	R column 3 at ω_3	R column 3 at ω_4
$1.0e-008^*$	$1.0e-008^*$	$1.0e-008^*$	$1.0e-008^*$
$-0.0042 - 0.3179i$	$-0.0342 - 0.0374i$	$-0.0264 + 0.1765i$	$0.00052 + 0.00186i$
$-0.0286 - 0.3536i$	$-0.0244 + 0.3811i$	$0.0281 - 0.1179i$	$-0.00005 - 0.00019i$
$0.0327 - 0.3468i$	$0.0050 - 0.2079i$	$-0.0046 - 0.2083i$	$-0.00717 - 0.00046i$
$-0.0024 - 0.1264i$	$-0.0152 - 0.0163i$	$-0.0122 + 0.0919i$	$0.00067 - 0.01321i$

Table E7.5.4(d) Mass-orthonormal mode shapes estimated from responses with force at q_3

$\underline{\psi}_1$	$\underline{\psi}_2$	$\underline{\psi}_3$	$\underline{\psi}_4$
0.0296	0.0077	-0.0309	-0.0022
0.0331	-0.0577	0.0210	0.0002
0.0325	0.0314	0.0361	0.0082
0.0118	0.0034	-0.0161	0.0151

$$\underline{\tilde{Q}} = \underline{R}(\omega)\underline{\tilde{F}} = \text{phasor displacements} \quad (5)$$

where from (4),

$$\underline{\tilde{F}} = (0 \ 0 \ 100e^{i0^\circ} \ 0)^T = (0 \ 0 \ 100 \ 0)^T \quad (6)$$

Thus,

$$\underline{\tilde{Q}} = \underline{R}_3(\omega) * 100 \Rightarrow \underline{R}_3(\omega) = \text{third column of } \underline{R} \text{ (receptance matrix)} = \frac{\underline{\tilde{Q}}(\omega)}{100} \quad (7)$$

where the vector $\underline{\tilde{Q}}(\omega)$ contains the displacement phasors at all four masses due to the force applied at mass q_3 .

The displacement phasor at dof k is

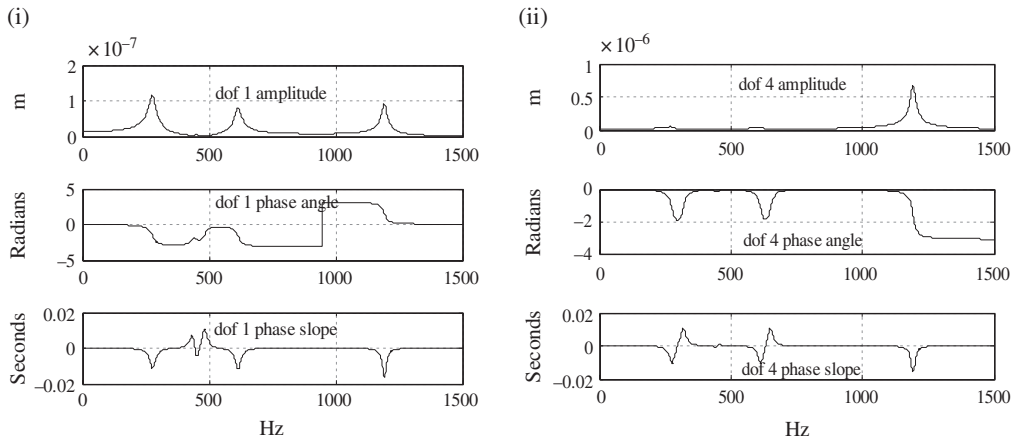
$$\tilde{Q}_k = |q_k| * e^{i\angle q_k} \quad (8)$$

The entries in $\underline{R}_3(\omega)$ are the receptances $R_{kj}(\omega)$ in (7.5.60), with $j=3$, $k=1$ through 4, and ω equals a natural frequency ω_p ($p=1,2,3,4$). Utilize (7) at each of the four resonant frequencies in Table E7.5.4(b) to obtain the receptances in Table E7.5.4(c).

These receptances and the ω_i and ξ_i from Table E7.5.4(b) are employed in formulas (7.5.62) and (7.5.67) to estimate the mass-orthonormal mode shapes in Table E7.5.4(d). The actual mass-orthonormal modes for this model are listed in Table E7.5.4(e).

Table E7.5.4(e) Exact mode shapes for the system model Figure E7.5.4(a)

$\underline{\psi}_1$	$\underline{\psi}_2$	$\underline{\psi}_3$	$\underline{\psi}_4$
0.0298	0.0056	-0.0310	-0.0110
0.0333	-0.0587	0.0210	0.0011
0.0323	0.0313	0.0361	0.0016
0.0118	0.0025	-0.0161	0.0791

**Figure E7.5.4(c)** Displacement amplitude, phase angle ϕ , and phase slope ($d\phi/d\omega$) at (i) q_1 and (ii) q_4 , due to a 100 N amplitude force at q_4

Comparison of these tables shows that modes 1, 2, and 3 have accurate estimates; however, the mode 4 estimate is poor. This is not surprising since a mode 4 peak is absent in the q_1 , q_2 , and q_3 plots and appears only as a small bump in the q_4 amplitude data in Figure E7.5.4(b). In actual practice, the shaker force would be moved from dof 3 to another location to try to more strongly excite mode 4. The mode 4 excitation is the corresponding “modal force” ($\underline{\psi}_4^T \tilde{\underline{F}}$) in (7.5.52). Table E7.5.4(e) shows that mode 4 has a relatively large component at q_4 so the “shaker” is placed at q_4 , that is, (6) becomes

$$\tilde{\underline{F}} = (0 \ 0 \ 0 \ 100)^T \quad (9)$$

The amplitude plots of q_1 and q_4 in Figure E7.5.4(c) confirm a strong mode 4 resonance results. The receptances corresponding to the force phasor in (9) are obtained from this figure using

$$\underline{R}_4(\omega_4) = \text{fourth column of } \underline{R} \text{ (receptance matrix)} = \frac{\tilde{\underline{Q}}(\omega_4)}{100}$$

which yields

$$\begin{aligned} R_{14} &= (-0.0028 + 0.0931i) \times 10^{-8} \\ R_{24} &= (0.0005 - 0.0096i) \times 10^{-8} \\ R_{34} &= (0.0007 - 0.0132i) \times 10^{-8} \\ R_{44} &= (0.0059 - 0.6728i) \times 10^{-8} \end{aligned} \quad (10)$$

The force is located at $j = 4$ (q_4), and the mode is $p = 4$, so the mode component at $k = 4$ (q_4) is from (7.5.62):

$$\psi_{jp} = \psi_{44} = \sqrt{2\xi_4\omega_4^2 |R_{44}(\omega_4)|} \quad (11)$$

The other components of mode 4 are obtained from (7.5.67) as

$$\psi_{kp} = \psi_{k4} = \text{sgn} * \psi_{44} * \frac{|R_{k4}(\omega_4)|}{|R_{44}(\omega_4)|} \quad (12)$$

where

$$\text{sgn} = \begin{cases} 1, & \text{if } \angle R_{k4}(\omega_4) - \angle R_{44}(\omega_4) \approx 0 \\ -1, & \text{if } \angle R_{k4}(\omega_4) - \angle R_{44}(\omega_4) \approx \pm 180^\circ \end{cases}$$

Utilizing (10) in (11) and (12) yields the new estimate for mode 4

$$\underline{\psi}_4 = (-0.0110 \ 0.0011 \ 0.0016 \ 0.0792)^T \quad (13)$$

which, by comparison to Table E7.5.4(e), is highly accurate.

7.5.7 Receptance-Based Modal Parameter Identification: Method II

The proceeding approach to Receptance-Based Modal Parameter Identification (RBMPI) requires taking measurements at near resonance conditions ($\omega \approx \omega_l$) and assumes that the modes are lightly damped. In practice, this may cause potentially damaging vibration and present a challenge of assuring that the measurements are very close to the resonances. Another approach to RBMPI is to utilize receptances that are measured at excitation frequencies (ω) well away from resonance frequencies (ω_l). Assume that the modes are to be measured in their mass-orthonormalized form (5.4.41) and that in an off-resonance condition

$$2\xi_l\omega_l\omega \ll \omega_l^2 - \omega^2 = (\omega_l + \omega)(\omega_l - \omega) \quad (7.5.68)$$

which is true if the system is lightly damped and if ω and ω_l are well separated.

Then from Equation (7.5.35),

$$R_{kj}(\omega) \approx \sum_{l=1}^m \frac{\psi_{kl}\psi_{jl}}{\omega_l^2 - \omega^2 + i2\xi_l\omega\omega_l} \approx \sum_{l=1}^m \frac{\psi_{kl}\psi_{jl}}{\omega_l^2 - \omega^2} = \sum_{l=1}^m \frac{\Lambda_{kj,l}}{\omega_l^2 - \Omega^2} \quad (7.5.69)$$

where only the m lowest modes have been included in the receptance summation and where

$$\Omega = \omega = \text{excitation frequency} \quad (7.5.70)$$

$$\Lambda_{kj,l} = \psi_{kl}\psi_{jl} \quad (7.5.71)$$

The receptance R_{kj} is measured at m separate excitation frequencies

$$\omega = \Omega_1, \Omega_2, \dots, \Omega_m \quad (7.5.72)$$

Equation (7.5.69) is written for these m frequencies as

$$\begin{Bmatrix} R_{kj}(\Omega_1) \\ R_{kj}(\Omega_2) \\ \vdots \\ R_{kj}(\Omega_m) \end{Bmatrix} = \begin{bmatrix} (\omega_1^2 - \Omega_1^2)^{-1} & (\omega_2^2 - \Omega_1^2)^{-1} & \cdots & (\omega_m^2 - \Omega_1^2)^{-1} \\ (\omega_1^2 - \Omega_2^2)^{-1} & (\omega_2^2 - \Omega_2^2)^{-1} & \cdots & (\omega_m^2 - \Omega_2^2)^{-1} \\ \vdots & \vdots & \cdots & \vdots \\ (\omega_1^2 - \Omega_m^2)^{-1} & (\omega_2^2 - \Omega_m^2)^{-1} & \cdots & (\omega_m^2 - \Omega_m^2)^{-1} \end{bmatrix} \begin{Bmatrix} \Lambda_{kj,1} \\ \Lambda_{kj,2} \\ \vdots \\ \Lambda_{kj,m} \end{Bmatrix} \quad (7.5.73)$$

and is solved for the $\Lambda_{kj,l}$ for $l = 1, 2, \dots, m$. From (7.5.71), the solution of (7.5.53) provides

$$\psi_{k1}\psi_{j1}, \psi_{k2}\psi_{j2}, \dots, \psi_{km}\psi_{jm} \quad (7.5.74)$$

for a fixed excitation point j and fixed response measurement point k . Let the excitation point (j) be fixed and measure the receptances at N response locations ($k = 1, \dots, N$). This step could be reversed with one response point and N excitation points, yielding similar results. Equation (7.5.73) is solved to obtain $\Lambda_{kj,l} = \psi_{kl}\psi_{jl}$ for each response point k utilizing the same (or different) excitation frequencies Ω_i as employed for the other response points. This yields numerical values for the following mode shape components:

$$\begin{array}{l} k=1 \rightarrow \\ k=2 \rightarrow \\ \vdots \\ k=j \rightarrow \\ \vdots \\ k=N \rightarrow \end{array} \begin{bmatrix} \psi_{11}\psi_{j1} & \psi_{12}\psi_{j2} & \psi_{13}\psi_{j3} & \cdots & \psi_{1m}\psi_{jm} \\ \psi_{21}\psi_{j1} & \psi_{22}\psi_{j2} & \psi_{23}\psi_{j3} & \cdots & \psi_{2m}\psi_{jm} \\ \vdots & \vdots & \vdots & \ddots & \vdots \\ \psi_{j1}\psi_{j1} & \psi_{j2}\psi_{j2} & \psi_{j3}\psi_{j3} & \cdots & \psi_{jm}\psi_{jm} \\ \vdots & \vdots & \vdots & \ddots & \vdots \\ \psi_{N1}\psi_{j1} & \psi_{N2}\psi_{j2} & \psi_{N3}\psi_{j3} & \cdots & \psi_{Nm}\psi_{jm} \end{bmatrix} \quad (7.5.75)$$

Taking the square root of the entries in the j th row of this matrix yields the j th component of all m mode shapes, that is,

$$\psi_{ji}, \quad i = 1, 2, \dots, m \text{ modes} \quad (7.5.76)$$

where j is the fixed, excitation location. Dividing the i th column of the matrix in (7.5.75) by ψ_{ji} yields the i th mode shape

$$\underline{\psi}_i = \begin{Bmatrix} \psi_{1i} \\ \psi_{2i} \\ \vdots \\ \psi_{Ni} \end{Bmatrix}, \quad i = 1, 2, \dots, m \quad (7.5.77)$$

Correct implementation of this method requires that the $R_{kj}(\omega)$ be nearly pure real numbers by (7.5.69). Thus, the excitation frequencies (Ω_i) should be selected so that $\angle R_{kj}$ is

nearly 0 or π , that is, 0° or 180° . To insure that the calculations produce real modes, utilize the approximation

$$R_{kj}(\Omega_l) \approx \text{Real}(R_{kj}(\Omega_l)) = |R_{kj}(\Omega_l)| * \cos(\angle R_{kj}(\Omega_l)) \quad (7.5.78)$$

at these frequencies.

EXAMPLE 7.5.5 *Experimental Identification of Piping System Mode Shapes by RBMPI: Method II*

Objective: Utilize the measurements of off-resonance receptances to estimate the lowest two mode shapes, $\underline{\psi}_1$ and $\underline{\psi}_2$, of the piping system studied in Example 7.5.4.

Assumption: The undamped natural frequencies, ω_1 and ω_2 , were determined by the “peak picking” or by the real (inverse receptance) crossover frequency (refer to Figure 7.5.2) methods to be

$$\omega_1 = 2\pi * 277 = 1740 \text{ rad/s}, \quad \omega_2 = 2\pi * 449 = 2821 \text{ rad/s} \quad (1)$$

For this example,

$$\begin{aligned} j &= 2 \quad (\text{excitation at dof 2}) \\ m &= 2 \quad (\text{modes to be identified}) \\ N &= 4 \quad (\text{number of components per mode shape}) \end{aligned} \quad (2)$$

Figure E7.5.5(a) shows valid frequencies for applying the off-resonance approach based on response phase angles that are near 0° or $\pm 180^\circ$, that is, π radians. These plots were obtained by applying the following force phasor at dof 2, that is,

$$\underline{\tilde{F}} = (0 \ 100 \ 0 \ 0)^T \quad (3)$$

Figure E7.5.5(a)-(i) shows the phase angle of q_1 is near 0° with an amplitude of 2.88×10^{-8} m at $f_1 = 100$ Hz and is near $-\pi$ with an amplitude of 5.57×10^{-8} m at $f_2 = 395$ Hz. Figure E7.5.5(a)-(ii) shows the phase angle of q_2 is near 0° with an amplitude of 9.1×10^{-8} m at $f_1 = 100$ Hz and is near zero with an amplitude of 1.3×10^{-7} m at $f_2 = 382$ Hz. Figure E7.5.5(a)-(iii) shows the phase angle of q_3 is near 0° with an amplitude of 2.2×10^{-8} m at $f_1 = 100$ Hz and is near $-\pi$ with an amplitude of 1.05×10^{-7} m at $f_2 = 364$ Hz. Figure E7.5.5(a)-(iv) shows the phase angle of q_4 is near 0° with an amplitude of 1.09×10^{-8} m at $f_1 = 100$ Hz and is near $-\pi$ with an amplitude of 2.36×10^{-8} m at $f_2 = 393$ Hz. Table E7.5.5(a) summarizes these results, where the receptance amplitudes $|R|$ listed equal the corresponding response amplitudes divided by 100 N, as in (7) of Example 7.5.4.

From (1), $\omega_1 = 1740$ rad/s and $\omega_2 = 2821$ rad/s. Then row 1 of Table E7.5.5(a) yields the following form for Equation (7.5.73):

$$\begin{Bmatrix} R_{12}(\Omega_1) \\ R_{12}(\Omega_2) \end{Bmatrix} = \begin{Bmatrix} 2.876 \times 10^{-10} \\ -5.57 \times 10^{-10} \end{Bmatrix} = \begin{bmatrix} 0.3798 \times 10^{-6} & 0.1322 \times 10^{-6} \\ -0.3192 \times 10^{-6} & 0.5563 \times 10^{-6} \end{bmatrix} \begin{Bmatrix} \Lambda_{12,1} \\ \Lambda_{12,2} \end{Bmatrix} \quad (4)$$

$$\Rightarrow \begin{Bmatrix} \Lambda_{12,1} \\ \Lambda_{12,2} \end{Bmatrix} = (\psi_{11}\psi_{21} \ \psi_{12}\psi_{22})^T = (0.9218 \times 10^{-3} \ -0.4724 \times 10^{-3})^T \quad (5)$$

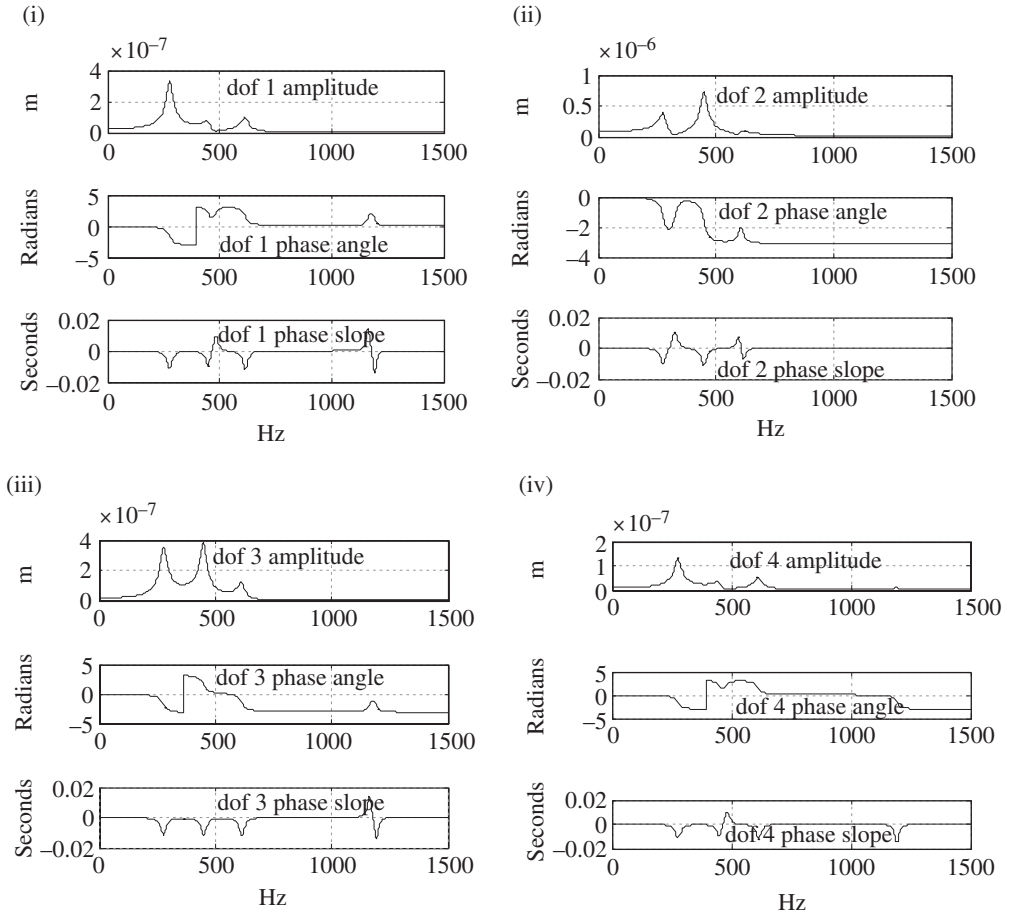


Figure E7.5.5(a) Displacement amplitude, phase angle ϕ , and phase slope ($d\phi/d\omega$) at (i) q_1 , (ii) q_2 , (iii) q_3 , and (iv) q_4 , due to a 100 N amplitude force at q_2

Table E7.5.5(a) Receptances at two selected forcing frequencies with phase near 0° or π

Dof	$\Omega_1 = 2\pi f_1$	$ R_1 $	$\angle R_1$	$R_1 \approx \text{Re}(R_1)$		$\Omega_2 = 2\pi f_2$	$ R_2 $	$\angle R_2$	$R_2 \approx \text{Re}(R_2)$	
				$= R_1 \cos(\angle R_1)$					$= R_2 \cos(\angle R_2)$	
$k=1$	628	2.88×10^{-10}	-0.051	2.876×10^{-10}		2482	5.53×10^{-10}	3.14	-5.57×10^{-10}	
$k=2$	628	9.06×10^{-10}	-0.0265	9.057×10^{-10}		2400	1.205×10^{-9}	-0.285	1.156×10^{-9}	
$k=3$	628	2.18×10^{-10}	-0.064	2.176×10^{-10}		2287	1.052×10^{-9}	3.138	-1.052×10^{-9}	
$k=4$	628	1.086×10^{-10}	-0.053	1.085×10^{-10}		2469	2.362×10^{-10}	3.14	-2.362×10^{-10}	

Table E7.5.5(b) Comparison of modes 1 and 2 for receptance and exact methods

	$\underline{\psi}_1$			$\underline{\psi}_2$		
	Exact	On-resonance (method I)	Off-resonance (method II)	Exact	On-resonance (method I)	Off-resonance (method II)
ψ_1	0.0298	0.0296	0.0266	0.0056	0.0077	0.0080
ψ_2	0.0333	0.0331	0.0346	-0.0587	-0.0577	-0.0591
ψ_3	0.0323	0.0325	0.0318	0.0313	0.0314	0.0253
ψ_4	0.0118	0.0118	0.0105	0.0025	0.0034	0.0037

Similarly, rows 2, 3, and 4 of Table E7.5.5(a) yield

$$\begin{aligned} \begin{Bmatrix} \Lambda_{22,1} \\ \Lambda_{22,2} \end{Bmatrix} &= (\psi_{21}\psi_{21} \quad \psi_{22}\psi_{22})^T = (0.12 \times 10^{-2} \quad 0.35 \times 10^{-2})^T \\ \begin{Bmatrix} \Lambda_{32,1} \\ \Lambda_{32,2} \end{Bmatrix} &= (\psi_{31}\psi_{21} \quad \psi_{32}\psi_{22})^T = (0.11 \times 10^{-2} \quad -0.15 \times 10^{-2})^T \\ \begin{Bmatrix} \Lambda_{42,1} \\ \Lambda_{42,2} \end{Bmatrix} &= (\psi_{41}\psi_{21} \quad \psi_{42}\psi_{22})^T = (0.362 \times 10^{-3} \quad -0.22 \times 10^{-3})^T \end{aligned} \quad (6)$$

The matrix in Equation (7.5.75) becomes

$$\begin{bmatrix} \psi_{11}\psi_{21} & \psi_{12}\psi_{22} \\ \psi_{21}\psi_{21} & \psi_{22}\psi_{22} \\ \psi_{31}\psi_{21} & \psi_{32}\psi_{22} \\ \psi_{41}\psi_{21} & \psi_{42}\psi_{22} \end{bmatrix} = \begin{bmatrix} 0.9218 \times 10^{-3} & -0.4724 \times 10^{-3} \\ 0.12 \times 10^{-2} & 0.35 \times 10^{-2} \\ 0.11 \times 10^{-2} & -0.15 \times 10^{-2} \\ 0.362 \times 10^{-3} & -0.22 \times 10^{-3} \end{bmatrix} \quad (7)$$

From the second row ($k=2$) of this equation,

$$\psi_{21} = \sqrt{0.0012} = 0.0346, \quad \psi_{22} = \sqrt{0.0035} = 0.0592 \quad (8)$$

Dividing the first column of (7) by ψ_{21} and the second column by ψ_{22} yields the first and second mode estimates

$$\underline{\psi}_1 = \begin{Bmatrix} \psi_{11} \\ \psi_{21} \\ \psi_{31} \\ \psi_{41} \end{Bmatrix} = \begin{Bmatrix} 0.0266 \\ 0.0346 \\ 0.0318 \\ 0.0105 \end{Bmatrix}, \quad \underline{\psi}_2 = \begin{Bmatrix} \psi_{12} \\ \psi_{22} \\ \psi_{32} \\ \psi_{42} \end{Bmatrix} = \begin{Bmatrix} -0.0080 \\ 0.0591 \\ -0.0253 \\ -0.0037 \end{Bmatrix} \quad (9)$$

The modal mass ($\underline{\psi}^T M \underline{\psi}$) is unchanged if $\underline{\psi}$ is replaced by $-\underline{\psi}$ so mode 2 can also be written as

$$\underline{\psi}_2 = (0.0080 \quad -0.0591 \quad 0.0253 \quad 0.0037)^T \quad (10)$$

and remain mass orthonormalized. Table E7.5.5(b) summarizes the receptance-based mode identification results for Examples 7.5.4 and 7.5.5. Both modes are mass orthonormalized.

7.5.8 Modal Assurance Criterion for Mode Shape Correlation

In practice, mode shape vectors must be compared for the following reasons: (i) comparing various measurements of the same mode shape, (ii) aiding to distinguish two mode shapes, and (iii) comparing the similarity between a measured mode shape and its model predicted counterpart. It is difficult to compare similarities of two large-order vectors (mode shapes) since each may possess many components. Consider the plotting of two mode shapes $\underline{\psi}_a$ and $\underline{\psi}_b$, which may be obtained by measurement, simulation (theory), or from both, as shown in Figure 7.5.3.

The slope of the curve fit is

$$\text{Mode scale factor} = \text{MSF} = \frac{\sum_{i=1}^N (\psi_{ia} \psi_{ib})}{\sum_{j=1}^N (\psi_{ia})^2} = \frac{\underline{\psi}_a^T \underline{\psi}_b}{\underline{\psi}_a^T \underline{\psi}_a} \quad (7.5.79)$$

Clearly, the mode scale factor (MSF) will equal 1.0 if $\underline{\psi}_a = \underline{\psi}_b$. A second parameter is defined to represent the deviation (scatter) of the points away from the linear curve fit

$$\text{Modal assurance criterion} = \text{MAC}(a, b) = \frac{(\underline{\psi}_a^T \underline{\psi}_b)^2}{(\underline{\psi}_a^T \underline{\psi}_a) (\underline{\psi}_b^T \underline{\psi}_b)} \quad (7.5.80)$$

For complex modes, this is generalized (Pandit, 1991) to the form

$$\text{MAC}(a, b) = \frac{|\bar{\underline{\psi}}_a^T \underline{\psi}_b|^2}{(\bar{\underline{\psi}}_a^T \underline{\psi}_a) (\bar{\underline{\psi}}_b^T \underline{\psi}_b)} \quad (7.5.81)$$

where the overbar ($\bar{\quad}$) indicates complex conjugate. Similar with the MSF, the modal assurance criterion (MAC) equals 1.0 if the modes are identical or if they differ by a scale factor. Two modes are considered to be strongly correlated if $\text{MAC} > 0.9$ and uncorrelated if $\text{MAC} < 0.05$.

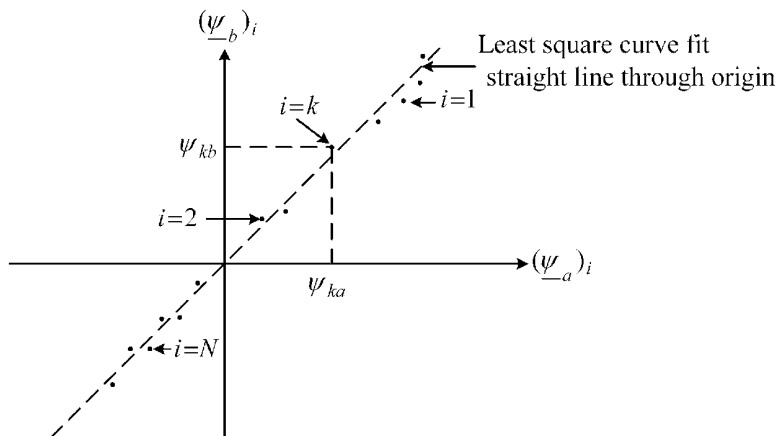


Figure 7.5.3 Plot of mode shape components $\underline{\psi}_b$ versus $\underline{\psi}_a$

Table E7.5.6(a) Estimated and exact mode shapes with a 100 N amplitude force at n

$\underline{\psi}_1^e$ estimated	$\underline{\psi}_1$ exact	$\underline{\psi}_2^e$ estimated	$\underline{\psi}_2$ exact	$\underline{\psi}_3^e$ estimated	$\underline{\psi}_3$ exact	$\underline{\psi}_4^e$ estimated	$\underline{\psi}_4$ exact
0.0296	0.0298	0.0077	0.0056	-0.0309	-0.0310	-0.0022	0.0110
0.0331	0.0333	-0.0577	-0.0587	0.0210	0.0210	0.0002	0.0011
0.0325	0.0323	0.0314	0.0313	0.0361	0.0361	0.0082	0.0016
0.0118	0.0118	0.0034	0.0025	-0.0161	-0.0161	0.0151	0.0791

EXAMPLE 7.5.6 *MAC Applied to Piping System Mode Shapes*

Objective: To apply the MAC between the estimated and exact mode shapes for the piping system of Examples 7.5.4 and 7.5.5.

Solution: The on-resonance, receptance-based estimates of the mode shapes for the 4 dof piping model shown in Figure E7.5.4(a) are listed in Tables E7.5.4(d) and E7.5.4(e) and repeated in Table E7.5.6(a).

The estimated modes were obtained with the excitation force at dof 3, which yielded a poor estimate of mode 4. The MAC matrix for this case is given by

$$\begin{bmatrix} \text{MAC}(\underline{\psi}_1^e, \underline{\psi}_1) & \text{MAC}(\underline{\psi}_1^e, \underline{\psi}_2) & \cdots & \text{MAC}(\underline{\psi}_1^e, \underline{\psi}_4) \\ \vdots & \vdots & \ddots & \vdots \\ \text{MAC}(\underline{\psi}_4^e, \underline{\psi}_1) & \cdots & \cdots & \text{MAC}(\underline{\psi}_4^e, \underline{\psi}_4) \end{bmatrix} = \begin{bmatrix} 1.0000 & 0.0377 & 0.0616 & 0.0240 \\ 0.0292 & 0.9987 & 0.0106 & 0.0010 \\ 0.0605 & 0.0076 & 1.0000 & 0.0385 \\ 0.1546 & 0.0546 & 0.0176 & 0.7924 \end{bmatrix} \quad (1)$$

These results show that the exact mode $\underline{\psi}_i$ and estimated mode $\underline{\psi}_j^e$ are strongly correlated for $i=j$ and weakly correlated if $i \neq j$. The exception is mode 4 in which case $\text{MAC}(\underline{\psi}_4^e, \underline{\psi}_4) = 0.7924$, which is less than the 0.9 good correlation limit. This is expected because of the poor estimate for mode 4. Swapping modes 3 and 4 in the estimated modal matrix yields the following MAC matrix:

$$\text{MAC} = \begin{bmatrix} 1.0000 & 0.0377 & 0.0616 & 0.0240 \\ 0.0292 & 0.9987 & 0.0106 & 0.0010 \\ 0.1546 & 0.0546 & 0.0176 & 0.7924 \\ 0.0605 & 0.0076 & 1.0000 & 0.0385 \end{bmatrix} \quad (2)$$

The $\text{MAC}(3,4) = 1.0$ result demonstrates the ability of the MAC method to match modes in two separate data sets, since the (3,4) corresponds to estimated and exact modes 3.

7.6 OTHER PHASOR RATIO MEASURES OF STEADY-STATE HARMONIC RESPONSE

The vibration literature contains several phasor ratios of (motion phasor)/(force phasor) and (force phasor)/(motion phasor), where phasor quantities are discussed in Section 2.5. It is useful to be aware of the definitions of these phasor ratios when reading the literature:

- (a) This chapter made extensive use of the receptance phasor (7.5.41)–(7.5.43):

$$\begin{aligned} R_{lj}(\omega) &= \text{displacement phasor at degree of freedom } l \text{ per force phasor at} \\ &\quad \text{degree of freedom } j \text{ with all other forces set to zero} \\ &= \frac{\tilde{Q}_l}{\tilde{F}_j} \left(\text{with } \tilde{F}_k = 0 \text{ for } k \neq j \right) = (l, j) \text{ entry of } \left(-\omega^2 \underline{M} + i\omega \underline{C} + \underline{K} \right)^{-1} \end{aligned} \quad (7.6.1)$$

The receptance R_{lj} is often referred to as a “dynamic flexibility.” This originates with the familiar static “flexibility” or “influence coefficient” defined as

$$\begin{aligned} r_{lj}(\omega) &= \text{static displacement at degree of freedom } l \text{ per static force} \\ &\quad \text{at degree of freedom } j \text{ with all other forces set to zero} \\ &= \frac{q_l}{f_j} \left(\text{with } f_k = 0 \text{ for } k \neq j \right) = (l, j) \text{ entry of } \underline{K}^{-1} \end{aligned} \quad (7.6.2)$$

The receptance R_{lj} is also referred to as “dynamic compliance” or “admittance.”

- (b) The inverse of the receptance $R_{lj}(\omega)$ is referred to as the “dynamic stiffness” or “dynamic modulus”:

$$\begin{aligned} K_{Dlj}(\omega) &= \text{force phasor at degree of freedom } l \text{ per displacement phasor at} \\ &\quad \text{degree of freedom } j \text{ with all other displacements set to zero} \\ &= \frac{\tilde{F}_l}{\tilde{Q}_j} \left(\text{with } \tilde{Q}_k = 0 \text{ for } k \neq j \right) = (l, j) \text{ entry of } \left(-\omega^2 \underline{M} + i\omega \underline{C} + \underline{K} \right) \end{aligned} \quad (7.6.3)$$

The dynamic stiffness equals the static stiffness when $\omega = 0$. The receptance $R_{lj}(\omega)$ is *not* the reciprocal of the dynamic stiffness $K_{Dlj}(\omega)$ except for SDOF systems.

- (c) The “mobility” is similar to the receptance but utilizes velocity instead of displacement:

$$\begin{aligned} M_{lj}(\omega) &= \text{velocity phasor at degree of freedom } l \text{ per force phasor at} \\ &\quad \text{degree of freedom } j \text{ with all other forces set to zero} \\ &= \frac{\tilde{V}_l}{\tilde{F}_j} \left(\text{with } \tilde{F}_k = 0 \text{ for } k \neq j \right) = \frac{i\omega \tilde{Q}_l}{\tilde{F}_j} = i\omega R_{lj}(\omega) \end{aligned} \quad (7.6.4)$$

- (d) The inverse quantity for $M_{lj}(\omega)$ is referred to as the “mechanical impedance”:

$$\begin{aligned} Z_{lj}(\omega) &= \text{force phasor at degree of freedom } l \text{ per velocity phasor at} \\ &\quad \text{degree of freedom } j \text{ with all other velocities set to zero} \\ &= \frac{\tilde{F}_l}{\tilde{V}_j} \left(\text{with } \tilde{V}_k = 0 \text{ for } k \neq j \right) \end{aligned} \quad (7.6.5)$$

- (e) The “inertance” of “acceleration” is similar to the receptance and mobility but utilizes acceleration:

$$\begin{aligned} A_{lj}(\omega) &= \text{acceleration phasor at degree of freedom } l \text{ per force phasor at} \\ &\quad \text{degree of freedom } j \text{ with all other forces set to zero} \\ &= \frac{\tilde{a}_l}{\tilde{F}_j} \left(\text{with } \tilde{F}_k = 0 \text{ for } k \neq j \right) = \frac{i\omega \tilde{V}_l}{\tilde{F}_j} = \frac{-\omega^2 \tilde{Q}_l}{\tilde{F}_j} \\ &= i\omega M_{lj}(\omega) = -\omega^2 R_{lj}(\omega) \end{aligned} \quad (7.6.6)$$

(f) The inverse quantity for $A_{lj}(\omega)$ is referred to as the “apparent mass”:

$$\begin{aligned}
 I_{lj}(\omega) &= \text{force phasor at degree of freedom } l \text{ per acceleration phasor at} \\
 &\quad \text{degree of freedom } j \text{ with all other accelerations set to zero} \\
 &= \frac{\tilde{F}_l}{\tilde{a}_j} \text{ (with } \tilde{a}_k = 0 \text{ for } k \neq j) \quad (7.6.7) \\
 &= \frac{\tilde{F}_l}{i\omega\tilde{V}_j} = \frac{\tilde{F}_l}{-\omega^2\tilde{Q}_j} = \frac{1}{i\omega}Z_{lj}(\omega) = \frac{-1}{\omega^2}K_{Dlj}(\omega)
 \end{aligned}$$

All of the preceding quantities (receptance, flexibility, compliance, admittance, stiffness, modulus, mobility, impedance, inertance, accelerance, and apparent mass) are defined for a specific force dof j and a response dof l . The quantity is referred to as “driving point” or “point,” that is, point impedance, if $l=j$. The quantity is referred to as “transfer” if $l \neq j$. In addition, the quantity may be referred to as “direct” if the directions ($x, y, z, \theta_x, \theta_y, \theta_z$) of dofs l and j are the same and “cross” if they are different.

From a measurement standpoint, it is much easier to set all forces to zero except for a single excitation force rather than to set all displacements equal to zero except for a single excitation displacement. Hence, only measurements of receptance, mobility, and inertance are typically performed. Harris (1988) provides a summary of impedance and mobility expressions for a variety of 1 and 2 dof system configurations.

7.7 SUMMARY

The topics covered in this chapter should provide the reader with an understanding and working knowledge of:

- (a) SSHR solution methodologies for 1, 2, and N dof systems
- (b) SSHR characteristics for constant amplitude, rotating imbalance, and ground motion disturbances
- (c) SSHR response amplitudes and phase angles
- (d) SSHR damping and resonance
- (e) Introductory rotor balancing methods
- (f) Principles of isolation of transmitted force and support motion
- (g) Analysis and design considerations for vibration absorber applications
- (h) SSHR solutions that utilize a modal expansion method
- (i) The use of receptances for predicting coupled system SSHR response of joined components and mode shapes
- (j) Introductory methods for modal parameter identification

7.8 CHAPTER 7 EXERCISES

7.8.1 Exercise Location

All exercises may be conveniently viewed and downloaded at the following website: **www.wiley.com/go/palazzolo**. This new feature greatly reduces the length of the printed book, yielding a significant cost savings for the college student, and the exercises are updated.

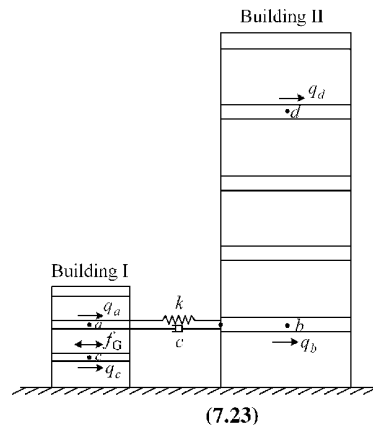
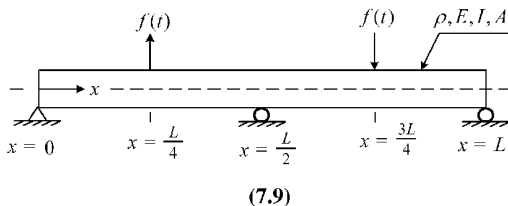
7.8.2 Exercise Goals

The goal of the Exercises in Chapter 7 is to strengthen the student's understanding and related engineering problem-solving skills in the following areas:

- Prediction of SSHR of vibrating systems to periodic forces. These periodic forces may be pure tone/single-frequency or multitone complex.
- Determination of SSHR of both lumped and continuous mass systems, the latter being modeled with finite elements or assumed modes.
- Implementation of vibration absorbers to translatory or rotational systems.
- Receptance-based synthesis of coupled systems joined by springs and dampers.
- Usage of receptances for parameter identification.
- Usage of the modal assurance criterion.

7.8.3 Sample Exercises: 7.9 and 7.23

Exercise 7.9 represents a large reciprocating compressor frame modeled as a continuous mass Euler–Bernoulli beam and utilizing the assumed modes approach. The system is subjected to periodic forces from crankshaft mass unbalance, resulting in SSHR. Exercise 7.23 treats two buildings that are under consideration for being joined together with a catwalk. Receptance synthesis must be utilized to determine if vibration caused by the punching operation in one building will adversely affect the precision inspection operation in the other building.



REFERENCES

- API Std 617, *Axial and Centrifugal Compressors and Expander-Compressors for Petroleum, Chemical and Gas Industry Services*, 7th ed., API Publishing Services, Washington, DC, R2002.
- BARLOW, M., *Balancing of High Speed Machinery*, Springer-Verlag, New York, 1989.
- BEARDS, C. T., *Vibration Analysis and Control System Dynamics*, Ellis Horwood, Chichester, 1981.
- DARLOW, M. S., MEHTA, R. K., SMALLEY, A. J., *NASA Contractor Report CR 135328 (N78-18460/TB)*, "Test parameters for elastomeric O-rings for range of materials, temperatures, amplitudes, squeeze values and stretch," August 1979.
- EWINS, D. J., *Modal Testing, Theory, Practice, and Application*, Research Studies Press, Baldock, 2001.
- HARRIS, C., *Shock and Vibration Handbook*, 3rd ed., McGraw Hill, New York, 1988.
- PANDIT, S., *Modal and Spectrum Analysis: Data Dependent Systems in State Space*, John Wiley & Sons, Inc., New York, 1991..

Chapter 8

Approximate Methods for Large-Order Systems

8.1 INTRODUCTION

The size (number of degrees of freedom (dofs)) of models continues to rapidly increase as machinery, structures, and other vibrating objects become more complex to increase performance and efficiency. This is somewhat a result of the development of automated finite element mesh generators that transform solid models into finely meshed finite element models (Example 10.10.1). Consequently, reducing computation time remains an important concern for many vibration simulation studies, especially for those that possess a large number of parameters to be varied in an intuitive or automated optimal design search.

Common approaches to reduce the computation time include:

- (a) **Kinematic constraints:** Simplify the model by imposing dependency relations between the dofs of a model as described in Section 2.11. This will reduce the model size and, depending on the engineering intuition and experience of the analyst, still preserve a sufficient level of prediction accuracy.
- (b) **Subspace condensation:** Restrict the solution space to a subspace spanned by a reduced set of basis vectors as described in Section 2.6. This step is typically applied to the model resulting from approach (a). The mode shape vectors are the most common basis vectors as illustrated in Chapters 5, 6, and 7. Other basis vector sets are also in widespread use such as Guyan basis vectors, which are treated in the next section.
- (c) **Receptance condensation:** Employ receptances to condense the number of dofs in the governing equations to those where forces are applied, interconnections between substructures are made, and local modifications are simulated. This approach is illustrated by the receptance synthesis shown in Example 7.5.3. The efficiency of this approach is enhanced by evaluating the receptances with truncated modal summation formulas such as (7.5.35) and (7.5.39).
- (d) **Reanalysis:** Utilize the solution to a “baseline model” to quickly obtain approximate solutions to the modified baseline model, which results from highly localized changes to the baseline model’s parameter values.
- (e) **Eigenproblem linearization:** The determinants in (2.8.9) and (2.8.10) clearly illustrate that eigenvalues, which provide mode natural frequencies and damping ratios, have a nonlinear dependence on system parameters. Solution for the eigenvalues for a multitude of parameter values can then become a computationally intensive task especially for large-order models. Two-term Taylor series approximations can be employed to obtain approximate, linearized relations between eigenvalues, eigenvectors (mode

shapes), and the model's parameters. These are particularly useful for obtaining an estimate of how an eigenvalue changes as a design parameter changes.

Some related approaches are discussed in this chapter.

8.2 GUYAN REDUCTION: STATIC CONDENSATION

Some dofs of most structural models typically have relatively small damping, inertia, and applied (external) forces associated with them. An example is bending rotation coordinates in beam-type models (frames or rotors) that have no added rotational inertia, damping, or external moments. The Guyan reduction method employs a special set of basis vectors (Section 2.6) to condense these dofs out of the model, thereby reducing the model size. Assume that the model dofs have been separated into two groups—retained (r) dofs and condensed (c) dofs—by ordering the dofs in the position vector as

$$\underline{q} = \begin{Bmatrix} \underline{q}_r \\ \underline{q}_c \end{Bmatrix} \quad (N \times 1) \quad (8.2.1)$$

where

$$N = n_r + n_c \quad (8.2.2)$$

The equilibrium equations will then have the form

$$\begin{bmatrix} \underline{m}_{rr} & \underline{m}_{rc} \\ \underline{m}_{cr} & \underline{m}_{cc} \end{bmatrix} \begin{Bmatrix} \underline{\ddot{q}}_r \\ \underline{\ddot{q}}_c \end{Bmatrix} + \begin{bmatrix} \underline{c}_{rr} & \underline{c}_{rc} \\ \underline{c}_{cr} & \underline{c}_{cc} \end{bmatrix} \begin{Bmatrix} \underline{\dot{q}}_r \\ \underline{\dot{q}}_c \end{Bmatrix} + \begin{bmatrix} \underline{k}_{rr} & \underline{k}_{rc} \\ \underline{k}_{cr} & \underline{k}_{cc} \end{bmatrix} \begin{Bmatrix} \underline{q}_r \\ \underline{q}_c \end{Bmatrix} = \begin{Bmatrix} \underline{f}_r \\ \underline{f}_c \end{Bmatrix} \quad (N \times 1) \quad (8.2.3)$$

or

$$\underline{M}\underline{\ddot{q}} + \underline{C}\underline{\dot{q}} + \underline{K}\underline{q} = \underline{f}(t) \quad (8.2.4)$$

The reordering of the matrices may be accomplished by utilizing a Boolean reordering matrix \underline{T} , as illustrated by the following example. Let \hat{q}_2 and \hat{q}_4 be retained dofs and \hat{q}_1 , \hat{q}_3 , and \hat{q}_5 the condensed dofs of a 5 dof system model. The original vector and reordered vector are then related by

$$\begin{Bmatrix} \hat{q}_1 \\ \hat{q}_2 \\ \hat{q}_3 \\ \hat{q}_4 \\ \hat{q}_5 \end{Bmatrix} = \begin{Bmatrix} q_{c1} \\ q_{r1} \\ q_{c2} \\ q_{r2} \\ q_{c3} \end{Bmatrix} = \begin{bmatrix} 0 & 0 & 1 & 0 & 0 \\ 1 & 0 & 0 & 0 & 0 \\ 0 & 0 & 0 & 1 & 0 \\ 0 & 1 & 0 & 0 & 0 \\ 0 & 0 & 0 & 0 & 1 \end{bmatrix} \begin{Bmatrix} q_{r1} \\ q_{r2} \\ q_{c1} \\ q_{c2} \\ q_{c3} \end{Bmatrix} = \begin{bmatrix} 0 & 0 & 1 & 0 & 0 \\ 1 & 0 & 0 & 0 & 0 \\ 0 & 0 & 0 & 1 & 0 \\ 0 & 1 & 0 & 0 & 0 \\ 0 & 0 & 0 & 0 & 1 \end{bmatrix} \begin{Bmatrix} \underline{q}_r \\ \underline{q}_c \end{Bmatrix} = \underline{T} \begin{Bmatrix} \underline{q}_r \\ \underline{q}_c \end{Bmatrix} \quad (8.2.5)$$

Let $\hat{\underline{M}}$, $\hat{\underline{C}}$, $\hat{\underline{K}}$, and $\hat{\underline{F}}$ be the mass, damping, and stiffness matrices and force vector, respectively, for the original unarranged dofs. The rearranged system's matrices and force vector, as shown in (8.2.3) or (8.2.4), are given by

$$\underline{M} = \underline{T}^T \hat{\underline{M}} \underline{T}, \quad \underline{C} = \underline{T}^T \hat{\underline{C}} \underline{T}, \quad \underline{K} = \underline{T}^T \hat{\underline{K}} \underline{T}, \quad \underline{F} = \underline{T}^T \hat{\underline{F}} \quad (8.2.6)$$

The assumption that the condensed (c) dofs have negligible inertia, damping, and external forces simplifies (8.2.3) to the form

$$\begin{bmatrix} \underline{m}_{rr} & \underline{0} \\ \underline{0} & \underline{0} \end{bmatrix} \begin{Bmatrix} \underline{\ddot{q}}_r \\ \underline{\ddot{q}}_c \end{Bmatrix} + \begin{bmatrix} \underline{c}_{rr} & \underline{0} \\ \underline{0} & \underline{0} \end{bmatrix} \begin{Bmatrix} \underline{\dot{q}}_r \\ \underline{\dot{q}}_c \end{Bmatrix} + \begin{bmatrix} \underline{k}_{rr} & \underline{k}_{rc} \\ \underline{k}_{cr} & \underline{k}_{cc} \end{bmatrix} \begin{Bmatrix} \underline{q}_r \\ \underline{q}_c \end{Bmatrix} = \begin{Bmatrix} \underline{f}_r \\ \underline{0} \end{Bmatrix} \quad (N \times 1) \quad (8.2.7)$$

Consider the bottom partition in this equation:

$$\underline{k}_{cr} \underline{q}_r + \underline{k}_{cc} \underline{q}_c = \underline{0} \quad (8.2.8)$$

$$\Rightarrow \underline{q}_c = -\underline{k}_{cc}^{-1} \underline{k}_{cr} \underline{q}_r \quad (n_c \times 1) \quad (8.2.9)$$

The inverse of matrix \underline{k}_{cc} in (8.2.9) will exist only if the retained dofs are selected such that *if all of the retained dofs are fixed*

$$\underline{q}_r = \underline{0} \quad (8.2.10)$$

then the remaining portion of the model is fully constrained against any rigid body motion. This is consistent with the notion from (8.2.9) that \underline{q}_c is dependent on \underline{q}_r since if \underline{q}_r is zero, (8.2.8) becomes

$$\underline{k}_{cc} \underline{q}_c = \underline{0} \quad (8.2.11)$$

which implies that $\underline{q}_c = 0$ if \underline{k}_{cc}^{-1} exists. On the other hand, if \underline{k}_{cc} was singular, \underline{q}_c could assume any value in the null space of \underline{k}_{cc} independent of \underline{q}_r . Thus, the dependency of \underline{q}_c on \underline{q}_r requires that \underline{k}_{cc}^{-1} exists. The dependency relation in (8.2.9) can be written for the complete system as

$$\underline{q} = \begin{Bmatrix} \underline{q}_r \\ \underline{q}_c \end{Bmatrix} = \begin{Bmatrix} \underline{q}_r \\ -\underline{k}_{cc}^{-1} \underline{k}_{cr} \underline{q}_r \end{Bmatrix} = \begin{bmatrix} \underline{I}_{nr} \\ -\underline{k}_{cc}^{-1} \underline{k}_{cr} \end{bmatrix} \begin{Bmatrix} \underline{q}_r \end{Bmatrix} \quad (8.2.12)$$

or

$$\underline{q} = \underline{T}_G \underline{q}_r \quad (8.2.13)$$

where the *Guyan transformation matrix* is given by

$$\underline{T}_G = \begin{bmatrix} \underline{T}_{G1} & \underline{T}_{G2} & \cdots & \underline{T}_{Gn_r} \end{bmatrix} = \begin{bmatrix} \underline{I}_{n_r} \\ \underline{k}_{cc}^{-1} \underline{k}_{cr} \end{bmatrix} \quad (8.2.14)$$

Equations (8.2.12)–(8.2.14) have the general form of the coordinate transformation, or change of basis, as shown in (2.6.9) and the related discussion. As discussed in Section 2.6, the column vectors of \underline{T}_G are the basis vectors of the transformation. These basis vectors have a physical interpretation as can be explained by expressing \underline{k}_{cr} column-wise as

$$\underline{k}_{cr} = \begin{bmatrix} \underline{k}_{cr1} & \underline{k}_{cr2} & \cdots & \underline{k}_{cm_r} \end{bmatrix} \quad (8.2.15)$$

Assume that all retained dofs (\underline{q}_r) are held fixed except for dof j , which is given a unit displacement so that

$$\underline{q}_{rj} = \left\{ \begin{array}{c} 0 \\ \vdots \\ 1 \\ \vdots \\ 0 \end{array} \right\} \leftarrow \text{row } j \quad (8.2.16)$$

and then by (8.2.9)

$$\underline{q}_{cj} = -\underline{k}_{cc}^{-1} \underline{k}_{cr} \underline{q}_{rj} = -\underline{k}_{cc}^{-1} \underline{k}_{crj} \quad (8.2.17)$$

= vector of all condensed degrees of freedom due to
imposing a unit displacement on the j th retained degree of freedom q_{rj}
while holding all other retained degrees of freedom fixed

The total system's deflection vector becomes

$$\underline{q}_j = \left\{ \begin{array}{c} \underline{q}_{rj} \\ \underline{q}_{cj} \end{array} \right\} = \left\{ \begin{array}{c} \underline{e}_j \\ -\underline{k}_{cc}^{-1} \underline{k}_{crj} \end{array} \right\} \quad (8.2.18)$$

where

$$\underline{e}_j = \left\{ \begin{array}{c} 0 \\ \vdots \\ 1 \\ \vdots \\ 0 \end{array} \right\} \leftarrow \text{row } j \quad (8.2.19)$$

Collect all \underline{q}_j as columns of a matrix

$$\begin{aligned} \left[\begin{array}{cccc} \underline{q}_{r1} & \underline{q}_{r2} & \cdots & \underline{q}_{rm_r} \\ \underline{q}_{c1} & \underline{q}_{c2} & \cdots & \underline{q}_{cm_r} \end{array} \right] &= \left[\begin{array}{cccc} \underline{e}_1 & \underline{e}_2 & \cdots & \underline{e}_{n_r} \\ -\underline{k}_{cc}^{-1} \underline{k}_{cr1} & -\underline{k}_{cc}^{-1} \underline{k}_{cr2} & \cdots & -\underline{k}_{cc}^{-1} \underline{k}_{cm_r} \end{array} \right] \\ &= \left[\begin{array}{c} \underline{I}_{n_r} \\ -\underline{k}_{cc}^{-1} \left[\underline{k}_{cr1} \quad \underline{k}_{cr2} \quad \cdots \quad \underline{k}_{cm_r} \right] \end{array} \right] = \left[\begin{array}{c} \underline{I}_{n_r} \\ -\underline{k}_{cc}^{-1} \underline{k}_{cr} \end{array} \right] \end{aligned} \quad (8.2.20a)$$

Comparing (8.2.14) and (8.2.2) shows that the j th column of the Guyan transformation matrix is

$$\begin{aligned} \underline{T}_{Gj} &= \text{the total system deflection vector } \underline{q} \text{ for the case} \\ &\text{when a unit displacement is imposed on the} \\ &\text{\textit{j}th retained degree of freedom } q_{rj} \text{ while all other} \\ &\text{retained degrees of freedom are held fixed} \end{aligned} \quad (8.2.20b)$$

The Guyan reduction method makes the approximation that the $N \times 1$ total system displacement vector \underline{q} in (8.2.1) is restricted to the subspace spanned by the n_r basis vectors $\underline{T}_{G1}, \underline{T}_{G2}, \dots, \underline{T}_{Gn_r}$, that is,

$$\underline{q} = \underline{T}_G \underline{q}_r = \begin{bmatrix} \underline{I}_{nr} \\ -\underline{k}_{cc}^{-1} \underline{k}_{cr} \end{bmatrix} \underline{q}_r = \sum_{j=1}^{n_r} q_{rj}(t) \underline{T}_{Gj} \quad (8.2.21)$$

This has the identical form with the general subspace condensation equation (2.6.9) and the modal subspace condensation equations (6.3.11)–(6.3.13):

$$\underline{q} = \underline{\Psi} \underline{\chi} = \sum_{j=1}^{n_m} \chi_j(t) \underline{\psi}_j \quad (8.2.22)$$

Substitute (8.2.21) into (8.2.4) and premultiply the results by \underline{T}_G^T to obtain

$$\underline{\tilde{M}} \underline{\ddot{q}}_r + \underline{\tilde{C}} \underline{\dot{q}}_r + \underline{\tilde{K}} \underline{q}_r = \underline{\tilde{f}} \quad (n_r \times 1) \quad (8.2.23)$$

where

$$\underline{\tilde{M}} = \underline{T}_G^T \underline{M} \underline{T}_G \quad (n_r \times n_r), \quad \underline{\tilde{C}} = \underline{T}_G^T \underline{C} \underline{T}_G \quad (n_r \times n_r), \quad \underline{\tilde{K}} = \underline{T}_G^T \underline{K} \underline{T}_G \quad (n_r \times n_r) \quad (8.2.24)$$

$$\underline{\tilde{f}} = \underline{T}_G^T \underline{f} \quad (n_r \times 1) \quad (8.2.25)$$

Thus, it is seen that the dimension of the equilibrium problem has been condensed from $(N \times N)$ in (8.2.4) to $(n_r \times n_r)$ in (8.2.23). The selection of which dofs are retained is somewhat based on experience but can be automated (Cook, 1989). A general rule is to retain dofs with relatively large concentrated mass, damping, external force, or moment.

EXAMPLE 8.2.1 Power Generation, Machinery Shaft Train Torsional Vibration

Statement: Large turbine-generator sets consist of high-pressure (HP), intermediate-pressure (IP), and low-pressure (LP) turbines and a generator and exciter. The exciter is a generator that supplies power to the field windings of the main generator. These sets may experience torsional vibration due to lack of damping (0.1% or lower) and electrical disturbance torques originating in the active part of the generator (Huster and Eckert, 1998). This vibration may lead to premature failure of the turbine blades, with potentially catastrophic consequences. The torque excitations are due to electromagnetic field disturbances in the air gap of the generator, and their effects propagate to all of the machinery components since they are rigidly coupled together. The excitation frequency occurs at 1 or 2 times line frequency (60 or 50 Hz). The disturbances are caused by:

Short circuits in the electrical grid, transformer, or generator stator windings
Synchronization failure

The duration of the excitation may be as short as 0.2 seconds and may be several times greater in magnitude than the nominal torque of the unit. Figure E8.2.1(a) depicts a large, power generating, turbine-generator set, and Figure E8.2.1(b) shows its simplified torsional vibration model. The lumped inertias represent rows of blade stages, coupling flanges, shaft

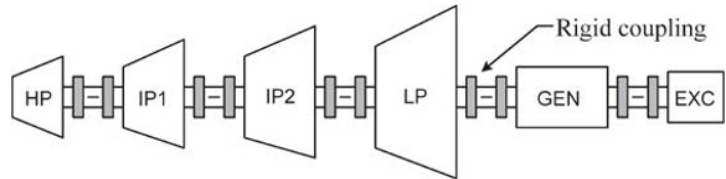
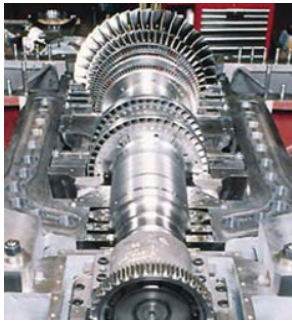


Figure E8.2.1(a) Turbine-generator set and typical machinery train layout. © Utilities & Energy Services | Texas A&M University

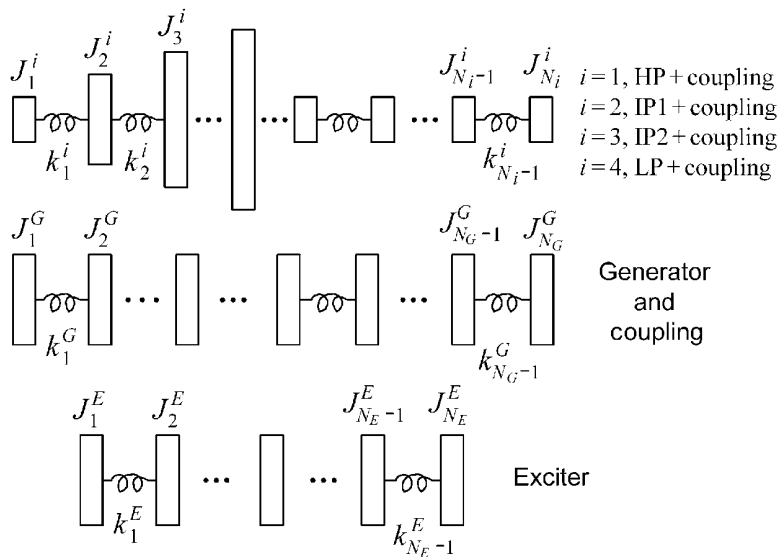


Figure E8.2.1(b) Simulation model for torsional vibration of machinery train

runs, bearing locations, and so on. The torsional stiffness results from twisting of the shaft and for a hollow circular shaft is $k_j = (G_j J_{Aj}) / L_j$ where G_j , J_{Aj} , and L_j are the j th shaft section's shear modulus, polar moment of inertia $[\pi(D_o^4 - D_i^4)/32]$, and length, respectively.

Objective: Compare the Guyan reduction, modal condensation, and exact solution approaches for predicting the transient, torsional response due to a sudden disturbance torque in the generator.

Assumptions: Linear model, and the only damping in the model is discrete (concentrated) damping at the bearings, that is, there is no orthogonal damping (5.4.93).

Parameter Values: The rotational inertias, torsional spring constants, and bearing torsional damping (drag) constants are listed in Table E8.2.1(a). Each station in this table consists of a lumped rotational inertia, rotational stiffness, and damping constant. This is illustrated in Figure E8.2.1(c).

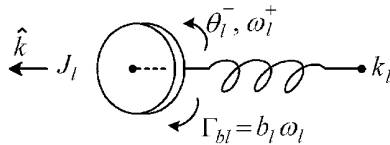
Table E8.2.1(a) Shaft and bearing model parameters

Machine	Global station no. l	Local station no.	J_l (kg m ²)	k_l (N/m $\times 10^8$)	b_l (N m s)
HPT	1	1	50	2.5	150
	2	2	75	3.5	0
	3	3	80	3.5	0
	4	4	200	3.5	0
	5	5	300	3.5	0
	6	6	75	2.5	0
	7	7	50	2.5	150
	8	8	50	2.5	0
	9	9	75	3.0	0
IP ₁ T	10	1	50	2.5	0
	11	2	50	2.5	0
	12	3	50	2.5	200
	13	4	100	4.5	0
	14	5	105	5.0	0
	15	6	300	5.0	0
	16	7	400	5.0	0
	17	8	105	5.0	0
	18	9	100	4.5	0
	19	10	50	2.5	200
IP ₂ T	20	11	50	2.5	0
	21	12	75	3.0	0
	22	1	50	2.5	0
	23	2	50	2.5	0
	24	3	50	2.5	200
	25	4	100	4.5	0
	26	5	105	5.0	0
	27	6	300	5.0	0
	28	7	400	5.0	0
	29	8	105	5.0	0
	30	9	100	4.5	0
	31	10	50	2.5	200
LPT	32	11	50	2.5	0
	33	12	75	3.0	0
	34	1	50	2.5	0
	35	2	50	2.5	0
	36	3	50	2.5	250
	37	4	100	5.0	0
	38	5	125	6.0	0
	39	6	125	6.0	0
	40	7	500	6.0	0
	41	8	600	6.0	0
	42	9	700	6.0	0
	43	10	125	5.0	0
	44	11	75	4.0	0
	45	13	50	2.5	250

(continued overleaf)

Table E8.2.1(a) (continued)

Machine	Global station no. l	Local station no.	J_l (kg m ²)	k_l (N/m × 10 ⁸)	b_l (N m s)
GEN	46	13	50	2.5	0
	47	14	75	3.0	0
	48	1	50	2.5	0
	49	2	50	2.5	150
	50	3	75	3.0	0
	51	4	250	3.0	0
	52	5	250	3.0	0
	53	6	75	3.0	0
	54	7	50	2.5	150
	55	8	50	2.5	0
EXC	56	9	75	3.0	0
	57	1	25	1.5	0
	58	2	25	1.5	75
	59	3	100	2.5	0
	60	4	100	2.5	0
	61	5	25	2.5	0
	62	6	25	0	75

**Figure E8.2.1(c)** Typical station in machinery train model

The transient load torque disturbance applied to generator stations 51 and 52 is given by

$$\Gamma_{\text{dist}} = \begin{cases} 0, & t < 0 \\ 0.5 \times 10^6 \sin(\omega_L t) + 0.25 \times 10^6 \sin(2\omega_L t), & 0 \leq t \leq 0.2 \\ 0, & t > 0.2 \text{ second} \end{cases} \quad (1)$$

where

$$\omega_L = \text{line frequency} = 2\pi * 60 \text{ rad/s} \quad (2)$$

Solution: The system matrices may be derived utilizing the finite element approach as discussed in Section 4.7 or by direct application of Lagrange's equation. The potential energy (4.5.88) and the $\partial U / \partial \underline{\theta}$ term in Lagrange's equation (4.5.106b) are

$$U = \frac{1}{2} \sum_{l=1}^{N-1} k_l (\theta_{l+1} - \theta_l)^2, \quad \frac{\partial U}{\partial \underline{\theta}} = \underline{K} \underline{\theta} = \begin{bmatrix} k_1 & -k_1 & 0 & \cdots & 0 & 0 \\ & k_1 + k_2 & -k_2 & \cdots & 0 & 0 \\ & & k_2 + k_3 & \cdots & 0 & 0 \\ & & & \ddots & \vdots & \vdots \\ \text{symmetric} & & & & k_{N-1} + k_{N-2} & -k_{N-1} \\ & & & & & k_{N-1} \end{bmatrix} \begin{Bmatrix} \theta_1 \\ \theta_2 \\ \theta_3 \\ \vdots \\ \theta_{N-1} \\ \theta_N \end{Bmatrix} \quad (3)$$

The kinetic energy (4.2.14) and the $(d/dt)(\partial T/\partial \dot{\underline{\theta}})$ term in Lagrange's equation (4.6.52) are

$$T = \frac{1}{2} \sum_{l=1}^N J_l \dot{\theta}_l^2, \quad \frac{d}{dt} \left(\frac{\partial T}{\partial \dot{\underline{\theta}}} \right) = \underline{M} \ddot{\underline{\theta}} = \begin{bmatrix} J_1 & 0 & 0 & \cdots & 0 & 0 \\ & J_2 & 0 & \cdots & 0 & 0 \\ & & J_3 & \cdots & 0 & 0 \\ & & & \ddots & \vdots & \vdots \\ \text{symmetric} & & & & J_{N-1} & 0 \\ & & & & & J_N \end{bmatrix} \begin{Bmatrix} \ddot{\theta}_1 \\ \ddot{\theta}_2 \\ \ddot{\theta}_3 \\ \vdots \\ \ddot{\theta}_{N-1} \\ \ddot{\theta}_N \end{Bmatrix} \quad (4)$$

The Rayleigh dissipation function (4.5.104) and the $\partial \mathfrak{S}^d/\partial \dot{\underline{\theta}}$ term in Lagrange's equation (4.6.52) are

$$\mathfrak{S}^d = \frac{1}{2} \sum_{l=1}^N b_l \dot{\theta}_l^2, \quad \frac{\partial \mathfrak{S}^d}{\partial \dot{\underline{\theta}}} = \underline{C} \dot{\underline{\theta}} = \begin{bmatrix} b_1 & 0 & 0 & \cdots & 0 & 0 \\ & b_2 & 0 & \cdots & 0 & 0 \\ & & b_3 & \cdots & 0 & 0 \\ & & & \ddots & \vdots & \vdots \\ \text{symmetric} & & & & b_{N-1} & 0 \\ & & & & & b_N \end{bmatrix} \begin{Bmatrix} \dot{\theta}_1 \\ \dot{\theta}_2 \\ \dot{\theta}_3 \\ \vdots \\ \dot{\theta}_{N-1} \\ \dot{\theta}_N \end{Bmatrix} \quad (5)$$

where b_l is zero except at the bearing stations as shown in Table E8.2.1(a). *The disturbance torques occur only at stations 51 and 52 and are defined by Equation (2).* The generalized torque (4.5.43) and the \underline{Q} term in Lagrange's equations (4.5.48) and (4.5.106b) are

$$Q_{\Gamma l} = \Gamma_{\text{dist}} \hat{k} \cdot \frac{\partial \omega_{51} \hat{k}}{\partial \theta_l} + \Gamma_{\text{dist}} \hat{k} \cdot \frac{\partial \omega_{52} \hat{k}}{\partial \theta_l}, \quad \underline{Q} = \begin{Bmatrix} Q_1 \\ Q_2 \\ \vdots \\ Q_{51} \\ Q_{52} \\ \vdots \\ Q_N \end{Bmatrix} = \begin{Bmatrix} 0 \\ 0 \\ \vdots \\ \Gamma_{\text{dist}}(t) \\ \Gamma_{\text{dist}}(t) \\ \vdots \\ 0 \end{Bmatrix} \quad (6)$$

The system Lagrange equation (4.5.106b) is

$$\frac{d}{dt} \left(\frac{\partial T}{\partial \dot{\underline{\theta}}} \right) + \frac{\partial \mathfrak{S}^d}{\partial \dot{\underline{\theta}}} + \frac{\partial U}{\partial \underline{\theta}} = \underline{Q} \quad (N \times 1) \quad (7)$$

or by substituting (3)–(6) into (7)

$$\underline{M} \ddot{\underline{\theta}} + \underline{C} \dot{\underline{\theta}} + \underline{K} \underline{\theta} = \underline{Q}(t) \quad (8)$$

which has the first-order form

$$\dot{\underline{\theta}} = \underline{\omega}, \quad \dot{\underline{\omega}} = \underline{M}^{-1} \left(\underline{Q}(t) - \underline{C} \underline{\omega} - \underline{K} \underline{\theta} \right) \quad (9)$$

The matrices and vector are rearranged according to the order shown in (8.2.1) and (8.2.3) with

$$\underline{q} = \begin{Bmatrix} \underline{q}_r \\ \underline{q}_c \end{Bmatrix} \quad (10)$$

The rearrangement operation was checked by confirming that the original and rearranged system's undamped natural frequencies were identical.

Results: The twenty lowest natural frequencies of the system including all dofs as retained are shown in Table E8.2.1(b). The undamped system's mass-orthonormalized (5.4.39) rigid body mode and five lowest flexible modes are shown in Figure E8.2.1(d).

The full, 62 dof system's transient responses at stations 5, 16, 28, 42, 52, and 60 are shown in Figure E8.2.1(e). These are the stations with the largest inertias in the HPT, IP1T, IP2T, LPT, GEN, and EXC machines, respectively. The numerical integration is performed using MATLAB's ODE45 integrator, and the maximum angular vibration amplitude over all of the stations in the model is 8.4° . The torsional excitation (1) is applied on the generator and takes time to affect the motion of the high-pressure (HP) turbine in Figure E8.2.1(a). This time delay is (0.025 seconds) indicated by the top plot in Figure E8.2.1(e)-(i). The high-frequency oscillation at stations 52 and 60 in Figure E8.2.1(e) is due to ringing of the lightly damped, -fifth flexible body mode (66.46 Hz) in Table E8.2.1(b). This is evident in the expanded plot of the angular displacement at station 60, as shown in Figure E8.2.1(e)-(ii). The

Table E8.2.1(b) Twenty lowest natural frequencies (Hz) of the full model

0	14.29	28.40	35.94	47.87	66.46	104.4	115.2	128.9	137.4
151.9	168.3	171.3	189.7	206.3	221.1	235.0	252.0	267.5	278.2

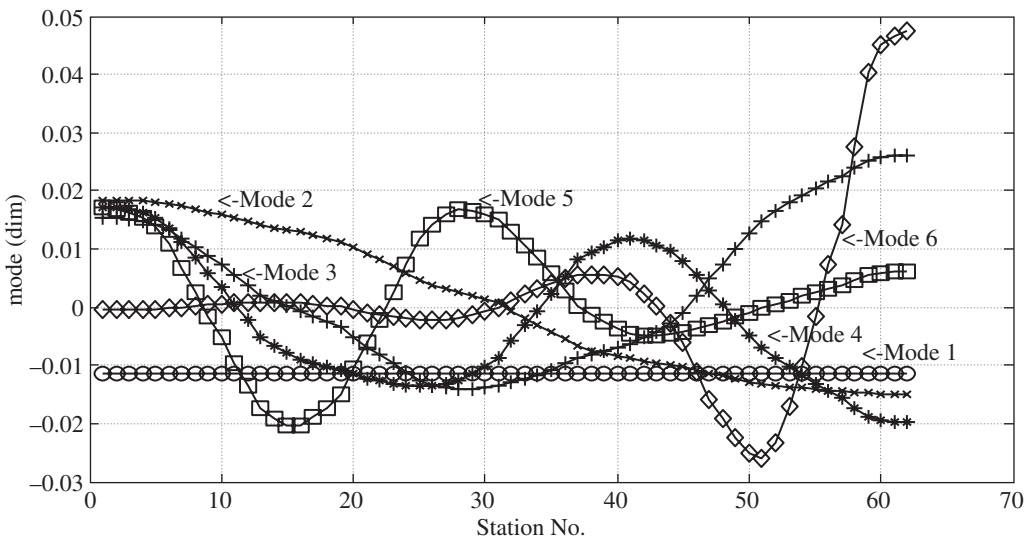


Figure E8.2.1(d) Rigid body mode (#1) and 5 lowest flexible mode shapes (#2, #3, #4, #5, #6) of the 62 dof system without Guyan reduction

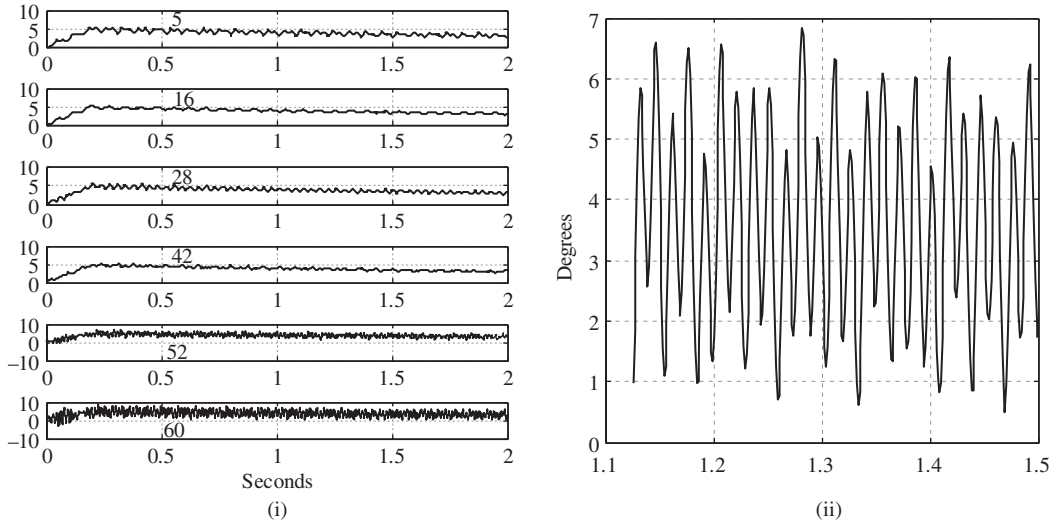


Figure E8.2.1(e) Angular deflections in degrees at (i) stations 5, 16, 28, 42, 52, and 60 and (ii) zoom of station 60, for the full system model without Guyan reduction

high-frequency oscillation is almost absent from the responses at stations 5, 16, 28, and 42 in Figure E8.2.1(e)-(i) since their components in the sixth mode are relatively small, as shown in Figure E8.2.1(d).

The following three cases illustrate the effect of varying the number of retained dofs on accuracy and efficiency in the Guyan reduction method:

- (I) Select the retained dofs as all major inertias, all dampings, and all external torques, that is, stations (1 4 5 7 12 15 16 19 24 27 28 31 36 40 41 42 45 49 51 52 54 58 59 60 62). Therefore, $n_r = 25$, $n_c = 37$, and $N = n_r + n_c = 62$.
- (II) Select the retained dofs with some major inertias, all dampings, and all external torques, that is, (1 5 7 12 16 19 24 28 31 36 42 45 49 51 52 54 58 60 62). Therefore, $n_r = 19$, $n_c = 43$, and $N = n_r + n_c = 62$.
- (III) Select the retained dofs with some major inertias and all external torques (5 16 28 42 51 52 60), that is, dofs with damping are not retained and $n_r = 7$, $n_c = 55$, and $N = n_r + n_c = 62$.

The Guyan transformation matrix (\underline{T}_G) in (8.2.14) and the Guyan condensed mass ($\tilde{\underline{M}}$), damping ($\tilde{\underline{C}}$), stiffness ($\tilde{\underline{K}}$), and force ($\tilde{\underline{f}}$) terms in (8.2.24) and (8.2.25) are formed in a MATLAB code. The Guyan basis vectors are columns of \underline{T}_G and are shown for case in Figure E8.2.1(f). By comparison, it is noted that the basis vectors of the original system are \underline{e}_i , that is,

$$\underline{\theta} = \sum_{i=1}^N \theta_i \underline{e}_i \quad (11)$$

where

$$\underline{e}_i = (0 \ 0 \ \cdots \ 1 \ \cdots \ 0)^T \quad (12)$$

↑
ith term

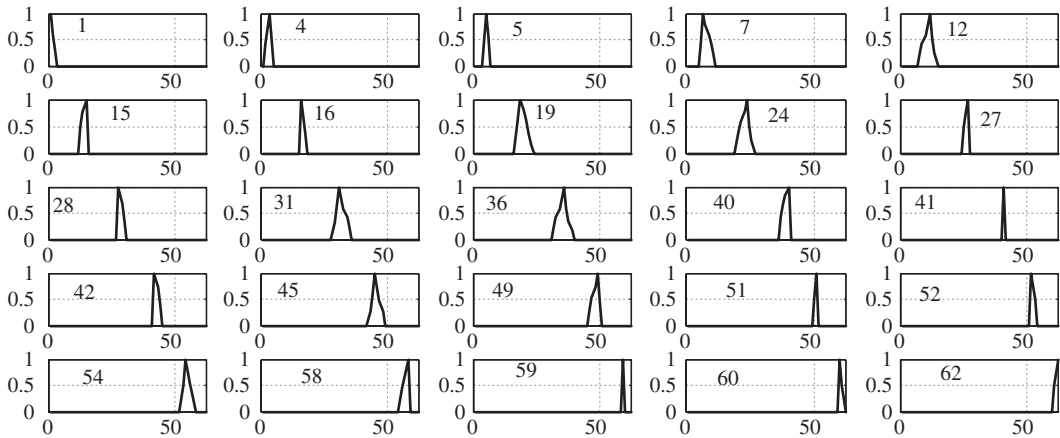


Figure E8.2.1(f) $n_r = 25$ Guyan basis vectors for each retained degree of freedom in case I ($n_r = 25$) versus station number

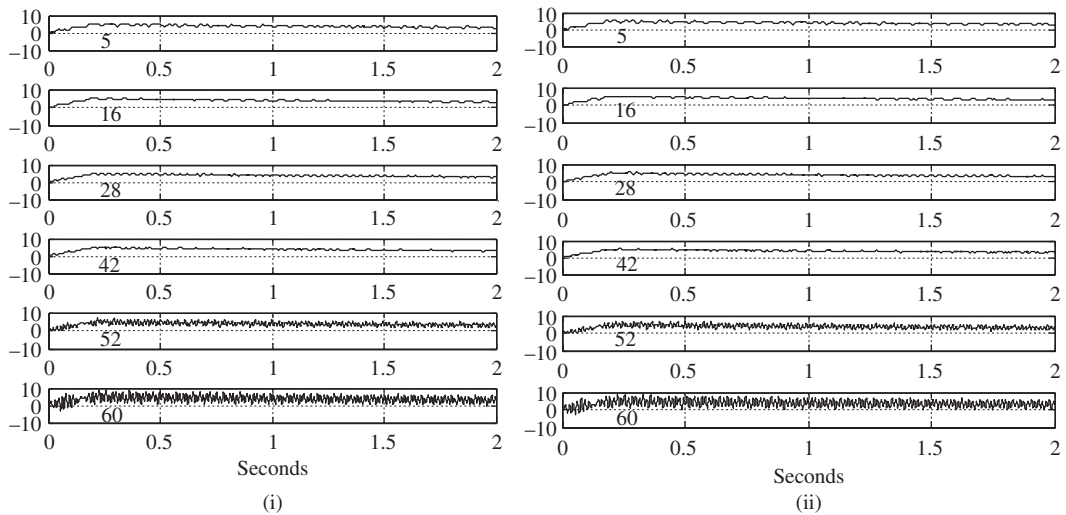


Figure E8.2.1(g) Angular deflections of degrees 5, 16, 28, 42, 52, and 60 for Guyan case (i) Model I ($n_r = 25$) and (ii) Model II ($n_r = 19$)

which are single vertical lines when plotted against dof number.

The condensed equations of motion in (8.2.23) are numerically integrated with MATLAB's ODE45 integrator. The angular deflections are shown for Guyan cases I, II, and III in Figures E8.2.1(g) and E8.2.1(h). The stations (5, 16, 28, 42, 52, 60) with displayed responses are the same as those for the "full system" response in Figure E8.2.1(e). The agreement between the Guyan reduced and full model deflections is excellent, especially as n_r increases from 7 to 25.

Table E8.2.1(c) compares the seven lowest undamped natural frequencies and damping ratios for the full system and the three Guyan reduced systems. The damping ratios are determined from the damped system eigenvalues utilizing (5.4.112) to obtain

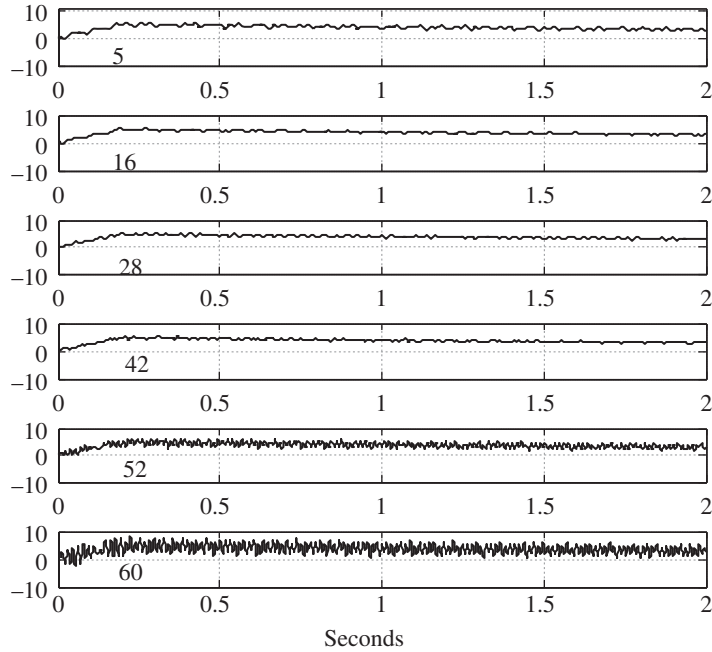


Figure E8.2.1(h) Angular deflections of degrees 5, 16, 28, 42, 52, and 60 for Guyan case Model III ($n_r = 7$)

Table E8.2.1(c) Seven lowest undamped natural frequencies (Hz) and damping ratios (%)

Quantity	Guyan reduced system			
	Entire 62 dof system	$n_r = 7$	$n_r = 19$	$n_r = 25$
<i>Frequencies</i>				
f_1	0 ^a	0	0	0
f_2	14.29	14.36	14.32	14.30
f_3	28.41	28.91	28.57	28.46
f_4	35.94	36.99	36.46	36.02
f_5	47.87	49.42	48.62	48.06
f_6	66.46	68.29	67.26	66.67
f_7	104.37	205.75	116.37	112.02
<i>Damping</i>				
ξ_1	100.0 ^a	100.0	100.0	100.0
ξ_2	0.161	0.159	0.162	0.161
ξ_3	0.087	0.082	0.089	0.088
ξ_4	0.052	0.047	0.053	0.052
ξ_5	0.033	0.028	0.035	0.034
ξ_6	0.040	0.034	0.040	0.040
ξ_7	0.042	0.009	0.063	0.051

^a Rigid body rotation mode.

$$\xi_{\%} = -100 * \frac{\text{Real}(\lambda)}{|\lambda|} \quad (13)$$

The agreement is very good for the lowest six modes and improves as n_r increases. The seventh mode only has good agreement for $n_r = 25$.

Table E8.2.1(d) Wall clock computation time and maximum angular deflection

Item	Entire 62 dof system	Guyan reduced system		
		$n_r = 7$	$n_r = 19$	$n_r = 25$
Wall clock time (seconds)	312.7	56.5	126.7	167.1
Maximum response angle (degrees)	8.41	7.92	8.77	8.55

Table E8.2.1(d) compares wall clock times and peak responses for the full and Guyan reduced system simulations. The Guyan approach produces significant time savings and high accuracy.

8.3 SUBSTRUCTURES: SUPERELEMENTS

Figure 8.3.1 is an illustration that shows some major components of the space shuttle main engine (SSME).

Each component will be typically modeled with finite elements including 1000s, 10,000s, or more dofs. A nonreduced model of the entire coupled system may be so large as to exceed practical computation limits. This problem is typically remedied by restricting the predicted response to a subspace spanned by a combination of modal and Guyan type basis vectors (Section 2.6). One approach is to apply Guyan reduction to each isolated component prior to assembling the model for the entire system. The retained dofs will include those with significant mass and damping, or with external forces, and all dofs that lie on any attachment interface(s) with the other components. For example, these interfaces are indicated by dashed lines in Figure 8.3.1. Let the model of the j th component have mass, damping, and stiffness matrices and external force vector represented by \underline{M}^j , \underline{C}^j , \underline{K}^j , and \underline{f}^j , respectively, and the Guyan transformation matrix given by (8.2.14)

$$\underline{T}_G^j = \begin{bmatrix} \underline{I}_{n_r}^j \\ -(\underline{k}_{cc}^j)^{-1} \underline{k}_{cr}^j \end{bmatrix} \quad (N_j \times n_{rj}) \quad (8.3.1)$$

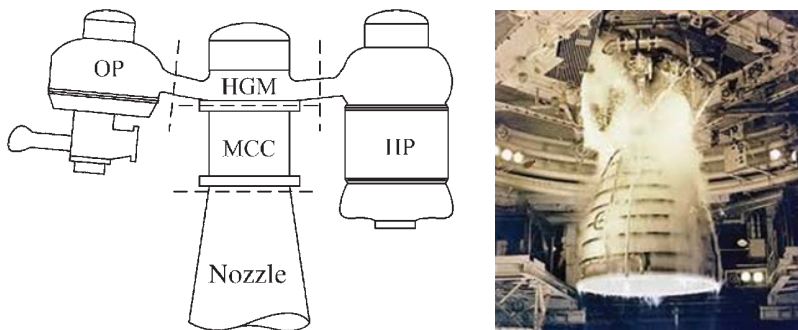


Figure 8.3.1 Some major components of the SSME. HGM, hot gas manifold; HP, hydrogen pump; MCC, main combustion chamber; Nozzle, exhaust nozzle; OP, oxygen pump. © NASA

Then the “substructure” or “superelement” matrices for components j are by (8.2.24) and (8.2.25):

$$\tilde{\underline{M}}^j = (\underline{T}_G^j)^T \underline{M}^j \underline{T}_G^j, \quad \tilde{\underline{C}}^j = (\underline{T}_G^j)^T \underline{C}^j \underline{T}_G^j, \quad \tilde{\underline{K}}^j = (\underline{T}_G^j)^T \underline{K}^j \underline{T}_G^j, \quad \tilde{\underline{f}}^j = (\underline{T}_G^j)^T \underline{f}^j \quad (8.3.2)$$

These substructure matrices are combined into a total system model using “modal synthesis.”

8.4 MODAL SYNTHESIS

The dictionary defines synthesis as “the composition or combination of parts or elements so as to form a whole.” In the field of structural modeling, “component mode synthesis” or simply “modal synthesis” describes the process of forming a system model from mode shapes or Guyan basis vectors of the isolated components. The motivation for utilizing modal synthesis is typically to reduce the number of dofs or to obtain a total system simulation model with component models that do not disclose design details of the components, which may be supplied by different, and possibly competing, companies.

The following analysis and example illustrate one of the many modal synthesis approaches. Consider the structure consisting of two components with a shared junction (J), or interface, as depicted in Figure 8.4.1.

The motion of each component is defined by a combination of modal (6.3.11), Guyan (8.2.21), and physical coordinates. These coordinates are summarized in the following list:

- (a) $\underline{\chi}_{\psi F}^1$: $n_\psi^1 \times 1$ vector of modal coordinates for the undamped system, free vibration modes of component 1, with interface 1-2 fixed in space
- (b) $\underline{\chi}_{\psi F}^2$: $n_\psi^2 \times 1$ vector of modal coordinates for the undamped system, free vibration modes of component 2, with interface 1-2 fixed in space
- (c) \underline{q}_J^1 : $n_J \times 1$ vector of Guyan retained dofs that are in component 1 and on interface (junction) 1-2
- (d) \underline{q}_J^2 : $n_J \times 1$ vector of Guyan retained dofs that are in component 2 and on interface (junction) 1-2
- (e) \underline{q}_I^1 : $n_I^1 \times 1$ vector of interior dofs that are in component 1
- (f) \underline{q}_I^2 : $n_I^2 \times 1$ vector of interior dofs that are in component 2

The total number of dofs in components 1 and 2 are

$$N^1 = n_I^1 + n_J, \quad N^2 = n_I^2 + n_J \quad (8.4.1)$$

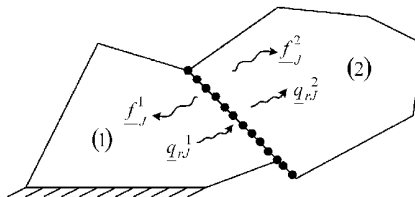


Figure 8.4.1 Two-component model of a structure showing junction (interface) forces and deflections

The forces in the model are categorized in a similar manner:

- (a) f_J^1 : $n_J \times 1$ vector of reaction forces acting on body 1 at interface (junction) 1-2
- (b) f_J^2 : $n_J \times 1$ vector of reaction forces acting on body 2 at interface (junction) 1-2
- (c) f_I^1 : $n_I^1 \times 1$ vector of external forces acting at interior dofs that are in component 1
- (d) f_I^2 : $n_I^2 \times 1$ vector of external forces acting at interior dofs that are in component 2

8.4.1 Uncoupled System Equations

The structure depicted in Figure 8.4.1 can be viewed as consisting of two isolated (uncoupled) substructures, each being subjected to the shared interface (junction) forces, external forces acting on the individual substructures, and boundary conditions acting on the individual substructures. The corresponding system equilibrium equation has stiffness, mass, and damping matrices that are uncoupled between the component 1 and component 2 coordinates. The uncoupling is clearly shown by the following partitioned forms:

$$\underline{M}\ddot{\underline{q}} + \underline{C}\dot{\underline{q}} + \underline{K}\underline{q} = \underline{f}(t) \quad (8.4.2)$$

or

$$\begin{bmatrix} \underline{M}^1 & \underline{0} \\ \underline{0} & \underline{M}^2 \end{bmatrix} \begin{Bmatrix} \ddot{\underline{q}}^1 \\ \ddot{\underline{q}}^2 \end{Bmatrix} + \begin{bmatrix} \underline{C}^1 & \underline{0} \\ \underline{0} & \underline{C}^2 \end{bmatrix} \begin{Bmatrix} \dot{\underline{q}}^1 \\ \dot{\underline{q}}^2 \end{Bmatrix} + \begin{bmatrix} \underline{K}^1 & \underline{0} \\ \underline{0} & \underline{K}^2 \end{bmatrix} \begin{Bmatrix} \underline{q}^1 \\ \underline{q}^2 \end{Bmatrix} = \begin{Bmatrix} \underline{f}^1 \\ \underline{f}^2 \end{Bmatrix} \quad (8.4.3)$$

where

$$\underline{q}^1 = \begin{Bmatrix} q_I^1 \\ q_J^1 \end{Bmatrix}, \quad \underline{q}^2 = \begin{Bmatrix} q_I^2 \\ q_J^2 \end{Bmatrix}, \quad \underline{f}^1 = \begin{Bmatrix} f_I^1 \\ f_J^1 \end{Bmatrix}, \quad \underline{f}^2 = \begin{Bmatrix} f_I^2 \\ f_J^2 \end{Bmatrix} \quad (8.4.4)$$

$$\underline{M}^1 = \begin{bmatrix} \underline{M}_{I,I}^1 & \underline{M}_{I,J}^1 \\ \underline{M}_{J,I}^1 & \underline{M}_{J,J}^1 \end{bmatrix}, \quad \underline{M}^2 = \begin{bmatrix} \underline{M}_{I,I}^2 & \underline{M}_{I,J}^2 \\ \underline{M}_{J,I}^2 & \underline{M}_{J,J}^2 \end{bmatrix} \quad (8.4.5)$$

$$\underline{C}^1 = \begin{bmatrix} \underline{C}_{I,I}^1 & \underline{C}_{I,J}^1 \\ \underline{C}_{J,I}^1 & \underline{C}_{J,J}^1 \end{bmatrix}, \quad \underline{C}^2 = \begin{bmatrix} \underline{C}_{I,I}^2 & \underline{C}_{I,J}^2 \\ \underline{C}_{J,I}^2 & \underline{C}_{J,J}^2 \end{bmatrix} \quad (8.4.6)$$

$$\underline{K}^1 = \begin{bmatrix} \underline{K}_{I,I}^1 & \underline{K}_{I,J}^1 \\ \underline{K}_{J,I}^1 & \underline{K}_{J,J}^1 \end{bmatrix}, \quad \underline{K}^2 = \begin{bmatrix} \underline{K}_{I,I}^2 & \underline{K}_{I,J}^2 \\ \underline{K}_{J,I}^2 & \underline{K}_{J,J}^2 \end{bmatrix} \quad (8.4.7)$$

The dimensions of these matrices are

$$\begin{bmatrix} n_I^1 \times n_I^1 & n_I^1 \times n_J \\ n_J \times n_I^1 & n_J \times n_J \end{bmatrix} \quad (8.4.8)$$

where $l=1$ (component 1) and $l=2$ (component 2). The junction is considered to be free (unconstrained) for forming the component matrices \underline{M}^l , \underline{C}^l , \underline{K}^l , and \underline{f}^l . The (1,1) diagonal blocks $\underline{M}_{I,I}^l$, $\underline{K}_{I,I}^l$, and $\underline{C}_{I,I}^l$ are property matrices corresponding to all junction dofs being

fixed. This method of modal synthesis requires that the mass, stiffness, and damping matrices for each component be available. The companies that manufacture the separate components may be more agreeable to contribute this information rather than detailed solid models and design details.

8.4.2 Coupled System Equations: Displacement Compatibility at Junction

The equations in (8.4.3) will become coupled by applying displacement compatibility and force equilibrium at the junction (J). The compatibility condition expresses the equality of displacements of the components at the junction when expressed in a common coordinate system. This condition is expressed mathematically by

$$\underline{q}_J^2 = \underline{T}_{J12} \underline{q}_J^1 \quad (8.4.9)$$

$n_J \times 1$ $n_J \times n_J$ $n_J \times 1$

The \underline{T}_{J12} matrix is block diagonal structure with each block being a two- or three-dimensional coordinate transformation matrix (2.7.1). This transforms the displacements at the junction nodes from the coordinate convention employed in component 1 to the coordinate convention employed in component 2. For example, the oxygen pump (OP) and hot gas manifold (HGM) dynamic models in Figure 8.3.1 may be developed by separate organizations using different displacement coordinate conventions so that compatibility of displacements at the junction requires the form in (8.4.9). Since \underline{T}_{J12} is a block diagonal matrix with each block being an orthogonal matrix, it follows the

$$\underline{T}_{J12}^{-1} = \underline{T}_{J12}^T \quad (8.4.10)$$

8.4.3 Coupled System Equations: Subspace Condensation

Motions within the components are restricted to user specified subspaces (Section 2.6) in order to reduce the number of dofs in each component model. The corresponding basis vectors (Section 2.6) consist of free vibration mode shapes and Guyan vectors. The mode shapes are computed with all junction (J) dofs fixed, since the junction motions are accounted for using the actual physical coordinates at the junction. Note the similarity of this with the fixed boundary node modes in the modal effective mass calculation (6.3.94). The interior dofs in component 1 are assumed to move with contributions from the undamped, junction fixed modes

$$\underline{q}_{(a)}^1 = \begin{Bmatrix} \underline{q}_J^1 \\ \underline{q}_J^1 \end{Bmatrix}_{(a)} = \begin{Bmatrix} \underline{\Psi}_J^1 \\ \underline{0} \end{Bmatrix}_{(a)} \begin{Bmatrix} \underline{\chi}_{\psi F}^1 \\ \underline{\chi}_{\psi F}^1 \end{Bmatrix} = \underline{\Psi}_1 \underline{\chi}_{\psi F}^1 \quad (8.4.11)$$

$n_J^1 \times n_{\psi}^1$ $n_J^1 \times n_{\psi}^1$

where $\underline{\Psi}_1$ is the modal matrix for component 1 with the junction fixed. The interior dofs in component 1 are assumed to also move with contributions from the Guyan constraint vectors (\underline{T}_{GJ}) in (8.2.14) with retained dofs on the interface (junction). Use of (8.2.12)–(8.2.14) shows

$$\underline{q}^1_{(b)} = \begin{Bmatrix} \underline{q}^1_I \\ \underline{q}^1_J \end{Bmatrix}_{(b)} = \begin{Bmatrix} -\left(\underline{K}^1_{I,I}\right)^{-1} \underline{K}^1_{I,J} \\ I \\ I \end{Bmatrix} \begin{Bmatrix} \underline{q}^1_J \\ \underline{q}^1_J \end{Bmatrix}_{n_J \times 1} = \underline{T}^1_{GI} \underline{q}^1_J \quad (8.4.12)$$

Therefore, the total deflections in component 1 are approximated by

$$\underline{q}^1 = \underline{q}^1_{(a)} + \underline{q}^1_{(b)} = \begin{Bmatrix} \underline{q}^1_I \\ \underline{q}^1_J \end{Bmatrix}_{n_I^1 \times 1} = \begin{bmatrix} \underline{\Psi}^1_I & \underline{G}^1_I \\ \underline{0} & I \end{bmatrix} \begin{Bmatrix} \underline{\chi}^1_{\psi F} \\ \underline{q}^1_J \end{Bmatrix}_{n_I^1 \times 1} \quad (8.4.13)$$

where

$$\underline{G}^1_I = -\left(\underline{K}^1_{I,I}\right)^{-1} \underline{K}^1_{I,J} \quad (n_I^1 \times n_J) \quad (8.4.14)$$

Similar definitions follow for component 2 so the uncoupled system displacements in (8.4.2) and (8.4.3) are approximated by

$$\underline{q} = \begin{Bmatrix} \underline{q}^1_I \\ \underline{q}^1_J \\ \underline{q}^2_I \\ \underline{q}^2_J \end{Bmatrix} = \begin{bmatrix} \underline{\Psi}^1_I & \underline{G}^1_I & \underline{0} & \underline{0} \\ \underline{0} & I_J & \underline{0} & \underline{0} \\ \underline{0} & \underline{0} & \underline{\Psi}^2_I & \underline{G}^2_I \\ \underline{0} & \underline{0} & \underline{0} & I_J \end{bmatrix} \begin{Bmatrix} \underline{\chi}^1_{\psi F} \\ \underline{q}^1_J \\ \underline{\chi}^2_{\psi F} \\ \underline{q}^2_J \end{Bmatrix} \quad (8.4.15)$$

Insert the compatibility relation (8.4.9) into (8.4.15) to remove the redundancy of including the same junction dofs for both components 1 and 2 in the vector on the RHS of (8.4.15). This step yields

$$\underline{q} = \begin{Bmatrix} \underline{q}^1_I \\ \underline{q}^1_J \\ \underline{q}^2_I \\ \underline{q}^2_J \end{Bmatrix} = \begin{bmatrix} \underline{\Psi}^1_I & \underline{G}^1_I & \underline{0} \\ \underline{0} & I_J & \underline{0} \\ \underline{0} & \underline{G}^2_I \underline{T}_{J12} & \underline{\Psi}^2_I \\ \underline{0} & \underline{T}_{J12} & \underline{0} \end{bmatrix} \begin{Bmatrix} \underline{\chi}^1_{\psi F} \\ \underline{q}^1_J \\ \underline{\chi}^2_{\psi F} \end{Bmatrix} \quad (8.4.16)$$

or

$$\underline{q}_{N_{\text{tot}} \times 1} = \underline{T}_{N_{\text{tot}} \times N} \underline{\chi}_{N \times 1} \quad (8.4.17)$$

where

$$N_{\text{tot}} = n_I^1 + n_J + n_I^2 + n_J, \quad N = n_{\psi}^1 + n_J + n_{\psi}^2 \quad (8.4.18)$$

The relationship defined in (8.4.17) expresses the underlying assumption that the motions of all physical coordinates of the coupled system will occur in a

N -dimensional subspace of N_{tot} space and that the subspace is spanned by the following basis vectors:

- Column 1 Partition of Equation (8.4.16)
These are the modes of the orthogonally damped, nongyroscopic, noncirculatory model of component 1 with component 2 and the interface (junction) fixed in space.
- Column 2 Partition of Equation (8.4.16)
These are the Guyan constraint vectors (8.2.18) for all interface (junction) dofs acting as “retained” dofs.
- Column 3 Partition of Equation (8.4.16)
These are the modes of the orthogonally damped, nongyroscopic, noncirculatory model of component 2 with component 1 and the interface (junction) fixed in space.

These and other types of basis vectors used for modal synthesis are described in Wang et al. (1983) and Craig (1981). The subspace condensation transformation in (8.4.17) is substituted into the uncoupled model EOM of (8.4.2). The result is then premultiplied by \underline{T}^T to obtain

$$\underline{\tilde{M}}\ddot{\underline{\chi}} + \underline{\tilde{C}}\dot{\underline{\chi}} + \underline{\tilde{K}}\underline{\chi} = \underline{\tilde{f}} \quad (N \times 1) \quad (8.4.19)$$

where

$$\underline{\tilde{M}} = \underline{T}^T \underline{M} \underline{T}, \quad \underline{\tilde{C}} = \underline{T}^T \underline{C} \underline{T}, \quad \underline{\tilde{K}} = \underline{T}^T \underline{K} \underline{T}, \quad \underline{\tilde{f}} = \underline{T}^T \underline{f} \quad (8.4.20)$$

and from (8.4.3)

$$\underline{M} = \begin{bmatrix} \underline{M}^1 & \underline{0} \\ \underline{0} & \underline{M}^2 \end{bmatrix}, \quad \underline{C} = \begin{bmatrix} \underline{C}^1 & \underline{0} \\ \underline{0} & \underline{C}^2 \end{bmatrix}, \quad \underline{K} = \begin{bmatrix} \underline{K}^1 & \underline{0} \\ \underline{0} & \underline{K}^2 \end{bmatrix}, \quad \underline{f} = \begin{Bmatrix} \underline{f}^1 \\ \underline{f}^2 \end{Bmatrix} \quad (8.4.21)$$

and $\underline{M}^l, \underline{C}^l, \underline{K}^l$, and \underline{f}^l are defined in (8.4.5)–(8.4.7) for $l=1,2$. Since all terms in $\underline{T}, \underline{M}, \underline{C}$, and \underline{K} are known, it follows that $\underline{\tilde{M}}, \underline{\tilde{C}}, \underline{\tilde{K}}$ are also known. From (8.4.3) and (8.4.4), the force vector \underline{f} in (8.4.20) contains the unknown junction forces, that is,

$$\underline{f} = \begin{Bmatrix} \underline{f}^1 \\ \underline{f}^2 \end{Bmatrix} = \begin{Bmatrix} \underline{f}_J^1 \\ \underline{f}_J^2 \end{Bmatrix} \quad (8.4.22)$$

The junction forces on the two components must obey Newton’s third law of equal and opposite reactions when expressed in a common coordinate system, similar to displacement compatibility in (8.4.9). Therefore,

$$\underline{f}_J^2 = -\underline{T}_{J12} \underline{f}_J^1 \quad (8.4.23)$$

and by using (8.4.10)

$$\underline{f}_J^1 = -\underline{T}_{J12}^T \underline{f}_J^2 \quad (8.4.24)$$

From (8.4.16), (8.4.20), and (8.4.22), the coupled system's force vector becomes

$$\begin{aligned} \tilde{\underline{f}} = \underline{T}^T \underline{f} &= \begin{bmatrix} (\underline{\Psi}_J^1)^T & \underline{0} & \underline{0} & \underline{0} \\ (\underline{G}_J^1)^T & \underline{I}_J & \underline{T}_{J12}^T (\underline{G}_J^2)^T & \underline{T}_{J12}^T \\ \underline{0} & \underline{0} & (\underline{\Psi}_J^2)^T & \underline{0} \end{bmatrix} \begin{Bmatrix} \underline{f}_J^1 \\ \underline{f}_J^1 \\ \underline{f}_J^2 \\ \underline{f}_J^2 \end{Bmatrix} \\ &= \begin{Bmatrix} (\underline{\Psi}_J^1)^T \underline{f}_J^1 \\ (\underline{G}_J^1)^T \underline{f}_J^1 + \underline{f}_J^1 + \underline{T}_{J12}^T (\underline{G}_J^2)^T \underline{f}_J^2 + \underline{T}_{J12}^T \underline{f}_J^2 \\ (\underline{\Psi}_J^2)^T \underline{f}_J^2 \end{Bmatrix} \end{aligned} \quad (8.4.25)$$

Substitute (8.4.24) into (8.4.25) to obtain

$$\tilde{\underline{f}} = \begin{Bmatrix} (\underline{\Psi}_J^1)^T \underline{f}_J^1 \\ (\underline{G}_J^1)^T \underline{f}_J^1 + (\underline{G}_J^2 \underline{T}_{J12})^T \underline{f}_J^2 \\ (\underline{\Psi}_J^2)^T \underline{f}_J^2 \end{Bmatrix} \quad (8.4.26)$$

This step eliminates the unknown junction forces \underline{f}_J^1 and \underline{f}_J^2 from the coupled system equations. Thus, all terms in (8.4.19) are known, so that it may then be solved for the generalized coordinates $\underline{\chi}(t)$. The physical coordinate responses may then be obtained via the transformation equation (8.4.17).

EXAMPLE 8.4.1 *Modal Synthesis Solution of Machinery Shaft Train Vibration*

Statement: This example illustrates the usage of modal synthesis to predict torsional vibrations of the turbine-generator machinery train subjected to a transient torque excitation as presented in Example 8.2.1. As a hypothetical scenario, assume that the four turbines are built by one vendor and modeled as train 1. The generator and exciter are built by a second vendor and modeled as train 2. Modal synthesis is utilized to couple the models and predict the transient response of the combined machinery shaft train.

Objective: Compare modal synthesis predicted responses to those presented in Example 8.2.1.

Assumptions and Parameter Values: Same as Example 8.2.1.

Solution: With reference to Figures E8.2.1(a) and E8.2.1(b) and also Table E8.2.1(a), the four-turbine model includes all global stations from 1 to 47, and the generator/exciter includes all global stations from 47 to 62. Therefore, 47 is the sole junction (J) dof and

$$n_J = 1, \quad n_I^1 = 46, \quad n_I^2 = 15, \quad N^1 = 47, \quad N^2 = 16 \quad (1)$$

$$N_{\text{tot}} = 2n_J + n_I^1 + n_I^2 = 63 \quad (2)$$

in Equations (8.4.1), (8.4.8), and (8.4.18). The train 1 and train 2 mass matrices (8.4.5) are given, similar to Equation (4) of Example 8.2.1, as

$$\underline{M}^1 = \begin{bmatrix} \underline{M}_{I,I}^1 & \underline{M}_{I,J}^1 \\ \underline{M}_{J,I}^1 & \underline{M}_{J,J}^1 \end{bmatrix} = \begin{bmatrix} J_1 & 0 & 0 & \cdots & 0 & 0 \\ & J_2 & 0 & \cdots & 0 & 0 \\ & & J_3 & \cdots & 0 & 0 \\ & & & \ddots & \vdots & \vdots \\ & & & & J_{46} & 0 \\ \hline 0 & 0 & 0 & \cdots & 0 & J_{47} \end{bmatrix} \quad (3)$$

$$\underline{M}^2 = \begin{bmatrix} \underline{M}_{I,I}^2 & \underline{M}_{I,J}^2 \\ \underline{M}_{J,I}^2 & \underline{M}_{J,J}^2 \end{bmatrix} = \begin{bmatrix} J_{48} & 0 & 0 & \cdots & 0 & 0 \\ & J_{49} & 0 & \cdots & 0 & 0 \\ & & J_{50} & \cdots & 0 & 0 \\ & & & \ddots & \vdots & \vdots \\ & & & & J_{62} & 0 \\ \hline 0 & 0 & 0 & \cdots & 0 & J_{47} \end{bmatrix} \quad (4)$$

The train 1 and train 2 stiffness matrices (8.4.7) are given, similar to Equation (3) of Example 8.2.1, as

$$\underline{K}^1 = \begin{bmatrix} \underline{K}_{I,I}^1 & \underline{K}_{I,J}^1 \\ \underline{K}_{J,I}^1 & \underline{K}_{J,J}^1 \end{bmatrix} = \begin{bmatrix} k_1 & -k_1 & 0 & \cdots & 0 & 0 \\ & k_1 + k_2 & -k_2 & \cdots & 0 & 0 \\ & & k_2 + k_3 & \cdots & 0 & 0 \\ & & & \ddots & \vdots & \vdots \\ & & & & k_{45} + k_{46} & -k_{46} \\ \hline 0 & 0 & 0 & \cdots & -k_{46} & k_{46} \end{bmatrix} \quad (5)$$

$$\underline{K}^2 = \begin{bmatrix} \underline{K}_{I,I}^2 & \underline{K}_{I,J}^2 \\ \underline{K}_{J,I}^2 & \underline{K}_{J,J}^2 \end{bmatrix} = \begin{bmatrix} k_{47} + k_{48} & -k_{48} & 0 & \cdots & 0 & -k_{47} \\ & k_{48} + k_{49} & -k_{49} & \cdots & 0 & 0 \\ & & k_{49} + k_{50} & \cdots & 0 & 0 \\ & & & \ddots & \vdots & \vdots \\ & & & & k_{61} & 0 \\ \hline -k_{47} & 0 & 0 & \cdots & 0 & k_{47} \end{bmatrix} \quad (6)$$

The train 1 and train 2 damping matrices (8.4.6) are given, similar to Equation (5) of Example 8.2.1, as

$$\underline{C}^1 = \begin{bmatrix} \underline{C}_{I,I}^1 & \underline{C}_{I,J}^1 \\ \underline{C}_{J,I}^1 & \underline{C}_{J,J}^1 \end{bmatrix} = \begin{bmatrix} b_1 & 0 & 0 & \cdots & 0 & 0 \\ & b_2 & 0 & \cdots & 0 & 0 \\ & & b_3 & \cdots & 0 & 0 \\ & & & \ddots & \vdots & \vdots \\ & & & & b_{46} & 0 \\ \hline 0 & 0 & 0 & \cdots & 0 & b_{47} \end{bmatrix} \quad (7)$$

$$\underline{C}^2 = \begin{bmatrix} \underline{C}_{I,I}^2 & \underline{C}_{I,J}^2 \\ \underline{C}_{J,I}^2 & \underline{C}_{J,J}^2 \end{bmatrix} = \begin{bmatrix} b_{48} & 0 & 0 & \cdots & 0 & 0 \\ & b_{49} & 0 & \cdots & 0 & 0 \\ & & b_{50} & \cdots & 0 & 0 \\ & & & \ddots & \vdots & \vdots \\ & & & & b_{62} & 0 \\ \hline 0 & 0 & 0 & \cdots & 0 & b_{47} \end{bmatrix} \quad (8)$$

The train 1 and train 2 force vectors (8.4.4) are given, similar to Equation (5) of Example 8.2.1, as

$$\underline{f}^1 = \begin{Bmatrix} 0 \\ 0 \\ \vdots \\ 0 \\ f_I^1 \\ \vdots \\ f_J^1 \end{Bmatrix} \begin{matrix} \leftarrow \text{position 1} \\ \\ \\ \leftarrow \text{position 46} \end{matrix}, \quad \underline{f}^2 = \begin{Bmatrix} 0 \\ 0 \\ 0 \\ \Gamma_{\text{dist}}(t) \\ \Gamma_{\text{dist}}(t) \\ \vdots \\ 0 \\ f_J^2 \end{Bmatrix} \begin{matrix} \leftarrow \text{position 1} \\ \\ \\ \leftarrow \text{position 4} \\ \leftarrow \text{position 5} \\ \\ \\ \leftarrow \text{position 15} \end{matrix} \quad (9)$$

where $\Gamma_{\text{dist}}(t)$ is defined by Equation (1) in Example 8.2.1. By Equations (8.4.5) and (8.4.7), the fixed junction component modes are obtained from

$$\begin{aligned} \omega_{I1j}^2 \underline{M}_{I,I}^1 \underline{\psi}_{I1j} &= \underline{K}_{I,I}^1 \underline{\psi}_{I1j} \quad (n_I^1 \times 1) \\ \omega_{I2j}^2 \underline{M}_{I,I}^2 \underline{\psi}_{I2j} &= \underline{K}_{I,I}^2 \underline{\psi}_{I2j} \quad (n_I^2 \times 1) \end{aligned} \quad (10)$$

The corresponding modal matrices are defined as

$$\begin{aligned} \underline{\Psi}_{I1} &= \begin{bmatrix} \underline{\psi}_{I11} & \underline{\psi}_{I12} & \cdots & \underline{\psi}_{I1n_I^1} \end{bmatrix} \\ \underline{\Psi}_{I2} &= \begin{bmatrix} \underline{\psi}_{I21} & \underline{\psi}_{I22} & \cdots & \underline{\psi}_{I2n_I^2} \end{bmatrix} \end{aligned} \quad (11)$$

From (8.4.14),

$$\begin{aligned} \underline{G}_J^1 &= -\left(\underline{K}_{I,I}^1\right)^{-1} \underline{K}_{I,J}^1 \quad (n_I^1 \times n_J) \\ \underline{G}_J^2 &= -\left(\underline{K}_{I,I}^2\right)^{-1} \underline{K}_{I,J}^2 \quad (n_I^2 \times n_J) \end{aligned} \quad (12)$$

The coordinate axes of each substructure in this example are parallel, so the coordinate transformation matrix in (8.4.10) is

$$\underline{T}_{J12} = \underline{I}_{n_J \times n_J} = 1 \quad (13)$$

Equations (10)–(13) yield the partitions in the system transformation matrix \underline{T} in (8.4.16):

$$\underline{T}_{n_{\text{tot}} \times N} = \begin{bmatrix} \underline{\Psi}_J^1 & \underline{G}_J^1 & \underline{0} \\ \underline{0} & \underline{I}_J & \underline{0} \\ \underline{0} & \underline{G}_J^2 \underline{T}_{J12} & \underline{\Psi}_J^2 \\ \underline{0} & \underline{T}_{J12} & \underline{0} \end{bmatrix} = \begin{bmatrix} \underline{\Psi}_J^1 & \underline{G}_J^1 & \underline{0} \\ \underline{0} & 1 & \underline{0} \\ \underline{0} & \underline{G}_J^2 & \underline{\Psi}_J^2 \\ \underline{0} & 1 & \underline{0} \end{bmatrix} \quad (14)$$

where

$$N = n_J + n_{\psi}^1 + n_{\psi}^2 = 1 + n_{\psi}^1 + n_{\psi}^2 \quad (15)$$

The coupled system's mass, damping, and stiffness matrices are (8.4.20)

$$\underline{\tilde{M}} = \underline{T}^T \underline{M} \underline{T}, \quad \underline{\tilde{C}} = \underline{T}^T \underline{C} \underline{T}, \quad \underline{\tilde{K}} = \underline{T}^T \underline{K} \underline{T} \quad (N \times N) \quad (16)$$

where from (8.4.21)

$$\underline{M} = \begin{bmatrix} \underline{M}^1 & \underline{0} \\ \underline{0} & \underline{M}^2 \end{bmatrix}, \quad \underline{C} = \begin{bmatrix} \underline{C}^1 & \underline{0} \\ \underline{0} & \underline{C}^2 \end{bmatrix}, \quad \underline{K} = \begin{bmatrix} \underline{K}^1 & \underline{0} \\ \underline{0} & \underline{K}^2 \end{bmatrix} \quad (17)$$

and from (8.4.26) the $\underline{\tilde{f}}$ vector becomes

$$\underline{\tilde{f}} = \begin{Bmatrix} (\underline{\Psi}_J^1)^T \underline{f}_J^1 \\ (\underline{G}_J^1)^T \underline{f}_J^1 + (\underline{G}_J^2 \underline{T}_{J12})^T \underline{f}_J^2 \\ (\underline{\Psi}_J^2)^T \underline{f}_J^2 \end{Bmatrix} = \begin{Bmatrix} \underline{0} \\ (\underline{G}_J^2)^T \underline{f}_J^2 \\ (\underline{\Psi}_J^2)^T \underline{f}_J^2 \end{Bmatrix} \quad (18)$$

Equations (8.4.17) and (8.4.19) are then utilized to obtain the following coupled system response characteristics:

$$\text{Undamped natural frequencies } (-\omega_l^2 \underline{\tilde{M}} + \underline{\tilde{K}}) \underline{\beta}_l = \underline{0} :$$

$$\underline{\psi}_l = \text{lth undamped system mode vector} = \begin{Bmatrix} \underline{\psi}_{Jl}^1 \\ \underline{\psi}_{Jl}^1 \\ \underline{\psi}_{Jl}^2 \\ \underline{\psi}_{Jl}^2 \end{Bmatrix} = \underline{T}_{N_{\text{tot}} \times N} \underline{\beta}_l \quad (N_{\text{tot}} \times 1) \quad (19)$$

Damped system modes:

$$\lambda_l^2 \underline{\tilde{M}} \underline{\gamma}_l + \lambda_l \underline{\tilde{C}} \underline{\gamma}_l + \underline{\tilde{K}} \underline{\gamma}_l = 0 \quad (N \times 1) \quad (20)$$

The physical coordinate mode vectors $\underline{\Delta}_l$ are obtained from the generalized coordinate mode vectors $\underline{\gamma}_l$ via (8.4.17) as

$$\underline{\Delta}_I = \begin{Bmatrix} \underline{\Delta}_{II}^1 \\ \underline{\Delta}_{II}^1 \\ \underline{\Delta}_{II}^2 \\ \underline{\Delta}_{II}^2 \end{Bmatrix} = \underset{N_{\text{tot}} \times N}{\underline{T}} \underset{N \times 1}{\underline{\gamma}_I} \quad (N_{\text{tot}} \times 1) \quad (21)$$

Transient response:

$$\underline{\tilde{M}} \underline{\ddot{\chi}} + \underline{\tilde{C}} \underline{\dot{\chi}} + \underline{\tilde{K}} \underline{\chi} = \underline{\tilde{f}} \quad (N \times 1) \quad (22)$$

or written in first-order form as

$$\underline{\dot{\chi}} = \underline{V}_{\underline{\chi}} \quad \text{and} \quad \underline{\dot{V}}_{\underline{\chi}} = \underline{\tilde{M}}^{-1} (\underline{\tilde{f}} - \underline{\tilde{C}} \underline{V}_{\underline{\chi}} - \underline{\tilde{K}} \underline{\chi}) \quad (N \times 1) \quad (23)$$

The physical coordinate displacements \underline{q} are obtained from the generalized coordinate displacements $\underline{\chi}$ via (8.4.17) as

$$\underline{q}(t) = \begin{Bmatrix} \underline{q}_I^1 \\ \underline{q}_I^1 \\ \underline{q}_I^2 \\ \underline{q}_I^2 \end{Bmatrix} = \underset{N_{\text{tot}} \times N}{\underline{T}} \underset{N \times 1}{\underline{\chi}} \quad (N_{\text{tot}} \times 1) \quad (24)$$

Figure E8.4.1(a) shows the lowest five, fixed junction ($\theta_{47} = 0$), free vibration mode shapes of components 1 and 2. The corresponding natural frequencies are listed in Table E8.4.1(a).

The number of free vibration modes utilized in the synthesis example is n_{ψ}^1 and n_{ψ}^2 for substructures 1 and 2, respectively. The number of Guyan modes utilized for the synthesis is ($n_J = 1$) for each substructure. The Guyan basis vectors are shown in Figure E8.4.1(b). This shows that imposing a unit rotation on the junction node 47 causes all of the other nodes to also move through a unit rotation. Equations (19) and (20) are utilized with $n_{\psi}^1 = n_{\psi}^2 = 6$ and

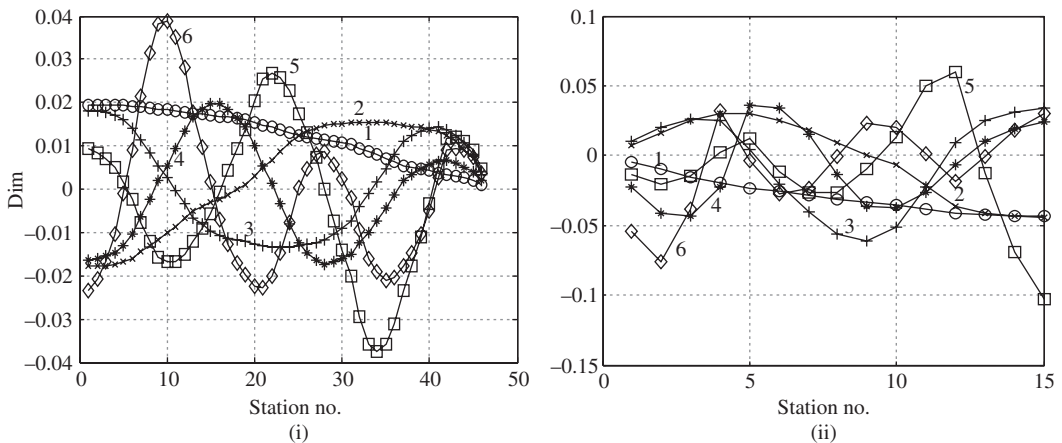
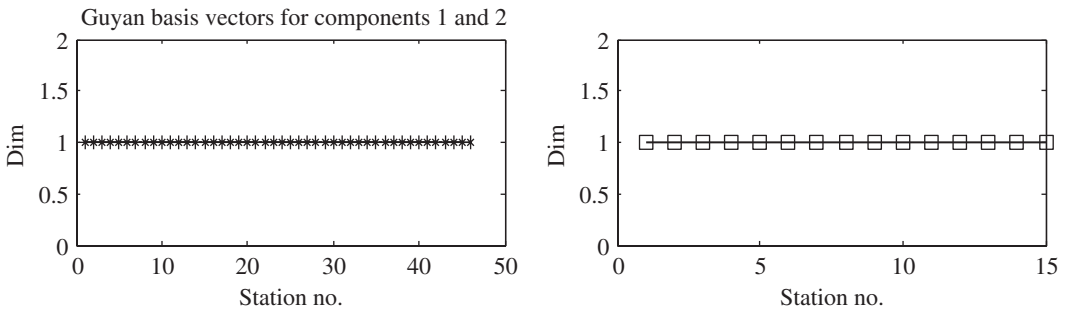
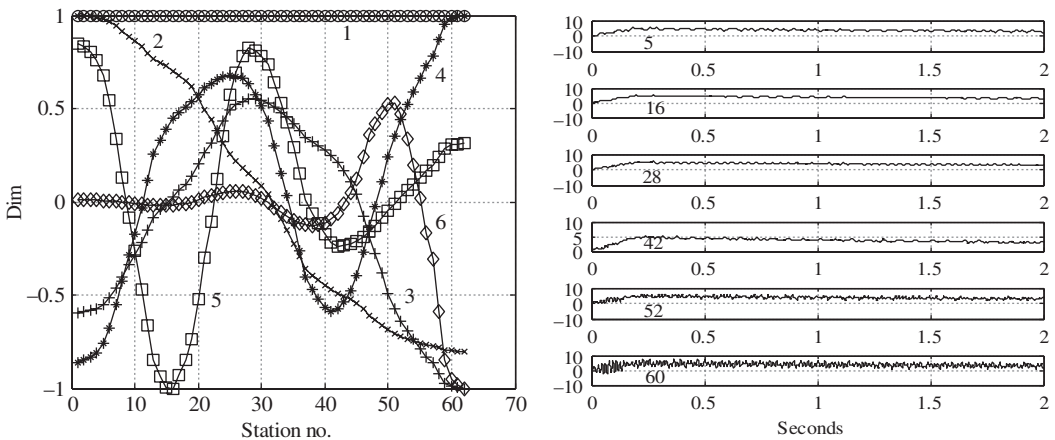


Figure E8.4.1(a) Five lowest fixed junction mode shapes for (i) substructure 1 and (ii) substructure 2

Table E8.4.1(a) Component mode natural frequencies for substructures 1 and 2

No.	Substructure 1 natural frequency (Hz)	Substructure 2 natural frequency (Hz)
1	9.44	32.6
2	25.60	73.5
3	37.0	155.3
4	48.3	226.0
5	106.4	288.2
6	116.5	316.9

**Figure E8.4.1(b)** Guyan basis vectors for components 1 and 2**Figure E8.4.1(c)** The $n_{\psi}^1 = n_{\psi}^2 = 6$ and $n_j = 1$ model results for (i) coupled, undamped system modes and (ii) angular deflections in degrees at stations 5, 16, 28, 42, 52, and 60

$n_j = 1$ to determine the undamped system modes of the coupled system as shown in Figure E8.4.1(c)-(i). These agree well with the exact modes in Figure E8.2.1(d).

Figure E8.4.1(c)-(ii) shows the coupled system's transient response predictions obtained by solving (23) and (24) with MATLAB ODE45 (ref. Example 2.3.1) for (n_{ψ}^1, n_{ψ}^2) equal (6,6). Table E8.4.1(b) shows good agreement between the exact

Table E8.4.1(b) Seven lowest undamped natural frequencies (Hz) and damping ratios (%) of the coupled system

Item	Complete 62 dof system	Modal synthesis model		
		$n_{\psi}^1 = 3, n_{\psi}^2 = 3$	$n_{\psi}^1 = 5, n_{\psi}^2 = 3$	$n_{\psi}^1 = 6, n_{\psi}^2 = 6$
f_1	0	0	0	0
f_2	14.29	14.22	14.22	14.22
f_3	28.41	28.38	28.38	28.38
f_4	35.94	35.93	35.93	35.93
f_5	47.87	—	47.86	47.86
f_6	66.46	65.27	65.86	65.83
f_7	104.37	116.41	103.88	103.61
ξ_1	100.0	100.0	100.0	100.0
ξ_2	0.161	0.16	0.16	0.16
ξ_3	0.087	0.087	0.087	0.087
ξ_4	0.052	0.052	0.052	0.052
ξ_5	0.033	—	0.033	0.033
ξ_6	0.040	0.041	0.039	0.040
ξ_7	0.042	0.024	0.041	0.041

(Table E8.2.1(c)) and modal synthesis predicted coupled system's natural frequencies and damping ratios. These quantities are calculated according to (5.4.112) as

$$\omega_i = |\lambda_i|, \quad \xi_i = \frac{-\text{Re}(\lambda_i)}{|\lambda_i|} \quad (25)$$

8.5 EIGENVALUE/NATURAL FREQUENCY CHANGES FOR PERTURBED SYSTEMS

The placement of natural frequencies to avoid resonance is a common objective for vibration engineers. This may occur at the initial design stage or in the “field” to troubleshoot and correct an existing resonance problem by shifting a natural frequency sufficiently away from all excitation frequencies. This may require extensive parameter searches with large-order simulation models utilizing much computer simulation time. There often is a need to quickly approximate predicted natural frequencies, mode shapes, and damping ratios. This is especially true when conducting a statistical-based study that requires varying multiple parameters within a given probability distribution (Barrett et al., 1996). The perturbation approach presented here provides a quick means for obtaining estimates of modal variables as system parameters vary. The formulas utilize results from a baseline (original) model as part of the approximate solution. This model's results are obtained by a single, exact solution step. The approximate approach provides modal variable estimates given model parameter changes or may be used in the inverse sense to provide required model changes given desired modal variables, such as natural frequencies.

8.5.1 Undamped, Nongyroscopic, Noncirculatory \underline{M} and \underline{K} Type Systems

Assume that the \underline{M} and \underline{K} matrices undergo changes

$$\underline{M} \Rightarrow \underline{M} + \Delta \underline{M}, \quad \underline{K} \Rightarrow \underline{K} + \Delta \underline{K} \quad (8.5.1)$$

that cause the following natural frequency and mode shape changes

$$\omega_l \Rightarrow \omega_l + \Delta\omega_l, \quad \underline{\psi}_l \Rightarrow \underline{\psi}_l + \Delta\underline{\psi}_l \quad (8.5.2)$$

as a result of changes in the dynamic equilibrium equation

$$\text{Original system} \Rightarrow (-\omega_l \underline{M} + \underline{K}) \underline{\psi}_l = 0 \quad (8.5.3)$$

$$\text{Modified system} \Rightarrow \{-[\omega_l^2 + \Delta(\omega_l^2)](\underline{M} + \Delta\underline{M}) + (\underline{K} + \Delta\underline{K})\}(\underline{\psi}_l + \Delta\underline{\psi}_l) = \underline{0} \quad (8.5.4)$$

Multiplying and canceling second-order terms for small $\Delta\underline{M}$ and $\Delta\underline{K}$ yields

$$(-\omega_l^2 \underline{M} + \underline{K}) \underline{\psi}_l - \omega_l^2 \Delta\underline{M} \underline{\psi}_l - \Delta(\omega_l^2) \underline{M} \underline{\psi}_l - \omega_l^2 \underline{M} \Delta\underline{\psi}_l + \underline{K} \Delta\underline{\psi}_l + \Delta\underline{K} \underline{\psi}_l \approx \underline{0} \quad (8.5.5)$$

Insert (8.5.3) and regroup terms

$$(\Delta\underline{K} - \omega_l^2 \Delta\underline{M}) \underline{\psi}_l + (\underline{K} - \omega_l^2 \underline{M}) \Delta\underline{\psi}_l - \Delta(\omega_l^2) \underline{M} \underline{\psi}_l \approx \underline{0} \quad (8.5.6)$$

Transpose (8.5.6) using symmetry of $\underline{M}, \underline{K}, \Delta\underline{M}$, and $\Delta\underline{K}$ to obtain

$$\Delta(\omega_l^2) \underline{\psi}_l^T \underline{M} \approx \Delta\underline{\psi}_l^T (\underline{K} - \omega_l^2 \underline{M}) + \underline{\psi}_l^T (\Delta\underline{K} - \omega_l^2 \Delta\underline{M}) \quad (8.5.7)$$

Postmultiply this equation by $\underline{\psi}_l$ and use (8.5.3) to obtain

$$\Delta(\omega_l^2) \approx \frac{\underline{\psi}_l^T (\Delta\underline{K} - \omega_l^2 \Delta\underline{M}) \underline{\psi}_l}{\tilde{m}_l} \quad (8.5.8)$$

where

$$\tilde{m}_l = \underline{\psi}_l^T \underline{M} \underline{\psi}_l \quad (8.5.9)$$

Note that

$$\Delta(\omega_l^2) \approx \frac{\partial \omega_l^2}{\partial \omega_l} \Delta\omega_l = 2\omega_l \Delta\omega_l \quad (8.5.10)$$

thus

Natural Frequency Perturbation Formula I

$$\Delta\omega_l \approx \frac{1}{2\tilde{m}_l \omega_l} \underline{\psi}_l^T (\Delta\underline{K} - \omega_l^2 \Delta\underline{M}) \underline{\psi}_l \quad l = 1, 2, \dots, N \quad (8.5.11)$$

In order to determine $\Delta\underline{\psi}_l$, let

$$\Delta\underline{\psi}_l = \sum_{k=1}^N c_{lk} \underline{\psi}_k \quad (8.5.12)$$

Substitute (8.5.12) into (8.5.7) and postmultiply the result by $\underline{\psi}_j$

$$\left(\sum_{k=1}^N c_{lk} \underline{\psi}_k^T \right) (\underline{K} - \omega_l^2 \underline{M}) \underline{\psi}_j \approx \Delta (\omega_l^2) \underline{\psi}_l^T \underline{M} \underline{\psi}_j - \underline{\psi}_l^T (\Delta \underline{K} - \omega_l^2 \Delta \underline{M}) \underline{\psi}_j \quad (8.5.13)$$

For $j \neq l$, use orthogonality (5.4.41) and (5.4.45)

$$\underline{\psi}_k^T \underline{M} \underline{\psi}_j = \delta_{kj} \tilde{m}_j, \quad \underline{\psi}_k^T \underline{K} \underline{\psi}_j = \delta_{kj} \tilde{m}_j \omega_j^2 \quad (8.5.14)$$

to obtain

$$c_{lj} = \frac{\underline{\psi}_l^T (\Delta \underline{K} - \omega_l^2 \Delta \underline{M}) \underline{\psi}_j}{\tilde{m}_j (\omega_l^2 - \omega_j^2)} \quad (8.5.15)$$

For $j = l$, the coefficient of c_{ll} in (8.5.13) is zero by (8.5.3) so c_{ll} is arbitrary and it may be set to zero. Substitution of (8.5.15) into (8.5.12) yields

Mode Shape Perturbation Formula I

$$\Delta \underline{\psi}_l \approx \sum_{\substack{k=1 \\ k \neq l}}^N \left(\frac{\underline{\psi}_l^T (\Delta \underline{K} - \omega_l^2 \Delta \underline{M}) \underline{\psi}_k}{\tilde{m}_k (\omega_l^2 - \omega_k^2)} \right) \underline{\psi}_k \quad (8.5.16)$$

EXAMPLE 8.5.1 *Approximate Natural Frequencies and Mode Shape Changes Due to Stiffness and Mass Change*

Statement: Existing machinery and structures often experience resonance problems after initial installation due to unmodeled effects such as attached piping, foundation flexibility, and so on. Quite often, the remedy is to shift a natural frequency by attaching stiffness (bracing) elements to ground or to add or subtract mass. The amount of stiffness or mass required to produce a desired shift in a natural frequency may be estimated with the above perturbation formulas.

Objective: Derive formulas for the approximate change in natural frequencies and mode shapes that result from adding mass or “stiffness to ground” to an existing machine or structure.

Assumptions: The mass and stiffness are small relative to their counterparts in the existing structure. The added mass is attached at the j_1, j_2 , and j_3 dofs. The added stiffness is attached to dof i .

Solution: The effect of attaching mass (m_A) is to add m_A to the (j_1, j_1) , (j_2, j_2) , and (j_3, j_3) locations in the \underline{M} matrix, so the increment in mass matrix is null except for three positions

$$\Delta \underline{M} = \begin{array}{c} \text{column} \\ \begin{array}{cccc} & j_1 & j_2 & j_3 \\ & \downarrow & \downarrow & \downarrow \\ \begin{bmatrix} 0 & \dots & & \dots & 0 \\ \vdots & & & & \vdots \\ & m_A & & & \\ & & m_A & & \\ & & & m_A & \\ \vdots & & & & \vdots \\ 0 & \dots & & \dots & 0 \end{bmatrix} & \begin{array}{l} \leftarrow \text{row } j_1 \\ \leftarrow \text{row } j_2 \\ \leftarrow \text{row } j_3 \end{array} \end{array} \end{array} \quad (1)$$

Similarly, the effect of adding a stiffness (k_A) between ground and dof i is to add k_A to the (i, i) location of the \underline{K} matrix, so the increment in stiffness matrix is null except for one position

$$\Delta \underline{K} = \begin{array}{c} \text{column } i \\ \downarrow \\ \begin{bmatrix} 0 & \dots & 0 \\ \vdots & k_A & \vdots \\ 0 & \dots & 0 \end{bmatrix} \leftarrow \text{row } i \end{array} \quad (2)$$

Therefore,

$$\underline{\psi}_l^T \Delta \underline{M} \underline{\psi}_l = m_A (\psi_{j_1 l}^2 + \psi_{j_2 l}^2 + \psi_{j_3 l}^2), \quad \underline{\psi}_l^T \Delta \underline{K} \underline{\psi}_l = k_A \psi_{il}^2 \quad (3)$$

Insert (3) into (8.5.11) to obtain

$$\Delta \omega_l \approx \frac{1}{2\tilde{m}_l \omega_l} \left[k_A \psi_{il}^2 - \omega_l^2 m_A (\psi_{j_1 l}^2 + \psi_{j_2 l}^2 + \psi_{j_3 l}^2) \right] \quad (4)$$

For a design application, the desired change in natural frequency is given and the required k_A or m_A must be determined. For example, from (4)

Mass modification at dof j for given $\Delta \omega_l$:

$$m_A \approx \frac{-2\tilde{m}_l}{\psi_{j_1 l}^2 + \psi_{j_2 l}^2 + \psi_{j_3 l}^2} \left(\frac{\Delta \omega_l}{\omega_l} \right) \quad (5)$$

Stiffness modification at dof j for given $\Delta \omega_l$:

$$k_A \approx \frac{-2\tilde{m}_l \omega_l \Delta \omega_l}{\psi_{il}^2} \quad (6)$$

The mode shape changes due to k_A and m_A are obtained from (8.5.16) as

$$\Delta \underline{\psi}_l \approx \sum_{\substack{k=1 \\ k \neq l}}^N \frac{\underline{\psi}_{il} \underline{\psi}_{ik} k_A - \omega_l^2 m_A (\underline{\psi}_{j_1 l} \underline{\psi}_{j_1 k} + \underline{\psi}_{j_2 l} \underline{\psi}_{j_2 k} + \underline{\psi}_{j_3 l} \underline{\psi}_{j_3 k})}{\tilde{m}_k (\omega_l^2 - \omega_k^2)} \quad (7)$$

Summary: This example has illustrated how the effect of $\Delta \underline{M}$ and $\Delta \underline{K}$ on the ω_l and $\underline{\psi}_l$ may be approximated. As expected, an increase in mass lowers the natural frequency so (5) has a negative sign, and an increase in stiffness raises the natural frequencies so (6) has a plus sign. Note from (5) and (6) that the amount of added mass and stiffness required to produce a desired change in the natural frequency is lowered as the mode shape component at the attachment point increases. The required added mass or stiffness becomes infinite if the attachment point is a node of the corresponding mode shape. This results since attaching a mass or stiffness at a node point of a mode will not affect the natural frequency of the mode.

8.5.2 Orthogonally Damped Systems

The next approach for estimating changes in the eigenvalues due to system parameter changes utilizes a two-term Taylor series expansion. Let d_i be the i th variable parameter in the model. These parameters are those that may be adjusted either in a design or a field troubleshooting type application:

$$\omega_l = \omega_{l0} + \sum_{i=1}^n \left. \frac{\partial \omega_l}{\partial d_i} \right|_0 \Delta d_i \quad (8.5.17)$$

and

$$\xi_l = \xi_{l0} + \sum_{i=1}^n \left. \frac{\partial \xi_l}{\partial d_i} \right|_0 \Delta d_i \quad (8.5.18)$$

where “0” indicates the original system, that is, before modifications. To illustrate this, consider the orthogonally damped, nongyroscopic, noncirculatory force system (5.4.108)

$$(\lambda^2 \underline{M} + \lambda \underline{C} + \underline{K}) \underline{\Lambda} = \underline{0} \quad (N \times 1) \quad (8.5.19)$$

where by (5.4.44), (5.4.46), (5.4.93), (5.4.100), and (5.4.114)

$$\underline{\Lambda} = \underline{\psi} = \text{an undamped, nongyroscopic, noncirculatory mode shape} \quad (8.5.20)$$

$$\underline{\psi}_j^T \underline{M} \underline{\psi}_k = \delta_{jk} \tilde{m}_j, \quad \underline{\psi}_j^T \underline{K} \underline{\psi}_k = \delta_{jk} \tilde{m}_j \omega_j^2, \quad \underline{\psi}_j^T \underline{C} \underline{\psi}_k = \delta_{jk} 2\xi_j \omega_j \tilde{m}_j \quad (8.5.21)$$

and by (5.4.112)

$$\lambda_j = -\xi_j \omega_j \pm i \omega_j \sqrt{1 - \xi_j^2} \quad (8.5.22)$$

Considering the partial derivative of (8.5.19) with respect to d_i yields

$$\left(2\lambda \frac{\partial \lambda}{\partial d_i} \underline{M} + \lambda^2 \frac{\partial \underline{M}}{\partial d_i} + \frac{\partial \lambda}{\partial d_i} \underline{C} + \lambda \frac{\partial \underline{C}}{\partial d_i} + \frac{\partial \underline{K}}{\partial d_i} \right) \underline{\psi} + (\lambda^2 \underline{M} + \lambda \underline{C} + \underline{K}) \frac{\partial \underline{\psi}}{\partial d_i} = \underline{0} \quad (8.5.23)$$

Transpose this equation for mode l and postmultiply this by $\underline{\psi}_l$ to obtain

$$\underline{\psi}_l^T \left(2\lambda_l \frac{\partial \lambda_l}{\partial d_i} \underline{M} + \lambda_l^2 \frac{\partial \underline{M}}{\partial d_i} + \frac{\partial \lambda_l}{\partial d_i} \underline{C} + \lambda_l \frac{\partial \underline{C}}{\partial d_i} + \frac{\partial \underline{K}}{\partial d_i} \right) \underline{\psi}_l + \frac{\partial \underline{\psi}_l}{\partial d_i} (\lambda_l^2 \underline{M} + \lambda_l \underline{C} + \underline{K}) \underline{\psi}_l = \underline{0} \quad (8.5.24)$$

Utilize (8.5.19) and (8.5.21) to simplify this to

$$\begin{aligned}\frac{\partial \lambda_l}{\partial d_i} &= \frac{\partial \lambda_{Rl}}{\partial d_i} + i \frac{\partial \lambda_{Il}}{\partial d_i} = -\frac{\underline{\psi}_l^T \left(\lambda_l^2 \frac{\partial \underline{M}}{\partial d_i} + \lambda_l \frac{\partial \underline{C}}{\partial d_i} + \frac{\partial \underline{K}}{\partial d_i} \right) \underline{\psi}_l}{\underline{\psi}_l^T (2\lambda_l \underline{M} + \underline{C}) \underline{\psi}_l} \\ &= \frac{-1}{\tilde{m}_l(2\lambda_l + 2\xi_l \omega_l)} \underline{\psi}_l^T \left(\lambda_l^2 \frac{\partial \underline{M}}{\partial d_i} + \lambda_l \frac{\partial \underline{C}}{\partial d_i} + \frac{\partial \underline{K}}{\partial d_i} \right) \underline{\psi}_l\end{aligned}\quad (8.5.25)$$

For an undamped (both before and after modification) system,

$$\xi_l = 0, \quad \underline{C} = 0, \quad \lambda_l = i\omega_l \quad (8.5.26)$$

then (8.5.25) implies

$$\frac{\partial \omega_l}{\partial d_i} = \left(\frac{1}{i} \right) \left(\frac{-1}{\tilde{m}_l 2i\omega_l} \right) \underline{\psi}_l^T \left(-\omega_l^2 \frac{\partial \underline{M}}{\partial d_i} + \frac{\partial \underline{K}}{\partial d_i} \right) \underline{\psi}_l = \frac{\underline{\psi}_l^T \left(-\omega_l^2 \frac{\partial \underline{M}}{\partial d_i} + \frac{\partial \underline{K}}{\partial d_i} \right) \underline{\psi}_l}{2\tilde{m}_l \omega_l} \quad (8.5.27)$$

For the damped case, the eigenvalues have the form of (8.5.22) so

$$\frac{\partial(\text{Real}(\lambda_l))}{\partial d_i} = \frac{\partial}{\partial d_i}(-\xi_l \omega_l) = -\omega_l \frac{\partial \xi_l}{\partial d_i} - \xi_l \frac{\partial \omega_l}{\partial d_i} = \frac{\partial \lambda_{Rl}}{\partial d_i} \quad (8.5.28)$$

and likewise

$$\frac{\partial(\text{Imag}(\lambda_l))}{\partial d_i} = \frac{\partial}{\partial d_i} \left(\omega_l \sqrt{1-\xi_l^2} \right) = \frac{\partial \omega_l}{\partial d_i} \sqrt{1-\xi_l^2} - \frac{\omega_l \xi_l}{\sqrt{1-\xi_l^2}} \frac{\partial \xi_l}{\partial d_i} = \frac{\partial \lambda_{Il}}{\partial d_i} \quad (8.5.29)$$

Equations (8.5.28) and (8.5.29) have the solutions

For $\xi_l \neq 0$

$$\frac{\partial \xi_l}{\partial d_i} = \frac{- \left[(1-\xi_l^2) \frac{\partial \lambda_{Rl}}{\partial d_i} + \xi_l \sqrt{1-\xi_l^2} \frac{\partial \lambda_{Il}}{\partial d_i} \right]}{\omega_l}, \quad \frac{\partial \omega_l}{\partial d_i} = \frac{- \left(\omega_l \frac{\partial \xi_l}{\partial d_i} + \frac{\partial \lambda_{Rl}}{\partial d_i} \right)}{\xi_l} \quad (8.5.30)$$

For $\xi_l = 0$

$$\frac{\partial \xi_l}{\partial d_i} = \frac{-1}{\omega_l} \frac{\partial \lambda_{Rl}}{\partial d_i}, \quad \frac{\partial \omega_l}{\partial d_i} = \frac{\partial \lambda_{Il}}{\partial d_i} \quad (8.5.31)$$

The $\partial \lambda_{Rl}/\partial d_i$ and $\partial \lambda_{Il}/\partial d_i$ terms in (8.5.30) and (8.5.31) are obtained from (8.5.25).

The modified system's undamped natural frequencies and damping factors are estimated from (8.5.17), (8.5.18), (8.5.30), and (8.5.25) as

$$\omega_l \approx \omega_{l0} + \sum_{i=1}^n \left. \frac{\partial \omega_l}{\partial d_i} \right|_0 \Delta d_i \quad (8.5.32)$$

$$\xi_l \approx \xi_{l0} + \sum_{i=1}^n \left. \frac{\partial \xi_l}{\partial d_i} \right|_0 \Delta d_i \quad (8.5.33)$$

where

$$\frac{\partial \omega_l}{\partial d_i} = \frac{-\left(\omega_l \frac{\partial \xi_l}{\partial d_i} + \frac{\partial \lambda_{Rl}}{\partial d_i}\right)}{\xi_l}, \quad \frac{\partial \xi_l}{\partial d_i} = \frac{-\left[(1-\xi_l^2) \frac{\partial \lambda_{Rl}}{\partial d_i} + \xi_l \sqrt{1-\xi_l^2} \frac{\partial \lambda_{Il}}{\partial d_i}\right]}{\omega_l} \quad (8.5.34)$$

and

$$\begin{aligned} \frac{\partial \lambda_l}{\partial d_i} &= \frac{\partial \lambda_{Rl}}{\partial d_i} + i \frac{\partial \lambda_{Il}}{\partial d_i} = \frac{-\underline{\psi}_l^T \left(\lambda_l^2 \frac{\partial \underline{M}}{\partial d_i} + \lambda_l \frac{\partial \underline{C}}{\partial d_i} + \frac{\partial \underline{K}}{\partial d_i} \right) \underline{\psi}_l}{\underline{\psi}_l^T (2\lambda_l \underline{M} + \underline{C}) \underline{\psi}_l} \\ &= \frac{-1}{\tilde{m}_l (2\lambda_l + 2\xi_l \omega_l)} \underline{\psi}_l^T \left(\lambda_l^2 \frac{\partial \underline{M}}{\partial d_i} + \lambda_l \frac{\partial \underline{C}}{\partial d_i} + \frac{\partial \underline{K}}{\partial d_i} \right) \underline{\psi}_l \end{aligned} \quad (8.5.35)$$

These equations simplify for the case of an originally undamped system with modifications that include damping. For this case,

$$\xi_l = 0, \quad \lambda_l = i\omega_l \quad (8.5.36)$$

Therefore, (8.5.25) simplifies to

$$\frac{\partial \lambda_l}{\partial d_i} = \frac{\partial \lambda_{lR}}{\partial d_i} + i \frac{\partial \lambda_{lI}}{\partial d_i} = \frac{-1}{2i\omega_l \tilde{m}_l} \underline{\psi}_l^T \left(-\omega_l^2 \frac{\partial \underline{M}}{\partial d_i} + i\omega_l \frac{\partial \underline{C}}{\partial d_i} + \frac{\partial \underline{K}}{\partial d_i} \right) \underline{\psi}_l \quad (8.5.37)$$

yielding

$$\frac{\partial \lambda_{lR}}{\partial d_i} = \frac{-1}{2\tilde{m}_l} \underline{\psi}_l^T \frac{\partial \underline{C}}{\partial d_i} \underline{\psi}_l, \quad \frac{\partial \lambda_{lI}}{\partial d_i} = \frac{1}{2\omega_l \tilde{m}_l} \underline{\psi}_l^T \left(-\omega_l^2 \frac{\partial \underline{M}}{\partial d_i} + \frac{\partial \underline{K}}{\partial d_i} \right) \underline{\psi}_l \quad (8.5.38)$$

where from (8.5.31)

$$\frac{\partial \xi_l}{\partial d_i} = \frac{-1}{\omega_l} \frac{\partial \lambda_{Rl}}{\partial d_i}, \quad \frac{\partial \omega_l}{\partial d_i} = \frac{\partial \lambda_{lI}}{\partial d_i} \quad (8.5.39)$$

Substitute (8.5.38) into (8.5.39) to obtain

$$\frac{\partial \xi_l}{\partial d_i} = \frac{1}{2\tilde{m}_l \omega_l} \underline{\psi}_l^T \frac{\partial \underline{C}}{\partial d_i} \underline{\psi}_l, \quad \frac{\partial \omega_l}{\partial d_i} = \frac{1}{2\omega_l \tilde{m}_l} \underline{\psi}_l^T \left(-\omega_l^2 \frac{\partial \underline{M}}{\partial d_i} + \frac{\partial \underline{K}}{\partial d_i} \right) \underline{\psi}_l \quad (8.5.40)$$

Equation (8.5.40) may then be substituted into (8.5.32) and (8.5.33).

EXAMPLE 8.5.2 *Approximate Natural Frequencies and Damping Ratios of a Truss*

Statement: The truss shown in Figure E8.5.2(a) has experienced resonance problems at its first mode (342 Hz). The excitation (forcing) frequency is fixed (unchangeable) so a decision is made to attach a stiffening element \bar{k} or mass \bar{m} to shift the natural frequency or attach a damper \bar{c} to decrease the amplification factor ($1/(2\xi)$). The modifications are to be attached at node 5.

The properties of all truss elements in the model are

$$A = 0.01 \text{ m}^2, \quad E_y = 2.0 \times 10^{11} \text{ N/m}^2, \quad \rho = 7000 \text{ kg/m}^3, \quad L = 1.0 \text{ m}$$

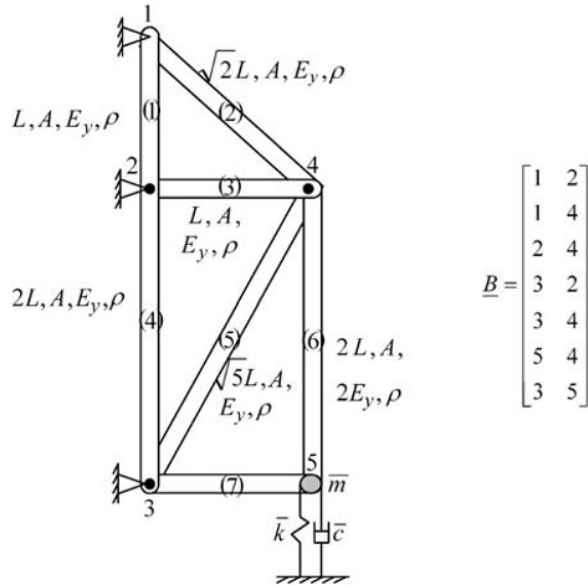


Figure E8.5.2(a) Truss with attached mass, spring, and dashpot

Objective: The objectives are to derive formulas for the approximate change in natural frequencies and damping ratios that result from adding mass, damping, or stiffness to the truss at node 5 and to plot the approximate and exact natural frequencies and damping ratios versus the modification variable values.

Assumptions: The modification mass and stiffness are small relative to their counterparts in the existing structure.

Solution: The approach shown in Section 4.8 is employed to obtain the mass and stiffness matrices for the free (nonfixed) dofs of the 2D truss model. The free dofs are

$$\begin{aligned} q_{f1} = q_7 &= \text{horizontal dof at node 4}, & q_{f2} = q_8 &= \text{vertical dof at node 4} \\ q_{f3} = q_9 &= \text{horizontal dof at node 5}, & q_{f4} = q_{10} &= \text{vertical dof at node 5} \end{aligned} \quad (1)$$

The equation of motion is (4.8.96)

$$\underline{M}_f \ddot{q}_f + \underline{C}_f \dot{q}_f + \underline{K}_f q_f = \underline{F}_f \quad (2)$$

$N_f \times N_f \quad N_f \times 1$
 $N_f \times N_f \quad N_f \times 1$
 $N_f \times N_f \quad N_f \times 1$
 $N_f \times 1$

Similar to the example of Figure 4.8.13, the original system mass and stiffness matrices are calculated to be

$$\underline{K}_f^o = 10^9 * \begin{bmatrix} 2.8859 & -0.3494 & -0.0000 & -0.0000 \\ -0.3494 & 3.4227 & -0.0000 & -2.0000 \\ -0.0000 & -0.0000 & 2.0000 & 0.0000 \\ -0.0000 & -2.0000 & 0.0000 & 2.0000 \end{bmatrix}, \quad \underline{M}_f^o = \begin{bmatrix} 155.2 & 0 & 23.3 & 0 \\ 0 & 155.2 & 0 & 23.3 \\ 23.3 & 0 & 70.0 & 0 \\ 0 & 23.3 & 0 & 70.0 \end{bmatrix} \quad (3)$$

The first natural frequency occurs at ($f_1 = 342\text{Hz}$, $\omega_1 = 2149\text{rad/s}$). The original system modes are shown in Figure E8.5.2(b). The first mode shape and its modal mass are

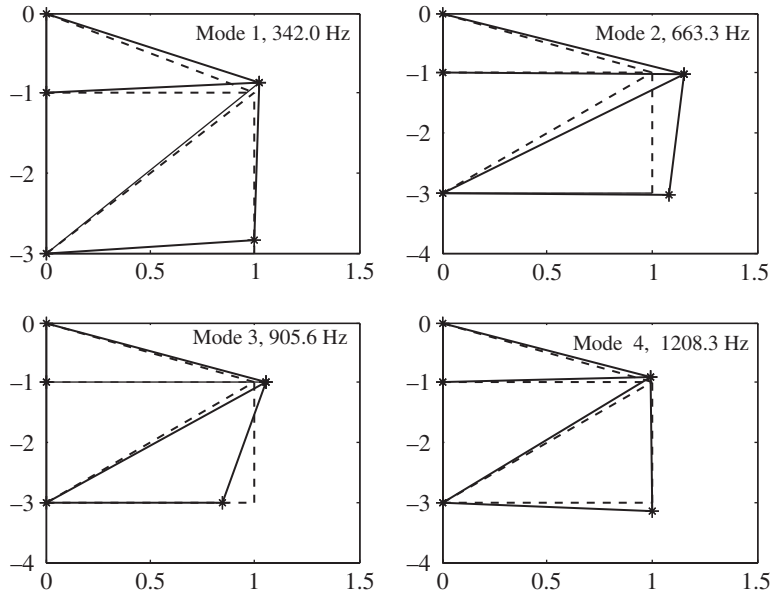


Figure E8.5.2(b) Modes of the original system

$$\underline{\psi}_{f1} = \{0.1285 \quad 0.7955 \quad 0.0083 \quad 1.0000\}^T, \quad \tilde{m}_1 = 207.9369, \quad \omega_1 = 2149 \text{ rad/s} \quad (4)$$

The modified system's natural frequency is estimated from (8.5.32) and (8.5.33) as

$$\begin{aligned} \omega_1|_{\text{modified}} &\approx \omega_{10} + \left. \frac{\partial \omega_1}{\partial \tilde{m}} \right|_0 \tilde{m} + \left. \frac{\partial \omega_1}{\partial \bar{k}} \right|_0 \bar{k} + \left. \frac{\partial \omega_1}{\partial \bar{c}} \right|_0 \bar{c} \\ \xi_1|_{\text{modified}} &\approx \xi_{10} + \left. \frac{\partial \xi_1}{\partial \tilde{m}} \right|_0 \tilde{m} + \left. \frac{\partial \xi_1}{\partial \bar{k}} \right|_0 \bar{k} + \left. \frac{\partial \xi_1}{\partial \bar{c}} \right|_0 \bar{c} \end{aligned} \quad (5)$$

where from (8.5.40)

$$\frac{\partial \xi_1}{\partial d_i} = \frac{1}{2\tilde{m}_1\omega_1} \underline{\psi}^T \frac{\partial \underline{C}_f}{\partial d_i} \underline{\psi}, \quad \frac{\partial \omega_1}{\partial d_i} = \frac{1}{2\omega_1\tilde{m}_1} \underline{\psi}^T \left(-\omega_1^2 \frac{\partial \underline{M}_f}{\partial d_i} + \frac{\partial \underline{K}_f}{\partial d_i} \right) \underline{\psi} \quad (6)$$

The mass, damping, and stiffness matrices with the modifications added become

$$\underline{M}_f = \underline{M}_f^o + \begin{bmatrix} 0 & 0 & 0 & 0 \\ 0 & 0 & 0 & 0 \\ 0 & 0 & \tilde{m} & 0 \\ 0 & 0 & 0 & \tilde{m} \end{bmatrix}, \quad \underline{K}_f = \underline{K}_f^o + \begin{bmatrix} 0 & 0 & 0 & 0 \\ 0 & 0 & 0 & 0 \\ 0 & 0 & 0 & 0 \\ 0 & 0 & 0 & \bar{k} \end{bmatrix}, \quad \underline{C}_f = \begin{bmatrix} 0 & 0 & 0 & 0 \\ 0 & 0 & 0 & 0 \\ 0 & 0 & 0 & 0 \\ 0 & 0 & 0 & \bar{c} \end{bmatrix} \quad (7)$$

Therefore,

$$\frac{\partial \underline{M}_f}{\partial \tilde{m}} = \begin{bmatrix} 0 & 0 & 0 & 0 \\ 0 & 0 & 0 & 0 \\ 0 & 0 & 1 & 0 \\ 0 & 0 & 0 & 1 \end{bmatrix}, \quad \frac{\partial \underline{M}_f}{\partial \bar{k}} = \underline{0}, \quad \frac{\partial \underline{M}_f}{\partial \bar{c}} = \underline{0}, \quad \frac{\partial \underline{K}_f}{\partial \tilde{m}} = \underline{0}, \quad \frac{\partial \underline{K}_f}{\partial \bar{k}} = \begin{bmatrix} 0 & 0 & 0 & 0 \\ 0 & 0 & 0 & 0 \\ 0 & 0 & 0 & 0 \\ 0 & 0 & 0 & 1 \end{bmatrix}, \quad \frac{\partial \underline{K}_f}{\partial \bar{c}} = \underline{0}$$

$$\frac{\partial C_f}{\partial \bar{m}} = 0, \quad \frac{\partial C_f}{\partial \bar{k}} = 0, \quad \frac{\partial C_f}{\partial \bar{c}} = \begin{bmatrix} 0 & 0 & 0 & 0 \\ 0 & 0 & 0 & 0 \\ 0 & 0 & 0 & 0 \\ 0 & 0 & 0 & 1 \end{bmatrix} \quad (8)$$

Substitution of (8) into (6) and then substituting values from (4) yield

$$\begin{aligned} \frac{\partial \omega_1}{\partial \bar{m}} &= \frac{1}{2\omega_1 \tilde{m}_1} \psi_{-fl}^T \left(-\omega_1^2 \frac{\partial M_f}{\partial \bar{m}} + \frac{\partial K_f}{\partial \bar{m}} \right) \psi_{-fl} = \frac{-\omega_1}{2\tilde{m}_1} (\psi_{fl3}^2 + \psi_{fl4}^2) \\ \frac{\partial \omega_1}{\partial \bar{k}} &= \frac{1}{2\omega_1 \tilde{m}_1} \psi_{-fl}^T \left(-\omega_1^2 \frac{\partial M_f}{\partial \bar{k}} + \frac{\partial K_f}{\partial \bar{k}} \right) \psi_{-fl} = \frac{\psi_{fl4}^2}{2\tilde{m}_1 \omega_1} \\ \frac{\partial \omega_1}{\partial \bar{c}} &= \frac{1}{2\omega_1 \tilde{m}_1} \psi_{-fl}^T \left(-\omega_1^2 \frac{\partial M_f}{\partial \bar{c}} + \frac{\partial K_f}{\partial \bar{c}} \right) \psi_{-fl} = 0 \end{aligned} \quad (9)$$

$$\frac{\partial \xi_1}{\partial \bar{m}} = \frac{\psi_{-fl}^T \frac{\partial C_f}{\partial \bar{m}} \psi_{-fl}}{2\tilde{m}_1 \omega_1} = 0, \quad \frac{\partial \xi_1}{\partial \bar{k}} = 0, \quad \frac{\partial \xi_1}{\partial \bar{c}} = \frac{\psi_{-fl}^T \frac{\partial C_f}{\partial \bar{c}} \psi_{-fl}}{2\tilde{m}_1 \omega_1} = \frac{\psi_{fl4}^2}{2\tilde{m}_1 \omega_1} \quad (10)$$

For mode 1, Equations (9) and (10) yield

$$\begin{aligned} \frac{\partial \omega_1}{\partial \bar{m}} &= -5.17 \frac{\text{rad/s}}{\text{kg}}, \quad \frac{\partial \omega_1}{\partial \bar{k}} = 1.12 \times 10^{-6} \frac{\text{rad/s}}{\text{N/m}}, \quad \frac{\partial \omega_1}{\partial \bar{c}} = 0, \\ \frac{\partial \xi_1}{\partial \bar{m}} &= 0, \quad \frac{\partial \xi_1}{\partial \bar{k}} = 0, \quad \frac{\partial \xi_1}{\partial \bar{c}} = 1.12 \times 10^{-6} \frac{\text{rad/s}}{\text{Ns/m}} \end{aligned} \quad (11)$$

Substitute (11) into (5) to obtain

$$\omega_1|_{\text{modified}} \approx 2149 - 5.17\bar{m} + (1.12 \times 10^{-6})\bar{k}, \quad \xi_1|_{\text{modified}} \approx (1.12 \times 10^{-6})\bar{c} \quad (12)$$

Figure E8.5.2(c) shows the variation of the first mode natural frequency versus the added mass value utilizing (12) and by exact solution. Figure E8.5.2(d) shows the variation of the first mode natural frequency versus the added stiffness value utilizing (12) and by exact solution. Figure E8.5.2(e) shows the variation of the first mode damper ratio ξ versus the added damping value utilizing (12) and by exact solution.

The exact damping ratios ξ in Figure E8.5.2(e) were obtained by solving the following eigenvalue problem from (5.4.218) and (5.4.219):

$$\lambda \underline{\Gamma} = \underline{A} \underline{\Gamma} \quad (2N \times 1) \quad (13)$$

$$\underline{A} = \underline{E}^{-1} \underline{H} = \begin{bmatrix} -\underline{M}^{-1} \underline{C} & -\underline{M}^{-1} \underline{K} \\ \underline{I}_N & \underline{0} \end{bmatrix} \quad (2N \times 2N) \quad (14)$$

$$\xi = \frac{-\text{Re}(\lambda)}{|\lambda|} \quad (15)$$

The final results in (9) and (10) are somewhat independent of the number of elements in the system, which illustrates the simplified form of the results. These results also show that the sensitivities increase as the square of the mode shape component at the modification attachment point. Consequently, selecting the attachment point location with a large mode component is a key step in a successful modification.

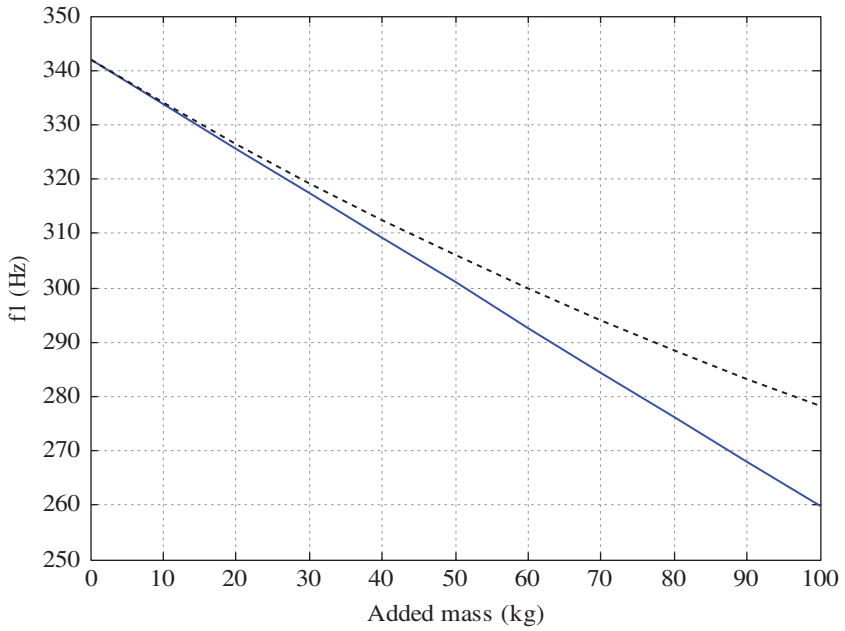


Figure E8.5.2(c) First natural frequency of the truss versus the added mass value. Exact (dashed)

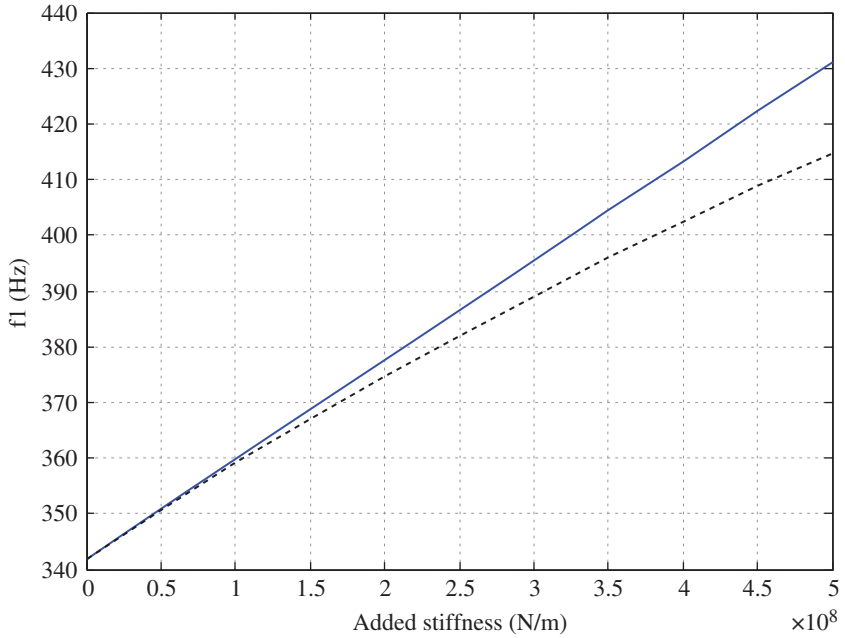


Figure E8.5.2(d) First natural frequency of the truss versus the added stiffness value. Exact (dashed)

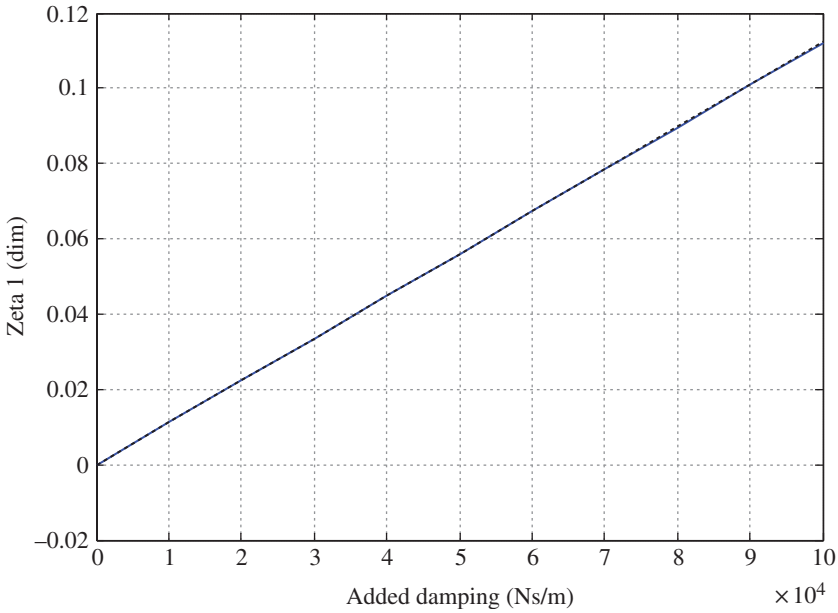


Figure E8.5.2(e) First mode damping ratio ξ versus the added damper value. Exact (dashed)

8.5.3 Rayleigh's Quotient

The Rayleigh quotient approach provides a means to estimate the lowest undamped natural frequency given the \underline{M} and \underline{K} matrices and a guess \underline{y} of the lowest mode shape $\underline{\psi}_1$. The Rayleigh quotient is defined as

$$R = \frac{\underline{y}^T \underline{K} \underline{y}}{\underline{y}^T \underline{M} \underline{y}} \quad (8.5.41)$$

The guess \underline{y} may be expressed in terms of the complete, linearly independent set of basis vectors $\underline{\psi}_i$ as

$$\underline{y} = a_1 \underline{\psi}_1 + a_2 \underline{\psi}_2 + \cdots + a_N \underline{\psi}_N \quad (8.5.42)$$

Assume that the error in \underline{y} , as a guess of $\underline{\psi}_1$, is of order ϵ . Then \underline{y} has the form

$$\underline{y} = \alpha \left(\underline{\psi}_1 + \epsilon_2 \underline{\psi}_2 + \cdots + \epsilon_N \underline{\psi}_N \right) \quad (8.5.43)$$

where

$$\epsilon_j \ll 1 \quad (8.5.44)$$

It can be shown with the use of orthogonality ((5.4.75), (5.4.77)) that if the $\underline{\psi}_i$ are mass orthonormalized, then

$$R \approx \omega_1^2 \left\{ 1 + \varepsilon_2^2 \left[\left(\frac{\omega_2}{\omega_1} \right)^2 - 1 \right] + \cdots + \varepsilon_N^2 \left[\left(\frac{\omega_N}{\omega_1} \right)^2 - 1 \right] \right\} \quad (8.5.45)$$

Equation (8.5.45) shows that:

- \sqrt{R} is an upper bound on ω_1 .
- If the \underline{y} guess of $\underline{\psi}_1$ is of order ε , the Rayleigh quotient prediction of ω_1^2 is of order ε^2 where

$$\varepsilon^2 \ll \varepsilon \quad (8.5.46)$$

Therefore, for a good guess \underline{y} “close” to $\underline{\psi}_1$, it results that

$$R \approx \omega_1^2 \quad (8.5.47)$$

EXAMPLE 8.5.3 Rayleigh’s Quotient Applied to a Simple Piping System

Description: A piping system is secured by flanges and bellows (expansion joints) and by vertical pipe hangers (not shown). The piping network experiences high-frequency vibration and resulting noise due to resonance between the pressure pulsations in the flowing gas and the piping axial natural frequencies. It is decided to model the network in order to assist in shifting the natural frequencies away from the pressure pulsation frequencies (Figure E8.5.3(a)).

Objective: Demonstrate Rayleigh’s quotient estimation of the lowest natural frequency.

Assumptions:

- Bellows stiffness is negligible.
- Piping enclosed by dashed box behaves rigidly.
- Masses of piping runs are lumped at the 4 dofs shown.
- Flanges are rigidly connected to ground.

Solution: The equations of motion for this system are

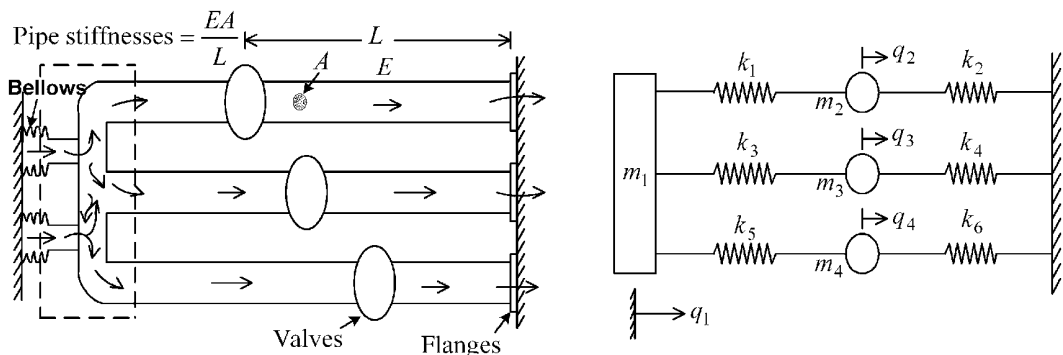


Figure E8.5.3(a) Simple piping system and lumped mass model

$$\underline{M}\ddot{\underline{q}} + \underline{K}\underline{q} = \underline{0} \quad (1)$$

$$\underline{q} = (q_1 \ q_2 \ q_3 \ q_4)^T \quad (2)$$

$$\underline{M} = \begin{bmatrix} m_1 & \underline{0} \\ & m_2 \\ \underline{0} & m_3 \\ & & m_4 \end{bmatrix}, \quad \underline{K} = \begin{bmatrix} k_1 + k_3 + k_5 & -k_1 & -k_3 & -k_5 \\ -k_1 & k_1 + k_2 & 0 & 0 \\ -k_3 & 0 & k_3 + k_4 & 0 \\ -k_5 & 0 & 0 & k_5 + k_6 \end{bmatrix} \quad (3)$$

and the numerical values are

$$m_1 = 500\text{kg}, \ m_2 = 200\text{kg}, \ m_3 = 300\text{kg}, \ m_4 = 150\text{kg} \quad (4)$$

i	1	2	3	4	5	6
$k_i(\text{N/m})$	10^9	0.5×10^9	2×10^9	0.75×10^9	3.0×10^9	5.0×10^9

Utilize MATLAB to determine the exact mode shapes and natural frequencies by solving

$$\underline{A} = \underline{M}^{-1}\underline{K}, \quad \lambda_j \underline{\psi}_j = \underline{A}\underline{\psi}_j, \quad \lambda_j = \omega_j^2 \quad (5)$$

The exact lowest natural frequency and mass-orthonormalized (5.4.40) mode shape are

$$\omega_1 = 1740.9\text{rad/s}, \quad \underline{\psi}_1 = (0.0298 \ 0.0333 \ 0.0323 \ 0.0118) \quad (6)$$

Consider the following guesses for $\underline{\psi}_1$ and their corresponding Rayleigh quotient (Eq. (8.5.41)) estimates for ω_1 :

Guess \underline{y} of $\underline{\psi}_1$	\sqrt{R} (rad/s)
$\underline{y} = (1 \ 1 \ 1 \ 1)$	2331
$\underline{y} = (1/m_1 \ 1/m_2 \ 1/m_3 \ 1/m_4)$	4345
k_6 restrains q_4 and k_6 is large so assume $\underline{y} = (1 \ 1 \ 1 \ 1/2)$	1770

Note all \sqrt{R} are greater than ω_1 , that is, Rayleigh provides an upper bound, and the use of some intuition in guess 3 results in an accurate estimate of the lowest natural frequency.

8.6 SUMMARY

This chapter should provide the reader with an understanding and working knowledge of some approximate methods in vibration analysis, specifically:

- (a) Guyan reduction and static condensation (GRSC) for condensing large-order systems by the use of constraint mode basis vectors

- (b) Modal synthesis-based modeling of large-order, multicomponent system using component mode and joint dof Guyan basis vectors
- (c) Eigenvalue perturbation estimates
- (d) Rayleigh quotient-based natural frequency estimates

8.7 CHAPTER 8 EXERCISES

8.7.1 Exercise Location

All exercises may be conveniently viewed and downloaded at the following website: **www.wiley.com/go/palazzolo**. This new feature greatly reduces the length of the printed book, yielding a significant cost savings for the college student, and the exercises are updated.

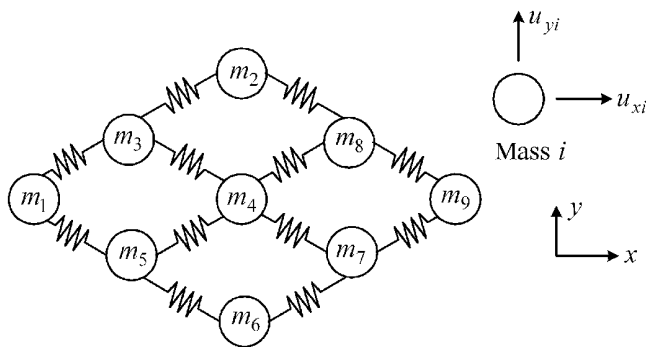
8.7.2 Exercise Goals

The goal of the Exercises in Chapter 8 is to strengthen the student's understanding and related engineering problem-solving skills in the following areas:

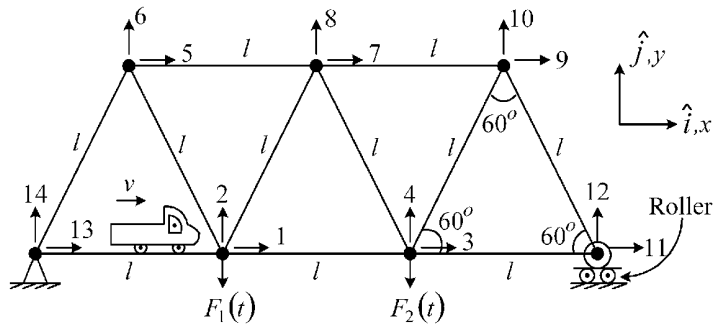
- (a) Determine Guyan basis vectors for a multi-dof vibrating system model given a set of retained dofs. The importance of Guyan reduction is increasing as more vibration-related models are finite element based with 1000s of dofs.
- (b) Model systems utilizing Guyan reduction.
- (c) Obtain natural frequency estimates using perturbation or Rayleigh quotient methods.

8.7.3 Sample Exercises 8.4 and 8.13

Exercise 8.4 requires identification of Guyan basis vectors and conditions when a set of dofs are inadmissible as being a valid set of retained dofs. Exercise (8.13) requires solution for vibration responses due to a truck passing over a bridge, utilizing numerical integration with all coordinates and with only Guyan retained coordinates.



(8.4)



(8.13)

REFERENCES

- BARRETT, T., PALAZZOLO, A., and KASCAK, A., "Probabilistic Critical Speed Determination by Receptance Based Reanalysis", *Proceedings of the 6th International Symposium on Transport Phenomena and Dynamics of Rotating Machinery*, pp. 272–288, Honolulu, March 1996.
- COOK, R., *Concepts and Applications of Finite Element Analysis*, John Wiley & Sons, Inc., New York, 1989.
- CRAIG, R. R., JR., *Structural Dynamics*, John Wiley & Sons, Inc., New York, 1981.
- HUSTER, J. and ECKERT, L., Calculation and measurement of torsional vibrations in large steam turbosets—new technique, *ABB Review*, June 1998. (or in *Machinery, Plant and Systems Monitor*, March/April 1999 or <http://multi-science.atypon.com/doi/abs/10.1260/0957456991496466>).
- WANG, B. P., PILKEY, W. D. and PALAZZOLO, A. B., "Reanalysis, Modal Synthesis and Dynamic Design," in A. K. Noor and W. D. Pilkey (eds.), *State of the Art Survey on Finite Element Technology*, ASME, New York, 1983, pp. 225–295.

Chapter 9

Beam Finite Elements for Vibration Analysis

9.1 INTRODUCTION

The finite element method (FEM) is utilized extensively in industry and research and development applications. Acquiring a good grasp of the corresponding theory presented here will provide the person utilizing commercial finite element software with a good understanding of its underlying assumptions and limitations. The FEM is utilized to model/simulate the vibration-related behavior of structural and machinery components possessing complex shapes, material property variations, boundary conditions, and loadings. This is accomplished in a “building block” approach as explained in Section 4.7 and illustrated for one-dimensional (1D) and two-dimensional (2D) truss structures in Section 4.8. The structure is divided into a multitude of elements that are joined by enforcing interelement equilibrium and displacement continuity. This “joining” or “assembling” yields the total system mass, stiffness, and damping matrices and force vector and is executed with assembly algorithms, as illustrated in Figures 4.8.5, 4.8.6, and 4.8.8, which utilize nodal or degree of freedom (dof) connectivity arrays (4.8.21, 4.8.83) and boundary condition/constraint-related arrays (4.8.30, 4.8.31). The element “building blocks” are the element matrices that are formed in two steps. The first step utilizes “shape functions” (4.7.5) to interpolate the displacements between user-located “node” points within each element. The node points are typically arranged in a regular pattern within the element, or within its geometrically transformed form. The second step is to apply Lagrange’s equations to the kinetic energy, potential energy, dissipation function, interelement forces, and external forces that exist within an individual element as shown by (4.7.60) and (4.7.61). The assembled total system matrices and force vector may then be utilized with the approaches presented in Chapters 5, 6, and 7 to predict free, transient, and steady-state harmonic displacement responses. The computed displacements may then be utilized for computing strains (4.7.22) and stresses (A.4.3), to ultimately predict component fatigue life (Section 1.4).

9.2 MODELING 2D FRAME STRUCTURES WITH EULER–BERNOULLI BEAM ELEMENTS

The 1D and 2D truss models, as depicted in Figure 4.8.11, assume ideal moment releases (pins at all joints). This is an approximation for actual truss structures that typically employ welded or riveted connections at the intersection of the truss structural members. The neglect of internal bending moments becomes unacceptable in structures that possess bolted and welded connections or experience in-span transverse force or bending moment loading. The frame model improves on the truss model by including bending moment and shear

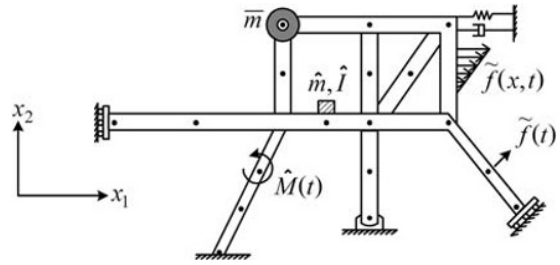


Figure 9.2.1 General planar frame model with 2D beam elements

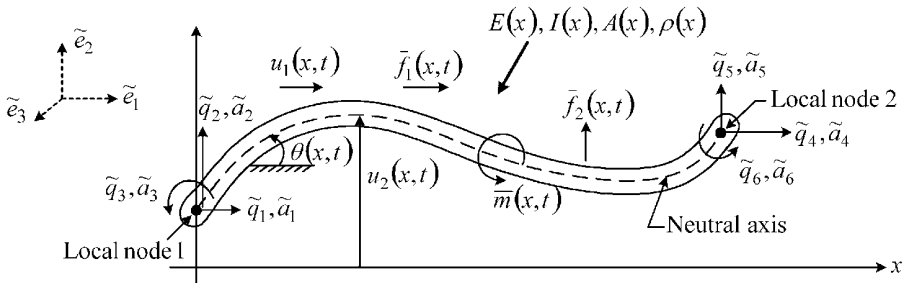


Figure 9.2.2 2D beam element showing displacements, rotations, forces, and moments in a local (element) coordinate system

force-induced deformation utilizing Euler–Bernoulli- or Timoshenko-type beam models. Inclusion of bending deformation requires that a rotation angle be added as a third dof to the 2-dof per node, 2D truss model depicted in Figure 4.8.12. Figure 9.2.1 depicts a generic 2D frame model including beam elements, forces, moments, boundary conditions, external springs, dampers and masses, etc.

Figure 9.2.2 shows an isolated 2-node beam element with deflections referenced to its own “local” coordinate system. Each node has 3 dofs, two mutually perpendicular translations and a bending rotation, totaling 6 dofs per element. Hence, following the development in Chapter 4, one should expect 6 by 6 mass and stiffness matrices and a 6 by 1 element force vector for this element.

The beam’s rotation θ is related to its transverse displacement u_2 by

$$\theta = \frac{\partial u_2}{\partial x} \quad (9.2.1)$$

which expresses the well-known Euler–Bernoulli beam kinematic assumption that

- plane cross sections remain plane and perpendicular to the neutral axis after deformation.

This assumption neglects warping and shear deformation effects. The other quantities in Figure 9.2.2 include:

$\bar{f}_1, \bar{f}_2, \bar{m}$: externally applied loads per unit length

\tilde{q}_j : displacement and rotation dofs at nodes

\tilde{a}_j : actions at nodes, where actions are the internal forces and moments that act between connected elements

9.2.1 2D Frame Element Stiffness Matrix and Strain Energy: Transverse Deflection

The transverse displacement of the beam element in Figure 9.2.2 is interpolated as

$$u_2(x_1, t) = N_2(x)\tilde{q}_2(t) + N_3(x)\tilde{q}_3(t) + N_5(x)\tilde{q}_5(t) + N_6(x)\tilde{q}_6(t) = \underline{N}_{2e} \underline{\tilde{q}}_{2e} \quad (9.2.2)$$

where

$$\underline{N}_{2e} = (N_2 \ N_3 \ N_5 \ N_6) \quad \text{and} \quad \underline{\tilde{q}}_{2e} = (\tilde{q}_2 \ \tilde{q}_3 \ \tilde{q}_5 \ \tilde{q}_6)^T \quad (9.2.3)$$

The shape functions ((2.11.36), (4.7.39)) in (9.2.2) are Hermite cubic polynomials

$$\begin{aligned} N_2(x) &= 1 - 3\frac{x^2}{L^2} + 2\frac{x^3}{L^3}, & N_3(x) &= L\left(\frac{x}{L} - 2\frac{x^2}{L^2} + \frac{x^3}{L^3}\right) \\ N_5(x) &= 3\frac{x^2}{L^2} - 2\frac{x^3}{L^3}, & N_6(x) &= L\left(-\frac{x^2}{L^2} + \frac{x^3}{L^3}\right) \end{aligned} \quad (9.2.4)$$

which satisfy the following consistency conditions (2.11.37):

	$N(0)$	$N'(0)$	$N(L)$	$N'(L)$
N_2	1	0	0	0
N_3	0	1	0	0
N_5	0	0	1	0
N_6	0	0	0	1

(9.2.5)

These conditions insure that the interpolations for u_2 in (9.2.2) and for θ in

$$\theta = \frac{\partial u_2}{\partial x} = N'_2(x)\tilde{q}_2(t) + N'_3(x)\tilde{q}_3(t) + N'_5(x)\tilde{q}_5(t) + N'_6(x)\tilde{q}_6(t) \quad (9.2.6)$$

yield the nodal values if evaluated at the nodal coordinates ($x=0, L$). From Figure 9.2.2, these conditions are:

	$x=0$	$x=L$
$u_2(x)$	$\tilde{q}_2(t)$	$\tilde{q}_5(t)$
$\theta(x)$	$\tilde{q}_3(t)$	$\tilde{q}_6(t)$

(9.2.7)

The Hermite polynomials also satisfy the rigid body displacement requirement that the entire element moves with a rigid body displacement if the nodes move with motions consistent with a rigid body displacement of the element. For example, let $\tilde{q}_2 = \tilde{q}_5 = \bar{u}_2$ and $\tilde{q}_3 = \tilde{q}_6 = 0$ in Figure 9.2.2, then by (9.2.2)

$$\begin{aligned} u_2(x, t) &= N_2(x)\tilde{q}_2 + N_3(x)\tilde{q}_3 + N_5(x)\tilde{q}_5 + N_6(x)\tilde{q}_6 \\ &= N_2(x)\bar{u}_2 + N_3(x) \cdot 0 + N_5(x)\bar{u}_2 + N_6(x) \cdot 0 \\ &= (N_2(x) + N_5(x))\bar{u}_2 = \bar{u}_2 \end{aligned} \quad (9.2.8)$$

since by (9.2.4)

$$N_2(x) + N_5(x) = 1 \quad (9.2.9)$$

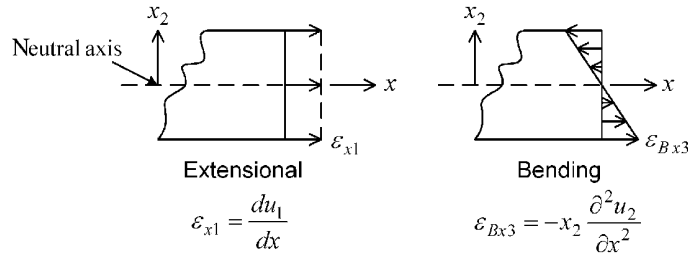


Figure 9.2.3 Strains acting on the cross section of a beam element

Thus, the entire element moves as a rigid body if its nodal coordinates move with rigid body motion. The extensional and bending strains occurring in a beam element are depicted in Figure 9.2.3. The bending strain–displacement relation for this element was given in Example 4.6.3 as

$$\varepsilon_{Bx3} = -x_2 \frac{\partial^2 u_2}{\partial x^2} = D_2(u_2) \quad \text{where } D_2 = -x_2 \frac{\partial^2}{\partial x^2} \quad (9.2.10)$$

Thus, the finite element \underline{B}_{2e} matrix in (4.7.56) is obtained from (9.2.2) and (9.2.10) as

$$\underline{B}_{2e} = \underline{D}_2 \underline{N}_{2e} = -x_2 (N_2'' \quad N_3'' \quad N_5'' \quad N_6'') \quad (9.2.11)$$

This result is substituted in (4.7.55) to obtain the element stiffness matrix for transverse deflection as

$$\begin{aligned} \tilde{\underline{K}}_{te} &= \int_V \underline{B}_{2e}^T \underline{E} \underline{B}_{2e} dV = \int_V \underline{B}_{2e}^T \underline{E} \underline{B}_{2e} dx dA \\ &= \int \int x_2^2 (N_2'' \quad N_3'' \quad N_5'' \quad N_6'')^T \underline{E} (N_2'' \quad N_3'' \quad N_5'' \quad N_6'') dA dx \\ &= \int_0^L \underline{E}(x) \underline{I}(x) \begin{bmatrix} N_2'' N_2'' & N_2'' N_3'' & N_2'' N_5'' & N_2'' N_6'' \\ & N_3'' N_3'' & N_3'' N_5'' & N_3'' N_6'' \\ \text{symmetric} & & N_5'' N_5'' & N_5'' N_6'' \\ & & & N_6'' N_6'' \end{bmatrix} dx \end{aligned} \quad (9.2.12)$$

where the element's cross-sectional area moment of inertia is defined by

$$I = \int_A x_2^2 dA \quad (9.2.13)$$

The strain energy in an element due to transverse deflections is given by (4.7.54) as

$$U_{te} = \frac{1}{2} \int_{V_e} \underline{\varepsilon}^T \underline{E}_e \underline{\varepsilon} dV_e = \frac{1}{2} \tilde{\underline{q}}_{2e}^T \tilde{\underline{K}}_{te} \tilde{\underline{q}}_{2e} \quad (9.2.14)$$

Elements that have a dominant influence on a natural frequency are often those that contribute the most strain energy for vibration in the respective mode shape. This fact is often utilized for deciding how to modify a beam structure to place natural frequencies.

9.2.2 2D Frame Element Stiffness Matrix and Strain Energy: Axial Deflection

The axial (x) displacement of the beam element in Figure 9.2.2 is interpolated as

$$u_1(x, t) = N_1(x)\tilde{q}_1(t) + N_4(x)\tilde{q}_4(t) = \underline{N}_{1e} \tilde{\underline{q}}_{1e} \quad (9.2.15)$$

where the axial shape functions (2.11.37) are

$$N_1(x) = 1 - \frac{x}{L}, \quad N_4(x) = \frac{x}{L} \quad (9.2.16)$$

and the corresponding arrays are

$$\underline{N}_{1e} = (N_1 \ N_4) \quad \text{and} \quad \tilde{\underline{q}}_{1e} = (\tilde{q}_1 \ \tilde{q}_4)^T \quad (9.2.17)$$

The axial (extensional) strain in a beam element is depicted in Figure 9.2.3. The strain–displacement relation is

$$\varepsilon_{x1} = \frac{\partial u_1}{\partial x} = D_1(u_1) \quad \text{where} \quad D_1 = \frac{\partial}{\partial x} \quad (9.2.18)$$

The finite element \underline{B}_{1e} matrix of (4.7.56) becomes

$$\underline{B}_{1e} = \underline{D}_1 \underline{N}_{1e} = (N'_1 \ N'_4) \quad (9.2.19)$$

The element stiffness matrix for transverse deflection is obtained from (9.2.19) and (4.7.55) as

$$\begin{aligned} \underline{K}_{ae} &= \int_V \underline{B}_{1e}^T \underline{E} \underline{B}_{1e} dV = \int_V \underline{B}_{1e}^T \underline{E} \underline{B}_{1e} dx dA \\ &= \int \int (N'_1 \ N'_4)^T \underline{E} (N'_1 \ N'_4) dA dx \\ &= \int_0^L \underline{E}(x) A(x) \begin{bmatrix} N'_1 N'_1 & N'_1 N'_4 \\ N'_1 N'_4 & N'_4 N'_4 \end{bmatrix} dx \end{aligned} \quad (9.2.20)$$

where the element's cross-sectional area is

$$A = \int_A dA \quad (9.2.21)$$

Elements that have the most effect (influence) on natural frequency placement are often those that have the most strain energy. The strain energy in an element due to axial deflections is given by (4.7.54) as

$$U_{ae} = \frac{1}{2} \int_V \underline{\varepsilon}^T \underline{E} \underline{\varepsilon} dV_e = \frac{1}{2} \tilde{\underline{q}}_{1e}^T \underline{K}_{ae} \tilde{\underline{q}}_{1e} \quad (9.2.22)$$

9.2.3 2D Frame Element Stiffness Matrix and Strain Energy

The quadratic forms in (9.2.14) and (9.2.22) are utilized to yield a combined axial-transverse deflection stiffness matrix for the 6-dof beam element:

$$\underline{\tilde{K}}_e = \begin{bmatrix} k_{a11} & 0 & 0 & k_{a12} & 0 & 0 \\ & k_{t11} & k_{t12} & 0 & k_{t13} & k_{t14} \\ & & k_{t22} & 0 & k_{t23} & k_{t24} \\ & & & k_{a22} & 0 & 0 \\ \text{symmetric} & & & & k_{t33} & k_{t34} \\ & & & & & k_{t44} \end{bmatrix} \quad (9.2.23a)$$

The integrals in these terms are performed for a uniform (constant E, I, A) beam element to obtain

$$\underline{\tilde{K}}_e = \begin{bmatrix} k_a & 0 & 0 & -k_a & 0 & 0 \\ 0 & 12k_t & 6Lk_t & 0 & -12k_t & 6Lk_t \\ 0 & 6Lk_t & 4L^2k_t & 0 & -6Lk_t & 2L^2k_t \\ -k_a & 0 & 0 & k_a & 0 & 0 \\ 0 & -12k_t & -6Lk_t & 0 & 12k_t & -6Lk_t \\ 0 & 6Lk_t & 2L^2k_t & 0 & -6Lk_t & 4L^2k_t \end{bmatrix} \quad (9.2.23b)$$

where

$$k_t = \frac{EI}{L^3}, \quad k_a = \frac{EA}{L} \quad (9.2.24)$$

The corresponding strain energy in this element becomes

$$U_e = \frac{1}{2} \underset{1 \times 1}{\tilde{q}}_e^T \underset{6 \times 6}{\underline{\tilde{K}}_e} \underset{6 \times 1}{\tilde{q}}_e \quad (9.2.25)$$

where

$$\underline{\tilde{q}}_e = (\tilde{q}_1 \quad \tilde{q}_2 \quad \tilde{q}_3 \quad \tilde{q}_4 \quad \tilde{q}_5 \quad \tilde{q}_6)^T \quad (9.2.26)$$

9.2.4 2D Frame Element Mass Matrix

The kinetic energy due to axial and transverse deflection and bending rotation is obtained from (4.2.14) and (5.5.85) as

$$\tilde{T}_e = \frac{1}{2} \int_0^L (\rho A dx) (\dot{u}_1^2 + \dot{u}_2^2) + (\rho dx I) \dot{\theta}^2 = \frac{1}{2} \int_0^L \rho A \dot{u}_1^2 dx + \frac{1}{2} \int_0^L \rho A \dot{u}_2^2 dx + \frac{1}{2} \int_0^L \rho I \dot{\theta}^2 dx \quad (9.2.27)$$

where I is the area moment of inertia about the x_3 axis passing through the neutral axis of the beam. Recall that

$$\theta = \frac{\partial u_2}{\partial x} \quad (9.2.28)$$

and substitute (9.2.2) and (9.2.15) into (9.2.27) to obtain

$$\begin{aligned} T_e = & \frac{1}{2} \int_0^L \rho A (N_1 \dot{q}_1 + N_4 \dot{q}_4)^2 dx + \frac{1}{2} \int_0^L \rho A (N_2 \dot{q}_2 + N_3 \dot{q}_3 + N_5 \dot{q}_5 + N_6 \dot{q}_6)^2 dx \\ & + \frac{1}{2} \int_0^L \rho I (N_2' \dot{q}_2 + N_3' \dot{q}_3 + N_5' \dot{q}_5 + N_6' \dot{q}_6)^2 dx \end{aligned} \quad (9.2.29)$$

Utilize (9.2.29) and the identity in (2.6.46) to obtain

$$T_e = \frac{1}{2} \dot{\underline{q}}_{1e}^T \underline{M}_{ae} \dot{\underline{q}}_{1e} + \frac{1}{2} \dot{\underline{q}}_{2e}^T \underline{M}_{te} \dot{\underline{q}}_{2e} + \frac{1}{2} \dot{\underline{q}}_{2e}^T \underline{M}_{Re} \dot{\underline{q}}_{2e} \quad (9.2.30)$$

where the axial mass matrix is

$$\underline{M}_{ae} = \int_0^L \rho(x) A(x) \begin{bmatrix} N_1 N_1 & N_1 N_4 \\ N_4 N_1 & N_4 N_4 \end{bmatrix} dx \quad (9.2.31)$$

the transverse displacement mass matrix is

$$\underline{M}_{te} = \int_0^L \rho(x) A(x) \begin{bmatrix} N_2 N_2 & N_2 N_3 & N_2 N_5 & N_2 N_6 \\ & N_3 N_3 & N_3 N_5 & N_3 N_6 \\ \text{symmetric} & & N_5 N_5 & N_5 N_6 \\ & & & N_6 N_6 \end{bmatrix} dx \quad (9.2.32)$$

and the transverse rotation (rotary inertia) mass matrix is

$$\underline{M}_{Re} = \int_0^L \rho(x) I(x) \begin{bmatrix} N_2' N_2' & N_2' N_3' & N_2' N_5' & N_2' N_6' \\ & N_3' N_3' & N_3' N_5' & N_3' N_6' \\ \text{symmetric} & & N_5' N_5' & N_5' N_6' \\ & & & N_6' N_6' \end{bmatrix} dx \quad (9.2.33)$$

The quadratic forms in (9.2.31)–(9.2.33) are combined to obtain the element mass matrix

$$\tilde{\underline{M}}_e = \tilde{\underline{M}}_e^{at} + \tilde{\underline{M}}_e^R \quad (9.2.34)$$

where the translational/axial and rotary inertia mass matrices are

$$\tilde{\underline{M}}_e^{at} = \begin{bmatrix} m_{a11} & 0 & 0 & m_{a12} & 0 & 0 \\ & m_{t11} & m_{t12} & 0 & m_{t13} & m_{t14} \\ & & m_{t22} & 0 & m_{t23} & m_{t24} \\ & & & m_{a22} & 0 & 0 \\ \text{symmetric} & & & & m_{t33} & m_{t34} \\ & & & & & m_{t44} \end{bmatrix}, \quad \tilde{\underline{M}}_e^R = \begin{bmatrix} 0 & 0 & 0 & 0 & 0 & 0 \\ & m_{R11} & m_{R12} & 0 & m_{R13} & m_{R14} \\ & & m_{R22} & 0 & m_{R23} & m_{R24} \\ & & & 0 & 0 & 0 \\ \text{symmetric} & & & & m_{R33} & m_{R34} \\ & & & & & m_{R44} \end{bmatrix} \quad (9.2.35)$$

The integrals in (9.2.31)–(9.2.33) are performed for the uniform (constant ρ, A, I) beam case to obtain

$$\tilde{\underline{M}}_e^{at} = m_B \begin{bmatrix} \frac{1}{3} & 0 & 0 & \frac{1}{6} & 0 & 0 \\ 0 & \frac{13}{35} & \frac{11}{210}L & 0 & \frac{9}{70} & -\frac{13}{420}L \\ 0 & 0 & \frac{1}{105}L^2 & 0 & \frac{13}{420}L & -\frac{1}{140}L^2 \\ 0 & 0 & 0 & \frac{1}{3} & 0 & 0 \\ \text{symmetric} & & & & \frac{13}{35} & -\frac{11}{210}L \\ 0 & 0 & 0 & 0 & 0 & \frac{1}{105}L^2 \end{bmatrix} \quad (9.2.36)$$

$$\tilde{\underline{M}}_e^R = I_B \begin{bmatrix} 0 & 0 & 0 & 0 & 0 & 0 \\ 0 & \frac{6}{5L^2} & \frac{1}{10L} & 0 & -\frac{6}{5L^2} & -\frac{1}{10L} \\ 0 & 0 & \frac{2}{15} & 0 & \frac{1}{10L} & -\frac{1}{30} \\ 0 & 0 & 0 & 0 & 0 & 0 \\ \text{symmetric} & & & & \frac{6}{5L^2} & -\frac{1}{10L} \\ 0 & 0 & 0 & 0 & 0 & \frac{2}{15} \end{bmatrix} \quad (9.2.37)$$

where

$$m_B = \rho AL, \quad I_B = \rho IL \quad (9.2.38)$$

9.2.5 2D Frame Element Force Vector

From Figure 9.2.2 and (4.5.52), the generalized forces are

$$\begin{aligned} \tilde{Q}_j = & \tilde{a}_1 \tilde{e}_1 \cdot \frac{\partial \dot{\tilde{q}}_1 \tilde{e}_1}{\partial \dot{\tilde{q}}_j} + \tilde{a}_2 \tilde{e}_2 \cdot \frac{\partial \dot{\tilde{q}}_2 \tilde{e}_2}{\partial \dot{\tilde{q}}_j} + \tilde{a}_3 \tilde{e}_3 \cdot \frac{\partial \dot{\tilde{q}}_3 \tilde{e}_3}{\partial \dot{\tilde{q}}_j} + \tilde{a}_4 \tilde{e}_1 \cdot \frac{\partial \dot{\tilde{q}}_4 \tilde{e}_1}{\partial \dot{\tilde{q}}_j} + \tilde{a}_5 \tilde{e}_2 \cdot \frac{\partial \dot{\tilde{q}}_5 \tilde{e}_2}{\partial \dot{\tilde{q}}_j} + \tilde{a}_6 \tilde{e}_3 \cdot \frac{\partial \dot{\tilde{q}}_6 \tilde{e}_3}{\partial \dot{\tilde{q}}_j} \\ & + \int_0^L \bar{f}_1 dx \tilde{e}_1 \cdot \frac{\partial \dot{u}_1 \tilde{e}_1}{\partial \dot{\tilde{q}}_j} + \int_0^L \bar{f}_2 dx \tilde{e}_2 \cdot \frac{\partial \dot{u}_2 \tilde{e}_2}{\partial \dot{\tilde{q}}_j} + \int_0^L \bar{m} dx \tilde{e}_3 \cdot \frac{\partial \dot{\theta} \tilde{e}_3}{\partial \dot{\tilde{q}}_j} \end{aligned} \quad (9.2.39)$$

Evaluation of the dot products results in the simplification

$$\begin{aligned} \tilde{Q}_j = & \tilde{a}_1 \cdot \frac{\partial \dot{\tilde{q}}_1}{\partial \dot{\tilde{q}}_j} + \tilde{a}_2 \cdot \frac{\partial \dot{\tilde{q}}_2}{\partial \dot{\tilde{q}}_j} + \tilde{a}_3 \cdot \frac{\partial \dot{\tilde{q}}_3}{\partial \dot{\tilde{q}}_j} + \tilde{a}_4 \cdot \frac{\partial \dot{\tilde{q}}_4}{\partial \dot{\tilde{q}}_j} + \tilde{a}_5 \cdot \frac{\partial \dot{\tilde{q}}_5}{\partial \dot{\tilde{q}}_j} + \tilde{a}_6 \cdot \frac{\partial \dot{\tilde{q}}_6}{\partial \dot{\tilde{q}}_j} \\ & + \int_0^L \bar{f}_1 dx \cdot \frac{\partial \dot{u}_1}{\partial \dot{\tilde{q}}_j} + \int_0^L \bar{f}_2 dx \cdot \frac{\partial \dot{u}_2}{\partial \dot{\tilde{q}}_j} + \int_0^L \bar{m} dx \cdot \frac{\partial \dot{\theta}}{\partial \dot{\tilde{q}}_j} \end{aligned} \quad (9.2.40)$$

Note that

$$\tilde{a}_1 \frac{\partial \dot{\tilde{q}}_1}{\partial \dot{\tilde{q}}_j} + \tilde{a}_2 \frac{\partial \dot{\tilde{q}}_2}{\partial \dot{\tilde{q}}_j} + \tilde{a}_3 \frac{\partial \dot{\tilde{q}}_3}{\partial \dot{\tilde{q}}_j} + \tilde{a}_4 \frac{\partial \dot{\tilde{q}}_4}{\partial \dot{\tilde{q}}_j} + \tilde{a}_5 \frac{\partial \dot{\tilde{q}}_5}{\partial \dot{\tilde{q}}_j} + \tilde{a}_6 \frac{\partial \dot{\tilde{q}}_6}{\partial \dot{\tilde{q}}_j} = \tilde{a}_j \quad (9.2.41)$$

Substitution of (9.2.41) and the interpolations in (9.2.2), (9.2.6), and (9.2.15) into (9.2.40) yield

$$\begin{aligned} \tilde{Q}_j = \tilde{a}_j + & \int_0^L \bar{f}_1 \frac{\partial [N_1(x)\dot{\tilde{q}}_1(t) + N_4(x)\dot{\tilde{q}}_4(t)]}{\partial \dot{\tilde{q}}_j} dx \\ & + \int_0^L \bar{f}_2 \frac{\partial [N_2(x)\dot{\tilde{q}}_2(t) + N_3(x)\dot{\tilde{q}}_3(t) + N_5(x)\dot{\tilde{q}}_5(t) + N_6(x)\dot{\tilde{q}}_6(t)]}{\partial \dot{\tilde{q}}_j} dx \\ & + \int_0^L \bar{m} \frac{\partial [N'_2(x)\tilde{q}_2(t) + N'_3(x)\tilde{q}_3(t) + N'_5(x)\tilde{q}_5(t) + N'_6(x)\tilde{q}_6(t)]}{\partial \dot{\tilde{q}}_j} dx \end{aligned} \quad (9.2.42)$$

Evaluation of the derivatives in (9.2.42) yields

$$\underline{\tilde{Q}}_e = (\tilde{Q}_1 \ \tilde{Q}_2 \ \tilde{Q}_3 \ \tilde{Q}_4 \ \tilde{Q}_5 \ \tilde{Q}_6)^T = \underline{\tilde{a}}_e + \underline{\tilde{f}}_e \quad (9.2.43)$$

where

$$\underline{\tilde{a}}_e = (\tilde{a}_1 \ \tilde{a}_2 \ \tilde{a}_3 \ \tilde{a}_4 \ \tilde{a}_5 \ \tilde{a}_6)^T \quad (9.2.44)$$

and

$$\underline{\tilde{f}}_e = \begin{Bmatrix} \tilde{f}_{e1} \\ \tilde{f}_{e2} \\ \tilde{f}_{e3} \\ \tilde{f}_{e4} \\ \tilde{f}_{e5} \\ \tilde{f}_{e6} \end{Bmatrix} = \int_0^{L_e} \begin{Bmatrix} N_1(x)\bar{f}_1(x) \\ N_2(x)\bar{f}_2(x) + N'_2(x)\bar{m}(x) \\ N_3(x)\bar{f}_2(x) + N'_3(x)\bar{m}(x) \\ N_4(x)\bar{f}_1(x) \\ N_5(x)\bar{f}_2(x) + N'_5(x)\bar{m}(x) \\ N_6(x)\bar{f}_2(x) + N'_6(x)\bar{m}(x) \end{Bmatrix} dx \quad (9.2.45)$$

The external force and moment distributions in Figure 9.2.2 may contain concentrated forces and moments. These are represented with Dirac delta functions as explained in Section 2.12. For example, concentrated forces ($\hat{F}_1(t), \hat{F}_2(t)$) and moment ($\hat{M}(t)$) in the \tilde{e}_1, \tilde{e}_2 , and \tilde{e}_3 directions, respectively, at $x = \hat{x}$ contribute the following element force vector from (9.2.45):

$$\underline{\tilde{f}}_e = \int_0^{L_e} \begin{Bmatrix} N_1(x)\hat{F}_1(t)\delta(x-\hat{x}) \\ N_2(x)\hat{F}_2(t)\delta(x-\hat{x}) + N'_2(x)\hat{M}(t)\delta(x-\hat{x}) \\ N_3(x)\hat{F}_2(t)\delta(x-\hat{x}) + N'_3(x)\hat{M}(t)\delta(x-\hat{x}) \\ N_4(x)\hat{F}_1(t)\delta(x-\hat{x}) \\ N_5(x)\hat{F}_2(t)\delta(x-\hat{x}) + N'_5(x)\hat{M}(t)\delta(x-\hat{x}) \\ N_6(x)\hat{F}_2(t)\delta(x-\hat{x}) + N'_6(x)\hat{M}(t)\delta(x-\hat{x}) \end{Bmatrix} dx = \begin{Bmatrix} N_1(\hat{x})\hat{F}_1(t) \\ N_2(\hat{x})\hat{F}_2(t) + N'_2(\hat{x})\hat{M}(t) \\ N_3(\hat{x})\hat{F}_2(t) + N'_3(\hat{x})\hat{M}(t) \\ N_4(\hat{x})\hat{F}_1(t) \\ N_5(\hat{x})\hat{F}_2(t) + N'_5(\hat{x})\hat{M}(t) \\ N_6(\hat{x})\hat{F}_2(t) + N'_6(\hat{x})\hat{M}(t) \end{Bmatrix} \quad (9.2.46)$$

where (2.12.5) has been used to evaluate the integrals. Collection of these results yields the final form of the element external force vector:

$$\tilde{f}_e = \int_0^{L_e} \begin{Bmatrix} N_1(x)\bar{f}_1(x) \\ N_2(x)\bar{f}_2(x) + N_2'(x)\bar{m}(x) \\ N_3(x)\bar{f}_2(x) + N_3'(x)\bar{m}(x) \\ N_4(x)\bar{f}_1(x) \\ N_5(x)\bar{f}_2(x) + N_5'(x)\bar{m}(x) \\ N_6(x)\bar{f}_2(x) + N_6'(x)\bar{m}(x) \end{Bmatrix} dx + \sum_{i=1}^{\beta} \begin{Bmatrix} N_1(\hat{x}_i)\hat{F}_{1i}(t) \\ N_2(\hat{x}_i)\hat{F}_{2i}(t) + N_2'(\hat{x}_i)\hat{M}_i(t) \\ N_3(\hat{x}_i)\hat{F}_{2i}(t) + N_3'(\hat{x}_i)\hat{M}_i(t) \\ N_4(\hat{x}_i)\hat{F}_{1i}(t) \\ N_5(\hat{x}_i)\hat{F}_{2i}(t) + N_5'(\hat{x}_i)\hat{M}_i(t) \\ N_6(\hat{x}_i)\hat{F}_{2i}(t) + N_6'(\hat{x}_i)\hat{M}_i(t) \end{Bmatrix} \quad (9.2.47)$$

where β is the number of concentrated force locations on the element. From (4.7.61), Lagrange's equations yield the following dynamic equilibrium equations for element e :

$$\frac{\tilde{M}_e}{6 \times 6} \ddot{\tilde{q}}_e + \frac{\tilde{K}_e}{6 \times 6} \tilde{q}_e = \frac{\tilde{a}_e}{6 \times 1} + \frac{\tilde{f}_e}{6 \times 1} \quad (9.2.48)$$

The element equilibrium equations are combined (assembled), while enforcing interelement displacement compatibility and equilibrium, to form the system equations. This process eliminates the interelement actions \tilde{a}_e . The actions are often utilized for computing beam stresses. The actions may be obtained by solving the total system equations for the nodal motions and then substituting the respective motions into the element equation (9.2.48) written as

$$\tilde{a}_e = \tilde{M}_e \ddot{\tilde{q}}_e + \tilde{K}_e \tilde{q}_e - \tilde{f}_e \quad (9.2.49)$$

9.2.6 2D Frame Element Stiffness and Mass Matrices and Force Vector: Transformation to Global Coordinates

The element matrices and force vector must be expressed in global coordinate form prior to being assembled into the total system matrices and force vector. Figure 9.2.4 shows a beam element with both local and global coordinate nodal variables.

The global and local (overhead tilde symbol) coordinate vectors are

$$\tilde{q}_e = (\tilde{q}_1 \ \tilde{q}_2 \ \tilde{q}_3 \ \tilde{q}_4 \ \tilde{q}_5 \ \tilde{q}_6)^T \quad (9.2.50)$$

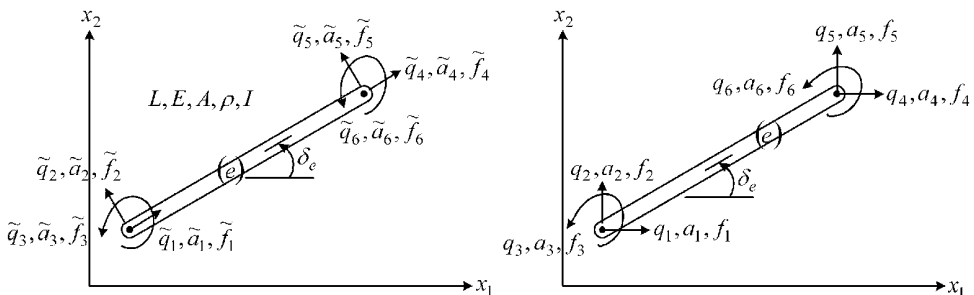


Figure 9.2.4 Beam element (e) in local and global coordinates

$$\underline{q}_e = (q_1 \ q_2 \ q_3 \ q_4 \ q_5 \ q_6)^T \quad (9.2.51)$$

$$\underline{\tilde{a}}_e = (\tilde{a}_1 \ \tilde{a}_2 \ \tilde{a}_3 \ \tilde{a}_4 \ \tilde{a}_5 \ \tilde{a}_6)^T \quad (9.2.52)$$

$$\underline{a}_e = (a_1 \ a_2 \ a_3 \ a_4 \ a_5 \ a_6)^T \quad (9.2.53)$$

$$\underline{\tilde{f}}_e = (\tilde{f}_1 \ \tilde{f}_2 \ \tilde{f}_3 \ \tilde{f}_4 \ \tilde{f}_5 \ \tilde{f}_6)^T \quad (9.2.54)$$

$$\underline{f}_e = (f_1 \ f_2 \ f_3 \ f_4 \ f_5 \ f_6)^T \quad (9.2.55)$$

The global and local coordinate vectors are related by

$$\underline{\tilde{q}}_e = \underline{T}_{Te} \underline{q}_e, \quad \underline{\tilde{a}}_e = \underline{T}_{Te} \underline{a}_e, \quad \underline{\tilde{f}}_e = \underline{T}_{Te} \underline{f}_e \quad (9.2.56)$$

where the coordinate transformation matrix is (2.7.1)

$$\underline{T}_{Te} = \begin{bmatrix} \underline{C}_{Te} & \underline{0} \\ \underline{0} & \underline{C}_{Te} \end{bmatrix}, \quad \underline{C}_{Te} = \begin{bmatrix} \cos \delta_e & \sin \delta_e & 0 \\ -\sin \delta_e & \cos \delta_e & 0 \\ 0 & 0 & 1 \end{bmatrix} \quad (9.2.57)$$

Substitute (9.2.56) into (9.2.25)

$$U_e = \frac{1}{2} \underline{q}_e^T (\underline{T}_{Te}^T \underline{\tilde{K}}_e \underline{T}_{Te}) \underline{q}_e \quad (9.2.58)$$

The potential energy may also be expressed with the global coordinate, element stiffness matrix as

$$U_e = \frac{1}{2} \underline{q}_e^T \underline{K}_e^e \underline{q}_e \quad (9.2.59)$$

Comparison of these two forms for the potential energy yields the global coordinate form of the element stiffness matrix as

$$\underline{K}_e^e = \underline{T}_{Te}^T \underline{\tilde{K}}_e \underline{T}_{Te} \quad (9.2.60)$$

This matrix may be expressed as

$$\underline{K}_e^e = \underline{T}_{Te}^T \underline{\tilde{K}}_e \underline{T}_{Te} = \underline{T}_{Te}^T (\underline{\tilde{K}}_e^a + \underline{\tilde{K}}_e^t) \underline{T}_{Te} = \underline{K}_e^a + \underline{K}_e^t \quad (9.2.61)$$

where “a” and “t” indicate axial and transverse contributions. The results of the multiplications in (9.2.61) are

$$\underline{K}_e^a = k_a \begin{bmatrix} a_{cc} & a_{cs} & 0 & -a_{cc} & -a_{cs} & 0 \\ & a_{ss} & 0 & -a_{cs} & -a_{ss} & 0 \\ & & 0 & 0 & 0 & 0 \\ & & & a_{cc} & a_{cs} & 0 \\ \text{symmetric} & & & & a_{ss} & 0 \\ & & & & & 0 \end{bmatrix} \quad (9.2.62)$$

where

$$k_a = \frac{E_e A_e}{L_e}, \quad a_{cc} = \cos^2 \delta_e, \quad a_{cs} = \cos \delta_e \sin \delta_e, \quad a_{ss} = \sin^2 \delta_e \quad (9.2.63)$$

$$\underline{K}_e^t = k_t \begin{bmatrix} 12a_{ss} & -12a_{cs} & -6La_s & -12a_{ss} & 12a_{cs} & -6La_s \\ & 12a_{cc} & 6La_c & 12a_{cs} & -12a_{cc} & 6La_c \\ & & 4L^2 & 6La_s & -6La_c & 2L^2 \\ & & & 12a_{ss} & -12a_{cs} & 6La_s \\ \text{symmetric} & & & & 12a_{cc} & -6La_c \\ & & & & & 4L^2 \end{bmatrix} \quad (9.2.64)$$

where

$$k_t = \frac{E_e I_e}{L_e^3}, \quad a_s = \sin \delta_e, \quad a_c = \cos \delta_e \quad (9.2.65)$$

Similar to (9.2.58), the kinetic energy is

$$T_e = \frac{1}{2} \dot{\underline{q}}_e^T \tilde{\underline{M}}_e \dot{\underline{q}}_e = \frac{1}{2} \dot{\underline{q}}_e^T (\underline{T}_{Te}^T \tilde{\underline{M}}_e \underline{T}_{Te}) \dot{\underline{q}}_e \quad (9.2.66)$$

The kinetic energy may also be expressed with the global coordinate, element mass matrix as

$$T_e = \frac{1}{2} \dot{\underline{q}}_e^T \underline{M}_e^e \dot{\underline{q}}_e \quad (9.2.67)$$

Comparison of these two forms for the kinetic energy yields the global coordinate form of the element mass matrix as

$$\underline{M}_e^e = \underline{T}_{Te}^T \tilde{\underline{M}}_e \underline{T}_{Te} \quad (9.2.68)$$

By (9.2.30), the global coordinate form of the element mass matrix is

$$\underline{M}_e^e = \underline{T}_{Te}^T \tilde{\underline{M}}_e \underline{T}_{Te} = \underline{T}_{Te}^T (\tilde{\underline{M}}_e^a + \tilde{\underline{M}}_e^t + \tilde{\underline{M}}_e^R) \underline{T}_{Te} = \underline{M}_e^a + \underline{M}_e^t + \underline{M}_e^R \quad (9.2.69)$$

where “a,” “t,” and “R” indicate the axial, transverse, and rotary inertia contributions as identified in (9.2.36) and (9.2.37). The results of the multiplications in (9.2.69) are

$$\underline{M}_e^a = \frac{mB}{3} \begin{bmatrix} a_{cc} & a_{cs} & 0 & \frac{a_{cc}}{2} & \frac{a_{cs}}{2} & 0 \\ & a_{ss} & 0 & \frac{a_{cs}}{2} & \frac{a_{ss}}{2} & 0 \\ & & 0 & 0 & 0 & 0 \\ & & & a_{cc} & a_{cs} & 0 \\ \text{symmetric} & & & & a_{ss} & 0 \\ & & & & & 0 \end{bmatrix} \quad (9.2.70)$$

$$\underline{M}_e^t = \frac{m_B}{35} \begin{bmatrix} 13a_{ss} & -13a_{cs} & -\frac{11}{6}La_s & \frac{9}{2}a_{ss} & -\frac{9}{2}a_{cs} & \frac{13}{12}La_s \\ & 13a_{cc} & \frac{11}{6}La_c & -\frac{9}{2}a_{cs} & \frac{9}{2}a_{cc} & -\frac{13}{12}La_c \\ & & \frac{L^2}{3} & -\frac{13}{12}La_s & \frac{13}{12}La_c & -\frac{L^2}{4} \\ & & & 13a_{ss} & -13a_{cs} & \frac{11}{6}La_s \\ & \text{symmetric} & & & 13a_{cc} & -\frac{11}{6}La_c \\ & & & & & \frac{L^2}{3} \end{bmatrix} \quad (9.2.71)$$

where

$$m_B = \rho_e A_e L_e \quad (9.2.72)$$

and

$$\underline{M}_e^R = \frac{I_B}{5L^2} \begin{bmatrix} 6a_{ss} & -6a_{cs} & -\frac{1}{2}La_s & -6a_{ss} & 6a_{cs} & -\frac{1}{2}La_s \\ & 6a_{cc} & \frac{1}{2}La_c & 6a_{cs} & -6a_{cc} & \frac{1}{2}La_c \\ & & \frac{2}{3}L^2 & \frac{1}{2}La_s & -\frac{1}{2}La_c & -\frac{1}{6}L^2 \\ & & & 6a_{ss} & -6a_{cs} & \frac{1}{2}La_s \\ & \text{symmetric} & & & 6a_{cc} & -\frac{1}{2}La_c \\ & & & & & \frac{2}{3}L^2 \end{bmatrix} \quad (9.2.73)$$

where

$$I_B = \rho_e I_e L_e \quad (9.2.74)$$

The transformation matrices \underline{C}_{TE} and \underline{T}_{TE} in (9.2.57) are orthogonal, that is,

$$\underline{C}_{TE}^{-1} = \underline{C}_{TE}^T, \quad \underline{T}_{TE}^{-1} = \underline{T}_{TE}^T \quad (9.2.75)$$

Therefore, from (9.2.56), the element force vector in global coordinates is

$$\underline{f}_e^e = \underline{T}_{TE}^T \tilde{\underline{f}}_e \quad (9.2.76)$$

where $\tilde{\underline{f}}_e$ is defined in (9.2.47).

EXAMPLE 9.2.1 *Single Element Model of Inclined, Guided Cantilever Beam with In-Span Concentrated Loading*

Statement: Figure E9.2.1(a) depicts a simple, one beam element model with distributed and concentrated loading. The beam is inclined from the horizontal direction by angle δ_e , fixed at

its lower end and guided (zero slope) at its upper end. The applied loading consists of transverse distributed load $\bar{f}_2(\tilde{x}, t)$ and:

- A concentrated force f_0 and moment m_0 at the midspan.
- A concentrated force f_1 at three-quarter span.
- A concentrated force \hat{f}_a at the upper node point (2).
- A concentrated mass, damper, and stiffness are attached at the upper end (node 2) of the beam. The beam's cross-sectional area and moment of inertia are A and I , respectively, and its density is ρ .

Objective: Determine the equation of motion for the only unconstrained nodal coordinate q_4 .

Assumptions: Utilize the Euler–Bernoulli beam theory model.

Solution: The element's local coordinate directions and external loads are shown in Figure E9.2.1(b).

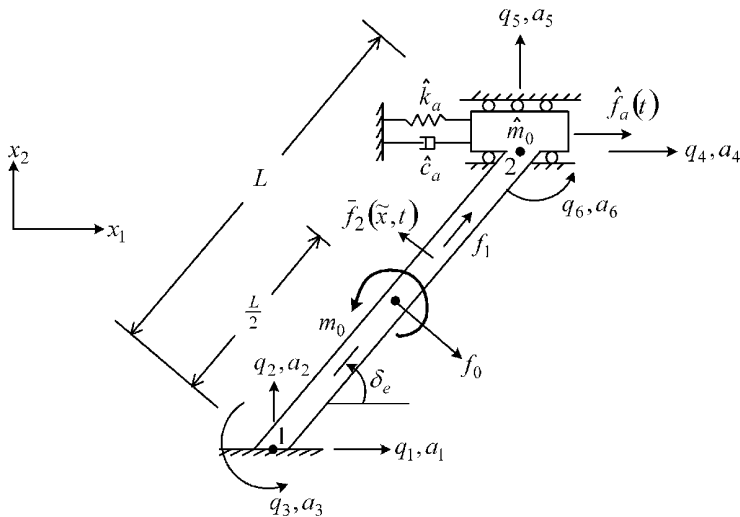


Figure E9.2.1(a) Single beam model geometry and loading

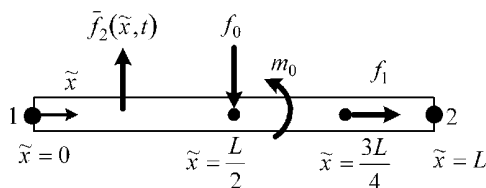


Figure E9.2.1(b) Local coordinate directions and loading

The element force vector (9.2.47) simplifies for this case to the form

$$\tilde{\mathbf{f}}_{-e} = \int_0^{L_e} \begin{Bmatrix} 0 \\ N_2(x)\bar{f}_2(\tilde{x},t) \\ N_3(x)\bar{f}_2(\tilde{x},t) \\ 0 \\ N_5(x)\bar{f}_2(\tilde{x},t) \\ N_6(x)\bar{f}_2(\tilde{x},t) \end{Bmatrix} d\tilde{x} + \begin{Bmatrix} N_1\left(\frac{3L}{4}\right)f_1(t) \\ -N_2\left(\frac{L}{2}\right)f_0(t) + N'_2\left(\frac{L}{2}\right)m_0(t) \\ -N_3\left(\frac{L}{2}\right)f_0(t) + N'_3\left(\frac{L}{2}\right)m_0(t) \\ N_4\left(\frac{3L}{4}\right)f_1(t) \\ -N_5\left(\frac{L}{2}\right)f_0(t) + N'_5\left(\frac{L}{2}\right)m_0(t) \\ -N_6\left(\frac{L}{2}\right)f_0(t) + N'_6\left(\frac{L}{2}\right)m_0(t) \end{Bmatrix} \quad (1)$$

For the sake of illustration, let

$$\bar{f}_2(\tilde{x}) = \bar{F}_2 \frac{\tilde{x}}{L} \cos(\omega t) \quad (2)$$

and note that from (9.2.4) and (9.2.16)

$$\begin{aligned} N_2\left(\frac{L}{2}\right) &= \frac{1}{2}, & N'_2\left(\frac{L}{2}\right) &= \frac{-3}{2L}, & N_3\left(\frac{L}{2}\right) &= \frac{L}{8}, & N'_3\left(\frac{L}{2}\right) &= \frac{-1}{4}, & N_1\left(\frac{3L}{4}\right) &= \frac{1}{4} \\ N_5\left(\frac{L}{2}\right) &= \frac{1}{2}, & N'_5\left(\frac{L}{2}\right) &= \frac{3}{2L}, & N_6\left(\frac{L}{2}\right) &= \frac{-L}{8}, & N'_6\left(\frac{L}{2}\right) &= \frac{-1}{4}, & N_4\left(\frac{3L}{4}\right) &= \frac{3}{4} \end{aligned} \quad (3)$$

Substitute (9.2.4), (2), and (3) into (1) to obtain

$$\tilde{\mathbf{f}}_{-e} = \int_0^{L_e} \begin{Bmatrix} 0 \\ \left(1 - 3\frac{x^2}{L^2} + 2\frac{x^3}{L^3}\right) * F_2 \frac{\tilde{x}}{L} \cos(\omega t) \\ L\left(\frac{x}{L} - 2\frac{x^2}{L^2} + \frac{x^3}{L^3}\right) * F_2 \frac{\tilde{x}}{L} \cos(\omega t) \\ 0 \\ \left(3\frac{x^2}{L^2} - 2\frac{x^3}{L^3}\right) * F_2 \frac{\tilde{x}}{L} \cos(\omega t) \\ L\left(-\frac{x^2}{L^2} + \frac{x^3}{L^3}\right) * F_2 \frac{\tilde{x}}{L} \cos(\omega t) \end{Bmatrix} d\tilde{x} + \begin{Bmatrix} \frac{f_1(t)}{4} \\ -\frac{f_0(t)}{2} - \frac{3}{2L}m_0(t) \\ -\frac{L}{8}f_0(t) - \frac{1}{4}m_0(t) \\ \frac{3}{4}f_1(t) \\ -\frac{1}{2}f_0(t) + \frac{3}{2L}m_0(t) \\ \frac{L}{8}f_0(t) - \frac{1}{4}m_0(t) \end{Bmatrix}$$

$$= \begin{pmatrix} \frac{f_1(t)}{4} \\ -\frac{f_0(t)}{2} - \frac{3}{2L}m_0(t) + \bar{F}_2 \frac{3L}{20} \cos(\omega t) \\ -\frac{L}{8}f_0(t) - \frac{1}{4}m_0(t) + \bar{F}_2 \frac{L^2}{30} \cos(\omega t) \\ \frac{3}{4}f_1(t) \\ -\frac{1}{2}f_0(t) + \frac{3}{2L}m_0(t) + \bar{F}_2 \frac{7L}{20} \cos(\omega t) \\ \frac{L}{8}f_0(t) - \frac{1}{4}m_0(t) - \bar{F}_2 \frac{L^2}{20} \cos(\omega t) \end{pmatrix} \quad (4)$$

The global coordinate form of the element force vector is obtained from (9.2.57) and (9.2.76) as

$$\underline{f}_e^e = \begin{pmatrix} f_{1e} \\ f_{2e} \\ f_{3e} \\ f_{4e} \\ f_{5e} \\ f_{6e} \end{pmatrix} = \underline{T}_{Te}^T \tilde{\underline{f}}_e = \begin{pmatrix} \cos(\delta_e) * \frac{f_1(t)}{4} + \sin(\delta_e) * \left(-\frac{f_0(t)}{2} - \frac{3}{2L}m_0(t) + \bar{F}_2 \frac{3L}{20} \cos(\omega t) \right) \\ -\sin(\delta_e) * \frac{f_1(t)}{4} + \cos(\delta_e) * \left(-\frac{f_0(t)}{2} - \frac{3}{2L}m_0(t) + \bar{F}_2 \frac{3L}{20} \cos(\omega t) \right) \\ -\frac{L}{8}f_0(t) - \frac{1}{4}m_0(t) + \bar{F}_2 \frac{L^2}{30} \cos(\omega t) \\ \cos(\delta_e) * \frac{3f_1(t)}{4} + \sin(\delta_e) * \left(-\frac{f_0(t)}{2} + \frac{3}{2L}m_0(t) + \bar{F}_2 \frac{7L}{20} \cos(\omega t) \right) \\ -\sin(\delta_e) * \frac{3f_1(t)}{4} + \cos(\delta_e) * \left(-\frac{f_0(t)}{2} + \frac{3}{2L}m_0(t) + \bar{F}_2 \frac{7L}{20} \cos(\omega t) \right) \\ \frac{L}{8}f_0(t) - \frac{1}{4}m_0(t) - \bar{F}_2 \frac{L^2}{20} \cos(\omega t) \end{pmatrix} \quad (5)$$

The global dofs are shown in Figure E9.2.1(c). Similar to (4.8.25) and (4.8.87), the nodal and dof connectivity arrays for the model are

$$\underline{B} = [1 \ 2], \quad \hat{\underline{B}} = [1 \ 2 \ 3 \ 4 \ 5 \ 6] \quad (6)$$

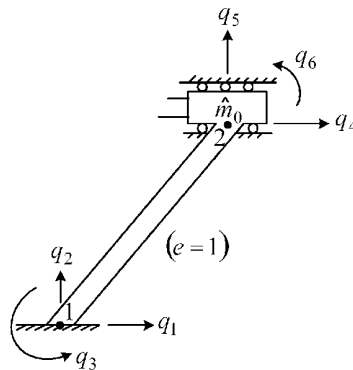


Figure E9.2.1(c) Global degrees of freedom and nodes 1 and 2

and similar to (4.8.35) or (4.8.94), the larray is

$$\tilde{L} = (l_1 \ l_2 \ l_3 \ l_4 \ l_5 \ l_6) = (0 \ 0 \ 0 \ 1 \ 0 \ 0) \quad (7)$$

since only the q_4 dof is not fixed. The assembly procedure is identical to that illustrated in Figure 4.8.14. The free dof system matrix $(\underline{M}_f, \underline{K}_f, \underline{C}_f)$ indices $(l_{\hat{B}_{er}}, l_{\hat{B}_{es}})$ in Figure 4.8.14 always contain at least 1 zero, unless $r = s = 4$, so most of the element matrix terms are not assembled. Therefore, from (9.2.69) to (9.2.74) and Figure 4.8.14

$$\begin{aligned} \underline{M}_f &= (\underline{M}^e)_{4,4} = (\underline{M}^a)_{4,4} + (\underline{M}^t)_{4,4} + (\underline{M}^R)_{4,4} \\ &= m_B \left(\frac{a_{cc}}{3} + \frac{13a_{ss}}{35} \right) + I_B \left(\frac{6a_{ss}}{5L^2} \right) = m_B \left(\frac{1}{3} \cos^2 \delta_e + \frac{13}{35} \sin^2 \delta_e \right) + \frac{6I_B}{5L^2} \sin^2 \delta_e \end{aligned} \quad (8)$$

where

$$m_B = \rho AL \quad \text{and} \quad I_B = \rho IL \quad (9)$$

Similarly from (9.2.61) to (9.2.65) and the assembly procedure illustrated in Figure 4.8.14

$$\underline{K}_f = (\underline{K}^e)_{4,4} = (\underline{K}^a)_{4,4} + (\underline{K}^t)_{4,4} = k_a a_{cc} + 12k_t a_{ss} = k_a \cos^2 \delta_e + 12k_t \sin^2 \delta_e \quad (10)$$

where

$$k_a = \frac{EA}{L}, \quad k_t = \frac{EI}{L^3} \quad (11)$$

Applying the assembly procedure of Figure 4.8.14 with (5) yields

$$\underline{f}_f = (\underline{f}^e)_4 = \cos(\delta_e) \frac{3f_1(t)}{4} + \sin(\delta_e) \left(-\frac{f_0(t)}{4} + \frac{3}{2L} m_0(t) + \bar{F}_2 \frac{7L}{20} \cos(\omega t) \right) \quad (12)$$

Next, consider the added mass, stiffness, damping, and force $(\hat{m}_a, \hat{k}_a, \hat{c}_a, \hat{f}_a)$ shown in Figure E9.2.1(a). The kinetic energy and additional term in Lagrange's equation due to concentrated mass m_a are

$$T_a = \frac{\hat{m}_a}{2} \dot{q}_4^2 \Rightarrow \frac{d}{dt} \left(\frac{\partial T}{\partial \dot{q}_4} \right) = \hat{m}_a \ddot{q}_4 \quad (13)$$

The potential energy and additional term in Lagrange's equation due to concentrated stiffness k_a are

$$U_a = \frac{\hat{k}_a}{2} q_4^2 \Rightarrow \frac{\partial U_a}{\partial q_4} = \hat{k}_a q_4 \quad (14)$$

The dissipation function and additional term in Lagrange's equation due to concentrated damping c_a are

$$\mathfrak{F}_a^d = \frac{\hat{c}_a}{2} \dot{q}_4^2 \Rightarrow \frac{\partial \mathfrak{F}_a^d}{\partial \dot{q}_4} = \hat{c}_a \dot{q}_4 \quad (15)$$

The generalized force in Lagrange's equation due to the applied force \hat{f}_a is

$$Q_a = \hat{f}_a \hat{e}_x \cdot \frac{\partial \dot{q}_4 \hat{e}_x}{\partial \dot{q}_4} = \hat{f}_a \quad (16)$$

Combining the results in (8)–(16) yields the equilibrium equations

$$m_{\text{equiv}} \ddot{q}_4 + c_{\text{equiv}} \dot{q}_4 + k_{\text{equiv}} q_4 = F_{\text{equiv}}(t) \quad (17)$$

where

$$m_{\text{equiv}} = \hat{m}_a + \left(\frac{1}{3} \cos^2 \delta_e + \frac{13}{35} \sin^2 \delta_e \right) m_B + \frac{6 I_B}{5 L^2} \sin^2 \delta_e, \quad c_{\text{equiv}} = \hat{c}_a$$

$$k_{\text{equiv}} = \hat{k}_a + k_a \cos^2 \delta_e + 12 k_t \sin^2 \delta_e, \quad F_{\text{equiv}} = \hat{f}_a(t) - \sin \delta_e \left(-\frac{f_0(t)}{2} + \frac{3 m_0(t)}{2L} \right) \quad (18)$$

$$m_B = \rho A L, \quad I_B = \rho I L, \quad k_a = \frac{EA}{L}, \quad k_t = \frac{EI}{L^3}$$

9.2.7 2D Frame: Beam Element Assembly Algorithm

The element mass \underline{M}^e and stiffness \underline{K}^e matrices, as expressed in global coordinates, are defined by (9.2.69)–(9.2.73) and (9.2.61)–(9.2.65), respectively. The element force vector \underline{f}^e , as expressed in global coordinates, is defined by (9.2.47) and (9.2.76). Algorithms are presented here for assembling these “building block” element matrices to form the system mass and stiffness matrices and force vector, including zero deflection constraints imposed on specified dofs. As depicted in Figure 9.2.5(a), the nodal connectivity array for element e stores the global node numbers corresponding to local node numbers $j = 1$ and $j = 2$ and is defined by

$$B_{ej} = \begin{cases} g_{1e}, & j = 1 \\ g_{2e}, & j = 2 \end{cases} \quad (9.2.77)$$

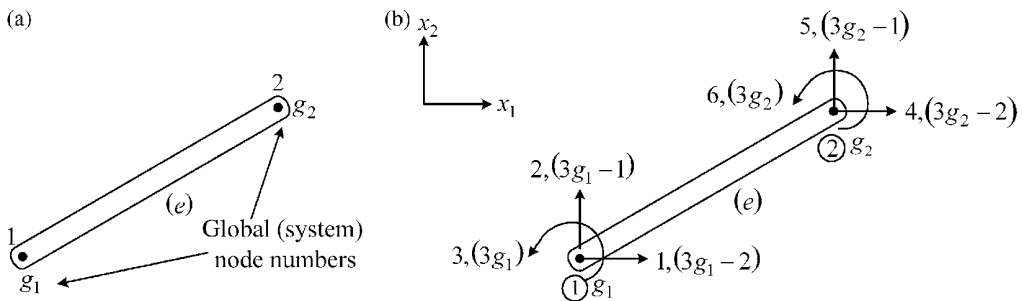


Figure 9.2.5 (a) Global node and (b) global degree of freedom numbering approach

As depicted in Figure 9.2.5(b), the dof connectivity array for element e stores the global dof numbers corresponding to local dof numbers $l = 1$ through $l = 6$ and is defined by

$$\hat{B}_{el} = \begin{cases} 3g_{1e}-2, & l=1 \\ 3g_{1e}-1, & l=2 \\ 3g_{1e}, & l=3 \\ 3g_{2e}-2, & l=4 \\ 3g_{2e}-1, & l=5 \\ 3g_{2e}, & l=6 \end{cases} \quad (9.2.78)$$

The dof array is not unique so (9.2.78) provides one illustrative approach. The pattern in (9.2.78) enables automated generation of the dof connectivity array \hat{B} utilizing the user-defined nodal connectivity array B . This is demonstrated by the following coding segment:

```

for e = 1 : 1 : E      (element index)
  for i = 1 : 1 : 2    (local node index)
    for k = 1 : 1 : 3  (dof index at a node)
      l = 3 * (i - 1) + k
       $\hat{B}_{el} = 3 * (B_{ei} - 1) + k$ 
    end
  end
end
end
end

```

(9.2.79)

As in (4.8.35) or (4.8.94), the *larray* indicates the locations of each dof in the condensed vector \underline{q}_f , which contains only free (unconstrained) dof displacements. The *larray* is again represented by

$$\tilde{L} = (l_1 \ l_2 \ \cdots \ l_N)$$

(9.2.80)

$l_i = \text{position of dof } q_i \text{ in the "free" dof vector } \underline{q}_f$
 $(l_i = 0 \text{ if } q_i \text{ is constrained})$

Suppose that the user input to a code requires entry of the nodes and corresponding dofs that are fixed to ground, that is, that have zero displacement. The user input instructions might read, that is,

For all constrained dofs, enter the global node number k_i and the corresponding dof d_i at global node number k_i which is fixed to ground, for $i = 1, m$, where m is the total number of fixed dofs in the model. The direction of a fixed dof is $d_i = 1$ (x_1 direction), $d_i = 2$ (x_2 direction), and $d_i = 3$ (rotation direction) in Figure 9.2.5.

The code internally defines an array *fixeddof* containing all of the global dof numbers that are fixed to ground, from

```

for i = 1 : 1 : m
  fixeddof(i) = 3 * (k_i - 1) + d_i
end

```

(9.2.81)

Let $Ndof$ be the total number of dofs in the entire model:

$$Ndof = 3 * (\text{Number of nodes in entire model}) \quad (9.2.82)$$

Then the $larray$ is generated from

```

ict=0
for i = 1 : 1 : Ndof
    iflag=0
    for j = 1 : 1 : m
        if i = fixeddof(j)
            iflag = 1
        end
    end
    larray(i) = 0
    if iflag = 0
        ict = ict + 1
        larray(i) = ict
    end
end
end
end

```

(9.2.83)

The assembly of the system matrices for the free (unconstrained) dofs is illustrated in Figure 9.2.6, which is identical to Figure 4.8.14.

Similar with (4.8.98) repeat the above “assembly” step for all E elements in the model and for all six local dofs, that is,

$$e = 1, 2, \dots, E, \quad r = 1, \dots, 6, \quad s = 1, \dots, 6 \quad (9.2.84)$$

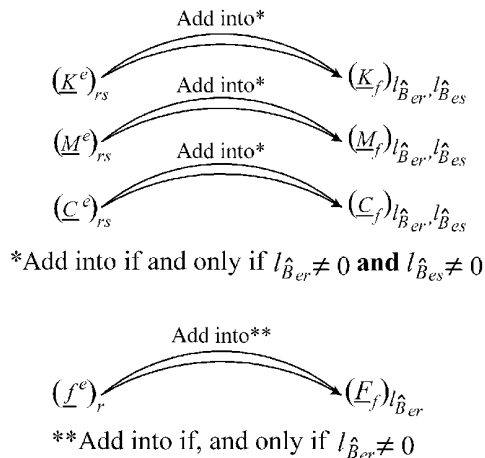


Figure 9.2.6 Assembly of free dof system matrices and force vector for a constrained system

As in (4.8.36), imposing the zero-displacement constraint conditions yields the following “condensed” dynamic equilibrium equation for the “free” (unconstrained) dofs of the constrained structure:

$$\underline{M}_f \ddot{\underline{q}}_f + \underline{C}_f \dot{\underline{q}}_f + \underline{K}_f \underline{q}_f = \underline{F}_f \quad (9.2.85)$$

$N_f \times N_f$ $N_f \times 1$ $N_f \times N_f$ $N_f \times 1$ $N_f \times N_f$ $N_f \times 1$ $N_f \times 1$

EXAMPLE 9.2.2 Three-Element Model of an Inclined Cantilever Beam

Statement: The simple cantilevered beam model in Figure E9.2.2(a) has $E = 3$ elements, $N = 4$ nodes, and a total of 12 dofs, only 9 of which are “free” (unconstrained) since node 1 is fixed in translation and rotation.

Objectives: Demonstrate a software-based assembly and solution, and as a verification case, show that the natural frequencies are the same for inclination angles of $\theta = 0^\circ$ and $\theta = 30^\circ$.

Assumptions: Euler–Bernoulli beam theory is applicable.

Solution: The fixed global dof numbers stored in the array `fixeddof(i)` are:

i	Global node k_i	Local dof d_i	<code>fixeddof(i)</code>
1	1	1	1
2	1	2	2
3	1	3	3

The `larray` of (9.2.80) is

$$\tilde{L} = (l_1 \ l_2 \ \cdots \ l_{12}) = (0 \ 0 \ 0 \ 1 \ 2 \ 3 \ 4 \ 5 \ 6 \ 7 \ 8 \ 9) \quad (1)$$

The `jarray` of (4.8.34) contains the full system, dof numbers for the dof which appear in the displacement vector \underline{q}_f of free dofs. For this example

$$\tilde{J} = (j_1 \ j_2 \ \cdots \ j_9) = (4 \ 5 \ 6 \ 7 \ 8 \ 9 \ 10 \ 11 \ 12) \quad (2)$$

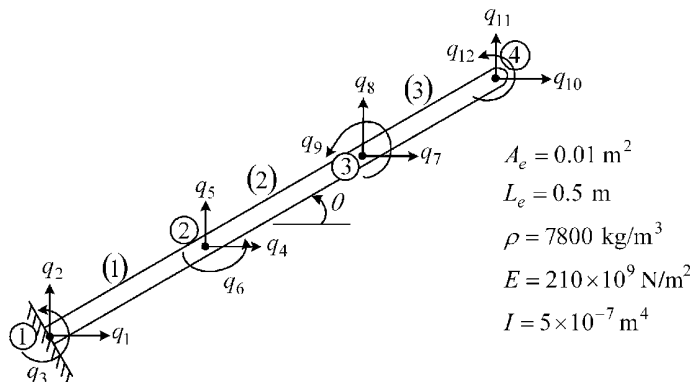
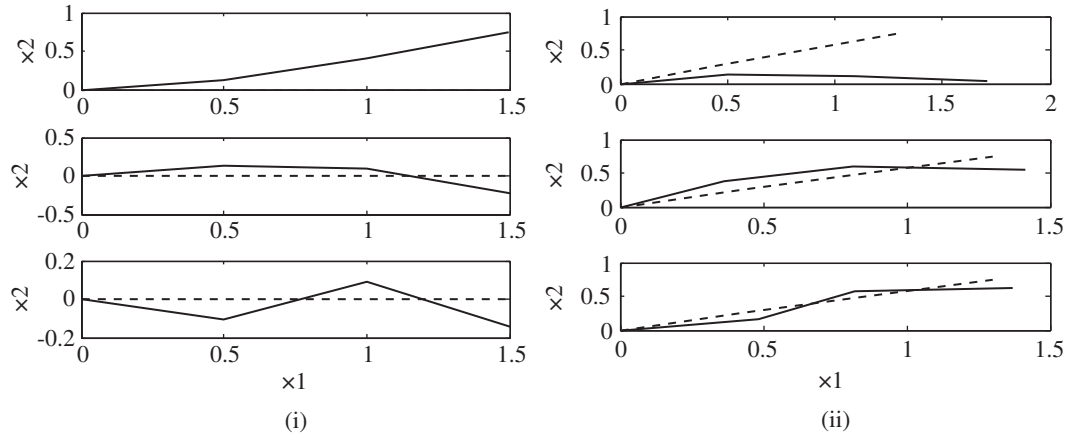


Figure E9.2.2(a) Inclined, cantilevered beam model

Table E9.2.2(a) Lowest three natural frequencies (rad/s)

	FE $\delta_e = \theta = 0^\circ$	FE $\delta_e = \theta = 30^\circ$	Analytical (continuous model)
Mode 1	57.34	57.34	57.4
Mode 2	360.49	360.49	359
Mode 3	1018.6	1018.6	1006

**Figure E9.2.2(b)** Mode shapes for the first (upper), second (middle), and third (bottom) modes for (i) $\theta = 0^\circ$ and (ii) $\theta = 30^\circ$. Dashed line indicates undeformed geometry

This array is used to assemble the full system response vector from the free dof response vector as demonstrated by the MATLAB code below. The \underline{B} and $\hat{\underline{B}}$ arrays are

$$\underline{B} = \begin{bmatrix} 1 & 2 \\ 2 & 3 \\ 3 & 4 \end{bmatrix}, \quad \hat{\underline{B}} = \begin{bmatrix} 1 & 2 & 3 & 4 & 5 & 6 \\ 4 & 5 & 6 & 7 & 8 & 9 \\ 7 & 8 & 9 & 10 & 11 & 12 \end{bmatrix} \quad (3)$$

The MATLAB code below defines and assembles the matrix quantities and determines the natural frequencies and mode shapes. The lowest three natural frequencies appear in Table E9.2.2(a) and the corresponding mode shapes appear in Figure E9.2.2(b). The $\delta_e = \theta = 0^\circ$ and $\delta_e = \theta = 30^\circ$ results are seen to be identical, as expected:

```
% Example 9.2.2 Inclined Cantilever Beam
clear
% INPUT NUMERICAL VALUES
N=4 ; % no. of nodes in model
B=[1 2 ; 2 3 ; 3 4] ; % Nodal connectivity matrix
dp=[1 2 3] ; % dof's with prescribed (known) displacements (u=0)
Modeplots=[9 8 7] ; % Mode numbers to be plotted
h=[0.5 0.5 0.5] ; % element lengths
A=[.01 .01 .01] ; % element cross sectional areas
Ey=210.0e+09*[1 1 1] ; % element Young's Moduli
```

```

Ix2=[5 5 5]*1.0e-07; % Area moments of inertia about the local
x2 axis
rho=(7800)*[1 1 1]; % Mass density of the beam material
zeta=[0 0 0]*pi/180.; % element angles in radians
scalefactor = 0.75;

% DETERMINE DIMENSIONS AND NODAL COORDINATES
E=size(B,1); % number of elements in the model
Npd=size(dp,2); % number of dof's with prescribed u's
edof=6; % number of dof's per element
Nplots = size(Modeplots,2); % Number of modelplots to be made
xnode = [0 0.5*cos(zeta(1)) 1.0*cos(zeta(1)) 1.5*cos
(zeta(1))];
ynode = [0 0.5*sin(zeta(1)) 1.0*sin(zeta(1)) 1.5*sin
(zeta(1))];

% DEFINE INTEGER ARRAYS
Nd = 3*N; % Total number of dof's in the model
% Degree of Connectivity Array ( global dof corresponding to
local dof in element e)
for e=1:1:E % element
    for i=1:1:2 % nodes per element
        for k=1:1:3 % dof per node
            alpha=3*(i-1)+k; % element dof
            Bhat(e,alpha)=3*(B(e,i)-1)+k; % global dof
                                     corresponding to
                                     % element dof
        end
    end
end
% Define L array from the dof's with prescribed u's
Nnpd=0; % counter for number of non-prescribed dof's
for i = 1:1:Nd
    flag=0;
    for k=1:1:Npd
        if i == dp(k)
            flag = 1;
        end
    end
    if flag == 0
        Nnpd = Nnpd + 1;
        jarray(Nnpd) = i;
    end
end
% Note at this point Nnpd is the total number of non-prescribed
u's .
% These u's must be solved for.
larray=zeros(1,Nd);
for i=1:1:Nnpd

```

```

    istore = jarray(i);
    larray(1,istore)=i;
end

% ASSEMBLE THE CONDENSED SYSTEM (GLOBAL) STIFFNESS AND MASS
MATRICES
% Initialize Kc and Mc to zero
Kc=zeros(Nnpd,Nnpd);
Mc=zeros(Nnpd,Nnpd);
for e =1:1:E
    % Form element stiffness matrix for element e
    a1=Ey(e)*A(e)/h(e); a4= 12*Ey(e)*Ix2(e)/h(e)^3;
    a5= -6*Ey(e)*Ix2(e)/h(e)^2; a7= 4*Ey(e)*Ix2(e)/h(e);
    a8=2*Ey(e)*Ix2(e)/h(e);
    A1=a1*cos(zeta(e))^2 + a4*sin(zeta(e))^2;
    A2=a4*cos(zeta(e))^2 + a1*sin(zeta(e))^2;
    A3=a7;
    A4=(a1-a4)*cos(zeta(e))*sin(zeta(e));
    A5=-a5*sin(zeta(e));
    A6=a5*cos(zeta(e));
    Ke=[A1 A4 A5 -A1 -A4 A5 ; A4 A2 A6 -A4 -A2 A6 ;
        A5 A6 A3 -A5 -A6 A3/2 ; -A1 -A4 -A5 A1 A4 -A5 ;
        -A4 -A2 -A6 A4 A2 -A6 ; A5 A6 A3/2 -A5 -A6 A3 ];

    % Mass Matrix for element e
    me = rho(e)*A(e)*h(e); % element mass
    Metilda=zeros(6,6);
    Metilda(2,2)=156; Metilda(2,3)=-22*h(e); Metilda(2,5)=54;
    Metilda(2,6)=13*h(e);
    Metilda(3,3)=4*h(e)^2; Metilda(3,5)=-13*h(e); Metilda
    (3,6)=-3*h(e)^2;
    Metilda(5,5)=156; Metilda(5,6)=22*h(e);
    Metilda(6,6)=4*h(e)^2;
    for i=1:1:6
        for j=i:1:6
            Metilda(j,i)=Metilda(i,j);
        end
    end
    Metilda=me/420*Metilda;
    Metilda(1,1)=me/3; Metilda(1,4)=me/6; Metilda(4,1)=me/6;
    Metilda(4,4)=me/3;

    CC=[cos(zeta(e)) sin(zeta(e)) 0; ...
        -sin(zeta(e)) cos(zeta(e)) 0; ...
        0 0 1];
    Te(1:3,1:3)=CC; Te(1:3,4:6)=zeros(3,3); Te(4:6,1:3)
    =zeros(3,3);
    Te(4:6,4:6)=CC;
    Me=Te'*Metilda*Te;

```

```

% Assemble Kc and Mc
for r=1:1:6
    for s=1:1:6
        % form the condensed Kc and Mc matrices
        lBhater=larray( Bhat(e,r) );
        lBhates=larray( Bhat(e,s) );
        if lBhater ~= 0
            if lBhates ~= 0
                % assemble Kc
                Kc(lBhater,lBhates) = Kc(lBhater,lBhates) + Ke(r,s) ;
                % assemble Mc
                Mc(lBhater,lBhates) = Mc(lBhater,lBhates) + Me(r,s) ;
            end
        end
    end % s loop
end % r loop
end % e loop

% SOLVE FOR THE CONDENSED SYSTEM NATURAL FREQUENCIES
format shortg
[Modes, Evalue]=eig(inv(Mc)*Kc);
natfreqhz=sqrt(diag(Evalue))/2/pi; % natural frequencies
                                        in hz

natfreq_rad_sec= natfreqhz*2*pi
Modes
pause
% Use the jarray to determine the complete mode shapes including
% constrained and free dofs
FullMode = zeros(Nd, Nnpd);
for j=1:1:Nnpd
    for i=1:1:Nnpd
        FullMode(jarray(i),j)=Modes(i,j);
    end
end
FullMode
% Normalize so that largest component in each mode shape
equals 1.0
for j=1:1:Nnpd
    mmax=0.;
    for i=1:1:Nd
        tst=FullMode(i,j);
        if abs(tst)>mmax
            stortst=tst;
            mmax=abs(tst);
        end
    end
    FullMode(1:Nd,j) = FullMode(1:Nd,j)/stortst;
end
FullMode

```

```

% Store mode components for plotting
for j=1:1:Nnpd
for i=1:1:N
  xplot(i,j) = xnode(i) + scalefactor*FullMode(3*(i-1)+1,j);
  yplot(i,j) = ynode(i) + scalefactor*FullMode(3*(i-1)+2,j);
end
end
for i=1:1:Nplots % Make Mode Shape Plots
  subplot(Nplots,1,i);
  plot(xplot(:,Modeplots(i)), yplot(:,Modeplots(i)), xnode,
  ynode, 'b- -');
  xlabel('x1')
  ylabel('x2')
  pause
end

```

EXAMPLE 9.2.3 Six-Element Model of a Portal Frame

Statement: The frame model in Figure E9.2.3(a) has $E = 6$ elements, $N = 7$ nodes, and a total of 21 dofs, only 15 of which are “free” (unconstrained) since nodes 1 and 7 are fixed in translation and rotation.

Objectives: Demonstrate calculation of natural frequencies and mode shapes of a frame.

Assumptions: Euler–Bernoulli beam theory is applicable.

Solution: The table below shows the fixed global dof numbers stored in the array $\text{fixeddof}(i)$:

i	Global node k_i	Local dof d_i	$\text{fixeddof}(i)$
1	1	1	1
2	1	2	2
3	1	3	3
4	7	1	19
5	7	2	20
6	7	3	21

The element orientation angles (ref. Figure 9.2.4) are

$$(\delta_1 \ \delta_2 \ \delta_3 \ \delta_4 \ \delta_5 \ \delta_6) = (90^\circ \ 90^\circ \ 0^\circ \ 0^\circ \ -90^\circ \ -90^\circ) \quad (1)$$

The *larray* of (9.2.80) is

$$\begin{aligned} \tilde{L} &= (l_1 \ l_2 \ \cdots \ l_{21}) \\ &= (0 \ 0 \ 0 \ 1 \ 2 \ 3 \ 4 \ 5 \ 6 \ 7 \ 8 \ 9 \ 10 \ 11 \ 12 \ 13 \ 14 \ 15 \ 0 \ 0 \ 0) \end{aligned} \quad (2)$$

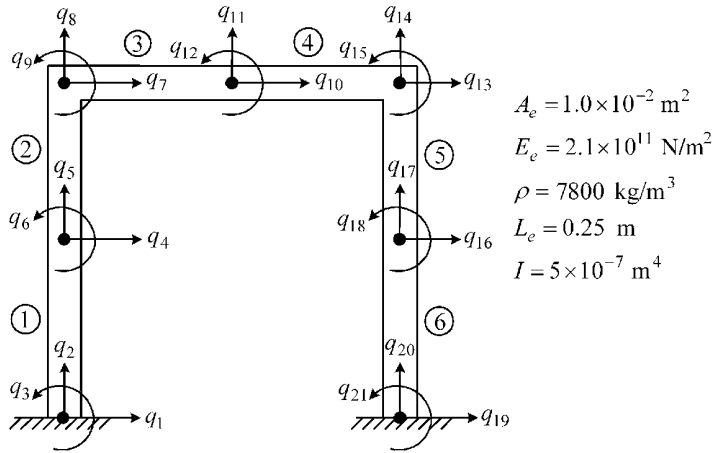


Figure E9.2.3(a) Portal frame beam model

Table E9.2.3(a) Lowest three natural frequencies

	ω_{ni} (rad/s)
Mode 1	470.13
Mode 2	1860
Mode 3	3061

The “ j array” of (4.8.34) contains the full system, dof numbers for the dof which appear in the displacement vector q_f of free dofs. For this example

$$\tilde{J} = (j_1 \ j_2 \ \cdots \ j_{15}) = (4 \ 5 \ 6 \ 7 \ 8 \ 9 \ 10 \ 11 \ 12 \ 13 \ 14 \ 15 \ 16 \ 17 \ 18) \quad (3)$$

This array is used to assemble the full system response vector from the free dof response vector as demonstrated in Example 9.2.2. The nodal \underline{B} and dof $\hat{\underline{B}}$ connectivity arrays are

$$\underline{B} = \begin{bmatrix} 1 & 2 \\ 2 & 3 \\ 3 & 4 \\ 4 & 5 \\ 5 & 6 \\ 6 & 7 \end{bmatrix}, \quad \hat{\underline{B}} = \begin{bmatrix} 1 & 2 & 3 & 4 & 5 & 6 \\ 4 & 5 & 6 & 7 & 8 & 9 \\ 7 & 8 & 9 & 10 & 11 & 12 \\ 10 & 11 & 12 & 13 & 14 & 15 \\ 13 & 14 & 15 & 16 & 17 & 18 \\ 16 & 17 & 18 & 19 & 20 & 21 \end{bmatrix} \quad (4)$$

A MATLAB code defines and assembles the matrix quantities and determines the natural frequencies and mode shapes. The lowest three natural frequencies appear in Table E9.2.3(a) and the corresponding mode shapes appear in Figure E9.2.3(b).

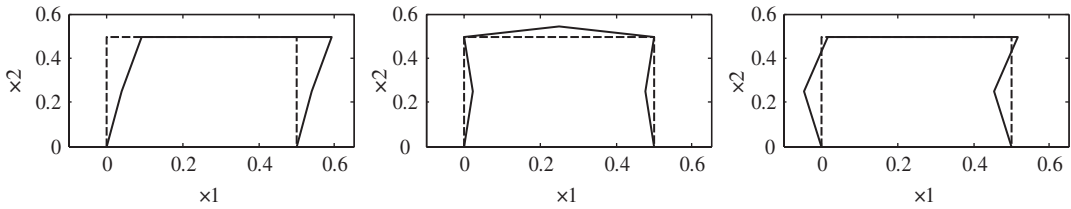


Figure E9.2.3(b) Mode shapes for the first (left), second (middle), and third (right) modes. Dashed line indicates undeformed geometry

EXAMPLE 9.2.4 *Finite Element Convergence Study for Ring Structure*

Statement: The ring model in Figure E9.2.4(a) has $E = n$ elements, $N = n$ nodes, and a total of $3 * n$ dofs, only $3 * (n - 1)$ of which are “free” (unconstrained) since node 1 is fixed in translation and rotation.

Objectives: Demonstrate element convergence and calculation of natural frequencies and mode shapes of the ring.

Assumptions: Euler–Bernoulli beam theory is applicable.

Solution: The table below shows the fixed global dof numbers stored in the array $\text{fixeddof}(i)$:

i	Global node k_i	Local dof d_i	$\text{fixeddof}(i)$
1	1	1	1
2	1	2	2
3	1	3	3

The nodal coordinates, element lengths, and orientation angles (ref. Figures 9.2.4 and E9.2.4(a)) are

$$x_{1i} = R * \cos((i-1)\Delta\theta), \quad x_{2i} = R * \sin((i-1)\Delta\theta) \quad (1)$$

$$L_e = \sqrt{(x_{1,e+1} - x_{1,e})^2 + (x_{2,e+1} - x_{2,e})^2} \quad e = 1, \dots, n-1 \quad (2)$$

$$\delta_e = \tan^{-1} \left(\frac{x_{2,e+1} - x_{2,e}}{x_{1,e+1} - x_{1,e}} \right) \quad e = 1, \dots, n-1 \quad (3)$$

The $larray$ of (9.2.80) is

$$\tilde{L} = (l_1 \quad l_2 \quad \dots \quad l_{3*n}) = (0 \quad 0 \quad 0 \quad 1 \quad 2 \quad 3 \quad \dots \quad 3*(n-1)) \quad (4)$$

The $jarray$ of (4.8.34) contains the full system, dof numbers for the dof which appear in the displacement vector \underline{q}_f of free dofs. For this example

$$\tilde{J} = (j_1 \quad j_2 \quad \dots \quad j_{3*(n-1)}) = (4 \quad 5 \quad 6 \quad 7 \quad 8 \quad 9 \quad \dots \quad 3*n) \quad (5)$$

This array is used to assemble the full system response vector from the free dof response vector as demonstrated in Example 9.2.2. The nodal \underline{B} connectivity array is

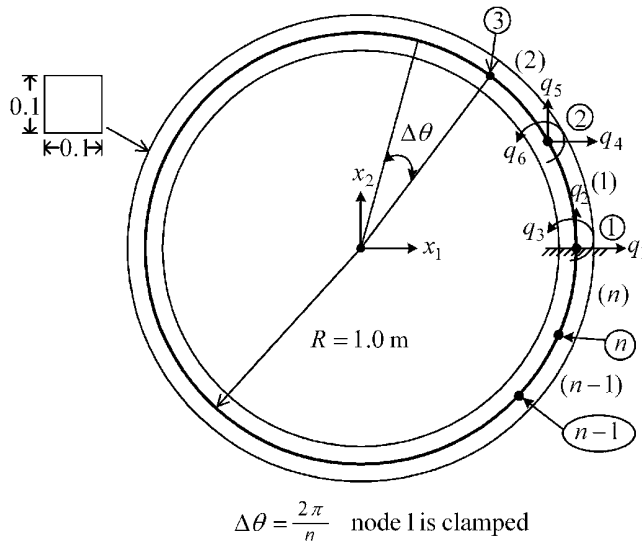


Figure E9.2.4(a) Ring structure beam model with a variable number of elements

Table E9.2.4(a) Lowest four natural frequencies in radian per second for node 1 fixed

E (no. of elements)	ω_1	ω_2	ω_3	ω_4
4	109	276	1016	1715
10	89	250	530	900
20	86	241	512	869
50	85	239	507	860
100	85	239	506	859

$$B_{e1} = e, \quad B_{e2} = \begin{cases} e + 1, & e \neq n \\ 1, & e = n \end{cases} \quad (6)$$

The dof \hat{B} connectivity array is obtained from (6) and (9.2.79). The geometric and material properties of the uniform ring are

$$A_e = 0.01 \text{ m}^2, \quad I_e = \frac{0.1^4}{12} = 8.333 \times 10^{-6} \text{ m}^4, \quad E = 210 \times 10^9 \text{ N/m}^2, \quad \rho = 7800 \text{ kg/m}^3 \quad (7)$$

A MATLAB code similar to that provided in Figure 9.2.2 defines and assembles the matrix quantities and determines the natural frequencies and mode shapes. The lowest four natural frequencies appear in Table E9.2.4(a) for various number (n) of elements. The results show convergence of the lowest 4 modes with approximately 50 elements.

The corresponding mode shapes for the 10- and 100-element cases are shown in Figures E9.2.4(b)-(i) and E9.2.4(b)-(ii), respectively.

Next, consider the ring with the same geometry and material properties however with the three constraints removed so that the ring is free to move with rigid body motion. The six lowest natural frequencies of a 100-element model are shown in Table E9.2.4(b).

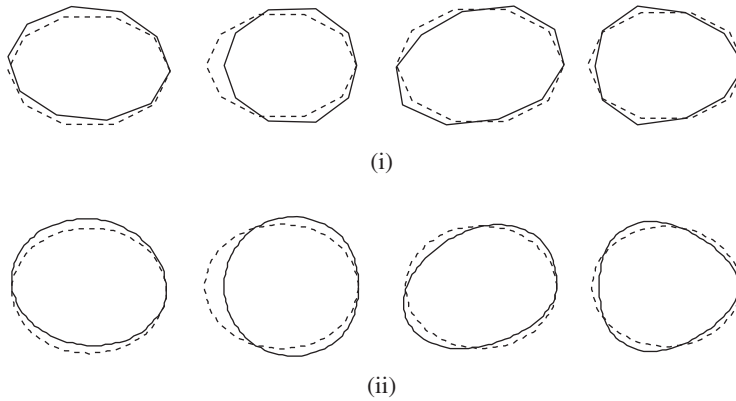


Figure E9.2.4(b) Mode shapes for the first through fourth modes (left to right) with a (i) 10-element model and (ii) 100-element model. Dashed line indicates undeformed geometry

Table E9.2.4(b) Lowest six natural frequencies of free (unconstrained) ring

i	f_i (Hz) finite elements	f_i (Hz) handbook ^a
1	0 ^b	—
2	0	—
3	0	—
4	15.99	15.99
5	45.24	45.23
6	86.74	79.8

^aHarris and Piersol (2002).

^bRigid body modes.

9.2.8 Imposed Support Excitation Modeling

The preceding sections treated the case where all imposed displacements were zero. The more general case is when some of the imposed displacements are nonzero, for example, a piping system which is vibrated by support motion at some locations but fixed to ground at other locations. The assembly procedure must be modified for this case to yield the following system equations:

$$\begin{matrix} \underline{M}_f & \ddot{\underline{q}}_f & + & \underline{C}_f & \dot{\underline{q}}_f & + & \underline{K}_f & \underline{q}_f & = & \underline{F}_f(t) & + & \underline{H}_M & \ddot{\underline{q}}_E(t) & + & \underline{H}_C & \dot{\underline{q}}_E(t) & + & \underline{H}_K & \underline{q}_E(t) \\ N_f \times N_f & N_f \times 1 & & N_f \times N_f & N_f \times 1 & & N_f \times N_f & N_f \times 1 & & N_f \times 1 & & N_f \times \bar{m} & \bar{m} \times 1 & & N_f \times \bar{m} & \bar{m} \times 1 & & N_f \times \bar{m} & \bar{m} \times 1 \end{matrix} \quad (9.2.86)$$

where $\underline{q}_E(t)$ is a $\bar{m} \times 1$ vector of nonzero, imposed (support) displacements and \bar{m} is the number of nonzero, imposed (support) displacements. The \underline{l} array is defined in the same manner as in (9.2.80):

$$\begin{aligned} \tilde{\underline{L}} &= (l_1 \quad l_2 \quad \cdots \quad l_N) \\ l_i &= \text{position of dof } q_i \text{ in the "free" dof vector } \underline{q}_f \\ & (l_i = 0 \text{ if } q_i \text{ is constrained}) \end{aligned} \quad (9.2.87)$$

The array of constrained (either zero or imposed) dofs *fixeddof* defined in (9.2.81) includes all dofs with either zero or nonzero imposed displacements. The mass, damping, and stiffness matrices and force vector in (9.2.86) are formed identically as previously as shown in Figure 9.2.6. The *larray* has zeros at all dofs with (zero or nonzero) imposed displacements. The remaining matrices H_M , H_C , H_K are obtained by considering the identity (2.6.30):

$$\underset{n \times m}{\underline{A}} \underset{m \times 1}{\underline{x}} = [\underline{A}_1 \ \underline{A}_2 \ \cdots \ \underline{A}_m] \underline{x} = \sum_{i=1}^m x_i \underline{A}_i \quad (n \times 1) \quad (9.2.88)$$

where \underline{A} represents the mass, damping, or stiffness matrices and \underline{x} represents the acceleration, velocity, or displacement vectors. Suppose $x(t)$ is given (imposed) at dof k . Then (9.2.88) may be written

$$\underset{n \times (n-1)}{\hat{\underline{A}}} \underset{(n-1) \times 1}{\hat{\underline{x}}} = \sum_{\substack{i=1 \\ i \neq k}}^{n-1} x_i \underline{A}_i = -x_k(t) \underline{A}_k \quad (n \times 1) \quad (9.2.89)$$

Thus, the term on the right-hand side of (9.2.89) becomes a pseudo forcing term with a coefficient vector \underline{A}_k . This is the basis for forming the right-hand side term in (9.2.86):

$$\underset{N_f \times \bar{m}}{\underline{H}_M} \ddot{\underset{\bar{m} \times 1}{\underline{q}}_E}(t) + \underset{N_f \times \bar{m}}{\underline{H}_C} \dot{\underset{\bar{m} \times 1}{\underline{q}}_E}(t) + \underset{N_f \times \bar{m}}{\underline{H}_K} \underset{\bar{m} \times 1}{\underline{q}}_E(t) \quad (9.2.90)$$

Recognition of this leads to the following algorithm for determining $\underline{H}_M, \underline{H}_C, \underline{H}_K$ in (9.2.86). With reference to Figure 9.2.6, allow r and s to range over all entries in the element matrix ($r = 1, 6$ and $s = 1, 6$ for the 2D beam element). Let e range over all elements in the model ($e = 1, E$). Denote the set of dofs with nonzero imposed displacements as members of the integer array

$$(i_1 \ i_2 \ \cdots \ i_p \ \cdots \ i_{\bar{m}}) \quad (9.2.91)$$

This is a subset of *fixeddof* defined in (9.2.81). Then add the following assembly step to Figure 9.2.6:

if $l_{\hat{B}_{es}} = 0$ AND if $l_{\hat{B}_{er}} \neq 0$ AND if $\hat{B}_{es} = i_p$ for some value of p ($p = 1, 2, \dots, \bar{m}$)

then

$$\begin{aligned} \text{Add: } -(\underline{K}^e)_{rs} \text{ into } (\underline{H}_K)_{(l_{\hat{B}_{er}}, p)}, \quad \text{Add: } -(\underline{C}^e)_{rs} \text{ into } (\underline{H}_C)_{(l_{\hat{B}_{er}}, p)}, \\ \text{Add: } -(\underline{M}^e)_{rs} \text{ into } (\underline{H}_M)_{(l_{\hat{B}_{er}}, p)} \end{aligned} \quad (9.2.92)$$

Equation (9.2.86) can be solved by using the numerical integration techniques presented in Section 6.4, or if steady-state vibrations due to harmonic loading are sought, then by using the complex variable approach in (7.5.1)–(7.5.8). In the latter approach, make the substitutions:

$$\underline{q}_f = \tilde{\underline{Q}}_f e^{i\omega t}, \quad \underline{F}_f = \tilde{\underline{F}}_f e^{i\omega t}, \quad \underline{q}_E = \tilde{\underline{Q}}_E e^{i\omega t} \quad (9.2.93)$$

The phasor displacement response vector $\underline{\tilde{Q}}_f$ is then obtained by solving the following set of complex, linear algebraic equations:

$$\left(-\omega^2 \underline{M}_f + i\omega \underline{C}_f + \underline{K}_f\right) \underline{\tilde{Q}}_f = \underline{\tilde{F}}_f + \left(-\omega^2 \underline{H}_M + i\omega \underline{H}_C + \underline{H}_K\right) \underline{\tilde{Q}}_E \quad (9.2.94)$$

The amplitude and phase angle of the j th dof are then obtained from (7.5.7) as

$$|\tilde{Q}_{jf}| = \sqrt{(\text{Re}(\tilde{Q}_{jf}))^2 + (\text{Im}(\tilde{Q}_{jf}))^2} \quad \text{and} \quad \phi_{Q_{jf}} = \tan^{-1} \left(\frac{\text{Im}(\tilde{Q}_{jf})}{\text{Re}(\tilde{Q}_{jf})} \right) \quad (9.2.95)$$

EXAMPLE 9.2.5 Piping System with Support Excitation

Statement: A run of piping is attached by flange to a large compressor mounted on an industrial steel frame platform. Mass imbalance forces in the compressor cause the compressor to vibrate in the vertical and fore and aft directions. The compressor vibration is treated as an imposed motion on the bottom of the piping run at the discharge flange connection to the compressor. The top end of the piping run is flanged connected and clamped to a concrete foundation block which constrains the piping from vibrating. The piping run and its boundary conditions are depicted in Figure E9.2.5(a). There are eight pipe elements of equal length (2 m), and the remaining material and geometric data is

$$A_e = 0.0264 \text{ m}^2, \quad I_e = 5.83 \times 10^{-4} \text{ m}^4, \quad E = 210 \times 10^9 \text{ N/m}^2, \quad \rho = 7800 \text{ kg/m}^3 \quad (1)$$

The imposed displacements at node 1 are

$$\text{Horiz: } q_1 = 1 \cos(\omega t) \text{ mm}, \quad \text{Vert: } q_2 = 0.5 \cos(\omega t) \text{ mm}, \quad \text{Rotation: } q_3 = 0 \quad (2)$$

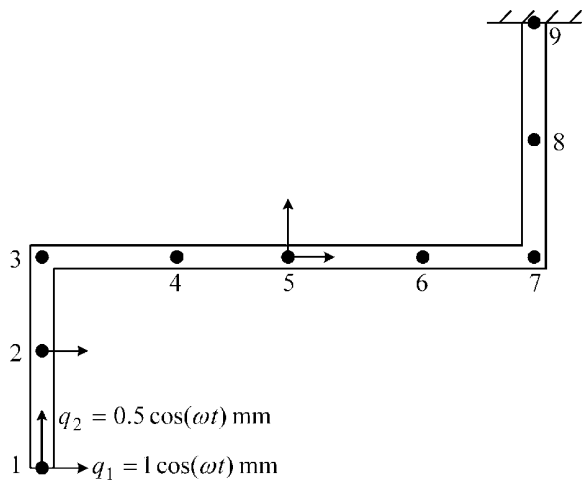


Figure E9.2.5(a) Discharge piping run of an industrial compressor with imposed vibration displacements at the compressor flange

The amplitudes and phase angles of the external forces and imposed displacements are expressed in phasor form as

$$\underline{\tilde{F}}_f = \underline{0}, \quad \underline{\tilde{Q}}_E = \left\{ \begin{array}{l} 0.001 \angle 0 \\ 0.0005 \angle 0 \end{array} \right\} \text{m} \quad (3)$$

An orthogonal damping matrix is included in the model using the formula (5.4.120):

$$\underline{C}_0 = \mu_m \underline{M} + \mu_k \underline{K} \quad (4)$$

with

$$\mu_m = 0, \quad \mu_k = 0.002 \quad (5)$$

Objectives: Determine the steady-state harmonic response at several locations on the piping system versus frequency ω of the imposed deflections.

Assumptions: Euler–Bernoulli beam theory is applicable. Amplitudes and phase angles of the imposed displacements are constant with frequency.

Solution: The theoretical equations (9.2.94) and (9.2.95) were programmed and solved for the example. Figure E9.2.5(b) shows the mode shapes and natural frequencies for fixed conditions at both ends of the run. Figure E9.2.5(c) shows the response amplitudes versus frequency at nodes 2 and 5.

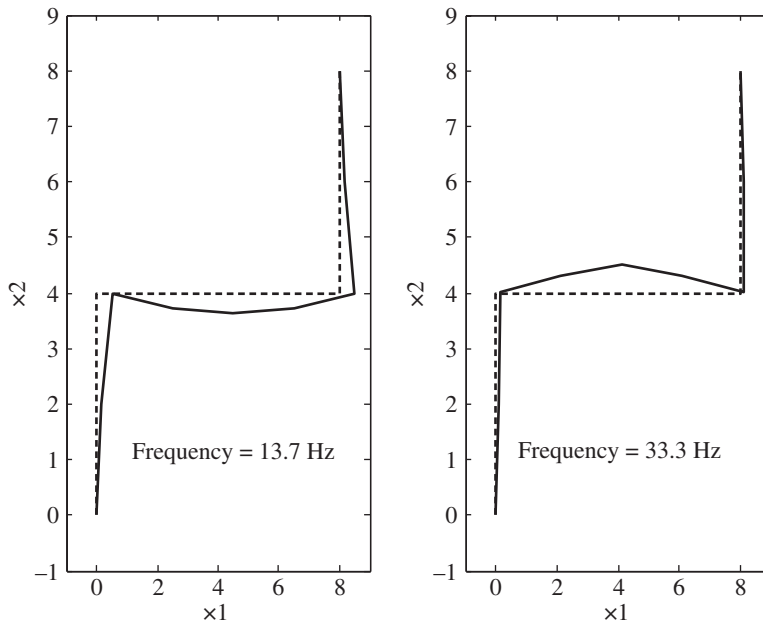


Figure E9.2.5(b) Lowest two mode shapes and natural frequencies for fixed end conditions

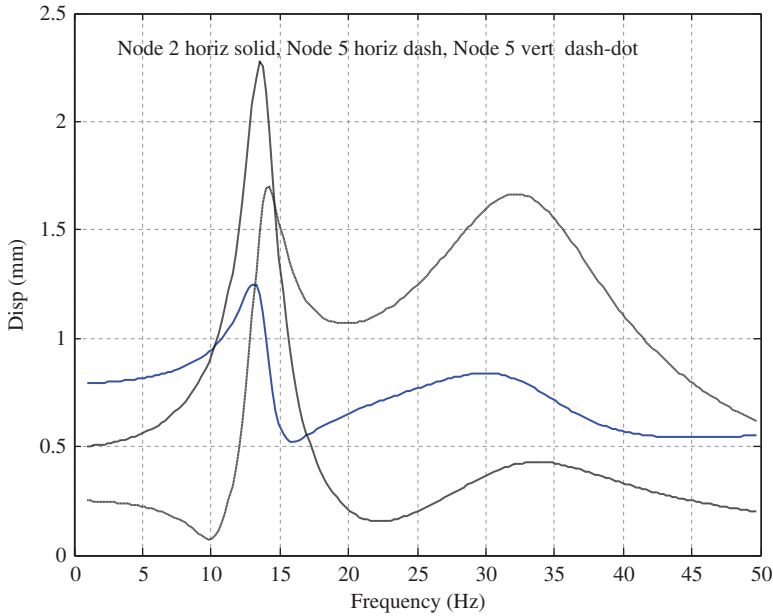


Figure E9.2.5(c) Steady-state harmonic response amplitude at nodes 2 and 5 versus imposed motion shaking frequency

9.3 THREE-DIMENSIONAL TIMOSHENKO BEAM ELEMENTS: INTRODUCTION

Almost all actual frame-type structures are three-dimensional (3D) in geometry, boundary conditions, or loading. Although 2D frames provide a good pedagogical tool to illustrate the procedure for forming a frame model, 3D beams are typically required for most engineering applications. A second improvement presented in this section is the replacement of Euler beam theory with Timoshenko beam (TB) theory. This provides higher accuracy by including shear deformation effects, that is, removal of the kinematic assumption that plane cross sections remain perpendicular to the neutral axis after deformation. Removing this assumption results in increased beam flexibility and reduced natural frequencies. Beam elements are commonly employed to model frame-type structures such as offshore and industrial equipment platforms and buildings and for modeling piping systems and rotating machinery shafting. Figure 9.3.1 represents the side view of a reciprocating compressor for natural gas transmission and its piping system. The cylinders and their support structures may be up to 2 m long and extend from the side of the compressor frame. Vertical suction and discharge pipes are connected to the cylinders and to large horizontal vessels. These vessels (bottles) contain specially designed baffles to attenuate dynamic pressure pulsations that originate in the piston/cylinder valves and if not suppressed can cause severe vibration and failure of the attached pipeline. Figure 9.3.2 shows a 3D beam model for the cylinders, suction and discharge bottles, and attached piping. Clamps and flanges are included in the model as spring attachments to ground and localized added inertias. The model was used to develop modifications to prevent repeated high-cycle fatigue failures in the attached high-pressure natural gas piping.

Figure 9.3.3 shows a photograph of the crankshaft of a large reciprocating compressor and a drawing of its beam and “brick” (solid) element models. These models were utilized to

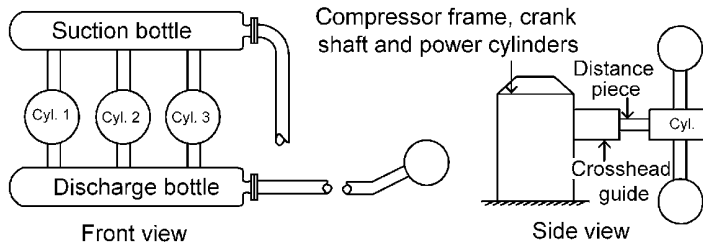


Figure 9.3.1 A three cylinder, natural gas transmission, reciprocating compressor

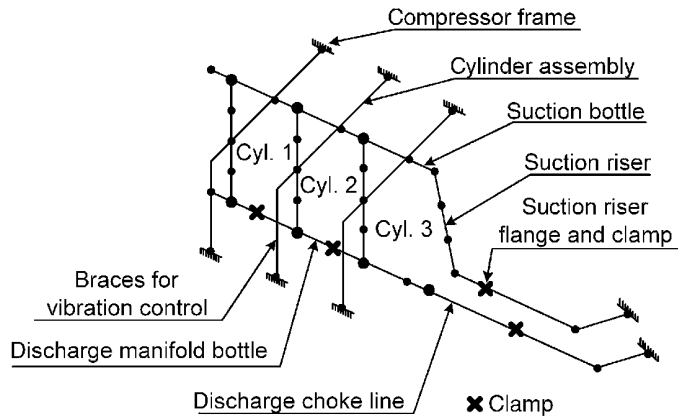


Figure 9.3.2 Frame – 3D beam model of the compressor and piping system

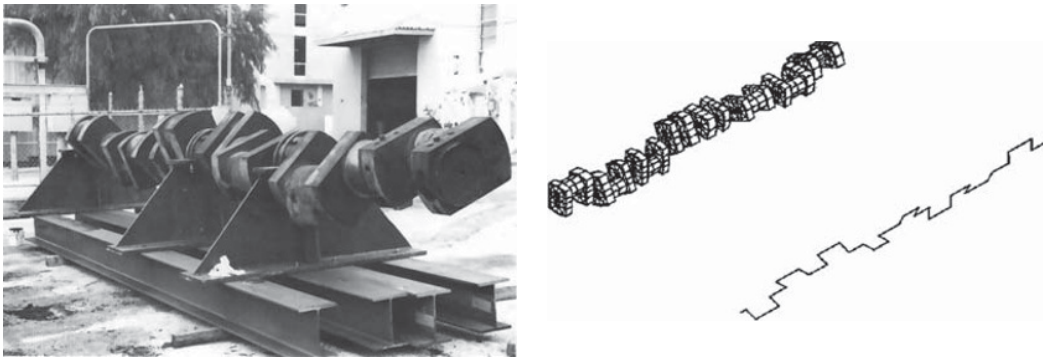


Figure 9.3.3 Reciprocating compressor crankshaft and its beam and brick element models

compare conventional crankshaft bearing alignment practice with related high-cycle fatigue life.

Figure 9.3.4 is a model of the drilling deck of an offshore platform that consists of scores of large I beams and pipes. This model was built to identify modifications to reduce intolerable vibration of the crew quarters due to forces from a gas reinjection compressor that was located on the deck. The figure illustrates a mode shape (solid line) of the deck structure.

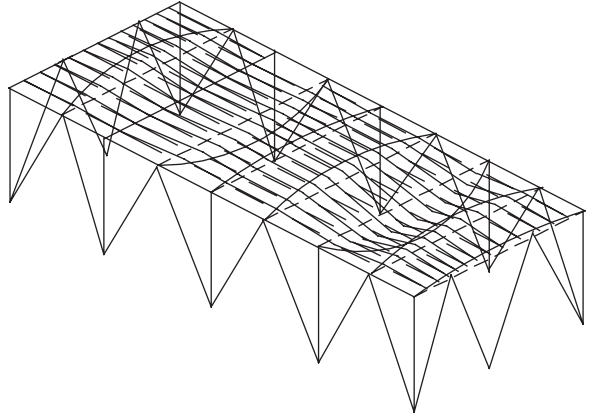


Figure 9.3.4 Frame model of an offshore platform drilling deck

9.4 3D TIMOSHENKO BEAM ELEMENTS: NODAL COORDINATES

Figure 9.4.1 shows a single 2-node, 3D beam element, with 6 dofs per node. The 12 dofs are shown directed in the global (x_1, x_2, x_3) directions. The local dofs and coordinate directions are shown by Figure 9.4.2 in 3D space and by Figure 9.4.3 as projections onto the local dof $\tilde{x}_1 - \tilde{x}_2$ and $\tilde{x}_1 - \tilde{x}_3$ planes. The local coordinate twist dofs are illustrated in Figure 9.4.4.

These figures indicate that the 12×1 vector of nodal displacements for this element can be expressed in either local or global coordinates as follows:

Local:

$$\underline{\tilde{q}}_e = (\tilde{q}_1^e \ \tilde{q}_2^e \ \tilde{q}_3^e \ \tilde{q}_4^e \ \tilde{q}_5^e \ \tilde{q}_6^e \ \tilde{q}_7^e \ \tilde{q}_8^e \ \tilde{q}_9^e \ \tilde{q}_{10}^e \ \tilde{q}_{11}^e \ \tilde{q}_{12}^e)^T \quad (9.4.1)$$

Global:

$$\underline{q}_e = (q_1^e \ q_2^e \ q_3^e \ q_4^e \ q_5^e \ q_6^e \ q_7^e \ q_8^e \ q_9^e \ q_{10}^e \ q_{11}^e \ q_{12}^e)^T \quad (9.4.2)$$

Typically, both local and global displacements are utilized in a frame structure vibration study, that is, local coordinate displacements are used to calculate reaction force and stresses, and global coordinate displacements aid in visualizing the motion of the overall structure. The coordinate transformation matrix between the two sets of coordinates is used to derive element stiffness and mass matrices and force vectors and for computing reaction forces and stresses. In order to derive an easily programmable (software) form of this matrix, begin by considering displacement vector \vec{V} in Figure 9.4.5, where

$$\vec{V} = V_1 \hat{e}_1 + V_2 \hat{e}_2 + V_3 \hat{e}_3 = \tilde{V}_1 \hat{\tilde{e}}_1 + \tilde{V}_2 \hat{\tilde{e}}_2 + \tilde{V}_3 \hat{\tilde{e}}_3 \quad (9.4.3)$$

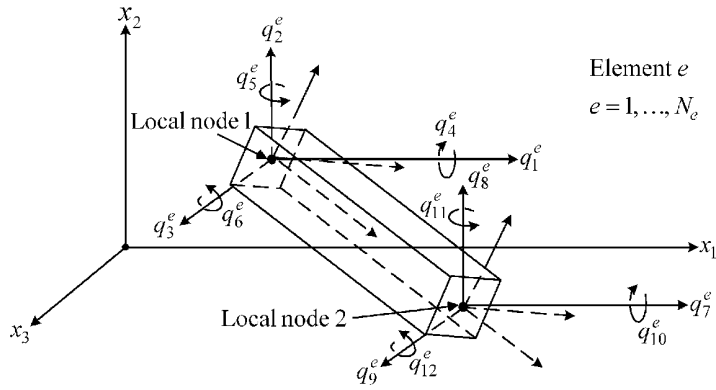


Figure 9.4.1 Nodal displacements for 3D beam element e in global coordinates

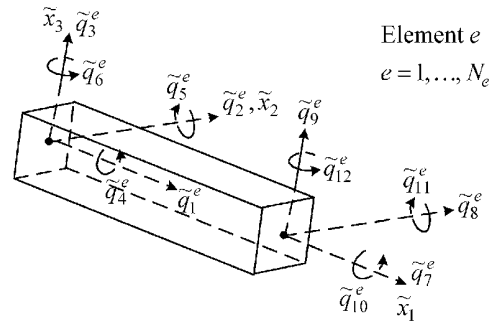


Figure 9.4.2 Nodal displacements of 3D beam element e in local coordinates

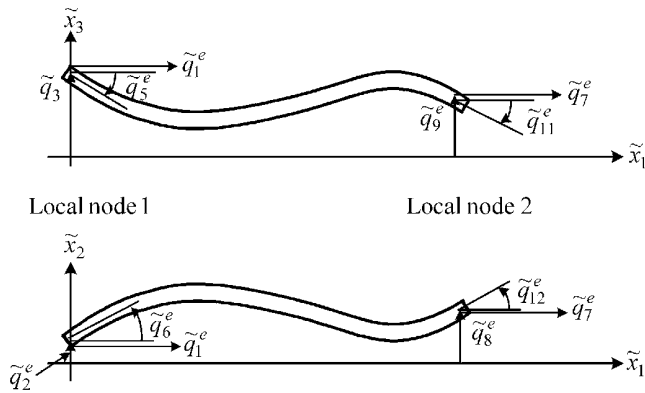


Figure 9.4.3 Projections of local coordinate displacements and slopes

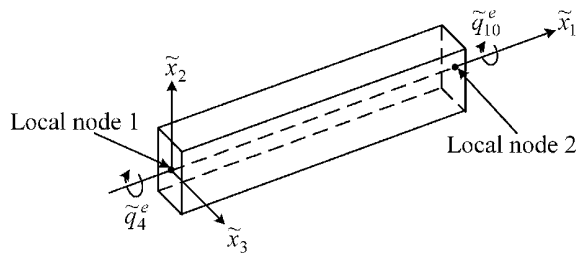


Figure 9.4.4 Twist dofs in the local coordinate system

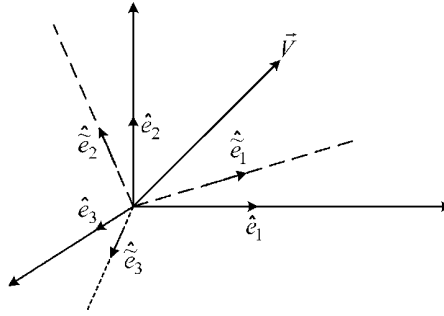


Figure 9.4.5 Vector \vec{V} and the local and global coordinate system unit vectors

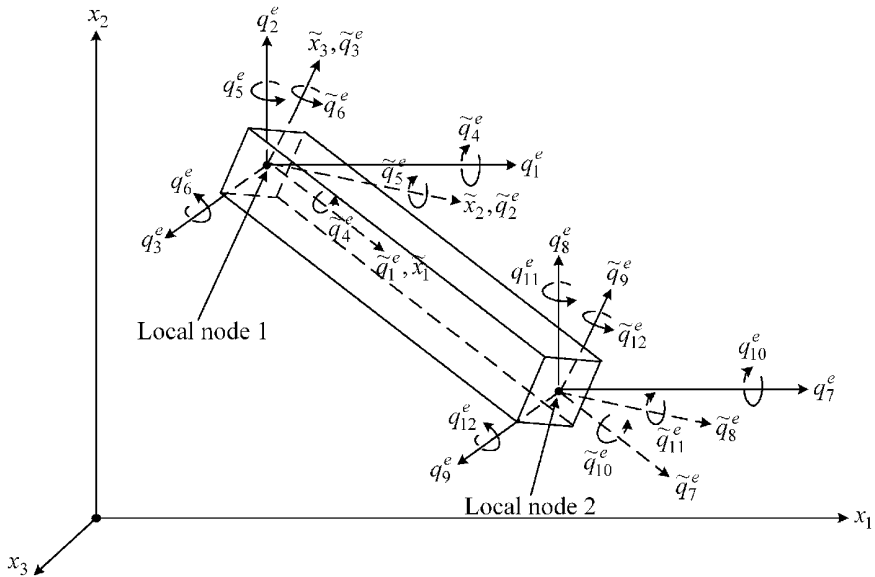


Figure 9.4.6 The 12 local and 12 global displacements at nodes 1 and 2 of element

Equations (2.7.5) and (2.7.6) apply for transforming the components of any vector between the two rotated coordinate systems in Figure 9.4.5, that is,

$$\begin{Bmatrix} \tilde{V}_1 \\ \tilde{V}_2 \\ \tilde{V}_3 \end{Bmatrix} = \begin{bmatrix} C_{11} & C_{12} & C_{13} \\ C_{21} & C_{22} & C_{23} \\ C_{31} & C_{32} & C_{33} \end{bmatrix} \begin{Bmatrix} V_1 \\ V_2 \\ V_3 \end{Bmatrix}, \quad C_{ij} = \cos(\angle \hat{e}_i, \hat{e}_j) \quad (9.4.4)$$

Figure 9.4.6 shows the local and global coordinate rotations and translations at each node on a 3D beam element. These are represented by displacement and small-angle rotation vectors in Figure 9.4.7.

The vectors in Figure 9.4.7 are expressed in both local and global coordinates as

$$\vec{V}_{T1} = q_1^e \hat{e}_1 + q_2^e \hat{e}_2 + q_3^e \hat{e}_3 = \tilde{q}_1^e \hat{e}_1 + \tilde{q}_2^e \hat{e}_2 + \tilde{q}_3^e \hat{e}_3 = \text{translation vector at local node 1} \quad (9.4.5)$$

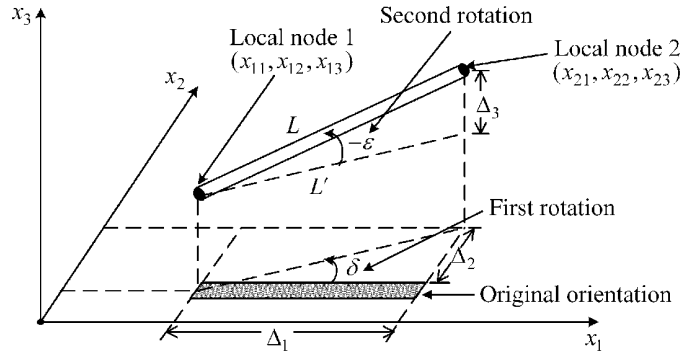


Figure 9.4.8 Orientation of beam element (e) via angles δ and ϵ

or

$$\begin{array}{ccc} \tilde{q}_e & = & \tilde{T}_e * q_e \\ \text{nodal displacement} & \text{transformation matrix} & \text{nodal displacement} \\ \text{in local coordinates} & & \text{in global coordinates} \end{array} \quad (9.4.11)$$

The direction cosines C_{ij} are expressed in terms of (Euler) angles through which the beam element is successively rotated starting with the beam element's local axes parallel to the global axes and ending with the beam element in its actual orientation in the system being modeled. The first two rotations (δ , ϵ) are depicted in Figure 9.4.8.

These rotation angles (δ , ϵ) are determined from the beam's nodal coordinates as follows. Let

$$\Delta_1 = X_{21} - X_{11}, \quad \Delta_2 = X_{22} - X_{12}, \quad \Delta_3 = X_{23} - X_{13} \quad (9.4.12)$$

$$L' = \sqrt{\Delta_1^2 + \Delta_2^2}, \quad L = \sqrt{\Delta_1^2 + \Delta_2^2 + \Delta_3^2} \quad (9.4.13)$$

then

$$\cos \delta = C\delta = \frac{\Delta_1}{L'}, \quad \sin \delta = S\delta = \frac{\Delta_2}{L'} \quad (9.4.14)$$

$$C\epsilon = \cos \epsilon = \cos(-\epsilon) = \frac{L'}{L}, \quad S\epsilon = \sin \epsilon = -\sin(-\epsilon) = -\frac{\Delta_3}{L} \quad (9.4.15)$$

The third (final) rotation γ is taken about the longitudinal axis of the beam and is usually determined from inspection by the modeler as illustrated by the example in Figure 9.4.9. The angle γ can be selected arbitrarily if the cross section is circular. In general, the beam will have two distinct area moments of inertia about its local \tilde{x}_2 and \tilde{x}_3 axes. Defining the angle γ then becomes an essential step for insuring the beam's cross section is properly oriented in the model.

The desired orientation is shown in Figure 9.4.9(a) and the local coordinates are shown in Figure 9.4.9(b). Imagine that the beam is originally oriented with its local coordinates ($\tilde{x}_1, \tilde{x}_2, \tilde{x}_3$) parallel to the global coordinates (x_1, x_2, x_3) as shown in Figure 9.4.9(c). Comparison with Figure 9.4.8 shows that successive rotations of

$$\delta = -90^\circ, \text{ then } \epsilon = 0^\circ, \text{ then } \gamma = +90^\circ \quad (9.4.16)$$

rotate the beam into its desired orientation in the frame model as shown in Figure 9.4.9(a).

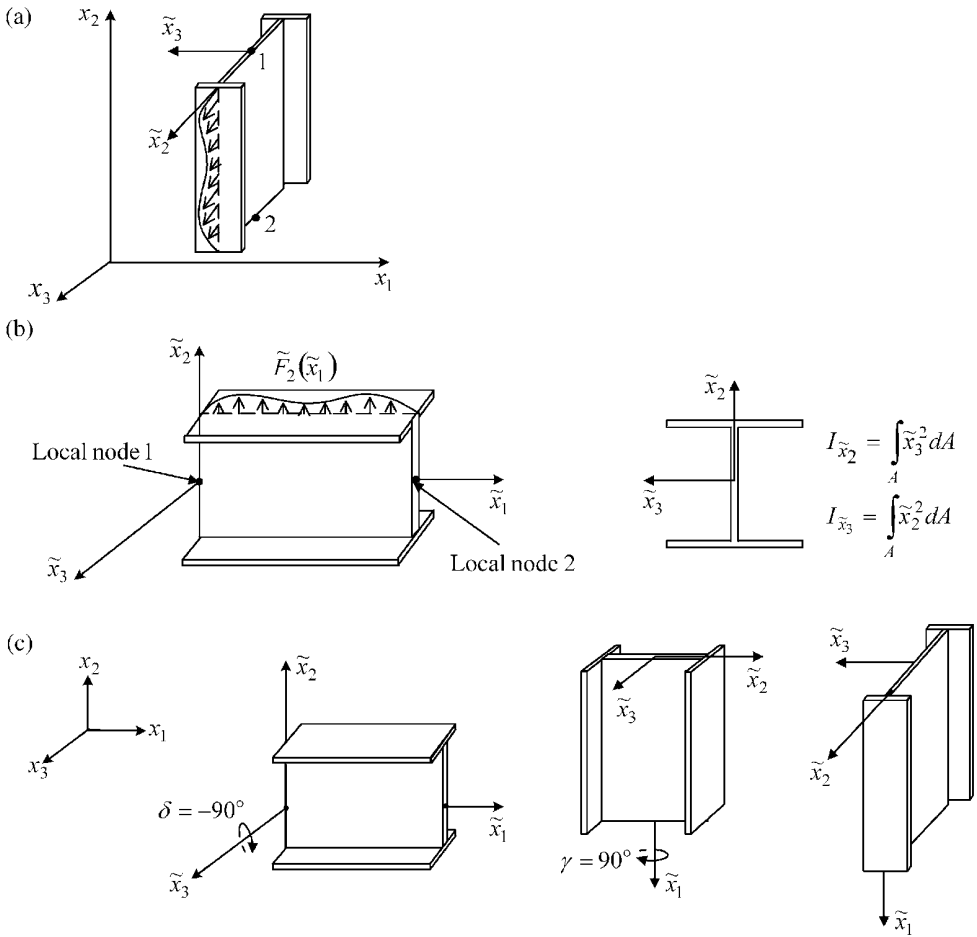


Figure 9.4.9 Determination of orientation angle γ for an I beam. (a) Actual orientation of element in assembled structure, (b) Starting orientation in sequence of rotations, and (c) Rotations between starting and actual orientations

The consecutive orientation angles for the general case are illustrated in Figure 9.4.10. Combining the rotations in Figure 9.4.10 yields

$$\begin{Bmatrix} \tilde{V}_1 \\ \tilde{V}_2 \\ \tilde{V}_3 \end{Bmatrix} = \begin{bmatrix} 1 & 0 & 0 \\ 0 & \cos\gamma & \sin\gamma \\ 0 & -\sin\gamma & \cos\gamma \end{bmatrix} \begin{bmatrix} \cos\varepsilon & 0 & -\sin\varepsilon \\ 0 & 1 & 0 \\ \sin\varepsilon & 0 & \cos\varepsilon \end{bmatrix} \begin{bmatrix} \cos\delta & \sin\delta & 0 \\ -\sin\delta & \cos\delta & 0 \\ 0 & 0 & 1 \end{bmatrix} \begin{Bmatrix} V_1 \\ V_2 \\ V_3 \end{Bmatrix} \quad (9.4.17)$$

or

$$\begin{Bmatrix} \tilde{V}_1 \\ \tilde{V}_2 \\ \tilde{V}_3 \end{Bmatrix} = \begin{bmatrix} C\varepsilon \cdot C\delta & C\varepsilon \cdot S\delta & -S\varepsilon \\ S\gamma \cdot S\varepsilon \cdot C\delta - C\gamma \cdot S\delta & S\gamma \cdot S\varepsilon \cdot S\delta + C\delta \cdot C\gamma & S\gamma \cdot C\varepsilon \\ S\varepsilon \cdot C\gamma \cdot C\delta + S\gamma \cdot S\delta & S\varepsilon \cdot C\gamma \cdot C\delta - S\gamma \cdot C\delta & C\gamma \cdot C\varepsilon \end{bmatrix} \begin{Bmatrix} V_1 \\ V_2 \\ V_3 \end{Bmatrix} = \begin{bmatrix} C_{11} & C_{12} & C_{13} \\ C_{21} & C_{22} & C_{23} \\ C_{31} & C_{32} & C_{33} \end{bmatrix} \begin{Bmatrix} V_1 \\ V_2 \\ V_3 \end{Bmatrix}$$

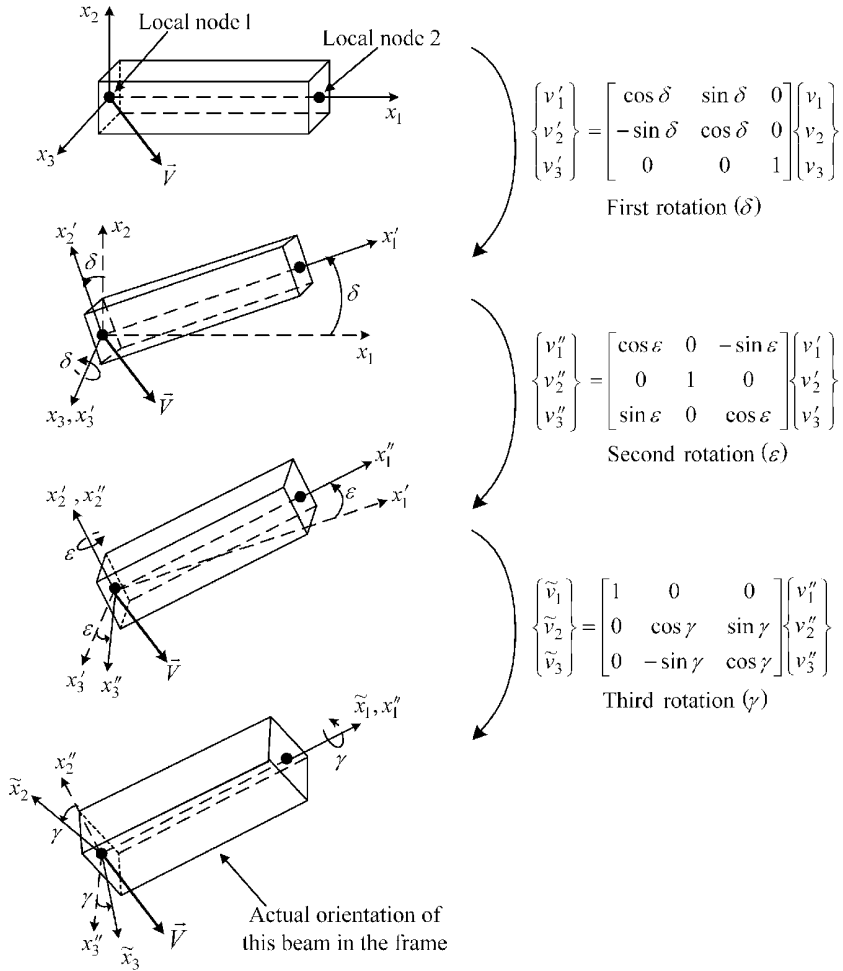


Figure 9.4.10 Orienting an element via three successive Euler angle rotations (δ, ϵ, γ)

where

$$C(\) \Rightarrow \cos(\) \text{ and } S(\) \Rightarrow \sin(\) \quad (9.4.18)$$

Substitution of (9.4.14) and (9.4.15) into (9.4.18) yields

$$\begin{Bmatrix} \tilde{V}_1 \\ \tilde{V}_2 \\ \tilde{V}_3 \end{Bmatrix} = \begin{bmatrix} \underbrace{\frac{\Delta_1}{L}}_{(C_{11})} & \underbrace{\frac{\Delta_2}{L}}_{(C_{12})} & \underbrace{\frac{\Delta_3}{L}}_{(C_{13})} \\ \underbrace{-\frac{\Delta_1 \Delta_3}{LL'} \sin \gamma - \frac{\Delta_2}{L'} \cos \gamma}_{(C_{21})} & \underbrace{-\frac{\Delta_2 \Delta_3}{LL'} \sin \gamma + \frac{\Delta_1}{L'} \cos \gamma}_{(C_{22})} & \underbrace{\frac{L'}{L} \sin \gamma}_{(C_{23})} \\ \underbrace{-\frac{\Delta_1 \Delta_3}{LL'} \cos \gamma + \frac{\Delta_2}{L'} \sin \gamma}_{(C_{31})} & \underbrace{-\frac{\Delta_2 \Delta_3}{LL'} \cos \gamma - \frac{\Delta_1}{L'} \sin \gamma}_{(C_{32})} & \underbrace{\frac{L'}{L} \cos \gamma}_{(C_{33})} \end{bmatrix} \times \begin{Bmatrix} V_1 \\ V_2 \\ V_3 \end{Bmatrix} \quad (9.4.19)$$

or

$$\tilde{\underline{V}} = \underline{C} \underline{V} \quad (9.4.20)$$

For the special case when the element is pointed along the x_3 axis

$$\Delta_1 = \Delta_2 = L' = 0 \quad (9.4.21)$$

which corresponds to

$$\delta = 0^\circ, \quad \varepsilon = \pm 90^\circ, \quad \gamma \text{ arbitrary} \quad (9.4.22)$$

Note that the $1/L'$ terms go to infinity in this case so Equation (9.4.19) should be replaced by

$$\begin{Bmatrix} \tilde{V}_1 \\ \tilde{V}_2 \\ \tilde{V}_3 \end{Bmatrix} = \begin{bmatrix} \underbrace{0}_{(C_{11})} & \underbrace{0}_{(C_{12})} & \underbrace{i_1}_{(C_{13})} \\ \underbrace{-i_1 \sin \gamma}_{(C_{21})} & \underbrace{\cos \gamma}_{(C_{22})} & \underbrace{0}_{(C_{23})} \\ \underbrace{-i_1 \cos \gamma}_{(C_{31})} & \underbrace{-\sin \gamma}_{(C_{32})} & \underbrace{0}_{(C_{33})} \end{bmatrix} \begin{Bmatrix} V_1 \\ V_2 \\ V_3 \end{Bmatrix} \quad \text{where } i_1 = \begin{cases} 1, & X_{13} < X_{23} \\ -1, & X_{13} > X_{23} \end{cases} \quad (9.4.23)$$

Equation (9.4.23) is obtained by substituting (9.4.22) into (9.4.18). The above transformation equations are also applicable to nodal force and moment vectors.

9.5 3D TIMOSHENKO BEAM ELEMENTS: SHAPE FUNCTIONS, ELEMENT STIFFNESS, AND MASS MATRICES

The Hermite cubic polynomial shape functions in (9.2.4) satisfy the static equilibrium equations and the consistency condition (9.2.5) for the unforced Euler–Bernoulli beam model. The shape functions satisfying similar conditions for the TB are not commonly shown in the literature and will be determined by solving the TB static equilibrium differential equations. The solution of the statics problem will also provide the element stiffness matrix in Lagrange's equations (4.7.61) for the element, that is,

$$\underline{M}_e \ddot{\underline{q}}_e + \underline{K}_e \underline{q}_e = \underline{Q}_e - \frac{\partial(\mathfrak{F}^c + \mathfrak{F}^d)}{\partial \dot{\underline{q}}_e} \quad (9.5.1)$$

The validity of obtaining the stiffness matrix by solving the static equilibrium equations instead of using the finite element equation (4.7.58)

$$\frac{\partial U}{\partial \underline{q}_e} = \underline{K}_e \underline{q}_e(t) \quad (9.5.2)$$

follows by noting that for statics problems the Lagrange equation

$$\frac{d}{dt} \left(\frac{\partial T}{\partial \dot{\underline{q}}_e} \right) - \frac{\partial T}{\partial \underline{q}_e} = \underline{Q}_e - \frac{\partial U}{\partial \underline{q}_e} - \frac{\partial(\mathfrak{F}^c + \mathfrak{F}^d)}{\partial \dot{\underline{q}}_e} \quad (9.5.3)$$

reduces to

$$\underline{Q}_e = \frac{\partial U}{\partial \underline{q}_e} \tag{9.5.4}$$

Thus, derivation of the stiffness matrix by relating forces and displacements in the statics problem solution (9.5.4) or by using the direct finite element approach (9.5.2) will produce identical results. The same shape functions obtained from the statics problem solution will also be used to derive the element mass matrix and force vector. So these terms may be referred to as the “consistent mass matrix” and “consistent element force” vector for the TB element. Related developments in the literature use the Euler–Bernoulli shape functions for determining the Timoshenko element mass matrix. This approach effectively expresses velocities in terms of shape functions that differ from those used for displacement interpolation when evaluating the element’s kinetic energy for obtaining the element mass matrix. The following development uses the same shape functions for deriving both the element mass and stiffness matrices, thereby producing a truly “consistent” element mass matrix.

The equations of motion utilize the strain–displacement relations for the element which differ from those used for Euler–Bernoulli beams. The Euler–Bernoulli beam kinematic constraint conditions are:

- (a) Plane sections remain plane.
- (b) Plane sections remain perpendicular to the neutral axis before and after deformation.

These assumptions imply that

$$\tilde{\epsilon}_{Bx3} = -\tilde{x}_2 \frac{\partial}{\partial \tilde{x}_1} \left(\frac{\partial \tilde{u}_2}{\partial \tilde{x}_1} \right) \tag{9.5.5}$$

where the coordinates and displacement are shown in Figure 9.5.1 and \tilde{u}_2 is the displacement of the neutral axis in the \tilde{x}_2 direction. This “beam curvature” formula previously appeared in Equation (14) of the Lagrange equation Example 4.6.3 and in (5.5.91) for the beam natural frequency derivation.

Constraint (b) was removed by (Timoshenko and Goodier, 1970) providing an additional deformation mode so that point a moves axially only to a'' instead of to a' , where $b-a'$ is perpendicular to the neutral axis.

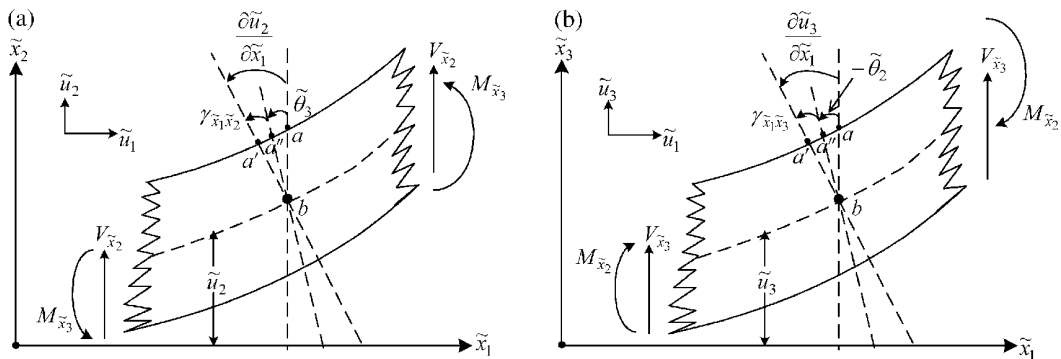


Figure 9.5.1 Kinematics for beam deformation in the (a) \tilde{x}_1 – \tilde{x}_2 and (b) \tilde{x}_1 – \tilde{x}_3 planes

9.5.1 Strain–Displacement Relations and Shear Form Factors

The neutral axis slope $\partial\tilde{u}_2/\partial\tilde{x}_1$ is replaced by the coordinate $\tilde{\theta}_3$ in (9.5.5) yielding

$$\tilde{\epsilon}_{Bx3} = -\tilde{x}_2 \frac{\partial\tilde{\theta}_3}{\partial\tilde{x}_1} \quad (9.5.6)$$

Similarly for the $\tilde{x}_1-\tilde{x}_3$ plane

$$\tilde{\epsilon}_{Bx2} = -\tilde{x}_3 \frac{\partial}{\partial\tilde{x}_1} (-\tilde{\theta}_2) = \tilde{x}_3 \frac{\partial\tilde{\theta}_2}{\partial\tilde{x}_1} \quad (9.5.7)$$

Shear strains are defined by Equation (A.3.16), that is,

$$\gamma_{\tilde{x}_1\tilde{x}_2} = \frac{\partial\tilde{u}_1}{\partial\tilde{x}_2} + \frac{\partial\tilde{u}_2}{\partial\tilde{x}_1}, \quad \gamma_{\tilde{x}_1\tilde{x}_3} = \frac{\partial\tilde{u}_1}{\partial\tilde{x}_3} + \frac{\partial\tilde{u}_3}{\partial\tilde{x}_1} \quad (9.5.8)$$

Note by Figure 9.5.1

$$\tilde{\theta}_3 = -\frac{\partial\tilde{u}_1}{\partial\tilde{x}_2}, \quad \tilde{\theta}_2 = \frac{\partial\tilde{u}_1}{\partial\tilde{x}_3} \quad (9.5.9)$$

so (9.5.8) may be written

$$\gamma_{\tilde{x}_1\tilde{x}_2} = -\tilde{\theta}_3 + \frac{\partial\tilde{u}_2}{\partial\tilde{x}_1}, \quad \gamma_{\tilde{x}_1\tilde{x}_3} = \tilde{\theta}_2 + \frac{\partial\tilde{u}_3}{\partial\tilde{x}_1} \quad (9.5.10)$$

which are consistent with Figure 9.5.1. Note if shear deformation is neglected

$$\gamma_{\tilde{x}_1\tilde{x}_2} = \gamma_{\tilde{x}_1\tilde{x}_3} = 0 \quad (9.5.11)$$

(9.5.10) implies

$$\tilde{\theta}_3 = \frac{\partial\tilde{u}_2}{\partial\tilde{x}_1}, \quad \tilde{\theta}_2 = -\frac{\partial\tilde{u}_3}{\partial\tilde{x}_1} \quad (9.5.12)$$

Substitution of (9.5.12) into (9.5.6) yields (9.5.5) as expected for Euler–Bernoulli beam theory.

Similar to shear strains, shear stresses vary over the cross section and with position along the beam, that is, from the constitutive law (A.4.3)

$$\tau_{\tilde{x}_1\tilde{x}_2} = G\gamma_{\tilde{x}_1\tilde{x}_2}(\tilde{x}_1, \tilde{x}_2, \tilde{x}_3), \quad \tau_{\tilde{x}_1\tilde{x}_3} = G\gamma_{\tilde{x}_1\tilde{x}_3}(\tilde{x}_1, \tilde{x}_2, \tilde{x}_3) \quad (9.5.13)$$

where G is the shear modulus of elasticity. The respective shear forces are

$$V_{\tilde{x}_2} = \int_{A(\tilde{x}_1)} \tau_{\tilde{x}_1\tilde{x}_2} dA = \tau_{\tilde{x}_1\tilde{x}_2}^{\text{ave}} A, \quad V_{\tilde{x}_3} = \int_{A(\tilde{x}_1)} \tau_{\tilde{x}_1\tilde{x}_3} dA = \tau_{\tilde{x}_1\tilde{x}_3}^{\text{ave}} A \quad (9.5.14)$$

where ave indicates the average value over the cross section. The “plane sections remain plane” assumption of Euler beam theory is retained by TB theory. Thus, from

Figure 9.5.1, the shear strains vary only with axial position (\tilde{x}_1). Define the “effective” shear stresses

$$\hat{\tau}_{\tilde{x}_1\tilde{x}_2}(\tilde{x}_1) = G\gamma_{\tilde{x}_1\tilde{x}_2}(\tilde{x}_1) \quad \text{and} \quad \hat{\tau}_{\tilde{x}_1\tilde{x}_3}(\tilde{x}_1) = G\gamma_{\tilde{x}_1\tilde{x}_3}(\tilde{x}_1) \quad (9.5.15)$$

which like the corresponding shear strains only vary with axial position (\tilde{x}_1). These are related to the average shear stresses by

$$\tau_{\tilde{x}_1\tilde{x}_2}^{\text{ave}} = k_2 \hat{\tau}_{\tilde{x}_1\tilde{x}_2}(\tilde{x}_1) = k_2 G\gamma_{\tilde{x}_1\tilde{x}_2}(\tilde{x}_1), \quad \tau_{\tilde{x}_1\tilde{x}_3}^{\text{ave}} = k_3 \hat{\tau}_{\tilde{x}_1\tilde{x}_3}(\tilde{x}_1) = k_3 G\gamma_{\tilde{x}_1\tilde{x}_3}(\tilde{x}_1) \quad (9.5.16)$$

Therefore, from (9.5.14) to (9.5.16),

$$V_{\tilde{x}_2} = k_2 A G \gamma_{\tilde{x}_1\tilde{x}_2}, \quad V_{\tilde{x}_3} = k_3 A G \gamma_{\tilde{x}_1\tilde{x}_3} \quad (9.5.17)$$

The factor k that relates the effective shear stresses to the average shear stresses

$$\tau_{\tilde{x}_1\tilde{x}_2}^{\text{ave}} = \frac{V_{\tilde{x}_2}}{A}, \quad \tau_{\tilde{x}_1\tilde{x}_3}^{\text{ave}} = \frac{V_{\tilde{x}_3}}{A} \quad (9.5.18)$$

has been determined so that the effective shear stresses in (9.5.15)

$$\hat{\tau}_{\tilde{x}_1\tilde{x}_2} = \frac{\tau_{\tilde{x}_1\tilde{x}_2}^{\text{ave}}}{k_2} = \frac{V_{\tilde{x}_2}}{k_2 A}, \quad \hat{\tau}_{\tilde{x}_1\tilde{x}_3} = \frac{\tau_{\tilde{x}_1\tilde{x}_3}^{\text{ave}}}{k_3} = \frac{V_{\tilde{x}_3}}{k_3 A} \quad (9.5.19)$$

acting over the effective areas

$$A_{s2} = k_2 A, \quad A_{s3} = k_3 A \quad (9.5.20)$$

produce the same strain energy as the actual shear stresses ($\tau_{\tilde{x}_1\tilde{x}_2}, \tau_{\tilde{x}_1\tilde{x}_3}$) acting over the actual cross section area A as discussed in Bathe (1982). Interesting discussions of k may be found in many references, such as Dym and Shames (1973) and Cowper (1966). Figure 9.5.2 shows the shear stress distribution on a rectangular cross section due to \tilde{x}_2 direction loading. The corresponding k value is from (Dym and Shames, 1973):

$$k = \frac{10(1+\nu)}{12+11\nu} \quad (9.5.21)$$

where ν is the Poisson’s ratio.

Shear form factors k from Cowper (1966) for other cross sections are provided in Figure 9.5.3. Note that from (9.5.17) the “no-shear” case can be studied by setting $1/(k_2 A G)$ and $1/(k_3 A G)$ to zero.

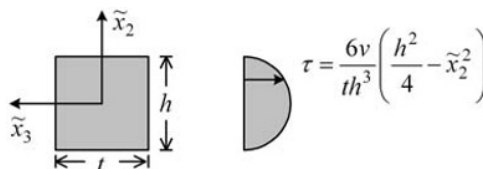


Figure 9.5.2 Shear stress distribution over the cross section of a rectangular-shaped beam

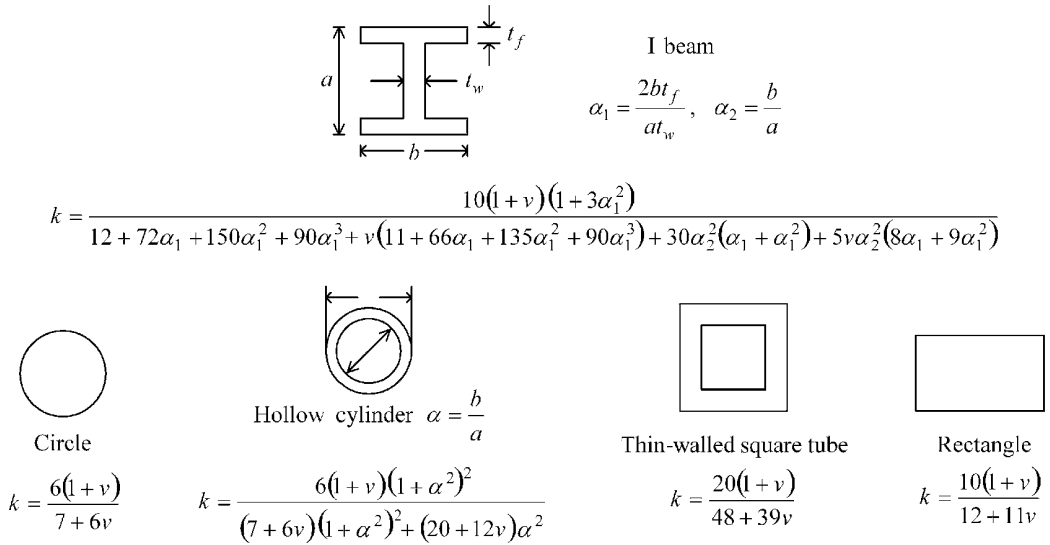
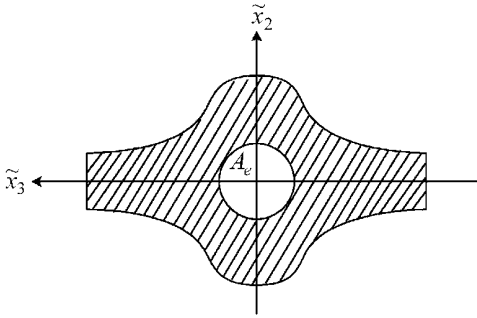


Figure 9.5.3 Shear form factors for some common cross sections (ν = Poisson ratio)

Other geometric properties of the beam's cross section include the area, and the area moments of inertia which are shown below:



Cross-Sectional Area:

$$A_e = \int_{A_e} d\tilde{x}_2 d\tilde{x}_3$$

Area Moments:

$$I_{\tilde{x}_2}^e = \int_{A_e} \tilde{x}_3^2 dA \quad \text{and} \quad I_{\tilde{x}_3}^e = \int_{A_e} \tilde{x}_2^2 dA \quad (9.5.22)$$

Torsion Constant:

$$J = \int_{A_e} f_T^2(\tilde{x}_2, \tilde{x}_3) dA$$

where f_T = torsion constant that depends on the shape of the cross section.

9.5.2 $\tilde{x}_1 - \tilde{x}_2$ Plane, Translational Differential Equations, Shape Functions, and Stiffness and Mass Matrices

The axial strain distribution due to an axial force $P_{\tilde{x}_1}$ and bending moment $M_{\tilde{x}_3}$ is illustrated in Figure 9.5.4.

The strain and stress are obtained from this figure and (9.5.6) as

$$\varepsilon_{\tilde{x}_1, \tilde{x}_1} = \frac{\partial \tilde{u}_1}{\partial \tilde{x}_1} - \tilde{x}_2 \frac{\partial \tilde{\theta}_3}{\partial \tilde{x}_1} \Rightarrow \sigma_{\tilde{x}_1, \tilde{x}_1} = E \varepsilon_{\tilde{x}_1, \tilde{x}_1} = E \frac{\partial \tilde{u}_1}{\partial \tilde{x}_1} - E \tilde{x}_2 \frac{\partial \tilde{\theta}_3}{\partial \tilde{x}_1} \quad (9.5.23)$$

The bending moment $\tilde{M}_{\tilde{x}_3}$ is the stress resultant

$$M_{\tilde{x}_3} = \int_A \tilde{x}_2 (-\sigma_{\tilde{x}_1, \tilde{x}_1}) dA = -E \frac{\partial \tilde{u}_1}{\partial \tilde{x}_1} \int_A \tilde{x}_2 dA + E \frac{\partial \tilde{\theta}_3}{\partial \tilde{x}_1} \int_A \tilde{x}_2^2 dA \quad (9.5.24)$$

The $\tilde{x}_2 dA$ integral is zero if the cross section is symmetric about the neutral axis. Therefore, substituting (9.5.22) into (9.5.24) yields

$$M_{\tilde{x}_3} = EI_{\tilde{x}_3} \frac{\partial \tilde{\theta}_3}{\partial \tilde{x}_1} \quad (9.5.25)$$

Consider equilibrium of the differential length beam with shear forces V and bending moments M as shown in Figure 9.5.5.

Taking moments about the left-hand side of the beam yields

$$M_{\tilde{x}_3} + \frac{\partial M_{\tilde{x}_3}}{\partial \tilde{x}_1} d\tilde{x}_1 + d\tilde{x}_1 \left(V_{\tilde{x}_2} + \frac{\partial V_{\tilde{x}_2}}{\partial \tilde{x}_1} d\tilde{x}_1 \right) - M_{\tilde{x}_3} = 0 \quad (9.5.26)$$

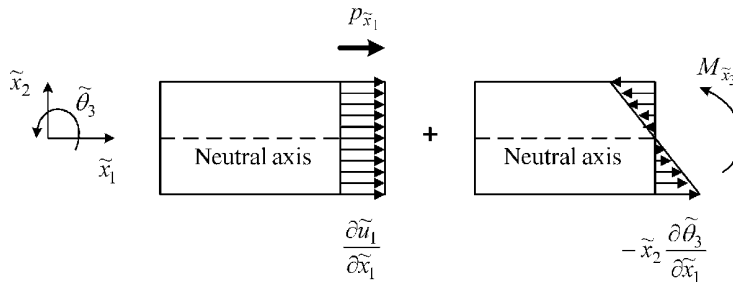


Figure 9.5.4 Axial strain distribution for $\tilde{x}_1 - \tilde{x}_2$ plane deformation

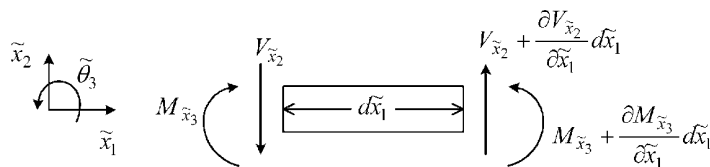


Figure 9.5.5 Free-body diagram of a differential beam in the $\tilde{x}_1 - \tilde{x}_2$ plane

and canceling second-order terms yields

$$\frac{\partial M_{\tilde{x}_3}}{\partial \tilde{x}_1} + V_{\tilde{x}_2} = 0 \quad (9.5.27)$$

Similarly, summing forces yields

$$-V_{\tilde{x}_2} + V_{\tilde{x}_2} + \frac{\partial V_{\tilde{x}_2}}{\partial \tilde{x}_1} d\tilde{x}_1 = 0 \Rightarrow \frac{\partial V_{\tilde{x}_2}}{\partial \tilde{x}_1} = 0 \quad (9.5.28)$$

Finally, recall from (9.5.10) and (9.5.17)

$$V_{\tilde{x}_2} = k_2 AG \gamma_{\tilde{x}_1 \tilde{x}_2} = k_2 AG \left(-\tilde{\theta}_3 + \frac{\partial \tilde{u}_2}{\partial \tilde{x}_1} \right) \quad (9.5.29)$$

or

$$\frac{\partial \tilde{u}_2}{\partial \tilde{x}_1} = \tilde{\theta}_3 + \frac{V_{\tilde{x}_2}}{k_2 AG} \quad (9.5.30)$$

Expressing Equations (9.5.25), (9.5.27), (9.5.28), and (9.5.30) in matrix form yields

Governing Equations for Static Beam Deformation in the $\tilde{x}_1 - \tilde{x}_2$ Plane

$$\frac{d\underline{z}^{12}}{d\tilde{x}_1} = \underline{G}^{12} \underline{z}^{12} \quad (4 \times 1) \quad (9.5.31)$$

where

$$\underline{z}^{12} = \begin{Bmatrix} \frac{D}{2 \times 1} \\ \frac{F}{2 \times 1} \end{Bmatrix} = \begin{Bmatrix} \tilde{u}_2 \\ \tilde{\theta}_3 \\ V_{\tilde{x}_2} \\ M_{\tilde{x}_3} \end{Bmatrix}, \quad \underline{G}^{12} = \begin{bmatrix} 0 & 1 & a_{12} & 0 \\ 0 & 0 & 0 & b_{12} \\ 0 & 0 & 0 & 0 \\ 0 & 0 & -1 & 0 \end{bmatrix}, \quad a_{12} = \frac{1}{k_2 AG}, \quad b_{12} = \frac{1}{EI_{\tilde{x}_3}} \quad (9.5.32)$$

The Maple code in Appendix B provides a symbolic solution of the system of ordinary differential equations in (9.5.31) and (9.5.32) for the state vector $\underline{z}^{12}(\tilde{x}_1)$ at an arbitrary location \tilde{x}_1 as shown in Figure 9.5.6 and with the initial conditions

$$\underline{z}^{12}(\tilde{x}_1 = 0) = (\tilde{u}_{20} \quad \tilde{\theta}_{30} \quad V_{\tilde{x}_2,0} \quad M_{\tilde{x}_3,0})^T \quad (9.5.33)$$

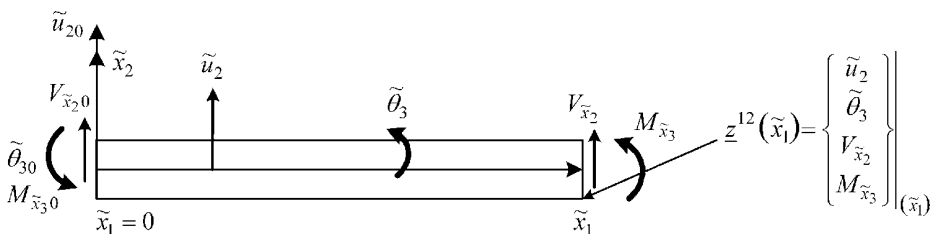


Figure 9.5.6 Free-body diagram of a beam in the $\tilde{x}_1 - \tilde{x}_2$ plane

The Appendix B Maple symbolic solution of (9.5.31) yields

$$\underline{z}(\tilde{x}_1) = \begin{Bmatrix} \underline{D} \\ \underline{F} \end{Bmatrix}_{2 \times 1} = \begin{Bmatrix} \tilde{u}_2 \\ \tilde{\theta}_3 \\ V_{\tilde{x}_2} \\ M_{\tilde{x}_3} \end{Bmatrix}_{(\tilde{x}_1)} = \begin{bmatrix} \underline{A}_{11} & \underline{A}_{12} \\ \underline{A}_{21} & \underline{A}_{22} \end{bmatrix}_{2 \times 2} \begin{Bmatrix} \tilde{u}_{20} \\ \tilde{\theta}_{30} \\ -V_{\tilde{x}_2 0} \\ -M_{\tilde{x}_3 0} \end{Bmatrix} \quad (9.5.34)$$

where

$$\underline{A}_{11} = \begin{bmatrix} 1 & \tilde{x}_1 \\ 0 & 1 \end{bmatrix}, \quad \underline{A}_{12} = \begin{bmatrix} -\frac{b_{12}}{6}\tilde{x}_1^3 + a_{12}\tilde{x}_1 & \frac{b_{12}}{2}\tilde{x}_1^2 \\ -\frac{b_{12}}{2}\tilde{x}_1^2 & b_{12}\tilde{x}_1 \end{bmatrix}, \quad \underline{A}_{21} = \begin{bmatrix} 0 & 0 \\ 0 & 0 \end{bmatrix}, \quad \underline{A}_{22} = \begin{bmatrix} 1 & 0 \\ -\tilde{x}_1 & 1 \end{bmatrix} \quad (9.5.35)$$

or

$$\begin{Bmatrix} \underline{D} \\ \underline{F} \end{Bmatrix}_{(\tilde{x}_1)} = \begin{bmatrix} \underline{A}_{11} & -\underline{A}_{12} \\ \underline{A}_{21} & -\underline{A}_{22} \end{bmatrix} \begin{Bmatrix} \underline{D}_0 \\ \underline{F}_0 \end{Bmatrix} \quad \text{where } \underline{D}_0 = \begin{Bmatrix} \tilde{u}_{20} \\ \tilde{\theta}_{30} \end{Bmatrix} \quad \text{and } \underline{F}_0 = \begin{Bmatrix} V_{\tilde{x}_2 0} \\ M_{\tilde{x}_3 0} \end{Bmatrix} \quad (9.5.36)$$

or

$$\underline{D}(\tilde{x}_1) = \underline{A}_{11}(\tilde{x}_1)\underline{D}_0 - \underline{A}_{12}(\tilde{x}_1)\underline{F}_0 \quad \text{and} \quad \underline{F}(\tilde{x}_1) = \underline{A}_{21}(\tilde{x}_1)\underline{D}_0 - \underline{A}_{22}(\tilde{x}_1)\underline{F}_0 \quad (9.5.37)$$

Evaluating at $\tilde{x}_1 = L$ yields

$$\underline{D}_L = \underline{D}(L) = \underline{A}_{11}(L)\underline{D}_0 - \underline{A}_{12}(L)\underline{F}_0 \quad \text{and} \quad \underline{F}_L = \underline{F}(L) = \underline{A}_{21}(L)\underline{D}_0 - \underline{A}_{22}(L)\underline{F}_0 \quad (9.5.38)$$

Solving for \underline{F}_0 yields

$$\underline{F}_0 = \underline{A}_{12}^{-1}(L) (-\underline{D}(L) + \underline{A}_{11}(L)\underline{D}_0) \quad (9.5.39)$$

Substitute (9.5.39) into $\underline{D}(\tilde{x}_1)$ in (9.5.37) to obtain

$$\underline{D}_{2 \times 1}(\tilde{x}_1) = \begin{Bmatrix} \tilde{u}_2(\tilde{x}_1) \\ \tilde{\theta}_3(\tilde{x}_1) \end{Bmatrix} = \underline{N}_{2 \times 4}^{12}(\tilde{x}_1) \begin{Bmatrix} \underline{D}_0 \\ \underline{D}_L \end{Bmatrix}_{2 \times 1} = \underline{N}_{2 \times 4}^{12}(\tilde{x}_1) \begin{Bmatrix} \tilde{u}_2(0) \\ \tilde{\theta}_3(0) \\ \tilde{u}_2(L) \\ \tilde{\theta}_3(L) \end{Bmatrix} \quad (9.5.40)$$

where

$$\begin{aligned} \underline{N}_{2 \times 4}^{12}(\tilde{x}_1) &= \begin{bmatrix} N_{11}^{12}(\tilde{x}_1) & N_{12}^{12}(\tilde{x}_1) & N_{13}^{12}(\tilde{x}_1) & N_{14}^{12}(\tilde{x}_1) \\ N_{21}^{12}(\tilde{x}_1) & N_{22}^{12}(\tilde{x}_1) & N_{23}^{12}(\tilde{x}_1) & N_{24}^{12}(\tilde{x}_1) \end{bmatrix} \\ &= [\underline{A}_{11}(\tilde{x}_1) - \underline{A}_{12}(\tilde{x}_1)\underline{A}_{12}^{-1}(L)\underline{A}_{11}(L) \quad \underline{A}_{12}(\tilde{x}_1)\underline{A}_{12}^{-1}(L)] \end{aligned} \quad (9.5.41)$$

The Maple code in Appendix B substitutes (9.5.35) into (9.5.41) to obtain the Timoshenko shape functions

$$\begin{aligned}
 N_{11}^{12} &= \gamma_1^{12} (L^3 + 2\tilde{x}_1^3 - 3\tilde{x}_1^2 L) + 12\gamma_2^{12} (L - \tilde{x}_1) \\
 N_{12}^{12} &= \gamma_1^{12} (\tilde{x}_1 L^3 + \tilde{x}_1^3 L - 2\tilde{x}_1^2 L^2) + 6\gamma_2^{12} \tilde{x}_1 (L - \tilde{x}_1) \\
 N_{13}^{12} &= -\gamma_1^{12} (2\tilde{x}_1^3 - 3\tilde{x}_1^2 L) + \gamma_2^{12} (12\tilde{x}_1) \\
 N_{14}^{12} &= \gamma_1^{12} (\tilde{x}_1^3 L - \tilde{x}_1^2 L^2) + 6\gamma_2^{12} \tilde{x}_1 (\tilde{x}_1 - L) \\
 N_{21}^{12} &= 6\gamma_1^{12} \tilde{x}_1 (\tilde{x}_1 - L) \\
 N_{22}^{12} &= \gamma_1^{12} (L^3 + 3\tilde{x}_1^2 L - 4\tilde{x}_1 L^2) + 12\gamma_2^{12} (L - \tilde{x}_1) \\
 N_{23}^{12} &= -6\gamma_1^{12} \tilde{x}_1 (\tilde{x}_1 - L) \\
 N_{24}^{12} &= \gamma_1^{12} \tilde{x}_1 (3\tilde{x}_1 L - 2L^2) + 12\gamma_2^{12} \tilde{x}_1
 \end{aligned} \tag{9.5.42}$$

where

$$\Phi_{12} = \frac{12EI_{\tilde{x}_3}}{k_2 AGL^2} = \frac{24I_{\tilde{x}_3}(1+\nu)}{k_2 AL^2}, \quad \gamma_1^{12} = \frac{1}{L^3(1+\Phi_{12})}, \quad \gamma_2^{12} = \frac{1}{12L(1+\Phi_{12}^{-1})} \tag{9.5.43}$$

and ν is the beam material's Poisson ratio. Note from (9.5.42)

$$\underline{N}^{12}(0) = \begin{bmatrix} 1 & 0 & 0 & 0 \\ 0 & 1 & 0 & 0 \end{bmatrix}, \quad \underline{N}^{12}(L) = \begin{bmatrix} 0 & 0 & 1 & 0 \\ 0 & 0 & 0 & 1 \end{bmatrix} \tag{9.5.44}$$

which must be the case since the interpolations in (9.5.40) must yield nodal values when evaluated at the node locations (consistency condition (2.11.37)). Shear deformation may be neglected by setting $1/(k_2 A)$ equal to zero, which from (9.5.43) yields

$$\Phi_{12} = 0, \quad \gamma_1^{12} = \frac{1}{L^3}, \quad \gamma_2^{12} = 0 \tag{9.5.45}$$

Substitution of (9.5.45) into (9.5.42) yields the Euler–Bernoulli beam, Hermite cubic polynomial shape functions, and their derivatives in (9.2.4) and (9.2.6). Thus, the TB shape functions differ from the Euler–Bernoulli shape functions.

From (9.5.38) and (9.5.39),

$$\underline{F}_L = (\underline{A}_{21}(L) - \underline{A}_{22}(L)\underline{A}_{12}^{-1}(L)\underline{A}_{11}(L))\underline{D}_0 + \underline{A}_{22}(L)\underline{A}_{12}^{-1}(L)\underline{D}_L \tag{9.5.46}$$

Equations (9.5.39) and (9.5.46) may be combined to form the matrix equation

$$\underline{F}^{12} = \begin{Bmatrix} \underline{F}_0 \\ \underline{F}_L \end{Bmatrix} = \begin{bmatrix} \underline{K}_{11}^{12} & \underline{K}_{12}^{12} \\ \underline{K}_{21}^{12} & \underline{K}_{22}^{12} \end{bmatrix} \begin{Bmatrix} \underline{D}_0 \\ \underline{D}_L \end{Bmatrix} = \tilde{\underline{K}}^{12} \underline{D}^{12} \tag{9.5.47}$$

where

$$\begin{aligned}
 \tilde{\underline{K}}_{11}^{12} &= \underline{A}_{12}^{-1}(L)\underline{A}_{11}(L), \quad \tilde{\underline{K}}_{12}^{12} = -\underline{A}_{12}^{-1}(L) \\
 \tilde{\underline{K}}_{21}^{12} &= \underline{A}_{21}(L) - \underline{A}_{22}(L)\underline{A}_{12}^{-1}(L)\underline{A}_{11}(L), \quad \tilde{\underline{K}}_{22}^{12} = \underline{A}_{22}(L)\underline{A}_{12}^{-1}(L)
 \end{aligned} \tag{9.5.48}$$

$$\underline{D}_0 = \begin{Bmatrix} \tilde{u}_{20} \\ \tilde{\theta}_{30} \end{Bmatrix}, \quad \underline{D}_L = \begin{Bmatrix} \tilde{u}_{2L} \\ \tilde{\theta}_{3L} \end{Bmatrix}, \quad \underline{D}^{12} = \begin{Bmatrix} \underline{D}_0 \\ \underline{D}_L \end{Bmatrix} = \begin{Bmatrix} \underline{D}_0 \\ \underline{D}_L \end{Bmatrix} = (\tilde{u}_{20} \quad \tilde{\theta}_{30} \quad \tilde{u}_{2L} \quad \tilde{\theta}_{3L})^T \quad (9.5.49)$$

$$\underline{F}_0 = \begin{Bmatrix} V_{\tilde{x}_2 0} \\ M_{\tilde{x}_3 0} \end{Bmatrix}, \quad \underline{F}_L = \begin{Bmatrix} V_{\tilde{x}_2 L} \\ M_{\tilde{x}_3 L} \end{Bmatrix} \quad (9.5.50)$$

The operations in (9.5.47) and (9.5.48) are performed symbolically in the Appendix B Maple code using the \underline{A}_{ij} in (9.5.35) yielding the $\tilde{x}_1 - \tilde{x}_2$ plane, bending plus shear, TB stiffness matrix

$$\tilde{K}_{4 \times 4}^{12} = \begin{bmatrix} \begin{matrix} (2) \\ \frac{12EI_{\tilde{x}_3}}{L^3(1+\Phi_{12})} \end{matrix} & \begin{matrix} (6) \\ \frac{6EI_{\tilde{x}_3}}{L^2(1+\Phi_{12})} \end{matrix} & \begin{matrix} (8) \\ \frac{-12EI_{\tilde{x}_3}}{L^3(1+\Phi_{12})} \end{matrix} & \begin{matrix} (12) \\ \frac{6EI_{\tilde{x}_3}}{L^2(1+\Phi_{12})} \end{matrix} \\ \begin{matrix} \frac{6EI_{\tilde{x}_3}}{L^2(1+\Phi_{12})} \end{matrix} & \begin{matrix} \frac{EI_{\tilde{x}_3}(4+\Phi_{12})}{L(1+\Phi_{12})} \end{matrix} & \begin{matrix} \frac{-6EI_{\tilde{x}_3}}{L^2(1+\Phi_{12})} \end{matrix} & \begin{matrix} \frac{EI_{\tilde{x}_3}(2-\Phi_{12})}{L(1+\Phi_{12})} \end{matrix} \\ \begin{matrix} \frac{-12EI_{\tilde{x}_3}}{L^3(1+\Phi_{12})} \end{matrix} & \begin{matrix} \frac{-6EI_{\tilde{x}_3}}{L^2(1+\Phi_{12})} \end{matrix} & \begin{matrix} \frac{12EI_{\tilde{x}_3}}{L^3(1+\Phi_{12})} \end{matrix} & \begin{matrix} \frac{-6EI_{\tilde{x}_3}}{L^2(1+\Phi_{12})} \end{matrix} \\ \begin{matrix} \frac{6EI_{\tilde{x}_3}}{L^2(1+\Phi_{12})} \end{matrix} & \begin{matrix} \frac{EI_{\tilde{x}_3}(2-\Phi_{12})}{L(1+\Phi_{12})} \end{matrix} & \begin{matrix} \frac{-6EI_{\tilde{x}_3}}{L^2(1+\Phi_{12})} \end{matrix} & \begin{matrix} \frac{EI_{\tilde{x}_3}(4+\Phi_{12})}{L(1+\Phi_{12})} \end{matrix} \end{bmatrix} \quad (9.5.51)$$

The numbers above and to the right of the matrix result from a comparison of Figures 9.4.3 and 9.5.6, which shows that the dofs for $\tilde{u}_{20}, \tilde{\theta}_{30}, \tilde{u}_{2L}$, and $\tilde{\theta}_{3L}$ are $\tilde{q}_2, \tilde{q}_6, \tilde{q}_8$, and \tilde{q}_{12} , respectively. Equation (9.5.45) may be substituted into (9.5.51) for the “no-shear deformation” case. This yields the previously obtained Euler–Bernoulli stiffness matrix (9.2.23b) (with rows and columns 1 and 4 deleted).

The element mass matrix is derived starting with consideration of the kinetic energy of the beam element. Figure 9.5.7 shows a differential slice of a uniform cross section beam element.

Generalization of (4.2.14) for small motions provides the kinetic energy of the differential length as

$$dT = \frac{1}{2} \bar{V}_G \cdot \bar{V}_G dm + \frac{1}{2} (\underline{\omega}^{b/n})^T \underline{I}_G^{B/b} \underline{\omega}^{b/n} \approx \frac{dm}{2} \left(\left(\frac{\partial \tilde{u}_1}{\partial t} \right)^2 + \left(\frac{\partial \tilde{u}_2}{\partial t} \right)^2 + \left(\frac{\partial \tilde{u}_3}{\partial t} \right)^2 \right) + \frac{\tilde{I}_1}{2} \left(\frac{\partial \tilde{\theta}_1}{\partial t} \right)^2 + \frac{\tilde{I}_2}{2} \left(\frac{\partial \tilde{\theta}_2}{\partial t} \right)^2 + \frac{\tilde{I}_3}{2} \left(\frac{\partial \tilde{\theta}_3}{\partial t} \right)^2 \quad (9.5.52)$$

where

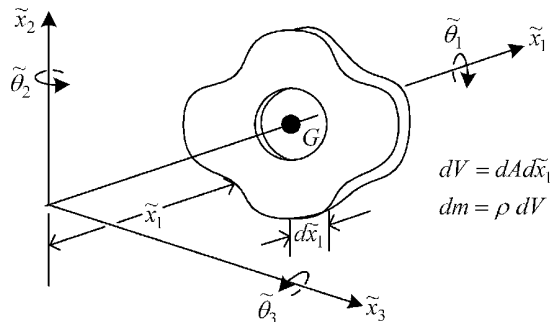


Figure 9.5.7 Differential length slice of a uniform beam element

$$\begin{aligned}
\tilde{I}_1 &= \int_A (\tilde{x}_2^2 + \tilde{x}_3^2) dm = \rho d\tilde{x}_1 \int_A (\tilde{x}_2^2 + \tilde{x}_3^2) dA = \rho J_p d\tilde{x}_1 \\
\tilde{I}_2 &= \int_A (d\tilde{x}_1^2 + \tilde{x}_3^2) dm \approx \int_A \tilde{x}_3^2 \rho dA d\tilde{x}_1 = \rho d\tilde{x}_1 I_{\tilde{x}_2} \\
\tilde{I}_3 &= \int_A (d\tilde{x}_1^2 + \tilde{x}_2^2) dm \approx \int_A \tilde{x}_2^2 \rho dA d\tilde{x}_1 = \rho d\tilde{x}_1 I_{\tilde{x}_3} \\
I_{\tilde{x}_2} &= \int_A \tilde{x}_3^2 dA = \text{area moment of inertia about the } \tilde{x}_2 \text{ axis} \\
I_{\tilde{x}_3} &= \int_A \tilde{x}_2^2 dA = \text{area moment of inertia about the } \tilde{x}_3 \text{ axis} \\
J_p &= \int_A (\tilde{x}_2^2 + \tilde{x}_3^2) dA = I_{\tilde{x}_2} + I_{\tilde{x}_3} = \text{area polar moment of inertia}
\end{aligned} \tag{9.5.53}$$

It then follows that the kinetic energy contributions from translation and rotation in the $\tilde{x}_1 - \tilde{x}_2$ plane are

$$T_{x_1x_2} = \underbrace{\frac{\rho A}{2} \int_0^L \left(\frac{\partial \tilde{u}_2}{\partial t} \right)^2 d\tilde{x}_1}_{\text{translation term}} + \underbrace{\frac{\rho I_{\tilde{x}_3}}{2} \int_0^L \left(\frac{\partial \tilde{\theta}_3}{\partial t} \right)^2 d\tilde{x}_1}_{\text{rotary inertia term}} \tag{9.5.54}$$

Recall from (9.5.40) and (9.5.41)

$$\tilde{u}_2(x, t) = \underline{N}_{12u}(\tilde{x}_1) \tilde{\underline{u}}_{12}(t) = [N_{11}^{12} \quad N_{12}^{12} \quad N_{13}^{12} \quad N_{14}^{12}] * (\tilde{u}_{20} \quad \tilde{\theta}_{30} \quad \tilde{u}_{2L} \quad \tilde{\theta}_{3L})^T \tag{9.5.55}$$

$$\tilde{\theta}_3(x, t) = \underline{N}_{12\theta}(\tilde{x}_1) \tilde{\underline{u}}_{12}(t) = [N_{21}^{12} \quad N_{22}^{12} \quad N_{23}^{12} \quad N_{24}^{12}] * (\tilde{u}_{20} \quad \tilde{\theta}_{30} \quad \tilde{u}_{2L} \quad \tilde{\theta}_{3L})^T \tag{9.5.56}$$

where the shape functions N_{ij}^{12} are defined in (9.5.42). Utilize (9.5.54)–(9.5.56) and the identity in (2.6.46) to obtain

$$T_{x_1x_2} = \frac{1}{2} \dot{\underline{u}}_{12}^T \tilde{\underline{M}}_{12u} \dot{\underline{u}}_{12} + \frac{1}{2} \dot{\underline{u}}_{12}^T \tilde{\underline{M}}_{12\theta} \dot{\underline{u}}_{12} \tag{9.5.57}$$

where $\tilde{\underline{u}}_{12} = (\tilde{u}_{20} \quad \tilde{\theta}_{30} \quad \tilde{u}_{2L} \quad \tilde{\theta}_{3L})^T$ and the translation and rotary inertia, consistent mass matrices are (as in (4.7.47))

$$\tilde{\underline{M}}_{12u} = \rho A \int_0^L \underline{N}_{12u}^T \underline{N}_{12u} d\tilde{x}_1, \quad \tilde{\underline{M}}_{12\theta} = \rho I_{\tilde{x}_3} \int_0^L \underline{N}_{12\theta}^T \underline{N}_{12\theta} d\tilde{x}_1 \tag{9.5.58}$$

The fact that these are the mass matrices in the Newton's law inertia force term follows from the Lagrange's equation expression (4.5.106b) and the quadratic form vector differentiation identity ((2.6.41), (2.6.42a), (2.6.42b)):

$$\underline{f}_{iner} = \frac{d}{dt} \left(\frac{\partial T}{\partial \dot{\underline{q}}} \right) = \frac{d}{dt} (\tilde{\underline{M}}_e \dot{\underline{u}}) = \tilde{\underline{M}}_e \ddot{\underline{u}} \tag{9.5.59}$$

Comparison of Figures 9.4.3 and 9.5.6 shows that $\tilde{u}_{20}, \tilde{\theta}_{30}, \tilde{u}_{2L}$, and $\tilde{\theta}_{3L}$ are dofs $\tilde{q}_2, \tilde{q}_6, \tilde{q}_8$, and \tilde{q}_{12} , respectively. The integrations in (9.5.58) are performed in the Appendix B Maple code yielding the results

$$\tilde{M}_{12u} = \frac{\rho AL}{420 * (b_{12}L^2 + 12a_{12})^2} \begin{bmatrix} a_1^{12u} & & & \\ a_2^{12u} & a_5^{12u} & \text{symmetric} & \\ a_3^{12u} & -a_4^{12u} & a_1^{12u} & \\ a_4^{12u} & a_6^{12u} & -a_2^{12u} & a_3^{12u} \end{bmatrix} \quad (9.5.60)$$

where

$$\begin{aligned} a_1^{12u} &= 156b_{12}^2L^4 + 3528a_{12}b_{12}L^2 + 20160a_{12}^2, & a_2^{12u} &= 2L(11b_{12}^2L^4 + 231a_{12}b_{12}L^2 + 1260a_{12}^2) \\ a_3^{12u} &= 54b_{12}^2L^4 + 1512a_{12}b_{12}L^2 + 10080a_{12}^2, & a_4^{12u} &= -L(13b_{12}^2L^4 + 378a_{12}b_{12}L^2 + 2520a_{12}^2) \\ a_5^{12u} &= L^2(4b_{12}^2L^4 + 84a_{12}b_{12}L^2 + 504a_{12}^2), & a_6^{12u} &= -3L^2(b_{12}^2L^4 + 28a_{12}b_{12}L^2 + 168a_{12}^2) \end{aligned} \quad (9.5.61)$$

$$\tilde{M}_{12\theta} = \frac{\rho I_{\bar{x}_3} L}{30 * (b_{12}L^2 + 12a_{12})^2} \begin{bmatrix} a_1^{12\theta} & & & \\ a_2^{12\theta} & a_3^{12\theta} & \text{symmetric} & \\ -a_1^{12\theta} & -a_2^{12\theta} & a_1^{12\theta} & \\ a_2^{12\theta} & a_4^{12\theta} & -a_2^{12\theta} & a_3^{12\theta} \end{bmatrix} \quad (9.5.62)$$

where

$$\begin{aligned} a_1^{12\theta} &= 36b_{12}^2L^2, & a_2^{12\theta} &= -3Lb_{12}(-b_{12}L^2 + 60a_{12}) \\ a_3^{12\theta} &= 4b_{12}^2L^4 + 60a_{12}b_{12}L^2 + 1440a_{12}^2, & a_4^{12\theta} &= -b_{12}^2L^4 - 60a_{12}b_{12}L^2 + 720a_{12}^2 \end{aligned} \quad (9.5.63)$$

where a_{12} and b_{12} are defined in (9.5.32). For the case of no-shear deformation ($a_{12} = 0$), these matrices become

$$\tilde{M}_{12u} \Big|_{a_{12}=0} = \frac{\rho AL}{420} \begin{bmatrix} 156 & & & \\ 22L & 4L^2 & \text{symmetric} & \\ 54 & 13L & 156 & \\ -13L & -3L^2 & -22L & 4L^2 \end{bmatrix} \quad (9.5.64)$$

$$\tilde{M}_{12\theta} \Big|_{a_{12}=0} = \frac{\rho I_{\bar{x}_3}}{30L} \begin{bmatrix} 36 & & & \\ 3L & 4L^2 & \text{symmetric} & \\ -36 & -3L & 36 & \\ 3L & -L^2 & -3L & 4L^2 \end{bmatrix} \quad (9.5.65)$$

The translational, consistent mass matrix in (9.5.64) appears in some finite element and vibration books, such as Cook et al. (1989).

9.5.3 $\tilde{x}_1 - \tilde{x}_3$ Plane, Translational Differential Equations, Shape Functions, and Stiffness and Mass Matrices

The axial strain distribution due to an axial force $P_{\tilde{x}_1}$ and bending moment $M_{\tilde{x}_2}$ is shown in Figure 9.5.8.

The strain and stress are obtained from this figure and Equation (9.5.7) as

$$\varepsilon_{\tilde{x}_1\tilde{x}_1} = \frac{\partial \tilde{u}_1}{\partial \tilde{x}_1} + \tilde{x}_3 \frac{\partial \tilde{\theta}_2}{\partial \tilde{x}_1} \Rightarrow \sigma_{\tilde{x}_1\tilde{x}_1} = E\varepsilon_{\tilde{x}_1\tilde{x}_1} = E \frac{\partial \tilde{u}_1}{\partial \tilde{x}_1} + E\tilde{x}_3 \frac{\partial \tilde{\theta}_2}{\partial \tilde{x}_1} \quad (9.5.66)$$

The bending moment $\tilde{M}_{\tilde{x}_2}$ is the stress resultant

$$\tilde{M}_{\tilde{x}_2} = \int_A \tilde{x}_3 (-\sigma_{\tilde{x}_1\tilde{x}_1}) dA = -E \frac{\partial \tilde{u}_1}{\partial \tilde{x}_1} \int_A \tilde{x}_3 dA + E \frac{\partial \tilde{\theta}_2}{\partial \tilde{x}_1} \int_A \tilde{x}_3^2 dA \quad (9.5.67)$$

The $\tilde{x}_3 dA$ integral is zero if the cross section is symmetric about the neutral axis. Therefore, substituting (9.5.22) into (9.5.67) yields

$$\tilde{M}_{\tilde{x}_2} = EI_{\tilde{x}_2} \frac{\partial \tilde{\theta}_2}{\partial \tilde{x}_1} \quad (9.5.68)$$

Consider the equilibrium of the differential length beam with shear force V and bending moment M , as shown in Figure 9.5.9.

Taking moments about the left-hand side of the beam yields

$$\tilde{M}_{\tilde{x}_2} + \frac{\partial \tilde{M}_{\tilde{x}_2}}{\partial \tilde{x}_1} d\tilde{x}_1 - d\tilde{x}_1 \left(V_{\tilde{x}_3} + \frac{\partial V_{\tilde{x}_3}}{\partial \tilde{x}_1} d\tilde{x}_1 \right) - \tilde{M}_{\tilde{x}_2} = 0 \quad (9.5.69)$$

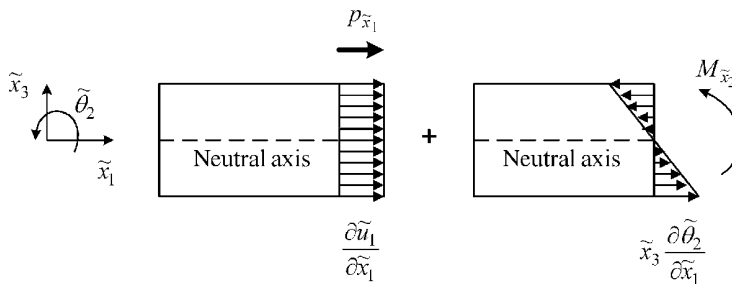


Figure 9.5.8 Axial strain distribution for $\tilde{x}_1 - \tilde{x}_3$ plane deformation

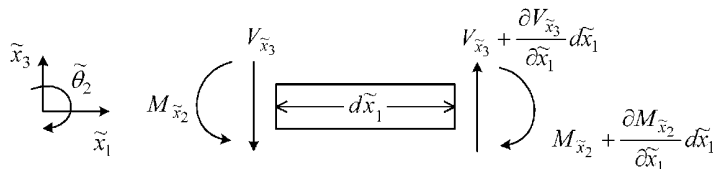


Figure 9.5.9 Free-body diagram of a differential beam in the $\tilde{x}_1 - \tilde{x}_3$ plane

and canceling second-order terms yields

$$\frac{\partial M_{\tilde{x}_2}}{\partial \tilde{x}_1} - V_{\tilde{x}_3} = 0 \quad (9.5.70)$$

Similarly, summing forces yields

$$-\tilde{V}_{\tilde{x}_3} + V_{\tilde{x}_3} + \frac{\partial V_{\tilde{x}_3}}{\partial \tilde{x}_1} d\tilde{x}_1 = 0 \Rightarrow \frac{\partial V_{\tilde{x}_3}}{\partial \tilde{x}_1} = 0 \quad (9.5.71)$$

Finally, recall from (9.5.10) and (9.5.17)

$$V_{\tilde{x}_3} = k_3 AG \gamma_{\tilde{x}_1, \tilde{x}_3} = k_3 AG \left(\tilde{\theta}_2 + \frac{\partial \tilde{u}_3}{\partial \tilde{x}_1} \right) \quad (9.5.72)$$

or

$$\frac{\partial \tilde{u}_3}{\partial \tilde{x}_1} = -\tilde{\theta}_2 + \frac{V_{\tilde{x}_3}}{k_3 AG} \quad (9.5.73)$$

Expressing Equations (9.5.68), (9.5.70), (9.5.71), and (9.5.73) in matrix form yields

Governing Equations for Static Beam Deformation in the $\tilde{x}_1 - \tilde{x}_3$ Plane

$$\frac{d\underline{z}^{13}}{dx_1} = \underline{G}^{13} \underline{z}^{13} \quad (4 \times 1) \quad (9.5.74)$$

where

$$\underline{z}^{13} = \begin{Bmatrix} \frac{D}{2 \times 1} \\ \frac{F}{2 \times 1} \end{Bmatrix} = \begin{Bmatrix} \tilde{u}_3 \\ \tilde{\theta}_2 \\ V_{\tilde{x}_3} \\ M_{\tilde{x}_2} \end{Bmatrix}, \quad \underline{G}_{13} = \begin{bmatrix} 0 & -1 & a_{13} & 0 \\ 0 & 0 & 0 & b_{13} \\ 0 & 0 & 0 & 0 \\ 0 & 0 & 1 & 0 \end{bmatrix}, \quad a_{13} = \frac{1}{k_3 AG}, \quad b_{13} = \frac{1}{EI_{\tilde{x}_2}} \quad (9.5.75)$$

The Maple code in Appendix B provides a symbolic solution of the system of ordinary differential equations in (9.5.74) and (9.5.75) yielding

$$\hat{\underline{z}}(\tilde{x}_1) = \begin{Bmatrix} \hat{D} \\ \hat{F} \end{Bmatrix}_{(\tilde{x}_1)} = \begin{Bmatrix} \tilde{u}_3 \\ \tilde{\theta}_2 \\ V_{\tilde{x}_3} \\ M_{\tilde{x}_2} \end{Bmatrix}_{(\tilde{x}_1)} = \begin{bmatrix} \hat{A}_{11} & \hat{A}_{12} \\ \hat{A}_{21} & \hat{A}_{22} \end{bmatrix}_{\substack{2 \times 2 & 2 \times 2 \\ 2 \times 2 & 2 \times 2}} \begin{Bmatrix} \tilde{u}_{30} \\ \tilde{\theta}_{20} \\ -V_{\tilde{x}_3 0} \\ -M_{\tilde{x}_2 0} \end{Bmatrix} \quad (9.5.76)$$

where

$$\hat{A}_{2 \times 2} = \begin{bmatrix} 1 & -\tilde{x}_1 \\ 0 & 1 \end{bmatrix}, \quad \hat{A}_{2 \times 2} = \begin{bmatrix} -\frac{b_{13}}{6} \tilde{x}_1^3 + a_{13} \tilde{x}_1 & -\frac{b_{13}}{2} \tilde{x}_1^2 \\ \frac{b_{13}}{2} \tilde{x}_1^2 & b_{13} \tilde{x}_1 \end{bmatrix}, \quad \hat{A}_{2 \times 2} = \begin{bmatrix} 0 & 0 \\ 0 & 0 \end{bmatrix}, \quad \hat{A}_{2 \times 2} = \begin{bmatrix} 1 & 0 \\ \tilde{x}_1 & 1 \end{bmatrix} \quad (9.5.77)$$

Eq. (9.5.76) becomes

$$\begin{Bmatrix} \hat{D} \\ \hat{F} \end{Bmatrix}_{(\tilde{x}_1)} = \begin{bmatrix} \hat{A}_{11} & -\hat{A}_{12} \\ \hat{A}_{21} & -\hat{A}_{22} \end{bmatrix} \begin{Bmatrix} \hat{D}_0 \\ \hat{F}_0 \end{Bmatrix} \quad (9.5.78)$$

where

$$\hat{D}_0 = \begin{Bmatrix} \tilde{u}_{30} \\ \tilde{\theta}_{20} \end{Bmatrix}, \quad \hat{F}_0 = \begin{Bmatrix} V_{\tilde{x}_3 0} \\ M_{\tilde{x}_2 0} \end{Bmatrix} \quad (9.5.79)$$

For arbitrary \tilde{x}_1 , Equation (9.5.78) becomes

$$\hat{D}(\tilde{x}_1) = \hat{A}_{11}(\tilde{x}_1)\hat{D}_0 - \hat{A}_{12}(\tilde{x}_1)\hat{F}_0, \quad \hat{F}(\tilde{x}_1) = \hat{A}_{21}(\tilde{x}_1)\hat{D}_0 - \hat{A}_{22}(\tilde{x}_1)\hat{F}_0 \quad (9.5.80)$$

Evaluating at $\tilde{x}_1 = L$ yields

$$\hat{D}_L = \hat{D}(L) = \hat{A}_{11}(L)\hat{D}_0 - \hat{A}_{12}(L)\hat{F}_0, \quad \hat{F}_L = \hat{F}(L) = \hat{A}_{21}(L)\hat{D}_0 - \hat{A}_{22}(L)\hat{F}_0 \quad (9.5.81)$$

Solving for \hat{F}_0 yields

$$\hat{F}_0 = \hat{A}_{12}^{-1}(L)(-\hat{D}(L) + \hat{A}_{11}(L)\hat{D}_0) \quad (9.5.82)$$

Substitute (9.5.82) into $\hat{D}(\tilde{x}_1)$ in (9.5.80) to obtain

$$\hat{D}_{\frac{2 \times 1}{\tilde{x}_1}}(\tilde{x}_1) = \begin{Bmatrix} \tilde{u}_3(\tilde{x}_1) \\ \tilde{\theta}_2(\tilde{x}_1) \end{Bmatrix} = \underline{N}_{\frac{2 \times 4}{\tilde{x}_1}}(\tilde{x}_1) \begin{Bmatrix} \hat{D}_0 \\ \hat{F}_0 \end{Bmatrix} = \underline{N}_{\frac{2 \times 4}{\tilde{x}_1}}(\tilde{x}_1) \begin{Bmatrix} \tilde{u}_3(0) \\ \tilde{\theta}_2(0) \\ \tilde{u}_3(L) \\ \tilde{\theta}_2(L) \end{Bmatrix} \quad (9.5.83)$$

where

$$\begin{aligned} \underline{N}_{13}(\tilde{x}_1) &= \begin{bmatrix} N_{11}^{13}(\tilde{x}_1) & N_{12}^{13}(\tilde{x}_1) & N_{13}^{13}(\tilde{x}_1) & N_{14}^{13}(\tilde{x}_1) \\ N_{21}^{13}(\tilde{x}_1) & N_{22}^{13}(\tilde{x}_1) & N_{23}^{13}(\tilde{x}_1) & N_{24}^{13}(\tilde{x}_1) \end{bmatrix} \\ &= \begin{bmatrix} \hat{A}_{11}(\tilde{x}_1) - \hat{A}_{12}(\tilde{x}_1)\hat{A}_{12}^{-1}(L)\hat{A}_{11}(L) & \hat{A}_{12}(\tilde{x}_1)\hat{A}_{12}^{-1}(L) \end{bmatrix} \end{aligned} \quad (9.5.84)$$

The manipulations indicated above are performed in the Maple code in Appendix B yielding the following “TB” shape functions:

$$\begin{aligned} N_{11}^{13} &= \gamma_1^{13}(L^3 + 2\tilde{x}_1^3 - 3\tilde{x}_1^2L) + 12\gamma_2^{13}(L - \tilde{x}_1) \\ N_{12}^{13} &= -\gamma_1^{13}(\tilde{x}_1L^3 + \tilde{x}_1^3L - 2\tilde{x}_1^2L^2) - 6\gamma_2^{13}\tilde{x}_1(L - \tilde{x}_1) \\ N_{13}^{13} &= -\gamma_1^{13}(2\tilde{x}_1^3 - 3\tilde{x}_1^2L) + \gamma_2^{13}(12\tilde{x}_1) \\ N_{14}^{13} &= -\gamma_1^{13}(\tilde{x}_1^3L - \tilde{x}_1^2L^2) - 6\gamma_2^{13}\tilde{x}_1(\tilde{x}_1 - L) \\ N_{21}^{13} &= -6\gamma_1^{13}\tilde{x}_1(\tilde{x}_1 - L) \\ N_{22}^{13} &= \gamma_1^{13}(L^3 + 3\tilde{x}_1^2L - 4\tilde{x}_1L^2) + 12\gamma_2^{13}(L - \tilde{x}_1) \\ N_{23}^{13} &= 6\gamma_1^{13}\tilde{x}_1(\tilde{x}_1 - L) \\ N_{24}^{13} &= \gamma_1^{13}\tilde{x}_1(3\tilde{x}_1L - 2L^2) + 12\gamma_2^{13}\tilde{x}_1 \end{aligned} \quad (9.5.85)$$

where

$$\Phi_{13} = \frac{12EI_{\tilde{x}_2}}{k_{13}AGL^2} = \frac{24I_{\tilde{x}_2}(1+\nu)}{k_{13}AL^2}, \quad \gamma_1^{13} = \frac{1}{L^3(1+\Phi_{13})}, \quad \gamma_2^{13} = \frac{\Phi_{13}}{12L(1+\Phi_{13})} = \frac{1}{12L(1+\Phi_{13}^{-1})} \quad (9.5.86)$$

where ν is the beam material's Poisson ratio.

Performing similar operations as in the $\tilde{x}_1-\tilde{x}_2$ plane case with the $\underline{A}_{i,j}$ from (9.5.77) yields the following result from the Maple code in Appendix B:

$$\underline{F}_{13} = \begin{Bmatrix} \underline{F}_0 \\ \underline{F}_L \end{Bmatrix} = \begin{bmatrix} \underline{K}_{11}^{13} & \underline{K}_{12}^{13} \\ \underline{K}_{21}^{13} & \underline{K}_{22}^{13} \end{bmatrix} \begin{Bmatrix} \underline{D}_0 \\ \underline{D}_L \end{Bmatrix} = \underline{\tilde{K}}^{13} \underline{D}_{13} \quad (9.5.87)$$

where

$$\underline{D}_0 = \begin{Bmatrix} \tilde{u}_{30} \\ \tilde{\theta}_{20} \end{Bmatrix}, \quad \underline{D}_L = \begin{Bmatrix} \tilde{u}_{3L} \\ \tilde{\theta}_{2L} \end{Bmatrix}, \quad \underline{F}_0 = \begin{Bmatrix} V_{\tilde{x}_3 0} \\ M_{\tilde{x}_2 0} \end{Bmatrix}, \quad \underline{F}_L = \begin{Bmatrix} V_{\tilde{x}_3 L} \\ M_{\tilde{x}_2 L} \end{Bmatrix} \quad (9.5.88)$$

The $\tilde{x}_1-\tilde{x}_3$ plane, bending plus shear, TB stiffness matrix is

$$\underline{\tilde{K}}_{4 \times 4}^{13} = \begin{bmatrix} \frac{12EI_{\tilde{x}_2}}{L^3(1+\Phi_{13})} & \frac{-6EI_{\tilde{x}_2}}{L^2(1+\Phi_{13})} & \frac{-12EI_{\tilde{x}_2}}{L^3(1+\Phi_{13})} & \frac{-6EI_{\tilde{x}_2}}{L^2(1+\Phi_{13})} \\ \frac{-6EI_{\tilde{x}_2}}{L^2(1+\Phi_{13})} & \frac{EI_{\tilde{x}_2}(4+\Phi_{13})}{L(1+\Phi_{13})} & \frac{6EI_{\tilde{x}_2}}{L^2(1+\Phi_{13})} & \frac{EI_{\tilde{x}_2}(2-\Phi_{13})}{L(1+\Phi_{13})} \\ \frac{-12EI_{\tilde{x}_2}}{L^3(1+\Phi_{13})} & \frac{6EI_{\tilde{x}_2}}{L^2(1+\Phi_{13})} & \frac{12EI_{\tilde{x}_2}}{L^3(1+\Phi_{13})} & \frac{6EI_{\tilde{x}_2}}{L^2(1+\Phi_{13})} \\ \frac{-6EI_{\tilde{x}_2}}{L^2(1+\Phi_{13})} & \frac{EI_{\tilde{x}_2}(2-\Phi_{13})}{L(1+\Phi_{13})} & \frac{6EI_{\tilde{x}_2}}{L^2(1+\Phi_{13})} & \frac{EI_{\tilde{x}_2}(4+\Phi_{13})}{L(1+\Phi_{13})} \end{bmatrix} \quad (9.5.89)$$

The numbers above and to the right of the matrix result from Figure 9.4.3 which shows that the $\tilde{x}_1-\tilde{x}_3$ plane dofs are $\tilde{q}_3, \tilde{q}_5, \tilde{q}_9$, and \tilde{q}_{11} in the 12-dof element. If shear effects are neglected,

$$\frac{1}{k_3A} = \Phi_{13} = 0 \quad (9.5.90)$$

and $\underline{\tilde{K}}_{13}$ becomes the standard Euler–Bernoulli-type beam stiffness matrix (Cook et al., 1989):

$$\underline{K}_{13} = \frac{EI_{\tilde{x}_2}}{L^3} \begin{bmatrix} 12 & -6L & -12 & -6L \\ -6L & 4L^2 & 6L & 2L^2 \\ -12 & 6L & 12 & 6L \\ -6L & 2L^2 & 6L & 4L^2 \end{bmatrix} \quad (9.5.91)$$

The element mass matrix is derived starting with the consideration of the kinetic energy of the beam element. Figure 9.5.7 shows a differential slice of a uniform cross section beam

element. From (9.5.52), the kinetic energy contributions from translation and rotation in the $\tilde{x}_1 - \tilde{x}_3$ plane are

$$T_{x1x3} = \underbrace{\frac{\rho A}{2} \int_0^L \left(\frac{\partial \tilde{u}_3}{\partial t} \right)^2 d\tilde{x}_1}_{\text{translation term}} + \underbrace{\frac{\rho I_{\tilde{x}_2}}{2} \int_0^L \left(\frac{\partial \tilde{\theta}_2}{\partial t} \right)^2 d\tilde{x}_1}_{\text{rotary inertia term}} \quad (9.5.92)$$

Recall from (9.5.83) and (9.5.84)

$$\tilde{u}_3(x, t) = \underline{N}_{13u}(\tilde{x}_1) \tilde{\underline{u}}_{13}(t) = [N_{11}^{13} \ N_{12}^{13} \ N_{13}^{13} \ N_{14}^{13}] * (\tilde{u}_{30} \ \tilde{\theta}_{20} \ \tilde{u}_{3L} \ \tilde{\theta}_{2L})^T \quad (9.5.93)$$

$$\tilde{\theta}_2(x, t) = \underline{N}_{13\theta}(\tilde{x}_1) \tilde{\underline{u}}_{13}(t) = [N_{21}^{13} \ N_{22}^{13} \ N_{23}^{13} \ N_{24}^{13}] * (\tilde{u}_{30} \ \tilde{\theta}_{20} \ \tilde{u}_{3L} \ \tilde{\theta}_{2L})^T \quad (9.5.94)$$

where N_{ij}^{13} are defined in (9.5.85). Utilize (9.5.92)–(9.5.94) and the identity in (2.6.46) to obtain

$$T_{x1x3} = \frac{1}{2} \dot{\underline{u}}_{13}^T \tilde{\underline{M}}_{13u} \dot{\underline{u}}_{13} + \frac{1}{2} \dot{\underline{u}}_{13}^T \tilde{\underline{M}}_{13\theta} \dot{\underline{u}}_{13} \quad (9.5.95)$$

where

$$\tilde{\underline{u}}_{13} = (\tilde{u}_{30} \ \tilde{\theta}_{20} \ \tilde{u}_{3L} \ \tilde{\theta}_{2L})^T \quad (9.5.96)$$

and the translation and rotary inertia, consistent mass matrices are (as in (4.7.47))

$$\tilde{\underline{M}}_{13u} = \rho A \int_0^L \underline{N}_{13u}^T \underline{N}_{13u} d\tilde{x}_1, \quad \tilde{\underline{M}}_{13\theta} = \rho I_{\tilde{x}_2} \int_0^L \underline{N}_{13\theta}^T \underline{N}_{13\theta} d\tilde{x}_1 \quad (9.5.97)$$

Figure 9.4.3 shows that $\tilde{u}_{30}, \tilde{\theta}_{20}, \tilde{u}_{3L}$, and $\tilde{\theta}_{2L}$ are dofs $\tilde{q}_3, \tilde{q}_5, \tilde{q}_9$, and \tilde{q}_{11} , respectively. The integrations in (9.5.97) are performed in the Appendix B Maple code yielding the results

$$\tilde{\underline{M}}_{13u} = \frac{\rho AL}{420 * (b_{13}L^2 + 12a_{13})^2} \begin{bmatrix} \overset{(3)}{a_1^{13u}} & \overset{(5)}{a_2^{13u}} & \overset{(9)}{a_3^{13u}} & \overset{(11)}{a_4^{13u}} \\ a_2^{13u} & a_5^{13u} & \text{symmetric} & \\ a_3^{13u} & -a_4^{13u} & a_1^{13u} & \\ a_4^{13u} & a_6^{13u} & -a_2^{13u} & a_5^{13u} \end{bmatrix} \begin{matrix} (3) \\ (5) \\ (9) \\ (11) \end{matrix} \quad (9.5.98)$$

where

$$\begin{aligned} a_1^{13u} &= 156b_{13}^2L^4 + 3528a_{13}b_{13}L^2 + 20160a_{13}^2, & a_2^{13u} &= -2L(11b_{13}^2L^4 + 231a_{13}b_{13}L^2 + 1260a_{13}^2) \\ a_3^{13u} &= 54b_{13}^2L^4 + 1512a_{13}b_{13}L^2 + 10080a_{13}^2, & a_4^{13u} &= L(13b_{13}^2L^4 + 378a_{13}b_{13}L^2 + 2520a_{13}^2) \\ a_5^{13u} &= L^2(4b_{13}^2L^4 + 84a_{13}b_{13}L^2 + 504a_{13}^2), & a_6^{13u} &= -3L^2(b_{13}^2L^4 + 28a_{13}b_{13}L^2 + 168a_{13}^2) \end{aligned} \quad (9.5.99)$$

and

$$\tilde{\underline{M}}_{13\theta} = \frac{\rho I_{\tilde{x}_2} L}{30 * (b_{13}L^2 + 12a_{13})^2} \begin{bmatrix} \overset{(3)}{a_1^{13\theta}} & \overset{(5)}{a_2^{13\theta}} & \overset{(9)}{a_3^{13\theta}} & \overset{(11)}{a_4^{13\theta}} \\ a_2^{13\theta} & a_3^{13\theta} & \text{symmetric} & \\ -a_1^{13\theta} & -a_2^{13\theta} & a_1^{13\theta} & \\ a_2^{13\theta} & a_4^{13\theta} & -a_2^{13\theta} & a_3^{13\theta} \end{bmatrix} \begin{matrix} (3) \\ (5) \\ (9) \\ (11) \end{matrix} \quad (9.5.100)$$

where

$$\begin{aligned} a_1^{13\theta} &= 36b_{13}^2L^2, \quad a_2^{13\theta} = 3Lb_{13}(-b_{13}L^2 + 60a_{13}) \\ a_3^{13\theta} &= 4b_{13}^2L^4 + 60a_{13}b_{13}L^2 + 1440a_{13}^2, \quad a_4^{13\theta} = -b_{13}^2L^4 - 60a_{13}b_{13}L^2 + 720a_{13}^2 \end{aligned} \quad (9.5.101)$$

and a_{13} and b_{13} are defined in (9.5.75). For the case of no-shear deformation ($a_{13} = 0$), these matrices become

$$\tilde{\underline{M}}_{13u} \Big|_{a_{13}=0} = \frac{\rho AL}{420} \begin{bmatrix} \overset{(3)}{156} & \overset{(5)}{0} & \overset{(9)}{0} & \overset{(11)}{0} \\ -22L & 4L^2 & \text{symmetric} & 0 \\ 54 & -13L & 156 & 0 \\ 13L & -3L^2 & 22L & 4L^2 \end{bmatrix} \quad (9.5.102)$$

$$\tilde{\underline{M}}_{13\theta} \Big|_{a_{13}=0} = \frac{\rho I_{\tilde{x}_2}}{30L} \begin{bmatrix} \overset{(3)}{36} & \overset{(5)}{0} & \overset{(9)}{0} & \overset{(11)}{0} \\ -3L & 4L^2 & \text{symmetric} & 0 \\ -36 & 3L & 36 & 0 \\ -3L & -L^2 & 3L & 4L^2 \end{bmatrix} \quad (9.5.103)$$

The fact that these are the mass matrices in the Newton's law inertia force term follows from the Lagrange's equation expression (4.5.106b) and the quadratic form vector differentiation identity ((2.6.41), (2.6.42)):

$$\underline{f}_{\text{-iner}} = \frac{d}{dt} \left(\frac{\partial T}{\partial \dot{\underline{q}}} \right) = \frac{d}{dt} (\tilde{\underline{M}}_e \dot{\underline{u}}) = \tilde{\underline{M}}_e \ddot{\underline{u}} \quad (9.5.104)$$

9.5.4 Axial (Longitudinal) \tilde{x}_1 Differential Equation, Shape Functions, and Stiffness and Mass Matrices

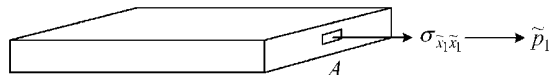
Figure 9.5.10 shows a normal stress acting on the cross section of a beam. Surface equilibrium (A.2.3) requires that

$$\tilde{p}_1 dA = \sigma_{\tilde{x}_1, \tilde{x}_1} dA = E \left(\frac{\partial \tilde{u}_1}{\partial \tilde{x}_1} + \text{bending strains} \right) dA \quad (9.5.105)$$

Integrating this equation over the symmetric cross section yields

$$EA \frac{\partial \tilde{u}_1}{\partial \tilde{x}_1} = \tilde{F}_1 \quad (9.5.106)$$

Figure 9.5.10 Axial stress acting on a beam cross section



since the bending strains are antisymmetric and thus integrate to zero. Assume that E, A , and \tilde{F}_1 are constant in the beam element and integrate (9.5.106)

$$\tilde{u}_1 = \frac{\tilde{F}_1}{EA} \tilde{x}_1 + \tilde{u}_{10} \quad (9.5.107)$$

Therefore, at $\tilde{x}_1 = L$,

$$\tilde{u}_{1L} = \frac{\tilde{F}_1 L}{EA} + \tilde{u}_{10} \Rightarrow \frac{\tilde{F}_1}{EA} = \frac{\tilde{u}_{1L} - \tilde{u}_{10}}{L} \quad (9.5.108)$$

Insert (9.5.108) into (9.5.107) to obtain

$$\tilde{u}_1(\tilde{x}_1) = N_1^{11}(\tilde{x}_1)\tilde{u}_{10} + N_2^{11}(\tilde{x}_1)\tilde{u}_{1L} \quad (9.5.109)$$

where the axial shape functions are

$$N_1^{11}(\tilde{x}_1) = 1 - \frac{\tilde{x}_1}{L}, \quad N_2^{11}(\tilde{x}_1) = \frac{\tilde{x}_1}{L} \quad (9.5.110)$$

Evaluation of (9.5.107) at $\tilde{x}_1 = L$ yields

$$\tilde{u}_{1L} = \frac{\tilde{F}_1 L}{EA} + \tilde{u}_{10} \Rightarrow \tilde{F}_1 = \frac{EA}{L}(\tilde{u}_{1L} - \tilde{u}_{10}) \quad (9.5.111)$$

From (9.5.111) and the static equilibrium condition in Figure 9.5.11, $\tilde{F}_{10} = -\tilde{F}_{1L}$

$$\begin{Bmatrix} \tilde{F}_{10} \\ \tilde{F}_{1L} \end{Bmatrix} = \begin{bmatrix} \frac{EA}{L} & -\frac{EA}{L} \\ -\frac{EA}{L} & \frac{EA}{L} \end{bmatrix} \begin{Bmatrix} \tilde{u}_{10} \\ \tilde{u}_{1L} \end{Bmatrix} \quad (9.5.112)$$

The axial stiffness matrix is seen to be

$$\underline{K}_{11} = \begin{bmatrix} \overset{(1)}{\frac{EA}{L}} & \overset{(7)}{-\frac{EA}{L}} \\ \underset{(7)}{-\frac{EA}{L}} & \underset{(1)}{\frac{EA}{L}} \end{bmatrix} \quad (9.5.113)$$

The numbers above and to the right of the matrix result from Figure 9.4.3 which shows that the axial dofs are \tilde{q}_1 and \tilde{q}_7 in the 12-dof element.

The kinetic energy contribution from axial motion is given in (9.5.52) as

$$T_{ax} = \frac{1}{2} \int \left(\frac{\partial \tilde{u}_1}{\partial t} \right)^2 dm = \rho \frac{A}{2} \int_0^L \left(\frac{\partial \tilde{u}_1}{\partial t} \right)^2 d\tilde{x}_1 \quad (9.5.114)$$

From (9.5.109) and (9.5.110)

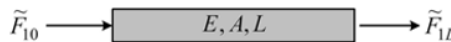


Figure 9.5.11 Axial nodal forces on a beam element

$$\tilde{u}_1(\tilde{x}_1) = \underline{N}_{\text{ax}} \tilde{u}_{\text{ax}} = [N_1^{11} \quad N_2^{11}] \begin{Bmatrix} \tilde{u}_{10} \\ \tilde{u}_{1L} \end{Bmatrix}, \quad N_1^{11} = 1 - \frac{\tilde{x}_1}{L}, \quad N_2^{11} = \frac{\tilde{x}_1}{L} \quad (9.5.115)$$

Therefore,

$$\begin{Bmatrix} \frac{\partial T_{\text{ax}}}{\partial \dot{u}_{10}} \\ \frac{\partial T_{\text{ax}}}{\partial \dot{u}_{1L}} \end{Bmatrix} = \rho A \int_0^L \begin{Bmatrix} \frac{\partial(\partial \tilde{u}_1 / \partial t)}{\partial \dot{u}_{10}} * \frac{\partial \tilde{u}_1}{\partial t} \\ \frac{\partial(\partial \tilde{u}_1 / \partial t)}{\partial \dot{u}_{1L}} * \frac{\partial \tilde{u}_1}{\partial t} \end{Bmatrix} d\tilde{x}_1 = \rho A \int_0^L \begin{Bmatrix} N_1^{11} \underline{N}_{\text{ax}} \dot{\tilde{u}}_{\text{ax}} \\ N_2^{11} \underline{N}_{\text{ax}} \dot{\tilde{u}}_{\text{ax}} \end{Bmatrix} d\tilde{x}_1 = \tilde{\underline{M}}_{\text{ax}} \dot{\tilde{u}}_{\text{ax}} \quad (9.5.116)$$

where, as in (4.7.47), the consistent mass matrix is

$$\tilde{\underline{M}}_{\text{ax}} = \rho A \int_0^L \begin{bmatrix} N_1^{11} N_1^{11} & N_1^{11} N_2^{11} \\ N_2^{11} N_1^{11} & N_2^{11} N_2^{11} \end{bmatrix} d\tilde{x}_1 = \rho A \int_0^L \underline{N}_{\text{ax}}^T \underline{N}_{\text{ax}} d\tilde{x}_1 \quad (9.5.117)$$

The integrations in (9.5.117) are performed in the Appendix B Maple code. Figure 9.4.3 shows that the dofs for \tilde{u}_{10} and \tilde{u}_{1L} are \tilde{q}_1 and \tilde{q}_7 , respectively. The integration therefore yields

$$\tilde{\underline{M}}_{\text{ax}} = \rho A L \begin{bmatrix} \overset{(1)}{1} & \overset{(7)}{1} \\ \overset{(1)}{3} & \overset{(7)}{6} \\ \overset{(7)}{1} & \overset{(7)}{3} \\ \overset{(7)}{6} & \overset{(7)}{3} \end{bmatrix} \quad (9.5.118)$$

9.5.5 Torsional $\tilde{\theta}_1$ Differential Equation, Shape Functions, and Stiffness and Mass Matrices

The torque along the longitudinal axis of a straight beam is given by Timoshenko and Goodier (1970):

$$\tilde{M}_1 = 2 \int_A \int \phi d\tilde{x}_2 d\tilde{x}_3 \quad (9.5.119)$$

where ϕ is a stress potential function that satisfies the Poisson equation

$$\nabla^2 \phi = -2G \frac{d\tilde{\theta}_1}{d\tilde{x}_1} \quad (9.5.120)$$

and where G is the shear modulus and $d\tilde{\theta}_1/d\tilde{x}_1$ is the axial derivative of the twist angle. Substitution of the solution of (9.5.120) into (9.5.119) yields the general form

$$\tilde{M}_1 = GJ \frac{d\tilde{\theta}_1}{d\tilde{x}_1} \quad (9.5.121)$$

where J is called the torsion constant, which is found in structural handbooks (e.g., AISC, 1980) for many different cross-sectional shapes. Integration of (9.5.121) yields

Figure 9.5.12 Twist torques at nodes of a beam element

$$\tilde{\theta}_1(\tilde{x}_1) = \frac{\tilde{M}_1 \tilde{x}_1}{GJ} + \tilde{\theta}_{10} \quad (9.5.122)$$

At $x=L$,

$$\tilde{\theta}_{1L} = \frac{\tilde{M}_1 L}{GJ} + \tilde{\theta}_{10} \Rightarrow \frac{\tilde{M}_1}{GJ} = \frac{\tilde{\theta}_{1L} - \tilde{\theta}_{10}}{L} \quad (9.5.123)$$

Insert (9.5.123) into (9.5.122) to obtain

$$\tilde{\theta}_1(\tilde{x}_1) = N_{\theta 1} \tilde{\theta}_{10} + N_{\theta L} \tilde{\theta}_{1L} \quad (9.5.124)$$

where the shape functions are

$$N_{\theta 1}(\tilde{x}_1) = 1 - \frac{\tilde{x}_1}{L}, \quad N_{\theta 2}(\tilde{x}_1) = \frac{\tilde{x}_1}{L} \quad (9.5.125)$$

From (9.5.123) and the static equilibrium condition from Figure 9.5.12, $\tilde{M}_{1L} = -\tilde{M}_{10}$

$$\begin{Bmatrix} \tilde{M}_{10} \\ \tilde{M}_{1L} \end{Bmatrix} = \begin{bmatrix} \frac{GJ}{L} & -\frac{GJ}{L} \\ -\frac{GJ}{L} & \frac{GJ}{L} \end{bmatrix} \begin{Bmatrix} \tilde{\theta}_{10} \\ \tilde{\theta}_{1L} \end{Bmatrix} \quad (9.5.126)$$

The matrix in (9.5.126) is the torsional stiffness matrix. The numbers above and to the right of the matrix result from Figure 9.4.2 which shows that the torsional dofs are \tilde{q}_4 and \tilde{q}_{10} in the 12-dof element.

The kinetic energy contribution from torsional motion is given in (9.5.52) as

$$T_{\text{tor}} = \frac{\rho J_p}{2} \int_0^L \left(\frac{\partial \tilde{\theta}_1}{\partial t} \right)^2 d\tilde{x}_1 \quad (9.5.127)$$

Recall from (9.5.124) and (9.5.125) that

$$\tilde{\theta}_1(\tilde{x}_1, t) = \underline{N}_{\theta 1} \underline{\tilde{u}}_{\theta 1} = [N_{\theta 1} \quad N_{\theta 2}] \begin{Bmatrix} \tilde{\theta}_{10} \\ \tilde{\theta}_{1L} \end{Bmatrix}, \quad N_{\theta 1} = 1 - \frac{\tilde{x}_1}{L}, \quad N_{\theta 2} = \frac{\tilde{x}_1}{L} \quad (9.5.128)$$

Therefore,

$$\begin{Bmatrix} \frac{\partial T_{\text{tor}}}{\partial \dot{\tilde{\theta}}_{10}} \\ \frac{\partial T_{\text{tor}}}{\partial \dot{\tilde{\theta}}_{1L}} \end{Bmatrix} = \rho J_p \int_0^L \begin{Bmatrix} \frac{\partial(\partial \tilde{\theta}_1 / \partial t)}{\partial \dot{\tilde{\theta}}_{10}} * \frac{\partial \tilde{\theta}_1}{\partial t} \\ \frac{\partial(\partial \tilde{\theta}_1 / \partial t)}{\partial \dot{\tilde{\theta}}_{1L}} * \frac{\partial \tilde{\theta}_1}{\partial t} \end{Bmatrix} d\tilde{x}_1 = \rho J_p \int_0^L \begin{Bmatrix} N_{\theta 1} \underline{N}_{\theta 1} \dot{\underline{\tilde{u}}}_{\theta 1} \\ N_{\theta 2} \underline{N}_{\theta 1} \dot{\underline{\tilde{u}}}_{\theta 1} \end{Bmatrix} d\tilde{x}_1 = \underline{\tilde{M}}_{\text{tor}} \dot{\underline{\tilde{u}}}_{\theta 1} \quad (9.5.129)$$

where, as in (4.7.47), the consistent mass matrix is

$$\underline{\tilde{M}}_{\text{tor}} = \rho J_p \int_0^L \begin{bmatrix} N_{\theta 1} N_{\theta 1} & N_{\theta 1} N_{\theta 2} \\ N_{\theta 2} N_{\theta 1} & N_{\theta 2} N_{\theta 2} \end{bmatrix} d\tilde{x}_1 = \rho J_p \int_0^L \underline{N}_{\theta 1}^T \underline{N}_{\theta 1} d\tilde{x}_1 \quad (9.5.130)$$

The integrations in (9.5.130) are performed in the Appendix B Maple code. Figure 9.4.2 shows that the dofs for $\tilde{\theta}_{10}$ and $\tilde{\theta}_{1L}$ are \tilde{q}_4 and \tilde{q}_{10} , respectively. This yields

$$\underline{\tilde{M}}_{\text{tor}} = \rho J_p L \begin{bmatrix} \overset{(4)}{1} & \overset{(10)}{1} \\ \overset{(4)}{\frac{1}{3}} & \overset{(10)}{\frac{1}{6}} \\ \overset{(4)}{1} & \overset{(10)}{\frac{1}{6}} \\ \overset{(4)}{\frac{1}{6}} & \overset{(10)}{\frac{1}{3}} \end{bmatrix} \quad (9.5.131)$$

9.5.6 Twelve-Dof Element Stiffness Matrix

Figure 9.5.13 shows all 12 nodal displacement and rotations and forces and moments in local (element-based) coordinates. In the notation of this figure, Equations (9.5.47) and (9.5.51) become

$$\begin{Bmatrix} \tilde{f}_2 \\ \tilde{f}_6 \\ \tilde{f}_8 \\ \tilde{f}_{12} \end{Bmatrix} = \underline{\tilde{K}}_{4 \times 4}^{12} \begin{Bmatrix} \tilde{q}_2 \\ \tilde{q}_6 \\ \tilde{q}_8 \\ \tilde{q}_{12} \end{Bmatrix} \quad (4 \times 1) \quad (9.5.132)$$

Equations (9.5.87) and (9.5.89) become

$$\begin{Bmatrix} \tilde{f}_3 \\ \tilde{f}_5 \\ \tilde{f}_9 \\ \tilde{f}_{11} \end{Bmatrix} = \underline{\tilde{K}}_{4 \times 4}^{13} \begin{Bmatrix} \tilde{q}_3 \\ \tilde{q}_5 \\ \tilde{q}_9 \\ \tilde{q}_{11} \end{Bmatrix} \quad (4 \times 1) \quad (9.5.133)$$

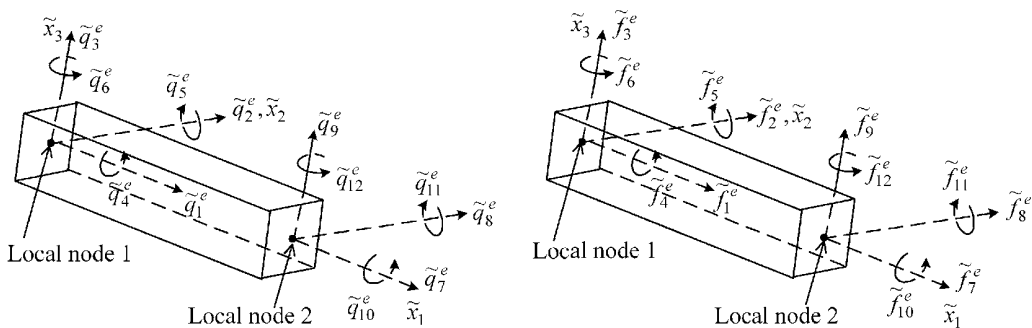


Figure 9.5.13 Nodal displacements and forces in local coordinates

The matrix in (9.5.136) is expressed in tabular form in Table 9.5.1.

Table 9.5.1 The local coordinate, 3D Timoshenko beam symmetric stiffness matrix $\tilde{\underline{K}}_e^a$

Entries	Term
(1,1), (7,7), (-7,-1)	$\frac{EA}{L}$
(4,4), (10,10), (-10,-4)	$\frac{GJ}{L}$
(2,2), (8,8), (-8,-2)	$\frac{12\beta_{12}^a}{L^3}$
(6,2), (-8,-6), (12,2), (-12,-8)	$\frac{6\beta_{12}^a}{L^2}$
(6,6), (12,12)	$\frac{\beta_{12}^b}{L}$
(12,6)	$\frac{\beta_{12}^c}{L}$
(3,3), (9,9), (-9,-3)	$\frac{12\beta_{13}^a}{L^3}$
(-5,-3), (9,5), (-11,-3), (11,9)	$\frac{6\beta_{13}^a}{L^2}$
(5,5), (11,11)	$\frac{\beta_{13}^b}{L}$
(11,5)	$\frac{\beta_{13}^c}{L}$

^aThe matrix is symmetric $\tilde{\underline{K}}_e^T = \tilde{\underline{K}}_e$.

All undefined terms in the 12×12 matrix are zero.

β_{ij}^k are defined in (9.5.137).

Negative entries (in parentheses) in the left column indicate to use the negative of the term shown in the right column.

The potential energy in a finite element has the form in (4.7.54), that is,

$$U_e = \frac{1}{2} \tilde{\underline{q}}_e^T \tilde{\underline{K}}_e \tilde{\underline{q}}_e \quad (9.5.138)$$

where $\tilde{\underline{K}}_e$ is the element stiffness matrix in local coordinates as defined in (9.5.136), and $\tilde{\underline{q}}_e$ is the nodal displacement vector in local coordinates as defined in (9.4.1) and shown in Figure 9.4.2. The potential energy is invariant with respect to the coordinate system utilized to define displacements so that it must also be true that

$$U_e = \frac{1}{2} \underline{q}_e^T \underline{K}_e \underline{q}_e \quad (9.5.139)$$

where \underline{K}_e is the stiffness matrix in global coordinates, and \underline{q}_e is the nodal displacement vector in global coordinates as defined in (9.4.2) and shown in Figure 9.4.1. Substitute the coordinate transformation (9.4.11) into (9.5.138) to obtain

$$U_e = \frac{1}{2} \underline{q}_e^T \underline{T}_e^T \tilde{\underline{K}}_e \underline{T}_e \underline{q}_e \quad (9.5.140)$$

Equating (9.5.139) and (9.5.140) yields

$$U_e = \frac{1}{2} \underline{q}_e^T \underline{K}_e \underline{q}_e = \frac{1}{2} \underline{q}_e^T \tilde{\underline{T}}_e \tilde{\underline{K}}_e \tilde{\underline{T}}_e \underline{q}_e \quad (9.5.141)$$

This relation holds for all possible vectors \underline{q}_e ; therefore, it follows that the global coordinate form of the element stiffness matrix may be determined from

$$\underline{K}_e = \tilde{\underline{T}}_e^T \tilde{\underline{K}}_e \tilde{\underline{T}}_e \quad (9.5.142)$$

where $\tilde{\underline{T}}_e$ is defined in (9.4.10), (9.4.11), (9.4.19), and (9.4.23). The total system model stiffness matrix is formed by assembling the element stiffness matrices in their global coordinate form (9.5.142).

9.5.7 Twelve-Dof Element Mass Matrix

The 12×12 , local coordinate, element mass matrix $\tilde{\underline{M}}_e$ is formed by combining $\tilde{x}_1 - \tilde{x}_2$ bending/shear contributions (9.5.60)–(9.5.63), $\tilde{x}_1 - \tilde{x}_3$ bending/shear contributions (9.5.98)–(9.5.101), axial contributions (9.5.118), and torsional contributions (9.5.131). The result is summarized in Table 9.5.2. The mass matrix $\tilde{\underline{M}}_e$ simplifies to the form given in Table 9.5.3 if shear deformation is neglected.

Table 9.5.2 The local coordinate, 3D Timoshenko beam, consistent inertia matrix $\tilde{\underline{M}}_e$ including rotary inertia and shear deformation^a

Term	Entry	Term	Entry
(4,4), (10,10)	$\frac{\rho J_p L}{3}$	(1,1), (7,7)	$\frac{\rho AL}{3}$
(10,4)	$\frac{\rho J_p L}{6}$	(7,1)	$\frac{\rho AL}{6}$
(2,2), (8,8)	$\gamma_{m12} \left(\frac{Aa_1^{12u}}{420} + \frac{I_{\tilde{x}_3} a_1^{12\theta}}{30} \right)$	(3,3), (9,9)	$\gamma_{m13} \left(\frac{Aa_1^{13u}}{420} + \frac{I_{\tilde{x}_2} a_1^{13\theta}}{30} \right)$
(6,2), (-12,-8)	$\gamma_{m12} \left(\frac{Aa_2^{12u}}{420} + \frac{I_{\tilde{x}_3} a_2^{12\theta}}{30} \right)$	(5,3), (-11,-9)	$\gamma_{m13} \left(\frac{Aa_2^{13u}}{420} + \frac{I_{\tilde{x}_2} a_2^{13\theta}}{30} \right)$
(8,2)	$\gamma_{m12} \left(\frac{Aa_3^{12u}}{420} - \frac{I_{\tilde{x}_3} a_1^{12\theta}}{30} \right)$	(9,3)	$\gamma_{m13} \left(\frac{Aa_3^{13u}}{420} - \frac{I_{\tilde{x}_2} a_1^{13\theta}}{30} \right)$
(12,2), (-8,-6)	$\gamma_{m12} \left(\frac{Aa_4^{12u}}{420} + \frac{I_{\tilde{x}_3} a_2^{12\theta}}{30} \right)$	(11,3), (-9,-5)	$\gamma_{m13} \left(\frac{Aa_4^{13u}}{420} + \frac{I_{\tilde{x}_2} a_2^{13\theta}}{30} \right)$
(6,6), (12,12)	$\gamma_{m12} \left(\frac{Aa_5^{12u}}{420} + \frac{I_{\tilde{x}_3} a_3^{12\theta}}{30} \right)$	(5,5), (11,11)	$\gamma_{m13} \left(\frac{Aa_5^{13u}}{420} + \frac{I_{\tilde{x}_2} a_3^{13\theta}}{30} \right)$
(12,6)	$\gamma_{m12} \left(\frac{Aa_6^{12u}}{420} + \frac{I_{\tilde{x}_3} a_4^{12\theta}}{30} \right)$	(11,5)	$\gamma_{m13} \left(\frac{Aa_6^{13u}}{420} + \frac{I_{\tilde{x}_2} a_4^{13\theta}}{30} \right)$

The matrix is symmetric $\tilde{\underline{M}}_e^T = \tilde{\underline{M}}_e$.

^a All undefined terms in the 12×12 matrix are zero

$$\gamma_{m12} = \frac{\rho L}{(b_{12}L^2 + 12a_{12})^2}, \quad \gamma_{m13} = \frac{\rho L}{(b_{13}L^2 + 12a_{13})^2}$$

a_{12} , b_{12} , a_{13} , b_{13} , and all a_i^{kl} are defined in (9.5.32), (9.5.61), (9.5.63), (9.5.75), (9.5.99), and (9.5.101). Negative terms (in parentheses) indicate to use the negative of the entries shown.

Table 9.5.3 The local coordinate, 3D Euler–Bernoulli beam, consistent inertia matrix \tilde{M}_e including rotary inertia^a

Term	Entry
(1,1), (7,7)	$\frac{\rho AL}{3}$
(7,1)	$\frac{\rho AL}{6}$
(4,4), (10,10)	$\frac{\rho J_p L}{3}$
(10,4)	$\frac{\rho J_p L}{6}$
(2,2), (8,8)	$\gamma_{m12}^u * 156 + \gamma_{m12}^\theta * 36$
(6,2), (-12,-8)	$\gamma_{m12}^u * 22L + \gamma_{m12}^\theta * 3L$
(6,6), (12,12)	$\gamma_{m12}^u * 4L^2 + \gamma_{m12}^\theta * 4L^2$
(8,2)	$\gamma_{m12}^u * 54 + \gamma_{m12}^\theta * (-36)$
(8,6), (-12,-2)	$\gamma_{m12}^u * 13L + \gamma_{m12}^\theta * (-3L)$
(12,6)	$\gamma_{m12}^u * (-3L^2) + \gamma_{m12}^\theta * (-L^2)$
(3,3), (9,9)	$\gamma_{m13}^u * 156 + \gamma_{m13}^\theta * 36$
(5,3), (-11,-9)	$\gamma_{m13}^u * (-22L) + \gamma_{m13}^\theta * (-3L)$
(5,5), (11,11)	$\gamma_{m13}^u * 4L^2 + \gamma_{m13}^\theta * 4L^2$
(9,3)	$\gamma_{m13}^u * 54 + \gamma_{m13}^\theta * (-36)$
(9,5), (-11,-3)	$\gamma_{m13}^u * (-13L) + \gamma_{m13}^\theta * 3L$
(11,5)	$\gamma_{m13}^u * (-3L^2) + \gamma_{m13}^\theta * (-L^2)$

^a The matrix is symmetric $\tilde{M}_e^T = \tilde{M}_e$.

All undefined terms in the 12×12 matrix are zero

$$\gamma_{m12}^u = \frac{\rho AL}{420}, \quad \gamma_{m12}^\theta = \frac{\rho I_{x_3}}{30L}, \quad \gamma_{m13}^u = \frac{\rho AL}{420}, \quad \gamma_{m13}^\theta = \frac{\rho I_{x_2}}{30L}$$

Negative terms (in parentheses) indicate to use the negative of the entries shown.

Similar to the derivation of (9.5.142), the invariance of the element's kinetic energy with respect to reference frame (coordinate system) yields the following formula for determining the element mass matrix in global coordinates:

$$\underline{M}_e = \tilde{T}_e^T \tilde{M}_e \tilde{T}_e \quad (9.5.143)$$

where \tilde{T}_e is defined in (9.4.10), (9.4.11), (9.4.19), and (9.4.23). The total system model mass matrix is formed by assembling the element mass matrices in their global coordinate form (9.5.143).

9.6 3D TIMOSHENKO BEAM ELEMENT FORCE VECTORS

Figure 9.6.1 shows distributed external forces and moments acting on a 3D beam element. In each case, it is assumed that the spatial force function is multiplied by a temporal function to produce the actual, spatially, and time-varying loading

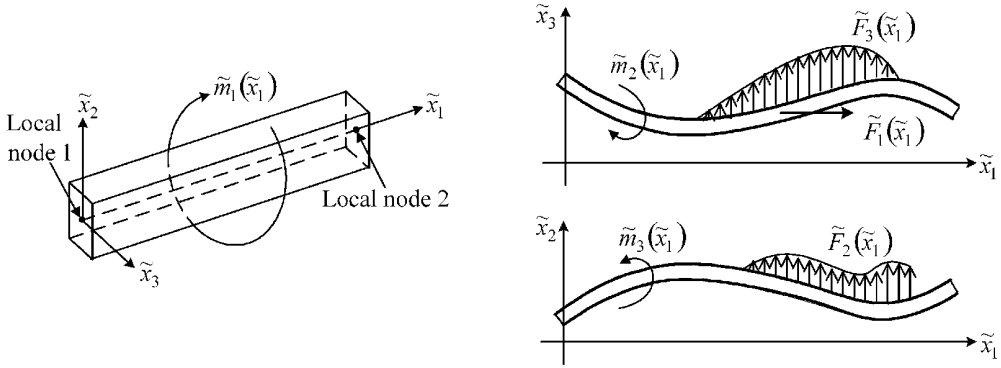


Figure 9.6.1 Applied force and moment functions in the element coordinate system

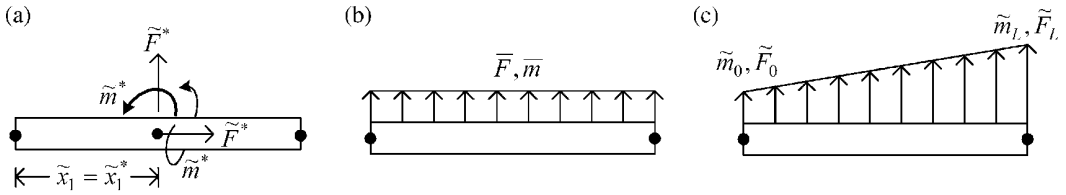


Figure 9.6.2 Various load distributions for a 3D beam element. (a) Point force, moment or torque at x_1^* . (b) Uniform force, moment or torque. (c) Spatially linear varying force, moment or torque

$$\begin{aligned}\tilde{F}_{1,\text{tot}}(\tilde{x}_1, t) &= \alpha_{F1}(t)\tilde{F}_1(\tilde{x}_1), & \tilde{F}_{2,\text{tot}}(\tilde{x}_1, t) &= \alpha_{F2}(t)\tilde{F}_2(\tilde{x}_1), & \tilde{F}_{3,\text{tot}}(\tilde{x}_1, t) &= \alpha_{F3}(t)\tilde{F}_3(\tilde{x}_1) \\ \tilde{m}_{1,\text{tot}}(\tilde{x}_1, t) &= \alpha_{m1}(t)\tilde{m}_1(\tilde{x}_1), & \tilde{m}_{2,\text{tot}}(\tilde{x}_1, t) &= \alpha_{m2}(t)\tilde{m}_2(\tilde{x}_1), & \tilde{m}_{3,\text{tot}}(\tilde{x}_1, t) &= \alpha_{m3}(t)\tilde{m}_3(\tilde{x}_1)\end{aligned}\quad (9.6.1)$$

The \tilde{F} and \tilde{m} in these formulas are forces and moments per unit length along \tilde{x}_1 . Therefore, \tilde{F} may be interpreted as a pressure multiplied by the beam width to convert force per area to force per length. The expression $\alpha(t)$ defines the time dependence of the respective loading. Three common load distributions will be treated here and are shown in Figure 9.6.2.

Case A: Point Load

In this case, the load acts only at a point $\tilde{x}_1 = \tilde{x}_1^*$, that is, from Section 2.12

$$\tilde{F} = \tilde{F}^* \delta(\tilde{x}_1 - \tilde{x}_1^*), \quad \tilde{m} = \tilde{m}^* \delta(\tilde{x}_1 - \tilde{x}_1^*) \quad (9.6.2)$$

where δ is a Dirac delta function.

Case B: Spatially Uniform Load

For this case, the loads per unit length are constant, that is,

$$\begin{aligned}\tilde{F} &= \bar{F} \quad 0 \leq \tilde{x}_1 \leq L \\ \tilde{m} &= \bar{m} \quad 0 \leq \tilde{x}_1 \leq L\end{aligned}\quad (9.6.3)$$

Case C: Spatially Linear Varying Load

For this case, the loads per unit length vary linearly with \tilde{x}_1 , that is,

$$\tilde{F} = \tilde{F}_0 \left(1 - \frac{\tilde{x}_1}{L}\right) + \tilde{F}_L \frac{\tilde{x}_1}{L} = \left[1 - \frac{\tilde{x}_1}{L} \quad \frac{\tilde{x}_1}{L}\right] \begin{Bmatrix} \tilde{F}_0 \\ \tilde{F}_L \end{Bmatrix} \quad (9.6.4)$$

The element force vectors are defined by the general formulas in (4.7.38). These are specialized for the different possible load directions in the following sections.

9.6.1 Axial Loads

From (4.7.38) and (9.6.1),

$$\begin{Bmatrix} \tilde{f}_{\text{ext},1} \\ \tilde{f}_{\text{ext},7} \end{Bmatrix} = \alpha_{F1}(t) \int_0^L \tilde{F}_1(\tilde{x}_1) \begin{Bmatrix} N_1^{11}(\tilde{x}_1) \\ N_2^{11}(\tilde{x}_1) \end{Bmatrix} d\tilde{x}_1 \quad (9.6.5)$$

and from (9.5.115),

$$N_1^{11}(\tilde{x}_1) = 1 - \frac{\tilde{x}_1}{L}, \quad N_2^{11}(\tilde{x}_1) = \frac{\tilde{x}_1}{L} \quad (9.6.6)$$

Point loading: Substitute (9.6.2) and (9.6.6) into (9.6.5) to obtain

$$\begin{Bmatrix} \tilde{f}_{\text{ext},1} \\ \tilde{f}_{\text{ext},7} \end{Bmatrix} = \alpha_{F1}(t) \int_0^L \tilde{F}_1^* \delta(\tilde{x}_1 - \tilde{x}_1^*) \begin{Bmatrix} 1 - \frac{\tilde{x}_1}{L} \\ \frac{\tilde{x}_1}{L} \end{Bmatrix} d\tilde{x}_1 = \alpha_{F1}(t) \tilde{F}_1^* \begin{Bmatrix} 1 - \frac{\tilde{x}_1^*}{L} \\ \frac{\tilde{x}_1^*}{L} \end{Bmatrix} \quad (9.6.7)$$

Uniform loading: Substitute (9.6.3) and (9.6.6) into (9.6.5) to obtain

$$\begin{Bmatrix} \tilde{f}_{\text{ext},1} \\ \tilde{f}_{\text{ext},7} \end{Bmatrix} = \alpha_{F1}(t) \int_0^L \bar{F}_1 \begin{Bmatrix} 1 - \frac{\tilde{x}_1}{L} \\ \frac{\tilde{x}_1}{L} \end{Bmatrix} d\tilde{x}_1 = \alpha_{F1}(t) \bar{F}_1 \frac{L}{2} \begin{Bmatrix} 1 \\ 1 \end{Bmatrix} \quad (9.6.8)$$

Linearly varying loading: Substitute (9.6.4) and (9.6.6) into (9.6.5) to obtain

$$\begin{Bmatrix} \tilde{f}_{\text{ext},1} \\ \tilde{f}_{\text{ext},7} \end{Bmatrix} = \alpha_{F1}(t) \int_0^L \begin{Bmatrix} 1 - \frac{\tilde{x}_1}{L} \\ \frac{\tilde{x}_1}{L} \end{Bmatrix} \left[1 - \frac{\tilde{x}_1}{L} \quad \frac{\tilde{x}_1}{L}\right] d\tilde{x}_1 \begin{Bmatrix} \tilde{F}_{10} \\ \tilde{F}_{1L} \end{Bmatrix} = \alpha_{F1}(t) \frac{L}{6} \begin{Bmatrix} 2\tilde{F}_{10} + \tilde{F}_{1L} \\ \tilde{F}_{10} + 2\tilde{F}_{1L} \end{Bmatrix} \quad (9.6.9)$$

9.6.2 Torsional Loads

From (4.7.38) and (9.6.1),

$$\begin{Bmatrix} \tilde{f}_{\text{ext},4} \\ \tilde{f}_{\text{ext},10} \end{Bmatrix} = \alpha_{m1}(t) \int_0^L \tilde{m}_1(\tilde{x}_1) \begin{Bmatrix} N_{\theta 1}(\tilde{x}_1) \\ N_{\theta 2}(\tilde{x}_1) \end{Bmatrix} d\tilde{x}_1 \quad (9.6.10)$$

where from (9.5.128)

$$N_{\theta 1}(\tilde{x}_1) = 1 - \frac{\tilde{x}_1}{L}, \quad N_{\theta 2}(\tilde{x}_1) = \frac{\tilde{x}_1}{L} \quad (9.6.11)$$

The nodal load vectors are identical in form to the axial load case since the shape functions are identical.

Point loading:

$$\begin{Bmatrix} \tilde{f}_{\text{ext},4} \\ \tilde{f}_{\text{ext},10} \end{Bmatrix} = \alpha_{m1}(t) \tilde{m}_1^* \begin{Bmatrix} 1 - \frac{\tilde{x}_1^*}{L} \\ \frac{\tilde{x}_1^*}{L} \end{Bmatrix} \quad (9.6.12)$$

Uniform loading:

$$\begin{Bmatrix} \tilde{f}_{\text{ext},4} \\ \tilde{f}_{\text{ext},10} \end{Bmatrix} = \alpha_{m1}(t) \tilde{m}_1 \frac{L}{2} \begin{Bmatrix} 1 \\ 1 \end{Bmatrix} \quad (9.6.13)$$

Linearly varying loading:

$$\begin{Bmatrix} \tilde{f}_{\text{ext},4} \\ \tilde{f}_{\text{ext},10} \end{Bmatrix} = \alpha_{m1}(t) \frac{L}{6} \begin{Bmatrix} 2\tilde{m}_{10} + \tilde{m}_{1L} \\ \tilde{m}_{10} + 2\tilde{m}_{1L} \end{Bmatrix} \quad (9.6.14)$$

9.6.3 $\tilde{x}_1 - \tilde{x}_2$ Plane Loads

From (4.7.38) and (9.6.1),

$$\begin{Bmatrix} \tilde{f}_{\text{ext},2} \\ \tilde{f}_{\text{ext},6} \\ \tilde{f}_{\text{ext},8} \\ \tilde{f}_{\text{ext},12} \end{Bmatrix} = \alpha_{F2}(t) \int_0^L \tilde{F}_2(\tilde{x}_1) \begin{Bmatrix} N_{11}^{12}(\tilde{x}_1) \\ N_{12}^{12}(\tilde{x}_1) \\ N_{13}^{12}(\tilde{x}_1) \\ N_{14}^{12}(\tilde{x}_1) \end{Bmatrix} d\tilde{x}_1 + \alpha_{m3}(t) \int_0^L \tilde{m}_3(\tilde{x}_1) \begin{Bmatrix} N_{21}^{12}(\tilde{x}_1) \\ N_{22}^{12}(\tilde{x}_1) \\ N_{23}^{12}(\tilde{x}_1) \\ N_{24}^{12}(\tilde{x}_1) \end{Bmatrix} d\tilde{x}_1 \quad (9.6.15)$$

where $N_{ij}^{12}(\tilde{x}_1)$ are defined in (9.5.42).

Point loading: Substitute (9.6.2) and (9.5.42) into (9.6.15) to obtain

$$\begin{Bmatrix} \tilde{f}_{\text{ext},2} \\ \tilde{f}_{\text{ext},6} \\ \tilde{f}_{\text{ext},8} \\ \tilde{f}_{\text{ext},12} \end{Bmatrix} = \alpha_{F2}(t) \tilde{F}_2^* \begin{Bmatrix} N_{11}^{12}(\tilde{x}_1^*) \\ N_{12}^{12}(\tilde{x}_1^*) \\ N_{13}^{12}(\tilde{x}_1^*) \\ N_{14}^{12}(\tilde{x}_1^*) \end{Bmatrix} + \alpha_{m3}(t) \tilde{m}_3^* \begin{Bmatrix} N_{21}^{12}(\tilde{x}_1^*) \\ N_{22}^{12}(\tilde{x}_1^*) \\ N_{23}^{12}(\tilde{x}_1^*) \\ N_{24}^{12}(\tilde{x}_1^*) \end{Bmatrix} \quad (9.6.16)$$

Uniform loading: Substitute (9.6.3) and (9.5.42) into (9.6.15) to obtain

$$\begin{aligned} \begin{Bmatrix} \tilde{f}_{\text{ext},2} \\ \tilde{f}_{\text{ext},6} \\ \tilde{f}_{\text{ext},8} \\ \tilde{f}_{\text{ext},12} \end{Bmatrix} &= \alpha_{F2}(t) \bar{F}_2 \int_0^L \begin{Bmatrix} N_{11}^{12}(\tilde{x}_1) \\ N_{12}^{12}(\tilde{x}_1) \\ N_{13}^{12}(\tilde{x}_1) \\ N_{14}^{12}(\tilde{x}_1) \end{Bmatrix} d\tilde{x}_1 + \alpha_{m3}(t) \bar{m}_3 \int_0^L \begin{Bmatrix} N_{21}^{12}(\tilde{x}_1) \\ N_{22}^{12}(\tilde{x}_1) \\ N_{23}^{12}(\tilde{x}_1) \\ N_{24}^{12}(\tilde{x}_1) \end{Bmatrix} d\tilde{x}_1 \\ &= \alpha_{F2}(t) \bar{F} \begin{Bmatrix} \frac{L}{2} \\ \frac{L^2}{12} \\ \frac{L}{2} \\ -\frac{L^2}{12} \end{Bmatrix} + \frac{\alpha_{m3}(t) \bar{m}_3}{b_{12}L^2 + 12a_{12}} \begin{Bmatrix} -b_{12}L^2 \\ 6a_{12}L \\ b_{12}L^2 \\ 6a_{12}L \end{Bmatrix} \end{aligned} \quad (9.6.17)$$

This simplifies for the no-shear deformation assumption to the form

$$\begin{Bmatrix} \tilde{f}_{\text{ext},2} \\ \tilde{f}_{\text{ext},6} \\ \tilde{f}_{\text{ext},8} \\ \tilde{f}_{\text{ext},12} \end{Bmatrix} = \alpha_{F2}(t) \bar{F}_2 \begin{Bmatrix} \frac{L}{2} \\ \frac{L^2}{12} \\ \frac{L}{2} \\ -\frac{L^2}{12} \end{Bmatrix} + \alpha_{m3}(t) \bar{m}_3 \begin{Bmatrix} -1 \\ 0 \\ 1 \\ 0 \end{Bmatrix} \quad (9.6.18)$$

Linearly varying loading: Substitute (9.6.4) and (9.5.42) into (9.6.15) to obtain

$$\begin{aligned} \begin{Bmatrix} \tilde{f}_{\text{ext},2} \\ \tilde{f}_{\text{ext},6} \\ \tilde{f}_{\text{ext},8} \\ \tilde{f}_{\text{ext},12} \end{Bmatrix} &= \alpha_{F2}(t) \int_0^L \begin{Bmatrix} N_{11}^{12}(\tilde{x}_1) \\ N_{12}^{12}(\tilde{x}_1) \\ N_{13}^{12}(\tilde{x}_1) \\ N_{14}^{12}(\tilde{x}_1) \end{Bmatrix} \left[1 - \frac{\tilde{x}_1}{L} \quad \frac{\tilde{x}_1}{L} \right] d\tilde{x}_1 \begin{Bmatrix} \tilde{F}_{20} \\ \tilde{F}_{2L} \end{Bmatrix} \\ &\quad + \alpha_{m3}(t) \int_0^L \begin{Bmatrix} N_{21}^{12}(\tilde{x}_1) \\ N_{22}^{12}(\tilde{x}_1) \\ N_{23}^{12}(\tilde{x}_1) \\ N_{24}^{12}(\tilde{x}_1) \end{Bmatrix} \left[1 - \frac{\tilde{x}_1}{L} \quad \frac{\tilde{x}_1}{L} \right] d\tilde{x}_1 \begin{Bmatrix} \tilde{m}_{30} \\ \tilde{m}_{3L} \end{Bmatrix} \end{aligned}$$

$$\begin{aligned}
&= \frac{\alpha_{F2}(t)}{60} \frac{\begin{bmatrix} 3L(7b_{12}L^2 + 80a_{12}) & 9b_{12}L^3 + 120a_{12}L \\ 3L^2(b_{12}L^2 + 10a_{12}) & 2b_{12}L^4 + 30a_{12}L^2 \\ 3L(3b_{12}L^2 + 40a_{12}) & 21b_{12}L^3 + 240a_{12}L \\ -2L^2(b_{12}L^2 + 15a_{12}) & -3b_{12}L^4 - 30a_{12}L^2 \end{bmatrix}}{b_{12}L^2 + 12a_{12}} \begin{Bmatrix} \tilde{F}_{20} \\ \tilde{F}_{2L} \end{Bmatrix} \\
&+ \frac{\alpha_{m3}(t)}{12} \frac{\begin{bmatrix} -6b_{12}L^2 & -6b_{12}L^2 \\ L(b_{12}L^2 + 48a_{12}) & -b_{12}L^3 + 24a_{12}L \\ 6b_{12}L^2 & 6b_{12}L^2 \\ L(-b_{12}L^2 + 24a_{12}) & b_{12}L^3 + 48a_{12}L \end{bmatrix}}{b_{12}L^2 + 12a_{12}} \begin{Bmatrix} \tilde{m}_{30} \\ \tilde{m}_{3L} \end{Bmatrix} \quad (9.6.19)
\end{aligned}$$

This simplifies for the no-shear deformation assumption to the form

$$\begin{Bmatrix} \tilde{f}_{\text{ext},2} \\ \tilde{f}_{\text{ext},6} \\ \tilde{f}_{\text{ext},8} \\ \tilde{f}_{\text{ext},12} \end{Bmatrix} = \frac{\alpha_{F2}(t)L}{60} \begin{bmatrix} 21 & 9 \\ 3L & 2L \\ 9 & 21 \\ -2L & -3L \end{bmatrix} \begin{Bmatrix} \tilde{F}_{20} \\ \tilde{F}_{2L} \end{Bmatrix} + \frac{\alpha_{m3}(t)}{12} \begin{bmatrix} -6 & -6 \\ L & -L \\ 6 & 6 \\ -L & L \end{bmatrix} \begin{Bmatrix} \tilde{m}_{30} \\ \tilde{m}_{3L} \end{Bmatrix} \quad (9.6.20)$$

9.6.4 \tilde{x}_1 - \tilde{x}_3 Plane Loads

From (4.7.38) and (9.6.1),

$$\begin{Bmatrix} \tilde{f}_{\text{ext},2} \\ \tilde{f}_{\text{ext},6} \\ \tilde{f}_{\text{ext},8} \\ \tilde{f}_{\text{ext},12} \end{Bmatrix} = \alpha_{F3}(t) \int_0^L \tilde{F}_3(\tilde{x}_1) \begin{Bmatrix} N_{11}^{13}(\tilde{x}_1) \\ N_{12}^{13}(\tilde{x}_1) \\ N_{13}^{13}(\tilde{x}_1) \\ N_{14}^{13}(\tilde{x}_1) \end{Bmatrix} d\tilde{x}_1 + \alpha_{m2}(t) \int_0^L \tilde{m}_2(\tilde{x}_1) \begin{Bmatrix} N_{21}^{13}(\tilde{x}_1) \\ N_{22}^{13}(\tilde{x}_1) \\ N_{23}^{13}(\tilde{x}_1) \\ N_{24}^{13}(\tilde{x}_1) \end{Bmatrix} d\tilde{x}_1 \quad (9.6.21)$$

where $N_{ij}^{13}(\tilde{x}_1)$ are defined by (9.5.85).

Point loading: Substitute (9.6.2) and (9.5.85) into (9.6.21) to obtain

$$\begin{Bmatrix} \tilde{f}_{\text{ext},3} \\ \tilde{f}_{\text{ext},5} \\ \tilde{f}_{\text{ext},9} \\ \tilde{f}_{\text{ext},11} \end{Bmatrix} = \alpha_{F3}(t) \tilde{F}_3^* \begin{Bmatrix} N_{11}^{13}(\tilde{x}_1^*) \\ N_{12}^{13}(\tilde{x}_1^*) \\ N_{13}^{13}(\tilde{x}_1^*) \\ N_{14}^{13}(\tilde{x}_1^*) \end{Bmatrix} + \alpha_{m2}(t) \tilde{m}_2^* \begin{Bmatrix} N_{21}^{13}(\tilde{x}_1^*) \\ N_{22}^{13}(\tilde{x}_1^*) \\ N_{23}^{13}(\tilde{x}_1^*) \\ N_{24}^{13}(\tilde{x}_1^*) \end{Bmatrix} \quad (9.6.22)$$

Uniform loading: Substitute (9.6.3) and (9.5.85) into (9.6.21) to obtain

$$\begin{aligned}
 \begin{Bmatrix} \tilde{f}_{\text{ext},3} \\ \tilde{f}_{\text{ext},5} \\ \tilde{f}_{\text{ext},9} \\ \tilde{f}_{\text{ext},11} \end{Bmatrix} &= \alpha_{F3}(t) \bar{F}_3 \int_0^L \begin{Bmatrix} N_{11}^{13}(\tilde{x}_1) \\ N_{12}^{13}(\tilde{x}_1) \\ N_{13}^{13}(\tilde{x}_1) \\ N_{14}^{13}(\tilde{x}_1) \end{Bmatrix} d\tilde{x}_1 + \alpha_{m2}(t) \bar{m}_2 \int_0^L \begin{Bmatrix} N_{21}^{13}(\tilde{x}_1) \\ N_{22}^{13}(\tilde{x}_1) \\ N_{23}^{13}(\tilde{x}_1) \\ N_{24}^{13}(\tilde{x}_1) \end{Bmatrix} d\tilde{x}_1 \\
 &= \alpha_{F3}(t) \bar{F}_3 \begin{Bmatrix} \frac{L}{2} \\ -\frac{L^2}{12} \\ \frac{L}{2} \\ \frac{L^2}{12} \end{Bmatrix} + \frac{\alpha_{m2}(t) \bar{m}_2}{b_{13}L^2 + 12a_{13}} \begin{Bmatrix} b_{13}L^2 \\ 6a_{13}L \\ -b_{13}L^2 \\ 6a_{13}L \end{Bmatrix}
 \end{aligned} \tag{9.6.23}$$

This simplifies for the no-shear deformation assumption to the form

$$\begin{Bmatrix} \tilde{f}_{\text{ext},3} \\ \tilde{f}_{\text{ext},5} \\ \tilde{f}_{\text{ext},9} \\ \tilde{f}_{\text{ext},11} \end{Bmatrix} = \alpha_{F3}(t) \bar{F}_3 \begin{Bmatrix} \frac{L}{2} \\ -\frac{L^2}{12} \\ \frac{L}{2} \\ \frac{L^2}{12} \end{Bmatrix} + \alpha_{m2}(t) \bar{m}_2 \begin{Bmatrix} 1 \\ 0 \\ -1 \\ 0 \end{Bmatrix} \tag{9.6.24}$$

Linear loading: Substitute (9.6.4) and (9.5.85) into (9.6.21) to obtain

$$\begin{aligned}
 \begin{Bmatrix} \tilde{f}_{\text{ext},3} \\ \tilde{f}_{\text{ext},5} \\ \tilde{f}_{\text{ext},9} \\ \tilde{f}_{\text{ext},11} \end{Bmatrix} &= \alpha_{F3}(t) \int_0^L \begin{Bmatrix} N_{11}^{13}(\tilde{x}_1) \\ N_{12}^{13}(\tilde{x}_1) \\ N_{13}^{13}(\tilde{x}_1) \\ N_{14}^{13}(\tilde{x}_1) \end{Bmatrix} \left[1 - \frac{\tilde{x}_1}{L} \quad \frac{\tilde{x}_1}{L} \right] d\tilde{x}_1 \begin{Bmatrix} \tilde{F}_{30} \\ \tilde{F}_{3L} \end{Bmatrix} \\
 &+ \alpha_{m2}(t) \int_0^L \begin{Bmatrix} N_{21}^{13}(\tilde{x}_1) \\ N_{22}^{13}(\tilde{x}_1) \\ N_{23}^{13}(\tilde{x}_1) \\ N_{24}^{13}(\tilde{x}_1) \end{Bmatrix} \left[1 - \frac{\tilde{x}_1}{L} \quad \frac{\tilde{x}_1}{L} \right] d\tilde{x}_1 \begin{Bmatrix} \tilde{m}_{20} \\ \tilde{m}_{2L} \end{Bmatrix}
 \end{aligned}$$

$$\begin{aligned}
& \frac{\alpha_{F3}(t)}{60} \frac{\begin{bmatrix} 3L(7b_{13}L^2 + 80a_{13}) & 9b_{13}L^3 + 120a_{13}L \\ -3L^2(b_{13}L^2 + 10a_{13}) & -2b_{13}L^4 - 30a_{13}L^2 \\ 3L(3b_{13}L^2 + 40a_{13}) & 21b_{13}L^3 + 240a_{13}L \\ 2L^2(b_{13}L^2 + 15a_{13}) & 3b_{13}L^4 + 30a_{13}L^2 \end{bmatrix} \begin{Bmatrix} \tilde{F}_{30} \\ \tilde{F}_{3L} \end{Bmatrix}}{b_{13}L^2 + 12a_{13}} \\
& + \frac{\alpha_{m2}(t)}{12} \frac{\begin{bmatrix} 6b_{13}L^2 & 6b_{13}L^2 \\ L(b_{13}L^2 + 48a_{13}) & -b_{13}L^3 + 24a_{13}L \\ -6b_{13}L^2 & -6b_{13}L^2 \\ -L(b_{13}L^2 - 24a_{13}) & b_{13}L^3 + 48a_{13}L \end{bmatrix} \begin{Bmatrix} \tilde{m}_{20} \\ \tilde{m}_{2L} \end{Bmatrix}}{b_{13}L^2 + 12a_{13}} \quad (9.6.25)
\end{aligned}$$

This simplifies for the no-shear deformation assumption ($a_{13} = 0$) to the form

$$\begin{Bmatrix} \tilde{f}_{\text{ext},3} \\ \tilde{f}_{\text{ext},5} \\ \tilde{f}_{\text{ext},9} \\ \tilde{f}_{\text{ext},11} \end{Bmatrix} = \frac{\alpha_{F3}(t)L}{60} \begin{bmatrix} 21 & 9 \\ -3L & -2L \\ 9 & 21 \\ 2L & 3L \end{bmatrix} \begin{Bmatrix} \tilde{F}_{30} \\ \tilde{F}_{3L} \end{Bmatrix} + \frac{\alpha_{m2}(t)}{12} \begin{bmatrix} 6 & 6 \\ L & -L \\ -6 & -6 \\ -L & L \end{bmatrix} \begin{Bmatrix} \tilde{m}_{20} \\ \tilde{m}_{2L} \end{Bmatrix} \quad (9.6.26)$$

9.6.5 Element Load Vector

The element load vector results are summarized in Table 9.6.1.

The external work is also invariant with respect to the coordinates in which it is expressed; therefore,

$$W_e^E = \tilde{f}_e^T \tilde{q}_e = f_e^T q_e \quad (9.6.27)$$

Substitution of (9.4.11) into (9.6.27) yields

$$\tilde{f}_e^T \tilde{T}_e q_e = f_e^T q_e \quad (9.6.28)$$

which is true for all q_e , if and only if

$$f_e = \tilde{T}_e^T \tilde{f}_e \quad (9.6.29)$$

where \tilde{T}_e is defined in (9.4.10), (9.4.11), (9.4.19), and (9.4.23). The total system model external force vector is formed by assembling the element force vectors in their global coordinate form (9.6.29).

Table 9.6.1 Element load vector \tilde{f}_e for point, uniform, and linearly varying loads

Term	Point load	Uniform load	Linearly varying load
$\tilde{f}_{\text{ext},1}$	$\alpha_{F1}(t)\tilde{F}_1^* \left(1 - \frac{\tilde{x}^*}{L}\right)$	$\alpha_{F1}(t)\tilde{F}_1 \frac{L}{2}$	$\alpha_{F1}(t)L \frac{(2\tilde{F}_{10} + \tilde{F}_{1L})}{6}$
$\tilde{f}_{\text{ext},2}$	$\alpha_{F2}(t)\tilde{F}_2^* N_{11}^{12}(\tilde{x}^*) + \alpha_{m3}(t)\tilde{m}_3^* N_{21}^{12}(\tilde{x}^*)$	$\alpha_{F2}(t)\tilde{F}_2 \frac{L}{2} - \alpha_{m3}(t)\tilde{m}_3 L^2 a_{F2}^{12}$	$\alpha_{F2}(t)(b_{F1}^{12}\tilde{F}_{20} + b_{F2}^{12}\tilde{F}_{2L}) + \alpha_{m3}(t)(-b_{F5}^{12}\tilde{m}_{30} - b_{F5}^{12}\tilde{m}_{3L})$
$\tilde{f}_{\text{ext},3}$	$\alpha_{F3}(t)\tilde{F}_3^* N_{11}^{13}(\tilde{x}^*) + \alpha_{m2}(t)\tilde{m}_2^* N_{21}^{13}(\tilde{x}^*)$	$\alpha_{F3}(t)\tilde{F}_3 \frac{L}{2} + \alpha_{m2}(t)\tilde{m}_2 L^2 a_{F2}^{13}$	$\alpha_{F3}(t)(b_{F1}^{13}\tilde{F}_{30} + b_{F4}^{13}\tilde{F}_{3L}) + \alpha_{m2}(t)(b_{F5}^{13}\tilde{m}_{20} + b_{F5}^{13}\tilde{m}_{2L})$
$\tilde{f}_{\text{ext},4}$	$\alpha_{m1}(t)\tilde{m}_1^* \left(1 - \frac{\tilde{x}^*}{L}\right)$	$\alpha_{m1}(t)\tilde{m}_1 \frac{L}{2}$	$\alpha_{m1}(t)L \frac{(2\tilde{m}_{10} + \tilde{m}_{1L})}{6}$
$\tilde{f}_{\text{ext},5}$	$\alpha_{F3}(t)\tilde{F}_3^* N_{12}^{13}(\tilde{x}^*) + \alpha_{m2}(t)\tilde{m}_2^* N_{22}^{13}(\tilde{x}^*)$	$-\alpha_{F3}(t)\tilde{F}_3 \frac{L^2}{12} + 6\alpha_{m2}(t)\tilde{m}_2 L a_{F1}^{13}$	$\alpha_{F3}(t)(-b_{F3}^{13}\tilde{F}_{30} - b_{F4}^{13}\tilde{F}_{3L}) + \alpha_{m2}(t)(b_{F6}^{13}\tilde{m}_{20} + b_{F7}^{13}\tilde{m}_{2L})$
$\tilde{f}_{\text{ext},6}$	$\alpha_{F2}(t)\tilde{F}_2^* N_{12}^{12}(\tilde{x}^*) + \alpha_{m3}(t)\tilde{m}_3^* N_{22}^{12}(\tilde{x}^*)$	$\alpha_{F2}(t)\tilde{F}_2 \frac{L^2}{12} + 6\alpha_{m3}(t)\tilde{m}_3 L a_{F1}^{12}$	$\alpha_{F2}(t)(b_{F3}^{12}\tilde{F}_{20} + b_{F4}^{12}\tilde{F}_{2L}) + \alpha_{m3}(t)(b_{F6}^{12}\tilde{m}_{30} + b_{F7}^{12}\tilde{m}_{3L})$
$\tilde{f}_{\text{ext},7}$	$\alpha_{F1}(t)\tilde{F}_1^* \frac{\tilde{x}^*}{L}$	$\alpha_{F1}(t)\tilde{F}_1 \frac{L}{2}$	$\alpha_{F1}(t)L \frac{(\tilde{F}_{10} + 2\tilde{F}_{1L})}{6}$
$\tilde{f}_{\text{ext},8}$	$\alpha_{F2}(t)\tilde{F}_2^* N_{13}^{12}(\tilde{x}^*) + \alpha_{m3}(t)\tilde{m}_3^* N_{23}^{12}(\tilde{x}^*)$	$\alpha_{F2}(t)\tilde{F}_2 \frac{L}{2} + \alpha_{m3}(t)\tilde{m}_3 L^2 a_{F2}^{12}$	$\alpha_{F2}(t)(b_{F2}^{12}\tilde{F}_{20} + b_{F1}^{12}\tilde{F}_{2L}) + \alpha_{m3}(t)(b_{F5}^{12}\tilde{m}_{30} + b_{F5}^{12}\tilde{m}_{3L})$
$\tilde{f}_{\text{ext},9}$	$\alpha_{F3}(t)\tilde{F}_3^* N_{13}^{13}(\tilde{x}^*) + \alpha_{m2}(t)\tilde{m}_2^* N_{23}^{13}(\tilde{x}^*)$	$\alpha_{F3}(t)\tilde{F}_3 \frac{L}{2} - \alpha_{m2}(t)\tilde{m}_2 L^2 a_{F2}^{13}$	$\alpha_{F3}(t)(b_{F2}^{13}\tilde{F}_{30} + b_{F1}^{13}\tilde{F}_{3L}) + \alpha_{m2}(t)(-b_{F5}^{13}\tilde{m}_{20} - b_{F5}^{13}\tilde{m}_{2L})$
$\tilde{f}_{\text{ext},10}$	$\alpha_{m1}(t)\tilde{m}_1^* \frac{\tilde{x}^*}{L}$	$\alpha_{m1}(t)\tilde{m}_1 \frac{L}{2}$	$\alpha_{m1}(t)L \frac{(\tilde{m}_{10} + 2\tilde{m}_{1L})}{6}$
$\tilde{f}_{\text{ext},11}$	$\alpha_{F3}(t)\tilde{F}_3^* N_{14}^{13}(\tilde{x}^*) + \alpha_{m2}(t)\tilde{m}_2^* N_{24}^{13}(\tilde{x}^*)$	$\alpha_{F3}(t)\tilde{F}_3 \frac{L^2}{12} + 6\alpha_{m2}(t)\tilde{m}_2 L a_{F1}^{13}$	$\alpha_{F3}(t)(b_{F4}^{13}\tilde{F}_{30} + b_{F3}^{13}\tilde{F}_{3L}) + \alpha_{m2}(t)(b_{F7}^{13}\tilde{m}_{20} + b_{F6}^{13}\tilde{m}_{2L})$
$\tilde{f}_{\text{ext},12}$	$\alpha_{F2}(t)\tilde{F}_2^* N_{14}^{12}(\tilde{x}^*) + \alpha_{m3}(t)\tilde{m}_3^* N_{24}^{12}(\tilde{x}^*)$	$-\alpha_{F2}(t)\tilde{F}_2 \frac{L^2}{12} + 6\alpha_{m3}(t)\tilde{m}_3 L a_{F1}^{12}$	$\alpha_{F2}(t)(-b_{F4}^{12}\tilde{F}_{20} - b_{F3}^{12}\tilde{F}_{2L}) + \alpha_{m3}(t)(b_{F7}^{12}\tilde{m}_{30} + b_{F6}^{12}\tilde{m}_{3L})$

Where $a_{F1}^{12} = \frac{a_{12}}{b_{12}L^2 + 12a_{12}}$, $a_{F2}^{12} = \frac{b_{12}}{b_{13}L^2 + 12a_{12}}$, $a_{F3}^{12} = \frac{a_{13}}{b_{13}L^2 + 12a_{13}}$, $a_{F1}^{13} = \frac{a_{13}}{b_{13}L^2 + 12a_{13}}$, $a_{F2}^{13} = \frac{b_{13}}{b_{13}L^2 + 12a_{13}}$, $a_{F3}^{13} = \frac{1}{b_{13}L^2 + 12a_{13}}$, $b_{F1}^{12} = 3L(7b_{12}L^2 + 80a_{12})\frac{a_{F3}^{12}}{60}$, $b_{F2}^{12} = (9b_{12}L^3 + 120a_{12}L)\frac{a_{F3}^{12}}{60}$, $b_{F3}^{12} = 3L^2(b_{12}L^2 + 10a_{12})\frac{a_{F3}^{12}}{60}$, $b_{F4}^{12} = 2b_{12}L^4 + 30a_{12}L^2\frac{a_{F3}^{12}}{60}$, $b_{F5}^{12} = L(b_{12}L^2 + 48a_{12})\frac{a_{F3}^{12}}{12}$, $b_{F6}^{12} = (-b_{12}L^3 + 24a_{12}L)\frac{a_{F3}^{12}}{12}$, $b_{F7}^{12} = (9b_{13}L^3 + 120a_{13}L)\frac{a_{F3}^{13}}{60}$, $b_{F1}^{13} = 3L^2(b_{13}L^2 + 10a_{13})\frac{a_{F3}^{13}}{60}$, $b_{F2}^{13} = (9b_{13}L^3 + 120a_{13}L)\frac{a_{F3}^{13}}{60}$, $b_{F3}^{13} = 3L^2(b_{13}L^2 + 10a_{13})\frac{a_{F3}^{13}}{60}$, $b_{F4}^{13} = 2b_{13}L^4 + 30a_{13}L^2\frac{a_{F3}^{13}}{60}$, $b_{F5}^{13} = 6b_{13}L^2\frac{a_{F3}^{13}}{12}$, $b_{F6}^{13} = L(b_{13}L^2 + 48a_{13})\frac{a_{F3}^{13}}{12}$, $b_{F7}^{13} = (-b_{13}L^3 + 24a_{13}L)\frac{a_{F3}^{13}}{12}$.

9.7 3D FRAME: BEAM ELEMENT ASSEMBLY ALGORITHM

The global coordinate form of the element mass \underline{M}^e and stiffness \underline{K}^e matrices and force vector are defined by (9.5.142), (9.5.143), and (9.6.29), respectively. Algorithms are presented here for assembling these “building block” element matrices to form the system mass and stiffness matrices and force vector, including zero deflection constraints imposed on specified dofs. As depicted in Figure 9.7.1, the nodal connectivity array for element e stores the global node numbers corresponding to local node numbers $j = 1$ and $j = 2$ and is defined by

$$B_{ej} = \begin{cases} g_{1e}, & j=1 \\ g_{2e}, & j=2 \end{cases} = \text{global node number corresponding to local node } j \text{ of element } e \quad (9.7.1)$$

As depicted in Figure 9.7.1, the dof connectivity array for element e stores the global dof numbers corresponding to local dof numbers $l = 1$ through $l = 12$, that is,

$$\hat{B}_{el} = \text{global degree of freedom number corresponding to local degree of freedom } l \text{ of element } e \quad (9.7.2)$$

and is defined in Table 9.7.1.

The pattern in Table 9.7.1 enables automated generation of the dof connectivity array utilizing the user-defined nodal connectivity array. This is demonstrated in the following coding segment:

```

for  $e = 1 : 1 : E$     (element index)
  for  $i = 1 : 1 : 2$     (local node index)
    for  $k = 1 : 1 : 6$  (dof index at a node)
       $l = 6 * (i - 1) + k$ 
       $\hat{B}_{el} = 6 * (B_{ei} - 1) + k$ 
    end
  end
end

```

(9.7.3)

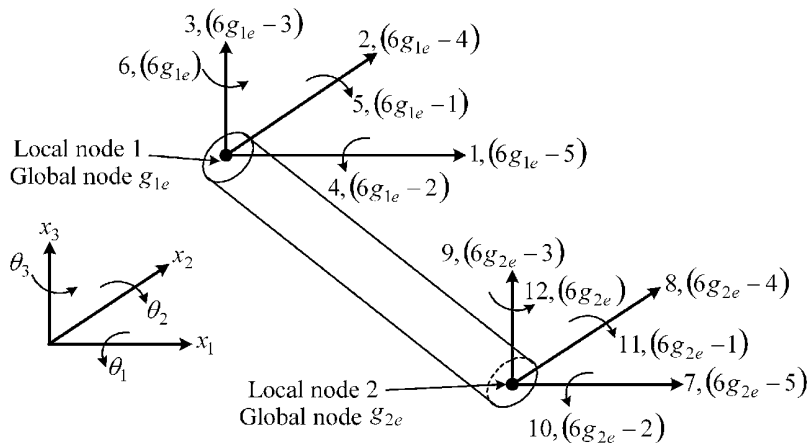


Figure 9.7.1 Local and global node and degree of freedom numbering convention

Table 9.7.1 3D beam element connectivity for element e

l	1	2	3	4	5	6	7	8	9	10	11	12
\hat{B}_{el}	$\begin{pmatrix} 6g_{1e} \\ -5 \end{pmatrix}$	$\begin{pmatrix} 6g_{1e} \\ -4 \end{pmatrix}$	$\begin{pmatrix} 6g_{1e} \\ -3 \end{pmatrix}$	$\begin{pmatrix} 6g_{1e} \\ -2 \end{pmatrix}$	$\begin{pmatrix} 6g_{1e} \\ -1 \end{pmatrix}$	$6g_{1e}$	$\begin{pmatrix} 6g_{2e} \\ -5 \end{pmatrix}$	$\begin{pmatrix} 6g_{2e} \\ -4 \end{pmatrix}$	$\begin{pmatrix} 6g_{2e} \\ -3 \end{pmatrix}$	$\begin{pmatrix} 6g_{2e} \\ -2 \end{pmatrix}$	$\begin{pmatrix} 6g_{2e} \\ -1 \end{pmatrix}$	$6g_{2e}$

This short list of commands generates the dof connectivity array \hat{B} given the nodal connectivity array B . As in (4.8.35) or (4.8.94), the *larray* indicates the locations of each “free” (unconstrained) dof in the condensed vector q_f of only free (unconstrained) dof displacements. The *larray* is again represented by

$$\begin{aligned} \tilde{L} &= (l_1 \ l_2 \ \cdots \ l_N) \\ l_i &= \text{position of dof } q_i \text{ in the “free” dof vector } q_f \\ & (l_i = 0 \text{ if } q_i \text{ is constrained}) \end{aligned} \quad (9.7.4)$$

Suppose that the user input to a code requires entry of the nodes and corresponding dofs that are fixed to ground, that is, that have zero displacement. This may be prompted as:

For all constrained dofs, enter the global node number k_i and the corresponding dof d_i at global node number k_i that is fixed to ground, for $i = 1, m$, where m is the total number of fixed dofs in the model. The direction of a fixed dof is $d_i = 1$ (x_1 direction), $d_i = 2$ (x_2 direction), $d_i = 3$ (x_3 direction), $d_i = 4$ (θ_1 direction), $d_i = 5$ (θ_2 direction), and $d_i = 6$ (θ_3 direction) in Figure 9.7.1.

The code internally defines an array *fixeddof* containing all of the global dof numbers that are fixed to ground:

$$\begin{aligned} &\text{for } i = 1 : 1 : m \\ &\quad \text{fixeddof}(i) = 6 * (k_i - 1) + d_i \\ &\text{end} \end{aligned} \quad (9.7.5)$$

Let *Ndof* be the total number of dofs in the entire model:

$$Ndof = 6 * (\text{Number of nodes in entire model}) \quad (9.7.6)$$

Then the *larray* is determined from

$$\begin{aligned} &ict = 0 \\ &\text{for } i = 1 : 1 : Ndof \\ &\quad iflag = 0 \\ &\quad \text{for } j = 1 : 1 : m \\ &\quad \quad \text{if } i = \text{fixeddof}(j) \\ &\quad \quad \quad iflag = 1 \\ &\quad \quad \text{end} \\ &\quad \text{end} \end{aligned}$$

$$\begin{aligned}
 & larray(i) = 0 \\
 & \text{if } iflag = 0 \\
 & \quad ict = ict + 1 \\
 & \quad larray(i) = ict \\
 & \text{end} \\
 & \text{end}
 \end{aligned} \tag{9.7.7}$$

The assembly of the system matrices for the free (unconstrained) dofs is illustrated in Figure 9.2.6. Similar with (9.2.84), repeat the above “assembly” step for all E elements in the model and for all 12 local dofs, that is,

$$e = 1, 2, \dots, E, \quad r = 1, \dots, 12, \quad s = 1, \dots, 12 \tag{9.7.8}$$

As in (9.2.85), imposing the zero-displacement constraint conditions yields the following “condensed” dynamic equilibrium equation for the “free” (unconstrained) dofs of the constrained structure:

$$\underset{N_f \times N_f}{\underline{M}_f} \ddot{\underset{N_f \times 1}{\underline{q}}_f} + \underset{N_f \times N_f}{\underline{C}_f} \dot{\underset{N_f \times 1}{\underline{q}}_f} + \underset{N_f \times N_f}{\underline{K}_f} \underset{N_f \times 1}{\underline{q}}_f = \underset{N_f \times 1}{\underline{F}_f} \tag{9.7.9}$$

EXAMPLE 9.7.1 *Natural Frequencies and Mode Shapes for 3D Pipe Run and Valve Support Stand*

Statement: Excessive vibration of piping in petrochemical, utility, and processing plants may lead to high-cycle fatigue failure (cracking), fastener looseness, and leakage. This is especially menacing when the pipe is transporting volatile gases. Therefore, it is very important to design piping systems with natural frequencies sufficiently displaced from source frequencies (rotating and reciprocating machinery, internal vortex shedding sources, etc.).

Objective: Determine the natural frequencies and mode shapes of the piping and support structure shown in Figure E9.7.1(a).

Assumptions:

- (a) Small (linear) motions of all nodes in the model.
- (b) Pipe clamps act as linear springs connecting nodes 11 and 17 and 21 and 30 to ground.
- (c) The valve may be treated as a rigid, concentrated inertia.
- (d) The structure is fixed to ground in all of its 6 dofs at nodes 1, 6, 16, 33, and 36.
- (e) The pipe is connected to a furnace metallic seal which acts as a set of springs at node 44.

Coding: The MATLAB code for this example is in Appendix C.

Solution:

- (a) Model Characteristics:

$$\begin{aligned}
 N_n &= 44 \text{ nodes} \\
 N_d &= 6N_n = 264 \text{ total degrees of freedom} \\
 E &= N_e = 43 \text{ elements (circled)}
 \end{aligned} \tag{1}$$

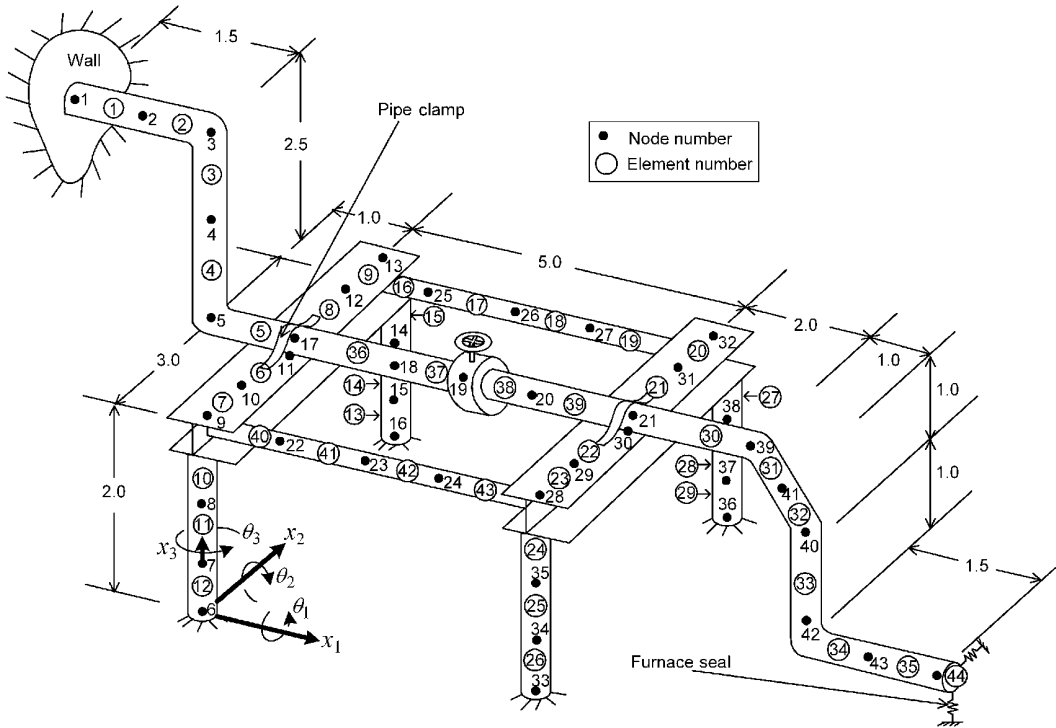


Figure E9.7.1(a) Beam model of pipe run and valve support stand (lengths in meters)

Table E9.7.1(a) Global degree of freedom ordering convention

Global dof no.	Location	Global dof no.	Location
1	x_1 dof at global node 1	259	x_1 dof at global node 44
2	x_2 dof at global node 1	260	x_2 dof at global node 44
3	x_3 dof at global node 1	261	x_3 dof at global node 44
4	θ_1 dof at global node 1	262	θ_1 dof at global node 44
5	θ_2 dof at global node 1	263	θ_2 dof at global node 44
6	θ_3 dof at global node 1	264	θ_3 dof at global node 44
⋮	⋮	⋮	⋮

The dof ordering convention follows Figure 9.7.1 and is shown in Table E9.7.1(a). Many of the beam elements in Figure E9.7.1(a) have identical properties. This fact can be utilized to reduce the amount of required input data for the code. This is facilitated by defining element “types.”

(b) Element Types:

(i) Type 1: Main Pipe Run Extending from Wall to Furnace

Nominal diameter = 0.127 m, pipe schedule = 40, wall thickness = 6.45×10^{-3} m
 OD = 0.141 m, $\rho = 7834 \text{ kg/m}^3$, $E = 2.14 \times 10^{11} \text{ N/m}^2$, $\nu = 0.3$,

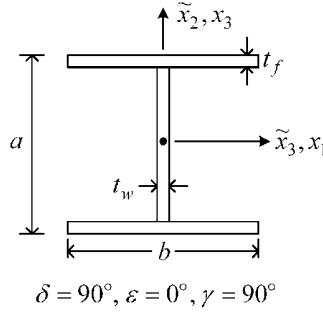


Figure E9.7.1(b) Cross section of I beam for the valve support stand

$$\begin{aligned}
 I_{\bar{x}_2} = I_{\bar{x}_3} &= \pi(OD^4 - ID^4)/64 = 6.3 \times 10^{-6} \text{ m}^4, \\
 J &= \pi(OD^4 - ID^4)/32 = 12.6 \times 10^{-6} \text{ m}^4, \\
 A &= \pi(OD^2 - ID^2)/4 = 2.77 \times 10^{-3} \text{ m}^2
 \end{aligned} \tag{2}$$

- (ii)** Type 2: Horizontal I Beams (Figures 9.4.8, 9.4.9, E9.7.1(a), and E9.7.1(b))
 From AISC (1980)
 Beam Type: W8 × 21

$$\begin{aligned}
 a &= 0.21 \text{ m}, \quad b = 0.134 \text{ m}, \quad \rho = 7834 \text{ kg/m}^3 \\
 t_w &= 6.35 \times 10^{-3} \text{ m}, \quad t_f = 1.02 \times 10^{-2} \text{ m}, \quad \nu = 0.3 \\
 E &= 2.14 \times 10^{11} \text{ N/m}^2 \\
 I_{\bar{x}_2} &= 4.07 \times 10^{-6} \text{ m}^4, \quad I_{\bar{x}_3} = 3.12 \times 10^{-5} \text{ m}^4, \\
 J &= 1.17 \times 10^{-7} \text{ m}^4, \quad A = 3.97 \times 10^{-3} \text{ m}^2
 \end{aligned} \tag{3}$$

- (iii)** Type 3: Vertical Support and Horizontal Support Stand Pipe
 Nominal diameter = 0.102 m, pipe schedule = 40, wall thickness = 6.02×10^{-3} m
 OD = 0.114 m, $\rho = 7834 \text{ kg/m}^3$, $E = 2.14 \times 10^{11} \text{ N/m}^2$, $\nu = 0.3$

$$\begin{aligned}
 I_{\bar{x}_2} = I_{\bar{x}_3} &= \frac{\pi(OD^4 - ID^4)}{64} = 3.01 \times 10^{-6} \text{ m}^4 \\
 J &= \frac{\pi(OD^4 - ID^4)}{32} = 6.02 \times 10^{-6} \text{ m}^4, \quad A = \frac{\pi(OD^2 - ID^2)}{4} = 2.05 \times 10^{-3} \text{ m}^2
 \end{aligned} \tag{4}$$

- (iv)** Type 4: Pipe Clamps and Furnace Seal (Both Clamps Have the Same Stiffness)
 Clamps:

$$\begin{aligned}
 k_{x_1 x_1}^c &= 8.75 \times 10^6 \text{ N/m}, \quad k_{\theta_1 \theta_1}^c = 111 \text{ Nm/rad}, \\
 k_{x_2 x_2}^c &= 17.5 \times 10^6 \text{ N/m}, \quad k_{\theta_2 \theta_2}^c = 111 \text{ Nm/rad}, \\
 k_{x_3 x_3}^c &= 26.3 \times 10^6 \text{ N/m}, \quad k_{\theta_3 \theta_3}^c = 222 \text{ Nm/rad}
 \end{aligned} \tag{5}$$

Furnace Seal:

$$\begin{aligned} k_{x_1x_1}^f &= 10.0 \times 10^6 \text{ N/m}, & k_{\theta_1\theta_1}^f &= 500 \text{ Nm/rad} \\ k_{x_2x_2}^f &= 15.0 \times 10^6 \text{ N/m}, & k_{\theta_2\theta_2}^f &= 250 \text{ Nm/rad} \\ k_{x_3x_3}^f &= 15.0 \times 10^6 \text{ N/m}, & k_{\theta_3\theta_3}^f &= 250 \text{ Nm/rad} \end{aligned} \quad (6)$$

(v) Type 5: Valve

$$m = 100 \text{ kg}, \quad (I_{x_1x_1} \quad I_{x_2x_2} \quad I_{x_3x_3}) = (1.25 \quad 1.0 \quad 0.75) \text{ kg} \cdot \text{m}^2 \quad (7)$$

where the inertias are referenced to the global x_1, x_2, x_3 axes in Figure E9.7.1(a).

(c) Element Summary by Nodal Connectivity and Element Type

Table E9.7.1(b) summarizes the elements in Figure E9.7.1(a).

The nodal connectivity array is given in Table E9.7.1(b). The dof connectivity array is automatically generated using the algorithm in (9.7.3).

Table E9.7.1(b) Element summary for Figure E9.7.1(a)

Element number (e)	Nodal connectivity			Element number (e)	Nodal connectivity		
	Local node 1 $ICON(e,1)$	Local node 2 $ICON(e,2)$	Type		Local node 1 $ICON(e,1)$	Local node 2 $ICON(e,2)$	Type
1	1	2	1	25	34	35	3
2	2	3	1	26	33	34	3
3	3	4	1	27	38	32	3
4	4	5	1	28	37	38	3
5	5	17	1	29	36	37	3
6	10	11	2	30	21	39	1
7	9	10	2	31	39	41	1
8	11	12	2	32	41	40	1
9	12	13	2	33	40	42	1
10	8	9	3	34	42	43	1
11	7	8	3	35	43	44	1
12	6	7	3	36	17	18	1
13	16	15	3	37	18	19	1
14	15	14	3	38	19	20	1
15	14	13	3	39	20	21	1
16	13	25	3	40	9	22	3
17	25	26	3	41	22	23	3
18	26	27	3	42	23	24	3
19	27	32	3	43	24	28	3
20	31	32	2	44	Clamp between nodes 11 and 17		4
21	30	31	2	45	Clamp between nodes 21 and 30		4
22	29	30	2	46	Furnace seal from node 44 to ground		4
23	28	29	2	47	Valve at node 19		5
24	35	28	3				

(d) Fixed Degrees of Freedom and the “ l ” and “ j ” Arrays

Table E9.7.1(c) summarizes the fixed dofs in Figure E9.7.1(a).

Thus, it is seen that the total number of nonprescribed dofs is

$$\begin{aligned} N_{\text{npd}} &= (\text{total no. of dofs}) - (\text{no. of prescribed dofs}) \\ &= N_d - N_{\text{pd}} = 6 * \text{no. of nodes} - 30 = 6 * 44 - 30 = 234 \end{aligned} \quad (8)$$

The last column in Table E9.7.1(c) is the “fixeddof” array in (9.7.7) which generates the $larray$ in the system matrix assembly algorithm (Figure 9.2.6).

As in Example 9.2.3, a “ $jarray$ ” is formed to “expand” the response vectors into their full dimension (N_d), which includes both fixed and free dofs. The $jarray(j_i)$ is

Table E9.7.1(c) Fixed degrees of freedom (dofs) in Figure E9.7.1(a)

Number l	Node	Direction	Global dof no. i_{pdl}
1	1	x_1	1
2	1	x_2	2
3	1	x_3	3
4	1	θ_1	4
5	1	θ_2	5
6	1	θ_3	6
7	6	x_1	31
8	6	x_2	32
9	6	x_3	33
10	6	θ_1	34
11	6	θ_2	35
12	6	θ_3	36
13	16	x_1	91
14	16	x_2	92
15	16	x_3	93
16	16	θ_1	94
17	16	θ_2	95
18	16	θ_3	96
19	33	x_1	193
20	33	x_2	194
21	33	x_3	195
22	33	θ_1	196
23	33	θ_2	197
24	33	θ_3	198
25	36	x_1	211
26	36	x_2	212
27	36	x_3	213
28	36	θ_1	214
29	36	θ_2	215
30	36	θ_3	216

formed by utilizing the input array of fixed dofs (i_{pd}) from Table E9.7.1(c) as shown below:

```

I = 0
for i = 1, Nd (= 264)
    flag = 0
    for l = 1, Npd (= 30)
        if i = ipdl
            flag = 1
        end
    end
    end
    if flag = 0
        I = I + 1
        JArray(I) = i
    end
end
end
Nnpd = I

```

(9)

(e) Form the Condensed System Stiffness Matrix

The system stiffness matrix (\underline{K}_f) with fixed constraints imposed is formed with the assembly algorithm illustrated in Figure 9.2.6. Each entry of all element stiffness matrices (9.5.142, which is the global coordinate form of 9.5.136) is added into the condensed form \underline{K}_f of the system stiffness matrix for

$$e = 1, 2, \dots, E, \quad r = 1, \dots, 12, \quad s = 1, \dots, 12 \quad (10)$$

where E is the total number of beam elements, which is 43 for this example. The assembly is described in the coding outline below, which is equivalent to Figure 9.2.6.

Initialize: $\underline{K}_f = \underline{0}$

for $e = 1, N_e (= 43)$

form the coordinate transformation matrix \tilde{T}_e utilizing Equations (9.4.10), (9.4.19), or (9.4.23)

form the e th element stiffness matrix \tilde{K}_e in local coordinates using Equation (9.5.136)

form the e th element stiffness matrix \underline{K}_e in global coordinates using Equation (9.5.142)

$$\underline{K}_e = \tilde{T}_e^T \tilde{K}_e \tilde{T}_e$$

for $r = 1, 12$

for $s = 1, 12$

```

       $\hat{B}_{er} = \text{ICONDOF}(e, r)$ 
       $\hat{B}_{es} = \text{ICONDOF}(e, s)$ 
       $l_{\hat{B}_{er}} = \text{larray}(\hat{B}_{er})$ 
       $l_{\hat{B}_{es}} = \text{larray}(\hat{B}_{es})$ 
      if  $l_{\hat{B}_{er}} \neq 0$  and  $l_{\hat{B}_{es}} \neq 0$ 
           $\underline{K}_f(l_{\hat{B}_{er}}, l_{\hat{B}_{es}}) = \underline{K}_f(l_{\hat{B}_{er}}, l_{\hat{B}_{es}}) + \underline{K}_e(r, s)$ 
      end
    end
  end
end

```

(11)

where **ICONDOF** is a 2D (coding) array that stores the dof connectivities (9.7.3) and **LArray** is a 1D (coding) array that stores the *larray* in (9.7.7). The above code segment (10) accounts only for the stiffness of the beam elements in the model. The stiffness of the clamps and furnace seal connecting nodes 11 and 17, 21 and 30, and 44 and 0 (ground) must still be assembled into the condensed form \underline{K}_f of the system stiffness matrix. These stiffness components and their locations are summarized in Table E9.7.1(d).

The force displacement law for a stiffness (\hat{k}) connected between 2 dofs d_1 and d_2 is given by

$$\begin{Bmatrix} F_{d1} \\ F_{d2} \end{Bmatrix} = \begin{bmatrix} \hat{k} & -\hat{k} \\ -\hat{k} & \hat{k} \end{bmatrix} \begin{Bmatrix} x_{d1} \\ x_{d2} \end{Bmatrix} \quad (12)$$

The force F_{d1} and F_{d2} will be added into the d_1 and d_2 rows of the full system equations, respectively. The terms multiplying x_{d1} in (12) will be added into the d_1 column of the full \underline{K} matrix and those multiplying x_{d2} will be added into the d_2 column of the full \underline{K} matrix. Therefore, assembly of the spring stiffness \hat{k} into the full \underline{K} matrix is performed as follows:

$$\begin{aligned} (\underline{K})_{d1,d1} &= (\underline{K})_{d1,d1} + \hat{k} \\ (\underline{K})_{d1,d2} &= (\underline{K})_{d1,d2} - \hat{k} \\ (\underline{K})_{d2,d1} &= (\underline{K})_{d2,d1} - \hat{k} \\ (\underline{K})_{d2,d2} &= (\underline{K})_{d2,d2} + \hat{k} \end{aligned} \quad (13)$$

Table E9.7.1(d) Pipe clamp and furnace seal stiffness connecting node I and J and their degrees of freedom (dofs)

Number m	Stiffness k_{sm}	Node I	Local dof	Global dof	Global dof in condensed system	Node J	Local dof	Global dof	Global dof in condensed system
1	k_{x_1, x_1}^c	11	1	61	$l_{61} = 49$	17	1	97	$l_{97} = 79$
2	k_{x_2, x_2}^c	11	2	62	$l_{62} = 50$	17	2	98	$l_{98} = 80$
3	k_{x_3, x_3}^c	11	3	63	$l_{63} = 51$	17	3	99	$l_{99} = 81$
4	k_{θ_1, θ_1}^c	11	4	64	$l_{64} = 52$	17	4	100	$l_{100} = 82$
5	k_{θ_2, θ_2}^c	11	5	65	$l_{65} = 53$	17	5	101	$l_{101} = 83$
6	k_{θ_3, θ_3}^c	11	6	66	$l_{66} = 54$	17	6	102	$l_{102} = 84$
7	k_{x_1, x_1}^c	30	1	175	$l_{175} = 157$	21	1	121	$l_{121} = 103$
8	k_{x_2, x_2}^c	30	2	176	$l_{176} = 158$	21	2	122	$l_{122} = 104$
9	k_{x_3, x_3}^c	30	3	177	$l_{177} = 159$	21	3	123	$l_{123} = 105$
10	k_{θ_1, θ_1}^c	30	4	178	$l_{178} = 160$	21	4	124	$l_{124} = 106$
11	k_{θ_2, θ_2}^c	30	5	179	$l_{179} = 161$	21	5	125	$l_{125} = 107$
12	k_{θ_3, θ_3}^c	30	6	180	$l_{180} = 162$	21	6	126	$l_{126} = 108$
13	k_{x_1, x_1}^f	44	1	259	$l_{259} = 229$	0	—	0	—
14	k_{x_2, x_2}^f	44	2	260	$l_{260} = 230$	0	—	0	—
15	k_{x_3, x_3}^f	44	3	261	$l_{261} = 231$	0	—	0	—
16	k_{θ_1, θ_1}^f	44	4	262	$l_{262} = 232$	0	—	0	—
17	k_{θ_2, θ_2}^f	44	5	263	$l_{263} = 233$	0	—	0	—
18	k_{θ_3, θ_3}^f	44	6	264	$l_{264} = 234$	0	—	0	—

Node 0 is ground (fixed point).

Assembly of \hat{k} into the condensed system stiffness matrix is performed by using the *larray* as follows:

$$\begin{aligned}
 \left(\underline{K}_f \right)_{l_{d1}, l_{d1}} &= \left(\underline{K}_f \right)_{l_{d1}, l_{d1}} + \hat{k} \\
 \left(\underline{K}_f \right)_{l_{d1}, l_{d2}} &= \left(\underline{K}_f \right)_{l_{d1}, l_{d2}} - \hat{k} \\
 \left(\underline{K}_f \right)_{l_{d2}, l_{d1}} &= \left(\underline{K}_f \right)_{l_{d2}, l_{d1}} - \hat{k} \\
 \left(\underline{K}_f \right)_{l_{d2}, l_{d2}} &= \left(\underline{K}_f \right)_{l_{d2}, l_{d2}} + \hat{k}
 \end{aligned} \tag{14}$$

This stiffness assembly procedure is utilized for all 18 stiffness terms in Table E9.7.1 (d). Note that if l_{d2} is zero, as is the case for node 44 in Table E9.7.1(d), the assembly simplifies to

$$\left(\underline{K}_f \right)_{l_{d1}, l_{d1}} = \left(\underline{K}_f \right)_{l_{d1}, l_{d1}} + \hat{k} \tag{15}$$

The constraint condensed form \underline{K}_f of the system stiffness matrix is completely assembled when this is finished. Appendix C has the MATLAB code for this and all steps in this example.

(f) Form the Condensed System Mass Matrix

The system mass matrix (M_f) with fixed constraints imposed is formed with the assembly algorithm illustrated in Figure 9.2.6. Each entry of all element mass matrices (9.5.143) is added into the condensed form \underline{M}_f of the system mass matrix for

$$e = 1, 2, \dots, E, \quad r = 1, \dots, 12, \quad s = 1, \dots, 12 \quad (16)$$

where E is the total number of beam elements, which is 43 for this example. The assembly is described in the coding outline below, which is equivalent to Figure 9.2.6, and where ICONDOF is a 2D code array that stores the dof connectivities \hat{B}_{el} (9.7.3), and $larray$ is a 1D code array that stores the $larray$ l_i in (9.7.4) and (9.7.7).

```

Initialize:  $\underline{M}_f = \underline{0}$ 

for  $e = 1, N_e$  ( $= 43$ )
    form the coordinate transformation matrix  $\tilde{T}_e$  utilizing (9.4.10), (9.4.19), or (9.4.23)
    form the  $e$ th element mass matrix  $\tilde{M}_e$  in local coordinates using Table 9.5.2
    form the  $e$ th element mass matrix  $\underline{M}_e$  in global coordinates using Equation (9.5.143)

         $\underline{M}_e = \tilde{T}_e^T \tilde{M}_e \tilde{T}_e$ 

        for  $r = 1, 12$ 
            for  $s = 1, 12$ 
                 $\hat{B}_{er} = ICONDOF(e, r)$ 
                 $\hat{B}_{es} = ICONDOF(e, s)$ 
                 $l_{\hat{B}_{er}} = larray(\hat{B}_{er})$ 
                 $l_{\hat{B}_{es}} = larray(\hat{B}_{es})$ 
                if  $l_{\hat{B}_{er}} \neq 0$  and  $l_{\hat{B}_{es}} \neq 0$ 
                     $\underline{M}_f(l_{\hat{B}_{er}}, l_{\hat{B}_{es}}) = \underline{M}_f(l_{\hat{B}_{er}}, l_{\hat{B}_{es}}) + \underline{M}_e(r, s)$ 
                end
            end
        end
    end
end

```

(17)

The above code segment (17) accounts for only the mass of the beam elements in the model.

The valve inertia must still be assembled into the mass matrix. The valve is at node 19 in the system model, Figure E9.7.1(a), so its inertias assemble into the full system mass matrix as

$$\begin{aligned}
 (\underline{M})_{109,109} &= (\underline{M})_{109,109} + m_{\text{valve}} \\
 (\underline{M})_{110,110} &= (\underline{M})_{110,110} + m_{\text{valve}} \\
 (\underline{M})_{111,111} &= (\underline{M})_{111,111} + m_{\text{valve}} \\
 (\underline{M})_{112,112} &= (\underline{M})_{112,112} + I_{x_1x_1}^{\text{valve}} \\
 (\underline{M})_{113,113} &= (\underline{M})_{113,113} + I_{x_2x_2}^{\text{valve}} \\
 (\underline{M})_{114,114} &= (\underline{M})_{114,114} + I_{x_3x_3}^{\text{valve}}
 \end{aligned} \tag{18}$$

The assembly into the condensed form \underline{M}_f of the system mass matrix is facilitated by using the *larray* to position the “added masses” into their appropriate constrained system positions as

$$\begin{aligned}
 (\underline{M}_f)_{l_{109},l_{109}} &= (\underline{M}_f)_{l_{109},l_{109}} + m_{\text{valve}} \cdots \Rightarrow (\underline{M}_f)_{91,91} = (\underline{M}_f)_{91,91} + m_{\text{valve}} \\
 (\underline{M}_f)_{l_{110},l_{110}} &= (\underline{M}_f)_{l_{110},l_{110}} + m_{\text{valve}} \cdots \Rightarrow (\underline{M}_f)_{92,92} = (\underline{M}_f)_{92,92} + m_{\text{valve}} \\
 (\underline{M}_f)_{l_{111},l_{111}} &= (\underline{M}_f)_{l_{111},l_{111}} + m_{\text{valve}} \cdots \Rightarrow (\underline{M}_f)_{93,93} = (\underline{M}_f)_{93,93} + m_{\text{valve}} \\
 (\underline{M}_f)_{l_{112},l_{112}} &= (\underline{M}_f)_{l_{112},l_{112}} + I_{x_1x_1}^{\text{valve}} \cdots \Rightarrow (\underline{M}_f)_{94,94} = (\underline{M}_f)_{94,94} + I_{x_1x_1}^{\text{valve}} \\
 (\underline{M}_f)_{l_{113},l_{113}} &= (\underline{M}_f)_{l_{113},l_{113}} + I_{x_2x_2}^{\text{valve}} \cdots \Rightarrow (\underline{M}_f)_{95,95} = (\underline{M}_f)_{95,95} + I_{x_2x_2}^{\text{valve}} \\
 (\underline{M}_f)_{l_{114},l_{114}} &= (\underline{M}_f)_{l_{114},l_{114}} + I_{x_3x_3}^{\text{valve}} \cdots \Rightarrow (\underline{M}_f)_{96,96} = (\underline{M}_f)_{96,96} + I_{x_3x_3}^{\text{valve}}
 \end{aligned} \tag{19}$$

At this point, the constraint condensed form \underline{M}_f of the system mass matrix is complete. Appendix C has the MATLAB code for this and all steps in this example.

(g) Determine the Natural Frequencies and Mode Shapes

As in (4.8.32) or (9.2.85), imposing the zero-displacement constraint conditions yields the following “condensed” dynamic equilibrium equation for the “free” (unconstrained) dofs of the constrained structure:

$$\underline{M}_f \ddot{\underline{q}}_f + \underline{K}_f \underline{q}_f = \underline{0} \tag{20}$$

$\begin{matrix} N_f \times N_f & N_f \times 1 \\ N_f \times 1 & N_f \times N_f \end{matrix}$

where $N_f = N_{\text{npd}}$ = number of free (nonfixed) dofs. Following Equations (5.4.3), (5.4.4), and (5.4.11) insertion of

$$\underline{q}_f = e^{i\omega t} \underline{\psi}_f \tag{21}$$

into (20) yields

$$\left(-\omega^2 \underline{M}_f + \underline{K}_f\right) \underline{\psi}_f = \underline{0} \quad (22)$$

The natural frequencies and mode shapes of the constrained, condensed system are obtained as described in Section 5.4. For mode shape plotting purposes, it is convenient to form the entire $\underline{\psi}$ vector, obtained from the free dof vector $\left(\underline{\psi}_f\right)$ and the zeros at fixed dofs. This is done with the *jarray* formed in (9) and the constrained dof index array i_{pd} in Table E9.7.1(c). The coding outline is:

Recovery of the Full System Mode Shape Vector $\underline{\psi}$ Using the *jarray*

Initialize $\underline{\psi} = \underline{0}$ ($N_d \times 1$)^a

for $l = 1, N_{npd}$

$k = jarray(l)$

$$\left(\underline{\psi}\right)_k = \left(\underline{\psi}_f\right)_l$$

end

^a Equation (1) shows $N_d = 264$ total number of free and fixed dofs.

Equation (8) shows $N_{npd} = 234$ free (nonfixed) dofs (23)

The full mode shape $\underline{\psi}$ now contains zeros at fixed and the motions in $\underline{\psi}_f$ at unconstrained dofs. The MATLAB code in Appendix C solves for the natural frequencies and mode shapes of the pipe run and valve support stand. Parameter values, nodal coordinates, nodal connectivities, and constrained dofs are defined at the beginning of the code. The shear form factors, polar area moments of inertia, dof connectivity array, *jarray*, and *larray* are then determined. The constraint condensed forms of the mass $\left(\underline{M}_f\right)$ and stiffness $\left(\underline{K}_f\right)$ matrices are formed from beam, clamp, furnace seal, and valve contributions. Mode shapes and natural frequencies are then obtained by solving Equation (22). Mode shapes 1–4 are shown in Figure E9.7.1(c).

9.8 2D FRAME MODELING WITH TIMOSHENKO BEAM ELEMENTS

Some machinery components, structures, or piping systems are constrained and loaded in a manner that makes out-of-plane deflection negligible and are accurately modeled as 2D frames. The 2D frame is a special case of the 3D model being constrained to move in the $x_1 - x_2$ plane. Imposing these constraints at the element level eliminates the requirement for explicitly constraining every out-of-plane-related deflection or slope similar with the list in Table E9.7.1(b). From Figures 9.4.2 and 9.4.3, it is seen that 2D motion allows freedom for the dofs shown in Figure 9.8.1 while imposing the out-of-plane and torsional motion constraints

$$\tilde{q}_3 = \tilde{q}_4 = \tilde{q}_5 = \tilde{q}_9 = \tilde{q}_{10} = \tilde{q}_{11} = 0 \quad (9.8.1)$$

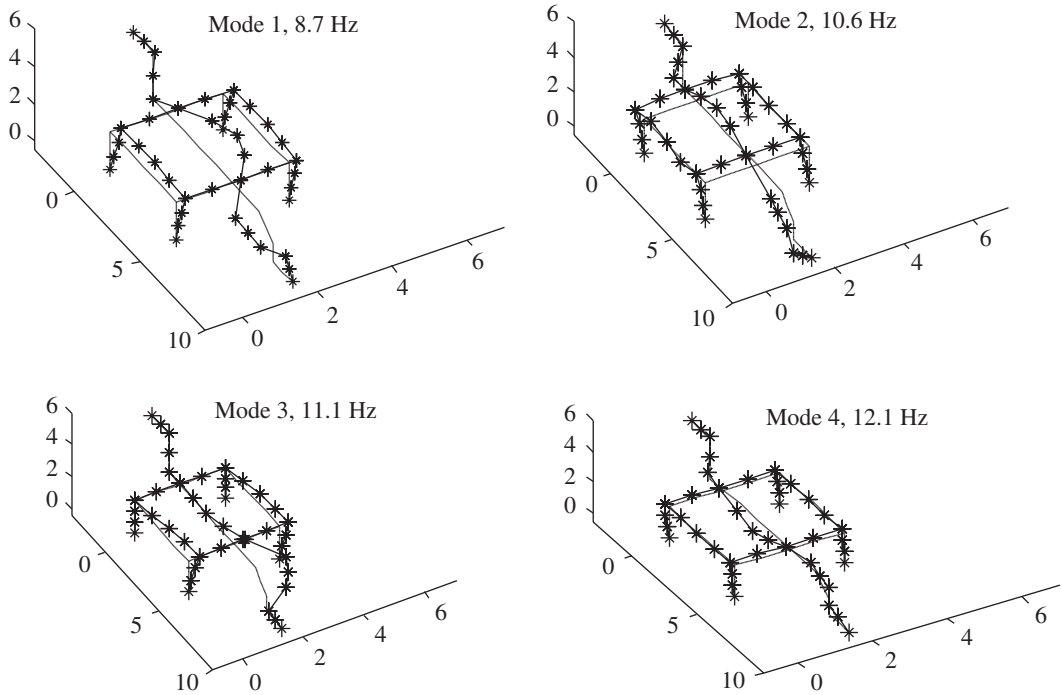


Figure E9.7.1(c) Mode shape 1–4 of piping system and support stand

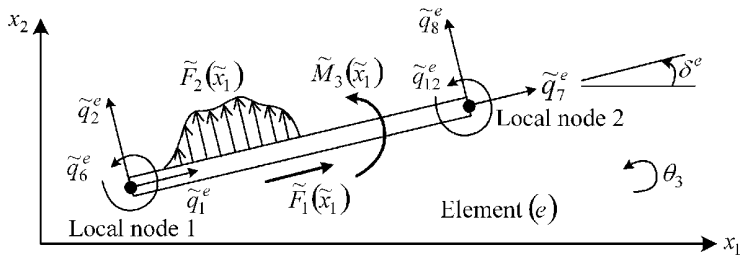


Figure 9.8.1 Local coordinate degrees of freedom for a 2D frame model

For convenience of notation, the 2D dofs are renumbered as

$$\tilde{V}_e = (\tilde{v}_1 \ v_2 \ \tilde{v}_3 \ \tilde{v}_4 \ \tilde{v}_5 \ \tilde{v}_6)^T = (\tilde{q}_1 \ \tilde{q}_2 \ \tilde{q}_6 \ \tilde{q}_7 \ \tilde{q}_8 \ \tilde{q}_{12})^T \tag{9.8.2}$$

in the element-based (local) coordinate system or as

$$V_e = (v_1 \ v_2 \ v_3 \ v_4 \ v_5 \ v_6)^T = (q_1 \ q_2 \ q_6 \ q_7 \ q_8 \ q_{12})^T \tag{9.8.3}$$

in the global coordinate system shown in Figure 9.8.2.

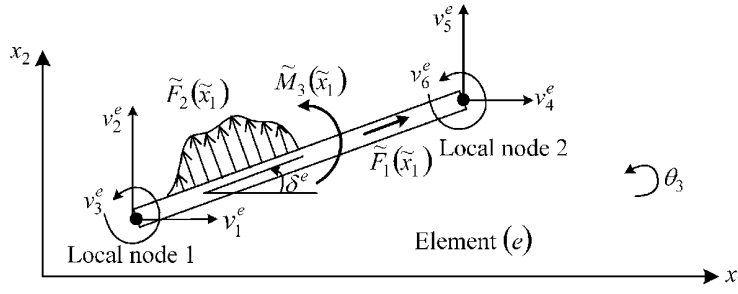


Figure 9.8.2 Global coordinate degrees of freedom (v_i^e) for a 2D frame model

Imposing the constraints of (9.8.1) on (9.5.136) yields the local coordinate, 2D TB element stiffness matrix shown in (9.8.4):

$$\underline{\tilde{K}}_e = \begin{matrix} & \begin{matrix} \tilde{v}_1 & \tilde{v}_2 & \tilde{v}_3 & \tilde{v}_4 & \tilde{v}_5 & \tilde{v}_6 \end{matrix} \\ \begin{matrix} \tilde{v}_1 \\ \tilde{v}_2 \\ \tilde{v}_3 \\ \tilde{v}_4 \\ \tilde{v}_5 \\ \tilde{v}_6 \end{matrix} & \left[\begin{array}{cccccc} \frac{EA}{L} & & & & & \\ 0 & \frac{12\beta_{12}^a}{L^3} & & & & \\ 0 & \frac{6\beta_{12}^a}{L^2} & \frac{\beta_{12}^b}{L} & & & \\ -\frac{EA}{L} & 0 & 0 & \frac{EA}{L} & & \\ 0 & \frac{-12\beta_{12}^a}{L^3} & \frac{-6\beta_{12}^a}{L^2} & 0 & \frac{12\beta_{12}^a}{L^3} & \\ 0 & \frac{6\beta_{12}^a}{L^2} & \frac{\beta_{12}^c}{L} & 0 & \frac{-6\beta_{12}^a}{L^2} & \frac{\beta_{12}^b}{L} \end{array} \right] \end{matrix} \quad (9.8.4)$$

where β_{12}^a and β_{12}^b are defined in (9.5.137). The 2D motion, local coordinate, element inertia matrix is obtained by imposing similar constraints on the terms in Table 9.5.2, yielding

$$\underline{\tilde{M}}_e = \begin{matrix} & \begin{matrix} \tilde{v}_1 & \tilde{v}_2 & \tilde{v}_3 & \tilde{v}_4 & \tilde{v}_5 & \tilde{v}_6 \end{matrix} \\ \begin{matrix} \tilde{v}_1 \\ \tilde{v}_2 \\ \tilde{v}_3 \\ \tilde{v}_4 \\ \tilde{v}_5 \\ \tilde{v}_6 \end{matrix} & \left[\begin{array}{cccccc} \frac{\rho AL}{3} & & & & & \\ 0 & \frac{\gamma_{m12} A a_1^{12u}}{420} & & & & \\ 0 & \frac{\gamma_{m12} A a_2^{12u}}{420} & \frac{\gamma_{m12} A a_5^{12u}}{420} & & & \\ \frac{\rho AL}{6} & 0 & 0 & \frac{\rho AL}{3} & & \\ 0 & \frac{\gamma_{m12} A a_3^{12u}}{420} & \frac{-\gamma_{m12} A a_4^{12u}}{420} & 0 & \frac{\gamma_{m12} A a_1^{12u}}{420} & \\ 0 & \frac{\gamma_{m12} A a_4^{12u}}{420} & \frac{\gamma_{m12} A a_6^{12u}}{420} & 0 & \frac{-\gamma_{m12} A a_2^{12u}}{420} & \frac{\gamma_{m12} A a_5^{12u}}{420} \end{array} \right] \end{matrix}$$

$$+ \frac{\gamma_{m12} I_{\tilde{x}_3}}{30} \begin{bmatrix} 0 \\ 0 & a_1^{12\theta} & & & & & \text{symmetric} \\ 0 & a_2^{12\theta} & a_3^{12\theta} & & & & \\ 0 & 0 & 0 & 0 & & & \\ 0 & -a_1^{12\theta} & -a_2^{12\theta} & 0 & a_1^{12\theta} & & \\ 0 & a_2^{12\theta} & a_4^{12\theta} & 0 & -a_2^{12\theta} & a_3^{12\theta} & \end{bmatrix} \quad (9.8.5)$$

where the a_j^{12u} and $a_j^{12\theta}$ terms are defined in (9.5.61) and (9.5.63), and the γ_{m12} is defined in Table 9.5.2. The element force vector for the 2D case is obtained from its 3D counterpart as

$$\underline{\tilde{f}}_{e,2D}^{6 \times 1} = \begin{Bmatrix} \tilde{v}_1 \\ \tilde{v}_2 \\ \tilde{v}_3 \\ \tilde{v}_4 \\ \tilde{v}_5 \\ \tilde{v}_6 \end{Bmatrix} \left\{ \begin{array}{l} \tilde{f}_{\text{ext},1} \\ \text{-----} \\ \tilde{f}_{\text{ext},2} \\ \text{-----} \\ \tilde{f}_{\text{ext},6} \\ \text{-----} \\ \tilde{f}_{\text{ext},7} \\ \text{-----} \\ \tilde{f}_{\text{ext},8} \\ \text{-----} \\ \tilde{f}_{\text{ext},12} \end{array} \right\} \quad (9.8.6)$$

where $\tilde{f}_{\text{ext},j}$ are given in Table 9.6.1. The element stiffness and mass matrices and force vector transform to global coordinates similar to the 3D case as in (9.5.142, 9.5.143, and 9.6.29)

$$\underline{K}_e = \underline{\tilde{T}}_e^T \underline{\tilde{K}}_e \underline{\tilde{T}}_e \quad 6 \times 6, \quad \underline{M}_e = \underline{\tilde{T}}_e^T \underline{\tilde{M}}_e \underline{\tilde{T}}_e \quad 6 \times 6, \quad \underline{f}_e = \underline{\tilde{T}}_e^T \underline{\tilde{f}}_e \quad 6 \times 1 \quad (9.8.7)$$

where the 2D coordinate transformation matrix is obtained from (9.4.10) using only the first rotation in Figure 9.4.8:

$$\underline{\tilde{T}}_e = \begin{bmatrix} c\delta^e & s\delta^e & 0 & 0 & 0 & 0 \\ -s\delta^e & c\delta^e & 0 & 0 & 0 & 0 \\ 0 & 0 & 1 & 0 & 0 & 0 \\ 0 & 0 & 0 & c\delta^e & s\delta^e & 0 \\ 0 & 0 & 0 & -s\delta^e & c\delta^e & 0 \\ 0 & 0 & 0 & 0 & 0 & 1 \end{bmatrix} \quad (9.8.8)$$

The 6×6 element matrices and 6×1 element force vector are assembled to form the constraint condensed system matrices using Figure 9.2.6, or (11) and (17) in Example 9.7.1, with

$$e = 1, 2, \dots, E, \quad r = 1, \dots, 6, \quad s = 1, \dots, 6 \quad (9.8.9)$$

where E is the total number of elements in the model. This will again yield the general form of the equilibrium equations

$$\underline{M}_f \ddot{\underline{q}}_f + \underline{K}_f \underline{q}_f = \underline{f}_f \quad (9.8.10)$$

for the “free” (unconstrained) dofs q_f . This equation may then be solved by the methods of Chapter 5 for free vibration, Chapter 6 for transient responses, and Chapter 7 for forced harmonic response.

EXAMPLE 9.8.1 Paint Station Frame Structure and Enclosure Vibrations

Statement: An automobile manufacturing plant utilizes an automated painting machine housed in a portable enclosure and supported by a frame. The enclosure is transported transversely to paint three parallel rows of automobiles, via an overhead crane. The lift hoists the enclosure and then transports it to the adjacent automobile as shown in Figure E9.8.1(a). An identical cable/hoist system is located on the other side of the I beam so that a total of four cables lift the enclosure. A study is commissioned to determine if increasing the hoisting speed, as characterized by a lifting time constant τ_L , will cause excessive vibration or dynamic cable stresses. A sudden cable failure event is also simulated to determine the resulting response of the crane’s support structure. The simulation model consists of the TB elements shown in Figure E9.8.1(b). A 2D beam element modeling approach is employed under the assumption that all disturbances and motions occur in the x_1-x_2 plane.

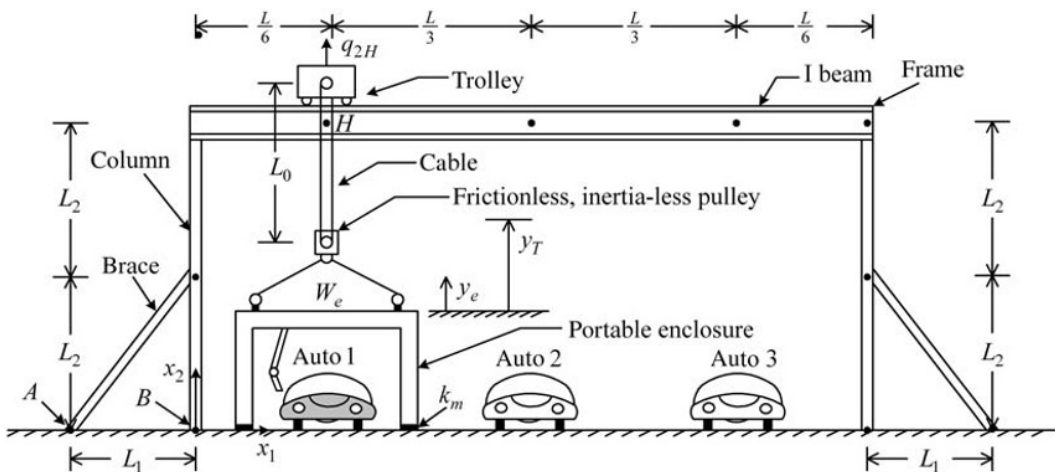


Figure E9.8.1(a) Painting enclosure, frame, and hoist

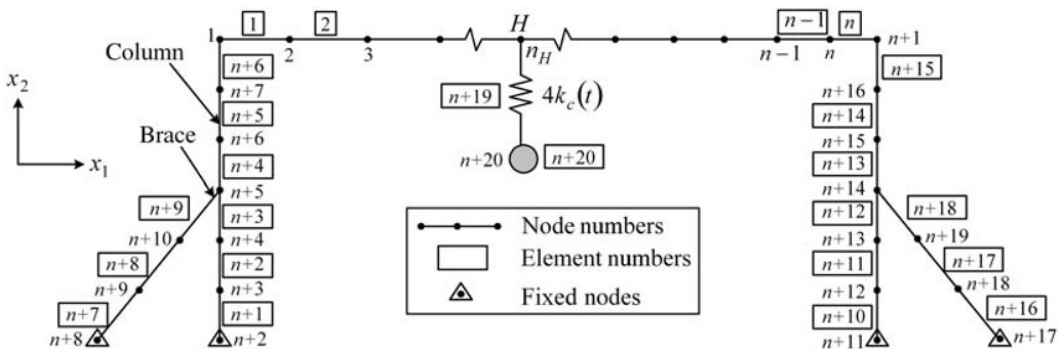


Figure E9.8.1(b) Node and element (boxed) numbering system

Objectives: The objectives of this problem include:

- (a) Determine the natural frequencies and mode shapes of the structure without the enclosure attached and with the enclosure attached and raised to a height y_T .
- (b) Determine the transient response of the system with several lifting rates of the enclosure.
- (c) Determine the transient response of the system to a sudden failure of the enclosure hoisting cables when the enclosure is stationary at its fully raised position (y_T).
- (d) Perform (c) with the enclosure at the $x_1=L/6$ and the $x_1=L/2$ positions in Figure E9.8.1(a)
- (e) Demonstrate convergence of the natural frequencies by increasing the number of elements in the I beam.

Assumptions:

- (a) The hoist raises the enclosure by winding in the upper end of the cable a distance

$$\Delta L_c(t) = 2y_T \left(1 - e^{-t/\tau_L}\right) \quad (1)$$

relative to the trolley.

- (b) The cable is initially taut and has length L_0 prior to lifting.
- (c) The trolley's reaction forces against the I beam are concentrated at the point H , and the trolley's vertical displacement is q_{2H} .
- (d) The cable's stiffness varies with its exposed length L_E as

$$k_c(t) = \frac{E_c A_c}{L_E(t)} \quad (2)$$

where

$$L_E(t) = L_0 + q_{2H} - y_e \quad (3)$$

and y_e is the enclosure's vertical displacement. The quantities E_c and A_c are the cable's Young's modulus and cross-sectional area, respectively. The tension in the cable is

$$f_c = k_c(t) \delta_c(t) \quad (4)$$

where δ_c is the stretch of the cable. This stretch is given by

$$\begin{aligned} \delta_c &= (\text{actual exposed length}) - (\text{exposed length without any loads or vibration}) \\ &= (L_0 + q_{2H} - y_e) - \left(L_0 - \frac{\Delta L_c(t)}{2}\right) = \frac{\Delta L_c(t)}{2} + q_{2H} - y_e \end{aligned} \quad (5)$$

where the $1/2$ factor in $\Delta L_c(t)/2$ accounts for the pulley kinematics in Figure E9.8.1(a). The total force exerted by the four cables (only two are shown in Figure E9.8.1(a)) on the enclosure is

$$f_{ce} = 4f_c = 4k_c \delta_c = 4k_c \left(\frac{\Delta L_c(t)}{2} + q_{2H} - y_e \right) = 4E_c A_c \frac{(\Delta L_c(t)/2) + q_{2H}(t) - y_e(t)}{L_0 + q_{2H}(t) - y_e(t)} \quad (6)$$

- (e) The cable is massless and remains tight at all times.

- (f) The frame's translational and rotational dofs are fixed to ground at the four locations indicated by triangles in Figure E9.8.1(b).
- (g) The enclosure is treated as a rigid mass.
- (h) The enclosure contacts the floor through two soft mounts with individual stiffness k_m .
- (i) The structural damping is 5% for the lowest 10 modes with the enclosure detached and follows equation (5.4.147) for the higher nodes.

Parameter Values:

- (a) System Values:

$$L_1 = 2.5 \text{ m}, L_2 = 3.0 \text{ m}, L = 20 \text{ m}, y_T = 2.5 \text{ m}, \tau_L = 1 \text{ and } 3 \text{ s}$$

$$\xi_l^d = 0.05 \text{ for } l = 1, 2, \dots, 10 = \text{desired damping ratios in (5.4.140) and (5.4.146)}$$

- (b) Element Types:

- (i) Overhead I Beam Element (Ref. Figures 9.4.2, 9.8.1, and E9.8.1(a)) and Equation (9.5.22)). The cross section of this beam is illustrated in Figure E9.8.1(c).
From the AISC (1980): Beam Type: W16 × 67

$$a = 0.415 \text{ m}, b = 0.26 \text{ m}, t_w = 0.01 \text{ m}, t_f = 0.017 \text{ m}, \nu = 0.3$$

$$I_{\tilde{x}_3} = 3.97 \times 10^{-4} \text{ m}^4, A = 0.0127 \text{ m}^2, E = 2.14 \times 10^{11} \text{ N/m}^2, \rho = 7834.0 \text{ kg/m}^3$$

- (ii) Vertical Columns: Square Structural Tubing (Figure E9.8.1(d))

From the AISC (1980)

Beam Type: 8 × 8

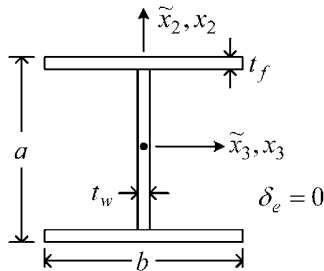


Figure E9.8.1(c) Cross section of overhead I beam

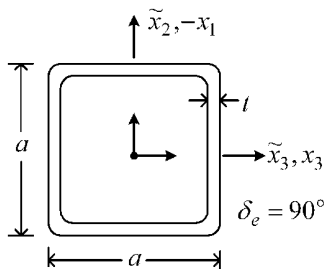


Figure E9.8.1(d) Cross section of vertical column-square tubing

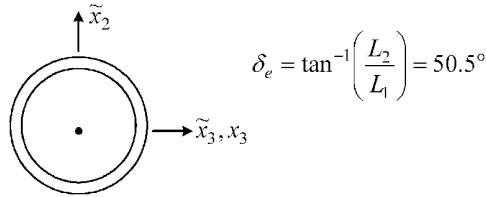


Figure E9.8.1(e) Cross section and angle of sloped pipe brace

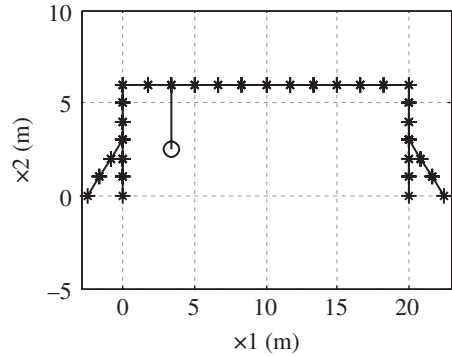


Figure E9.8.1(f) Model geometry verification plot

$$a = 0.203 \text{ m}, \quad t = 0.0095 \text{ m}, \quad I_{\tilde{x}_3} = 4.4 \times 10^{-5} \text{ m}^4, \quad A = 0.0072 \text{ m}^2, \\ E = 2.14 \times 10^{11} \text{ N/m}^2, \quad \nu = 0.3, \quad \rho = 7834.0 \text{ kg/m}^3$$

(iii) Sloped Column Braces (Figure E9.8.1(e))

Pipe (nominal diameter 5'' (0.127 m) schedule 40), wall thickness = $6.45 \times 10^{-3} \text{ m}$

$$\text{OD} = 0.141 \text{ m}, \quad I_{\tilde{x}_3} = 6.3 \times 10^{-6} \text{ m}^4, \quad A = 2.77 \times 10^{-3} \text{ m}^2, \quad E = 2.14 \times 10^{11} \text{ N/m}^2 \\ \nu = 0.3, \quad \rho = 7834.0 \text{ kg/m}^3$$

(iv) Hoist Cable: $L_0 = 3.5 \text{ m}, A_c = 1.3 \times 10^{-4} \text{ m}^2, E_c = 2.14 \times 10^{11} \text{ N/m}^2$

(v) Enclosure: $W_e = 9870.0 \text{ N}, m_e = 1000.0 \text{ kg}, k_m = 200000.0 \text{ N/m}$

(c) Element Summary by Nodal Connectivity and Element Type

Table E9.8.1(a) provides a element summary. Figure E9.8.1(f) shows a model geometry verification plot of the frame structure from the corresponding MATLAB code in Appendix D.

Fixed Degrees of Freedom: Similar to Figure 9.2.5, the full system dofs at global node i are

$$x_1 \text{ direction} : 3 * (i - 1) + 1, \quad x_2 \text{ direction} : 3 * (i - 1) + 2, \quad \theta_3 \text{ direction} : 3 * (i - 1) + 3 \quad (7)$$

Table E9.8.1(b) summarizes the fixed dofs in the model (Figure E9.8.1(b)) utilizing the numbering convention in (7).

Table E9.8.1(a) Element summary for Figure E9.8.1(a)

Nodal connectivity				Nodal connectivity			
Element number (e)	Local node 1 B_{e1} $ICON(e,1)$	Local node 2 B_{e2} $ICON(e,2)$	Type	Element number (e)	Local node 1 B_{e1} $ICON(e,1)$	Local node 2 B_{e2} $ICON(e,2)$	Type
1	1	2	1	$n+9$	$n+10$	$n+5$	3
2	2	3	1	$n+10$	$n+11$	$n+12$	2
3	3	4	1	$n+11$	$n+12$	$n+13$	2
\vdots	\vdots	\vdots	\vdots	$n+12$	$n+13$	$n+14$	2
$n-1$	$n-1$	n	1	$n+13$	$n+14$	$n+15$	2
n	n	$n+1$	1	$n+14$	$n+15$	$n+16$	2
$n+1$	$n+2$	$n+3$	2	$n+15$	$n+16$	$n+1$	2
$n+2$	$n+3$	$n+4$	2	$n+16$	$n+17$	$n+18$	3
$n+3$	$n+4$	$n+5$	2	$n+17$	$n+18$	$n+19$	3
$n+4$	$n+5$	$n+6$	2	$n+18$	$n+19$	$n+14$	3
$n+5$	$n+6$	$n+7$	2				
$n+6$	$n+7$	1	2	$n+19$	Cable between nodes H^a and $n+20$		4
$n+7$	$n+8$	$n+9$	3				
$n+8$	$n+9$	$n+10$	3	$n+20$	Enclosure mass at node $n+20$		5

^a Node H is node $(n/6+1)$ for the enclosure above auto 1 and is node $(n/2+1)$ for the enclosure above auto 2. The integer n is selected to be some multiple of 6.

Table E9.8.1(b) Fixed degrees of freedom (dofs) in Figure E9.8.1(b)

Number l	Node	Direction	Global dof no. i_{pd}	Number l	Node	Direction	Global dof no. i_{pd}
1	$n+2$	x_1	$3*(n+1)+1$	7	$n+11$	x_1	$3*(n+10)+1$
2	$n+2$	x_2	$3*(n+1)+2$	8	$n+11$	x_2	$3*(n+10)+2$
3	$n+2$	θ_3	$3*(n+1)+3$	9	$n+11$	θ_3	$3*(n+10)+3$
4	$n+8$	x_1	$3*(n+7)+1$	10	$n+17$	x_1	$3*(n+16)+1$
5	$n+8$	x_2	$3*(n+7)+2$	11	$n+17$	x_2	$3*(n+16)+2$
6	$n+8$	θ_3	$3*(n+7)+3$	12	$n+17$	θ_3	$3*(n+16)+3$

Thus, it is seen that the total number of “free” nonprescribed dofs is

$$\begin{aligned}
 n_f &= N_{\text{npd}} = (\text{total no. of dofs}) - (\text{no. of prescribed dofs}) = N_d - N_{\text{pd}} \\
 &= 3 * (\text{no. of nodes}) + 1 (\text{dof for mass } m_e) - 12 = 3(n+19) + 1 - 12 = 3n + 46
 \end{aligned} \quad (8)$$

Solution: The following describes the steps employed in the MATLAB code in Appendix D:

(a) Form Degree of Freedom (dof) Connectivity Array

The dof connectivities are defined as in (9.2.79) as

for $e=1, n+18 \leftarrow$ (elements)

for $j=1, 2 \leftarrow$ (nodes/element)

```

for  $k=1, 3 \leftarrow (\text{dof/node})$ 
     $l=3*(j-1)+k$ 
     $ICONDOF(e,l)=3*(ICON(e,j)-1)+k$ 
end
end
end

```

(9)

where $ICONDOF(e, l)$ is the dof connectivity array \hat{B}_{el} , and $ICON$ is the nodal connectivity array B_{el} defined in Table E9.8.1(a). The coding logic in (9) only applies to the beam elements (types 1, 2, 3), and not to the spring and mass in Figure E9.8.1(b). The cable spring connects the x_2 dof of node n_H to the dof (y_e) for vertical motion of the enclosure mass (m_e). Therefore,

$$n_H = \frac{n}{6} + 1 \quad (\text{if the enclosure is above auto 1})$$

$$n_H = \frac{n}{2} + 1 \quad (\text{if the enclosure is above auto 2})$$

(10)

The cable spring is a 2-dof element (vertical displacement at each end of the spring) and its dof connectivity is

$$\hat{B}_{n+19,1} = ICONDOF(n+19, 1) = 3*(n_H-1) + 2 = x_2 \text{ dof at node } n_H$$

$$\hat{B}_{n+19,2} = ICONDOF(n+19, 2) = 3*(n+19) + 1 = y_e \text{ displacement of enclosure}$$

(11)

The enclosure mass element's node is not shared by any other element; therefore, its dof connectivity becomes

$$\hat{B}_{n+20,1} = ICONDOF(n+20, 1) = 3*(n+19) + 1 = y_e \text{ displacement of enclosure}$$

(12)

(b) Form the *jarray*

The *jarray* contains the nonfixed (free) dof numbers in increasing order. As in Example 9.2.3, a *jarray* is formed to “expand” the response vectors into their full dimension (N_d), which includes both fixed and free dofs. The *jarray*(j_i) is formed by utilizing the input array of fixed dofs (i_{pd}) from Table E9.8.1(b) as

```

 $I=0$ 
for  $i=1, N_d (= 3*(n+19)+1) \leftarrow (\text{total no. of dofs})$ 
     $flag=0$ 
    for  $l=1, N_{pd} (= 12) \leftarrow (\text{no. of prescribed dofs})$ 
        if  $i=i_{pd} \leftarrow (\text{see Table E9.8.1(b)})$ 
             $flag=1$ 
        end
    end
end
if  $flag=0$ 

```

$$\begin{aligned}
 & I = I + 1 \\
 & \text{jarray}(I) = i \\
 & \text{end} \\
 & \mathbf{end} \\
 & N_{npd} = I \leftarrow (\text{no. of non-prescribed dofs}) \tag{13}
 \end{aligned}$$

(c) Form the *larray*

The *larray* contains the locations of the full system dofs in the condensed dof vector \underline{x}_f in increasing order. All fixed dofs are assigned the number 0 in the *larray*. The *jarray(j_i)* is utilized to form the *larray(l_i)* as

$$\begin{aligned}
 & \text{for } i = 1, N_d (= 3 * (\mathbf{n} + \mathbf{19}) + \mathbf{1}) \leftarrow (\text{total no. of dofs}) \\
 & \quad \text{larray}(i) = 0 \\
 & \text{end} \\
 & \text{for } I = 1, N_{npd} \leftarrow \text{from jarray coding (Eq. 13)} \\
 & \quad i_{st} = \text{jarray}(I) \\
 & \quad \text{larray}(i_{st}) = I \\
 & \text{end} \tag{14}
 \end{aligned}$$

(d) Form the Constraint Condensed System Stiffness Matrix for the Frame

Consider the structure with the enclosure detached in Figures E9.8.1(a) or E9.8.1

(b). The system stiffness matrix $\left(\underline{K}_f\right)$ with fixed constraints imposed is formed according to Figure 9.2.6 with indices r and s running from 1 to 6 and by using the dof connectivity and L arrays:

$$\begin{aligned}
 & \underline{K}_f = \underline{0} \quad n_f \times n_f \quad \text{initialize stiffness matrix to zero} \\
 & \quad \mathbf{for } e = \mathbf{1}, \mathbf{E} (= \mathbf{n} + \mathbf{18}) \leftarrow (\text{beam elements only}) \\
 & \quad \text{-- form the coordinate transformation matrix } \tilde{T}_e \text{ utilizing Equation (9.8.8)} \\
 & \quad \text{-- form the } e\text{th element stiffness matrix } \tilde{K}_e \text{ in local coordinates using Equation (9.8.4)} \\
 & \quad \text{-- form the } e\text{th element stiffness matrix } \underline{K}_e \text{ in global coordinates using Equation (9.8.7)} \\
 & \quad \underline{K}_e = \tilde{T}_e^T \tilde{K}_e \tilde{T}_e \\
 & \quad \mathbf{for } r = \mathbf{1}, \mathbf{6} \\
 & \quad \quad \mathbf{for } s = \mathbf{1}, \mathbf{6} \\
 & \quad \quad \quad \hat{B}_{er} = \text{ICONDOF}(e, r) \\
 & \quad \quad \quad \hat{B}_{es} = \text{ICONDOF}(e, s) \\
 & \quad \quad \quad l_{\hat{B}_{er}} = \text{larray}(\hat{B}_{er}) \\
 & \quad \quad \quad l_{\hat{B}_{es}} = \text{larray}(\hat{B}_{es})
 \end{aligned}$$


```

                                if  $l_{\hat{B}_{er}} \neq 0$  and  $l_{\hat{B}_{es}} \neq 0$ 
                                    
$$\underline{K}_f(l_{\hat{B}_{er}}, l_{\hat{B}_{es}}) = \underline{K}_f(l_{\hat{B}_{er}}, l_{\hat{B}_{es}}) + \underline{K}_e(r, s)$$

                                end
                            end
                        end
                    end
                end
            end
        end
    end
end

```

(e) Form the Constraint Condensed System Mass Matrix for the Frame

Consider the structure with the enclosure detached in Figures E9.8.1(a) or E9.8.1

(b). The system mass matrix (\underline{M}_f) with fixed constraints imposed is formed according to Figure 9.2.6 with indices r and s running from 1 to 6 and by using the dof connectivity and L arrays:

```

 $\underline{M}_f = \underline{0}$     $n_f \times n_f$    initialize mass matrix to zero
    for  $e = 1, E$  ( $= n + 18$ ) ← (beam elements only)
        – form the coordinate transformation matrix  $\underline{\tilde{T}}_e$  utilizing Equation (9.8.8)
        – form the  $e$ th element mass matrix  $\underline{\tilde{M}}_e$  in local coordinates using Equation (9.8.5)
        – form the  $e$ th element mass matrix  $\underline{M}_e$  in global coordinates using Equation (9.8.7)

        
$$\underline{M}_e = \underline{\tilde{T}}_e^T \underline{\tilde{M}}_e \underline{\tilde{T}}_e$$

        for  $r = 1, 6$ 
            for  $s = 1, 6$ 
                 $\hat{B}_{er} = \text{ICONDOF}(e, r)$ 
                 $\hat{B}_{es} = \text{ICONDOF}(e, s)$ 
                 $l_{\hat{B}_{er}} = \text{larray}(\hat{B}_{er})$ 
                 $l_{\hat{B}_{es}} = \text{larray}(\hat{B}_{es})$ 
                if  $l_{\hat{B}_{er}} \neq 0$  and  $l_{\hat{B}_{es}} \neq 0$ 
                    
$$\underline{M}_f(l_{\hat{B}_{er}}, l_{\hat{B}_{es}}) = \underline{M}_f(l_{\hat{B}_{er}}, l_{\hat{B}_{es}}) + \underline{M}_e(r, s)$$

                end
            end
        end
    end
end

```

(f) Modes of the Frame-Only Model

The undamped equation of motion for the frame structure (i.e., no cable and enclosure) is

$$\underline{M}_f \ddot{\underline{q}}_f + \underline{K}_f \underline{q}_f = \underline{0} \quad (n_f \times 1) \quad (17)$$

where \underline{M}_f and \underline{K}_f are the constraint condensed mass and stiffness matrices formed in (d) and (e), n_f is the number of nonfixed (free) dofs in the frame-only model

$$n_f = 3(n + 19) - 12 = 3n + 45 \quad (18)$$

and \underline{q}_f is the $n_f \times 1$ vector of all “free” nonfixed displacements in the frame-only model. The algebraic form of the undamped, free vibration equation is (5.4.12)

$$-\omega_{fi}^2 \underline{M}_f \underline{\psi}_{fi} + \underline{K}_f \underline{\psi}_{fi} = \underline{0} \quad (n_f \times 1) \quad (19)$$

Equation (19) is solved to obtain the natural frequencies and mode shapes of the frame structure without the enclosure. The mode shapes $\underline{\psi}_{fi}$ for the free dofs are “expanded” into full system mode shapes $\underline{\psi}_l$ by using the *jarray* (13) to include the fixed dofs as follows:

$$\begin{aligned} &\text{for } l=1, N_{pd} (=12) \\ &\quad k = i_{pd}l \\ &\quad \left(\underline{\psi} \right)_k = 0 \quad (\text{fixed dof}) \\ &\text{end} \\ &\text{for } l=1, N_{pd} \\ &\quad k = jarray(l) \\ &\quad \left(\underline{\psi} \right)_k = \left(\underline{\psi}_f \right)_l \\ &\text{end} \end{aligned} \quad (20)$$

The full system mode shapes $\underline{\psi}_l$ now contains zeros at all fixed dofs. Figure E9.8.1(g) shows that the lowest 4 modes are nearly identical for $n=6$ and $n=12$, where n is the mesh parameter defined in Figure E9.8.1(b). This demonstrates “mesh convergence.”

The first (4.7 Hz), third (15.2 Hz), and fourth (30.5 Hz) modes resemble the lowest three bending modes of a simply supported beam (SSB). The Euler–Bernoulli SSB frequencies are

$$\begin{aligned} f_j^{\text{EB}} &= \frac{1}{2\pi} \left(\frac{j\pi}{L} \right)^2 \sqrt{\frac{EI}{\rho A}} = \frac{1}{2\pi} \left(\frac{j\pi}{20} \right)^2 \sqrt{\frac{(2.14 \times 10^{11})(3.97 \times 10^{-4})}{(7834)(0.0127)}} \\ &= 3.63j^2 = (3.63, 14.52, 32.67) \text{ Hz} \end{aligned} \quad (21)$$

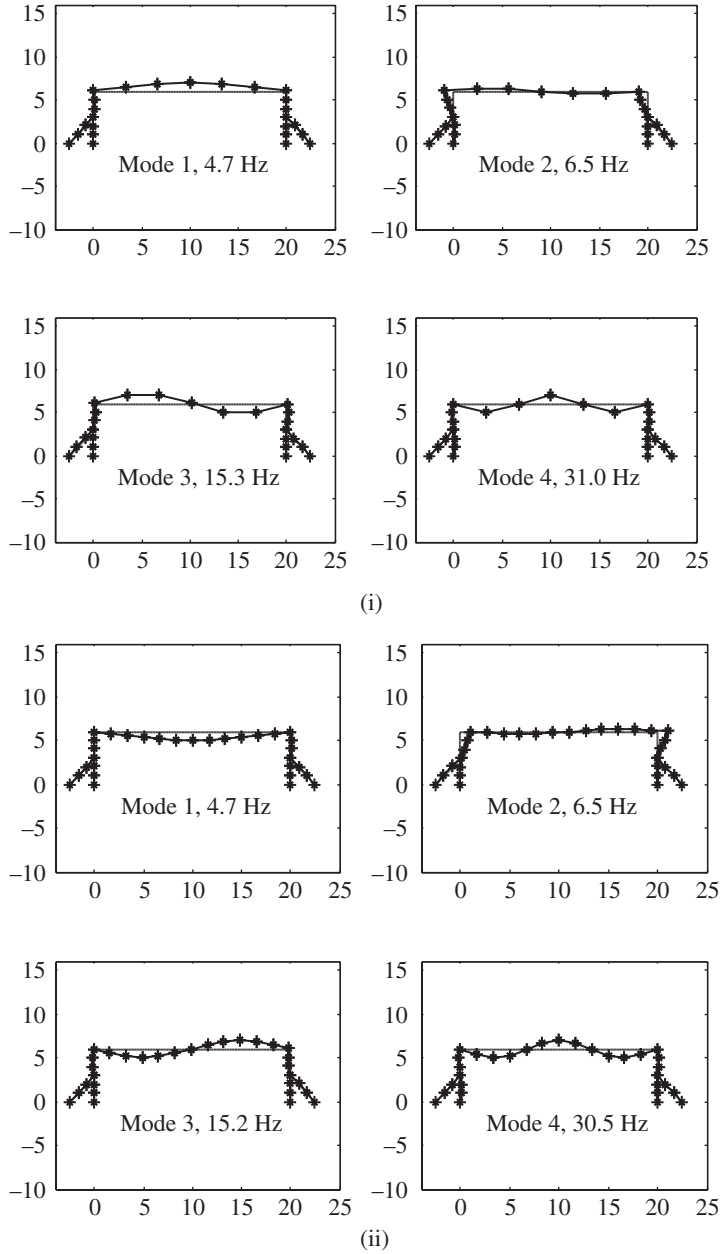


Figure E9.8.1(g) Modes with enclosure detached for (i) $n=6$ and (ii) $n=12$ in Figure E9.8.1(b)

The Timoshenko SSB frequencies (without rotary inertia effects) are

$$f_j^T = \frac{f_j^{\text{EB}}}{\sqrt{1 + \left(\frac{j\pi}{L}\right)^2 \frac{I}{A} \frac{2(1+\nu)}{k}}} = \frac{3.63j^2}{\sqrt{1 + \left(\frac{j\pi}{20}\right)^2 \left(\frac{3.97 \times 10^{-4}}{0.0127}\right) \frac{2(1+0.3)}{0.0819}}} = \frac{3.63j^2}{\sqrt{1 + 0.0245j^2}}$$

$$= (3.59, 13.86, 29.6) \text{ Hz}$$

The results in (21) and (22) are very similar to the finite element model results in Figure E9.8.1(g), that is,

$$(f_1^{\text{FE}}, f_2^{\text{FE}}, f_4^{\text{FE}}) = (4.7, 15.2, 30.5) \text{ Hz} \quad (23)$$

The difference arises from the stiffer rotational constraints and the rotary inertia effects (second matrix in 9.8.5) in the finite element model. The above discussion is included to illustrate how formulas for simple models can be used to perform approximate “reality” checks on a complex finite element model.

(g) The Constraint Condensed System Damping Matrix for the Frame-Only Model

The orthogonal damping matrix for the frame without the enclosure is by (5.4.140), (5.4.142), and (5.4.146)

$$\underline{C}_{f0} = \mu_1 \underline{K}_f + \sum_{l=1}^{m-1} \frac{2\kappa_l \omega_{fl}}{\dot{m}_{fl}} \underline{M}_f \underline{\psi}_{fl} \underline{\psi}_{fl}^T \underline{M}_f \quad (24)$$

where

$$\mu_1 = \frac{2\xi_m^d}{\omega_{cm}} \quad \text{and} \quad \kappa_l = \xi_l^d - \xi_m^d \frac{\omega_{fl}}{\omega_{fm}} \quad (25)$$

and ξ_l^d is the specified (desired) damping ratio of the l th mode in the frame-only structure. For this example, let

$$m = 10, \quad \xi_1^d = \xi_2^d = \dots = \xi_m^d = 0.05 \quad (26)$$

The lowest 20 natural frequencies and damping ratios of the frame-only structure with $n = 12$ are listed in Table E9.8.1(c).

(h) Equations of Motion for the Coupled Frame: Enclosure System

Parts (d)–(g) pertain to the frame-only model (no enclosure). The enclosure and frame models are coupled in this section to form the entire system model. The constraint condensed displacement vector of the coupled system is

$$\hat{\underline{q}}_f = \left\{ \begin{array}{c} \underline{q}_f \\ \underline{y}_e \end{array} \right\} \hat{n}_f \times 1 \quad (27)$$

Table E9.8.1(c) Natural frequencies and damping ratios for frame-only structure

Mode	Natural frequency (Hz)	Damping ratio	Mode	Natural frequency (Hz)	Damping ratio
1	4.7	0.05	11	96.8	0.054
2	6.5	0.05	12	102.4	0.057
3	15.2	0.05	13	106.8	0.060
4	30.5	0.05	14	125.4	0.070
5	49.9	0.05	15	131.1	0.074
6	54.8	0.05	16	152.9	0.086
7	54.9	0.05	17	156.6	0.088
8	72.4	0.05	18	157.4	0.102
9	87.3	0.05	19	181.4	0.113
10	89.2	0.05	20	201.3	0.119

where

$$\hat{n}_f = n_f + 1 \quad (28)$$

The cable that connects the enclosure and frame is attached in the x_2 direction at frame node n_H in (10). This is the

$$3 * (n_H - 1) + 2 \quad (29)$$

dof of the total system and the

$$l^* = l_{3 * (n_H - 1) + 2} = \text{larray}(3 * (n_H - 1) + 2) \quad (30)$$

dof of the constraint condensed system. A free-body diagram of the isolated enclosure is shown in Figure E9.8.1(h).

The sum of the cable forces $f_{ce}(t)$ in Figure E9.8.1(h) is defined by (2), (3), and (6) as

$$f_{ce}(t) = \frac{4E_c A_c (\Delta L_c(t)/2 + q_{2H}(t) - y_e(t))}{L_0 + q_{2H}(t) - y_e(t)} \quad (31)$$

where

$$\Delta L_c(t) = 2y_T (1 - e^{-t/\tau_L}) \quad (32)$$

and $q_{2H}(t)$ is the vertical deflection of the frame at node n_H in (10). The force in (31) may be rewritten in terms of the components in the coupled system displacement vector (27) as

$$f_{ce}(t) = \frac{4E_c A_c \left(\Delta L_c(t)/2 + \left(\hat{q}_f \right)_{l^*} - \left(\hat{q}_f \right)_{\hat{n}_f} \right)}{L_0 + \left(\hat{q}_f \right)_{l^*} - \left(\hat{q}_f \right)_{\hat{n}_f}} \quad (33)$$

which is clearly a nonlinear function of the enclosure and frame displacements. Soft stiffness mounts k_m are attached to the bottom of the enclosure to reduce its impact force on the concrete floor. The weight of the enclosure compresses the mounts by an amount

$$\Delta_e = \frac{W_e}{2k_m} \quad (34)$$

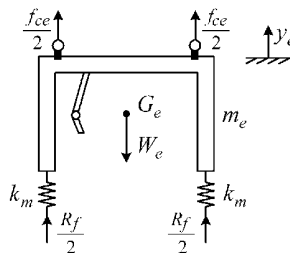


Figure E9.8.1(h) Free-body diagram of the enclosure

The enclosure's vertical displacement y_e in Figures E9.8.1(a) and E9.8.1(h) is referenced from the static equilibrium position of the enclosure with the cables slack. The reaction force between the floor and enclosure becomes

$$R_f = \begin{cases} 2k_m(\Delta_e - y_e), & y_e \leq \Delta_e \\ 0, & y_e > \Delta_e \end{cases} = \begin{cases} 2k_m \left(\Delta_e - \left(\hat{q}_f \right)_{\hat{n}_f} \right), & \left(\hat{q}_f \right)_{\hat{n}_f} \leq \Delta_e \\ 0, & \left(\hat{q}_f \right)_{\hat{n}_f} > \Delta_e \end{cases} \quad (35)$$

The equation of motion for the enclosure is

$$m_e \ddot{y}_e = f_{ce} + R_f - W_e \quad (36)$$

and the equation of motion for the frame portion of the system is

$$\underline{M}_f \ddot{\underline{q}}_f + \underline{C}_{f0} \dot{\underline{q}}_f + \underline{K}_f \underline{q}_f = \underline{f}_f \quad (n_f \times 1) \quad (37)$$

where the constraint condensed force vector is

$$\underline{f}_f = \begin{matrix} n_f \times 1 \\ \left(\begin{array}{c} 0 \\ \vdots \\ -f_{ce} \\ \vdots \\ 0 \end{array} \right) \leftarrow \text{row } l^* \end{matrix} \quad (38)$$

The frame node deflections are referenced to the statically deflected state with the enclosure removed, so beam element weights are ignored in (38). The following first-order (state) forms of (36) and (37) may be numerically integrated using the methods of Section 6.4 to obtain the response at any node in the frame model and of the enclosure, given the lift height y_T and time constant τ_L in (32). The first-order forms are

$$\dot{y}_e = v_e, \quad \dot{v}_e = \frac{1}{m_e} (f_{ce} + R_f - W_e) \quad (39)$$

$$\dot{\underline{q}}_f = \underline{v}_f \quad (n_f \times 1), \quad \dot{\underline{v}}_f = \underline{M}_f^{-1} (\underline{f}_f - \underline{C}_f \underline{v}_f - \underline{K}_f \underline{q}_f) \quad (n_f \times 1) \quad (40)$$

with f_{ce} defined in (33), R_f defined in (35), and \underline{f}_f defined in (38).

A linearized model is also formed by considering the system with the enclosure in a stationary state so that the cable has constant length and stiffness k_c values. The coupled, linear system equations have the form

$$\hat{\underline{M}}_f \ddot{\hat{\underline{q}}}_f + \hat{\underline{C}}_{f0} \dot{\hat{\underline{q}}}_f + \hat{\underline{K}}_f \hat{\underline{q}}_f = \hat{\underline{f}}_f \quad (\hat{n}_f \times 1) \quad (41)$$

The $(\hat{n}_f \times \hat{n}_f)$ $\hat{\underline{M}}_f$, $\hat{\underline{C}}_{f0}$, and $\hat{\underline{K}}_f$ matrices are formed by initializing each to a zero matrix. The corresponding frame-only, $(n_f \times n_f)$ \underline{M}_f , \underline{C}_{f0} , and \underline{K}_f matrices are then added into the upper n_f rows and columns of $\hat{\underline{M}}_f$, $\hat{\underline{C}}_{f0}$, and $\hat{\underline{K}}_f$, respectively. Finally, the enclosure and cable-related terms are added, as described next. The cable stiffness

k_c connects the x_2 dof of frame node n_H to the x_2 dof of the enclosure node $n + 20$ in Figure E9.8.1(b). The corresponding full system dofs are

$$g_H = 3 * (n_H - 1) + 2 \quad \text{and} \quad g_e = 3 * (n + 19) + 1 \quad (42)$$

and the corresponding dofs in the constraint condensed system are from (28) and (30) l^* and \hat{n}_f , respectively. The element stiffness matrix for the cable spring is

$$\underline{K}_{\text{cable}} = \begin{bmatrix} l^* & \hat{n}_f \\ 4k_c & -4k_c \\ -4k_c & 4k_c \end{bmatrix} l^* \quad (43)$$

where the bordering symbols show the rows and columns of the constraint condensed matrix \hat{K}_f into which the four entries in $\underline{K}_{\text{cable}}$ are added, for example,

$$\begin{aligned} &\text{Add } 4k_c \text{ into (row } l^*, \text{ column } l^*) \text{ of } \hat{K}_f, \text{ Add } -4k_c \text{ into (row } l^*, \text{ column } \hat{n}_f) \text{ of } \hat{K}_f \\ &\text{Add } -4k_c \text{ into (row } \hat{n}_f, \text{ column } l^*) \text{ of } \hat{K}_f, \text{ Add } 4k_c \text{ into (row } \hat{n}_f, \text{ column } \hat{n}_f) \text{ of } \hat{K}_f \end{aligned} \quad (44)$$

The enclosure mount stiffness $2k_m$ (Figure E9.8.1(h)) is added into the (\hat{n}_f, \hat{n}_f) position of \hat{K}_f only if the enclosure is in contact with the floor. Likewise, the enclosure mass m_e is added into the (\hat{n}_f, \hat{n}_f) position of \hat{M}_f for all cases.

(i) Natural Frequencies and Mode Shapes for the Coupled Frame–Cable–Enclosure System

The mesh parameter in Figure E9.8.1(b) is $n = 12$ for this study. The cable stiffness (Eqs. 2 and 3) varies with length so consider the following two cases:

Case (a): Enclosure above auto 2, ($x_1 = \frac{L}{2}$), and resting on floor ($2k_m$ included) $y_T = 0$

$$k_c = \frac{E_c A_c}{L_0} = \frac{(2.14 \times 10^{11})(1.3 \times 10^{-4})}{3.5} = 7.95 \times 10^6 \text{ N/m} \quad (45)$$

Case (b): Enclosure above auto 2, ($x_1 = \frac{L}{2}$), and raised above floor $y_T = 2.5$ m

$$k_c = \frac{E_c A_c}{L_0 - y_T} = \frac{(2.14 \times 10^{11})(1.3 \times 10^{-4})}{1.0} = 27.8 \times 10^6 \text{ N/m} \quad (46)$$

Figure E9.8.1(i) shows the lowest 4 mode shapes for both cases (a) and (b).

Table E9.8.1(d) shows the lowest 10 natural frequencies for both cases.

(j) Transient Response during an Enclosure Lift

Equations (39) and (40) are numerically integrated with MATLAB ODE45 (Appendix D) to simulate vibrations of the frame and enclosure due to raising the enclosure according with (1). The ordering of the state variables in the ODE45 subfunction is

$$\underline{Q}_c = \begin{Bmatrix} \underline{q}_f \\ \underline{v}_f \\ y_e \\ \underline{v}_e \end{Bmatrix} \quad ((2n_f + 2) \times 1) \quad (47)$$

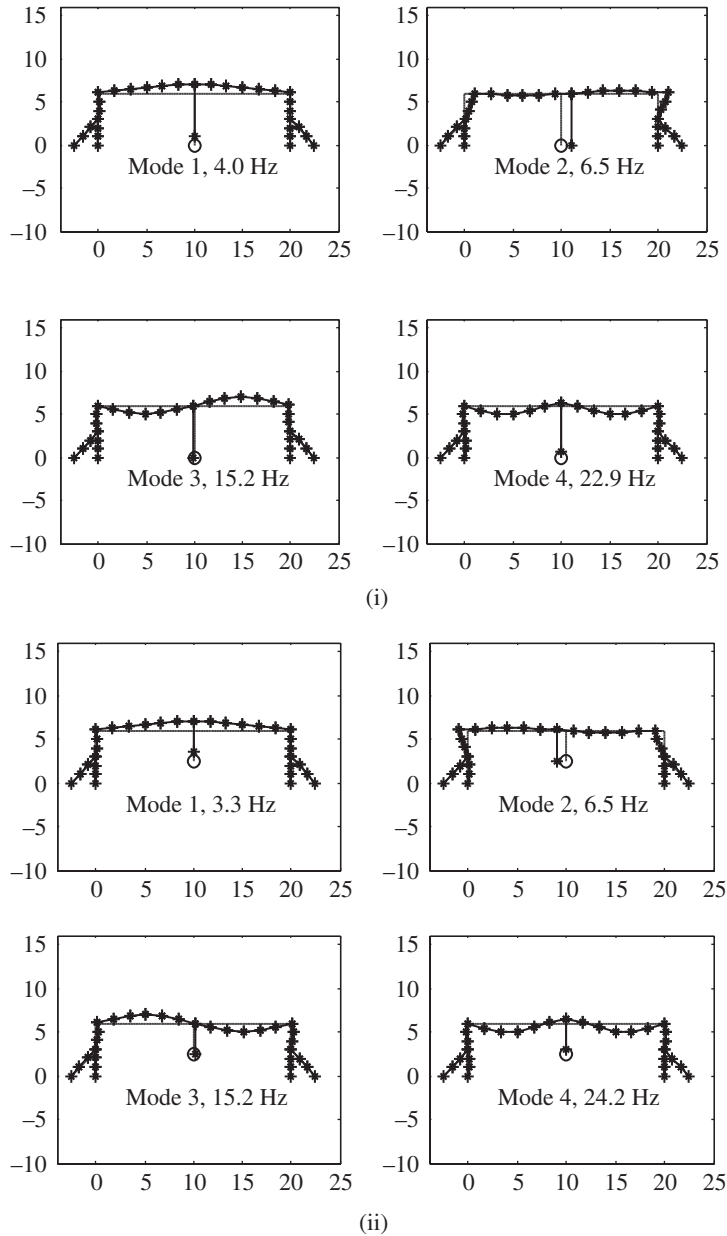


Figure E9.8.1(i) Modes for (i) case (a), and for (ii) case (b)

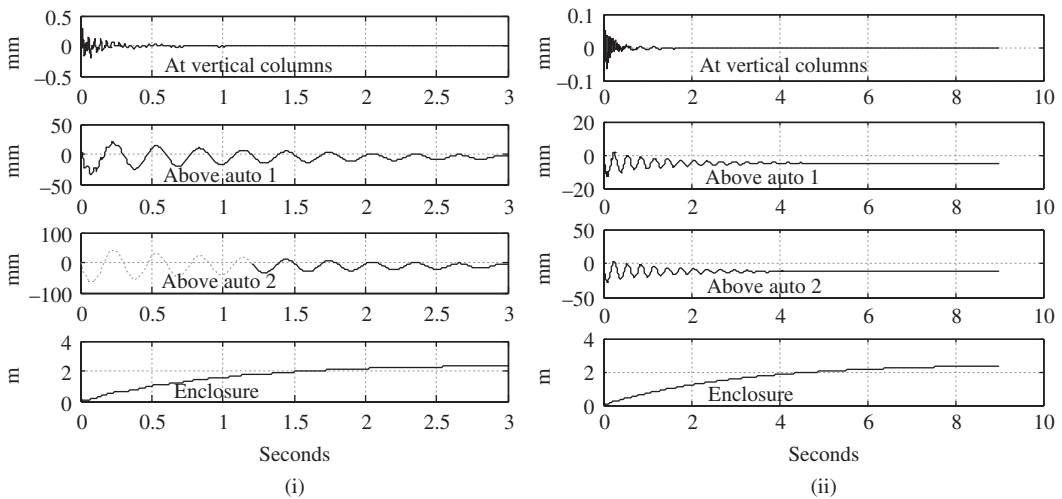
The dimension of this vector is from (18)

$$2N_{\text{npd}} = 2n_f + 2 = 2(3n + 45) + 2 = 2(3n + 46) \quad (48)$$

Equation (1) shows that the time required for the enclosure to be raised to 87% of its target value is approximately $2\tau_L$. Consider the case when the enclosure is above auto 2 and the I beam is modeled with $n = 12$ elements. Figure E9.8.1(j) shows the displacements of the frame and enclosure for $\tau_L = 1$ s and $\tau_L = 3$ s. Figure E9.8.1(k) shows the corresponding cable force (f_c , Eq. 4), cable stress (f_c/A_c), and enclosure mount force (R_f , Eq. 35). These figures clearly show that (a) increasing the hoist time significantly

Table E9.8.1(d) Natural frequency summary with enclosure attached above auto 2

Mode	Natural frequencies (Hz)		
	Without enclosure	Case (a) Enclosure attached $y_T = 0$	Case (b) Enclosure attached at $y_e = 2.5$ m
1	4.7	4.0	3.3
2	6.5	6.5	6.5
3	15.2	15.2	15.2
4	30.5	22.9	24.2
5	49.9	46.2	49.9
6	54.8	49.9	54.7
7	54.9	54.8	54.9
8	72.4	54.9	56.6
9	87.3	79.4	87.1
10	89.2	87.4	89.2

**Figure E9.8.1(j)** Vertical displacement of the I beam at the locations indicated and of the enclosure for (i) $\tau_L = 1$ s and (ii) $\tau_L = 3$ s

reduces vibrations and cable stress and force and (b) dynamic peak stresses are much larger than their static load counterparts so it is essential to perform a vibration simulation. For comparison purposes, the static cable force is one-fourth of the enclosure weight, $f_{\text{cable}}^{\text{static}} = W_e/4 = 2468$ N, and the corresponding static stress in the cable is $\sigma_{\text{cable}}^{\text{static}} = f_{\text{cable}}^{\text{static}}/A_c = 0.19 \times 10^8$ N/m². The peak dynamic displacement (41.0 mm) of the I beam midspan is also much larger than its static response value 12.0 mm.

(k) Response of Frame to Sudden Failure of Cables

A worst-case scenario study is requested for considering simultaneous failure of all four cables when the enclosure is stationary and raised off of the floor. The objective is to predict the vibration of the frame and forces at reaction (fixed) points on the frame (A and B in Figure E9.8.1(a)). Similar to the gravel truck loading Example 5.3.1, the

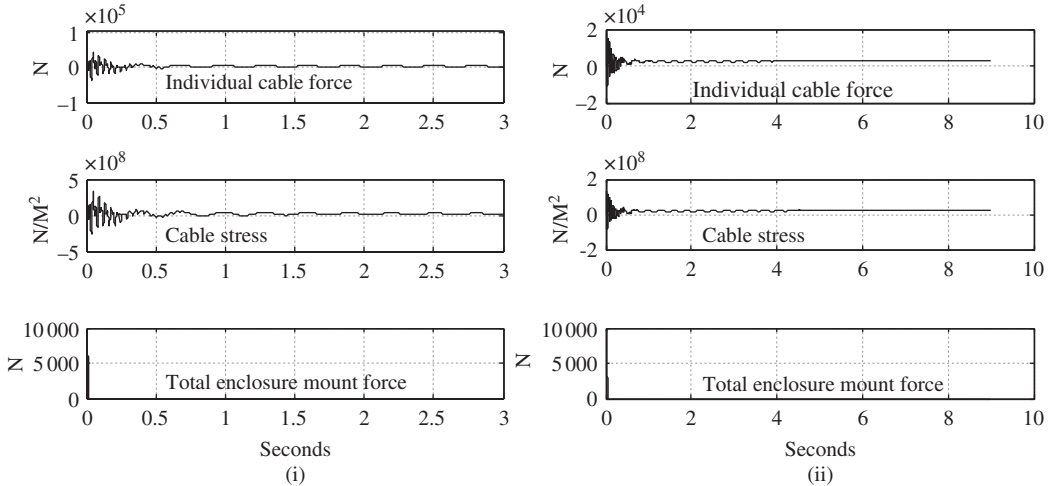


Figure E9.8.1(k) Forces and cable stress for the enclosure at midspan and (i) $\tau_L = 1$ s and (ii) $\tau_L = 3$ s

frame is initially, statically deflected due to the weight of the suspended enclosure. These deflections are obtained by solving the static form of Equation (41):

$$\hat{\underline{q}}_{-f} \Big|_{\text{static}} = \hat{\underline{K}}_{-f}^{-1} \hat{\underline{f}}_{-f} \quad (49)$$

where similar to (38) the static load vector is

$$\hat{\underline{f}}_{-f} = \begin{Bmatrix} 0 \\ \vdots \\ -W_e \\ \vdots \\ 0 \end{Bmatrix} \leftarrow \text{row } l^* \quad (50)$$

W_e is the enclosure weight and

$$n_H = \begin{cases} \frac{n}{6} + 1, & \text{enclosure above auto 1} \\ \frac{n}{2} + 1, & \text{enclosure above auto 2} \end{cases} \quad (51)$$

in (30). These static deflections are imposed as initial conditions for the sudden cable failure model. Figure E9.8.1(l) shows the initial static deflection patterns just prior to the cable failure, for the case of the enclosure positioned above auto 1 and above auto 2.

The frame static displacements become the initial conditions for solving the transient response condition (37)

$$\underline{M}_f \ddot{\underline{q}}_f + \underline{C}_{f0} \dot{\underline{q}}_f + \underline{K}_f \underline{q}_f = \underline{f}_f \quad (n_f \times 1) \quad (52)$$

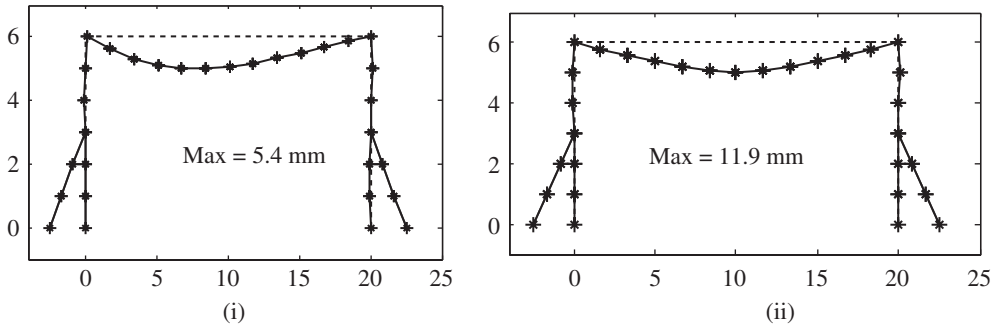


Figure E9.8.1(i) Deflection of frame due to enclosure weight prior to cable failure. Enclosure above (i) auto 1 and above (ii) auto 2

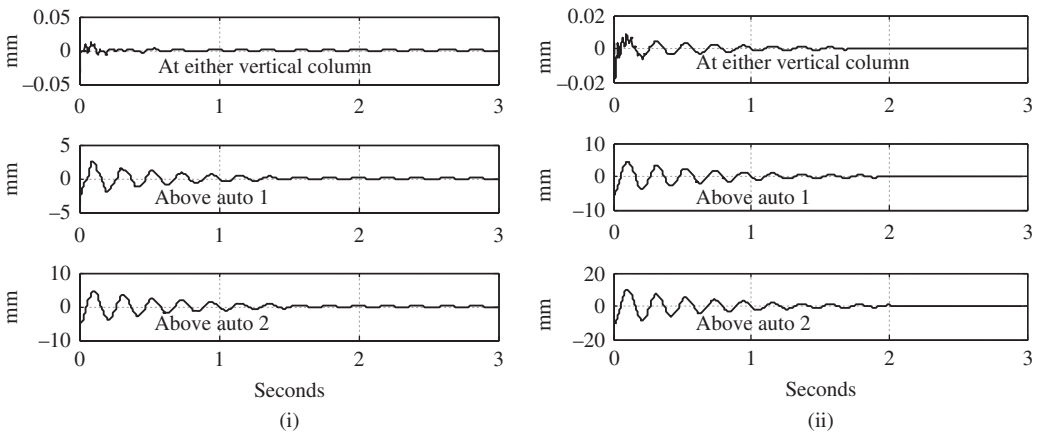


Figure E9.8.1(m) Vertical displacement of the I beam at the locations indicated, for the enclosure above (i) auto 1 and above (ii) auto 2

with $f_f = \underline{0}$. The state vector for the MATLAB ODE45 numerical integration solution is

$$\underline{Q}_c = \begin{Bmatrix} \underline{q}_f \\ \underline{v}_f \end{Bmatrix} \quad (2n_f \times 1) \quad (53)$$

Figure E9.8.1(m) shows the predicted vibrations at selected locations along the I beam after the cables fail.

The reaction forces at *A* and *B* in Figure E9.8.1(a) are obtained by considering the dynamic equilibrium of the beam element that contains the fixed node at *A* or *B*. This figure and Table E9.8.1(a) show that these elements and nodes are

$$\begin{aligned} \mathbf{A} : \text{fixed node } n + 8 \text{ is local node 1 of element } n + 7 \\ \mathbf{B} : \text{fixed node } n + 2 \text{ is local node 1 of element } n + 1 \end{aligned} \quad (54)$$

The inertia and damping terms of the element equation are ignored as an approximation, which improves as the element size diminishes, yielding the condition

$$\underline{F}_e = \underline{K}_e \underline{V}_e \quad (55)$$

where

$$\underline{F}_e = (F_{11}^e \quad F_{21}^e \quad M_1^e \quad F_{12}^e \quad F_{22}^e \quad M_2^e)^T \quad (56)$$

$$\underline{K}_e = \text{element stiffness matrix in Equation (9.8.7)} \quad (57)$$

$$\underline{V}_e = (v_1^e \quad v_2^e \quad v_3^e \quad v_4^e \quad v_5^e \quad v_6^e)^T = (u_{11}^e \quad u_{21}^e \quad \theta_1^e \quad u_{12}^e \quad u_{22}^e \quad \theta_2^e)^T \quad (58)$$

$$F_{ij}^e = \text{force in global } x_i \text{ direction at local node } j \text{ of element } e \quad (59)$$

$$M_j^e = \text{moment at local node } j \text{ of element } e \quad (60)$$

$$u_{ij}^e = \text{translational displacement in global } x_i \text{ direction at local node } j \text{ of element } e \quad (61)$$

$$\theta_j^e = \text{translational rotation at local node } j \text{ of element } e \quad (62)$$

Represent \underline{K}_e in the partitioned matrix form

$$\underline{K}_e = \begin{bmatrix} \frac{K_{11}^e}{3 \times 3} & \frac{K_{12}^e}{3 \times 3} \\ \frac{K_{21}^e}{3 \times 3} & \frac{K_{22}^e}{3 \times 3} \end{bmatrix} \quad (63)$$

The reaction forces at local node 1 are then obtained from (55) with zero displacements at local node 1 as

$$\begin{Bmatrix} F_{11}^e \\ F_{21}^e \\ M_1^e \end{Bmatrix} = \begin{bmatrix} \frac{K_{12}^e}{3 \times 3} \\ \frac{K_{21}^e}{3 \times 3} \end{bmatrix} \begin{Bmatrix} u_{12}^e \\ u_{22}^e \\ \theta_2^e \end{Bmatrix} \quad (64)$$

Inspection of Figures E9.8.1(a) and E9.8.1(b) shows that the displacements $(u_{12}^e, u_{22}^e, \theta_2^e)$ in (64) are those at node $(n+9)$ for the reaction forces at A and $(n+3)$ for the reaction forces at B. Table E9.8.1(e) provides the positions of these displacements in the solution vector $(\underline{q}_f(t))$ of (52).

Figure E9.8.1(n) shows the reaction forces versus time at the fixed point locations A and B in Figure E9.8.1(a), following the simultaneous failure of the cables.

Table E9.8.1(e) Positions of the displacements in Equation (64)

		Locations in \underline{q}_f		
		u_{12}^e	u_{22}^e	θ_2^e
A	node : $n+9$	$\text{larray}(3(n+8)+1)$	$\text{larray}(3(n+8)+2)$	$\text{larray}(3(n+8)+3)$
B	node : $n+3$	$\text{larray}(3(n+2)+1)$	$\text{larray}(3(n+2)+2)$	$\text{larray}(3(n+2)+3)$

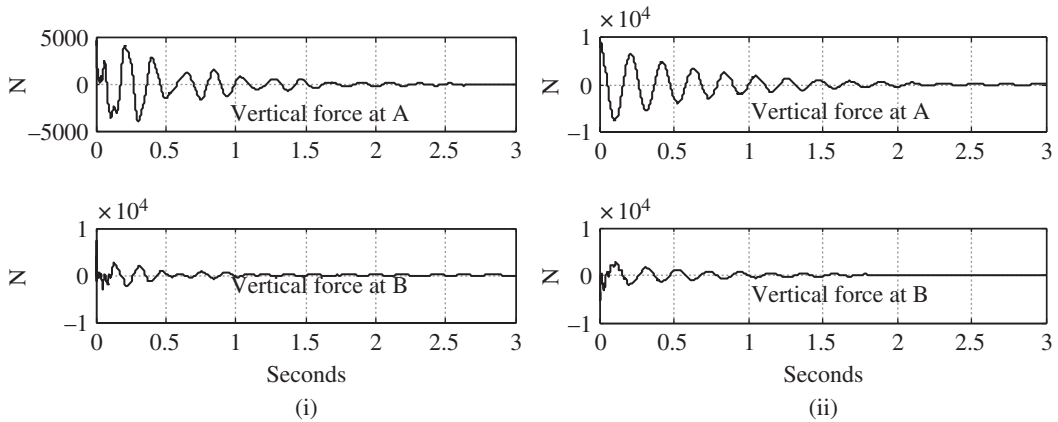


Figure E9.8.1(n) Reaction force time history at the constraint locations A and B in Figure E9.8.1(a) for the enclosure above (i) auto 1 and above (ii) auto 2

Summary: This example provides the following results and techniques:

- **Mesh Convergence:** The $n = 6$ and $n = 12$ modes and natural frequencies in Figure E9.8.1 (g) are nearly identical.
- **Statics versus Dynamics Model:** The dynamic (vibratory) displacements, forces, and stresses were shown to be much higher (20 times for cable stress) than their static solution counterparts for the enclosure lift simulation.
- **Analysis Types:** Transient-forced, mode and natural frequency, initial condition, and static response analyses are presented.
- **Special Features:** Orthogonal damping, time-dependent stiffness, and nonlinear forces (Eqs. 2, 24, and 33).
- **Reaction Force Determination:** The analysis in Equations (55)–(64) provided the reaction forces at A and B in Figure E9.8.1(a), as shown in Figure E9.8.1(n) for the sudden cable failure case.

9.9 SUMMARY

This chapter presented a thorough discussion and development of modeling beam-like structures (frames) for vibration simulation studies. The math models required for programming were developed for both 3D and 2D frames. The results were presented with detailed algorithms for assembling the beam elements into system matrices and subsequent solutions for modal data and time domain responses. The assembly procedures were shown to be nearly identical to those given in Chapter 4 for truss-type structures. The theory was demonstrated with complex 3D and 2D frame-type structures.

9.10 CHAPTER 9 EXERCISES

9.10.1 Exercise Location

All exercises may be conveniently viewed and downloaded at the following website: www.wiley.com/go/palazzolo. This new feature greatly reduces the length of the printed book, yielding a significant cost savings for the college student, and the exercises are updated.

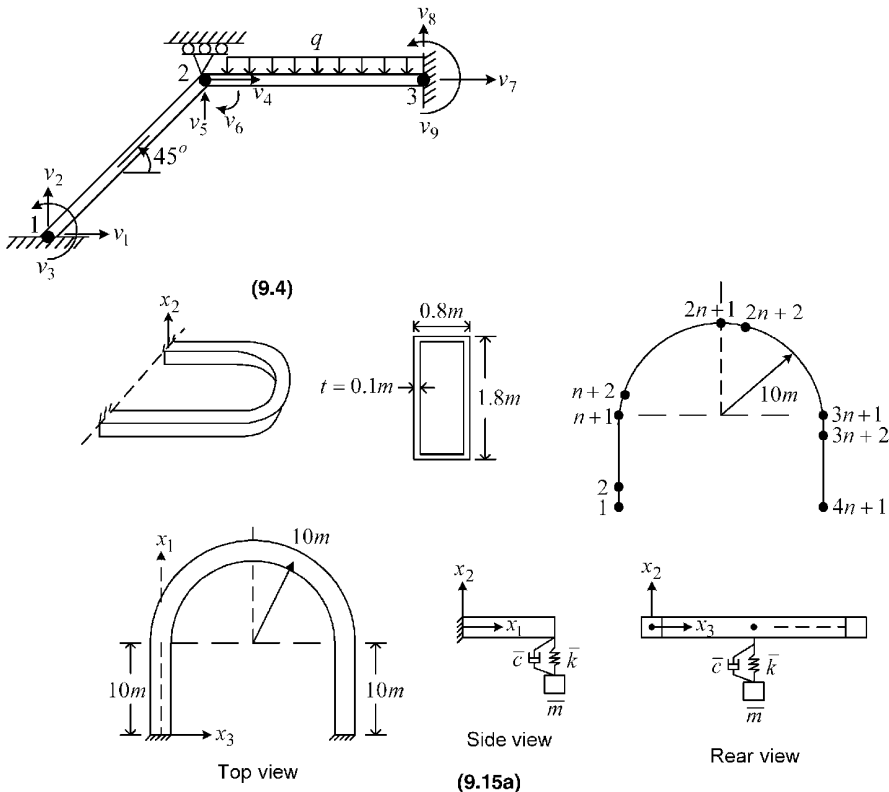
9.10.2 Exercise Goals

The goal of the Exercises in Chapter 9 is to strengthen the student's understanding and related engineering problem solving skills in the following areas:

- Understanding the underlying theory of beam element and frame models
- Ability to formulate a frame-type finite element model with arbitrary geometry, loading, and boundary conditions
- Calculating the free and forced vibration responses of frames including natural frequencies and mode shapes

9.10.3 Sample Exercises: 9.4 and 9.15a

The frame in 9.4 is constrained as shown and is subjected to a sudden uniform load. The objective is to determine the resulting vibration at node 2 and the reaction forces, moments, and stresses at node 3. The U-shaped frame in 9.15a represents the Skywalk that is perched over the edge of the Grand Canyon. A vibration absorber is attached to its underside to aid in suppressing pedestrian-induced vibrations. The objective is to calculate its natural frequencies and mode shapes.



REFERENCES

- American Institute of Steel Construction (AISC). *Manual of Steel Construction*, 8th ed. AISC, Chicago, IL, 1980.
- BATHE, K. J. *Finite Element Procedures in Engineering Analysis*. Prentice Hall, Englewood Cliffs, NJ, 1982.
- COOK, R., MALKUS, D. and PLESHA, M. *Concepts and Applications of Finite Element Analysis*, 3rd ed. John Wiley & Sons, New York, 1989.
- COWPER, G. R. "The Shear Coefficient in Timoshenko's Beam Theory". *J. Appl. Mech.* 335–340, 1966.
- DYM, C. and SHAMES, I. *Solid Mechanics—A Variational Approach*. McGraw Hill, New York, 1973.
- HARRIS, C. and PERSOL, A. *Harris Shock and Vibration Handbook*, 5th ed. McGraw Hill, New York, 2002.
- TIMOSHENKO, S. and GOODIER, J. *Theory of Elasticity*. McGraw Hill, New York, 1970.

Chapter 10

2D Planar Finite Elements for Vibration Analysis

10.1 INTRODUCTION

Design optimization algorithms, such as genetic algorithms, often utilize lower fidelity (detailed) models to narrow the range of prospective designs to a smaller set of candidate designs. The model fidelity is then increased for screening the surviving designs for more accurate predictions of stress, deflection, natural frequency, etc. The simplified models typically impose deflection or stress assumptions to reduce the dimensions of the model resulting in a reduction of modeling and simulation times. Excessive simulation time can be a serious impediment to analyzing a requisite number of design configurations even with modern, ultra-fast computers. This results from the extremely large numbers of degrees of freedom in many automated mesh finite element models. Imposing of deflection assumptions was previously illustrated in Chapter 9 where the condition “plane sections remain plane” was imposed on beam deflections. A similar, but less restrictive, approach is used in this chapter for developing plane stress, plane strain, and axisymmetric finite element models. These models are called 2D since finite element discretization (meshing) is applied only to a 2D area and not to a volume. The finite element method FEM is the approach of preference in most industrial and research and development environments. Acquiring a good grasp of the corresponding theory can assist commercial finite element software users in recognizing the limitations of the software that result from the inherent assumptions of the theory that the codes are based on.

10.2 PLANE STRAIN ($P\epsilon$)

The assumptions utilized for plane strain modeling are that the ratio of depth to width is very large, and the loading and boundary conditions are only in the 2D plane and nonvarying in the depth direction. Although the construction and loads on the object being modeled rarely meet these assumptions to a high degree of precision, the results of the model are frequently of sufficient accuracy to guide the initial design development, with the final candidate designs employing more precise models. Figure 10.2.1 illustrates some possible applications where the plane strain assumption may be very accurate due to in-plane loading and loading and boundary conditions that are approximately invariant in the depth direction. Euler–Bernoulli and Timoshenko beams assume invariance of deflection and loading in the depth direction and thus act similar to $P\epsilon$ models. The beam models also have additional kinematic constraints, that is, “plane sections remain plane” which disregards warping behavior of the beam’s cross section.

It is important to note that for dynamics, the $P\epsilon$ model is useful only for studying vibration mode shapes and response that are invariant in the depth direction. For example,

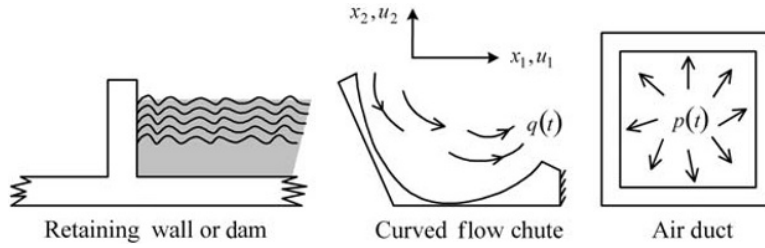


Figure 10.2.1 Some structural dynamics systems appropriate for plane strain modeling

twisting would invalidate $P\epsilon$ as an appropriate model for some turbomachinery blades. The assumptions of plane strain may be mathematically expressed in terms of the notation of Section A.3 as

$$u_3 = 0, \quad u_1 = u_1(x_1, x_2), \quad u_2 = u_2(x_1, x_2) \quad (10.2.1)$$

Therefore, the normal and shear strains from (A.3.21) become

$$\epsilon_{33} = \frac{\partial u_3}{\partial x_3} = 0, \quad \epsilon_{23} = \frac{1}{2} \left(\frac{\partial u_2}{\partial x_3} + \frac{\partial u_3}{\partial x_2} \right) = 0, \quad \epsilon_{13} = \frac{1}{2} \left(\frac{\partial u_1}{\partial x_3} + \frac{\partial u_3}{\partial x_1} \right) = 0 \quad (10.2.2)$$

Substitution of these strains into the isotropic material law equation (A.4.3) yields

$$\sigma_{11} = \alpha_{P\epsilon} [(1-\nu)\epsilon_{11} + \nu\epsilon_{22}] \quad (10.2.3)$$

$$\sigma_{22} = \alpha_{P\epsilon} [\nu\epsilon_{11} + (1-\nu)\epsilon_{22}] \quad (10.2.4)$$

$$\sigma_{33} = \alpha_{P\epsilon} (\nu\epsilon_{11} + \nu\epsilon_{22}) \quad (10.2.5)$$

where

$$\alpha_{P\epsilon} = \frac{E}{(1+\nu)(1-2\nu)} \quad (10.2.6)$$

Sum (10.2.3) and (10.2.4) to obtain

$$\nu(\sigma_{11} + \sigma_{22}) = \alpha_{P\epsilon} \nu (\epsilon_{11} + \epsilon_{22}) \quad (10.2.7)$$

Equations (10.2.5) and (10.2.7) then show that

$$\sigma_{33} = \nu(\sigma_{11} + \sigma_{22}) \quad (10.2.8)$$

The shear stresses are obtained from (A.4.3) and (10.2.2) as

$$\sigma_{13} = \sigma_{23} = 0, \quad \sigma_{12} = \alpha_{P\epsilon} (1-2\nu)\epsilon_{12} \quad (10.2.9)$$

Since σ_{33} can be obtained from σ_{11} and σ_{22} in (10.2.8), the nonzero stresses become

$$\begin{Bmatrix} \sigma_{11} \\ \sigma_{22} \\ \sigma_{12} \end{Bmatrix} = \alpha_{P\epsilon} \begin{bmatrix} 1-\nu & \nu & 0 \\ \nu & 1-\nu & 0 \\ 0 & 0 & \frac{1-2\nu}{2} \end{bmatrix} \begin{Bmatrix} \epsilon_{11} \\ \epsilon_{22} \\ 2\epsilon_{12} \end{Bmatrix} \quad (10.2.10)$$

or in matrix–vector notation,

$$\underline{\sigma}_{Pe} = \underline{E}_{Pe} \underline{\varepsilon}_{Pe} \quad 3 \times 1 \quad (10.2.11)$$

10.3 PLANE STRESS ($P\sigma$)

In one aspect, the plane stress assumption is opposite from that of the plain strain assumption. Plane stress structures must generally have very thin plate-like geometry. The assumption of only in-plane loading is still required for the plane stress model. Figure 10.3.1 illustrates some possible applications of the plane stress modeling approach. Plane stress assumptions are frequently imposed for formulating the in-plane deformation model of plates, and plate theory is applied to the Kirchhoff out-of-plane bending and Mindlin shear deformation of plates.

To better understand the plane stress approximation, assume that no external loading exists on the x_3 surface of the plate, that is, in-plane loads may be treated as internal loads. Applying the equilibrium conditions on the top and bottom surfaces of the plate, Equation (A.2.3), with

$$n_1 = n_2 = 0, \quad n_3 = 1 \quad (\text{unit normal}) \quad (10.3.1)$$

and

$$\Phi_1 = \Phi_2 = \Phi_3 = 0 \quad (\text{surface traction on } \pm x_3 \text{ surface}) \quad (10.3.2)$$

yields the results

$$\sigma_{13} = \sigma_{23} = \sigma_{33} = 0 \quad (10.3.3)$$

Assume that this conditions hold approximately in the interior, and thus from (10.3.3) and the isotropic material law (A.4.3),

$$\sigma_{11} = \alpha_{Pe} [(1-\nu)\varepsilon_{11} + \nu\varepsilon_{22} + \nu\varepsilon_{33}] \quad (10.3.4)$$

$$\sigma_{22} = \alpha_{Pe} [\nu\varepsilon_{11} + (1-\nu)\varepsilon_{22} + \nu\varepsilon_{33}] \quad (10.3.5)$$

$$\sigma_{33} = \alpha_{Pe} [\nu\varepsilon_{11} + \nu\varepsilon_{22} + (1-\nu)\varepsilon_{33}] = 0 \quad (10.3.6)$$

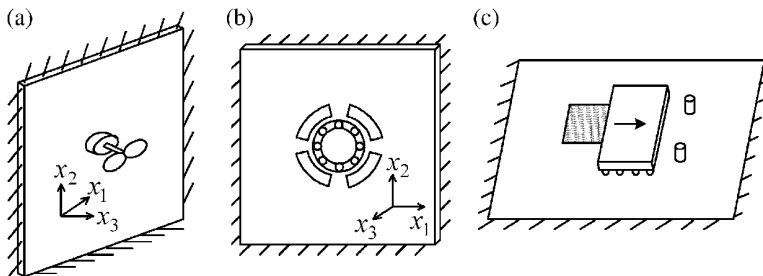


Figure 10.3.1 Some structural dynamics systems appropriate for plane stress modeling. (a) Furnace wall mounted fan, (b) panel mounted ball bearing with cutouts and (c) floor plate with quick open hatch and bumper stops

where $\alpha_{Pe} = E/(1+\nu)(1-2\nu)$. From (10.3.6),

$$\varepsilon_{33} = \frac{(-\nu\varepsilon_{11} - \nu\varepsilon_{22})}{(1-\nu)} \quad (10.3.7)$$

Substitute (10.3.7) into (10.3.4) and (10.3.5) to obtain

$$\sigma_{11} = \frac{E}{1-\nu^2}(\varepsilon_{11} + \nu\varepsilon_{22}), \quad \sigma_{22} = \frac{E}{1-\nu^2}(\nu\varepsilon_{11} + \varepsilon_{22}) \quad (10.3.8)$$

and from (A.4.3),

$$\sigma_{12} = \frac{E}{1+\nu}\varepsilon_{12} \quad (10.3.9)$$

These relations are written in matrix form as

$$\begin{Bmatrix} \sigma_{11} \\ \sigma_{22} \\ \sigma_{12} \end{Bmatrix} = \frac{E}{1-\nu^2} \begin{bmatrix} 1 & \nu & 0 \\ \nu & 1 & 0 \\ 0 & 0 & \frac{1-\nu}{2} \end{bmatrix} \begin{Bmatrix} \varepsilon_{11} \\ \varepsilon_{22} \\ 2\varepsilon_{12} \end{Bmatrix} \quad (10.3.10)$$

or

$$\underline{\sigma}_{P\sigma} = \underline{E}_{P\sigma} \underline{\varepsilon}_{P\sigma} \quad (10.3.11)$$

It is interesting to note that the $P\sigma$ material matrix $\underline{E}_{P\sigma}$ may be obtained from the Pe matrix \underline{E}_{Pe} (10.2.8) by making the substitutions

$$\nu \Rightarrow \frac{\nu}{1+\nu}, \quad E \Rightarrow \frac{E(1+2\nu)}{(1+\nu)^2} \quad (10.3.12)$$

This simplifies coding since the ρe and $\rho\sigma$ models differ only by an “effective” Poisson ratio ν and Young’s Modulus E .

10.4 PLANE STRESS AND PLANE STRAIN: ELEMENT STIFFNESS AND MASS MATRICES AND FORCE VECTOR

The area of the model in the x_1-x_2 plane may be meshed with various orders and types of elements. The 4-node quadrilateral, isoparametric finite element shown in Figure 10.4.1 is utilized here for sake of illustration. The element numbers are ($e = 1, 2, \dots, N_E$), and the node numbers ($i = 1, 2, \dots, N_N$).

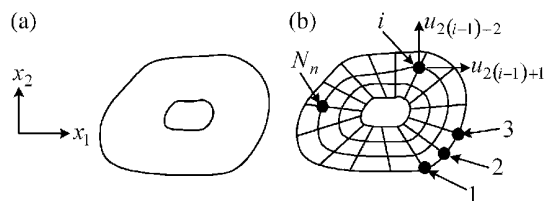


Figure 10.4.1 Plane stress/strain model (a) without FE mesh and (b) with FE mesh including N_n nodes and a degree of freedom numbering convention

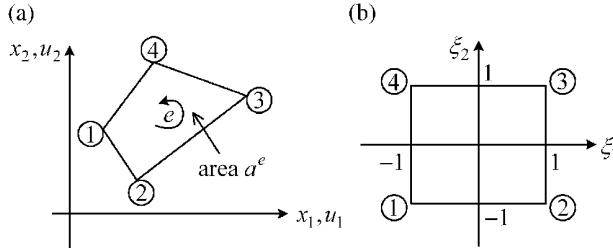


Figure 10.4.2 Four-node quadrilateral element in (a) actual coordinates and (b) natural (parent) coordinates

Each element in the model has the general geometry description depicted in Figure 10.4.2.

As discussed in Section 2.11 (2.11.36), the u_1 and u_2 displacements are interpolated within the element according to

$$u_i = \sum_{k=1}^4 N_k(\xi_1, \xi_2) u_{ik}^{(e)} \quad i = 1, 2 \quad (10.4.1)$$

where the shape functions are defined in this case by the Lagrangian polynomials,

$$\begin{aligned} N_1 &= \frac{1}{4}(1-\xi_1)(1-\xi_2), & N_2 &= \frac{1}{4}(1+\xi_1)(1-\xi_2) \\ N_3 &= \frac{1}{4}(1+\xi_1)(1+\xi_2), & N_4 &= \frac{1}{4}(1-\xi_1)(1+\xi_2) \end{aligned} \quad (10.4.2)$$

$$u_{ik}^{(e)} = u_i \text{ displacement of local node } k \text{ of element } e \quad (10.4.3)$$

The geometry of the element is mapped from its actual shape into a square as depicted in Figure 10.4.2. This mapping is expressed by

$$x_i = \sum_{k=1}^4 N_k(\xi_1, \xi_2) x_{ik}^{(e)} \quad i = 1, 2 \quad (10.4.4)$$

where ξ_i are the “natural” or “parent” coordinates and

$$x_{ik}^{(e)} = x_i \text{ coordinate of local node } k \text{ of element } e \quad (10.4.5)$$

This is referred to as an “isoparametric” formulation since both the displacement interpolation and geometry mapping utilize the same shape functions $N_k(\xi_1, \xi_2)$. The general formulation of the finite element stiffness matrix, Equations (4.7.16)–(4.7.34), applied to the 2D approximation case yields

$$\underline{\underline{u}}^e = \left\{ \begin{matrix} u_1 \\ u_2 \end{matrix} \right\} = \underline{\underline{N}} \underline{\underline{q}}^e \quad (10.4.6)$$

$$\underline{\underline{q}}^e = (u_{11}^e \ u_{21}^e \ u_{12}^e \ u_{22}^e \ u_{13}^e \ u_{23}^e \ u_{14}^e \ u_{24}^e)^T \quad (10.4.7)$$

$$\underline{\underline{N}} = \begin{bmatrix} N_1 & 0 & N_2 & 0 & N_3 & 0 & N_4 & 0 \\ 0 & N_1 & 0 & N_2 & 0 & N_3 & 0 & N_4 \end{bmatrix} \quad (10.4.8)$$

$$\underline{\varepsilon} = \begin{Bmatrix} \varepsilon_{11} \\ \varepsilon_{22} \\ 2\varepsilon_{12} \end{Bmatrix} = \begin{bmatrix} \frac{\partial}{\partial x_1} & 0 \\ 0 & \frac{\partial}{\partial x_2} \\ \frac{\partial}{\partial x_2} & \frac{\partial}{\partial x_1} \end{bmatrix} \begin{Bmatrix} u_1 \\ u_2 \end{Bmatrix} = \underline{D}\underline{u} \quad (10.4.9)$$

$$\underline{\varepsilon}^e = \underline{B}^e \underline{q}^e \quad (10.4.10)$$

$\begin{matrix} 3 \times 1 & & 3 \times 8 & 8 \times 1 \end{matrix}$

and finally by (4.7.30),

$$\underline{K}^e = \int_{V_e} \underline{B}_e^T \underline{E}_e \underline{B}_e dV \quad (10.4.11)$$

Equation (10.4.11) is not in a form that is conducive to programming and numerical evaluation. The following steps convert the integrand and integration into a more easily programmable form. To begin, rewrite (10.4.9) as

$$\underline{\varepsilon} = \begin{bmatrix} 1 & 0 & 0 & 0 \\ 0 & 0 & 0 & 1 \\ 0 & 1 & 1 & 0 \end{bmatrix} \begin{Bmatrix} \frac{\partial u_1}{\partial x_1} \\ \frac{\partial u_1}{\partial x_2} \\ \frac{\partial u_2}{\partial x_1} \\ \frac{\partial u_2}{\partial x_2} \end{Bmatrix} \quad (10.4.12)$$

The derivatives with respect to x_j in (10.4.12) are not readily evaluated since the displacements u_j are interpolated with natural coordinates ξ_j . The differentiations are transformed to derivatives taken with respect to the ξ_j coordinates as follows. By the chain rule of differentiation,

$$\begin{Bmatrix} \frac{\partial}{\partial \xi_1} \\ \frac{\partial}{\partial \xi_2} \end{Bmatrix} = \begin{bmatrix} \frac{\partial x_1}{\partial \xi_1} & \frac{\partial x_2}{\partial \xi_1} \\ \frac{\partial x_1}{\partial \xi_2} & \frac{\partial x_2}{\partial \xi_2} \end{bmatrix} \begin{Bmatrix} \frac{\partial}{\partial x_1} \\ \frac{\partial}{\partial x_2} \end{Bmatrix} \quad (10.4.13)$$

or in matrix–vector symbols (2.6.42a),

$$\frac{\partial}{\partial \underline{\xi}} = \underline{J} \frac{\partial}{\partial \underline{x}} \quad (10.4.14)$$

where the “Jacobian” matrix \underline{J} is expressed with Equation (10.4.4) as

$$\underline{J} = \begin{bmatrix} \sum_{k=1}^4 \frac{\partial N_k}{\partial \xi_1} x_{1k}^e & \sum_{k=1}^4 \frac{\partial N_k}{\partial \xi_1} x_{2k}^e \\ \sum_{k=1}^4 \frac{\partial N_k}{\partial \xi_2} x_{1k}^e & \sum_{k=1}^4 \frac{\partial N_k}{\partial \xi_2} x_{2k}^e \end{bmatrix} = \begin{bmatrix} \frac{\partial N_1}{\partial \xi_1} & \frac{\partial N_2}{\partial \xi_1} & \frac{\partial N_3}{\partial \xi_1} & \frac{\partial N_4}{\partial \xi_1} \\ \frac{\partial N_1}{\partial \xi_2} & \frac{\partial N_2}{\partial \xi_2} & \frac{\partial N_3}{\partial \xi_2} & \frac{\partial N_4}{\partial \xi_2} \end{bmatrix} \begin{bmatrix} x_{11}^e & x_{21}^e \\ x_{12}^e & x_{22}^e \\ x_{13}^e & x_{23}^e \\ x_{14}^e & x_{24}^e \end{bmatrix} = \begin{bmatrix} J_{11} & J_{12} \\ J_{21} & J_{22} \end{bmatrix} \quad (10.4.15)$$

The second form of \underline{J} in (10.4.15) provides an efficient manner for its evaluation. The shape function derivatives will soon be shown to be evaluated at the same ‘‘Gauss points’’ in every element, and so these matrices need be calculated (and stored) only once. These matrices may then be multiplied by the matrix of nodal coordinates in (10.4.15), which does change between elements, to obtain the matrix \underline{J} evaluated at the Gauss points. Apply (10.4.14) to the derivatives of u_1 and u_2 in (10.4.12),

$$\begin{Bmatrix} \frac{\partial u_1}{\partial x_1} \\ \frac{\partial u_1}{\partial x_2} \\ \frac{\partial u_2}{\partial x_1} \\ \frac{\partial u_2}{\partial x_2} \end{Bmatrix} = \begin{bmatrix} \underline{J}^{-1} & \underline{0} \\ \underline{0} & \underline{J}^{-1} \end{bmatrix} \begin{Bmatrix} \frac{\partial u_1}{\partial \xi_1} \\ \frac{\partial u_1}{\partial \xi_2} \\ \frac{\partial u_2}{\partial \xi_1} \\ \frac{\partial u_2}{\partial \xi_2} \end{Bmatrix} \quad (10.4.16)$$

Substitute (10.4.16) into (10.4.12) to obtain

$$\underline{\varepsilon} = \underline{A}_1^e \underline{r} \quad (10.4.17)$$

$\begin{matrix} 3 \times 1 & & 3 \times 4 & 4 \times 1 \end{matrix}$

where

$$\underline{r} = \begin{Bmatrix} \frac{\partial u_1}{\partial \xi_1} \\ \frac{\partial u_1}{\partial \xi_2} \\ \frac{\partial u_2}{\partial \xi_1} \\ \frac{\partial u_2}{\partial \xi_2} \end{Bmatrix} \quad (10.4.18)$$

and

$$\underline{A}_1^e = \begin{bmatrix} 1 & 0 & 0 & 0 \\ 0 & 0 & 0 & 1 \\ 0 & 1 & 1 & 0 \end{bmatrix} \begin{bmatrix} \underline{J}^{-1} & \underline{0} \\ \underline{0} & \underline{J}^{-1} \end{bmatrix} \quad (10.4.19)$$

$\begin{matrix} 3 \times 4 & & 2 \times 2 & 2 \times 2 \\ & & 2 \times 2 & 2 \times 2 \end{matrix}$

Substitute (10.4.6)–(10.4.8) into (10.4.18) to obtain

$$\underline{r} = \begin{Bmatrix} \frac{\partial u_1}{\partial \xi_1} \\ \frac{\partial u_1}{\partial \xi_2} \\ \frac{\partial u_2}{\partial \xi_1} \\ \frac{\partial u_2}{\partial \xi_2} \end{Bmatrix} = \begin{bmatrix} \frac{\partial N_1}{\partial \xi_1} & 0 & \frac{\partial N_2}{\partial \xi_1} & 0 & \frac{\partial N_3}{\partial \xi_1} & 0 & \frac{\partial N_4}{\partial \xi_1} & 0 \\ \frac{\partial N_1}{\partial \xi_2} & 0 & \frac{\partial N_2}{\partial \xi_2} & 0 & \frac{\partial N_3}{\partial \xi_2} & 0 & \frac{\partial N_4}{\partial \xi_2} & 0 \\ 0 & \frac{\partial N_1}{\partial \xi_1} & 0 & \frac{\partial N_2}{\partial \xi_1} & 0 & \frac{\partial N_3}{\partial \xi_1} & 0 & \frac{\partial N_4}{\partial \xi_1} \\ 0 & \frac{\partial N_1}{\partial \xi_2} & 0 & \frac{\partial N_2}{\partial \xi_2} & 0 & \frac{\partial N_3}{\partial \xi_2} & 0 & \frac{\partial N_4}{\partial \xi_2} \end{bmatrix} \begin{Bmatrix} u_{11}^e \\ u_{21}^e \\ u_{12}^e \\ u_{22}^e \\ u_{13}^e \\ u_{23}^e \\ u_{14}^e \\ u_{24}^e \end{Bmatrix} \quad (10.4.20)$$

or in matrix–vector symbols,

$$\underline{r} = \underline{A}_2^e \underline{q}^e \quad (10.4.21)$$

Note that as described above for evaluating the Jacobian matrix \underline{J} , the matrix of shape function derivatives in (10.4.20) need be evaluated only once at each Gauss point in a single element, since the Gauss points will be the same for every element in the mesh. Substitution of (10.4.21) into (10.4.17) yields

$$\underline{\varepsilon} = \underline{A}_1^e \underline{A}_2^e \underline{q}^e \quad (10.4.22)$$

Comparison of (10.4.10) and (10.4.22) shows that

$$\underline{B}^e = \underline{A}_1^e \underline{A}_2^e \quad (10.4.23)$$

The stiffness matrix integral in (10.4.11) can now be considered utilizing (10.4.23). The integration domain includes the $x_1 - x_2$ area of the element as shown in Figure 10.4.2 and a finite thickness in the x_3 direction. Let the thickness of an element in the x_3 direction of Figure 10.4.2 be represented by \hat{t}^e . For plane strain models, all loads are considered per unit depth, in which case $\hat{t}^e = 1$. The stiffness matrix integral in (10.4.11) may then be written as

$$\underline{K}^e = \hat{t}^e \int_{a^e} (\underline{B}^e)^T \underline{E}^e \underline{B}^e da^e \quad (10.4.24)$$

where a^e is the area of element e in the $x_1 - x_2$ plane. The differential area da^e transforms between actual and natural coordinates as (Hildebrand, 1976)

$$da^e = dx_1 dx_2 = \det(\underline{J}_e) d\xi_1 d\xi_2 \quad (10.4.25)$$

Equation (10.4.24) then becomes

$$\underline{K}^e = \hat{t}^e \int_{-1}^1 \int_{-1}^1 (\underline{B}^e)^T \underline{E}^e \underline{B}^e \det(\underline{J}_e) d\xi_1 d\xi_2 \quad (10.4.26)$$

where the plane strain or plane stress, isotropic, material property matrix is given by (10.2.10) or (10.3.10), respectively. Although the integration domain now assumes a very simple unit square shape, the integrand terms in (10.4.26) are more complicated than polynomial expressions and generally have the form of rational functions of ξ_1 and ξ_2 . The denominator in the rational functions results from the \underline{J}^{-1} term in (10.4.16). Consequently, the double integral must be performed numerically and the usual method is by using “Gauss Quadrature” (GQ), as implemented with the following steps:

- (a) The integrand matrix $(\underline{B}^e)^T \underline{E}^e \underline{B}^e \det(\underline{J}_e)$ is evaluated at a set of discrete “Gauss integration point” locations (ξ_{1s}, ξ_{2t}) in the integration domain $(-1 \leq \xi_1 \leq +1, -1 \leq \xi_2 \leq +1)$. The indices s and t range between $s = 1, 2, \dots, n_G$ and $t = 1, 2, \dots, n_G$ yielding a set of n_G^2 Gauss integration point locations within $(-1 \leq \xi_1 \leq +1, -1 \leq \xi_2 \leq +1)$. The parameter n_G is referred to as the GQ order and typically equals 2 or 3 for the 4 node, quadrilateral element shown in Figure 10.4.2. The coordinates (ξ_{1s}, ξ_{2t}) of these special locations are called “Gauss integration points.” Table 10.4.1 shows the Gauss integration points for various Gauss integration orders.

Table 10.4.1 Gauss Quadrature (GQ) points and weight factors for order 1–4

Order n_G	Point no. (i)	Location of GQ point ξ_i	Weight factor \bar{w}_i
1	1	0	2
2	1	$-1/\sqrt{3}$	1
	2	$1/\sqrt{3}$	1
3	1	$-\sqrt{0.6}$	5/9
	2	0	8/9
	3	$+\sqrt{0.6}$	5/9
4	1	$-\sqrt{\frac{3+2r}{7}}$	$\frac{1}{2} - \frac{1}{6r}$
	2	$-\sqrt{\frac{3-2r}{7}}$	$\frac{1}{2} + \frac{1}{6r}$
	3	$+\sqrt{\frac{3-2r}{7}}$	$\frac{1}{2} + \frac{1}{6r}$
	4	$+\sqrt{\frac{3+2r}{7}}$	$\frac{1}{2} - \frac{1}{6r}$

- (b) The set of n_G^2 matrices in (a) are then multiplied by their respective weighting factors $\bar{w}_s \bar{w}_t$, which are shown in Table 10.4.1.
- (c) The double integral in (10.4.26) is then replaced by a double sum over $s = 1, 2, \dots, n_G$ and $t = 1, 2, \dots, n_G$.

The net effect of applying these steps converts the integral in (10.4.26) into the sum

$$\underline{K}^e \approx \hat{t}^e \sum_{s=1}^{n_G} \sum_{t=1}^{n_G} \bar{w}_s \bar{w}_t \underline{B}_e^T(\xi_{1s}, \xi_{2t}) \underline{E}_e \underline{B}_e(\xi_{1s}, \xi_{2t}) \det(\underline{J}_e(\xi_{1s}, \xi_{2t})) \quad (10.4.27)$$

Notably, GQ of order n_G will provide the exact value for

$$\int_{-1}^1 f(\xi) d\xi \quad (10.4.28)$$

if $f(\xi)$ is a polynomial in ξ of degree $(2n_G - 1)$ or less. The general form of the element mass matrix is given by (4.7.10) as

$$\underline{M}^e = \int_{V_e} \rho \underline{N}^T \underline{N} dV \quad (10.4.29)$$

where \underline{N} is defined in (10.4.8). The isoparametric transformation is applied to obtain

$$\underline{M}^e = \hat{t}^e \int_{-1}^1 \int_{-1}^1 \rho \underline{N}^T \underline{N} \det(\underline{J}_e) d\xi_1 d\xi_2 \quad (10.4.30)$$

and finally, applying GQ yields the formula

$$\underline{M}^e \approx \hat{t}^e \sum_{s=1}^{n_G} \sum_{t=1}^{n_G} \bar{w}_s \bar{w}_t \rho(\xi_{1s}, \xi_{2t}) \underline{N}^T(\xi_{1s}, \xi_{2t}) \underline{N}(\xi_{1s}, \xi_{2t}) \det(\underline{J}_e(\xi_{1s}, \xi_{2t})) \quad (10.4.31)$$

10.4.1 External Forces

The external forces acting on the element may be distributed throughout its volume or applied on one or more of its four edges. The volume force densities (force per unit volume) are F_{Vx1}^e and F_{Vx2}^e , and the surface (edge) force densities (force per unit area) are $F_{\Gamma x1}^e$ and $F_{\Gamma x2}^e$. Examples of the former include gravity (weight) and imposed acceleration, and examples of the latter include pressure and concentrated surface loads. The element force vector may then be expressed by (4.7.59) as

$$\underset{8 \times 1}{f}^e = \begin{pmatrix} f_{11}^e \\ f_{21}^e \\ f_{12}^e \\ f_{22}^e \\ f_{13}^e \\ f_{23}^e \\ f_{14}^e \\ f_{24}^e \end{pmatrix} = \int_{\Gamma^e} \underline{N}^T \begin{Bmatrix} F_{\Gamma x1}^e \\ F_{\Gamma x2}^e \end{Bmatrix} d\Gamma + \int_{V^e} \underline{N}^T \begin{Bmatrix} F_{Vx1}^e \\ F_{Vx2}^e \end{Bmatrix} dV \quad (10.4.32)$$

where Γ^e represents all edges of the element that lie on the surface of the structure being modeled, and the shape function matrix \underline{N} is defined in (10.4.8).

10.4.2 Concentrated Forces

Consider the general case where all nodes in an element are subjected to concentrated forces, where in actual applications many of these loads will be zero. Let $F_{ik}^A(t)$ represent a concentrated external force acting at local node k in direction x_i . This loading can be included in the volume force integral of (10.4.32) by using Dirac delta functions as explained in Section 2.12, that is,

$$\underset{8 \times 1}{f}_{-c}^e = \int_V \underline{N}^T \sum_{k=1}^4 \begin{Bmatrix} F_{1k}^A(t) \delta(x_1 - x_{1k}, x_2 - x_{2k}) \\ F_{2k}^A(t) \delta(x_1 - x_{1k}, x_2 - x_{2k}) \end{Bmatrix} dV = \int_V \left\{ \begin{array}{l} \sum_{k=1}^4 F_{1k}^A(t) N_1 \delta(x_1 - x_{1k}, x_2 - x_{2k}) \\ \sum_{k=1}^4 F_{2k}^A(t) N_1 \delta(x_1 - x_{1k}, x_2 - x_{2k}) \\ \sum_{k=1}^4 F_{1k}^A(t) N_2 \delta(x_1 - x_{1k}, x_2 - x_{2k}) \\ \sum_{k=1}^4 F_{2k}^A(t) N_2 \delta(x_1 - x_{1k}, x_2 - x_{2k}) \\ \sum_{k=1}^4 F_{1k}^A(t) N_3 \delta(x_1 - x_{1k}, x_2 - x_{2k}) \\ \sum_{k=1}^4 F_{2k}^A(t) N_3 \delta(x_1 - x_{1k}, x_2 - x_{2k}) \\ \sum_{k=1}^4 F_{1k}^A(t) N_4 \delta(x_1 - x_{1k}, x_2 - x_{2k}) \\ \sum_{k=1}^4 F_{2k}^A(t) N_4 \delta(x_1 - x_{1k}, x_2 - x_{2k}) \end{array} \right\} dV = \begin{Bmatrix} F_{11}^A(t) \\ F_{21}^A(t) \\ F_{12}^A(t) \\ F_{22}^A(t) \\ F_{13}^A(t) \\ F_{23}^A(t) \\ F_{14}^A(t) \\ F_{24}^A(t) \end{Bmatrix} \quad (10.4.33)$$

which follows from (2.12.4) and since the shape functions defined in (10.4.2) satisfy

$$N_k(x_{1j}, x_{2j}) = \begin{cases} 0, & j \neq k \\ 1, & j = k \end{cases} \quad (10.4.34)$$

The concentrated load at a node should be included in only one element force vector to avoid redundancy.

Alternatively, concentrated forces applied at nodes may be placed directly into the total system force vector at the degrees of freedom where they are applied. This procedure permits bypassing the step of assembling the element force vector into the total system force vector.

10.4.3 General Volumetric Loading

Next consider volumetric forces that are distributed within the domain of an element. Consider the distributed volumetric load having components

$$\underline{F}_v^e = \begin{Bmatrix} F_{vx1}^e \\ F_{vx2}^e \end{Bmatrix} = \begin{Bmatrix} f_{vx1}^e(x_1, x_2) \alpha_{vx1}^e(t) \\ f_{vx2}^e(x_1, x_2) \alpha_{vx2}^e(t) \end{Bmatrix} \quad (10.4.35)$$

where the $\alpha(t)$ terms contain the temporal dependence of the loading. This may occur for example when a deformable object is subjected to a time-varying acceleration field. The element force vector is determined from (10.4.25) and (10.4.32) as

$$\underline{f}_v^e(t) = \hat{t}^e \int_{-1}^1 \int_{-1}^1 \underline{N}^T(\xi_1, \xi_2) \begin{Bmatrix} f_{vx1}^e(\xi_1, \xi_2) \alpha_{vx1}^e(t) \\ f_{vx2}^e(\xi_1, \xi_2) \alpha_{vx2}^e(t) \end{Bmatrix} \det(\underline{J}_e) d\xi_1 d\xi_2 \quad (10.4.36)$$

Substitution of (10.4.8) and use of GQ converts (10.4.36) into a form that may be readily programmed and evaluated

$$\underline{f}_v^e(t) = \hat{t}^e \begin{Bmatrix} \alpha_{vx1}^e(t) \sum_{r=1}^{n_G} \sum_{s=1}^{n_G} \bar{w}_r \bar{w}_s N_1(\xi_{1r}, \xi_{2s}) f_{vx1}^e(\xi_{1r}, \xi_{2s}) \det(\underline{J}_e(\xi_{1r}, \xi_{2s})) \\ \alpha_{vx2}^e(t) \sum_{r=1}^{n_G} \sum_{s=1}^{n_G} \bar{w}_r \bar{w}_s N_1(\xi_{1r}, \xi_{2s}) f_{vx2}^e(\xi_{1r}, \xi_{2s}) \det(\underline{J}_e(\xi_{1r}, \xi_{2s})) \\ \alpha_{vx1}^e(t) \sum_{r=1}^{n_G} \sum_{s=1}^{n_G} \bar{w}_r \bar{w}_s N_2(\xi_{1r}, \xi_{2s}) f_{vx1}^e(\xi_{1r}, \xi_{2s}) \det(\underline{J}_e(\xi_{1r}, \xi_{2s})) \\ \alpha_{vx2}^e(t) \sum_{r=1}^{n_G} \sum_{s=1}^{n_G} \bar{w}_r \bar{w}_s N_2(\xi_{1r}, \xi_{2s}) f_{vx2}^e(\xi_{1r}, \xi_{2s}) \det(\underline{J}_e(\xi_{1r}, \xi_{2s})) \\ \alpha_{vx1}^e(t) \sum_{r=1}^{n_G} \sum_{s=1}^{n_G} \bar{w}_r \bar{w}_s N_3(\xi_{1r}, \xi_{2s}) f_{vx1}^e(\xi_{1r}, \xi_{2s}) \det(\underline{J}_e(\xi_{1r}, \xi_{2s})) \\ \alpha_{vx2}^e(t) \sum_{r=1}^{n_G} \sum_{s=1}^{n_G} \bar{w}_r \bar{w}_s N_3(\xi_{1r}, \xi_{2s}) f_{vx2}^e(\xi_{1r}, \xi_{2s}) \det(\underline{J}_e(\xi_{1r}, \xi_{2s})) \\ \alpha_{vx1}^e(t) \sum_{r=1}^{n_G} \sum_{s=1}^{n_G} \bar{w}_r \bar{w}_s N_4(\xi_{1r}, \xi_{2s}) f_{vx1}^e(\xi_{1r}, \xi_{2s}) \det(\underline{J}_e(\xi_{1r}, \xi_{2s})) \\ \alpha_{vx2}^e(t) \sum_{r=1}^{n_G} \sum_{s=1}^{n_G} \bar{w}_r \bar{w}_s N_4(\xi_{1r}, \xi_{2s}) f_{vx2}^e(\xi_{1r}, \xi_{2s}) \det(\underline{J}_e(\xi_{1r}, \xi_{2s})) \end{Bmatrix} \quad (10.4.37)$$

10.4.4 Edge Loads

Finally, consider the case of a time-varying, spatially uniform load acting on edge 1–2 of the 4-node, quadrilateral, isoparametric element shown in Figure 10.4.3. This may occur for example when a deformable object is subjected to a time-varying acoustic or fluid pressure-induced surface load. The natural coordinate ξ_2 has the value (-1) on edge 1–2. Therefore on this edge, the shape functions in (10.4.2) become

$$N_1 = \frac{1}{2}(1 - \xi_1), \quad N_2 = \frac{1}{2}(1 + \xi_1), \quad N_3 = N_4 = 0 \quad (10.4.38)$$

and the coordinate mapping Equations (10.4.4), (10.4.5) become

$$x_1 = \frac{1}{2}(1 - \xi_1)x_{11}^e + \frac{1}{2}(1 + \xi_1)x_{12}^e, \quad x_2 = \frac{1}{2}(1 - \xi_1)x_{21}^e + \frac{1}{2}(1 + \xi_1)x_{22}^e \quad (10.4.39)$$

The differential surface area along edge 1–2 is

$$d\Gamma_{12}^e = \hat{t}^e dl_{12} = \hat{t}^e \sqrt{dx_1^2 + dx_2^2} = \hat{t}^e \sqrt{\left(\frac{dx_1}{d\xi_1}\right)^2 + \left(\frac{dx_2}{d\xi_1}\right)^2} d\xi_1 \quad (10.4.40)$$

Substitution of (10.4.39) into (10.4.40) yields

$$d\Gamma_{12}^e = \frac{\hat{t}^e}{2} \sqrt{(x_{12}^e - x_{11}^e)^2 + (x_{22}^e - x_{21}^e)^2} d\xi_1 = \frac{\hat{t}^e}{2} l_{12}^e d\xi_1 \quad (10.4.41)$$

where l_{12}^e is the length of edge 1–2. Substitute (10.4.38) and (10.4.41) and the time-varying, spatially uniform surface load vector,

$$\underline{F}_\Gamma = \begin{Bmatrix} F_{\Gamma x1}^e \\ F_{\Gamma x2}^e \end{Bmatrix} = \begin{Bmatrix} \bar{f}_{\Gamma x1}^e \alpha_{\Gamma x1}^e(t) \\ \bar{f}_{\Gamma x2}^e \alpha_{\Gamma x2}^e(t) \end{Bmatrix} \quad (10.4.42)$$

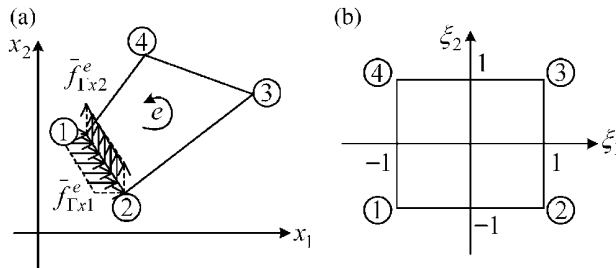


Figure 10.4.3 Uniform loads on edge 1–2 of 4-node isoparametric element. (a) actual coordinates and (b) natural coordinates

into the general expression for the element force vector (10.4.32) to obtain

$$f_{\Gamma_{12}}^e(t) = \frac{\hat{l}_{12}^e}{2} \begin{Bmatrix} \alpha_{\Gamma_{x1}}^e(t) \bar{f}_{\Gamma_{x1}}^e \int_{-1}^1 N_1 d\xi \\ \alpha_{\Gamma_{x2}}^e(t) \bar{f}_{\Gamma_{x2}}^e \int_{-1}^1 N_1 d\xi \\ \alpha_{\Gamma_{x1}}^e(t) \bar{f}_{\Gamma_{x1}}^e \int_{-1}^1 N_2 d\xi \\ \alpha_{\Gamma_{x2}}^e(t) \bar{f}_{\Gamma_{x2}}^e \int_{-1}^1 N_2 d\xi \\ \alpha_{\Gamma_{x1}}^e(t) \bar{f}_{\Gamma_{x1}}^e \int_{-1}^1 N_3 d\xi \\ \alpha_{\Gamma_{x2}}^e(t) \bar{f}_{\Gamma_{x2}}^e \int_{-1}^1 N_3 d\xi \\ \alpha_{\Gamma_{x1}}^e(t) \bar{f}_{\Gamma_{x1}}^e \int_{-1}^1 N_4 d\xi \\ \alpha_{\Gamma_{x2}}^e(t) \bar{f}_{\Gamma_{x2}}^e \int_{-1}^1 N_4 d\xi \end{Bmatrix} = \begin{Bmatrix} \frac{\alpha_{\Gamma_{x1}}^e(t) f_{\Gamma_{x1}}^{eT}}{2} \\ \frac{\alpha_{\Gamma_{x2}}^e(t) f_{\Gamma_{x2}}^{eT}}{2} \\ \frac{\alpha_{\Gamma_{x1}}^e(t) f_{\Gamma_{x1}}^{eT}}{2} \\ \frac{\alpha_{\Gamma_{x2}}^e(t) f_{\Gamma_{x2}}^{eT}}{2} \\ 0 \\ 0 \\ 0 \\ 0 \end{Bmatrix} \quad (10.4.43)$$

where

$$f_{\Gamma_{x1}}^{eT} = \bar{f}_{\Gamma_{x1}}^e \hat{l}_{12}^e, \quad f_{\Gamma_{x2}}^{eT} = \bar{f}_{\Gamma_{x2}}^e \hat{l}_{12}^e \quad (10.4.44)$$

are the resultant forces of the uniform load distributions in the x_1 and x_2 directions on edge 1–2.

10.5 ASSEMBLY PROCEDURE FOR 2D, 4-NODE, QUADRILATERAL ELEMENTS

The preceding section showed how the element force vector and element mass and stiffness matrices may be evaluated in a numerical integration form that is conducive to programming. These terms must be assembled to form counterparts for the entire system, thereby providing a system mathematical model for obtaining the response of the system to initial conditions, periodic loading, or transient loading. This section explains the detailed assembly procedure needed to obtain the system matrices from the element matrices. Figure 10.4.1 shows a generic meshed cross-sectional area with N_n nodes. The system degrees of freedom (dofs) are ordered according to the convention

$$\begin{aligned} \text{Global (system) node } i, \quad x_1 \text{ direction,} \quad \text{system dof: } u_{2*(i-1)+1} \\ \text{Global (system) node } i, \quad x_2 \text{ direction,} \quad \text{system dof: } u_{2*(i-1)+2} \end{aligned} \quad (10.5.1)$$

which is also illustrated in Table 10.5.1.

The system has a combination of constrained (fixed) and free degrees of freedom. ‘‘Global free’’ is utilized to describe the system that is free from constraints. The total number of dofs in the global-free system is

Table 10.5.1 System degree of freedom ordering convention

System node number	Direction: plane stress/strain	System dof number
1	x_1	1
1	x_2	2
2	x_1	3
2	x_2	4
\vdots	\vdots	\vdots
N_n	x_1	$2 * (N_n - 1) + 1$
N_n	x_2	$2 * (N_n - 1) + 2$

Table 10.5.2 Plane stress/strain element local dof ordering convention

Local dof (m)	Local node	Direction
1	1	x_1
2	1	x_2
3	2	x_1
4	2	x_2
5	3	x_1
6	3	x_2
7	4	x_1
8	4	x_2

$$N_d = N_n(\text{number of nodes in the model}) * 2 \text{ dofs/node} = 2N_n \quad (10.5.2)$$

The nodal connectivity array is defined by

$$B_{ej} = ICON(e, j) = \text{global node number for local node } j \text{ of element } e, \quad (10.5.3)$$

for $j = 1, 2, 3, 4$, and $e = 1, \dots, N_e$

where N_e is the total number of elements in the model. The local nodes are ordered CCW starting at any of the 4 nodes in the element as shown in Figure 10.4.2. Table 10.5.2 shows the ordering of the 8 local degrees of freedom (dofs) in the element displacement vector \underline{q}_e as defined in (10.4.20) and (10.4.21).

A dof connectivity array may be defined similar to the nodal connectivity array in (10.5.3) as

$$\hat{B}_{em} = ICONDOF(e, m) = \text{system dof number for local dof number } m \quad (10.5.4)$$

of element e , for $m = 1, 2, \dots, 8$, and $e = 1, \dots, N_e$

The conventions for global dof numbering (10.5.1) and element dof numbering (Table 10.5.2) provide an easily programmable means to generate the dof connectivities from the nodal connectivities as follows:

$$\hat{B}_{em} = ICONDOF(e, m) = 2 * (ICON(e, j) - 1) + k \quad (10.5.5)$$

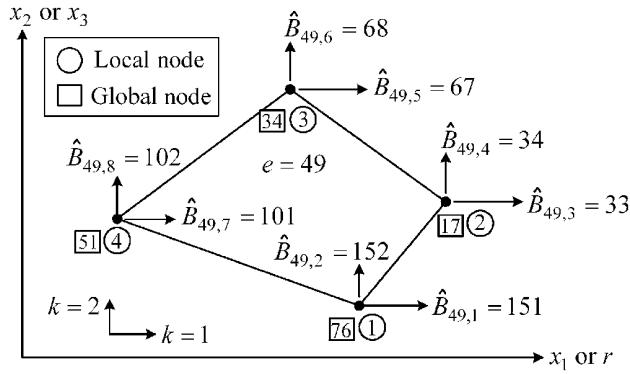


Figure 10.5.1 System degrees of freedom for a typical 2D element (element number $e = 49$)

Table 10.5.3 System dofs for the 2D, 4-node, quadrilateral element in Figure 10.5.1

Element (e)	Local node (j)	x_k direction index (k)	Local dof $m = 2*(j-1) + k$	Global node number $ICON(e, j) B_{ej}$	Global dof number $\hat{B}_{em} = 2*(ICON(e, j) - 1) + k$
49	1	1	1	76	151
49	1	2	2	76	152
49	2	1	3	17	33
49	2	2	4	17	34
49	3	1	5	34	67
49	3	2	6	34	68
49	4	1	7	51	101
49	4	2	8	51	102

where

$$\begin{aligned}
 k &= 1, 2 && \text{(direction index } x_1, x_2) \\
 j &= 1, 2, 3, 4 && \text{(local node index)} \\
 m &= 2*(j-1) + k && \text{(local dof index)}
 \end{aligned} \tag{10.5.6}$$

Figure 10.5.1 and Table 10.5.3 provide an example illustrating how the dof connectivity array is formed for a typical element.

Completion of the model requires explicitly imposing the displacement constraints (zero-displacement degrees of freedom). The $larray$ is defined for this purpose in an identical manner as with the beam element model in (9.2.83).

Assembly of the mass and stiffness matrices also follows the same procedure as for the beam element (Figure 9.2.6) and is illustrated in Figure 10.5.2. Similar to (4.8.98), repeat the Figure 10.5.2 “assembly” step for all N_e elements in the model and for all 8 local degrees of freedom, that is,

$$e = 1, 2, \dots, E, \quad r = 1, \dots, 8, \quad s = 1, \dots, 8 \tag{10.5.7}$$

The element matrices and force vectors (\underline{K}^e , \underline{M}^e , \underline{f}^e) in Figure 10.5.2 are obtained from

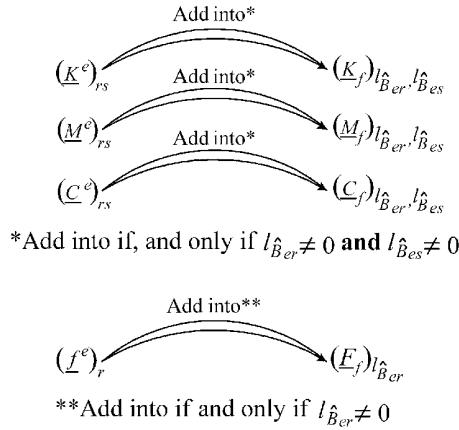


Figure 10.5.2 Assembly of constraint condensed system matrices and force vector from element matrices and force vector

Plane Stress/Plane Strain: Element Stiffness Matrix: Equation (10.4.27)

$$\underline{K}^e \approx \hat{i}^e \sum_{s=1}^{n_G} \sum_{t=1}^{n_G} \bar{w}_s \bar{w}_t \underline{B}_e^T(\xi_{1s}, \xi_{2t}) \underline{E}_e \underline{B}_e(\xi_{1s}, \xi_{2t}) \det(\underline{J}_e(\xi_{1s}, \xi_{2t})) \quad (10.5.8)$$

where from (10.4.19) through (10.4.23),

$$\underline{B}_e(\xi_1, \xi_2) = \underline{A}_1^e(\xi_1, \xi_2) \underline{A}_2^e(\xi_1, \xi_2) \quad (10.5.9)$$

Plane Stress/Plane Strain: Element Mass Matrix: Equation (10.4.31)

$$\underline{M}^e \approx \hat{i}^e \sum_{s=1}^{n_G} \sum_{t=1}^{n_G} \bar{w}_s \bar{w}_t \rho(\xi_{1s}, \xi_{2t}) \underline{N}^T(\xi_{1s}, \xi_{2t}) \underline{N}(\xi_{1s}, \xi_{2t}) \det(\underline{J}_e(\xi_{1s}, \xi_{2t})) \quad (10.5.10)$$

Plane Stress/Strain: Element Force Vectors: See Equations (10.4.33), (10.4.37), (10.4.43)

Similar to the case of a 1D bar finite element in (4.8.36), imposing the zero-displacement constraint conditions yields the following “condensed” dynamic equilibrium equation for the “free” (unconstrained) degrees of freedom \underline{q}_f of the constrained structure.

$$\frac{\underline{M}_f}{N_f \times N_f} \frac{\dot{\underline{q}}_f}{N_f \times 1} + \frac{\underline{C}_f}{N_f \times N_f} \frac{\dot{\underline{q}}_f}{N_f \times 1} + \frac{\underline{K}_f}{N_f \times N_f} \frac{\underline{q}_f}{N_f \times 1} = \frac{\underline{F}_f}{N_f \times 1} \quad (10.5.11)$$

Equation (10.5.11) is solved for all of the nonfixed (free) dofs in the system, which comprise the \underline{q}_f vector. The entire system (fixed plus free dofs) displacement vector \underline{q} may be formed from \underline{q}_f using the *jarray* as was defined (4.8.34). The *jarray* contains the complete system degree of freedom numbers for all degrees of freedom which appear in the displacement vector \underline{q}_f of free degrees of freedom. Let

$$i_{pdl} = l\text{th fixed dof number for } l = 1, \dots, N_{pd} \quad (10.5.12)$$

Then the *jarray* is defined as follows:

$I = 0$

for $i = 1, N_d$ ← (total no. of dofs)

$flag = 0$

for $l = 1, N_{pd}$ ← (no. of fixed dofs)

if $i = i_{pdl}$

$flag = 1$ (indicates that this dof is a fixed dof)

end

end

if $flag = 0$

$I = I + 1$

$jarray(I) = i$

end

end

$N_{npd} = I$ ← no. of free (non-prescribed) dofs (10.5.13)

The entire system (fixed plus free dofs) displacement vector \underline{q} may then be formed utilizing the *jarray* from \underline{q}_f as

for $l = 1, N_{pd}$ (no. of fixed dofs)

$k = i_{pdl}$

$q_k = 0$ (set prescribed displacements equal to zero in the system displacement vector)

end

for $l = 1, N_{npd}$ (no. of non-fixed dofs)

$k = jarray(l)$

$q_k = (q_f)_l$ (load calculated displacements to the system displacement vector)

end

(10.5.14)

Conversely, the *larray* contains the locations of the full system (fixed plus free) degrees of freedom in the condensed degree of freedom vector \underline{x}_f in increasing order, as illustrated in (4.8.35). All fixed degrees of freedom are assigned the number 0 in the *larray*. The *jarray*(j_i) may be utilized to form the *larray*(l_i) as

for $i = 1, N_d (= 3 * (n + 19) + 1)$ ← (total no. of dofs)

$larray(i) = 0$ initialize array to zero (null)

end

for $I = 1, N_{npd}$

$i_{st} = \text{jarray}(I) \leftarrow$ (from *jarray* coding)

$\text{larray}(i_{st}) = I$

end

(10.5.15)

10.6 COMPUTATION OF STRESSES IN 2D SOLID ELEMENTS

In many cases, vibration studies will include computation and examination of stresses to evaluate the goodness of a design concept. This is illustrated in Figures 1.4.3 and 1.4.8 which shows that machinery or structural members may fail from high-cycle fatigue (HCF) even with stress levels far below the ultimate/tensile strength S_{ut} , while undergoing cyclic stress due to vibrations. Therefore, it is often required to evaluate vibratory stresses at interior locations in the elements and on the surface of the object being modeled. The procedure for achieving this is provided in the following discussion.

10.6.1 Interior Stress Determination

It is generally accepted that the most accurate evaluation of stresses occurs at the GQ points (Table 10.4.1) as discussed by Barlow (1976). Stresses at other points in an element are then interpolated from the GQ point values. The stress in a plane strain model obeys (10.2.11)

$$\underline{\sigma} = \underline{E}_{pe} \underline{\varepsilon} \quad (3 \times 1) \quad (10.6.1)$$

and in a plane stress model (10.3.11),

$$\underline{\sigma} = \underline{E}_{ps} \underline{\varepsilon} \quad (3 \times 1) \quad (10.6.2)$$

where

$$\underline{\sigma} = (\sigma_{11} \quad \sigma_{22} \quad \sigma_{12})^T, \quad \underline{\varepsilon} = (\varepsilon_{11} \quad \varepsilon_{22} \quad 2\varepsilon_{12})^T$$

$$\underline{E}_{pe} = \frac{E}{(1+\nu)(1-2\nu)} \begin{bmatrix} 1-\nu & \nu & 0 \\ \nu & 1-\nu & 0 \\ 0 & 0 & \frac{1-2\nu}{2} \end{bmatrix}, \quad \underline{E}_{ps} = \frac{E}{1-\nu^2} \begin{bmatrix} 1 & \nu & 0 \\ \nu & 1 & 0 \\ 0 & 0 & \frac{1-\nu}{2} \end{bmatrix} \quad (10.6.3)$$

Let \underline{E} represent either \underline{E}_{pe} or \underline{E}_{ps} , and then by (10.6.1), (10.6.2), (10.4.10), and (10.4.23),

$$\underline{\sigma}^e = \underline{E}^e \underline{\varepsilon}^e = \underline{E}^e \underline{B}^e \underline{q}^e = \underline{E}^e \underline{A}_1^e \underline{A}_2^e \underline{q}^e \quad (10.6.4)$$

3×1 3×3 3×1 3×3 3×8 8×1 3×3 3×4 4×8 8×1

So that the stress at any integration point pair (ξ_{1i}, ξ_{2k}) is obtained from

$$\underline{\sigma}(\xi_{1i}, \xi_{2k}, t) = \underline{E}^e \underline{A}_1^e(\xi_{1i}, \xi_{2k}) \underline{A}_2^e(\xi_{1i}, \xi_{2k}) \underline{q}^e(t) \quad (10.6.5)$$

3×1 3×3 3×4 4×8 8×1

The displacements in the element displacement vector $\underline{q}^e(t)$ (10.4.7) are obtained from the total system displacement vector $\underline{q}(t)$ that results from solving (10.5.11) and using (10.5.14).

The system dofs corresponding to the local dofs in $\underline{q}^e(t)$ are obtained from the dof connectivity array \hat{B}_{em} (10.5.4). Therefore,

$$\left(\underline{q}^e(t)\right)_m = \left(\underline{q}(t)\right)_{\hat{B}_{em}} \quad \text{for } m = 1, \dots, 8 \quad (10.6.6a)$$

alternatively,

$$\left(\underline{q}^e\right)_m = \begin{cases} \left(\underline{q}_f\right)_{l_{\hat{B}_{em}}}, & l_{\hat{B}_{em}} \neq 0 \\ 0, & l_{\hat{B}_{em}} = 0 \end{cases}, \quad m = 1, \dots, 8 \quad (10.6.6b)$$

Summary of Steps to Obtain Stresses at Gauss Quadrature Point Locations (ξ_{1i}, ξ_{2k}) within any Element “e”

- (a) Solve for $\underline{q}(t)$ from (10.5.11) and (10.5.14) at some time t . This solution may correspond to free (Chapter 5), transient forced (Chapter 6), or steady-state harmonic forced (Chapter 7) vibrations.
- (b) Obtain the element “e” nodal displacement vector $\underline{q}_e(t)$ from (10.6.6a) and (10.6.6b).
- (c) Evaluate the shape functions $N_l(\xi_1, \xi_2)$ and their derivatives $\partial N_l / \partial \xi_1$ and $\partial N_l / \partial \xi_2$ from (10.5.2) for $l = 1, 2, 3, 4$ at the integration point locations $(\xi_{1i}, \xi_{2k}) = (\xi_{1i}, \xi_{2k})$ in Table 10.4.1.
- (d) Compute the locations of the integration point pairs (ξ_{1i}, ξ_{2k}) in the actual physical coordinates (10.4.4),

$$x_1 = \sum_{l=1}^4 N_l(\xi_{1i}, \xi_{2k}) x_{1l}^e, \quad x_2 = \sum_{l=1}^4 N_l(\xi_{1i}, \xi_{2k}) x_{2l}^e \quad (10.6.7)$$

- (e) Compute the Jacobian matrix \underline{J}_e at ξ_{1i}, ξ_{2k} via (10.4.15).
- (f) Form the \underline{A}_1^e and \underline{A}_2^e matrices at (ξ_{1i}, ξ_{2k}) via Equations (10.4.19)–(10.4.21), respectively.
- (g) Compute the \underline{B}^e matrix (10.4.23),

$$\underline{B}^e = \underline{A}_1^e \underline{A}_2^e \quad (10.6.8)$$

- (h) Compute the strains at (ξ_{1i}, ξ_{2k}) via (10.4.22), (10.4.23), and (10.6.8),

$$\underline{\epsilon}^e(\xi_{1i}, \xi_{2k}, t) = \underline{B}^e(\xi_{1i}, \xi_{2k}) \underline{q}^e(t) \quad (10.6.9)$$

- (i) Compute the stresses at (ξ_{1i}, ξ_{2k}) at the given time t by (10.6.4)

$$\underline{\sigma}^e(\xi_{1i}, \xi_{2k}, t) = \underline{E}^e \underline{\epsilon}^e(\xi_{1i}, \xi_{2k}, t) \quad (10.6.10)$$

- (j) Repeat steps (b)–(h) for all integration points in element “e.” Interpolate stresses within element “e” given all integration point stresses $\underline{\sigma}^e(\xi_{1i}, \xi_{2k})$ and their physical coordinate locations $\{x_1^e(\xi_{1i}, \xi_{2k}), x_2^e(\xi_{1i}, \xi_{2k})\}$, in element “e.”
- (k) Determine fatigue life utilizing computed stresses and the methods of Section 1.4

10.6.2 Surface Stresses

Maximum stresses often occur on the surface of a vibrating member and are those that are most likely to cause failure in a machine or structure. Surface stresses may be obtained by extrapolating integration point stresses to the surface or by directly considering strains and equilibrium on the surface. The former approach was explained above and the latter approach is explained below.

Consider the plane stress/strain model shown in Figure 10.6.1. Suppose that element (e) has its edge 1–2 on the surface of the member. A surface–tangent coordinate system is defined for edge 1–2 with unit vectors \hat{e}_1 and \hat{e}_2 . The global coordinate (\hat{e}_1, \hat{e}_2) and surface–tangent coordinate (\hat{e}_1, \hat{e}_2) unit vectors are related by

$$\hat{e}_2 = \bar{e}_{12} \hat{e}_1 + \bar{e}_{22} \hat{e}_2 = \frac{x_{1,2}^e - x_{1,1}^e}{l_{12}^e} \hat{e}_1 + \frac{x_{2,2}^e - x_{2,1}^e}{l_{12}^e} \hat{e}_2 \quad (10.6.11)$$

The vector cross product of two vectors is perpendicular to the two vectors. Therefore,

$$\hat{e}_1 = \bar{e}_{11} \hat{e}_1 + \bar{e}_{21} \hat{e}_2 = -\hat{e}_3 \times \hat{e}_2 = \frac{x_{2,2}^e - x_{2,1}^e}{l_{12}^e} \hat{e}_1 - \frac{x_{1,2}^e - x_{1,1}^e}{l_{12}^e} \hat{e}_2 \quad (10.6.12)$$

Clearly, \hat{e}_1 and \hat{e}_2 are perpendicular since from (10.6.11) and (10.6.12),

$$\hat{e}_1 \cdot \hat{e}_2 = 0 \quad (10.6.13)$$

The nodal displacements at local node k may be expressed in the (\hat{e}_1, \hat{e}_2) coordinate system as (2.7.1)

$$\begin{Bmatrix} \bar{u}_{1,k}^e \\ \bar{u}_{2,k}^e \end{Bmatrix} = \begin{bmatrix} \cos \theta^e & \sin \theta^e \\ -\sin \theta^e & \cos \theta^e \end{bmatrix} \begin{Bmatrix} u_{1,k}^e \\ u_{2,k}^e \end{Bmatrix} = \begin{bmatrix} \bar{e}_{11} & \bar{e}_{21} \\ -\bar{e}_{21} & \bar{e}_{11} \end{bmatrix} \begin{Bmatrix} u_{1,k}^e \\ u_{2,k}^e \end{Bmatrix} \quad (10.6.14)$$

where

$\bar{u}_{j,k}^e$ = displacement in the surface coordinate direction \hat{e}_j at local node k of element e

$u_{j,k}^e$ = displacement in the physical coordinate direction \hat{e}_j at local node k of element e

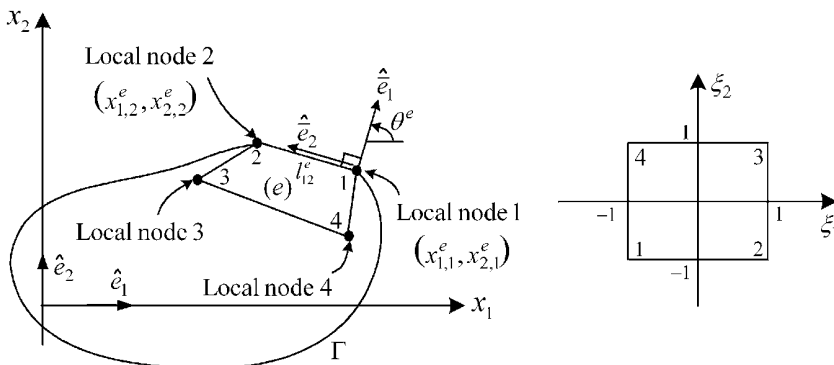


Figure 10.6.1 Geometry for determining surface stresses on edge 1–2 of element “ e ”

$$j=1, 2, \quad k=1, 2 \quad (10.6.15)$$

Edge 1–2 of element e is assumed to be subjected to the tractions shown in Figure 10.6.2.

The tractions can be transformed between the surface–tangent and global coordinate systems similar to the displacements in (10.6.14), that is,

$$\begin{Bmatrix} \bar{F}_{\Gamma 1} \\ \bar{F}_{\Gamma 2} \end{Bmatrix} = \begin{bmatrix} \bar{e}_{11} & \bar{e}_{21} \\ -\bar{e}_{21} & \bar{e}_{11} \end{bmatrix} \begin{Bmatrix} F_{\Gamma 1} \\ F_{\Gamma 2} \end{Bmatrix} \quad (10.6.16)$$

The Cauchy boundary formulas relate surface tractions and stresses at the surface according to (Equation A.2.3)

$$\begin{Bmatrix} F_{\Gamma 1} \\ F_{\Gamma 2} \end{Bmatrix} = \begin{bmatrix} n_1^e & 0 & n_2^e \\ 0 & n_2^e & n_1^e \end{bmatrix} \begin{Bmatrix} \sigma_{11} \\ \sigma_{22} \\ \sigma_{12} \end{Bmatrix} \quad (10.6.17)$$

These formulas apply in all coordinate systems so that in surface–tangent coordinates,

$$\begin{Bmatrix} \bar{F}_{\Gamma 1} \\ \bar{F}_{\Gamma 2} \end{Bmatrix} = \begin{bmatrix} \bar{n}_1^e & 0 & \bar{n}_2^e \\ 0 & \bar{n}_2^e & \bar{n}_1^e \end{bmatrix} \begin{Bmatrix} \bar{\sigma}_{11} \\ \bar{\sigma}_{22} \\ \bar{\sigma}_{12} \end{Bmatrix} \quad (10.6.18)$$

where \bar{n}_1^e and \bar{n}_2^e are the components of the unit normal vector to edge 1–2, as expressed in the surface–tangent coordinate system. The tractions and stresses in this coordinate system are shown in Figure 10.6.3.

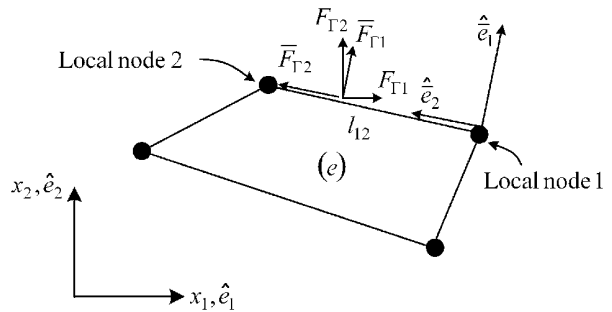


Figure 10.6.2 Tractions on edge 1–2 expressed in the surface–tangent and global coordinate systems

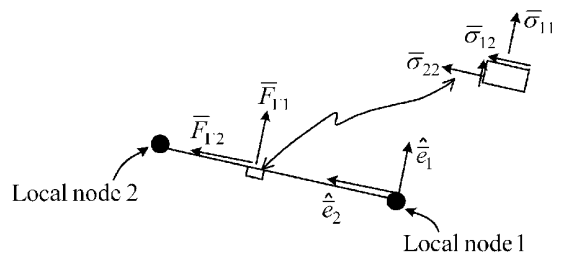


Figure 10.6.3 Tractions and stresses in the surface–tangent coordinate system

The surface–tangent coordinate system’s unit normal vector components are

$$\bar{n}_1^e = 1, \quad \bar{n}_2^e = 0 \quad (10.6.19)$$

Substitute (10.6.19) into (10.6.18) to obtain

$$\bar{\sigma}_{11} = \bar{F}_{\Gamma 1}, \quad \bar{\sigma}_{12} = \bar{F}_{\Gamma 2} \quad (10.6.20)$$

This shows that two of the three stresses in the surface–tangent coordinate system are obtained from the known applied surface tractions. The third is obtained from the surface–tangent coordinate system strains as illustrated below. Figure 10.6.1 shows that ξ_2 equals -1 on edge 1–2, therefore the shape functions (10.4.2) on this edge become

$$N_1 = \frac{1}{2}(1 - \xi_1), \quad N_2 = \frac{1}{2}(1 + \xi_1), \quad N_3 = N_4 = 0 \quad (10.6.21)$$

The \bar{x}_2 coordinate and \bar{u}_2 displacement on this edge may then be expressed with (10.4.1) and (10.4.4) as

$$\begin{aligned} \bar{x}_2 &= \sum_{k=1}^4 N_k \bar{x}_{2,k}^e = \frac{1}{2}(1 - \xi_1) \bar{x}_{2,1}^e + \frac{1}{2}(1 + \xi_1) \bar{x}_{2,2}^e \\ \bar{u}_2 &= \sum_{k=1}^4 N_k \bar{u}_{2,k}^e = \frac{1}{2}(1 - \xi_1) \bar{u}_{2,1}^e + \frac{1}{2}(1 + \xi_1) \bar{u}_{2,2}^e \end{aligned} \quad (10.6.22)$$

where from Figure 10.6.4,

$$\bar{x}_{2,1}^e = 0, \quad \bar{x}_{2,2}^e = l_{12}^e \quad (10.6.23)$$

Substitution of (10.6.23) in (10.6.22) yields

$$\bar{x}_2 = \frac{1}{2}(1 + \xi_1) l_{12}^e \quad (10.6.24)$$

Figure 10.6.4 shows that

$$\bar{x}_1 = 0 \quad (10.6.25)$$

on edge 1–2, therefore

$$\frac{\partial \bar{x}_1}{\partial \xi_1} = 0 \quad \text{on edge 1–2} \quad (10.6.26)$$

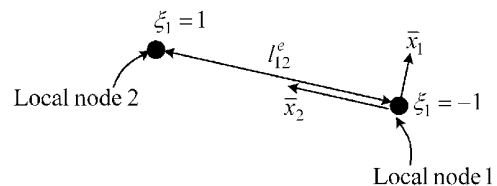


Figure 10.6.4 Interpolations of \bar{x}_2 on edge 1–2

Utilize (10.6.24) and the chain rule of differentiation to obtain

$$\frac{\partial}{\partial \xi_1} = \frac{\partial \bar{x}_1}{\partial \xi_1} \frac{\partial}{\partial \bar{x}_1} + \frac{\partial \bar{x}_2}{\partial \xi_1} \frac{\partial}{\partial \bar{x}_2} = 0 + \frac{l_{12}^e}{2} \frac{\partial}{\partial \bar{x}_2} \quad (10.6.27)$$

to obtain the 2-dimensional “surface” Jacobian expression

$$\frac{\partial}{\partial \bar{x}_2} = \frac{2}{l_{12}^e} \frac{\partial}{\partial \xi_1} \quad (10.6.28)$$

Apply (10.6.28) to obtain the strain $\bar{\epsilon}_{22}$ in the surface–tangent coordinate system as

$$\bar{\epsilon}_{22} = \frac{\partial \bar{u}_2}{\partial \bar{x}_2} = \frac{2}{l_{12}^e} \frac{\partial \bar{u}_2}{\partial \xi_1} \quad (10.6.29)$$

Substitute (10.6.22) into (10.6.29) to obtain

$$\bar{\epsilon}_{22} = \frac{2}{l_{12}^e} \left(-\frac{\bar{u}_{2,1}^e}{2} + \frac{\bar{u}_{2,2}^e}{2} \right) = \frac{1}{l_{12}^e} (\bar{u}_{2,2}^e - \bar{u}_{2,1}^e) \quad (10.6.30)$$

The third surface stress $\bar{\sigma}_{22}$ is obtained by substituting the strain in (10.6.30) into the isotropic, plane stress/strain material law (10.2.10) or (10.3.10), which when expressed in the surface–tangent coordinate system becomes

$$\begin{Bmatrix} \bar{\sigma}_{11} \\ \bar{\sigma}_{22} \\ \bar{\sigma}_{12} \end{Bmatrix} = \frac{E}{(1+\nu)e_2} \begin{bmatrix} e_1 & \nu & 0 \\ \nu & e_1 & 0 \\ 0 & 0 & e_3 \end{bmatrix} \begin{Bmatrix} \bar{\epsilon}_{11} \\ \bar{\epsilon}_{22} \\ 2\bar{\epsilon}_{12} \end{Bmatrix} \quad (10.6.31)$$

The terms e_j are defined for plane strain in (10.2.10) and for plane stress in (10.3.10). The first two equations in (10.6.31) are

$$\bar{\sigma}_{11} = \frac{E}{(1+\nu)e_2} (e_1 \bar{\epsilon}_{11} + \nu \bar{\epsilon}_{22}) \quad (10.6.32)$$

and

$$\bar{\sigma}_{22} = \frac{E}{(1+\nu)e_2} (\nu \bar{\epsilon}_{11} + e_1 \bar{\epsilon}_{22}) \quad (10.6.33)$$

Solving these equations for $\bar{\epsilon}_{11}$ yields

$$\bar{\epsilon}_{11} = \left[\frac{(1+\nu)e_2}{E} \bar{\sigma}_{11} - \nu \bar{\epsilon}_{22} \right] \frac{1}{e_1} \quad (10.6.34)$$

Substitution of (10.6.34) into (10.6.32) yields

$$\begin{aligned} \bar{\sigma}_{22} &= \frac{E}{(1+\nu)e_2} \left[\frac{\nu(1+\nu)e_2}{e_1 E} \bar{\sigma}_{11} - \frac{\nu^2}{e_1} \bar{\epsilon}_{22} \right] + \frac{Ee_1}{(1+\nu)e_2} \bar{\epsilon}_{22} \\ &= \frac{E}{(1+\nu)e_2} \bar{\epsilon}_{22} \left(-\frac{\nu^2}{e_1} + e_1 \right) + \frac{\nu}{e_1} \bar{\sigma}_{11} \end{aligned} \quad (10.6.35)$$

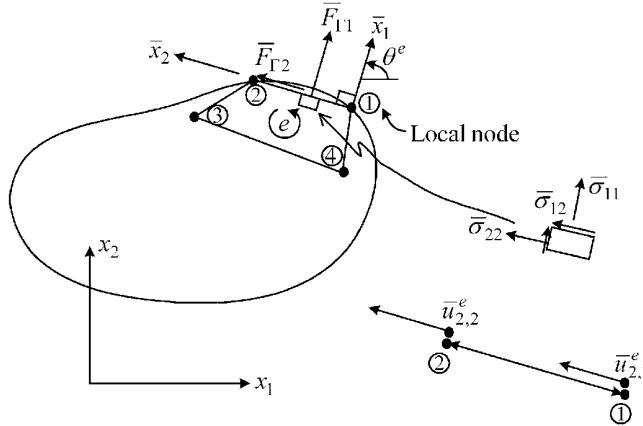


Figure 10.6.5 Plane stress/plane strain surface stress summary diagram

Finally, substitution of (10.6.20) and (10.6.30) into (10.6.35) yields the following summary of formulas for the surface stresses illustrated in Figure 10.6.5:

$$\bar{\sigma}_{11} = \bar{F}_{\Gamma 1}, \quad \bar{\sigma}_{12} = \bar{F}_{\Gamma 2}, \quad \bar{\sigma}_{22} = \frac{\nu}{e_1} \bar{F}_{\Gamma 1} + \frac{E}{(1+\nu) e_2} \left(e_1 - \frac{\nu^2}{e_1} \right) \frac{(\bar{u}_{2,2}^e - \bar{u}_{2,1}^e)}{l_{12}^e} \quad (10.6.36)$$

where

e_i	e_1	e_2	e_3
Plane stress	1	$1-\nu$	$\frac{1-\nu}{2}$
Plane strain	$1-\nu$	$1-2\nu$	$\frac{1-2\nu}{2}$

The surface-tangent coordinate displacements in (10.6.36) are obtained from the system coordinate displacements utilizing the transformation in (10.6.14).

10.7 EXTRA SHAPE FUNCTIONS TO IMPROVE ACCURACY

The elements discussed in Section 10.4 work fine for modeling general 2D deformations but may act overly “stiff” for some bending-type problems, thereby requiring a large number of elements to obtain highly accurate results. This “excessively stiff in bending” behavior may be mitigated by using a higher-order (quadratic) element or by adding two additional terms in the interpolation of the displacements (10.4.1):

$$u_i = \sum_{k=1}^4 N_k u_{i,k}^e + \sum_{k=5}^6 N_k u_{i,k}^e \quad (10.7.1)$$

where

$$N_5 = 1 - \xi_2^2, \quad N_6 = 1 - \xi_1^2 \quad (10.7.2)$$

The $k=5$ and $k=6$ displacements are not associated with any particular nodal position and are ultimately condensed out of the element by using a condensation similar with the Guyan reduction procedure discussed in Chapter 8. The extra shape function approach still utilizes only 4 nodes, which simplifies meshing compared with use of 8- or 9-node quadratic elements.

The geometrical mapping from natural to physical coordinates, expressed by (10.4.4), is unaffected by the N_5 and N_6 terms. Thus, the Jacobian matrix (10.4.15) and A_1 matrix (10.4.19) are similarly unaffected. The A_2 matrix in (10.4.20) is altered only by appending columns 9–12:

$$\underline{A}_2^e = \left[\begin{array}{cc|cc} & & \frac{\partial N_5}{\partial \xi_1} & 0 & \frac{\partial N_6}{\partial \xi_1} & 0 \\ & & \frac{\partial N_5}{\partial \xi_2} & 0 & \frac{\partial N_6}{\partial \xi_2} & 0 \\ \underline{A}_2^e & & & & & \\ 4 \times 8 & & & & & \\ \text{from Eq. (10.4.20)} & & & & & \\ \text{and Eq. (10.4.21)} & & 0 & \frac{\partial N_5}{\partial \xi_1} & 0 & \frac{\partial N_6}{\partial \xi_1} \\ & & 0 & \frac{\partial N_5}{\partial \xi_2} & 0 & \frac{\partial N_6}{\partial \xi_2} \end{array} \right] \quad (10.7.3)$$

The \underline{B}^e matrix of (10.4.23) now has the dimensions shown in

$$\underline{B}^e = \underline{A}_1^e \underline{A}_2^e \quad (10.7.4)$$

$$3 \times 12 \quad 3 \times 4 \quad 4 \times 12$$

The element stiffness matrix in (10.4.24) now becomes the 12×12 matrix

$$\underline{K}^e = \hat{t}^e \int_{a^e} (\underline{B}^e)^T \underline{E}^e \underline{B}^e da^e = \begin{bmatrix} \underline{k}_{rr} & \underline{k}_{rc} \\ \underline{k}_{cr} & \underline{k}_{cc} \end{bmatrix} \quad (10.7.5)$$

$$12 \times 12 \quad \int_{a^e} \quad 12 \times 3 \quad 3 \times 3 \times 12 \quad \begin{matrix} 8 \times 8 & 8 \times 4 \\ 4 \times 8 & 4 \times 4 \end{matrix}$$

It is assumed that the extra nodes associated with N_5 and N_6 are not subjected to interelement, external, inertial, or damping forces. This assumption allows the motions of these nodes to be related to motions of nodes 1–4 in terms of the stiffness matrix in (10.7.5) and is shown by considering equilibrium for a single element:

$$\begin{bmatrix} \underline{m}_{rr}^e & \underline{0} \\ \underline{0} & \underline{0} \end{bmatrix} \begin{Bmatrix} \underline{\dot{q}}_r^e \\ \underline{\dot{q}}_c^e \end{Bmatrix} + \begin{bmatrix} \underline{c}_{rr}^e & \underline{0} \\ \underline{0} & \underline{0} \end{bmatrix} \begin{Bmatrix} \underline{\dot{q}}_r^e \\ \underline{\dot{q}}_c^e \end{Bmatrix} + \begin{bmatrix} \underline{k}_{rr}^e & \underline{k}_{rc}^e \\ \underline{k}_{cr}^e & \underline{k}_{cc}^e \end{bmatrix} \begin{Bmatrix} \underline{q}_r^e \\ \underline{q}_c^e \end{Bmatrix} = \begin{Bmatrix} \underline{f}_r^e \\ \underline{0} \end{Bmatrix} \quad (N \times 1) \quad (10.7.6)$$

The bottom row implies

$$\underline{q}_c^e = -(\underline{k}_{cc}^e)^{-1} \underline{k}_{cr}^e \underline{q}_r^e \quad (10.7.7)$$

which is identical to (8.2.9) for Guyan reduction—static condensation. Substitute (10.7.7) into the top row of (10.7.6) to obtain

$$\underline{m}_{rr}^e \underline{\ddot{q}}_r^e + \underline{c}_{rr}^e \underline{\dot{q}}_r^e + \hat{\underline{k}} \underline{q}_r^e = \underline{f}_r^e \quad (10.7.8)$$

where

$$\hat{\underline{k}}^e = \underline{k}_{rr}^e - \underline{k}_{rc} (\underline{k}_{cc}^e)^{-1} \underline{k}_{cr}^e \quad (10.7.9)$$

The dimensions of $\hat{\underline{k}}^e$ are 8×8 , the same as the original 4-node element without extra shape functions. The matrix $\hat{\underline{k}}^e$ is used as the element stiffness matrix \underline{K}_e in the constraint condensed stiffness matrix assembly procedure shown in Figure 10.5.2. The “extra” shape functions N_5 and N_6 are employed only to soften the stiffness in bending and not to change the element mass matrix in (10.4.31) nor the element force vector in (10.4.32). A further discussion of this topic may be found in (Hughes, 1987).

In summary, this section has presented a modification of the bilinear interpolation, quadrilateral element to include quadratic interpolation terms. This is accomplished without increasing the number of nodes or degrees of freedom.

10.8 ILLUSTRATIVE EXAMPLE

EXAMPLE 10.8.1 *Comparison Between 2D Solid and Beam Element Models for a Simply Supported Beam*

Statement: This example utilizes a simply supported beam to illustrate the use of plane strain FE models for natural frequencies and forced response predictions.

Objectives: The objectives of this example include:

- (a) Build a plane strain, 4-node, quadrilateral, isoparametric model of a simply supported beam.
- (b) Determine the natural frequencies, mode shapes, and forced response.
- (c) Repeat (a) and (b) with a Timoshenko beam element model (Section 9.8).
- (d) Compare the results of the Timoshenko beam model with the plane strain model.
- (e) Compare natural frequencies with and without the extra shape functions of Section 10.7.

Assumptions: The assumptions for this example are:

- (a) Small motions, that is, small motion stress–strain and strain–displacement relations (10.2.10), (10.3.10), (10.6.1), and (10.6.2) are valid.
- (b) Motions, loads, and boundary conditions are invariant in the depth (z) directions. All loads are given as per unit depth.

Coding: The MATLAB Code for this example is in Appendix E.

Parameter Values: The Young’s modulus, Poisson’s ratio, weight density, and lengths are

$$E = 2.1 \times 10^{11} \text{ N/m}, \quad \nu = 0.3, \quad \rho g = 7.69 \times 10^4 \text{ N/m}^3, \quad L_1 = 1.0 \text{ m}, \quad L_2 = 0.1 \text{ m} \quad (1)$$

The mass, stiffness, and force all increase linearly with depth for the plane strain structural model, so the depth dimension cancels out of the equilibrium equation (10.5.11)

$$\underline{M}_f \ddot{\underline{q}}_f + \underline{C}_f \dot{\underline{q}}_f + \underline{K}_f \underline{q}_f = \underline{F}_f \quad (2)$$

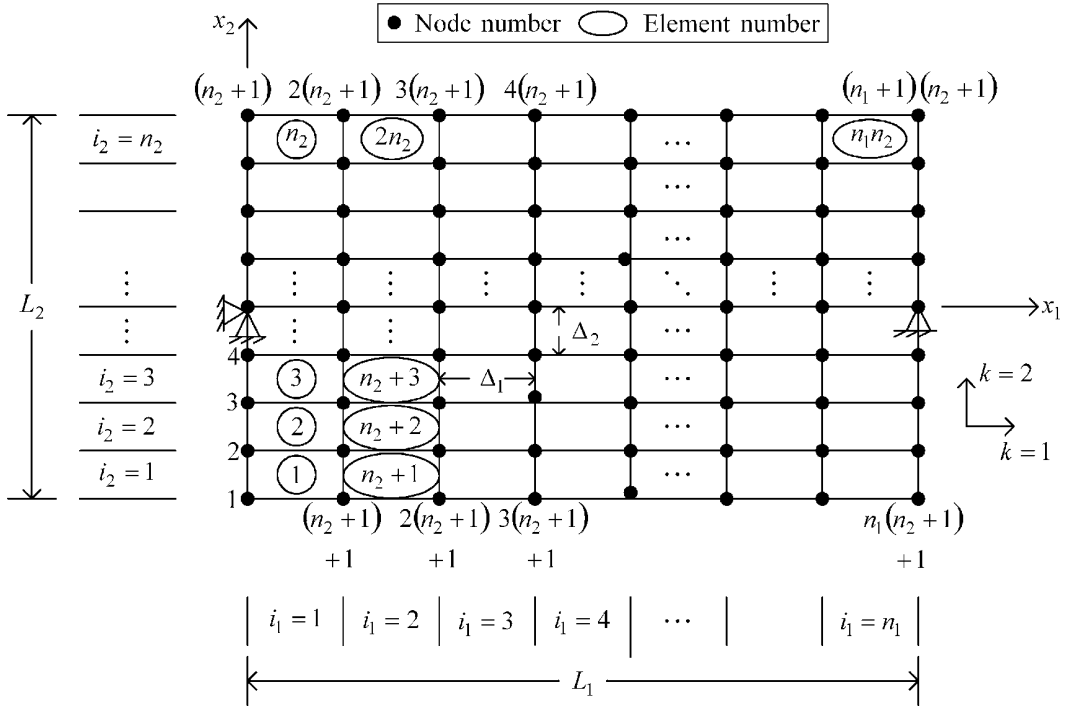


Figure E10.8.1(a) Simply supported beam model with 4-node P_e elements

Model Mesh: The beam model is meshed with the uniformly spaced grid shown in Figure E10.8.1(a). The x_1 and x_2 lengths are divided into n_1 and n_2 sections with lengths

$$\Delta_1 = \frac{L_1}{n_1}, \quad \Delta_2 = \frac{L_2}{n_2} \quad (3)$$

where n_2 must be even to locate the neutral axis at $x_2 = 0$. Any element number or node number may be expressed in terms of the integer indices i_1 and i_2 .

From this figure, the mesh integer parameters are

$$\begin{aligned} N_n &= \text{number of nodes} = (n_1 + 1) * (n_2 + 1), & N_e &= \text{number of elements} = n_1 n_2 \\ N_d &= \text{number of dofs} = 2 * N_n, & N_{pd} &= \text{number of fixed dofs} = 3 \\ N_{npd} &= \text{number of free dofs} = N_d - 3 \end{aligned} \quad (4)$$

Integer Arrays for the Model: The node numbers for an arbitrary element e are shown in Figure E10.8.1(b).

(a) Form the Nodal Connectivity Array

The nodal connectivity array (10.5.3) is evaluated from the following code logic:

$$\begin{aligned} &\text{for } i_1 = 1, n_1 \quad (\text{Horizontal intervals}) \\ &\quad \text{for } i_2 = 1, n_2 \quad (\text{vertical intervals}) \\ &\quad \quad e = i_2 + n_2 * (i_1 - 1) \quad (\text{element number}) \\ &\quad \quad \text{ICON}(e, 1) = i_1 * (n_2 + 1) + i_2 + 1 \quad (\text{element connectivities}) \end{aligned}$$

$$ICON(e,2) = ICON(e,1) - (n_2 + 1)$$

$$ICON(e,3) = ICON(e,2) - 1$$

$$ICON(e,4) = ICON(e,1) - 1$$

end

end

where $ICON(e,j) = B_{ej}$ = element connectivity

= global node number for local node j of element e ,

$$j = 1, \dots, 4, \quad e = 1, \dots, N_e$$

Appendix E has the MATLAB Code for this and all steps in this example.

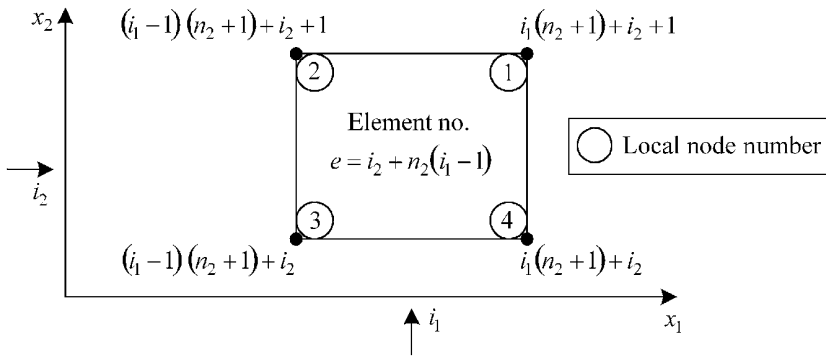


Figure E10.8.1(b) Global node numbers for element e of the simply supported beam model

(b) Form the Degree of Freedom dof Connectivity Array from the Nodal Connectivity Array

The dof connectivity array \hat{B}_{em} (10.5.4) is evaluated from the following code logic:

for $e = 1, N_e$ (elements)

 for $j = 1, 4$ (local nodes)

 for $k = 1, 2$ (direction)

$$l = 2 * (j - 1) + k \quad (\text{local dof number})$$

$$ICONDOF(e,l) = 2 * (ICON(e,j) - 1) + k$$

 end

 end

end

where $ICONDOF(e,l) = \hat{B}_{el}$ = dof connectivity

= global dof number for local dof l of element e , $l = 1 \dots 8$, $e = 1 \dots N_e$

and $k = 1(x_1)$ and $k = 2(x_2)$ directions

(c) Form the $jarray(j_i)$

The requirement that n_2 is even and inspection of Figure E10.8.1(a) shows that the *fixed* dofs for simply supported boundary conditions are

At $(x_1 = x_2 = 0)$:

$$i_{pd1} = \left(\frac{n_2}{2} + 1 - 1\right) * 2 + 1 = n_2 + 1, \quad i_{pd2} = n_2 + 2 \quad (5)$$

At $(x_1 = L_1, x_2 = 0)$:

$$i_{pd3} = 2 * \left[n_1(n_2 + 1) + \frac{n_2}{2} + 1 - 1 \right] + 1 = 2n_1(n_2 + 1) + n_2 + 2 \quad (6)$$

where

$$i_{pdl} = \text{dof number of the } l\text{th fixed dof, } l = 1, \dots, N_{pd}, \quad N_{pd} = 3 = \text{total number of fixed dofs} \quad (7)$$

Recall that the $jarray$ is defined as (4.8.34)

$$j_i = \text{system dof number of the } i\text{th non-fixed dof, where } i = 1, \dots, N_{npd} \quad (8)$$

and

$$\begin{aligned} N_{npd} &= N_d - N_{pd} = \text{total number of non-fixed dofs in the system model} \\ &= 2 * N_n - 3 = 2(n_1 + 1)(n_2 + 1) - 3 \end{aligned} \quad (9)$$

The $jarray$ may be formed with (10.5.13) and (7).

(d) Form the $larray(l_i)$

The $larray(l_i)$ (4.8.35) stores either the position of system dof i in the constraint condensed system or a zero if i is fixed. The $larray(l_i)$ is formed from the $jarray(j_i)$, (4) and (9) as

for $i = 1, N_d \leftarrow$ (total no. of dofs)

$$larray(i) = 0$$

end

for $I = 1, N_{npd}$

$$i_{st} = jarray(I)$$

$$larray(i_{st}) = I$$

end

Nodal Coordinate Arrays: The coordinates of the nodes in Figure E10.8.1(a) are determined from the following code logic:

$$\Delta_1 = \frac{L_1}{n_1}, \quad \Delta_2 = \frac{L_2}{n_2}, \quad nc = 0, \quad p_1 = -\Delta_1, \quad p_2 = -\frac{L_2}{2} - \Delta_2$$

for $i_1 = 1, n_1 + 1$

$$p_1 = p_1 + \Delta_1$$

for $i_2 = 1, n_2 + 1$

$$p_2 = p_2 + \Delta_2$$

$$nc = nc + 1$$

$$x_1(nc) = p_1$$

$$x_2(nc) = p_2$$

end

$$p_2 = -\frac{L_2}{2} - \Delta_2 \quad (10)$$

end

Mass and Stiffness Matrices and Force Vector: The constraint condensed stiffness \underline{K}_f and mass \underline{M}_f matrices are assembled according to Figure 10.5.2. Simulation results are provided for the vertical force shown in Figure E10.8.1(c).

The force is applied at the 1/4 span position on the top surface of the beam. Figure E10.8.1(a) shows that this is at degree of freedom (dof),

$$i_F = \left(\frac{n_1}{4} + 1\right)(n_2 + 1) * 2 \quad (11)$$

which requires that n_1 be a multiple of 4. The corresponding constraint condensed dof is obtained from the *larray* (9.2.83) as l_{i_F} . The global-condensed system force vector therefore has the form

$$\underline{F}_f = \underset{N_f \times 1}{(0 \ 0 \ \dots \ 0 \ \underset{\substack{\uparrow \\ \text{row } l_{i_F}}}{f(t)} \ 0 \ \dots \ 0)^T} \quad (12)$$

2D Beam Model with Rotary Inertia and Shear Deformation Effects: Figure E10.8.1(d) shows the beam finite element model corresponding to the plane strain model in Figure E10.8.1(a).

From (9.8.4), (9.8.5), (9.5.61), (9.5.63), and Table 9.5.2, the properties of element e in this figure include

$$E^e, A^e = L_2 * 1, L^e = \frac{L_1}{n_1}, \rho^e, I_{\bar{x}_3} = \frac{L_y^3}{12} * 1, k_2, G^e, v^e \quad (13)$$

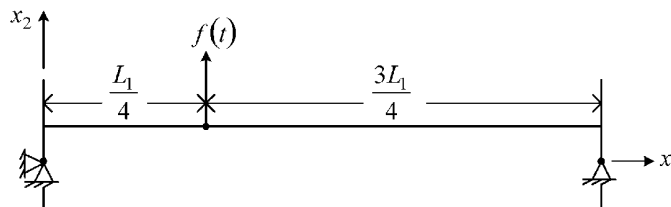


Figure E10.8.1(c) External force $f(t)$ for transient and harmonic response simulation

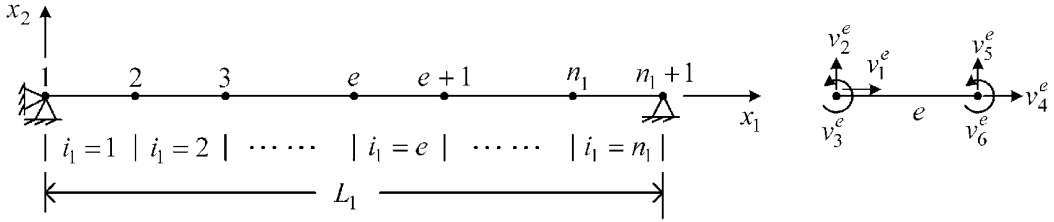


Figure E10.8.1(d) Simply supported beam model with Timoshenko-type beam elements

where L_1 and L_2 are shown in Figure E10.8.1(a), the multiplications by 1 indicate properties per unit depth, and from Figure 9.5.3, the shear form factor formula for a rectangular cross section is

$$k_2 = \frac{10(1+\nu)}{12+11\nu} \quad (14)$$

which is independent of the beam's dimensions. The nodal coordinates, element connectivities, and fixed degrees of freedom for the beam model are

$$x_{1j} = (j-1)\Delta_1, \quad x_{2j} = 0 \quad j = 1, 2, \dots, n_1 + 1 \quad (15)$$

$$ICON(e,1) = e, \quad ICON(e,2) = e + 1 \quad e = 1, 2, \dots, n_1 \quad (16)$$

$$i_{pd1} = 1, \quad i_{pd2} = 2, \quad i_{pd3} = 3n_1 + 2 \quad (17)$$

Natural Frequencies and Mode Shapes: The free vibration matrix equilibrium equation for the undamped, constraint condensed system is given by (2)

$$\underline{M}_f \ddot{\underline{q}}_f + \underline{K}_f \underline{q}_f = \underline{0} \quad (N_{npd} \times 1) \quad (18)$$

Similar to (5.4.3) and (5.4.12), insertion of

$$\underline{q}_f = e^{i\omega t} \underline{\psi}_f \quad (19)$$

into (18) yields

$$\left(-\omega^2 \underline{M}_f + \underline{K}_f \right) \underline{\psi}_f = \underline{0} \quad (20)$$

The natural frequencies and mode shapes of the constraint condensed system are obtained via the MATLAB code in Appendix E. For mode shape plotting purposes, it is convenient to form the entire $\underline{\psi}$ vector, which is the union of the fixed (zero displacement) dof and the calculated free dof ($\underline{\psi}_f$) modal components. This is implemented by utilizing the *jarray* (8) and the fixed dof index array i_{pdI} (7). The coding is

for $l=1, N_{pd}$ ($=3$)

$$k = i_{pdI}$$

$$\left(\underline{\psi} \right)_k = 0 \quad (\text{fixed dof})$$

end

for $l = 1, N_{npd}$

$$k = jarray(l)$$

$$\left(\underline{\psi}\right)_k = \left(\underline{\psi}_f\right)_l$$

end

(21)

The full $\underline{\psi}$ mode shape now contains zeros at fixed dofs and the motions in $\underline{\psi}_f$ at the nonfixed dofs. Figure E10.8.1(e) shows the 6 lowest modes of the plane strain model ($n_1 = 20, n_2 = 6$) utilizing the extra shape functions (N_5, N_6) of Section 10.7, 3rd Order GQ from Table 10.4.1, and the mesh parameters $n_1 = 20$ and $n_2 = 6$. The corresponding results with 4th Order GQ are virtually identical.

Figure E10.8.1(f) shows the 6 lowest modes of the Timoshenko beam model with shear deformation, rotary inertia, and $n_1 = 20$.

The closed form, analytical formulas for the related frequencies f_i are

- Lateral Vibration with Rotary Inertia and Shear Deformation

$$\omega_i^4 \left(\frac{\rho r^2}{kG}\right) - \omega_i^2 \left[1 + \frac{i^2 \pi^2 r^2}{L^2} \left(1 + \frac{E}{kG}\right)\right] + \frac{\alpha^2 \pi^4 i^4}{L^4} = 0 \quad (22)$$

where

$$r^2 = \frac{I}{A}, \quad \alpha^2 = \frac{EI}{\rho A}, \quad f_i = \frac{\omega_i}{2\pi}$$

- f_i^{EB} Euler–Bernoulli: lateral vibration without shear deformation. Without rotary inertia
- f_i^{T} Timoshenko: lateral vibration with shear deformation. Without rotary inertia

$$f_i^{\text{EB}} = \frac{1}{2\pi} \left(\frac{i\pi}{L}\right)^2 \sqrt{\frac{EI}{\rho A}}, \quad f_i^{\text{T}} = \frac{f_i^{\text{EB}}}{\sqrt{1 + \left(\frac{i\pi}{L}\right)^2 \frac{I 2(1+\nu)}{A k}}} \quad (23)$$

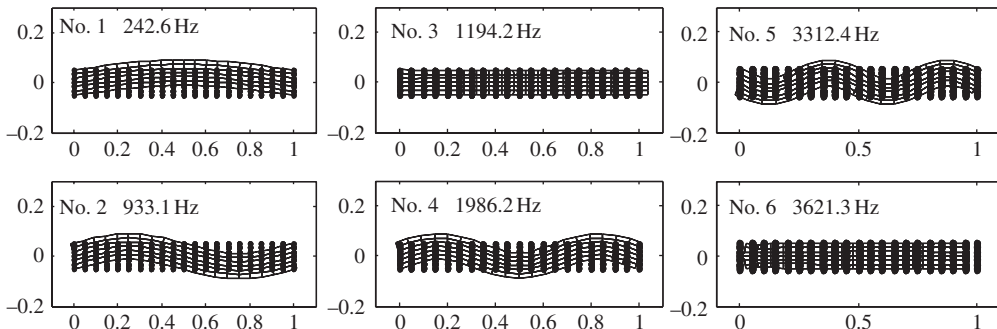


Figure E10.8.1(e) Six lowest modes of plane strain mode ($n_1 = 20, n_2 = 6$)

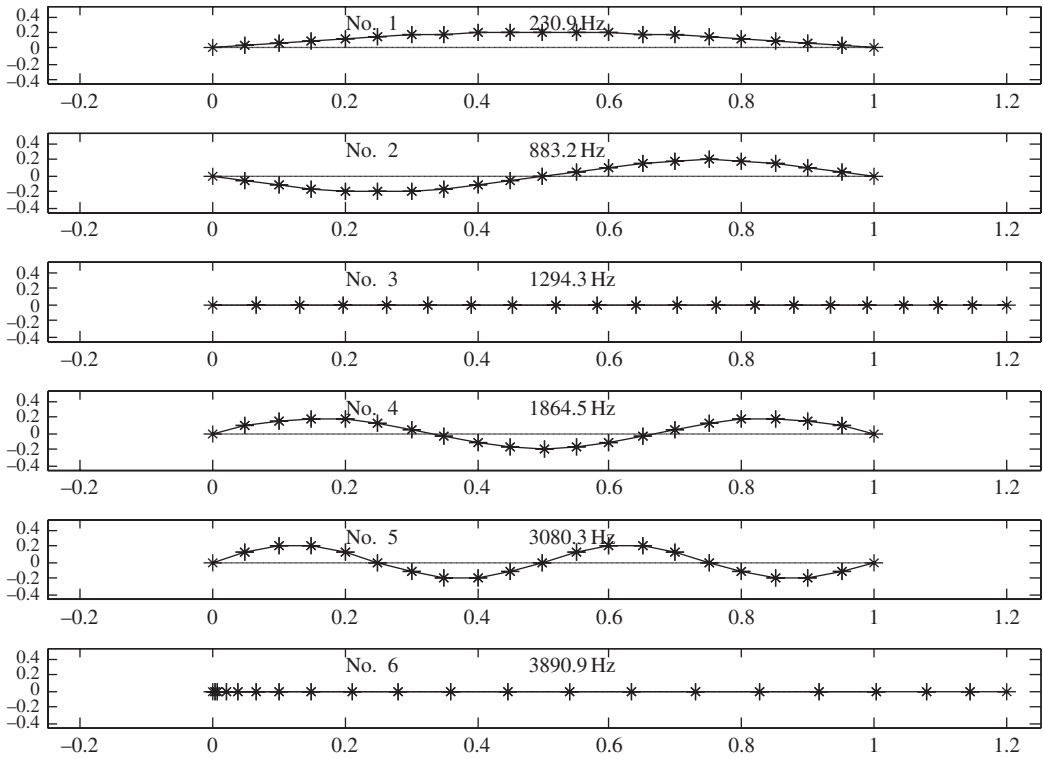


Figure E10.8.1(f) Six lowest modes of the Timoshenko finite element FE beam model

(a) Axial Vibration

$$f_i = \frac{(2i+1)}{4\pi L} \pi * C \quad \text{where } C = \sqrt{\frac{E}{\rho}} \quad \text{and } i=0, 1, 2, \dots \quad (24)$$

The analytical and finite element model results are summarized in Table E10.8.1(a). Considering only the analytical results shows that shear deformation (9.5.5) has a softening effect (A_T frequencies are lower than A_{EB} frequencies), and similarly, rotary inertia lowers the frequencies even further (A_{SRI} vs. A_T frequencies). The finite element results are listed for various mesh density parameter values (n_1 and n_2 in Figure E10.8.1(a)). The results indicate that the natural frequencies are nearly converged with respect to mesh density even with the coarsest mesh densities shown and that increasing mesh density slightly lowers the higher natural frequencies.

As expected, the Timoshenko beam finite element model B results are nearly identical with the analytical model which includes shear deformation and rotary inertia. The plane strain model lateral results are within 5% of the beam and analytical models. The differences result from the assumed boundary conditions on the finite element model and the beam's kinematic deformation assumptions (9.2.1) and (9.5.5). The two axial mode frequencies of the plane strain (extra shape function) model have the following values if all x_1 dof's are constrained at the left end ($x_1=0$):

$$\begin{aligned} (n_1, n_2) = (20, 6) &\Rightarrow (f_1, f_2)_{\text{axial}} = (1357, 4073) \text{ Hz} \\ (n_1, n_2) = (40, 6) &\Rightarrow (f_1, f_2)_{\text{axial}} = (1356, 4065) \text{ Hz} \end{aligned} \quad (25)$$

Table E10.8.1(a) Natural frequency summary for $L_1 = 1.0$ m and $L_2 = 0.1$ m

Analytical A , plane strain PS_i , FE beam B_i	Natural frequencies (Hz)								
	n_1	n_2	Lateral				Axial		
			f_1	f_2	f_3	f_4	f_1	f_2	
A_{Ax}	—	—	—	—	—	—	—	1294	3881
A_{EB}	—	—	235	939	2112	3755	—	—	—
A_T	—	—	232	895	1907	3171	—	—	—
A_{SRI}	—	—	231	883	1862	3067	—	—	—
B_1	20	—	231	883	1864	3080	1294	3891	—
B_2	40	—	231	883	1862	3070	1294	3884	—
PS_1	20	6	253	973	2064	3433	1236	3728	—
PS_2	20	10	253	971	2059	3423	1230	3710	—
PS_3	40	6	245	935	1967	3236	1208	—	—
PS_4	60	8	243	926	1943	3185	1186	—	3597
PS_{ESF1}	20	6	243	933	1986	3312	1194	—	3621
PS_{ESF2}	40	6	242	923	1942	3196	1188	—	3600
PS_{ESF3}	40	10	242	923	1942	3196	1188	—	3600

Subscripts: Ax, axial; EB, Euler–Bernoulli; ESF, include extra shape function (N_5, N_6); SRI, includes shear deformation and rotary inertia effects; T, Timoshenko.

These results are also within 5% of the analytical beam model results which neglects “Poisson contraction” effects. The results (PS_{ESF2} vs. PS_3) also show that the extra shape functions (N_5, N_6) lower the natural frequencies and accelerate convergence.

Damped, Forced Response: The preceding discussion focused on comparison of free vibration characteristics for various modeling approaches. The following results compare plane strain and beam finite element model results for forced dynamic response. A time-varying concentrated force is applied at the quarter-span location as shown in Figure E10.8.1(c). The time history of this force (per meter of depth) is given by

$$f(t) = \begin{cases} 5.0 \times 10^5 * \frac{t}{0.01} \text{ N} & 0 \leq t \leq 0.01 \text{ s} \\ 5.0 \times 10^5 \text{ N} & t > 0.01 \text{ s} \end{cases} \quad (26)$$

The damping model employed is given by (5.4.140), (5.4.142), and (5.4.146) with $m = 6$ prescribed damping ratios, that is, the orthogonal damping matrix is given by

$$\underline{C}_{of} = \mu_1 \underline{K}_f + \underline{M}_f \left(\sum_{l=1}^{m-1} \frac{2\kappa_l \omega_l}{\tilde{m}_l} \underline{\psi}_{fl} \underline{\psi}_{fl}^T \right) \underline{M}_f \quad (27)$$

$$\xi_1^d = \xi_2^d = 0.02, \quad \xi_3^d = \xi_4^d = 0.04, \quad \xi_5^d = \xi_6^d = 0.06, \quad \mu_1 = \frac{2\xi_m^d}{\omega_m}, \quad \text{and} \quad \kappa_l = \xi_l^d - \xi_m^d \frac{\omega_l}{\omega_m} \quad (28)$$

The force is applied at the following degree of freedom (refer to Figures E10.8.1(a) and E10.8.1(d)).

$$i_F = \begin{cases} \left(\frac{n_1}{4} + 1 \right) (n_2 + 1) * 2, & \text{plane strain model} \\ 3 * \frac{n_1}{4} + 2, & \text{beam model} \end{cases} \quad (29)$$

The mesh index n_1 must be a multiple of 4 to locate the force at the quarter-span location, and the constraint condensed force vector $\underline{F}_f(t)$ is given by (12) and (26). The damped dynamic equilibrium equation (2) is integrated with MATLAB's ODE45 numerical integration routine (ref. Example 2.3.1) as shown in Appendix E. The first-order equations integrated with ODE45 are

$$\dot{\underline{q}}_f = \underline{V}_f \quad (N_{\text{npd}} \times 1), \quad \dot{\underline{V}}_f = \underline{M}_f^{-1} \left(\underline{F}_f(t) - \underline{C}_{\text{of}} \underline{V}_f - \underline{K}_f \underline{q}_f \right) \quad (N_{\text{npd}} \times 1) \quad (30)$$

with zero displacement and velocity initial conditions,

$$\underline{q}_f(0) = \underline{V}_f(0) = \underline{0} \quad (31)$$

Figure E10.8.1(g) shows the x_2 displacement on the top surface ($x_2 = L_2/2$) at the quarter, mid, and three-quarter-span locations for the plane strain model with extra shape functions and (i) $n_1 = 20$, $n_2 = 6$, and (ii) $n_1 = 40$, $n_2 = 6$. The responses are seen to be nearly unaffected by increasing the mesh density to $n_1 = 40$, $n_2 = 6$ which confirms that the mesh has converged with respect to the n_1 mesh parameter. The plane strain model's static responses, that is, from (2)

$$\underline{q}_{f\infty} = \underline{K}_f^{-1} \underline{F}_{f\infty} \quad (32)$$

to the steady-state force (5.0×10^5 N) in (26) are 0.317 mm at $L_1/4$, 0.379 mm at $L_1/2$, and 0.24 mm at $3L_1/4$. These agree with the steady-state results in Figure E10.8.1(g).

For comparison, the responses of the beam element model B_1 with $n_1 = 20$ elements, shear deformation, and rotary inertia are shown in Figure E10.8.1(h). These represent responses along the neutral axis of the beam ($x_2 = 0$ in Figure E10.8.1(a)). The plane strain PS_{ESF1} model responses along the neutral axis are shown in the same figure for comparison. The results of the two models are seen to be nearly identical. These examples show very close results between the plane strain model and the beam model, which begs the question, "So why not just use a beam model?" Well for beam-like structures, that is certainly a valid point. However, in engineering applications, many, if not most, structures and structural components do not possess the geometry, loading, or boundary conditions consistent with

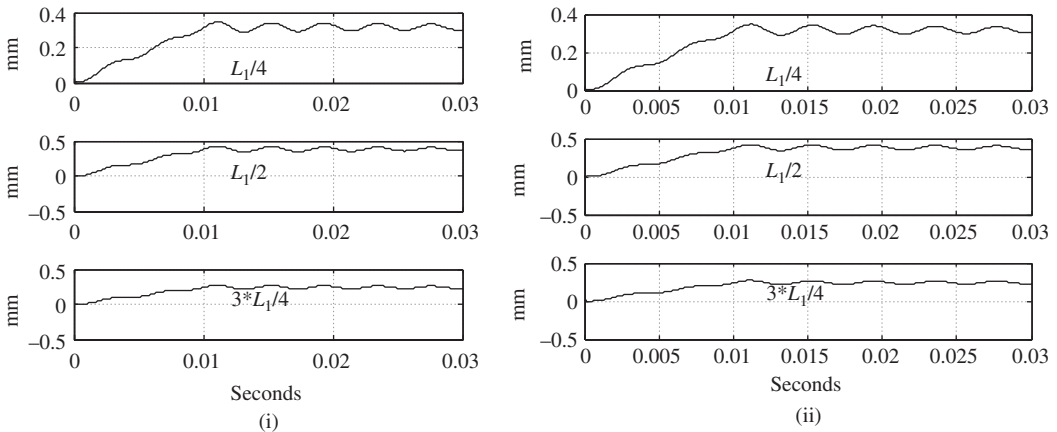


Figure E10.8.1(g) Top surface x_2 direction displacements at x_1 locations indicated for the plane strain model with mesh parameters (i) $n_1 = 20$, $n_2 = 6$, and (ii) $n_1 = 40$, $n_2 = 6$

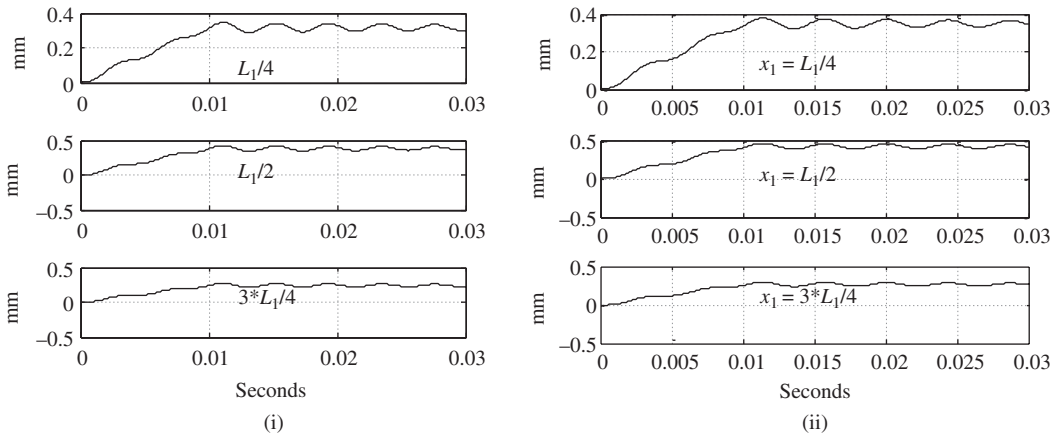


Figure E10.8.1(h) Neutral axis ($x_2=0$) x_2 direction displacements on the x_1 locations indicated for the (i) plane strain model PS_{ESF1} and the (ii) beam model B_1

the beam model's assumptions. In those cases, a more general finite element model such as plane strain or plane stress is required.

10.9 2D AXISYMMETRIC MODEL

An axisymmetric model is used for structures that can be generated by revolving a cross section about the axis of longitudinal symmetry. Typical examples include pipes, vessels, circular ducts, etc. Figure 10.9.1(a) illustrates an example where an internal dynamic pressure $p(t)$ results from vortex shedding within a pipeline due to internal flow past a branch pipe. The dynamic pressure acts uniformly around the pipe creating an axisymmetric dynamic pressure. The pipeline may be clamped to foundation blocks in a manner that constrains the pipe nearly around its entire circumference creating an axisymmetric boundary condition. Thus, the conditions for utilizing an axisymmetric model, namely, axisymmetric geometry, loads, and boundary conditions are satisfied. In practice, some assumptions must be made to justify the use of an axisymmetric, or for that matter, any other finite element modeling approach. The model is useful only for obtaining axisymmetric vibrations, modes, deflections, and stresses. Figure 10.9.1(b) depicts a heat exchanger vessel with internal pressure pulsation, which may be the result of an upstream reciprocating compressor.

10.9.1 Axisymmetric Model Stresses and Strains

Failure of a vibrating machinery component is typically caused by cyclic stresses exceeding the fatigue life of its material. The accurate prediction of the stresses therefore becomes an essential part of the simulation process. Figure 10.9.2 shows a differential volume element and its strains and stresses in a cylindrical coordinate system.

The general strain–displacement relationship in cylindrical coordinates is given by (Fung, 1965) as

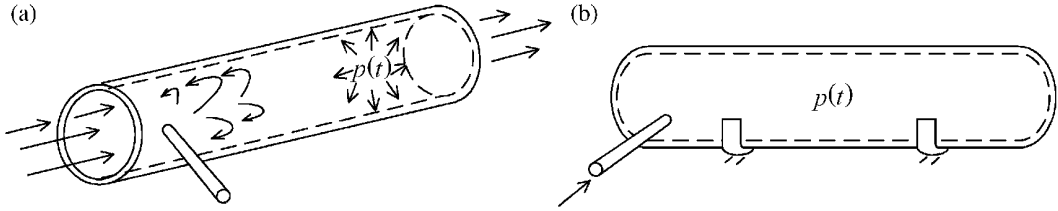


Figure 10.9.1 Structural dynamics examples for axisymmetric modeling. (a) Long natural gas pipeline with side branch-induced vortex shedding and (b) heat exchanger vessel with internal pressure pulsation

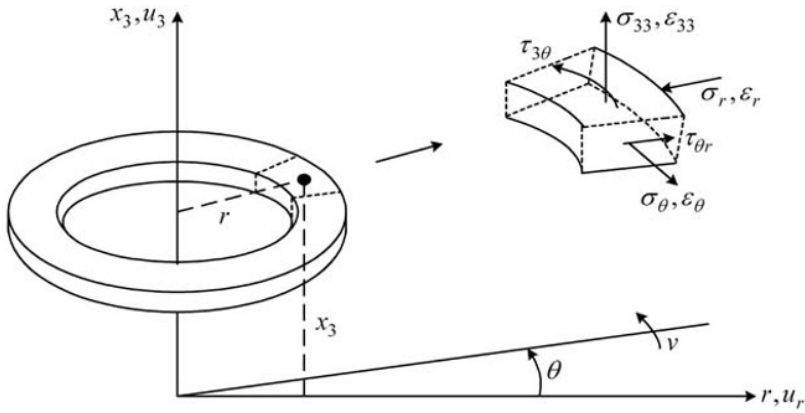


Figure 10.9.2 Axisymmetric ring region and differential volume in cylindrical coordinates

$$\begin{Bmatrix} \epsilon_r \\ \epsilon_\theta \\ \epsilon_{33} \\ \gamma_{3r} \\ \gamma_{r\theta} \\ \gamma_{\theta 3} \end{Bmatrix} = \begin{bmatrix} \frac{\partial}{\partial r} & 0 & 0 \\ \frac{1}{r} & \frac{1}{r} \frac{\partial}{\partial \theta} & 0 \\ 0 & 0 & \frac{\partial}{\partial x_3} \\ \frac{\partial}{\partial x_3} & 0 & \frac{\partial}{\partial r} \\ \frac{1}{r} \frac{\partial}{\partial \theta} & \frac{\partial}{\partial r} - \frac{1}{r} & 0 \\ 0 & \frac{\partial}{\partial x_3} & \frac{1}{r} \frac{\partial}{\partial \theta} \end{bmatrix} \begin{Bmatrix} u_r \\ v \\ u_3 \end{Bmatrix} \tag{10.9.1}$$

or

$$\epsilon = \underset{6 \times 1}{D} \underset{6 \times 13 \times 1}{U} \tag{10.9.2}$$

The kinematic constraint assumptions for axisymmetric geometry and loading are

$$v = 0, \quad \frac{\partial u_r}{\partial \theta} = 0, \quad \frac{\partial u_3}{\partial \theta} = 0 \tag{10.9.3}$$

where v , u_r , and u_3 are the circumferential, radial, and axial components of displacement, respectively. Substitution of (10.9.3) into (10.9.1) yields

$$\gamma_{r\theta} = 0, \quad \gamma_{\theta 3} = 0 \quad (10.9.4)$$

and

$$\begin{Bmatrix} \varepsilon_r \\ \varepsilon_{33} \\ \varepsilon_\theta \\ \gamma_{3r} \end{Bmatrix} = \begin{bmatrix} \frac{\partial}{\partial r} & 0 \\ 0 & \frac{\partial}{\partial x_3} \\ \frac{1}{r} & 0 \\ \frac{\partial}{\partial x_3} & \frac{\partial}{\partial r} \end{bmatrix} \begin{Bmatrix} u_r \\ u_3 \end{Bmatrix} \quad (10.9.5)$$

or

$$\underline{\varepsilon}_{4 \times 1} = \underline{D}_{4 \times 2} \underline{U}_{2 \times 1} \quad (10.9.6)$$

The corresponding material law matrix for an axisymmetric geometry and loading with an isotropic material is from (Cook et al., 1989)

$$\underline{\sigma} = \begin{Bmatrix} \sigma_r \\ \sigma_{33} \\ \sigma_\theta \\ \tau_{r3} \end{Bmatrix} = \underline{E}_{\text{ax}} \begin{Bmatrix} \varepsilon_r \\ \varepsilon_{33} \\ \varepsilon_\theta \\ \gamma_{3r} \end{Bmatrix} = \underline{E}_{\text{ax}} \underline{\varepsilon} \quad (10.9.7)$$

where

$$\underline{E}_{\text{ax}} = \frac{E}{(1+\nu)e_2} \begin{bmatrix} e_1 & \nu & \nu & 0 \\ \nu & e_1 & \nu & 0 \\ \nu & \nu & e_1 & 0 \\ 0 & 0 & 0 & e_3 \end{bmatrix} \quad (10.9.8)$$

$$e_1 = 1 - \nu, \quad e_2 = 1 - 2\nu, \quad e_3 = \frac{e_2}{2} \quad (10.9.9)$$

10.9.2 4-Node, Bilinear Axisymmetric Element

Figure 10.9.3 depicts a generic axisymmetric object and the corresponding 2D finite element mesh of the cross section that generates the object when rotated about the x_3 axis.

Figure 10.9.4 shows a typical element in the actual (physical) and natural coordinates.

The total element is a toroidal solid as shown in Figure 10.9.5; hence, the quadrilateral shape shown in Figure 10.9.4 is only a slice through the full element in the r - x_3 plane.

The displacement interpolations and geometry mapping for this 4-node element are

$$u_r = \sum_{k=1}^4 N_k u_{rk}^{(e)} \quad (\text{radial displacement}), \quad u_3 = \sum_{k=1}^4 N_k u_{3k}^{(e)} \quad (\text{axial displacement}) \quad (10.9.10)$$

$$r = \sum_{k=1}^4 N_k r_k^{(e)} \quad (\text{radial position}), \quad x_3 = \sum_{k=1}^4 N_k x_{3k}^{(e)} \quad (\text{axial position}) \quad (10.9.11)$$

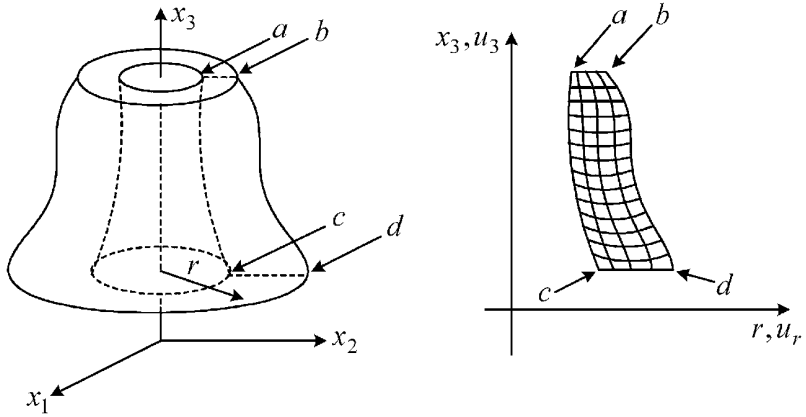


Figure 10.9.3 Axisymmetric model and meshed 2D section

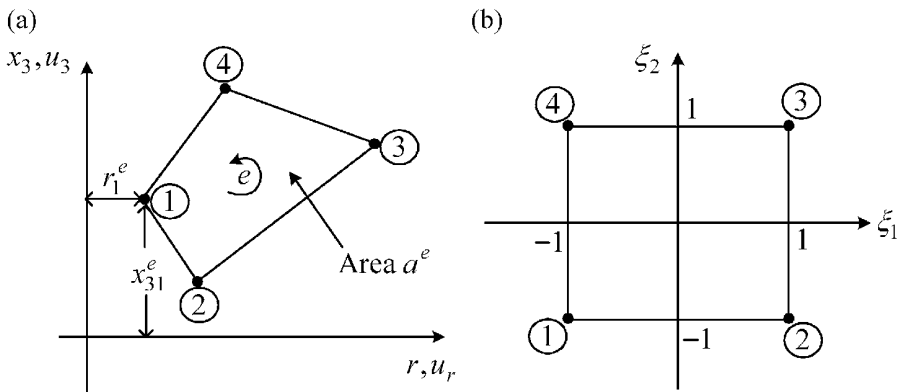


Figure 10.9.4 Isoparametric, quadrilateral element for axisymmetric modeling. (a) actual coordinates and (b) natural coordinates

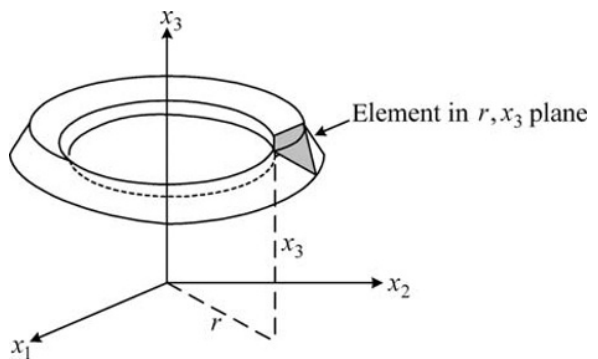


Figure 10.9.5 Toroidal solid axisymmetric, quadrilateral element

where $([]_k^{(e)})$ = value of $[]$ at local node k of element e) and the $N_k(\xi_1, \xi_2)$ are defined in (10.4.2).

The strain–displacement relationship (10.9.5) may be written as

$$\begin{Bmatrix} \varepsilon_r \\ \varepsilon_{33} \\ \varepsilon_\theta \\ \gamma_{3r} \end{Bmatrix} = \begin{bmatrix} 1 & 0 & 0 & 0 & 0 \\ 0 & 0 & 0 & 1 & 0 \\ 0 & 0 & 0 & 0 & \frac{1}{r} \\ 0 & 1 & 1 & 0 & 0 \end{bmatrix} \begin{Bmatrix} \frac{\partial u_r}{\partial r} \\ \frac{\partial u_r}{\partial x_3} \\ \frac{\partial u_3}{\partial r} \\ \frac{\partial u_3}{\partial x_3} \\ u_r \end{Bmatrix} \quad (10.9.12)$$

Use of the Jacobian-derivative transformation yields

$$\begin{Bmatrix} \frac{\partial u_r}{\partial r} \\ \frac{\partial u_r}{\partial x_3} \\ \frac{\partial u_3}{\partial r} \\ \frac{\partial u_3}{\partial x_3} \\ u_r \end{Bmatrix} = \begin{bmatrix} J_e^{-1} & \underline{0} & \underline{0} \\ \underline{0} & J_e^{-1} & \underline{0} \\ \underline{0} & \underline{0} & 1 \\ \underline{0} & \underline{0} & \underline{0} \end{bmatrix} \begin{Bmatrix} \frac{\partial u_r}{\partial \xi_1} \\ \frac{\partial u_r}{\partial \xi_2} \\ \frac{\partial u_3}{\partial \xi_1} \\ \frac{\partial u_3}{\partial \xi_2} \\ u_r \end{Bmatrix} = \begin{bmatrix} J_e^{-1} & \underline{0} & \underline{0} \\ \underline{0} & J_e^{-1} & \underline{0} \\ \underline{0} & \underline{0} & 1 \\ \underline{0} & \underline{0} & \underline{0} \end{bmatrix} * \underline{R}^e \quad (10.9.13)$$

where the Jacobian matrix is

$$\underline{J}_e = \begin{bmatrix} \frac{\partial r}{\partial \xi_1} & \frac{\partial x_3}{\partial \xi_1} \\ \frac{\partial r}{\partial \xi_2} & \frac{\partial x_3}{\partial \xi_2} \end{bmatrix} = \begin{bmatrix} \frac{\partial N_1}{\partial \xi_1} & \frac{\partial N_2}{\partial \xi_1} & \frac{\partial N_3}{\partial \xi_1} & \frac{\partial N_4}{\partial \xi_1} \\ \frac{\partial N_1}{\partial \xi_2} & \frac{\partial N_2}{\partial \xi_2} & \frac{\partial N_3}{\partial \xi_2} & \frac{\partial N_4}{\partial \xi_2} \end{bmatrix} \begin{bmatrix} r_1^e & x_{31}^e \\ r_2^e & x_{32}^e \\ r_3^e & x_{33}^e \\ r_4^e & x_{34}^e \end{bmatrix} \quad (10.9.14)$$

Combining (10.9.12) and (10.9.13) yields

$$\begin{Bmatrix} \varepsilon_r \\ \varepsilon_{33} \\ \varepsilon_\theta \\ \gamma_{3r} \end{Bmatrix} = \begin{bmatrix} 1 & 0 & 0 & 0 & 0 \\ 0 & 0 & 0 & 1 & 0 \\ 0 & 0 & 0 & 0 & \frac{1}{r} \\ 0 & 1 & 1 & 0 & 0 \end{bmatrix} \begin{bmatrix} J_e^{-1} & \underline{0} & \underline{0} \\ \underline{0} & J_e^{-1} & \underline{0} \\ \underline{0} & \underline{0} & 1 \end{bmatrix} \begin{Bmatrix} \frac{\partial u_r}{\partial \xi_1} \\ \frac{\partial u_r}{\partial \xi_2} \\ \frac{\partial u_3}{\partial \xi_1} \\ \frac{\partial u_3}{\partial \xi_2} \\ u_r \end{Bmatrix} = \begin{bmatrix} 1 & 0 & 0 & 0 & 0 \\ 0 & 0 & 0 & 1 & 0 \\ 0 & 0 & 0 & 0 & \frac{1}{r} \\ 0 & 1 & 1 & 0 & 0 \end{bmatrix} \begin{bmatrix} J_e^{-1} & \underline{0} & \underline{0} \\ \underline{0} & J_e^{-1} & \underline{0} \\ \underline{0} & \underline{0} & 1 \end{bmatrix} * \underline{R}^e \quad (10.9.15)$$

or

$$\underline{\varepsilon}^e = \underline{A}_1^e(\xi_1, \xi_2) \underline{R}^e \quad (10.9.16)$$

The \underline{R}^e vector (10.9.15) may be expressed in terms of the shape functions and nodal displacements using (10.9.10)

$$\underline{R}^e = \begin{Bmatrix} \frac{\partial u_r}{\partial \xi_1} \\ \frac{\partial u_r}{\partial \xi_2} \\ \frac{\partial u_3}{\partial \xi_1} \\ \frac{\partial u_3}{\partial \xi_2} \\ u_r \\ u_3 \end{Bmatrix} = \begin{bmatrix} \frac{\partial N_1}{\partial \xi_1} & 0 & \frac{\partial N_2}{\partial \xi_1} & 0 & \frac{\partial N_3}{\partial \xi_1} & 0 & \frac{\partial N_4}{\partial \xi_1} & 0 \\ \frac{\partial N_1}{\partial \xi_2} & 0 & \frac{\partial N_2}{\partial \xi_2} & 0 & \frac{\partial N_3}{\partial \xi_2} & 0 & \frac{\partial N_4}{\partial \xi_2} & 0 \\ 0 & \frac{\partial N_1}{\partial \xi_1} & 0 & \frac{\partial N_2}{\partial \xi_1} & 0 & \frac{\partial N_3}{\partial \xi_1} & 0 & \frac{\partial N_4}{\partial \xi_1} \\ 0 & \frac{\partial N_1}{\partial \xi_2} & 0 & \frac{\partial N_2}{\partial \xi_2} & 0 & \frac{\partial N_3}{\partial \xi_2} & 0 & \frac{\partial N_4}{\partial \xi_2} \\ N_1 & 0 & N_2 & 0 & N_3 & 0 & N_4 & 0 \end{bmatrix} \begin{Bmatrix} u_{r1} \\ u_{31} \\ u_{r2} \\ u_{32} \\ u_{r3} \\ u_{33} \\ u_{r4} \\ u_{34} \end{Bmatrix} \quad (10.9.17)$$

or

$$\underline{R}^e = \underline{A}_2^e \underline{q}^e \quad (10.9.18)$$

Substitution of (10.9.18) into (10.9.16) yields

$$\underline{\varepsilon}^e = \underline{A}_1^e \underline{A}_2^e \underline{q}^e \quad 4 \times 1 \quad (10.9.19)$$

Therefore, by (10.4.10),

$$\underline{B}^e(\xi_1, \xi_2) = \underline{A}_1^e(\xi_1, \xi_2) \underline{A}_2^e(\xi_1, \xi_2) \quad (10.9.20)$$

The stiffness matrix is obtained from (10.4.11) as

$$\underline{K}^e = \int_V (\underline{B}^e)^T \underline{E}_{ax}^e \underline{B}^e dV = \int_{a^e} \int_0^{2\pi} \int_0^r (\underline{B}^e)^T \underline{E}_{ax}^e \underline{B}^e r dr d\theta dz \quad (10.9.21)$$

The θ integral in (10.9.21) may be easily performed, since neither \underline{B}^e or \underline{E}^e depends on θ in the axisymmetric model, yielding

$$\underline{K}^e = 2\pi \int_{a^e} (\underline{B}^e)^T \underline{E}_{ax}^e \underline{B}^e r dr dz \quad (10.9.22)$$

This relation expressed in natural (ξ_1, ξ_2) coordinates becomes

$$\underline{K}^e = 2\pi \int_{-1}^1 \int_{-1}^1 (\underline{B}^e(\xi_1, \xi_2))^T \underline{E}_{ax}^e \underline{B}^e(\xi_1, \xi_2) r(\xi_1, \xi_2) \det(\underline{J}_e(\xi_1, \xi_2)) d\xi_1 d\xi_2 \quad (10.9.23)$$

The integral in (10.9.23) is performed with GQ:

$$\underline{K}^e = 2\pi \sum_{s=1}^{n_G} \sum_{t=1}^{n_G} \bar{w}_s \bar{w}_t (\underline{B}^e(\xi_{1s}, \xi_{2t}))^T \underline{E}_{\text{ax}}^e \underline{B}^e(\xi_{1s}, \xi_{2t}) r(\xi_{1s}, \xi_{2t}) \det(\underline{J}_e(\xi_{1s}, \xi_{2t})) \quad (10.9.24)$$

Likewise, the general form of the element mass matrix is obtained from (10.4.29) as

$$\begin{aligned} \underline{M}^e &= \int_{V^e} \rho \underline{N}^T \underline{N} dV = \int \int_0^{2\pi} \int_0^a \rho \underline{N}^T \underline{N} r dr d\theta dz = 2\pi \int_{-1}^1 \int_{-1}^1 \rho \underline{N}^T \underline{N} r \det(\underline{J}_e) d\xi_1 d\xi_2 \\ &\approx 2\pi \sum_{s=1}^{n_G} \sum_{t=1}^{n_G} \bar{w}_s \bar{w}_t \rho \underline{N}^T(\xi_{1s}, \xi_{2t}) \underline{N}(\xi_{1s}, \xi_{2t}) r(\xi_{1s}, \xi_{2t}) \det(\underline{J}_e(\xi_{1s}, \xi_{2t})) \end{aligned} \quad (10.9.25)$$

The body forces (force/volume) and surface forces (force/area) acting on the axisymmetric structure may act in either the r (radial) or x_3 (axial) directions. The corresponding element force vector is derived from the general form in (10.4.32), that is,

$$\underline{f}_{8 \times 1}^e = \begin{Bmatrix} f_{11}^e \\ f_{21}^e \\ f_{12}^e \\ f_{22}^e \\ f_{13}^e \\ f_{23}^e \\ f_{14}^e \\ f_{24}^e \end{Bmatrix} = \int_{\Gamma^e} \underline{N}^T \begin{Bmatrix} F_{\Gamma r}^e \\ F_{\Gamma x3}^e \end{Bmatrix} d\Gamma + \int_{V^e} \underline{N}^T \begin{Bmatrix} F_{Vr}^e \\ F_{Vx3}^e \end{Bmatrix} dV \quad (10.9.26)$$

where Γ represents all edges of the element that are subjected to surface loading.

In order to illustrate a load vector determination, consider the case of a spatially uniform surface load acting on edge 2–3 of element e as depicted in Figure 10.9.6.

This is fairly general since the connectivity of the element may be defined so that edge 2–3 occurs on the desired surface of the model. The natural coordinate $\xi_1 = +1$ on edge 2–3, thus the shape functions in (10.4.2) become

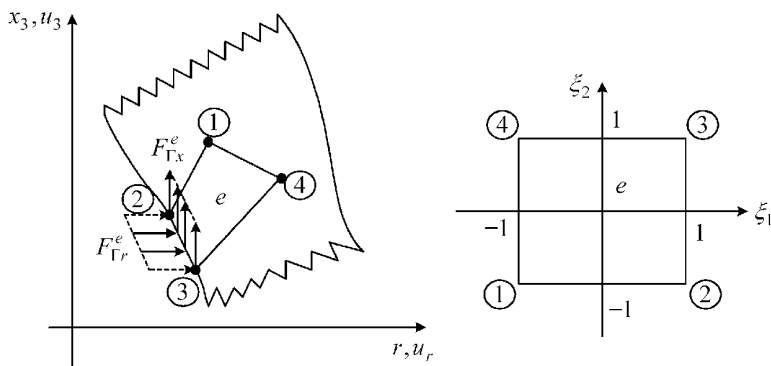


Figure 10.9.6 Uniform surface loading applied to edge 2–3 of an axisymmetric 4-node element e

$$N_1 = N_4 = 0, \quad N_2 = \frac{1}{2}(1 - \xi_2), \quad N_3 = \frac{1}{2}(1 + \xi_2) \quad (10.9.27)$$

The geometry mapping (10.9.11) on edge 2–3 becomes

$$r = \frac{1}{2}(1 - \xi_2) r_2^e + \frac{1}{2}(1 + \xi_2) r_3^e, \quad x_3 = \frac{1}{2}(1 - \xi_2) x_{32}^e + \frac{1}{2}(1 + \xi_2) x_{33}^e \quad (10.9.28)$$

The differential surface area along edge 2–3 is

$$\begin{aligned} d\Gamma_{23} &= 2\pi * r * dl_{23} = 2\pi * r \sqrt{dr^2 + dx_3^2} = 2\pi * r \sqrt{\left(\frac{\partial r}{\partial \xi_2}\right)^2 + \left(\frac{\partial x_3}{\partial \xi_2}\right)^2} d\xi_2 \\ &= \pi * r \sqrt{(r_3^e - r_2^e)^2 + (x_{33}^e - x_{32}^e)^2} d\xi_2 = \pi r l_{23}^e d\xi_2 \end{aligned} \quad (10.9.29)$$

where l_{23}^e is the length of edge 2–3 on element e . Substitute (10.4.8), (10.9.27), and (10.9.29) into (10.9.26) and express the tractions (force/area) as the product of a constant, spatial factor (\bar{f}), and a temporal factor ($\alpha(t)$) to obtain

$$\begin{aligned} \bar{f}_{\Gamma_{23}}^e = \begin{Bmatrix} f_{11}^e \\ f_{21}^e \\ f_{12}^e \\ f_{22}^e \\ f_{13}^e \\ f_{23}^e \\ f_{14}^e \\ f_{24}^e \end{Bmatrix}_{8 \times 1} &= \int_{\Gamma_{23}^e} \underline{N}^T \left\{ \begin{array}{l} \bar{f}_{\Gamma_r}^e \alpha_{\Gamma_r}(t) \\ \bar{f}_{\Gamma_{x3}}^e \alpha_{\Gamma_{x3}}(t) \end{array} \right\} d\Gamma_{23} = \pi l_{23}^e \int_{-1}^1 \begin{Bmatrix} 0 & 0 \\ 0 & 0 \\ \frac{(1-\xi_2)}{2} & 0 \\ 0 & \frac{(1-\xi_2)}{2} \\ \frac{(1+\xi_2)}{2} & 0 \\ 0 & \frac{(1+\xi_2)}{2} \\ 0 & 0 \\ 0 & 0 \end{Bmatrix} \left\{ \begin{array}{l} \bar{f}_{\Gamma_r}^e \alpha_{\Gamma_r}(t) \\ \bar{f}_{\Gamma_{x3}}^e \alpha_{\Gamma_{x3}}(t) \end{array} \right\} (r_2^e N_2 + r_3^e N_3) d\xi_2 \\ &= \frac{\pi}{4} l_{23}^e \int_{-1}^1 \begin{Bmatrix} 0 \\ 0 \\ \alpha_{\Gamma_r}(t) \bar{f}_{\Gamma_r}^e (1-\xi_2) [r_2^e (1-\xi_2) + r_3^e (1+\xi_2)] \\ \alpha_{\Gamma_{x3}}(t) \bar{f}_{\Gamma_{x3}}^e (1-\xi_2) [r_2^e (1-\xi_2) + r_3^e (1+\xi_2)] \\ \alpha_{\Gamma_r}(t) \bar{f}_{\Gamma_r}^e (1+\xi_2) [r_2^e (1-\xi_2) + r_3^e (1+\xi_2)] \\ \alpha_{\Gamma_{x3}}(t) \bar{f}_{\Gamma_{x3}}^e (1+\xi_2) [r_2^e (1-\xi_2) + r_3^e (1+\xi_2)] \\ 0 \\ 0 \end{Bmatrix} d\xi_2 = \frac{\pi}{3} l_{23}^e \begin{Bmatrix} 0 \\ 0 \\ \alpha_{\Gamma_r}(t) \bar{f}_{\Gamma_r}^e (2r_2^e + r_3^e) \\ \alpha_{\Gamma_{x3}}(t) \bar{f}_{\Gamma_{x3}}^e (2r_2^e + r_3^e) \\ \alpha_{\Gamma_r}(t) \bar{f}_{\Gamma_r}^e (r_2^e + 2r_3^e) \\ \alpha_{\Gamma_{x3}}(t) \bar{f}_{\Gamma_{x3}}^e (r_2^e + 2r_3^e) \\ 0 \\ 0 \end{Bmatrix} \end{aligned} \quad (10.9.30)$$

Equation (10.9.30) is applicable for general loading and geometry. Let's consider a very special case to illustrate a physical interpretation of this element load vector. Consider an element that has a vertical edge subjected to constant pressure,

$$r_2^e = r_3^e = r_{23}^e, \quad \bar{f}_{\Gamma_{x3}} = 0, \quad \bar{f}_{\Gamma_r} = p \text{ (pressure)} \quad (10.9.31)$$

Then the total pressure force on edge 2–3 as

$$f_p^{\text{TOT}} = \text{pressure} * \text{area} = p * (2\pi * r_{23}^e l_{23}^e) \tag{10.9.32}$$

In this case, (10.9.30) simplifies to

$$f_{\Gamma 23}^e = \begin{pmatrix} f_{11}^e \\ f_{21}^e \\ f_{12}^e \\ f_{22}^e \\ f_{13}^e \\ f_{23}^e \\ f_{14}^e \\ f_{24}^e \end{pmatrix}_{8 \times 1} = \begin{pmatrix} 0 \\ 0 \\ \alpha_{\Gamma r}(t) f_p^{\text{TOT}} / 2 \\ 0 \\ \alpha_{\Gamma r}(t) f_p^{\text{TOT}} / 2 \\ 0 \\ 0 \\ 0 \end{pmatrix} \tag{10.9.33}$$

which is depicted in Figure 10.9.7.

The element force vector in (10.9.33) contains one-half of the total pressure load acting on edge 2–3, applied on the radial degrees of freedom at nodes 2 and 3. These results intuitively make sense and result from the linear interpolation and mappings employed. Higher-order element formulations yields equivalent force vectors which are mathematically consistent with the corresponding stiffness and mass matrices, yet are generally not intuitive.

Summarizing, the element matrices and force vectors in Figure 10.5.2 are:

Axisymmetric Element Stiffness Matrix: Equation (10.9.24)

$$\underline{K}^e \approx 2\pi \sum_{s=1}^{n_G} \sum_{t=1}^{n_G} \bar{w}_s \bar{w}_t (\underline{B}^e(\xi_{1s}, \xi_{2t}))^T \underline{E}_{\text{ax}}^e \underline{B}^e(\xi_{1s}, \xi_{2t}) r(\xi_{1s}, \xi_{2t}) \det(\underline{J}_e(\xi_{1s}, \xi_{2t})), \tag{10.9.34}$$

where by (10.9.20),

$$\underline{B}^e(\xi_1, \xi_2) = \underline{A}_1^e(\xi_1, \xi_2) \underline{A}_2^e(\xi_1, \xi_2) \tag{10.9.35}$$

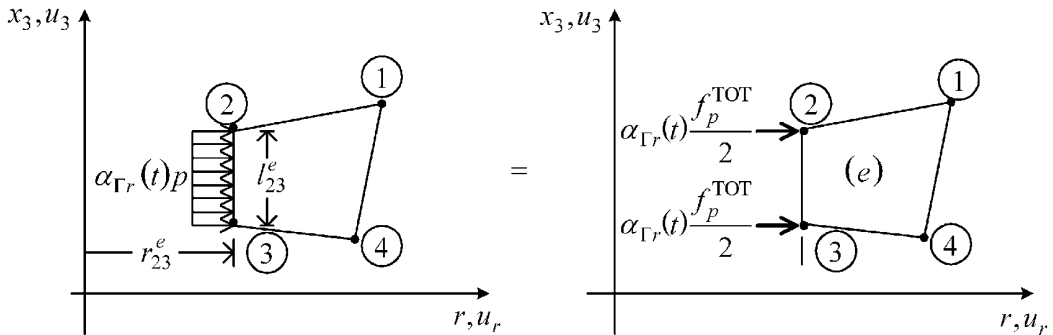


Figure 10.9.7 Time-varying, spatially uniform pressure on edge 2–3 and equivalent forces

Axisymmetric Element Mass Matrix: Equation (10.9.25)

$$\underline{M}^e \approx 2\pi \sum_{s=1}^{n_G} \sum_{t=1}^{n_G} \bar{w}_s \bar{w}_t \rho \underline{N}^T(\xi_{1s}, \xi_{2t}) \underline{N}(\xi_{1s}, \xi_{2t}) r(\xi_{1s}, \xi_{2t}) \det(\underline{J}_e(\xi_{1s}, \xi_{2t})) \quad (10.9.36)$$

Axisymmetric Element: Assembly and Stress Evaluation

Assembly of the system matrices from the element matrices is facilitated by defining degree of freedom ordering conventions. As illustrated in Figure 10.4.1, the system degrees of freedom dofs are ordered according to the convention

$$\begin{aligned} \text{Global (system) node } i, r \text{ direction, system dof : } u_{2*(i-1)+1} \\ \text{Global (system) node } i, x_3 \text{ direction, system dof : } u_{2*(i-1)+2} \end{aligned} \quad (10.9.37)$$

This is illustrated in tabular form in Table 10.9.1.

Please note that the local nodes are ordered CCW starting at any of the 4 nodes in the element as shown in Figure 10.9.4. Table 10.9.2 shows the ordering of 8 local degrees of freedom dofs within the element \underline{q}_e vector as indicated in (10.9.17) and (10.9.18).

The system equations (10.5.11)

$$\underset{N_f \times N_f}{\underline{M}_f} \underset{N_f \times 1}{\ddot{\underline{q}}_f} + \underset{N_f \times N_f}{\underline{C}_f} \underset{N_f \times 1}{\dot{\underline{q}}_f} + \underset{N_f \times N_f}{\underline{K}_f} \underset{N_f \times 1}{\underline{q}_f} = \underset{N_f \times 1}{\underline{F}_f} \quad (10.9.38)$$

Table 10.9.1 System degree of freedom ordering convention

System node number	Direction in axisymmetric model	System dof number
1	r	1
1	x_3	2
2	r	3
2	x_3	4
\vdots	\vdots	\vdots
N_n	r	$2*(N_n-1)+1$
N_n	x_3	$2*(N_n-1)+2$

Table 10.9.2 Plane stress/strain element local dof ordering convention

Local dof (m)	Local node	Direction
1	1	r
2	1	x_3
3	2	r
4	2	x_3
5	3	r
6	3	x_3
7	4	r
8	4	x_3

are assembled identically to the plane strain/stress mode, that is, by use of Figure 10.5.2 and Equations (10.5.11)–(10.5.15). These equations may be solved for the free, transient force and harmonic force cases as illustrated in Chapters 5, 6, and 7, respectively. The resulting deflections can then be used in the post-processing stage to determine stresses.

The stresses in an axisymmetric model obey (10.9.7)

$$\underline{\sigma} = \frac{E_{ax}}{4 \times 1} \underline{\varepsilon} \quad (10.9.39)$$

where

$$\underline{\sigma} = (\sigma_r \ \sigma_{33} \ \sigma_\theta \ \tau_{r3})^T, \quad \underline{\varepsilon} = (\varepsilon_r \ \varepsilon_{33} \ \varepsilon_\theta \ \gamma_{3r})^T \quad (10.9.40)$$

$$\frac{E_{ax}}{4 \times 4} = \frac{E}{(1+\nu)e_2^a} \begin{bmatrix} e_1^a & \nu & \nu & 0 \\ \nu & e_1^a & \nu & 0 \\ \nu & \nu & e_1^a & 0 \\ 0 & 0 & 0 & e_3^a \end{bmatrix}, \quad e_1^a = 1-\nu, \quad e_2^a = 1-2\nu, \quad e_3^a = \frac{e_2^a}{2} \quad (10.9.41)$$

The following procedure may be used for determining axisymmetric solid model stresses at any integration point pair (ξ_{1i}, ξ_{2k}) within element e .

GQ Point Stress Evaluation Procedure

- (a) Solve (10.9.38) for $q_f(t)$ at some time t by numerical integration (Section 6.4) or other means. The solution may correspond to zero (Chapter 5), arbitrary (Chapter 6), or harmonic (Chapter 7) forces.
- (b) Obtain the element e nodal displacements $q_e(t)$ from (10.6.6b)

$$\left(q^e \right)_m = \begin{cases} \left(q_f \right)_{l_{\hat{B}_{em}}} & , \quad l_{\hat{B}_{em}} \neq 0 \\ 0, & l_{\hat{B}_{em}} = 0 \end{cases}, \quad m = 1, \dots, 8 \quad (10.9.42)$$

- (c) Evaluate the shape functions $N_l(\xi_1, \xi_2)$ and their derivatives $\partial N_l / \partial \xi_1$ and $\partial N_l / \partial \xi_2$ from (10.4.2) for $l = 1, 2, 3, 4$ at the integration point locations $(\xi_1, \xi_2) = (\xi_{1i}, \xi_{2k})$ in Table 10.4.1.
- (d) Compute the locations of the integration point pairs (ξ_{1i}, ξ_{2k}) in the actual coordinates (10.9.11),

$$r = \sum_{l=1}^4 N_l(\xi_{1i}, \xi_{2k}) r_l^e, \quad x_3 = \sum_{l=1}^4 N_l(\xi_{1i}, \xi_{2k}) x_{3l}^e \quad (10.9.43)$$

- (e) Compute the Jacobian matrix J_e at ξ_{1i}, ξ_{2k} via (10.9.14).
- (f) Form the \underline{A}_1^e and \underline{A}_2^e matrices at (ξ_{1i}, ξ_{2k}) via Equations (10.9.16) through (10.9.18).
- (g) Compute the \underline{B}^e matrix (10.9.20),

$$\underline{B}^e = \underline{A}_1^e \underline{A}_2^e \quad (10.9.44)$$

- (h) Compute the strains at (ξ_{1i}, ξ_{2k}) via (10.9.19) and (10.9.20),

$$\underline{\varepsilon}^e(\xi_{1i}, \xi_{2k}, t) = \underline{B}^e(\xi_{1i}, \xi_{2k}) q^e(t) \quad (10.9.45)$$

(i) Compute the stresses at (ξ_{1i}, ξ_{2k}) at the given time t by (10.9.39)

$$\underline{\sigma}^e(\xi_{1i}, \xi_{2k}, t) = \underline{E}_{\text{ax}}^e \underline{\epsilon}^e(\xi_{1i}, \xi_{2k}, t) \quad (10.9.46)$$

(j) Repeat steps (b)–(i) for all integration points in element e . Interpolate stresses within element e given all integration point stresses $\underline{\sigma}^e(\xi_{1i}, \xi_{2k})$ and their actual locations $\{ r^e(\xi_{1i}, \xi_{2k}), x_3^e(\xi_{1i}, \xi_{2k}) \}$ in element e .

(k) Determine fatigue life utilizing computed stresses and the methods of Section 1.4.

EXAMPLE 10.9.1 Axisymmetric Modes and Natural Frequencies of a Steel Disk

Statement: This example illustrates the use of 4-node, bilinear isoparametric elements to determine the axisymmetric modes of the disk illustrated in Figure E10.9.1(a). The results are compared with usage of 9-node quadratic, isoparametric elements for the same model. The disk has free boundary conditions and may be viewed as a rotor or similarly shaped structural or machinery component. The material properties of the disk are

$$E = 2.0 \times 10^{11} \text{ N/m}^2, \quad \nu = 0.3, \quad \rho = 8000 \text{ kg/m}^3 \quad (1)$$

Solution: The tapered, equally spaced parameterized mesh pattern for this problem is shown in Figure E10.9.1(b). The mesh pattern and connectivities are the same as utilized in Figures E10.8.1(a) and E10.8.1(b), respectively. Figure E10.9.1(c) shows the 4 lowest mode shapes. The zero-frequency mode corresponds to a rigid body motion along the x_3 direction. The other modes shown are radial (breathing) and bending modes.

9-Node Quadratic Element Model The axisymmetric model in the above example illustrated the theory for the 4-node, bilinear quadrilateral element. The steps for employing a higher-order 9-node, quadratic, quadrilateral, isoparametric element are identical to those shown in (10.9.1)–(10.9.25). The main difference is that the interpolation and mapping will have 9 terms instead of 4, that is,

$$u_r = \sum_{k=1}^9 N_k u_{rk}^{(e)} \quad (\text{radial displacement}), \quad u_3 = \sum_{k=1}^9 N_k u_{3k}^{(e)} \quad (\text{axial displacement}) \quad (2)$$

$$r = \sum_{k=1}^9 N_k r_k^{(e)} \quad (\text{radial position}), \quad x_3 = \sum_{k=1}^9 N_k x_{3k}^{(e)} \quad (\text{axial position}) \quad (3)$$

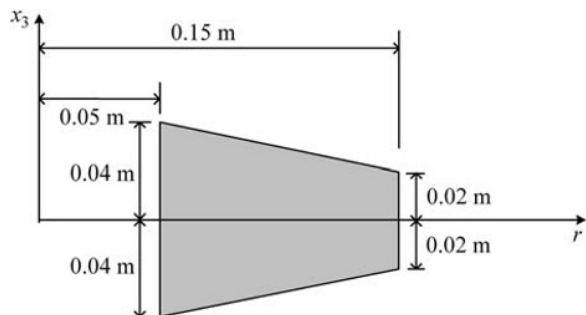


Figure E10.9.1(a) Cross section of the axisymmetric disk

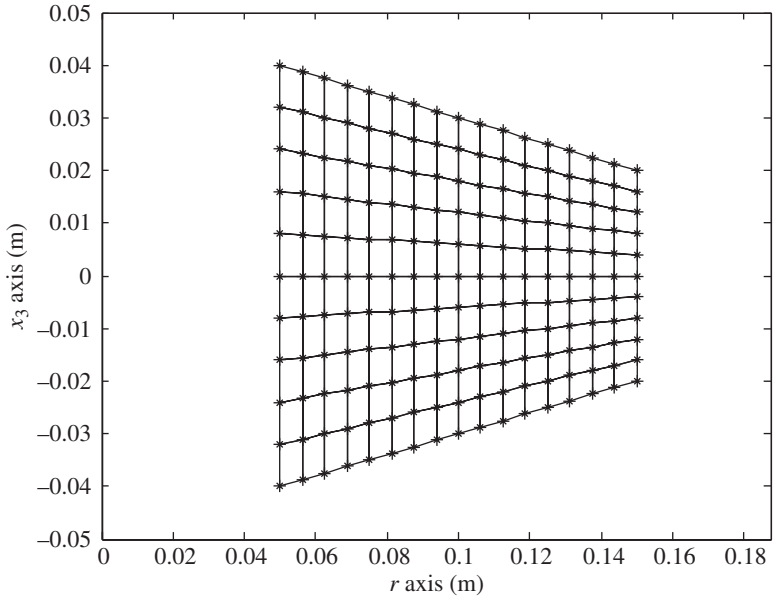


Figure E10.9.1(b) 4-node isoparametric element mesh for the axisymmetric disk

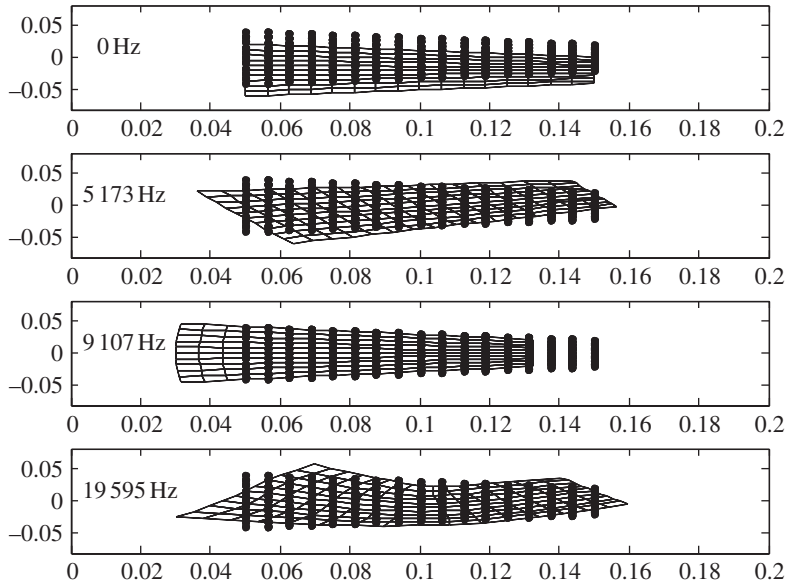


Figure E10.9.1(c) The 4 lowest modes of the axisymmetric disk determined with 4-node bilinear, isoparametric elements

Figure E10.9.1(d) shows a typical 9-node element in both physical and natural coordinates. The 9-node element shape functions are generated from one-dimensional Lagrange polynomials:

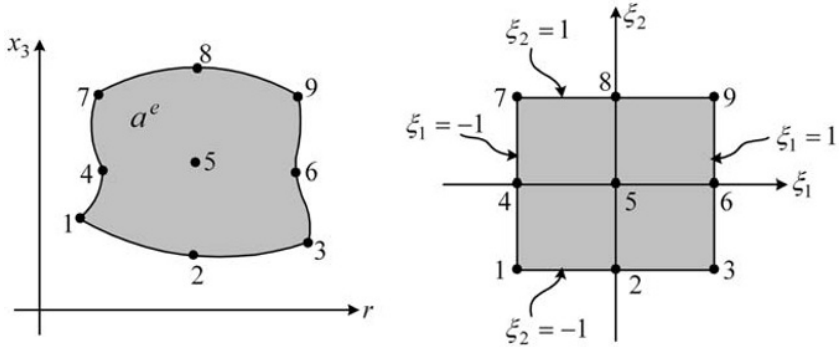


Figure E10.9.1(d) Typical 9-node, quadratic element in physical and natural coordinates

$$\psi_i(\xi) = \frac{\prod_{\substack{j=1 \\ j \neq i}}^n (\xi_j - \xi)}{\prod_{\substack{j=1 \\ j \neq i}}^n (\xi_j - \xi_i)} \quad (4)$$

= 1 dimensional, n th order shape function for node i , where ξ_j is the natural coordinate of local node j , $j = 1 \dots n$, and π denotes a series product

The 9-node, quadratic element shape functions are given by (Reddy, 2005)

$$\begin{aligned} N_1 &= \frac{\xi_2(\xi_2-1)}{2} * \frac{\xi_1(\xi_1-1)}{2}, & N_2 &= -\frac{\xi_2(\xi_2-1)}{2} * (\xi_1+1)(\xi_1-1) \\ N_3 &= \frac{\xi_2(\xi_2-1)}{2} * \frac{\xi_1(\xi_1+1)}{2}, & N_4 &= -(\xi_2+1)(\xi_2-1) * \frac{\xi_1(\xi_1-1)}{2} \\ N_5 &= (\xi_2+1)(\xi_2-1) * (\xi_1+1)(\xi_1-1), & N_6 &= -(\xi_2+1)(\xi_2-1) * \frac{\xi_1(\xi_1+1)}{2} \\ N_7 &= \frac{\xi_2(\xi_2+1)}{2} * \frac{\xi_1(\xi_1-1)}{2}, & N_8 &= -\frac{\xi_2(\xi_2+1)}{2} * (\xi_1+1)(\xi_1-1) \\ N_9 &= \frac{\xi_2(\xi_2+1)}{2} * \frac{\xi_1(\xi_1+1)}{2} \end{aligned} \quad (5)$$

These shape functions satisfy the consistency conditions of (2.11.37).

The 9-node quadratic element mesh is generated with the node and element patterns depicted in Figure E10.9.1(e). In this figure, $\bar{N} = \frac{N-1}{2}$, $\bar{m} = \frac{m-1}{2}$ and $N_e = \bar{N} \bar{m}$ = number of elements.

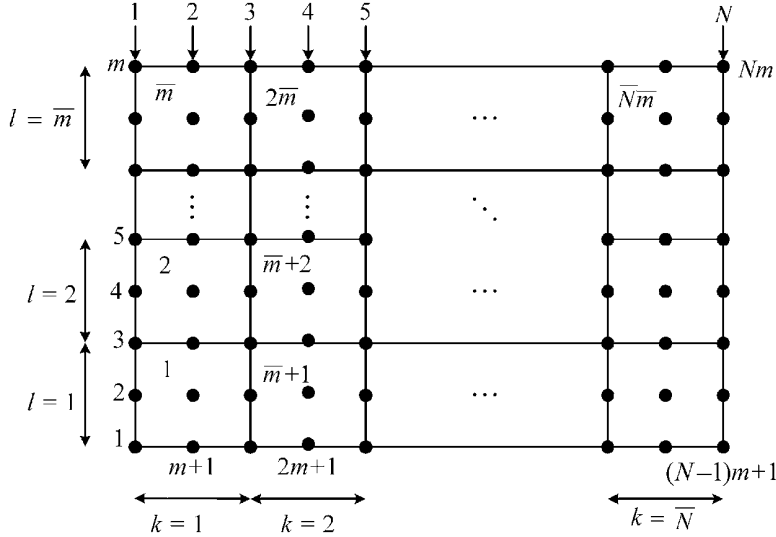


Figure E10.9.1(e) Node and element mesh patterns for 9-node quadratic element

The nodal connectivity array is defined in (10.5.3) as

$$B_{ej} = ICON(e, j) = \text{global node number for local node } j \text{ of element } e, \quad (6)$$

for $j = 1, 2, \dots, 9$ and $e = 1, \dots, N_e$

where N_e is the total number of elements in the model. This array is defined by the following coding logic for the 9-node elements:

$$\begin{aligned} &\text{for } k = 1 : 1 : \bar{N} \\ &\quad \text{for } l = 1 : 1 : \bar{m} \\ &\quad\quad e = (k-1)\bar{m} + l \quad (\text{element number}) \\ &\quad\quad B_{e1} = 2l - 1 + 2m(k-1); \quad B_{e2} = B_{e1} + m; \quad B_{e3} = B_{e1} + 2m; \\ &\quad\quad B_{e4} = B_{e1} + 1; \quad B_{e5} = B_{e2} + 1; \quad B_{e6} = B_{e3} + 1; \\ &\quad\quad B_{e7} = B_{e4} + 1; \quad B_{e8} = B_{e5} + 1; \quad B_{e9} = B_{e6} + 1; \\ &\quad \text{end} \\ &\text{end} \end{aligned} \quad (7)$$

Figure E10.9.1(f) shows the 9-node, quadratic isoparametric element mesh for the axisymmetric disk model. The total system dynamic equilibrium equations (10.9.38) are assembled identically to the plane strain/stress mode, that is, by use of Figure 10.5.2 and Equations (10.5.11)–(10.5.15), with the indices r and s both ranging from 1 to 18. Figure E10.9.1(g) shows the 4 lowest mode shapes and corresponding natural frequencies. The zero-frequency mode corresponds to a rigid body motion along the x_3 direction. The other modes shown are radial (breathing) and bending modes. Comparison of Figures E10.9.1(c) and E10.9.1(f) shows that the 4-node and 9-node element models yield modes and frequencies in close agreement.

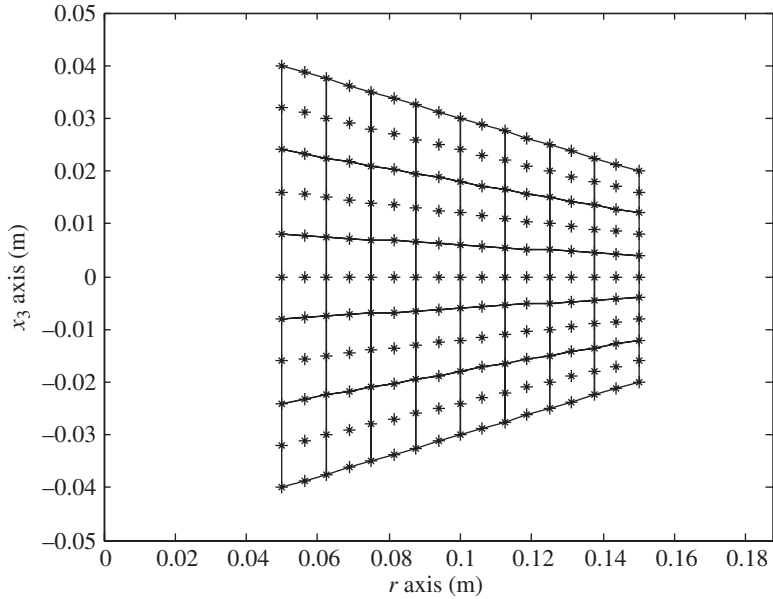


Figure E10.9.1(f) 9-node isoparametric element mesh for axisymmetric disk

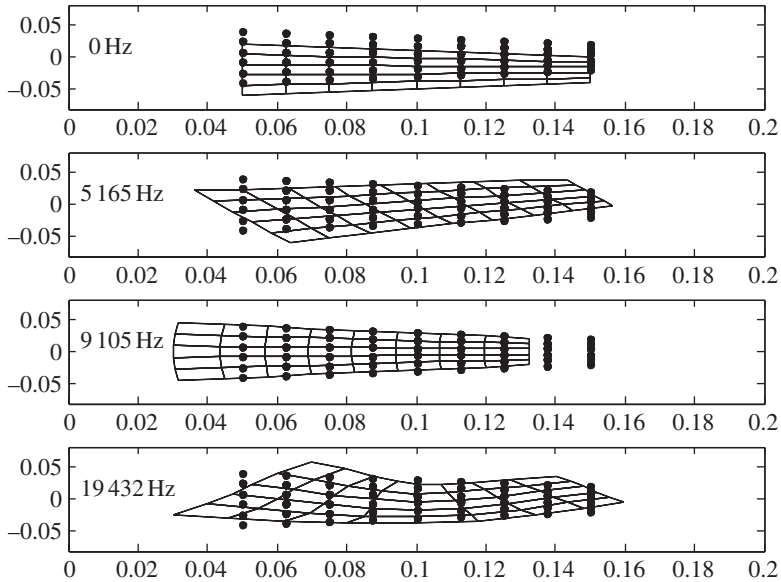


Figure E10.9.1(g) The 4 lowest modes of the axisymmetric disk determined with 9-node, quadratic, isoparametric elements

10.10 AUTOMATED MESH GENERATION: CONSTANT STRAIN TRIANGLE ELEMENTS

Defining the nodal coordinates and element connectivities may be a very time consuming and difficult task, especially for irregular-shaped model domains, and with the need to perform convergence studies with mesh refinement. Commercially available finite element

software presently has the capability to perform automated mesh generation over general 2D and 3D domains. The domain may be defined by the user within the finite element code with mesh generation features or may be defined directly from a solid model of the object. This section shows examples using the MATLAB 2D triangular mesh generation code MESH2D

<http://www.mathworks.com/matlabcentral/fileexchange/25555-mesh2d-automatic-mesh-generation>

MESH2D is a toolbox of 2D meshing routines written by Dr. Darren Engwirda, Massachusetts Institute of Technology, NASA Goddard Institute for Space Studies. The input consists of the vertex (key) points of the domain being modeled and a mesh refinement parameter h_{\max} that maintains the maximum triangular element dimension less than this upper limit. The outputs of MESH2D include the nodal connectivity \underline{B} and nodal coordinate arrays. A 3-node triangle element is presented in order to use with MESH2D to solve plane stress/plane strain vibration problems. The element utilizes linear displacement interpolation (shape) functions, which result in the strains and stresses being constants within each element. Example 10.10.1 demonstrates the use of MESH2D for establishing and refining meshes and obtaining natural frequencies and mode shapes.

Figure 10.10.1 shows a typical triangle element with its 3 local node numbers and 6 local degree of freedom numbers. For sake of illustration, it is assumed that the density, Young's modulus, and Poisson's ratio are constants within any given element.

The displacement interpolation relation within the element is

$$\begin{Bmatrix} u_1(x_1, x_2) \\ u_2(x_1, x_2) \end{Bmatrix} = \begin{bmatrix} \psi_1(x_1, x_2) & 0 & \psi_2(x_1, x_2) & 0 & \psi_3(x_1, x_2) & 0 \\ 0 & \psi_1(x_1, x_2) & 0 & \psi_2(x_1, x_2) & 0 & \psi_3(x_1, x_2) \end{bmatrix} \begin{Bmatrix} u_1^e \\ u_2^e \\ u_3^e \\ u_4^e \\ u_5^e \\ u_6^e \end{Bmatrix} \quad (10.10.1)$$

or

$$\underline{u}(x_1, x_2) = \underline{N}(x_1, x_2) \underline{q}^e \quad (10.10.2)$$

where the shape functions have the general form

$$\psi_i(x_1, x_2) = \frac{1}{2a^e} (\alpha_i + \beta_i x_1 + \gamma_i x_2) \quad (10.10.3)$$

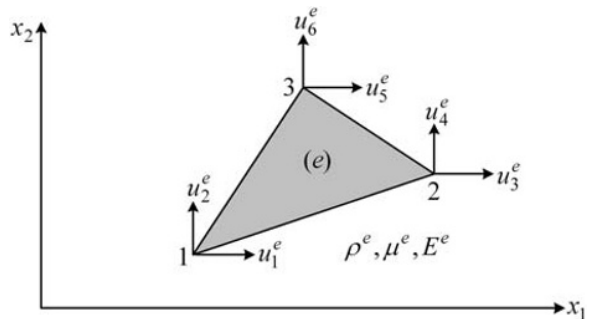


Figure 10.10.1 Typical 3-node triangle element with linear displacement interpolation

and a^e is the element area,

$$\begin{bmatrix} \alpha_1 & \alpha_2 & \alpha_3 \\ \beta_1 & \beta_2 & \beta_3 \\ \gamma_1 & \gamma_2 & \gamma_3 \end{bmatrix} = \begin{bmatrix} x_{12}x_{23} - x_{13}x_{22} & x_{13}x_{21} - x_{11}x_{23} & x_{11}x_{22} - x_{12}x_{21} \\ x_{22} - x_{23} & x_{23} - x_{21} & x_{21} - x_{22} \\ x_{13} - x_{12} & x_{11} - x_{13} & x_{12} - x_{11} \end{bmatrix} \quad (10.10.4)$$

and x_{ik} is the x_i coordinate of local node k of element e .

10.10.1 Element Stiffness Matrix

Recall from (10.4.9), (10.4.10), and (10.10.2),

$$\underline{\varepsilon} = \begin{Bmatrix} \varepsilon_{11} \\ \varepsilon_{22} \\ 2\varepsilon_{12} \end{Bmatrix} = \begin{bmatrix} \frac{\partial}{\partial x_1} & 0 \\ 0 & \frac{\partial}{\partial x_2} \\ \frac{\partial}{\partial x_2} & \frac{\partial}{\partial x_1} \end{bmatrix} \begin{Bmatrix} u_1 \\ u_2 \end{Bmatrix} = \underline{D} \underline{u} = (\underline{D} \underline{N}) \underline{q}^e = \underline{B}_e \underline{q}^e \quad (10.10.5)$$

Substitution of (10.10.1)–(10.10.3) into (10.10.5) yields

$$\underline{B}_e = \underline{D} \underline{N} = \begin{bmatrix} \frac{\partial}{\partial x_1} & 0 \\ 0 & \frac{\partial}{\partial x_2} \\ \frac{\partial}{\partial x_2} & \frac{\partial}{\partial x_1} \end{bmatrix} \begin{bmatrix} \psi_1 & 0 & \psi_2 & 0 & \psi_3 & 0 \\ 0 & \psi_1 & 0 & \psi_2 & 0 & \psi_3 \end{bmatrix} = \frac{1}{2a^e} \begin{bmatrix} \beta_1 & 0 & \beta_2 & 0 & \beta_3 & 0 \\ 0 & \gamma_1 & 0 & \gamma_2 & 0 & \gamma_3 \\ \gamma_1 & \beta_1 & \gamma_2 & \beta_2 & \gamma_3 & \beta_3 \end{bmatrix} \quad (10.10.6)$$

Finally, the element stiffness matrix is given by (10.4.11)

$$\underline{K}^e = \int_{V_e} \underline{B}_e^T \underline{E}_e \underline{B}_e dV = t^e a^e \underline{B}_e^T \underline{E}_e \underline{B}_e \quad (10.10.7)$$

where t^e is the thickness of element e , which equals 1 for a plane strain model. The plane strain P_ε and plane stress P_σ constitutive matrices \underline{E}_e are defined in (10.2.10) and (10.3.10) as

$$P_\varepsilon : \underline{E}_e = \frac{E}{(1+\nu)(1-2\nu)} \begin{bmatrix} 1-\nu & \nu & 0 \\ \nu & 1-\nu & 0 \\ 0 & 0 & \frac{1-2\nu}{2} \end{bmatrix}, \quad P_\sigma : \underline{E}_e = \frac{E}{1-\nu^2} \begin{bmatrix} 1 & \nu & 0 \\ \nu & 1 & 0 \\ 0 & 0 & \frac{1-\nu}{2} \end{bmatrix} \quad (10.10.8)$$

10.10.2 Element Mass Matrix

The element mass matrix is defined in (10.4.29) as

$$\underline{M}^e = \int_{V_e} \rho \underline{N}^T \underline{N} dV = \int_{a^e} \rho \underline{N}^T \underline{N} t da^e \quad (10.10.9)$$

Substitute (10.10.1) and (10.10.2) into (10.10.9), and assume the density and thickness are constants within the element to obtain:

$$\underline{M}^e = \int_{V^e} \rho \underline{N}^T \underline{N} dV = \rho t \int_{a^e} \begin{bmatrix} \psi_1^2 & 0 & \psi_1 \psi_2 & 0 & \psi_1 \psi_3 & 0 \\ 0 & \psi_1^2 & 0 & \psi_1 \psi_2 & 0 & \psi_1 \psi_3 \\ \psi_1 \psi_2 & 0 & \psi_2^2 & 0 & \psi_2 \psi_3 & 0 \\ 0 & \psi_1 \psi_2 & 0 & \psi_2^2 & 0 & \psi_2 \psi_3 \\ \psi_1 \psi_3 & 0 & \psi_2 \psi_3 & 0 & \psi_3^2 & 0 \\ 0 & \psi_1 \psi_3 & 0 & \psi_2 \psi_3 & 0 & \psi_3^2 \end{bmatrix} da^e \quad (10.10.10)$$

A general integration formula for “simplex” shape functions (10.10.3) taken over the triangular element area may be found in (Huebner et al., 1994)

$$\int_{a^e} \psi_1^i \psi_2^j \psi_3^k da^e = \frac{(i!)(j!)(k!)}{(i+j+k+2)!} * 2a^e \quad (10.10.11)$$

where ! indicates the factorial operation. Utilizing (10.10.11) to evaluate (10.10.10) yields

$$\underline{M}^e = \frac{\rho t a^e}{12} \begin{bmatrix} 2 & 0 & 1 & 0 & 1 & 0 \\ 0 & 2 & 0 & 1 & 0 & 1 \\ 1 & 0 & 2 & 0 & 1 & 0 \\ 0 & 1 & 0 & 2 & 0 & 1 \\ 1 & 0 & 1 & 0 & 2 & 0 \\ 0 & 1 & 0 & 1 & 0 & 2 \end{bmatrix} \quad (10.10.12)$$

An alternative lumped-mass approach consists simply of lumping one-third of the entire mass of the element at each node, yielding

$$\underline{M}^e = \frac{\rho t a^e}{3} \begin{bmatrix} 1 & 0 & 0 & 0 & 0 & 0 \\ 0 & 1 & 0 & 0 & 0 & 0 \\ 0 & 0 & 1 & 0 & 0 & 0 \\ 0 & 0 & 0 & 1 & 0 & 0 \\ 0 & 0 & 0 & 0 & 1 & 0 \\ 0 & 0 & 0 & 0 & 0 & 1 \end{bmatrix} \quad (10.10.13)$$

10.10.3 System Matrix Assembly

The element mass and stiffness matrices for the 3 node, 2 dof per node, triangle elements are both 6 by 6. Therefore, the assembly procedure to obtain \underline{M}_f and \underline{K}_f is identical to that shown in Figure 10.5.2 with the indices spanning the ranges

$$e = 1, 2, \dots, E \text{ (no. of elements)}, \quad r = 1, \dots, 6, \quad s = 1, \dots, 6 \quad (10.10.14)$$

The modes and natural frequencies are then obtained using the MATLAB eig command:

```
[modalmatrix, otemp] = eig(Kf,Mf) ;
omegasquared = diag(otemp) ;
omega =real(sqrt(omegasquared)) ;
natfreq = omega/2/pi;
```

EXAMPLE 10.10.1 *Use of 3-Node Triangle, Plane Strain Elements to Obtain the Natural Frequencies and Mode Shapes of a Simply Supported Beam*

Statement: The system in Example 10.8.1 is resolved using 3-node triangle, plane strain elements. The identical, simply supported boundary conditions are applied and the material properties and dimensions are also the same as in Example 10.8.1. Natural frequencies and mode shapes are obtained first by using an equally spaced mesh and then by using the MATLAB MESH2D code to generate the mesh. The mass and stiffness matrices are obtained as outlined in this section for both approaches.

Solution: The equally spaced parameterized mesh pattern for this problem is shown in Figure E10.10.1(a).

The coding logic for defining the element connectivity matrix B is shown below.

```
for i = 1 : 1 : N-1
    for j = 1 : 1 : M-1
        e = 2*(i-1)*(M-1) + 2*j - 1    element number for odd elements
        B(e,1) = M*(i-1) + j
        B(e,2) = B(e,1) + M
        B(e,3) = B(e,1) + 1
        e = e + 1    element number for even elements
        B(e,1) = i*M + j
        B(e,2) = B(e,1) + 1
        B(e,3) = B(e,2) - M
    end
end
```

(1)

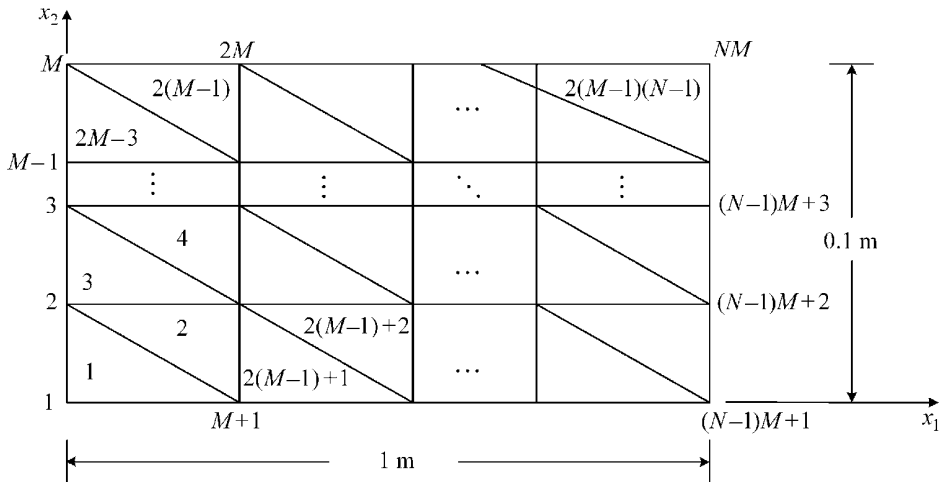


Figure E10.10.1(a) Parametric mesh pattern for 3-node triangle meshed simply supported beam

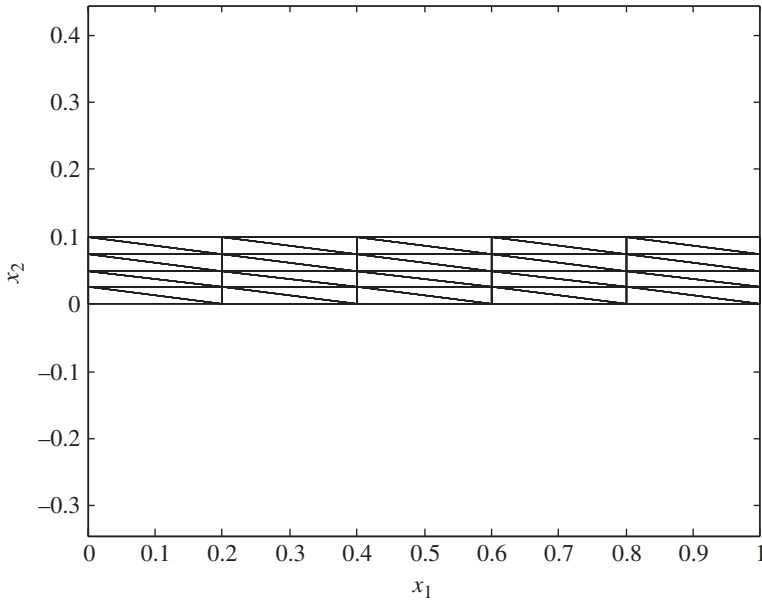


Figure E10.10.1(b) Mesh pattern for $M = 5$ and $N = 6$

Table E10.10.1(a) Natural frequency (in Hertz) versus mesh refinement parameters M and N

M	N	Consistent mass model				Lumped mass model			
		First	Second	Third	Fourth	First	Second	Third	Fourth
5	6	560	1335	2152	4192	542	1325	1888	3450
11	12	333	1278	1297	2720	331	1244	1295	2559
21	22	269	1031	1259	2179	269	1024	1258	2142
31	32	255	973	1234	2049	255	970	1234	2034

The fixed degrees of freedom dof for the simply supported boundary condition are

$$\begin{aligned}
 &\text{At } x_1 = 0, x_2 = 0.1/2 = 0.05 \text{ dof: } M \text{ and dof: } M + 1 \\
 &\text{At } x_1 = 1, x_2 = 0.1/2 = 0.05 \text{ dof: } 2 * (N - 1) * M + M + 1
 \end{aligned} \tag{2}$$

Figure E10.10.1(b) shows the mesh pattern for the case $M = 5$ and $N = 6$.

Table E10.10.1(a) provides a comparison of the four lowest natural frequencies as the mesh density is increased, utilizing consistent mass (10.10.12) and lumped mass (10.10.13) models.

The results show convergence of the natural frequencies as the mesh is further refined and the close agreement between the lumped mass and consistent mass approaches. By comparison from Table E10.8.1(a), the 4-node isoparametric element prediction was (242, 923, 1188, 1942), and the Timoshenko beam model prediction was (231, 883, 1294, 1862) for the 4 lowest modes. Figure E10.10.1(c) shows the corresponding mode shapes for the case $M = 21$, $N = 22$. Mode 3 is clearly an axial mode.

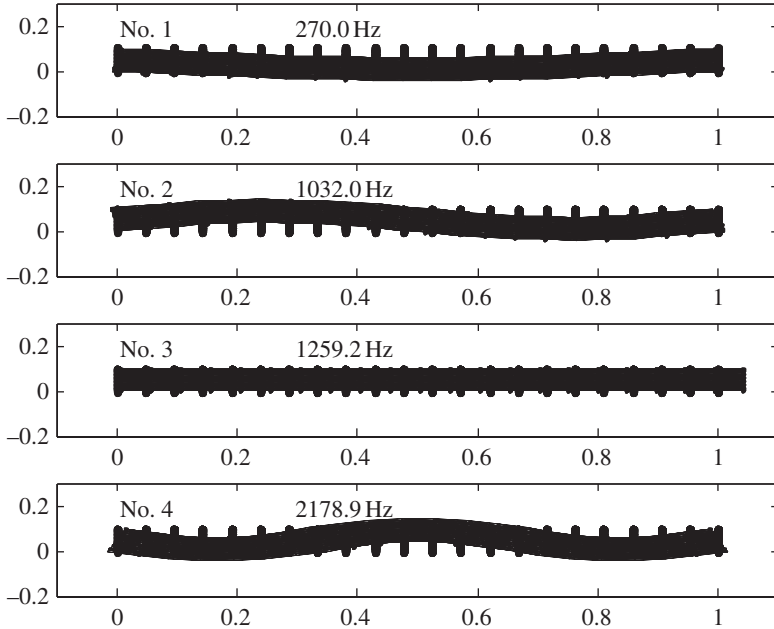


Figure E10.10.1(c) Mode shapes for the 4 lowest modes

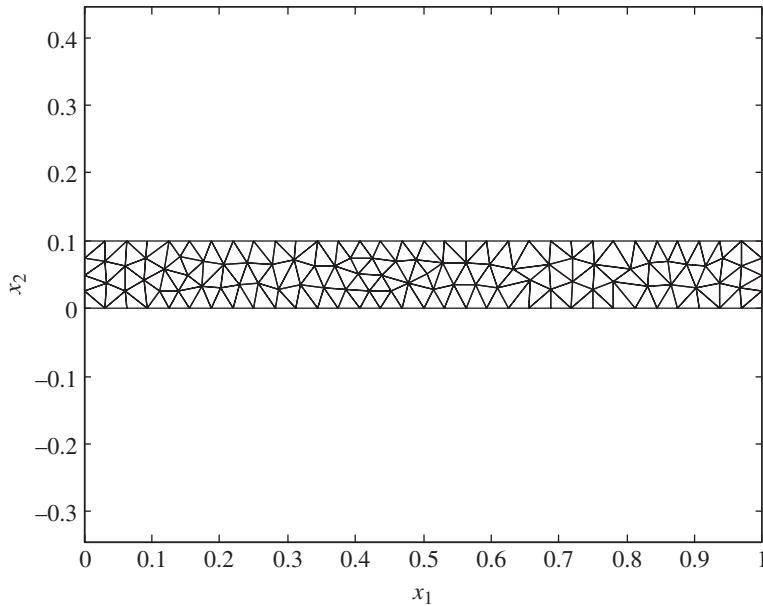


Figure E10.10.1(d) MESH2D-generated mesh for $h_{\max} = 0.03$ m

MESH2D provides a mesh refinement capability that keeps the max triangle dimension below a user-defined upper limit h_{\max} . Figure E10.10.1(d) shows the mesh produced by MESH2D for $h_{\max} = 0.03$ m. The keypoints input into MESH2D for this domain are the corner points

$$\text{KP1} = (0, 0), \text{KP2} = (1.0, 0.0), \text{KP3} = (1.0, 0.10), \text{KP4} = (0.0, 0.1) \quad (3)$$

The following domain boundary, keypoint connection pairs are also input:

$$\text{KP1 to KP2, KP2 to KP3, KP3 to KP4, KP4 to KP1} \quad (4)$$

The mesh generated consists of 198 elements with 136 nodes. The nodes with fixed dofs are obtained by searching for those nearest to the actual simple support point locations: (0, 0.05) and (1.0, 0.05). The former has x_1 and x_2 constraints, and the latter has an x_2 constraint.

Figure E10.10.1(e) shows the mode shapes and natural frequencies for the mesh in Figure E10.10.1(d).

Decreasing the mesh refinement parameter to $h_{\max} = 0.02$ m yields the mesh shown in Figure E10.10.1(f), with 772 elements, 459 nodes, and the 4 lowest natural frequencies:

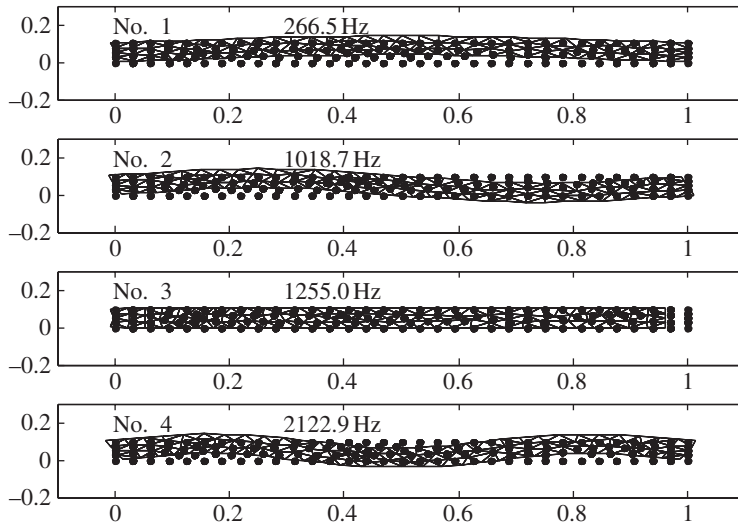


Figure E10.10.1(e) Modes and natural frequencies for mesh in Figure E10.10.1(d)

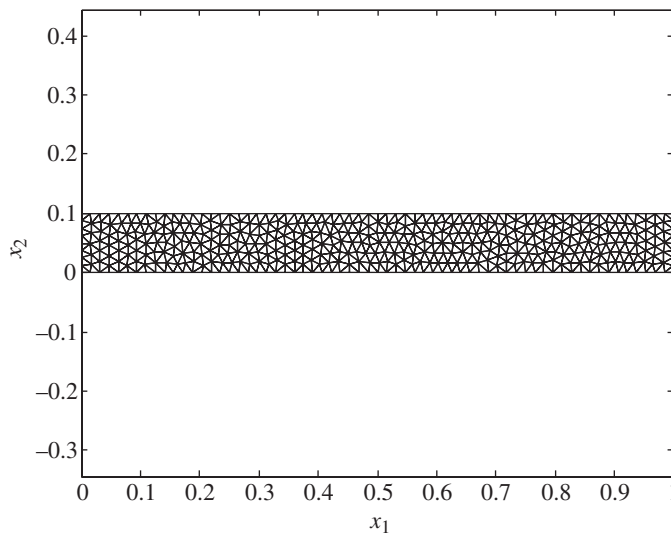


Figure E10.10.1(f) MESH2D-generated mesh for $h_{\max} = 0.02$ m

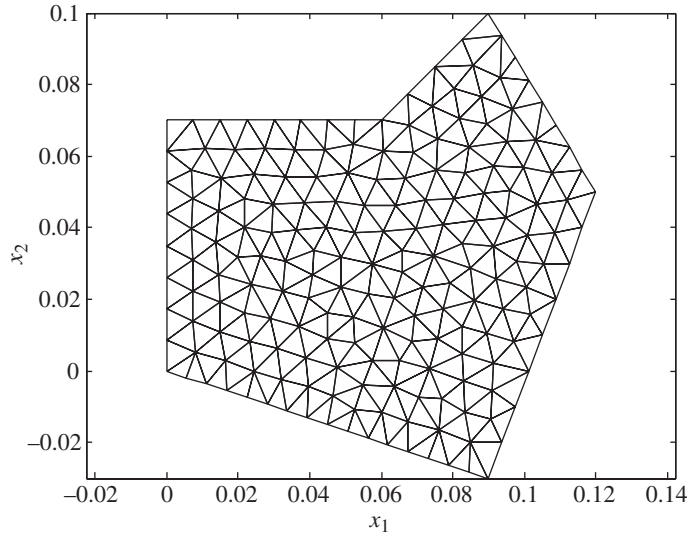


Figure E10.10.1(g) MESH2D-generated mesh for domain with 6 vertices and $h_{\max} = 0.01$ m

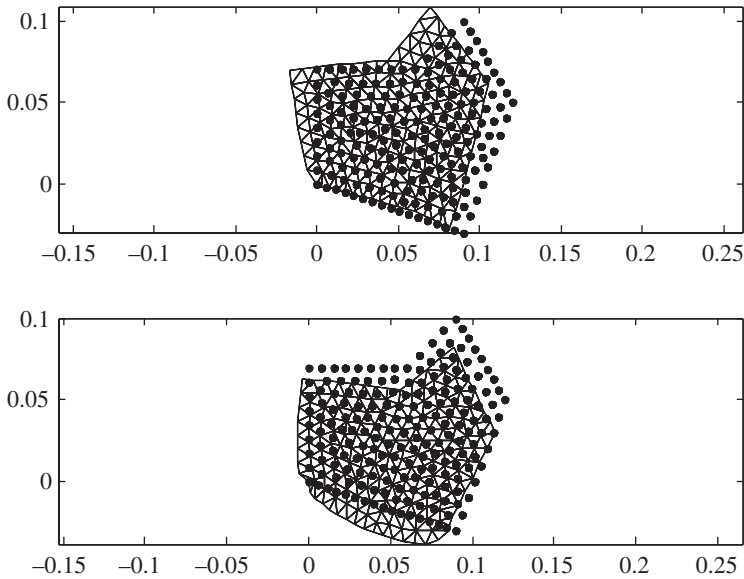


Figure E10.10.1(h) First mode at 4157 Hz (top) and second mode at 6816 Hz (bottom) for mesh in Figure E10.10.1(g)

(248, 944, 1226, 1980) Hz. These frequencies are very similar to those listed in Table E10.10.1(a).

Figure E10.10.1(g) demonstrates the powerful capability of MESH2D for generating a mesh for a more general domain with six vertices (keypoints) and $h_{\max} = 0.01$ m. This plane strain model has the same material properties as the previous simply supported beam.

The lower left vertex has both dofs fixed and the lower middle vertex has only its vertical dof fixed. The lowest 2 mode shapes and natural frequencies are shown in Figure E10.10.1(h).

10.11 MEMBRANES

Membranes are thin, drum skin-like members that are unable to resist bending moments and in-plane shear force, and therefore only possess in-plane tensile, internal loads. Figure 10.11.1(a) shows a membrane that has both free and fixed boundary conditions. The free-body diagram of a differential piece of the membrane is shown in Figure 10.11.1(b), with a cross-sectional cut through the piece shown in Figure 10.11.1(c). The two types of boundary conditions for the membrane are:

1. Fixed edge: $w(x, t) = 0$ on some portion of the boundary Γ .
2. Free edge: $T \frac{\partial w}{\partial n} = 0 \Rightarrow \frac{\partial w}{\partial n} = \vec{\nabla}(w) \cdot \hat{n} = 0$ on some portion of the boundary Γ .

One may note that the membrane is a 2-dimensional form of the string problem as shown in Figure 5.5.1.

The membrane is initially stretched to obtain the tensions per unit length, T_x and T_y , which are assumed to be time invariant. The transverse deflection $w(x, t)$ is assumed to be very small relative to the overall dimensions of the membrane.

10.11.1 Kinetic Energy and Element Mass Matrix

The area density $\hat{\rho}$ of the membrane is defined by

$$\hat{\rho} = \text{mass per unit area} = \frac{m_m}{A_m} = \frac{\rho V_m}{A_m} = \frac{\rho A_m d}{A_m} = \rho d, \Rightarrow dm = \hat{\rho} dx dy \quad (10.11.1)$$

where A_m , ρ , and d are the area, density, and thickness of the membrane. The kinetic energy of the membrane is

$$T = \frac{1}{2} \int_{A_m} \dot{w}^2 dm = \frac{1}{2} \int_{A_m} \dot{w}^2 \hat{\rho} dx dy = \sum_{e=1}^E \frac{1}{2} \int_{a_e} \dot{w}^2 \hat{\rho}_e dx dy \quad (10.11.2)$$

where a_e is the area of the e th element as depicted in Figure 10.4.2, and E is the total number of elements in the model. For illustration, assume that the membrane area is meshed into E 4-node, isoparametric, quadrilateral elements as shown in Figures 10.4.1 and 10.4.2. The transverse displacement is interpolated as (10.4.1)

$$w = \sum_{k=1}^4 N_k(\xi_1, \xi_2) w_k^{(e)} = \underline{N} \underline{q}^e \Rightarrow \dot{w} = \sum_{k=1}^4 N_k(\xi_1, \xi_2) \dot{w}_k^{(e)} = \underline{N} \dot{\underline{q}}^e = (\dot{\underline{q}}^e)^T \underline{N}^T \quad (10.11.3)$$

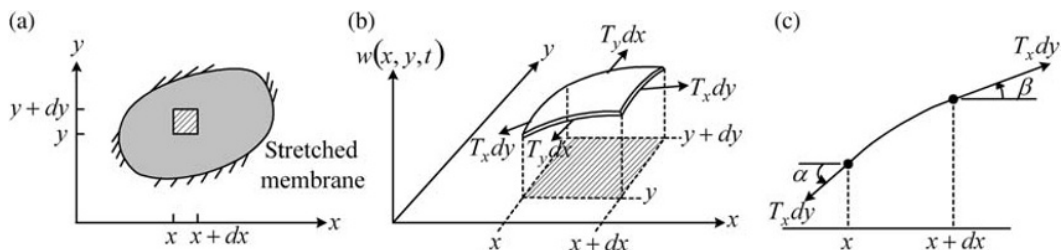


Figure 10.11.1 (a) Stretched membrane and its (b) differential element and (c) free-body diagram

where the element's nodal displacement vector and shape function matrix are

$$\underline{q}^e = (w_1^e \ w_2^e \ w_3^e \ w_4^e)^T, \quad \underline{N} = (N_1 \ N_1 \ N_1 \ N_1) \quad (10.11.4)$$

The individual shape functions are defined in (10.4.2). The kinetic energy of the e th element may then be written as

$$T_e = \frac{1}{2} \int_{a_e} \dot{w}^2 \hat{\rho}_e \, dx dy = \frac{1}{2} \int_{a_e} \hat{\rho}_e \left(\dot{q}_e \right)^T \underline{N}^T \underline{N} \dot{q}_e \, dx dy = \frac{1}{2} \left(\dot{q}_e \right)^T \underline{M}_e \dot{q}_e \quad (10.11.5)$$

where the element mass matrix is given by

$$\underline{M}_e = \int_{a_e} \hat{\rho}_e \underline{N}^T \underline{N} \, dx dy \quad (10.11.6)$$

or in scalar form

$$m_{ij}^e = \int_{a_e} \hat{\rho}_e N_i N_j \, dx dy \quad (10.11.7)$$

Similar to (10.4.30) and (10.4.31), transforming the integral to natural coordinates and use of GQ yields

$$\underline{M}_e = \int_{-1}^1 \int_{-1}^1 \hat{\rho}_e \underline{N}^T \underline{N} \det(\underline{J}_e) \, d\xi_1 \, d\xi_2 \quad (10.11.8)$$

$$\underline{M}_e \approx \sum_{s=1}^{n_G} \sum_{t=1}^{n_G} \bar{w}_s \bar{w}_t \hat{\rho}_e(\xi_{1s}, \xi_{2t}) \underline{N}^T(\xi_{1s}, \xi_{2t}) \underline{N}(\xi_{1s}, \xi_{2t}) \det(\underline{J}_e(\xi_{1s}, \xi_{2t})) \quad (10.11.9)$$

where the sums extend over the Gauss points in Table 10.4.1.

10.11.2 Strain Potential Energy and Element Stiffness Matrix

Similar to Example 4.6.5, the second-order strains corresponding to transverse vibration of the tensioned membranes are

$$\varepsilon_x = \frac{1}{2} \left(\frac{dw}{dx} \right)^2, \quad \varepsilon_y = \frac{1}{2} \left(\frac{dw}{dy} \right)^2 \quad (10.11.10)$$

and the strain energy is

$$\begin{aligned} U_e &= \int_{V_e} (\sigma_x \varepsilon_x + \sigma_y \varepsilon_y) \, dV = \int_{V_e} (\sigma_x \varepsilon_x + \sigma_y \varepsilon_y) \, dV = \int_{a_e} \left(\frac{F_x}{A_x} \varepsilon_x + \frac{F_y}{A_y} \varepsilon_y \right) d^* dx dy \\ &= \int_{a_e} \left(\frac{T_x dy}{d^* dy} \varepsilon_x + \frac{T_y dx}{d^* dx} \varepsilon_y \right) d^* dx dy = \int_{a_e} (T_x \varepsilon_x + T_y \varepsilon_y) \, dx dy \\ &= \frac{1}{2} \int_{a_e} \left(T_x \left(\frac{dw}{dx} \right)^2 + T_y \left(\frac{dw}{dy} \right)^2 \right) \, dx dy \end{aligned} \quad (10.11.11)$$

Substitution of the interpolated form of $w(x, y)$, Equation (10.11.3), into (10.11.11) yields

$$U_e = \frac{1}{2} \int_{a_e} \left(T_x(\underline{q}_e)^T \frac{\partial N^T}{\partial x} \frac{\partial N}{\partial x} \underline{q}_e + T_y(\underline{q}_e)^T \frac{\partial N^T}{\partial y} \frac{\partial N}{\partial y} \underline{q}_e \right) dx dy = \frac{1}{2} (\underline{q}_e)^T \underline{K}^e \underline{q}_e \quad (10.11.12)$$

where the element stiffness matrix is identified as

$$\underline{K}^e = \int_{a_e} \left(T_x \frac{\partial N^T}{\partial x} \frac{\partial N}{\partial x} + T_y \frac{\partial N^T}{\partial y} \frac{\partial N}{\partial y} \right) dx dy \quad (10.11.13)$$

or in scalar form,

$$k_{ij}^e = \int_{a_e} \left(T_x \frac{\partial N_i}{\partial x} \frac{\partial N_j}{\partial x} + T_y \frac{\partial N_i}{\partial y} \frac{\partial N_j}{\partial y} \right) dx dy \quad (10.11.14)$$

Note from (10.4.16),

$$\left\{ \begin{array}{c} \frac{\partial N}{\partial x} \\ \frac{\partial N}{\partial y} \end{array} \right\} = \begin{bmatrix} J_{11}^* & J_{12}^* \\ J_{21}^* & J_{22}^* \end{bmatrix} \left\{ \begin{array}{c} \frac{\partial N}{\partial \xi_1} \\ \frac{\partial N}{\partial \xi_2} \end{array} \right\}, \quad \text{where} \quad \begin{bmatrix} J_{11}^* & J_{12}^* \\ J_{21}^* & J_{22}^* \end{bmatrix} = \underline{J}^{-1}_{2 \times 2} \quad (10.11.15)$$

Substitute (10.11.15) into (10.11.14) to obtain

$$k_{ij}^e = \int_{-1}^1 \int_{-1}^1 \left[T_x \left(J_{11}^* \frac{\partial N_i}{\partial \xi_1} + J_{12}^* \frac{\partial N_i}{\partial \xi_2} \right) \left(J_{11}^* \frac{\partial N_j}{\partial \xi_1} + J_{12}^* \frac{\partial N_j}{\partial \xi_2} \right) + T_y \left(J_{21}^* \frac{\partial N_i}{\partial \xi_1} + J_{22}^* \frac{\partial N_i}{\partial \xi_2} \right) \left(J_{21}^* \frac{\partial N_j}{\partial \xi_1} + J_{22}^* \frac{\partial N_j}{\partial \xi_2} \right) \right] \det(J) d\xi_1 d\xi_2 \quad (10.11.16)$$

Application of GQ to perform the integrations yields

$$k_{ij}^e = \sum_{s=1}^{n_G} \sum_{t=1}^{n_G} \bar{w}_s \bar{w}_t \left[T_x \left(J_{11}^*(\xi_{1s}, \xi_{2t}) \frac{\partial N_i}{\partial \xi_1}(\xi_{1s}, \xi_{2t}) + J_{12}^*(\xi_{1s}, \xi_{2t}) \frac{\partial N_i}{\partial \xi_2}(\xi_{1s}, \xi_{2t}) \right) * \left(J_{11}^*(\xi_{1s}, \xi_{2t}) \frac{\partial N_j}{\partial \xi_1}(\xi_{1s}, \xi_{2t}) + J_{12}^*(\xi_{1s}, \xi_{2t}) \frac{\partial N_j}{\partial \xi_2}(\xi_{1s}, \xi_{2t}) \right) + T_y \left(J_{21}^*(\xi_{1s}, \xi_{2t}) \frac{\partial N_i}{\partial \xi_1}(\xi_{1s}, \xi_{2t}) + J_{22}^*(\xi_{1s}, \xi_{2t}) \frac{\partial N_i}{\partial \xi_2}(\xi_{1s}, \xi_{2t}) \right) * \left(J_{21}^*(\xi_{1s}, \xi_{2t}) \frac{\partial N_j}{\partial \xi_1}(\xi_{1s}, \xi_{2t}) + J_{22}^*(\xi_{1s}, \xi_{2t}) \frac{\partial N_j}{\partial \xi_2}(\xi_{1s}, \xi_{2t}) \right) \right] \det(J(\xi_{1s}, \xi_{2t})) \quad (10.11.17)$$

where the sums extend over the Gauss points in Table 10.4.1.

10.11.3 Matrix Assembly

The membrane has only one degree of freedom (dof) per node, similar to the one-dimensional truss element in Section 4.8. Thus, similar to Figure 4.8.8, assembly of

the condensed form of the mass and stiffness matrices can be achieved with just the nodal connectivity array \underline{B} and the $larray$. This is depicted in Figure 10.11.2. Recall from (4.8.21) the “nodal connectivity array” is defined as

$$\underline{B}_{ej} = \text{“global” node number for local node } j \text{ of element } e \quad (10.11.18)$$

$$e = 1, 2, \dots, E, \quad j = 1, 2, 3, 4$$

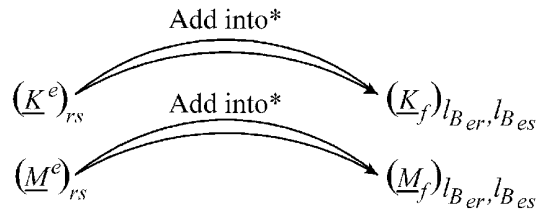
Recall from (4.8.35) the “ l ” array indicates the locations of each free (unconstrained) node in the vector \underline{q}_f of only free (unconstrained) node displacements.

The forced response of the membrane is obtained by solving (4.8.36), which is repeated here as

$$\underset{N_f \times N_f}{\underline{M}_f} \ddot{\underline{q}}_f + \underset{N_f \times N_f}{\underline{C}_f} \dot{\underline{q}}_f + \underset{N_f \times N_f}{\underline{K}_f} \underline{q}_f = \underset{N_f \times 1}{\underline{F}_f} \quad (10.11.19)$$

EXAMPLE 10.11.1 Natural Frequencies and Mode Shapes of a Square Membrane

Objective: The objective is to utilize isoparametric, 4-node, quadrilateral elements to determine the 5 lowest natural frequencies and plot the corresponding mode shapes of the square membrane with fixed edges shown in Figure E10.11.1(a). The finite element results will then be compared with the results from an analytical approach (exact solution). The analytical approach is the solution of Exercise 5.44.



for $e = 1, 2, \dots, E$ (no. of elements)
 $r = 1, 2, 3, 4$ (no. of nodes per element)
 $s = 1, 2, 3, 4$ (no. of node per element)

Figure 10.11.2 Assembly of the condensed form of the system stiffness and mass matrices

*Add into if and only if $l_{B_{er}} \neq 0$ and $l_{B_{es}} \neq 0$

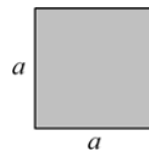


Figure E10.11.1(a) Square membrane with fixed edges of length “ a ”

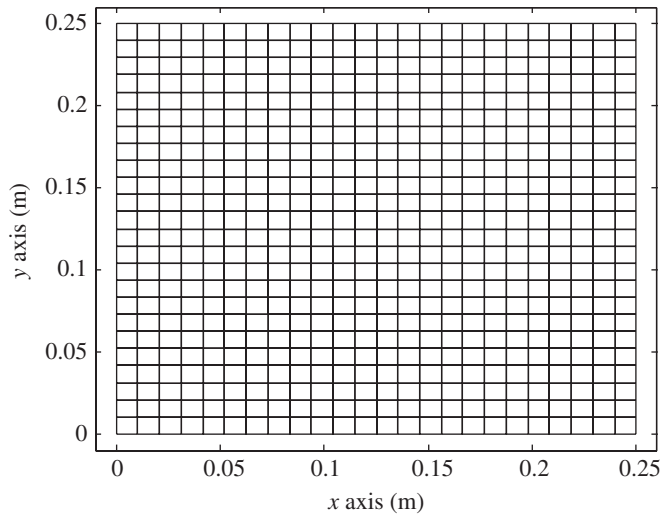


Figure E10.11.1(b) Finite element model mesh for the square membrane

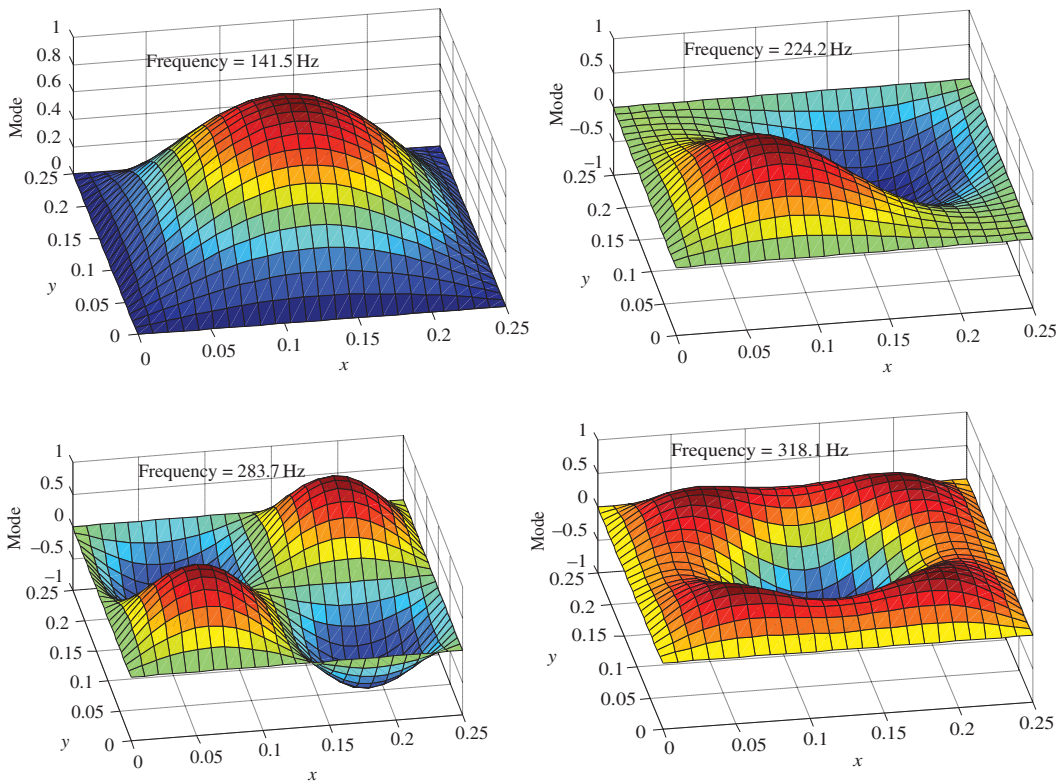


Figure E10.11.1(c) Finite element model mode shapes for the 4 lowest modes

Parameter Values

$$\rho = 20 \text{ kg/m}^3, \quad d = 0.001 \text{ m}, \quad a = 0.25 \text{ m}, \quad T_x = T_y = 50 \text{ N/m}$$

Mesh Plot: Figure E10.11.1(b) shows the a 25×25 square element mesh for the membrane model.

Table E10.11.1(a) Comparison of finite element and analytical membrane natural frequencies

Method	Mode 1	Mode 2	Mode 3	Mode 4	Mode 5
Analytical	141.4 Hz	223.6 Hz	282.8 Hz	316.2 Hz	360.55 Hz
FE: 15 × 15	141.7	225.2	285.2	321.7	366.2
FE: 25 × 25	141.5	224.2	283.7	318.1	362.5

Results: Figure E10.11.1(c) shows the modes and natural frequencies for the 4 lowest modes. Table E10.11.1(a) shows that the natural frequencies are very close to their analytical counterparts for the two meshes examined.

10.12 BANDED STORAGE

The examples and results in this chapter demonstrate that the number of degrees of freedom in a detailed, high-fidelity, finite element model may become very large and in some cases 10s, if not 100s, of thousands of degrees of freedom. Computation time reduction may become a top priority, especially if design variables are being searched for an optimal design, requiring many simulations with the model. In some models, judicious node numbering of a finite element mesh may result in the stiffness and mass matrices having a “banded” structure as illustrated in (10.12.1). This matrix structure may facilitate a more economical solution.

$$\underline{A} = \begin{bmatrix} X & x & x & 0 & 0 & 0 & 0 & 0 & 0 & \dots & \dots & 0 & 0 & 0 \\ x & X & x & x & 0 & 0 & 0 & 0 & 0 & \dots & \dots & 0 & 0 & 0 \\ x & x & X & x & x & 0 & 0 & 0 & 0 & \dots & \dots & 0 & 0 & 0 \\ 0 & x & x & X & x & x & 0 & 0 & 0 & \dots & \dots & 0 & 0 & 0 \\ 0 & 0 & x & x & X & x & x & 0 & 0 & \dots & \dots & 0 & 0 & 0 \\ 0 & 0 & 0 & x & x & X & x & x & 0 & \dots & \dots & 0 & 0 & 0 \\ 0 & 0 & 0 & 0 & x & x & X & x & x & \dots & \dots & 0 & 0 & 0 \\ \cdot & \cdot & \cdot & \cdot & \cdot & \cdot & \cdot & \cdot & \cdot & \cdot & \cdot & \cdot & \cdot & \cdot \\ \cdot & \cdot & \cdot & \cdot & \cdot & \cdot & \cdot & \cdot & \cdot & \cdot & \cdot & \cdot & \cdot & \cdot \\ \cdot & \cdot & \cdot & \cdot & \cdot & \cdot & \cdot & \cdot & \cdot & \cdot & \cdot & \cdot & \cdot & \cdot \\ 0 & 0 & 0 & 0 & 0 & 0 & \dots & \dots & x & x & X & x & x & 0 \\ 0 & 0 & 0 & 0 & 0 & 0 & \dots & \dots & 0 & x & x & X & x & x \\ 0 & 0 & 0 & 0 & 0 & 0 & \dots & \dots & 0 & 0 & x & x & X & x \\ 0 & 0 & 0 & 0 & 0 & 0 & \dots & \dots & 0 & 0 & 0 & x & x & X \end{bmatrix} \quad (10.12.1)$$

The matrix \underline{A} typically represents \underline{M} or \underline{K} but could also represent the complex coefficient matrix used to obtain steady-state harmonic response in (7.5.5)

$$\left(-\omega^2 \frac{\underline{M}}{N \times N} + i\omega \frac{\underline{C}_T}{N \times N} + \frac{\underline{K}_T}{N \times N} \right) \frac{\tilde{\underline{Q}}}{N \times 1} = \frac{\tilde{\underline{F}}}{N \times 1} \quad (10.12.2)$$

The structure of only null diagonals above a certain upper or below a certain lower diagonal in these matrices allows for a significantly faster solution for natural frequencies

(Chapter 5), transient response (Chapter 6), and steady-state harmonic response (Chapter 7). The banded character of a Hermitian matrix ($\underline{A} = \text{complex conjugate transpose of } \underline{A}$) is quantified by

$$\begin{aligned} h &= \text{semibandwidth of } \underline{A} \\ &= \text{highest nonnull upper diagonal of } \underline{A} \text{ (including the main diagonal)} \end{aligned} \quad (10.12.3)$$

Franklin (1968, p.211) shows that the total number of multiplications required to solve an N th order set of linear equations with a Hermitian coefficient matrix and semibandwidth h is

$$\mu = \frac{1}{6}(h-1)[3(h+2)N - 2h(h+1)] + (2h-1)N - h(h-1) \quad (10.12.4)$$

with the number of additions and subtractions substantially the same. To illustrate, suppose that $N = 100$, then the number of multiplications for several values of h become

h	10	20	40	100
μ	6880	21 760	66 920	175 600

This result illustrates that banded solvers may provide a significant reduction in operations and hence computation time. An easily programmable means to determine h is with the equation

$$h = \max(j-i+1) \text{ for which } A_{ij} \neq 0, \quad i=1, N, \quad j=1, N \quad (10.12.5)$$

Applying (10.12.5) to the matrix in (10.12.1) yields $h = 3$. The shortcoming of this formula is it requires that the matrix \underline{A} be assembled in full storage form as depicted in (10.12.1). This may require significant computer memory for storage and further increase computation time. Clearly from (10.12.1), there is only a need to store the main and upper nonnull diagonals resulting in significantly less storage memory. Reflection on Figure 10.12.1 (from Figure 10.5.2) reveals a means to determine h from the element connectivities and the *larray* prior to assembly.

The required formulas are

$$\text{Unconstrained structure: } h = \max(\hat{B}_{es} - \hat{B}_{er} + 1), \quad e=1, \dots, E, \quad r=1, \dots, N_{de}, \quad s=1, \dots, N_{de} \quad (10.12.6)$$

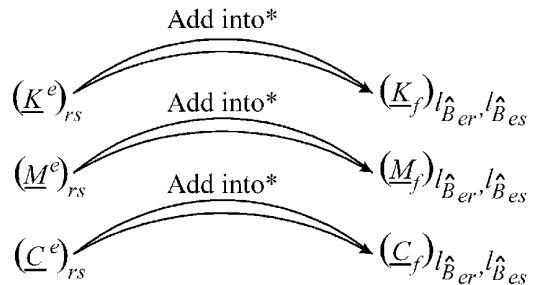


Figure 10.12.1 System matrix assembly from element matrices

*Add into if, and only if $l_{\hat{B}_{er}} \neq 0$ and $l_{\hat{B}_{es}} \neq 0$

Constrained structure: $h_f = \max(l_{\hat{B}_{es}} - l_{\hat{B}_{er}} + 1)$, $e = 1, \dots, E$, $r = 1, \dots, N_{de}$, $s = 1, \dots, N_{de}$
 (do not include terms in the maximum search for which either
 $l_{\hat{B}_{er}}$ or $l_{\hat{B}_{es}}$ are zero) (10.12.7)

where E is the total number of elements in the model, N_{de} is the number of degrees of freedom in element e , l represents the *larray* in (10.5.15), and \hat{B} is the dof connectivity array in (10.5.4).

These formulas permit the semibandwidth to be determined at the element level prior to assembly of the system matrices. This is required to assemble the element matrices directly into the banded storage form of the system matrices, as will be shown below.

The example in (10.12.8) and (10.12.9) illustrates a common approach for the banded storage form.

Full storage:

$$\underline{A} = \begin{bmatrix} A_{11} & A_{12} & A_{13} & 0 & 0 & 0 \\ & A_{22} & A_{23} & A_{24} & 0 & 0 \\ & & A_{33} & A_{34} & A_{35} & 0 \\ & & & A_{44} & A_{45} & A_{46} \\ \text{symmetric} & & & & A_{55} & A_{56} \\ & & & & & A_{66} \end{bmatrix} \quad (10.12.8)$$

Banded storage:

$$\underline{A}_B = \begin{bmatrix} A_{B11} & A_{B12} & A_{B13} \\ A_{B21} & A_{B22} & A_{B23} \\ A_{B31} & A_{B32} & A_{B33} \\ A_{B41} & A_{B42} & A_{B43} \\ A_{B51} & A_{B52} & A_{B53} \\ A_{B61} & A_{B62} & A_{B63} \end{bmatrix} = \begin{bmatrix} A_{11} & A_{12} & A_{13} \\ A_{22} & A_{23} & A_{24} \\ A_{33} & A_{34} & A_{35} \\ A_{44} & A_{45} & A_{46} \\ A_{55} & A_{56} & 0 \\ A_{66} & 0 & 0 \end{bmatrix} \quad (10.12.9)$$

In this approach, the main diagonal of the N by N matrix \underline{A} is stored as the first column of the N by h_f matrix \underline{A}_B , the first upper diagonal of \underline{A} is stored as the second column of \underline{A}_B , the second upper diagonal of \underline{A} is stored as the third column of \underline{A}_B , and so on. The entries in matrix \underline{A} may be transferred into the banded storage matrix \underline{A}_B with the following rules:

- $(A_B)_{m, n-m+1} = A_{mn}$ $m = 1, 2, \dots, N$ $n = 1, 2, \dots, N$
 - If $n < m$, do not add A_{mn} into \underline{A}_B (only store upper triangle and main diagonal
 since \underline{A} is symmetric)
 - If $n > (m + h - 1)$, do not add A_{mn} into \underline{A}_B (do not store zeros outside of the bandwidth)
- (10.12.10)

Combining these rules with the procedure shown in Figure 10.12.1 yields the means to assemble the banded storage form of the constraint condensed, system mass or stiffness

matrix (\underline{K}_f or \underline{M}_f) directly from the element matrices (\underline{K}^e or \underline{M}^e) according to the following rules:

$$\begin{aligned} \left(\underline{K}_f\right)_{l_{\hat{B}_{er}}, l_{\hat{B}_{es}}-l_{\hat{B}_{er}}+1} &= \left(\underline{K}_f\right)_{l_{\hat{B}_{er}}, l_{\hat{B}_{es}}-l_{\hat{B}_{er}}+1} + \left(\underline{K}^e\right)_{rs} \\ \left(\underline{M}_f\right)_{l_{\hat{B}_{er}}, l_{\hat{B}_{es}}-l_{\hat{B}_{er}}+1} &= \left(\underline{M}_f\right)_{l_{\hat{B}_{er}}, l_{\hat{B}_{es}}-l_{\hat{B}_{er}}+1} + \left(\underline{M}^e\right)_{rs} \end{aligned} \quad (10.12.11)$$

Perform the sums in (10.12.11) if all of the following conditions are satisfied:

$$l_{\hat{B}_{er}} \neq 0, \quad l_{\hat{B}_{es}} \neq 0, \quad l_{\hat{B}_{es}} \geq l_{\hat{B}_{er}}, \quad l_{\hat{B}_{es}} \leq \left(l_{\hat{B}_{er}} + h_f - 1\right) \quad (10.12.12)$$

where the semibandwidth h_f of the constraint condensed system matrices is obtained in (10.12.7). The indices in these equations range as follows: e varies from 1 to the total number of elements in the model, and r and s range from 1 to the number of degrees of freedom dof in element e .

EXAMPLE 10.12.1 *Steady-State Harmonic Response of the Simply Supported Beam in Example 10.8.1 Utilizing Banded Storage and Solver*

Statement: This example utilizes the simply supported beam in Example 10.8.1 to illustrate the use of plane strain FE models for steady-state forced harmonic response prediction and to illustrate programming of the above algorithms for banded storage.

Parameter Values: The Young's modulus, Poisson's ratio, and weight density and lengths are given in (1) of Example 10.8.1.

Excitation: The grid pattern shown in Figure E10.8.1(a) is employed with $n_1 = 40$ and $n_2 = 6$ for this example. The force is applied at the 1/4 span position on the top surface of the beam. Figure E10.8.1(a) shows that this is at degree of freedom (dof),

$$i_F = \left(\frac{n_1}{4} + 1\right)(n_2 + 1) * 2 \quad (1)$$

The corresponding constraint condensed dof is obtained from the *larray* (9.2.83) as l_{i_F} . The global-condensed system force vector therefore has the form

$$\underline{F}_f = \underset{N_f \times 1}{(0 \ 0 \ \dots \ 0 \ f(t) \ 0 \ \dots \ 0)^T} \quad (2)$$

\uparrow
 row l_{i_F}

The sinusoidal force has the same amplitude as the peak transient force in Example 10.8.1; however, the force is applied sinusoidally, that is,

$$f(t) = 500,000 \cos(\omega t) \text{ N} \quad (3)$$

Solution: Recall from Chapter 7 that the steady-state harmonic response phasors are determined by solving (7.5.5)

$$\left(-\omega^2 \underline{M}_f + i\omega \underline{C}_f + \underline{K}_f\right) \tilde{\underline{Q}}_f = \underline{R}(\omega) \tilde{\underline{Q}}_f = \tilde{\underline{F}}_f \quad N_{\text{npd}} \times 1 \quad (4)$$

The amplitude and phase angle at degree of freedom j are then obtained from (7.5.7)

$$|\tilde{Q}_{fj}| = \sqrt{[\operatorname{Re}(\tilde{Q}_{fj})]^2 + [\operatorname{Im}(\tilde{Q}_{fj})]^2} \quad \text{and} \quad \phi_{Q_{fj}} = \tan^{-1} \left(\frac{\operatorname{Im}(\tilde{Q}_{fj})}{\operatorname{Re}(\tilde{Q}_{fj})} \right) \quad (5)$$

From (2), (3), and (7.5.3), the phasor force vector for this system is

$$\underset{N_f \times 1}{\tilde{\underline{F}}_f} = (0 \ 0 \ \cdots \ 0 \ 500,000 \ 0 \ \cdots \ 0)^T \quad (6)$$

↑
row l_{fF}

The damping model is obtained from (5.4.120)

$$\underline{C}_f = \mu_m \underline{M}_f + \mu_k \underline{K}_f \quad (7)$$

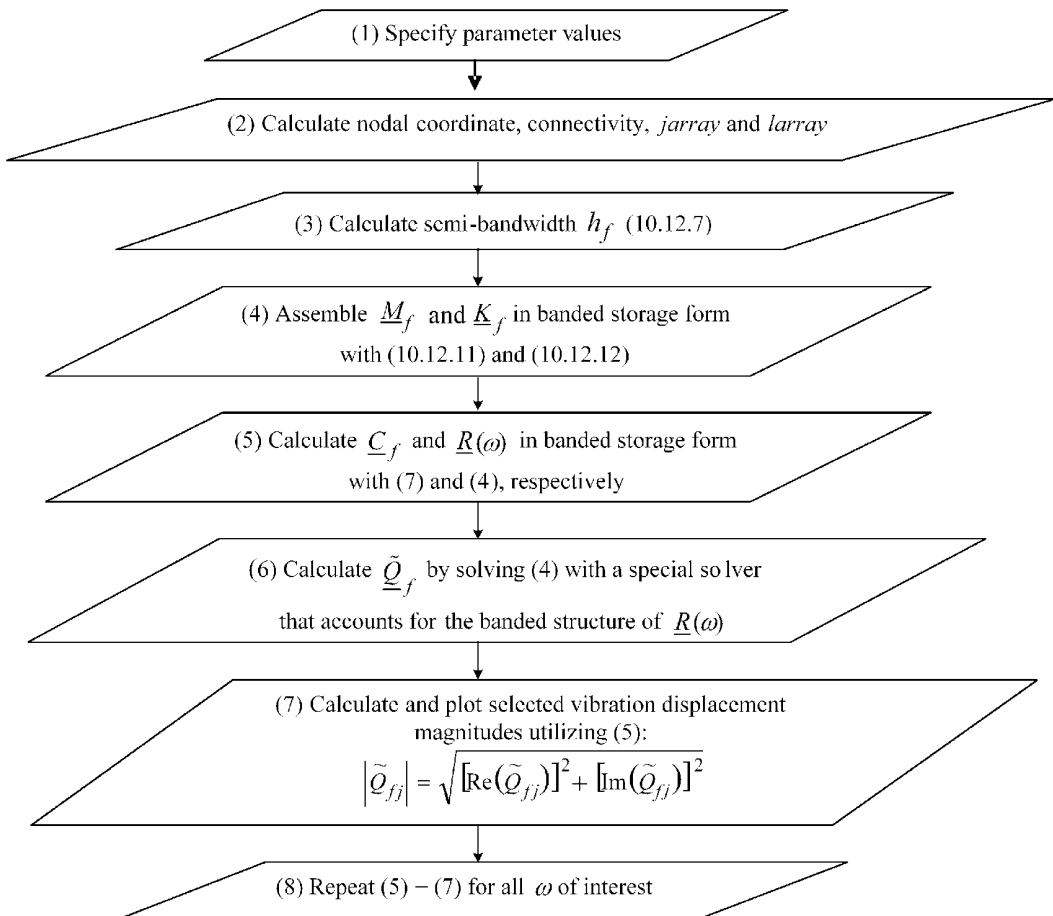


Figure E10.12.1(a) Flow diagram for obtaining steady-state, harmonic response utilizing a banded solver

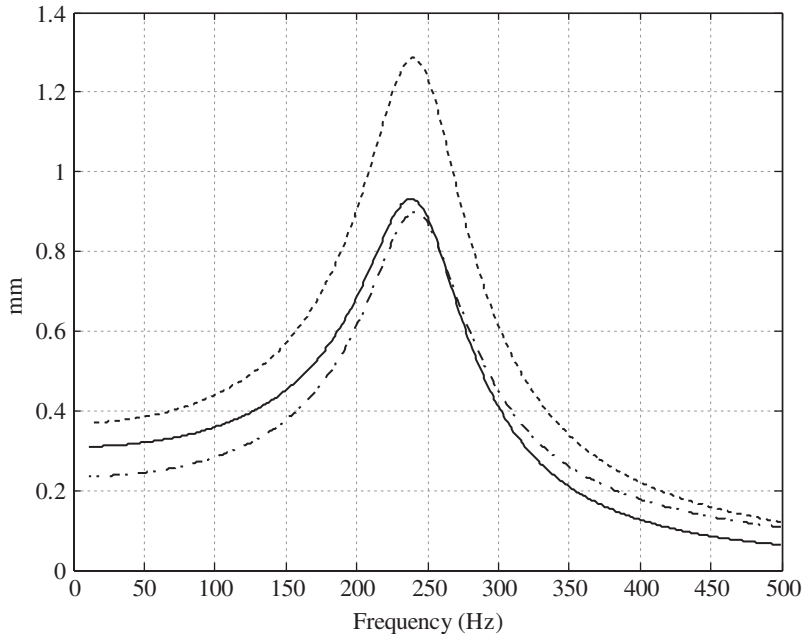


Figure E10.12.1(b) Vibration displacement amplitude on the top surface of the beam at $x_1 = L_1/4$ (solid), $x_1 = L_1/2$ (dashed), and $x_1 = 3L_1/4$ (dash-dot)

The damping is prescribed to be 15% ($\xi = 0.15$) at 250 Hz which is nearly identical with the first bending mode (245 Hz) in Table E10.8.1(a) and Figure E10.8.1(e). This is achieved by setting $\mu_m = 0$ in (7) and determining μ_k from (5.4.122) as

$$\mu_k = \frac{2\xi}{\omega} = \frac{2 * 0.15}{2 * \pi * 250} = 1.9 \times 10^{-4} \quad (8)$$

By (7), all matrices in (4), that is, \underline{M}_f , \underline{C}_f , \underline{K}_f , and $\underline{R}(\omega)$ have the same semibandwidth. Applying (10.12.7) to the mesh pattern in Figure E10.8.1(a) with $n_1 = 40$ and $n_2 = 6$ yields a semibandwidth of $h_f = 18$. Figure E10.12.1(a) shows a flow diagram for obtaining the steady-state, harmonic response of the simply supported beam model to a sinusoidal excitation. The corresponding code is listed in Appendix E.

Figure E10.12.1(b) shows the vibration displacement amplitude versus forcing frequency at three locations on the top surface of the beam model. The dimensional characteristics of this example are 574 degrees of freedom, 571 nonprescribed degrees of freedom, 240 elements, constrained system semibandwidth = 18, number of excitation frequencies = 500, and total execution time = 33 seconds (wall clock time) on a 2.67 GHz, 64-bit laptop.

10.13 CHAPTER 10 EXERCISES

10.13.1 Exercise Location

All exercises may be conveniently viewed and downloaded at the following website: www.wiley.com/go/palazzolo. This new feature greatly reduces the length of the printed book, yielding a significant cost savings for the college student, and is updated.

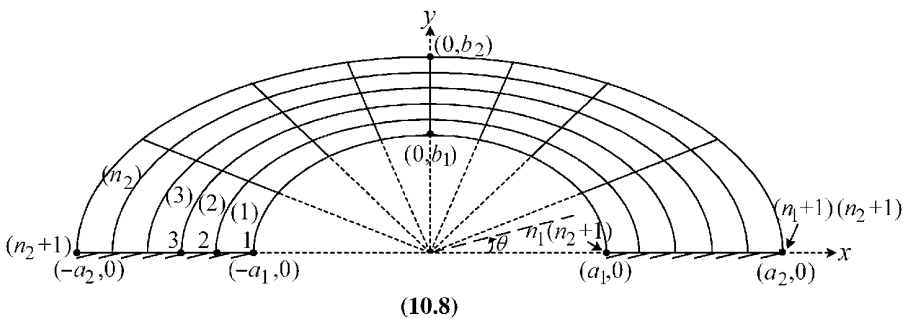
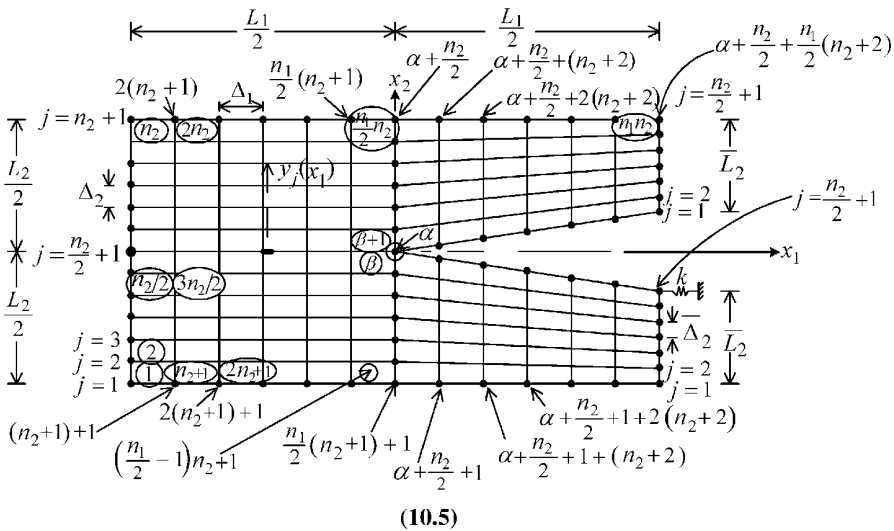
10.13.2 Exercise Goals

The goal of the Exercises in Chapter 10 is to strengthen the student’s understanding and related engineering problem solving skills in the following areas:

- (a) Develop a skill for meshing a 2D solid element model for plane stress/strain analyses.
- (b) Determining natural frequencies of plane stress/strain models and visualizing accompanying modes
- (c) Evaluating benefit of utilizing extra shape functions to accelerate convergence of predicted natural frequencies versus mesh refinement.

10.13.3 Sample Exercises: 10.5 and 10.8

The component in Exercise 10.5 is a plane stress/strain model that is cantilevered at its left end and constrained by a spring at its lower right end. The half ellipse-shaped component in Exercise 10.8 is represented with a plane stress/strain model. Its bottom surface is totally constrained. Suggestions for node/element patterns are provided. The student must calculate the natural frequencies and mode shapes. Solutions may be obtained by modifying a given MATLAB code.



REFERENCES

- BARLOW, J. "Optimal Stress Locations in Finite Element Models". *Int. J. Numer. Methods Eng.*, Vol. **10**, 243–251, 1976.
- COOK, R., MALKUS, D. and PLESHA, M. *Concepts and Applications of Finite Element Analysis*, 3rd ed. John Wiley & Sons, 1989.
- FRANKLIN, J. N. *Matrix Theory*. Prentice Hall, 1968.
- FUNG, Y. C. *Foundations of Solid Mechanics*. Prentice Hall, 1965.
- HILDEBRAND, F. *Advanced Calculations for Applications*, 2nd ed. Prentice Hall, 1976.
- HUEBNER, K., THORNTON, E. A., BYROM, T. G. *The Finite Element Method for Engineers*, 3rd ed. John Wiley & Sons, 1994.
- HUGHES, T. *The Finite Element Method*. Prentice Hall, 1987.
- REDDY, J. N. *An Introduction to the Finite Element Method*, 3rd ed. McGraw Hill, 2005.

Chapter 11

3D Solid Elements for Vibration Analysis

11.1 INTRODUCTION

Powerful automated meshing codes and solvers presently make 3D solid finite element modeling the preferred approach for vibration simulations of many structures and machines. The mesh generators can quickly fill an arbitrarily shaped solid model of a machine, vehicle, or structural component with 3D solid elements. These codes even refine mesh densities in an automated manner to improve the predictions. The 3D solid elements have the potential to yield more accurate results, being free from the kinematic constraints imposed on beam, plane strain/stress, axisymmetric, plate, or truss elements as discussed in Chapters 4, 9, and 10. A disadvantage of these large degree of freedom (dof) models is the added computational time, which may be reduced by using the approximate methods discussed in Chapter 8, or by the judicious use of the lower-fidelity models in Chapters 9 and 10 for preliminary design studies. Table 11.1.1 summarizes some of the kinematic assumptions of the elements in these generally lower-fidelity models.

Figure 11.1.1 shows some 3D solid element shapes that appear in the literature and/or in the element menus of commercially available finite element software.

For the sake of illustration, the 3D solid element presented in detail in this chapter is an 8-node hexahedron “brick” as shown with actual (x_1, x_2, x_3) and natural (ξ_1, ξ_2, ξ_3) coordinates in Figure 11.1.2. The 8 local node numbers (k), nodal coordinates $(x_{1,k}^e, x_{2,k}^e, x_{3,k}^e)$, and nodal displacements $(u_{1,k}^e, u_{2,k}^e, u_{3,k}^e)$ are shown in this figure. The displacements and coordinates are directed along the axes of the same global coordinate system (x_1, x_2, x_3) utilized by all elements in the model. The element has six faces, any of which could possibly be on the surface of the modeled system and acted on by external forces in the form of a pressure or more general surface traction. Surface stresses may be evaluated directly on these faces or extrapolated from interior points out to the surfaces. Interior stresses are typically evaluated at the Gauss points (GP) to improve their accuracy. The interior of the element possesses mass and could be subjected to a body force such as centrifugal or gravity loading. The irregular shape of the element precludes analytical evaluation of the integrals associated with the stiffness and mass matrices and force vector. These integrals must first be transformed to a parent coordinate system and then performed with Gauss integration. The 8-node solid element has a 6-node (degenerate) pentahedral shape counterpart formed by coalescing two pairs of nodes as shown in Figure 11.1.3.

Figure 11.1.4 shows a reciprocating compressor crankshaft and axial air compressor blade comprised of 8- and 6-node brick elements. These are relatively coarse meshes. The intended purpose of these models was to determine the fatigue life of these components

Table 11.1.1 Summary of FE model assumptions

Element type	Kinematic or kinetic assumption
Plane strain	Depth-to-width and depth-to-height ratios large. All strains, stresses, displacements, and loads are independent of depth coordinate. Strain $\epsilon_{33} = 0$. All motion occurs only in the $x_1 - x_2$ plane (Figure 10.2.1)
Plane stress	Depth-to-width and height ratios small. In plane loading only. All motion occurs only in the $x_1 - x_2$ plane (Figure 10.3.1)
Beams	Plane sections remain plane. Symmetric geometry about the neutral axis at $\tilde{x}_2 = \tilde{x}_3 = 0$ (Figure 9.5.1)
Axisymmetric	All strains, stresses, displacements, and loads are independent of θ (Figures 10.9.2 and 10.9.3)

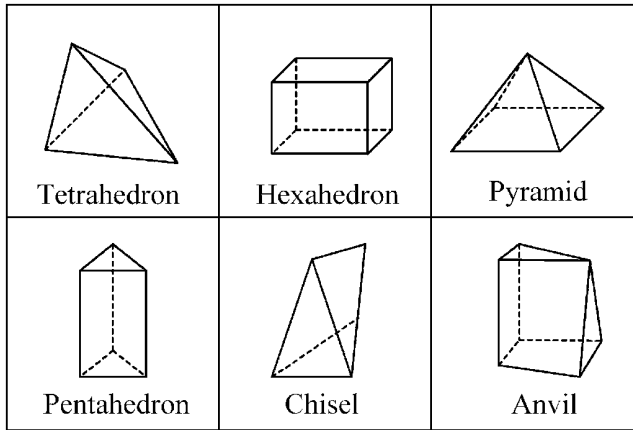


Figure 11.1.1 Shapes utilized for 3D solid modeling with FE

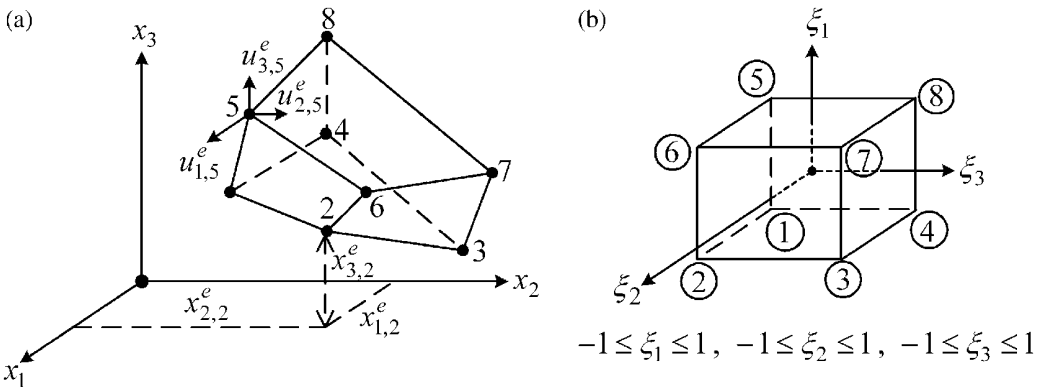


Figure 11.1.2 Hexahedral, 8-node, isoparametric 3D solid element in (a) actual and (b) parent (natural) coordinates

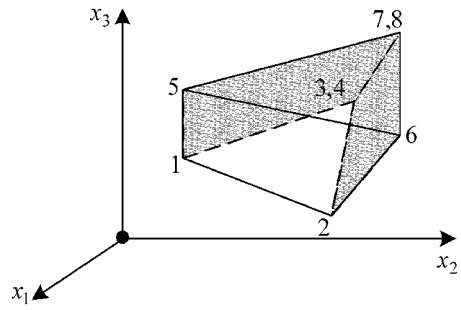


Figure 11.1.3 Degenerate, 6-node form of 8-node brick element

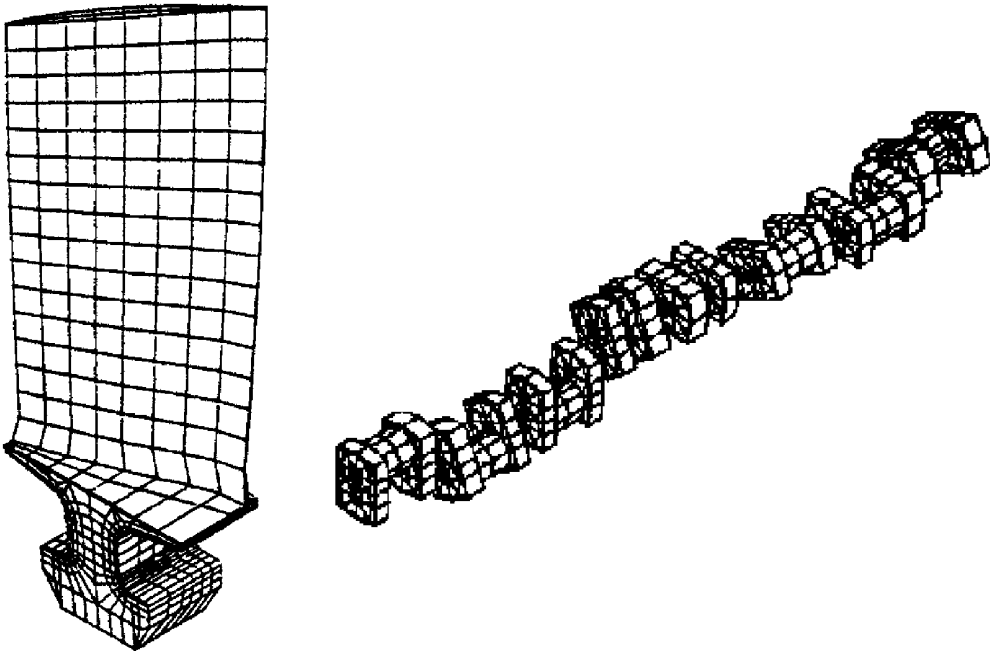


Figure 11.1.4 Axial air compressor blade and reciprocating compressor crankshaft finite element models composed of 8-node brick element

as subjected to cyclic loading. Vibratory stresses were predicted for this purpose and were of greater use than the vibratory displacements.

11.2 ELEMENT STIFFNESS MATRIX

11.2.1 Shape Functions

Figure 11.1.2 shows that each of the 8 nodes in the hexahedral element has three coordinates $(x_{1,k}^e, x_{2,k}^e, x_{3,k}^e)$ and three displacements $(u_{1,k}^e, u_{2,k}^e, u_{3,k}^e)$ in the global coordinate system (x_1, x_2, x_3) . The global displacement functions (u_1, u_2, u_3) are interpolated throughout the element utilizing natural coordinates, shape functions, and nodal displacements. The

element geometry (x_1, x_2, x_3) is mapped into natural coordinates using the isoparametric approach, where the same shape functions as the displacement interpolations are utilized. The natural coordinates vary within the limits

$$-1 \leq \xi_1 \leq 1, \quad -1 \leq \xi_2 \leq 1, \quad -1 \leq \xi_3 \leq 1 \quad (11.2.1)$$

The eight trilinear Lagrange-type shape functions for the hexahedral solid element are given by

$$\begin{aligned} N_1 &= \frac{(1-\xi_1)(1-\xi_2)(1-\xi_3)}{8}, & N_2 &= \frac{(1-\xi_1)(1+\xi_2)(1-\xi_3)}{8} \\ N_3 &= \frac{(1-\xi_1)(1+\xi_2)(1+\xi_3)}{8}, & N_4 &= \frac{(1-\xi_1)(1-\xi_2)(1+\xi_3)}{8} \\ N_5 &= \frac{(1+\xi_1)(1-\xi_2)(1-\xi_3)}{8}, & N_6 &= \frac{(1+\xi_1)(1+\xi_2)(1-\xi_3)}{8} \\ N_7 &= \frac{(1+\xi_1)(1+\xi_2)(1+\xi_3)}{8}, & N_8 &= \frac{(1+\xi_1)(1-\xi_2)(1+\xi_3)}{8} \end{aligned} \quad (11.2.2)$$

The locations of the 8 nodes in the natural coordinate system are shown in Table 11.2.1.

Utilizing these nodal coordinates, it can be easily verified that the shape functions in (11.2.2) satisfy the consistency conditions (2.11.37)

$$N_j(\xi_{1r}, \xi_{2s}, \xi_{3t}) = \begin{cases} 0, & r \neq j \text{ or } s \neq j \text{ or } t \neq j \\ 1, & r = s = t = j \end{cases} \quad (11.2.3)$$

where ξ_{kl} = value of ξ_k at local node l , $k = 1, 3$, and $l = 1, 8$.

This condition insures that the node locations in the natural coordinates map onto the node locations in the actual coordinates and likewise that the nodal displacements are recovered from the interpolation expressions when they are evaluated at the nodal coordinates in the natural coordinate system. This was previously explained in (2.11.37).

The element geometry is mapped from natural to actual coordinates with the isoparametric transformation

$$x_i = \sum_{k=1}^8 N_k x_{i,k}^e, \quad i = 1, 2, 3 \quad (11.2.4)$$

where $x_{i,k}^e = x_i$ coordinate of local node k of element e .

Table 11.2.1 Nodal natural coordinates for 8-node hexahedral solid element

Local node no.	ξ_1	ξ_2	ξ_3
1	-1	-1	-1
2	-1	1	-1
3	-1	1	1
4	-1	-1	1
5	1	-1	-1
6	1	1	-1
7	1	1	1
8	1	-1	1

The displacements throughout the element are interpolated with the shape functions and nodal displacements as

$$u_i = \sum_{k=1}^8 N_k u_{i,k}^e, \quad i = 1, 2, 3 \quad (11.2.5)$$

where $u_{i,k}^e = u_i$ displacement of local node k of element e .

Similar to the 2D models in Chapter 10, improvement of the hexahedral element's accuracy in bending problems may be obtained by adding extra shape functions to its displacement interpolation as per Cook et al. (1989):

$$u_i = \sum_{k=1}^8 N_k u_{i,k}^e + \sum_{k=9}^{11} N_k u_{i,k}^e \quad (11.2.6)$$

where nodes 9, 10, and 11 are not assigned any specific locations within the element. The three additional shape functions are

$$N_9 = 1 - \xi_2^2, \quad N_{10} = 1 - \xi_3^2, \quad N_{11} = 1 - \xi_1^2 \quad (11.2.7)$$

The addition of the three extra shape functions causes the interpolated displacements to be different on the shared face of two joined elements, when evaluated with the interpolation expressions in the two elements. Hence, the elements with the three extra shape functions are referred to as "incompatible" elements. Including the extra shape functions is most effective for rectangular-shaped elements as described in Hughes (1987). Nodes 9, 10, and 11 will be reduced out in the final form of the element stiffness matrix yielding a 24×24 K^e matrix instead of a 33×33 matrix.

A pentahedral-shaped "degenerate" element may be formed by coalescing node 3 with node 4 and node 7 with node 8. The resulting element is shown in Figure 11.1.3. The shape functions for this element are easily obtained by setting

$$x_{1,3}^e = x_{1,4}^e, \quad x_{1,7}^e = x_{1,8}^e \quad (11.2.8)$$

Equation (11.2.4) becomes

$$\begin{aligned} x_i = & N_1 x_{i,1}^e + N_2 x_{i,2}^e + (N_3 + N_4) x_{i,3}^e + N_5 x_{i,5}^e + N_6 x_{i,6}^e + (N_7 + N_8) x_{i,7}^e \\ & + \hat{N}_1 \hat{x}_{i,1}^e + \hat{N}_2 \hat{x}_{i,2}^e + \hat{N}_3 \hat{x}_{i,3}^e + \hat{N}_4 \hat{x}_{i,4}^e + \hat{N}_5 \hat{x}_{i,5}^e + \hat{N}_6 \hat{x}_{i,6}^e \end{aligned} \quad (11.2.9)$$

where $\hat{\cdot}$ indicates local node number in the pentahedral element shown in Figure 11.2.1.

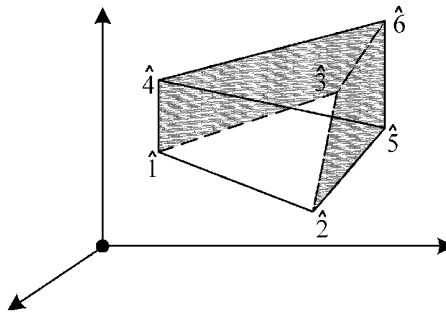


Figure 11.2.1 Pentahedral element node numbers

Comparison of Figures 11.1.3 and 11.2.1 and consideration of (11.2.9) yield the pentahedral shape functions and nodal coordinates as

$$\begin{aligned} \hat{N}_1 &= N_1, \quad \hat{N}_2 = N_2, \quad \hat{N}_3 = N_3 + N_4, \quad \hat{N}_4 = N_5, \quad \hat{N}_5 = N_6, \quad \hat{N}_6 = N_7 + N_8 \\ \hat{x}_{i,1}^e &= x_{i,1}^e, \quad \hat{x}_{i,2}^e = x_{i,2}^e, \quad \hat{x}_{i,3}^e = x_{i,3}^e, \quad \hat{x}_{i,4}^e = x_{i,5}^e, \quad \hat{x}_{i,5}^e = x_{i,6}^e, \quad \hat{x}_{i,6}^e = x_{i,7}^e \end{aligned} \quad (11.2.10)$$

11.2.2 Element Stiffness Matrix Integral and Summation Forms

The following linear strain–displacement relation for an elastic solid is derived in (A.3.18)

$$\begin{Bmatrix} \varepsilon_{11} \\ \varepsilon_{22} \\ \varepsilon_{33} \\ 2\varepsilon_{12} \\ 2\varepsilon_{23} \\ 2\varepsilon_{13} \end{Bmatrix} = \begin{bmatrix} \partial/\partial x_1 & 0 & 0 \\ 0 & \partial/\partial x_2 & 0 \\ 0 & 0 & \partial/\partial x_3 \\ \partial/\partial x_2 & \partial/\partial x_1 & 0 \\ 0 & \partial/\partial x_3 & \partial/\partial x_2 \\ \partial/\partial x_3 & 0 & \partial/\partial x_1 \end{bmatrix} \begin{Bmatrix} u_1 \\ u_2 \\ u_3 \end{Bmatrix} = \begin{bmatrix} 1 & 0 & 0 & 0 & 0 & 0 & 0 & 0 & 0 \\ 0 & 0 & 0 & 0 & 1 & 0 & 0 & 0 & 0 \\ 0 & 0 & 0 & 0 & 0 & 0 & 0 & 0 & 1 \\ 0 & 1 & 0 & 1 & 0 & 0 & 0 & 0 & 0 \\ 0 & 0 & 0 & 0 & 0 & 1 & 0 & 1 & 0 \\ 0 & 0 & 1 & 0 & 0 & 0 & 1 & 0 & 0 \end{bmatrix} \begin{Bmatrix} \partial u_1/\partial x_1 \\ \partial u_1/\partial x_2 \\ \partial u_1/\partial x_3 \\ \partial u_2/\partial x_1 \\ \partial u_2/\partial x_2 \\ \partial u_2/\partial x_3 \\ \partial u_3/\partial x_1 \\ \partial u_3/\partial x_2 \\ \partial u_3/\partial x_3 \end{Bmatrix} \quad (11.2.11)$$

The displacement derivatives with respect to x_i in (11.2.1) cannot be evaluated directly since the displacement field is expressed in terms of natural coordinates ξ_j by (11.2.5) or (11.2.6). The derivatives with respect to physical coordinates x_i in (11.2.11) must be transformed to derivatives with respect to the natural coordinates. This transformation of derivatives is obtained by applying the chain rule of differentiation

$$\begin{Bmatrix} \frac{\partial}{\partial \xi_1} \\ \frac{\partial}{\partial \xi_2} \\ \frac{\partial}{\partial \xi_3} \end{Bmatrix} = \begin{bmatrix} \frac{\partial x_1}{\partial \xi_1} & \frac{\partial x_2}{\partial \xi_1} & \frac{\partial x_3}{\partial \xi_1} \\ \frac{\partial x_1}{\partial \xi_2} & \frac{\partial x_2}{\partial \xi_2} & \frac{\partial x_3}{\partial \xi_2} \\ \frac{\partial x_1}{\partial \xi_3} & \frac{\partial x_2}{\partial \xi_3} & \frac{\partial x_3}{\partial \xi_3} \end{bmatrix} \begin{Bmatrix} \frac{\partial}{\partial x_1} \\ \frac{\partial}{\partial x_2} \\ \frac{\partial}{\partial x_3} \end{Bmatrix} = (\underline{J}) \begin{Bmatrix} \frac{\partial}{\partial x_1} \\ \frac{\partial}{\partial x_2} \\ \frac{\partial}{\partial x_3} \end{Bmatrix} \quad (11.2.12)$$

where \underline{J} is the 3D Jacobian matrix. Note that from (11.2.4)

$$\frac{\partial x_i}{\partial \xi_m} = \sum_{k=1}^8 \frac{\partial N_k}{\partial \xi_m} x_{i,k}^e \quad i=1,3 \quad m=1,3 \quad (11.2.13)$$

Substitute (11.2.13) into (11.2.12) to obtain

$$\underline{J} = \begin{bmatrix} \frac{\partial N_1}{\partial \xi_1} & \frac{\partial N_2}{\partial \xi_1} & \frac{\partial N_3}{\partial \xi_1} & \frac{\partial N_4}{\partial \xi_1} & \frac{\partial N_5}{\partial \xi_1} & \frac{\partial N_6}{\partial \xi_1} & \frac{\partial N_7}{\partial \xi_1} & \frac{\partial N_8}{\partial \xi_1} \\ \frac{\partial N_1}{\partial \xi_2} & \frac{\partial N_2}{\partial \xi_2} & \frac{\partial N_3}{\partial \xi_2} & \frac{\partial N_4}{\partial \xi_2} & \frac{\partial N_5}{\partial \xi_2} & \frac{\partial N_6}{\partial \xi_2} & \frac{\partial N_7}{\partial \xi_2} & \frac{\partial N_8}{\partial \xi_2} \\ \frac{\partial N_1}{\partial \xi_3} & \frac{\partial N_2}{\partial \xi_3} & \frac{\partial N_3}{\partial \xi_3} & \frac{\partial N_4}{\partial \xi_3} & \frac{\partial N_5}{\partial \xi_3} & \frac{\partial N_6}{\partial \xi_3} & \frac{\partial N_7}{\partial \xi_3} & \frac{\partial N_8}{\partial \xi_3} \end{bmatrix} \begin{bmatrix} x_{1,1}^e & x_{2,1}^e & x_{3,1}^e \\ x_{1,2}^e & x_{2,2}^e & x_{3,2}^e \\ x_{1,3}^e & x_{2,3}^e & x_{3,3}^e \\ x_{1,4}^e & x_{2,4}^e & x_{3,4}^e \\ x_{1,5}^e & x_{2,5}^e & x_{3,5}^e \\ x_{1,6}^e & x_{2,6}^e & x_{3,6}^e \\ x_{1,7}^e & x_{2,7}^e & x_{3,7}^e \\ x_{1,8}^e & x_{2,8}^e & x_{3,8}^e \end{bmatrix} \quad (11.2.14)$$

The second matrix in (11.2.14) contains the nodal coordinates which are different for all elements. The first matrix may be evaluated at each Gauss integration point (Table 10.4.1) in any element, stored, and then reused for all other elements in the mesh. The derivatives of the shape functions in (11.2.2) and (11.2.7) are expressed in terms of the natural coordinates ξ_1, ξ_2, ξ_3 in Table 11.2.2. The nodal coordinates $(x_{1,k}^e, x_{2,k}^e, x_{3,k}^e)$ are user defined or may be code generated.

Application of the derivative transformation in (11.2.12) to the three displacement functions u_1, u_2 , and u_3 yields

Table 11.2.2 Shape function derivatives for the 8-node incompatible hexahedral element where $(N_{k,e} = \partial N_k / \partial \xi_e)$

$N_{1,1} = -\frac{1}{8}(1-\xi_2)(1-\xi_3)$	$N_{1,2} = -\frac{1}{8}(1-\xi_1)(1-\xi_3)$	$N_{1,3} = -\frac{1}{8}(1-\xi_1)(1-\xi_2)$
$N_{2,1} = -\frac{1}{8}(1+\xi_2)(1-\xi_3)$	$N_{2,2} = \frac{1}{8}(1-\xi_1)(1-\xi_3)$	$N_{2,3} = -\frac{1}{8}(1-\xi_1)(1+\xi_2)$
$N_{3,1} = -\frac{1}{8}(1+\xi_2)(1+\xi_3)$	$N_{3,2} = \frac{1}{8}(1-\xi_1)(1+\xi_3)$	$N_{3,3} = \frac{1}{8}(1-\xi_1)(1+\xi_2)$
$N_{4,1} = -\frac{1}{8}(1-\xi_2)(1+\xi_3)$	$N_{4,2} = -\frac{1}{8}(1-\xi_1)(1+\xi_3)$	$N_{4,3} = \frac{1}{8}(1-\xi_1)(1-\xi_2)$
$N_{5,1} = \frac{1}{8}(1-\xi_2)(1-\xi_3)$	$N_{5,2} = -\frac{1}{8}(1+\xi_1)(1-\xi_3)$	$N_{5,3} = -\frac{1}{8}(1+\xi_1)(1-\xi_2)$
$N_{6,1} = \frac{1}{8}(1+\xi_2)(1-\xi_3)$	$N_{6,2} = \frac{1}{8}(1+\xi_1)(1-\xi_3)$	$N_{6,3} = -\frac{1}{8}(1+\xi_1)(1+\xi_2)$
$N_{7,1} = \frac{1}{8}(1+\xi_2)(1+\xi_3)$	$N_{7,2} = \frac{1}{8}(1+\xi_1)(1+\xi_3)$	$N_{7,3} = \frac{1}{8}(1+\xi_1)(1+\xi_2)$
$N_{8,1} = \frac{1}{8}(1-\xi_2)(1+\xi_3)$	$N_{8,2} = -\frac{1}{8}(1+\xi_1)(1+\xi_3)$	$N_{8,3} = \frac{1}{8}(1+\xi_1)(1-\xi_2)$
$N_{9,1} = 0$	$N_{9,2} = -2\xi_2$	$N_{9,3} = 0$
$N_{10,1} = 0$	$N_{10,2} = 0$	$N_{10,3} = -2\xi_3$
$N_{11,1} = -2\xi_1$	$N_{11,2} = 0$	$N_{11,3} = 0$

$$\begin{pmatrix} \frac{\partial u_1}{\partial x_1} \\ \frac{\partial u_1}{\partial x_2} \\ \frac{\partial u_1}{\partial x_3} \\ \frac{\partial u_2}{\partial x_1} \\ \frac{\partial u_2}{\partial x_2} \\ \frac{\partial u_2}{\partial x_3} \\ \frac{\partial u_3}{\partial x_1} \\ \frac{\partial u_3}{\partial x_2} \\ \frac{\partial u_3}{\partial x_3} \end{pmatrix} = \begin{bmatrix} \underline{J}^{-1} & \underline{0} & \underline{0} \\ \underline{0} & \underline{J}^{-1} & \underline{0} \\ \underline{0} & \underline{0} & \underline{J}^{-1} \end{bmatrix} \begin{pmatrix} \frac{\partial u_1}{\partial \xi_1} \\ \frac{\partial u_1}{\partial \xi_2} \\ \frac{\partial u_1}{\partial \xi_3} \\ \frac{\partial u_2}{\partial \xi_1} \\ \frac{\partial u_2}{\partial \xi_2} \\ \frac{\partial u_2}{\partial \xi_3} \\ \frac{\partial u_3}{\partial \xi_1} \\ \frac{\partial u_3}{\partial \xi_2} \\ \frac{\partial u_3}{\partial \xi_3} \end{pmatrix} \quad (11.2.15)$$

Substitution of (11.2.15) into the strain–displacement relation (11.2.11) yields

$$\underline{\varepsilon} = \begin{pmatrix} \varepsilon_{11} \\ \varepsilon_{22} \\ \varepsilon_{33} \\ 2\varepsilon_{12} \\ 2\varepsilon_{23} \\ 2\varepsilon_{13} \end{pmatrix} = \begin{bmatrix} 1 & 0 & 0 & 0 & 0 & 0 & 0 & 0 & 0 \\ 0 & 0 & 0 & 0 & 1 & 0 & 0 & 0 & 0 \\ 0 & 0 & 0 & 0 & 0 & 0 & 0 & 0 & 1 \\ 0 & 1 & 0 & 1 & 0 & 0 & 0 & 0 & 0 \\ 0 & 0 & 0 & 0 & 0 & 1 & 0 & 1 & 0 \\ 0 & 0 & 1 & 0 & 0 & 0 & 1 & 0 & 0 \end{bmatrix} \begin{bmatrix} \underline{J}^{-1} & \underline{0} & \underline{0} \\ \underline{0} & \underline{J}^{-1} & \underline{0} \\ \underline{0} & \underline{0} & \underline{J}^{-1} \end{bmatrix} \begin{pmatrix} \frac{\partial u_1}{\partial \xi_1} \\ \frac{\partial u_1}{\partial \xi_2} \\ \frac{\partial u_1}{\partial \xi_3} \\ \frac{\partial u_2}{\partial \xi_1} \\ \frac{\partial u_2}{\partial \xi_2} \\ \frac{\partial u_2}{\partial \xi_3} \\ \frac{\partial u_3}{\partial \xi_1} \\ \frac{\partial u_3}{\partial \xi_2} \\ \frac{\partial u_3}{\partial \xi_3} \end{pmatrix} \quad (11.2.16)$$

The Jacobian matrix is evaluated in (11.2.14) and its inverse is represented in scalar form by

$$\underline{J}^{-1} = \begin{bmatrix} J_{11}^* & J_{12}^* & J_{13}^* \\ J_{21}^* & J_{22}^* & J_{23}^* \\ J_{31}^* & J_{32}^* & J_{33}^* \end{bmatrix} \quad (11.2.17)$$

Substitution of (11.2.17) into (11.2.16) yields

$$\underline{\varepsilon} = \begin{bmatrix} J_{11}^* & J_{12}^* & J_{13}^* & 0 & 0 & 0 & 0 & 0 & 0 \\ 0 & 0 & 0 & J_{21}^* & J_{22}^* & J_{23}^* & 0 & 0 & 0 \\ 0 & 0 & 0 & 0 & 0 & 0 & J_{31}^* & J_{32}^* & J_{33}^* \\ J_{21}^* & J_{22}^* & J_{23}^* & J_{11}^* & J_{12}^* & J_{13}^* & 0 & 0 & 0 \\ 0 & 0 & 0 & J_{31}^* & J_{32}^* & J_{33}^* & J_{21}^* & J_{22}^* & J_{23}^* \\ J_{31}^* & J_{32}^* & J_{33}^* & 0 & 0 & 0 & J_{11}^* & J_{12}^* & J_{13}^* \end{bmatrix} \begin{pmatrix} \frac{\partial u_1}{\partial \xi_1} \\ \frac{\partial u_1}{\partial \xi_2} \\ \frac{\partial u_1}{\partial \xi_3} \\ \frac{\partial u_2}{\partial \xi_1} \\ \frac{\partial u_2}{\partial \xi_2} \\ \frac{\partial u_2}{\partial \xi_3} \\ \frac{\partial u_3}{\partial \xi_1} \\ \frac{\partial u_3}{\partial \xi_2} \\ \frac{\partial u_3}{\partial \xi_3} \end{pmatrix} \quad (11.2.18)$$

which may be expressed more succinctly as

$$\underline{\varepsilon} = \underline{A}_1 \underline{q} \quad (11.2.19)$$

The \underline{A}_1 matrix may be programmed and evaluated quite easily since it only depends on the Jacobian matrix, which is evaluated by (11.2.14). The vector \underline{q} in (11.2.19) will next be expressed in terms of the nodal displacement vector \underline{u}_{eN} . Differentiating the x_i direction displacement u_i , Equation (11.2.6), with respect to the l th natural coordinate ξ_l yields

$$\frac{\partial u_i}{\partial \xi_l} = \sum_{k=1}^{11} N_{k,l} u_{i,k}^e \quad (11.2.20)$$

where, as in Table 11.2.2, the “comma” notation implies

$$N_{k,l} = \frac{\partial N_k}{\partial \xi_l} \quad (11.2.21)$$

Equation (11.2.20) generates nine equations, since $i=1,2, \text{ and } 3$ and $l=1,2, \text{ and } 3$, which may be written in matrix form as

$$\underline{q} = \underline{A}_2 \underline{u}_{eN} \quad (11.2.22)$$

where

$$\underline{q} = \begin{Bmatrix} \partial u_1 / \partial \xi_1 \\ \partial u_1 / \partial \xi_2 \\ \partial u_1 / \partial \xi_3 \\ \hline \partial u_2 / \partial \xi_1 \\ \partial u_2 / \partial \xi_2 \\ \partial u_2 / \partial \xi_3 \\ \hline \partial u_3 / \partial \xi_1 \\ \partial u_3 / \partial \xi_2 \\ \partial u_3 / \partial \xi_3 \end{Bmatrix}_{9 \times 1}, \quad \underline{A}_2 = \begin{bmatrix} N_{1,1} & 0 & 0 & N_{2,1} & 0 & 0 & \cdots & N_{11,1} & 0 & 0 \\ N_{1,2} & 0 & 0 & N_{2,2} & 0 & 0 & \cdots & N_{11,2} & 0 & 0 \\ N_{1,3} & 0 & 0 & N_{2,3} & 0 & 0 & \cdots & N_{11,3} & 0 & 0 \\ \hline 0 & N_{1,1} & 0 & 0 & N_{2,1} & 0 & \cdots & 0 & N_{11,1} & 0 \\ 0 & N_{1,2} & 0 & 0 & N_{2,2} & 0 & \cdots & 0 & N_{11,2} & 0 \\ 0 & N_{1,3} & 0 & 0 & N_{2,3} & 0 & \cdots & 0 & N_{11,3} & 0 \\ \hline 0 & 0 & N_{1,1} & 0 & 0 & N_{2,1} & \cdots & 0 & 0 & N_{11,1} \\ 0 & 0 & N_{1,2} & 0 & 0 & N_{2,2} & \cdots & 0 & 0 & N_{11,2} \\ 0 & 0 & N_{1,3} & 0 & 0 & N_{2,3} & \cdots & 0 & 0 & N_{11,3} \end{bmatrix}_{9 \times 33} \quad (11.2.23)$$

$$\underline{u}_{eN} = (u_{1,1}^e \ u_{2,1}^e \ u_{3,1}^e \ u_{1,2}^e \ u_{2,2}^e \ u_{3,2}^e \ \cdots \ u_{1,11}^e \ u_{2,11}^e \ u_{3,11}^e)^T \quad (11.2.24)$$

Note that the matrix \underline{A}_2 may be easily programmed and evaluated at any point ξ_1, ξ_2, ξ_3 within the element by utilizing Table 11.2.2 and (11.2.23). This matrix may be evaluated at each Gauss integration point (Table 10.4.1) in any element, stored, and then reused for all other elements in the mesh. Combine the two relations (11.2.19) and (11.2.22) to obtain

$$\underline{\varepsilon} = \underline{A}_1 \underline{q} = \underline{A}_1 \underline{A}_2 \underline{u}_{eN} \quad (11.2.25)$$

Table 11.2.3 Gauss integration points and weight factors for a $3 \times 3 \times 3$ mesh

α	β	γ	$\xi_{1\alpha}$	$\xi_{2\beta}$	$\xi_{3\gamma}$	W_α	W_β	W_γ
1	1	1	$-\epsilon$	$-\epsilon$	$-\epsilon$	5/9	5/9	5/9
		2			0			8/9
	↓	3		↓	ϵ		↓	5/9
	2	1		0	$-\epsilon$		8/9	5/9
		2			0			8/9
	↓	3		↓	ϵ		↓	5/9
	3	1		ϵ	$-\epsilon$		5/9	5/9
		2			0			8/9
↓	↓	3	↓	↓	ϵ	↓	↓	5/9
2	1	1	0	$-\epsilon$	$-\epsilon$	8/9	5/9	5/9
		2			0			8/9
	↓	3		↓	ϵ		↓	5/9
	2	1		0	$-\epsilon$		8/9	5/9
		2			0			8/9
	↓	3		↓	ϵ		↓	5/9
	3	1		ϵ	$-\epsilon$		5/9	5/9
		2			0			8/9
↓	↓	3	↓	↓	ϵ	↓	↓	5/9
3	1	1	ϵ	$-\epsilon$	$-\epsilon$	5/9	5/9	5/9
		2			0			8/9
	↓	3		↓	ϵ		↓	5/9
	2	1		0	$-\epsilon$		8/9	5/9
		2			0			8/9
	↓	3		↓	ϵ		↓	5/9
	3	1		ϵ	$-\epsilon$		5/9	5/9
		2			0			8/9
↓	↓	3	↓	↓	ϵ	↓		5/9

Note: $n_G = 3$ and $\epsilon = \sqrt{0.6}$.

Comparison of (11.2.25) with (4.7.22)

$$\underline{\epsilon} = \underline{B}_e \underline{u}_{eN} \quad (11.2.26)$$

shows that

$$\underline{B}_e = \underline{A}_1 \underline{A}_2 \quad (11.2.27)$$

$6 \times 33 \quad 6 \times 99 \times 33$

Recall that by (4.7.30) the stiffness matrix is

$$\underline{K}^e = \int_{V_e} \underline{B}_e^T \underline{E}_e \underline{B}_e dV \quad (11.2.28)$$

$33 \times 33 \quad 33 \times 6 \quad 6 \times 6 \quad 6 \times 33$

The constitutive relation matrix \underline{E}_e is defined for a general isotropic material in (A.4.3) as

$$\underline{E}_e = \frac{E}{(1+\nu)(1-2\nu)} \begin{bmatrix} 1-\nu & \nu & \nu & 0 & 0 & 0 \\ \nu & 1-\nu & \nu & 0 & 0 & 0 \\ \nu & \nu & 1-\nu & 0 & 0 & 0 \\ 0 & 0 & 0 & \frac{1-2\nu}{2} & 0 & 0 \\ 0 & 0 & 0 & 0 & \frac{1-2\nu}{2} & 0 \\ 0 & 0 & 0 & 0 & 0 & \frac{1-2\nu}{2} \end{bmatrix} \quad (11.2.29)$$

where E and ν are the element's Young's modulus and Poisson's ratio, respectively.

The integral in (11.2.28) is over the element volume depicted in Figure 11.1.2(a). In general, the integration domain is very complex so a closed form solution is unobtainable. This obstacle is removed by utilizing the isoparametric mapping in (11.2.4) to transform the element geometry into the cube-shaped, natural coordinate domain shown in Figure 11.1.2(b). Gauss quadrature may be easily applied to evaluate \underline{K}_e in the cube-shaped domain. The differential volume in (11.2.28) transforms according to (10.4.25) as

$$dV = \det \underline{J} d\xi_1 d\xi_2 d\xi_3 \quad (11.2.30)$$

where the Jacobian matrix \underline{J} is defined in (11.2.14), and its determinant becomes

$$\det(\underline{J}) = J_{11}(J_{22}J_{33} - J_{32}J_{23}) - J_{12}(J_{21}J_{33} - J_{23}J_{31}) + J_{13}(J_{21}J_{32} - J_{22}J_{31}) \quad (11.2.31)$$

Substitute (11.2.30) into (11.2.28) and change the integration limits to those of the cube geometry to obtain

$$\underline{K}^e = \int_{-1}^1 \int_{-1}^1 \int_{-1}^1 \underline{B}_e^T(\xi_1, \xi_2, \xi_3) \underline{E} \underline{B}_e(\xi_1, \xi_2, \xi_3) * \det(\underline{J}(\xi_1, \xi_2, \xi_3)) d\xi_1 d\xi_2 d\xi_3 \quad (11.2.32)$$

Similar to (10.4.27), the stiffness matrix in (11.2.32) is evaluated with the following 3D Gauss quadrature formula:

$$\int_{-1}^1 \int_{-1}^1 \int_{-1}^1 f(\xi_1, \xi_2, \xi_3) d\xi_1 d\xi_2 d\xi_3 = \sum_{\alpha=1}^{n_G} \sum_{\beta=1}^{n_G} \sum_{\gamma=1}^{n_G} \bar{w}_\alpha \bar{w}_\beta \bar{w}_\gamma f(\xi_{1\alpha}, \xi_{2\beta}, \xi_{3\gamma}) \quad (11.2.33)$$

where $\xi_{1\alpha}, \xi_{2\beta}, \xi_{3\gamma}$ are Gauss quadrature (integration) points and $\bar{w}_\alpha, \bar{w}_\beta, \bar{w}_\gamma$ are the corresponding weight factors. Applying (11.2.33) to (11.2.32) yields

$$\underline{K}^e_{33 \times 33} = \sum_{\alpha=1}^{n_G} \sum_{\beta=1}^{n_G} \sum_{\gamma=1}^{n_G} \bar{w}_\alpha \bar{w}_\beta \bar{w}_\gamma \underline{B}_e^T(\xi_{1\alpha}, \xi_{2\beta}, \xi_{3\gamma}) * \frac{E}{6 \times 6 \times 33} \underline{B}_e(\xi_{1\alpha}, \xi_{2\beta}, \xi_{3\gamma}) \det(\underline{J}(\xi_{1\alpha}, \xi_{2\beta}, \xi_{3\gamma})) \quad (11.2.34)$$

This form of the element stiffness matrix may be easily programmed to evaluate it in a numerical form. The $3 \times 3 \times 3$ grid of integration points in Table 11.2.3 is recommended for evaluating (11.2.34).

Nine additional dofs result from including the three extra shape functions in the displacement interpolation (11.2.6) and (11.2.7). Setting the internal forces on these nodes

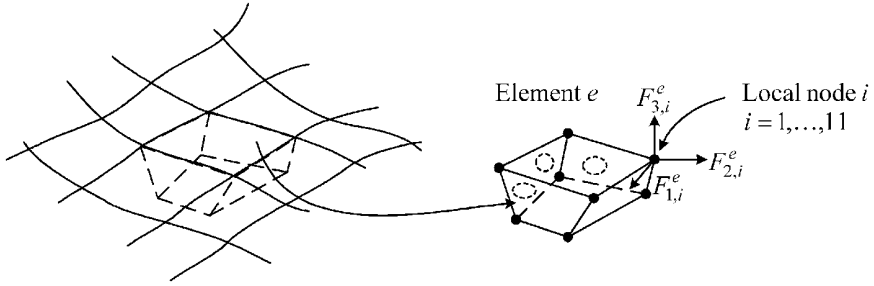


Figure 11.2.2 An 11-node, incompatible solid brick element isolated from a finite element model

to zero provides the condition to eliminate the corresponding dof at the element level, utilizing a Guyan reduction (Section 8.2) type approach.

Consider a single, isolated element from a structural model’s mesh as shown in Figure 11.2.2.

The equilibrium equation for the single element is

$$\underline{K}^e \underline{u}_{eN} = \underline{f}^e + \underline{f}_{-A}^e \tag{11.2.35}$$

$33 \times 33 \quad 33 \times 1 \quad 33 \times 1 \quad 33 \times 1 \quad 33 \times 1$

where \underline{f}^e is the element external load vector and \underline{f}_{-A}^e represents reaction forces between this element and its neighbor’s nodes. Let nodes 1–8 be retained (*r*) nodes and nodes 9–11 condensed (*c*) nodes, and then equation (11.2.34) may be written in partitioned matrix form, similar to (8.2.3) as

$$\begin{bmatrix}
 K_{G1,1}^e & K_{G1,2}^e & \cdots & K_{G1,24}^e & K_{G1,25}^e & \cdots & K_{G1,33}^e \\
 \vdots & \vdots & \ddots & \vdots & \vdots & \ddots & \vdots \\
 K_{G24,1}^e & K_{G24,2}^e & \cdots & K_{G24,24}^e & K_{G24,25}^e & \cdots & K_{G24,33}^e \\
 K_{G25,1}^e & K_{G25,2}^e & \cdots & K_{G25,24}^e & K_{G25,25}^e & \cdots & K_{G25,33}^e \\
 \vdots & \vdots & \ddots & \vdots & \vdots & \ddots & \vdots \\
 K_{G33,1}^e & K_{G33,2}^e & \cdots & K_{G33,24}^e & K_{G33,25}^e & \cdots & K_{G33,33}^e
 \end{bmatrix}
 \begin{Bmatrix}
 u_{1,1}^e \\
 u_{2,1}^e \\
 u_{3,1}^e \\
 \vdots \\
 u_{1,8}^e \\
 u_{2,8}^e \\
 u_{3,8}^e \\
 u_{1,9}^e \\
 u_{2,9}^e \\
 u_{3,9}^e \\
 \vdots \\
 u_{1,11}^e \\
 u_{2,11}^e \\
 u_{3,11}^e
 \end{Bmatrix}
 =
 \begin{Bmatrix}
 f_{1,1}^e \\
 f_{2,1}^e \\
 f_{3,1}^e \\
 \vdots \\
 f_{1,8}^e \\
 f_{2,8}^e \\
 f_{3,8}^e \\
 f_{1,9}^e \\
 f_{2,9}^e \\
 f_{3,9}^e \\
 \vdots \\
 f_{1,11}^e \\
 f_{2,11}^e \\
 f_{3,11}^e
 \end{Bmatrix}
 +
 \begin{Bmatrix}
 f_{A1,1}^e \\
 f_{A2,1}^e \\
 f_{A3,1}^e \\
 \vdots \\
 f_{A1,8}^e \\
 f_{A2,8}^e \\
 f_{A3,8}^e \\
 f_{A1,9}^e \\
 f_{A2,9}^e \\
 f_{A3,9}^e \\
 \vdots \\
 f_{A1,11}^e \\
 f_{A2,11}^e \\
 f_{A3,11}^e
 \end{Bmatrix}
 \tag{11.2.36}$$

or

$$\begin{bmatrix} \underline{K}_{rr}^e & \underline{K}_{rc}^e \\ \underline{K}_{cr}^e & \underline{K}_{cc}^e \end{bmatrix} \begin{Bmatrix} \underline{u}_r^e \\ \underline{u}_c^e \end{Bmatrix} = \begin{Bmatrix} \underline{f}_r^e \\ \underline{f}_c^e \end{Bmatrix} + \begin{Bmatrix} \underline{f}_{Ar}^e \\ \underline{f}_{Ac}^e \end{Bmatrix} \quad (11.2.37)$$

The (9×1) vector \underline{f}_{Ac}^e is set to zero since the condensed nodes (9, 10, 11) in one element are not coincident with or connected to the nodes in any adjacent element, that is, there are no reaction forces between neighboring elements at the condensed nodes. Equation (11.2.37) becomes

$$\underline{K}_{rr}^e \underline{u}_r^e + \underline{K}_{rc}^e \underline{u}_c^e = \underline{f}_r^e + \underline{f}_{Ar}^e \quad (11.2.38)$$

$$\underline{K}_{cr}^e \underline{u}_r^e + \underline{K}_{cc}^e \underline{u}_c^e = \underline{f}_c^e \quad (11.2.39)$$

Solving (11.2.39) for \underline{u}_c^e yields

$$\underline{u}_c^e = (\underline{K}_{cc}^e)^{-1} \underline{f}_c^e - (\underline{K}_{cc}^e)^{-1} \underline{K}_{cr}^e \underline{u}_r^e \quad (11.2.40)$$

Substituting (11.2.40) into (11.2.38) yields

$$\left(\underline{K}_{rr}^e - \underline{K}_{rc}^e \left(\underline{K}_{cc}^e \right)^{-1} \underline{K}_{cr}^e \right) \underline{u}_r^e = - \underline{K}_{rc}^e \left(\underline{K}_{cc}^e \right)^{-1} \underline{f}_c^e + \underline{f}_r^e + \underline{f}_{Ar}^e \quad (11.2.41)$$

Equation (11.2.41) represents the equilibrium equation for a single element. The system equilibrium equation is formed by adding (assembling) Equation (11.2.41) into a system stiffness matrix and force vector, for $e = 1, N_e$ (total number of elements). By Newton's third law, the adjacent elements to any particular element would contribute equal and opposite actions to their shared nodes, and consequently, all \underline{f}_{Ar}^e terms will cancel. For this reason, \underline{f}_{Ar}^e can be ignored in (11.2.41), and it can be concluded that the element stiffness matrix for an 8-node, incompatible solid element with three extra shape functions is

$$\hat{\underline{K}}_{24 \times 24}^e = \underline{K}_{24 \times 24}^e - \underline{K}_{24 \times 9}^e \left(\underline{K}_{9 \times 9}^e \right)^{-1} \underline{K}_{9 \times 24}^e \quad (11.2.42)$$

Note that this matrix has the same dimension (24×24) and dofs as an 8-node element with no extra shape functions; therefore, it is treated in the same manner as an 8-node brick for assembly into the system matrix.

11.3 THE ELEMENT MASS MATRIX AND FORCE VECTOR

Books on statics would limit the discussion to only the stiffness matrix, but of course in vibrations, the inertia (mass) matrix is equally important. In addition, the requirement to model forced vibrations makes it necessary to discuss the element and system force vectors. The extra "incompatible" shape functions in (11.2.7) are utilized to "soften" the bending stiffness of the elements. Consequently, from Hughes (1987), they are not employed to

modify the mass matrix or force vector formulations, which will only use shape functions $N_1 - N_8$ in Equation (11.2.2).

11.3.1 Element Mass Matrix

The general form of the element mass matrix is given by (4.7.47) as

$$\underline{M}^e = \int_{V^e} \rho \underline{N}^T \underline{N} dV \quad (11.3.1)$$

where for the 8-node solid brick element

$$\underline{N}_{3 \times 24} = \begin{bmatrix} N_1 & 0 & 0 & | & N_2 & 0 & 0 & | & | & N_8 & 0 & 0 \\ 0 & N_1 & 0 & | & 0 & N_2 & 0 & | & \cdots & 0 & N_8 & 0 \\ 0 & 0 & N_1 & | & 0 & 0 & N_2 & | & | & 0 & 0 & N_8 \end{bmatrix} \quad (11.3.2)$$

Substitution of (11.2.30) into (11.3.1) yields

$$\underline{M}^e = \int_{-1}^1 \int_{-1}^1 \int_{-1}^1 \rho \underline{N}^T \underline{N} \det(\underline{J}_e) d\xi_1 d\xi_2 d\xi_3 \quad (11.3.3)$$

Apply Gauss quadrature (11.2.33) for evaluating (11.3.3) to obtain

$$\underline{M}^e \approx \sum_{\alpha=1}^{n_G} \sum_{\beta=1}^{n_G} \sum_{\gamma=1}^{n_G} \bar{w}_\alpha \bar{w}_\beta \bar{w}_\gamma \rho (\xi_{1\alpha}, \xi_{2\beta}, \xi_{3\gamma}) \underline{N}^T(\xi_{1\alpha}, \xi_{2\beta}, \xi_{3\gamma}) \underline{N}(\xi_{1\alpha}, \xi_{2\beta}, \xi_{3\gamma}) \det(\underline{J}(\xi_{1\alpha}, \xi_{2\beta}, \xi_{3\gamma})) \quad (11.3.4)$$

11.3.2 Element External Force Vector

The external forces acting on an element may be divided into two categories: (i) internal or volume based and (ii) surface forces that are applied on one or more of the element's six faces. The volume force densities (force per unit volume) are F_{Vx1}^e, F_{Vx2}^e , and F_{Vx3}^e and are typically associated with gravity or imposed acceleration such as centrifugal acceleration. The surface (edge) force densities (force per unit area) are $F_{\Gamma x1}^e, F_{\Gamma x2}^e$, and $F_{\Gamma x3}^e$ and are typically associated with pressure, friction, point or distributed surface loads, and so on. The total element force vector is given by (4.7.59) as

$$\underline{f}_{24 \times 1}^e = \begin{Bmatrix} f_{1,1}^e \\ f_{2,1}^e \\ f_{3,1}^e \\ \vdots \\ f_{1,8}^e \\ f_{2,8}^e \\ f_{3,8}^e \end{Bmatrix} = \int_{\Gamma^e} \underline{N}^T \begin{Bmatrix} F_{\Gamma x1}^e \\ F_{\Gamma x2}^e \\ F_{\Gamma x3}^e \end{Bmatrix} d\Gamma + \int_{V^e} \underline{N}^T \begin{Bmatrix} F_{Vx1}^e \\ F_{Vx2}^e \\ F_{Vx3}^e \end{Bmatrix} dV \quad (11.3.5)$$

where Γ^e represents all faces of the element that lie on the surface of the structure being modeled.

11.3.3 Force Vector: Concentrated Nodal Forces

It is common practice to apply concentrated loads at specified nodal locations and directions in finite element modeling. A simplified element force vector and assembly process result for this case. Let $F_{ik}^A(t)$ be a concentrated external force acting at local node k in direction x_i . Then from Section 2.12 and Equations (11.3.2) and (11.3.5)

$$\begin{aligned} \underline{f}_C^e = \int_V \underline{N}^T \begin{Bmatrix} F_{1k}^A(t)\delta(x_1-x_{1k},x_2-x_{2k},x_3-x_{3k}) \\ F_{2k}^A(t)\delta(x_1-x_{1k},x_2-x_{2k},x_3-x_{3k}) \\ F_{3k}^A(t)\delta(x_1-x_{1k},x_2-x_{2k},x_3-x_{3k}) \end{Bmatrix} dV \\ = \int_V \begin{Bmatrix} F_{1k}^A(t)N_1\delta(x_1-x_{1k},x_2-x_{2k},x_3-x_{3k}) \\ F_{2k}^A(t)N_1\delta(x_1-x_{1k},x_2-x_{2k},x_3-x_{3k}) \\ F_{3k}^A(t)N_1\delta(x_1-x_{1k},x_2-x_{2k},x_3-x_{3k}) \\ \vdots \\ F_{1k}^A(t)N_8\delta(x_1-x_{1k},x_2-x_{2k},x_3-x_{3k}) \\ F_{2k}^A(t)N_8\delta(x_1-x_{1k},x_2-x_{2k},x_3-x_{3k}) \\ F_{3k}^A(t)N_8\delta(x_1-x_{1k},x_2-x_{2k},x_3-x_{3k}) \end{Bmatrix} dV = \begin{Bmatrix} 0 \\ 0 \\ 0 \\ \vdots \\ F_{1k}^A(t) \\ F_{2k}^A(t) \\ F_{3k}^A(t) \\ \vdots \\ 0 \\ 0 \\ 0 \end{Bmatrix} \quad (11.3.6) \end{aligned}$$

where δ is the Kronecker delta and the shape functions defined in (11.2.2) satisfy

$$N_k(x_{1j},x_{2j},x_{3j}) = \begin{cases} 0, & j \neq k \\ 1, & j = k \end{cases} \quad (11.3.7)$$

The concentrated force at a node should be included in only one element force vector to avoid redundancy.

Alternatively, consideration of the assembly procedure shows that a *concentrated force applied at a node may be added directly into the total system force vector at the location corresponding to the global dof that the force is applied on*. This avoids forming and assembling element force vectors (11.3.6) for concentrated nodal forces.

11.3.4 Force Vector: Volumetric Loads

Next, consider forces that act throughout the volume of a component of the system model. This type of force is referred to as a distributed volumetric load (force per unit volume) and may be mathematically represented by

$$\underline{F}_v = \begin{Bmatrix} F_{Vx1}^e \\ F_{Vx2}^e \\ F_{Vx3}^e \end{Bmatrix} = \begin{Bmatrix} f_{Vx1}^e(x_1, x_2, x_3) \alpha_{Vx1}^e(t) \\ f_{Vx2}^e(x_1, x_2, x_3) \alpha_{Vx2}^e(t) \\ f_{Vx3}^e(x_1, x_2, x_3) \alpha_{Vx3}^e(t) \end{Bmatrix} \quad (11.3.8)$$

where the $\alpha(t)$ terms represent the temporal dependence of the loading. This may occur, for example, when a deformable object is subjected to a time-varying imposed acceleration.

The corresponding element force vector is determined from (11.2.30) and (11.3.5) as

$$\underline{f}_{-V}^e(t) = \int_{-1}^1 \int_{-1}^1 \int_{-1}^1 \underline{N}^T(\xi_1, \xi_2, \xi_3) \begin{Bmatrix} f_{Vx1}^e(\xi_1, \xi_2, \xi_3) \alpha_{Vx1}^e(t) \\ f_{Vx2}^e(\xi_1, \xi_2, \xi_3) \alpha_{Vx2}^e(t) \\ f_{Vx3}^e(\xi_1, \xi_2, \xi_3) \alpha_{Vx3}^e(t) \end{Bmatrix} \det(\underline{J}_e) d\xi_1 d\xi_2 d\xi_3 \quad (11.3.9)$$

Substitution of (11.3.2) and use of Gauss quadrature yield the result in 11.3.10, which may be readily programmed:

$$\underline{f}_{-V}^e(t) = \begin{Bmatrix} \alpha_{Vx1}^e(t) \sum_{\alpha=1}^{n_G} \sum_{\beta=1}^{n_G} \sum_{\gamma=1}^{n_G} \bar{w}_\alpha \bar{w}_\beta \bar{w}_\gamma N_1(\xi_{1\alpha}, \xi_{2\beta}, \xi_{3\gamma}) f_{Vx1}^e(\xi_{1\alpha}, \xi_{2\beta}, \xi_{3\gamma}) \det(\underline{J}_e(\xi_{1\alpha}, \xi_{2\beta}, \xi_{3\gamma})) \\ \alpha_{Vx2}^e(t) \sum_{\alpha=1}^{n_G} \sum_{\beta=1}^{n_G} \sum_{\gamma=1}^{n_G} \bar{w}_\alpha \bar{w}_\beta \bar{w}_\gamma N_1(\xi_{1\alpha}, \xi_{2\beta}, \xi_{3\gamma}) f_{Vx2}^e(\xi_{1\alpha}, \xi_{2\beta}, \xi_{3\gamma}) \det(\underline{J}_e(\xi_{1\alpha}, \xi_{2\beta}, \xi_{3\gamma})) \\ \alpha_{Vx3}^e(t) \sum_{\alpha=1}^{n_G} \sum_{\beta=1}^{n_G} \sum_{\gamma=1}^{n_G} \bar{w}_\alpha \bar{w}_\beta \bar{w}_\gamma N_1(\xi_{1\alpha}, \xi_{2\beta}, \xi_{3\gamma}) f_{Vx3}^e(\xi_{1\alpha}, \xi_{2\beta}, \xi_{3\gamma}) \det(\underline{J}_e(\xi_{1\alpha}, \xi_{2\beta}, \xi_{3\gamma})) \\ \alpha_{Vx1}^e(t) \sum_{\alpha=1}^{n_G} \sum_{\beta=1}^{n_G} \sum_{\gamma=1}^{n_G} \bar{w}_\alpha \bar{w}_\beta \bar{w}_\gamma N_2(\xi_{1\alpha}, \xi_{2\beta}, \xi_{3\gamma}) f_{Vx1}^e(\xi_{1\alpha}, \xi_{2\beta}, \xi_{3\gamma}) \det(\underline{J}_e(\xi_{1\alpha}, \xi_{2\beta}, \xi_{3\gamma})) \\ \alpha_{Vx2}^e(t) \sum_{\alpha=1}^{n_G} \sum_{\beta=1}^{n_G} \sum_{\gamma=1}^{n_G} \bar{w}_\alpha \bar{w}_\beta \bar{w}_\gamma N_2(\xi_{1\alpha}, \xi_{2\beta}, \xi_{3\gamma}) f_{Vx2}^e(\xi_{1\alpha}, \xi_{2\beta}, \xi_{3\gamma}) \det(\underline{J}_e(\xi_{1\alpha}, \xi_{2\beta}, \xi_{3\gamma})) \\ \alpha_{Vx3}^e(t) \sum_{\alpha=1}^{n_G} \sum_{\beta=1}^{n_G} \sum_{\gamma=1}^{n_G} \bar{w}_\alpha \bar{w}_\beta \bar{w}_\gamma N_2(\xi_{1\alpha}, \xi_{2\beta}, \xi_{3\gamma}) f_{Vx3}^e(\xi_{1\alpha}, \xi_{2\beta}, \xi_{3\gamma}) \det(\underline{J}_e(\xi_{1\alpha}, \xi_{2\beta}, \xi_{3\gamma})) \\ \vdots \\ \alpha_{Vx1}^e(t) \sum_{\alpha=1}^{n_G} \sum_{\beta=1}^{n_G} \sum_{\gamma=1}^{n_G} \bar{w}_\alpha \bar{w}_\beta \bar{w}_\gamma N_8(\xi_{1\alpha}, \xi_{2\beta}, \xi_{3\gamma}) f_{Vx1}^e(\xi_{1\alpha}, \xi_{2\beta}, \xi_{3\gamma}) \det(\underline{J}_e(\xi_{1\alpha}, \xi_{2\beta}, \xi_{3\gamma})) \\ \alpha_{Vx2}^e(t) \sum_{\alpha=1}^{n_G} \sum_{\beta=1}^{n_G} \sum_{\gamma=1}^{n_G} \bar{w}_\alpha \bar{w}_\beta \bar{w}_\gamma N_8(\xi_{1\alpha}, \xi_{2\beta}, \xi_{3\gamma}) f_{Vx2}^e(\xi_{1\alpha}, \xi_{2\beta}, \xi_{3\gamma}) \det(\underline{J}_e(\xi_{1\alpha}, \xi_{2\beta}, \xi_{3\gamma})) \\ \alpha_{Vx3}^e(t) \sum_{\alpha=1}^{n_G} \sum_{\beta=1}^{n_G} \sum_{\gamma=1}^{n_G} \bar{w}_\alpha \bar{w}_\beta \bar{w}_\gamma N_8(\xi_{1\alpha}, \xi_{2\beta}, \xi_{3\gamma}) f_{Vx3}^e(\xi_{1\alpha}, \xi_{2\beta}, \xi_{3\gamma}) \det(\underline{J}_e(\xi_{1\alpha}, \xi_{2\beta}, \xi_{3\gamma})) \end{Bmatrix} \quad (11.3.10)$$

11.3.5 Force Vector: Face Loading

This type of loading characterizes applied, time-varying surface loads such as pressure, wind gusts, contact loading, distributed friction forces, magnetic fields, and so on. The general mathematical expression for surface loading is obtained from (11.3.5) as

$$\underline{f}^e_{24 \times 1} = \int_{\Gamma^e} \underline{N}^T \begin{Bmatrix} F_{\Gamma x1}^e \\ F_{\Gamma x2}^e \\ F_{\Gamma x3}^e \end{Bmatrix} d\Gamma \tag{11.3.11}$$

For the sake of illustration, assume that a traction (surface force per area) is applied to face 1 of the element shown in Figure 11.3.1. The analysis developed below also applies to loading on the other faces with the appropriate change in indices.

Since $\xi_1 = -1$ on face 1, it follows from (11.2.2) that

$$N_5 = N_6 = N_7 = N_8 = 0 \tag{11.3.12}$$

on face 1. Substituting (11.3.12) into the \underline{N} matrix of (11.3.2) and then into (11.3.11) shows that \underline{f}^e has zero entries in rows 13, 14, 15, 16, 17, 18, 19, 20, 21, 22, 23, and 24. In other words, \underline{f}^e has zero entries for every dof not on face 1. The remaining entries in \underline{f}^e are obtained by transforming the surface integral in (11.3.11) into 2D natural coordinates and then applying Gauss quadrature as discussed below. Figure 11.3.2 shows face 1 in actual and natural coordinates.

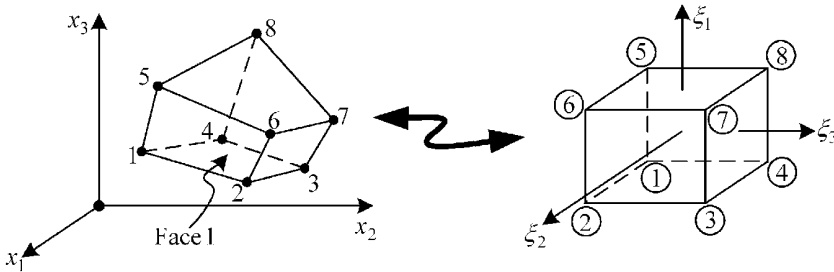


Figure 11.3.1 Face 1 as defined by local nodes 1, 2, 3, and 4

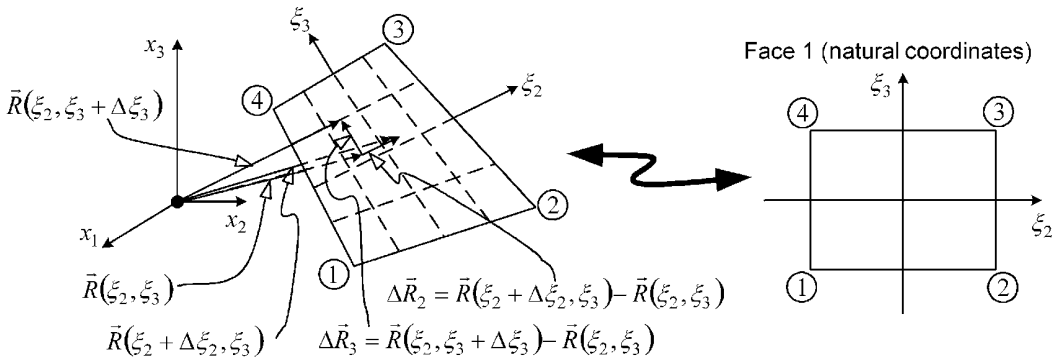


Figure 11.3.2 Face 1 ($\xi_1 = -1$) of the hexahedral 8-node brick element

From Figure 11.3.2,

$$\frac{d\bar{R}}{d\xi_2} = \lim_{\Delta\xi_2 \rightarrow 0} \frac{\Delta\bar{R}_2}{\Delta\xi_2}, \quad \frac{d\bar{R}}{d\xi_3} = \lim_{\Delta\xi_3 \rightarrow 0} \frac{\Delta\bar{R}_3}{\Delta\xi_3} \quad (11.3.13)$$

where $(d\bar{R}/d\xi_2)$ is along a line of constant ξ_3 and $(d\bar{R}/d\xi_3)$ is along a line of constant ξ_2 . A differential of surface area on face 1 of the element is shown in Figure 11.3.3.

From vector geometry, the area of the parallelogram in Figure 11.3.3 can be calculated from the formula

$$d\Gamma = \left| \frac{d\bar{R}}{d\xi_3} d\xi_3 \times \frac{d\bar{R}}{d\xi_2} d\xi_2 \right| = \left| \frac{d\bar{R}}{d\xi_3} \times \frac{d\bar{R}}{d\xi_2} \right| d\xi_2 d\xi_3 = \tilde{J} d\xi_2 d\xi_3 \quad (11.3.14)$$

The “surface” Jacobian is defined as (Hildebrand, 1976)

$$\tilde{J} = \left| \frac{d\bar{R}}{d\xi_3} \Big|_{\xi_1=-1} \times \frac{d\bar{R}}{d\xi_2} \Big|_{\xi_1=-1} \right| \quad (11.3.15)$$

where \bar{R} is defined in Figure 11.3.2 as

$$\bar{R} = x_1 \hat{e}_1 + x_2 \hat{e}_2 + x_3 \hat{e}_3 \quad (11.3.16)$$

therefore,

$$\frac{\partial \bar{R}}{\partial \xi_3} \times \frac{\partial \bar{R}}{\partial \xi_2} = \det \begin{bmatrix} \hat{e}_1 & \hat{e}_2 & \hat{e}_3 \\ \frac{\partial x_1}{\partial \xi_3} & \frac{\partial x_2}{\partial \xi_3} & \frac{\partial x_3}{\partial \xi_3} \\ \frac{\partial x_1}{\partial \xi_2} & \frac{\partial x_2}{\partial \xi_2} & \frac{\partial x_3}{\partial \xi_2} \end{bmatrix} = g_1 \hat{e}_1 + g_2 \hat{e}_2 + g_3 \hat{e}_3 \quad (11.3.17)$$

where

$$g_1 = \frac{\partial x_2}{\partial \xi_3} \frac{\partial x_3}{\partial \xi_2} - \frac{\partial x_2}{\partial \xi_2} \frac{\partial x_3}{\partial \xi_3}, \quad g_2 = \frac{\partial x_1}{\partial \xi_2} \frac{\partial x_3}{\partial \xi_3} - \frac{\partial x_1}{\partial \xi_3} \frac{\partial x_3}{\partial \xi_2}, \quad g_3 = \frac{\partial x_1}{\partial \xi_3} \frac{\partial x_2}{\partial \xi_2} - \frac{\partial x_2}{\partial \xi_3} \frac{\partial x_1}{\partial \xi_2} \quad (11.3.18)$$

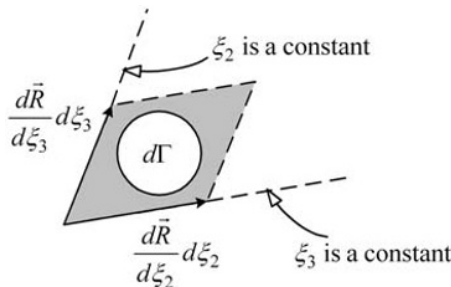


Figure 11.3.3 Differential of surface area on face 1

From (11.3.14) and (11.3.17), the surface Jacobian may be expressed as

$$\tilde{J} = \sqrt{g_1^2 + g_2^2 + g_3^2} \quad (11.3.19)$$

Recall from (11.2.4)

$$x_i = \sum_{k=1}^8 N_k x_{i,k}^e \quad i = 1, 2, 3 \quad (11.3.20)$$

Therefore, it follows that

$$\frac{\partial x_i}{\partial \xi_m} = \sum_{k=1}^8 \frac{\partial N_k}{\partial \xi_m} x_{i,k}^e \quad i = 1, 2, 3 \quad m = 2, 3 \quad (11.3.21)$$

Table 11.2.2 shows that

$$\left. \frac{\partial N_k}{\partial \xi_m} \right|_{\xi_1 = -1} = 0 \quad \text{for } k = 5, 6, 7, 8 \quad m = 2, 3 \quad (11.3.22)$$

therefore,

$$\left. \frac{\partial x_i}{\partial \xi_m} \right|_{\xi_1 = -1} = \sum_{k=1}^4 \left. \frac{\partial N_k}{\partial \xi_m} \right|_{\xi_1 = -1} x_{i,k} \quad i = 1, 2, 3 \quad m = 2, 3 \quad (11.3.23)$$

The $(\partial N_k / \partial \xi_m)$ terms in (11.3.23) are obtained from the shape function derivative formulas in Table 11.2.2 and are evaluated at all integration point pairs (ξ_2, ξ_3) on face 1. The resulting $(\partial x_i / \partial \xi_m)$ terms may then be inserted into (11.3.18) to obtain $g_1, g_2,$ and g_3 . Finally, from (11.3.15) and (11.3.17), the surface Jacobian determinant is evaluated from

$$|\tilde{J}| = \left| \frac{\partial \bar{R}}{\partial \xi_3} \times \frac{\partial \bar{R}}{\partial \xi_2} \right|_{\xi_1 = -1} = (g_1^2 + g_2^2 + g_3^2)^{1/2} \Big|_{\xi_1 = -1} \quad (11.3.24)$$

Substitution of (11.3.14) into (11.3.11) yields

$$\begin{aligned} \underline{f}_{24 \times 1}^e &= \int_{-1}^1 \int_{-1}^1 \underline{N}_e^T \underline{F}_\Gamma^e |\tilde{J}| d\xi_2 d\xi_3 \\ &= \int_{-1}^1 \int_{-1}^1 \left\{ \underline{N}_e^T(\xi_1, \xi_2, \xi_3) \underline{F}_\Gamma^e(x_1(\xi_1, \xi_2, \xi_3), x_2(\xi_1, \xi_2, \xi_3), x_3(\xi_1, \xi_2, \xi_3)) \right\} \Big|_{\xi_1 = -1} * |\tilde{J}(\xi_2, \xi_3)| d\xi_2 d\xi_3 \end{aligned} \quad (11.3.25)$$

Equation (11.3.25) is in a form suitable for Gauss quadrature, as expressed by

$$\underline{f}_{24 \times 1}^e = \sum_{\beta=1}^{n_G} \sum_{\gamma=1}^{n_G} \bar{w}_\beta \bar{w}_\gamma * \left[\underline{N}_e^T(\xi_1, \xi_{2\beta}, \xi_{3\gamma}) \underline{F}_\Gamma^e(x_i(\xi_1, \xi_{2\beta}, \xi_{3\gamma})) \right] |\tilde{J}(\xi_{2\beta}, \xi_{3\gamma})| \Big|_{\xi_1 = -1} \quad (11.3.26)$$

A final point of interest is that both $\left(\frac{\partial \vec{R}}{\partial \xi_2}\right)\Big|_{\xi_1=-1}$ and $\left(\frac{\partial \vec{R}}{\partial \xi_3}\right)\Big|_{\xi_1=-1}$ are parallel to the surface in Figure 11.3.2; therefore, the cross product

$$g_1 \hat{e}_1 + g_2 \hat{e}_2 + g_3 \hat{e}_3 = \frac{\partial \vec{R}}{\partial \xi_3}\Big|_{\xi_1=-1} \times \frac{\partial \vec{R}}{\partial \xi_2}\Big|_{\xi_1=-1} \quad (11.3.27)$$

is normal to the surface. This outward normal vector will be employed in Section 11.5 for computing the surface stresses with Cauchy's surface equilibrium boundary formula (A.2.6)

$$\Phi_j = n_i \sigma_{ij} \quad (11.3.28)$$

11.4 ASSEMBLY PROCEDURE FOR THE 3D, 8-NODE, HEXAHEDRAL ELEMENT MODEL

As indicated in the discussion of truss, beam, and planar solid elements, the total system model consists of all dofs including both free and fixed. The fixed dofs are zero and need not be solved for so a constraint condensed model is formed consisting of only free (nonfixed) dofs. This follows the same approach used for truss elements in Chapter 4, beam elements in Chapter 9, and plane strain/stress and axisymmetric elements in Chapter 10. The global dofs are ordered in the global-free system displacement vector as shown in Table 11.4.1.

The total number of dofs in the system is

$$N_d = N_n * \frac{3\text{dofs}}{\text{node}} = 3N_n \quad (11.4.1)$$

where N_n is the number of nodes in the model.

The nodal connectivity array for the 8-node elements is

$$B_{ej} = \text{ICON}(e,j) = \text{global node number for local node } j \text{ of element } e, \quad (11.4.2)$$

for $j = 1, 8$ and $e = 1, \dots, N_e$

Table 11.4.1 Degree of freedom (dof) ordering convention in the total system displacement vector

System node number	Direction	System dof number
1	x_1	1
1	x_2	2
1	x_3	3
2	x_1	4
2	x_2	5
2	x_3	6
\vdots	\vdots	\vdots
N_n	x_1	$3 * (N_n - 1) + 1$
N_n	x_2	$3 * (N_n - 1) + 2$
N_n	x_3	$3 * (N_n - 1) + 3$

where N_e is the number of elements in the model. The local nodes are ordered as shown in Figure 11.1.2. The ordering of local dofs within an element is shown in the \underline{u}_r^e vector in (11.2.36)

$$\underline{u}_r^e = (u_{1,1}^e \ u_{2,1}^e \ u_{3,1}^e \ u_{1,2}^e \ u_{2,2}^e \ u_{3,2}^e \ \cdots \ u_{1,8}^e \ u_{2,8}^e \ u_{3,8}^e)^T \quad (24 \times 1) \quad (11.4.3)$$

and is also shown in Table 11.4.2. Similar with the nodal connectivity array, a dof connectivity array is defined by

$$\hat{B}_{el} = \text{ICONDOF}(e, l) = \text{system dof number for local dof number } l \text{ of element } e, \quad (11.4.4)$$

for $l = 1, \dots, 24$ and $e = 1, \dots, N_e$

and is evaluated using the nodal connectivities and the formula

$$\hat{B}_{el} = \text{ICONDOF}(e, l) = 3 * (\text{ICON}(e, j) - 1) + k \quad (11.4.5)$$

where

$$\begin{aligned} k &= 1, 2, 3 \text{ (direction index } x_1, x_2, x_3), \\ j &= 1, 8 \text{ (local node index),} \\ l &= 3 * (j - 1) + k \text{ (local dof index)} \end{aligned} \quad (11.4.6)$$

Figure 11.4.1 and Table 11.4.3 illustrate the dof connectivity array for an example 3D solid element.

Similar to (10.5.12) for planar solids, let

$$i_{pdl} = l\text{th fixed dof number for } l = 1, \dots, N_{pd}$$

be an array defined by the modeler to store the dofs that are fixed (constrained). The $jarray$ (j_i) contains the system dof numbers that are free (not fixed) and is determined via the algorithm defined in (10.5.13) for models with any type of elements (truss, beam, 2D solid, 3D solid, and so on). The counterpart $larray$ (l_i) stores either the location of system dof i in the constraint condensed vector \underline{x}_f or a zero if system dof i is fixed. The algorithm for forming

Table 11.4.2 Local degrees of freedom (dofs) in a 3D hexahedral solid element

Local dof (l)	Local node	Direction	Local dof (l)	Local node	Direction
1	1	x_1	13	5	x_1
2	1	x_2	14	5	x_2
3	1	x_3	15	5	x_3
4	2	x_1	16	6	x_1
5	2	x_2	17	6	x_2
6	2	x_3	18	6	x_3
7	3	x_1	19	7	x_1
8	3	x_2	20	7	x_2
9	3	x_3	21	7	x_3
10	4	x_1	22	8	x_1
11	4	x_2	23	8	x_2
12	4	x_3	24	8	x_3

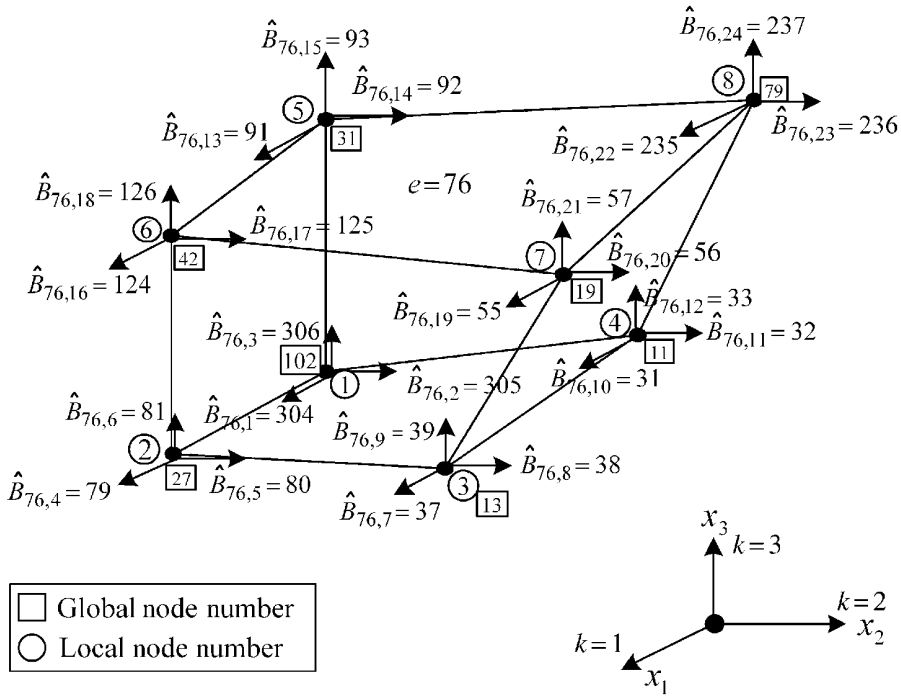


Figure 11.4.1 System dofs example for a hypothetical 8-node solid element with element number $e = 76$

Table 11.4.3 System degrees of freedom (dofs) for the 3D element shown in Figure 11.4.1

Element (e)	Local node (j)	Direction index (k)	Local dof $l = 3 * (j - 1) + k$	Global node number $\underline{B}_{ej} = \text{ICON}(e, j)$	Global dof number $\hat{B}_{el} = \text{ICONDOF}(e, l)$ $= 3 * (\text{ICON}(e, j) - 1) + k$
76	1	1	1	102	304
76	1	2	2	102	305
76	1	3	3	102	306
76	2	1	4	27	79
76	2	2	5	27	80
76	2	3	6	27	81
76	3	1	7	13	37
76	3	2	8	13	38
76	3	3	9	13	39
76	4	1	10	11	31
76	4	2	11	11	32
76	4	3	12	11	33
76	5	1	13	31	91
76	5	2	14	31	92
76	5	3	15	31	93
76	6	1	16	42	124
76	6	2	17	42	125
76	6	3	18	42	126
76	7	1	19	19	55
76	7	2	20	19	56
76	7	3	21	19	57
76	8	1	22	79	235
76	8	2	23	79	236
76	8	3	24	79	237

the *larray* is given in (10.5.13)–(10.5.15) for models with any type of elements (truss, beam, 2D, 3D, and so on). The local dof numbers within an element are defined in Table 11.4.2 and transform into global system and constraint condensed system dof numbers according with Table 11.4.4.

From these results, it follows that the constraint condensed system mass and stiffness matrices and force vector may be formed directly from the corresponding element matrices as shown in Figure 11.4.2.

As in (9.2.85), imposing the zero-displacement constraint conditions yields the following “condensed” dynamic equilibrium equation for the “free” (unconstrained) dofs of the constrained structure:

$$\underset{N_f \times N_f}{\underline{M}_f} \ddot{\underset{N_f \times 1}{\underline{q}}_f} + \underset{N_f \times N_f}{\underline{C}_f} \dot{\underset{N_f \times 1}{\underline{q}}_f} + \underset{N_f \times N_f}{\underline{K}_f} \underset{N_f \times 1}{\underline{q}}_f = \underset{N_f \times 1}{\underline{F}_f} \quad (11.4.7)$$

Equation (11.4.7) is solved for all of the nonfixed dofs in the system, that is, the \underline{q}_f vector. The entire system (fixed and free dofs) displacement vector \underline{q} may be formed from \underline{q}_f using the *jarray* as demonstrated in Example 9.2.2 or (10.5.14):

Table 11.4.4 Degree of freedom (dof) conventions for element matrices, full system, and constraint condensed dof system

Element <i>e</i> local dofs (= 1, ..., 24)	System dofs (= 1, 2, ..., <i>N_d</i>)	Constraint condensed dofs ^a (= 1, 2, ..., <i>N_{npd}</i>)
<i>m</i>	<i>B_{em}</i>	<i>l_{B_{em}}</i>
<i>n</i>	<i>B_{en}</i>	<i>l_{B_{en}}</i>

^a *l_{B_{em}}* or *l_{B_{en}}* will be zero if the dof is fixed, that is, it will not appear in the constraint condensed system vector \underline{q}_f .

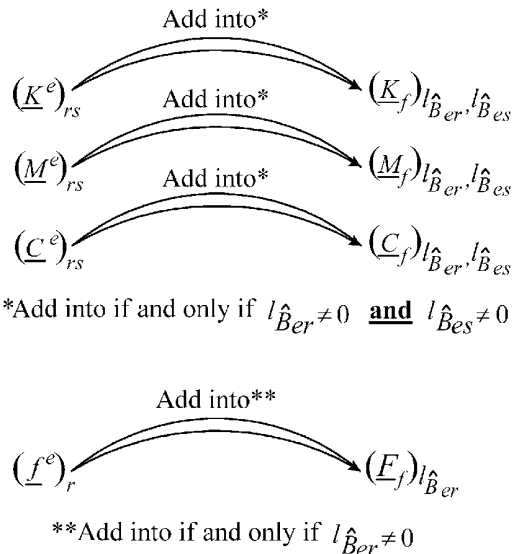


Figure 11.4.2 Assembly of constraint condensed system matrices and force vector from the element matrices and force vector

$$\begin{aligned}
& \text{for } l=1, N_{pd} \text{ (no. of fixed dofs)} \\
& \quad k = i_{pdl} \\
& \quad q_k = 0 \\
& \text{end} \\
& \text{for } l=1, N_{npd} \text{ (no. of nonfixed dofs)} \\
& \quad k = jarray(l) \\
& \quad (q)_k = (q_f)_l \\
& \text{end}
\end{aligned} \tag{11.4.8}$$

The element stiffness matrix \underline{K}^e in Figure 11.4.2 is obtained from (11.2.42) if extra shape functions are included or directly from the 24×24 version of (11.2.34) if the 8-node element is used. The element mass matrix \underline{M}^e in Figure 11.4.2 is obtained from (11.3.4). The element force vector \underline{f}^e in Figure 11.4.2 is obtained from (11.3.6) for concentrated nodal forces, from (11.3.10) for distributed volume loads, and from (11.3.26) for face loading.

11.5 COMPUTATION OF STRESSES FOR A 3D HEXAHEDRAL SOLID ELEMENT

The prediction of dynamic stresses is an essential step in most vibration studies, since vibratory stresses may lead to high-cycle fatigue-induced fracture failure as discussed in Section 1.4. Stresses may be evaluated at locations inside of an element or on an element face that lies on the surface of the object being modeled.

11.5.1 Computation of Interior Stress

A general practice is to evaluate the stresses at the Gauss integration points since for certain element geometries, this yields the most accurate stress predictions (Cook et al., 1989). Stress at other locations in an element may then be interpolated or extrapolated from the GQ point values. The stress in a 3D solid element model of a structure with isotropic material properties is given by (A.4.3)

$$\begin{Bmatrix} \sigma_{11} \\ \sigma_{22} \\ \sigma_{33} \\ \sigma_{23} \\ \sigma_{13} \\ \sigma_{12} \end{Bmatrix} = \frac{E}{(1+\nu)(1-2\nu)} \begin{bmatrix} 1-\nu & \nu & \nu & 0 & 0 & 0 \\ \nu & 1-\nu & \nu & 0 & 0 & 0 \\ \nu & \nu & 1-\nu & 0 & 0 & 0 \\ 0 & 0 & 0 & \frac{1-2\nu}{2} & 0 & 0 \\ 0 & 0 & 0 & 0 & \frac{1-2\nu}{2} & 0 \\ 0 & 0 & 0 & 0 & 0 & \frac{1-2\nu}{2} \end{bmatrix} \begin{Bmatrix} \epsilon_{11} \\ \epsilon_{22} \\ \epsilon_{33} \\ 2\epsilon_{23} \\ 2\epsilon_{13} \\ 2\epsilon_{12} \end{Bmatrix} \tag{11.5.1}$$

or

$$\underline{\sigma} = \underline{E}\underline{\epsilon} \tag{11.5.2}$$

where $\nu = \text{Poisson's ratio}$ and $E = \text{Young's modulus}$.

Substitution of (11.2.25) and (11.2.27) into (11.5.2) yields

$$\underline{\sigma}^e = \underline{E}^e \underline{\epsilon}^e = \underline{E}^e \underline{B}^e \underline{u}_{eN} = \underline{E}^e \underline{A}_1^e \underline{A}_2^e \underline{u}_{eN} \quad (11.5.3)$$

The stress at any integration point $(\xi_{1\alpha}, \xi_{2\beta}, \xi_{3\gamma})$ is obtained from

$$\underline{\sigma}^e(\xi_{1\alpha}, \xi_{2\beta}, \xi_{3\gamma}) = \underline{E}^e \underline{B}^e(\xi_{1\alpha}, \xi_{2\beta}, \xi_{3\gamma}) \underline{u}_{eN} \quad (11.5.4)$$

The element displacements \underline{u}_{eN} in (11.5.4) may be obtained from the constraint condensed displacement vector \underline{q}_f in (11.4.7) at any time t using the dof connectivity array \hat{B}_{em} from (11.4.4) and the *larray* (10.5.15). Recall that $m = 1, \dots, 24$ indicates the 24 local dofs in \underline{u}_{eN} as shown in Table 11.4.2. Therefore,

$$(\underline{u}_{eN})_m = \begin{cases} (\underline{q}_f)_{l_{\hat{B}_{em}}}, & l_{\hat{B}_{em}} \neq 0 \\ 0, & l_{\hat{B}_{em}} = 0 \end{cases}, \quad \text{for } m = 1, \dots, 24 \quad (11.5.5)$$

The \underline{u}_{eN} in (11.5.5) only include the 24 retained dofs (nodes 1–8) in element e . The remaining 9 dofs, that is, 25–33, are obtained via (11.2.40) with $f_c^e = \underline{0}$, as recommended in Cook et al. (1989), if extra shape functions are employed, that is, N_9, N_{10} , and N_{11} , in (11.2.7).

Steps to obtain stresses at Gauss integration point $\xi_{1\alpha}, \xi_{2\beta}, \xi_{3\gamma}$ within element e :

- (a) At some time t , obtain the element e nodal displacements $\underline{u}_{eN}(t)$ from the displacement vector $\underline{q}_f(t)$ via (11.5.5). Treat these as the retained dofs (\underline{u}_r^e) in (11.2.40) and solve for \underline{u}_c^e by setting f_c^e equal to zero. Finally, set $(\underline{u}_{eN})_m$ equal to \underline{u}_c^e for $m = 25, \dots, 33$.
- (b) Compute the shape functions $N_l(\xi_1, \xi_2, \xi_3)$ and their derivatives $\partial N_l / \partial \xi_1$, $\partial N_l / \partial \xi_2$, and $\partial N_l / \partial \xi_3$ from (11.2.2), (11.2.7), and Table 11.2.2 for $l = 1, 11$, at the GP locations, $(\xi_1, \xi_2, \xi_3) = (\xi_{1\alpha}, \xi_{2\beta}, \xi_{3\gamma})$, in Table 11.2.3.
- (c) Compute the locations of the GP integration point $(\xi_{1\alpha}, \xi_{2\beta}, \xi_{3\gamma})$ in the actual coordinates (11.2.4)

$$x_i = \sum_{l=1}^8 N_l(\xi_{1\alpha}, \xi_{2\beta}, \xi_{3\gamma}) x_{il}^e \quad i = 1, 2, 3 \quad (11.5.6)$$

- (d) Compute the Jacobian matrix \underline{J}_e at $\xi_{1\alpha}, \xi_{2\beta}, \xi_{3\gamma}$ via (11.2.14).
- (e) Form the \underline{A}_1^e and \underline{A}_2^e matrices at $(\xi_{1\alpha}, \xi_{2\beta}, \xi_{3\gamma})$ via Equations (11.2.18), (11.2.19), and (11.2.23), respectively.
- (f) Compute the \underline{B}^e matrix (11.2.27)

$$\underline{B}^e = \underline{A}_1^e \underline{A}_2^e \quad (11.5.7)$$

Note that \underline{B}^e is 6×33 if the three extra nodes (9, 10, 11) are included and is 6×24 if only 8 nodes per element are utilized.

- (g) Compute the strains at $(\xi_{1\alpha}, \xi_{2\beta}, \xi_{3\gamma})$ via (11.2.26)

$$\underline{\epsilon}^e(\xi_{1\alpha}, \xi_{2\beta}, \xi_{3\gamma}, t) = \underline{B}^e(\xi_{1\alpha}, \xi_{2\beta}, \xi_{3\gamma}) \underline{u}_{eN}(t) \quad (11.5.8)$$

(h) Compute the stresses at $(\xi_{1\alpha}, \xi_{2\beta}, \xi_{3\gamma})$ at the given time t by (11.5.4)

$$\underline{\sigma}^e(\xi_{1\alpha}, \xi_{2\beta}, \xi_{3\gamma}, t) = \underline{E}^e \underline{\epsilon}^e(\xi_{1\alpha}, \xi_{2\beta}, \xi_{3\gamma}, t) = \underline{E}^e \underline{B}^e(\xi_{1\alpha}, \xi_{2\beta}, \xi_{3\gamma}) \underline{u}_{eN} \quad (11.5.9)$$

(i) Repeat steps (b)–(h) for all integration points in element e . Interpolate/extrapolate stresses within element e given all integration point stresses $\underline{\sigma}^e(\xi_{1\alpha}, \xi_{2\beta}, \xi_{3\gamma})$ and their actual locations $\{x_1^e(\xi_{1\alpha}, \xi_{2\beta}, \xi_{3\gamma}), x_2^e(\xi_{1\alpha}, \xi_{2\beta}, \xi_{3\gamma}), x_3^e(\xi_{1\alpha}, \xi_{2\beta}, \xi_{3\gamma})\}$ in element e .

The above procedure yields the six component stresses at any location within an element. Ductile material failure methods typically employ the von Mises or equivalent stresses, defined using the above component stresses, as given in (1.4.15)–(1.4.17).

11.5.2 Computation of Surface Stresses

This section explains how to obtain surface stresses directly without extrapolation of integration point stresses to the surface. Surface stress evaluation is very important since failures often initiate on the surface of a component (Figure 11.5.1).

Strain is typically measured by cementing a strain gage to the surface, which provides strains in a coordinate system that is tangent to the surface at the location where the gage is attached. Assume that face 6 of an element is located on the surface of the object being modeled. Figure 11.5.2 shows the face 6 surface and a local (surface) coordinate system attached to it. This face is selected arbitrarily and the surface stresses may be obtained in a similar manner on any of the other five faces.

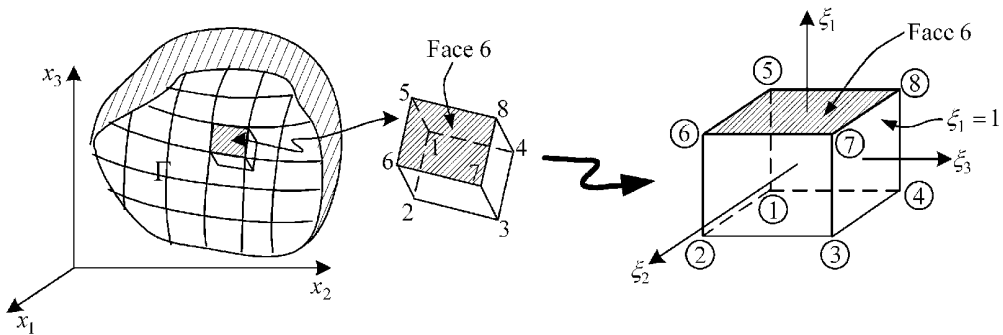


Figure 11.5.1 Surface stress computation on face 6 of element e

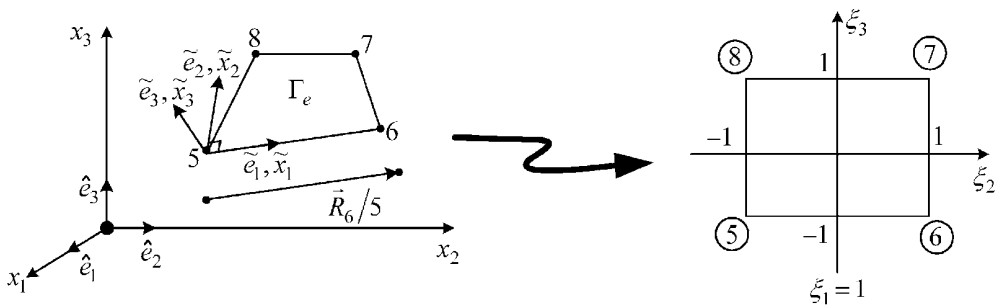


Figure 11.5.2 Transformation of face 6 to natural coordinates

For simplicity, assume that nodes 5, 6, 7, and 8 are coplanar. This will insure that the \tilde{x}_1, \tilde{x}_2 axes are tangent to the surface throughout Γ_e . If the surface is warped due to non-coplanar nodes or interpolation of quadratic or higher orders, one must define a different “surface” coordinate system at each point of interest on face 6. This may be accomplished by utilizing the tangent vector $\left(d\vec{R}/d\xi_2 \right) \Big|_{\xi_1=1}$ and normal vector

$$\hat{n} = \frac{\frac{\partial \vec{R}}{\partial \xi_2} \times \frac{\partial \vec{R}}{\partial \xi_3}}{\left| \frac{\partial \vec{R}}{\partial \xi_2} \times \frac{\partial \vec{R}}{\partial \xi_3} \right|} \quad (11.5.10)$$

as discussed in the derivation of (11.3.27). In order to compute surface stress, all quantities (displacements, strains, tractions, and so on) need to be expressed in the local $\tilde{x}_1, \tilde{x}_2, \tilde{x}_3$ coordinates, which requires a coordinate transformation matrix between the global axes (x_1, x_2, x_3) and surface tangent axes ($\tilde{x}_1, \tilde{x}_2, \tilde{x}_3$).

11.5.3 Coordinate Transformation

Consider the following analysis used to obtain the coordinate transformation matrix between the (x_1, x_2, x_3) and ($\tilde{x}_1, \tilde{x}_2, \tilde{x}_3$) orthogonal triads. The local unit vector \tilde{e}_3 is normal to the surface; therefore,

$$\tilde{e}_3 = \tilde{e}_{31}\hat{e}_1 + \tilde{e}_{32}\hat{e}_2 + \tilde{e}_{33}\hat{e}_3 = \hat{n} = n_1\hat{e}_1 + n_2\hat{e}_2 + n_3\hat{e}_3 = \frac{\vec{R}_{6/5} \times \vec{R}_{8/5}}{\left| \vec{R}_{6/5} \times \vec{R}_{8/5} \right|} \quad (11.5.11)$$

by the assumption that face 6 is planar. Note that $\vec{R}_{6/5}$ and $\vec{R}_{8/5}$ are vectors that start at node 5 and end at nodes 6 and 8, respectively. The local unit vector \tilde{e}_1 is obtained from

$$\tilde{e}_1 = \tilde{e}_{11}\hat{e}_1 + \tilde{e}_{12}\hat{e}_2 + \tilde{e}_{13}\hat{e}_3 = \frac{\vec{R}_{6/5}}{\left| \vec{R}_{6/5} \right|} \quad (11.5.12)$$

The remaining local unit vector \tilde{e}_2 is obtained from the condition of orthogonal unit vectors:

$$\begin{aligned} \tilde{e}_2 &= \tilde{e}_{21}\hat{e}_1 + \tilde{e}_{22}\hat{e}_2 + \tilde{e}_{23}\hat{e}_3 = \tilde{e}_3 \times \tilde{e}_1 = \det \begin{bmatrix} \hat{e}_1 & \hat{e}_2 & \hat{e}_3 \\ \tilde{e}_{31} & \tilde{e}_{32} & \tilde{e}_{33} \\ \tilde{e}_{11} & \tilde{e}_{12} & \tilde{e}_{13} \end{bmatrix} \\ &= \hat{e}_1(\tilde{e}_{32}\tilde{e}_{13} - \tilde{e}_{33}\tilde{e}_{12}) + \hat{e}_2(\tilde{e}_{33}\tilde{e}_{11} - \tilde{e}_{31}\tilde{e}_{13}) + \hat{e}_3(\tilde{e}_{31}\tilde{e}_{12} - \tilde{e}_{32}\tilde{e}_{11}) \end{aligned} \quad (11.5.13)$$

Figure 11.5.3 shows both the global and surface tangent coordinate systems.

The components \tilde{A}_i of any vector \vec{A} expressed in the $\tilde{x}_1, \tilde{x}_2, \tilde{x}_3$ coordinates can be obtained from the components A_i of the same vector expressed in the global axes (x_1, x_2, x_3) utilizing (2.7.5)

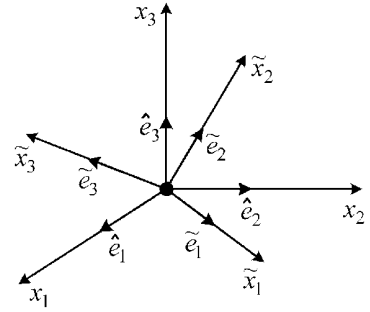


Figure 11.5.3 The global and surface tangent (local) coordinate systems

$$\begin{Bmatrix} \tilde{A}_1 \\ \tilde{A}_2 \\ \tilde{A}_3 \end{Bmatrix} = \begin{bmatrix} C_{11} & C_{12} & C_{13} \\ C_{21} & C_{22} & C_{23} \\ C_{31} & C_{32} & C_{33} \end{bmatrix} \begin{Bmatrix} A_1 \\ A_2 \\ A_3 \end{Bmatrix} \quad (11.5.14)$$

where the direction cosine is defined in (2.7.6) as

$$C_{ij} = \cos(\tilde{x}_i, x_j) = \text{cosine of the angle between the } \tilde{x}_i \text{ direction and the } x_j \text{ direction} \quad (11.5.15)$$

The C_{ij} are obtained by noting

$$\tilde{e}_i \cdot \hat{e}_j = |\tilde{e}_i| |\hat{e}_j| \cos(\tilde{e}_i, \hat{e}_j) = (1)(1) \cos(\tilde{x}_i, x_j) = C_{ij} \quad (11.5.16)$$

Inspection of Equations (11.5.11)–(11.5.13) shows that

$$\tilde{e}_i \cdot \hat{e}_j = \tilde{e}_{ij} \quad (11.5.17)$$

Therefore,

$$C_{ij} = \tilde{e}_{ij} \quad (11.5.18)$$

where \tilde{e}_{ij} are obtained from the nodal coordinates via Equations (11.5.11)–(11.5.13).

11.5.4 Geometry Mapping in Surface Tangent Coordinates

The relative position vector from node 5 to any other node (k) is expressed in system coordinates as

$$\vec{r}_{k/5} = \begin{Bmatrix} x_{1,k} - x_{1,5} \\ x_{2,k} - x_{2,5} \\ x_{3,k} - x_{3,5} \end{Bmatrix} = \begin{Bmatrix} x_{\text{rel}1,k} \\ x_{\text{rel}2,k} \\ x_{\text{rel}3,k} \end{Bmatrix} \quad k = 5, 6, 7, 8 \quad (11.5.19)$$

These relative position vectors may be expressed in surface tangent coordinates via (11.5.14)–(11.5.18) as

$$\begin{Bmatrix} \tilde{x}_{\text{rel}1,k} \\ \tilde{x}_{\text{rel}2,k} \\ \tilde{x}_{\text{rel}3,k} \end{Bmatrix} = \begin{bmatrix} \tilde{e}_{11} & \tilde{e}_{12} & \tilde{e}_{13} \\ \tilde{e}_{21} & \tilde{e}_{22} & \tilde{e}_{23} \\ \tilde{e}_{31} & \tilde{e}_{32} & \tilde{e}_{33} \end{bmatrix} \begin{Bmatrix} x_{\text{rel}1,k} \\ x_{\text{rel}2,k} \\ x_{\text{rel}3,k} \end{Bmatrix} \quad k = 5, 6, 7, 8 \quad (11.5.20)$$

Equation (11.5.20) provides the nodal coordinates of all 4 nodes *as measured in the surface tangent coordinate system*. To obtain the coordinates of other points on Γ_e (as measured in the surface tangent coordinates), apply the standard isoparametric mapping formula

$$\tilde{x}_i = \sum_{k=5}^8 N_k(\xi_2, \xi_3) \Big|_{\xi_1=1} \tilde{x}_{\text{rel},i,k} \quad i = 1, 2, 3 \quad (11.5.21)$$

where from (11.2.2)

$$\begin{aligned} N_5 \Big|_{\xi_1=1} &= \frac{1}{4}(1-\xi_2)(1-\xi_3), & N_6 \Big|_{\xi_1=1} &= \frac{1}{4}(1+\xi_2)(1-\xi_3) \\ N_7 \Big|_{\xi_1=1} &= \frac{1}{4}(1+\xi_2)(1+\xi_3), & N_8 \Big|_{\xi_1=1} &= \frac{1}{4}(1-\xi_2)(1+\xi_3) \end{aligned} \quad (11.5.22)$$

11.5.5 Displacements in the Surface Tangent Coordinate System

Let $u_{i,k}$ represent the global coordinate displacement of node k in the i th direction. The nodal displacements measured in the surface tangent coordinate system are then obtained from (11.5.14)–(11.5.18) as

$$\begin{Bmatrix} \tilde{u}_{1,k} \\ \tilde{u}_{2,k} \\ \tilde{u}_{3,k} \end{Bmatrix} = \begin{bmatrix} \tilde{e}_{11} & \tilde{e}_{12} & \tilde{e}_{13} \\ \tilde{e}_{21} & \tilde{e}_{22} & \tilde{e}_{23} \\ \tilde{e}_{31} & \tilde{e}_{32} & \tilde{e}_{33} \end{bmatrix} \begin{Bmatrix} u_{1,k} \\ u_{2,k} \\ u_{3,k} \end{Bmatrix} \quad k = 5, 6, 7, 8 \quad (11.5.23)$$

The displacements are interpolated in the surface coordinate system via

$$\tilde{u}_i = \sum_{k=5}^8 N_k(\xi_2, \xi_3) \tilde{u}_{i,k} \quad (11.5.24)$$

where $\tilde{u}_{i,k}$ is the i th direction displacement, at node k , as measured in the surface tangent coordinate system.

11.5.6 Strains in the Surface Tangent Coordinate System

The three strains that are required for determining the surface stresses are (A.3.21)

$$\tilde{\varepsilon}_{11} = \frac{\partial \tilde{u}_1}{\partial \tilde{x}_1}, \quad \tilde{\varepsilon}_{12} = \frac{1}{2} \left(\frac{\partial \tilde{u}_1}{\partial \tilde{x}_2} + \frac{\partial \tilde{u}_2}{\partial \tilde{x}_1} \right), \quad \tilde{\varepsilon}_{22} = \frac{\partial \tilde{u}_2}{\partial \tilde{x}_2} \quad (11.5.25)$$

To obtain these strains, consider the following analysis. The \tilde{u}_i are differentiated with respect to \tilde{x}_i in (11.5.25) but are instead functions of ξ_j as expressed in (11.5.24). Use the chain rule to show

$$\begin{Bmatrix} \frac{\partial}{\partial \xi_2} \\ \frac{\partial}{\partial \xi_3} \end{Bmatrix} = \begin{bmatrix} \frac{\partial \tilde{x}_1}{\partial \xi_2} & \frac{\partial \tilde{x}_2}{\partial \xi_2} \\ \frac{\partial \tilde{x}_1}{\partial \xi_3} & \frac{\partial \tilde{x}_2}{\partial \xi_3} \end{bmatrix} \begin{Bmatrix} \frac{\partial}{\partial \tilde{x}_1} \\ \frac{\partial}{\partial \tilde{x}_2} \end{Bmatrix} = (\tilde{J}) \begin{Bmatrix} \frac{\partial}{\partial \tilde{x}_1} \\ \frac{\partial}{\partial \tilde{x}_2} \end{Bmatrix} = \begin{bmatrix} \tilde{J}_{11} & \tilde{J}_{12} \\ \tilde{J}_{21} & \tilde{J}_{22} \end{bmatrix} \begin{Bmatrix} \frac{\partial}{\partial \tilde{x}_1} \\ \frac{\partial}{\partial \tilde{x}_2} \end{Bmatrix} \quad (11.5.26)$$

This is rewritten as

$$\begin{Bmatrix} \frac{\partial}{\partial \tilde{x}_1} \\ \frac{\partial}{\partial \tilde{x}_2} \end{Bmatrix} = \frac{1}{\frac{\partial \tilde{x}_1}{\partial \xi_2} \frac{\partial \tilde{x}_2}{\partial \xi_3} - \frac{\partial \tilde{x}_2}{\partial \xi_2} \frac{\partial \tilde{x}_1}{\partial \xi_3}} \begin{bmatrix} \frac{\partial \tilde{x}_2}{\partial \xi_3} & -\frac{\partial \tilde{x}_2}{\partial \xi_2} \\ -\frac{\partial \tilde{x}_1}{\partial \xi_3} & \frac{\partial \tilde{x}_1}{\partial \xi_2} \end{bmatrix} \begin{Bmatrix} \frac{\partial}{\partial \xi_2} \\ \frac{\partial}{\partial \xi_3} \end{Bmatrix} \quad (11.5.27)$$

where from (11.5.21)

$$\frac{\partial \tilde{x}_i}{\partial \xi_m} = \sum_{k=5}^8 \frac{\partial N_k}{\partial \xi_m} \Big|_{\xi_1=1} \tilde{x}_{\text{rel},k} \quad m=2,3 \quad (11.5.28)$$

Application of (11.5.27) to the surface tangent displacements yields

$$\begin{Bmatrix} \frac{\partial \tilde{u}_1}{\partial \tilde{x}_1} \\ \frac{\partial \tilde{u}_1}{\partial \tilde{x}_2} \\ \frac{\partial \tilde{u}_2}{\partial \tilde{x}_1} \\ \frac{\partial \tilde{u}_2}{\partial \tilde{x}_2} \end{Bmatrix} = \frac{1}{\det(\tilde{J})} \begin{bmatrix} \frac{\partial \tilde{x}_2}{\partial \xi_3} & -\frac{\partial \tilde{x}_2}{\partial \xi_2} & 0 & 0 \\ -\frac{\partial \tilde{x}_1}{\partial \xi_3} & \frac{\partial \tilde{x}_1}{\partial \xi_2} & 0 & 0 \\ 0 & 0 & \frac{\partial \tilde{x}_2}{\partial \xi_3} & -\frac{\partial \tilde{x}_2}{\partial \xi_2} \\ 0 & 0 & -\frac{\partial \tilde{x}_1}{\partial \xi_3} & \frac{\partial \tilde{x}_1}{\partial \xi_2} \end{bmatrix} \begin{Bmatrix} \frac{\partial \tilde{u}_1}{\partial \xi_2} \\ \frac{\partial \tilde{u}_1}{\partial \xi_3} \\ \frac{\partial \tilde{u}_2}{\partial \xi_2} \\ \frac{\partial \tilde{u}_2}{\partial \xi_3} \end{Bmatrix} \quad (11.5.29)$$

where

$$\det \tilde{J} = \frac{\partial \tilde{x}_1}{\partial \xi_2} \frac{\partial \tilde{x}_2}{\partial \xi_3} - \frac{\partial \tilde{x}_2}{\partial \xi_2} \frac{\partial \tilde{x}_1}{\partial \xi_3} \quad (11.5.30)$$

from (11.5.24)

$$\frac{\partial \tilde{u}_i}{\partial \xi_m} = \sum_{k=5}^8 \frac{\partial N_k}{\partial \xi_m} (\xi_2, \xi_3) \Big|_{\xi_1=1} \tilde{u}_{i,k} \quad (11.5.31)$$

and $\partial \tilde{x}_i / \partial \xi_m$ are determined from (11.5.28). Note that given any parent coordinate pair (ξ_2, ξ_3) , all terms like $\partial \tilde{u}_i / \partial \tilde{x}_j$ may be computed from (11.5.29) to (11.5.31); therefore, the required strains in (11.5.25) may also be computed.

11.5.7 Surface Stresses Obtained from Cauchy's Boundary Formula

The next step is to require that the surface stresses satisfy Cauchy's formula (A.2.3), as applied in the surface tangent coordinate system shown in Figure 11.5.4.

From this figure,

$$\hat{n} = \tilde{n}_1 \tilde{e}_1 + \tilde{n}_2 \tilde{e}_2 + \tilde{n}_3 \tilde{e}_3 = \tilde{e}_3 \quad (11.5.32)$$

Therefore,

$$\tilde{n}_1 = 0, \quad \tilde{n}_2 = 0, \quad \tilde{n}_3 = 1 \quad (11.5.33)$$

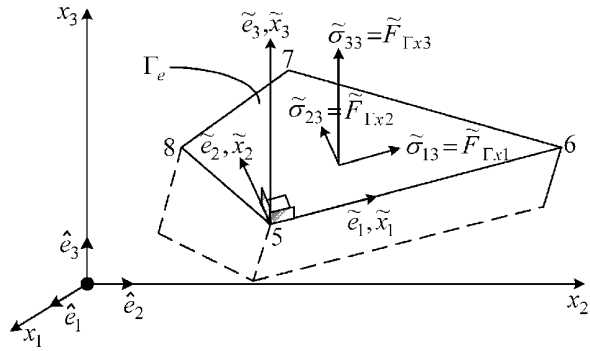


Figure 11.5.4 Applied tractions in the surface tangent coordinate system

The Cauchy boundary formula (A.2.3) applied in the surface tangent coordinates is

$$\begin{Bmatrix} \tilde{F}_{\Gamma x1} \\ \tilde{F}_{\Gamma x2} \\ \tilde{F}_{\Gamma x3} \end{Bmatrix} = \begin{bmatrix} \tilde{n}_1 & 0 & 0 & \tilde{n}_2 & 0 & \tilde{n}_3 \\ 0 & \tilde{n}_2 & 0 & \tilde{n}_1 & \tilde{n}_3 & 0 \\ 0 & 0 & \tilde{n}_3 & 0 & \tilde{n}_2 & \tilde{n}_1 \end{bmatrix} \begin{Bmatrix} \tilde{\sigma}_{11} \\ \tilde{\sigma}_{22} \\ \tilde{\sigma}_{33} \\ \tilde{\sigma}_{12} \\ \tilde{\sigma}_{23} \\ \tilde{\sigma}_{13} \end{Bmatrix} \quad (11.5.34)$$

where the overhead “~” indicates evaluation in the surface tangent coordinate system. Substitution of (11.5.33) into (11.5.34) yields

$$\tilde{\sigma}_{13} = \tilde{F}_{\Gamma x1}, \quad \tilde{\sigma}_{23} = \tilde{F}_{\Gamma x2}, \quad \tilde{\sigma}_{33} = \tilde{F}_{\Gamma x3} \quad (11.5.35)$$

where the three stresses are shown in Figure 11.5.4. Since the surface tractions $\tilde{F}_{\Gamma xi}$ are known, Equation (11.5.35) shows that three of the six surface stresses may easily be obtained from the prescribed surface tractions (zero or nonzero) as expressed in the surface tangent coordinate system. The remaining three must be obtained utilizing the material law and the strain–displacement relations.

11.5.8 Surface Stresses Obtained from the Constitutive Law and Surface Strains

From (A.4.3), the isotropic material law in the surface tangent coordinate system is

$$\begin{Bmatrix} \tilde{\sigma}_{11} \\ \tilde{\sigma}_{22} \\ \tilde{\sigma}_{33} \\ \tilde{\sigma}_{23} \\ \tilde{\sigma}_{13} \\ \tilde{\sigma}_{12} \end{Bmatrix} = \frac{E}{(1+\nu)(1-2\nu)} \begin{bmatrix} 1-\nu & \nu & \nu & 0 & 0 & 0 \\ \nu & 1-\nu & \nu & 0 & 0 & 0 \\ \nu & \nu & 1-\nu & 0 & 0 & 0 \\ 0 & 0 & 0 & \frac{1-2\nu}{2} & 0 & 0 \\ 0 & 0 & 0 & 0 & \frac{1-2\nu}{2} & 0 \\ 0 & 0 & 0 & 0 & 0 & \frac{1-2\nu}{2} \end{bmatrix} \begin{Bmatrix} \tilde{\epsilon}_{11} \\ \tilde{\epsilon}_{22} \\ \tilde{\epsilon}_{33} \\ 2\tilde{\epsilon}_{23} \\ 2\tilde{\epsilon}_{13} \\ 2\tilde{\epsilon}_{12} \end{Bmatrix} \quad (11.5.36)$$

Solve the third equation in (11.5.36) for $\tilde{\epsilon}_{33}$:

$$\tilde{\epsilon}_{33} = \frac{\tilde{\sigma}_{33} - \gamma v \tilde{\epsilon}_{11} - \gamma v \tilde{\epsilon}_{22}}{\gamma(1-v)} \quad (11.5.37)$$

where

$$\gamma = \frac{E}{(1+\nu)(1-2\nu)} = \frac{2G}{1-2\nu} \quad (11.5.38)$$

Substitute (11.5.37) into the first and second rows of (11.5.36) and note the last row of (11.5.36) to obtain

$$\tilde{\sigma}_{11} = \frac{\nu \tilde{\sigma}_{33} + 2G(\tilde{\epsilon}_{11} + \nu \tilde{\epsilon}_{22})}{1-\nu}, \quad \tilde{\sigma}_{22} = \frac{\nu \tilde{\sigma}_{33} + 2G(\nu \tilde{\epsilon}_{11} + \tilde{\epsilon}_{22})}{1-\nu}, \quad \tilde{\sigma}_{12} = 2G \tilde{\epsilon}_{12} \quad (11.5.39)$$

11.5.9 Summary of Surface Stress Computation

The geometry and prescribed surface tractions of face 6 are shown in Figure 11.5.5.

The following steps summarize the procedure for determining surface stresses:

(a) Compute unit vectors along the surface tangent coordinate system's axes

$$\begin{aligned} \tilde{e}_1 &= \tilde{e}_{11} \hat{e}_1 + \tilde{e}_{12} \hat{e}_2 + \tilde{e}_{13} \hat{e}_3 = \frac{\vec{R}_{6/5}}{|\vec{R}_{6/5}|}, \\ \tilde{e}_2 &= \tilde{e}_{21} \hat{e}_1 + \tilde{e}_{22} \hat{e}_2 + \tilde{e}_{23} \hat{e}_3 = \tilde{e}_3 \times \tilde{e}_1, \\ \tilde{e}_3 &= \tilde{e}_{31} \hat{e}_1 + \tilde{e}_{32} \hat{e}_2 + \tilde{e}_{33} \hat{e}_3 = \frac{\vec{R}_{6/5} \times \vec{R}_{8/5}}{|\vec{R}_{6/5} \times \vec{R}_{8/5}|} \end{aligned} \quad (11.5.40)$$

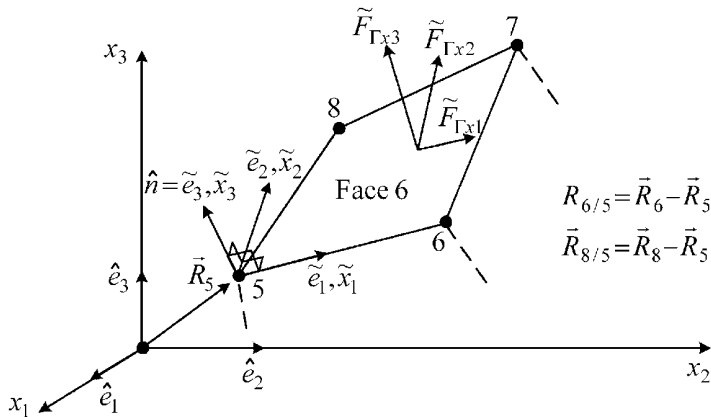


Figure 11.5.5 Hexahedral solid element surface stress calculation

(b) Obtain nodal coordinates in the surface tangent coordinate system

$$\begin{Bmatrix} \tilde{x}_{\text{rel}1,k} \\ \tilde{x}_{\text{rel}2,k} \\ \tilde{x}_{\text{rel}3,k} \end{Bmatrix} = \begin{bmatrix} \tilde{e}_{11} & \tilde{e}_{12} & \tilde{e}_{13} \\ \tilde{e}_{21} & \tilde{e}_{22} & \tilde{e}_{23} \\ \tilde{e}_{31} & \tilde{e}_{32} & \tilde{e}_{33} \end{bmatrix} \begin{Bmatrix} x_{1,k} - x_{1,5} \\ x_{2,k} - x_{2,5} \\ x_{3,k} - x_{3,5} \end{Bmatrix} \quad k = 5, 6, 7, 8 \quad (11.5.41)$$

(c) Interpolate element geometry in the surface tangent coordinate system

$$\tilde{x}_i = \sum_{k=5}^8 N_k(\xi_2, \xi_3) \Big|_{\xi_1=1} \tilde{x}_{\text{rel}i,k} \quad i = 1, 2, 3 \quad (11.5.42)$$

where, at $\xi_1 = 1$,

$$\begin{aligned} N_5 &= \frac{1}{4}(1-\xi_2)(1-\xi_3), & N_6 &= \frac{1}{4}(1+\xi_2)(1-\xi_3) \\ N_7 &= \frac{1}{4}(1+\xi_2)(1+\xi_3), & N_8 &= \frac{1}{4}(1-\xi_2)(1+\xi_3) \end{aligned} \quad (11.5.43)$$

(d) Obtain nodal displacements in the surface coordinate system

$$\begin{Bmatrix} \tilde{u}_{1,k} \\ \tilde{u}_{2,k} \\ \tilde{u}_{3,k} \end{Bmatrix} = \begin{bmatrix} \tilde{e}_{11} & \tilde{e}_{12} & \tilde{e}_{13} \\ \tilde{e}_{21} & \tilde{e}_{22} & \tilde{e}_{23} \\ \tilde{e}_{31} & \tilde{e}_{32} & \tilde{e}_{33} \end{bmatrix} \begin{Bmatrix} u_{1,k} \\ u_{2,k} \\ u_{3,k} \end{Bmatrix} \quad k = 5, 6, 7, 8 \quad (11.5.44)$$

where $u_{i,k}$ is the local node k displacement in direction x_i , for $i = 1, 2, 3$, as obtained from (11.4.7) at any time t .

(e) Interpolate displacements in the surface tangent coordinate system

$$\tilde{u}_i = \sum_{k=5}^8 N_k(\xi_2, \xi_3) \Big|_{\xi_1=1} \tilde{u}_{i,k} \quad i = 1, 2, 3 \quad (11.5.45)$$

(f) Compute strains in the surface tangent coordinate system

$$\tilde{\varepsilon}_{11} = \frac{\partial \tilde{u}_1}{\partial \tilde{x}_1}, \quad \tilde{\varepsilon}_{12} = \frac{1}{2} \left(\frac{\partial \tilde{u}_1}{\partial \tilde{x}_2} + \frac{\partial \tilde{u}_2}{\partial \tilde{x}_1} \right), \quad \tilde{\varepsilon}_{22} = \frac{\partial \tilde{u}_2}{\partial \tilde{x}_2} \quad (11.5.46)$$

$$\begin{Bmatrix} \frac{\partial \tilde{u}_1}{\partial \tilde{x}_1} \\ \frac{\partial \tilde{u}_1}{\partial \tilde{x}_2} \\ \frac{\partial \tilde{u}_2}{\partial \tilde{x}_1} \\ \frac{\partial \tilde{u}_2}{\partial \tilde{x}_2} \end{Bmatrix} = \frac{1}{\det(\tilde{J})} \begin{bmatrix} \frac{\partial \tilde{x}_2}{\partial \xi_3} & -\frac{\partial \tilde{x}_2}{\partial \xi_2} & 0 & 0 \\ -\frac{\partial \tilde{x}_1}{\partial \xi_3} & \frac{\partial \tilde{x}_1}{\partial \xi_2} & 0 & 0 \\ 0 & 0 & \frac{\partial \tilde{x}_2}{\partial \xi_3} & -\frac{\partial \tilde{x}_2}{\partial \xi_2} \\ 0 & 0 & -\frac{\partial \tilde{x}_1}{\partial \xi_3} & \frac{\partial \tilde{x}_1}{\partial \xi_2} \end{bmatrix} \begin{Bmatrix} \frac{\partial \tilde{u}_1}{\partial \xi_2} \\ \frac{\partial \tilde{u}_1}{\partial \xi_3} \\ \frac{\partial \tilde{u}_2}{\partial \xi_2} \\ \frac{\partial \tilde{u}_2}{\partial \xi_3} \end{Bmatrix} \quad (11.5.47)$$

$$\det \tilde{J} = \frac{\partial \tilde{x}_1}{\partial \xi_2} \frac{\partial \tilde{x}_2}{\partial \xi_3} - \frac{\partial \tilde{x}_2}{\partial \xi_2} \frac{\partial \tilde{x}_1}{\partial \xi_3} \quad (11.5.48)$$

$$\frac{\partial \tilde{x}_i}{\partial \xi_m} = \sum_{k=5}^8 \frac{\partial N_k}{\partial \xi_m} \Big|_{\xi_1=1} \tilde{x}_{\text{rel},k} \quad m=2,3 \quad (11.5.49)$$

$$\frac{\partial \tilde{u}_i}{\partial \xi_m} = \sum_{k=5}^8 \frac{\partial N_k}{\partial \xi_m} \Big|_{\xi_1=1} \tilde{u}_{i,k} \quad m=2,3 \quad (11.5.50)$$

Let $(\partial N_k / \partial \xi_m)|_{\xi_1=1}$ be represented by $N_{k,m}$, and then from (11.5.43)

$$\begin{aligned} N_{5,2} &= -\frac{1}{4}(1-\xi_3), & N_{5,3} &= -\frac{1}{4}(1-\xi_2) \\ N_{6,2} &= \frac{1}{4}(1-\xi_3), & N_{6,3} &= -\frac{1}{4}(1+\xi_2) \\ N_{7,2} &= \frac{1}{4}(1+\xi_3), & N_{7,3} &= \frac{1}{4}(1+\xi_2) \\ N_{8,2} &= -\frac{1}{4}(1+\xi_3), & N_{8,3} &= \frac{1}{4}(1-\xi_2) \end{aligned} \quad (11.5.51)$$

- (g) Obtain three surface stresses in the surface tangent coordinate system directly from the prescribed tractions

$$\tilde{\sigma}_{13} = \tilde{F}_{\Gamma x1}, \quad \tilde{\sigma}_{23} = \tilde{F}_{\Gamma x2}, \quad \tilde{\sigma}_{33} = \tilde{F}_{\Gamma x3} \quad (11.5.52)$$

where $\tilde{F}_{\Gamma xi}$ is the component of the prescribed surface traction on face 6 in the \tilde{e}_i direction. Note for pure pressure loading $\tilde{F}_{\Gamma x1} = \tilde{F}_{\Gamma x2} = 0$ and $\tilde{F}_{\Gamma x3} = -P$.

- (h) Obtain three surface stresses in the surface tangent coordinate system from the constitutive law

$$\tilde{\sigma}_{11} = \frac{v\tilde{\sigma}_{33} + 2G(\tilde{\epsilon}_{11} + v\tilde{\epsilon}_{22})}{1-v}, \quad \tilde{\sigma}_{22} = \frac{v\tilde{\sigma}_{33} + 2G(v\tilde{\epsilon}_{11} + \tilde{\epsilon}_{22})}{1-v}, \quad \tilde{\sigma}_{12} = 2G\tilde{\epsilon}_{12} \quad (11.5.53)$$

where $\tilde{\sigma}_{33}$ is obtained from (11.5.52) and $\tilde{\epsilon}_{11}, \tilde{\epsilon}_{22}$, and $\tilde{\epsilon}_{33}$ are obtained from (11.5.46).

11.6 3D SOLID ELEMENT MODEL EXAMPLE

EXAMPLE 11.6.1 Correlation Study for a Simply Supported Beam Model with Beam, 2D Solid, and 3D Solid Elements

Statement: This example utilizes a simply supported beam to illustrate the use of 8-node solid elements and to compare results with Timoshenko beam and 2D solid element models.

Objectives: The objectives of this example are:

- Build a 3D, 8-node hexahedral element model of a simply supported beam with arbitrary aspect ratio and mesh density.
- Determine natural frequencies, mode shapes, and transient responses.
- Compare response to those obtained with the beam and 2D solid element models in Example 10.8.1.

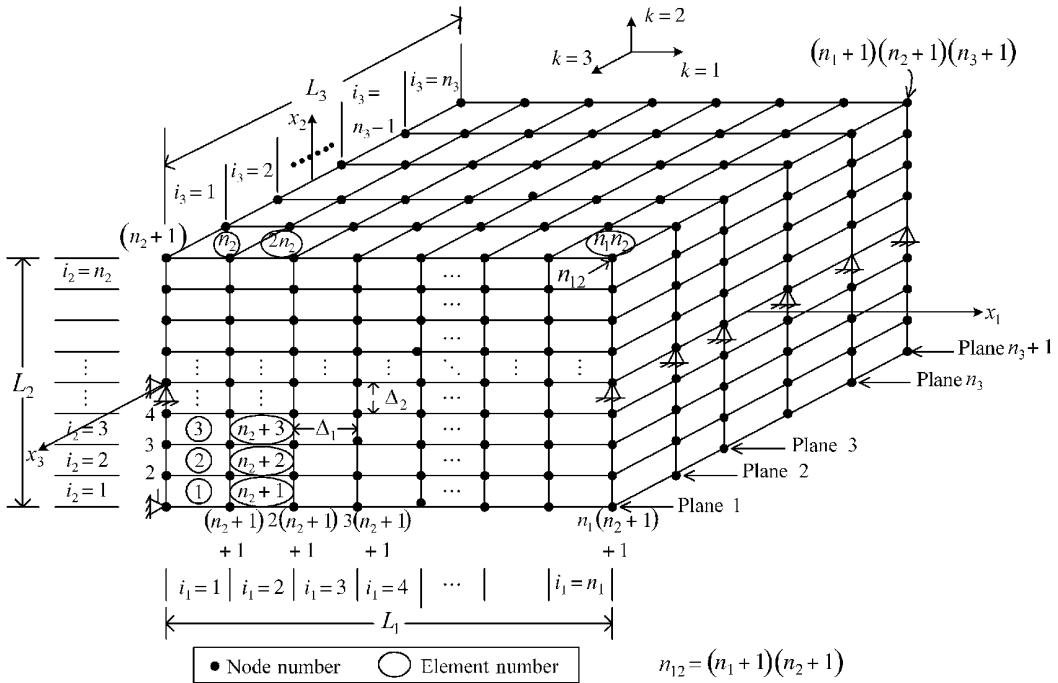


Figure E11.6.1(a) Simply supported beam model with 8-node hexahedral elements

Assumptions: The assumptions for this example are:

Small motions, that is, small-motion strain–displacement and stress–strain relations (A.3.21) and (A.4.4), are valid.

Material Properties: The Young's modulus, Poisson's ratio, and weight density are

$$E = 2.0 \times 10^{11} \text{ N/m}^2, \quad \nu = 0.3, \quad \rho g = 7.69 \times 10^4 \text{ N/m}^3$$

Model Mesh: The beam model is meshed with the uniformly spaced grid shown in Figure E11.6.1(a). The x_1 , x_2 , and x_3 dimensions are divided into n_1 , n_2 , and n_3 sections, respectively; thus,

$$\Delta_i = \frac{L_i}{n_i} \quad (1)$$

where n_i are all even numbers to symmetrically locate the boundary conditions and

$$L_1 = 1.0 \text{ m}, \quad L_2 = 0.1 \text{ m}, \quad L_3 = 0.1 \text{ m} \quad (2)$$

From this figure, it is seen that the plane i_3 node numbers are obtained from their plane 1 counterparts by adding $(i_3 - 1) * n_{12}$ and the layer i_3 element numbers are obtained from their layer $i_3 = 1$ counterparts by adding $(i_3 - 1) * n_1 n_2$. In addition,

$$\begin{aligned} N_n &= \text{number of system nodes} = (n_1 + 1)(n_2 + 1)(n_3 + 1), \\ N_e &= \text{number of system elements} = n_1 n_2 n_3, \\ N_d &= \text{number of system dofs} = 3 * N_n, \\ N_{pd} &= \text{number of fixed dofs} = 3 * (n_3 + 1) + 1, \\ N_{npd} &= \text{number of nonfixed dofs} = N_d - N_{pd} \end{aligned} \quad (3)$$

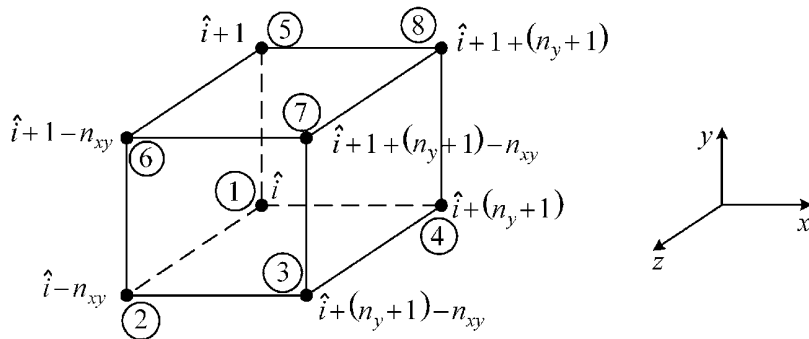
The expression for N_{pd} is the sum of $(n_3 + 1)$ “ u_2 ” constraints at $x_1 = L_1$, $2(n_3 + 1)$ “ u_y ” and “ u_1 ” constraints at $x = 0$, and one “ u_3 ” constraint at node 1 to prevent rigid body motion in the x_3 direction.

Integer Arrays: The node numbers for a typical element are shown in Figure E11.6.1(b).

(a) Form Node Connectivity Array ICON. The nodal connectivity array is defined below:

$$\begin{aligned}
 &\text{for } i_1 = 1, n_1 \text{ (horizontal intervals)} \\
 &\quad \text{for } i_2 = 1, n_2 \text{ (vertical intervals)} \\
 &\quad \quad \text{for } i_3 = 1, n_3 \text{ (depth intervals)} \\
 &\quad \quad \quad e = n_1 * n_2 (i_3 - 1) + n_2 (i_1 - 1) + i_2 \\
 &\quad \quad \quad \hat{i} = (n_1 + 1)(n_2 + 1)i_3 + (n_2 + 1)(i_1 - 1) + i_2 \\
 &\quad \quad \quad \text{ICON}(e, 1) = \hat{i} \\
 &\quad \quad \quad \text{ICON}(e, 2) = \hat{i} - n_{12} \\
 &\quad \quad \quad \text{ICON}(e, 3) = \hat{i} - n_{12} + n_2 + 1 \\
 &\quad \quad \quad \text{ICON}(e, 4) = \hat{i} + n_2 + 1 \\
 &\quad \quad \quad \text{ICON}(e, 5) = \hat{i} + 1 \\
 &\quad \quad \quad \text{ICON}(e, 6) = \hat{i} + 1 - n_{12} \\
 &\quad \quad \quad \text{ICON}(e, 7) = \hat{i} + 1 + n_2 + 1 - n_{12} \\
 &\quad \quad \quad \text{ICON}(e, 8) = \hat{i} + 1 + n_2 + 1 \\
 &\quad \quad \quad \text{end} \\
 &\quad \quad \quad \text{end} \\
 &\quad \quad \quad \text{end}
 \end{aligned} \tag{4}$$

where $\text{ICON}(e, j) = B_{ej}$ = global node number for local node j of element e ,
 $j = 1, \dots, 8, e = 1, \dots, N_e$



Element indices: (i_x, i_y, i_z)

Element no.: $e = n_x n_y (i_z - 1) + n_y (i_x - 1) + i_y$

Global node no. for local node 1: $\hat{i} = (n_x + 1)(n_y + 1)i_z + (n_y + 1)(i_x - 1) + i_y$

Figure E11.6.1(b) Global node numbers for element e of the simply supported beam model

(b) Form DOF Connectivity Array.

The dof connectivity array \hat{B}_{el} is then determined based on (11.4.4):

$$\begin{aligned}
 &\text{for } e = 1, N_e \text{ (elements)} \\
 &\quad \text{for } j = 1, 8 \text{ (local nodes)} \\
 &\quad\quad \text{for } k = 1, 3 \text{ (directions)} \\
 &\quad\quad\quad l = 3 * (j - 1) + k \text{ (local dof numbers)} \\
 &\quad\quad\quad \text{ICONDOF}(e, l) = 3 * (\text{ICON}(e, j) - 1) + k \\
 &\quad\quad \text{end} \\
 &\quad \text{end} \\
 &\text{end} \\
 &\text{where } \text{ICONDOF}(e, l) = \hat{B}_{el} = \text{global dof number for local dof } l \text{ of element } e, \\
 &j = 1, \dots, 24, \quad e = 1, \dots, N_e, \quad \text{and } k = 1(x_1), k = 2(x_2), k = 3(x_3)
 \end{aligned} \tag{5}$$

(c) Form the $jarray(j_i)$.

The requirement that n_2 is even and inspection of Figure E11.6.1(a) shows that the fixed dofs for the simply supported boundary conditions are stored in the array i_{pdl} below:

$$\begin{aligned}
 &l = 0 \\
 &\text{for } i = 1, n_3 + 1 \\
 &\quad l1 = 3 * \frac{n_2}{2} + 1 + (i - 1) * 3 * n_{12} \text{ (} u_1 \text{ direction at } x_1 = 0) \\
 &\quad l2 = l1 + 1 \text{ (} u_2 \text{ direction at } x_1 = 0) \\
 &\quad l3 = l2 + n_1(n_2 + 1) * 3 \text{ (} u_2 \text{ direction at } x = L_1) \\
 &\quad l = l + 1 \\
 &\quad i_{pdl} = l1 \\
 &\quad l = l + 1 \\
 &\quad i_{pdl} = l2 \\
 &\quad l = l + 1 \\
 &\quad i_{pdl} = l3 \\
 &\text{end} \\
 &l = l + 1 \\
 &i_{pdl} = 3 \text{ (restrict rigid body } u_3 \text{ motion at global node 1)} \\
 &N_{pd} = 3 * (n_3 + 1) + 1 \text{ (total number of prescribed dofs)}
 \end{aligned} \tag{6}$$

The $jarray$ is defined in (10.5.12) and (10.5.13) utilizing the array i_{pdl} of fixed dofs from (6):

j_i = system dof number of the i th nonfixed dof

where

$$\begin{aligned}
 i = 1, \dots, N_{npd} \text{ and } N_{npd} = N_d - N_{pd} = \text{total number of fixed dofs in the system model} \\
 = 3 * N_d - N_{pd} = 3(n_1 + 1)(n_2 + 1)(n_3 + 1) - 3(n_3 + 1) - 1
 \end{aligned} \tag{7}$$

(d) Form the $larray(l_i)$.

The $larray(l_i)$ stores either the position of system dof i in the condensed system or zero if i is fixed. The $larray$ is formed from the $jarray(j_i)$ as described in (10.5.15) with N_d, N_{npd} from (2).

(e) Nodal Coordinates. The coordinates of the model nodes in Figure E11.6.1(a) are determined as follows:

$$\begin{aligned}
 \Delta_1 &= \frac{L_1}{n_1}, \quad \Delta_2 = \frac{L_2}{n_2}, \quad \Delta_3 = \frac{L_3}{n_3} \\
 nc &= 0, \quad p1 = -\Delta_1, \quad p2 = -\frac{L_2}{2} - \Delta_2, \quad p3 = \frac{L_3}{2} + \Delta_3 \\
 \text{for } j_3 &= 1, n_3 + 1 \\
 \quad p3 &= p3 - \Delta_3 \\
 \quad \quad \text{for } j_1 &= 1, n_1 + 1 \\
 \quad \quad \quad p1 &= p1 + \Delta_1 \\
 \quad \quad \quad \quad \text{for } j_2 &= 1, n_2 + 1 \\
 \quad \quad \quad \quad \quad p2 &= p2 + \Delta_2 \\
 \quad \quad \quad \quad \quad nc &= nc + 1 \\
 \quad \quad \quad \quad \quad x_1(nc) &= p1 \\
 \quad \quad \quad \quad \quad x_2(nc) &= p2 \\
 \quad \quad \quad \quad \quad x_3(nc) &= p3 \\
 \quad \quad \quad \quad \quad \quad \text{end} \\
 \quad \quad \quad \quad \quad p2 &= -\frac{L_2}{2} - \Delta_2 \\
 \quad \quad \quad \quad \quad \quad \text{end} \\
 \quad \quad \quad p1 &= -\Delta_1 \\
 \quad \quad \text{end}
 \end{aligned} \tag{8}$$

Mass and Stiffness Matrices and Force Vector: The stiffness and mass matrices for the system with fixed dofs removed are assembled from the element stiffness and mass matrices following the algorithm illustrated in Figure 11.4.2.

Natural Frequencies and Mode Shapes: The simply supported beam of Example 10.8.1 with dimensions $L_1 = 1.0\text{m}$, $L_2 = 0.1\text{m}$, and $L_3 = 0.1\text{m}$ is modeled here with 8-node brick-type solid elements. The related MATLAB code is shown in Appendix F. From (6), the constrained dofs for the $n_1 = 12$, $n_2 = 4$, and $n_3 = 4$ case are

$$7 \ 8 \ 188 \ 202 \ 203 \ 383 \ 397 \ 398 \ 578 \ 592 \ 593 \ 773 \ 787 \ 788 \ 968 \ 3 \quad (9)$$

Third-order Gauss quadrature is employed in obtaining the element mass and stiffness matrices in (11.2.34) and (11.3.4). The two lowest $x_1 - x_2$ plane bending modes and an axial mode for this case using extra shape functions (11.2.7) are shown in Figure E11.6.1(c). The corresponding natural frequencies are 233.1, 915.6, and 1173.1 Hz with extra shape functions (11.2.7) and 262.7, 1024.5, and 1215 without extra shape functions.

Figure E11.6.1(d) shows a mode of the $n_1 = 12$, $n_2 = 4$, and $n_3 = 4$ with extra shape functions, model that occurs at 1441.9 Hz. This is a combined expansion (breathing)–torsion mode that cannot be predicted by a beam or plane stress/strain model. Table E11.6.1(a)

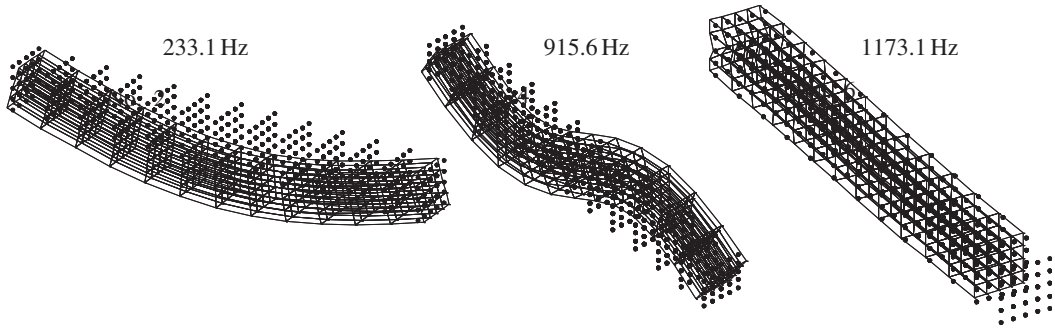


Figure E11.6.1(c) The two lowest x_1 – x_2 bending and lowest axial modes for $n_1 = 12$, $n_2 = 4$, and $n_3 = 4$ with extra shape functions

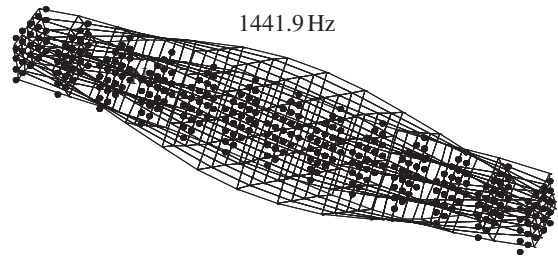


Figure E11.6.1(d) A combined expansion (breathing)–torsion mode of the $n_1 = 12$, $n_2 = 4$, and $n_3 = 4$ with extra shape functions model

Table E11.6.1(a) Natural frequencies for various mesh densities

Case	n_1	n_2	n_3	Extra shape function	$f_1^{\text{bend}, x_1-x_2}$ Hz	$f_2^{\text{bend}, x_1-x_2}$ Hz	f_{axial} Hz
1	12	4	4	No	262.7	1024.5	1215
2	12	4	4	Yes	233.1	915.6	1173.1
3	12	6	6	Yes	233.1	914.7	1154
4	16	6	6	Yes	232	900.6	1151
5	16	6	6	No	249.1	962.9	1197.2
6	18	8	8	Yes	232	896.4	1136

shows these mode frequencies for different mesh densities. The trends shown include convergence to the natural frequencies from above as the number of elements increase and quicker convergence when extra shape functions (11.2.7) are included. As expected, the results are very close to those of the plane strain and beam models in Table E10.8.1(a).

Tripling the x_3 direction length yields nearly identical x_1 – x_2 plane bending mode frequencies since the mass and stiffness characteristics both increase proportionately. More general, nonbeam, nonplane strain-type modes also result as shown in Figure E11.6.1(e).

Damped, Forced Response: The objective here is to predict the transient vibration response (Chapter 6) of the beam to a suddenly applied force. The damped dynamic equilibrium equation

$$\dot{\underline{q}}_f = \underline{V}_f (N_{npd} \times 1), \quad \dot{\underline{V}}_f = \underline{M}_f^{-1} (\underline{f}_f(t) - \underline{C}_{of} \underline{V}_f - \underline{K}_f \underline{q}_f) \quad (10)$$

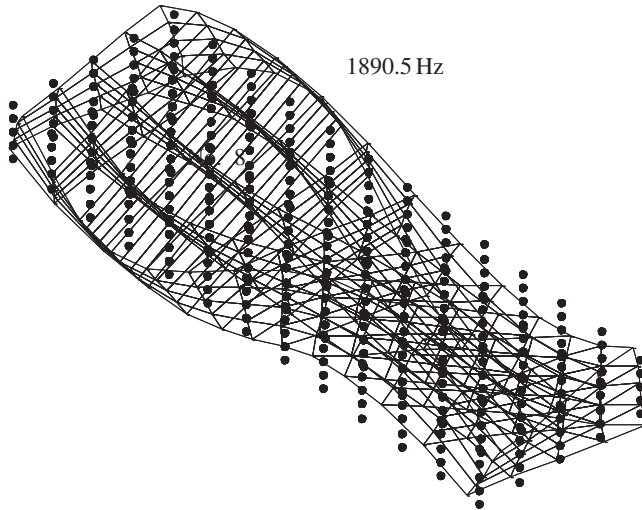


Figure E11.6.1(e) A combined bending plus torsion mode of the $n_1 = 12$, $n_2 = 4$, and $n_3 = 4$ with extra shape functions and $L_3 = 0.3\text{m}$ model

with zero initial conditions

$$\underline{q}_f(0) = \underline{V}_f(0) = \underline{0} \quad (11)$$

is numerically integrated with MATLAB's ODE45 numerical integration routine as shown in Appendix F. As in Example 10.8.1, a set of external concentrated forces are applied as shown in Figure E10.8.1(c). The time history of these forces is given by

$$f(t) = \begin{cases} \frac{0.1}{n_3 + 1} * 5.0 \times 10^5 * \frac{t}{0.01} \text{ N}, & 0 \leq t \leq 0.01 \text{ s} \\ \frac{0.1}{n_3 + 1} * 5.0 \times 10^5 \text{ N}, & t > 0.01 \text{ s} \end{cases} \quad (12)$$

where the factor of 0.1 is applied since the beam depth is only $L_3 = 0.1 \text{ m}$, that is, not 1 m, and the factor of $(1/n_3 + 1)$ appears since the forces are applied at $n_3 + 1$ nodes occurring along the x_3 direction at the quarter span location. The forces are applied in the x_2 direction on the top of the beam in Figure E11.6.1(a) at $x_1 = (L_1/4)$:

$$\text{Forced nodes: } N_{Fi} = \left(\frac{n_1}{4} + 1\right) * (n_2 + 1) + (i-1) * n_{12} \quad \text{for } i = 1, 2, \dots, n_3 + 1 \quad (13)$$

$$\text{Forced dofs: } k_i = (N_{Fi} - 1) * 3 + 2 \quad \text{for } i = 1, 2, \dots, n_3 + 1$$

The forces are input into rows of the constraint condensed force vector $\underline{f}_f(t)$ at positions defined using the *larray* ((6) and (10.5.12), (10.5.13), (10.5.15)) by

for $i = 1, n_3 + 1$

$$i_{fnode} = (i-1)n_{12} + (n_2 + 1) * \left(\frac{n_1}{4} + 1\right)$$

$$i_{fdof} = 3 * (i_{fnode} - 1) + 2 \quad (14)$$

$$i_{fdofc} = 1(i_{fdof})$$

end

where $n_{12} = (n_1 + 1) * (n_2 + 1)$ and the mesh index n_1 must be selected to be a multiple of 4. Thus, the constraint condensed force vector $\underline{f}_f(t)$ has the following form:

$$\underset{N_{npd} \times 1}{\underline{f}_f} = \{0 \ 0 \ \cdots \ 0 \ \underset{\substack{\uparrow \\ \text{row } i_{fdof}^{(1)}}}{f(t)} \ 0 \ \cdots \ 0 \ \underset{\substack{\uparrow \\ \text{row } i_{fdof}^{(2)}}}{f(t)} \ 0 \ \cdots \ 0 \ \underset{\substack{\uparrow \\ \text{row } i_{fdof}^{(n_3+1)}}}{f(t)} \ 0 \ \cdots \ 0\}^T \quad (15)$$

where the nonzero row numbers are defined in (14). The damping model employed in Example 10.8.1 imposed prescribed values of modal damping for the six lowest modes of the plane strain model, which according to Figure E10.8.1(e) and Equation (29) of Example 10.8.1 were

$\xi^d = 0.02$ for the two lowest $x_1 - x_2$ plane bending modes

$\xi^d = 0.04$ for the lowest axial mode and the third $x_1 - x_2$ plane bending mode (16)

$\xi^d = 0.06$ for the fourth $x_1 - x_2$ plane bending mode and the second axial mode

The two lowest $x_1 - x_2$ plane bending modes of the 3D solid element model are modes 2 and 4, so the damping is specified as $\xi^d = 0.02$ for modes 1–4. The lowest axial mode and the third $x_1 - x_2$ plane bending mode are modes 6 and 9, respectively, of the 3D solid element model, so the damping is specified as $\xi^d = 0.04$ for modes 5–9. The second axial mode and the fourth $x_1 - x_2$ plane bending mode are modes 13 and 12, respectively, of the 3D solid element model, so the damping is specified as $\xi^d = 0.06$ for modes 10–13. The damping matrix is given by (5.4.140), (5.4.142), and (5.4.146) as

$$\underline{C}_{of} = \mu_1 \underline{K}_f + \underline{M}_f \left(\sum_{l=1}^{m-1} \frac{2\kappa_l \omega_l}{\tilde{m}_l} \underline{\psi}_{fl} \underline{\psi}_{fl}^T \right) \underline{M}_f \quad (17)$$

with $m = 13$, $\xi^d = 0.02$ for modes 1–4, $\xi^d = 0.04$ for modes 5–9, $\xi^d = 0.06$ for modes 10–13, and

$$\mu_1 = \frac{2\xi_m^d}{\omega_m}, \quad \kappa_l = \xi_l^d - \xi_m^d \frac{\omega_l}{\omega_m} \quad (18)$$

The resulting x_2 direction displacements are plotted at the quarter, half, and three-quarter span locations at the center of the beam in the x_3 direction. These dofs must be located in the \underline{q}_f vector in order to be plotted. The corresponding dofs in the constraint condensed displacement vector \underline{q}_f are given using the *larray* ((6) and (10.5.12), (10.5.13), (10.5.15)). Recall that $l(w)$ provides the row number in \underline{q}_f that contains the displacement of dof w in the unconstrained (total system) model. Therefore, the x_2 direction dofs at the 1/4, 1/2, and 3/4 locations are

on top surface $x_2 = L_2/2$

$$\text{dof in } \underline{q}_f = l\left(\left\{\left[(n_2 + 1)\left(\alpha * \frac{n_1}{4} + 1\right) + \frac{n_3}{2} * n_{12}\right] - 1\right\} * 3 + 2\right) \quad (19)$$

on midplane (neutral axis) $x_2 = 0$

$$\text{dof in } \underline{q}_f = l\left(\left\{\left[(n_2 + 1)\left(\alpha * \frac{n_1}{4}\right) + \frac{n_2}{2} + 1 + \frac{n_3}{2} * n_{12}\right] - 1\right\} * 3 + 2\right) \quad (20)$$

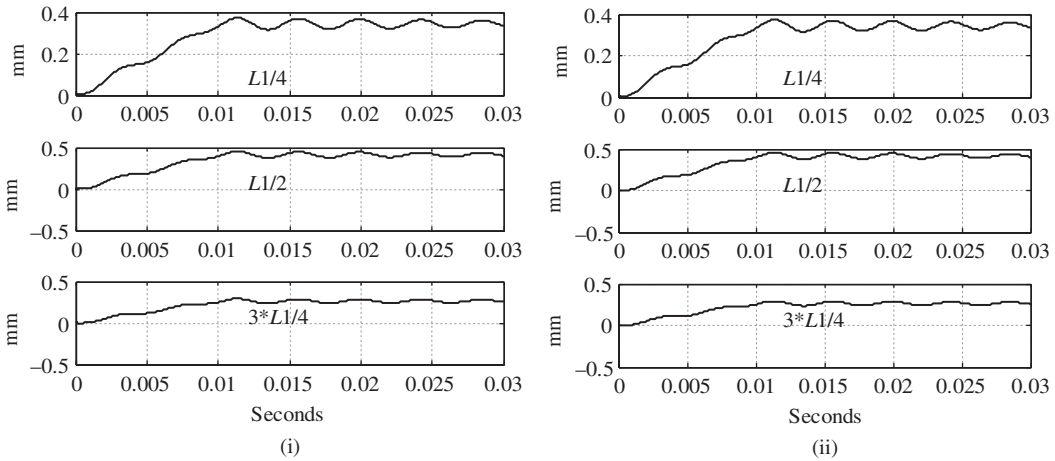


Figure E11.6.1(f) x_2 Displacements on the (i) top surface ($x_2 = L_2/2$) and (ii) mid surface ($x_2 = 0$) locations at the x_1 locations indicated

where $\alpha = 1$ at the quarter span $x_1 = L_1/4$, $\alpha = 2$ at the half span $x_1 = L_1/2$, $\alpha = 3$ at the three-quarter span $x_1 = 3L_1/4$, and $l(\)$ is the *larray* value of $(\)$. Figure E11.6.1(f) shows the x_2 displacement on the top ($x_2 = L_2/2$) and neutral ($x_2 = 0$) surfaces, at the quarter, mid, and three-quarter span locations for the 8-node solid element model with extra shape functions and with mesh parameters $n_1 = 12$, $n_2 = 6$, and $n_3 = 6$.

The displacements are seen to be nearly identical to the plane strain and beam model predictions in Figures E10.8.1(g) and E10.8.1(h).

11.7 3D SOLID ELEMENT SUMMARY

Powerful commercial automated meshing codes and solvers now make 3D solid finite elements the element of preference for the modeling of many structures and machines for vibration response prediction. The use of solid elements removes the kinematic deformation assumptions inherent in more approximate elements such as beams, plates, and so on as summarized in Table 11.1.1. This reveals coupled modes involving breathing, torsion, extension, and so on as illustrated in Figures E11.6.1(d) and E11.6.1(e). The use of extra shape functions as illustrated in this chapter and Chapter 10 accelerates convergence, in particular when bending deformation is significant. This benefit is achieved while maintaining the simpler meshing task of linear elements, as compared with quadratic elements. Failures frequently initiate on the surface of a component where stresses peak and defects and damage may occur. The text provides a detailed derivation for surface stress evaluation and for determining stresses at Gauss integration points which may then be extrapolated for obtaining surface stresses. A detailed example is provided comparing results of the 3D hexahedral element with a plane strain example presented in Chapter 10.

Some key topics covered include 3D solid element related:

- (a) Stiffness and mass matrices, including the extra shape function stiffness matrix
- (b) Element force vectors for interior and surface applied loads

- (c) Assembly procedure for system matrices
- (d) Interior and surface stress calculation
- (e) Determination of mode shapes, natural frequencies, and forced transient response

11.8 CHAPTER 11 EXERCISES

11.8.1 Exercise Location

All exercises may be conveniently viewed and downloaded at the following website: www.wiley.com/go/palazzolo. This new feature greatly reduces the length of the printed book, yielding a significant cost savings for the college student, and is updated.

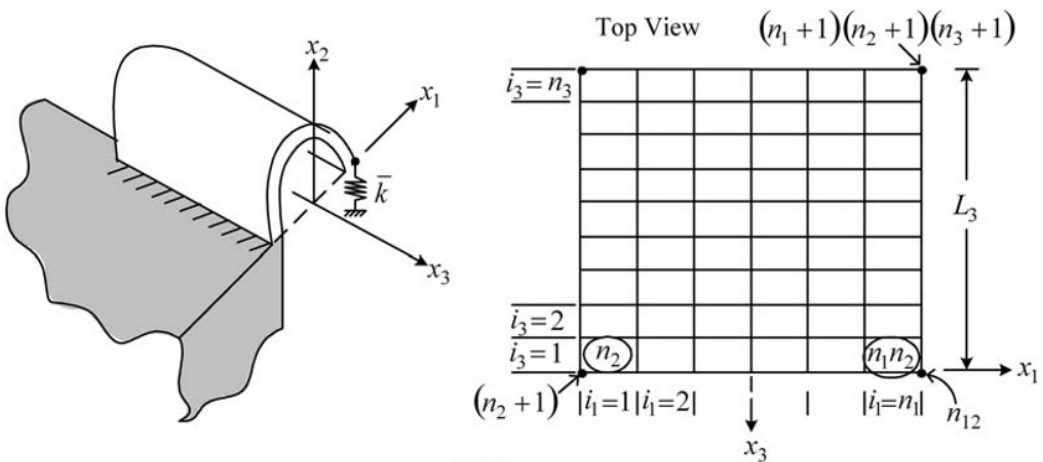
11.8.2 Exercise Goals

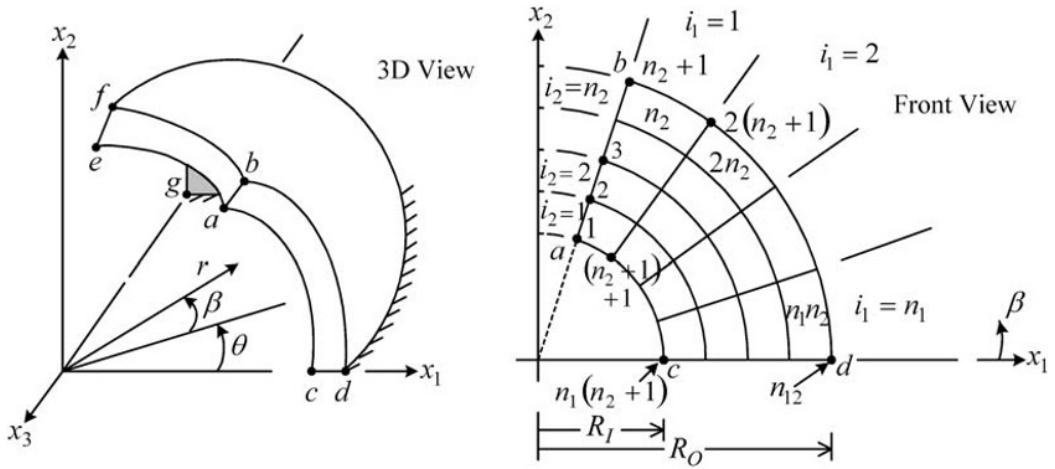
The goal of the Exercises in Chapter 11 is to strengthen the student's understanding and related engineering problem-solving skills in the following areas:

- (a) Developing a skill for meshing a 3D solid element model
- (b) Determining natural frequencies of 3D solid element models and visualizing accompanying mode shapes
- (c) Evaluating benefit of utilizing extra shape functions to accelerate convergence of predicted natural frequencies versus mesh refinement

11.8.3 Sample Exercises: 11.2 and 11.3

The component in Exercise 11.2 is a semicircular arch that is cantilevered on its left end. The component in Exercise 11.3 is a one-eighth hollow sphere with its bottom edge fixed to ground. Suggestions for node/element patterns are provided. The student must calculate the natural frequencies and mode shapes. The models in both exercises are comprised of 8-node, 3D solid elements. Solutions may be obtained by modifying a given MATLAB code.





(11.3)

REFERENCES

COOK, R., MALKUS, D., and PLESHA, M. *Concepts and Applications of Finite Element Analysis*, 3rd ed., John Wiley, New York, 1989.

HILDEBRAND, F. *Advanced Calculus for Applications*, 2nd ed., Prentice Hall, Englewood Cliffs, NJ, 1976.

HUGHES, T. *The Finite Element Method*, Prentice Hall, Englewood Cliffs, NJ, 1987.

Chapter 12

Active Vibration Control

12.1 INTRODUCTION

Common goals of vibration control include reduction of dynamic stress (fatigue) or displacement (interference/wear), machining imperfections, optical alignment errors, fastener looseness, human discomfort, and so on. Passive vibration control seeks to achieve these goals via structural modification and installation of devices such as absorber masses, spring, and dampers to reduce the system sensitivity to external disturbances and to self-excitation forces, that is, instability (Section 5.6). Limitations of passive control devices include the following:

- (a) The force–motion relationships are generally simple in form, that is,

$$F = kx, \quad F = c\dot{x} \quad (12.1.1)$$

Passive device forces are generally determined solely by the motions at the points of attachment of the passive force device. Often, for example, in the case of gyroscopic spinning systems, a more effective control requires force distributions that are determined by combinations of motions at various locations on the body.

- (b) It may be impractical for the passive control device to adapt to various operating conditions such as rotational speeds, pressures, temperatures, amplitudes of disturbances, and so on.
- (c) Active vibration control (AVC) devices may be programmed to adapt to variations in the plant (structure, vehicle, or machine) that is vibrating, for example, a vehicle that experiences a large mass change between loaded and unloaded states.
- (d) Passive force devices that typically utilize oil or elastomers may have limited temperature ranges that would preclude operation in extremely cold or hot environments.

AVC devices can replicate the behavior of a passive device as described by (12.1.1) and also produce forces with a more general dependence on motion variables. AVC devices may also adapt to changing operating condition variables and function well even in extreme temperature and pressure environments, including vacuum conditions. Figure 12.1.1 illustrates the major components of an AVC system. The plant (structure, machine, etc.) is subjected to dynamic external forces that cause vibrations. These vibrations are measured with motion sensors such as accelerometers, noncontact displacement sensors, and other transducers. The vibration signals are treated as deviations, or errors, relative to the desired target positions, which are typically zero. The errors are routed through a control law, having the physical realization as a digital or analog controller. The controller's input and output signals are typically low voltage, current, and power and thus unable to deliver the required power to operate force/moment actuation devices. Consequently, they are routed into a servo power amplifier (SPA) that outputs power sufficient to operate actuation devices. The control

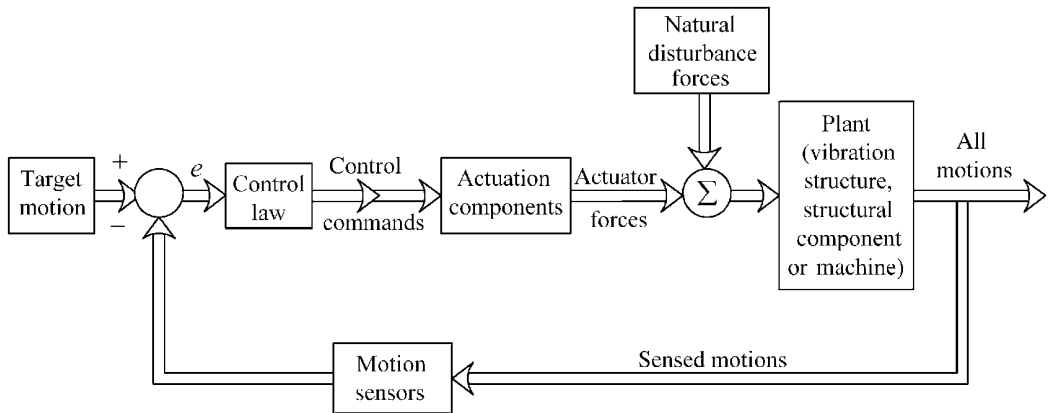


Figure 12.1.1 Feedback control loop diagram for “core” AVC implementation

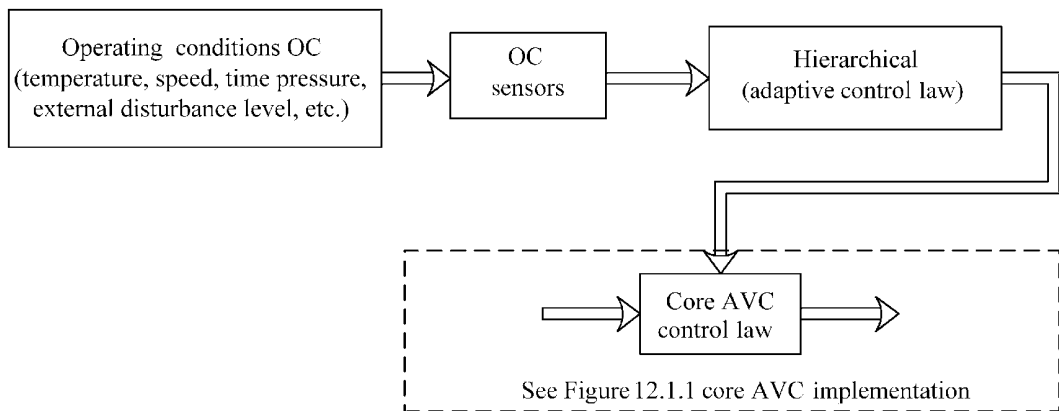


Figure 12.1.2 Hierarchical (adaptive) implementation of AVC

forces that are produced exert forces that are of appropriate amplitude, phase, and frequency to counter the effect of the external “natural” loads. The net effect is reduced vibration and sound.

The “core” AVC approach in Figure 12.1.1 may be nested within a supervisory or hierarchical control architecture as shown in Figure 12.1.2. The higher-level control updates control parameters such as feedback gains in response to operating condition changes. The higher-order control may utilize a neural network to provide real-time parameter identification which in turn is used to update control gains or a fuzzy logic expert system which utilizes preprogrammed rules to determine how control parameters must change as operating conditions change (Lei and Palazzolo, 2000).

Although AVC has an obvious advantage in versatility over passive means, trade-offs occur in complexity, cost, and reliability. Widespread implementation has been impeded by these trade-offs; however, the rapid pace of technology advancements will enhance acceptance of this new technology as illustrated by the following examples.

A research team at the Center for Electromechanics at the University of Texas (Buckner et al., 2001) were successful in reducing vehicle body accelerations from over 8g’s to under 0.3g’s on an off-road vehicle by developing an AVC suspension system. Electromechanical actuators are attached in parallel with soft springs between the wheel (unsprung) and body

(sprung) masses. Sensors measure body acceleration and wheel–body relative displacements and velocities which are sampled at 1000 times/s and routed to a digital controller. The control law develops commands to simultaneously cancel nonlinear forces in the passive suspension and to produce forces on the body which are proportional to its absolute velocity and to its relative displacement, with respect to the wheel. This produces a desired suspension stiffness and “skyhook” damping between the body and inertial space. A neural network-based supervisory controller updated the core controller parameters (Figure 12.1.2) in response to terrain changes.

Dohner et al. (2002) successfully developed an AVC system to increase the chatter-free depth of cut of a milling machine by one order of magnitude. Chatter is a violent vibration that results from the tool bits reaction to the cutting pattern it encounters from previous cuts. This limits the depth of cut and slows down completion of a milling task. The R&D team mounted the rotating spindle on an electrorestrictive actuator (EA) that can dynamically move (vibrate) its centerline in response to commands of a controller. The EA can expand or contract in response to an applied voltage across it. The sensed motion quantities in Figure 12.1.1 were strain gages that are cemented onto the root of the spinning cutting tool. Strain signals are transmitted from the spindle to the nonrotating frame via telemetry. Minimizing the dynamic, time-varying strain was the objective for the AVC system.

Researchers at Texas A&M University and NASA Glenn also used feedback-based AVC on a spinning shaft to avoid or dampen resonances, suppress instabilities (Section 5.6), and attenuate transient vibrations due to sudden imbalance (ref. Example 6.4.1) in Palazzolo et al. (1989, 1991) and Manchala et al. (1997). The ball bearings that support the shaft were retained in housings supported by soft springs to allow lateral motion but prevent rotation of the outer race. A piezoelectric stack actuator acted in parallel with the soft antirotating spring to support the bearing house and impart AVC forces to it. The stacks had a 400 N dynamic load capacity and 0.08 mm stroke for a 100 V input. These actuators only push so a pair of out-of-phase actuators acts on diametrically opposite sides of the housing in both the horizontal and vertical directions. The sensors utilized were noncontacting eddy-current relative displacement probes that have a gain of 8.0 V/mm and a bandwidth of 10 kHz. The analog and digital controller components implemented various types of filtering and proportional-integral-derivative (PID) control, and the digital components were utilized to implement feedforward cancellation of rotor imbalance response. Feedforward command voltages were determined by minimizing residual synchronous vibrations in Manchala et al. (1997). Actuator force limitations were accounted for by using a constrained quadratic programming approach to determine the control voltages. The feedforward control represents another type of supervisory control (Figure 12.1.2) in the sense that the control law was automatically adapted to the amplitude and phase angles of the system vibrations.

The International Space Station (ISS) provides an ideal platform for protein crystal growth, semiconductor fabrication, and experimentation in combustion and fluid mechanics due to the extremely low-gravitation environment. This environment can be degraded through by disturbances which occur in three frequency ranges:

- (a) Gravity gradients and atmospheric drag (10^{-5} – 10^{-3} Hz)
- (b) Crew motion and low-frequency components of thruster firings (10^{-3} –1 Hz)
- (c) Machinery (pumps, compressors, electric motors, fans) impact and high-frequency components of thruster firings (1–1000 Hz)

These sources may produce accelerations three orders of magnitude larger than allowable levels for microgravity experiments (ME) and manufacturing. Thus, isolation of these experiments on soft mounts is essential (ref. Figure 7.3.3 and Example 7.3.1). There are no

known passive soft mounts with the required extremely low stiffness, so researchers at NASA Marshall and McDonnell Douglas Aerospace developed an active suspension system (Edberg et al., 1996). This yielded a 30-fold level of isolation in test conducted on the US Space Shuttle. The ME is free to float in space except for its umbilical cord which carries power and sensor signals. The AVC system imparts isolation forces to the ME via an electromagnetic noncontacting Lorentz force actuator over a ± 1 cm “rattle space.” Feedback sensors consist of accelerometers for ME acceleration attenuation and laser-based optical sensors for relative position control. The accelerometers have a submicro-g noise floor, which determines the bound on the isolation system performance since motions that produce a smaller signal than the noise floor cannot be distinguished from noise. The power required for this AVC application is 100 W, and the controller hardware was a digital signal processor (DSP) for the position control and radiation-hardened analog components for the acceleration control.

A second space application of the AVC is the strut support structure for a Hubble-class, 102" diameter telescope structure, reported in Henderson (1996). Piezoelectric stack actuators were implemented along with collocated force sensors to provide a high static stiffness plus good isolation of higher-frequency disturbances. The actuators expand or contract 25×10^{-6} m when ± 100 V is applied across them. A digital controller was utilized at a sampling rate of 20 kHz to implement both single input–single output (SISO) and multiple input–multiple output (MIMO) core control laws (Figure 12.1.1). The AVC system provided a means to shift the fundamental mode of the telescope on the struts from 29 Hz down to 5 Hz. This softening effect provided a 20 dB decrease in telescope motions.

The Dowa Kasai Phoenix Tower is a 50-story building in Osaka, Japan, that employs AVC to reduce building sway due to strong wind gusts. A motion reduction of 50% for wind velocities up to 15 m/s resulted from the AVC as reported in Culshaw (1996). The actuators in this application consist of two 6 ton (5000 kg) masses that are translated via a motor/ball screw arrangement producing inertial forces that are designed to counter building sway. Two- to threefold reductions in the feedback acceleration sensor signals typically result by employing AVC.

Piezo actuators are available in a stack form and also in a thin “patch” or “wafer” form that is cemented onto thin-walled structural panels. Electrically induced deflections of the piezo are adjusted to cancel the forced vibration of the panels due to natural disturbances. An interesting application is the piezoelectric patch-equipped vertical tails on the 1/6 scale F-18 airplane wind tunnel model described in Moses (1997). The objective of this effort at NASA Langley was to demonstrate reduction of the dynamic stresses at the root of the vertical tail due to buffeting by the wake from the wing/fuselage leading-edge extensions. These stresses could lead to high-cycle fatigue cracking at the root of the tail. Mock tails made of aluminum with modes (14 Hz bending and 62 Hz torsion) similar to actual tails were equipped with piezoelectric patch actuators at the root and elsewhere. The wind tunnel air speed was maintained at 40 m/s, while the angle of attack was varied from 20° to 34°. A frequency domain control law (Figure 12.1.1) was implemented utilizing a digital controller with a bandwidth of about 75 Hz. Accelerometer signals were time delayed to produce control signals proportional to velocity at the first mode frequency, that is, to produce damping of the bending mode. Results showed a 60% reduction of root strains utilizing AVC.

One of the earlier descriptions (Palazzolo et al., 1991) discussed the successful application of AVC to attenuate rotating shaft vibrations utilizing diametrically opposed, piezoelectric stack pairs to dynamically push the shaft center toward a target position and (zero) velocity. Magnetic bearings (MB) provide a similar role for combined shaft support plus AVC. In contrast to piezo stacks which can only push the shaft through its bearings, the EM actuators can only pull the shaft. Hence, the EMs are also arranged in diametrically

opposite pairs. An important application of MB is for suspending high-speed energy storage flywheels that will be used for electrochemical battery replacements on the ISS and on satellites. The R&D efforts in Palazzolo et al. (2001a) and Lei and Palazzolo (2008) describe the steps that led to stable and low-vibration operation of a 12 kg–350 watt-hr flywheel at 60 000 rpm. The position of the spinning shaft's centerline was sensed with a noncontacting eddy-current-based sensor. Its signal was routed to a digital controller sampling at a rate of 8000/s. A MIMO control law (Palazzolo et al., 2001) especially designed to provide damping and cancel gyro torque perturbations was implemented to control nutation and precession modes that vary dramatically with speed. The high-frequency nutation mode required a controller bandwidth out to nearly 1500 Hz. The controller outputs are routed to power amplifiers which supply current to the electromagnetic actuator control coils. The control coils drive flux through the stationary and rotating parts of the actuator which are separated by a 0.5 mm air gap. The flux produces a control force which pulls the shaft toward its target position and zero vibration velocity.

The objective of this chapter is to introduce the reader to some important aspects of AVC that are directly related to the areas of vibration discussed in the prior chapters. These include active stiffness and damping, vibratory stability and forced harmonic response, vibration measurement, actuator control forces, and mode shape. In addition, this chapter illustrates the beneficial effects of AVC for providing stiffness and damping in an easily adjustable, yet bounded manner. The technical literature abounds with papers that have incorporated advanced control topics into AVC. The reader is referred to the vast literature on AVC to pursue a more in-depth knowledge including such areas as LQR, H-infinity, and sliding mode (Minihan et al., 2003) control approaches, MIMO control systems, magnetostrictive and shape memory alloy actuators, fuzzy logic (Lei et al., 2000) and neural network-based adaptive control schemes, genetic algorithm-based controller design (Zhong and Palazzolo, 2014), and so on.

12.2 AVC SYSTEM MODELING

Nearly all AVC systems share major common traits; therefore, much can be learned about AVC by treating a single type of AVC with significant detail. This is the present approach which utilizes a flexible structure with an electromagnetic actuator for AVC. Piezoelectric actuator-based AVC is also presented utilizing much of the methodology of the electromagnetic actuator example. The following electromagnetic actuator-based example includes key areas that appear in nearly all AVC applications:

(a) AVC systems are generally composed of the following major parts:

- The plant, a flexible body such as a machine, structure, and so on with vibration caused by external disturbances.
- Disturbances (forces, imposed support motions) that cause the plant to vibrate.
- Sensors that measure the instantaneous vibrations.
- Controllers that receive the sensor outputs and process these to form an effective control signal to reduce the vibration level.
- Power amplifiers or SPAs that increase the power of the control signals and convert them into an appropriate form (electric current or voltage, pressure, and so on) for the actuation (forcing) devices to operate. “Servo” indicates the device has an internal feedback loop that senses its output and regulates it to obtain the targeted output (typically current or voltage to the actuator).

- Actuators (magnetic, magnetostrictive, piezoelectric, hydraulic, pneumatic, and others) then apply the vibration control (suppression) forces to the plant. The above components are generally arranged in series (cascaded) in the order listed above.
- (b) The input/output characteristics of all isolated components in a feedback loop vary with the frequency of their inputs. This is indicated by the significant variation of the output amplitude and phase angle of a feedback component as its input frequency changes while holding the input amplitude and phase angle constant. The output amplitude rolls off (reduces) and the output phase lag angle increases as the input frequency increases. This property is characterized by “bandwidth” which is generally defined as the frequency at which the output amplitude is reduced to $-3\text{dB} = 1/\sqrt{2} = 0.707$ of its static (frequency = 0) value. The increase in phase lag is a source of instability in AVC systems and is generally compensated for by including lead or derivative stages in the controller. Wider bandwidth translates to higher cost for most feedback components.
- (c) Modeling the frequency response characteristics of the feedback components requires the use of additional control states which are coupled with the structural states (positions and velocities) to form the complete coupled system model. The natural frequency, modal damping, mode shape, stability, transient response, and steady-state harmonic response characteristics of the AVC system depend on both the structural states and the control states. Ignoring control states by assuming “infinite bandwidth” behavior of the feedback components can provide useful first approximations of the system response but may also fail to accurately predict stability or vibration levels in the as-built system. The frequency response characteristics of an isolated feedback component are typically measured. In most cases, this is the only practical approach for modeling the component which may consist of 100s of circuit elements as seen in Figure 12.2.1(a) for an SPA. The corresponding output/input frequency response amplitude and phase angle response of this SPA are shown in Figure 12.2.1(b). These responses can be adjusted on commercial units by potentiometer or circuit component adjustments.
- (d) The major feedback components—sensors, controllers, power amplifiers, and actuators—all have output saturation limits related to power limitations or protection measures installed to prevent damage to the parts of the components. The input/output behavior of these components may also become highly nonlinear beyond their specified “linear” operating ranges, yielding ineffective feedback control. AVC system designs that neglect limitations of the feedback components in linear range and frequency response may lead to overoptimistic simulation results and ultimate failure of the as-built system. The most common approach to incorporating saturation limits is to include a limiter in the component model that sets the quantity, such as voltage, current, flux density, etc., to its saturation value if the predicted value exceeds its saturation limits. The saturation limits are typically specified by the manufacturer or may be readily measured.
- (e) Accurate dynamic response modeling of all components in the feedback loop and the plant is imperative to develop an accurate system dynamic response model. Actuators are custom designed for many AVC applications, so they must receive special attention in the component modeling process. AVC actuators may share with passive components or bear the full static as well as dynamic loads. Comprehensive AVC design must therefore consider static load bearing performance of the actuators along with their performance in mitigating vibration. In addition, installation of an AVC actuator typically results in addition of passive forces as well as active forces. The passive forces may result from the structural stiffness of the actuator, that is, piezoelectric patch or stack

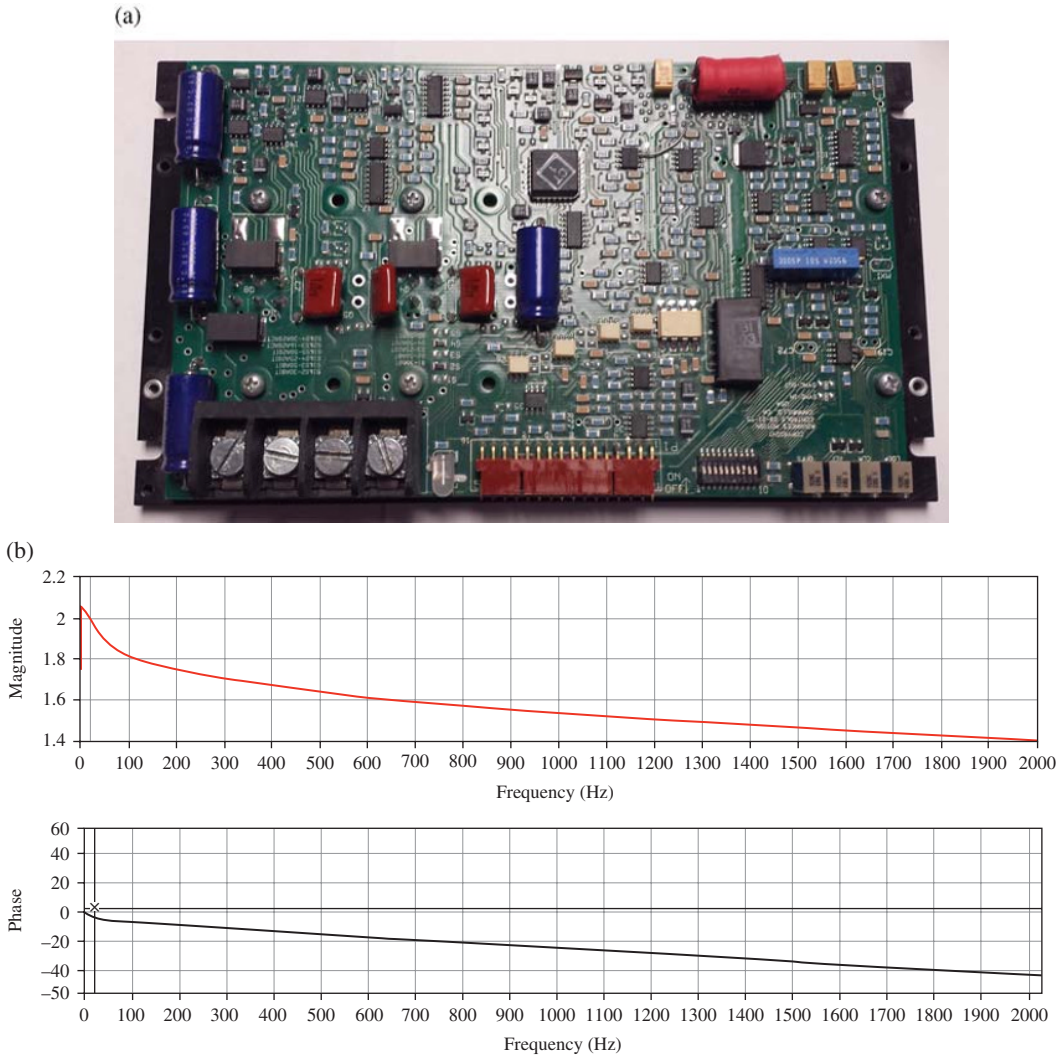


Figure 12.2.1 (a) Servo power amplifier SPA with surface mount electronics populated printed circuit board. (b) Output/input frequency response amplitude and phase angle response for the servo power amplifier in Figure 12.2.1(a)

stiffness, or in the case of a magnetic actuator the field due to the bias flux to which the control (active) flux is added or subtracted. Detailed models of electromagnetic and piezoelectric actuators are presented in this chapter.

- (f) Vibratory instability (Section 5.6) of an AVC system results mainly from two phenomena: phase lag and noncollocated sensor and actuator pairs. Phase lag results from time delay in the feedback loop which causes a delay between when the target error is sensed and when the corresponding corrective force is applied by the actuator. The error changes during the delay which can result in the force amplifying the motion instead of suppressing the motion. The measured target error may be measured at a location displaced away from where the corrective force is applied in some applications. This may result from the size of the actuator or from a maintenance or operating temperature-related consideration. This is referred to as a noncollocated sensor/actuator pair. The motions at the sensor and actuator may be out of phase in certain vibration modes,

so the corrective force is applied with the wrong phase, inducing vibratory instabilities in these modes.

Sections 12.3–12.7 utilize the example of an imbalanced rotor supported on MB to illustrate AVC modeling, simulation, and response. The development begins with an infinite bandwidth model and progresses to a model that includes the finite bandwidths of the feedback path components. The latter model may result in closed-loop instability which is shown to be alleviated by using lead compensation. The development presented is for a “Jeffcott” rigid rotor model which provides a simplified representation of an actual rotor-bearing system. Tilt motion of the rotor is neglected in this pure translation model. The Jeffcott rotor was previously discussed in Section 7.3 (ref. Figures 7.3.12, 7.3.13, and 7.3.14). The techniques presented in Sections 12.4. to 12.7 may be readily extended to more complex multi-degree-of-freedom vibrating systems.

12.3 AVC ACTUATOR MODELING

Successful modeling of AVC systems typically requires an accurate model of the actuator and an understanding of its saturation limits. The following discussion illustrates this by providing an analysis of an electromagnetic actuator for MB. Figure 12.3.1 shows a photo and diagram of a simplified MB. The two opposing C-cores in a four-pole arrangement provide a bidirectional force in the vertical “y” direction. The C-core pair in the horizontal “x” direction is not shown for clarity. A coil is removed in the photo to display the laminated pole.

The magnetic actuator model parameters include:

$$\begin{aligned}
 L_J &= \text{flux path length in journal,} \\
 L_S &= \text{flux path length in stator,} \\
 L_g &= \text{air gap with journal centered,} \\
 \mu_0 &= \text{permeability in free space,} \\
 \bar{\mu}_J &= \text{relative permeability of journal material,} \\
 \bar{\mu}_S &= \text{relative permeability of stator material,} \\
 A_g &= \text{flux cross-sectional area in air gap (per pole),} \\
 A_J &= \text{flux cross-sectional area in journal,} \\
 A_S &= \text{flux cross-sectional area in stator,} \\
 I_B &= \text{bias current in pole pair } q, \\
 i_{Cq} &= \text{control current in pole pair } q, \\
 q &= \text{displacement of the shaft away from its centered} \\
 &\quad \text{position in the } q \text{ direction,} \\
 N &= \text{number of wire turns in coil.}
 \end{aligned} \tag{12.3.1}$$

The magnetic actuator in Figure 12.3.1 operates in accordance with Ampere’s law, Gauss’s law, Faraday’s law, and constitutive relations (Ohm’s law, B – H curves, and so on). Ampere’s law may be stated as

$$\oint \vec{H} \cdot d\vec{l} = NI \tag{12.3.2}$$

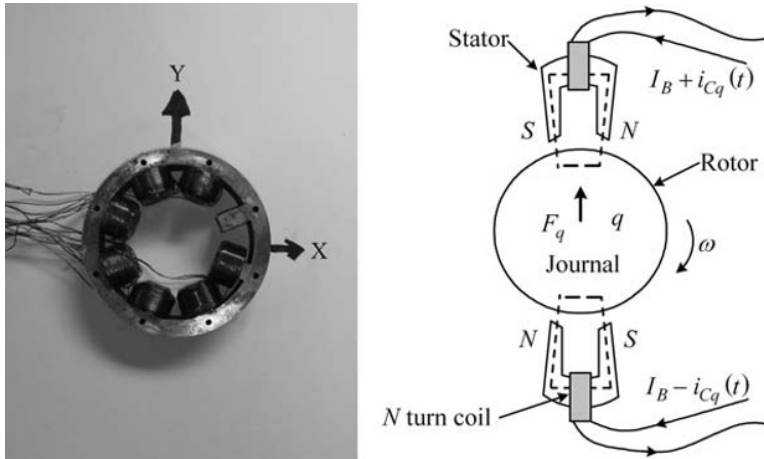


Figure 12.3.1 Oposing C-core pair in a heteropolar magnetic bearing actuator

where \vec{H} is the magnetic field intensity, $d\vec{l}$ is a differential of path length along the closed magnetic circuit (dashed lines in Figure 12.3.1), and N is the number of turns of the enclosed current I . One-dimensional (1D) magnetic circuit analysis makes the assumption that \vec{H} is parallel to the path and is constant in a given material. Application of (12.3.2) to the upper pole flux path in Figure 12.3.1 yields

$$H_S L_S + H_J L_J + 2H_g(L_g - q) = NI \quad (12.3.3)$$

The magnetic intensity and flux density for a linear material are related by the constitutive law

$$B = \mu H \quad (12.3.4)$$

where μ is the magnetic permeability. Leakage is ignored so that magnetic flux is conserved (Gauss's law for magnetism) around the loop, yielding

$$\phi = B_S A_S = B_J A_J = B_g A_g \quad (12.3.5)$$

where A represents the cross-sectional area of the flux path. The flux is obtained by substituting (12.3.4) and (12.3.5) into (12.3.3) to obtain

$$(R_S + R_J + 2R_g)\phi = NI \quad (12.3.6)$$

where the reluctances are defined by

$$R_S = \frac{L_S}{\mu_S A_S}, \quad R_J = \frac{L_J}{\mu_J A_J}, \quad R_g = \frac{L_g - q}{\mu_0 A_g} \quad (12.3.7)$$

From (12.3.5) and (12.3.6), the air gap flux density becomes

$$B_g = d_B \frac{NI}{A_g (R_S + R_J + 2R_g)} \quad (12.3.8)$$

where the flux derate factor d_B accounts for leakage and fringing effects and is typically taken as about 0.8–0.9. The Maxwell stress tensor formula determines the force exerted by the magnetic field across the air gap at a pole and has the one dimensional form

$$F = \frac{B_g^2 A_g}{2\mu_0} \quad (12.3.9)$$

From this formula, the maximum possible magnetic pressure is limited to

$$P_{\max} = \frac{F_{\max}}{A} = \frac{B_{\max}^2}{2\mu_0}, \quad F_{\max} = \frac{B_{\max}^2 A}{2\mu_0} \quad (12.3.10)$$

where B has units of Tesla (1 T = 1 N/Am), A has the unit of square meter, and $\mu_0 = 4\pi \times 10^{-7}$ N/A². The best magnetic conducting medium (iron–cobalt alloy) has a saturation flux density of about 2.3 T, which from (12.3.10) yields a maximum magnetic pressure of 2.1 MPa (294 lb/in.²). This is an example of “saturation,” where the output of a feedback component in an AVC system is limited.

The total force on the journal (length of shaft in the bearing) in Figure 12.3.1 is obtained by applying (12.3.8) and (12.3.9) to the top and bottom pole pairs as

$$F_q = \frac{d_B^2 N^2}{\mu_0 A_g} \left[\frac{(I_B + i_{Cq})^2}{\left(R_S + R_J + 2\frac{L_g - q}{\mu_0 A_g}\right)^2} - \frac{(I_B - i_{Cq})^2}{\left(R_S + R_J + 2\frac{L_g + q}{\mu_0 A_g}\right)^2} \right] \quad (12.3.11)$$

Linearization (Section 2.4) of (12.3.11) about the centered position $q=0$ and $i_{Cq}=0$ yields

$$F_q = k_i^q i_{Cq} - k_p^q q \quad (12.3.12)$$

where

$$k_i^q = \frac{d_B^2 N^2}{\mu_0 A_g} \left[\frac{4I_B}{\left(R_S + R_J + 2\frac{L_g}{\mu_0 A_g}\right)^2} \right] \quad \text{and} \quad k_p^q = - \left(\frac{d_B N}{\mu_0 A_g} \right)^2 \left[\frac{8I_B^2}{\left(R_S + R_J + 2\frac{L_g}{\mu_0 A_g}\right)^3} \right] \quad (12.3.13)$$

which are the current and position stiffness coefficients for a single opposing C-core pair aligned along direction q . The position stiffness force ($k_p^q q$) is a passive term and is unaffected by the feedback control. This must be included in the system model similar with any other passive force acting in the system. A passive force term will be present with all types of AVC actuators including piezoelectric, magnetostrictive, hydraulic, and so on.

At first glance, equations (12.3.11) and (12.3.12) would appear to imply that the C-core pair actuator system could produce an infinitely large force if the electrical current was increased to an infinitely large value. The flaw in this view lies in the limit of the linearized approximation (12.3.4) of the C-core material's B – H curve. In reality, the B curve departs from linearity, bends, and gradually flattens as H is continually increased. All materials have a saturation limit on flux density B which is represented by B_{\max} in (12.3.10). The max force per pole is then given in (12.3.10) as $F_{\max} = (B_{\max}^2 A)/(2\mu_0)$. Thus, if the flux density is near its maximum value, the force can be increased only by increasing the pole area.

A more extensive treatment of magnetic actuators including permanent magnet bias may be found in Palazzolo et al. (2012).

EXAMPLE 12.3.1 Force and Stiffness of a C-Core Pair

Statement: This numerical example provides familiarization with magnetic units and typical values for reluctances, flux density, magnetic pressure, and force and stiffness of the opposing C-core pair actuator.

Parameter Values

$$\begin{aligned}
 L_J &= \text{flux path length in journal} = 0.1 \text{ m}, \\
 L_S &= \text{flux path length in stator} = 0.2 \text{ m}, \\
 L_g &= \text{air gap with journal centered} = 0.0005 \text{ m}, \\
 \mu_0 &= \text{permeability in free space} = 4 \times 10^{-7} \text{ N/A}^2, \\
 \bar{\mu}_J &= \text{relative permeability of journal material} = 5000, \\
 \bar{\mu}_S &= \text{relative permeability of stator material} = 5000, \\
 A_g &= \text{flux cross-sectional area in air gap (per pole)} = 0.0025 \text{ m}^2, \\
 A_J &= \text{flux cross-sectional area in journal} = 0.0025 \text{ m}^2, \\
 A_S &= \text{flux cross-sectional area in stator} = 0.0025 \text{ m}^2, \\
 d_B &= \text{flux derate factor} = 1 \\
 I_B &= \text{bias current in pole pair } q = 10 \text{ A}, \\
 i_{Cq} &= \text{control current in pole pair } q = 0 \text{ A}, \\
 N &= \text{number of wire turns in coil} = 100.
 \end{aligned} \tag{1}$$

Calculated Values

Reluctances:

$$R_S = \frac{L_S}{\mu_S A_S} = 12732, \quad R_J = \frac{L_J}{\mu_J A_J} = 6366, \quad R_g = \frac{L_g}{\mu_0 A_g} = 160000 \tag{2}$$

Note $R_g \gg R_J$ and $R_g \gg R_S$; therefore, R_J and R_S are typically neglected.

Flux:

$$\phi = \frac{NI}{(R_S + R_J + 2R_g)} = 0.0029 \text{ Wb/m}^2 \tag{3}$$

Flux Densities:

$$B_g = \frac{\phi}{A_g} = 1.18 \text{ T}, \quad B_S = \frac{\phi}{A_S} = 1.18 \text{ T}, \quad B_J = \frac{\phi}{A_J} = 1.18 \text{ T} \tag{4}$$

$$\text{Air gap magnetic pressure (neglecting leakage and fringing)} = \frac{B_g^2}{2\mu_0} = 0.56 \text{ MPa (75 psi)} \tag{5}$$

$$\text{Air gap magnetic force per pole (neglecting leakage and fringing)} = \frac{B_g^2 A_g}{2\mu_0} = 1398 \text{ N (308 lb)} \tag{6}$$

Current Stiffness:

$$k_i = 1184 \text{ N/A (246 lb/A)}, \quad (7)$$

reference (12.3.13)

Position Stiffness:

$$k_p = -21.1 \times 10^6 \text{ N/m (-118050 lb/in.)}, \quad (8)$$

reference (12.3.13)

12.4 SYSTEM MODEL WITH AN INFINITE BANDWIDTH FEEDBACK APPROXIMATION

Ideally, the feedback path would operate free from electrical noise, and the output of any component in the feedback path would be invariant with respect to the frequency of its input. This is never the case with real physical systems as shown in Figure 12.2.1. However, the study of the ideal case can provide some initial design guidance. Figure 12.4.1 illustrates a Jeffcott rotor supported on MB. The MB support the weight and other static loads on the rotor and provide the AVC actuator function in Figure 12.1.1.

The damper c_e represents damping due to vibration of the rotor in the surrounding gas or liquid medium. Manufacturing limitations result in the mass center G of the rotor being off-set from its geometric (spin) center O by the “mass eccentricity” distance e . The offset causes unbalanced forces (7.3.74) and (7.3.75) that shake the rotor at its spinning frequency ω . Forces produced by the MB actuators are represented by the symbol F_M . The symbols f_{dist}^x and f_{dist}^y represent nonimbalance forces that may also act on the rotor. Applying Newton’s law to this system yields

$$m \frac{d^2(x + e \cos(\omega t))}{dt^2} = 2F_{MX}(t) - c_e \dot{x}, \quad m \frac{d^2(y + e \sin(\omega t))}{dt^2} = 2F_{MY}(t) - c_e \dot{y} - mg \quad (12.4.1)$$

Both x and y sensors are shown and provide instantaneous location of the shaft center for comparison to its desired target values, x_T, y_T , as depicted in Figure 12.4.1. An actual

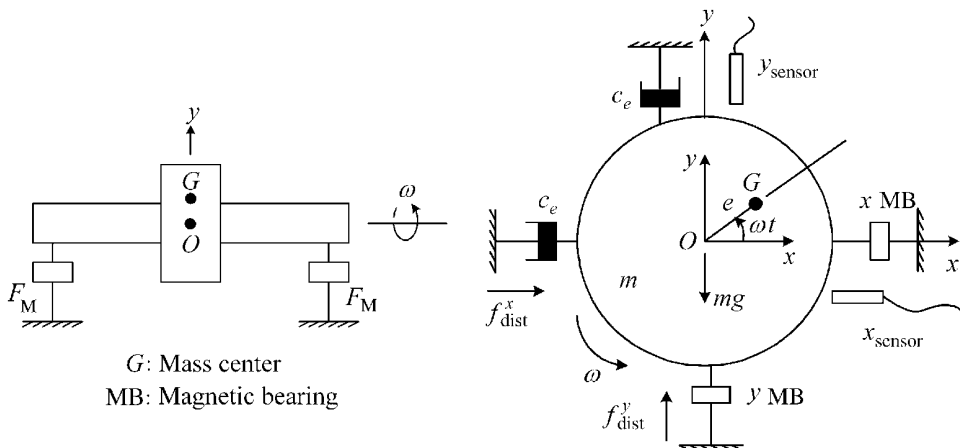


Figure 12.4.1 Front and end views of the Jeffcott rotor model (JRM) with magnetic bearings (MB)



Figure 12.4.2 Noncontacting sensor to measure position of the spinning shaft

noncontacting eddy-current position sensor is shown in Figure 12.4.2. The threaded portion is fastened into the stationary housing of the machine. The brown ceramic tip contains a coil of fine wire that emits a high-frequency (1 MHz) magnetic field in the air gap between the tip and the spinning shaft's surface. The field and resulting inductance change with air gap. The output of the sensor is a voltage that is approximately proportional to the air gap distance.

For a perfectly round rotating shaft, the position sensors will produce 0 volts when the shaft center O is at the bearing center and in general produce voltages proportional to the distance of the shaft center from the center of the bearing O_B (origin of the x - y coordinates):

$$V_{SX} = G_S x, \quad V_{SY} = G_S y \quad (12.4.2)$$

The constant G_S is the sensor sensitivity, which is typically about 8 V/mm. The relations in (12.4.2) do not vary with frequency, so they represent an infinite bandwidth idealization. In general due to the rotation of the shaft, surface imperfections such as out-of-roundness and nonuniform magnetic, optical, and electrical properties produce a repeatable sensor output pattern called “runout,” even if the shaft and bearing centers are coincident ($x=y=0$). The shaft runout at a sensor location is depicted in Figure 12.4.3 and is typically very difficult to measure. This phenomenon is also a controls challenge in compensating for the repeatable runout patterns in hard disk drives. Shaft runout typically lies within the range 0.01–0.1 mm.

The total sensor output voltages become

$$V_{SX} = G_S x + V_X^{RO}(t), \quad V_{SY} = G_S y + V_Y^{RO}(t) \quad (12.4.3)$$

The sensor voltages corresponding to the target location $O_T = (x_T, y_T)$ in the absence of runout are

$$V_{SXT} = G_S x_T, \quad V_{SYT} = G_S y_T \quad (12.4.4)$$

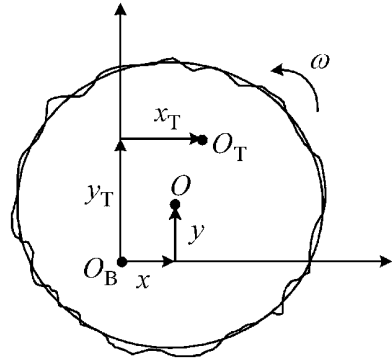


Figure 12.4.3 Highly magnified runout pattern and target position

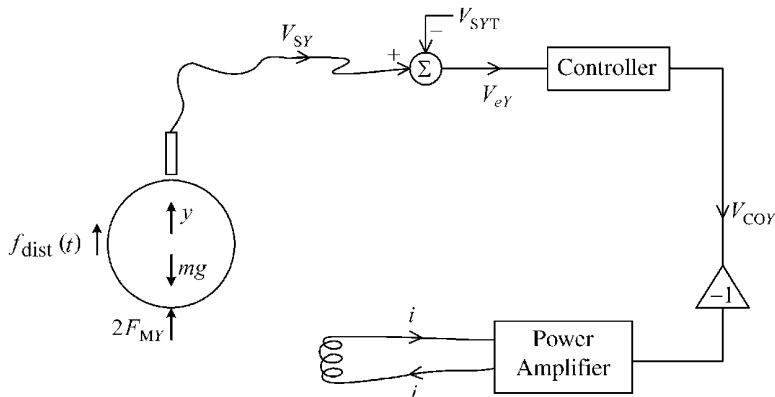


Figure 12.4.4 Feedback path for the y direction magnetic suspension control

The feedback control is assumed to be uncoupled between the x and y directions. The y direction feedback control is illustrated in Figure 12.4.4. The shaft is seen to be loaded in the $-y$ direction by the weight W .

The sensor outputs a voltage V_{SY} due to the shaft displacement y combined with the runout. The target voltage V_{SYT} is subtracted from the sensor voltage to form the “error” voltage:

$$V_{eY} = V_{SY} - V_{SYT} \quad (12.4.5)$$

The error voltage is acted on by the compensation stages in the controller producing a controller output voltage V_{COY} . This signal is inverted and routed to a servo power amplifier. The SPA is itself a feedback control system that varies its switched output voltage’s duty cycle in order to produce a control current i_{CY} that is proportional to the SPA input voltage V_{COY} . This is an important point since the internal feedback on current may allow the modeler to ignore the electrical subsystem model that converts voltage to current, that is, coil inductance and resistance and so on. The magnetic force is a nonlinear function of both

i_{CY} and y but is linearized as shown in Example 2.4.2. The control current, current stiffness, displacement y , and position stiffness produce the magnetic force F_{MY} .

Mathematical descriptions of the major feedback components

Sensors (ref. Figure 12.4.2):

From (12.4.3),

$$V_{SX} = G_S x + V_X^{\text{RO}}(t), \quad V_{SY} = G_S y + V_Y^{\text{RO}}(t) \quad (12.4.6)$$

which neglects the gradual roll-off of the sensor output voltage as frequency increases.

Controller:

For the sake of illustration, assume that the controller is an ideal proportional-derivative (PD) type. Therefore,

$$V_{COX} = G_{PX} e_x + G_{DX} \dot{e}_x, \quad V_{COY} = G_{PY} e_y + G_{DY} \dot{e}_y \quad (12.4.7)$$

where the control errors are defined by

$$e_x = V_{SX} - V_{SXT}, \quad e_y = V_{SY} - V_{SYT} \quad (12.4.8)$$

and

$$G_{PX}, G_{DX}, G_{PY}, \text{ and } G_{DY} \quad (12.4.9)$$

are the tunable proportional and derivative gains. This model has an infinite bandwidth unlike an actual controller which would “roll off” the derivative gain at high frequencies to reduce noise amplification. The model also lacks an output voltage limiter which is present on all analog and digital controllers.

Servo Power Amplifiers (ref. Figure 12.2.1):

The SPA current output equations are

$$i_{CX} = -G_{PA} V_{COX}, \quad i_{CY} = -G_{PA} V_{COY} \quad (12.4.10)$$

where G_{PA} is the DC gain of the SPA. This is an idealized model lacking roll-off of the output at very high frequencies and current and voltage output limiters. The operational characteristic in (12.4.10) is enabled by the internal servo control of SPA output current.

Magnetic Force Actuators (ref. Figure 12.3.1):

The control forces are nonlinear functions of current and gap as explained in Example 2.4.2 and (12.3.13). The linearized force models were shown in these to be

$$F_{MX} = -k_P x + k_i i_{CX}, \quad F_{MY} = -k_P y + k_i i_{CY} \quad (12.4.11)$$

where k_P and k_i are the position and current stiffness, respectively. In actuality, actuators have maximum output force limits due to flux saturation of the actuator steel and have finite bandwidth due to eddy currents.

12.4.1 Closed-Loop Feedback Controlled System Model

Substituting (12.4.6)–(12.4.10) into (12.4.11) yields

$$\begin{aligned}
 F_{MX} &= -k_p x + k_i i_{CX} = -k_p x + k_i (-G_{PA} V_{COX}) \\
 &= -k_p x - k_i G_{PA} (G_{PX} e_x + G_{DX} \dot{e}_x) = -k_p x - k_i G_{PA} G_{PX} e_x - k_i G_{PA} G_{DX} \dot{e}_x \\
 &= -k_p x - k_i G_{PA} G_{PX} (V_{SX} - V_{SXT}) - k_i G_{PA} G_{DX} (\dot{V}_{SX} - \dot{V}_{SXT}) \\
 &= -k_p x - k_i G_{PA} G_{PX} V_{SX} + k_i G_{PA} G_{PX} V_{SXT} - k_i G_{PA} G_{DX} \dot{V}_{SX} \\
 &= -k_p x - k_i G_{PA} G_{PX} (G_S x + V_X^{RO}(t)) + k_i G_{PA} G_{PX} V_{SXT} - k_i G_{PA} G_{DX} (G_S \dot{x} + \dot{V}_X^{RO}(t)) \\
 &= -k_p x - k_i G_{PA} G_{PX} G_S x - k_i G_{PA} G_{PX} V_X^{RO}(t) + k_i G_{PA} G_{PX} V_{SXT} - k_i G_{PA} G_{DX} G_S \dot{x} \\
 &\quad - k_i G_{PA} G_{DX} \dot{V}_X^{RO}(t) \tag{12.4.12}
 \end{aligned}$$

Note from (12.4.4) that $V_{SXT} = G_S x_T$ allows (12.4.12) to be written as

$$F_{MX} = -k_p x - k_{actX} x - c_{actX} \dot{x} - k_i G_{PA} G_{PX} V_X^{RO}(t) + k_{actX} x_T - k_i G_{PA} G_{DX} \dot{V}_X^{RO}(t) \tag{12.4.13}$$

where

$$\begin{aligned}
 k_{actX} &= \text{active stiffness in the } x \text{ direction} = k_i G_{PA} G_{PX} G_S \\
 c_{actX} &= \text{active damping in the } x \text{ direction} = k_i G_{PA} G_{DX} G_S
 \end{aligned} \tag{12.4.14}$$

Likewise, in the y direction,

$$F_{MY} = -k_p y - k_{actY} y - c_{actY} \dot{y} - k_i G_{PA} G_{PY} V_Y^{RO}(t) + k_{actY} y_T - k_i G_{PA} G_{DY} \dot{V}_Y^{RO}(t) \tag{12.4.15}$$

where

$$\begin{aligned}
 k_{actY} &= \text{active stiffness in the } y \text{ direction} = k_i G_{PA} G_{PY} G_S \\
 c_{actY} &= \text{active damping in the } y \text{ direction} = k_i G_{PA} G_{DY} G_S
 \end{aligned} \tag{12.4.16}$$

Thus, it is seen that the closed-loop MB force has a negative (destabilizing) position stiffness component, positive active stiffness and damping components, a constant component due to the target, and a shaking component due to runout. This last component acts as an undesirable disturbance on the rotor. Substitution of these magnetic force expressions into Newton's law (Equation (12.4.1)) yields the following:

$$\begin{aligned}
 m \frac{d^2(x + e \cos(\omega t))}{dt^2} &= 2F_{MX}(t) - c_e \dot{x} \\
 &= 2(-k_p x - k_{actX} x - c_{actX} \dot{x} - k_i G_{PA} G_{PX} V_X^{RO}(t) \\
 &\quad + k_{actX} x_T - k_i G_{PA} G_{DX} \dot{V}_X^{RO}(t)) - c_e \dot{x} \\
 \Rightarrow m \ddot{x} + (c_e + 2c_{actX}) \dot{x} + 2(k_p + k_{actX}) x \\
 &= 2(-k_i G_{PA} G_{PX} V_X^{RO}(t) - k_i G_{PA} G_{DX} \dot{V}_X^{RO}(t)) + m e \omega^2 \cos(\omega t) + 2k_{actX} x_T
 \end{aligned} \tag{12.4.17}$$

$$\begin{aligned}
m \frac{d^2(y + e \sin(\omega t))}{dt^2} &= 2F_{MY}(t) - c_e \dot{y} - mg \\
&= 2(-k_{PY} - k_{actY}y - c_{actY}\dot{y} - k_i G_{PA} G_{PY} V_Y^{RO}(t) \\
&\quad + k_{actY}y_T - k_i G_{PA} G_{DY} \dot{V}_Y^{RO}(t)) - c_e \dot{y} - mg \\
\Rightarrow m\ddot{y} + (c_e + 2c_{actY})\dot{y} + 2(k_P + k_{actY})y & \\
= 2\left(-k_i G_{PA} G_{PY} V_Y^{RO}(t) - k_i G_{PA} G_{DY} \dot{V}_Y^{RO}(t)\right) + me\omega^2 \sin(\omega t) + 2k_{actY}y_T - mg & \quad (12.4.18)
\end{aligned}$$

Consider the special case with no runout and no imbalance. The above equations simplify as:

$$m\ddot{x} + (c_e + 2c_{actX})\dot{x} + 2(k_P + k_{actX})x = 2k_{actX}x_T \quad (12.4.19)$$

$$m\ddot{y} + (c_e + 2c_{actY})\dot{y} + 2(k_P + k_{actY})y = 2k_{actY}y_T - mg \quad (12.4.20)$$

Equations (12.4.16), (12.4.19), and (12.4.20) clearly show how the MB's active stiffness and damping may be adjusted by changing the proportional G_{PY} and derivative G_{DY} feedback gains in the controller. The ability to control the stiffness and damping allows them to be adapted to varying operating or environmental conditions and is a clear advantage of active over passive vibration control.

Equations (12.4.19) and (12.4.20) simplify to the following forms at steady state ($\ddot{x} = \dot{x} = 0$):

$$2(k_P + k_{actX})x_{SS} = 2k_{actX}x_T \quad (12.4.21)$$

$$2(k_P + k_{actY})y_{SS} = 2k_{actY}y_T - mg \quad (12.4.22)$$

Therefore, at steady state,

$$x_{SS} = \frac{k_{actX}}{k_P + k_{actX}}x_T, \quad y_{SS} = \frac{k_{actY}y_T - (mg/2)}{k_P + k_{actY}} \quad (12.4.23)$$

Note that the shaft's x position coordinate will not attain its target position with PD control and static loading, unless the target position is at the center of the bearing $x_{SS} = x_T = 0$. The steady-state error in the x direction shaft position is

$$e_{SSX} = x_{SS} - x_T = \frac{k_{actX}}{k_P + k_{actX}}x_T - x_T = \frac{k_P}{k_P + k_{actX}}x_T \quad (12.4.24)$$

which is zero only if $x_T = 0$ or $k_P = 0$ or $k_{actX} \rightarrow \infty$. Thus, high proportional gain G_{PX} in Equation (12.4.14) will reduce the positioning error since $k_{actX} = k_i G_{PA} G_{PX} G_S$. Alternatively, lag or integral compensation could be used for this purpose. The corresponding control current is obtained from as

$$\begin{aligned}
i_{CXSS} &= -G_{PA} V_{COX_SS} = -G_{PA} G_{PX} e_x \\
&= -G_{PA} G_{PX} G_S (x_{SS} - x_T) = -G_{PA} G_{PX} G_S \frac{k_P}{k_P + k_{actX}} x_T
\end{aligned} \quad (12.4.25)$$

The required control current is zero if the x direction target is set at the center of the bearing $x_T = 0$. This is an unstable equilibrium point though because the position stiffness

is negative. Increasing the proportional gain to reduce the steady-state positioning error yields the following asymptotic limit as $G_{PX} \rightarrow \infty$:

$$\begin{aligned} i_{CXSS}|_{G_{PX} \rightarrow \infty} &= -G_{PA} G_{PX} G_S \frac{k_P}{k_P + k_{actX}} x_T = -G_{PA} G_{PX} G_S \frac{k_P}{k_P + k_i G_{PA} G_{PX} G_S} x_T \\ &= -\frac{k_P}{k_i} x_T \end{aligned} \quad (12.4.26)$$

which is nonzero and increases with x_T . The steady-state y position y_{SS} of the shaft is (12.4.23) which will not attain its target position y_T even if $y_T = 0$, or if $k_P = 0$, but will reach it if $k_{actY} \rightarrow \infty$. An interesting and useful case is if the target position is selected in a manner that results in the position stiffness effect cancelling the weight effect, that is,

$$2k_P y_T = -mg \Rightarrow y_T = \frac{-mg}{2k_P} \quad (12.4.27)$$

Substitution of (12.4.27) into (12.4.23) yields

$$y_{SS} = \frac{k_{actY} y_T - \frac{mg}{2}}{k_P + k_{actY}} = \frac{k_{actY} \frac{-mg}{2k_P} - \frac{mg}{2}}{k_P + k_{actY}} = \frac{-mg}{2} * \frac{\frac{k_{actY}}{k_P} + 1}{k_P + k_{actY}} = \frac{-mg}{2k_P} = y_T \quad (12.4.28)$$

Thus, it is seen that setting the y target at the position defined in (12.4.27) yields a zero steady-state position error in the y direction. The benefit of this is that the required y direction control current i_{CY} becomes zero at steady state. The position stiffness is seen to support the weight with the aid of very little control current. Thus, if permanent magnets are employed to supply the bias flux density (which provides the position stiffness k_P), the weight, or any other constant side load for that matter, can be reacted solely by the permanent magnets, with only a very small cost for electric power.

The vibration stability (Section 5.6) of this system is determined by considering the free vibration for either (12.4.19) or (12.4.20):

$$m\ddot{x} + (c_e + 2c_{actX})\dot{x} + 2(k_P + k_{actX})x = 0 \quad (12.4.29)$$

Substitution of the assumed form for the solution of x

$$x(t) = \tilde{x}e^{\lambda t} \quad (12.4.30)$$

yields

$$[m\lambda^2 + (c_e + 2c_{actX})\lambda + 2(k_P + k_{actX})]\tilde{x} = 0 \quad (12.4.31)$$

The term \tilde{x} cannot be zero or the vibration would be zero for all time t (by 12.4.30); therefore, the bracketed term must be zero, yielding the ‘‘characteristic equation’’

$$m\lambda^2 + (c_e + 2c_{actX})\lambda + 2(k_P + k_{actX}) = 0 \quad (12.4.32)$$

The roots of this equation may be real or complex numbers, having the general form

$$\lambda_1 = a - i\omega_d \quad \text{and} \quad \lambda_2 = a + i\omega_d \quad (12.4.33)$$

Equation (12.4.30) may be written as

$$x(t) = \tilde{x}e^{(a \pm i\omega_d)t} = \tilde{x}e^{at} [\cos(\omega_d t) \pm i \sin(\omega_d t)] \quad (12.4.34)$$

Clearly, the response $x(t)$ will diverge to ∞ if $a > 0$ or converge to 0 if $a < 0$. Thus, the sign of the real part of the eigenvalue determines stability of the system. The roots of (12.4.32) may be written as

$$\lambda_1 = -\frac{c_{\text{eff}}}{2m} - \sqrt{\left(\frac{c_{\text{eff}}}{2m}\right)^2 - \frac{k_{\text{eff}}}{m}}, \quad \lambda_2 = -\frac{c_{\text{eff}}}{2m} + \sqrt{\left(\frac{c_{\text{eff}}}{2m}\right)^2 - \frac{k_{\text{eff}}}{m}} \quad (12.4.35)$$

where

$$k_{\text{eff}} = 2(k_P + k_{\text{act}X}) \quad \text{and} \quad c_{\text{eff}} = c_e + 2c_{\text{act}X} \quad (12.4.36)$$

Note that λ_1 will be a negative real number and λ_2 will be a positive real number if k_{eff} is negative, in which case the system will be unstable. Thus, the total stiffness in (12.4.19) and (12.4.20) must be positive for stable levitation; therefore,

$$k_{\text{eff}} = 2(k_P + k_{\text{act}X}) > 0 \quad (12.4.37)$$

where by (12.4.14)

$$k_{\text{act}X} = \text{active stiffness in the } x \text{ direction} = k_i G_{PA} G_{PX} G_S \quad (12.4.38)$$

Therefore, the proportional feedback gains G_{PX} and G_{PY} must satisfy

$$G_{PX} > \frac{-k_P}{k_i G_{PA} G_S} \quad \text{and} \quad G_{PY} > \frac{-k_P}{k_i G_{PA} G_S} \quad (12.4.39)$$

for stable control. Next, consider the case when k_{eff} is positive. Dividing (12.4.19) and (12.4.20) by the mass m yields

$$\ddot{x} + 2\xi\omega_n\dot{x} + \omega_n^2 x = \frac{2k_{\text{act}X} * x_T}{m} \quad (12.4.40)$$

$$\ddot{y} + 2\xi\omega_n\dot{y} + \omega_n^2 y = \frac{2k_{\text{act}X} * y_T}{m} - g \quad (12.4.41)$$

where

$$\omega_n = \sqrt{\frac{2(k_P + k_{\text{act}X})}{m}} = \sqrt{\frac{2(k_P + k_i G_{PA} G_{PX} G_S)}{m}} \quad (12.4.42)$$

is the closed-loop system's undamped natural frequency. Likewise, the closed-loop system's damping ratio and amplification factor ((7.3.52), (7.3.53)) are

$$\xi = \frac{c_e + 2c_{\text{act}X}}{2m\omega_n}$$

$$\text{AF} = \frac{1}{2\xi} = \frac{m\omega_n}{c_e + 2c_{\text{act}X}} = \frac{\sqrt{m * 2(k_P + k_{\text{act}X})}}{c_e + 2c_{\text{act}X}} = \frac{\sqrt{m * 2(k_P + k_i G_{PA} G_{PX} G_S)}}{c_e + 2k_i G_{PA} G_{DX} G_S} \quad (12.4.43)$$

Thus, within the assumptions of the infinite bandwidth model, the natural frequency and amplification factors can be varied by changing the controller's proportional G_{PX} and derivative G_{DX} feedback gains. Conversely, the desired natural frequency and amplification factor can be prescribed and the proportional and derivative feedback gains solved for by using (12.4.42) and (12.4.43), that is,

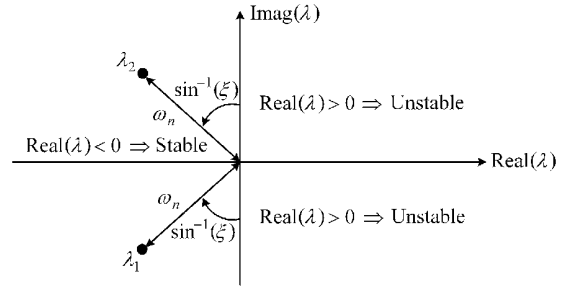


Figure 12.4.5 Closed-loop system poles when $k_{\text{eff}} > 0$

$$G_P = \frac{m\omega_n^2 - 2k_P}{2k_i G_{PA} G_S}, \quad G_D = \frac{2\xi m\omega_n - c_e}{2k_i G_{PA} G_S} \quad (12.4.44)$$

Equation (12.4.44) provides initial values for these gains, which may be further improved by tuning or by using a more refined model. The eigenvalues of (12.4.40) and (12.4.41) are obtained from the characteristic equation

$$\lambda^2 + 2\xi\omega_n\lambda + \omega_n^2 = 0 \quad (12.4.45)$$

yielding

$$\lambda_1 = -\xi\omega_n - i\omega_d \quad \text{and} \quad \lambda_2 = -\xi\omega_n + i\omega_d \quad (12.4.46)$$

where

$$\omega_d = \omega_n \sqrt{1 - \xi^2} = \text{damped natural frequency} \quad (12.4.47)$$

Figure 12.4.5 provides a geometric interpretation of the locations of these poles in the complex plane. Clearly, increased damping ratio moves the poles farther into the left-hand plane yielding increased stability.

12.5 SYSTEM MODEL WITH FINITE BANDWIDTH FEEDBACK

The output displacement amplitude of a simple spring–mass–damper oscillator excited by a constant amplitude input force will vary with input frequency and ultimately decrease as the frequency of the input becomes very large as shown in Figure 7.3.5(a). Figure 7.3.5(b) shows that the phase lag of the output behind the input also varies with frequency. In like manner, all physical systems exhibit frequency response characteristics. This includes electrical, electromagnetic, piezoelectric, pneumatic, hydraulic, and other systems and for the present purpose sensors, controllers, power amplifiers, and actuators. These systems must be represented by dynamic models, with corresponding dynamic states, unless their required operating frequency range is well below their respective bandwidths. All components in the feedback path (Figure 12.4.4) generally possess low-pass filters (LPF) to suppress high-frequency noise amplification and prevent control signal aliasing in digital controllers by reducing output amplitudes at high frequencies. A similar filtering behavior also occurs in the electromagnetic actuator due to the presence of eddy currents that strengthen with increased frequency and cancels the actuator's magnetic flux. The filtering action, whether by intent or by nature, is detrimental due to the increased phase lag that it introduces along

with the amplitude roll-off. The phase lag results in a loss of phase margin and corresponding loss in stability.

For the sake of illustration, a second-order LPF is employed in the following analysis to explain the effect of filtering and roll-off on the stability and forced response of the Jeffcott rotor. Figure 12.5.1 shows the closed-loop feedback controlled Jeffcott rotor with MB model. The filter block is shown in series with the power amplifier although it could be located anywhere in the closed-loop shown in Figure 12.4.4 and have the same effect on the system, since the model does not include saturation effects. A lead compensation stage will be included in subsequent analysis but is treated as a simple gain = 1 at this point in the development. Figure 12.5.2 depicts the isolated filter stage.

The amplitude and phase angle frequency response of the filter are shown in Figure 12.5.3. Resonance is avoided by using large ξ . The transfer function and corresponding differential equation for the filter are given by

$$T_f(s) = \frac{V_{out}(s)}{V_{in}(s)} = \frac{\omega_f^2}{s^2 + 2\xi_f\omega_f s + \omega_f^2} \quad (12.5.1)$$

and

$$\ddot{V}_{out} + 2\xi_f\omega_f\dot{V}_{out} + \omega_f^2 V_{out} = \omega_f^2 V_{in} \quad (12.5.2)$$

where ω_f is the corner frequency and ξ_f is the damping ratio of the filter, and $r = \omega/\omega_f$.

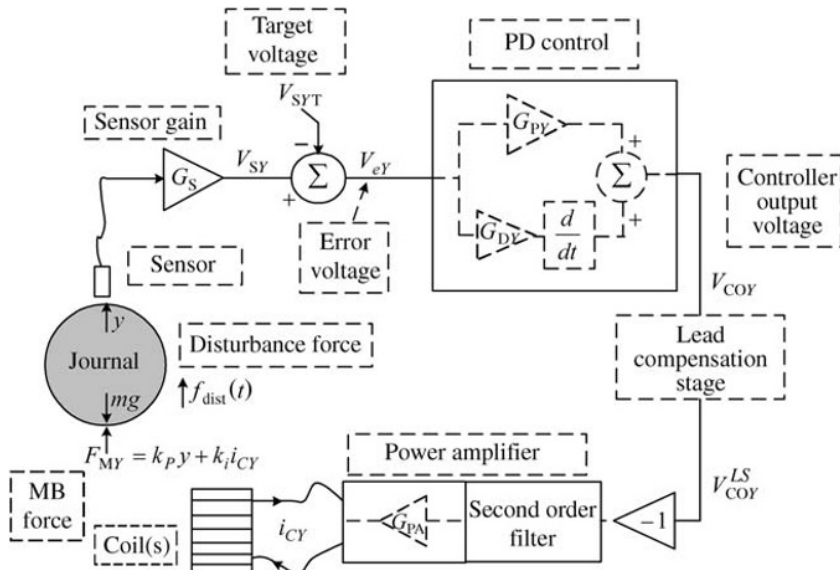


Figure 12.5.1 Closed-loop feedback controlled Jeffcott rotor with magnetic bearing model

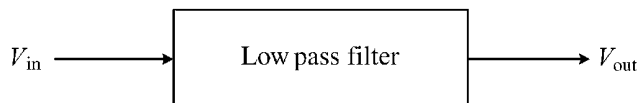


Figure 12.5.2 Low-pass filter block

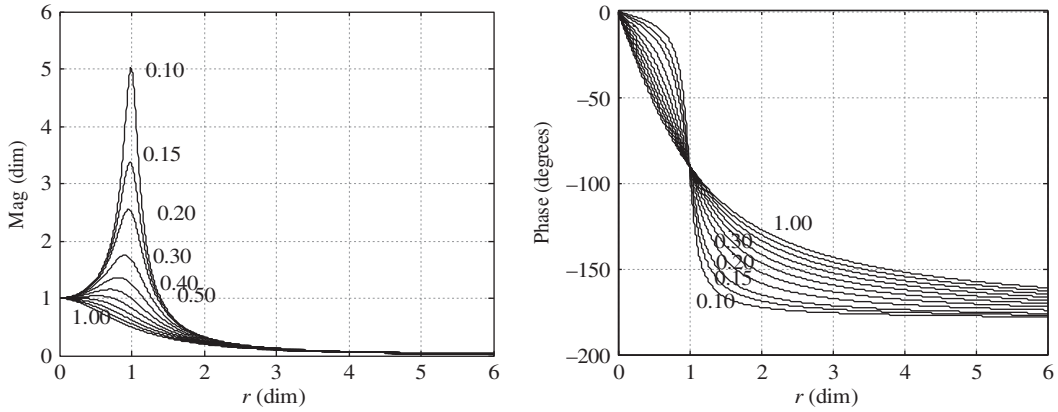


Figure 12.5.3 Amplitude and phase angle responses of a second-order filter for $0.1 < \xi < 1.0$

The amplitude and phase angle of the output are obtained from (7.3.28) and (7.3.29) as

$$\left| \frac{V_{\text{out}}}{V_{\text{in}}} \right| = \frac{1}{\sqrt{(1-r^2)^2 + (2\xi r)^2}} \quad (12.5.3)$$

$$\angle V_{\text{out}} - \angle V_{\text{in}} = -\tan^{-1} \left(\frac{2\xi r}{1-r^2} \right) \quad (12.5.4)$$

Equation (12.5.2) may also be obtained from the transfer function $T_f(s)$ in (12.5.1) with the “control canonical form” approach. This approach is generally applicable for converting an experimentally or analytically derived transfer function into a set of first-order state differential equations for the purpose of coupling with the governing dynamic differential equations of the flexible structure model. This provides the basis for forming the total feedback controlled system model. Given the general transfer function,

$$T(s) = \frac{\text{out}(s)}{\text{in}(s)} = \frac{b_1 s^{n-1} + b_2 s^{n-2} + \cdots + b_n}{s^n + a_1 s^{n-1} + \cdots + a_n} \quad (12.5.5)$$

The equivalent state space differential equation in control canonical form is

$$\dot{\underline{W}} = \underline{A} \underline{W} + \underline{B} * \text{in}(t) \quad (12.5.6)$$

and the output is obtained from

$$\text{out}(t) = \underline{C} \underline{W}(t) \quad (12.5.7)$$

where $\underline{W} = \{w_1 \ w_2 \ \cdots \ w_n\}^T$,

$$\underline{A} = \begin{bmatrix} -a_1 & -a_2 & \cdots & -a_{n-1} & -a_n \\ 1 & 0 & \cdots & 0 & 0 \\ \vdots & \vdots & \ddots & \vdots & \vdots \\ 0 & 0 & \cdots & 0 & 0 \\ 0 & 0 & \cdots & 1 & 0 \end{bmatrix}, \quad \underline{B} = \begin{bmatrix} 1 \\ 0 \\ \vdots \\ 0 \\ 0 \end{bmatrix}, \quad \underline{C} = [b_1 \ b_2 \ \cdots \ b_n] \quad (12.5.8)$$

The MATLAB utility TF2SS will provide the \underline{A} , \underline{B} , and \underline{C} matrices in (12.5.8) given the numerator and denominator coefficients in the transfer function (12.5.5):

TF2SS transfer function to state space conversion:

$[A,B,C,D] = \text{TF2SS}(\text{NUM},\text{DEN})$ calculates the state space representation

The ideal (infinite bandwidth) power amplifier transfer function was given by (12.4.10) as

$$\frac{i_{CY}}{V_{COY}} = -G_{PA} \quad (12.5.9)$$

An improved model with a second-order filter is derived from (12.5.2) and (12.5.9) as

$$\frac{d^2 i_{CY}}{dt^2} + 2\xi_f \omega_f \frac{d(i_{CY})}{dt} + \omega_f^2 i_{CY} = -G_{PA} \omega_f^2 V_{COY} \quad (12.5.10)$$

For this analysis, the other components in the MB feedback loop for the Jeffcott rotor will retain their ideal infinite bandwidth models.

Sensor:

$$V_{SY} = G_S y + V_Y^{\text{RO}}(t), \quad V_{SYT} = G_S y_T \quad (12.5.11)$$

Controller:

$$V_{COY} = G_{PY} e_y + G_{DY} \dot{e}_y \quad (12.5.12)$$

where the error is defined as

$$e_y = V_{SY} - V_{SYT} \quad (12.5.13)$$

Actuator:

$$F_{MY} = -k_P y + k_I i_{CY} \quad (12.5.14)$$

System Equation of Motion:

$$m \frac{d^2 y}{dt^2} = 2F_{MY}(t) - c_e \dot{y} - mg + me\omega^2 \sin(\omega t) \quad (12.5.15)$$

Consider the case of zero runout. Equations (12.5.10)–(12.5.15) combine to yield

$$\begin{aligned} \frac{d^2 i_{CY}}{dt^2} + 2\xi_f \omega_f \frac{d(i_{CY})}{dt} + \omega_f^2 i_{CY} &= -G_{PA} \omega_f^2 V_{COY} = -G_{PA} \omega_f^2 (G_{PY} e_y + G_{DY} \dot{e}_y) \\ &= -G_{PA} \omega_f^2 G_{PY} e_y - G_{PA} \omega_f^2 G_{DY} \dot{e}_y \\ &= -G_{PA} \omega_f^2 G_{PY} (V_{SY} - V_{SYT}) - G_{PA} \omega_f^2 G_{DY} (\dot{V}_{SY} - \dot{V}_{SYT}) \\ &= -G_{PA} \omega_f^2 G_{PY} G_S (y - y_T) - G_{PA} \omega_f^2 G_{DY} G_S \dot{y} \end{aligned} \quad (12.5.16)$$

and

$$\begin{aligned} m \frac{d^2 y}{dt^2} &= 2F_{MY}(t) - c_e \dot{y} - mg + me\omega^2 \sin(\omega t) \\ &= 2(-k_P y + k_I i_{CY}) - c_e \dot{y} - mg + me\omega^2 \sin(\omega t) \end{aligned} \quad (12.5.17)$$

Consider the zero-imbalance steady-state case ($d^2i_{CY}/dt^2 = di_{CY}/dt = \dot{y} = \ddot{y} = 0$). Equations (12.5.16) and (12.5.17) become

$$i_{CYSS} = -G_{PA}G_{PY}G_S(y_{SS} - y_T), \quad 0 = 2(-k_P y_{SS} + k_i i_{CYSS}) - mg \quad (12.5.18)$$

Solving these equations for i_{CYSS} and y_{SS} yields

$$y_{SS} = \frac{k_{actY} y_T - (mg/2)}{k_P + k_{actY}}, \quad i_{CYSS} = \frac{k_{actY} * [k_P y_T + (mg/2)]}{k_i (k_P + k_{actY})} \quad (12.5.19)$$

where from (12.4.16)

$$\begin{aligned} k_{actY} &= \text{active stiffness in the } y \text{ direction} = k_i G_{PA} G_{PY} G_S \\ c_{actY} &= \text{active damping in the } y \text{ direction} = k_i G_{PA} G_{DY} G_S \end{aligned} \quad (12.5.20)$$

Comparison of (12.5.19) with (12.4.23) shows that the filter does not affect the steady-state position error. The same result holds also for the steady-state current. Consider the homogenous forms of (12.5.16) and (12.5.17) by setting

$$-mg = me = y_T = 0 \quad (12.5.21)$$

yielding

$$\begin{aligned} \frac{d^2 i_{CY}}{dt^2} + 2\xi_f \omega_f \frac{di_{CY}}{dt} + \omega_f^2 i_{CY} &= -G_{PA} \omega_f^2 G_{PY} G_S y - G_{PA} \omega_f^2 G_{DY} G_S \dot{y} \\ &= -\frac{k_{actY}}{k_i} \omega_f^2 y - \frac{c_{actY}}{k_i} \omega_f^2 \dot{y} \end{aligned} \quad (12.5.22)$$

$$m \frac{d^2 y}{dt^2} = 2(-k_P y + k_i i_{CY}) - c_e \dot{y} \quad (12.5.23)$$

The matrix-vector form of these equations is

$$\tilde{\underline{A}} \ddot{\underline{Y}} + \tilde{\underline{B}} \dot{\underline{Y}} + \tilde{\underline{C}} \underline{Y} = \underline{0} \quad (12.5.24)$$

where

$$\underline{Y} = \begin{Bmatrix} i_{CY} \\ y \end{Bmatrix}, \quad \tilde{\underline{A}} = \begin{bmatrix} 1 & 0 \\ 0 & m \end{bmatrix}, \quad \tilde{\underline{B}} = \begin{bmatrix} 2\xi_f \omega_f & \frac{c_{actY}}{k_i} \omega_f^2 \\ 0 & c_e \end{bmatrix}, \quad \tilde{\underline{C}} = \begin{bmatrix} \omega_f^2 & \frac{k_{actY}}{k_i} \omega_f^2 \\ -2k_i & 2k_P \end{bmatrix} \quad (12.5.25)$$

Substitute the following form for the solution of \underline{Y}

$$\underline{Y} = \tilde{\underline{Y}} e^{\lambda t} \quad (12.5.26)$$

into (12.5.24) to obtain

$$\left(\lambda^2 \tilde{\underline{A}} + \lambda \tilde{\underline{B}} + \tilde{\underline{C}} \right) \tilde{\underline{Y}} = \underline{0} \quad (12.5.27)$$

The determinant of the coefficient matrix in (12.5.27) must be zero if vibrations are to exist, that is, $\tilde{\underline{Y}} \neq \underline{0}$. Therefore,

$$\det \begin{bmatrix} \lambda^2 + 2\xi_f \omega_f \lambda + \omega_f^2 & \frac{c_{actY}}{k_i} \omega_f^2 \lambda + \frac{k_{actY}}{k_i} \omega_f^2 \\ -2k_i & m\lambda^2 + c_e \lambda + 2k_P \end{bmatrix} = 0 \quad (12.5.28)$$

Expanding this determinant yields

$$\lambda^4 + a_1 \lambda^3 + a_2 \lambda^2 + a_3 \lambda + a_4 = 0 \quad (12.5.29)$$

where

$$\begin{aligned} a_1 &= 2\xi_f \omega_f + \frac{c_e}{m}, \\ a_2 &= \frac{2\xi_f \omega_f c_e + 2k_P}{m} + \omega_f^2, \\ a_3 &= \frac{4\xi_f \omega_f k_P + \omega_f^2 c_e + 2c_{actY} \omega_f^2}{m}, \\ a_4 &= \frac{2\omega_f^2 (k_P + k_{actY})}{m} \end{aligned} \quad (12.5.30)$$

EXAMPLE 12.5.1 Closed-Loop Stability of Magnetic Bearing Supported Jeffcott Rotor

Statement: This example demonstrates the effect of the low-pass filter corner frequency ω_f on closed-loop system stability. While lowering the low-pass filter corner frequency always increases noise suppression, the closed-loop stability may be diminished in the process as shown by this example.

Parameter Values

A Jeffcott rotor model with magnetic bearings and a finite bandwidth power amplifier has the following values:

$$\begin{aligned} m &= 10 \text{ kg}; \quad \xi_f = 0.5, \text{ low-pass filter corner frequency } \omega_f = \text{variable}, \\ k_{actY} &= 10\,000\,000 \text{ N/m}; \quad c_{actY} = 2000 \text{ N s/m}; \quad c_e = 100 \text{ N s/m}, \\ k_P &= -1\,000\,000 \text{ N/m}. \end{aligned}$$

Results: The corresponding undamped natural frequency, damping ratio, and damped natural frequency of the ideal (infinite bandwidth) system are:

Equation (12.4.42)

$$\omega_{ny} = \sqrt{\frac{2(k_P + k_{actY})}{m}} \Rightarrow f_{ny} = \frac{\omega_{ny}}{2\pi} = 213 \text{ Hz} \quad (1)$$

Equation (12.4.43)

$$\xi_y = \frac{c_e + 2c_{actY}}{2m\omega_{ny}} = 0.15 \quad (2)$$

Equation (12.4.47)

$$\omega_{dy} = \omega_{ny} \sqrt{1 - \xi_y^2} \Rightarrow f_{dy} = \frac{\omega_{dy}}{2\pi} = 211 \text{ Hz} \quad (3)$$

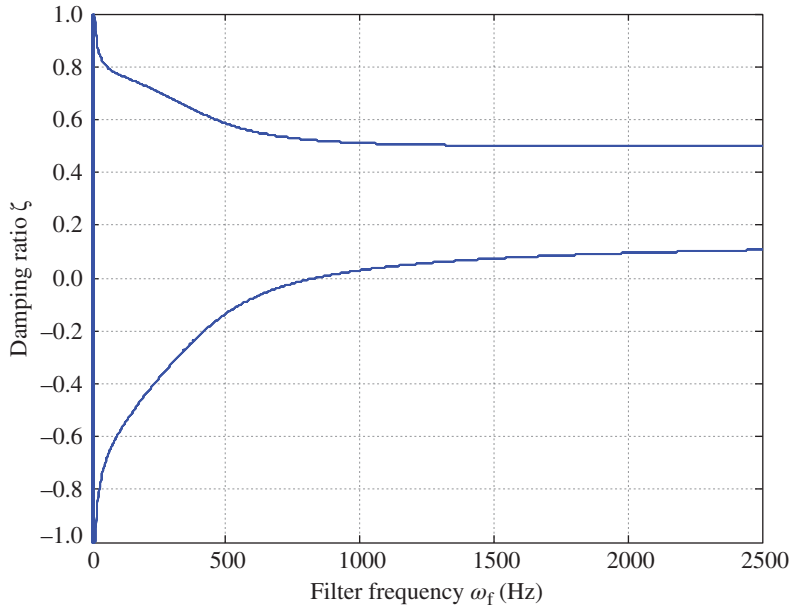


Figure E12.5.1(a) (a) Damping ratios of closed-loop system poles versus low-pass filter corner frequency $f_f = \omega_f/2\pi$

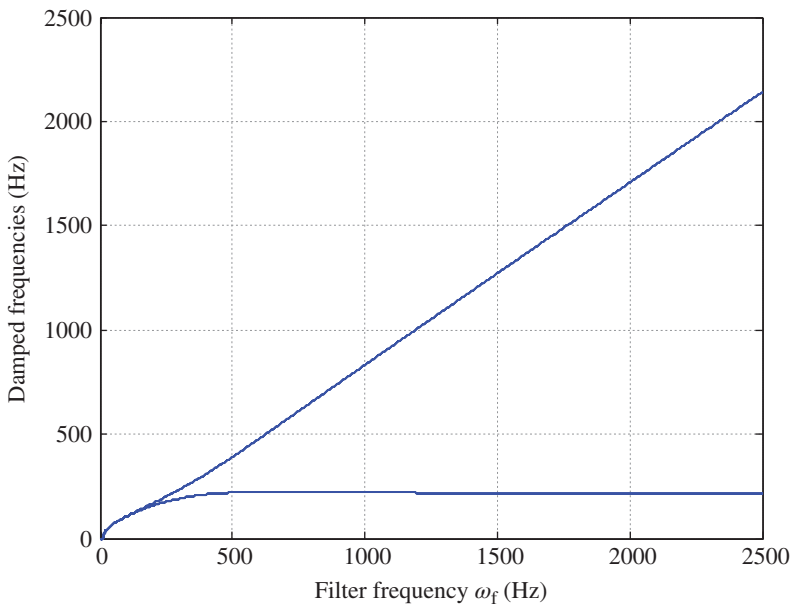


Figure E12.5.1(b) Damped natural frequencies of the closed-loop system poles versus low-pass filter frequency $f_f = \omega_f/2\pi$

Figure E12.5.1(a) shows a plot of the closed-loop system damping ratios versus the filter corner frequency $f_f = \omega_f/2\pi$ in Hz for the Jeffcott rotor model with magnetic bearings including a finite bandwidth power amplifier (with second-order filter). Note that the lower damping ratio is negative (system is unstable) for f_f less than approximately 835 Hz. This damping ratio approaches the ideal (infinite bandwidth) system value 0.15 as $f_f \rightarrow \infty$. The

negative damping ratio clearly shows that although a filter is beneficial in reducing noise in the feedback loop, it may cause the system to become unstable if the filter's corner frequency is set too low. This is an engineering example of too much of a good thing!

Figure E12.5.1(b) shows a plot of the damped natural frequencies versus filter corner frequency $f_f = \omega_f/2\pi$ for the Jeffcott rotor model with magnetic bearings including a finite bandwidth power amplifier. The lower damped natural frequency approaches the ideal (infinite bandwidth) system value 211 Hz as $f_f \rightarrow \infty$. Note that a second vibratory mode occurs due to the filter dynamics.

12.6 SYSTEM MODEL WITH FINITE BANDWIDTH FEEDBACK AND LEAD COMPENSATION

Lead compensation is a standard approach for improving the stability of the closed-loop feedback controlled system with far less penalty of excessive noise amplification at high frequencies, as may result when using a high-gain differentiator stage (derivative feedback). Lead compensators are typically cascaded in series with other control stages and may be easily realized by analog or digital means. Figure 12.5.1 shows the lead compensation stage located just before the power amplifier.

12.6.1 Transfer Function Approach

The transfer functions across the power amplifier (with filter) are obtained from (12.5.10) as

$$\frac{i_{CY}(s)}{V_{COY}^{LS}(s)} = T_{PA}(s) = \frac{-G_{PA}\omega_f^2}{s^2 + 2\xi_f\omega_f s + \omega_f^2} \quad (12.6.1)$$

The transfer functions across the lead stage are

$$\frac{V_{COY}^{LS}(s)}{V_{COY}(s)} = T_{lead}(s) = \frac{p}{z} \frac{s+z}{s+p} \quad (12.6.2)$$

where p and z are the pole and zero of the lead stage, respectively. The zero and infinite frequency gains of the lead stage are seen to be 1 and p/z , respectively. The combined transfer function from the PD control output to the control current is the product of the transfer functions in (12.6.1) and (12.6.2):

$$\frac{i_{CY}(s)}{V_{COY}(s)} = T_{PA}(s) * T_{lead}(s) = \frac{-G_{PA}\omega_f^2}{s^2 + 2\xi_f\omega_f s + \omega_f^2} * \frac{p}{z} * \frac{s+z}{s+p} \quad (12.6.3)$$

The y equilibrium equation is still (12.5.23)

$$m \frac{d^2 y}{dt^2} = 2(-k_p y + k_i i_{CY}) - c_e \dot{y} \quad (12.6.4)$$

with transfer function form

$$\frac{y(s)}{i_{CY}(s)} = T_M(s) = \frac{2k_i}{ms^2 + c_e s + 2k_p} \quad (12.6.5)$$

Combining this with (12.6.3) yields

$$\frac{y(s)}{V_{COY}(s)} = T_{PA}(s) * T_{lead}(s) * T_M(s) = \frac{-G_{PA}\omega_f^2}{s^2 + 2\xi_f\omega_f s + \omega_f^2} * \frac{p}{z} * \frac{s+z}{s+p} * \frac{2k_i}{ms^2 + c_e s + 2k_p} \quad (12.6.6)$$

Rewrite (12.5.11)–(12.5.13) with the target voltage and runout omitted since they do not affect stability to obtain

$$V_{COY}(s) = G_{PY}V_{SY} + G_{DY} s V_{SY} = (G_{PY} + G_{DY} s)G_S y(s) \quad (12.6.7)$$

Substitution of (12.6.7) into (12.6.6) yields

$$\left[1 - \frac{-G_{PA}\omega_f^2}{s^2 + 2\xi_f\omega_f s + \omega_f^2} * \frac{p}{z} * \frac{s+z}{s+p} * \frac{2k_i}{ms^2 + c_e s + 2k_p} * (G_{PY} + G_{DY} s)G_S \right] y(s) = 0 \quad (12.6.8)$$

Motion is impossible if $y(s)$ is zero; hence, Equation (12.6.8) implies

$$\left[1 - \frac{-G_{PA}\omega_f^2}{s^2 + 2\xi_f\omega_f s + \omega_f^2} * \frac{p}{z} * \frac{s+z}{s+p} * \frac{2k_i}{ms^2 + c_e s + 2k_p} * (G_{PY} + G_{DY} s)G_S \right] = 0 \quad (12.6.9)$$

Setting the numerator of (12.6.9) to zero yields

$$(s^2 + 2\xi_f\omega_f s + \omega_f^2) * (s+p) * (ms^2 + c_e s + 2k_p) + G_{PA}\omega_f^2 * \frac{p}{z} * (s+z) * 2k_i * (G_{PY} + G_{DY} s)G_S = 0 \quad (12.6.10)$$

Recall from (12.4.14) for the ideal infinite bandwidth system that

$$\begin{aligned} k_{actY} &= \text{active stiffness in the } y \text{ direction} = k_i G_{PA} G_{PY} G_S \\ c_{actY} &= \text{active damping in the } y \text{ direction} = k_i G_{PA} G_{DY} G_S \end{aligned} \quad (12.6.11)$$

Thus, (12.6.10) becomes

$$(s^2 + 2\xi_f\omega_f s + \omega_f^2) * (s+p) * (ms^2 + c_e s + 2k_p) + \omega_f^2 * \frac{p}{z} * (s+z) * 2(k_{actY} + c_{actY}s) = 0 \quad (12.6.12)$$

$$\Rightarrow s^5 + a_1 s^4 + a_2 s^3 + a_3 s^2 + a_4 s + a_5 = 0 \quad (12.6.13)$$

where

$$\begin{aligned} a_1 &= \frac{c_e}{m} + 2\xi_f\omega_f + p, \\ a_2 &= \omega_f^2 + 2\xi_f\omega_f p + (2\xi_f\omega_f + p) * \frac{c_e}{m} + 2\frac{k_p}{m}, \\ a_3 &= \frac{[2\omega_f^2 p c_{actY} / z + \omega_f^2 p m + (\omega_f^2 + 2\xi_f\omega_f p) c_e + 2(2\xi_f\omega_f + p) k_p]}{m}, \\ a_4 &= \frac{[\omega_f^2 p c_e + 2(\omega_f^2 + 2\xi_f\omega_f p) k_p + 2\omega_f^2 p c_{actY} + 2\omega_f^2 p k_{actY} / z]}{m}, \\ a_5 &= \frac{2\omega_f^2 p (k_p + k_{actY})}{m} \end{aligned} \quad (12.6.14)$$

Note that the gains k_i , G_{PA} , G_{PY} , and G_S do not appear in this expression, since they are collected in a group as either k_{actY} or c_{actY} . The closed-loop system poles, frequencies, and damping ratios are obtained by solving for the roots of (12.6.13).

EXAMPLE 12.6.1 *Closed-Loop Stability of Magnetic Bearing Supported Jeffcott Rotor Including Lead Compensation*

Statement: This example demonstrates the beneficial effect of lead compensation for improving closed-loop system vibration stability.

Parameter Values: A Jeffcott rotor model with magnetic bearings, a finite bandwidth power amplifier, and a lead compensation stage has the following values:

$$m = 10 \text{ kg}, \xi_f = 0.5, \omega_f = 2\pi * 700 \text{ rad/s}, k_{actY} = 10\,000\,000 \text{ N/m}, \\ c_{actY} = 2000 \text{ N s/m}, c_e = 100 \text{ N s/m}, k_p = -1\,000\,000 \text{ N/m}$$

These values are identical to those used for Example 12.5.1. The filter corner frequency (700 Hz) is selected to produce an unstable closed-loop system response for the case of no lead compensation as shown in Figure E12.5.1(a). One may ask, “Why not just raise the filter frequency to stabilize the system, instead of using a lead compensation stage?” The filter in Example 12.5.1 may not be adjustable since it may be embedded in a power amplifier or other device containing 100s of miniaturized soldered components that are surface mounted on a printed circuit board (Figure 12.2.1). Alternatively, the “filter” may not be a filter in the electrical sense but instead represents the experimentally measured frequency response (transfer function) of an actuator with an output that naturally “rolls off” due to eddy-current effects, capacitance effects, and so on.

Results: The infinite bandwidth damping ratio and damped natural frequency were given in (2) and (3) of Example 12.5.1 as

$$\xi_y = \frac{(c_e + 2c_{actY})}{2m\omega_{ny}} = 0.15 \quad (1)$$

$$\omega_{dy} = \omega_{ny} \sqrt{1 - \xi_y^2} \Rightarrow f_{dy} = \frac{\omega_{dy}}{2\pi} = 211 \text{ Hz} \quad (2)$$

The eigenvalues, damping ratios, and damped natural frequencies of this system with the power amplifier filter ($\xi_f = 0.5$; $\omega_f = 2\pi 700$) before adding a lead compensation stage are shown in Table E12.6.1(a), where the damping ratios and damped natural frequencies are defined by

Table E12.6.1(a) Eigenvalues, natural frequencies, and damping ratios for the system without lead compensation

Eigenvalue no.	Eigenvalue	Damped natural frequency (Hz)	Damping ratio (dim)
1	$52 + i1402$	223	-0.037
2	$52 - i1402$	223	-0.037
3	$-2260 + i3550$	565	0.54
4	$-2260 - i3550$	565	0.54

$$\xi = -\frac{\text{Real}(\lambda)}{|\lambda|}, \quad \omega_{dy} = \text{Imaginary}(\lambda) \quad (3)$$

Clearly, this system is unstable (negative damping ratio) with the filter corner frequency set at $\omega_f = 700$ Hz which is consistent with Figure E12.5.1(a). A properly designed phase lead compensation stage will help stabilize this system. A phase lead compensation stage is typically designed using the following approach. The transfer function of the lead compensation stage is given by (12.6.2)

$$\text{TF}_{\text{lead}}(s) = \frac{p}{z} * \frac{s+z}{s+p} \quad (4)$$

Define the following terms:

$$\text{Infinite frequency gain} = G_{L\infty} = \frac{p}{z} \quad (5)$$

$$\text{Desired maximum phase lead (in radians) of the lead stage} = \phi_{\text{peak}} \quad (6)$$

$$\text{Desired frequency (in Hz) where maximum } \phi_{\text{peak}} \text{ should occur} = f_{\text{peak}} \quad (7)$$

Then the pole p and zero z in (4) may be determined from

$$G_{L\infty} = \frac{1 + \sin(\phi_{\text{peak}})}{1 - \sin(\phi_{\text{peak}})}, \quad z = \frac{2\pi}{\sqrt{G_{L\infty}}} f_{\text{peak}}, \quad p = z * G_{L\infty} \quad (8)$$

A design objective is to determine the values of ϕ_{peak} and f_{peak} that yield the maximum value of the minimum damping ratio, considered over all five eigenvalues of the closed-loop system. A search over ϕ_{peak} and f_{peak} was conducted. Each set of these parameters produces five eigenvalues that are the roots of (12.6.13). A fine grid (100 × 100) was searched over the ranges

$$0 < \phi_{\text{peak}} < 60^\circ \quad \text{and} \quad 200 < f_{\text{peak}} < 700 \text{ Hz} \quad (9)$$

The results for maximizing the minimum value of the closed-loop eigenvalue damping ratio were

$$\phi_{\text{peak}} = 30.6^\circ, \quad f_{\text{peak}} = 320 \text{ Hz}, \quad \max \text{ of } \xi_{\text{min}} = 0.49, \quad p = 3525, \quad z = 1147 \quad (10)$$

The eigenvalues, damped natural frequencies, and damping ratios for this case are shown in Table E12.6.1(b). The addition of the optimal phase lead compensation stage is seen to increase the damping much above the ideal (infinite bandwidth) model (see Eq. (1) $\Rightarrow \xi_y = 0.15$).

Table E12.6.1(b) Eigenvalues, natural frequencies, and damping ratios for the system with the optimized lead compensator ($p = 3525$, $z = 1147$)

Eigenvalue no.	Eigenvalue	Damped natural frequency (Hz)	Damping ratio (dim)
1	-2720	0	1.0
2	-1499 ± i2550	406	0.51
3	-1108 ± i1982	315.5	0.49

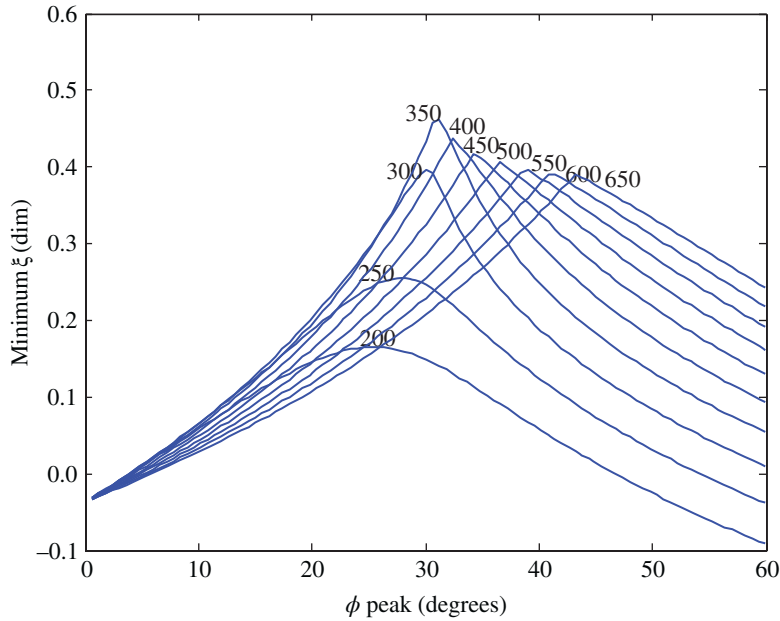


Figure E12.6.1(a) Plot of minimum damping ratio ξ_{\min} versus ϕ_{peak} , for $f_{\text{peak}} \in (200, 250, 300, \dots, 650)$ Hz

Figure E12.6.1(a) shows the variation of the minimum value of closed-loop eigenvalue damping ratio versus ϕ_{peak} .

12.6.2 State Space Approach

A transfer function approach was utilized to obtain the characteristic polynomial in (12.6.13), which was solved to obtain the closed-loop system eigenvalues, damped natural frequencies, and damping ratios. This approach is effective in this case but is not feasible for large-order vibrating structure models. In that case, it is best to utilize the state space approach as outlined for the same example below. The transfer function across the lead stage and power amplifier was given in (12.6.3) as

$$\frac{i_{CY}(s)}{V_{COY}(s)} = T_{PA}(s) * T_{\text{lead}}(s) = \frac{-G_{PA}\omega_f^2(p/z) * (s+z)}{s^3 + (p+2\xi_f\omega_f)s^2 + (2\xi_f\omega_f p + \omega_f^2)s + \omega_f^2 p} \quad (12.6.15)$$

The general control canonical form transformation for any transfer function was provided in (12.5.5)–(12.5.8). Applying the transformation to (12.6.15) yields

$$\text{in} = V_{COY}, \quad \text{out} = i_{CY} = \underline{C}\underline{W}, \quad \dot{\underline{W}} = \underline{A}\underline{W} + \underline{B} * \text{in}(t) \quad (12.6.16)$$

$$\underline{C} = \left[0 \quad -G_{PA}\omega_f^2 \left(\frac{p}{z} \right) \quad -G_{PA}\omega_f^2 p \right], \quad \underline{W} = \{w_1 \quad w_2 \quad w_3\}^T \quad (12.6.17)$$

$$\underline{A} = \begin{bmatrix} -(p+2\xi_f\omega_f) & -(2\xi_f\omega_f p + \omega_f^2) & -\omega_f^2 p \\ 1 & 0 & 0 \\ 0 & 1 & 0 \end{bmatrix}, \quad \underline{B} = \begin{bmatrix} 1 \\ 0 \\ 0 \end{bmatrix} \quad (12.6.18)$$

where from (12.5.11) to (12.5.13)

$$\begin{aligned} V_{COY} &= G_{PY}e_y + G_{DY}\dot{e}_y = G_{PY}(V_{SY} - V_{SYT}) + G_{DY}(\dot{V}_{SY} - \dot{V}_{SYT}) \\ &= G_{PY}(G_{SY} + V_Y^{RO}(t) - G_{SYT}) + G_{DY}(G_S\dot{y} + \dot{V}_Y^{RO}(t) - G_S\dot{y}_T) \end{aligned} \quad (12.6.19)$$

Thus, the complete set of differential equations for the combined lead stage and power amplifier become

$$\begin{aligned} \begin{Bmatrix} \dot{w}_1 \\ \dot{w}_2 \\ \dot{w}_3 \end{Bmatrix} &= \begin{bmatrix} -(p + 2\xi_f\omega_f) & -(2\xi_f\omega_f p + \omega_f^2) & -\omega_f^2 p \\ 1 & 0 & 0 \\ 0 & 1 & 0 \end{bmatrix} \begin{Bmatrix} w_1 \\ w_2 \\ w_3 \end{Bmatrix} \\ &+ \begin{Bmatrix} G_{PY}(G_{SY} + V_Y^{RO}(t) - G_{SYT}) + G_{DY}(G_S\dot{y} + \dot{V}_Y^{RO}(t) - G_S\dot{y}_T) \\ 0 \\ 0 \end{Bmatrix} \end{aligned} \quad (12.6.20)$$

Newton's law for the rotor mass is still (12.5.17)

$$m \frac{d^2 y}{dt^2} = 2(-k_P y + k_i i_{CY}) - c_e \dot{y} - mg + m e \omega^2 \sin(\omega t) \quad (12.6.21)$$

Note from (12.6.16) to (12.6.17)

$$\text{out} = i_{CY} = \underline{C} \underline{W} = \begin{bmatrix} 0 & -G_{PA}\omega_f^2 \left(\frac{p}{z}\right) & -G_{PA}\omega_f^2 p \end{bmatrix} \begin{Bmatrix} w_1 \\ w_2 \\ w_3 \end{Bmatrix} = -G_{PA}\omega_f^2 p * \left(\frac{w_2}{z} + w_3\right) \quad (12.6.22)$$

Substitute (12.6.22) into (12.6.21) to obtain

$$\begin{aligned} m \frac{d^2 y}{dt^2} &= 2(-k_P y + k_i i_{CY}) - c_e \dot{y} - mg + m e \omega^2 \sin(\omega t) \\ &= -2k_P y - 2k_i G_{PA}\omega_f^2 p \left(\frac{w_2}{z} + w_3\right) - c_e \dot{y} - mg + m e \omega^2 \sin(\omega t) \end{aligned} \quad (12.6.23)$$

The state (first-order) form of this differential equation is

$$\dot{y} = v_Y \quad (12.6.24)$$

$$\dot{v}_Y = -\frac{2k_P y}{m} - \frac{2k_i G_{PA}\omega_f^2 p (w_2/z + w_3)}{m} - \frac{c_e v_Y}{m} - g + e \omega^2 \sin(\omega t) \quad (12.6.25)$$

Similar equations can be derived for an arbitrary number of degree-of-freedom structural system and coupled with feedback-related state equations like (12.6.16), but of arbitrary order. This is the advantage of the state space approach over the previously discussed transfer function approach. Equations (12.6.20), (12.6.24), and (12.6.25) can be combined into a single set of closed-loop system equations as

$$\dot{\underline{X}}_{\text{sys}} = \underline{A}_{\text{sys}} \underline{X}_{\text{sys}} + \underline{F}_{\text{sys}}^{\text{F}} + \underline{F}_{\text{sys}}^{\text{RO}} + \underline{F}_{\text{sys}}^{\text{T}}, \quad \underline{X}_{\text{sys}} = \{w_1 \ w_2 \ w_3 \ y \ v_Y\}^{\text{T}} \quad (12.6.26)$$

where the system matrix is

$$\underline{A}_{\text{sys}} = \begin{bmatrix} -(p + 2\xi_f \omega_f) & -(2\xi_f \omega_f p + \omega_f^2) & -\omega_f^2 p & G_{PY} G_S & G_{DY} G_S \\ 1 & 0 & 0 & 0 & 0 \\ 0 & 1 & 0 & 0 & 0 \\ 0 & 0 & 0 & 0 & 1 \\ 0 & \frac{-2k_i G_{PA} \omega_f^2 p / z}{m} & \frac{-2k_i G_{PA} \omega_f^2 p}{m} & \frac{-2 * k_P}{m} & \frac{-c_e}{m} \end{bmatrix} \quad (12.6.27)$$

and the excitation vectors are

$$\underline{F}_{\text{sys}}^{\text{F}} = \text{system force vector} = \{0 \ 0 \ 0 \ 0 \ -g + e\omega^2 \sin(\omega t)\}^{\text{T}} \quad (12.6.28)$$

$$\underline{F}_{\text{sys}}^{\text{RO}} = \text{system runout vector} = \{G_{PY} V_Y^{\text{RO}}(t) + G_{DY} \dot{V}_Y^{\text{RO}}(t) \ 0 \ 0 \ 0 \ 0\}^{\text{T}} \quad (12.6.29)$$

$$\underline{F}_{\text{sys}}^{\text{T}} = \text{system target vector} = \{-G_{PY} G_S y_T - G_{DY} G_S \dot{y}_T \ 0 \ 0 \ 0 \ 0\}^{\text{T}} \quad (12.6.30)$$

The homogenous form of (12.6.26)

$$\dot{\underline{X}}_{\text{sys}} = \underline{A}_{\text{sys}} \underline{X}_{\text{sys}} \quad (12.6.31)$$

may be solved for the eigenvalues of the closed-loop system similar with (5.4.183):

$$\lambda \underline{\psi}_{\text{sys}} = \underline{A}_{\text{sys}} \underline{\psi}_{\text{sys}} \quad (12.6.32)$$

The results are identical to those obtained from the transfer function approach (12.6.13).

The steady-state harmonic response of the closed-loop system may also be obtained using the methods of Chapter 7, that is, (7.5.1)–(7.5.5). For the sake of illustration, consider the case when gravity, runout, and target position terms are omitted (set to zero). Then, (12.6.26) becomes

$$\dot{\underline{X}}_{\text{sys}} = \underline{A}_{\text{sys}} \underline{X}_{\text{sys}} + \underline{F}_{\text{sys}}^{\text{F}}(t) \quad (12.6.33)$$

where $\underline{F}_{\text{sys}}^{\text{F}}(t)$ is the sinusoidal function of t :

$$\underline{F}_{\text{sys}}^{\text{F}} = \text{system force vector} = \{0 \ 0 \ 0 \ 0 \ e\omega^2 \sin(\omega t)\}^{\text{T}} \quad (12.6.34)$$

Similar to (7.5.3), equation $\underline{F}_{\text{sys}}^{\text{F}}(t)$ may be written in complex variable form as

$$\underline{F}_{\text{sys}}^{\text{F}} = \text{Real}(\tilde{\underline{F}}_{\text{sys}}^{\text{F}} * e^{i\omega t}) \quad (12.6.35)$$

where

$$\tilde{\underline{F}}_{\text{sys}}^{\text{F}} = \{0 \ 0 \ 0 \ 0 \ -ie\omega^2\}^{\text{T}} \quad (12.6.36)$$

Thus, (12.6.33) becomes

$$\dot{\underline{X}}_{\text{sys}} = \underline{A}_{\text{sys}} \underline{X}_{\text{sys}} + \underline{\tilde{F}}_{\text{sys}}^{\text{F}} * e^{i\omega t} \quad (12.6.37)$$

Assume a solution to (12.6.37) of the form

$$\underline{X}_{\text{sys}} = \underline{\tilde{X}}_{\text{sys}} e^{i\omega t} \quad (12.6.38)$$

Therefore,

$$\begin{aligned} \Rightarrow i\omega \underline{\tilde{X}}_{\text{sys}} &= \underline{A}_{\text{sys}} \underline{\tilde{X}}_{\text{sys}} + \underline{\tilde{F}}_{\text{sys}}^{\text{F}}, \\ \Rightarrow \left(\underline{A}_{\text{sys}} - i\omega \underline{I} \right) \underline{\tilde{X}}_{\text{sys}} &= -\underline{\tilde{F}}_{\text{sys}}^{\text{F}}, \\ \Rightarrow \underline{\tilde{X}}_{\text{sys}} &= - \left(\underline{A}_{\text{sys}} - i\omega \underline{I} \right)^{-1} \underline{\tilde{F}}_{\text{sys}}^{\text{F}} \end{aligned} \quad (12.6.39)$$

EXAMPLE 12.6.2 *Steady-State Harmonic Imbalance Response of the Closed-Loop Feedback Controlled Magnetic Bearing Supported Jeffcott Rotor, with Lead Compensator*

Statement: This example demonstrates the effect of low-pass filter corner frequency on the steady-state vibration amplitude of a Jeffcott rotor supported by magnetic bearings.

Parameter Values: Consider the optimal phase lead case examined in Example 12.6.1 where the Jeffcott rotor on magnetic bearings has a finite bandwidth power amplifier, a phase lead compensation stage, and the following values:

$$m = 10 \text{ kg}, \quad \xi_f = 0.5, \quad \omega_f = 2\pi * 700 \text{ rad/s}, \quad c_e = 100 \text{ N s/m}, \quad k_p = -1000000 \text{ N/m},$$

$$G_S = 8000, \quad G_{PA} = 1.0, \quad k_i = 125, \quad G_{PY} = 10, \quad G_{DY} = 0.002$$

$$\Rightarrow k_{actY} = 10\,000\,000 \text{ N/m}, \quad \Rightarrow c_{actY} = 2000 \text{ N s/m}, \quad e = 0.0001 \text{ m}$$

$$\phi_{\text{peak}} = 30.6^\circ, \quad f_{\text{peak}} = 320 \text{ Hz}, \quad \max \text{ of } \xi_{\text{min}} = 0.49, \quad p = 3525, \quad z = 1147 \quad (1)$$

where from (12.4.14)

$$k_{\text{act}} = \text{active stiffness} = k_i G_{PA} G_P G_S, \quad c_{\text{act}} = \text{active damping} = k_i G_{PA} G_D G_S \quad (2)$$

Results: From (12.6.26), the amplitude and phase angle of y are given by

$$|y| = \left| \left(\underline{\tilde{X}}_{\text{sys}} \right)_4 \right| \quad \text{and} \quad \phi_y = \angle \left(\underline{\tilde{X}}_{\text{sys}} \right)_4 \quad (3)$$

where $\underline{\tilde{X}}_{\text{sys}}$ is obtained by solving (12.6.39). Figure E12.6.2(a) shows the amplitude and phase angle of the y vibration versus rotational speed frequency for five values of filter corner frequency. The amplification factor increases as the filter corner frequency is decreased which is consistent with the loss of stability with decreased corner frequency shown in Figure E12.5.1(a).

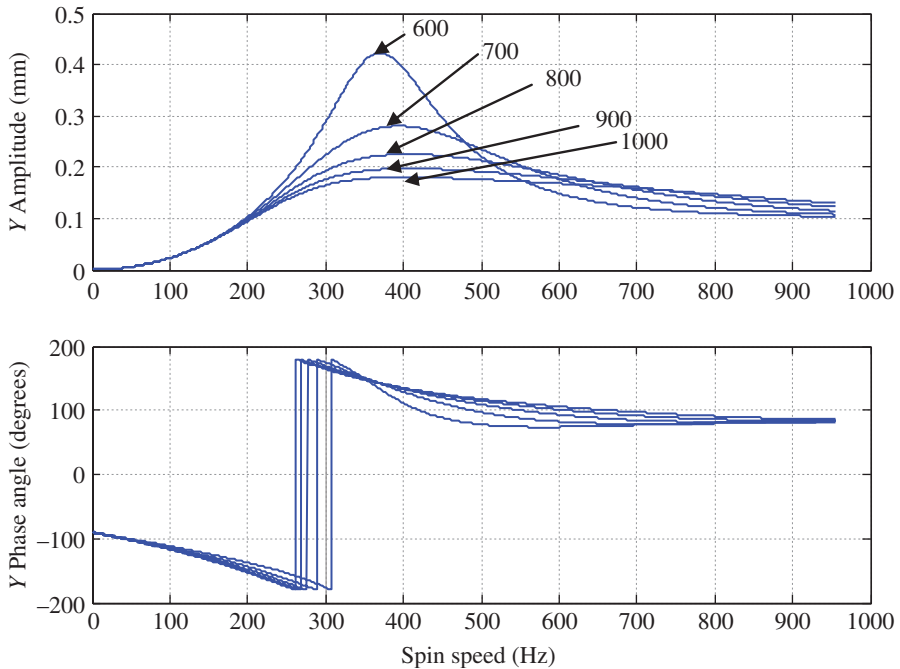


Figure E12.6.2(a) Amplitude and phase angle of y versus spin speed for five values of the filter corner frequency $f_t = \omega_t/2\pi$ in Hz

12.7 SENSOR/ACTUATOR NONCOLLOCATION EFFECT ON VIBRATION STABILITY

The preceding sections demonstrated that time delay (phase lag) in the feedback loop can contribute to vibratory instability. A second source of closed-loop control instability is non-collocation of sensor/actuator pairs. Locating the sensor away from the point of application of the actuator force will result in some modes having in-phase components at the sensor and actuator locations and other modes having out-of-phase components. The modes with out-of-phase components may be driven unstable by the feedback control depending on the control gains and the tare passive damping in the modes. This is demonstrated by again considering the Jeffcott rotor supported by MB. Figure 12.7.1 depicts a Jeffcott-type rotor model with MB represented by the linearized forces (12.3.12):

$$F_M = -k_p y + k_i i \quad (12.7.1)$$

The sensor and actuator are positioned at different locations, a so-called noncollocated arrangement.

Similar with the assumed modes approach in Section 4.6, the total motion of the rotor may be viewed as the superposition of vibration modes $\phi_i(x)$, as expressed mathematically by

$$y(x, t) = \sum q_i(t) \phi_i(x) \quad (12.7.2)$$

A more rigorous analysis of the rotor-bearing system would include coupling between the modes which accounts for the effect that motion in certain modes cause in the response of

the other modes. This coupling diminishes for the higher-order modes. The objective of the present analysis is to illustrate the qualitative effects of positioning the sensors and actuators at different positions, an assembly constraint that is typically dictated by available space in the machine and its operating temperature limits. The spatial separation of the sensor and its actuator pair may destabilize some higher-order modes while having little effect on lower-order modes. This may result when utilizing derivative gain to increase the active damping ((12.4.14) and (12.4.16)) of a lower mode, resulting in the destabilization of a higher mode.

To illustrate these points, consider the single symmetric vibration mode shown in Equation (12.7.3) and Figure 12.7.2:

$$y(x,t) = q(t)\phi(x) = q(t)\cos\left(\frac{2\pi x}{L}\right) \quad (12.7.3)$$

The kinetic energy stored in the rotor has contributions from the shaft and the central disk:

$$T = \frac{\bar{m}}{2} * \left(\frac{dy}{dt}\right)^2 \Big|_{x=0} + \int_{-L/2}^{L/2} \left(\frac{dy}{dt}\right)^2 \frac{dm}{2} \quad (12.7.4)$$

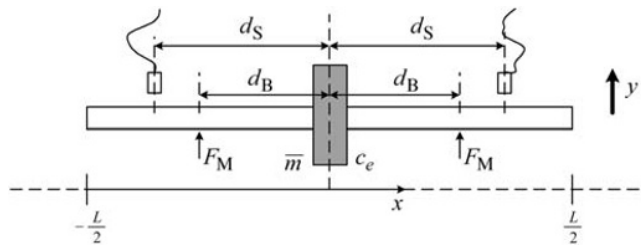


Figure 12.7.1 Jeffcott-type rotor model with noncollocated magnetic bearings

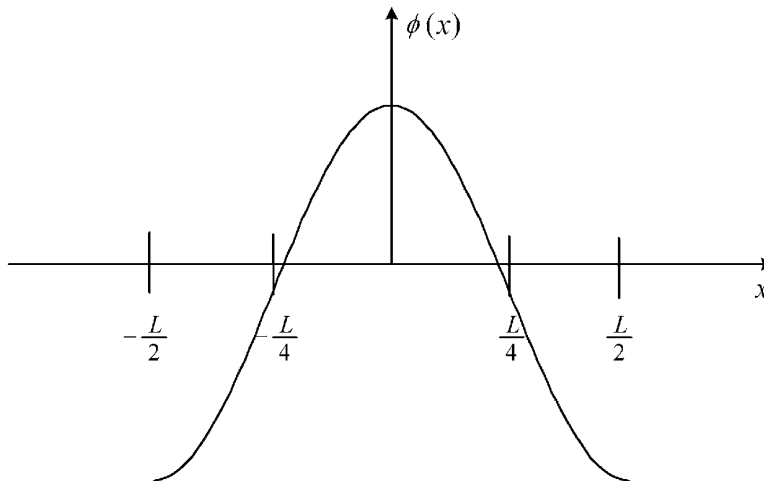


Figure 12.7.2 Vibration mode for illustrating noncollocation effect on closed-loop stability

Substitution of (12.7.3) yields

$$T = \frac{\bar{m}}{2} \dot{q}^2 + \frac{\rho A}{2} \int_{-L/2}^{L/2} (\dot{q} \phi(x))^2 dx = \frac{1}{2} \left(\bar{m} + \rho A \frac{L}{2} \right) \dot{q}^2 \quad (12.7.5)$$

The strain energy has contributions from the position stiffness and the strain energy in the shaft (9.2.10, 9.2.14):

$$U = 2 \left(\frac{k_P}{2} \right) y^2(x=d_B) + \frac{EI}{2} \int_{-L/2}^{L/2} \left(\frac{d^2 y}{dx^2} \right)^2 dx \quad (12.7.6)$$

Substitution of (12.7.3) into (12.7.6) yields

$$\begin{aligned} U &= k_P q^2(t) \phi^2(x=d_B) + \frac{EI}{2} * \frac{16\pi^4}{L^4} * q^2(t) * \int_{-L/2}^{L/2} \left(\cos\left(\frac{2\pi x}{L}\right) \right)^2 dx \\ &= \frac{q^2(t)}{2} \left(2k_P \phi^2(x=d_B) + EI * \frac{16\pi^4}{L^3} \right) \end{aligned} \quad (12.7.7)$$

The Rayleigh dissipation function (4.5.78) for the disk damping is

$$\mathfrak{F} = \frac{c_e}{2} * \left(\frac{dy}{dt} \right)^2 \Big|_{x=0} = \frac{c_e}{2} * \dot{q}^2 \phi^2(x=0) \quad (12.7.8)$$

Note that the effective damping, $c_e \phi^2(x=0)$, becomes zero if the mode has a node at the location of c_e . The MB forces due to the control currents ($F_{M_i} = k_i i$) are treated as external forces and create the following effective control force based on assumed modes theory (4.6.86 and Example 4.6.4, Eq. 44):

$$F_{\text{eff}, M_i} = 2k_i i \phi(x=d_B) \quad (12.7.9)$$

Note that the effective control force will become zero if the mode has a node at the location of the MB. The feedback control current is obtained by assuming an ideal (infinite bandwidth) feedback control loop (12.4.2, 12.4.7, 12.4.10) and utilizing (12.7.3)

$$\begin{aligned} i &= -G_{PA} V_{COY} = -G_{PA} (G_P V_Y + G_D \dot{V}_Y) \\ &= -G_{PA} (G_P G_S y(x=d_S) + G_D G_S \dot{y}(x=d_S)) \\ &= -G_{PA} G_S (G_P \phi(x=d_S) q(t) + G_D \phi(x=d_S) \dot{q}(t)) \end{aligned} \quad (12.7.10)$$

Combining (12.7.9) and (12.7.10) yields

$$F_{\text{eff}, M_i} = -2k_i * \phi(x=d_B) * G_{PA} G_S * (G_P \phi(x=d_S) q(t) + G_D \phi(x=d_S) \dot{q}(t)) \quad (12.7.11)$$

The equilibrium-Lagrange equation (4.6.52) for this system is

$$\frac{d}{dt} \left(\frac{\partial T}{\partial \dot{q}} \right) + \frac{\partial U}{\partial q} + \frac{\partial \mathfrak{F}}{\partial \dot{q}} = F_{\text{eff}, M_i} \quad (12.7.12)$$

Substitution of (12.7.5), (12.7.7), (12.7.8), and (12.7.11) into (12.7.12) yields

$$\begin{aligned} & \left(\bar{m} + \rho A \frac{L}{2} \right) \ddot{q} + q(t) \left(2k_P * \phi^2(x=d_B) + EI * \frac{16\pi^4}{L^3} \right) + c_e \dot{q} \phi^2(0) \\ & = F_{\text{eff}, M_i} = -2k_i * \phi(d_B) * G_{PA} G_S * (G_P * \phi(d_S) * q(t) + G_D * \phi(d_S) * \dot{q}(t)) \end{aligned} \quad (12.7.13)$$

or

$$m_{\text{eff}} \ddot{q} + c_{\text{eff}} \dot{q} + k_{\text{eff}} q = 0 \quad (12.7.14)$$

where

$$\begin{aligned} m_{\text{eff}} &= \left(\bar{m} + \rho A \frac{L}{2} \right) \\ c_{\text{eff}} &= c_e * \phi^2(x=0) + 2k_i G_{PA} G_S G_D * \phi(x=d_B) * \phi(x=d_S) \\ k_{\text{eff}} &= 2k_P * \phi^2(x=d_B) + EI * \frac{16\pi^4}{L^3} + 2k_i G_{PA} G_S G_P * \phi(x=d_B) * \phi(x=d_S) \end{aligned} \quad (12.7.15)$$

Divide (12.7.14) by m_{eff} and define

$$\begin{aligned} \omega_n &= \sqrt{\frac{k_{\text{eff}}}{m_{\text{eff}}}} = \text{undamped natural frequency,} \\ \xi &= \frac{c_{\text{eff}}}{2m_{\text{eff}}\omega_n} = \text{damping ratio,} \\ \omega_d &= \omega_n \sqrt{1 - \xi^2} = \text{damped natural frequency} \end{aligned} \quad (12.7.16)$$

to obtain

$$\ddot{q} + 2\xi\omega_n \dot{q} + \omega_n^2 q = 0 \quad (12.7.17)$$

which has the solution

$$\begin{aligned} q(t) &= e^{-\xi\omega_n t} (A \cos(\omega_d t) + B \sin(\omega_d t)) \\ \Rightarrow y(x, t) &= q(t)\phi(x) = e^{-\xi\omega_n t} (A \cos(\omega_d t) + B \sin(\omega_d t))\phi(x) \end{aligned} \quad (12.7.18)$$

Equation (12.7.16) shows that the damping ratio ξ in (12.7.18) is in direct proportion to and has the same sign as c_{eff} . Damping ratio is inversely proportional to amplification factor:

$$A_f = \frac{1}{2\xi} = \frac{m_{\text{eff}}\omega_n}{c_{\text{eff}}} \quad (12.7.19)$$

Thus, decreasing the effective damping will increase the amplification factor A_f , which is an undesirable result according to API 617 (Section 1.4). Equations (12.7.15)–(12.7.18) show that mode ϕ will become unstable (negative damping c_{eff} and damping ratio ξ) if

$$\phi(x=d_B) \text{ and } \phi(x=d_S) \text{ have opposite signs} \quad (12.7.20)$$

and

$$|2k_i G_{PA} G_S G_D * \phi(x=d_B) * \phi(x=d_S)| > c_e * \phi^2(x=0) \quad (12.7.21)$$

which implies

$$G_D > \frac{c_e \phi^2(x=0)}{|2k_i G_{PA} G_S \phi(x=d_B) \phi(x=d_S)|} \quad (12.7.22)$$

From (12.7.15), the effect of increasing the derivative gain G_D will be to increase the damping in a mode $\phi(x)$ if both $\phi(d_B)$ and $\phi(d_S)$ have the same sign. This is typically the case for the lower modes that have few nodes or antinodes. However, the likelihood of the mode shape having opposite signs at the sensor and actuator locations increases for the higher-order modes. Thus, a high derivative gain G_D may be beneficial for stabilizing a lower-order mode, but destabilizing for a higher-order mode according with (12.7.21). This is a very important result for the designer of an MB to consider since it reveals that there are inherent upper bounds on the value of G_D that can be utilized at the design stage even if other bounds related to saturation are neglected. In addition, a rigid rotor model will not indicate destabilization of flexible modes due to noncollocation, since the rigid rotor model does not include flexible modes. From (12.7.21), the tare, or passive, damping $c_e * \phi^2(0)$ in a mode is the only term that prevents the mode from becoming unstable if $\phi(x=d_B)$ and $\phi(x=d_S)$ have opposite signs. Thus, experimental measurement of higher-order modal damping (5.4.105) provides critical information for accurate design of a control law. As was previously demonstrated, the presence of a filter in the feedback loop will diminish the positive damping and exacerbate the destabilizing effect of the uncollocated sensor. Increasing the external passive damping c_e will allow G_D and therefore the active damping (12.4.16)

$$c_{actY} = \text{active damping in the y direction} = k_i G_{PA} G_{DY} G_S \quad (12.7.23)$$

to be increased before encountering instability.

The static (levitation) stability of the rotor may also be affected by noncollocation since by (12.7.15) the effective modal stiffness will become negative if

$$k_{eff} = 2k_P \phi^2(x=d_B) + EI \frac{16\pi^4}{L^3} + 2k_i G_{PA} G_S G_P \phi(x=d_B) \phi(x=d_S) < 0 \quad (12.7.24)$$

This will occur if

$$\phi(x=d_B) \text{ and } \phi(x=d_S) \text{ have opposite signs}$$

and

$$16\pi^4 \frac{EI}{L^3} < |2k_P * \phi^2(x=d_B) + 2k_i G_{PA} G_S G_P \phi(x=d_B) \phi(x=d_S)| \quad (12.7.25)$$

This establishes an upper bound on stable proportional gain, since the instability condition (12.7.15) may be written as

$$\phi(x=d_B) \text{ and } \phi(x=d_S) \text{ have opposite signs}$$

and

$$G_P > \frac{16\pi^4 \frac{EI}{L^3} + 2k_P * \phi^2(x=d_B)}{2k_i G_{PA} G_S * |\phi(x=d_B) \phi(x=d_S)|} \quad (12.7.26)$$

Recall from (12.4.16) that the active stiffness of the bearing for an infinite bandwidth model is

$$k_{actY} = \text{active stiffness in the y direction} = k_i G_{PA} G_{PY} G_S \quad (12.7.27)$$

Therefore, by (12.7.26) and (12.7.27), the stable level of active stiffness becomes bounded due to a noncollocated sensor/actuator pair. This is detrimental to an application requiring ultrahigh MB stiffness such as for milling machines or lathes that need high bearing stiffness to produce a high-quality surface finish on machined parts. The sensor and actuator pairs should be nearly collocated in these applications.

EXAMPLE 12.7.1 *Noncollocation Effect on Proportional and Derivative Gain and Active Stiffness and Damping Upper Bounds*

Statement: The following numerical example elucidates the above analysis for determining the maximum active stiffness and maximum active damping for a mode that has an out-of-phase noncollocated actuator/sensor pair.

Parameter Values: The example mode shape is

$$\phi(x) = \cos\left(\frac{2\pi x}{L}\right) \quad (1)$$

and the parameter values are

$$\begin{aligned} L &= 0.762 \text{ m}, \quad d_B = \frac{5}{16}L \Rightarrow \phi(d_B) = \cos\left(\frac{2\pi * 5}{16}\right) = -0.383, \quad G_S = 7874 \text{ V/m}, \quad G_{PA} = 1 \text{ A/V}, \\ d_S &= \frac{3}{16}L \Rightarrow \phi(d_S) = \cos\left(\frac{2\pi * 3}{16}\right) = 0.383, \quad D = 0.0254 \text{ m}, \quad A = \pi \frac{D^2}{4} = 5.07 \times 10^{-4} \text{ m}^2, \\ I &= \pi \frac{D^4}{64} = 2.043 \times 10^{-8} \text{ m}^4, \quad E = 2.07 \times 10^{11} \text{ N/m}^2, \quad \rho = 7786 \text{ kg/m}^3, \quad c_e = 1752 \text{ Ns/m}, \\ m_{\text{shaft}} &= \rho AL = 3 \text{ kg}, \quad \bar{m} = 2m_{\text{shaft}} = 6 \text{ kg}, \quad k_i = 89 \text{ N/A}, \quad k_p = -350393 \text{ N/m} \end{aligned} \quad (2)$$

Results: By (12.7.15),

$$m_{\text{eff}} = \left(\bar{m} + \rho A \frac{L}{2}\right) = 7.5 \text{ kg} \quad (3)$$

The condition for instability (12.7.20), or the first condition in (12.7.26), is satisfied by (2) since $\phi(d_S) = 0.383$ and $\phi(d_B) = -0.383$ have opposite signs. The maximum stable derivative gain is obtained from (12.7.22) as

$$G_{D, \text{max}} = \frac{c_e \phi^2(x=0)}{|2k_i G_{PA} G_S \phi(x=d_B) \phi(x=d_S)|} = 0.0085 \quad (4)$$

The maximum stable proportional gain is obtained from (12.7.26) as

$$G_P = \frac{16\pi^4 \frac{EI}{L^3} + 2k_p * \phi^2(x=d_B)}{2k_i G_{PA} G_S * |\phi(x=d_B) \phi(x=d_S)|} = 72.1 \quad (5)$$

The corresponding ideal active stiffness and damping values are obtained from (12.4.16) as

$$k_{\text{act}Y} = \text{active stiffness in the } y \text{ direction} = k_i G_{PA} G_{PY} G_S = 5 \times 10^7 \text{ N/m} \quad (6)$$

$$c_{\text{act}Y} = \text{active damping in the } y \text{ direction} = k_i G_{PA} G_{DY} G_S = 5981 \text{ Ns/m} \quad (7)$$

12.8 PIEZOELECTRIC ACTUATORS

The author and his graduate students and colleagues at NASA Glenn performed extensive studies on the usage of piezoelectric actuator stacks for vibration control of a rotating shaft (Palazzolo et al., 1989, 1991; Tang et al., 1995). The results of this research were experimental demonstrations of the AVC suppression of unstable (Chapter 5), transient (Chapter 6), and steady-state harmonic (Chapter 7) vibrations of the spinning shaft. The piezoelectric actuator supports the ball bearings which in turn supports the rotating shaft. The control forces are transmitted from the piezoelectric actuators through the ball bearings to the rotating shaft and are caused by expansion and contraction of the piezoelectric actuator material in response to applied voltages. The piezoelectric actuators mainly act in a push mode since the stacks are brittle in tension. This is accounted for by internal preload springs in the actuators and in some applications by installing the actuators in opposing pairs so that one actuator produces a (+) direction force on one side of the bearing and the other actuator provides a force in the opposing (−) direction on the opposite side of the bearing.

Unlike the SPA shown in Figure 12.2.1(a) for magnetic bearing usage, which acts in current control mode, the power amplifier for piezoelectric actuators acts in a voltage control mode outputting voltages proportional to the control voltages. The output voltages range up to 150 V for low-voltage applications and 1000 V for high-voltage applications. Expansion factors vary with piezoelectric stack vendor and model, but a typical value for a 10 cm long stack is 10^{-6} m/V with a peak expansion of 0.1 mm. The forces generated by commercially available stacks can exceed 3000 N depending on the stiffness of the internal preload spring and the stiffness of the surface in contact with the tip of the actuator. Thus, for a high-performance stack of net internal stiffness of 40 N/ μ m and a peak expansion of 90 μ m, the load capacity in compression is approximately 40 N/ μ m * 90 μ m = 3600 N. The piezoelectric actuator stacks are composed of 100s of thin piezoelectric wafers separated by conducting electrodes that are held at the impressed voltage to the stack. The many wafers then expand in series, yielding the maximum expansion and force possible for the given length of the actuator.

The electrical response of a piezo stack is dominated by its capacitance, so its bandwidth may become limited by the maximum available current for a constant level of expansion, since $|i| \approx |C * (dV/dt)| = C\omega|V|$. Typical capacitance values range from 5 to 50 μ F. Stack resonance frequencies typically range from 5 to 10 kHz which is usually ideal for high-frequency AVC applications.

Figure 12.8.1 depicts a thin piezo layer sandwiched by two electrodes with differential voltage $V(t)$. The electrodes are cemented to the top and bottom faces in this figure. The free

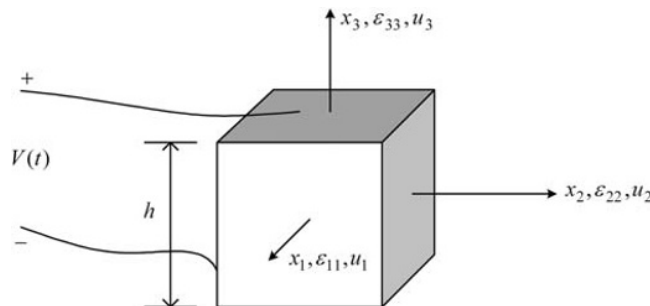


Figure 12.8.1 Piezoelectric cube with applied voltage $V(t)$ and resulting strains

unconstrained layer experiences strains in all three directions due to application of the voltage, as expressed by

$$\varepsilon_{33f} = d_{33} \frac{V(t)}{h}, \quad \varepsilon_{11f} = d_{31} \frac{V(t)}{h}, \quad \varepsilon_{22f} = d_{32} \frac{V(t)}{h} \quad (12.8.1)$$

The piezoelectric material is classified according to the level of difficulty in polarizing the material, that is, soft material is easily polarized and hard material is significantly more difficult to polarize. Typical values of the piezoelectric charge constants (moduli) are as follows:

Soft Piezo Material:

$$d_{33} = 250 \times 10^{-12} \text{ m/V (or C/N)}, \quad d_{31} = d_{32} = -125 \times 10^{-12} \text{ m/V}$$

Hard Piezo Material:

$$d_{33} = 600 \times 10^{-12} \text{ m/V (or C/N)}, \quad d_{31} = d_{32} = -250 \times 10^{-12} \text{ m/V} \quad (12.8.2)$$

By (12.8.1), the free expansion/contraction of the layer in the x_3 direction is

$$\delta_3 = h\varepsilon_{33f} = d_{33}V(t) \quad (12.8.3a)$$

12.8.1 Piezoelectric Stack Actuator

The piezoelectric stack actuator is typically arranged in a stack of n_p layers, each separated by an extremely thin electrically conducting foil electrode. The total length of the stack is $H = n_p h$, so the total expansion contraction becomes

$$\Delta_3 = H\varepsilon_{33f} = n_p d_{33} V(t) \quad (12.8.3b)$$

Figure 12.8.2 depicts the internal operation of a piezoelectric stack-type actuator neglecting piezo material inertial effects. The latter effects are treated in Tang et al. (1995).

The stiffness k_p is an internal preload spring that maintains the piezo stack in compression to prevent tensile failure. The stiffness k_E is a stiffness inserted between the piezo stack and the object being actuated for the purpose of maintaining a preload between the actuator and the object. The stack stiffness is (4.8.17):

$$k_S = \frac{A_p E_p}{H} \quad (12.8.4)$$

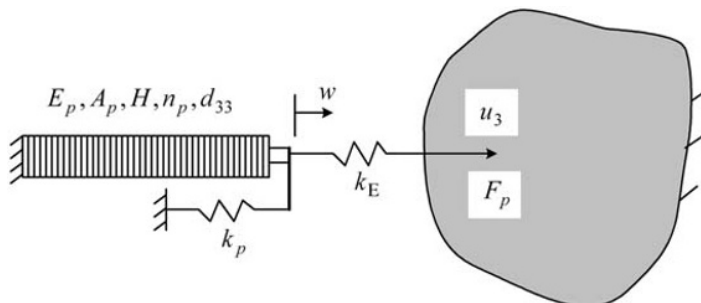


Figure 12.8.2 Static model of piezoelectric stack actuator

Equilibrium of the piezo actuator tip requires

$$\frac{E_p A_p}{L_p} (\Delta_3 - w) - k_p w - k_E (w - u_3) = 0 \quad (12.8.5)$$

The MATLAB symbolic code (Section 2.2) below solves (12.8.3a)–(12.8.5) to obtain

$$w = \alpha_1 u_3 + \alpha_2 V(t) \quad (12.8.6)$$

where

$$\alpha_1 = \frac{k_E}{k_E + k_p + k_S}, \quad \alpha_2 = \frac{k_S d_{33} n_p}{k_E + k_p + k_S} \quad (12.8.7)$$

The force applied to the object being controlled becomes

$$F_p = k_E (w - u_3) \quad (12.8.8)$$

Equation (12.8.6) is substituted into (12.8.8) in the symbolic MATLAB code below to obtain

$$F_p = -k_E \frac{k_p + k_S}{k_E + k_p + k_S} u_3 + \frac{k_E k_S d_{33} n_p}{k_E + k_p + k_S} V(t) \quad (12.8.9)$$

MATLAB Symbolic Code (Section 2.2)

```
clear all

syms Ep Ap Lp np d33 V Kp Ke u3 H Ks FP FPa FPb Fpc

a1 = Ks+Kp+Ke; a2 = Ks*np*d33

w = (a2*V + Ke*u3) / a1

w1 = collect(w, u3)

w2 = collect(w1, V)

FP = Ke*(w-u3)

FPa = collect(FP, V)

FPb = collect(FPa, u3)

Fpc = simplify(FPb)
```

EXAMPLE 12.8.1 *Active Vibration Control of a Cantilevered Beam Mounted Mass with Piezoelectric Stack Actuator AVC*

Statement: An enclosure containing a motor and sensitive electronic instrumentation is mounted on a cantilevered beam-type rail as shown in Figure E12.8.1(a). The vibration is considered excessive, so it is decided to install a piezoelectric stack actuator-based AVC system.

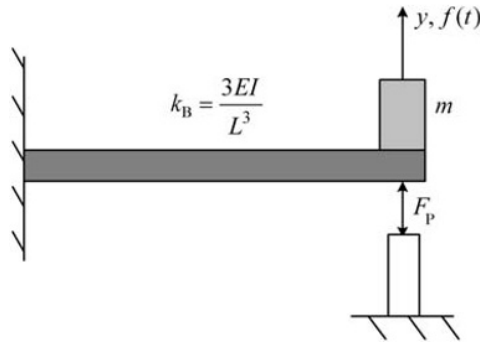


Figure E12.8.1(a) Cantilevered rail mounted instrumentation enclosure with piezoelectric stack AVC

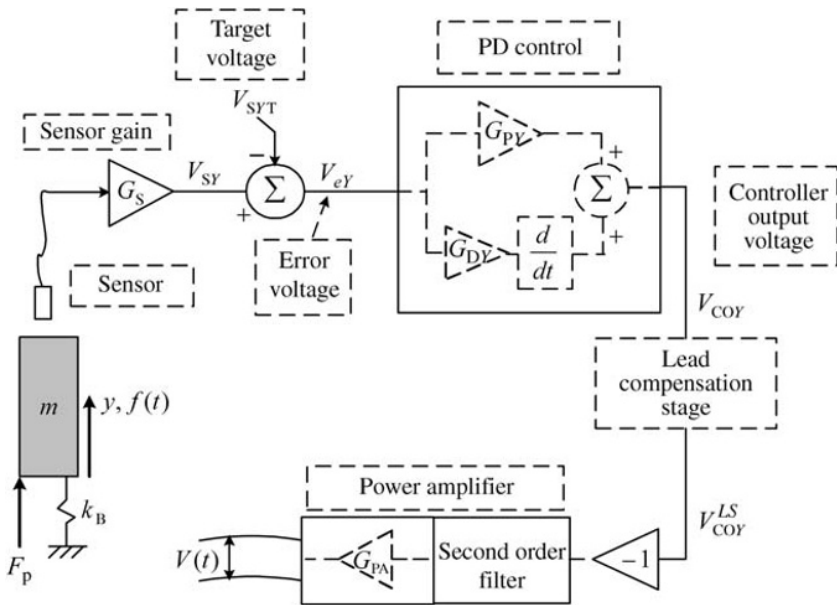


Figure E12.8.1(b) Closed feedback control model with piezoelectric stack AVC

Objective: Derive the state equations for the closed-loop system which includes a lead compensation stage, PD stage, and a second-order representation of the power amplifier that supplies the voltage to the piezoelectric actuator.

Solution: Figure E12.8.1(b) shows the complete AVC feedback loop. Unlike the magnetic bearing control in Figure 12.5.1, the input to the piezoelectric actuator is a voltage that is internally controlled in a voltage feedback loop.

The transfer function between the controller output and the voltage across the piezoelectric actuator stack is obtained from (12.6.15) as

$$\frac{V(s)}{V_{COR}(s)} = T_{PA}(s) * T_{lead}(s) = \frac{-G_{PA}\omega_f^2(p/z)(s+z)}{s^3 + (p + 2\xi_f\omega_f)s^2 + (2\xi_f\omega_f p + \omega_f^2)s + \omega_f^2 p} \quad (1)$$

The control canonical form of this relation is obtained from (12.6.16) to (12.6.18) as

$$\text{in} = V_{\text{COY}}, \quad \text{out} = V = \underline{C} \underline{W}, \quad \dot{\underline{W}} = \underline{A} \underline{W} + \underline{B} * \text{in}(t) \quad (2)$$

$$\underline{C} = \begin{bmatrix} 0 & -G_{\text{PA}} \omega_f^2 \left(\frac{p}{z} \right) & -G_{\text{PA}} \omega_f^2 p \end{bmatrix}, \quad \underline{W} = \{w_1 \ w_2 \ w_3\}^T \quad (3)$$

$$\underline{A} = \begin{bmatrix} -(p + 2\xi_f \omega_f) & -(2\xi_f \omega_f p + \omega_f^2) & -\omega_f^2 p \\ 1 & 0 & 0 \\ 0 & 1 & 0 \end{bmatrix}, \quad \underline{B} = \begin{bmatrix} 1 \\ 0 \\ 0 \end{bmatrix} \quad (4)$$

Equation (12.6.19) relates the controller output voltage to the deflection y as

$$\begin{aligned} V_{\text{COY}} &= G_{\text{PY}} e_y + G_{\text{DY}} \dot{e}_y = G_{\text{PY}} (V_{\text{SY}} - V_{\text{SYT}}) + G_{\text{DY}} (\dot{V}_{\text{SY}} - \dot{V}_{\text{SYT}}) \\ &= G_{\text{PY}} (G_{\text{SY}} y + V_Y^{\text{RO}}(t) - G_{\text{SYT}}) + G_{\text{DY}} (G_{\text{SY}} \dot{y} + \dot{V}_Y^{\text{RO}}(t) - G_{\text{SYT}} \dot{y}) \end{aligned} \quad (5)$$

Substitution of (5) into (2)–(4) yields the state equations in the form

$$\begin{aligned} \begin{Bmatrix} \dot{w}_1 \\ \dot{w}_2 \\ \dot{w}_3 \end{Bmatrix} &= \begin{bmatrix} -(p + 2\xi_f \omega_f) & -(2\xi_f \omega_f p + \omega_f^2) & -\omega_f^2 p \\ 1 & 0 & 0 \\ 0 & 1 & 0 \end{bmatrix} \begin{Bmatrix} w_1 \\ w_2 \\ w_3 \end{Bmatrix} \\ &+ \begin{Bmatrix} G_{\text{PY}} (G_{\text{SY}} y + V_Y^{\text{RO}}(t) - G_{\text{SYT}}) + G_{\text{DY}} (G_{\text{SY}} \dot{y} + \dot{V}_Y^{\text{RO}}(t) - G_{\text{SYT}} \dot{y}) \\ 0 \\ 0 \end{Bmatrix} \end{aligned} \quad (6)$$

The equation of motion for m is obtained utilizing (12.8.9) as

$$m\ddot{y} = -k_{\text{BY}} y - c\dot{y} + F_{\text{p}} + f(t) = -k_{\text{BY}} y - c\dot{y} - k_{\text{E}} \frac{k_{\text{p}} + k_{\text{S}}}{k_{\text{E}} + k_{\text{p}} + k_{\text{S}}} y + \frac{k_{\text{E}} k_{\text{S}} d_{33} n_{\text{p}}}{k_{\text{E}} + k_{\text{p}} + k_{\text{S}}} V(t) + f(t) \quad (7)$$

Therefore,

$$m\ddot{y} = -c\dot{y} - \frac{k_{\text{B}} (k_{\text{E}} + k_{\text{p}} + k_{\text{S}}) + k_{\text{E}} (k_{\text{p}} + k_{\text{S}})}{k_{\text{E}} + k_{\text{p}} + k_{\text{S}}} y + \frac{k_{\text{E}} k_{\text{S}} d_{33} n_{\text{p}}}{k_{\text{E}} + k_{\text{p}} + k_{\text{S}}} V(t) + f(t) \quad (8)$$

As in (12.6.22), the piezo stack voltage V in (8) may be obtained from (2) and (3) as

$$V(t) = \underline{C} \underline{W} = \begin{bmatrix} 0 & -G_{\text{PA}} \omega_f^2 \left(\frac{p}{z} \right) & -G_{\text{PA}} \omega_f^2 p \end{bmatrix} \begin{Bmatrix} w_1 \\ w_2 \\ w_3 \end{Bmatrix} = -G_{\text{PA}} \omega_f^2 p * \left(\frac{w_2(t)}{z} + w_3(t) \right) \quad (9)$$

Substitute (9) into (8) to obtain

$$m\ddot{y} = -c\dot{y} - \alpha_k y - \alpha_w * \left(\frac{w_2(t)}{z} + w_3(t) \right) + f(t) \quad (10)$$

where

$$k_{\text{eff}} = k_B + \frac{k_E(k_p + k_S)}{k_E + k_p + k_S}, \quad \alpha_w = \frac{k_E k_S d_{33} n_p}{k_E + k_p + k_S} G_{PA} \omega_f^2 p \quad (11)$$

The state (first-order) form of (10) is

$$\dot{y} = v_Y \quad (12)$$

$$\dot{v}_Y = -\frac{c}{m} v_Y - \frac{\alpha_k}{m} y - \frac{\alpha_w}{m} * \left(\frac{w_2(t)}{z} + w_3(t) \right) + \frac{1}{m} f(t) \quad (13)$$

Equations (6), (12), and (13) can be combined into a single set of closed-loop system equations as

$$\dot{\underline{X}}_{\text{sys}} = \underline{A}_{\text{sys}} \underline{X}_{\text{sys}} + \underline{F}_{\text{sys}}^F, \quad \underline{X}_{\text{sys}} = \{w_1 \ w_2 \ w_3 \ y \ v_Y\}^T \quad (14)$$

where the system matrix is

$$\underline{A}_{\text{sys}} = \begin{bmatrix} -(p + 2\xi_f \omega_f) & -(2\xi_f \omega_f p + \omega_f^2) & -\omega_f^2 p & G_{PY} G_S & G_{DY} G_S \\ 1 & 0 & 0 & 0 & 0 \\ 0 & 1 & 0 & 0 & 0 \\ 0 & 0 & 0 & 0 & 1 \\ 0 & \frac{\alpha_w}{m * z} & \frac{-\alpha_w}{m} & \frac{-k_{\text{eff}}}{m} & \frac{-c}{m} \end{bmatrix} \quad (15)$$

and the excitation vector is

$$\underline{F}_{\text{sys}}^F = \text{system force vector} = \left\{ 0 \ 0 \ 0 \ 0 \ \frac{f(t)}{m} \right\}^T \quad (16)$$

The homogenous form of (14)

$$\dot{\underline{X}}_{\text{sys}} = \underline{A}_{\text{sys}} \underline{X}_{\text{sys}} \quad (17)$$

may be solved for the eigenvalues of the closed-loop system similar with (5.4.183):

$$\lambda \underline{\psi}_{\text{sys}} = \underline{A}_{\text{sys}} \underline{\psi}_{\text{sys}} \quad (18)$$

The preceding analysis accounts for the finite bandwidth of the feedback loop. It may also be helpful for selecting gains to consider the ideal infinite bandwidth case, without lead compensation. Recall from (12.8.9) that

$$F_p = -k_E \frac{k_p + k_S}{k_E + k_p + k_S} u_3 + \frac{k_E k_S d_{33} n_p}{k_E + k_p + k_S} V(t) \quad (19)$$

In Figure E12.8.1(b), the actuator voltage for the ideal infinite bandwidth case, without lead compensation, is

$$V(t) = -(G_{PA} G_{PY} G_S y + G_{PA} G_{DY} G_S \dot{y}) \quad (20)$$

Substitute (20) into (19) to obtain

$$F_{p,ideal} = -k_E \frac{k_p + k_S}{k_E + k_p + k_S} u_3 - \frac{k_E k_S d_{33} n_p}{k_E + k_p + k_S} (G_{PA} G_{PY} G_{SY} + G_{PA} G_{DY} G_{SY}) \quad (21)$$

Thus, the ideal active stiffness and damping become

$$k_{act} = \frac{k_E k_S d_{33} n_p}{k_E + k_p + k_S} G_{PA} G_{PY} G_S, \quad c_{act} = \frac{k_E k_S d_{33} n_p}{k_E + k_p + k_S} G_{PA} G_{DY} G_S \quad (22)$$

The ideal case natural frequency and damping ratios become

$$f_{n,ideal} = \frac{1}{2\pi} \sqrt{\frac{k_{eff} + k_{act}}{m}}, \quad \xi_{ideal} = \frac{c + c_{act}}{2m(2\pi f_{n,ideal})} \quad (23)$$

If given $f_{n,ideal}$ and ξ_{ideal} the required G_{PY} and G_{DY} are from (22) and (23)

$$G_{PY} = \frac{m(2\pi f_{n,ideal})^2 - k_{eff}}{\frac{k_E k_S d_{33} n_p}{k_E + k_p + k_S} G_{PA} G_S}, \quad G_{DY} = \frac{2m(2\pi f_{n,ideal}) \xi_{ideal} - c}{\frac{k_E k_S d_{33} n_p}{k_E + k_p + k_S} G_{PA} G_S} \quad (24)$$

Numerical Example:

Structure : Original (without piezo attached) natural frequency = $f_{n0} = 100\text{Hz}$,

and damping ratio = $\xi_0 = 0.02$,

$$m = 10\text{kg}, \quad k_B = m(2\pi * 100)^2 \approx 4 \times 10^6 \text{N/m},$$

$$c = 2m(2\pi * 100) * 0.02 \approx 250 \text{Ns/m}$$

$$\text{Power amplifier : } \omega_f = 2\pi * 400 \text{rad/s}, \quad \xi_f = 0.5, \quad G_{PA} = 20 \text{V/V} \quad (25)$$

Sensor : $G_S = 8000 \text{V/m}$

Piezoelectric stack : $k_S = 5 \times 10^7 \text{N/m}$, $k_p = 5 \times 10^6 \text{N/m}$,

$$d_{33} = 250 \times 10^{-12} \text{m/V}, \quad n_p = 800 \text{ layers}$$

External preload stiffness between beam and piezo : $k_E = 3 \times 10^6 \text{N/m}$

From the above data, the natural frequency and damping ratio of the structure without the piezo stack attached are f_{n0} and ξ_0 , respectively. One objective of the AVC is to increase the damping ratio of the vibration mode. Installing the piezo stack increases the effective stiffness supporting the mass to be

$$k_{eff} = k_B + \frac{k_E(k_S + k_p)}{k_S + k_p + k_E} = 4 \times 10^6 + 3 \times 10^6 * \frac{5 \times 10^7 + 5 \times 10^6}{5 \times 10^7 + 5 \times 10^6 + 3 \times 10^6} = 6.8 \times 10^6 \text{N/m} \quad (26)$$

The corresponding natural frequency and damping ratio are

$$f_{np} = \frac{1}{2\pi} \sqrt{\frac{k_{eff}}{m}} = \frac{1}{2\pi} \sqrt{\frac{6.86 \times 10^6}{10}} = 132 \text{Hz}, \quad \xi_p = \frac{c}{2m(2\pi f_{np})} = 0.015 \quad (27)$$

Table E12.8.1(a) Eigenvalues, natural frequencies, and damping ratios for the system with the optimized lead compensator ($p = 3618$, $z = 868$)

Eigenvalue no.	Eigenvalue	Damped natural frequency (Hz)	Damping ratio (dim)
1	-2551	0	1.0
2	$-817 \pm i944$	150	0.65
3	$-985 \pm i1139$	180	0.65

Therefore, attaching the passive piezo stack has increased the natural frequency by 32% and lowered the damping by 25%. The feedback control is seen to be required to improve the damping ratio.

The equation in (24) may be used to obtain initial values of the PD gains G_{PY} and G_{DY} . For this purpose, select

$$f_{n,ideal} = 100\text{Hz}, \quad \xi_{ideal} = 0.1 \quad (28)$$

This will lower the support stiffness and raise the damping to a higher level without depending excessively on derivative gain. Too much derivative gain may cause the power amplifier to become saturated if significant high-frequency electrical noise is present in the feedback loop. Solving (24) for G_{PY} and G_{DY} yields

$$G_{PY} = -34.375, \quad G_{DY} = 0.0121 \quad (29)$$

As in Example 12.6.1, the pole p and zero z of the lead stage are determined from

$$G_{L\infty} = \frac{1 + \sin(\phi_{peak})}{1 - \sin(\phi_{peak})}, \quad z = \frac{2\pi}{\sqrt{G_{L\infty}}} f_{peak}, \quad p = zG_{L\infty} \quad (30)$$

A design objective is to determine the values of ϕ_{peak} and f_{peak} that yield the maximum value of the minimum damping ratio, considered over all five eigenvalues of the closed-loop system matrix \underline{A}_{sys} in (15). The closed-loop system damping ratios and damped natural frequencies are determined from the eigenvalues λ of \underline{A}_{sys} in (15) as

$$\xi_i = \frac{-\text{Real}(\lambda)}{|\lambda|}, \quad f_{di} = \frac{1}{2\pi} \text{Imag}(\lambda) \quad (31)$$

A search over ϕ_{peak} and f_{peak} was conducted. A fine grid (100×100) was searched over the ranges

$$0 < \phi_{peak} < 60^\circ \quad \text{and} \quad 10 < f_{peak} < 410\text{Hz} \quad (32)$$

The results for maximizing the minimum value of the closed-loop eigenvalue damping ratio were

$$\phi_{peak} = 37.8^\circ, \quad f_{peak} = 282\text{Hz}, \quad \max \text{ of } \xi_{min} = 0.65, \quad p = 3618, \quad z = 868 \quad (33)$$

The eigenvalues, damped natural frequencies, and damping ratios for this case are shown in Table E12.8.1(a). The addition of the optimal phase lead compensation stage is seen to increase the damping much above the ideal (infinite bandwidth) PD control model (see Eq. (28) $\Rightarrow \xi_{ideal} = 0.1$).

12.8.2 Piezoelectric Layer (Patch) Actuator

The piezoelectric layer actuator (PLA) utilizes the cross expansion property constant d_{31} in (12.8.1) and Figure 12.8.1 to stretch or compress outer fibers of a thin beam or plate, thereby inducing bending moments to actuate the AVC. Seminal work in this approach was performed by Crawley and deLuis (1987) and has since been expanded by many researchers for active vibration and noise control and for energy harvesting, notably Bilgen et al. (2011), Morgan and Wang (1998), and Wang (2009).

The PLA is bonded to the outer surface(s) and induces strains in the structural component with AVC. The strains in turn produce moments and forces in the component which provide actuation for the AVC approach. The outcome of the following derivation is relations between voltages applied to the AVC and the forces and moments that result and are applied to the component. The structural component is assumed to act linearly so that only the strains and stresses due to the PLA are considered in deriving the forces and moments due to the PLA. Strains and stresses due to external or inertial loading may be temporarily ignored for the purpose of identifying the PLA forces and added later by superposition. Figure 12.8.3 illustrates a pair of identical PLAs bonded to opposing sides of a thin elastic beam which is assumed to bend in a manner consistent with Euler–Bernoulli beam theory (Example 4.6.3 and Section 9.2). The voltages applied to the opposing PLAs are assumed to be of opposite polarity, inducing tensile strains on the top surface and compressive strains on the bottom surface, or vice versa.

The moment $m_p(x_1)$ impressed on the beam by the PLA is equal and opposite to the moment $m_b(x_1)$; it induces internally in the beam, which may be expressed by

$$m_b(x_1) + m_p(x_1) = 0 \quad (12.8.10)$$

This may be expressed in terms of stresses and by noting symmetry of the stresses about the neutral axis to obtain

$$2 \int_0^d x_3 \sigma_{11b} dA + 2 \int_d^{d+h} x_3 \sigma_{11p} dA = 0 \quad (12.8.11)$$

where σ_{11b} and σ_{11p} are the x_1 normal stresses in the beam and piezo layer, respectively. In terms of strain, (12.8.11) becomes

$$\int_0^d x_3 E_b \varepsilon_{11b} dA + \int_d^{d+h} x_3 E_p \varepsilon_{11p} dA = 0 \quad (12.8.12)$$

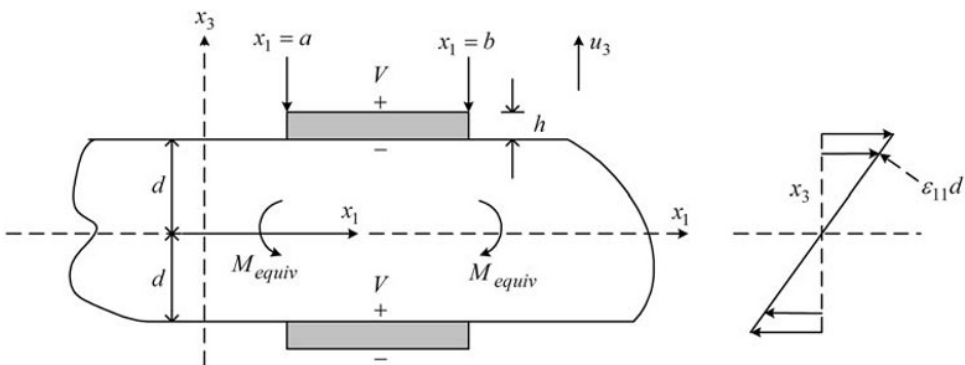


Figure 12.8.3 Model of piezoelectric stack actuator and equivalent end moments

The strains are assumed to vary linearly through the thickness so

$$\varepsilon_{11b} = \frac{x_3}{d} \varepsilon_{11d} \quad (12.8.13)$$

where ε_{11d} is the x_1 normal strain at the interface of the beam and the piezo layer, $x_3 = d$. The piezo layer strain field is a superposition of the bending strain plus the compressive strain resulting from the piezo crosswise expansion term $\varepsilon_{11f} = d_{31} \frac{V(t)}{h}$ in (12.8.1). Thus,

$$\varepsilon_{11p} = \frac{x_3}{d} \varepsilon_{11d} - \varepsilon_{p,\text{free}} = \frac{x_3}{d} \varepsilon_{11d} - \frac{d_{31}}{h} V(t) \quad (12.8.14)$$

The strain $\varepsilon_{p,\text{free}}$ is the free expansion strain of the piezo layer due to voltage $V(t)$ which is impressed across the piezo layer in the x_3 direction. The symbolic MATLAB code provided below substitutes (12.8.13) and (12.8.14) into (12.8.12) and solves for ε_{11d} to obtain

$$\begin{aligned} \varepsilon_{11d} &= \beta \varepsilon_{p,\text{free}} \\ \text{where } \beta &= \frac{3E_p d h (2d + h)}{2(E_b d^3 + 3E_p d^2 h + 3E_p d h^2 + E_p h^3)} \\ \text{and } \varepsilon_{p,\text{free}} &= \frac{d_{31}}{h} V(t) \end{aligned} \quad (12.8.15)$$

From (12.8.10) to (12.8.13), the total moment applied on the beam by the piezo patch becomes

$$\begin{aligned} m_b &= \int_{-d}^d x_3 \sigma_{11b} dA = \int_{-d}^d x_3 E_b \varepsilon_{11b} dA = \int_{-d}^d x_3 E_b \frac{x_3}{d} \varepsilon_{11d} dA \\ &= \int_{-d}^d x_3 E_b \frac{x_3}{d} \beta \varepsilon_{p,\text{free}} dA = \beta \varepsilon_{p,\text{free}} \frac{E_b I}{d} \end{aligned} \quad (12.8.16)$$

$$\text{where } I = \text{area moment of inertia} = \int_{-d}^d x_3^2 dA$$

Figure 12.8.3 shows that the piezoelectric patch (layer) extends from $x_1 = a$ to $x_1 = b$. Therefore,

$$m_b(x_1) = \beta \varepsilon_{p,\text{free}} \frac{E_b I}{d} [H(x_1 - a) - H(x_1 - b)] \quad (12.8.17)$$

where the Heaviside function H is discussed in Section 2.12 and (6.2.42). Recall from (5.5.90) that

$$\rho A \frac{\partial^2 u_3}{\partial t^2} = \rho I \frac{\partial^4 u_3}{\partial x_1^2 \partial t^2} - \frac{\partial^2 M}{\partial x_1^2} - \frac{\partial \tilde{\Gamma}}{\partial x_1} + \tilde{f} \quad (12.8.18)$$

The term $\tilde{\Gamma}(x_1)$ is an applied moment per unit length. Thus, in the present case from (12.8.17) and Section 2.12,

$$\begin{aligned} \tilde{\Gamma}(x_1) &= \frac{\partial(-m_b)}{\partial x_1} = -\beta \varepsilon_{p,\text{free}} \frac{\partial}{\partial x_1} \left(\frac{E_b I}{d} [H(x_1 - a) - H(x_1 - b)] \right) \\ &= -\beta \varepsilon_{p,\text{free}} \frac{E_b I}{d} [\delta(x_1 - a) - \delta(x_1 - b)] \end{aligned} \quad (12.8.19)$$

As explained in the derivation in (9.2.46), the Dirac delta terms in (12.8.19) represent concentrated line moments applied at the two ends of the piezo patch. Therefore, within the approximations of the present derivation, the excitation imposed by the piezo patch may be represented by a pair of equivalent opposing moments applied at the ends of the piezo patch and of value

$$M_{\text{equiv}} = \beta \varepsilon_{\text{p,free}} \frac{E_b I}{d} \text{ in units of Nm where } \varepsilon_{\text{p,free}} = \frac{d_{31}}{h} V(t) \quad (12.8.20)$$

This is illustrated in Figure 12.8.3. A second means for applying the piezoelectric patch excitation may be derived as follows. Recall from (5.5.84) that

$$\tilde{f}(x, t) = \text{Applied load per unit length} \quad (12.8.21)$$

From (12.8.18), \tilde{f} can be interpreted as an equivalent $\partial \tilde{\Gamma} / \partial x_1$ term, where from (12.8.19)

$$\tilde{f} = \frac{\partial \tilde{\Gamma}(x_1)}{\partial x_1} = \frac{\partial^2 (-m_b)}{\partial x_1^2} = -\beta \varepsilon_{\text{p,free}} \frac{E_b I}{d} [\delta'(x-a) - \delta'(x-b)] \quad (12.8.22)$$

Similar with the Dirac delta function, its derivative also has integration properties in Section 2.12 that enables the force density in (12.8.22) to be included in the model as illustrated by Example 12.8.2.

MATLAB Symbolic Code (for obtaining the result in (12.8.14))

```
clear all

syms Eb Ep d h x3 t eps_p_free eps11d sol_eps11d WW a x b c
sol_eps11d sol_eps11d_collect sol_eps11d_collect_simplify
ER K P

check abc

% Section 12.8 Piezoelectric Patch Actuator

% Perform Integrations:
WW = int(x3*Eb*x3/d*eps11d*t,x3,0,d) + int(x3*Ep*(x3/
d*eps11d-eps_p_free)*t,x3,d,d+h)

eqn = WW == 0

sol_eps11d = solve(eqn,eps11d)

sol_eps11d_collect = collect(sol_eps11d,eps_p_free)

sol_eps11d_collect_simplify = simplify(sol_eps11d_collect)

ER = Ep/Eb;
```

```

K = -3*h*d*(d+2*h)/(2*(h^3 + ER*d^3)+3*ER*h*d^2);

P=K*ER;

check = sol_eps11d_collect_simplify + P/(1-P)

abc = simplify(check)

```

Code Output

```

>> PiezoAnalysisCh12_Patch_bbb
WW = (Eb*d^2*eps11d*t)/3 + (Ep*h*t*(2*d*eps11d -
2*d*eps_p_free + 2*eps11d*h - eps_p_free*h))/2 +
(Ep*eps11d*h^3*t)/(3*d)
eqn = (Eb*d^2*eps11d*t)/3 + (Ep*h*t*(2*d*eps11d -
2*d*eps_p_free + 2*eps11d*h - eps_p_free*h))/2 +
(Ep*eps11d*h^3*t)/(3*d) == 0

sol_eps11d = (Ep*h*t*(2*d*eps_p_free + eps_p_free*h))/(2*
((Eb*d^2*t)/3 + (Ep*h*t*(2*d + 2*h))/2 + (Ep*h^3*t)/(3*d)))

sol_eps11d_collect = ((Ep*h*t*(2*d + h))/(2*((Eb*d^2*t)/3 +
(Ep*h*t*(2*d + 2*h))/2 + (Ep*h^3*t)/(3*d))))*eps_p_free

sol_eps11d_collect_simplify = (3*Ep*d*eps_p_free*h*(2*d +
h))/(2*Eb*d^3 + 6*Ep*d^2*h + 6*Ep*d*h^2 + 2*Ep*h^3)

check = (3*Ep*d*eps_p_free*h*(2*d + h))/(2*Eb*d^3 + 6*Ep*d^2*h
+ 6*Ep*d*h^2 + 2*Ep*h^3) - (3*Ep*d*h*(d + 2*h))/(Eb*((3*Ep*d*h*
(d + 2*h))/(Eb*((2*Ep*d^3)/Eb + (3*Ep*d^2*h)/Eb + 2*h^3)) + 1)*
((2*Ep*d^3)/Eb + (3*Ep*d^2*h)/Eb + 2*h^3))

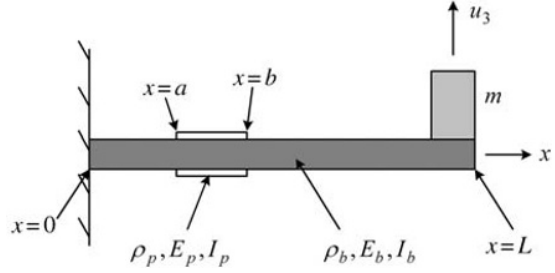
abc = (3*Ep*d*eps_p_free*h*(2*d + h))/(2*Eb*d^3 + 6*Ep*d^2*h +
6*Ep*d*h^2 + 2*Ep*h^3) - (3*Ep*d*h*(d + 2*h))/(2*Ep*d^3 +
6*Ep*d^2*h + 6*Ep*d*h^2 + 2*Eb*h^3)

```

EXAMPLE 12.8.2 *Assumed Modes Model of a Cantilevered Beam Mounted Mass with a Piezoelectric Patch Actuator*

Statement: The mass m shown in Figure E12.8.2(a) is a miniature container holding a solution to be shaken as part of a biological experiment. The assumed modes approach F_p discussed in Section 4.6 is utilized to model transverse vibrations of the beam and mass m with piezoelectric patch actuators as shown in Figure E12.8.2(a).

Figure E12.8.2(a) Cantilevered rail mounted instrumentation enclosure with piezoelectric patch AVC



Objective: Determine the equations of motion for the open-loop system where $V(t)$ is the input and $u_3(x, t)$ is the output.

Solution: As in Example 4.6.3, utilize the two term assumed modes expansion

$$u(x, t) = q_1(t)\phi_1(x) + q_2(t)\phi_2(x) \quad (1)$$

where

$$\phi_1(x) = \frac{3x^2}{L^2} - \frac{2x^3}{L^3}, \quad \phi_2(x) = \frac{-x^2}{L^2} + \frac{x^3}{L^3} \quad (2)$$

The stiffness matrix is determined from (20) of Example 4.6.3 as

$$\underline{K} = \int_V \underline{B}^T \underline{E} \underline{B} dV = \int_V E \begin{bmatrix} \phi_1'' \\ \phi_2'' \end{bmatrix} [\phi_1'' \ \phi_2''] y^2 dA dx \quad (3)$$

which for the present example yields

$$k_{ij} = \int_0^a E_b I_b \phi_i'' \phi_j'' dx + \int_a^b E_b \bar{I} \phi_i'' \phi_j'' dx + \int_b^L E_b I_b \phi_i'' \phi_j'' dx \quad (4)$$

where

$$\bar{I} = \frac{E_b I_b + 2E_p I_p}{E_b}, \quad I_b = \int_{-d}^d y^2 dA, \quad I_p = \int_d^{d+h} y^2 dA$$

The mass matrix is determined from (6–11) of Example 4.6.3 as

$$m_{ij} = \int_0^a \rho_b A_b \phi_i \phi_j dx + \int_a^b \rho_b \bar{A} \phi_i \phi_j dx + \int_b^L \rho_b A_b \phi_i \phi_j dx \quad (5)$$

where

$$\bar{A} = \frac{\rho_b A_b + 2\rho_p A_p}{\rho_b}, \quad A_b = \int_{-d}^d dA, \quad A_p = \int_d^{d+h} dA$$

As shown in Example 4.6.4, the mass matrix resulting from the tip mass m is given by

$$\underline{M}_m = m \begin{bmatrix} \phi_1 \phi_1 & \phi_1 \phi_2 \\ \phi_2 \phi_1 & \phi_2 \phi_2 \end{bmatrix}_{x=L} = m \begin{bmatrix} 1 & 0 \\ 0 & 0 \end{bmatrix} \quad (6)$$

The integrals in (4) and (5) are evaluated with the following MATLAB symbolic code:

```
clear all

syms x L phi phidd k m Eb I Ibar a b rhob A Abar K M

% Example 12.8.2 Piezoelectric Patch ( Layer ) Actuator

phi(1) = 3*x^2/L^2 - 2*x^3/L^3;
phi(2) = -x^2/L^2 + x^3/L^3;
phi

for i=1:1:2
    phidd(i) = diff(phi(i),x,2);
end
phidd

for i=1:1:2
    for j=1:1:2
        k(i,j) = int(phidd(i)*phidd(j)*Eb*I,x,0,a) +
            int(phidd(i)*phidd(j)*Eb*Ibar,x,a,b) +
            int(phidd(i)*phidd(j)*Eb*I,x,b,L);
        m(i,j) = int(phi(i)*phi(j)*rhob*A,x,0,a) +
            int(phi(i)*phi(j)*rhob*Abar,x,a,b) +
            int(phi(i)*phi(j)*rhob*A,x,b,L);
    end
end

K = simplify(k)

M = simplify(m)
```

The results are listed below:

$$m_{11} = (A*rhob*(13*L^7 - 63*L^2*b^5 + 70*L*b^6 - 20*b^7))/(35*L^6) - (L^2*((9*Abar*rhob*a^5)/5 - (9*Abar*b^5*rhob)/5) - L*(2*Abar*rhob*a^6 - 2*Abar*rhob*b^6) + (4*Abar*a^7*rhob)/7 - (4*Abar*b^7*rhob)/7)/L^6 + (A*a^5*rhob*(63*L^2 - 70*L*a + 20*a^2))/(35*L^6)$$

$$m_{12} = m_{21} = - (rhob*(11*A*L^7 + 60*A*a^7 - 60*Abar*a^7 - 60*A*b^7 + 60*Abar*b^7 + 126*A*L^2*a^5 - 126*Abar*L^2*a^5 - 126*A*L^2*b^5 + 126*Abar*L^2*b^5 - 175*A*L*a^6 + 175*Abar*L*a^6 + 175*A*L*b^6 - 175*Abar*L*b^6))/(210*L^6)$$

$$m_{22} = (rhob*(A*L^7 + 15*A*a^7 - 15*Abar*a^7 - 15*A*b^7 + 15*Abar*b^7 + 21*A*L^2*a^5 - 21*Abar*L^2*a^5 - 21*A*L^2*b^5 + 21*Abar*L^2*b^5 - 35*A*L*a^6 + 35*Abar*L*a^6 + 35*A*L*b^6 - 35*Abar*L*b^6))/(105*L^6)$$

$$k_{11} = (12 * E_b * I * (L^3 - 3 * L^2 * b + 6 * L * b^2 - 4 * b^3)) / L^6 - (12 * E_b * I_{bar} * (a - b) * (3 * L^2 - 6 * L * a - 6 * L * b + 4 * a^2 + 4 * a * b + 4 * b^2)) / L^6 + (12 * E_b * I * a * (3 * L^2 - 6 * L * a + 4 * a^2)) / L^6$$

$$k_{12} = k_{21} = (6 * E_b * I_{bar} * (a - b) * (2 * L^2 - 5 * L * a - 5 * L * b + 4 * a^2 + 4 * a * b + 4 * b^2)) / L^6 - (6 * E_b * I * (L^3 - 2 * L^2 * b + 5 * L * b^2 - 4 * b^3)) / L^6 - (6 * E_b * I * a * (2 * L^2 - 5 * L * a + 4 * a^2)) / L^6$$

$$k_{22} = (4 * E_b * I * (L^3 - L^2 * b + 3 * L * b^2 - 3 * b^3)) / L^6 + (4 * E_b * I * a * (L^2 - 3 * L * a + 3 * a^2)) / L^6 - (4 * E_b * I_{bar} * (a - b) * (L^2 - 3 * L * a - 3 * L * b + 3 * a^2 + 3 * a * b + 3 * b^2)) / L^6$$

The generalized forces resulting from the piezo patch are obtained from (25) of Example 4.6.3 as

$$\begin{Bmatrix} Q_1 \\ Q_2 \end{Bmatrix} = \begin{Bmatrix} \int_0^L \tilde{f}(x,t) \phi_1(x) dx \\ \int_0^L \tilde{f}(x,t) \phi_2(x) dx \end{Bmatrix} \quad (7)$$

where the applied force density is obtained from (12.8.22) as

$$\tilde{f} = -\beta \epsilon_{p,free} \frac{E_b I_b}{d} [\delta'(x-a) - \delta'(x-b)] \quad (8)$$

As discussed in Section 2.12,

$$\int f(x) \delta'(x-c) dx = -f'(c) \quad (9)$$

Apply this to (7) and (8) and utilize (12.8.20) to obtain

$$\begin{aligned} \begin{Bmatrix} Q_1 \\ Q_2 \end{Bmatrix} &= -\beta \frac{d_{31}}{h} V(t) \frac{E_b I_b}{d} \begin{Bmatrix} \int_0^L [\delta'(x-a) - \delta'(x-b)] \phi_1(x) dx \\ \int_0^L [\delta'(x-a) - \delta'(x-b)] \phi_2(x) dx \end{Bmatrix} \\ &= -\beta \frac{d_{31}}{h} V(t) \frac{E_b I_b}{d} \begin{Bmatrix} \phi_1'(b) - \phi_1'(a) \\ \phi_2'(b) - \phi_2'(a) \end{Bmatrix} \\ &= -\beta \frac{d_{31}}{h} V(t) \frac{E_b I_b}{d} \begin{Bmatrix} \frac{6b}{L^2} - \frac{6b^2}{L^3} - \frac{6a}{L^2} + \frac{6a^2}{L^3} \\ \frac{-2b}{L^2} + \frac{3b^2}{L^3} + \frac{2a}{L^2} - \frac{3a^2}{L^3} \end{Bmatrix} \end{aligned} \quad (10)$$

The system differential equation becomes

$$\begin{aligned} & \begin{bmatrix} m_{11} + m & m_{12} \\ m_{21} & m_{22} \end{bmatrix} \begin{Bmatrix} \ddot{q}_1 \\ \ddot{q}_2 \end{Bmatrix} + \begin{bmatrix} k_{11} & k_{12} \\ k_{21} & k_{22} \end{bmatrix} \begin{Bmatrix} q_1 \\ q_2 \end{Bmatrix} = \begin{Bmatrix} Q_1 \\ Q_2 \end{Bmatrix} \\ & = -\beta \frac{d_{31}}{h} V(t) \frac{E_b I_b}{d} \begin{Bmatrix} \frac{6b}{L^2} - \frac{6b^2}{L^3} - \frac{6a}{L^2} + \frac{6a^2}{L^3} \\ -\frac{2b}{L^2} + \frac{3b^2}{L^3} + \frac{2a}{L^2} - \frac{3a^2}{L^3} \end{Bmatrix} \end{aligned} \quad (11)$$

The physical coordinate displacements are then obtained from

$$u(x, t) = q_1(t)\phi_1(x) + q_2(t)\phi_2(x) \quad (12)$$

The coefficients in (11) are obtained from the MATLAB symbolic code above as

$$\begin{aligned} m_{11} = & \frac{A_b \rho_b (13L^7 - 63L^2 b^5 + 70Lb^6 - 20b^7)}{35L^6} \\ & - \frac{\{L^2 [(9\bar{A}\rho_b a^5)/5 - (9\bar{A}b^5 \rho_b)/5] - L(2\bar{A}\rho_b a^6 - 2\bar{A}\rho_b b^6) + (4\bar{A}a^7 \rho_b)/7 - (4\bar{A}b^7 \rho_b)/7\}}{L^6} \\ & + \frac{A_b a^5 \rho_b (63L^2 - 70La + 20a^2)}{35L^6} \end{aligned} \quad (13)$$

$$m_{12} = m_{21} = \frac{\rho_b \begin{pmatrix} 11A_b L^7 + 60A_b a^7 - 60\bar{A}a^7 - 60A_b b^7 + 60\bar{A}b^7 \\ + 126A_b L^2 a^5 - 126\bar{A}L^2 a^5 - 126A_b L^2 b^5 + 126\bar{A}L^2 b^5 \\ - 175A_b L a^6 + 175\bar{A}L a^6 + 175A_b L b^6 - 175\bar{A}L b^6 \end{pmatrix}}{210L^6} \quad (14)$$

$$m_{22} = \frac{\rho_b \begin{pmatrix} A_b L^7 + 15A_b a^7 - 15\bar{A}a^7 - 15A_b b^7 + 15\bar{A}b^7 \\ + 21A_b L^2 a^5 - 21\bar{A}L^2 a^5 - 21A_b L^2 b^5 + 21\bar{A}L^2 b^5 \\ - 35A_b L a^6 + 35\bar{A}L a^6 + 35A_b L b^6 - 35\bar{A}L b^6 \end{pmatrix}}{105L^6} \quad (15)$$

$$\begin{aligned} k_{11} = & \frac{[12E_b I_b (L^3 - 3L^2 b + 6Lb^7 - 4b^3)]}{L^6} \\ & - \frac{12E_b \bar{I}(a-b) (3L^2 - 6La - 6Lb + 4a^2 + 4ab + 4b^2)}{L^6} + \frac{[12E_b I_b a (3L^2 - 6La + 4a^2)]}{L^6} \end{aligned} \quad (16)$$

$$\begin{aligned} k_{12} = k_{21} = & \frac{6E_b \bar{I}(a-b) (2L^2 - 5La - 5Lb + 4a^2 + 4ab + 4b^2)}{L^6} \\ & - \frac{6E_b I_b (L^3 - 2L^2 b + 5Lb^2 - 4b^3)}{L^6} - \frac{[6E_b I_b a (2L^2 - 5La + 4a^2)]}{L^6} \end{aligned} \quad (17)$$

$$k_{22} = \frac{4E_b I_b (L^3 - L^2 b - 3Lb^2 - 3b^3)}{L^6} + \frac{4E_b I_b a (L^2 - 3Lb + 3a^2)}{L^6} - \frac{[4E_b \bar{I} (a-b) (L^2 - 3La - 3Lb + 3a^2 + 3ab + 3b^2)]}{L^6} \quad (18)$$

12.9 SUMMARY

AVC is increasingly implemented for applications where the vibration control system must adapt to a changing plant, environment, or operating conditions. They are also used in extreme environments that are not conducive to passive damper materials. The presence of filters to suppress electrical noise and finite bandwidth feedback components degrade closed-loop system stability. Likewise, an inability to collocate all sensor and actuator pairs for flexible structure AVC also may contribute to closed-loop feedback system instability. Lead compensation is discussed as a means to improve stability. An infinite bandwidth, linearized, saturation-free AVC system model was presented. Although limited in predicting control instability, this simple model still provides initial approximations for feedback gain values (12.4.44) to achieve a desired natural frequency and damping ratio.

This chapter provides modeling methods to include feedback component frequency response characteristics, stabilizing control stages such as a lead compensator, and noncollocation of sensor/actuator pairs. Also included is an example of detailed modeling of actuators, which is an essential step for successful AVC implementation. Actuator modeling is an important step for all AVC applications whether using piezoelectric, magnetostrictive, shape memory alloy, hydraulic, pneumatic, or electromagnetic actuators. The state modeling approach presented can be easily extended to AVC models including flexible structures with many degrees of freedom.

Examples are provided for determining closed-loop feedback AVC system natural frequencies, modal damping, stability, and forced harmonic response.

12.10 CHAPTER 12 EXERCISES

12.10.1 Exercise Location

All exercises may be conveniently viewed and downloaded at the following website: **www.wiley.com/go/palazzolo**. This new feature greatly reduces the length of the printed book, yielding a significant cost savings for the college student, and is updated.

12.10.2 Exercise Goals

The goal of the exercises in Chapter 12 is to strengthen the student's understanding and related engineering problem-solving skills in the following area:

- (a) Modeling of closed-loop feedback AVC systems

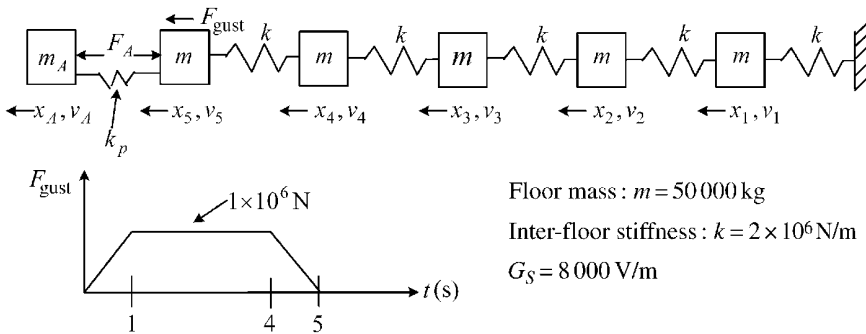
12.10.3 Sample Exercise: 12.1

The building model has an absorber mass on its top floor to suppress sway induced by wind gusts. The AVC hydraulic actuator applies an actuation force horizontally in equal and

opposite directions on the top floor and absorber mass. The feedback loop consists of (i) a sensor that outputs a voltage proportional to the relative displacement between the absorber mass and the top floor, $V_S = G_S(x_{\text{abs mass}} - x_{\text{top floor}})$; (ii) a PD controller with input V_S , output V_{CO} , and adjustable proportional and derivative feedback gains G_P and G_D , respectively (Ref. Figure 12.5.1); (iii) a lead compensation stage with input V_{CO} , output V_{CO}^{LS} , and adjustable pole p and zero z (Ref. Figure 12.5.1); and (iv) an actuator consisting of pressure control valves and hydraulic cylinders that produce an actuation force with the following transfer function (12.5.1):

$$T_f(s) = \frac{F_A(s)}{V_{CO}^{LS}(s)} = \frac{G_A \omega_f^2}{s^2 + 2\xi_f \omega_f s + \omega_f^2}, \quad \xi_f = 0.9, \quad \omega_f = 2\pi * 20, \quad G_A = 50000 \text{ N/V}$$

The passive stiffness of the actuator is $k_p = 5 \times 10^7 \text{ N/m}$.



- (a) For the entire feedback controlled model, identify the following terms in (12.6.26): $\underline{A}_{\text{sys}}$ and $\underline{F}_{\text{sys}}^F$. Utilize the state vector

$$\underline{X}_{\text{sys}} = \{x_1 \ x_2 \ x_3 \ x_4 \ x_5 \ x_A \ v_1 \ v_2 \ v_3 \ v_4 \ v_5 \ v_A \ w_1 \ w_2 \ w_3\}^T$$

- (b) Use any integration method in Section 6.4 or MATLAB (see Example 2.3.1), MAPLE, MATHCAD, and so on to determine the top floor peak displacement without m_A attached.
- (c) Adjust the feedback parameters—pole p , zero z , G_P , and G_D —to identify values that maximize the minimum value of the damping ratios $\xi_j = -\text{Real}(\lambda_j)/|\lambda_j|$ for the closed-loop feedback controlled system.
- (d) Repeat (b) for the controlled system using the values from (c). Compare results.

REFERENCES

- BILGEN, O., KARAMI, M., INMAN, D., and FRISWELL, M., "The Actuation Characterization of Cantilevered Unimorph Beams with Single Crystal Piezoelectric Materials," *Smart Materials and Structures*, 2011, Vol. 20, Article No. 055024.
- BUCKNER, G. D., SCHUETZE, K. T., and BENO, J. H., "Intelligent Feedback Linearization for Active Vehicle Suspension Control," *Journal of Dynamic Systems, Measurement, and Control*, 2001, Vol. 123, pp. 727–733.
- CRAWLEY, E. and DELUIS, J., "Use of Piezoelectric Actuators as Elements of Intelligent Structures," *AIAA Journal*, 1987, Vol. 25, No. 10, pp. 1373–1385.

- CULSHAW, B., *Smart Structures and Materials*, Artech House, Inc., Boston, MA, 1996.
- DOHNER, J. L., LAUFFER, J. P., HINNERICHS, T. D., SHANKAR, N., REGELBRUGGE, M. E., KWAN, C.-M., XU, R., WINTERBAUER, W., and BRIDGER, K., "On the Use of Active Structural Control to Enhance the Cutting Performance of a Milling Machine," *Smart Structures and Materials 2002, Proceedings of the SPIE*, 2002, Vol. **4698**, pp. 519–527.
- EDBERG, D., BOUCHER, R., SCHENCK, D., NURRE, G., WHORTON, M., KIM, Y., and ALHORN, D., "Results of the Stable Microgravity Vibration Isolation Flight Experiment," *Proceedings of the Guidance and Control, American Astronautical Society*, 1996, Vol. **92** (Advances in the Astronautical Sciences), pp. 567–581.
- HENDERSON, T. C., "Design and Testing of a Broadband Active Vibration Isolation System Using Stiff Actuators," *Proceedings of the Guidance and Control, American Astronautical Society*, 1996, Vol. **92** (Advances in the Astronautical Sciences), pp. 481–500.
- LEI, S. and PALAZZOLO, A., "Control of Flexible Rotor Systems with Active Magnetic Bearings," *Journal of Sound and Vibrations*, 2008, Vol. **314**, pp. 19–38.
- LEI, S., PALAZZOLO, A., and KASCAK, A., "Nonlinear Fuzzy Logic Control for Forced Large Motions of Spinning Shafts," *Journal of Sound and Vibrations*, 2000, Vol. **235**, No. 3, pp. 435–449.
- MANCHALA, D., PALAZZOLO, A., KASCAK, A., MONTAGUE, G., and BROWN, G., "Constrained Quadratic Programming, Active Control of Rotating Mass Imbalance," *Journal of Sound and Vibration*, 1997, Vol. **205**, No. 5, pp. 561–580.
- MINIHAN, T., LEI, S., SUN, G., and PALAZZOLO, A., "Large Motion Tracking Control for Thrust Magnetic Bearings with Fuzzy Logic, Sliding Mode, and Direct Linearization," *Journal of Sound and Vibration*, 2003, Vol. **263**, pp. 549–567.
- MORGAN, R. and WANG, K.-W., "An Integrated Active-Parametric Control Approach for Active-Passive Hybrid Piezoelectric Network with Variable Resistance," *Journal of Intelligent Material Systems and Structures*, 1998, Vol. **9**, No. 7, pp. 564–573.
- MOSES, R. W., "Vertical Tail Buffeting Alleviation Using Piezoelectric Actuators—Some Results of the Actively Controlled Response of Buffet—Affected Tails (ACROBAT) Program," *Proceedings of SPIE—Smart Structures and Materials 1997*, 4–6 March 1997, pp. 87–98.
- PALAZZOLO, A., LIN, R., ALEXANDER, R., KASCAK, A., and MONTAGUE, G., "Piezoelectric Pushers for Active Vibration Control of Rotating Machinery," *Journal of Vibration, Acoustics, Stress, and Reliability in Design*, 1989, Vol. **111**, pp. 298–305.
- PALAZZOLO, A., LIN, R., ALEXANDER, R., KASCAK, A., and MONTAGUE, G., "Test and Theory for Piezoelectric Actuator—Active Vibration Control of Rotating Machinery," *Journal of Vibration and Acoustics*, 1991, Vol. **113**, pp. 167–175.
- PALAZZOLO, A., KIM, Y., KENNY, A., NA, U., LEI, S., THOMAS, T., BEACH, R., KASCAK, A., and MONTAGUE, G., "Magnetic Suspensions for Flywheel Batteries," *Proceedings of IECEC'01, 36th Inter-society Energy conversion Engineering Conference*, July 29–August 2, 2001a, Paper No. IECEC2001-AT-81, pp. 97–103.
- PALAZZOLO, A., LI, M., JOO NA, U., and THOMAS, E., "System and Method for Controlling Suspension Using a Magnetic Field," *US Patent: (US 6,323,614B1)*; Date of Patent: November 27, 2001b.
- PALAZZOLO, A. B., WANG, Z., LEE, J.-G., KASCAK, A., and PROVENZA, A., "Magnetic Bearings," a chapter section (Section 4.6), *Handbook of Lubrication and Tribology, Volume II: Theory and Design*, Second Edition, ed. R. Bruce, CRC Press, Boca Raton, FL, 2012.
- TANG, P., PALAZZOLO, A., et al., "Combined Piezoelectric-Hydraulic Actuator Based Active Vibration Control for Rotordynamic System," *Journal of Vibration and Acoustics*, 1995, Vol. **117**, pp. 285–293.
- WANG, K.-W., *Adaptive Structural Systems with Piezoelectric Transducer Circuitry*, Springer, New York, 2009.
- ZHONG, W. and PALAZZOLO, A., "Magnetic Bearing Rotordynamic System Optimization Using Multi-Objective Genetic Algorithms," *Journal of Dynamic Systems, Measurement, and Control*, 2014, Vol. **137**, No. 2, Article No. 021012.

Appendix A

Fundamental Equations of Elasticity

This appendix provides a background of the fundamental equations of elasticity to understand the internal strain energy expressions for deformable bodies utilized in the Lagrange equations and the derivations for the finite element stiffness matrices.

A.1 EQUILIBRIUM

The equilibrium equations are expressions of Newton's second law at a point in a structure. Figure A.1.1 shows a general structure and a differential volume element in its interior.

The variation of stresses on the differential element is shown in Figure A.1.2. Newton's second law can be written in the x_1 direction as

$$\begin{aligned} & \left(\sigma_{11} + \frac{\partial \sigma_{11}}{\partial x_1} dx_1 \right) dx_2 dx_3 - \sigma_{11} dx_2 dx_3 + \left(\sigma_{31} + \frac{\partial \sigma_{31}}{\partial x_3} dx_3 \right) dx_1 dx_2 - \sigma_{31} dx_1 dx_2 \\ & + \left(\sigma_{21} + \frac{\partial \sigma_{21}}{\partial x_2} dx_2 \right) dx_1 dx_3 - \sigma_{21} dx_1 dx_3 + \bar{F}_{v1} dx_1 dx_2 dx_3 - \rho dx_1 dx_2 dx_3 \ddot{x}_1 = 0 \end{aligned} \quad (\text{A.1.1})$$

The acceleration term may be viewed as an equivalent body force by D'Alembert's principle, so (A.1.1) simplifies, after cancelations, to the form

$$\frac{\partial \sigma_{11}}{\partial x_1} + \frac{\partial \sigma_{21}}{\partial x_2} + \frac{\partial \sigma_{31}}{\partial x_3} + \bar{F}_{v1} = 0 \quad (\text{A.1.2})$$

The analogous equations for the x_2 and x_3 directions may be written in a similar fashion. Next, consider Newton's rotational equations (sum of the moments equals zero) as applied about line A-A in Figure A.1.2:

$$\begin{aligned} & \left(\sigma_{11} + \frac{\partial \sigma_{11}}{\partial x_1} dx_1 \right) dx_2 dx_3 \left(-\frac{dx_2}{2} \right) + \sigma_{11} dx_2 dx_3 \left(\frac{dx_2}{2} \right) + \left(\sigma_{12} + \frac{\partial \sigma_{12}}{\partial x_1} dx_1 \right) dx_2 dx_3 (dx_1) \\ & + \left(\sigma_{22} + \frac{\partial \sigma_{22}}{\partial x_2} dx_2 \right) dx_1 dx_3 \left(\frac{dx_1}{2} \right) + \sigma_{22} dx_1 dx_3 \left(-\frac{dx_1}{2} \right) + \left(\sigma_{21} + \frac{\partial \sigma_{21}}{\partial x_2} dx_2 \right) dx_1 dx_3 (-dx_2) \\ & + \sigma_{31} dx_1 dx_2 \left(\frac{dx_2}{2} \right) + \sigma_{32} dx_1 dx_2 \left(-\frac{dx_1}{2} \right) + \left(\sigma_{32} + \frac{\partial \sigma_{32}}{\partial x_3} dx_3 \right) dx_1 dx_2 \left(\frac{dx_1}{2} \right) \\ & + \left(\sigma_{31} + \frac{\partial \sigma_{31}}{\partial x_3} dx_3 \right) dx_1 dx_2 \left(-\frac{dx_2}{2} \right) + \bar{F}_{v1} dx_1 dx_2 dx_3 \left(-\frac{dx_2}{2} \right) + \bar{F}_{v2} dx_1 dx_2 dx_3 \left(\frac{dx_1}{2} \right) = 0 \end{aligned} \quad (\text{A.1.3})$$

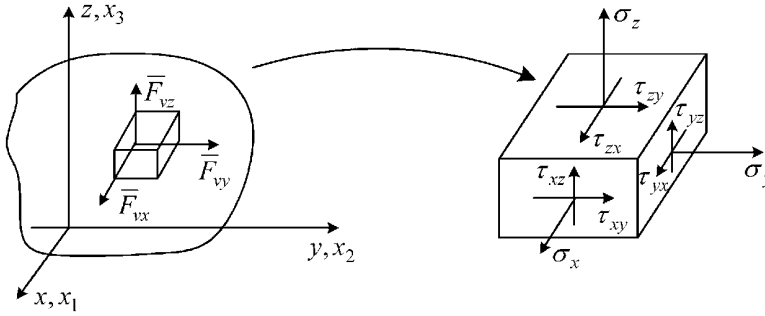


Figure A.1.1 General state of stress of a differential volume element. \bar{F}_{vx} , \bar{F}_{vy} , \bar{F}_{vz} are forces per unit volume acting at point P

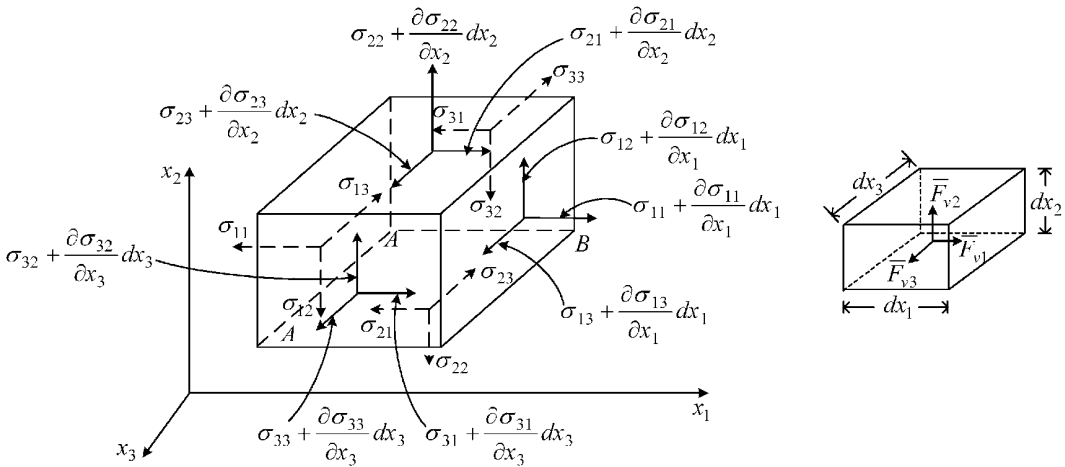


Figure A.1.2 Stress distribution on a differential element

Divide this equation by $dx_1 dx_2 dx_3$ and cancel terms to obtain

$$-\frac{\partial \sigma_{11}}{\partial x_1} \frac{dx_2}{2} + \sigma_{12} + \frac{\partial \sigma_{12}}{\partial x_1} dx_1 + \frac{\partial \sigma_{22}}{\partial x_2} \frac{dx_1}{2} - \sigma_{21} - \frac{\partial \sigma_{21}}{\partial x_2} dx_2 - \frac{\partial \sigma_{31}}{\partial x_3} dx_2 + \bar{F}_{v1} \frac{-dx_2}{2} + \bar{F}_{v2} \frac{dx_1}{2} = 0 \tag{A.1.4}$$

Finally, allowing dx_1, dx_2 and dx_3 to go to zero yields the moment equilibrium equation

$$\sigma_{12} = \sigma_{21} \tag{A.1.5}$$

Similar relations between σ_{13} and σ_{31} and σ_{23} and σ_{32} can be obtained in the same fashion, proving that the stress tensor is symmetric:

$$\sigma_{ij} = \sigma_{ji} \quad i = 1, 3 \quad j = 1, 3 \tag{A.1.6}$$

The translational and rotational equilibrium equations may now be written as

$$\begin{bmatrix} \partial_{x_1} & 0 & 0 & 0 & \partial_{x_3} & \partial_{x_2} \\ 0 & \partial_{x_2} & 0 & \partial_{x_3} & 0 & \partial_{x_1} \\ 0 & 0 & \partial_{x_3} & \partial_{x_2} & \partial_{x_1} & 0 \end{bmatrix} \begin{Bmatrix} \sigma_{11} \\ \sigma_{22} \\ \sigma_{33} \\ \sigma_{23} \\ \sigma_{13} \\ \sigma_{12} \end{Bmatrix} + \begin{Bmatrix} \bar{F}_{v1} \\ \bar{F}_{v2} \\ \bar{F}_{v3} \end{Bmatrix} = \begin{Bmatrix} 0 \\ 0 \\ 0 \end{Bmatrix} \tag{A.1.7}$$

where

$$\partial_{xi} = \frac{\partial}{\partial x_i} \quad (\text{A.1.8})$$

or in the $x = x_1, y = x_2, z = x_3$ notation

$$\begin{bmatrix} \partial_x & 0 & 0 & 0 & \partial_z & \partial_y \\ 0 & \partial_y & 0 & \partial_z & 0 & \partial_x \\ 0 & 0 & \partial_z & \partial_y & \partial_x & 0 \end{bmatrix} \begin{Bmatrix} \sigma_x \\ \sigma_y \\ \sigma_z \\ \tau_{yz} \\ \tau_{xz} \\ \tau_{xy} \end{Bmatrix} + \begin{Bmatrix} \bar{F}_{vx} \\ \bar{F}_{vy} \\ \bar{F}_{vz} \end{Bmatrix} = \begin{Bmatrix} 0 \\ 0 \\ 0 \end{Bmatrix} \quad (\text{A.1.9})$$

This may be expressed in matrix–vector notation as

$$\underline{D}^T \underline{\sigma} + \underline{\bar{F}}_v = \underline{0} \quad (3 \times 1) \quad (\text{A.1.10})$$

where \underline{D}^T , $\underline{\sigma}$ and $\underline{\bar{F}}_v$ can be easily identified by comparison with Equation (A.1.7) or (A.1.9). The Einstein summation convention follows the simple rule that repeated indices imply summation over those indices, that is,

$$b_k a_{ik} = b_1 a_{i1} + b_2 a_{i2} + b_3 a_{i3} = \sum_{k=1}^3 b_k a_{ik} \quad (\text{A.1.11})$$

It can be easily verified that (A.1.7) may be expressed with the Einstein summation conventions as

$$\sigma_{ij,j} + \bar{F}_{vi} = 0 \quad (\text{A.1.12})$$

where the comma denotes partial differentiation. For example, if $i = 1$, Equation (A.1.12) becomes

$$\frac{\partial \sigma_{11}}{\partial x_1} + \frac{\partial \sigma_{12}}{\partial x_2} + \frac{\partial \sigma_{13}}{\partial x_3} + \bar{F}_{v1} = 0 \quad (\text{A.1.13})$$

which is identical to the first of Equation (A.1.7).

A.2 TRACTION BOUNDARY CONDITIONS (CAUCHY'S FORMULA)

The tractions (force/area) applied to an object must equilibrate with its stresses at the surface according to Cauchy's formula (Fung, 1965). This formula is derived in the following analysis. Consider the pyramid-shaped differential element shown in Figure A.2.1. Face ABC lies on the surface of the object.

The following definitions pertain to this figure:

$$\begin{aligned} n_i &= \cos(\angle x_i, \hat{n}) = \text{cosine of the angle between } x_i \text{ and } \hat{n} \\ dS_i &= n_i dS \\ \Phi_i &= \text{surface traction in } x_i \text{ direction (force per unit area)} \\ \bar{F}_{vi} &= \text{body force in } x_i \text{ direction (force per unit volume)} \\ \text{Volume} &= 2 \sqrt{\frac{n_1 n_2 n_3}{3}} dS^{3/2} \\ n_1^2 + n_2^2 + n_3^2 &= 1 \end{aligned} \quad (\text{A.2.1})$$

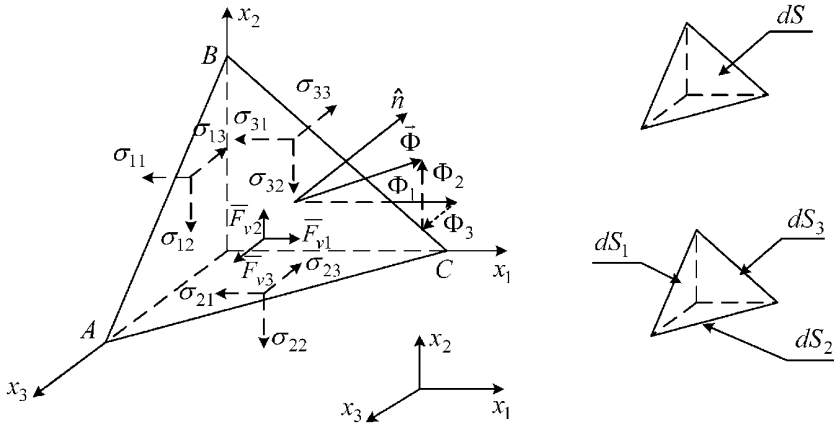


Figure A.2.1 Surface equilibrium diagram

The equilibrium condition in the x_1 direction is

$$\Phi_1 dS - \sigma_{31} dS_3 - \sigma_{21} dS_2 - \sigma_{11} dS_1 + \bar{F}_{v1} \left(2\sqrt{\frac{n_1 n_2 n_3}{3}} dS^{3/2} \right) = 0$$

or

$$\Phi_1 dS - \sigma_{31} n_3 dS - \sigma_{21} n_2 dS - \sigma_{11} n_1 dS + \bar{F}_{v1} \left(2\sqrt{\frac{n_1 n_2 n_3}{3}} dS^{3/2} \right) = 0$$

Canceling dS yields

$$\Phi_1 - \sigma_{31} n_3 - \sigma_{21} n_2 - \sigma_{11} n_1 + \bar{F}_{v1} \left(2\sqrt{\frac{n_1 n_2 n_3}{3}} dS^{1/2} \right) = 0$$

Then, as dS approaches zero,

$$\Phi_1 = n_1 \sigma_{11} + n_2 \sigma_{21} + n_3 \sigma_{31} \quad (\text{A.2.2})$$

Consideration of x_2 and x_3 equilibrium equations yields

$$\begin{Bmatrix} \Phi_1 \\ \Phi_2 \\ \Phi_3 \end{Bmatrix} = \begin{bmatrix} n_1 & 0 & 0 & 0 & n_3 & n_2 \\ 0 & n_2 & 0 & n_3 & 0 & n_1 \\ 0 & 0 & n_3 & n_2 & n_1 & 0 \end{bmatrix} \begin{Bmatrix} \sigma_{11} \\ \sigma_{22} \\ \sigma_{33} \\ \sigma_{23} \\ \sigma_{13} \\ \sigma_{12} \end{Bmatrix} \quad (\text{A.2.3})$$

or in the $x = x_1, y = x_2, z = x_3, l = n_1, m = n_2, n = n_3$ notation

$$\begin{Bmatrix} \Phi_x \\ \Phi_y \\ \Phi_z \end{Bmatrix} = \begin{bmatrix} l & 0 & 0 & 0 & n & m \\ 0 & m & 0 & n & 0 & l \\ 0 & 0 & n & m & l & 0 \end{bmatrix} \begin{Bmatrix} \sigma_x \\ \sigma_y \\ \sigma_z \\ \tau_{yz} \\ \tau_{xz} \\ \tau_{xy} \end{Bmatrix} \quad (\text{A.2.4})$$

These relationships may be written in matrix–vector notation as

$$\underline{\Phi} = \underline{N}^T \underline{\sigma} \quad (3 \times 1) \quad (\text{A.2.5})$$

where $\underline{\Phi}$, \underline{N}^T and $\underline{\sigma}$ are easily identified by comparison to Equation (A.2.3).

In tensor notation, Cauchy's formulae are written as

$$\Phi_j = n_i \sigma_{ji} = n_i \sigma_{ij} \quad (\text{A.2.6})$$

since

$$\sigma_{ij} = \sigma_{ji} \quad (\text{A.2.7})$$

A.3 THE STRAIN–DISPLACEMENT RELATIONS (KINEMATICS OF DEFORMATION)

A body is said to undergo a rigid body motion if the distance between any two points in the body remains unchanged. Thus, a measure of the deformation (i.e., change in geometry) in a body is provided by the change in the distance between points in the body. This is quantified by the difference

$$(dL')^2 - (dL)^2 \quad (\text{A.3.1})$$

where dL and dL' are the distances between A and B in Figure A.3.1, before and after deformation. This measure of deformation (A.3.1) can be related to strains.

The coordinates of A, B, A' and B' are

$$\begin{aligned} A(x, y, z), \quad B(x + dx, y + dy, z + dz) \\ A'(x + u, y + v, z + w), \quad B'(x + u + dx', y + v + dy', z + w + dz') \end{aligned} \quad (\text{A.3.2})$$

Therefore,

$$dL^2 = dx^2 + dy^2 + dz^2 \quad (\text{A.3.3})$$

$$(dL')^2 = (dx')^2 + (dy')^2 + (dz')^2 \quad (\text{A.3.4})$$

The displacements of points A and B can be expressed in terms of their position changes as shown in Figure A.3.2 and the following analysis.

The coordinates of A are (x, y, z) and the coordinates of A' are (x', y', z') . Therefore,

$$u = x' - x \quad v = y' - y \quad w = z' - z \quad (\text{A.3.5})$$

Note

$$dL^2 = dx^2 + dy^2 + dz^2, \quad (dL')^2 = (dx')^2 + (dy')^2 + (dz')^2 \quad (\text{A.3.6})$$

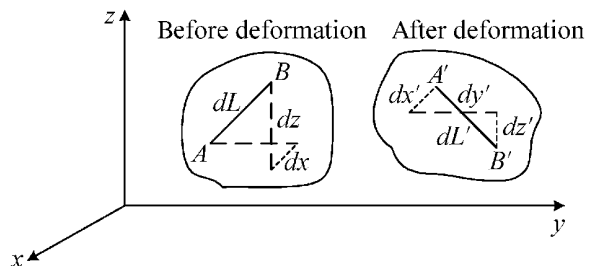


Figure A.3.1 Generic structure before and after deformation

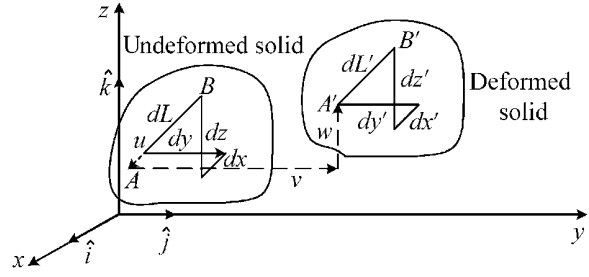


Figure A.3.2 Displacements of A and B

The displacement of point A is given by

$$\bar{u}_A = u\hat{i} + v\hat{j} + w\hat{k} \quad (\text{A.3.7})$$

The displacement of point B is given by

$$\bar{u}_B = (u + du)\hat{i} + (v + dv)\hat{j} + (w + dw)\hat{k} \quad (\text{A.3.8})$$

where by the chain rule of differentiation

$$\begin{aligned} du &= \frac{\partial u}{\partial x} dx + \frac{\partial u}{\partial y} dy + \frac{\partial u}{\partial z} dz \\ dv &= \frac{\partial v}{\partial x} dx + \frac{\partial v}{\partial y} dy + \frac{\partial v}{\partial z} dz \\ dw &= \frac{\partial w}{\partial x} dx + \frac{\partial w}{\partial y} dy + \frac{\partial w}{\partial z} dz \end{aligned} \quad (\text{A.3.9})$$

Equation (A.3.5) implies

$$dx' = du + dx \quad dy' = dv + dy \quad dz' = dw + dz \quad (\text{A.3.10})$$

Substituting (A.3.10) into (A.3.6) yields

$$(dL')^2 = dx^2 + dy^2 + dz^2 + 2dudx + 2dvdy + 2dwdz + du^2 + dv^2 + dw^2 \quad (\text{A.3.11})$$

Substituting dL^2 from (A.3.6) and (A.3.11) into (A.3.1) yields

$$(dL')^2 - (dL)^2 = 2(dudx + dvdy + dwdz) + du^2 + dv^2 + dw^2 \quad (\text{A.3.12})$$

Substituting (A.3.9) into (A.3.12) yields

$$\begin{aligned} (dL')^2 - (dL)^2 &= 2 \left\{ \frac{\partial u}{\partial x} + \frac{1}{2} \left[\left(\frac{\partial u}{\partial x} \right)^2 + \left(\frac{\partial v}{\partial x} \right)^2 + \left(\frac{\partial w}{\partial x} \right)^2 \right] \right\} dx^2 \\ &+ 2 \left\{ \frac{\partial v}{\partial y} + \frac{1}{2} \left[\left(\frac{\partial u}{\partial y} \right)^2 + \left(\frac{\partial v}{\partial y} \right)^2 + \left(\frac{\partial w}{\partial y} \right)^2 \right] \right\} dy^2 \\ &+ 2 \left\{ \frac{\partial w}{\partial z} + \frac{1}{2} \left[\left(\frac{\partial u}{\partial z} \right)^2 + \left(\frac{\partial v}{\partial z} \right)^2 + \left(\frac{\partial w}{\partial z} \right)^2 \right] \right\} dz^2 \\ &+ 2 \left\{ \frac{\partial u}{\partial y} + \frac{\partial v}{\partial x} + \frac{\partial u \partial u}{\partial x \partial y} + \frac{\partial v \partial v}{\partial x \partial y} + \frac{\partial w \partial w}{\partial x \partial y} \right\} dx dy \\ &+ 2 \left\{ \frac{\partial u}{\partial z} + \frac{\partial w}{\partial x} + \frac{\partial u \partial u}{\partial x \partial z} + \frac{\partial v \partial v}{\partial x \partial z} + \frac{\partial w \partial w}{\partial x \partial z} \right\} dx dz \\ &+ 2 \left\{ \frac{\partial v}{\partial z} + \frac{\partial w}{\partial y} + \frac{\partial u \partial u}{\partial y \partial z} + \frac{\partial v \partial v}{\partial y \partial z} + \frac{\partial w \partial w}{\partial y \partial z} \right\} dy dz \end{aligned} \quad (\text{A.3.13})$$

Note that if $(dL)^2 = (dL')^2$ for all A and B on the body, the body is unstrained and it is said to have undergone a rigid body displacement. Therefore, $(dL)^2 - (dL')^2$ provides an appropriate measure of deformation of the solid. To define the strains, write (A.3.13) as

$$(dL')^2 - (dL)^2 = 2\varepsilon_x dx^2 + 2\varepsilon_y dy^2 + 2\varepsilon_z dz^2 + 2\gamma_{xy} dx dy + 2\gamma_{xz} dx dz + 2\gamma_{yz} dy dz \quad (\text{A.3.14})$$

where the normal strain is defined by

$$\begin{aligned} \varepsilon_x &= \frac{\partial u}{\partial x} + \frac{1}{2} \left[\left(\frac{\partial u}{\partial x} \right)^2 + \left(\frac{\partial v}{\partial x} \right)^2 + \left(\frac{\partial w}{\partial x} \right)^2 \right] \\ \varepsilon_y &= \frac{\partial v}{\partial y} + \frac{1}{2} \left[\left(\frac{\partial u}{\partial y} \right)^2 + \left(\frac{\partial v}{\partial y} \right)^2 + \left(\frac{\partial w}{\partial y} \right)^2 \right] \\ \varepsilon_z &= \frac{\partial w}{\partial z} + \frac{1}{2} \left[\left(\frac{\partial u}{\partial z} \right)^2 + \left(\frac{\partial v}{\partial z} \right)^2 + \left(\frac{\partial w}{\partial z} \right)^2 \right] \end{aligned}$$

and the engineering shear strains by

$$\begin{aligned} \gamma_{xy} &= \frac{\partial u}{\partial y} + \frac{\partial v}{\partial x} + \frac{\partial u}{\partial x} \frac{\partial u}{\partial y} + \frac{\partial v}{\partial x} \frac{\partial v}{\partial y} + \frac{\partial w}{\partial x} \frac{\partial w}{\partial y} \\ \gamma_{xz} &= \frac{\partial u}{\partial z} + \frac{\partial w}{\partial x} + \frac{\partial u}{\partial x} \frac{\partial u}{\partial z} + \frac{\partial v}{\partial x} \frac{\partial v}{\partial z} + \frac{\partial w}{\partial x} \frac{\partial w}{\partial z} \\ \gamma_{yz} &= \frac{\partial v}{\partial z} + \frac{\partial w}{\partial y} + \frac{\partial u}{\partial y} \frac{\partial u}{\partial z} + \frac{\partial v}{\partial y} \frac{\partial v}{\partial z} + \frac{\partial w}{\partial y} \frac{\partial w}{\partial z} \end{aligned} \quad (\text{A.3.15})$$

Equation (A.3.15) is the nonlinear “large deflection” or finite strain–displacement relations. In many cases of practical importance, the deformations in a structure are sufficiently small, so that the quadratic terms in (A.3.15) are insignificant. In this case, the “linearized” strain–displacement relations become

$$\begin{aligned} \varepsilon_x &= \frac{\partial u}{\partial x}, \quad \varepsilon_y = \frac{\partial v}{\partial y}, \quad \varepsilon_z = \frac{\partial w}{\partial z} \\ \gamma_{xy} &= \frac{\partial u}{\partial y} + \frac{\partial v}{\partial x}, \quad \gamma_{xz} = \frac{\partial u}{\partial z} + \frac{\partial w}{\partial x}, \quad \gamma_{yz} = \frac{\partial v}{\partial z} + \frac{\partial w}{\partial y} \end{aligned} \quad (\text{A.3.16})$$

The strains $\gamma_{xy}, \gamma_{xz}, \gamma_{yz}$ are the “engineering strains” that are typically discussed in strength of materials books. A convenient shear strain definition for tensor notation is given by

$$\varepsilon_{yz} = \frac{1}{2} \left(\frac{\partial v}{\partial z} + \frac{\partial w}{\partial y} \right) = \frac{1}{2} \gamma_{yz}, \quad \varepsilon_{xz} = \frac{1}{2} \left(\frac{\partial u}{\partial z} + \frac{\partial w}{\partial x} \right) = \frac{1}{2} \gamma_{xz}, \quad \varepsilon_{xy} = \frac{1}{2} \left(\frac{\partial u}{\partial y} + \frac{\partial v}{\partial x} \right) = \frac{1}{2} \gamma_{xy} \quad (\text{A.3.17})$$

Combining (A.3.16) and (A.3.17) yields the relationship

$$\begin{Bmatrix} \varepsilon_x \\ \varepsilon_y \\ \varepsilon_z \\ \gamma_{yz} \\ \gamma_{xz} \\ \gamma_{xy} \end{Bmatrix} = \begin{bmatrix} \partial_x & 0 & 0 \\ 0 & \partial_y & 0 \\ 0 & 0 & \partial_z \\ 0 & \partial_z & \partial_y \\ \partial_z & 0 & \partial_x \\ \partial_y & \partial_x & 0 \end{bmatrix} \begin{Bmatrix} u \\ v \\ w \end{Bmatrix} \quad (\text{A.3.18})$$

or in matrix–vector notation

$$\underline{\varepsilon} = \underline{D} \underline{U} \quad (\text{A.3.19})$$

By defining

$$\begin{Bmatrix} \varepsilon_{11} \\ \varepsilon_{22} \\ \varepsilon_{33} \\ 2\varepsilon_{23} \\ 2\varepsilon_{13} \\ 2\varepsilon_{12} \end{Bmatrix} = \begin{Bmatrix} \varepsilon_x \\ \varepsilon_y \\ \varepsilon_x \\ 2\varepsilon_{yz} \\ 2\varepsilon_{xz} \\ 2\varepsilon_{xy} \end{Bmatrix} = \begin{Bmatrix} \varepsilon_x \\ \varepsilon_y \\ \varepsilon_z \\ \gamma_{yz} \\ \gamma_{xz} \\ \gamma_{xy} \end{Bmatrix} \quad (\text{A.3.20})$$

Equation (A.3.18) implies

$$\varepsilon_{ij} = \frac{1}{2}(u_{i,j} + u_{j,i}) \quad (\text{A.3.21})$$

which shows that

$$\varepsilon_{ij} = \varepsilon_{ji} \quad (\text{A.3.22})$$

A.4 MATERIAL LAW (CONSTITUTIVE RELATIONS)

The relations between the kinetic (i.e., force, stress) and kinematic (i.e., displacement, strains) variables depend upon the constitution (physical properties) of the material and are thus called “constitutive equations.” For a linear, isotropic solid, these become

$$\begin{Bmatrix} \varepsilon_{11} \\ \varepsilon_{22} \\ \varepsilon_{33} \\ 2\varepsilon_{23} \\ 2\varepsilon_{13} \\ 2\varepsilon_{12} \end{Bmatrix} = \frac{1}{E} \begin{bmatrix} 1 & -\nu & -\nu & 0 & 0 & 0 \\ -\nu & 1 & -\nu & 0 & 0 & 0 \\ -\nu & -\nu & 1 & 0 & 0 & 0 \\ 0 & 0 & 0 & 2(1+\nu) & 0 & 0 \\ 0 & 0 & 0 & 0 & 2(1+\nu) & 0 \\ 0 & 0 & 0 & 0 & 0 & 2(1+\nu) \end{bmatrix} \begin{Bmatrix} \sigma_{11} \\ \sigma_{22} \\ \sigma_{33} \\ \sigma_{23} \\ \sigma_{13} \\ \sigma_{12} \end{Bmatrix} \quad (\text{A.4.1})$$

or

$$\underline{\varepsilon} = \underline{E}^{-1} \underline{\sigma} \quad (\text{A.4.2})$$

and

$$\begin{Bmatrix} \sigma_{11} \\ \sigma_{22} \\ \sigma_{33} \\ \sigma_{23} \\ \sigma_{13} \\ \sigma_{12} \end{Bmatrix} = \frac{E}{(1+\nu)(1-2\nu)} \begin{bmatrix} 1-\nu & \nu & \nu & 0 & 0 & 0 \\ \nu & 1-\nu & \nu & 0 & 0 & 0 \\ \nu & \nu & 1-\nu & 0 & 0 & 0 \\ 0 & 0 & 0 & \frac{1-2\nu}{2} & 0 & 0 \\ 0 & 0 & 0 & 0 & \frac{1-2\nu}{2} & 0 \\ 0 & 0 & 0 & 0 & 0 & \frac{1-2\nu}{2} \end{bmatrix} \begin{Bmatrix} \varepsilon_{11} \\ \varepsilon_{22} \\ \varepsilon_{33} \\ 2\varepsilon_{23} \\ 2\varepsilon_{13} \\ 2\varepsilon_{12} \end{Bmatrix} \quad (\text{A.4.3})$$

or

$$\underline{\sigma} = \underline{E} \underline{\varepsilon} \quad (\text{A.4.4})$$

where ν = Poisson’s ratio and E = Young’s modulus. To account for the thermal strains, consider an element of an elastic solid subjected to a temperature change ΔT . If an element of length dx is not constrained, it expands to a new length of $dx + (dx)\alpha\Delta T$ where α is the coefficient of thermal expansion which may depend on temperature. In an isotropic body,

the thermal expansion is the same in all direction, so that an unrestrained 3D element experiences a uniform expansion but no angular distortions. Thus, in the unrestrained isotropic body, the temperature change leads to thermal normal strains while not producing thermal shear strains:

$$\varepsilon_x^0 = \varepsilon_y^0 = \varepsilon_z^0 = \alpha \Delta T, \quad \gamma_{xy}^0 = \gamma_{xz}^0 = \gamma_{yz}^0 = 0 \quad (\text{A.4.5})$$

The material law in this case becomes

$$\underline{\varepsilon} = \underline{E}^{-1} \underline{\sigma} + \underline{\varepsilon}^0 \quad (\text{A.4.6})$$

or

$$\underline{\sigma} = \underline{E} \underline{\varepsilon} - \underline{E} \underline{\varepsilon}^0 \quad (\text{A.4.7})$$

where \underline{E} , $\underline{\varepsilon}$, $\underline{\sigma}$ are defined in Equations (A.4.1)–(A.4.4) and

$$\underline{\varepsilon}^0 = \alpha \Delta T (1 \ 1 \ 1 \ 0 \ 0 \ 0)^T \quad (\text{A.4.8})$$

Utilizing (A.4.3) and (A.4.8), it can be shown that (A.4.7) may be written as

$$\underline{\sigma} = \underline{E} \underline{\varepsilon} + \underline{\sigma}_0 \quad (6 \times 1) \quad (\text{A.4.9})$$

where

$$\underline{\sigma}_0 = \frac{-E\alpha\Delta T}{1-2\nu} (1 \ 1 \ 1 \ 0 \ 0 \ 0)^T \quad (\text{A.4.10})$$

In these equations, it should be noted that ΔT is the difference between the actual temperature and a reference (strain-free) temperature at the point where stresses and strains are under consideration. The coefficient of thermal expansion is around $6 \times 10^{-6} \text{ cm/cm/}^\circ\text{F}$ for various types of steel and may range as high as $5 \times 10^{-4} \text{ cm/cm/}^\circ\text{F}$ for some elastomers. For an orthotropic material (Cook, 1989),

$$\underline{\varepsilon} = \underline{E}^{-1} \underline{\sigma} + \underline{\varepsilon}^0 \quad (\text{A.4.11})$$

where

$$\underline{E}^{-1} = \begin{bmatrix} \frac{1}{E_x} & -\frac{\nu_{xy}}{E_y} & -\frac{\nu_{xz}}{E_z} & 0 & 0 & 0 \\ -\frac{\nu_{yx}}{E_x} & \frac{1}{E_y} & -\frac{\nu_{yz}}{E_z} & 0 & 0 & 0 \\ -\frac{\nu_{zx}}{E_x} & -\frac{\nu_{zy}}{E_y} & \frac{1}{E_z} & 0 & 0 & 0 \\ 0 & 0 & 0 & \frac{1}{G_{yz}} & 0 & 0 \\ 0 & 0 & 0 & 0 & \frac{1}{G_{xz}} & 0 \\ 0 & 0 & 0 & 0 & 0 & \frac{1}{G_{xy}} \end{bmatrix} \quad (\text{A.4.12})$$

This matrix must be symmetric by the Betti–Maxwell theorem:

$$\frac{\nu_{yx}}{E_x} = \frac{\nu_{xy}}{E_y}, \quad \frac{\nu_{zx}}{E_x} = \frac{\nu_{xz}}{E_z}, \quad \frac{\nu_{zy}}{E_y} = \frac{\nu_{yz}}{E_z} \quad (\text{A.4.13})$$

The $\underline{\varepsilon}^0$ term for the orthotropic case is

$$\underline{\varepsilon}^0 = (\alpha_x \Delta T \quad \alpha_y \Delta T \quad \alpha_z \Delta T \quad 0 \quad 0 \quad 0)^T \quad (\text{A.4.14})$$

A.5 COMPATIBILITY RELATIONSHIPS

It can be shown that the strains are not independent, that is, from (A.3.16):

$$\frac{\partial^2}{\partial x \partial y} (\gamma_{xy}) - \frac{\partial^2}{\partial y^2} (\varepsilon_x) - \frac{\partial^2}{\partial x^2} (\varepsilon_y) = \frac{\partial^2}{\partial x \partial y} \left(\frac{\partial u}{\partial y} + \frac{\partial v}{\partial x} \right) - \frac{\partial^2}{\partial y^2} \left(\frac{\partial u}{\partial x} \right) - \frac{\partial^2}{\partial x^2} \left(\frac{\partial v}{\partial y} \right) = 0$$

The full set of compatibility relations is

$$\begin{bmatrix} 0 & \partial_z^2 & \partial_y^2 & -\partial_y \partial_z & 0 & 0 \\ \partial_z^2 & 0 & \partial_x^2 & 0 & -\partial_z \partial_x & 0 \\ \partial_y^2 & \partial_x^2 & 0 & 0 & 0 & -\partial_x \partial_y \\ -\partial_y \partial_z & 0 & 0 & -\frac{1}{2} \partial_x^2 & \frac{1}{2} \partial_x \partial_y & \frac{1}{2} \partial_x \partial_z \\ 0 & -\partial_z \partial_x & 0 & \frac{1}{2} \partial_y \partial_x & -\frac{1}{2} \partial_y^2 & \frac{1}{2} \partial_y \partial_z \\ 0 & 0 & -\partial_x \partial_y & \frac{1}{2} \partial_z \partial_x & \frac{1}{2} \partial_z \partial_y & -\frac{1}{2} \partial_z^2 \end{bmatrix} \begin{Bmatrix} \varepsilon_x \\ \varepsilon_y \\ \varepsilon_z \\ \gamma_{yz} \\ \gamma_{xz} \\ \gamma_{xy} \end{Bmatrix} = \begin{Bmatrix} 0 \\ 0 \\ 0 \\ 0 \\ 0 \\ 0 \end{Bmatrix} \quad (\text{A.5.1})$$

or

$$D_1 \underline{\varepsilon} = \underline{0} \quad (\text{A.5.2})$$

A.6 WORK AND POTENTIAL ENERGY

A.6.1 Internal Work and Potential Energy

From elementary physics, the work performed by a force \vec{F} on a particle equals

$$W_{ab} = \int_a^b \vec{F} \cdot \vec{ds} \quad (\text{A.6.1})$$

where \vec{ds} is the differential displacement vector of the particle. The internal work performed in deforming a body is defined in a similar manner. Figure A.6.1 shows the stresses that act on a differential volume contained in the body as discussed in (Reddy, 1984). The dashed lines indicate the undeformed differential volume and the solid lines indicate the deformed. The internal forces that resist the deformation shown in Figure A.6.1 are

$$F_{11} = -\sigma_{11} dx_2 dx_3, \quad F_{21} = -\sigma_{21} dx_1 dx_3 \quad (\text{A.6.2})$$

Recall that work is performed throughout the entire strain cycle during the deformation of a spring, that is,

$$W_{ab} = \int_a^b dW = \int_a^b F dx = \int_a^b -kx dx = -\frac{k}{2} x^2 \Big|_a^b \quad (\text{A.6.3})$$

where the minus sign indicates work performed by the internal force of the spring in resisting deformation.

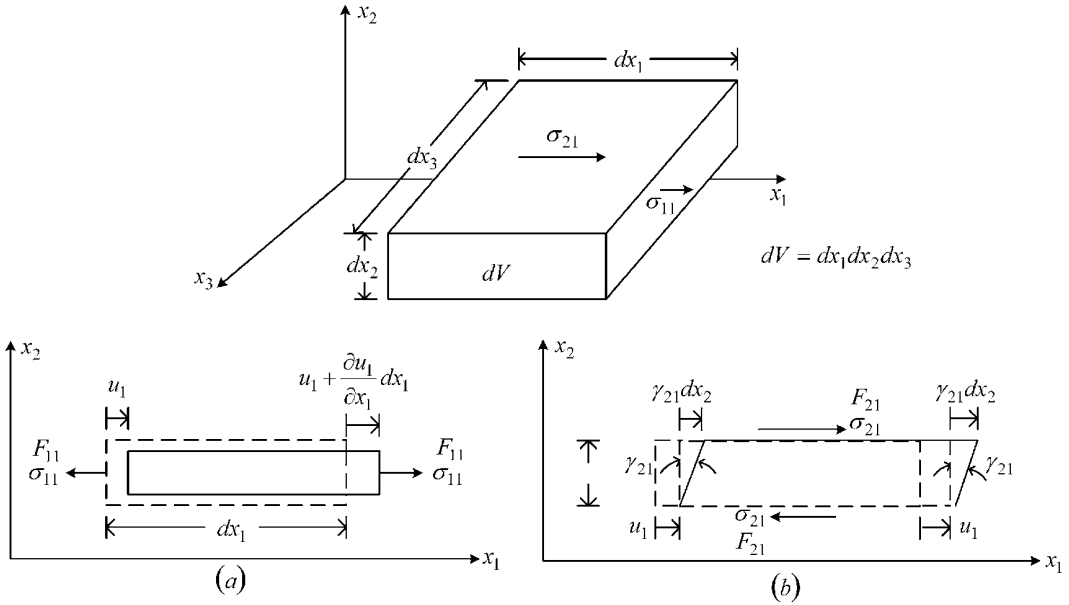


Figure A.6.1 Original and deformed states of differential volume for (a) normal and (b) shear stresses

Likewise, the work performed by the forces in (A.6.2) must be evaluated by considering all contributions from the original to the deformed state. The differential work contributed by the normal internal forces in Figure A.6.1 is

$$dW_{11} = F_{11} d\left(u_1 + \frac{\partial u_1}{\partial x_1} dx_1\right) - F_{11} du_1 = F_{11} d\varepsilon_{11} dx_1 = -\sigma_{11} d\varepsilon_{11} dV \quad (\text{A.6.4})$$

where from (A.3.21)

$$\varepsilon_{11} = \frac{du_1}{dx_1} \quad (\text{A.6.5})$$

Similarly, for the shear forces,

$$dW_{21} = -F_{21} du_1 + F_{21} d(u_1 + \gamma_{21} dx_2) = F_{21} d\gamma_{21} dx_2 = -\sigma_{21} d\gamma_{21} dV \quad (\text{A.6.6})$$

Similar results hold for the remaining normal (σ_{22}, σ_{33}) and shear (σ_{23}, σ_{13}) stresses, yielding

$$\begin{aligned} dW &= -(\sigma_{11} d\varepsilon_{11} + \sigma_{22} d\varepsilon_{22} + \sigma_{33} d\varepsilon_{33} + \sigma_{12} d\gamma_{12} + \sigma_{23} d\gamma_{23} + \sigma_{13} d\gamma_{13}) dV \\ &= -\underset{1 \times 6}{\underline{\underline{\sigma}}}^T \underset{6 \times 1}{d\underline{\underline{\varepsilon}}} dV \end{aligned} \quad (\text{A.6.7})$$

The total internal work performed is then given by

$$W_1 = - \int_V \int_0^\varepsilon \underline{\underline{\sigma}}^T d\underline{\underline{\varepsilon}} dV \quad (\text{A.6.8})$$

Substitution of the material law for a linear, elastic solid (A.4.4) into (A.6.8) yields

$$W_1 = - \int_V \int_0^\varepsilon \underline{\underline{\varepsilon}}^T \underline{\underline{E}} \underline{\underline{\varepsilon}} dV \quad (\text{A.6.9})$$

The inner integral may be performed if \underline{E} is symmetric, yielding the strain energy density function

$$U_\rho = \int_0^\underline{\varepsilon} \underline{\varepsilon}^T \underline{E} d\underline{\varepsilon} = \frac{1}{2} \underline{\varepsilon}^T \underline{E} \underline{\varepsilon} \quad (\text{A.6.10})$$

The total internal strain energy becomes

$$U_1 = -W_1 = \frac{1}{2} \int_V U_\rho dV = \frac{1}{2} \int_V \underline{\varepsilon}^T \underline{E} \underline{\varepsilon} dV \quad (\text{A.6.11})$$

A.6.2 Work of External Forces Acting on a Deformable Body

Externally applied forces perform work on a deformable body with surface S and volume V according to the equation

$$W^E = \int_V \int_0^{\underline{u}} \underline{\bar{F}}_{EV}^T d\underline{u} dV + \int_S \int_0^{\underline{u}} \underline{\bar{F}}_{ES}^T d\underline{u} dS \quad (\text{A.6.12})$$

where

$$\underline{\bar{F}}_{EV} = \left\{ \begin{array}{l} \bar{F}_{EV1}(x_1, x_2, x_3) \\ \bar{F}_{EV2}(x_1, x_2, x_3) \\ \bar{F}_{EV3}(x_1, x_2, x_3) \end{array} \right\} = \text{the applied distributed body forces acting inside the body} \\ (\text{force per unit volume}) \quad (\text{A.6.13})$$

$$\underline{\bar{F}}_{ES} = \left\{ \begin{array}{l} \bar{F}_{ES1}(x_1, x_2, x_3) \\ \bar{F}_{ES2}(x_1, x_2, x_3) \\ \bar{F}_{ES3}(x_1, x_2, x_3) \end{array} \right\} = \text{the applied surface tractions (force per unit area)} \\ \text{acting on the body's surface} \quad (\text{A.6.14})$$

$$\underline{u} = \left\{ \begin{array}{l} u_1(x_1, x_2, x_3) \\ u_2(x_1, x_2, x_3) \\ u_3(x_1, x_2, x_3) \end{array} \right\} = \text{displacement field in or on the body where } \underline{\bar{F}}_{EV} \text{ or } \underline{\bar{F}}_{ES} \text{ are applied} \\ (\text{A.6.15})$$

Figure A.6.2 illustrates a body force such as gravity, that is,

$$\underline{\bar{F}}_{EV} \Big|_{\text{gravity}} = \left\{ \begin{array}{l} 0 \\ 0 \\ -\frac{dm * g}{dV} \end{array} \right\} = \left\{ \begin{array}{l} 0 \\ 0 \\ -\frac{\rho dV * g}{dV} \end{array} \right\} = \left\{ \begin{array}{l} 0 \\ 0 \\ -\rho g \end{array} \right\} \quad (\text{A.6.16})$$

The pressure p is an example of a surface traction, that is,

$$\underline{\bar{F}}_{ES} \Big|_{\text{pressure}} = \left\{ \begin{array}{l} 0 \\ 0 \\ -p \end{array} \right\} \quad (\text{A.6.17})$$

If the forces are independent of displacements, the inner integral of (A.6.12) may be performed, yielding

$$W^E = \int_V \underline{\bar{F}}_{EV}^T \underline{u} dV + \int_S \underline{\bar{F}}_{ES}^T \underline{u} dS \quad (\text{A.6.18})$$

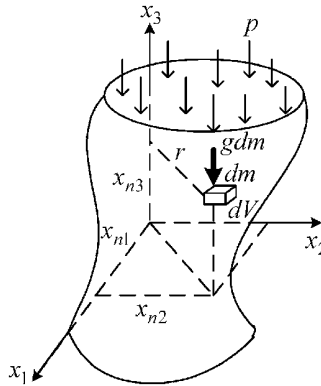


Figure A.6.2 Illustration of externally applied forces

REFERENCES

- COOK, R. *Concepts and Applications of Finite Element Analysis*, 3rd ed. New York: John Wiley & Sons, Inc., 1989.
- FUNG, Y.C. *Foundation of Solid Mechanics*. Englewood Cliffs: Prentice Hall, 1965.
- REDDY, J.N. *Energy and Variational Methods in Applied Mechanics*. New York: John Wiley & Sons, Inc., 1984.

Index

- absorber, 560, 563
- accelerance, 592
- acceleration vector formula, 90
- active vibration control, 37, 867
- actuator, 868, 871, 872, 889
 - magnetic, 874–878, 881
- admittance, 592
- Ampere's law, 874
- amplification factor *see* Quality factor
 - Q under damping
- API Standards, 22, 29, 548, 551
- apparent mass, 593
- assumed modes, 96
 - active vibration control, 919
 - damping matrix, 241, 249, 263
 - examples, 214, 222, 229, 235, 245, 254, 261
 - external forces, 222, 228, 234, 242, 247, 264
 - global shape functions, 97, 219, 226
 - kinematically admissible function, 97
 - kinetic energy, 223
 - Lagrange equation, 212, 219
 - mass matrix, 212, 225, 237, 246, 259, 262, 357
 - natural frequencies and mode shapes, 355, 359
 - potential energy, 226
 - rotating structures, 215
 - stiffness matrix, 220, 227, 233, 239, 258, 263, 357
- atomic clock, 6
- atomic force microscope AFM, 28
- AVC *see* active vibration control

- backward mode, 340, 385
- balancing rotating machinery, 24, 545, 549
- banded storage, 817
- bandwidth of matrices, 815
- bandwidth of response, 872, 886
- bar finite elements, 275–307
 - assembly of matrices, 281–285, 288, 299
 - constrained system *jarray*, 287, 298
 - constrained system *larray*, 287, 298, 301
 - degree of freedom dof connectivity array, 296, 300
 - nodal connectivity array, 279
- one dimensional (1D), 275–289
 - damping matrix, 277
 - force vector, 278
 - mass matrix, 277
 - stiffness matrix, 277
- two dimensional (2D), 289–307
 - coordinate transform, 291
 - damping matrix, 294
 - element actions, 296
 - embedded rigid sections, 303, 362
 - external force vector, 295
 - mass matrix, 293, 302
 - mode shapes, 363
 - natural frequency, 332, 362
 - stiffness matrix, 292, 302
- base excitation, 445, 475
- basis vector, Guyan, 69
- basis vectors, 65
- beam finite elements
 - Euler, 637–670
 - assembly of matrices, 656
 - constrained system *jarray*, 657, 663, 664
 - constrained system *larray*, 653, 656, 657, 662, 664, 666
 - degree of freedom dof connectivity array, 654, 655, 658, 663
 - nodal connectivity array, 654, 658, 663
 - coordinates, 639
 - damping matrix, 669
 - force vector, 644–646, 651, 669
 - global coordinates, 646–648, 652
 - harmonic response, 669
 - imposed support motion, 666
 - mass matrix, 642–644, 648
 - mode shapes, 658, 664, 666, 669
 - natural frequency, 658, 664, 666, 669
 - shape function, 639
 - stiffness matrix, 639–642, 647
 - strain energy, 639–642, 647
 - strains, 640
 - three dimensional (3D), 680, 688, 694
 - Timoshenko
 - two dimensional (2D), 725–750
 - assembly of matrices
 - constrained system *jarray*, 734, 737
 - constrained system *larray*, 735
 - degree of freedom dof connectivity array, 733
 - nodal connectivity array, 713, 718, 733

- beam finite elements (*cont'd*)
 - coordinates, 726
 - coordinate transformation, 728
 - damping matrix, 739
 - force vector, 728, 741
 - mass matrix, 727, 728, 736
 - mode shapes, 737, 743
 - natural frequency, 737, 743
 - shape function, 639
 - stiffness matrix, 727, 728, 735
 - strain energy, 639–642
 - strains, 640
 - transient response, 746
- three dimensional (3D), 670–726
 - assembly of matrices, 281–285, 288, 299, 656, 766, 812–813, 816, 845
 - constrained system *jarray*, 719, 720, 725
 - constrained system *larray*, 714, 719, 721
 - degree of freedom dof connectivity array, 713
 - nodal connectivity array, 713, 718
 - coordinate transform, 673–679, 703, 711
 - coordinates, 672, 685, 700, 713, 716
 - external force vector, 704–712
 - mass matrix, 688–690, 695–700, 703, 723
 - mode shapes, 726
 - moment of inertia, 683
 - natural frequency, 726
 - shape function, 687, 693, 697, 699
 - shear form factor, 682, 683
 - stiffness matrix, 688, 694, 697, 701, 702, 703, 720
 - strain energy, 682, 702, 703
 - strains, 680, 681, 691, 696
- beam strain, 232
- bearing instability, 411–413
- beat vibrations, 331
- Belleville washer, 56
- bi-orthogonality *see* orthogonality
- boundary condition, essential, 99

- C-core, 876
- cable constraint, 93
- cable vibrations, 390
- Campbell diagram, 254
- canonical form, 85
- Cauchy's formula *see* traction boundary condition
- central difference *see* numerical integration algorithms
- change of basis, 67
- characteristic equation, 80
 - single degree of freedom (dof), 311
 - two degrees of freedom (dof), 320
- Cholesky factorization, 348
- circulatory matrix, 19, 344, 506
- collocation *see* noncollocation

- complex variables, 60
 - differential equation solution, 62, 526, 528, 566
- compliance, 592
- compressor, 552
- constitutive relation *see* material law
- continuous distributed mass systems, 390
 - Euler Bernoulli beam, 400
 - longitudinal bars, 394
 - strings and cables, 390
 - Timoshenko beam, 404
 - torsion bars, 396
- control *see* feedback control
- control canonical form, 888, 911
- convolution integral, 434
- coordinate transformation, 67, 75
- corner frequency, 887
- current stiffness, 876, 878

- damping, 3, 29
 - active, 882, 890, 896, 906, 913
 - elastomeric, 556
 - half power point measurement, 538, 579
 - log decrement, 313
 - measurement, 313, 538, 541, 543, 579, 582
 - orthogonal damping matrix, 364, 367–377, 457, 486, 569, 669, 739, 863
 - phase slope measurement, 541
 - proportional *see* orthogonal damping matrix under damping
 - Quality factor Q, 540, 547, 885, 904
 - ratio, 309, 540
 - active, 891
 - derivative, 624
 - multi degree of freedom system (dof), 364
 - single degree of freedom system (dof), 311
 - in a rotating frame, 343
- degrees of freedom, 63
 - independent, 97
- differential equations, 50
- Dirac delta, 86, 100, 434, 917, 921
- distributed mass, continuous systems, 390

- earthquake, 8, 446, 475
- effective mass *see* modal effective mass
- eigenvalue, 79
 - circulatory system, 343
 - conjugate, 311
 - derivative, 595, 620, 624
 - gyroscopic system, 334, 339, 380
 - linearization, 595
 - orthogonally damped system, 365, 374–377
 - perturbation, 621
 - reanalysis, 595
 - single degree of freedom (dof), 310
- eigenvector, 79
 - derivatives, 595
 - gyroscopic system, 334, 339, 380
 - non-uniqueness, 80
 - perturbation, 621

- elastomer, 556
- electrorestrictive actuator, 869
- endurance limit, 13
- energy methods, advantages, 143
- equilibrium (general equations for a solid), 927
- equilibrium position, 30
- equivalent stress, 17
- Euler angles, 77
- Euler numerical integration *see* numerical integration algorithms
- Euler's identity, 60, 527
- fatigue
 - damage, 18
 - failure, 11
- feedback control, 868, 878
 - compensation, 880
 - control law, 869, 871, 881, 882
 - error, 880
 - steady state, 883
 - gains, 881, 883, 906, 914
 - lead compensation, 893, 896, 914
 - piezoelectric stack actuator, 907
 - poles, 886
 - sensors, 868–869, 871, 879, 881, 889
 - stability, 873, 884, 885, 891, 895, 905, 906
- filter of elastic modes, 468
- finite elements *see* individual element types: bars, beams-2DEuler, beams-2DTimoshenko, beams-3DTimoshenko, solid-2D, membrane, solid-3D
- finite elements, 211 *see also* Lagrange equation
 - "*J*" array *see* individual element types
 - "*L*" array *see* individual element types
 - assembly of matrices *see* individual element types
 - automated mesh, 801
 - banded storage, 815
 - degree of freedom connectivity array *see* individual element types
 - external forces, 272, 275
 - Gauss integration points, 757–759
 - ground excitation, 666
 - introduction, 35
 - isoparametric, 755, 826
 - kinematic constraint, 98, 99
 - kinetic energy, 267, 272
 - Lagrange equation, 275
 - mass matrix, 267, 269, 272
 - nodal connectivity array *see* individual element types
 - nodal displacements, 268, 272
 - potential energy, 274
 - shape function consistency condition, 99, 276, 639, 679, 687, 826
 - shape function interpolation, 99, 268, 272
 - stiffness matrix, 269, 271, 274
 - strain-displacement relation, 271
 - support excitation, 666
- flexibility, 592
- flexible modes, 68
- force transmissibility *see* transmissibility
- force types
 - base excitation, 445, 446, 475
 - exponential, 422, 429, 432
 - impulse, 435
 - modal, 453, 489
 - periodic, 525, 552
 - pulse, 437, 440, 442
 - ramp, 422, 429
 - rotating imbalance, 504, 525, 529, 538–540, 546, 549, 551, 561, 567, 900
 - step, 422, 429
 - successive, 438
- forward mode shape, 340, 385, 548
- Fourier series, 4, 80, 552, 554
- free vibration, 3 *see also* initial condition
 - response, natural frequency, mode shape
- frequency, 2
- frequency response function (FRF), 83, 872
- gains *see* feedback control
- Gauss quadrature, 759
- generalized coordinates, 67
- Goodman diagram, 14
- good vibrations, 9
- Green's function, 435
- Guyan reduction
 - basis vectors, 596, 599, 606, 619
 - reordering of matrices, 596
 - selection of retained degrees of freedom, 597
 - transformation matrix, 597
- gyroscopic system, 319, 335
 - bi-orthogonality, 387
 - matrix, 319, 332, 338, 506
 - mode shapes, 335, 339
 - natural frequencies, 334, 339, 380
- half power point *see* half power point
 - measurement under damping
- harmonic response, 525
 - active controlled system, 899
 - modal approach, 570
- N degrees of freedom, 566, 567, 815, 818
- receptances *see* receptances
- single degree of freedom, 527–559
 - force input, 529
 - support motion input, 535
 - two (2) degrees of freedom, 559–565
- harmonics, 4
- Heaviside function, 86, 100, 435, 439, 440
- heavy spot, 548
- Hertzian contact, 56
- high spot, 548
- human body vibrations, 6, 9

- identification of parameters, 543
 - imbalance *see* force types rotating imbalance
 - impedance, 592
 - impulse function, 86
 - incompatible elements, 774
 - inertance, 592
 - inertia, 29, 32, 33
 - influence coefficient
 - definition, 592
 - balancing, 549
 - initial condition response
 - continuous, distributed mass systems, 394, 395, 399
 - gyroscopic system, 335, 340
 - modal distribution initial conditions, 363
 - N degrees of freedom (dof) , 351, 354, 359
 - orthogonally damped systems, 366, 372
 - rigid body modes, 354
 - single degree of freedom (dof), 312, 317
 - Two (2) degrees of freedom (dof), 324, 327, 330, 335
 - inner product, 70
 - instability, 344, 408–418, 510
 - instability *see* stability under feedback control
 - international space station, 869
 - ISO standards, 9, 29
 - isolation of support motion input, 536, 537
 - isoparametric, 35

 - Jeffcott rotor, 55, 874, 878, 891, 900

 - kinematic constraints, 86, 92
 - kinetic energy
 - flexible body
 - assumed modes *see* assumed modes
 - finite elements *see* finite elements
 - particle, 144
 - rigid body, 145, 146, 155
 - examples, 156, 185, 188, 191, 201, 206

 - Lagrange equation, 35
 - assumed modes *see* assumed modes
 - compared with Newton's law, 207
 - finite elements *see* finite elements
 - flexible bodies, 211, 223
 - generalized force, 166
 - flexible bodies
 - internal force, 218, 220
 - external force, 221, 222, 228
 - rigid bodies
 - forces, 166, 184
 - examples, 186, 191, 193, 201, 207
 - torques, 166, 186
 - examples, 185, 186, 191, 193
 - potential energy, 168
 - flexible body, 216, 225
 - rotational stiffness, 176
 - examples, 185, 191
 - translational stiffness symmetric
 - matrix, 169
 - examples, 185, 188, 191, 193
 - Rayleigh dissipation
 - rotational damping, 180
 - example, 185, 188, 191, 206
 - translational damping, 174
 - examples, 188, 191, 201
 - rigid bodies, 162, 164, 166, 182
 - static equilibrium position reference, 196–199
 - symbolic math code automation, 201
 - system of particles, 157, 162
- Laplace transforms, 83, 428, 440
- lead compensation *see* feedback control
- linear dependent, 67
- linear independent, 67
- linearization, 56, 118, 207, 876
- log decrement, 313
- loss factor, 557
- low pass filter (LPF), 886, 889
-
- MAC *see* assurance criterion under modal
- magnetic
 - bearing actuator, 871, 874, 875
 - circuit, 875
 - field intensity, 875
 - flux density, 875, 877
- magnetic force, 58
- MAPLE
 - 3D plot, 260
 - determinant, 320
 - differential equation solution, 53, 426
 - differentiation, 426, 531
 - eigenvalues, 47, 358
 - function integration or differentiation, 215, 232, 252, 260
 - Laplace transform, 430, 434
 - matrix, 253, 260
 - numerical integration, 50, 54
 - plot, 531
 - simplify, 253
 - solve algebraic equation–find roots, 311, 342, 531
 - square root, 531
 - substitution (subs), 434
 - symbolic, 45, 122
 - Taylor series, 57
- material law (general equations for a solid), 934
- MATLAB, 42
 - eigenvalues, 43, 462, 511, 805, 661
 - format, 661
 - global command, 51, 510
 - mode shapes, 462, 805, 661
 - numerical integration, 50, 54, 463, 507, 513, 516
 - error tolerance, 474

- plots, 450, 455, 514, 521, 662
- symbolic
 - collect, 907, 917
 - diff (differentiation), 920
 - differential equation solution, 428
 - int (integration), 917, 920
 - Laplace transform, 431
 - simplify, 907, 917, 920
 - solve (solve equations), 917
 - syms, 45, 428, 431, 907, 917
- transfer function to state space, 889
- matrix
 - circulatory, 70, 319, 342, 344
 - direction cosine, 76
 - gyroscopic, 70, 319, 332, 338
 - lower triangular, 348
 - orthogonal, 70, 77
 - orthogonal damping, 367, 373, 377
 - partitioned, 73
 - positive definite, 70, 346
 - rank, 352
 - skew symmetric, 70, 344, 338
- Maxwell stress tensor, 876
- membrane finite elements, 810–820
 - assembly of matrices, 812–813, 816
 - mass matrix, 810–811
 - mode shape, 813, 814
 - natural frequencies, 813
 - potential energy, 811–812
 - shape functions, 811
 - stiffness matrix, 811–812
 - strains, 811–812
- MESH2D, 802
- microgravity vibration isolation, 169
- MIL Military standards, 27, 29
- Miner–Palmgren Rule, 18
- mobility, 592
- modal
 - acceleration method, 453, 455
 - analysis, 79
 - assurance criterion, 590, 591
 - condensation, 451, 492
 - coordinates, 452, 466, 479, 489, 491
 - dominance, 577, 578
 - effective mass, 477, 484
 - force, 453, 489
 - mass, 349
 - parameter identification, 578, 580, 581
 - participation factor, 477
 - synthesis, 609
 - basis vectors, 609
 - junction degrees of freedom, 611
 - subspace condensation, 611
- mode shape, 36, 64, 68, 80, 309
 - comparison, 590
 - continuous distributed mass systems, 392, 395, 398, 402, 407
 - gyroscopic system, 339, 380
 - measurement, 580, 581, 585, 587
 - N degrees of freedom, 347, 362
 - orthogonally damped system, 364, 366, 375
 - orthonormal, 350
 - perturbation, 621
 - scale factor, 590
 - Two (2) degrees of freedom, 324, 326, 330, 339
- momentum and impulse method
 - angular, 134
 - linear, 129
- music, 6
- natural frequency, 3, 6, 36, 79, 309
 - active, 891, 896, 913
 - continuous distributed mass systems, 393, 395, 398, 402, 407
 - damped, 311, 364
 - derivative, 624
 - gyroscopic system, 334, 339, 380
 - measurement, 541, 543, 579, 584
 - N degrees of freedom (dof), 347, 353, 355
 - orthogonal damped system, 362, 372, 377
 - 1 degree of freedom (dof), 309, 311, 317
 - perturbation, 621, 624
 - rigid body mode, 352
 - Two (2) degrees of freedom (dof), 323, 326, 330, 332, 339
- Newmark Beta *see* numerical integration algorithms
- Newton's law, 34
 - compared with Lagrange's equation, 207
 - examples, 104, 105, 112, 117, 121, 122, 138, 207
 - rotational, 110, 111,
 - static equilibrium position reference, 120
 - symbolic math code automation, 122
 - translational, 108
- node (of finite element model), 35, 99
- node (of mode shape), 65
- noncollocation, 873, 901, 906
- numerical integration, 51, 54, 494
- numerical integration algorithms, 494
 - central difference, 495
 - Euler, 501
 - Euler–Improved, 501
 - Newmark Beta, 496, 507, 518
 - Runge–Kutta, 503, 507, 519
 - time step, 508, 515
- Nyquist plot *see* polar plot
- O ring, 558
- orbit, 547
- orthogonality, 68
 - bi-orthogonality
 - general \underline{M} , \underline{K} , \underline{C} systems, 388–390, 489
 - gyroscopic modes, 385, 387
 - continuous distributed mass systems, 393
 - orthogonally damped system mode shapes, 364, 373

- orthogonality (*cont'd*)
 - symmetric mass, stiffness and damping systems, 377
 - trigonometric, 82
 - undamped system mode shapes, 349, 353, 354, 358
- parameter identification *see* modal parameter identification
- participation factor *see* modal participation factor
- particle motion, 103
- periodic excitation, 552
- permeability, 875, 877
- phase angle, 2
- phasors, 60, 525, 557, 566
- piezoelectric, 6
- piezoelectric actuator
 - capacitance, 907
 - expansion factors, 907, 913
 - internal preload, 907
 - patch or layer (PLA), 870, 915
 - cantilever, 918, 919
 - force, 917, 921
 - moment, 916, 917
 - polarization, 907
 - preload, 907, 913
 - resonance, 907
 - soft and hard materials, 907
 - stack, 869, 908, 910, 913
 - voltage requirement, 907
- polar plot, 543
- potential energy, 151
 - assumed modes *see* assumed modes
 - finite elements *see* finite elements
 - general equations for a solid, 936
 - Lagrange equation *see* Lagrange equation
- power, 35
- power and work, 151, 155, 156
- power amplifier, 84, 867
- power conservation principle, 153, 155, 156
- pressure pulsation, 552
- proportional damping *see* orthogonal damping matrix under damping
- pulley system, 95
- pulse disturbances, 440, 442
- quadratic form, 73
- quality factor *Q see* Quality factor *Q* under damping
- rainflow cycle counting, 18
- Rayleigh's quotient, 631
- reanalysis, 595
- receptances, 572, 574, 592
 - measurement, 580, 581, 584, 587, 592
 - modal formula with accelerated convergence, 574
 - mode dominance, 577
 - of orthogonally damped system, 573
 - synthesis of substructures, 575, 576, 595
- reluctance (magnetic), 875, 877
- resonance, 3, 79, 531, 540, 556, 559, 560, 572, 584, 820
- response spectrum, 444
- rigid body motions (modes), 63, 465, 471, 485
- rms root mean square, 4
- rolling contact, 93
- rotating machinery standards, 22
- rotating structures assumed modes, 215, 245
- rotordynamic instability, 413
- RungeKutta *see* numerical integration algorithms
- runout, 879, 882
- sand pattern, 64
- saturation, 872, 876
- sawtooth, 554
- seismic, 8
- self excited vibrations *see* instability
- separation margin (resonance), 22
- servo power amplifier (SPA), 867, 871, 873, 881, 907
- shaker, 538, 582, 584
- S-N curve, 13, 21
- solid finite elements
 - two dimensional (2D), 751–821
 - assembly of matrices, 766
 - assembly of matrices
 - constrained system *jarray*, 766, 767, 779
 - constrained system *larray*, 765, 766, 767, 779
 - degree of freedom dof connectivity array, 764, 778
 - nodal connectivity array, 764, 777, 800
 - axisymmetric, 786–801
 - coordinates, 754, 755, 763, 764
 - external force vector, 760–763, 780, 792–794
 - extra shape functions, 774
 - Gauss integration points, 757, 759
 - harmonic response, 820
 - incompatible, 774
 - isoparametric, 755
 - Jacobian, 756, 790
 - mass matrix, 759, 766, 795, 803
 - mesh, 777, 801, 805–809
 - mode shapes, 781–786, 797, 806
 - natural frequency, 781–786, 797, 806
 - plane strain, 751
 - plane stress, 753
 - shape functions, 755, 775, 788, 799, 802
 - stiffness matrix, 756, 758, 759, 766, 775, 791, 792, 794, 803
 - strains, 752, 756, 787
 - stress calculation, 768–774, 796
 - triangular elements, 801–809
- three dimensional (3D)
 - assembly of matrices, 845
 - constrained system *jarray*, 845, 859
 - constrained system *larray*, 845, 860

- degree of freedom dof connectivity array, 843, 844, 859
 - nodal connectivity array, 842, 858
 - coordinates, 824, 842–844
 - degenerate (6 node), 827
 - external force vector, 834, 836–842, 863
 - extra shape functions, 827, 834
 - Gauss integration points, 832, 860
 - incompatible, 827, 834
 - isoparametric, 824, 826
 - Jacobian, 828, 830
 - mass matrix, 835
 - mesh, 857
 - mode shapes, 861
 - natural frequency, 861
 - shape functions, 826, 829
 - stiffness matrix, 832–835
 - strains, 828
 - stress calculation, 846–856
 - transient response, 861
- span a subspace, 65
- spectrum (response), 444, 446, 475
- state space model, 897, 898, 912
- static condensation *see* Guyan reduction
- Static Equilibrium Position SEP reference, 120
- steady state harmonic response *see* harmonic response
- stiffness, 29, 31
- dynamic, 543, 592
 - measurement, 543
- stiffness (active), 882, 890, 906, 913
- stiffness (position), 876, 878, 882
- stiffness matrix assumed modes, 220, 227, 248
- strain
- beam, 232
 - general equations for a solid, 931
 - plate, 256
- stress
- stiffening, 247
 - calculation, 768–774
 - concentration factor, 18
 - general equations for a solid, 929
- strings, 390
- subspace, 63, 67
- subspace condensation, 69, 453, 489, 491, 492, 595, 611
- substructures, 608 *see also* synthesis of substructures
- successive disturbances, 438
 - superelements, 608
 - support excitation *see* base excitation
 - Symbolic Math Code solution, 122, 201
 - synthesis *see* modal synthesis
 - synthesis of substructures, 575, 576, 608, 609
- Taylor series, 56
- tesla, 876
- Timoshenko beam theory, continuous distributed mass model, 404
- traction boundary condition (general equations for a solid), 929
- transfer function, 84, 431, 872, 888, 893, 910
- convert to canonical form, 888, 898, 911
 - rolloff, 883
- transient response, 421
- N degrees of freedom, 451
 - N degrees of freedom unconstrained system, 465
 - 1 degree of freedom, 421
 - Analytical solution, 422
 - convolution integral, 434
 - Laplace Transform solution, 428
- transmissibility ratio, 530
- transport theorem, 90
- trial weight, 549
- unbalance *see* force types rotating imbalance
- uncollocation *see* noncollocation
- uncoupling of equations of motion *see* orthogonality
- units, 5
- unstable vibrations *see* instability
- valve instability, 408
- variable mass systems, 138
- velocity vector formula, 90
- vibration absorber *see* absorber
- viscoelastic material, 261
- von Mises stress, 17
- whirl, 547
- work
- and potential energy, 147, 150
 - energy principle, 153, 154, 155
 - forces that do not perform work, 149
 - general equations for a solid, 936
 - rotational, 148

WILEY END USER LICENSE AGREEMENT

Go to www.wiley.com/go/eula to access Wiley's ebook EULA.